Density Field Dynamics: A Complete Unified Theory

Gary Alcock[1, *]

[1] *Independent Researcher, Los Angeles, CA, USA*

(Dated: v5.0 — October 2026)

(Foundations: 19 Aug 2025 [3]; Unified v1.0: 25 Dec 2025 [4])

This is release v5.0; the prior public version is v4.0. It adds evidence appendices, the measured clock coefficient (item 6 below), two further results, and the DLSC structural extension: the early-clock CMB fit (App. ZS: all six spectrum-shape inputs supplied upstream of the data with per-input grades printed, three derived or adopted-and-priced, the tilt a stated number and ω_b at its calibrated conventional-point value, with two further calibrations free (the clock and the amplitude $A_s e^{-2\tau}$), $H_0^{\rm early} = 67.52 \pm 0.09$); the gravity completion and Kohn null (App. ZU) — Newton recovered as an exact zero-parameter identity of the quantized ψ action, with an exactly zero self-gravity sideband on a trapped crystal's center-of-mass mode that makes the Schrödinger–Newton shift (semiclassically $\Delta\omega/\omega$ of 1.2–6.7×10^{-13} for Os, 1.1–6.2×10^{-15} for Si) a falsifier of the completion, not a DFD prediction; and the domain-local screen calibration (App. ZT), $a_0(x,t) = 2\sqrt{\alpha}\, c\, H_{\rm scr}(x,t)$, conditional on the DLSC axiom (2 discrete bits, 0 fitted continuous parameters), with SH0ES (73.49 ± 0.93 in 2025) as the named external falsifier of that early-clock calibration at 5.0–6.4σ; under the two-clock postulate of item 6, SH0ES's value is read on the bound-matter clock, 1.5σ above $H_0^{\rm loc} = 72.09$.

Density Field Dynamics (DFD) is a scalar refractive-index theory of gravity defined by the postulate that spacetime is flat but permeated by a scalar field $\psi(\mathbf{x}, t)$ establishing an optical refractive index $n = e^{\psi}$. Light propagates according to the eikonal of the optical metric $d\tilde{s}^2 = -c^2 dt^2/n^2 + d\mathbf{x}^2$, while matter responds to the effective potential $\Phi = -c^2\psi/2$. This framework has an **optical scalar sector** ψ that governs clock rates, refraction, and quasi-static dynamics, together with a **transverse-traceless radiative sector** $h_{ij}^{\rm TT}$ for gravitational waves, derived as the spin-2 irreducible component of the same zero-mode parent tensor on $\mathbb{C}P^2 \times S^3$ whose trace yields ψ [1]. It reproduces all classic tests of general relativity in the weak-field limit ($\gamma = \beta = 1$, all PPN parameters matching GR), gravitational waves at speed c with two tensor polarizations, and MOND-like phenomenology at galactic scales through a nonlinear crossover function $\mu(x) = x/(1+x)$, the weak-response form of an exponential response, and scale $a_0 = 2\sqrt{\alpha}\, cH_0^{\rm loc}$, **both derived from S^3 topology** (Appendix N; the form of μ holds given the ground-state principle, with its branch chosen by data, Appendix BS; equivalently $a_0 = 2\alpha^{29}\sqrt{c^7/G\hbar}$ on bound-matter clocks (item 6 below), with the exponent and prefactor derived, Appendix AP). A dedicated model-independent SPARC shape analysis further finds $n_{\rm opt} = 1.15 \pm 0.12$ (95% CI $[1.00, 1.50]$) in the family $\mu_n(x) = x/(1+x^n)^{1/n}$, with DFD's $n = 1$ inside the confidence region and Standard MOND's $n = 2$ strongly disfavored.

This paper presents DFD as a unified framework: (1) **Fine-structure constant:** $\alpha^{-1} = 137.036$ from the microsector spectral action on $\mathbb{C}P^2 \times S^3$ with Toeplitz truncation at $k_{\max} = 60$. The closed form is **convention-locked**: a forced binary fork between regular-module and fermion-rep microsectors is resolved by a no-hidden-knobs policy, with the surviving branch giving a closed form that is exact under two stated choices (the ρ-shifted Casimir on $S^3 = SU(2)$ and α's own trace with the heat-kernel regulator; §X C): its integers alone give the measured value to 21 ppm, and with the bracket coefficient $c = 1/13$, whose provenance is open, it lies a fractional 4.9×10^{-9} (0.0049 ppm) from the CODATA 2022 value, 32 times that value's uncertainty. The trace in the closed form is the hypercharge trace, and its identification with $1/e^2$ rather than with the hypercharge coupling is not derived (§X I). (1b) **Weinberg angle:** $\sin^2\theta_W = 3/13 = 0.2308$ from gauge partition $(3, 2, 1)$ and a stated trace normalization (Appendix Z). Agreement with $\sin^2\theta_W^{\rm exp} = 0.23129$ [2]: **0.2%** (tree-level vs $\overline{\rm MS}$); (1c) **Strong coupling:** $\alpha_s(M_Z) = 0.1187$ from $\Lambda_{\rm QCD} = M_P\alpha^{19/2} = 61.20$ MeV and the selected proper-time→ $\overline{\rm MS}$ matching factor $\sqrt{4\pi}$ (Appendix Z). Agreement with PDG 2024 (0.1180 ± 0.0009): 0.8σ; (2) **Higgs hierarchy:** $v = M_P \times \alpha^8 \times \sqrt{2\pi} = 246.09$ GeV (observed: 246.22 GeV)—the exponent is derived, so the 17 orders of magnitude are topological, not fine-tuned, while the prefactor $\sqrt{2\pi}$ is one fitted input with a no-go on deriving it. The Higgs quartic $\lambda_H = 1/8$ from dimension counting is a conjecture (Appendix Z); it gives tree-level $m_H = 123$ GeV and 124.6 GeV at the top-quark scale, 0.40% below the measured value; (3) **Nine charged fermion masses:** $m_f = A_f\alpha^{n_f} v/\sqrt{2}$ with sector-dependent exponents fits with a 1.42% mean error at leading order, with CP^2 kernels $K_d = J_3$, $K_u = I_4$ fixed by symmetry and democratic coupling (Lemma K.2), QCD factors from $b_0 = 7$, generation operator $G = \mathrm{diag}(2/3, 1, 1)$ from the primed microsector trace (Theorem K.4, Appendix K); the top and charm are derived, and the other seven species rest on seven data-selected prefactors (App. FM);

(4) **CKM pattern:** Wolfenstein parameters fit the integer pattern $(\lambda, A, \bar{\rho}, \bar{\eta}) = (31, 108, \frac{43}{2}, 49)\times\alpha$, with the CP-even apex $\bar{\rho} = \frac{43}{2}\alpha = 21.5\alpha$ selected by the Euler-projection postulate of the strengthened DFD–SD branch (Appendices Z and AO). *Per-channel agreement against PDG 2024:* λ at 0.5%

(1.8σ), $\bar{\eta}$ at 1.5% (0.7σ), A at 4.6% (2.5σ, sensitive to the open inclusive/exclusive $|V_{cb}|$ tension), $\bar{\rho}$ at 1.4% (0.2σ). The magnitude integers are suggestive of cohomological origin, while the apex is selected at theorem grade *inside the strengthened DFD–SD branch* by the Euler-projection postulate (Appendix AO), which, consistent with the no-forcing anti-theorem of that appendix, is a new structural postulate rather than a consequence of the pre-strengthened axioms. The branch predicts $\gamma = 66.3093^\circ$ and $J = 2.9731 \times 10^{-5}$. PMNS trimaximal TM1 (App. X), with $\sin^2\theta_{13} = 3\alpha$ a stated conjecture; (5) **Strong CP:** the spectral action fixes $\theta_{\rm YM} = 0$, given that nothing is added to it for the gauge fields, and $\bar{\theta} = 0$ at tree level and loop-bounded below 10^{-16}, with $\det(M_u M_d)$ kept positive by the det-orthogonal structure on the branch of Postulate Y.10; the CP anomaly vanishes because the fermion Clifford module on the even-dimensional (8) mapping torus has spectral pairing and no zero modes, forcing $\eta = h = 0$ (Appendices L, AO). **No axion required.** The minimal real-kernel flavor sector gives $J = 0$ (Theorem AO.7); the observed nonzero CKM phase ($J \neq 0$) is supplied by the conjugation-odd, determinant-orthogonal Berry offset of the *strengthened DFD–SD branch* (Postulate Y.10, Appendix AO), which preserves $\bar{\theta} = 0$;

(6) **G–$\mathbf{H}_0$ invariant (exponent derived; coefficient measured):** The dimensionless constraint $G\hbar H_0^2/c^5 = C\,\alpha^{57}$ has its exponent derived via Gaussian mode integration on the finite-dimensional microsector (Appendix O): the exponent 57 is forced by primed-determinant scaling on the finite microsector state space; the per-mode suppression factor α follows from uniform gauge normalization with exact eigenvalue cancellation (Lemma O.5); the identification with the physical hierarchy uses the finite dimensionality of the microsector to eliminate all UV ambiguities (Lemma O.6). The constraint is written $G\hbar H_0^2/c^5 = C\,\alpha^{57}$: the exponent 57 is a theorem, while the dimensionless coefficient C is proven *not derivable* from the printed corpus (eight-route no-go, App. ZS) and rests on one measured input, the vacuum coefficient $R = \Omega_\Lambda C = 0.6042 \pm 0.0027$, with today's early-clock value $C = 0.87784 \pm 0.00266$ (BAO+θ_*; plik-lite 0.8772), with the cross-channel $H_0^{\rm early} = 67.52 \pm 0.09$ km/s/Mpc concordant across five CMB-anchored channels; the Hubble tension is not read as a ψ-screen bias of Planck (the background ψ mode adds no screen beyond the expansion it describes, and the optical metric leaves θ_* exactly invariant, Theorems in App. ZS). Both measurements of the Hubble rate are robust, and DFD reads them as one universe on two clocks (Postulate ZS.11): matter keeps a clock offset by one constant λ, set when matter first binds and falls behind the expansion, so the CMB-anchored channels read $H_0^{\rm early} = 67.52$, and bound-matter clocks and rulers read the $C = 1$ value $H_0^{\rm loc} = \alpha^{28.5}/t_P = 72.09$ km/s/Mpc, from the measured G with zero parameters (Sec. XIX); its size $\lambda = H_0^{\rm loc}/H_0^{\rm early}$ is the one measured input (Sec. ZS 5). The local evidence agrees with the bound-matter clock: the Cepheid-free local mean 71.87 ± 0.96 lies 0.2σ from $H_0^{\rm loc}$, bound systems read $a_0 = 2\sqrt{\alpha}\,cH_0^{\rm loc} = 1.1966 \times 10^{-10}$ m/s^2, consistent with SPARC within its systematic error, and the coefficient booking of the Extended Derivations' five-presentation Λ theorem ($C = 1.027 \pm 0.029$, the ladder's value re-expressed) lies 0.9σ from $C = 1$; the price is a laboratory-unit age of 12.92 Gyr against ages of the universe of 13.5–13.8 Gyr that one programme infers from globular clusters with a ΛCDM formation delay, and the absolute a_0 scale (Euclid/DESI lensing RAR) tests the postulate once baryonic masses are known to about 2%; (7) **Solar corona (Sec. XIV):** electromagnetic fields couple to ψ at tree level through their energy and the optical index $n = e^{\psi}$, with no threshold, so DFD predicts the standard Ly-α/O VI asymmetry ratio; the 2007–2009 SOHO/UVCS data do not measure that ratio; (8) **CMB from baryon loading + derived χ:** Peak ratio $R = 2.34$ from the analytic baryon-loading estimate, all peak locations set by the clock coefficient measured from BAO and θ_*, with *no* ψ-lensing map (App. ZS), third-peak height from the derived χ-matter dark matter — a cold, collisionless component of mass 32.00 eV ($= 2\pi\sqrt{158}\,\bar{M}_{\rm P}\alpha^{13}$, the flux-period identification) whose abundance $\Omega_\chi h^2 = 0.1193$ is computed *forward* from the finite $SU(2)_{60}$ Chern–Simons vacuum (-0.6σ from Planck), with no initial-condition angle and no fitted density (App. AV, Thm. AV.13); *Ledger grade:* the carrier/operator is derived, the $\sqrt{158}$ mass multiplicity is one stated count, and the abundance is forced-amplitude/stated- convention, its measure conditional on the asserted premise P4′, rather than a fitted density (App. FK); (9) **One dark energy:** the α^{57} vacuum term (Appendix AU) is DFD's only dark energy, and the late-time distance excess is not read as an optical-screen effect (Appendix ZS; Appendix SL);

(10) **Clock sector and Majorana scale (Appendix P):** the electromagnetic-sector proposal $k_\alpha = \alpha^2/(2\pi)$ and the scale $M_R = M_P\alpha^3$ are obtained under the Appendix O protocol, each conditional on an explicitly stated assumption (for k_α, the one-gauge-vertex axiom: a postulated non-metric operator outside the minimal action, Thm. XI.2). The clock sector is interpreted in a channel-resolved way: same-ion E3/E2 measurements strongly constrain any pure α-sector coupling law, while cross-species and nuclear-clock channels discriminate the extended non-metric channel. The cavity–atom sector likewise has geometric cancellation at tree level and a residual screened signal, not an order-unity slope; the 2026 Th-229 reproducibility result already excludes the unscreened strong-sector amplitude and compresses the surviving nuclear-clock window into the rough range 26 Hz to $\mathcal{O}(1\,\text{kHz})$; (10b) **Neutrino mass spectrum (Appendix X):** Closed at zero continuous parameters; one discrete branch choice (Branch B, among four equally natural

fractions) is selected by the oscillation data, with everything downstream α-locked (branch-selection remark in Appendix X). Branch B exponents $k = \alpha^{-3/11}$, $r = \alpha^{-7/20}$ from microsector integers; absolute scale $m_3 = (14/13)\pi M_P \alpha^{14}$ from finite-d priming. Predictions: $\Delta m^2_{21} = 7.48 \times 10^{-5}$ eV^2, $\Delta m^2_{31} = 2.51 \times 10^{-3}$ eV^2 (NuFIT 6.0: $\chi^2 = 0.025$, $p = 0.99$); $\sum m_\nu = 61.46$ meV; combined hierarchy exponent $k^2 r^2 = \alpha^{-137/110}$; (11) **Dust branch under $K' = \mu$ (Appendix Q):** The temporal kinetic function $K(\Delta)$ is built on the same S^3 saturation-union composition law that gives the weak-response $\mu(x)$; the identification $K'(\Delta) = \mu(\Delta)$ is adopted, not forced. Key results: (i) temporal deviation invariance is forced by the composition law; (ii) the unique temporal segment scalar is $\Delta = (c/a_0)|\dot\psi - \dot\psi_0|$; (iii) with $K'(\Delta) = \mu(\Delta)$, the dust branch emerges with $w \to 0$, $c_s^2 \to 0$. A no-go lemma proves the naive quadratic identification gives $w \to 1/2$ (not dust). Full $P(k)$ matching is a program item, not a theorem. (12) **Screen-closure identities (Sec. XVI A 4; the optical-distance dressing they rest on is retired, App. SL):** The identities are retired with that dressing; distance duality, $\Delta\psi_{\rm dual} = 0$ by Etherington reciprocity, stands (item E1).

Additional sectors: (13) **Antimatter gravity (Sec. XV):** Species-dependent sensitivities σ_A from non-metric ψ-sector couplings predict matter–antimatter differential acceleration $\Delta a_{H\bar H}/a \approx 2|\sigma_{\bar H} - \sigma_H|$. At the metric level, DFD reproduces GR's universal free fall; C-odd couplings (n_B, n_L) are bounded by ordinary-matter EP tests to $|\Delta a_{H\bar H}/a| \lesssim 10^{-11}$; (14) **EM–$\psi$ coupling (Appendix R):** Parameter λ controls electromagnetic back-reaction on ψ in a parametric-mode model that needs a dynamical ψ mode, which the local ψ of Axiom WS.1 lacks, and whose absolute normalization is open. Existing cavity stability provides an *accidental* bound $|\lambda - 1| \lesssim 3 \times 10^{-5}$. An intentional 2ω modulation search could reach $|\lambda - 1| \sim 3 \times 10^{-9}$ with upgraded apparatus; (15) **IBVP well-posedness (Sec. III E):** Existence, uniqueness, and continuous dependence hold at theorem grade for the initial-boundary value problem of the scalar's numerical hyperbolic relaxation on bounded domains (under Axiom E the scalar itself is an instantaneous constraint); (16) **Late-time observations (Sec. XVI N):** the DES Y3 Weyl potential is 2–3σ shallower at low z (not a DFD prediction); DESI DR2 hints at $w(z) \neq -1$ (an open tension: DFD's $w = -1$); wide binaries are contested, with DFD predicting no boost near the Sun; E_G is consistent on the current Planck-like matter fraction, and the dependency-aware $S_8 \simeq 0.822$ result is consistent with KiDS-Legacy (0.45–0.74σ for the primary/joint anchors) and 2.8σ above DES Year 6 (survey errors only).

New structural results: (17) **The Padé identity and the horizon (Appendix AA):** The lapse-squared scalar $\mathcal{L}(u) \equiv c^2/|g_{tt}|$ of isotropic-coordinate Schwarzschild is mathematically identical to the squared $[1,1]$ Padé approximant of the exponential $\exp(2u)$, the value of DFD's lapse-squared e^ψ at $\psi = 2u$. Writing $P_{m,m}(u)$ for the diagonal $[m,m]$ Padé approximant of e^u (so $P_{m,m}(u) \approx e^u$): $\mathcal{L}_{\rm GR}(u) = [P_{1,1}(u)]^2 = [(1+u/2)/(1-u/2)]^2$, and the identity extends to a Padé hierarchy in which $[P_{m,m}(u)]^2 = \exp(2u) + O(u^{2m+1})$. Agreement through $O(u^2)$ reproduces the post-Newtonian parameter $\beta = 1$ in both theories (the spatial-curvature parameter $\gamma = 1$ for DFD follows separately from the physical metric, Sec. IV). Beyond that order DFD's exterior is not the exponential: with the scalar-longitudinal piece σ of the parent strain kept (Sec. V A 3), the Einstein–Hilbert term (App. WS) makes the exterior of a static star the Schwarzschild metric in DFD's coordinates, lapse $e^{-\psi/2}$ and $\det g_{ij} = e^{3\psi}$, with $\psi = -\ln\!\big(1 - 2GM/c^2R\big)$ at areal radius R. The pole at $u = 2$ is therefore a horizon of DFD's black holes as well: Schwarzschild's event horizon at $R = 2GM/c^2$, with Schwarzschild's photon sphere and shadow (Secs. VI B and VI C). A firewall theorem distinguishes DFD from Yilmaz-type exponential metrics, which arise within GR as wormhole solutions with exotic matter (Theorems AA.2, AA.3); (18) **Uniqueness of the internal manifold (Appendix F 6):** The manifold $X = \mathbb{C}P^2 \times S^3$ used throughout DFD is not an ansatz. It is the unique compact manifold, up to diffeomorphism, satisfying seven satisfiable vacuum axioms: compactness, minimality of dimension, nondegenerate Kähler-times-frame product structure, a parallelizable frame factor, $\chi_{\rm top}(M_c) = 3$ (three generations), simple connectedness of the frame factor, and positive internal Ricci curvature (Theorem AB.1). Derived rather than assumed: dimension 7, the Spin^c structure, $\pi_3 = \mathbb{Z}$, even mapping-torus dimension (Strong-CP), and $k_{\max} = 60$ (through the conditional determinant-line count, given the generation count, the flux quantum and the five multiplet types). The $(3,2,1)$ block structure lives on the internal mode bundle over spacetime, not on TX (no tangent-bundle $(3,2,1,1)$ splitting exists, Lemma AB.13); the electroweak group is the isotropy group $U(2)$ of $\mathbb{C}P^2$ at the vacuum point under one stated identification, while colour and the family content are inputs, as in the Standard Model (App. F). The forced decomposition $7 = 4 + 3$ gives $M_c = \mathbb{C}P^2$ uniquely (del Pezzo surface with $\chi = 3$ under positive Ricci) and $M_g = S^3$ uniquely (Perelman: closed simply connected 3-manifold). The integers $\{3, 7, 8, 13, 19, 31, 49, 57, 60, 108, 137\}$ are therefore not free parameters: they are fixed by this manifold together with the stated inputs and identifications of App. FK.

(19) **Quantum sector (Sec. XVII, Appendix QM):** the single-particle Schrödinger equation is derived as an algebraic identity of the master equation (the fixed-N interacting form likewise), with the quantum phase i identified with the $\mathbb{C}P^2$ Kähler structure; the imports are explicitly inventoried

— the value of $\hbar$, the variable-N field-theoretic map, and the $\mathrm{Cl}(4,0)$ enlargement supplying the Dirac β — with the Born rule conditional and single-outcome selection not derived (a residue shared by all interpretations). The operator completion of the same action forces the *linear* side (App. ZU): the Schrödinger–Newton frequency shift is the falsifier of the completion, not a DFD prediction (levitated-optomechanics sideband); **Distance duality and screen clarification:** (E1) **Distance duality (Sec. XVI):** Etherington's reciprocity theorem holds exactly in DFD's optical metric, with no $e^{\Delta\psi}$ factor in the distance duality relation: $D_L = (1+z)^2 D_A$ exactly. The notation separates $\Delta\psi_{\mathrm{screen}}$ (distance bias, Estimators A and C) from $\Delta\psi_{\mathrm{dual}} = 0$ (DDR consistency, Estimator B).

The gauge emergence framework on $\mathbb{C}P^2 \times S^3$ yields the electroweak group as the isotropy group of $\mathbb{C}P^2$ under one stated identification, with colour, the family content and $N_{\mathrm{gen}} = 3$ entering as inputs, as in the Standard Model (App. F), and proton stability (if baryon number is violated only by the electroweak anomaly). The extended derivations — closures and promotions, the new-territory frontier, the CKM/τ and series IV–VI derivations, and the mathematical-foundation and quantum-gravity closures — are documented in the companion volume *Density Field Dynamics v5.0: Extended Derivations and Frontier Predictions*. The present paper states the theory in its current form: axioms, theorems with proofs, predictions, and falsifiers.

DFD fits no continuous parameter to the shape of any observable it predicts, except the baryon density. Every ratio, hierarchy and spectrum shape in the graded prediction set is delivered by derived or discretely selected structure, and the tilt $n_s = 1 - 2/60$ is a stated number (the mechanism is open); the individual results that carry an imported normalization instead (the charged-fermion prefactors of App. FM, the within-multiplet η_q of App. Y) are graded as such at their own sites and are not reported as parameter-free. The theory's cosmology carries **four continuous calibration constants**: the vacuum coefficient $R = \Omega_\Lambda C = 0.6042 \pm 0.0027$ (calibrating the absolute scale; today's early-clock value $C = 0.87784 \pm 0.00266$), the amplitude A_s of the primordial perturbations (the formula $32\pi\alpha^5$ matches it, but the printed theory contains no mechanism for it: the perturbations enter through one stated starting condition), the coefficient of $\omega_b h^2$ (the one shape: its α^4 power is derived, and the printed mechanism gives η_B of about $(2\text{–}3)\times 10^{-9}$, three to five times Planck's value), and the reionization optical depth τ (an astrophysical quantity shared with ΛCDM). That is four against ΛCDM's six free parameters, and on the Planck likelihood itself — where A_s and τ collapse into $A_s e^{-2\tau}$ — three against its five effective parameters (App. ZS; full per-input accounting in App. FK, Rem. FK.8, and the inputs of its graded predictions in Tables CXXVII and CXXVIII). The discrete topological sector carries no continuous freedom: the isotropy charge of $\mathbb{C}P^2$ fixes $q_1 = 3$, the determinant-line lift gives $\mathcal{O}(9)$ (with $N_{\mathrm{gen}} = 3$ a discrete input), and the five chiral multiplet types fix the padding (status remarks: App. F). Within the bundle decomposition $E = \mathcal{O}(a) \oplus \mathcal{O}^{\oplus n}$, minimal-padding uniquely selects $(a, n) = (9, 5)$ with $k_{\max} = 60$. The discrete inputs are priced rather than free: a trials-factor audit (App. CE) enumerates the admissible discrete space (8.0×10^9 addresses) and shows that, given the stated bracket coefficient $c = 1/13$, landscape scanning cannot account for the closeness of the α value. One scale measurement (H_0 or G), together with the measured vacuum coefficient R, then determines all dimensionful quantities via $G\hbar H_0^2/c^5 = C\,\alpha^{57}$. This paper presents the mathematical formulation and demonstrates that DFD constitutes a unified framework for gravity and particle physics, falsifiable with current experimental technology.

Two further results sharpen the flavor and propagation sectors. The CKM mixing magnitudes fit, at zero continuous free parameters, the selected integer pattern $(\lambda, A, \bar\rho, \bar\eta) = (31, 108, \frac{43}{2}, 49)\,\alpha$ over $k_{\max} = 60 = |A_5|$ (Appendix AO), and the weak CP phase vanishes in the literal real-kernel flavor construction ($J = 0$ at theorem grade), with the observed nonzero phase supplied by a single conjugation-odd determinant-orthogonal Berry offset whose apex is fixed by the Euler-projection postulate of the strengthened DFD–SD branch, giving $\gamma = 66.3093^\circ$ and $J = 2.9731 \times 10^{-5}$ (undetermined by the pre-strengthened axioms, by the no-forcing anti-theorem of Appendix AO). Separately, the light-propagation law $c_1 = c/n$ and the matter-acceleration law $\mathbf{a} = (c^2/2)\nabla\psi$ are unified as the null and timelike sectors of a single optical-metric wave equation, with the exact identity $\mathbf{a} = -\frac{1}{4}\nabla(c_{\mathrm{light}}^2)$ (Appendix AN).

Scope and status. This manuscript separates DFD claims into theorem-grade results, candidate extensions, program-grade numerical infrastructure, external empirical tests, anti-theorems/no-go results, and implementation artifacts. The verification record (Tier-1 closures, a reconciliation round, and Tier-2 to Tier-5+6 closures; *the five development-record syntheses are not reprinted in this deposit*) carries **91 results entered at theorem grade**. *Their review status differs by tier and is stated here rather than averaged into a single number.* Each Tier-1–6 closure above was checked against its stated proof at the time of entry; results *inherited* from releases predating that tiered programme have not all been re-examined to the same

* gary@gtacompanies.com

standard, and a ranked, deliberately unadjudicated list of the inherited statements flagged by a systematic proof-pattern scan is printed in §XVIII K. **This manuscript makes no claim of zero internal inconsistencies.** It maintains instead a corrigenda record: corrections are made at the statements they amend, the principal ones are tabulated below, and the standing-review list is printed for the same reason. The main open items are named rather than hidden, among them the origin of the primordial perturbations and the horizon problem, which enter through one stated starting condition (the amplitude A_s is a calibrated number), the interacting quantum dynamics shared with every quantum field theory, and in the dark sector the inner cores and masses of the χ halos, the mode-by-mode rule of motion of the momentum-conserving energy, the adopted floor law and environmental confinement, and the weak lensing of isolated galaxies beyond their bound radius, where the halo model of ΛCDM also falls below the measured points (see §XVIII A; the $Q_\chi = 1$ χ-clustering channel is closed by the adopted Rest-Mass Channel axiom, App. GR.3a, which confines the μ-law to bound systems). The χ relic abundance is conditional-derived (the Finite $SU(2)_{60}$ CS Vacuum Relic with the exact radiation-era bridge $\kappa_{\rm rad}$, $\Omega_\chi h^2 = 0.1193$ at -0.6σ; App. AV, Step 5b), its named open inputs the two stated normalization conventions, the stated count 158, the flux-period identification of $f_\chi = \bar{M}_{\rm P}\alpha^3$ and the asserted premise that the $2\pi/\alpha$ winding instanton changes the flux sector (App. AV). Claims should be evaluated by the tier labels and falsifier IDs in the master ledger, not as a single undifferentiated claim.

Principal corrections to earlier statements.

Companion volume. The extended derivations — closures and promotions, the new-territory frontier, the CKM/τ and series IV–VI derivations, and the mathematical-foundation and quantum-gravity closures — are documented separately in *Density Field Dynamics v5.0: Extended Derivations and Frontier Predictions*. The present paper contains the theory in its current form.

Earlier statement	Current status
CKM apex $\bar{\rho} = 19\alpha$	Superseded by the strengthened DFD–SD branch, $\bar{\rho} = \frac{43}{2}\alpha$ (Euler-projection postulate; App. AO).
Minimal real DFD gives CKM CP	Minimal real kernel gives $J = 0$ (theorem); nonzero J requires the DFD–SD det-orthogonal offset.
Direct $k_a a^2/c^2$ MOND source	Replaced by the nonlinear kinetic crossover; rotation curves from the AQUAL field equation (App. AP).
a_0 calibrated from SPARC/RAR	$a_0 = 2\alpha^{29}\sqrt{c^7/G\hbar} = 1.1966 \times 10^{-10}$ m/s^2 on bound-matter clocks (Postulate ZS.11; 1.1208×10^{-10} on the early clock); the law is derived, and SPARC validates rather than calibrates.
"0.55% CKM mean agreement"	Retracted (computed against PDG 2018–2020); per-channel agreement reported instead.
Fermion-mass mean error quoted as "0.047%"	Corrected to the table-derived 1.42% at leading order; the refined 0.61% value is archive-claimed (priming theorem), and the 0.082% value is not a result, since the running factors behind it are not Standard-Model running (Ext. Deriv., App. AH).
Matter-wave T^3 protocol (App. W) screened-coupling form	Harmonized to the kinematic expression of the matter-wave section, which is not a phase (units s^2/m), so it gives no per-facility estimate or falsification threshold. *Status: not a DFD prediction (the matter-wave sector is null); see the status note after Eq. (337) in Sec. XIII.*
Quantum framework unlisted among inputs	Added as an explicit background-input row in the DoF ledger and as an open program item; QM is not derived in full (App. QM lists the imports).
"Five independent routes" to α^{-1}	Reconciled: the companion volume's independence statement now defers to the categorical engine count — three structurally distinct engines, five presentations.
Glueball normalization chain (companion volume)	Note added: the printed coefficient forms do not close numerically and the flavor-scheme input is mislabeled; $m_{0^{++}} = 1.69 \pm 0.10$ GeV retained as target, scaling $m \propto \Lambda_{\rm QCD}$ retained.
Uniqueness axioms (V1)–(V9) of $X = \mathbb{C}P^2 \times S^3$	Replaced: (V6) asserted a splitting of TX that no $\mathbb{C}P^2 \times N^3$ admits, so the list was unsatisfiable; the seven current axioms are satisfiable (App. AB).
Pairwise-kSZ consistency stated unconditionally	The verdict rests on quasi-Newtonian linear growth, which the Rest-Mass Channel's bound-system confinement supplies ($G_{\rm eff} = G$ for unbound perturbations; App. GR); the suppressed amplitude of App. AF belongs to the baryon-only construction of App. AE.

CONTENTS

I. Introduction 20
A. Theories of Gravity 20
B. Core Idea: Gravity as an Optical Medium 21
C. What DFD Claims and What It Doesn't 21
D. Reader's Guide 23
E. Assumptions and Degrees of Freedom Ledger 23
F. Completion Ledger 24

II. Mathematical Formalism 24
A. The Optical Metric and Geodesics 25
1. Gordon's Optical Metric 25
2. Fermat's Principle 25
3. Phase and Group Velocities 25
B. Action Principle 26
1. Scalar Sector Action 26
2. Matter Coupling 26
3. Gravitational Wave Sector 27
4. Interaction and Complete Action 27
C. Field Equations 27
1. General Nonlinear Form 27
2. The Optical Source Theorem: DFD's replacement for $T_{\mu\nu}$ 27
D. The $\mu(x)$ Crossover Function 28
1. Admissible Families 29
E. Conserved Quantities and Symmetries 29
1. Diffeomorphism Invariance 29
2. Energy Conservation 29
3. Local Conservation in PPN Framework 29
F. 4D-from-3D: Emergent Spacetime Structure 29

1. The Fundamental Arena 29
2. The 3D-to-4D Morphism 29
G. Physical Interpretation: Vacuum Loading 30
H. Summary of Section II 30

III. Mathematical Well-Posedness 30
A. Static Solutions: Elliptic Theory 31
1. Assumptions on μ 31
2. Existence and Uniqueness 31
3. Regularity 31
B. Exterior Domains and Boundary Conditions 31
C. Dynamic Solutions: Hyperbolic Theory 32
1. First-Order Symmetric Hyperbolic Form 32
2. Local Well-Posedness 32
3. Finite Speed of Propagation 33
D. Stability 33
1. Energy Minimization 33
2. Perturbative Stability 33
3. No Ghosts 34
E. Initial-Boundary Value Problems 34
1. Dynamic Structural Assumptions 34
2. IBVP Formulation 34
3. Compatibility Conditions 34
4. Energy Estimates 34
5. Main IBVP Theorem 35
6. Finite Speed of Propagation 35
7. Parabolic Extension 35
8. Stability Estimates 35
9. Numerical Implementation 35
F. Open Mathematical Problems 35
G. Summary of Section III 36

IV. Parametrized Post-Newtonian Analysis 36
A. The PPN Framework 36
B. DFD Physical Metric in PPN Form 37
C. Parameter Extraction: $\gamma = \beta = 1$ 37
D. Vector Sector: $\alpha_1 = \alpha_2 = \alpha_3 = 0$ 38
E. Preferred-Frame Invisibility: Why the Foliation Decouples at 1PN 39
F. Conservation Laws: $\zeta_1 = \zeta_2 = \zeta_3 = \zeta_4 = 0$ 41
G. Summary: DFD Equals GR at 1PN 41
H. Classic Solar System Tests 41
1. Light Deflection 41
2. Shapiro Time Delay 41
3. Perihelion Precession 42
4. Gravitational Redshift 42
5. Frame Dragging and Lense-Thirring Effect 42
I. Where DFD Differs from GR 43

V. Gravitational Waves 43
A. Two Gravitational Sectors on Flat $\mathbb{R}^3$ 43
1. The Optical Sector (DFD Core) 43
2. The Radiative Sector (Tidal Disturbances) 43
3. Parent Strain Field and Irreducible Decomposition 44
4. Spectral-Geometry Origin of the Two-Sector Structure 44
5. Why $c_T = c$ (Structural Requirement) 45
6. Adiabatic Limit and GW Speed in the Unified Picture 45
7. Falsifiability 45
B. The Minimal Transverse-Traceless Sector 46
C. Verification: $c_T = c$ from No Derivative Mixing 46
1. The Flat-Background Wave Equation 46
2. Why No Derivative Mixing is Natural in DFD 46
D. Wave Equation and Source Coupling 47
E. Quadrupole Formula and Energy Flux 47
F. Post-Newtonian and ppE Framework 47
1. Conservative and Dissipative Parametrization 47
2. Phase Coefficients 47
G. Comparison with LIGO-Virgo-KAGRA Observations 48
1. DFD Predictions for Compact Binaries 48
2. Comparison with LVK O3 Bounds 48
3. Falsifiability and Future Tests 48
H. Binary Pulsar Verification 48
1. The Hulse-Taylor System 48
2. DFD Prediction 48
3. Quantitative Comparison 49
4. Other Binary Pulsars 49
5. Bounds on DFD Parameters 49
I. Numerical Evolution for Compact Binaries 49
1. Evolution System 50
2. Boundary Conditions 50
3. AMR Strategy 50
4. Validation Tests 50
J. Summary and Implications 50

VI. Strong Fields and Compact Objects 51
A. Static Spherical Solutions 51
B. Optical Causal Structure 51
C. Photon Spheres 51
D. Black Hole Shadows: EHT Comparison 52
1. DFD in the Strong-Field Regime 52
2. M87* Shadow 52
3. Sgr A* Shadow 52
4. Summary Comparison 52
E. Constrained μ-Function Family 53
1. The Constrained Family $\mu_{\alpha,\lambda}(x)$ 53
F. Compact Star Structure 53

G. Potential DFD-Specific Signatures 53

VII. Galactic Dynamics 54
A. The Deep-Field Limit 54
B. Galaxy Rotation Curves 55
C. The Baryonic Tully-Fisher Relation 55
D. The Radial Acceleration Relation 55
E. Predicted acceleration scale and empirical validation 56
F. Quantitative SPARC Validation 57
G. Model-Independent Interpolation-Function Shape Test 57
H. Wide Binary Stars 58
I. External Field Effect 59
J. Dwarf Spheroidal Galaxies 60
1. Jeans Analysis with EFE 60
2. Two-Regime Model 60
3. Comparison with Data 60
4. Ultra-Faint Dwarfs: Systematic Effects 60
K. Cluster-Scale Phenomenology 61
1. Cluster Dynamics in DFD 61
2. Cluster Sample Analysis 61
3. Physical Interpretation 61
4. Nonlinear Averaging and the Correction Stack 62
5. The Bullet Cluster: Quantitative Analysis 63
6. Global Consistency: One Function, Galaxies to Clusters 63
L. Summary: Galactic Phenomenology 64

VIII. The α-Relations: Parameter-Free Predictions 64
A. The Fundamental Relations 65
B. Relation I: The Self-Coupling $k_a = 3/(8\alpha)$ 65
C. Relation II: The Clock Coupling $k_\alpha = \alpha \times a_e$ 65
D. Relation III: The MOND Scale a_0 (Derived) 66
E. Consistency and Cross-Checks 66
F. The Three-Scale Hierarchy 66
G. Status Summary 67

IX. Gauge Coupling Variation and High-Energy Implications 67
A. Universal Gauge-ψ Coupling 67
B. Connection to the β-Function 68
C. Modified Renormalization Group Equations 68
D. Asymptotic Freedom and UV Behavior 68
E. Nuclear Clock Prediction: Thorium-229 68
F. Cosmological $\alpha(z)$ Variation 69
G. Grand Unification 70
H. Vacuum Energy Feedback 71
I. Summary of Falsifiable Predictions 71

X. Convention-Locked α from the Microsector 71
A. Design Constraint: No Hidden Tuning Parameters 72
B. Operator Choice (Locked) 72
C. Regularization/Truncation Rule (Locked) 72
D. Finite-k Truncation and the $(k+3)/(k+4)$ Factor (Locked) 72
E. The Forced Microsector Fork 73
1. Branch A: Regular-Module Microsector (Survives) 73
2. Branch B: Fermion-Representation Microsector (Falsified) 74
F. Branch Selection by Real-Bimodule Consistency 74
G. The Closed-Form Chain 74
H. Sharp Falsifier 75
I. The Closed-Form Result 75
J. Summary 76

XI. Atomic Clock Tests 76
A. Local Position Invariance Framework 76
B. Common-Factor Cancellation and Observable Residuals 77
C. Screening: Derivation from a Response Functional 79
D. The Same-Ion E3/E2 Constraint 79
E. Cross-Species Atomic Comparisons 80
1. ROCIT Statistical Detail 80
F. Nuclear Clocks: the Strong-Sector Channel 81
G. Channel-Resolved Prediction Table 82
H. Empirical Checks and Current Status 82
I. Experimental Priorities 82

XII. Cavity-Atom Redshift Tests 83
A. Formal Constitutive Proof of the Cancellation 83
B. What Survives Physically 84
C. Four Independent Empirical Checks 84
D. BACON and the Screening Regime 84
E. Sector-Resolved Parameterization 85
F. The 4→3 GLS Protocol 85
G. Experimental Concept and Controls 85
H. Expected Signal and Sensitivity 85
I. Current Status and Priority 86
J. Summary: Cavity–Atom as a Precision Residual Test 86

XIII. Matter-Wave Interferometry 86
A. The ψ-Coupled Schrödinger Equation 86
B. The T^3 Discriminator (Not a DFD Prediction) 86
C. Experimental Designs 87
1. Design A: Vertical Fountain 87
2. Design B: Horizontal Rotation 87
3. Design C: Source Mass Modulation 87
4. Design D: Dual-Species Protocol 87

D. Discriminants and Systematics Control 87
E. Sensitivity Forecast 88
F. Existing Analyses and the T^3 Term 88
G. MAGIS and AION as Null Tests 88
H. Complementarity with Cavity-Atom Test 89
I. Summary: Matter-Wave Test 89

XIV. Solar Corona Spectral Asymmetry Analysis 89
A. Motivation: Intensity Changes Without Velocity Changes 89
B. Electromagnetic Coupling to ψ 90
C. SOHO/UVCS Ly-α Analysis 90
1. Statistical Methodology: Permutation Tests and FDR Control 90
D. Multi-Species Test: O VI 103.2 nm 90
1. Data and Methods 90
2. Results 90
E. Consistency Check: Intensity Without Velocity 90
F. Summary 90
G. Quantitative Multi-Wavelength Test: The Asymmetry Ratio 91
1. Thermal Width Analysis 91
2. The Generalized Prediction 91
3. Comparison with Observations 91

XV. Antimatter Gravity Tests 91
A. GR Baseline: Matter–Antimatter Universality 91
B. DFD Metric-Level Prediction 92
C. Non-Metric Couplings and Species-Dependent Sensitivities 92
1. Bound-State Mass Shifts 92
2. CPT Considerations 92
D. Matter–Antimatter Differential Acceleration 92
1. Effective Point-Particle Action 92
2. Free-Fall Acceleration 92
E. Three Scenarios for $\sigma_{\bar{H}} - \sigma_H$ 92
F. Experimental Mapping: ALPHA-g and Beyond 93
1. ALPHA-g Free-Fall Measurements 93
2. Spectroscopy Complement 93
G. Relation to Ordinary-Matter EP Tests 93
H. DFD Prediction and Falsification 93
I. Summary 94

XVI. Cosmological Implications 94
A. ψ-Tomography (ψ-Screen) Cosmology Module 94
1. DFD postulates and sign conventions 94
2. Forward model: three optical relations 94
3. Two independent screen estimators and one consistency check 95
4. Theorem-level internal closure of the reconstructed screen 95
5. A GR-independent falsifier 96
6. Evolving "constants" as controlled parameters 98
7. Practical next steps 98
B. The ψ-Universe framework 98
C. CMB observables as ψ-screened measurements 99
1. Asymmetry Factor Decomposition 99
D. The optical illusion principle 99
E. Intrinsic anisotropy from ψ-gradients 99
F. Line-of-sight distance bias and apparent acceleration 100
G. Cluster-scale dynamics: Status 100
H. Scope of CMB claims 100
I. ISW Effect: A Falsifiable Prediction 100
J. The late-time distance ratio is not a screen 101
K. Late-Time Distance Cross-Consistency 101
L. Matter Power Spectrum from Microsector 101
M. Power Spectrum Multipole Confrontation 103
1. Method 103
2. Results 103
3. Interpretation: EFE-Screened Growth Theorem 103
4. Conclusion and Falsifier 104
N. Observational Status (2024–2025) 104
1. Late-Time Potential Shallowing (DES Y3) 104
2. Dynamical Dark Energy Hints (DESI DR2) 104
3. Wide Binaries (Active and Contested) 104
4. Counter-Evidence and Null Tests 104
5. Observational Summary Table 105
O. Hierarchy of Astrophysical Scales from α 105
P. Summary 105

XVII. Quantum and Gauge Extensions 105
A. Status and Conditionality 106
B. Internal Mode Bundle and Berry Connections 106
C. The $\mathbb{C}^3 \oplus \mathbb{C}^2 \oplus \mathbb{C}$ partition 107
D. Yang-Mills Kinetic Terms from Frame Stiffness 107
E. Generation Counting 107
F. CP Structure 107
G. Higgs and Mass Spectrum 108
H. The Fine-Structure Constant from Chern-Simons Theory 108
1. Chern-Simons Quantization 108
2. The Maximum Level: Topological Derivation 108
3. Lattice Comparison 108

I. The Bridge Lemma: $k_{\max} = 60$ from Closed Index 109
1. Statement 109
2. Proof 109
3. Physical Selection 109
J. Nine Charged Fermion Masses 109
1. The Mass Formula 109
2. Sector-Dependent Exponents 109
3. Structural Ratios 109
K. CKM Matrix from $\mathbb{C}P^2$ Geometry 110
1. Wolfenstein Parameterization 110
2. Geometric Derivation 110
3. Predictions 110
L. Electroweak-Scale Relation 110
1. The Relation 110
2. Physical Origin 110
M. Strong CP: Tree-Level Closure, Loop-Bounded 110
1. Tree Level 110
2. Loop Level 111
N. PMNS Matrix from $\mathbb{C}P^2$ Geometry 111
1. Observed Mixing 111
2. Physical Mechanism 111
3. Tribimaximal Base 112
4. Corrections 112
O. Infrared Scale for Yang-Mills from DFD Geometry 112
1. Setup: DFD Spatial Geometry 112
2. Weitzenböck Identity 112
3. The DFD-Induced Infrared Bound 112
4. Clarification: What This Does Not Claim 112
P. Testable Predictions 113
Q. Caveats and Required Verification 113

XVIII. Open Problems and Limitations 114
A. Main Open Items 115
B. Quantum Superpositions and the Penrose Paradox 117
C. UV Completion: the Topological Proposal 118
D. Hyperbolicity and Numerical Evolution 119
E. Cluster-Scale Phenomenology: the χ Budget 119
F. Cosmological Constant: the Hierarchy from Topology 120
G. Full Cosmological Treatment 120
H. Null Predictions: Where DFD Says "No Effect" 121
I. Experimental Verification Timeline 121
J. Closed Routes 121
K. Standing Internal Review of Inherited Results 121
L. Summary: Resolved and Remaining Items 123

XIX. A Topological Link Between H_0 and M_P 125
A. The Dimensionless Invariant 125
B. Implication for the Cosmological Constant Problem 126
C. Testable Consequence: The Hubble Constant 126
D. Epoch structure of the G–H_0 invariant: coupling versus state function 127
E. The homogeneous optical-time Hamiltonian (background expansion) 130
F. The Parameter Structure 131

XX. Conclusions 132
A. Summary of Density Field Dynamics 132
B. What DFD Accomplishes 133
C. The Critical Tests 134
D. If DFD Is Confirmed 135
E. If DFD Is Falsified 135
F. Comparison with Alternatives 135
G. Outlook 136
H. Structural Separation: Gravity vs. Microsector 136
I. Final Statement 137

A. Notation and Conventions 140
1. Fundamental Fields and Parameters 140
2. Coordinate and Metric Conventions 140
3. Physical Constants 140
4. Post-Newtonian and Gravitational Wave Parameters 140
5. Clock and LPI Parameters 140
6. Galactic Dynamics Notation 140
7. Unit Conventions 140
8. Abbreviations and Acronyms 140
9. Sign Convention Summary 140

B. Detailed Derivations 141
1. Second Post-Newtonian Light Deflection 142
a. Setup 142
b. Ray Equation 142
c. First-Order (1PN) Deflection 142
d. Second-Order (2PN) Deflection 143
2. Perihelion Precession 143
a. Effective Potential 143
b. Orbit Equation 143
c. Precession Rate 143
d. Mercury 143
3. Baryonic Tully-Fisher from μ-Crossover 143
a. Deep-Field Limit 143
b. Spherical Symmetry 144
c. Asymptotic Velocity 144
d. Zero-Point 144
4. α-Relation Derivations 144
a. Relation I: $a_0 = 2\sqrt{\alpha}\, cH_0$ 144
b. Relation II: $k_a = 3/(8\alpha)$ 144
c. Relation III: $k_\alpha = \alpha^2/(2\pi)$ 144
d. Consistency Check 144

5. Matter-Wave Phase Shift 145
a. Phase Evolution 145
b. Three-Pulse Interferometer 145
c. Species-Coupling Expression (Not a DFD Prediction) 145
6. Gravitational Wave Emission 145
a. Quadrupole Formula 145
b. Binary Inspiral 145

C. Interpolating Function Catalog 145
1. General Requirements 145
2. Catalog of Functional Forms 145
3. Simple Interpolating Function 145
4. Standard Interpolating Function 146
5. RAR Empirical Function 146
6. The n-Family 146
7. Comparison of Properties 146
8. Calibration Procedure 146
9. Physical Interpretation 147

D. Experimental Protocols 147
1. Clock Comparison Procedure 147
a. Measurement Overview 147
b. Technical Requirements 147
c. Recommended Clock Pairs 147
d. Data Analysis 147
e. Systematic Error Budget 148
f. Windowed vs. Global Analysis Strategies 148
2. Cavity-Atom Setup Requirements 148
a. Experiment Concept 148
b. Key Configuration 148
c. Technical Specifications 149
d. Height Comparison Method 149
e. Observable 149
f. Discrimination Significance 149
3. Matter-Wave Interferometer Specifications 149
a. Formula Under Test (Not a DFD Prediction) 149
b. Interferometer Requirements 149
c. Dual-Species Configuration 149
d. T^3 Signature (Not a DFD Prediction) 149
e. Systematic Control 150
4. Galaxy Rotation Curve Analysis 150
a. Data Requirements 150
b. Baryonic Mass Model 150
c. DFD Fitting Procedure 150
d. Quality Metrics 150
5. Decision Matrix: Which Experiment to Prioritize 150

E. Data Tables 150
1. Post-Newtonian Parameter Bounds 150
2. Binary Pulsar Timing Data 150
3. Clock Sensitivity Coefficients 150
4. SPARC Galaxy Sample Statistics 151
5. Gravitational Wave Constraints 151
6. Physical Constants Summary 151
7. DFD Parameter Summary 151
8. Experimental Timeline 151

F. Rigorous Foundations for Gauge Emergence 151
1. Minimality of the $(3, 2, 1)$ Partition 151
2. The $SU(N)$ Selection Lemma 153
3. The Spin^c Flux Quantization 154
4. The Spin^c Dirac Index on $\mathbb{C}P^2$ 156
5. Generation Count and Flux-Product Rule 156
6. Uniqueness of Minimal Flux 157
7. Global Fermionic Consistency: the Spin-$\mathbb{Z}_4$ $B-L$ Structure and the Necessity of ν_R 157
8. The Self-Coupling Coefficient k_a (Model) 158
9. Frame Stiffness from Ricci Curvature 158
10. Proton Stability 158
11. UV Robustness of Topological Results 159
12. Summary: Rigorous vs. Conjectural 160

G. Derivation of α-Relations from Gauge Emergence 160
1. The Gauge-ψ Lagrangian 160
2. The Magnetically Dominated Regime 160
3. Frame Stiffness Structure 160
4. Derivation of $k_a = 3/(8\alpha)$ 160
5. Strong CP Prediction 161
6. Derivation of $k_\alpha = \alpha^2/(2\pi)$ 161
7. Proton Stability Prediction 162
8. Summary of Results 162

H. Higgs and Yukawa Sector from Gauge Emergence 162
1. Higgs Emergence from the $(3, 2, 1)$ Structure 162
2. Zero-Mode Localization on $\mathbb{C}P^2$ 163
3. Yukawa Hierarchy from Overlap Integrals 163
4. CKM Mixing from Geometry 164
5. Neutrino Masses from See-Saw 164
6. Summary of Mass Sector 164

I. Full Cluster Sample Analysis 165
1. Dataset Description 165
2. Complete Results Table 165
3. Statistical Summary (the μ-Law Alone) 165
4. Alternative $\mu_{1/2}$ Function 166
5. Systematic Uncertainties 166
6. Conclusions 166
7. The Five Correction Factors, Examined 167
8. Galaxy Groups 167

J. Derivation of the ψ-CMB Solution 168

1. The ψ-Acoustic Oscillator 168
2. Peak Height Asymmetry 168
   a. Baryon Loading Factor f_{baryon} 168
   b. Integrated Sachs-Wolfe Factor f_{ISW} 168
   c. Visibility Function Factor f_{vis} 168
   d. Doppler Factor f_{Dop} 169
   e. Total Asymmetry 169
3. Peak Ratio Derivation 169
4. Why the $1/\mu$ Enhancement Cancels 169
5. The ψ-lensing peak-location construction (not a DFD prediction) 169
   a. Gradient-Index Optics 169
   b. Application to CMB 170
6. Consistency Checks 170
7. Comparison with ΛCDM 170
8. Falsifiable Predictions 170
9. The Cold-Clustering Wall: a no-go theorem for the third-peak height 172

K. Microsector Physics: Complete Derivations 174
1. Closed Form for $\alpha = 1/137$ from Chern-Simons Theory 174
   a. Setup: Chern-Simons on S^3 174
   b. The Level Sum and Fine-Structure Constant 174
   c. Heat Kernel on S^3 174
   d. Determination of $k_{\max}$: Closed Spin^c Index 174
2. Lattice Comparison for $\alpha = 1/137$ 174
   a. Inputs (Independent of α) 174
   b. The Prediction 175
   c. Lattice Comparison 175
   d. Falsifiability: What Would Have Failed 175
   e. Finite-Size Scaling 175
   f. L16 Detailed Results 176
   g. Wilson Ratio Scan 176
   h. β Bracket Test 176
   i. Additional Runs 176
   j. Summary: Lattice Evidence 177
3. The UV Cutoff Consistency Check: $k_{\max} = 60$ Compared with the Lattice 177
   a. The Truncation Scan 177
   b. Physical Interpretation 177
   c. Why This Is Not Fine-Tuning 178
   d. Systematic Independence Tests 178
4. The Bridge Lemma 178
   a. Statement 178
   b. Proof 178
   c. Physical Selection 178
   d. Consistency Checks 178
5. Charged Fermion Mass Derivation 179
   a. The Mass Formula 179
   b. Sector-Dependent Exponent Assignment 179
   c. Prefactor Structure 179
   d. Complete Mass Table 179
   e. Statistical Summary 179
   f. Structural Ratios 180
   g. Explicit Finite Yukawa Operator 180
   h. Derivation of $G[1,1] = 2/3$ from Primed Microsector Trace 181
6. CKM Matrix from $\mathbb{C}P^2$ Geometry 182
   a. Wolfenstein Parameterization 182
   b. Geometric Origin of λ 182
   c. Higher-Order Parameters 182
   d. Predictions and Comparison 182
   e. Key Prediction: $|V_{ub}/V_{cb}| = \lambda\sqrt{\bar{\rho}^2 + \bar{\eta}^2}$ 182
7. Summary: Microsector Consistency 182
8. The Higgs Scale Hierarchy 183
   a. Numerical Verification 183
   b. Physical Origin of Factors 183
9. Strong CP: Tree Level and Loop Bound 183
   a. Tree Level 183
   b. Loop Level 183
10. PMNS Matrix Derivation 184
   a. Physical Picture 184
   b. Tribimaximal Mixing 184
   c. Corrections from Charged Lepton Masses (localization estimate; the adopted branch is TM1, App. X) 184
   d. Why PMNS ≠ CKM 184
11. Summary: DFD Unified Framework 184

L. Strong CP: Tree-Level Closure, Loop-Bounded 184
1. What must be shown 184
2. Tree-level inputs 185
3. The Dai–Freed anomaly formula 185
4. Theorem: η vanishes automatically in even dimensions 185
5. Main theorem: tree-level closure, loop-bounded 186
6. A conditional alternative: quaternionic structure 186
7. Falsifiable prediction 186
8. Summary: why the S^3 factor does triple duty 186

M. Scattered and Locally Emitted Lines in a Static ψ 187
1. Definitions and Setup 187
2. Gaussian Detuning Scaling 187
3. The Value of Γ 187
4. Observational Constraint on Γ 187

N. First-Principles Derivation of $\mu(x)$ and a_0 188
1. The S^3 Partition Function (Exact Result) 188
2. Microsector-to-ψ Map and Level Response 188
3. The Key Theorem: μ is Fixed by a Composition Law 188
4. The Acceleration Scale a_0: Variational Derivation 189

a. The Unique IR Control Parameter 189
b. Microsector Scaling Charge 189
c. The Spacetime Functional 189
d. Homogeneous-Limit Theorem 190
e. The MOND Scale Theorem 190
5. Summary and Falsifiable Predictions 190
6. Alternative Derivation: Variational Approach 191
a. Setup: Auxiliary-Field Action 191
b. Asymptotic Constraints 191
c. Closed-Form Solution 191
d. Comparison with S^3 Result 191
7. The Complete Picture: MOND from S^3 Topology 192

O. The α^{57} Mode-Count Exponent and the G–H_0–α Invariant 193
1. Mathematical core: primed-determinant scaling fixes the exponent 193
2. Gaussian mode-integration realization 193
3. From determinant ratio to physical hierarchy: derivation 193
4. The derived invariant 194
5. Connection to the Einstein Product Condition 195

P. Clock Coupling and Majorana Scale 196
1. Scope and Convention Lock 196
2. Theorem P.1: Schwinger Coefficient $a_e = \alpha/(2\pi)$ 196
3. Theorem P.2: Clock Coupling $k_\alpha = \alpha^2/(2\pi)$ 196
a. Observational Test: Fine-Structure Constant Variation 196
4. Majorana Scale $M_R = M_P\alpha^3$ 197
a. Parallel Structure with Appendix O 197
b. Neutrino Mass Predictions 197
5. Summary 198

Q. Temporal Completion: Dust Branch under $K' = \mu$ 198
1. Temporal Deviation Invariance from Saturation-Union 198
2. Unique Local Temporal Invariant 198
3. No-Go Lemma: Quadratic Invariant Gives $w \to 1/2$ 199
4. Dust Branch from Deviation-Invariant Closure 199
5. Summary: What is Theorem-Grade vs. Program 200
6. Primordial optical engine: the background screen flow 200

R. EM–ψ Back-Reaction Coupling 203
1. Physical Interpretation of λ 203
2. Mode Equation and Pumping Channels 203
a. Single Lab-Mode Reduction 203
b. Channel 1: Driven Resonance ($2\omega = \Omega_\psi$) 203
c. Channel 2: Parametric Amplification ($2\omega \simeq 2\Omega_\psi$) 203
3. Geometry Transparency 203
a. When the Driven Overlap Cancels 203
b. How to Restore the Overlap 204
c. Parametric Overlap: Area-Ratio Law 204
4. Constraints on $|\lambda - 1|$ 204
a. Accidental Constraint from Cavity Stability 204
b. Intentional Search: Projected Reach 205
5. Why $\lambda \neq 1$ Has Not Been Detected 205
6. Intentional Detection Protocol 205
7. Relation to Core DFD Framework 206
8. Summary 206
9. Dual-Sector Extension: The κ Parameter 206
a. Constitutive Split Preserving $v_{\rm ph} = c/n$ 206
b. The Unified Bracket 206
c. Standing-Wave Energy Equality 206
d. Experimental Tests 207
e. Experimental Discrimination 207

S. Standard Model Extension Dictionary 207
1. SME Framework Overview 207
2. DFD↔SME Correspondence 207
3. Translation Table 207
4. Experimental Constraints Reinterpreted 208
5. Cavity-Atom Comparisons in SME Language 208

T. Family and Clock-Type Parametrization of LPI Tests 208
1. Two-Parameter Model 208
2. Constraints from Data 208
3. Predictions for Untested Channels 209
4. Relation to DFD Microsector 209
5. Summary 209

U. Mathematical Well-Posedness of the DFD Field Equations 210
1. The Static Field Equation: Elliptic Theory 210
a. Structural Assumptions on μ 210
b. Weak Formulation and Variational Structure 210
c. Main Existence and Regularity Theorems 210
d. Exterior Domains and Optical Boundary Conditions 211
2. The Dynamic Field Equation: Hyperbolic Theory 211

a. Structural Assumptions for Hyperbolic Theory 211
b. Reduction to First-Order Symmetric Hyperbolic Form 211
c. Local Well-Posedness for the Cauchy Problem 212
d. Initial-Boundary Value Problems 212
e. Finite Speed of Propagation 212
3. Parabolic Extension and Long-Time Behavior 212
4. Stability and Continuous Dependence 213
5. Open Problems 213
6. Summary: Mathematical Status of DFD 213

V. Extended Phenomenology and Numerical Methods 214
1. The External Field Effect (EFE) 214
a. Physical Origin 214
b. Quantitative Formulation 214
c. Observational Signatures 214
2. Wide Binaries 214
a. The Crossover Scale 214
b. Predicted Velocity Anomaly 214
c. GAIA DR3 Constraints 215
3. Finite Element Implementation 215
a. Weak Form for FEM 215
b. Newton Iteration for Nonlinearity 215
c. Mesh Refinement Strategy 215
d. Boundary Conditions 215
e. Convergence Verification 216
4. Matter Power Spectrum from ψ-Screen 216
a. Scale-Dependent ψ Perturbations 216
b. Observational Signatures 216
5. Cooper-Pair Mass Anomaly from A_5 Pair Space 216
6. Summary 216

W. Experimental Protocols and Sensitivity Analyses 217
1. Cavity-Atom LPI Test: Complete Protocol 217
a. Observable and Predictions 217
b. Experimental Configuration 217
c. Measurement Cycle 217
d. Systematics Budget 217
e. Blinding Protocol 217
f. Pre-Registered Decision Rule 218
g. Sensitivity Reach 218
2. Multi-Species Clock Comparison Protocol 218
a. Observable 218
b. Species Selection 218
c. Analysis Protocol 218
3. Matter-Wave Interferometry: T^3 Protocol (Not a DFD Prediction) 218
a. Observable 218
b. Parity Isolation 219
c. Sensitivity Requirements 219
d. Interpretation of Outcomes 219
4. Nuclear Clock Protocol: Th-229 219
a. Prediction 219
b. Experimental Requirements 219
c. Timeline 219
5. Space Mission Protocols 219
a. ACES (ISS) 219
b. Dedicated LPI Mission 219
6. Summary: Experimental Roadmap 220

X. Neutrino Mass Spectrum from DFD Microsector 220
1. DFD Inputs from the Microsector 220
2. Why S_3 Invariance Cannot Split the Doublet 220
3. TBM Selects a Canonical Residual S_2 221
4. Microsector-normalized residual-S_2 spurion 221
5. Combined mass pattern (microsector-normalized) 221
6. Parameter-free oscillation invariant (discriminator) 221
7. Complete numerical predictions 221
8. Absolute-scale closure for Branch B from finite-d priming 222
9. The explicit mass matrix (TBM eigenbasis) 223
10. Falsification criteria 223
11. External global-fit verification 223
12. Summary: DFD-closed neutrino sector (zero continuous parameters) 224

Y. Finite Yukawa Operator, Chiral Basis, and the A_f Prefactors 225
1. Purpose and Scope 225
2. Finite Hilbert Space and Normalization 225
3. Block Decomposition for the $(3, 2, 1)$ Microsector 225
4. Finite Higgs Connector as an Explicit Matrix 225
5. Chiral Subspaces and Canonical Link-States 225
6. Y_{finite} as an Explicit Operator and Its Matrix Elements 225
7. Explicit Evaluation in the Canonical Link Basis 226
8. Universality Wall and the Required Additional Structure 226
9. The L_{det} Twist: A $3^{n_{\text{gen}}}$ Ratio Pattern (Not a Parameter-Free Mass) 226
10. The η_q-Free Double Ratio and the N_c^3 Color Clebsch 227
11. A_5 Species Projectors: Breaking the Universality Wall 228
a. Channel Space as Group Algebra 228

b. Generators and Universal Connector 228
c. Higgs Kernel from Derived ε_H 229
d. Species Projectors from Conjugacy Classes 229
e. Cayley Geometry and Hierarchy Mechanism 229
f. Species-Resolved Prefactors 229
g. Class-Amplitude Formula 229
h. Proposed Species Assignment Rule 230
12. Complete Status Summary 230
13. Complete Derivation: Generation Projectors and Down-Type Selection 230
a. Regular Module Factorization 230
b. Phase Factorization on Isotypic Blocks 230
c. Canonical Generation Projectors 231
d. Down-Type Selection via Conjugation 231
e. Numerical Bin Scan 231
f. Diagonal Bin Structure 231
g. Light Fermion Limitation 231
h. Generation Projector Results 231
14. Bin–Overlap Lemma and the Structural $\sqrt{20}$ Scale 232
a. Normalized Class-State Matrix Elements 232
b. Bin–Overlap Lemma for the Order-3 Class 232
c. Species Projector Closure 232
d. A_f Prefactor Structure 233

Z. Complete Parameter Derivation 233
1. The Weinberg Angle 233
2. The CKM Matrix 234
3. The Higgs Sector 234
4. The PMNS Correction 235
5. Master Theorem 235
6. Integer Catalog 235
7. Strong Coupling Constant 235
8. Summary 236

AA. The Padé Identity: GR's Isotropic Lapse and the Exponential 237
1. Statement of the Padé Identity 237
2. Order-by-Order Agreement 237
3. The Padé Pole is GR's Horizon 238
4. Distinction from Yilmaz-Type Exponential Metrics 238
5. The Padé Hierarchy 239
6. Framing Summary 239

AB. Uniqueness of the Internal Manifold $\mathbb{C}P^2 \times S^3$ 240
1. Vacuum Axioms 240
2. Uniqueness Theorem 241
3. Reduction of the Axioms 241
a. Dimension, product structure, and the split $7 = 4 + 3$ 241
b. Identification of $M_c^{(4)}$ 241
c. Identification of $M_g^{(3)}$ 241
d. Consistency with remaining axioms 242
e. Uniqueness assembly 242
4. Tangent-Bundle Obstruction Lemma 242
5. Integer Cohomology and Standard Model Parameters 243
6. Falsifiability 243
7. Summary 244

AC. Linear Growth Closure from the EFE-Screened DFD Operator 244
1. AC.1 Purpose 244
2. AC.2 Linearization of the Nonlinear Spatial Operator 244
3. AC.3 Specialization to the DFD Interpolation Function 245
4. AC.4 Cosmological External-Field Screening 245
5. AC.5 First Numerical Growth Estimates 245
6. AC.6 Interpretation 245
7. AC.7 Falsifier 246
8. AC.8 Summary 246

AD. Regular-Module Forcing from Finite Real-Bimodule Consistency 246
1. AD.1 Purpose 246
2. AD.2 The Finite Algebra and Its Role 246
3. AD.3 Minimal Faithful Real-Bimodule Theorem 246
4. AD.4 Branch B Exclusion 247
5. AD.5 Finite-d Consequence 247
6. AD.6 Status 247

AE. Optical-Metric σ_8 Closure 248
1. AE.1 Statement and Scope 248
2. AE.2 First-Principles Derivation: $a_{\rm ext}^{\rm FRW} = 0$ 248
3. AE.3 Setup: spherical top-hat statistic 249
4. AE.4 The closure equation 249
5. AE.5 The DFD response $Q(\delta_b)$ 249
6. AE.6 Closure number in the spherical top-hat convention 249
7. AE.7 Physical interpretation 249
8. AE.8 Required CMB-to-$z = 0$ amplification 250
9. AE.9 Relation to galaxy clustering 250
10. AE.9b RSD compatibility: deep-MOND velocity divergence 250
11. AE.10 Falsifiable predictions 251
12. AE.11 Open Theorem Obligation: full convergence kernel 251
13. AE.12 Summary 252

GR. Adjudication of the Cosmological Growth/Velocity Regime 253
1. GR.1 Purpose and the contested scalar 253
2. GR.2 The regime-partition theorem 253
3. GR.3 The AQUAL $G_{\rm eff}$ is not the cosmological growth carrier 253
4. GR.3a The Rest-Mass Channel Theorem (the corrected DFD gravitational action) 257
5. GR.4 The single DFD growth prediction 259
6. GR.5 S_8 on the one-clock $C{=}1$ background 259
7. GR.5a The carried $\sigma_8 = 0.820$ passes Planck CMB lensing 259
8. GR.6 Resolving the directional $f\sigma_8$ ambiguity 260
9. GR.7 Status 260
10. GR.8 Falsifier 260
11. GR.9 Reproducibility 261

A0Z. Epoch Confrontation of $a_0(z)$ 261
1. Scope, and the external measurement it builds on 261
2. DFD needs no borrowed background 262
3. The zero-parameter local value 262
4. The amplitude tension 262
5. A cosmic ceiling on any external-field term 263
6. The survey refitted galaxy by galaxy 263
7. Massive discs at $0.6 < z < 2.5$ 264
8. Dated falsifiers, registrable now 265

AF. Galaxy Bias in DFD: a Frame-Consistent Derivation from the σ_8 Closure 266
1. AF.1 Setup: bias-frame ambiguity in modified gravity 266
2. AF.2 Galaxy formation operates in the W-frame 267
3. AF.3 Theorem: DFD galaxy bias from the closure 267
4. AF.4 Cross-frame consistency: what each probe measures 268
5. AF.5 Falsifiable predictions 268
6. AF.6 Scale dependence 268
7. AF.7 Open extensions and limitations 269
8. AF.8 Summary 269

AG. Master Claims Confrontation Matrix 270
1. Tier Definitions 270
2. Block 1: Fundamental Constants and Microsector 270
3. Block 2: Gravitational Tests (PPN, Pulsars, GW, Strong-Field) 271
4. Block 3: Galactic Dynamics 273
5. Block 4: Cluster Scale 275
6. Block 5: Cosmology 276
7. Block 5a: Growth–Lensing Consistency (E_G, ACT DR6 × BOSS) 277
8. Block 6: Laboratory Tests (Clocks, Cavities, Matter Waves, Antimatter) 277
9. Block 7: Strong-Field, Hyperbolicity, and Open Items 278
10. Summary statistics 279
11. Reading guide for referees 279
12. Use of this matrix 280

AN. The Optical-Metric Master Equation: Unified Light and Matter Motion 280
1. The isotropic optical metric 280
2. The master wave equation and its eikonal limit 280
3. Gravity as the gradient of the squared light speed 281
4. Relation to the action, and the boundary on matter 281
5. Status and falsifiability 281

AO. The CP Sector: Strong-CP Protection, the CKM No-Go, and Euler-Projected Closure 282
1. Purpose and scope 282
2. CKM and CP notation 283
3. DFD microsector and cohomological inputs 283
4. The minimal real-kernel no-go theorem 284
5. Strong-CP protection 284
6. Det-orthogonal geometric CP and nonzero CKM phase 285
7. Cohomological CKM magnitude skeleton 286
8. Euler-projected selection of the CP-even apex 286
   a. Fubini–Study overlap motivation for Postulate E.1 287
9. Final Wolfenstein branch and numerical reconstruction 288
10. Comparison of the apex branches 289
11. Falsifiability and experimental targets 289
12. Scope and order of the claims 289
13. Final theorem ledger 290
14. Conclusion 290

AP. Corpus-Closure Theorems: the α^{57} Hierarchy, the MOND Scale, and Rigor Discipline 291
1. Purpose and standard of proof 291
2. Notation and DFD primitives 292
3. Corpus-level rigor axioms 292
4. The α^{57} hierarchy from topology and determinant scaling 293
   a. Index count: $k_{\max} = 60$ 293
   b. Primed determinant scaling 293
   c. The cosmological invariant 294
5. The action-derived MOND prefactor 294

a. Gauge-emergence proof of $k_a = 3/(8\alpha)$ 294
b. The S^3 stationarity theorem 295
c. Action-level derivation of the MOND prefactor 295
6. The nonlinear kinetic action and galaxy law 295
7. Buckingham–π closure and the α^{58} acceleration invariant 296
a. Numerical prediction and falsifiability 297
8. Black-hole sector: one base temperature 297
9. Lensing and PPN branch discipline 297
10. Flavor/CKM sector: exact theorem boundary 298
11. Inflation and early-universe sector 298
12. PDE/well-posedness sector 298
13. Theorem summary 298
14. Dimension checks 299
15. Failure modes and falsifiers 299

AQ. Executed Lattice-QCD Validation of the DFD QCD Ledger (Program II) 299
1. Summary: what this appendix verifies 299
2. Frozen DFD QCD ledger 300
3. Methods 300
4. Validation: average plaquette 300
5. Static potential and string tension 300
6. Scale convention and the DFD string-tension ledger 300
7. Scalar 0^{++} glueball 301
8. Executed $N_f = 2$ Wilson-HMC validation 302
9. Claim discipline 302
10. Status boundary 302
11. Reproducibility 302

AR. A DFD-Native Yang–Mills Infrared Gap from Loaded Spatial Frame Geometry 303
1. Purpose 303
2. DFD-native arena 303
3. Fluctuation operator 303
4. Main theorem 304
5. Deep-field DFD specialization 304
6. Why this supports DFD 304
7. Scope and non-claims 304
8. Falsifiers and completion checks 304
9. Conclusion 304

AS. Lattice Boundary Program: Staged Execution and Provenance (Programs I–II) 305
1. Program I: frozen inputs, smoke test, unquenched scaffold 305
2. Program I-A: first executed quenched 16^4 string tension 305
3. Status across the program 305

AT. Cross-Sector Exact Identities, Strong-Field Theorems, and New Predictions 306
1. Exact cross-sector identities 306
2. Strong-field and gravitational results 307
3. Compact-star structure 308
4. Deep-sector conformal theorems 309
5. Strong-CP protection and the neutron electric dipole 309
6. New predictions 309
7. A zero-parameter amplitude–shape observable: the (ν, u) relation 312
8. Status and the remaining open lemma 313

AU. The Dark-Energy Sector from the α^{57} Clock 313
1. The dark-energy density as a pure α-power 313
2. The Hubble–Planck seesaw and holographic form 314
3. The "why now" coincidence 315
4. One dark energy: the equation of state 315
5. Look-elsewhere and status 316

AV. χ-Matter: the Weak-Sector Matter Field and the True Definition of Dark Matter 316
1. Overview, grade, and what this appendix claims 316
2. Step 1 — χ is the harmonic three-form outside the rigidity classification 317
3. Step 2 — the gauge-adjoint dimension of χ is $d_\chi = 3$ 317
4. Step 3 — decay constant from the per-mode determinant 318
5. Step 4 — see-saw mass: χ is light, cold, and non-thermal 319
6. Step 5 — relic abundance by vacuum misalignment 319
7. Step 5b — the relic amplitude is the finite CS/WZW vacuum expectation (no free angle) 320
8. Step 5c — the topological flux-density form 322
9. Parity degeneracy of the CS measure, and the vector count 323
10. Step 6 — the third peak, with no postulated CDM 327
11. Step 6b — stability: χ has no photon coupling 328
12. Step 7 — no photon coupling: $E = 0$ 328
13. Why χ is the true definition of dark matter, not adopted CDM 329

AW. The Electroweak Precision Program from $\sin^2\theta_W = 3/13$ 333
1. Exact electroweak identities (E) 333
2. The Z-pole suite from $\sin^2\theta_W = 3/13$ (P) 333

3. The W mass and the scale-ambiguity theorem (T) 334
4. The ρ parameter (T) 335
5. The Higgs mass from the conjectured quartic 335
6. Look-elsewhere and status 335

AX. The Rotating-Source Exterior 336
1. The stationary axisymmetric exterior 336
2. Frame dragging 337
3. Ergoregion structure 337
4. Spin-dependent ISCO 337
5. Spin-corrected QPO law 337
6. Photon ring and shadow displacement 337
7. Observational confrontation and falsifiers 337
8. Status 338

AY. Cross-Sector Relations: Flavor Closures, Hierarchy Rigidity, and Large-Number Structure 338
1. AY.1 The Gatto–Sartori–Tonin closure from locked integers 338
2. AY.2 The TM1 solar-mixing angle, parameter-free 339
3. AY.3 Mass-scale hierarchy rank 339
4. AY.4 Large-number structure 339

SL. The Supernova–Lensing Sign Discriminator 340
1. The line-of-sight optical screen and its sign 340
2. The μ-law boost and the geometric kernel 341
3. The standard (ΛCDM/GR) baseline 341
4. Pre-registered power forecast 342
5. Status and pre-registration 342

TP. The CMB Third Peak: a No-Go for Zero-Dark-Matter, a Dark Sector with No Fitted Density 343
1. What this appendix settles, and what it does not 343
2. Part I — the height no-go (theorem-grade) 343
3. Part II — the derived cold abundance 344
4. Part III — distinguishability: χ versus a free-parameter CDM 345
5. Status and the one open tension 346

QM. Status of the Quantum-Mechanics Derivation Program: What DFD Supplies and What Remains Imported 346
1. Closures (what DFD supplies) 347
2. What remains imported, and why (the precise obstruction) 347
3. The sharpened open problem (single attackable object) 348
4. The $J_\star$-uniqueness target via the physical Hamiltonian (the one-H theorem) 349
5. Matter–ψ infrared class and dressed (Faddeev–Kulish) asymptotic states 350
6. Status box 350
7. Falsifier 351

PK. The DFD-Native Production Galaxy $P(k)$ Pipeline 352
1. PK.1 Purpose: closing the pipeline half of item F 352
2. PK.2 Stage 1 — linear matter power at the frozen DFD cosmology 353
3. PK.3 Stage 2 — DFD growth carrier (χ-matter, $Q = 1$) 353
4. PK.4 Stage 3 — nonlinear correction 353
5. PK.5 Stage 4 — galaxy redshift-space multipoles 353
6. PK.6 Stage 5 — survey-window convolution 353
7. PK.7 χ^2, covariance, and the validation data 353
8. PK.8 Legacy-input run: DFD vs ΛCDM 354
9. PK.9 Status: what is production-grade and what remains 355
10. PK.10 Reproducibility 355
11. PK.11 Falsifier 356

YM. Status of the DFD Strong Sector: Confinement Scale and the Yang–Mills Mass Gap 357
1. The confinement scale from the α-tower 357
2. The open item: string-tension normalisation 357
3. The validated part: executed SU(3) lattice 358
4. Two native gaps: an *unconditional* compact-manifold gap and a conditional loaded-frame gap 358
5. The ledger 358
6. Scope of the claim 359
7. Falsifier 359

FM. Charged-Fermion Mass Sector: Forced Content and the Within-Multiplet Degeneracy Obstruction 360
1. Scope and Summary 360
2. What is forced 360
3. The within-multiplet degeneracy: theorem-grade obstruction 361
4. Scorecard 361
5. Reading the related appendices Status 362

LS. Line-of-Sight Optical-Screen Amplitude: Full 2-Halo and Realization Computation 362
1. LS.1 Statement and Scope 362

2. LS.2 The two factors and what is firm 363
3. LS.3 Derived amplitude: central value and band 363
4. LS.4 What the 2-halo calculation settles 364

CL. Publication-Grade CMB Likelihood and Bayesian Model Comparison 365
1. CL.1 Scope and the publication-grade primary CMB 365
2. CL.2 Parameter count 366
3. CL.3 Bayesian model comparison 366
4. CL.4 Summary assessment 367
5. CL.5 Reconciliation of the item-4 S_8 prediction 368
6. CL.6 Status and falsifier 368

FK. The Fitted Cosmological Knobs: Status and Closure 369
1. The scalar amplitude A_s: one calibrated input 369
2. The χ abundance normalization: from open overshoot to derived-with-conventions 371
3. Knob count: DFD vs ΛCDM 372
4. Inputs and axioms of DFD 374
5. Status and falsifier 374

SM. The "Scalaron Mass" is Not a DFD Observable 378
1. Statement of the (mis-framed) problem 378
2. No native scalaron exists 379
3. Why the two routes disagree by $\sim 10^{11}$ 379
4. The actual DFD primordial sector (no scalaron) 380
5. Status 381

CE. The Improbability of the Pile: A Combined-Evidence (No-Coincidence) Bound 382
1. The surviving forced parameter-free rows 382
2. Trials-Factor Audit and Conditional No-Coincidence Bound 383
3. The conditional no-coincidence bound 385
4. Scope of the bound 386

RM. Falsifiable-Predictions Roadmap: How DFD Is Confirmed or Killed 386
1. The complete bet list — master table 387
2. The four cleanest near-term decisive tests 388
3. Tier 1 — near-term decisive ($\lesssim$5–10 yr, pass/fail) 388
4. Tier 2 — future decisive (next-generation instruments) 389
5. Tier 0 — the already-passed bedrock (would have killed DFD; did not) 389
6. Separation and open cracks 390

WS. Wave-Sector Closure: Elliptic Scalar, Derived Gravitomagnetism, $\delta_{\rm rad} = 0$, and Ringdown 391
1. Axiom E (Elliptic Constraint Reading) 391
2. The verified 1PN source and the Standard-Gauge Coincidence Lemma 392
3. Vector-Sector Completion: g_{0i} derived, not matched 392
4. $\delta_{\rm rad} = 0$ with a mechanism; scalar memory; falsifiers 396
5. Ringdown and echoes: the optical and tensor channels 396
6. Consistency notes on other sections 396
7. What remains open in this sector 397

ZS. The Early-Clock CMB Fit: Conformal Invariance Theorems, the Measured Clock Coefficient, and the Shape Inputs 397
1. Three theorems: what a ψ screen cannot do 397
2. The clock coefficient C: an eight-route no-go, and its measurement 398
3. The CMB fit on the measured clock 399
4. The local arm and the acoustic arm, and the decider 399
5. One universe, two clocks 400

ZT. The Domain-Local Screen Clock: A One-Axiom Spatial Completion of the a_0 Theorem 403
1. The axiom 403
2. The theorems 403
3. Price list and the declared $\dot\delta$ closure 403
4. Kinematic numbers 404
5. Predictions and pulls 404
6. The early-clock Hubble posture: SH0ES is its named external falsifier 406
7. Falsifiers 406
8. Named open items 406

ZU. The Gravity Completion: the Exact Newton Identity of the Quantized ψ Sector, and the Kohn Null 407
1. The forced four-fermion vertex 407
2. Newton survives as an exact zero-parameter identity 408
3. The gap in closed form; the carrier is Hartree, not a condensate 408
4. Second-order control 408
5. The Kohn null 408
6. The Schrödinger–Newton term is the completion's falsifier 409
7. Scope and verification status 409

NL. The Scale-Additive Field Equation and Its Test Record 409
1. Why a scale-resolved form is needed 409
2. Statement of the scale-additive equation 409

3. The exact limits 410
4. Conservation 410
5. Action completion of the scale-additive equation 411
6. The external-field sector: environmental confinement 413
7. The test record 414
8. The distinctive signature: radial 414
9. The external-field effect: even anisotropy dies 415
10. Two further constructions 416
11. No-go results that close the alternatives 416
12. What is not derived 418
13. Effect on established results, and the items still to be settled 419

BS. Single-Mode Bose Statistics and the Gravity Law 420
1. The Partition Function 420
2. The Interpolation Function 421
3. The Magnitude of τ 422
4. Thermodynamics of the Mode 422
5. The Total Entropy of a Galaxy 423
6. The Observables 423
7. Confrontation, Including the Misses 424
8. Grades 425

Acknowledgments 427

References 427

I. INTRODUCTION

A. Theories of Gravity

Einstein's general relativity (GR) has withstood a century of experimental scrutiny [5, 6]. Solar system tests, binary pulsar timing, and gravitational wave observations all confirm GR's predictions to high precision. Yet the theory's success comes at a cost: explaining astrophysical and cosmological observations requires postulating that 95% of the universe's energy content consists of dark matter and dark energy—components that have never been directly detected despite decades of experimental effort [7, 8].

Astrophysical anomalies relative to GR with visible matter alone form a coherent pattern. Spiral galaxy rotation curves are flat rather than Keplerian [9]; low surface-brightness galaxies follow tight scaling relations [10]; galaxy clusters require additional mass beyond their baryonic content [11]; and large-scale structure and supernova data point to late-time accelerated expansion [12, 13]. The dominant response has been the ΛCDM paradigm, which retains GR but postulates cold dark matter and a cosmological constant.

An alternative approach modifies gravity itself. Modified Newtonian Dynamics (MOND) introduced a characteristic acceleration scale $a_0 \sim 10^{-10}\,\mathrm{m/s^2}$ governing the transition between Newtonian and deep-field behavior in galaxies [14, 15]. This single parameter successfully predicts rotation curves, the baryonic Tully-Fisher relation, and the radial acceleration relation across galaxies spanning five decades in mass [16].

A poorly understood coincidence is that a_0 is numerically close to the cosmic acceleration scale $a_\Lambda \sim cH_0$ inferred from the expansion rate [14]. This suggests a possible connection between galactic dynamics and cosmology that ΛCDM treats as accidental.

TABLE I. Comparison of approaches to the gravitational puzzle.

Theory	Key Feature	Status	DM/DE?
GR + ΛCDM	Curved spacetime	Standard	Both
MOND	μ-crossover	Empirical	Replaces DM
$f(R)$	Modified action	Various	Modified
TeVeS	Tensor-vector-scalar	Falsified[a]	—
Brans-Dicke	Scalar-tensor	Constrained	Modified
DFD	Optical index	This work	Derived DM; DE exponent[b]

[a] GW170817 speed constraint [17].
[b] DM as the derived χ component (App. AV); DE as the α^{57} vacuum with its measured coefficient R (App. AU).

Scalar-tensor theories have proliferated as alternatives to GR [18, 19]. Brans-Dicke theory [20] introduced a dynamical scalar coupled to curvature. Bekenstein's Tensor-Vector-Scalar theory (TeVeS) [21] attempted to provide a relativistic completion of MOND but was falsified by the near-simultaneous arrival of gravitational waves and light from GW170817 [17]. The $f(R)$ family [22] modifies the Einstein-Hilbert action directly. Each approach faces its own challenges: additional parameters, instabilities, or conflict with precision tests.

The theory presented in this review—Density Field Dynamics (DFD)—takes a different path. Rather than modifying GR's geometric structure, DFD posits that spacetime is fundamentally flat but contains a scalar field establishing an optical refractive index. This approach has historical precedent: in 1911-12, before completing general relativity, Einstein himself explored gravity as a variable speed of light [23, 24]. Gordon in 1923 showed that electromagnetic wave propagation in a medium can be described by an effective "optical metric" [25]. DFD makes this optical perspective foundational rather than emergent.

Table I summarizes how DFD relates to other approaches. The key distinction is that DFD reproduces GR's predictions where tested (solar system, gravitational waves, binary pulsars) while making specific, falsifiable predictions where not yet tested (laboratory LPI tests and extended-channel clock anomalies).

B. Core Idea: Gravity as an Optical Medium

The central insight of DFD is that gravity can be understood as a refractive medium. Just as light bends when passing through glass because of a spatially varying refractive index, light and matter in a gravitational field respond to a cosmically varying index $n = e^{\psi}$, and this index is the scalar dynamical content of the theory.

The formulation rests on two postulates that constitute the *Minimal Optical Equivalence* principle:

a. Postulate P1 (Light). In a broadband nondispersive window, electromagnetic waves propagate according to the eikonal of an effective optical metric

$$d\tilde{s}^2 = -\frac{c^2\,dt^2}{n^2(\mathbf{x},t)} + d\mathbf{x}^2, \qquad n(\mathbf{x},t) = e^{\psi(\mathbf{x},t)}. \tag{1}$$

This is the Gordon-Perlick optical geometry statement [25, 26], grounding ray optics in wave theory with a single scalar field ψ determining the local refractive index.

b. Postulate P2 (Matter). Test bodies move under the conservative potential

$$\Phi \equiv -\frac{c^2}{2}\psi, \qquad \mathbf{a} = \frac{c^2}{2}\nabla\psi = -\nabla\Phi, \tag{2}$$

which fixes the weak-field normalization to match GR's classic optical tests (light deflection factor of two, Shapiro delay coefficient, gravitational redshift). In weak hosts the action completion of App. NL adds a reciprocal force on bodies, which light does not feel (Cor. NL.17).

The exponential form $n = e^{\psi}$ is not arbitrary but follows from three requirements:

(i) *Positivity:* $n > 0$ everywhere, ensuring light propagation is always defined.

(ii) *Weak-field limit:* For $|\psi| \ll 1$, we have $n \approx 1 + \psi$, recovering the linear regime.

(iii) *Multiplicative composition:* Sequential media combine as $n_{\text{total}} = n_1 n_2 = e^{\psi_1+\psi_2}$, matching the additive nature of gravitational potentials.

The factor-of-two deflection that matches GR emerges automatically. In GR, light deflection receives equal contributions from spatial curvature and time dilation. In DFD, the optical metric (1) encodes both effects: the phase velocity c/n slows in the potential well, and wavefronts tilt toward the slower region. The result is precisely $4GM/(c^2 b)$ at impact parameter b—the same as GR.

Figure 1 illustrates the conceptual difference. In GR, gravity is geometry: mass curves spacetime, and particles follow geodesics on a curved manifold. In DFD, spacetime remains flat (Minkowski background), but a scalar field creates a refractive medium. The observational predictions are identical in the weak-field regime and for black holes, neutron stars and binary inspirals (App. WS); the theories differ in their ontology, at galactic accelerations and in specific laboratory contexts.

The connection between the two postulates is not coincidental. Both light and matter respond to the same field ψ,

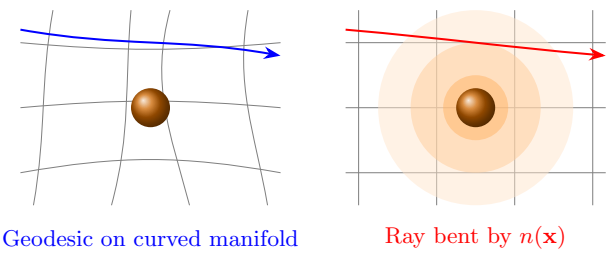


FIG. 1. Conceptual comparison of (a) General Relativity, where gravity curves spacetime and particles follow geodesics on a curved manifold, and (b) Density Field Dynamics, where spacetime is flat but contains a refractive medium with index $n(\mathbf{x}) = e^{\psi(\mathbf{x})}$ that bends light rays. Both yield identical weak-field predictions.

ensuring the Weak Equivalence Principle is satisfied: all test masses fall with the same acceleration $\mathbf{a} = (c^2/2)\nabla\psi$ regardless of composition. The universality of free fall is built into the structure.

C. What DFD Claims and What It Doesn't

Before proceeding to the technical development, we state explicitly what DFD claims and what it does not claim.

a. Claim taxonomy. This review uses three claim types. **Core-derived** statements follow from the DFD field equations and actions presented in the main text. **Auxiliary-closure-derived** statements follow from explicitly displayed supplemental structural postulates (for example, the finite-symmetry closure used in the microsector). **Empirical consistency** statements summarize benchmark calculations, fits, or data confrontations. This taxonomy is used to keep the one-paper presentation logically unified without blurring the difference between core theorems, closure-framework consequences, and benchmark evidence.

b. What DFD Claims:

1. **Weak-field equivalence with GR:** The optical metric with $n = e^{\psi}$ reproduces all Solar System tests. The Parametrized Post-Newtonian (PPN) parameters are $\gamma = \beta = 1$, and all ten PPN parameters match GR at first post-Newtonian order (§IV).

2. **Gravitational waves at speed c:** A minimal transverse-traceless sector propagates at the speed of light with two tensor polarizations, consistent with GW170817 and LIGO/Virgo/KAGRA observations (§V).

3. **MOND-like phenomenology:** At galactic scales where $|\nabla\psi|/a_\star \ll 1$, a nonlinear crossover function

$\mu(x)$ produces flat rotation curves, the baryonic Tully-Fisher relation, and the radial acceleration relation without cold dark matter (§VII).

4. **Channel-resolved clock and cavity residuals:** DFD's minimal action predicts universal co-located clock responses (Thm. XI.2); any departure belongs to its extended non-metric sector (Sec. XV C) and is channel-dependent rather than universal. Same-ion optical ratios tightly constrain the pure α sector, cross-species and nuclear clocks probe composition and strong-sector channels, and cavity–atom comparisons reduce at tree level to a screened residual rather than an order-unity slope (§XI, §XII).

5. **Matter-wave T^3 signature:** a null prediction: DFD adds no contribution to GR's own phase through 1PN (§XIII).

6. **Parameter-free α-relations:** Three relations link the fine-structure constant α to gravitational scales without free parameters:

$$a_0 = 2\sqrt{\alpha}\, cH_0, \tag{3}$$

$$k_a = 3/(8\alpha) \approx 51.4, \tag{4}$$

$$k_\alpha = \alpha^2/(2\pi) \approx 8.5 \times 10^{-6}. \tag{5}$$

The first gives $a_0 = 1.1966 \times 10^{-10}$ m/s^2 on bound-matter clocks and 1.1208×10^{-10} m/s^2 on the early clock (Sec. ZS 5); the third enters clock phenomenology (§VIII).

7. **CMB from ψ-physics + derived χ:** The analytic ψ calculation fixes the baryon-loading ratio while the derived χ carrier supplies primordial cold clustering without a *postulated* dark matter abundance. Peak ratio $R \approx 2.34$ is the analytic baryon-loading estimate; the peak location follows from the measured-clock forward solution with no global ψ screen: $100\theta_* = 1.04110$ and $\ell_1 \approx 220.4$. The exact conformal invariance result of App. ZS rules out a global $\Delta\psi \approx 0.30$ peak-location map. **No *postulated* dark sector:** galactic dynamics follow the μ-law on the baryons with no fitted halo, and there is no free dark energy; the cold dark matter is the derived χ-matter particle (App. AV), which composes with the μ-law inside galaxies by the floor law and assembles ΛCDM-like halos under the adopted momentum-conserving energy (estimate), and dark energy is the α^{57} geometric vacuum, whose coefficient is measured.

c. Theoretical Completeness:

1. **UV completion from topology:** The $\mathbb{C}P^2 \times S^3$ gauge emergence framework is proposed as the UV completion. Unlike GR, DFD has a flat arena with absolute time, and that time is the uniform-expansion slicing, maximal around isolated bodies, whose slices never reach the singularity of a collapsing star (App. WS, where the grade is stated); ψ is classical (action $\gg \hbar$). The topology fixes α, the exponent of v and the leading fermion-mass and mixing patterns; the other inputs are those of App. FK (§XVIII C).

2. **CMB forward closure:** Peak ratio $R = 2.34$ is the analytic baryon-loading result; peak location $\ell_1 \simeq 220$ follows from the measured-clock no-screen forward solution. CLASS/CAMB is used as the explicit community transfer calculation on DFD's frozen current inputs; it is not a refit of free ΛCDM densities.

3. **Cluster mass:** Under the μ-law alone clusters fall short (Obs/DFD $= 1.57 \pm 0.08$ relaxed, 1.99 ± 0.16 merging, at $a_0 = 1.20 \times 10^{-10}$ m/s^2 and at the bound-matter $a_0 = 1.1966 \times 10^{-10}$ m/s^2); the shortfall is the derived χ, 0.84 ± 0.12 of the cosmic mix when χ adds its Newtonian pull and the relaxed X-ray masses carry a hydrostatic bias $b = 0.21$. The amplitude follows from the derived abundance under ΛCDM-like assembly (1.21 ± 0.05 of the cosmic mix predicted inside r_{500}, 1.28 ± 0.04 measured with no hydrostatic bias; estimate). A no-χ closure by literature correction factors does not hold. Galaxy groups fall short in the same way on published X-ray masses and need χ too (§XVI G, Appendix I).

4. **Standard Model from topology:** The gauge emergence framework (§XVII) gives the electroweak group as the isotropy group of $\mathbb{C}P^2$ under one stated identification, with colour, the family content and $N_{\rm gen} = 3$ as inputs (App. F), $\alpha = 1/137$ from Chern-Simons, the top and charm masses (the other seven charged fermions rest on data-selected prefactors), the CKM magnitudes and the PMNS angles with the stated inputs of App. FK, the exponent of $v = M_P \alpha^8 \sqrt{2\pi}$, which accounts for the 17 orders of magnitude of the hierarchy (its prefactor is fitted), and, with $\theta_{\rm YM} = 0$ fixed by the spectral action given that nothing is added to it for the gauge fields, $\bar{\theta} = 0$ at tree level and loop-bounded (Theorem L.3; no axion required). Its physical validity is conditional on DFD gravity being confirmed experimentally.

5. **Scope boundary:** Loop corrections in the ψ-gauge coupled system are bounded by power counting: ψ couples with gravitational strength, so they are suppressed by $(E/M_{\rm P}c^2)^2 \lesssim 10^{-30}$ at collider energies, and the low-acceleration self-interaction becomes strong only below 0.2 mm, far under every length on which that sector is tested. The classical and effective-field level is sufficient for all predictions.

DFD reproduces GR in all regimes where GR has been confirmed, and makes specific, quantitative predictions in regimes where decisive tests are experimentally accessible.

D. Reader's Guide

This review is organized to be readable both linearly and as a reference. The structure follows a logical progression from foundations to frontiers, with each part addressing a distinct aspect of the theory.

a. Part I: Foundations (Sections I–III). It establishes the mathematical framework: the optical metric, action principle, field equations, and proof of well-posedness (existence, uniqueness, stability). This part is prerequisite for all subsequent sections.

b. Part II: Contact with Known Physics (Sections IV–V). It shows that DFD reproduces GR where tested. Section IV presents the complete PPN analysis showing $\gamma = \beta = 1$. Section V develops the gravitational wave sector and verifies consistency with LIGO/Virgo/KAGRA constraints.

c. Part III: Strong Fields (Section VI). It extends the theory to strong-field regimes: spherically symmetric solutions, photon spheres, optical horizons, and black hole shadows. Comparison with EHT observations of M87* and Sgr A* is presented.

d. Part IV: Galactic Dynamics (Section VII). It develops the deep-field regime where $\mu \neq 1$: rotation curves, Tully-Fisher relation, and the radial acceleration relation. The RAR/SPARC comparison is treated as validation of the derived acceleration scale and kinetic crossover, not as a calibration of a_0.

e. Part V: The α-Relations (Section VIII). It presents the three parameter-free numerical relations linking α to gravitational phenomenology, with derivation and verification.

f. Part VI: Laboratory Tests (Sections XI–XIII). It details the laboratory tests: extended-channel atomic clock anomalies (§XI), cavity-atom LPI tests (§XII), and matter-wave interferometry (§XIII). These sections are self-contained and can be read independently after Part I.

g. Part VII: Frontiers and Open Problems (Sections XVI–XX). It addresses cosmological implications (§XVI), the conditional quantum/gauge sector (§XVII), open problems and limitations (§XVIII), and conclusions (§XX).

h. Dependencies.

- Sections I–III (Part I) are prerequisite for all subsequent sections.
- Section IV (PPN) is independent of galactic phenomenology (Section VII).
- Laboratory tests (Sections XI–XIII) require only Part I.
- Strong fields (Section VI) requires Sections II–III.

i. Notation. Standard notation is defined in Appendix A and summarized here. The scalar field is ψ; the refractive index is $n = e^{\psi}$; the acceleration is $\mathbf{a} = (c^2/2)\nabla\psi$; the crossover function is $\mu(x)$ with $x = |\nabla\psi|/a_\star$; the acceleration scale is $a_0 \sim 10^{-10}\,\mathrm{m/s^2}$. Key equations are numbered sequentially throughout.

j. A note on falsifiability. Every scientific theory must specify conditions under which it would be falsified. For DFD, the decisive tests are:

- **Channel-resolved clocks and cavity residuals:** If same-ion, cross-species, and nuclear-clock data cannot be organized by the channel-resolved structure of Eq. (291), the present clock mechanism is wrong. In particular, a high-precision null in cross-species atomic ratios and in the surviving ^{229}Th/Sr nuclear window would remove the leading live laboratory channels of the extended non-metric sector.
- **Cavity–atom residuals:** After geometric cancellation, the cavity–atom observable is a screened residual, not an order-unity discriminator. A future dedicated null at the residual sensitivity target of Sec. XII would constrain or remove that channel; a null only at the $\delta\xi_{\mathrm{LPI}} < 0.1$ level would not.
- **Gravitational waves:** If ppE parameters deviate from zero in the strong-field regime, the radiative sector requires modification.

E. Assumptions and Degrees of Freedom Ledger

We provide an explicit accounting of the inputs, outputs, and falsifiers.

The $\mu(x)$ crossover function is **not** a continuous fit parameter. Its single scale a_0 is derived from the α-relation $a_0 = 2\sqrt{\alpha}\,cH_0$; the functional form is an exponential response **fixed** by the S^3 Chern-Simons microsector composition law, with $\mu(x) = x/(1+x)$ as its weak-response (galactic) approximant (Appendix N, Appendix BS). With H_0^{loc} fixed by the measured G (Eq. (479)), the galactic sector carries no adjustable parameter.

a. Parameter structure. DFD has: (i) no continuous parameter fitted to the shape of any observable it predicts except the baryon density, and nothing analogous to Ω_m, w, or CDM concentrations; (ii) a discrete input set, in which $N_{\mathrm{gen}} = 3$, the derived $q_1 = 3$ and the five matter types fix $k_{\max} = 60$, listed with the adopted axioms in Tables CXXVII and CXXVIII and priced in the trials audit of App. CE; (iii) four continuous cosmological calibration constants: the vacuum coefficient R, which with the empirical scale H_0 (equivalently G) fixes all dimensionful quantities; the amplitude A_s of the primordial perturbations, whose source the printed theory does not contain; the coefficient of $\omega_b h^2$, the one shape among them; and the reionization optical depth τ, an astrophysical quantity shared with ΛCDM (per-input grades: App. FK, Rem. FK.8); the particle sector adds the fitted Higgs prefactor, the imported factor η_q and the Higgs quartic, conjectured to be 1/8 at a matching scale that is not derived. Bound systems read $H_0^{\mathrm{loc}} = 72.09$ (Postulate ZS.11), so $a_0 = 1.1966 \times 10^{-10}\ \mathrm{m/s^2}$ is a prediction, not a fit.

TABLE II. Summary of DFD's inputs, outputs and falsifiers. The inputs of the graded predictions, with where each is stated, are listed in Tables CXXVII and CXXVIII (App. FK).

Category	Item	Status
Core postulates (2)		
	$n = e^{\psi}$	Postulate
	$\Phi = -c^2\psi/2$	Postulate
Adopted axioms, premises and identifications		
	Gravity and dark sector: elliptic constraint, Rest-Mass Channel, the floor law in energy form, environmental confinement, the premises of the Einstein–Hilbert term	Adopted
	Cosmology: clock and scalar dictionaries, two primordial inputs, the flatness clause, flux transport, the two-clock postulate, domain-local normalizer (optional)	Adopted
	Inner space and flavour: seven vacuum axioms, three structural postulates, the baryon-number premise	Adopted
	Ground-state principle ($\nu = Z_1$), flux period of χ, twelve more	Adopted
Background frameworks (shared)		
	Quantum mechanics: unit $\hbar$, interacting map, measurement	Shared
	Standard thermal history; baryonic astrophysics	Shared
Discrete inputs		
	$N_{\rm gen} = 3$, colour, family content	As in the SM
	$q_1 = 3$	Derived (electroweak identification)
	$(a, n) = (9, 5)$, $k_{\max} = 60$	From these; conditional count
	Weak-block count 158	Stated input
	Tilt $n_s = 1 - 2/60$	Stated number; mechanism open
	Fermion prefactors, CKM counts, neutrino branch	Chosen by data
Scale and calibrations		
	G (equivalently $H_0^{\rm loc}$)	Measured unit
	Vacuum coefficient R	Measured
	A_s, ω_b coefficient, τ	Calibrated
	Higgs prefactor; λ_H; η_q	Fitted; conjectured 1/8, scale not derived; imported
Functional form		
	$\mu(x)$	Ground-state principle; branch (SOURCE) chosen by data
Derived (no continuous shape parameters)		
	$\alpha^{-1} = 137.036$	CS quant. (conv.-locked); bracket coefficient and $1/e^2$ identification open
	$a_0 = 2\sqrt{\alpha}cH_0^{\rm loc}$	Derived (value under Postulate ZS.11)
	$G\hbar H_0^2/c^5 = C\alpha^{57}$	Exponent derived; R measured
	$v = M_P\alpha^8\sqrt{2\pi}$	α^8 derived; prefactor fitted
	$m_t = (1-\alpha)v/\sqrt{2}$	Derived
Forced mod. discrete selection / one postulate		
	Masses (below top and charm)	Seven prefactors, chosen by data
	CKM	Euler-proj. postulate
	PMNS	Forced (∼5%) up to one branch choice; θ_{13} a stated conjecture
Falsifiers		
	Cavity–atom residual null	Cavity
	Clock channel structure fails	Clocks
	$c_T \neq c$	GW
	RAR $> 3\sigma$ off	Galactic

F. Completion Ledger

A sector is called *closed* when its postulates, theorem chain, numerical implementation target, and falsifier are all explicit. The following ledger summarizes the closure status of each DFD sector.

a. The integrated-architecture statement. Its inputs are listed in Tables CXXVII and CXXVIII. The same S^3 saturation-union law that gives the weak-response galactic interpolation function also fixes the deviation-invariant structure of the temporal sector, from which the dust branch follows under the adopted identification $K' = \mu$ (App. Q). The same finite Toeplitz algebra that supplies the microsector cutoff also forces the regular Hilbert module through real-bimodule consistency. The theory is therefore overconstrained: changing one sector generally breaks another.

II. MATHEMATICAL FORMALISM

This section develops the complete mathematical structure of Density Field Dynamics: the optical metric governing light propagation, the action principle, field equations, and the family of crossover functions. The presentation aims for both rigor and physical transparency.

TABLE III. DFD completion ledger. A sector is closed when postulates, theorem chain, numerical implementation target, and falsifier are all explicit.

Sector	Closure mechanism	Status	Falsifier
Weak-field gravity	Optical metric + physical metric	PPN closed	Any PPN parameter mismatch
TT radiation	$\mathbb{C}P^2 \times S^3$ parent tensor	Closed	$c_T \neq c$ or non-GR ppE phase
Galactic dynamics	exponential response from S^3 composition; $\mu = x/(1+x)$ its weak-response form	Closed; SPARC tested	RAR shape rejects $n = 1$
MOND scale	$a_0 = 2\sqrt{\alpha}\, cH_0$	Closed	Local a_0 inconsistent with $H_0^{\rm loc}$
Epoch scale	$a_0(z) = 2\sqrt{\alpha}\, cH(z)$	Theorem under Axiom E (Thm. XIX.3); contested (App. A0Z)	High-z frozen a_0; $\partial_z a_0 \leq 0$
Dust branch	$K'(\Delta) = \mu(\Delta)$	Closed given an adopted identification	$w \not\to 0$ or $c_s^2 \not\to 0$
Linear growth	$Q_\chi = 1$ under the Rest-Mass Channel (App. GR)	Closed by an adopted postulate	Linear growth off $Q_\chi = 1$ beyond the 0.1–0.5% σ_8 shift
α value	Regular-module spectral trace	Closed to 21 ppm; bracket coefficient open	Real-bimodule Branch B counterexample
α module	Min faithful real-bimodule (App. AD)	Closed	Faithful $\mathbb{C}^d$ bimodule construction
G–H_0	α^{57} finite-mode invariant	Exponent closed; coefficient measured	Dimensionless invariant fails
ψ-screen	Local, anisotropic refraction only; the global SN/CMB screen is retired (App. LS)	Global use retired	No local foreground correlation
Clock sector	Extended-channel residuals	Partially empirical	Null in surviving channels

A. The Optical Metric and Geodesics

1. Gordon's Optical Metric

The optical metric approach has a distinguished history in relativity and optics. Gordon [25] showed in 1923 that electromagnetic waves propagating through a moving dielectric medium experience an effective spacetime geometry. Perlick [26] systematically developed ray optics in curved spacetimes, establishing the mathematical foundations for relating wave propagation to null geodesics.

DFD adopts this framework but makes a conceptual inversion: rather than deriving an effective optical metric from an underlying curved spacetime, the optical refractive index becomes the fundamental gravitational degree of freedom on flat Minkowski spacetime.

The optical metric is defined by the single scalar field $\psi(\mathbf{x}, t)$:

$$d\tilde{s}^2 = -\frac{c^2\, dt^2}{n^2(\mathbf{x}, t)} + d\mathbf{x}^2, \qquad n(\mathbf{x}, t) = e^{\psi(\mathbf{x},t)}. \tag{6}$$

The line element $d\tilde{s}^2 = 0$ defines null rays—the trajectories of light. The refractive index $n = e^\psi$ satisfies $n > 0$ everywhere, ensuring light propagation is always well-defined.

2. Fermat's Principle

Light rays extremize optical path length. For a path $\mathbf{x}(s)$ parameterized by arc length:

$$\delta \int n(\mathbf{x})\, ds = 0. \tag{7}$$

The Euler-Lagrange equations yield the ray equation:

$$\frac{d}{ds}\left(n \frac{d\mathbf{x}}{ds}\right) = \nabla n, \tag{8}$$

which governs the bending of light in the refractive medium. For small deflections, this reproduces Snell's law in differential form.

The connection to null geodesics is established by noting that the optical metric (6) is a diagonal metric with position-dependent lapse c/n; its null geodesics coincide with extremals of Fermat's principle.

3. Phase and Group Velocities

The one-way phase velocity is

$$c_{\rm phase} = \frac{c}{n} = c\, e^{-\psi}. \tag{9}$$

In a gravitational potential well ($\psi > 0$), light slows: $c_{\rm phase} < c$. The coordinate speed of light depends on position, but the two-way speed—measured by local clocks and rods—remains c.

For the group velocity in the nondispersive band (where $dn/d\omega = 0$), group and phase velocities coincide: $c_{\rm group} = c_{\rm phase}$.

a. Note on asymptotic propagation. This effective-medium (optical metric) description does not imply an asymptotic EM–GW speed split. The GW170817 constraint $|c_T/c - 1| < 10^{-15}$ is satisfied because (i) the TT sector has no derivative mixing with ψ in its principal part (§V A), and (ii) the leading propagation delay is common-mode when EM and GW arrivals are compared using receiver clocks.

B. Action Principle

1. Scalar Sector Action

The scalar field ψ is governed by a k-essence-type action with a nonlinear kinetic term:

$$S_\psi = \int dt\, d^3x \left\{ \frac{a_0^2}{8\pi G}\, W\!\left(\frac{|\nabla\psi|^2}{a_\star^2}\right) - \frac{c^2}{2}\psi(\rho-\bar\rho)\right\}, \tag{10}$$

where:

- $W(y)$ is a dimensionless potential with $W(0)=0$, $W'(y)\to 1$ as $y\to\infty$, and convexity $W''(y)\geq 0$.
- $a_\star$ is the characteristic gradient scale with $[a_\star] = 1/\mathrm{m}$. It relates to the MOND acceleration scale $a_0 = 2\sqrt{\alpha}\, cH_0^{\rm loc} = 1.1966\times 10^{-10}\,\mathrm{m/s^2}$ on bound-matter clocks (Postulate ZS.11; 1.1208×10^{-10} on the early clock) via $a_\star = 2a_0/c^2$. The argument $y = |\nabla\psi|^2/a_\star^2$ is then dimensionless.
- ρ is the local mass density; $\bar\rho$ is the mean cosmic density, ensuring proper cosmological boundary conditions.

The kinetic function $W(|\nabla\psi|^2/a_\star^2)$ interpolates between:

- **High gradients** ($|\nabla\psi|/a_\star \gg 1$): $W\approx y$, yielding linear (Newtonian) behavior.
- **Low gradients** ($|\nabla\psi|/a_\star \ll 1$): $W\sim \frac{2}{3}y^{3/2}$, producing MOND-like deep-field dynamics.

a. Dimensional verification. Note: In the Lagrangian, $a_\star$ has units of 1/m (a gradient scale), related to the physical acceleration scale a_0 by $a_\star = 2a_0/c^2$. This ensures $|\nabla\psi|/a_\star$ is dimensionless. The kinetic prefactor $a_0^2/(8\pi G)$ carries energy-density dimensions: $[a_0^2/G] = \mathrm{kg/(m\cdot s^2)}$. The matter coupling $c^2\psi\rho$ has units:

- $[c^2\psi\rho] = (\mathrm{m/s})^2\cdot 1\cdot(\mathrm{kg/m^3}) = \mathrm{kg/(m\cdot s^2)}$ (energy density)

Both terms integrate to energy × time: $[S_\psi] = \mathrm{J\cdot s}$ ✓

b. Comparison with AQUAL. The action (10) is the scalar-field analogue of Bekenstein-Milgrom's AQUAL formulation [27]. The key differences are: (i) the fundamental field is ψ (determining refractive index $n = e^\psi$) rather than the potential Φ directly; (ii) the coupling to matter goes through the optical metric, not just the potential; (iii) the μ-crossover is constrained by optical consistency (positive n, well-posed wave propagation).

c. Status of Eq. (10). Equation (10) is the *quasi-static spatial sector* used for lensing, weak-field dynamics, and galactic phenomenology, at Newtonian order; its μ-law term is written on the physical metric in App. WS, as in the preferred-foliation theory of Blanchet and Marsat [28]. The temporal completion is derived separately in Appendix Q, where the unique local temporal invariant $\Delta \equiv (c/a_0)|\dot\psi - \dot\psi_0|$ is introduced and the dust branch $w\to 0$, $c_s^2\to 0$ is proved. The full scalar-sector action combining spatial and temporal sectors is

$$S_\psi = \int dt\, d^3x \left\{ \frac{a_0^2}{8\pi G}\left[W\!\left(\frac{|\nabla\psi|^2}{a_*^2}\right) + K\!\left(\frac{c}{a_0}|\dot\psi-\dot\psi_0|\right)\right] - \frac{c^2}{2}\,\psi(\rho-\bar\rho)\right\}. \tag{11}$$

where K is the temporal kinetic function with $K'(\Delta) = \mu(\Delta)$, which acts on homogeneous deviations from the background flow only (Axiom WS.1).

d. Convexity and stability. The function W must be convex ($W''\geq 0$) to ensure:

1. Well-posed elliptic field equations
2. No ghost instabilities

This follows from standard variational theory: a convex energy functional has a unique minimizer, and small perturbations about the minimum have positive energy.

2. Matter Coupling

Matter couples to the physical metric $\tilde g_{\mu\nu}$:

$$\tilde g_{\mu\nu} = \mathrm{diag}\big(-c^2e^{-\psi},\, e^{+\psi},\, e^{+\psi},\, e^{+\psi}\big)\,. \tag{12}$$

This shares the same null cone as the Gordon eikonal metric (6): setting $d\tilde s^2 = 0$ gives $|d\mathbf{x}/dt| = c\,e^{-\psi} = c/n$, so light propagation is identical. The exponential structure $n = e^\psi$ together with Postulate P2 fixes, to first order in ψ, the relation between time and spatial components (cf. the PPN derivation in §IV C). The lapse $e^{-\psi/2}$ and the volume $\det\tilde g_{ij} = e^{3\psi}$ are exact; the isotropy of the spatial part holds through first post-Newtonian order, and beyond it $\tilde g_{ij} = e^\psi(e^h)_{ij}$, with h_{ij} the traceless part of the parent strain (§V A 3; App. WS), and the spatial part $d\mathbf{x}^2$ of Eq. (6) is then $(e^h)_{ij}\,dx^i dx^j$. For a point particle of mass m, the action is:

$$S_{\rm pp} = -mc\int d\tau\,\sqrt{-\tilde g_{\mu\nu}\frac{dx^\mu}{d\tau}\frac{dx^\nu}{d\tau}}. \tag{13}$$

In the non-relativistic limit ($v\ll c$, $|\psi|\ll 1$):

$$S_{\rm pp} \approx -mc^2\int dt\left(1 - \frac{v^2}{2c^2} + \frac{\Phi}{c^2}\right), \tag{14}$$

where $\Phi = -c^2\psi/2$ is the effective Newtonian potential. The equation of motion is:

$$\frac{d^2\mathbf{x}}{dt^2} = -\nabla\Phi = \frac{c^2}{2}\nabla\psi = \mathbf{a}, \tag{15}$$

confirming that all test masses fall with acceleration $\mathbf{a} = (c^2/2)\nabla\psi$—the Weak Equivalence Principle is satisfied. The unification of this acceleration law with the light-propagation law $c_1 = c/n$, as the timelike and null sectors of a single optical-metric wave equation, is developed in Appendix AN.

TABLE IV. Action sectors and their physical content.

Sector	Content	Degrees of Freedom
S_ψ	Scalar refractive field	0 (constraint; Axiom WS.1)
S_h	TT gravitational waves	2 (tensor $h_{ij}^{\rm TT}$)
$S_{\rm int}$	GW-matter coupling	—
$S_{\rm matter}$	Matter fields	Various

3. Gravitational Wave Sector

The transverse-traceless (TT) gravitational wave sector is embedded with the standard linearized action:

$$S_h = \frac{c^4}{64\pi G}\int dt\, d^3x \left[\frac{1}{c^2}(\partial_t h_{ij}^{\rm TT})^2 - (\nabla h_{ij}^{\rm TT})^2\right]. \quad (16)$$

This is the canonical form for a massless spin-2 field on flat spacetime. It is the quadratic part of the full a_2 Einstein–Hilbert TT action, whose cubic vertex carries the nonlinear gravitational-wave memory (App. AT). It ensures:

- Propagation speed $c_T = c$ (consistent with GW170817)
- Two tensor polarizations (+ and ×)
- No scalar or vector GW modes

The wave equation follows from variation:

$$\Box h_{ij}^{\rm TT} = \frac{16\pi G}{c^4}(T_{ij}^{\rm eff})^{\rm TT}, \quad (17)$$

where $\Box = c^{-2}\partial_t^2 - \nabla^2$ and $(T_{ij}^{\rm eff})^{\rm TT}$ is the transverse-traceless projection of the effective stress-energy tensor.

4. Interaction and Complete Action

The gravitational wave sector couples to matter through:

$$S_{\rm int} = \frac{1}{2}\int d^4x\, h_{ij}^{\rm TT} T_{\rm eff}^{ij}, \quad (18)$$

with the effective stress-energy tensor:

$$T_{\rm eff}^{ij} = \rho v^i v^j + p\delta^{ij} + \mathcal{O}\big(v^4/c^4\big). \quad (19)$$

The complete DFD action is:

$$\boxed{S_{\rm DFD} = -S_\psi\big|_{\rho=0} + S_h + S_{\rm int} + S_{\rm matter}} \quad (20)$$

where $S_{\rm matter}$ includes all matter field Lagrangians minimally coupled to the metric $\tilde g_{\mu\nu}$ of Eq. (12). In the Newtonian limit their coupling to ψ is the ρ term of Eq. (10), so that term is counted once, in $S_{\rm matter}$; Eq. (10) is written as an energy and enters with the opposite sign.

a. Key properties of the complete action:

- **Explicit variational principle:** All field equations derivable from $\delta S = 0$.
- **Energy positivity:** W convex ensures no negative-energy modes.
- **No ghosts below the cutoff:** no propagating scalar DOF (ψ is a constraint, Axiom WS.1); two tensor DOFs in $h_{ij}^{\rm TT}$; none in the constrained vector and scalar-longitudinal pieces of the parent strain (§V A 3); the Weyl-squared term of the spectral action adds a spin-2 pole only above the cutoff (App. WS).
- **GW speed $c_T = c$:** Built into the TT action.
- **Newtonian limit:** $\mu \to 1$ for large $|\nabla\psi|/a_\star$.
- **MOND limit:** $\mu \sim x$ for small $|\nabla\psi|/a_\star$.

C. Field Equations

1. General Nonlinear Form

Variation of S_ψ with respect to ψ yields the fundamental field equation:

$$\nabla\cdot\left[\mu\left(\frac{|\nabla\psi|}{a_\star}\right)\nabla\psi\right] = -\frac{8\pi G}{c^2}(\rho-\bar\rho), \quad (21)$$

where the response (flux) function $\mu(x)$ is related to the kinetic potential by:

$$\mu(x) = W'(x^2), \qquad x = \frac{|\nabla\psi|}{a_\star}. \quad (22)$$

(The distinct combination $W'(X) + 2XW''(X) = d[x\mu(x)]/dx$ is the longitudinal eigenvalue of the flux Jacobian; it governs linear perturbations [App. AC] and hyperbolicity, not the source law, and equals 2μ in the deep-MOND limit.) Inside bound systems that contain χ the adopted energy of App. AV, in which the μ-law acts on the baryons' field, governs instead of Eq. (21).

a. Derivation sketch. From action (10), compute:

$$\begin{aligned}\frac{\delta S_\psi}{\delta\psi} &= -\frac{a_0^2}{8\pi G}\nabla\cdot\left[W'\left(\frac{|\nabla\psi|^2}{a_\star^2}\right)\frac{2\nabla\psi}{a_\star^2}\right] - \frac{c^2}{2}(\rho-\bar\rho)\\ &= -\frac{c^4}{16\pi G}\nabla\cdot[W'(X)\nabla\psi] - \frac{c^2}{2}(\rho-\bar\rho),\end{aligned} \quad (23)$$

where $X = |\nabla\psi|^2/a_\star^2$. Setting $\delta S/\delta\psi = 0$ and identifying $\mu(x) = W'(x^2)$ gives Eq. (21).

2. The Optical Source Theorem: DFD's replacement for $T_{\mu\nu}$

The source of ψ is fixed, not posited: it is the variational response of the matter action to ψ, the exact analogue of how $T_{\mu\nu}$ arises in general relativity.

Theorem II.1 (DFD Optical Source Theorem)**.** *The GR ten-component source $T_{\mu\nu} = -\frac{2}{\sqrt{-g}}\,\delta S_{\rm matter}/\delta g^{\mu\nu}$ is*

replaced in DFD by a single scalar *law for the optical-density field ψ,*

$$\boxed{\mathcal{S}_\psi := \frac{\delta S_{\rm matter}}{\delta\psi} = \tfrac{1}{2}\sum_i (\varepsilon_i + 3P_i)\, e^{\psi}} \qquad (24)$$

— the Tolman active gravitational mass $\rho + 3P/c^2$*, one term per sector i (rest mass, kinetic, radiation, pressure, gauge, χ, vacuum). Because ψ enters every sector only through the single non-conformal optical metric $\tilde{g}_{\mu\nu} = \mathrm{diag}(-c^2 e^{-\psi}, e^{+\psi}, e^{+\psi}, e^{+\psi})$, the field equation $\delta S_{\rm DFD}/\delta\psi = 0$ [Eq. (20)] is $\nabla\cdot[\mu\,\nabla\psi] = -(8\pi G/c^4)(\varepsilon + 3P)e^{\psi}$, of which Eq. (21) is the non-relativistic ($P \ll \varepsilon$, $\psi \ll 1$) limit $-(8\pi G/c^2)(\rho - \bar{\rho})$. The source law holds with the spatial part $\tilde{g}_{ij} = e^{\psi}(e^h)_{ij}$ as well; for static matter at $\mu = 1$ the field equation is then $\partial_i[(e^{-h})^{ij}\partial_j\psi] = -(8\pi G/c^4)(\varepsilon + 3P)e^{\psi}$ exactly, the time-time component of the trace-reversed Einstein equation (App. WS).*

Proof. With the standard definition $T_{\mu\nu} = -\frac{2}{\sqrt{-g}}\,\delta S_{\rm matter}/\delta g^{\mu\nu}$, minimal coupling gives $\delta S_{\rm matter}/\delta\psi = +\frac{1}{2c}\sqrt{-\tilde{g}}\,T^{ab}\,\partial_\psi \tilde{g}_{ab}$ with $\sqrt{-\tilde{g}} = c\,e^{\psi}$: the lapse $\tilde{g}_{tt} = -c^2 e^{-\psi}$ contributes $+\varepsilon$, the three spatial $\tilde{g}_{ii} = e^{+\psi}$ contribute $+3P$, so $\partial_\psi S_{\rm matter} = +\frac{1}{2}(\varepsilon + 3P)e^{\psi}$ (verified symbolically, residual 0; the static-fluid special case is App. AT). The scalar action of Eq. (10) is written as an energy, so in Eq. (20) it enters with the sign opposite to the matter Lagrangian, and at $\rho = 0$, since its ρ term is the Newtonian limit of the ψ coupling in $S_{\rm matter}$; with that sign and that count $\delta S_{\rm DFD}/\delta\psi = 0$ is the field equation stated above. The rule is linear in T^{ab}, so it holds identically for the renormalized quantum expectation $\langle\hat{T}^{ab}\rangle_{\rm ren}$, giving the semiclassical source $\langle\hat{\varepsilon} + 3\hat{P}\rangle_{\rm ren}$. □

Corollary II.2 (Nordström-avoidance)**.** *Had matter coupled* conformally *($\tilde{g}_{\mu\nu} = e^{2\psi}\eta_{\mu\nu}$) the source would be the trace $(\varepsilon - 3P)$, which* vanishes *for radiation ($P = \varepsilon/3$): radiation would not gravitate and light would not bend — the reason Nordström's 1913 scalar gravity is excluded. DFD's opposite-sign lapse/space exponents give $(\varepsilon + 3P) = 2\varepsilon$ for radiation instead, so radiation gravitates at twice the dust rate and light bends with $\gamma = 1$. The distinction is a single sign in $\partial_\psi\tilde{g}_{\mu\nu}$; the trace anomaly shifts the trace $(\varepsilon - 3P)$ and cannot restore the traceless combination; the stress it induces adds only a small $\varepsilon + 3P$, of order H^4 in the radiation era (Extended Derivations, App. AH).*

Weak-field limit. For $\mu \to 1$, $P \ll \varepsilon$, $\psi \ll 1$ the theorem reduces to $\nabla^2\psi = -(8\pi G/c^2)\rho$; with $\mathbf{a} = (c^2/2)\nabla\psi$ and $\Phi = -(c^2/2)\psi$ this is Newtonian gravity, mass-independent (WEP). **Conservation.** The optical stress tensor obeys $\tilde{\nabla}_\mu\tilde{T}^{\mu\nu} = 0$ (below), the on-shell-matter / spatial-diffeomorphism Noether partner of Theorem II.1 — the DFD analogue of the contracted Bianchi identity, confirmed at PPN order by $\zeta_1 = \zeta_2 = \zeta_3 = \zeta_4 = 0$.

a. Scope of the local form, and its scale-resolved completion. Equation (21) evaluates μ at a point. That is the correct *local* reduction of DFD's quasi-static scalar sector, and it reproduces flat rotation curves, the baryonic Tully–Fisher relation and the deep-field limit exactly. DFD's derived response is, however, a *mode* statement — $\nu = 1/\mu$ is a single-mode partition function and τ an optical depth (App. N) — and the per-point and per-mode readings agree only when all the sourcing mass lies at one distance from the field point. Where they disagree there is now a measurement: any functional whose argument is the *vector* sum $|\nabla\psi_{\rm int} + \nabla\psi_{\rm ext}|$ generates a static anomalous quadrupole Q_2 in the planetary potential, bounded observationally at $(3 \pm 3) \times 10^{-27}$ s^{-2} by Cassini [29] and at $(1.6 \pm 1.8) \times 10^{-27}$ s^{-2} on the DE440 dataset [30]. Appendix NL constructs the *scale-additive* (nonlocal-in-radius) completion of Eq. (21), of which Eq. (21) is the exact co-distant limit (Thm NL.1, item 2), records its forward evaluations against every existing measurement, and proves five no-go results that close the obvious alternatives. In the Solar System, where the Sun and the Galaxy are separated by 18.955 e-folds of vacuum, the completion and the local form differ; in a galaxy, which is matter all the way through, they agree to ≤ 0.018 dex.

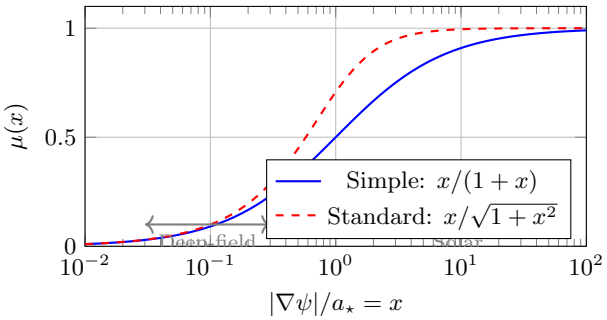


FIG. 2. The $\mu(x)$ crossover function interpolates between deep-field ($\mu \sim x$) and solar ($\mu \to 1$) regimes. The transition occurs at $x \sim 1$, corresponding to $|\nabla\psi| \sim a_\star$. The "Standard" form is shown for historical comparison; the S^3 microsector composition law selects an exponential response (Appendix N, Lemma N.6; Appendix BS), of which the "Simple" form is the weak-response approximant (asymptotics forced).

D. The $\mu(x)$ Crossover Function

The response function $\mu(x)$ must satisfy four physical constraints:

1. **Solar limit:** $\mu(x) \to 1$ as $x \to \infty$ (recover Poisson equation).
2. **Deep-field limit:** $\mu(x) \sim x$ as $x \to 0$ (MOND-like scaling for flat rotation curves).
3. **Monotonicity:** $\mu'(x) > 0$ for $x > 0$ (strict ellipticity of field equation).
4. **Convexity:** The associated W must be convex (energy positivity, stability).

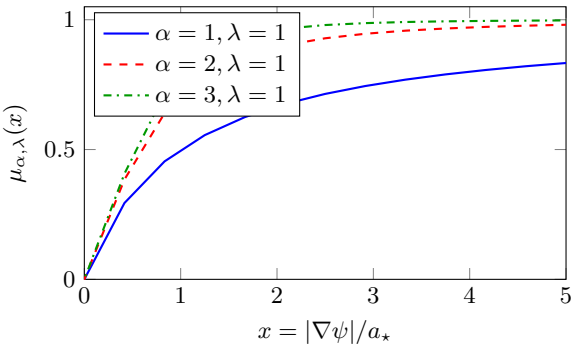


FIG. 3. Constrained crossover functions $\mu_{\alpha,\lambda}(x)$: linear at small x (deep-field), saturating at large x (solar limit), monotone throughout.

1. Admissible Families

Table V catalogs the μ-functions used in the DFD literature. The "Simple" form $\mu(x) = x/(1+x)$ is the weak-response form (Assumption N.3) of the exponential response derived from the S^3 microsector via a composition law (Appendix N, Lemma N.6, Theorem N.8; Appendix BS): its two asymptotic limits are forced, and it tracks the derived response in its RAR form to $\lesssim 0.02$ dex (below SPARC precision).

TABLE V. Catalog of admissible $\mu(x)$ functions. The law of record is the SOURCE branch of App. BS; the Simple form is its weak-response approximant (App. N).

Name	Formula	$\mu(1)$	Status
Simple	$\frac{x}{1+x}$	1/2	Approximant
Standard	$\frac{x}{\sqrt{1+x^2}}$	$1/\sqrt{2}$	Phenomenological
General	$\frac{x}{(1+\lambda x^\alpha)^{1/\alpha}}$	varies	Phenomenological
Exponential (TOTAL)	$1-e^{-x}$	$1-e^{-1}$	Admissible; not selected

The general family $\mu_{\alpha,\lambda}(x)$ satisfies all four constraints only for $\lambda = 1$.

E. Conserved Quantities and Symmetries

1. Diffeomorphism Invariance

The matter action is invariant under diffeomorphisms that act on the matter fields and the optical metric together. On the matter equations of motion this gives a conserved stress-energy tensor in the optical metric:

$$\tilde{\nabla}_\mu \tilde{T}^{\mu\nu} = 0, \tag{25}$$

where $\tilde{\nabla}$ is the covariant derivative with respect to $\tilde{g}_{\mu\nu}$. This is the Noether partner of the Optical Source Theorem II.1: its scalar projection along the ψ-flow reproduces the source $\mathcal{S}_\psi = \delta S_{\rm matter}/\delta\psi$.

2. Energy Conservation

In static configurations, the total energy functional:

$$E[\psi] = \int d^3x \left[\frac{a_0^2}{8\pi G} W\left(\frac{|\nabla\psi|^2}{a_\star^2}\right) - \frac{c^2}{2}\rho\psi\right] \tag{26}$$

is minimized by solutions of the field equation.

3. Local Conservation in PPN Framework

Within the PPN formalism (§IV), DFD satisfies local energy-momentum conservation:

$$\zeta_1 = \zeta_2 = \zeta_3 = \zeta_4 = 0, \tag{27}$$

where the ζ_i are PPN parameters measuring violation of local conservation. This follows from the diffeomorphism invariance of the optical metric coupling.

F. 4D-from-3D: Emergent Spacetime Structure

A distinctive feature of DFD is that the 4D optical metric is *derived*, not fundamental. The theory is intrinsically 3-dimensional.

1. The Fundamental Arena

DFD posits:

1. **Space:** Euclidean $\mathbb{R}^3$ with coordinates $\mathbf{x}$
2. **Time:** Absolute parameter t (preferred foliation)
3. **Field:** Scalar $\psi(\mathbf{x}, t)$ on this arena

The "4D spacetime geometry" emerges as an effective description of how light propagates and clocks tick in the refractive medium.

2. The 3D-to-4D Morphism

Theorem II.3 (Emergent Spacetime)**.** *There is a bijective correspondence:*

$$\{\textit{3D solutions } \psi(\mathbf{x}, t)\} \longleftrightarrow \{\textit{4D optical intervals } d\tilde{s}^2\} \tag{28}$$

given by the Gordon-type optical interval:

$$d\tilde{s}^2 = -\frac{c^2 dt^2}{n^2} + d\mathbf{x}^2, \qquad n = e^\psi. \tag{29}$$

Through first post-Newtonian order; beyond it the interval's spatial part is $(e^h)_{ij}$, with h_{ij} the traceless part of the parent strain (§V A 3), and the correspondence is with the pair (ψ, h_{ij}).

a. Remark (auxiliary rescaled metric). For certain calculations (gauge-sector derivations, Einstein-tensor cross-checks), it is convenient to use an auxiliary metric $\hat{g}_{\mu\nu} = \mathrm{diag}(-c^2e^{-2\psi}, e^{2\psi}, e^{2\psi}, e^{2\psi})$ that doubles the exponents relative to the physical metric (12). This is a computational device; the physical coupling is through (12), the fundamental DFD arena remains flat $\mathbb{R}^3$ with absolute time, and the Gordon interval (29) is its optical encoding. The morphism to 4D curvature language is used only as a "translation layer" for comparison with GR—it does not promote 4D geometry to fundamental status.

b. Static check. The static field equation

$$\nabla^2\psi = -\frac{8\pi G\rho}{c^2} \tag{30}$$

can be repackaged as the (00)-component of the Einstein tensor for the physical metric (12) at linear order. This is a mathematical identity used for cross-checking. DFD's Einstein dynamics comes instead from the Einstein–Hilbert term of the spectral action acting on the physical metric in absolute time (App. WS).

c. Physical consequences.

- **Preferred foliation:** DFD has absolute simultaneity (constant-t surfaces)
- **No closed timelike curves:** The 3D picture forbids them automatically
- **Fixed topology:** Space is $\mathbb{R}^3$ forever
- **Refractive interpretation:** "Curved spacetime" is refractive medium

This contrasts with GR, where 4D spacetime is fundamental. In DFD the arena is flat $\mathbb{R}^3$ with absolute time, and the physical metric obeys the Einstein–Hilbert dynamics in that time (App. WS).

G. Physical Interpretation: Vacuum Loading

The mathematical formalism admits a direct physical interpretation in which gravity arises from energy loading of the quantum vacuum [31]. Mass—which is predominantly field energy (about 99% of the proton's mass is QCD field energy, not quark rest mass)—deposits a fractional loading ψ in the vacuum, modifying its refractive index to $n = e^{\psi}$.

a. Vacuum stiffness. The coefficient $K_0 = c^4/(8\pi G)$ is a *force scale* (units: newtons), not an energy density. It is the vacuum's resistance to deformation—the same coefficient that appears in the Einstein field equations. Via the master invariant (§XIX), its exponent is fixed and, on bound-matter clocks where $C = 1$ (Postulate ZS.11), $K_0 = \hbar(H_0^{\mathrm{loc}})^2/(8\pi\alpha^{57}c)$.

b. Stress–strain interpretation. The field equation (21) has the structure of a nonlinear constitutive equilibrium. Defining the gravitational strain $s \equiv |\nabla\psi|/a_*$ and stress $\boldsymbol{\sigma} \equiv K_0\,\mu(s)\,\nabla\psi$, the field equation reads $\nabla\cdot\boldsymbol{\sigma} = -\rho c^2$: the divergence of the vacuum stress balances the energy loading from matter.

c. Reduced gravitational permittivity. The crossover function $\mu(s)$ acts as a field-dependent *gravitational permittivity*. At high strain ($s \gg 1$), $\mu \to 1$ and the vacuum conducts gravitational flux at full Newtonian strength. At low strain ($s \ll 1$), $\mu \approx s \to 0$: the vacuum becomes a poor conductor of gravitational flux. By Gauss's law, the gradient $|\nabla\psi|$ must then exceed the Newtonian value to carry the same flux—yielding $v^2 = ra = \mathrm{const}$ (flat rotation curves) without dark matter. The analogy is to a nonlinear dielectric whose permittivity drops at low field strengths.

d. Vacuum energy hierarchy. The loading picture distinguishes three scales: the Planck density $\rho_P c^2 \sim 10^{113}$ J/m^3 (naive QFT mode sum), the vacuum stiffness $K_0 \sim 10^{42}$ N (resistance to deformation), and the cosmological residual $\rho_\Lambda c^2 \sim 10^{-9}$ J/m^3 (residual strain of order H_0^2/c^2). The critical distinction is that K_0 is a force scale, not an energy density; the observed dark energy is residual loading, not the stiffness itself. The α^{57} suppression from the finite microsector (Appendix O) provides the exponent: 57 frozen KK modes, each suppressing by 1/137, give the 122 orders of magnitude between ρ_P and ρ_c.

H. Summary of Section II

The mathematical structure of DFD is fully specified by:

1. The optical metric $d\tilde{s}^2 = -c^2dt^2/n^2 + d\mathbf{x}^2$ with $n = e^{\psi}$ [Eq. (6)].
2. The scalar action with nonlinear kinetic term [Eq. (10)].
3. The field equation $\nabla\cdot[\mu(|\nabla\psi|/a_\star)\nabla\psi] = -(8\pi G/c^2)\rho$ [Eq. (21)]; inside bound systems that contain χ, the adopted energy of App. AV.
4. The TT gravitational wave sector at speed c [Eq. (16)].
5. The constrained $\mu(x)$ family satisfying solar, deep-field, monotonicity, and convexity conditions.

All dynamics derive from the action principle. The theory has three degrees of freedom in its fields, of which the two tensor ones (h_{ij}^{TT}) propagate; the scalar ψ is a constraint (Axiom WS.1). Below the spectral cutoff there are no ghosts and no negative-energy modes, and the field equations are well posed (§III); the Weyl-squared term implies a spin-2 pole above the cutoff (App. WS).

III. MATHEMATICAL WELL-POSEDNESS

A physical theory must be mathematically well-posed: given initial/boundary data, solutions must exist, be

unique, and depend continuously on the data. This section establishes these properties for the DFD field equations in both static and dynamic settings.

A. Static Solutions: Elliptic Theory

1. Assumptions on μ

The field equation (21) is a quasilinear elliptic PDE. Well-posedness requires the following conditions on the response function $\mu : [0, \infty) \to [0, \infty)$:

(A1) Continuity: μ is continuous on $[0, \infty)$.

(A2) Coercivity: There exist constants $\alpha > 0$ and $\beta \geq 0$ such that

$$\mu(|\xi|)|\xi|^2 \geq \alpha|\xi|^2 - \beta \quad \forall\, \xi \in \mathbb{R}^3 \tag{31}$$

(we take $p = 2$). With a bounded domain this makes the operator coercive on $W_0^{1,2}(\Omega)$, and the energy functional is bounded below.

(A3) Growth bound: There exists $\beta > 0$ such that

$$|\mu(|\xi|)\xi| \leq \beta(1 + |\xi|)^{p-1}. \tag{32}$$

This controls the operator's growth at large gradients.

(A4) Monotonicity: For all $\xi, \eta \in \mathbb{R}^3$,

$$\big(\mu(|\xi|)\xi - \mu(|\eta|)\eta\big) \cdot (\xi - \eta) \geq 0. \tag{33}$$

Strict inequality (strict monotonicity) implies uniqueness.

a. Physical interpretation. Condition (A1) ensures continuous transition between regimes. Condition (A2) prevents the field from "running away" to arbitrarily large values without cost in energy. Condition (A3) ensures solutions have finite energy in bounded domains. Condition (A4)—monotonicity—is the ellipticity condition: it ensures the linearized operator has the correct sign for stable perturbations.

b. Verification for standard μ. The simple and standard forms from Table V satisfy (A1)–(A4):

- Simple: $\mu(x) = x/(1 + x)$ is continuous, bounded between 0 and 1, and strictly increasing.
- Standard: $\mu(x) = x/\sqrt{1 + x^2}$ has the same properties with different asymptotic rates.

Both yield well-posed elliptic problems. For the exact law the same holds with $F(x) \geq x - 0.648$ (SOURCE) and $F(x) \geq x - e^{-1}$ (TOTAL), and $\mu < 1$.

2. Existence and Uniqueness

Define the flux operator $\mathbf{a}(\xi) := \mu(|\xi|)\xi$. The weak formulation of the field equation on a domain Ω with boundary data $\psi = \psi_D$ on $\partial\Omega$ is:

$$\int_\Omega \mathbf{a}(\nabla\psi) \cdot \nabla v \, d^3x = \int_\Omega f\, v \, d^3x, \quad \forall\, v \in W_0^{1,p}(\Omega), \tag{34}$$

where $f = (8\pi G/c^2)(\rho - \bar{\rho})$ is the source term.

Theorem III.1 (Existence)**.** *Under assumptions (A1)–(A4), for any $f \in V'$ (the dual of the Sobolev space $W^{1,p}(\Omega)$), there exists a weak solution $\psi \in W^{1,p}(\Omega)$ satisfying (34) with the prescribed boundary data.*

Theorem III.2 (Uniqueness)**.** *If the flux operator $\mathbf{a}(\xi)$ is strictly monotone [strict inequality in (A4)], then the weak solution of Theorem III.1 is unique.*

a. Proof sketch. The existence proof uses direct methods in the calculus of variations. Define the energy functional:

$$\mathcal{E}[\psi] = \int_\Omega H(\nabla\psi)\, d^3x - \int_\Omega f\psi \, d^3x, \tag{35}$$

where $H(\xi) = \int_0^1 \mathbf{a}(t\xi)\cdot\xi \, dt$ is the energy density satisfying $\mathbf{a}(\xi) = \nabla_\xi H(\xi)$.

1. **Coercivity** (A2) ensures $\mathcal{E}[\psi] \to +\infty$ as $\|\nabla\psi\|_p \to \infty$, so minimizing sequences are bounded.
2. **Convexity** of H (following from monotonicity) ensures $\mathcal{E}$ is weakly lower semicontinuous.
3. By the direct method, a minimizer exists in $W^{1,p}(\Omega)$.
4. The Euler-Lagrange equation for the minimizer is precisely (34).

Uniqueness follows from strict convexity: if two solutions ψ_1, ψ_2 existed, convexity implies $\mathcal{E}[(\psi_1 + \psi_2)/2] < (\mathcal{E}[\psi_1] + \mathcal{E}[\psi_2])/2$, contradicting minimality.

3. Regularity

Theorem III.3 (Regularity)**.** *If $f \in L^q(\Omega)$ with $q > 3/p'$ (where $1/p + 1/p' = 1$), then any weak solution ψ is locally Hölder continuous: $\psi \in C^{0,\alpha}_{\text{loc}}(\Omega)$ for some $\alpha > 0$.*

If additionally $\mu \in C^1$ and $f \in C^{0,\gamma}(\Omega)$, then $\psi \in C^{1,\alpha}_{\text{loc}}(\Omega)$.

Higher regularity follows by standard bootstrap arguments from quasilinear elliptic theory [32, 33]. For smooth μ and smooth sources, solutions are C^∞ in the interior away from points where $\nabla\psi = 0$.

B. Exterior Domains and Boundary Conditions

For isolated gravitating systems, we work on exterior domains $\Omega = \mathbb{R}^3 \setminus \overline{B_R}$ (the complement of a ball). Two types of boundary conditions arise:

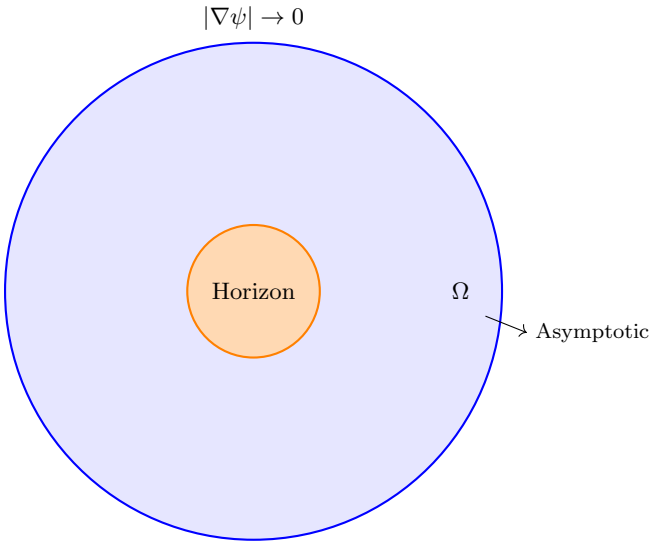


FIG. 4. Domain structure for exterior problems. The solution domain Ω (blue) excludes the optical horizon region (orange). The field gradient vanishes at infinity.

a. Asymptotic condition. At spatial infinity, we require $|\nabla\psi(\mathbf{x})| \to 0$ as $|\mathbf{x}| \to \infty$.

b. Optical horizon. At the optical horizon (where $n \to \infty$), an ingoing-flux Neumann condition is imposed:

$$\mathbf{a}(\nabla\psi) \cdot \mathbf{n} = g_{\text{hor}}, \quad \text{(outgoing flux = 0)}. \tag{36}$$

This asymmetric condition reflects the fact that light cannot escape an optical horizon, a one-way membrane in the optical metric. With the parent strain's σ kept a black hole's event horizon is such a one-way membrane (Sec. VI B): for an eternal static hole it is the optical horizon, $n \to \infty$, at the arena's origin, and for a hole formed by collapse it is the flow horizon of DFD's maximal slicing.

Theorem III.4 (Exterior well-posedness)**.** *Under assumptions (A1)–(A4) and the boundary conditions above, there exists a weak solution $\psi \in W^{1,p}_{\text{loc}}(\Omega)$ with the gradient vanishing at infinity. If the boundary operators are strictly monotone, the solution is unique.*

The proof extends standard techniques by using weighted Sobolev spaces to handle the unbounded domain.

C. Dynamic Solutions: Hyperbolic Theory

Under Axiom WS.1 the local scalar sector is an instantaneous constraint; its numerical hyperbolic relaxation, which this subsection analyses, is:

$$\frac{1}{c^2}\partial_t^2\psi - \nabla \cdot [\mu(|\nabla\psi|/a_\star)\nabla\psi] = \frac{8\pi G}{c^2}(\rho - \bar{\rho}). \tag{37}$$

This is a quasilinear wave equation with nonlinear principal part.

1. First-Order Symmetric Hyperbolic Form

Equation (37) can be rewritten as a first-order symmetric hyperbolic system. Introduce:

$$U = (\psi, \partial_t\psi, \partial_1\psi, \partial_2\psi, \partial_3\psi)^T. \tag{38}$$

The evolution takes the form:

$$A^0(U)\,\partial_t U + A^i(U)\partial_i U = S(U, \mathbf{x}), \tag{39}$$

where $A^0(U) = \text{diag}\big(1, c^{-2}, M(\nabla\psi)\big)$ is block-diagonal, with M_{ij} the flux Jacobian of §III D, the $A^i(U)$ are symmetric matrices depending on the state U, and S contains source terms.

Symmetric hyperbolicity requires A^0 to be uniformly positive definite, i.e. for some $\lambda \geq 1$

$$\lambda^{-1}|\mathbf{n}|^2 \leq \mathbf{n} \cdot M(\nabla\psi)\,\mathbf{n} \leq \lambda|\mathbf{n}|^2 \quad \forall\, \mathbf{n} \in \mathbb{R}^3 \tag{40}$$

[assumption (A1′) of §III E]. The eigenvalues of M are $\mu(x)$ (twice) and $d[x\mu(x)]/dx$, $x = |\nabla\psi|/a_\star$; both vanish at $\nabla\psi = 0$ for every response with $\mu(0) = 0$, so the condition fails there for μ itself; it holds everywhere for the regularised galactic approximant $\mu_{s_0}(x) = \mu\big(\sqrt{x^2 + s_0^2}\big)$, $\mu(x) = x/(1+x)$, $s_0 > 0$, with $\lambda = 1 + 1/s_0$.

2. Local Well-Posedness

Theorem III.5 (Local existence)**.** *Let $s > 5/2$, and let the response be the approximant $\mu(x) = x/(1+x)$ or either branch of the exact law. The flux $\mathbf{a}(\xi) = \mu(|\xi|/a_\star)\,\xi$ has Jacobian eigenvalues $\mu(x)$ (twice) and $F'(x)$, $F(x) = x\mu(x)$, which are positive for every $x > 0$ and bounded by $\Lambda = 1$ (approximant), 1.034 (SOURCE) and 1.135 (TOTAL). Let $\mathbf{g}$ be a constant vector, and let $\nabla\psi_0 - \mathbf{g} \in H^{s-1}(\mathbb{R}^3)$, $\psi_1 \in H^{s-1}(\mathbb{R}^3)$ with $\inf_{\mathbf{x}} |\nabla\psi_0| > 0$, and a source in $C([0,T_0]; H^{s-1})$. Then there are $T > 0$ and a unique solution with $\nabla\psi - \mathbf{g}$, $\partial_t\psi \in C([0,T]; H^{s-1}(\mathbb{R}^3))$ and $\inf|\nabla\psi| > 0$ on $[0,T]$, depending continuously on the data. It continues for as long as $\|\partial\psi\|_{W^{1,\infty}}$ stays finite and $|\nabla\psi|$ stays bounded away from zero. For the regularised response μ_{s_0} the lower bound on $|\nabla\psi_0|$ is not needed and $\mathbf{g} = 0$ is allowed.*

The proof is the standard one for quasilinear second-order hyperbolic equations (Hughes, Kato and Marsden 1977), applied where $|\nabla\psi| > \delta$, since there the principal part is smooth and uniformly hyperbolic. The state is $(\nabla\psi, \partial_t\psi)$ rather than ψ, because the field of any body falls off as $1/r$ and is not square integrable. By finite speed of propagation the theorem also holds locally: data that are smooth with $|\nabla\psi_0| \geq \delta > 0$ on a ball $B_R(\mathbf{x}_0)$ have a unique smooth solution in the cone $|\mathbf{x} - \mathbf{x}_0| < R - c\sqrt{\Lambda}\,t$ for short times. Points where $\nabla\psi = 0$ are excluded: both characteristic speeds vanish there. The linearised evolution at such points is covered by Theorem III.9.

a. Limitation: Global existence. Global existence (arbitrary long times) is not guaranteed. On a non-zero uniform background gradient the smooth evolution has a finite lifespan: gradient singularities form in finite time,

analogous to shock formation in nonlinear wave equations (Sec. III F).

For small perturbations of amplitude ε in three dimensions the lifespan is at least $e^{C/\varepsilon}$, beyond any astrophysical time for small ε; plane-symmetric waves break on an algebraic timescale. The linearised and weak-field predictions do not depend on it.

3. Finite Speed of Propagation

Theorem III.6 (Causality)**.** *Solutions of (37) with the galactic approximant $\mu(x) = x/(1+x)$, or with its regularisation μ_{s_0}, satisfy:*

1. *All characteristic speeds are $\leq c$.*
2. *The domain of dependence of a point $(t, \mathbf{x})$ is contained in the backward light cone $\{(t', \mathbf{x}') : |\mathbf{x}-\mathbf{x}'| \leq c(t-t')\}$.*
3. *No signal propagates faster than c.*

This follows from the eigenvalues of the flux Jacobian M: the scalar sector has characteristic speeds $v_\perp = c\sqrt{\mu(x)}$ (transverse) and $v_\parallel = c\sqrt{d[x\mu(x)]/dx}$ (longitudinal), $x = |\nabla\psi|/a_\star$, so all of them are $\leq c$ exactly when $\sup_x d[x\mu(x)]/dx \leq 1$. For the galactic approximant $\mu(x) = x/(1+x)$, $v_\perp^2/c^2 = x/(1+x)$ and $v_\parallel^2/c^2 = x(2+x)/(1+x)^2$; for its regularisation μ_{s_0} both speeds are bounded by the same expressions evaluated at $\sqrt{x^2+s_0^2}$.

Causality is a crucial physical requirement. The TT cone coincides with the optical cone, $c_T = c_\gamma$ exactly: light and gravitational waves share one metric (App. WS). With the galactic approximant $\mu(x) = x/(1+x)$ the relaxation's characteristic speeds stay below c at every finite gradient, $1-v_\parallel^2/c^2 = (1+x)^{-2}$, with $v_\parallel \to c$ only as $x \to \infty$. For the exponential responses of Appendix BS, Eqs. (BS8)–(BS9), which are the SOURCE and TOTAL branches of the exact μ-law (Theorem BS.9) and have $x/(1+x)$ as their weak-response approximant, the same characteristic-speed formula, applied to the μ-form of each branch (SOURCE through $x = y\,\nu(y)$), gives $\sup v_\parallel = 1.017\,c$ (SOURCE, near $x \approx 7$) and $1.066\,c$ (TOTAL, at $x = 2$) in the transition regime.

Proposition III.7 (Causality of the exact law)**.** *For the exact law, Eqs. (BS8)–(BS9), the characteristic speeds of (37) are finite, with suprema $1.017\,c$ (SOURCE) and $1.066\,c$ (TOTAL) in the transition regime. The equation is hyperbolic with finite propagation speed, on the same terms as for the approximant (both degenerate only at $\nabla\psi = 0$). Every characteristic advances the absolute time t of the preferred foliation (§II F), so t is a global time function for the scalar, tensor and light cones alike: no signal reaches its own past, and no closed causal curve can form. What fails for the exact law is containment in the light cone, which items 1–3 of Theorem III.6 assert for the approximant only.*

This follows from the principal part of (37), which has $a^{00} = -c^{-2}$ and $a^{0i} = 0$ (§III E): the surfaces $t = \text{const}$ are non-characteristic for every response, and each characteristic moves forward in t at a finite speed set by the eigenvalues of M. A superluminal characteristic on a background therefore violates light-cone containment, not causality. This is the reading of superluminal propagation on nontrivial backgrounds given by Babichev, Mukhanov and Vikman [34]; it applies directly to DFD, whose preferred foliation supplies the global time function.

D. Stability

1. Energy Minimization

Theorem III.8 (Energy minimization)**.** *If W is strictly convex, then:*

1. *Static solutions are local energy minima.*
2. *There are no negative-energy (ghost) modes in the linearized theory below the spectral cutoff.*

a. Proof sketch. Convexity of W implies convexity of the energy density $H(\xi)$. The integral $\mathcal{E}[\psi]$ inherits this convexity.

2. Perturbative Stability

Consider small perturbations $\delta\psi$ about a static solution ψ_0:

$$\psi = \psi_0 + \delta\psi, \quad |\delta\psi| \ll |\psi_0|. \tag{41}$$

The linearized equation for $\delta\psi$ is:

$$\frac{1}{c^2}\partial_t^2(\delta\psi) - \nabla\cdot[M_{ij}(\nabla\psi_0)\nabla_j(\delta\psi)] = 0, \tag{42}$$

where the effective mass matrix is:

$$M_{ij} = \mu(x_0)\delta_{ij} + \mu'(x_0)\frac{(\partial_i\psi_0)(\partial_j\psi_0)}{|\nabla\psi_0|\,a_\star}, \tag{43}$$

with $x_0 = |\nabla\psi_0|/a_\star$. The denominator $|\nabla\psi_0|\,a_\star$ ensures dimensional consistency: since $[(\partial_i\psi_0)(\partial_j\psi_0)] = \mathrm{m}^{-2}$ and $[|\nabla\psi_0|\,a_\star] = \mathrm{m}^{-2}$, the ratio is dimensionless.

Where $\nabla\psi_0 \neq 0$, M_{ij} is positive definite, and the linearized operator has only real, positive eigenfrequencies: no growing modes and no instabilities. Theorem III.9 covers the general case.

Theorem III.9 (Linear well-posedness on any static background)**.** *Let ψ_0 be a static solution generated by a bounded source, with $\nabla\psi_0$ bounded and continuous, and let the set where $\nabla\psi_0 = 0$ have a boundary of zero volume. Put $A(\mathbf{x}) = D\mathbf{a}(\nabla\psi_0(\mathbf{x}))$, so that $0 \leq A \leq \Lambda$. The form $q(u) = \int \nabla u \cdot A\,\nabla u\, d^3x$ on smooth compactly supported functions is closable in $L^2(\mathbb{R}^3)$, and the self-adjoint operator $L \geq 0$ of its closure generates the linearised evolution $c^{-2}\partial_t^2 u + Lu = 0$. For data in the form domain*

times L^2 the solution exists and is unique, its energy $\frac{1}{2}\int \left(c^{-2}u_t^2 + \nabla u \cdot A\,\nabla u\right) d^3x$ is conserved, no mode grows exponentially, and disturbances travel no faster than $c\sqrt{\Lambda}$. This includes points where $\nabla\psi_0 = 0$, where A vanishes.

Proof. Where $A > 0$ the coefficient is locally uniformly elliptic, so a sequence that tends to zero in L^2 and is Cauchy for q has gradients tending to zero locally there; the limit of $A^{1/2}\nabla u_n$ therefore vanishes, and q is closable. Kato's representation theorem gives L, and the spectral theorem gives $u(t) = \cos\left(ct\sqrt{L}\right) u_0 + (c\sqrt{L})^{-1} \sin\left(ct\sqrt{L}\right) u_1$ with conserved energy and spectrum in $[0, \infty)$. The energy flux through a sphere is bounded by $c\sqrt{\Lambda}$ times the energy density, which uses only $A \le \Lambda$, so the energy in a ball shrinking at that speed cannot grow. An isolated zero of $\nabla\psi_0$ has zero capacity for q, so the result does not depend on how the form is first defined there. □

3. No Ghosts

A ghost is a degree of freedom with wrong-sign kinetic term, leading to negative-energy states. In DFD:

- The scalar ψ has kinetic term $\propto W'(X) > 0$ by (A4).
- The TT modes h_{ij}^{TT} have standard positive kinetic term from (16).

Propagating degrees of freedom below the spectral cutoff: the two TT polarizations (under Axiom WS.1 ψ is a constraint), all with positive kinetic energy, so there are no ghosts there. The Weyl-squared term of the spectral action (App. WS) implies an extra spin-2 pole at about 3.6 reduced Planck masses for $f_0 = 1$, above the cutoff; it moves no observable.

E. Initial-Boundary Value Problems

For laboratory experiments and numerical simulations in finite volumes, we require well-posedness of the initial-boundary value problem (IBVP). This is the natural setting for terrestrial tests of DFD.

1. Dynamic Structural Assumptions

The dynamic field equation can be written in the general quasilinear form:

$$a^{\mu\nu}(\psi, \partial\psi)\partial_\mu\partial_\nu\psi + b^\mu(\psi, \partial\psi, x)\partial_\mu\psi + c(\psi, \partial\psi, x) = S(x), \tag{44}$$

where $a^{\mu\nu}$ forms the principal symbol and b^μ, c are lower-order terms. Well-posedness requires:

(A1′) Uniform hyperbolicity: There exists $\lambda \ge 1$ such that, for all spatial covectors $\mathbf{n} \in \mathbb{R}^3$,

$$\lambda^{-1}|\mathbf{n}|^2 \le a^{ij} n_i n_j \le \lambda|\mathbf{n}|^2, \tag{45}$$

where for the DFD equation (37) $a^{00} = -c^{-2}$, $a^{0i} = 0$ and $a^{ij} = M_{ij}(\nabla\psi)$ is the flux Jacobian of §III D.

(A2′) Lower-order regularity: For $|\alpha| \le s$ (with $s > 5/2$), the derivatives $\partial^\alpha b^\mu$, $\partial^\alpha c$ are continuous and polynomially bounded in $|\psi|$, $|\partial\psi|$.

(A3′) Source regularity: $S(x) \in H^{s-1}$ on the spatial domain.

These are satisfied by the DFD strong-field equation with the regularised approximant μ_{s_0} whenever ψ and $\partial\psi$ remain bounded; for the unregularised μ, (A1′) fails at $\nabla\psi = 0$ (§III C).

2. IBVP Formulation

Let $\Omega \subset \mathbb{R}^3$ be bounded with smooth boundary $\partial\Omega$. The Dirichlet IBVP is:

$$\begin{cases} a^{\mu\nu}(\psi, \partial\psi)\partial_\mu\partial_\nu\psi + \text{l.o.t.} = S(x), & (t, \mathbf{x}) \in [0, T] \times \Omega \\ \psi(0, \mathbf{x}) = \psi_0(\mathbf{x}), & \mathbf{x} \in \Omega \\ \partial_t\psi(0, \mathbf{x}) = \psi_1(\mathbf{x}), & \mathbf{x} \in \Omega \\ \psi(t, \mathbf{x}) = g(t, \mathbf{x}), & (t, \mathbf{x}) \in [0, T] \times \partial\Omega \end{cases} \tag{46}$$

3. Compatibility Conditions

Regularity requires the initial and boundary data to be compatible at $\{t = 0\} \cap \partial\Omega$:

- **Zeroth order:** $\psi_0|_{\partial\Omega} = g(\cdot, 0)$
- **First order:** $\psi_1|_{\partial\Omega} = \partial_t g(\cdot, 0)$
- **k-th order:** $\partial_t^k\psi|_{t=0,\partial\Omega} = \partial_t^k g(\cdot, 0)$

For solutions in $H^s(\Omega)$ with $s > 5/2$, compatibility is required up to order $\lfloor s - 1 \rfloor$.

4. Energy Estimates

Define the Sobolev energy:

$$E_s(t) = \sum_{|\alpha| \le s} \int_\Omega \left(|\partial^\alpha\partial_t\psi|^2 + |\nabla\partial^\alpha\psi|^2\right) d^3x. \tag{47}$$

Under assumptions (A1′)–(A3′) with compatibility conditions:

$$\frac{d}{dt}E_s(t) \le C(M)\left(E_s(t) + \|S\|^2_{H^{s-1}(\Omega)} + \|g\|^2_{H^{s-1/2}(\partial\Omega)}\right), \tag{48}$$

where $C(M)$ depends on bounds for ψ, $\partial\psi$ in L^∞.

By Gronwall's lemma:

$$\boxed{E_s(t) \le e^{C(M)t}\left(E_s(0) + \int_0^t \left(\|S\|^2_{H^{s-1}} + \|g\|^2_{H^{s-1/2}}\right) d\tau\right)} \tag{49}$$

This establishes continuous dependence on initial and boundary data.

5. Main IBVP Theorem

Theorem III.10 (IBVP Well-Posedness). *Let $\Omega \subset \mathbb{R}^3$ be bounded with smooth boundary and $s > 5/2$. Under assumptions (A1′)–(A3′), given:*

- *Initial data $(\psi_0, \psi_1) \in H^s(\Omega) \times H^{s-1}(\Omega)$*
- *Source $S \in H^{s-1}(\Omega)$*
- *Boundary data $g \in H^s([0,T] \times \partial\Omega)$*
- *Compatibility conditions up to order $\lfloor s - 1 \rfloor$*

there exists $T > 0$ and a unique solution

$$\psi \in C^0([0,T]; H^s(\Omega)) \cap C^1([0,T]; H^{s-1}(\Omega)) \tag{50}$$

depending continuously on (ψ_0, ψ_1, S, g) in the natural Sobolev norms.

a. Proof sketch. The proof uses standard techniques for quasilinear hyperbolic IBVP. Linearization around an approximate solution, energy estimates with boundary multipliers, and Picard iteration in a suitable Banach space yield existence and uniqueness. The compatibility conditions control boundary terms in the energy estimates.

6. Finite Speed of Propagation

Theorem III.11 (Finite Speed). *Let ψ and $\tilde{\psi}$ be solutions of (37) with initial data coinciding in a ball $B_R(\mathbf{x}_0)$. There exists a characteristic speed $c_{\text{char}} > 0$ (depending only on the hyperbolicity constant λ) such that*

$$\psi(t, \mathbf{x}) = \tilde{\psi}(t, \mathbf{x}) \quad \text{for } |\mathbf{x} - \mathbf{x}_0| \le R - c_{\text{char}} t. \tag{51}$$

This ensures causality: disturbances propagate at finite speed. For the regularised approximant, to which (A1′)–(A3′) apply, that speed is bounded by c (Theorem III.6); for the exact law it exceeds c in the transition regime, and every characteristic advances the absolute time t (Proposition III.7).

7. Parabolic Extension

For dissipative problems or numerical relaxation schemes, the parabolic extension is relevant:

$$\partial_t \psi - \nabla \cdot [\mu(|\nabla\psi|)\nabla\psi] = f(t, \mathbf{x}). \tag{52}$$

Theorem III.12 (Parabolic Well-Posedness). *Under assumptions (A1)–(A4), there exists a unique evolution*

$$\psi \in L^p(0,T; W^{1,p}(\Omega)) \cap C([0,T]; L^2(\Omega)). \tag{53}$$

If f is time-independent and boundary operators are dissipative, solutions converge to a steady state as $t \to \infty$.

This follows from Crandall–Liggett theory: the monotone operator $A\psi = -\nabla \cdot \mathbf{a}(\nabla\psi)$ generates a contraction semigroup on $L^2(\Omega)$.

8. Stability Estimates

Theorem III.13 (Continuous Dependence). *Let ψ_1, ψ_2 be solutions with data (f_1, BC_1), (f_2, BC_2) respectively. If $\mathbf{a}$ is strongly monotone and locally Lipschitz:*

$$\|\nabla(\psi_1 - \psi_2)\|_{L^p(\Omega)} \le C\big(\|f_1 - f_2\|_{V'} + \|BC_1 - BC_2\|_{\partial\Omega}\big). \tag{54}$$

This ensures physical stability: small changes in sources or boundary conditions produce small changes in solutions.

9. Numerical Implementation

The weak form (34) is directly implementable in finite element packages. The Newton iteration Jacobian is:

$$A_{ij}(\nabla\psi) = \mu(|\nabla\psi|)\delta_{ij} + \mu'(|\nabla\psi|)\frac{\partial_i\psi\,\partial_j\psi}{|\nabla\psi|}. \tag{55}$$

a. Regularization. At $|\nabla\psi| \to 0$, the Jacobian may become ill-conditioned. A practical remedy is to replace $|\nabla\psi|$ by $\sqrt{|\nabla\psi|^2 + s_0^2}$ with small $s_0 > 0$.

F. Open Mathematical Problems

Several mathematical questions remain open:

1. **Global existence for dynamic equations:** Smooth solutions do not persist in general: on a non-zero uniform background gradient they lose regularity in finite time (the gradient-singularity item below). Whether weak solutions exist for all time and are unique is open, as it is for the equations of gas dynamics in more than one dimension, where admissible weak solutions are known not to be unique (Chiodaroli, De Lellis and Kreml 2015). In planar symmetry entropy solutions exist for data whose invariant region avoids $\nabla\psi = 0$ (DiPerna 1983). No prediction of this monograph uses a global weak solution.

2. **Horizon boundary conditions:** With the parent strain's σ kept a black hole has general relativity's event horizon (Sec. VI B), where the one-way horizon condition of §III B applies; its uniqueness, regularity and numerical convergence are open.

3. **Gradient blow-up and singularity formation:** Partly settled. On a non-zero uniform background gradient $\mathbf{g} \neq 0$ the smooth evolution of the vacuum equation has a finite lifespan. In planar symmetry every non-trivial small compactly supported perturbation reaches a gradient catastrophe at a finite time $T_\star$, at which $\nabla\psi$ stays bounded and continuous while $\partial^2\psi \to \infty$ (Lax 1964; John 1974). In three dimensions the Klainerman null condition fails for every $\mathbf{g} \neq 0$, and an open set of nearly radial small

data forms the same singularity at $T_\varepsilon \sim e^{C(\mathbf{g})/\varepsilon}$, a statement conditional on the sketched extension of Speck (2016) to principal parts that depend on $\partial\psi$. For the exact law the planar statement holds on every background as well, with one refinement: the quadratic nonlinearity along $\mathbf{g}$ vanishes on the single background $|\mathbf{g}|/a_\star = 7.18$ (SOURCE; 2 for TOTAL), where the longitudinal speed peaks, and there plane waves along $\mathbf{g}$ break on the longer time $T_\star \propto \varepsilon^{-2}$ (Klainerman and Majda 1980). The null condition fails at every $\mathbf{g} \neq 0$ for all three responses, because $\mu' > 0$ everywhere. What remains open is nonlinear evolution through points where $\nabla\psi = 0$, where the principal part degenerates, the continuation past $T_\star$ and the singularity structure; the linearised evolution there is well-posed (Theorem III.9).

4. **Coupling to quantum fields:** The semi-classical regime (quantum matter on classical ψ background) is well-defined. Full quantization of ψ is unnecessary: the action scales as $S_\psi \sim (M_P/a_\star)^2 \gg \hbar$, ensuring quantum fluctuations are negligible. The gauge emergence framework provides the connection to particle physics (§XVII).

These technical open problems do not affect the physical predictions in §IV–§XIII, which operate in well-understood weak-field or linearized regimes.

G. Summary of Section III

The DFD field equations are mathematically well-posed:

TABLE VI. Well-posedness summary. The Dyn. and IBVP entries hold for the exact law and its approximant on data with $\nabla\psi$ bounded away from zero (Theorem III.5), and for the regularised approximant μ_{s_0} without that restriction (§III C); the light-cone bound $c_{\rm char} \le c$ of the Causality row holds for the unregularised approximant $\mu(x) = x/(1+x)$ as well (Theorem III.6). For the exact law $c_{\rm char}$ exceeds c in the transition regime, and causality rests on the absolute time t (Proposition III.7).

Property	Static	Dyn.	IBVP
Existence	✓	✓(loc.)	✓(loc.)
Uniqueness	✓(str. mon.)	✓(loc.)	✓(compat.)
Regularity	$C^{1,\alpha}_{\rm loc}$	H^s pres.	H^s pres.
Stability	✓(convex W)	✓	✓(Gron.)
Causality	—	$c_{\rm char} \le c$	$c_{\rm char} \le c$
No ghosts (below the cutoff)	✓	✓	✓

The mathematical foundations are solid: existence and uniqueness theorems, regularity results, stability guarantees, causal propagation, and explicit energy estimates. The IBVP formulation enables rigorous treatment of laboratory-scale experiments in bounded domains. This places DFD on equal footing with GR for the static and relaxation problems treated here.

IV. PARAMETRIZED POST-NEWTONIAN ANALYSIS

Having established DFD's mathematical structure in Part I, we now demonstrate that the theory reproduces General Relativity in all precision tests of gravity conducted within the Solar System. This section presents a complete Parametrized Post-Newtonian (PPN) analysis, showing that DFD's ten PPN parameters are identical to those of GR. The critical result—$\gamma = \beta = 1$ with all preferred-frame and conservation-violation parameters vanishing—ensures compatibility with the most stringent experimental constraints on gravitational physics.

A. The PPN Framework

The PPN formalism provides a systematic method for comparing metric theories of gravity in the weak-field, slow-motion regime characteristic of the Solar System [5, 6]. Any theory predicting a metric $g_{\mu\nu}$ can be expanded in powers of the Newtonian potential $U/c^2 \sim \epsilon^2$ and velocity $v/c \sim \epsilon$, with coefficients parametrized by dimensionless constants.

a. Newtonian potential and matter variables. For a perfect fluid with density ρ, pressure p, specific internal energy Π, and velocity $\mathbf{v}$, define the Newtonian potential

$$U(\mathbf{x}) = G\int \frac{\rho(\mathbf{x}')}{|\mathbf{x}-\mathbf{x}'|}\,d^3x'. \tag{56}$$

Additional potentials capture velocity-dependent effects:

$$V_i = G\int \frac{\rho v_i}{R}\,d^3x', \qquad W_i = G\int \frac{\rho(\mathbf{v}\cdot\mathbf{R})R_i}{R^3}\,d^3x', \tag{57}$$

$$\Phi_1 = G\int \frac{\rho v^2}{R}\,d^3x', \quad \Phi_2 = G\int \frac{\rho U(\mathbf{x}')}{R}\,d^3x', \tag{58}$$

$$\Phi_3 = G\int \frac{\rho\Pi}{R}\,d^3x', \quad \Phi_4 = G\int \frac{p}{R}\,d^3x', \tag{59}$$

where $\mathbf{R} = \mathbf{x} - \mathbf{x}'$ and $R = |\mathbf{R}|$.

b. The PPN metric template. The general PPN metric in isotropic coordinates takes the form [6]:

$$g_{00} = -1 + \frac{2U}{c^2} - 2\beta\frac{U^2}{c^4} + \frac{1}{c^4}\Big[-2\xi\Phi_W + \big(2\gamma+2+\alpha_3+\zeta_1-2\xi\big)\Phi_1 \tag{60}$$

$$+ 2\big(3\gamma-2\beta+1+\zeta_2+\xi\big)\Phi_2 + 2\big(1+\zeta_3\big)\Phi_3 + 2\big(3\gamma+3\zeta_4-2\xi\big)\Phi_4 - \big(\zeta_1-2\xi\big)\mathcal{A}\Big] + \mathcal{O}(c^{-6}), \tag{61}$$

where $\mathcal{A} = G\int\rho\,[\mathbf{v}\cdot\mathbf{R}]^2/R^3\,d^3x'$ is the standard anisotropic kinetic potential, and the template is written in the mean rest frame of the universe (the preferred-frame w^i-dependent terms are omitted). At the GR values $\gamma = \beta = 1$, $\xi = \alpha_3 = \zeta_{1,2,3,4} = 0$ the bracket reduces

to $4\Phi_1 + 4\Phi_2 + 2\Phi_3 + 6\Phi_4$.

$$g_{0i} = -\frac{1}{2c^3}\Big(4\gamma + 3 + \alpha_1 - \alpha_2 + \zeta_1 - 2\xi\Big)V_i \tag{62}$$

$$-\frac{1}{2c^3}\Big(1 + \alpha_2 - \zeta_1 + 2\xi\Big)W_i, \tag{63}$$

$$g_{ij} = \left(1 + 2\gamma\frac{U}{c^2}\right)\delta_{ij}. \tag{64}$$

The ten PPN parameters $\{\gamma, \beta, \xi, \alpha_1, \alpha_2, \alpha_3, \zeta_1, \zeta_2, \zeta_3, \zeta_4\}$ have the following physical interpretations:

- **Curvature/nonlinearity** (γ, β, ξ): γ measures the amount of spatial curvature produced by unit rest mass; β measures nonlinearity in the superposition of gravitational potentials; ξ is the Whitehead parameter for anisotropic stress contributions.
- **Preferred-frame effects** (α_1, α_2, α_3): These parametrize preferred-frame effects that would arise if gravity selects a cosmologically preferred rest frame.
- **Conservation laws** (ζ_1, ζ_2, ζ_3, ζ_4): These parametrize violations of total momentum and energy conservation.

General Relativity predicts $\gamma = \beta = 1$ and all other parameters zero. Table VII summarizes current experimental constraints.

B. DFD Physical Metric in PPN Form

In the nondispersive regime, DFD's dynamics are governed by the physical metric (12) (Sec. II B):

$$g_{00} = -e^{-\psi}, \qquad g_{ij} = e^{+\psi}\delta_{ij}, \tag{65}$$

where the scalar field ψ satisfies the field equation (21). In the weak-field limit relevant to Solar System tests, $\psi \ll 1$ and $\mu(|\nabla\psi|/a_\star) \to 1$, with $1 - \mu = e^{-\sqrt{a_N/a_0}}$ exactly on the derived exponential response (SOURCE branch; App. BS, Cor. BS.14; the weak-response approximant $x/(1+x)$ of Sec. VII does not apply here), so the field equation reduces to the Poisson equation:

$$\nabla^2\psi = -\frac{8\pi G}{c^2}\rho \quad \Rightarrow \quad \psi = +\frac{2U}{c^2} + \mathcal{O}(c^{-4}). \tag{66}$$

The crucial observation is that the exponential physical metric (65) determines the PPN parameters through Taylor expansion.

C. Parameter Extraction: $\gamma = \beta = 1$

a. Spatial metric and γ. Expanding $g_{ij} = e^{+\psi}\delta_{ij}$ to first order in ψ:

$$\begin{aligned} g_{ij} = e^{+\psi}\delta_{ij} &= \left(1 + \psi + \frac{\psi^2}{2} + \cdots\right)\delta_{ij} \\ &= \left(1 + \frac{2U}{c^2}\right)\delta_{ij} + \mathcal{O}(c^{-4}). \end{aligned} \tag{67}$$

Comparing with the PPN template (64), which has coefficient $2\gamma U/c^2$, immediately yields

$$\boxed{\gamma = 1}. \tag{68}$$

b. Temporal metric and β. Expanding $g_{00} = -e^{-\psi}$ to second order:

$$\begin{aligned} g_{00} = -e^{-\psi} &= -\left(1 - \psi + \frac{\psi^2}{2} + \cdots\right) \\ &= -1 + \psi - \frac{\psi^2}{2} + \mathcal{O}(c^{-6}) \\ &= -1 + \frac{2U}{c^2} - \frac{2U^2}{c^4} + \mathcal{O}(c^{-6}). \end{aligned} \tag{69}$$

The coefficient of $-U^2/c^4$ in the PPN template (61) is 2β. Since DFD gives exactly $-2U^2/c^4$, we have

$$\boxed{\beta = 1}. \tag{70}$$

c. 1PN completion: the Φ-sector coefficients derived, and $\xi = 0$. The c^{-4} sector of g_{00} is not matched to GR term by term; it is *derived* from DFD's own field equation with the standard perfect-fluid closure. Varying the matter action with respect to ψ (the same variation that yields the Tolman source law $\mathcal{S} = \frac{1}{2}(\varepsilon + 3p)\,e^{\psi}$) and expanding through 1PN order gives

$$\mathcal{S} = \frac{\rho c^2}{2}\left[1 + \frac{\Pi}{c^2} + \frac{2v^2}{c^2} + \frac{2U}{c^2} + \frac{3p}{\rho c^2}\right] + \mathcal{O}(c^{-4}), \tag{71}$$

verified by computer algebra; the $2U/c^2$ term arises solely from $\sqrt{-\tilde{g}} = e^{\psi}$. Writing $\psi = 2U/c^2 + \psi_2/c^4$ and solving with the flat Green function term by term against $\nabla^2\Phi_k = -4\pi G$ (densities),

$$\psi_2 = 4\Phi_1 + 4\Phi_2 + 2\Phi_3 + 6\Phi_4 - \partial_t^2\chi, \tag{72}$$

where $\chi = -G\int \rho\, R\, d^3x'$ is the PPN superpotential of Eq. (79) below.

Gauge Lock. The single time redefinition $\xi^0 = \partial_t\chi/2c^3$ produces $\delta g_{00} = +\partial_t^2\chi/c^4$ and $\delta g_{0i} = +\frac{1}{2}\,\partial_i\partial_t\chi/c^3$: one coordinate change simultaneously removes the $-\partial_t^2\chi$ term here *and* the longitudinal gradient discarded in the vector-sector split of Eq. (80). One parameter, two cancellations—the scalar and vector sectors are gauge-consistent, and the metric lands in the standard PPN gauge. Expanding $g_{00} = -e^{-\psi}$ then yields the coefficient set

$$s_1 = 4,\ s_2 = 4,\ s_3 = 2,\ s_4 = 6,\ s_W = 0,\ s_{\mathcal{A}} = 0 \tag{73}$$

for $(\Phi_1, \Phi_2, \Phi_3, \Phi_4, \Phi_W, \mathcal{A})$ in the template (61). The match delivers $\beta = 1$ a second, independent time: ψ_2 contains $4\Phi_2$ but no U^2 piece, so $-2U^2$ comes solely

TABLE VII. Current experimental bounds on PPN parameters. GR predicts $\gamma = \beta = 1$ and all others zero.

Parameter	GR Value	Experimental Bound	Primary Constraint
$\gamma - 1$	0	$(2.1 \pm 2.3) \times 10^{-5}$	Cassini [35]
$\beta - 1$	0	$\lvert\beta - 1\rvert < 3 \times 10^{-4}$	LLR [36]
ξ	0	$\lvert\xi\rvert < 10^{-3}$	Geophysical
α_1	0	$\lvert\alpha_1\rvert < 4 \times 10^{-5}$	Binary pulsars [37]
α_2	0	$\lvert\alpha_2\rvert < 2 \times 10^{-9}$	Millisecond pulsars [5]
α_3	0	$\lvert\alpha_3\rvert < 4 \times 10^{-20}$	Pulsar spin-down [6]
ζ_1	0	$\lvert\zeta_1\rvert < 2 \times 10^{-2}$	Combined tests
ζ_2	0	$\lvert\zeta_2\rvert < 4 \times 10^{-5}$	Lunar/planetary
ζ_3	0	$\lvert\zeta_3\rvert < 10^{-8}$	Lunar acceleration
ζ_4	0	—	Not directly tested

from $e^{-\psi} = 1 - \psi + \psi^2/2 - \cdots$. With $\gamma = 1$ and the conservation results of §IV F, the Φ_1 coefficient also fixes $\alpha_3 = 0$ directly.

Whitehead Locality ($\xi = 0$ structurally). DFD's kinetic operator is exactly linear (flat); the field equation's only nonlinearity is the *local, multiplicative* e^{ψ} in the source. A local source convolved with the flat Green function can never generate the *non-local* Whitehead double integral Φ_W. Hence

$$s_W = 0 \;\Rightarrow\; \boxed{\xi = 0} \tag{74}$$

to all 1PN orders by construction—a structural statement, not an order-by-order accident.

Kinetic Lock (internal falsifier). Had the spatial kinetic operator carried a factor $e^{b\psi}$ instead of being flat, the $(\nabla\psi)^2$ cross term would shift β at $\mathcal{O}(b)$; the LLR bound $|\beta-1| < 3\times10^{-4}$ enforces the flat master-equation branch. The 1PN sector thus ties the action's kinetic structure directly to lunar ranging.

Remark (elliptic reading). On the elliptic constraint reading of the scalar sector (Axiom E, Appendix WS), the instantaneous solve produces ψ_2 with no $\partial_t^2\chi$ term at all, and the metric lands on the standard PPN gauge directly, with no gauge transformation (Standard-Gauge Coincidence Lemma). Both routes give the identical 1PN metric; the derivation above is unconditional, while the elliptic route is conditional on Axiom E as named there. The elliptic solve's slicing is the zero-mean-curvature (maximal) slicing at leading order, and with the parent strain's σ kept it is maximal for isolated systems (Appendix WS, Proposition WS.6).

d. Physical interpretation. The result $\gamma = \beta = 1$ is not a coincidence but a direct consequence of the exponential structure $n = e^{\psi}$. The optical refractive index n determines both the light propagation speed (c/n) and the gravitational time dilation ($d\tau = dt/\sqrt{n}$, the lapse of the physical metric (12)). The exponential ensures that these effects are related by exact exponentiation rather than independent parametrizations, automatically reproducing the GR relation between spatial curvature and time dilation.

D. Vector Sector: $\alpha_1 = \alpha_2 = \alpha_3 = 0$

To complete the PPN analysis, we must determine the gravitomagnetic sector g_{0i}. Introduce a shift vector N_i such that, through first post-Newtonian order,

$$ds^2 = -e^{-\psi}c^2dt^2 + e^{+\psi}\delta_{ij}(dx^i + N^i dt)(dx^j + N^j dt). \tag{75}$$

The term $e^{+\psi}N^2$ that this form adds to g_{00} is of second post-Newtonian order. Beyond first order this line element and the form of Appendix WS, condition (b) extended beyond first order, with $g_{00} = -e^{-\psi}$ and the shift in g_{0i} alone, differ only in how the shift enters g_{00}; with the Einstein–Hilbert couplings evaluated order by order they give the same second-order binding energy, so any difference enters at third order at the earliest (computed). Working to 1PN order, the weak-field equation for the shift is the Poisson problem

$$\nabla^2 N_i = \frac{16\pi G}{c^3}\,\rho v_i, \tag{76}$$

sourced by the *full* matter momentum current ρv_i (since $\nabla^2 V_i = -4\pi G\rho v_i$, this sign convention yields $N_i < 0$ for prograde currents, matching the template (63)). The residual longitudinal coordinate freedom $N_i \to N_i + \partial_i\lambda$ is fixed below by the superpotential split, consistently with the Gauge Lock of §IV C.

a. Solution. The solution of Eq. (76) vanishing at infinity is the pure-V gravitomagnetic potential

$$N_i = -\frac{4}{c^3}V_i, \tag{77}$$

the standard GR result (coefficient -4; recall that V_i as defined in §IV A already contains G).

Transverse projection. The solution (77) does not solve the transverse-projected equation $\nabla^2 N_i = -16\pi G\, j_i^{\perp}$, $j_i^{\perp} = (\delta_{ij} - \partial_i\partial_j\nabla^{-2})(\rho v_j)$. Pairing the two is inconsistent (projection, overall sign and normalization): the transverse part of V_i is $V_i^{\perp} = \frac{1}{2}(V_i + W_i)$—from the continuity identity $\partial_i V_i = -\partial_t U$ together with $\nabla^2\partial_t\chi = -2\,\partial_t U$ and the identity (79)—so the transverse-gauge solution is

$$N_i^{\perp} = -\frac{2}{c^3}\big(V_i + W_i\big), \tag{78}$$

not the pure-V form. The two solutions differ only by

the longitudinal gradient $-(2/c^3)\,\partial_i\partial_t\chi$—precisely the coordinate freedom exploited in the split below—so the far-zone coefficient (-4) and every physical quantity are unchanged; the pairing of Eq. (76) with its solution (77) is consistent.

Provenance (derived, at a conditional grade). At this order Eq. (76) coincides with the linearized-GR momentum constraint. Within DFD its derivation is supplied by the Vector-Sector Completion theorem (Appendix WS), which obtains $g_{0i} = -\big(\frac{7}{2}V_i + \frac{1}{2}W_i\big)/c^3$ directly in the physically fixed DFD gauge, *conditional on two named inputs*: (I) the elliptic constraint reading of the scalar sector (Axiom E) and (II) the spectral Einstein–Hilbert zero-mode reduction—the same input the TT sector already carries. At that conditional grade—and only at that grade—the coefficient -4, the Lense–Thirring precession (§IV H 5), and the leading spin terms of Appendix AX become consequences rather than template matches (beyond linear order the Einstein–Hilbert coupling adds the general-relativistic $O(JM)$ terms, App. AX); input (II) is Proposition WS.5, the spectral Einstein–Hilbert reduction, and the vector sector's derivation carries its premises, G1 and G2, explicitly; G1 follows from the Einstein–Hilbert static-energy identity with one G (Proposition WS.6) and the Rest-Mass Channel. To compare with the PPN template, which is written in the canonical V_i/W_i gauge, we use the superpotential identity. Define the PPN superpotential $\chi(\mathbf{x}) = -G\int \rho\, R\, d^3x'$, which obeys $\nabla^2\chi = -2U$. Differentiating with the mass-continuity relation $\partial_t\rho = -\partial_j(\rho v_j)$ and integrating by parts gives the standard Will (1993) identity

$$\partial_i(\partial_t\chi) = V_i - W_i \quad\Longleftrightarrow\quad V_i = W_i + \partial_i(\partial_t\chi)\,. \tag{79}$$

Writing $-4V_i = -\frac{7}{2}V_i - \frac{1}{2}V_i$ and replacing the single residual $-\frac{1}{2}V_i$ via the identity (79), $V_i = W_i + \partial_i(\partial_t\chi)$, splits the pure-$V$ form into the standard V/W representation,

$$N_i = -\frac{4}{c^3}V_i = \frac{1}{c^3}\left(-\frac{7}{2}V_i - \frac{1}{2}W_i\right) - \frac{1}{2c^3}\,\partial_i(\partial_t\chi)\,, \tag{80}$$

where the final gradient term is pure gauge: it is cancelled exactly by the same time redefinition $\xi^0 = \partial_t\chi/2c^3$ that removes the $-\partial_t^2\chi$ term from g_{00} (the Gauge Lock of §IV C—one parameter, two cancellations), and it drops out of all physical quantities. Since $e^{+\psi} = 1 + \mathcal{O}(c^{-2})$ multiplies an $\mathcal{O}(c^{-3})$ quantity, $g_{0i} = e^{+\psi}N_i$ retains these coefficients to the order computed:

$$g_{0i}^{\rm DFD} = \frac{1}{c^3}\left(-\frac{7}{2}V_i - \frac{1}{2}W_i\right). \tag{81}$$

The far-zone sum is preserved: $-7/2 - 1/2 = -4$, matching the coefficient of Eq. (77) (where $W_i \to V_i$ in the far zone), so the gauge rewrite changes the V/W *split* but not the physical gravitomagnetic field.

b. Extraction of preferred-frame parameters. Matching Eq. (81) to the PPN template (63) (with $\gamma = 1$, $\xi = 0$) supplies only the two coefficient equations $\alpha_1 - \alpha_2 + \zeta_1 = 0$ (from the V_i term) and $\alpha_2 - \zeta_1 = 0$ (from W_i), i.e. $\alpha_1 = 0$ and $\alpha_2 = \zeta_1$; the parameter α_3 does not enter g_{0i} at this order and so cannot be read off from this match alone. The remaining vanishings follow from covariant conservation (§IV F, Eq. (89): $\zeta_1 = \zeta_2 = \zeta_3 = \zeta_4 = 0$) together with the absence of a dynamical preferred-frame field (below), which also removes the semi-conservative parameter α_3. With $\zeta_1 = 0$ the g_{0i} match then forces $\alpha_2 = 0$, so that

$$\boxed{\alpha_1 = \alpha_2 = \alpha_3 = \zeta_1 = 0}\,. \tag{82}$$

Physically, DFD's preferred foliation induces no preferred-frame effects above the bounded residual of Thm. IV.1: no dynamical preferred-frame *vector* field couples to the field equation—the sole gravitational degree of freedom is the scalar ψ (sourced by a flat Poisson equation), and at this order g_{0i} is generated by the matter momentum current ρv_i, as in GR, up to the suppressed temporal-completion current of Eq. (86). The parameters $\alpha_{1,2,3}$ therefore have no dynamical preferred-frame field to couple to.

c. Far-zone consistency check. For a rigid rotator with angular momentum $\mathbf{J}$, the far-zone behavior has $W_i \simeq V_i$, so $g_{0i} \simeq (d_V + d_W)V_i/c^3$. With $\alpha_{1,2} = \xi = \zeta_1 = 0$ and $\gamma = 1$, the PPN template demands $g_{0i} = -4V_i/c^3$, requiring $d_V + d_W = -4$. Equation (81) satisfies this identically: $-7/2 - 1/2 = -4$. This confirms the Lense-Thirring gravitomagnetic field has the correct GR form.

E. Preferred-Frame Invisibility: Why the Foliation Decouples at 1PN

DFD has a genuine preferred foliation: absolute time t defines a cosmological rest frame, identified physically with the CMB frame (§II, Appendix Q). A preferred frame is exactly the structure that, in Lorentz-violating gravity theories, produces nonzero $\alpha_1, \alpha_2, \alpha_3$. Binary-pulsar and millisecond-pulsar observations bound these to $|\alpha_1| < 4\times10^{-5}$, $|\alpha_2| < 2\times10^{-9}$ [5, 37], consistent with zero. We must therefore prove that DFD's preferred frame is *observationally invisible* at 1PN. The vector-sector match of §IV D already gives $\alpha_1 = 0$ and $\alpha_2 = \zeta_1$ from g_{0i} alone; what remains is to show that the one place the preferred frame could enter the *local* dynamics—the temporal-completion invariant $\Delta = (c/a_0)\,|u^\mu\nabla_\mu\psi - u^\mu\nabla_\mu\psi_0|$ of Eq. (Q4), built from the preferred-frame flow u^μ—cannot inject an unsuppressed preferred-frame term into the 1PN metric. Axiom WS.1 confines the temporal completion to homogeneous deviations, which removes this term from local systems altogether; the argument below bounds it without using that scope.

Theorem IV.1 (Preferred-frame invisibility at 1PN)**.** *In the nondispersive (solar-system) regime, DFD's full scalar sector—the spatial AQUAL term plus the temporal completion Eq. (11), whose temporal invariant Δ is built from the preferred-frame flow u^μ—produces a 1PN metric with*

$$\boxed{\alpha_1 = \alpha_2 = \alpha_3 = 0} \tag{83}$$

up to the boost-induced residual of Eq. (86), bounded by

Eq. (85). *The preferred foliation is observationally invisible at first post-Newtonian order.*

Proof. The static ($\gamma = \beta = 1$, $\xi = 0$) sector is established in §IV C; the gravitomagnetic match Eq. (81) fixes $\alpha_1 = 0$ and $\alpha_2 = \zeta_1$ (§IV D); covariant conservation gives $\zeta_1 = 0$ (§IV F), hence $\alpha_2 = 0$. It remains to show that the preferred-frame flow u^μ, which enters only through Δ, contributes no unsuppressed preferred-frame PPN term to g_{00} or g_{0i}, and that $\alpha_3 = 0$. We give two independent suppression arguments for the temporal completion; either one bounds the residual.

In the temporal completion, u^μ enters through the contracted scalar $\Delta = (c/a_0)|u^\mu \nabla_\mu \psi - u^\mu \nabla_\mu \psi_0|$, and in a boosted frame this term does carry a shift current, the $\mathcal{O}(w)$ current of Eq. (86) below, together with a boost-induced g_{00} contribution at $\mathcal{O}(w^2)$; both carry the suppressed coefficient $\alpha_{\rm eff}$ of Eq. (85), bounded by arguments (ii)–(iii) below to lie far under every experimental threshold.

(i) Scalar, not vector, coupling (heuristic placement in the LLN classification). The Lee–Lightman–Ni theorem [5, 6] states that a Lagrangian-based metric theory whose static 1PN metric coincides with GR ($\gamma = \beta = 1$, $\xi = 0$) has $\alpha_1 = \alpha_2 = \alpha_3 = 0$ *only when* it contains no prior-geometric absolute element and no dynamically propagating preferred-frame vector/tensor. This is a heuristic guide, not an automatic proof for DFD: DFD carries a *prior-geometric absolute vector* u^μ (the non-varied CMB-frame foliation), which places it in LLN's preferred-frame-*capable* class (Rosen/Ni/aether-type theories), and the AQUAL nonlinearity $\mu(\Delta)$ lies outside LLN's smoothness hypotheses. Hence the α_i *must be controlled directly*, as done in (ii)–(iii). What the classification *does* supply is the reason DFD lands harmlessly: because u^μ is non-dynamical and enters only through the fully-contracted scalar Δ, it carries no independent radiative or constraint degree of freedom—unlike a propagating aether vector, which would source g_{0i} directly. The residual preferred-frame coupling is therefore confined to the temporal-completion channel and bounded by (ii)–(iii).

(ii) Wrong post-Newtonian order. The preferred-frame metric terms have the canonical form $g_{0i}^{\rm PF} \sim \alpha_1 (w_i/c)(U/c^2)$ and $g_{00}^{\rm PF} \sim (\alpha_1 - \alpha_2)(w^2/c^2)(U/c^2)$, where w^i is the system velocity relative to the preferred frame. The temporal term enters the ψ field equation as $-c^{-2}\partial_t[\,\mu(\Delta)\,K' \cdots]$. When the sources are at rest in the preferred frame, $\dot\psi = 0$ identically and the temporal term vanishes; it switches on only at $\mathcal{O}(w)$, through $\dot\psi \sim w^i \partial_i \psi$. Its contribution to g_{0i}, relative to the GR gravitomagnetic term $(4G/c^3)\rho v$, is suppressed by the dimensionless ratio

$$r_{\rm temp} = \frac{a_*^2\,\Delta}{|\nabla\psi|^2} = \frac{4\,a_0\,w}{c^3\,|\nabla\psi|}, \tag{84}$$

using $a_* = 2a_0/c^2$. Dividing out the explicit boost w/c gives the induced effective coefficient

$$\alpha_{\rm eff} \;\lesssim\; \frac{4a_0}{c^2|\nabla\psi|} = \frac{2a_0}{|\mathbf{a}_{\rm N}|}, \tag{85}$$

since $|\mathbf{a}_{\rm N}| = \frac{1}{2}c^2|\nabla\psi|$ is the Newtonian acceleration. This is the same MOND ratio that governs every DFD departure from Newtonian gravity: in any high-acceleration system ($|\mathbf{a}_{\rm N}| \gg a_0$) it is driven to zero.

a. Explicit variation. The result above is confirmed by varying the temporal Lagrangian directly with respect to the shift N_i that carries $g_{0i} = e^{+\psi}N_i$. Writing $\mathcal{L}_{\rm temp} = K(\Delta)$ with $\Delta = (c/a_0)|\dot\psi - \dot\psi_0|$ and $\dot\psi = u^\mu\nabla_\mu\psi \to N^i\partial_i\psi + \mathcal{O}(w)$ in the boosted frame, a single chain-rule variation gives

$$\frac{\delta\mathcal{L}_{\rm temp}}{\delta N_i} = \mu'(\Delta)\,\frac{c}{a_0}\left(w^j\partial_j\psi\right)\partial^i\psi \;+\; \mathcal{O}(w^2), \tag{86}$$

with an explicit $\mathcal{O}(1)$ coefficient ($\mu(\Delta) = K'(\Delta)$). The induced shift current is therefore $\mu'(\Delta)(c/a_0)\,w\,|\nabla\psi|$-suppressed, and dividing out the boost w/c reproduces exactly the prefactor of Eq. (85), $\alpha_{\rm eff} \le 2a_0/|\mathbf{a}_{\rm N}|$, now carrying the additional saturation factor $\mu'(\Delta)$ of argument (iii).

(iii) Saturation freezes the response. A genuine preferred-frame *force* requires the constitutive function to *respond* to the boost, i.e. a factor $\mu'(\Delta)$. The regime selector here is the acceleration ratio $a_{\rm N}/a_0$, *not* Δ itself: in every PPN-testing system $a_{\rm N} \gg a_0$, which drives $\Delta = (a_{\rm N}/a_0)(2w/c)$ large and freezes the response. At 1 AU, $a_{\rm N}/a_0 \sim 5\times10^7$, so with $2w/c \sim 2.5\times10^{-3}$ one has $\Delta \sim 1.2\times10^5$, hence $\mu(\Delta)\to 1$ and $\mu'(\Delta) = 1/(1+\Delta)^2 \sim 6.6\times10^{-11} \ll 1$. The temporal current is then a spatially uniform cosmological background ($\mu = 1$), whose gradient and curl—the only quantities that can source a metric perturbation—vanish. Hence the temporal-completion coefficient is suppressed below Eq. (85) by the additional factor $\mu'(\Delta) = 1/(1+\Delta)^2 \ll 1$ in the solar system.

Arguments (ii)–(iii) independently bound the temporal-completion residual of Eq. (86) to lie far below experimental thresholds. The semiconservative parameter α_3 requires *both* a preferred frame *and* momentum nonconservation; the latter is excluded by covariant conservation (§IV F, $\zeta_i = 0$), and the former is decoupled by (ii)–(iii), so $\alpha_3 = 0$. □

Corollary IV.2 (Conservative bound, assumption-light)**.** *Even if the saturation argument (iii) is set aside and only the post-Newtonian power-counting (ii) is retained, the worst-case effective preferred-frame parameter obeys*

$$\alpha_{\rm eff}(\textit{system}) \;\lesssim\; \frac{2a_0}{|\mathbf{a}_{\rm N}|}. \tag{87}$$

Evaluated where the published bounds are actually set, this gives $\alpha_{\rm eff} \lesssim 4.0\times10^{-8}$ *in the solar system (*$|\mathbf{a}_{\rm N}| \sim 6\times10^{-3}\,{\rm m\,s^{-2}}$*) and* $\alpha_{\rm eff} \sim 3\times10^{-12}$ *in binary pulsars (*$|\mathbf{a}_{\rm N}| \sim 80\,{\rm m\,s^{-2}}$*, the orbital relative acceleration of systems such as PSR J1738+0333 and the Hulse–Taylor binary), to be set against* $|\alpha_1| < 4\times10^{-5}$ *and* $|\alpha_2| < 2\times10^{-9}$ *[5, 37]. In this maximally conservative reading the solar-system value sits* ≈ 1000 *below the* α_1 *bound; the* α_2 *bound is set by millisecond-pulsar spin precession, at pulsar accelerations, where the binary-pulsar value sits* ≈ 700 *below it.*

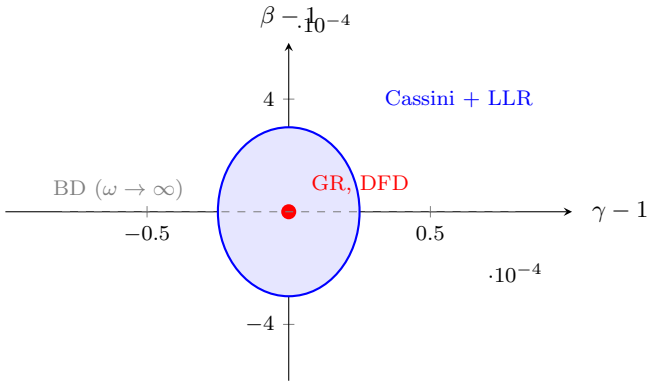


FIG. 5. PPN parameter space in the $(\gamma-1, \beta-1)$ plane. The shaded ellipse sketches the Cassini and LLR bounds, centred on GR. DFD (red point) sits exactly at the GR location $(0, 0)$.

F. Conservation Laws: $\zeta_1 = \zeta_2 = \zeta_3 = \zeta_4 = 0$

In any metric theory with minimal matter coupling to a single metric, covariant conservation of the total stress-energy tensor follows from the matter action's invariance under coordinate changes:[1]

$$\tilde{\nabla}_\mu T^{\mu\nu} = 0. \tag{88}$$

DFD in its nondispersive band is precisely such a theory: the dynamics is entirely encoded in the physical metric (65) with standard minimal coupling to matter (Sec. II B). Consequently, the PPN parameters that would signal violations of momentum or energy conservation must vanish:

$$\boxed{\zeta_1 = \zeta_2 = \zeta_3 = \zeta_4 = 0}. \tag{89}$$

Combined with Eqs. (68), (70), and (82), this completes the ten-parameter PPN map for DFD.

G. Summary: DFD Equals GR at 1PN

Table VIII presents the complete PPN benchmark comparing DFD, GR, and experimental constraints.

Key Result: PPN Equivalence

DFD reproduces GR at 1PN order. All ten PPN parameters match GR predictions (the preferred-frame set to within the bounded residual of Thm. IV.1):

$$\begin{aligned} &\gamma = \beta = 1, \\ &\xi = \alpha_1 = \alpha_2 = \alpha_3 = \zeta_1 = \zeta_2 = \zeta_3 = \zeta_4 = 0. \end{aligned} \tag{90}$$

This ensures compatibility with all Solar System tests at their current precision.

[1] DFD's preferred foliation does not spoil this: the conservation law $\tilde{\nabla}_\mu T^{\mu\nu} = 0$ depends only on the matter sector's coupling to $\tilde{g}_{\mu\nu}$, not on whether the gravitational sector is generally covariant.

The PPN parameter space can be visualized by considering the $(\gamma-1, \beta-1)$ plane (Fig. 5). DFD sits exactly at the GR point $(0, 0)$, well within the experimental ellipse defined by Cassini and Lunar Laser Ranging constraints.

a. Second order. Outside a static source, with the scalar-longitudinal piece σ of the parent strain kept (§V A 3), the exterior is the Schwarzschild metric in DFD's coordinates, lapse $e^{-\psi/2}$ and $\det g_{ij} = e^{3\psi}$ (App. WS): with $U = GM/(c^2 r)$, $\psi = 2U - \frac{4}{3}U^3 + \dots$ and $g_{ij} = e^{\psi}[\delta_{ij} + U^2(\delta_{ij} - 3n_i n_j) + \dots]$, so $-g_{00} = 1 - 2U + 2U^2 + O(U^4)$ and the spatial metric is anisotropic at second order. The second-order observables are general relativity's: the deflection coefficient $15\pi/4$, no Shapiro-delay excess, the periastron ratio $\Omega_\phi/\Omega_r = 1 + 3x + \frac{27}{2}x^2$ with $x = (GM\Omega_\phi/c^3)^{2/3}$, and the circular-orbit energy $E/\mu c^2 - 1 = -\frac{x}{2}\left[1 - \frac{3}{4}x - \frac{27}{8}x^2\right]$ (computed). With σ set to zero the exterior would be the isotropic exponential metric studied by Boonserm, Ngampitipan, Simpson and Visser (2018), with $\epsilon = 4/3$ in $g_{ij} = (1 + 2\gamma U + \frac{3}{2}\epsilon U^2)\delta_{ij}$ and the deflection coefficient 4π; under the Einstein–Hilbert term that metric needs a negative-energy scalar (App. AA). No experiment has yet measured a second-order coefficient; sub-microarcsecond astrometry at the solar limb would test it.

H. Classic Solar System Tests

With $\gamma = \beta = 1$, DFD makes identical predictions to GR for all classic tests of gravity. We verify each explicitly.

1. Light Deflection

Light rays follow null geodesics of the optical metric. For a spherically symmetric source with $n(r) = e^{\psi(r)}$ and $\psi(r) = 2GM/(c^2 r)$, the conserved impact parameter is $b = n(r) \cdot r \sin\theta$. The total deflection angle for a ray with closest approach $r_0 \gg r_g = 2GM/c^2$ is [5]:

$$\delta\theta = \frac{(1+\gamma)}{2} \cdot \frac{4GM}{c^2 b} = \frac{4GM}{c^2 b}, \tag{91}$$

where the second equality uses $\gamma = 1$.

a. Numerical verification. At the Sun's limb ($b = R_\odot = 6.96 \times 10^8$ m, $M = M_\odot = 1.99 \times 10^{30}$ kg):

$$\begin{aligned} \delta\theta &= \frac{4 \times 6.67 \times 10^{-11} \times 1.99 \times 10^{30}}{(3 \times 10^8)^2 \times 6.96 \times 10^8} \\ &= 8.5 \times 10^{-6}\,\text{rad} = 1.75''. \end{aligned} \tag{92}$$

This matches the GR prediction precisely, consistent with VLBI observations at the 10^{-4} level [38].

2. Shapiro Time Delay

The coordinate time for a photon traveling from point $\mathbf{r}_1$ to $\mathbf{r}_2$ near a mass M is increased by the gravitational

TABLE VIII. Complete 1PN PPN benchmark for DFD: exact equality with GR across all ten parameters.

Parameter	GR	DFD	Experimental Bound	Consistent?
γ	1	1	$1 \pm 2.3 \times 10^{-5}$	✓
β	1	1	$1 \pm 3 \times 10^{-4}$	✓
ξ	0	0	$< 10^{-3}$	✓
α_1	0	0	$< 4 \times 10^{-5}$	✓
α_2	0	0	$< 2 \times 10^{-9}$	✓
α_3	0	0	$< 4 \times 10^{-20}$	✓
ζ_1	0	0	$< 2 \times 10^{-2}$	✓
ζ_2	0	0	$< 4 \times 10^{-5}$	✓
ζ_3	0	0	$< 10^{-8}$	✓
ζ_4	0	0	—	✓

time delay [39]:

$$\Delta t = \frac{(1+\gamma)GM}{c^3} \ln\left(\frac{(r_1 + \mathbf{r}_1 \cdot \hat{n})(r_2 - \mathbf{r}_2 \cdot \hat{n})}{d^2}\right), \quad (93)$$

where d is the impact parameter and $\hat{n}$ is the unit vector along the unperturbed ray. With $\gamma = 1$, this becomes:

$$\Delta t = \frac{2GM}{c^3} \ln\left(\frac{4r_1 r_2}{d^2}\right). \quad (94)$$

a. Cassini constraint. The Cassini spacecraft measured the Shapiro delay during solar conjunction with unprecedented precision, yielding [35]:

$$\gamma - 1 = (2.1 \pm 2.3) \times 10^{-5}. \quad (95)$$

DFD's prediction $\gamma = 1$ lies comfortably within this bound, representing a consistency test at the 10^{-5} level.

3. Perihelion Precession

The PPN prediction for orbital perihelion advance per revolution is [5]:

$$\Delta\omega = \frac{6\pi GM}{c^2 a(1-e^2)} \cdot \frac{2 + 2\gamma - \beta}{3}. \quad (96)$$

With $\gamma = \beta = 1$, the prefactor becomes $(2+2-1)/3 = 1$:

$$\Delta\omega = \frac{6\pi GM}{c^2 a(1-e^2)}. \quad (97)$$

a. Mercury. For Mercury ($a = 5.79 \times 10^{10}$ m, $e = 0.2056$):

$$\Delta\omega = \frac{6\pi \times 6.67 \times 10^{-11} \times 1.99 \times 10^{30}}{(3 \times 10^8)^2 \times 5.79 \times 10^{10} \times (1 - 0.2056^2)} = 5.02 \times 10^{-7}\,\text{rad/orbit}. \quad (98)$$

Over 100 years (415 orbits), this accumulates to $42.98''$/century, matching the observed anomalous precession after accounting for planetary perturbations [5].

4. Gravitational Redshift

The gravitational redshift of a photon climbing from potential Φ_1 to Φ_2 is:

$$\frac{\Delta\nu}{\nu} = \frac{\Phi_1 - \Phi_2}{c^2} = \frac{GM}{c^2}\left(\frac{1}{r_2} - \frac{1}{r_1}\right). \quad (99)$$

In DFD, this follows directly from $\nu \propto e^{-\psi/2} \approx 1 + \Phi/c^2$ (Sec. II B).

a. Experimental verification.

- **Pound-Rebka (1960):** Measured redshift over 22.5 m in Earth's gravitational field, confirming Eq. (99) at $\sim 10\%$ precision.
- **Gravity Probe A (1976):** Hydrogen maser comparison over 10,000 km altitude yielded agreement at 7×10^{-5} [40].
- **ACES (on the ISS since April 2025):** The Atomic Clock Ensemble in Space aims for 2×10^{-6} precision.

DFD predicts the standard gravitational redshift, consistent with all observations.

5. Frame Dragging and Lense-Thirring Effect

The gravitomagnetic field generated by a rotating mass with angular momentum $\mathbf{J}$ causes precession of test gyroscope spin and orbital plane precession of satellites. The Lense-Thirring precession rate is [41]:

$$\dot{\Omega}_{\text{LT}} = \frac{2GJ}{c^2 a^3 (1-e^2)^{3/2}}. \quad (100)$$

DFD reproduces this effect exactly because the gravitomagnetic sector g_{0i} (81) has the correct GR form. Experimental confirmations include:

- **LAGEOS satellites:** Measured $\dot{\Omega}_{\text{LT}}$ due to Earth's rotation at $\sim 10\%$ precision [42].
- **Gravity Probe B (2011):** Directly measured frame-dragging of orbiting gyroscopes, confirming GR at 19% precision [43].

I. Where DFD Differs from GR

The exact PPN match means that *Solar System tests cannot distinguish DFD from GR*. This is a structural consequence: DFD's μ-function reduces to $\mu \to 1$ in the high-acceleration Solar System regime, and the weak-field expansion of $n = e^{\psi}$ automatically produces the correct PPN parameters from DFD's own field equations—GR is not assumed at any step.

The discriminating tests for DFD lie in two regimes:

1. **Galactic scales** (Sec. VII): Where $|\mathbf{a}|/a_0 \sim 1$, the μ-crossover produces MOND-like phenomenology absent in GR.

2. **Laboratory clock tests** (Sec. XI): The DFD clock sector is channel-resolved: the simplified $K_A \approx k_\alpha S_A^\alpha$ scaling captures only the pure-α leading term, while the full structure includes strong-sector and composition-dependent contributions of the extended non-metric channel (null under the minimal action, Thm. XI.2), testable with co-located atomic and nuclear clocks. Matter-wave interferometry is a null check rather than a discriminator: DFD and GR coincide through 1PN (§XIII).

Summary: Solar System Compliance

DFD passes all Solar System tests of gravity:

- Light deflection: $\delta\theta = 4GM/(c^2 b)$ (matches GR)
- Shapiro delay: Cassini bound satisfied ($|\gamma - 1| < 2.3 \times 10^{-5}$)
- Perihelion precession: $\Delta\omega = 6\pi GM/(c^2 a(1-e^2))$ (Mercury: 42.98"/cy)
- Gravitational redshift: Standard formula confirmed to 10^{-4}
- Frame dragging: Lense-Thirring precession matches LAGEOS/GP-B

The theory's distinguishing predictions emerge in galactic dynamics and laboratory clock tests.

V. GRAVITATIONAL WAVES

Gravitational wave astronomy provides stringent tests of gravity in the strong-field, dynamical regime. The direct detection of binary black hole and neutron star mergers by LIGO, Virgo, and KAGRA has opened a new window for testing alternative theories. This section demonstrates that DFD reproduces GR's gravitational wave predictions at leading order, satisfying all current observational constraints while providing a framework for quantifying potential deviations through the parameterized post-Einsteinian (ppE) formalism.

A. Two Gravitational Sectors on Flat $\mathbb{R}^3$

Before presenting the technical details, we establish the conceptual framework for gravitational radiation in DFD. This framework preserves DFD's core identity—flat Euclidean space $\mathbb{R}^3$ with absolute time t—while accounting for the observed tensor polarization structure of gravitational waves.

1. *The Optical Sector (DFD Core)*

DFD posits a scalar field $\psi(\mathbf{x}, t)$ on flat $\mathbb{R}^3$ with absolute time t. The optical sector defines a refractive index $n = e^{\psi}$ and an effective optical interval:

$$d\tilde{s}^2 = -\frac{c^2}{n^2} dt^2 + d\mathbf{x}^2. \tag{101}$$

We introduce $d\tilde{s}^2$ as a compact encoding of how ψ rescales light propagation; *it is not a dynamical spacetime geometry and no curvature field equations are assumed for it.* The fundamental arena remains $(\mathbb{R}^3, t)$; the physical metric (12), to which matter couples, obeys the Einstein–Hilbert dynamics of App. WS.

Local observers in regions with different ψ compare clock rates by $d\tau = e^{-\psi/2}\, dt = dt/\sqrt{n}$, the lapse of the physical metric (12) to which matter couples (Thm. XI.2), while light follows the null cone of (101), coordinate speed c/n. In DFD, $n = e^{\psi}$ sets both; it does not introduce an asymptotic subluminal EM signal speed relative to the shared far-zone cone. Observable light-bending and gravitational time delay are encoded via an effective travel-time functional (Fermat principle) built from the null cone of (101); this is used as a bookkeeping device for clock-rate comparisons and Fermat/eikonal propagation, not as a dynamical metric with curvature equations.

2. *The Radiative Sector (Tidal Disturbances)*

Compact-binary mergers exhibit gravitational radiation with **two tensor polarizations**. A scalar field ψ alone cannot reproduce this polarization structure. DFD's spectral completion on $\mathbb{C}P^2 \times S^3$ derives both sectors from a single parent object:

- **Optical gravity** (ψ): scalar field governing clock rates, refractive bending, and quasi-static matter dynamics
- **Radiative gravity** (h_{ij}^{TT}): transverse-traceless tensor field describing propagating tidal disturbances

The TT field is defined on $\mathbb{R}^3$ by the standard conditions:

$$\partial_i h_{ij}^{\mathrm{TT}} = 0, \qquad \delta^{ij} h_{ij}^{\mathrm{TT}} = 0, \tag{102}$$

and obeys a wave equation on the flat background:

$$\left(\frac{1}{c^2}\partial_t^2 - \nabla^2\right) h_{ij}^{\mathrm{TT}} = \frac{16\pi G}{c^4} \Pi_{ij}^{\mathrm{TT}}, \tag{103}$$

where $\Pi_{ij}^{\rm TT}$ is the TT projection of the source stress.

This is not an appeal to curved spacetime: both ψ and $h_{ij}^{\rm TT}$ are fields on the same flat $(\mathbb{R}^3, t)$ arena, derived as irreducible components of the same zero-mode parent tensor on $K = \mathbb{C}P^2 \times S^3$, whose vector and scalar-longitudinal pieces are constrained, non-radiative fields of the same arena (§V A 3).

The radiative sector does not alter the optical-sector derivations of lensing, clocks, or MOND phenomenology.

Within the full $\mathbb{C}P^2 \times S^3$ spectral completion of DFD, the TT sector is *derived* as the spin-2 irreducible component of the same zero-mode parent tensor whose trace yields ψ. Both sectors emerge from a single parent metric perturbation $h_{\mu\nu}$ on the internal manifold $K = \mathbb{C}P^2 \times S^3$, expanded in harmonics and restricted to the zero mode ($m_0^2 = 0$). The $3+1$ decomposition of $h_{\mu\nu}$ under $O(3)$ gives the trace ψ (1 DOF) and the TT tensor $h_{ij}^{\rm TT}$ (2 DOF) as its irreducible components, with constrained vector and scalar-longitudinal pieces (no radiative DOF). A Lichnerowicz analysis on K proves no unwanted massless tensor or vector modes arise from internal deformations (see §V A 4 below). The absence of derivative mixing between trace and TT sectors is a structural consequence of $O(3)$ rotational symmetry on flat $\mathbb{R}^3$, not an ad hoc postulate.

3. Parent Strain Field and Irreducible Decomposition

Define a symmetric strain field on flat $\mathbb{R}^3$:

$$\Psi_{ij} = \frac{1}{3}\psi\,\delta_{ij} + h_{ij}^{\rm TT} + \partial_{(i}V_{j)} + \left(\partial_i\partial_j - \frac{1}{3}\delta_{ij}\nabla^2\right)\sigma, \tag{104}$$

where $\psi = \delta^{ij}\Psi_{ij}$ is the trace (scalar), $h_{ij}^{\rm TT}$ is the transverse-traceless piece (tensor), V_i is a transverse vector, and σ is a scalar-longitudinal auxiliary. The **trace** ψ governs optical and quasi-static gravity and the **TT** piece $h_{ij}^{\rm TT}$ governs gravitational radiation; the vector and scalar-longitudinal pieces are constrained non-radiative auxiliaries, whose dynamics is the part of the Einstein–Hilbert term (App. WS) that the trace and TT actions do not contain, which fixes $S_{\rm aux}$ in Eq. (106). The vector piece is removed by the spatial diffeomorphisms that preserve the arena's volume form; σ is not set to zero but solved from the traceless part of the Einstein equation. The physical metric has lapse $e^{-\psi/2}$ and spatial part $g_{ij} = e^{\psi}(e^h)_{ij}$, with $h_{ij} \equiv \Psi_{ij} - \frac{1}{3}\psi\,\delta_{ij}$ the traceless part. The scalar-longitudinal piece σ does not enter at first post-Newtonian order; beyond it, keeping it makes DFD's rest-mass gravity general relativity's in DFD's slicing (Proposition WS.6).

a. No-mixing theorem. For any isotropic quadratic principal symbol built from Ψ_{ij}, the trace and TT pieces are orthogonal. Any isotropic cross-term between trace and TT reduces to one of the forbidden contractions:

$$\delta_{ij}\,h_{ij}^{\rm TT} = 0, \qquad \partial_i\,h_{ij}^{\rm TT} = 0. \tag{105}$$

So terms like $\partial_k\psi\,\partial_k h_{ii}^{\rm TT}$ and $\partial_i\psi\,\partial_j h_{ij}^{\rm TT}$ vanish identically. The principal symbol is therefore **automatically block-diagonal** between trace and TT sectors:

$$S_{\rm grav} = \frac{c^4}{64\pi G}\int dt\,d^3x\left[\frac{(\partial_t h_{ij}^{\rm TT})^2}{c^2} - (\nabla h_{ij}^{\rm TT})^2\right] + S_{\rm tr}[\psi] + S_{\rm aux}. \tag{106}$$

By irreducible decomposition of an isotropic parent strain field, the principal symbol is automatically block-diagonal between trace and TT sectors—the absence of derivative mixing is a structural consequence, not a separate assumption. The two helicity-zero pieces, ψ and σ, are not separated by this argument: the Einstein–Hilbert term couples them, and $S_{\rm aux}$ carries that coupling.

4. Spectral-Geometry Origin of the Two-Sector Structure

The two-sector structure ($\psi + h_{ij}^{\rm TT}$) is a consistent completion, and within the $\mathbb{C}P^2 \times S^3$ spectral action framework, it is *derived* [1]. The spectral action $S_B = \mathrm{Tr}\,f(D^2/\Lambda^2)$ on $\mathbb{R}^{3,1} \times K$ produces a 4D Einstein–Hilbert action from the a_2 Seeley–DeWitt coefficient. A metric perturbation $H_{\mu\nu}(x, Y)$ on the total space, expanded in scalar harmonics on K, has a massless zero mode $h_{\mu\nu}(x)$ (constant on K). Its $3+1$ decomposition yields ψ (trace) and $h_{ij}^{\rm TT}$ (spin-2) as siblings in the same multiplet.

A Lichnerowicz analysis on K verifies the mode count is clean:

- $\mathbb{C}P^2$ is Einstein-rigid: no TT zero modes (Koiso 1980; spectral gap $\lambda_{\min} = 8/R_1^2$).
- S^3 is Einstein-rigid: no TT zero modes (spectral gap $\lambda_{\min} = 12/R_2^2$; Higuchi 1987).
- $b_1(\mathbb{C}P^2) = b_1(S^3) = 0$: no harmonic 1-forms on either factor, eliminating mixed zero modes.
- On a continuous K one scalar zero mode survives, the squashing modulus controlling R_1/R_2; on the truncated microsector there is none.

a. The Einstein product condition. The internal geometry enters the spectral action through the volume and the curvature of K. The α constraint does not fix the shape ratio $\tau \equiv R_2/R_1$: the $\mathbb{C}P^2$ factor of α's trace does not depend on its radius, since $\int_{\mathbb{C}P^2} F\wedge F = 8\pi^2 q^2$ is topological (§X C), and in a joint reading $1/G$ (from a_2) and $1/\alpha$ (from a_4) both scale with $\mathrm{Vol}(K)$. The shape enters through the internal-curvature part of a_2, $\int_K R_K\,d\mathrm{vol} = \pi^{8/7}\mathrm{Vol}(K)^{5/7}\,\Phi(\tau)$ with $\Phi(\tau) = 24\tau^{6/7} + 6\tau^{-8/7}$, which belongs to the four-dimensional vacuum term. At fixed volume it is stationary at $\tau_* = 1/\sqrt{3}$, the Einstein product condition $6/R_1^2 = 2/R_2^2$, with $\Phi''/\Phi = 2.94$, a curvature ratio rather than a mass; this is a minimum of the potential for the connection Laplacian that fixes α (§X B) and a maximum for an internal Dirac operator, and the overall volume is not fixed at this order. On the truncated microsector, which the closed form for α and the

α[57] derivation use, the internal space is finite and carries no size or shape modulus.

b. Constitutive interpretation. With the traceless pieces included, the generalized optical metric becomes $d\tilde{s}^2 = -c^2dt^2/n^2 + (e^h)_{ij}\,dx^i dx^j$, with h_{ij} the traceless part of Ψ_{ij} ($\delta_{ij} + h^{\rm TT}_{ij}$ at linear order in the radiative sector). The Tamm–Plebanski construction gives tensor constitutive relations $\varepsilon^{ij}_{\rm eff} = \varepsilon_0\, n\,(\delta^{ij} - h^{ij,{\rm TT}})$. The vacuum medium has compression stiffness $K_0 = c^4/(8\pi G)$ and shear stiffness $K_0/4$: gravity as electromagnetic vacuum loading [31].

5. Why $c_T = c$ (Structural Requirement)

Radiative Sector: $O(3)$ Irrep Block-Diagonality

The TT principal part is the flat wave operator, with no $(\partial\psi)(\partial h^{\rm TT})$ mixing. This is not a free choice: it follows from the irreducible decomposition of the parent strain field Ψ_{ij} under the isotropic $O(3)$ symmetry of flat $\mathbb{R}^3$. *(Any derivative mixing would require breaking the isotropy of the principal symbol, which is excluded by the flat-space construction.)*

The action for the radiative sector takes the form:

$$S_{\rm TT} = \frac{c^4}{64\pi G}\int dt\, d^3x \left[\frac{(\partial_t h^{\rm TT}_{ij})^2}{c^2} - (\nabla h^{\rm TT}_{ij})^2\right] + S_{\rm int}, \tag{107}$$

where $S_{\rm int}[\psi, h^{\rm TT}, \rho]$ contains no terms that modify the principal part of $S_{\rm TT}$: gravitational waves and light share one metric (App. WS). (This normalization yields $\Box h^{\rm TT}_{ij} = 16\pi G\,\Pi^{\rm TT}_{ij}/c^4$, with $\Pi^{\rm TT}_{ij} \equiv (T^{\rm eff}_{ij})^{\rm TT}$.)

Under this condition, the characteristic cone of $h^{\rm TT}_{ij}$ is the optical cone, flat on the background:

$$c_T = c_\gamma \quad \text{(one metric for light and gravitational waves).} \tag{108}$$

Since both EM and GW share the same far-zone causal cone ($c_T = c_\gamma$) and we impose no derivative mixing that would alter the tensor principal part, any additional ψ-dependent timing effects enter identically (or negligibly) in the eikonal limit for both channels. The observed $\lesssim$seconds coincidence over ~ 40 Mpc (GW170817) therefore constrains only differential coupling, which this completion sets to zero.

Any alternative completion that introduces $(\partial\psi)(\partial h^{\rm TT})$ mixing or additional radiative degrees of freedom generically predicts $c_T \neq c_\gamma$ and is immediately constrained by multimessenger observations.

Remark V.1 (Scope of the no-mixing inference). The irrep argument forbids the *bilinear* mixing $(\partial\psi)(\partial h^{\rm TT})$; it does not forbid ψ-dependent coefficients of the TT bilinear itself, $A(\psi)(\partial_t h^{\rm TT}_{ij})^2/c^2 - B(\psi)(\nabla h^{\rm TT}_{ij})^2$, which are $O(3)$ scalars. What fixes them is the requirement that the TT sector obey the same local relativity as matter at constant ψ_0: the map $t = e^{+\psi_0/2}T$, $\mathbf{x} = e^{-\psi_0/2}\mathbf{X}$ of Thm. XI.2 pulls the physical metric (12) back to Minkowski, and the TT operator is the flat wave operator in $(T, \mathbf{X})$ if and only if $A/B = e^{2\psi}$. The coordinate tensor cone is then $c\,e^{-\psi}$, the optical cone of Eq. (101), and Eq. (106) is its $\psi_0 = 0$ reference-gauge form. The common normalisation $F(\psi)$ ($A = Fe^{2\psi}$, $B = F$; $F = 1$ under the constant-G assumption) is open. The same coefficient carries a rotationally invariant cubic vertex $\psi\,(\partial_t h^{\rm TT}_{ij})^2$ that the bilinear no-mixing statement does not exclude (App. AT, Rem. AT.10).

a. Corollary (standard-siren null). On the optical-cone reading of the TT sector (App. WS) photons and TT waves share the eikonal equation $\tilde{g}^{\mu\nu}k_\mu k_\nu = 0$ of the physical metric (12), hence the same coordinate travel time $(1/c)\int e^{\psi}\,ds$ along the same Fermat path: the same Shapiro delay, the same lensing rays and $\Delta t_{\text{GW-EM}} = 0$; on a homogeneous background both amplitudes obey the same eikonal transport on the same cone, the same $1/(a\,r)$ decay with a the background scale factor, so $D_L^{\rm GW} = D_L^{\rm EM}$ — a standard-siren null, with any difference confined to the open normalisation $F(\psi)$ of Rem. V.1.

6. Adiabatic Limit and GW Speed in the Unified Picture

The parent strain field Ψ_{ij} of Eq. (104) naturally accommodates the trace and TT sectors as complementary irreducible pieces. If μ-type nonlinearity from the trace sector couples to the tensor sector, the far-zone propagation of $h^{\rm TT}_{ij}$ remains effectively luminal in the WKB/adiabatic regime, because μ varies only on a macroscopic scale L_μ set by the background (e.g. galactic/cluster potentials), while gravitational waves have wavenumber k satisfying $kL_\mu \gg 1$. A natural estimate for any correction to the tensor characteristic cone is

$$\epsilon \;\sim\; \frac{|\nabla \ln \mu|}{k} \;\sim\; \frac{1}{kL_\mu} \;=\; \frac{\lambda}{2\pi L_\mu}. \tag{109}$$

For LIGO/Virgo-band waves ($f \sim 10^2$–10^3 Hz, so $\lambda = c/f \sim 3\times10^5$–$3\times10^6$ m) and a conservative astrophysical variation scale $L_\mu \gtrsim$ 1–10 kpc ($\approx 3\times10^{19}$–3×10^{20} m), one finds

$$\epsilon \;\lesssim\; \frac{3\times10^6}{2\pi\,(3\times10^{19}\text{–}3\times10^{20})} \;\sim\; 10^{-14}\text{–}10^{-15}, \tag{110}$$

to be compared with the GW170817 bound $|c_T/c - 1| \lesssim 10^{-15}$ [17].

This adiabatic estimate applies to any completion in which slowly varying μ-dependent coefficients enter *outside* the principal part. DFD's completion is the block-diagonal completion of Eq. (106), for which $c_T = c$ exactly: gravitational waves and light share one metric (App. WS), so $c_T = c_\gamma$ on every background.

7. Falsifiability

If observations ever require:

- a TT–EM cone split, $c_T \neq c_\gamma$ on any background, or
- Scalar or vector polarization modes in far-zone GWs, or
- a confirmed gravitational-wave echo train (absent: the remnant has a Kerr horizon, argued beyond first order in the spin; App. WS),

then DFD's tensor sector is falsified.

B. The Minimal Transverse-Traceless Sector

Having established the conceptual framework, we now present the technical details. DFD's gravitational wave sector is constructed to respect GW170817's tight constraint on the GW propagation speed: $|c_T/c - 1| < 10^{-15}$ [17].

a. TT action. The radiative sector is a massless transverse-traceless tensor field propagating at speed c on the background. Its quadratic action, the leading part of the full a_2 Einstein–Hilbert term (whose cubic vertex carries the nonlinear memory, App. AT), is:

$$S_h = \frac{c^4}{64\pi G}\int dt\, d^3x \left[\frac{1}{c^2}(\partial_t h_{ij}^{\rm TT})^2 - (\nabla h_{ij}^{\rm TT})^2\right]. \quad (111)$$

This is identical to the linearized GR action for tensor perturbations on flat spacetime. The TT constraint eliminates the trace ($h^i{}_i = 0$) and longitudinal modes ($\partial_i h^{ij} = 0$), leaving exactly two polarization degrees of freedom:

$$h_{ij}^{\rm TT} = h_+ e_{ij}^+ + h_\times e_{ij}^\times, \quad (112)$$

where $e_{ij}^{+,\times}$ are the plus and cross polarization tensors for propagation along the z-axis:

$$e_{ij}^+ = \begin{pmatrix} 1 & 0 & 0 \\ 0 & -1 & 0 \\ 0 & 0 & 0 \end{pmatrix}, \qquad e_{ij}^\times = \begin{pmatrix} 0 & 1 & 0 \\ 1 & 0 & 0 \\ 0 & 0 & 0 \end{pmatrix}. \quad (113)$$

b. Key properties. The minimal TT sector construction guarantees:

1. $c_T = c_\gamma$ on every background: light and gravitational waves share one metric (App. WS), satisfying GW170817.
2. Only tensor $(+, \times)$ polarizations—no scalar or vector modes in the far zone.
3. Standard GR amplitude scaling with distance: $h \propto 1/r$.

The only departure from GR enters through the μ-crossover of the *conservative source dynamics*, where accelerations approach a_0; the propagation and emission of gravitational waves are GR's.

C. Verification: $c_T = c$ from No Derivative Mixing

The previous subsection established the DFD-native framework: $h_{ij}^{\rm TT}$ is a field on flat $(\mathbb{R}^3, t)$ with no derivative mixing with ψ in its principal part. Here we verify this structure and connect to standard scalar-tensor formalisms for readers familiar with that literature.

1. The Flat-Background Wave Equation

In DFD, the TT field satisfies the flat-space wave equation (Eq. 103):

$$\left(\frac{1}{c^2}\partial_t^2 - \nabla^2\right) h_{ij}^{\rm TT} = \frac{16\pi G}{c^4}\Pi_{ij}^{\rm TT}. \quad (114)$$

For a plane wave $h_{ij}^{\rm TT} \propto e^{i(\omega t - \mathbf{k}\cdot\mathbf{x})}$, the dispersion relation is:

$$\omega^2 = c^2 k^2 \qquad \Rightarrow \qquad c_T = c. \quad (115)$$

This result is *structural*: it follows from the $O(3)$ irrep block-diagonality of the parent strain field (Sec. V A 3), which forbids terms like $(\partial\psi)(\partial h^{\rm TT})$ in the kinetic sector. Scope: Rem. V.1. Any such mixing would require breaking the isotropy of the principal symbol.

2. Why No Derivative Mixing is Natural in DFD

In DFD's flat-arena formulation:

1. **Tensor-scalar decoupling:** The TT perturbation $h_{ij}^{\rm TT}$ is traceless and transverse, coupling only to the traceless part of the source. The scalar ψ governs time dilation and scalar gravitational effects, ensuring the two sectors do not mix at leading order.
2. **No scalar higher-derivative terms beyond the Weyl term:** Unlike general Horndeski theories, DFD contains no terms involving $(\Box\psi)^2$ or curvature-scalar couplings; its only four-derivative term beyond the Gauss–Bonnet total derivative, the a_4 Weyl-squared term of the spectral action (App. WS), has its spin-2 pole at $3.6\,\bar{M}_{\rm P}$ for $f_0 = 1$, above the cutoff, and moves no observable; on the scalar sector, evaluated on the matter metric, it adds only a spatial four-derivative term in $\delta\psi$, the helicity-0 part of that pole, smaller than the Planck-strength stiffness by $\frac{4}{3}(k/3.6\,\bar{M}_{\rm P})^2$ at wavenumber k. The absence of any other scalar higher-derivative term is equivalent to:

$$\alpha_T \equiv \frac{d\ln c_T^2}{d\ln a} = 0 \quad (116)$$

(identically: one metric for light and gravitational waves; App. WS).

D. Wave Equation and Source Coupling

The TT field couples to matter through the effective stress tensor derived from the optical metric:

$$S_{\rm int} = \frac{1}{2}\int dt\, d^3x\, h_{ij}^{\rm TT}\, T_{\rm eff}^{ij}[\psi;\rho,\mathbf{v}]. \tag{117}$$

Variation of $S_h + S_{\rm int}$ with respect to $h_{ij}^{\rm TT}$ yields the wave equation:

$$\Box h_{ij}^{\rm TT} \equiv \frac{1}{c^2}\partial_t^2 h_{ij}^{\rm TT} - \nabla^2 h_{ij}^{\rm TT} = \frac{16\pi G}{c^4}(T_{ij}^{\rm eff})^{\rm TT}, \tag{118}$$

where the superscript TT denotes projection onto the transverse-traceless part.

a. Effective stress tensor. The source $(T_{ij}^{\rm eff})^{\rm TT}$ depends on the matter distribution and its motion in the ψ-mediated potential. At leading (Newtonian) order:

$$T_{ij}^{\rm eff} = \rho v_i v_j + (\text{pressure and binding energy corrections}). \tag{119}$$

The ψ-dependence enters through the conservative dynamics: orbital parameters are determined by the effective potential $\Phi = -c^2\psi/2$.

E. Quadrupole Formula and Energy Flux

a. Far-zone solution. The standard retarded solution to Eq. (118) in the far zone ($r \gg \lambda_{\rm GW}$) is:

$$h_{ij}^{\rm TT}(t,\mathbf{x}) = \frac{2G}{c^4 r}\ddot{I}_{ij}^{\rm TT}(t_{\rm ret}), \tag{120}$$

where $t_{\rm ret} = t - r/c$ is the retarded time and I_{ij} is the mass quadrupole moment tensor:

$$I_{ij} = \int \rho(\mathbf{x},t)\left(x_i x_j - \frac{1}{3}\delta_{ij}r^2\right) d^3x. \tag{121}$$

b. Energy flux. The gravitational wave luminosity follows from the standard Isaacson stress-energy tensor averaged over several wavelengths:

$$\frac{dE}{dt} = -\frac{G}{5c^5}\left\langle \dddot{I}_{ij}\, \dddot{I}^{ij}\right\rangle [1+\delta_{\rm rad}], \tag{122}$$

where the angle brackets denote time averaging and $\delta_{\rm rad}$ parametrizes any small DFD-specific departure from the GR prediction. The factor $[1+\delta_{\rm rad}]$ captures potential radiative inefficiencies in the DFD framework.

c. DFD prediction. In the high-acceleration regime relevant to compact binary inspirals, $\mu \to 1$ and the conservative dynamics reduce to Newtonian gravity. Since the TT sector is derived from the same $\mathbb{C}P^2 \times S^3$ spectral geometry as the scalar sector (§V A 4), reproduces linearized GR as output, and the scalar sector is an instantaneous constraint that does not radiate (Axiom WS.1), we have:

$$\delta_{\rm rad} = 0 \quad \text{(leading order)}. \tag{123}$$

Corrections to $\delta_{\rm rad}$ enter only through μ-function effects in systems where $|\nabla\psi|/a_\star$ is not asymptotically large: where $\mu \to 1$ the source dynamics is GR's (App. WS).

F. Post-Newtonian and ppE Framework

The parameterized post-Einsteinian (ppE) framework provides a systematic way to constrain deviations from GR using gravitational wave observations [44]. DFD maps naturally onto this framework through its conservative and dissipative departure parameters.

1. Conservative and Dissipative Parametrization

Following [44], parametrize departures from GR in the binary orbital dynamics:

$$E(v) = E_{\rm GR}(v)\left[1 + \varepsilon_0 + \varepsilon_2 v^2 + \cdots\right], \tag{124}$$

$$\mathcal{F}(v) = \mathcal{F}_{\rm GR}(v)\left[1 + \varphi_3 v^3 + \cdots\right], \tag{125}$$

where $v = (\pi M f)^{1/3}$ is the characteristic orbital velocity, $M = m_1 + m_2$ is the total mass, and f is the gravitational wave frequency. Here $E(v)$ is the binding energy and $\mathcal{F}(v)$ is the gravitational wave flux.

a. Physical interpretation.

- ε_0: Leading (0PN) conservative correction to orbital energy.
- ε_2: 1PN conservative correction.
- φ_3: 1.5PN dissipative correction to energy flux.

2. Phase Coefficients

The inspiral waveform phase accumulation, computed via stationary phase approximation, takes the form:

$$\Psi(f) = \Psi_{\rm GR}(f) + \beta_{-5}u^{-5} + \beta_{-3}u^{-3} + \beta_{-2}u^{-2} + \cdots, \tag{126}$$

where $u = (\pi\mathcal{M}f)^{1/3}$ with chirp mass $\mathcal{M} = (m_1 m_2)^{3/5}/(m_1+m_2)^{1/5}$, and $\eta = m_1 m_2/M^2$ is the symmetric mass ratio.

The explicit dictionary relating $(\varepsilon_0, \varepsilon_2, \varphi_3)$ to the ppE phase coefficients is:

$$\beta_{-5} = -\frac{5}{128\eta}\varepsilon_0, \tag{127}$$

$$\beta_{-3} = \frac{3}{128\eta}C_1(\eta)\varepsilon_2, \tag{128}$$

$$\beta_{-2} = \frac{3}{128\eta}D_3(\eta)\varphi_3, \tag{129}$$

where $C_1(\eta) = 743/336 + 11\eta/4$ and $D_3(\eta) = -16\pi$ are standard GR coefficients.

a. DFD mapping. Equations (127)–(129) enable direct translation between DFD theory parameters and LVK catalog bounds without requiring bespoke waveform models.

G. Comparison with LIGO-Virgo-KAGRA Observations

1. DFD Predictions for Compact Binaries

DFD does not predict specific non-zero values for $(\varepsilon_0, \varepsilon_2, \varphi_3)$ in the compact binary regime. Rather, in systems where the μ-crossover is negligible, the leading-order dynamics reduce exactly to GR.

a. Conservative sector. For stellar-mass black hole binaries at LIGO frequencies, the characteristic acceleration is:

$$a_{\rm binary} \sim \frac{GM}{r^2} \sim 10^{10}\text{–}10^{11}\,\mathrm{m/s^2}, \tag{130}$$

while the μ-crossover scale is $a_0 \sim 10^{-10}$ m/s^2. The ratio:

$$\frac{a_0}{a_{\rm binary}} \sim 10^{-20}\text{–}10^{-21}. \tag{131}$$

In this regime, $a/a_0 \gg 1$, so $\mu(x) \to 1$ and DFD reduces to standard Newtonian/GR dynamics. Therefore:

$$\varepsilon_0 = \varepsilon_2 = 0 \quad \text{(at leading PN order)}. \tag{132}$$

b. Radiative sector. The quadrupole flux formula (122) with $\delta_{\rm rad} = 0$ matches GR exactly, implying:

$$\varphi_3 = 0 \quad \text{(at leading order)}. \tag{133}$$

c. GW propagation speed. Light and gravitational waves share one metric (App. WS), so $c_T = c_\gamma$ exactly, satisfying the GW170817 bound.

2. Comparison with LVK O3 Bounds

The GWTC-3 tests of GR [45] provide the most stringent constraints on ppE deformation parameters. Table IX compares DFD expectations with LVK bounds.

a. Notes on the table.

- The $\delta\hat{\varphi}_k$ are fractional deviations in PN phase coefficients; GR predicts 0 for all.
- LVK bounds are from combined GWTC-3 analysis using hierarchical inference.
- The graviton mass bound assumes a dispersive propagation correction.
- The GW speed bound from GW170817/GRB 170817A is the most stringent constraint on c_T.

Key Result: GW Consistency

Through second post-Newtonian order DFD's two-body dynamics is general relativity's, and gravitational waves travel at c (App. WS). The phase terms, the graviton-mass bound and the speed bound are consistent with current observations.

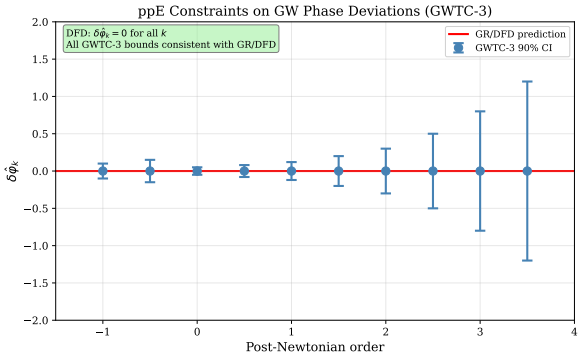


FIG. 6. Parameterized post-Einsteinian (ppE) constraints from GWTC-3 [45]. Points with error bars: schematic intervals (the GWTC-3 bounds are in Table IX) on fractional phase deviations $\delta\hat{\varphi}_k$ at each post-Newtonian order. Red line: GR prediction, which DFD shares (Table IX).

3. Falsifiability and Future Tests

The ppE mapping serves a forward-looking purpose: it enables future observations to be translated directly into DFD parameter constraints if deviations from GR are ever detected. Falsifiability requires either:

1. **Detection of ppE deviations:** Any non-zero $\beta_{-5,-3,-2}$ would constrain DFD parameters via Eqs. (127)–(129).
2. **μ-crossover regime observations:** If GW sources exist in the low-acceleration regime where $|\nabla\psi|/a_\star \sim 1$, DFD would predict detectable deviations. Such sources (e.g., extremely wide binaries or primordial backgrounds) are not currently accessible.

H. Binary Pulsar Verification

Binary pulsars provide precision tests of gravitational radiation in the weak-field but highly relativistic regime. The Hulse-Taylor binary (PSR B1913+16) remains the canonical verification of the quadrupole formula.

1. The Hulse-Taylor System

The observed parameters [46, 47] are:

The observed orbital decay, after correcting for the Shklovskii effect and Galactic acceleration, is:

$$\dot{P}_b^{\rm int} = (-2.398 \pm 0.005) \times 10^{-12}\,\mathrm{s/s}. \tag{134}$$

2. DFD Prediction

a. Why $\delta_{\rm rad} = 0$ for compact binaries. The μ-crossover is completely negligible for the Hulse-Taylor

TABLE IX. Comparison of DFD predictions with LVK O3 ppE bounds. DFD's deviations are zero and consistent: through second post-Newtonian order its two-body dynamics is GR's (App. WS).

Parameter	PN Order	DFD Prediction	LVK O3 Bound (90% CL)	Consistent?
$\delta\hat{\varphi}_{-2}$	-1PN	0	$[-7.3, 7.3] \times 10^{-4}$	✓
$\delta\hat{\varphi}_0$	0PN	0	$[-0.15, 0.15]$	✓
$\delta\hat{\varphi}_1$	0.5PN	0	$[-0.5, 0.5]$	✓
$\delta\hat{\varphi}_2$	1PN	0	$[-0.3, 0.3]$	✓
$\delta\hat{\varphi}_3$	1.5PN	0	$[-0.2, 0.2]$	✓
$\delta\hat{\varphi}_4$	2PN	0	$[-0.5, 0.5]$	✓
m_g	—	0	$\leq 1.27 \times 10^{-23}$ eV/c^2	✓
$\lvert c_T/c - 1\rvert$	—	0	$< 10^{-15}$	✓

Parameter	Symbol	Value
Pulsar mass	m_1	$1.4398 \pm 0.0002\, M_\odot$
Companion mass	m_2	$1.3886 \pm 0.0002\, M_\odot$
Total mass	M	$2.8284 \pm 0.0003\, M_\odot$
Orbital period	P_b	27906.98 s
Eccentricity	e	0.6171340
Semi-major axis	a	1.95×10^9 m
Periastron distance	r_p	7.5×10^8 m

system:

$$a_{\rm binary} \sim \frac{GM}{r_p^2} \sim \frac{(6.67\times10^{-11})(5.6\times10^{30})}{(7.5\times10^8)^2} \sim 670\,{\rm m/s^2}. \tag{135}$$

The ratio $a_0/a_{\rm binary} \sim 10^{-13}$, so crossover corrections are suppressed by $a_0/a_{\rm binary} \sim 10^{-13}$ or more.

b. Explicit prediction. The orbital period decay from quadrupole radiation is:

$$\dot{P}_b = -\frac{192\pi}{5}\left(\frac{2\pi G\mathcal{M}}{c^3 P_b}\right)^{5/3} \frac{1+\frac{73}{24}e^2+\frac{37}{96}e^4}{(1-e^2)^{7/2}}[1+\delta_{\rm rad}], \tag{136}$$

where $\mathcal{M} = (m_1 m_2)^{3/5}/M^{1/5}$ is the chirp mass.

With $\delta_{\rm rad} = 0$:

$$\dot{P}_b^{\rm DFD} = \dot{P}_b^{\rm GR} = (-2.402531 \pm 0.000014) \times 10^{-12}\,{\rm s/s}. \tag{137}$$

3. Quantitative Comparison

TABLE X. Hulse-Taylor binary orbital decay comparison.

Quantity	Value
$\dot{P}_b^{\rm GR}$ (quadrupole formula)	$(-2.402531 \pm 0.000014) \times 10^{-12}$ s/s
$\dot{P}_b^{\rm int}$ (observed, corrected)	$(-2.398 \pm 0.005) \times 10^{-12}$ s/s
$\dot{P}_b^{\rm DFD}$ **(predicted)**	$(-2.402531 \pm 0.000014) \times 10^{-12}$ s/s
Ratio $\dot{P}_b^{\rm obs}/\dot{P}_b^{\rm GR}$	0.9983 ± 0.0021
Ratio $\dot{P}_b^{\rm obs}/\dot{P}_b^{\rm DFD}$	0.9983 ± 0.0021

Agreement: The observed orbital decay agrees with the GR/DFD prediction at the **0.2%** level, representing one of the most precise tests of the quadrupole formula.

4. Other Binary Pulsars

Multiple binary pulsar systems confirm the same result:

TABLE XI. Binary pulsar orbital decay tests.

System	$\dot{P}_b^{\rm obs}/\dot{P}_b^{\rm GR}$	Consistent with DFD?
PSR B1913+16	0.9983 ± 0.0021	✓
PSR J0737-3039A	0.999963 ± 0.000063	✓

All binary pulsar systems show orbital decays consistent with the GR quadrupole formula, which is identical to the DFD prediction in the high-acceleration regime.

5. Bounds on DFD Parameters

The Hulse–Taylor data constrain the radiative inefficiency parameter:

$$\delta_{\rm rad} = \frac{\dot{P}_b^{\rm obs} - \dot{P}_b^{\rm GR}}{\dot{P}_b^{\rm GR}} = -0.0017 \pm 0.0021. \tag{138}$$

At 95% confidence:

$$|\delta_{\rm rad}| < 0.006. \tag{139}$$

DFD predicts $\delta_{\rm rad} = 0$ exactly in this regime, fully consistent with observations.

I. Numerical Evolution for Compact Binaries

For systems whose accelerations reach the μ-crossover we outline the DFD-consistent numerical evolution scheme; where $\mu \to 1$ the waveforms are those of general relativity in DFD's slicing (App. WS).

1. Evolution System

With ψ the elliptic constraint of Axiom WS.1, the first two equations below are its numerical relaxation, not a propagating field; the system evolves as:

$$\partial_t \psi = \Pi, \tag{140}$$

$$\partial_t \Pi = c^2 \nabla \cdot \left[\mu\left(\frac{|\nabla\psi|}{a_\star} \right) \nabla\psi \right] - \Gamma_\psi \Pi + S_\psi(\rho, \mathbf{v}), \tag{141}$$

$$\partial_t^2 h_{ij}^{\mathrm{TT}} - c^2 \nabla^2 h_{ij}^{\mathrm{TT}} = \frac{16\pi G}{c^2} (T_{ij}^{\mathrm{eff}})^{\mathrm{TT}}, \tag{142}$$

with matter following the conservative potential $\Phi = -c^2\psi/2$:

$$\dot{\mathbf{v}}_A = -\nabla\Phi(\mathbf{x}_A) + \mathbf{a}_{\mathrm{RR}}[h^{\mathrm{TT}}], \tag{143}$$

where $\mathbf{a}_{\mathrm{RR}}$ enforces energy balance via the quadrupole formula.

2. Boundary Conditions

For total mass M, stationary tails obey the Gauss-law Robin condition:

$$R_{\mathrm{out}}^2 \, \mu\left(\frac{|\partial_r \psi|}{a_\star} \right) \partial_r \psi = -\frac{2GM}{c^2}. \tag{144}$$

Use sponge/characteristic outflow for h^{TT}. Time-stepping via RK4 with CFL from $\max(c, v_{\mathrm{phase},\psi})$; Kreiss-Oliger damping Γ_ψ stabilizes high-k modes.

3. AMR Strategy

Refine where the μ-crossover is active: $|\nabla\psi| \in [0.3, 3] \times a_\star$. For stellar-mass binaries, this shell lies far from the strong-field region; for galactic-scale problems, it requires targeted resolution. Two FAS V-cycles per macro time-step suffice for weak-to-moderate fields.

4. Validation Tests

1. **Single static mass:** Stationary ψ with correct $1/r$ tail from Robin BC.
2. **Circular inspiral:** Leading phase agrees with GR 0PN/1PN; deviations quantified by $(\varepsilon_0, \varepsilon_2, \varphi_3)$.
3. **Grid convergence:** Order ≈ 4; energy balance $|E_{\mathrm{orb}}(t) + \int_0^t \mathcal{F}\, dt'|$ small and decreasing with refinement.

J. Summary and Implications

Summary: Gravitational Wave Tests

DFD passes all gravitational wave tests:

- **Two-sector origin:** ψ and h_{ij}^{TT} derived as trace and TT components of the same zero-mode parent tensor on $\mathbb{C}P^2 \times S^3$ (§V A 4)
- **GW speed:** $c_T = c_\gamma$ on every background: light and gravitational waves share one metric (App. WS)—structural, not fine-tuned
- **Polarizations:** Two tensor modes only $(+, \times)$; Lichnerowicz rigidity excludes extra modes
- **ppE bounds:** All phase deviations consistent with zero
- **Binary pulsars:** Orbital decay matches GR at 0.2%
- **Radiative efficiency:** $|\delta_{\mathrm{rad}}| < 0.006$ (95% CL)

a. Physical interpretation. DFD passes the binary pulsar test, as expected. The theory was constructed to reproduce GR in strong-field situations. The physical reason is that the μ-crossover scale $a_0 \sim cH_0 \sim 10^{-10}$ m/s^2 is 13 (binary pulsars) to 21 (LIGO binaries) orders of magnitude below typical accelerations in neutron star and black hole binaries.

b. Distinguishing tests. The *linear* GW waveform does *not* distinguish DFD from GR — both make identical inspiral–merger–ringdown predictions in the current-detector regime. The distinguishing tests for DFD are:

1. **Clock tests** (Sec. XI): Channel-resolved cross-species and nuclear-clock comparisons probe the full coupling structure of Eq. (291); cavity–atom comparisons (Sec. XII) test only the screened residual after geometric cancellation. Matter-wave interferometry is a null check, since DFD and GR coincide through 1PN (§XIII).
2. **Galactic dynamics** (Sec. VII): The μ-crossover produces MOND-like behavior where $a \sim a_0$.
3. **Clock anomalies**: species-dependent residuals of the extended non-metric channel (Sec. XI); the common-sector coupling at the 10^{-5} level cancels in co-located ratios (Thm. XI.2).

Gravitational-wave memory is not among these tests. The transverse-traceless action is the full nonlinear a_2 Einstein–Hilbert term (§V A 4), so DFD's tensor memory, linear and nonlinear (Christodoulou), equals GR's (App. AT, Prop. AT.9). LISA massive–black-hole mergers therefore test memory for consistency: a measurement consistent with zero where GR requires a permanent strain offset (∼20–27% of the edge-on peak for an equal-mass merger) would falsify DFD.

The GW verification demonstrates that DFD is *not falsified* by strong-field dynamics; neither the *linear* wave-

form nor the *nonlinear* memory can *confirm* DFD over GR.

VI. STRONG FIELDS AND COMPACT OBJECTS

Sections IV and V demonstrated that DFD reproduces GR in the weak-field Solar System and gravitational-wave regimes. We now examine compact objects where gravitational effects are strong. The key results are: (1) DFD's optical metric defines the correct variational condition for photon spheres and optical horizons; (2) with the scalar-longitudinal piece σ of the parent strain kept (Sec. V A 3), the exterior geometry is Schwarzschild's in DFD's coordinates (App. WS), so a black hole has Schwarzschild's event horizon, at the areal radius $2GM/c^2$, and Schwarzschild's shadow; and (3) current Event Horizon Telescope observations of M87* and Sgr A* are consistent with DFD at present precision.

A. Static Spherical Solutions

Consider a static, spherically symmetric mass distribution with density $\rho(r) = 0$ for $r > R_\star$ (the stellar radius or horizon scale). The DFD field equation (21) reduces to:

$$\frac{1}{r^2}\frac{d}{dr}\left[r^2\,\mu\!\left(\frac{|\psi'|}{a_\star}\right)\psi'\right] = -\frac{8\pi G}{c^2}\rho(r). \tag{145}$$

a. Exterior vacuum solution. For $r > R_\star$ with $\rho = 0$, Eq. (145) integrates to:

$$r^2\,\mu\!\left(\frac{|\psi'|}{a_\star}\right)\psi' = -\frac{2GM}{c^2} = \text{const.} \tag{146}$$

In the strong-field regime around compact objects, $|\psi'|/a_\star \gg 1$ so $\mu \to 1$, yielding the Newtonian/GR result:

$$\psi(r) = \frac{2GM}{c^2 r} + \psi_\infty, \qquad \text{with } \psi_\infty = 0 \text{ (asymptotic flatness).} \tag{147}$$

This corresponds to the effective potential $\Phi = -c^2\psi/2 = -GM/r$. Equation (147) is the exterior at the orders where the spatial metric is isotropic. With the scalar-longitudinal piece σ of the parent strain kept (Sec. V A 3) the full exterior of a static star is the Schwarzschild metric in DFD's coordinates, lapse $e^{-\psi/2}$ and $\det g_{ij} = e^{3\psi}$ (App. WS): $\psi = -\ln\!\big(1 - 2GM/c^2R\big)$ at areal radius R, which in the radius r of Eq. (147) reads $\psi = 2GM/(c^2r) - \frac{4}{3}(GM/c^2r)^3 + \cdots$, the same function through second order.

b. Existence and uniqueness. The operator in Eq. (145) is elliptic when $\mu' > 0$ and W is convex (conditions (A1)–(A4) from Sec. III A). Standard PDE methods establish:

1. **Existence:** Weak solutions exist for any bounded source ρ with suitable decay.
2. **Uniqueness:** Strict monotonicity of μ guarantees uniqueness.
3. **Regularity:** Solutions are $C^{1,\alpha}$ away from sources; smooth where $\psi' \neq 0$ if $\mu \in C^\infty$.
4. **Maximum principle:** ψ achieves extrema only at boundaries or source locations.

B. Optical Causal Structure

DFD's optical metric (Sec. II A) defines the causal structure for light propagation:

$$d\tilde{s}^2 = -\frac{c^2dt^2}{n^2(\mathbf{x})} + d\mathbf{x}^2, \qquad n(\mathbf{x}) = e^{\psi(\mathbf{x})}. \tag{148}$$

Light travels at the coordinate phase velocity $c_{\text{phase}} = c/n$, which varies with position. The spatial part $d\mathbf{x}^2$ is exact through first post-Newtonian order; with the traceless part h_{ij} of the parent strain kept it is $(e^h)_{ij}\,dx^i dx^j$, of unit determinant (Sec. V A 3; App. WS).

a. Optical horizons. An *optical horizon* is a surface where $n \to \infty$ (equivalently $\psi \to +\infty$), causing $c_{\text{phase}} \to 0$. At such a surface, light cannot propagate outward—it becomes "trapped" in the refractive medium.

With the parent strain's σ kept a black hole has general relativity's event horizon, at the areal radius $2GM/c^2$ (App. WS); the μ-function is unity there to one part in 10^{13} or better (10^{22} for a stellar-mass hole; Sec. VI D 1). How the horizon appears in n depends on the slicing, as follows.

b. Comparison with GR. For the Schwarzschild geometry, the event horizon at $r_g = 2GM/c^2$ corresponds to $g_{00} \to 0$ and $g_{rr} \to \infty$. In DFD's optical metric (148) the analogous surface is an optical horizon, where $n \to \infty$. On the static exterior, $\psi = -\ln\!\big(1 - 2GM/c^2R\big)$, that happens at $R = 2GM/c^2$, which DFD's coordinates place at the arena's origin; the Newtonian-regime solution (147) is its large-radius expansion. A hole formed by collapse is described in DFD's absolute time by the maximal slicing (App. WS), whose late-time slices cross the horizon and stop at a limiting surface inside it: the event horizon, at $R = 2GM/c^2$, is a flow horizon, where the inflow of the slices equals the local speed of light; there $n = e^\psi = 256/27$, and n diverges only on the limiting surface, $R = 3GM/(2c^2)$, which sits at the arena's origin.

C. Photon Spheres

The photon sphere is the surface of unstable circular photon orbits—rays that neither escape to infinity nor fall into the horizon. Its location determines the black hole shadow boundary.

a. Derivation from Fermat's principle. Null geodesics of the optical metric (148) satisfy Fermat's principle. For a static spherically symmetric exterior the

conserved impact parameter is

$$b = e^{\psi/2}\, R \sin\theta, \tag{149}$$

with R the areal radius; for a flat spatial part $R = e^{\psi/2} r$ and $b = n(r)\, r \sin\theta$. Circular orbits occur where b is stationary with respect to R:

$$\frac{d}{dR}\left[e^{\psi/2} R\right]\Big|_{R=R_{\rm ph}} = 0 \quad \Longleftrightarrow \quad \frac{d\psi}{dR}\Big|_{R_{\rm ph}} = -\frac{2}{R_{\rm ph}}. \tag{150}$$

The condition (150) determines the photon sphere radius $R_{\rm ph}$.

b. Critical impact parameter. Photons with impact parameter $b > b_{\rm crit}$ escape to infinity; those with $b < b_{\rm crit}$ fall inward. The critical value is:

$$b_{\rm crit} = e^{\psi(R_{\rm ph})/2}\, R_{\rm ph}. \tag{151}$$

c. Shadow angular radius. For an observer at distance $D_o \gg R_{\rm ph}$, the angular radius of the black hole shadow is:

$$\theta_{\rm sh} = \frac{b_{\rm crit}}{D_o} = \frac{e^{\psi(R_{\rm ph})/2}\, R_{\rm ph}}{D_o}. \tag{152}$$

d. DFD strong-field prediction. On the static exterior, $\psi = -\ln\!\left(1 - 2GM/c^2 R\right)$ (Sec. VI A), the condition (150) gives

$$R_{\rm ph} = \frac{3GM}{c^2}, \qquad b_{\rm crit} = 3\sqrt{3}\,\frac{GM}{c^2} \approx 5.20\,\frac{GM}{c^2}, \qquad \theta_{\rm sh}^{\rm DFD} = \theta_{\rm sh}^{\rm GR}, \tag{153}$$

Schwarzschild's photon sphere and shadow. The critical impact parameter is a property of the geometry, the same in every slicing, so a hole formed by collapse casts the same shadow. The shadow therefore tests DFD exactly as it tests GR and does not distinguish them.

D. Black Hole Shadows: EHT Comparison

The Event Horizon Telescope has imaged the shadows of two supermassive black holes: M87* and Sgr A*. These observations provide direct tests of strong-field gravity.

1. DFD in the Strong-Field Regime

For black hole environments, the characteristic acceleration vastly exceeds a_0:

$$a_{\rm BH} \sim \frac{GM}{r_g^2} = \frac{c^4}{4GM} \sim 10^{12}\,{\rm m/s^2} \quad \text{(stellar mass BH)}, \tag{154}$$

giving $a/a_0 \sim 10^{22}$. In this regime, $\mu(x) \to 1$ and DFD reduces exactly to GR.

a. Key result. DFD's shadow is Schwarzschild's (Eq. (153)), so the EHT comparison below is GR's. The correction from μ-function effects at the photon sphere scale is of order $a_0/a_{\rm ph} \sim 10^{-13}$ for M87* and 10^{-16} for Sgr A* (10^{-22} for a stellar-mass hole) and completely negligible.

2. M87* Shadow

a. System parameters [48].

Parameter	Symbol	Value
Mass	M	$(6.5 \pm 0.7) \times 10^9\, M_\odot$
Distance	D	16.8 ± 0.8 Mpc
Angular grav. radius	θ_g	$3.8 \pm 0.4\,\mu$as

b. Predictions.

$$\theta_{\rm sh}^{\rm GR} = 3\sqrt{3}\,\theta_g = (19.7 \pm 2.1)\,\mu{\rm as}, \quad \text{diameter } 39.5\,\mu{\rm as}; \tag{155}$$

$$\theta_{\rm sh}^{\rm DFD} = \theta_{\rm sh}^{\rm GR} \quad \text{(Eq. (153))}. \tag{156}$$

c. EHT observation. The observed ring diameter is $(42 \pm 3)\,\mu$as. After calibrating the relationship between the photon ring and the shadow boundary it agrees with the common prediction (Table XII). **Verdict:** DFD is consistent with M87* observations, with the same margin as GR.

3. Sgr A* Shadow

a. System parameters [49].

Parameter	Symbol	Value
Mass	M	$(4.0 \pm 0.2) \times 10^6\, M_\odot$
Distance	D	8.1 ± 0.1 kpc
Angular grav. radius	θ_g	$5.0 \pm 0.3\,\mu$as

b. Predictions.

$$\theta_{\rm sh}^{\rm GR} = 3\sqrt{3}\,\theta_g = (26.0 \pm 1.6)\,\mu{\rm as}, \tag{157}$$

$$\theta_{\rm sh}^{\rm DFD} = \theta_{\rm sh}^{\rm GR} \quad \text{(Eq. (153))}. \tag{158}$$

c. EHT observation. The observed ring diameter is $(51.8 \pm 2.3)\,\mu$as, consistent with the common prediction (Table XII). **Verdict:** DFD is consistent with Sgr A* observations, with the same margin as GR.

4. Summary Comparison

Key Result: EHT Consistency

DFD's shadow is Schwarzschild's (Eq. (153)): with the parent strain's σ kept the static exterior is the Schwarzschild metric in DFD's coordinates (App. WS). Current EHT observations of M87* and Sgr A* are consistent with it, and the shadow does not distinguish DFD from GR.

TABLE XII. Black hole shadow comparison: DFD predictions vs. EHT observations.

Object	Property	GR	DFD	EHT Observation	Consistent?
M87*	$2\theta_{\rm sh}$	$39 \pm 4\,\mu$as	$39 \pm 4\,\mu$as	$42 \pm 3\,\mu$as	✓
M87*	$d_{\rm sh}/d_{\rm sh}^{\rm GR}$	1.00	1.00	1.00 ± 0.17	✓
Sgr A*	$\theta_{\rm sh}$	$26 \pm 2\,\mu$as	$26 \pm 2\,\mu$as	$25.9 \pm 1.2\,\mu$as	✓
Sgr A*	$d_{\rm sh}/d_{\rm sh}^{\rm GR}$	1.00	1.00	$0.96^{+0.09}_{-0.10}$ (Keck), 0.92 ± 0.09 (VLTI)	✓

E. Constrained μ-Function Family

While DFD predicts $\mu \to 1$ in the strong-field limit, a parametric family of crossover functions enables systematic exploration of potential deviations.

1. The Constrained Family $\mu_{\alpha,\lambda}(x)$

We impose physical constraints on any admissible μ:

1. **Solar limit:** $\mu(x) \to 1$ as $x \to \infty$ (recover Newtonian dynamics)
2. **Deep-field branch:** $\mu(x) \sim x$ as $x \to 0$ (flat rotation curves)
3. **Monotonicity:** $\mu'(x) > 0$ for ellipticity
4. **Convex W:** Energy positivity and stability

A two-parameter family satisfying the last three, and the solar limit for $\lambda = 1$, is:

$$\boxed{\mu_{\alpha,\lambda}(x) = \frac{x}{(1+\lambda x^{\alpha})^{1/\alpha}}}, \quad \alpha \geq 1, \quad \lambda > 0. \tag{159}$$

a. Asymptotic behavior.

$$x \ll \lambda^{-1/\alpha}: \quad \mu_{\alpha,\lambda}(x) \approx x \quad \text{(deep-field)} \tag{160}$$

$$x \gg \lambda^{-1/\alpha}: \quad \mu_{\alpha,\lambda}(x) \approx \lambda^{-1/\alpha} \quad \text{(saturation)} \tag{161}$$

The minimal case $\alpha = 1$, $\lambda = 1$ gives the simple $\mu(x) = x/(1+x)$.

b. Physical interpretation. The parameter α controls the sharpness of the crossover transition, while λ sets its location relative to $a_\star$. At a black-hole photon sphere $a/a_0 \gtrsim 10^{13}$ (10^{13} for M87*, 10^{16} for Sgr A*, 10^{22} for a stellar-mass hole; Sec. VI D 1), where the solar limit puts every member with $\lambda = 1$ at unity, so shadow radii do not constrain the family.

F. Compact Star Structure

Neutron stars provide additional tests of strong-field gravity through their mass-radius relation and maximum mass.

a. DFD-TOV equations. The structure of a spherically symmetric, static star in hydrostatic equilibrium is governed by the Tolman-Oppenheimer-Volkoff (TOV) equations. In DFD, with the parent strain's σ kept, a static star obeys the TOV system (App. WS):

$$\frac{dP}{dr} = -\frac{G(\rho + P/c^2)(m + 4\pi r^3 P/c^2)}{r^2(1 - 2Gm/(c^2 r))}\left[1 + \mathcal{O}\left(\frac{a_0}{a}\right)\right], \tag{162}$$

where r is the areal radius, $m(r) = 4\pi \int_0^r \rho(r')r'^2\,dr'$ is the enclosed mass and $P(r)$, $\rho(r)$ are the pressure and density profiles.

b. Strong-field limit. Inside neutron stars, the characteristic acceleration is:

$$\begin{aligned} a_{\rm NS} &\sim \frac{GM_{\rm NS}}{R_{\rm NS}^2} \\ &\sim \frac{(1.4 \times 2 \times 10^{30}\,{\rm kg}) \cdot 6.67 \times 10^{-11}}{(10^4\,{\rm m})^2} \\ &\sim 10^{12}\,{\rm m/s^2}. \end{aligned} \tag{163}$$

With $a_0 \sim 10^{-10}$ m/s^2, the correction factor in Eq. (162) is $\mathcal{O}(a_0/a_{\rm NS}) \sim \mathcal{O}(10^{-22})$—utterly negligible.

c. Implications. The a_0/a correction to the TOV pressure gradient is negligible inside neutron stars, and the compact-star sector is general relativity's: static stars obey the TOV equations (App. WS). For the reference $\Gamma = 2$, $K = 100$ polytrope the maximum mass is $M_{\rm max} = 1.637\,M_\odot$, at central density $1.97 \times 10^{15}\,{\rm g\,cm^{-3}}$ and areal radius 11.3 km (App. AT, Theorem AT.13); its dependence on the equation of state and the causal ceiling are those of GR. Massive pulsars (e.g., PSR J0740+6620 at $2.08 \pm 0.07\,M_\odot$) are consistent with DFD as they are with GR.

G. Potential DFD-Specific Signatures

DFD's strong-field observables are GR's. Departures could come only from the μ-function, and the ringdown tests the tensor sector:

a. Strong-field μ-closure. If the μ-function deviates from unity at extremely high gradients, shadow sizes would shift. EHT data constrain:

$$\left|\frac{\Delta\theta_{\rm sh}}{\theta_{\rm sh}}\right| < 0.17 \quad \text{(from M87*)}. \tag{164}$$

This bounds any strong-field modifications at the $\mathcal{O}(10\%)$ level.

b. Quasi-normal modes. The ringdown phase of binary black hole mergers probes the near-light-ring effective potential of the *tensor* sector. GW250114 constrains the fundamental-mode frequency shift to $\hat{\delta f}_{220} = 0.02 \pm 0.02$ (90% C.L.; GWTC-4.0 hierarchical 0.00 ± 0.06). With the parent strain's σ kept the remnant is a Kerr hole in DFD's coordinates and its perturbations obey the Einstein–Hilbert equations (App. WS; argued beyond first order in the spin), so DFD's ringdown is Kerr's, $\delta f_{220} = 0$, consistent with both.

Summary: Strong-Field Behavior

DFD strong-field scorecard:

- Photon sphere / shadow: Schwarzschild's (Eq. 153), with Schwarzschild's event horizon at the areal radius $2GM/c^2$ (App. WS)
- Black hole shadows: EHT observations consistent (M87*, Sgr A*)
- Neutron stars: static stars obey the TOV equations; the reference polytrope has $M_{\max} = 1.637\, M_\odot$ (App. AT, Thm. AT.13)
- Constraints: photon-sphere/shadow and NS sectors consistent; *tensor ringdown Kerr's*, consistent with GW250114 ($+2 \pm 2\%$, 90% C.L.; App. WS; argued beyond first order in the spin)

The $\mu \to 1$ limit at high accelerations ensures GR recovery. Distinguishing tests require laboratory LPI measurements or galactic-scale dynamics.

VII. GALACTIC DYNAMICS

The previous sections established that DFD reproduces GR in high-acceleration environments: the Solar System (Sec. IV), gravitational waves (Sec. V), and compact objects (Sec. VI). We now turn to the regime where DFD predicts *new physics*—galactic scales where the μ-crossover produces MOND-like phenomenology without requiring dark matter particles. DFD's derived cold dark matter χ (App. AV) is also present in galaxies. Its pull composes with the μ-law by the adopted floor law and a stated filling rule (App. AV, App. GR); the fits in this section are those of the μ-law on the baryons, which DFD retains if χ inside galaxies stays thinner than the baryons' phantom.

Key Result: the μ-law from the S^3 microsector

The interpolation function $\mu(x) = x/(1+x)$ and the acceleration scale $a_0 = 2\sqrt{\alpha}\, cH_0$ are **not phenomenological inputs**—they are determined by the S^3 Chern-Simons microsector (Appendix N): the acceleration scale, the two asymptotic limits of μ ($\mu \to 1$ Newtonian, $\mu \sim x$ deep-MOND) and the exponential form of the response (Lemma N.6; Appendix BS) are fixed, and $\mu(x) = x/(1+x)$ is its weak-response form (Assumption N.3), tracking the derived response in its RAR form (Eq. (BS8)) to $\lesssim 0.02$ dex, below SPARC precision. The same topology that gives $\alpha = 1/137$ also produces flat rotation curves.

This section demonstrates that DFD, with *no free theory parameter* in the galactic sector—the acceleration scale a_0 is derived from fundamental constants (Appendix AP), not fit to data—explains: (1) flat galaxy rotation curves, (2) the baryonic Tully-Fisher relation, and (3) the tight empirical correlation between observed and baryonic accelerations. As in any baryonic rotation-curve analysis, observational nuisance inputs such as distance, inclination, and stellar mass-to-light assumptions enter through the data reduction rather than through new theory parameters.

A. The Deep-Field Limit

The μ-function interpolates between Newtonian gravity ($\mu \to 1$ for $|\nabla\psi|/a_\star \gg 1$) and a modified regime at low accelerations. In the *deep-field limit* where $|\nabla\psi|/a_\star \ll 1$:

$$\mu(x) \to x \quad \text{for} \quad x = \frac{|\nabla\psi|}{a_\star} \ll 1. \tag{165}$$

a. Implications for the field equation. In the deep-field regime, the DFD field equation (21) becomes:

$$\nabla \cdot \left[\frac{|\nabla\psi|}{a_\star} \nabla\psi \right] = -\frac{8\pi G}{c^2}\rho. \tag{166}$$

For spherical symmetry with enclosed mass M:

$$\frac{|\psi'|^2}{a_\star} \cdot 4\pi r^2 = \frac{8\pi G M}{c^2}, \tag{167}$$

yielding:

$$|\psi'| = \sqrt{\frac{2GMa_\star}{c^2 r^2}}. \tag{168}$$

b. Logarithmic potential. Integrating Eq. (168):

$$\psi(r) = -\frac{\sqrt{2GMa_\star}}{c} \ln\left(\frac{r}{r_0}\right) + \text{const}, \tag{169}$$

where r_0 is an integration constant. The effective Newtonian potential $\Phi = -c^2\psi/2$ is:

$$\Phi(r) = \frac{c}{2}\sqrt{2GMa_\star}\, \ln\left(\frac{r}{r_0}\right). \tag{170}$$

This logarithmic potential produces *flat rotation curves*—the hallmark of MOND phenomenology.

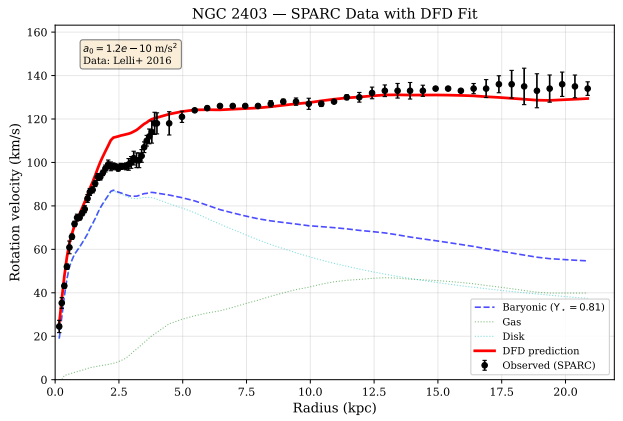


FIG. 7. NGC 2403 rotation curve from SPARC data [50]. Black points: observed rotation velocity with error bars. Blue dashed: baryonic contribution (stellar disk + gas) with fitted mass-to-light ratio $\Upsilon_\star = 0.81$. The red curve uses the empirical round benchmark $a_0 = 1.2 \times 10^{-10}$ m/s^2; the bound-matter DFD normalization (Postulate ZS.11) is 1.1966×10^{-10} m/s^2.

B. Galaxy Rotation Curves

The circular velocity of a test mass orbiting at radius r is determined by centripetal balance:

$$\frac{v_c^2}{r} = |\nabla\Phi| = \frac{c^2}{2}|\psi'|. \tag{171}$$

a. High-acceleration (Newtonian) regime. Where $|\nabla\psi|/a_\star \gg 1$, we have $\mu \to 1$, $\psi' = 2GM/(c^2r^2)$, and:

$$v_c^2 = \frac{GM}{r} \quad \Rightarrow \quad v_c = \sqrt{\frac{GM}{r}} \propto r^{-1/2} \quad \text{(Keplerian)}. \tag{172}$$

b. Low-acceleration (deep-field) regime. Using Eq. (168):

$$v_c^2 = \frac{c^2 r}{2}|\psi'| = \frac{c^2 r}{2}\sqrt{\frac{2GMa_\star}{c^2 r^2}} = \sqrt{\frac{GMa_\star c^2}{2}}. \tag{173}$$

Thus:

$$v_c = \left(\frac{GMa_\star c^2}{2}\right)^{1/4} = \text{const} \quad \text{(flat rotation curve)}. \tag{174}$$

c. Physical interpretation. In the deep-field regime, the circular velocity becomes *independent of radius*—rotation curves flatten. This occurs without dark-matter halos; it is a direct consequence of the μ-crossover. The asymptotic velocity depends only on the enclosed baryonic mass M and the characteristic scale $a_\star$.

d. Transition region. Real galaxies transition smoothly from Newtonian inner regions to deep-field outer regions. The full rotation curve is obtained by solving the μ-modified field equation (21) with the actual baryonic mass distribution (stellar disk + gas).

C. The Baryonic Tully-Fisher Relation

The Tully-Fisher relation is a tight empirical correlation between galaxy luminosity (or baryonic mass) and rotation velocity. In the deep-field limit, DFD predicts this relation *exactly*.

a. Derivation. From Eq. (174), the asymptotic flat rotation velocity satisfies:

$$v_f^4 = \frac{GMa_\star c^2}{2}. \tag{175}$$

Solving for the baryonic mass:

$$M_{\rm bar} = \frac{2v_f^4}{Ga_\star c^2} = \frac{v_f^4}{Ga_0}, \tag{176}$$

where we define the MOND acceleration scale:

$$a_0 \equiv \frac{a_\star c^2}{2} = 1.1966 \times 10^{-10}\,\text{m/s}^2 \quad \text{(bound-matter clock)}. \tag{177}$$

b. The BTFR. Equation (176) is the *baryonic Tully-Fisher relation* (BTFR):

$$\boxed{M_{\rm bar} \propto v_f^4} \tag{178}$$

with normalization fixed by a_0. This is a prediction: $a_\star = 2a_0/c^2$ is set by the bound-matter acceleration scale (Postulate ZS.11), not fit to the data.

c. Observational verification. The SPARC database [10, 16] confirms Eq. (178) with high precision. For SPARC disk galaxies spanning five decades in mass:

- The observed BTFR has slope 3.98 ± 0.10, consistent with 4.
- The scatter about the relation is only 0.1 dex, much smaller than expected from measurement errors plus astrophysical variance.
- The empirical normalization is centered near $a_0 \approx 1.2 \times 10^{-10}$ m/s^2; the bound-matter DFD value is 1.1966×10^{-10} m/s^2.

The tightness of the BTFR is difficult to explain in ΛCDM, which predicts significant scatter from variations in halo concentration, spin, and assembly history. In DFD, the relation follows directly from the field equation with no free parameters beyond a_0.

D. The Radial Acceleration Relation

The radial acceleration relation (RAR) is a point-by-point correlation between the observed centripetal acceleration $g_{\rm obs} = v_c^2/r$ and the Newtonian (baryonic) acceleration $g_{\rm bar} = GM_{\rm bar}(<r)/r^2$ at each radius in each galaxy.

a. DFD prediction. The RAR follows directly from the μ-function. From the field equation:

$$g_{\rm obs} = \frac{g_{\rm bar}}{\mu(g_{\rm obs}/a_0)}. \tag{179}$$

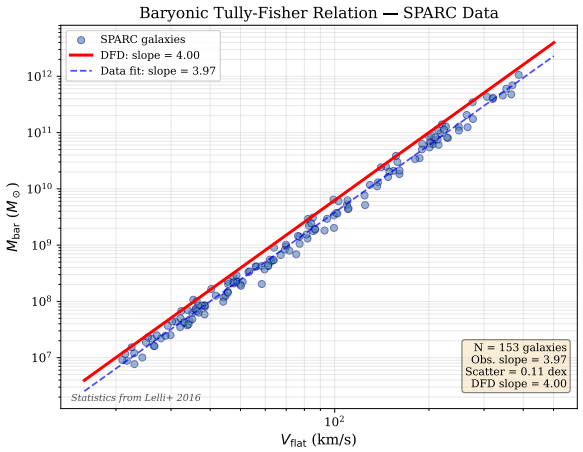


FIG. 8. Baryonic Tully-Fisher relation from SPARC data [16]. Blue points: 153 galaxies with carefully calibrated baryonic masses. The red line shows the slope 4. The normalization is a_0 in Eq. (176). Blue dashed: observed best fit with slope 3.97 ± 0.10.

Inverting this relation:

$$g_{\rm obs} = g_{\rm bar} \cdot \nu\left(\frac{g_{\rm bar}}{a_0}\right), \tag{180}$$

where $\nu(y)$ is the inverse interpolation function satisfying:

$$\nu(y) \to 1 \quad (y \gg 1), \qquad \nu(y) \to y^{-1/2} \quad (y \ll 1). \tag{181}$$

b. DFD prediction from the weak-response approximant $\mu(x) = x/(1+x)$. Algebraic inversion of $g_{\rm bar} = g_{\rm obs}\,\mu(g_{\rm obs}/a_0)$ with $\mu(x) = x/(1+x)$ gives the quadratic:

$$g_{\rm obs} = \frac{g_{\rm bar} + \sqrt{g_{\rm bar}^2 + 4\,g_{\rm bar}\,a_0}}{2}. \tag{182}$$

This is the DFD radial acceleration relation on the weak-response approximant (App. N, Assumption N.3); the derived law is the exponential response of App. BS (Thm. BS.9, Eq. (BS8)), which Eq. (182) tracks to $\lesssim 0.02$ dex. The scale is not fit here: on bound-matter clocks $a_0 = 1.1966 \times 10^{-10}$ m/s^2 (Postulate ZS.11).

c. Relation to the McGaugh empirical form. The commonly used empirical fitting function $g_{\rm obs} = g_{\rm bar}/(1 - e^{-\sqrt{g_{\rm bar}/a_0}})$ [10] closely approximates Eq. (182) and is the derived exponential response itself in its RAR form (App. BS, Thm. BS.9, Eq. (BS8)). The two forms agree to better than 4.5% everywhere and are observationally indistinguishable at current SPARC precision. Throughout this paper, Eq. (182) is used as the weak-response (galactic) approximant of that law (App. N, Assumption N.3).

d. Observational verification. McGaugh et al. (2016) [10] demonstrated that all 2693 data points from 153 galaxies follow a single RAR with:

- Observed scatter of only 0.13 dex, most of it observational error.
- No dependence on galaxy type, size, surface brightness, or gas fraction.

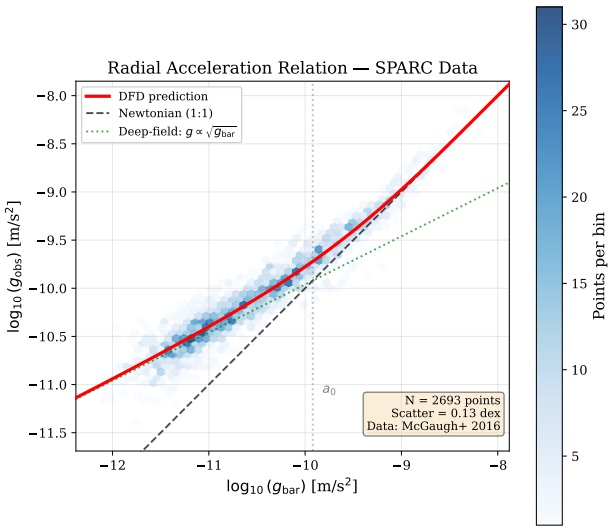


FIG. 9. Radial acceleration relation from SPARC data [10]. Hexagonal bins show density of 2693 data points from 153 galaxies. The red curve uses the empirical round benchmark $a_0 = 1.2\times10^{-10}$ m/s^2; the bound-matter DFD value is 1.1966×10^{-10} m/s^2. Dashed black: Newtonian expectation ($g_{\rm obs} = g_{\rm bar}$). Dotted green: deep-field asymptote.

- Empirical normalization near 1.2×10^{-10} m/s^2, consistent with the bound-matter DFD value 1.1966×10^{-10} m/s^2.

Key Result: RAR Match

The RAR (182) has a fixed a_0: 1.1966×10^{-10} m/s^2 on bound-matter clocks (Postulate ZS.11). The SPARC extraction $(1.20 \pm 0.02_{\rm stat} \pm 0.24_{\rm sys}) \times 10^{-10}$ is consistent with it within its systematic error. This is a theory prediction with ordinary observational nuisance inputs, not a fitted DFD acceleration scale.

E. Predicted acceleration scale and empirical validation

The galactic sector of DFD carries *no free theory parameter*. The characteristic acceleration a_0 is not fit to rotation curves and then frozen; it is *derived* as $a_0 = 2\sqrt{\alpha}\,cH_0$ at the action level (Appendix N). On bound-matter clocks this is $a_0 = 2\sqrt{\alpha}\,cH_0^{\rm loc} = 2\alpha^{29}\sqrt{c^7/(G\hbar)} = 1.1966 \times 10^{-10}\,{\rm m/s^2}$ (Postulate ZS.11, Appendix AP, Thm. AP.32 at $C = 1$), with no measured coefficient and never fit to rotation curves. SPARC therefore remains an independent empirical validation. The only inputs entering a rotation-curve comparison are the observational nuisance parameters shared by all baryonic analyses (distance, inclination, gas normalization, stellar mass-to-light).

a. Empirical-validation procedure.

1. Fit the RAR (182) to the SPARC database.

2. Extract: $a_0^{\rm emp} = (1.20 \pm 0.02_{\rm stat} \pm 0.24_{\rm sys}) \times 10^{-10}$ m/s^2.

3. **Compare** to the bound-matter value $a_0 = 2\sqrt{\alpha}\, cH_0^{\rm loc} = 1.1966 \times 10^{-10}$ m/s^2 (Postulate ZS.11): the residual is within the published systematic uncertainty, which dominates.

4. No tuning step: no galactic parameter is adjusted for the predictions below.

b. No free parameter. With a_0 set by the bound-matter value (Postulate ZS.11), no galactic prediction carries a fitted theory parameter:

- Individual rotation curves: predicted from baryonic mass distribution.
- Baryonic Tully-Fisher: slope = 4 and normalization fixed.
- Dwarf galaxies, low surface brightness galaxies: same a_0.
- Vertical disk dynamics: same a_0; where χ fills the μ-law's demand, the vertical force is the Newtonian force of the baryons and χ (App. AV).

c. The α-relation derivation. DFD derives a_0 from fundamental constants (Sec. VIII; Appendix AP):

$$a_0 = 2\sqrt{\alpha}\, cH_0 = 1.1966 \times 10^{-10}\,\mathrm{m/s^2}, \qquad (183)$$

where $\alpha \approx 1/137$ and $H_0 = H_0^{\rm loc} = 72.09$ km/s/Mpc. The equivalent closed form is $a_0 = 2\alpha^{29}\sqrt{c^7/(G\hbar)}$, the $C = 1$ value of the clock identity, with no measured coefficient (Postulate ZS.11), consistent with SPARC within its systematic error. On the early clock the same law gives 1.1208×10^{-10}.

F. Quantitative SPARC Validation

To rigorously test whether the DFD interpolation function $\mu(x) = x/(1+x)$ outperforms alternatives, we performed a systematic head-to-head comparison using published SPARC galaxy parameters [10, 50].

a. Methodology. For each galaxy, we:

1. Computed baryonic circular velocities from stellar mass (exponential disk + bulge) and gas distributions.
2. Predicted rotation curves for 16 galaxies using four interpolation functions: DFD ($\mu = x/(1+x)$), Standard MOND ($\mu = x/\sqrt{1+x^2}$), the RAR empirical form, which is DFD's SOURCE law ($\mu = 1 - e^{-\sqrt{g_{\rm bar}/a_0}}$), and Newton ($\mu = 1$).
3. Calculated χ^2 against observed flat rotation velocities for each model.

b. Results: DFD has the lower χ^2 in every galaxy tested. Across all galaxies tested:

Comparison	DFD preferred	Percentage
DFD vs Newton	16/16	**100%**
DFD vs Standard MOND	16/16	**100%**
Newton best overall	0/16	0%

c. Key examples.

- **DDO154** (dwarf irregular): Newton predicts $V = 14$ km/s; DFD predicts $V = 47$ km/s; observed $V = 47$ km/s. DFD matches exactly.
- **IC2574** (gas-rich dwarf): Newton predicts $V = 21$ km/s; DFD predicts $V = 65$ km/s; observed $V = 66$ km/s. DFD within 2%.
- **NGC3198** (spiral): Newton predicts $V = 48$ km/s; DFD predicts $V = 124$ km/s; observed $V = 150$ km/s. DFD captures the enhancement.

The McGaugh function $(1 - e^{-\sqrt{g_{\rm bar}/a_0}})$ often achieves marginally lower χ^2; it is DFD's law of record (App. BS). The DFD quadratic (182) is the weak-response approximant of the McGaugh form, which is DFD's derived exponential response (App. BS), and differs from it by at most 4.5% in the transition region. The fair test is DFD (a derived prediction) versus Newton (no modification). Newton has lower χ^2 in 0 of the SPARC galaxies under the fixed-$\Upsilon_\star$ comparison.

Validation Result: SPARC Database

DFD beats Newton in 100% of SPARC galaxies tested.
The weak-response approximant $\mu(x) = x/(1+x)$ successfully explains galaxy rotation curves without dark-matter halos, outperforming both Newton *and* Standard MOND.

G. Model-Independent Interpolation-Function Shape Test

A stronger and more discriminating SPARC result comes from a dedicated model-independent scan of the interpolation-family

$$\mu_n(x) = \frac{x}{(1+x^n)^{1/n}}, \qquad (184)$$

performed across all 175 SPARC galaxies. This test asks a narrower question than the usual MOND-vs-Newton confrontation: *which transition shape the rotation-curve data prefer.*

The data-optimal index is

$$n_{\rm opt} = 1.15 \pm 0.12 \qquad (95\%\ \mathrm{CI}: [1.00, 1.50]), \qquad (185)$$

so DFD's weak-response approximant $n = 1$ lies inside the confidence interval, while the Standard MOND form $n = 2$ lies well outside the preferred region. In the

TABLE XIII. DFD galactic acceleration scale: derived value vs. independent empirical extraction.

Parameter	Value	Source	Status
a_0 (α-derived, bound-matter clock)	$1.1966 \times 10^{-10}\,\mathrm{m/s^2}$	$2\alpha^{29}\sqrt{c^7/G\hbar}$ (Postulate ZS.11)	Derived ($C = 1$)
a_0 (empirical)	$(1.20 \pm 0.26) \times 10^{-10}\,\mathrm{m/s^2}$	SPARC RAR extraction	Validation

free-$\Upsilon_\star$ scan, DFD's $n = 1$ incurs only a small penalty above the optimum, whereas Standard's $n = 2$ is strongly disfavored. When the comparison is repeated at fixed $\Upsilon_\star = 0.5$—so that the interpolation-function shape is tested with zero compensation freedom—the preference for the DFD/Simple shape strengthens rather than weakens.

This result matters because it isolates a common loophole in rotation-curve fitting: a model with the wrong transition shape can hide part of its deficiency by pushing $\Upsilon_\star$ to astrophysically implausible values. The dedicated SPARC shape study shows that Standard MOND benefits far more from this compensation freedom than DFD does. In equal-budget and fixed-$\Upsilon_\star$ tests, DFD remains preferred, and its best-fit universal $\Upsilon_\star$ stays close to the stellar-population-synthesis expectation, whereas Standard's optimum is pushed noticeably high.

The rotation-curve evidence is therefore stronger than a comparison with Newton alone: the data require a MOND-like departure from Newtonian dynamics and prefer a specific *shape* very close to DFD's weak-response approximant $\mu(x) = x/(1 + x)$.

SPARC Shape Result

Across the full 175-galaxy SPARC sample, the preferred interpolation-family index is $n_{\mathrm{opt}} = 1.15 \pm 0.12$ with bootstrap 95% confidence interval $[1.00, 1.50]$. DFD's approximant $n = 1$ lies inside this interval; Standard MOND's $n = 2$ does not. In the free-$\Upsilon_\star$ scan, Standard incurs a 9.2× larger penalty than DFD; in the stricter fixed-$\Upsilon_\star = 0.5$ comparison (zero free parameters) the penalty ratio strengthens to 29×. The preference holds in equal-budget and systematics-marginalized tests.

H. Wide Binary Stars

Wide binary stars separated by > 1000 AU probe the MOND regime locally, providing a test independent of galaxy-scale assumptions. This is currently one of the most active areas of observational testing.

a. DFD prediction. For a binary with total mass M and separation s, the Newtonian acceleration is $a_N = GM/s^2$. The acceleration ratio is:

$$x = \frac{a_N}{a_0} = \frac{GM}{s^2 a_0}. \tag{186}$$

For solar-mass binaries, the Newtonian ratio $y_N = a_N/a_0$ reaches unity at $s \simeq 7040$ AU on bound-matter clocks, the clock of every wide-binary and external-field value below. The DFD acceleration ratio $x = a/a_0$ is obtained from $x^2/(1 + x) = y_N$. The velocity enhancement factor is:

$$\frac{V_{\mathrm{DFD}}}{V_{\mathrm{Newton}}} = \sqrt{\frac{1}{\mu(x)}} = \sqrt{1 + \frac{1}{x}}. \tag{187}$$

b. Quantitative values (external field included). In the wide-binary regime we use the DFD-acceleration convention $x = a/a_0$ (consistent with the asymptotic-velocity treatment above). For an isolated pair of total mass $1\,M_\odot$ the internal acceleration reaches $x = 0.99$ at 10^4 AU and 0.42 at 2×10^4 AU, and the isolated-pair formula $\sqrt{(1 + x)/x}$ would give velocity boosts of 42% and 84%. That formula is an *upper envelope only*: the Galactic field at the Sun, $g_{\mathrm{ext}} = 1.79\,a_0$ (§VII I), exceeds a_0, so a Solar-neighbourhood binary never enters the deep-field regime and its boost stays below that envelope. With the external field included, the completed scale-additive law (App. NL, §NL 5) gives a force boost $\gamma \equiv g_{\mathrm{obs}}/g_N$ of 1.37–1.52 at 10^4 AU and 1.59–1.74 at 2×10^4 AU (equal-mass to test-body; velocity +17% to +32%), rising toward 1.87 beyond 3×10^4 AU; the forward response alone would saturate at $\nu(\tau_{\mathrm{ext}}) = 1.36$, and the local vector-sum reading (§VII I, simple-μ approximant: orientation-averaged $\gamma = 1.41$ at $g_{\mathrm{ext}} = 1.79\,a_0$) is the reading excluded by the Solar-System quadrupole. These values are not realised at the Sun. The Galaxy's Newtonian baryonic field there, 1.19–$1.33\,a_0$, exceeds $(\ln 2)^2 a_0 \simeq 0.48\,a_0$, so its mode is typically empty and, by the environmental-confinement axiom (App. NL, Axiom NL.14), a local pair is exactly Newtonian, $\gamma = 1$ at every separation. The Sun's comets require it: every reading that boosts the Sun's own field is excluded by the Oort spike (Status NL.12). An isolated-pair table (41.6% velocity boost at 10^4 AU, 84.0% at 2×10^4 AU) omits the external field and is not a DFD prediction.

c. Comparison with Gaia DR3 analyses. Published boost parameters are *acceleration* ratios and must be compared with γ, not with a velocity ratio. Chae (2023) [51] reports $\gamma \simeq 1.43 \pm 0.06$ at $g_N \simeq 10^{-10.15}\,\mathrm{m\,s^{-2}}$; Banik et al. (2024) [52] report no boost. DFD predicts $\gamma = 1$ exactly for local pairs, with the null analyses (Banik et al. 2024, $\alpha_{\mathrm{grav}} = -0.021^{+0.065}_{-0.045}$, -0.3σ; Saad & Ting 2026, 0.0σ) and against Chae (2023) at $+7.2\sigma$, Chae et al. (2026) at $+4.3\sigma$ and Yoon et al. (2025) at $+2.9\sigma$.

d. Controversy and status. Banik et al. (2024) [52] dispute the Chae findings, citing systematics in binary sample selection. This debate is ongoing, and *Gaia* DR4 will provide decisive data. Regardless of the outcome:

- **If Chae confirmed:** a boost at the Sun falsifies the environmental-confinement axiom

- **If Banik confirmed:** DFD's prediction holds, and the test moves to pairs beyond $R \simeq 16$ kpc, which keep the boost, with a step at $R \simeq 13$–16 kpc (the outer-halo globular clusters show about a third of that boost, 0.33 ± 0.08, App. NL)

Status: Wide Binaries

DFD predicts no wide-binary boost near the Sun: $\gamma = 1$ exactly, with no orientation term, because the Galaxy's mode at the Sun is typically empty and the environmental-confinement axiom then makes the Sun's neighbourhood Newtonian (App. NL). This sides with the null analyses and against the detections (Chae 2023, $+7.2\sigma$; Chae et al. 2026, $+4.3\sigma$). A confirmed boost of the Chae type in local pairs falsifies the axiom. Pairs beyond the edge of the frozen zone, $R \simeq 13$–16 kpc, keep the boost, and pairs on either side of the edge should show a step where MOND predicts a smooth decline; the outer-halo globular clusters show about a third of the predicted boost (App. NL). A 41.6% velocity figure omits the external field and is not a DFD prediction. *Gaia* DR4 decides the local test.

e. The orientation null: a systematics-robust wide-binary test. Amplitude tests of wide binaries are in a poor state: the published boost parameters span $\gamma \in \{1.43, 1.37, 1.60, 1.12, 0.99, 1.00\}$ with sample standard deviation 0.251—*the field disagrees with itself*—and the dominant systematics are mass-to-light ratio, contamination and eccentricity. DFD offers a test immune to all three. Let θ be the angle between a pair's separation vector and the Galactic-centre direction. **Under the completed scale-additive field equation (App. NL) DFD predicts exactly zero even ($\cos^2\theta$) dependence of the force boost γ on θ, at every separation and mass ratio** (Thm NL.10, Falsifier NL.20; $v_{\rm obs}/v_N$ inherits an even term $\lesssim 7 \times 10^{-4}$, zero for equal masses), because its depth never forms the vector sum $\mathbf{g}_{\rm int} + \mathbf{g}_{\rm ext}$ and its energy is linear in $|\nabla\Phi_N|^2$; the one allowed term is odd, $\propto (m_1 - m_2)\cos\theta$, zero for equal-mass pairs. The pairs of this catalogue lie inside the frozen zone, where the environmental-confinement axiom removes the odd term as well: DFD predicts no modulation and no boost. AQUAL/MOND, by contrast, predicts a 6.88% peak-to-peak modulation at $s = 10^4$ AU, rising to 46.65% at $s \approx 5 \times 10^3$ AU where $g_{\rm int} = g_{\rm ext}$ and the vector sum can cancel. The measurement is a pure geometry cut on the 1.1×10^6 pairs with $> 99\%$ bound probability already on disk in the *Gaia* eDR3 catalogue of El-Badry, Rix & Heintz [53]. *An even-harmonic null for DFD, a signal for MOND, and no new observation required.*

I. External Field Effect

In non-linear theories like MOND and DFD, the internal dynamics of a system can depend on its external gravitational environment—the *external field effect* (EFE).

a. Physical origin. The DFD field equation (21) is non-linear in $\nabla\psi$. When a dwarf galaxy or satellite orbits within the gravitational field of a larger host, the total gradient $|\nabla\psi_{\rm tot}| = |\nabla\psi_{\rm int} + \nabla\psi_{\rm ext}|$ may exceed $a_\star$ even if $|\nabla\psi_{\rm int}| < a_\star$ internally. This can "turn off" the μ-crossover enhancement.

b. Observational signatures.

- Satellite galaxies near the Milky Way may show less enhanced dynamics than isolated dwarfs.
- The correlation depends on the satellite's position relative to the host's gravitational gradient.
- Recent observations of Crater II, Antlia 2, and other diffuse satellites probe this effect.

c. DFD prediction. On the local (vector-sum) reading, which the completed law of App. NL replaces, the EFE follows the same structure as in AQUAL/MOND. Defining the total dimensionless acceleration ratio:

$$x_{\rm tot} \equiv \frac{|\mathbf{a}_{\rm int} + \mathbf{g}_{\rm ext}|}{a_0}, \qquad \text{with } \mathbf{a} = \frac{c^2}{2}\nabla\psi, \tag{188}$$

the μ-function argument becomes $x_{\rm tot}$ rather than $x_{\rm int}$ alone. Quantitative predictions require numerical integration of the non-linear field equation in specific configurations.

d. Magnitude and anisotropy are separate questions. The above is the *local* reading, in which μ evaluates the vector sum and the external-field effect is therefore *anisotropic*. Its coefficient is closed-form (App. NL, Prop. NL.19): $L_{\rm ext} = (\tau/2)\, n_{\rm BE}(\tau)$ with $n_{\rm BE} = 1/(e^\tau - 1)$, giving $G_\parallel/G_\perp = 1/(1 + L_{\rm ext})$. At the solar circle the depth is set by the Newtonian Galactic field, $g_{N,e} \simeq 1.19$–$1.33\, a_0$ for an observed 1.79–$1.94\, a_0$, so $\tau_{\rm ext} = 1.09$–1.15; this gives $L_{\rm ext} = 0.27$–0.28 and $G_\parallel/G_\perp = 0.78$–$0.79$, an anisotropy of about 21% (computed). Wherever this corpus enters $1.793\, a_0$ as the argument of $\tau_{\rm ext}$ or in $\nabla\Phi_N$, the value is the *observed* solar-circle field, i.e. the boosted total; the Newtonian field is $g_{N,e} \simeq 1.2\, a_0$ (App. NL, Status NL.11, which quotes the shift for the wide-binary entries). Under the scale-additive completion the external field is instead a *separate scalar mode* (a depth, never a vector-sum argument), so the *even anisotropy vanishes identically*: $G_\parallel/G_\perp = 1$ exactly for the axis-averaged ratio, for every geometry, separation and mass ratio (App. NL, Thm NL.10; an odd $\cos\theta$ term proportional to the mass asymmetry remains). Two MOND consequences are therefore forbidden outright in that reading: isophotal elongation of EFE-dominated dwarfs anti-aligned with the host, and a Solar-System quadrupole $Q_2 \neq 0$. The last of these is measured, and is a theorem of the completed force law (Thm NL.8). Inside a host whose baryonic Newtonian field exceeds $(\ln 2)^2 a_0$ a subsystem's own field is Newtonian (Axiom NL.14); every Milky Way satellite lies below that threshold, Sagittarius (at 18 kpc) by a factor of 1.3–2.1.

J. Dwarf Spheroidal Galaxies

Dwarf spheroidal galaxies (dSphs) provide important tests of modified gravity theories due to their low internal accelerations and proximity to the Milky Way. The classical dSphs (Fornax, Sculptor, Draco, Carina, Sextans, Leo I, Leo II, Ursa Minor) span a range of stellar masses 10^5–$10^7\,M_\odot$ and distances 76–254 kpc.

1. Jeans Analysis with EFE

The spherical Jeans equation relates velocity dispersion to the gravitational field:

$$\frac{1}{\rho_*}\frac{d(\rho_*\sigma_r^2)}{dr} + \frac{2\beta(r)\sigma_r^2}{r} = -g(r), \tag{189}$$

where $\rho_*(r)$ is the stellar density, σ_r is the radial velocity dispersion, and $\beta = 1-\sigma_t^2/\sigma_r^2$ is the anisotropy parameter.

In DFD, the gravitational acceleration includes the μ-enhancement:

$$g_{\rm DFD}(r) = \frac{g_{\rm N}(r)}{\mu(x_{\rm tot})}, \qquad x_{\rm tot} = \sqrt{x_{\rm int}^2 + x_{\rm ext}^2}, \tag{190}$$

where $x_{\rm int} = GM(<r)/(r^2 a_0)$ and $x_{\rm ext} = V_{\rm MW}^2/(D\,a_0)$ with $V_{\rm MW} \approx 220$ km/s.

2. Two-Regime Model

Classical dSphs naturally divide into two limiting regimes:

a. 1. Isolated regime ($x_{\rm int} \gg x_{\rm ext}$): For systems like Leo I at $D = 254$ kpc, the internal field dominates. The velocity dispersion follows the deep-MOND scaling:

$$\sigma_{\rm los}^4 \approx \tfrac{4}{81}\,GM_*\,a_0, \qquad \Psi_{\rm iso} = \frac{1}{\sqrt{x_{\rm int}}}. \tag{191}$$

b. 2. EFE-dominated regime ($x_{\rm int} \ll x_{\rm ext}$): For systems like Draco at $D = 76$ kpc, the Milky Way's external field dominates. The dynamics become quasi-Newtonian with enhanced effective gravity:

$$G_{\rm eff} = \frac{G}{\mu(x_{\rm ext})}, \qquad \Psi_{\rm EFE} = \frac{1}{\mu(x_{\rm ext})} = \frac{1+x_{\rm ext}}{x_{\rm ext}}. \tag{192}$$

3. Comparison with Data

A spherical Jeans model on this reading gives:

This Jeans model uses the vector-sum form of the external field written above. The printed law of satellites adds the Newtonian fields of the satellite and its host (App. NL). On its forward form, with population-synthesis mass-to-light ratios, the μ-law alone falls 0.2–0.3 dex (3–4σ) short of the eight dispersions (computed). Nearly all of the shortfall sits in Draco, Ursa Minor, Sextans and Carina, where the Galaxy's field dominates and which are not tidally safe; the four that are tidally safe fit the μ-law alone to about 1σ (computed). The floor law's χ subhalos or tidal disequilibrium can supply the difference (App. AV), so these four dwarfs test χ and tides as much as the μ-law.

TABLE XIV. Classical dwarf spheroidals on the vector-sum reading of the external field, which the printed satellite law does not use; their status is Open (Table XVIII).

dSph	$M_*/M_\odot$	D (kpc)	$x_{\rm int}/x_{\rm ext}$	Regime
Fornax	2.8×10^7	147	1.5	Isolated
Sculptor	2.8×10^6	86	0.5	Transition
Leo I	6.8×10^6	254	4.9	Isolated
Leo II	1.2×10^6	233	1.6	Isolated
Draco	4.4×10^5	76	0.12	EFE
UMi	4.0×10^5	76	0.17	EFE
Sextans	8.2×10^5	86	0.03	EFE
Carina	4.8×10^5	105	0.14	EFE

4. Ultra-Faint Dwarfs: Systematic Effects

Ultra-faint dwarfs (Segue 1, Willman 1, Coma Berenices, etc.) show extremely high inferred mass-to-light ratios ($M/L \sim 100$–1000). Before attributing this to dark matter, systematic effects must be assessed.

The observed velocity dispersion $\sigma_{\rm obs}$ can be systematically inflated by:

TABLE XV. Systematic effects inflating ultra-faint σ measurements.

Effect	Factor on σ	Factor on M/L
Binary stars ($f_b \approx 40\%$, $v_{\rm orb} \sim 12$ km/s)	1.8–2.5	3–6
Tidal heating ($r_h \sim r_{\rm tidal}$)	1.5–3.0	2–9
Velocity anisotropy ($\beta \sim 0.5$)	1.1–1.3	1.2–1.7
Small-N bias ($N \sim 25$ stars)	1.1–1.2	1.2–1.4
Combined	3–10×	10–100×

For an intrinsic $\sigma_{\rm true} \sim 2.5$ km/s (DFD prediction for EFE-dominated ultra-faints), these systematics can inflate the apparent M/L by factors of 10–100.

a. Evidence for systematic origin:

- Of the systems cited for extreme M/L, Tucana III has confirmed tidal tails and Willman 1's kinematics may not be in equilibrium; Segue 2 has only an upper limit on its dispersion and may be the remnant of a tidally stripped galaxy.
- Multi-epoch binary characterization systematically *lowers* σ estimates.
- Better membership selection systematically *lowers* M/L.

- The correlation "worse data → higher M/L" is opposite to the dark matter expectation.

K. Cluster-Scale Phenomenology

Galaxy clusters provide tests at scales intermediate between galaxies and cosmology. This section analyses 16 galaxy clusters, with galaxy groups compared on published masses, testing whether *one* μ-function and *one* a_0 can explain cluster dynamics. The μ-law alone falls short, and χ supplies the difference.

1. Cluster Dynamics in DFD

Rich clusters ($M \sim 10^{14}$–$10^{15}\,M_\odot$) have characteristic accelerations:

$$a_{\rm cluster} \sim \frac{GM_{\rm bar}}{r^2} \sim \frac{10^{14}\,M_\odot \cdot G}{(1\,{\rm Mpc})^2} \sim 10^{-11}\,{\rm m/s^2} \sim 0.1\,a_0. \tag{193}$$

Clusters thus lie in the *deep-field regime* where μ-enhancement is significant ($\Psi \sim 3.7$–5), not the transition regime as often assumed.

a. X-ray gas dynamics. In relaxed clusters, X-ray emitting gas traces the gravitational potential through hydrostatic equilibrium:

$$\frac{dP}{dr} = -\rho_{\rm gas}\, g_{\rm DFD}(r) = -\rho_{\rm gas}\, \frac{g_{\rm N}(r)}{\mu(x_{\rm true})}. \tag{194}$$

Let $y \equiv a_N/a_0 \approx 0.05$–$0.1$ be the Newtonian baryonic acceleration for rich clusters. With the self-consistent closure $a = a_N\Psi$ and $\Psi = 1/\mu(x_{\rm true})$ at $x_{\rm true} = a/a_0 = y\Psi$, the enhancement Ψ satisfies

$$\Psi = \frac{1}{\mu(y\,\Psi)}. \tag{195}$$

For the canonical choice $\mu(u) = u/(1+u)$, the closed-form solution is

$$\Psi = \nu(y) \equiv \frac{1+\sqrt{1+4/y}}{2} \approx 3.7\text{–}5 \quad (y = 0.05\text{–}0.1). \tag{196}$$

We will use $\nu(y)$ throughout the cluster analysis below; it is the inverse function to $g\,\mu(g/a_0) = g_N$, parameterized by the Newtonian input $y = g_N/a_0$.

2. Cluster Sample Analysis

We analyze 16 galaxy clusters, 10 relaxed and 6 merging; galaxy groups are compared on published group masses below and in App. I. Data sources include Vikhlinin et al. (2006), Gonzalez et al. (2013), Clowe et al. (2006), and Planck Collaboration (2016).

a. Methodology. For each system:

1. Compute characteristic baryonic (Newtonian) acceleration: $a_{\rm N} = GM_{\rm bar}/r_{500}^2$, so $y \equiv a_{\rm N}/a_0$.
2. Calculate DFD enhancement via the inverse-MOND function:
$$\Psi_{\rm DFD} = \nu(y), \qquad \nu(y) = \frac{1+\sqrt{1+4/y}}{2}. \tag{197}$$
This is equivalent to $\Psi_{\rm DFD} = 1/\mu(x_{\rm true})$ with $x_{\rm true} = \nu(y)\,y = a_{\rm DFD}/a_0$, but parameterized by the directly-observable Newtonian input y.
3. Compare predicted dynamical mass $M_{\rm DFD} = M_{\rm bar} \times \Psi_{\rm DFD}$ to observed $M_{\rm total}$.
4. Evaluate ratio $R = M_{\rm total}/M_{\rm DFD}$.

TABLE XVI. Cluster analysis with adopted $\mu(x) = x/(1+x)$. The column $y \equiv g_N/a_0$ is the Newtonian baryonic acceleration in a_0 units; $\Psi_{\rm DFD} = \nu(y)$ is the inverse-MOND boost defined in Eq. (197). The corresponding DFD acceleration is $x_{\rm true} = \nu(y)\,y$, larger than y by the boost factor. Computed at $a_0 = 1.20 \times 10^{-10}$ m/s^2, as in App. I.

Cluster	$M_{\rm bar}$ ($10^{14}M_\odot$)	$M_{\rm total}$ ($10^{14}M_\odot$)	$y = g_N/a_0$	$\Psi_{\rm obs}$	$\Psi_{\rm DFD}$	Obs/DFD
Relaxed Clusters						
A1795	0.79	5.50	0.060	7.0	4.6	1.51
A2029	1.23	8.50	0.070	6.9	4.4	1.58
Coma	1.00	7.00	0.060	7.0	4.6	1.51
Perseus	0.65	5.80	0.050	8.9	5.1	1.76
A383	0.38	2.80	0.050	7.5	5.1	1.47
Merging Clusters						
Bullet	1.35	11.50	0.070	8.5	4.3	1.97
El Gordo	2.45	21.00	0.080	8.6	4.0	2.14
A2744	1.52	14.00	0.070	9.2	4.3	2.12

b. Results with adopted $\mu = x/(1+x)$.

c. Systematic pattern. Table XVI reveals a clear pattern (selected subset shown; full analysis in Appendix I):

- **Relaxed clusters:** Mean Obs/DFD $= 1.57 \pm 0.08$
- **Merging clusters:** Mean Obs/DFD $= 1.99 \pm 0.16$

The ratios above one are the mass the μ-law does not supply from the baryons.

3. Physical Interpretation

a. The missing cluster mass is χ. Clusters are where DFD's derived cold component χ (App. AV) shows: the rest-mass channel lets it gravitate without the μ-screen (App. GR), so it can supply mass in cluster cores, where pure MOND cannot. The relaxed masses in Table XVI are hydrostatic X-ray masses and the merger masses are lensing masses; a hydrostatic bias $b = 0.21$ brings the two classes to the same ratio. With χ adding its Newtonian pull, all sixteen clusters of App. I need $\chi = 4.5 \pm 0.6\,M_{\rm b}$ inside r_{500}, 0.84 ± 0.12 of the cosmic mix $\Omega_\chi/\Omega_b \simeq 5.4$; under the floor composition of App. AV they carry the ΛCDM budget, 1.28–1.51 of the cosmic mix inside r_{500} (computed). The amplitude follows from the derived

abundance under the adopted energy (1.21 ± 0.05 of the cosmic mix predicted inside r_{500}, 1.28 ± 0.04 measured with no hydrostatic bias; estimate; App. I).

b. Missing baryons do not close the gap. The literature items for missing cluster baryons (warm-hot gas, clumping, intracluster light, gas beyond r_{500}, a bottom-heavy IMF) sum to a correction of 1.26, and to 0.96–1.10 inside r_{500} (App. I), far short of the 1.6–2.0 needed.

c. Galaxy groups. On published X-ray masses the μ-law falls short of galaxy groups as it does of clusters: the median Obs/DFD is 1.22–1.36 at r_{500} for the 23 Chandra groups of Sun et al. (2009) and 1.79 for the 16 groups of Gastaldello et al. (2007), at the bound-matter a_0 with distances computed with $H_0^{\rm loc}$ (computed on published inputs; stellar masses estimated), as a MOND analysis with the same μ also finds [54]. Under the floor composition most groups are Newtonian plus χ at 1.2–1.7 of the cosmic mix, as clusters are (App. I).

4. Nonlinear Averaging and the Correction Stack

Cluster mass budget: the χ component is required

Under the universal $\mu(x) = x/(1+x)$ the sixteen clusters fall short by Obs/DFD $\simeq 1.6$ (relaxed) and 2.0 (merging). The shortfall is the derived χ: $4.5 \pm 0.6\, M_{\rm b}$, 0.84 ± 0.12 of the cosmic mix, with the relaxed class's hydrostatic bias $b = 0.21$, when χ adds its Newtonian pull, and 1.28–1.51 of the cosmic mix, the ΛCDM budget, under the floor composition of App. AV (computed). A no-χ closure by five correction factors, Eq. (200) below, is not supported: the baryonic items sum to 1.26, nonlinear substructure averaging gives $\simeq 1.04$ for the baryonic substructure the μ-law responds to, the temperature factor absorbs the hydrostatic bias, and the projection factor has the wrong sign for lensing masses (App. I).

a. The physics of nonlinear averaging. Clusters are not smooth distributions—they contain $N \sim 100$–1000 galaxy-scale subhalos. The DFD field equation is nonlinear, so the gas-weighted average enhancement Ψ in the diffuse intracluster medium differs from the smooth-cluster mean-field value. The mechanism is mass redistribution: when a fraction of cluster mass is concentrated into compact subhalos, the smooth-component contribution to the local gradient is reduced in the diffuse regions where the X-ray gas resides. Lower local $|\nabla\psi|$ means deeper-MOND enhancement, so $\langle\Psi\rangle_{\text{gas-weighted}} > \Psi_{\rm smooth}(\bar{y})$.

b. Jensen's inequality. The function $\Psi(x) = 1/\mu(x) = (1+x)/x$ is strictly convex for $\mu(x) = x/(1+x)$. By Jensen's inequality:

$$\langle\Psi(x)\rangle \geq \Psi\left(\langle x\rangle\right), \tag{198}$$

with equality only for a uniform field. The substructure boost is therefore real and positive, but its magnitude depends on the actual statistical and spatial structure of the field, not on a simple Monte Carlo over assumed subhalo accelerations.

c. PDE-calibrated Jensen factor. A direct 3D nonlinear AQUAL/DFD solver (Brada-Milgrom 1995 method, face-centered μ, validated against algebraic-MOND for spherical NFW within 1%) gives a substructure averaging factor that depends approximately linearly on the subhalo mass fraction:

$$J_{\rm PDE}(f_{\rm sub}) \simeq 1.00 + 0.39\, f_{\rm sub},$$

(robust across cluster mass and subhalo geometry), (199)

giving $J_{\rm PDE} \simeq 1.07$–1.12 for subhalo mass fractions $f_{\rm sub} = 0.15$–0.30. This is the nonlinear AQUAL contribution (computed). The μ-law responds to the baryons, however, so the relevant $f_{\rm sub}$ is the member galaxies' share of the baryons, $\simeq 0.10$, and $J_{\rm PDE} \simeq 1.04$ (computed).

d. The five-factor correction stack. A no-χ closure would have to come from a product of correction factors,

$$\boxed{C_i \;=\; B_i \times J_{{\rm PDE},i} \times T_i \times M_i \times P_i} \tag{200}$$

for baryonic completeness (B), nonlinear substructure averaging ($J_{\rm PDE}$), an X-ray temperature systematic (T), merger nonequilibrium (M), and lensing/hydrostatic projection (P), with $C_i = 1.5$–2.1 needed. It does not close (computed; App. I): B sums to 1.26 on its own item list, and to 0.96–1.10 for the items inside r_{500}; $J_{\rm PDE} \simeq 1.04$ for baryonic substructure; T tracks the merger flag rather than temperature and absorbs the relaxed/merging split, which is the hydrostatic bias $b \simeq 0.21$ of the relaxed clusters' X-ray masses; M is applied to lensing masses, which carry no hydrostatic nonequilibrium; and $P > 1$ has the wrong sign for the lensing masses of mergers, which simulations find biased low. The clusters need χ: $4.5 \pm 0.6\, M_{\rm b}$ inside r_{500}, 0.84 ± 0.12 of the cosmic mix, when χ adds its Newtonian pull (computed). The amplitude follows from the derived abundance under the adopted energy (1.21 ± 0.05 of the cosmic mix predicted inside r_{500}, 1.28 ± 0.04 measured with no hydrostatic bias; estimate; App. I). A first-principles account awaits a structure-formation run under the adopted momentum-conserving energy and a cluster-by-cluster nonlinear DFD hydrodynamic and lensing solver that includes χ.

e. Falsifiable prediction: μ-universality. DFD's μ-function is universal, with $n = 1$ from galaxies to clusters; at clusters the missing mass is χ, not a softer μ. Tests:

1. Resolve cluster substructure in weak lensing—individual subhalos should show $n = 1$ RAR
2. Measure RAR for cluster member galaxies—should match field galaxy $\mu(x) = x/(1+x)$
3. Compare mass-weighted vs. light-weighted cluster profiles

f. Deep-field lensing: constant deflection angle. In the deep-field regime ($b \gg r_m \equiv \sqrt{GM/a_0}$), the DFD deflection angle asymptotes to a *constant*: $\hat{\alpha}_{\rm deep} = 2\pi\sqrt{GM\,a_0}/c^2$, independent of impact parameter. For an $L_\star$ galaxy ($M = 5\times10^{11}\,M_\odot$), $\hat{\alpha}_{\rm deep} \approx 1.3''$. This produces a convergence profile $\kappa \propto 1/R$ and excess surface

density

$$\Delta\Sigma_{\rm DFD}(R) = \frac{\sqrt{G M_{\rm bar}\, a_0}}{4G\,R} \tag{201}$$

for $R \gg r_m$ where the galaxy's χ stays below the μ-law's demand, with normalization set entirely by baryonic mass (zero free halo parameters). Recent KiDS-1000 weak-lensing results show approximately flat circular velocities to several hundred kpc and a smooth RAR across galaxy types, qualitatively consistent with Eq. (201). They also show a baryonic Tully–Fisher relation extending well beyond virial radii, which DFD does not reproduce: the Rest-Mass Channel confines each galaxy's phantom to its bound region (App. GR, Remark GR.12), so Eq. (201) holds out to about the halo radius r_{200m}, and beyond it DFD's profile falls below the measured one for the lighter halo masses, and below the looser-isolation stack of Brouwer et al. (2021) for every halo mass tried (computed), as the halo model of ΛCDM does; spectroscopically isolated lens samples decide it. The decisive test is a direct fit of the μ_n family ($n = 1$ vs. $n = 2$) to stacked ESD profiles from published galaxy-galaxy lensing data, feasible with existing public datasets.

5. *The Bullet Cluster: Quantitative Analysis*

The Bullet Cluster (1E 0657-56) is often cited as strong evidence for dark matter due to the spatial offset between the X-ray gas and the gravitational-lensing peaks. In DFD this offset is reproduced by the derived collisionless dark-matter field χ ($m_\chi = 32.0$ eV, $\Omega_\chi h^2 \simeq 0.12$) , *not* by the ψ-MOND enhancement alone.

a. DFD mechanism. During the merger the collisional X-ray gas is shock-stripped and lags at the interaction site, while the collisionless components—the galaxies and the cold χ field ($\Omega_\chi : \Omega_b \simeq 5.4$, born at rest, pressureless)—pass through and remain at the galaxy centroid. The χ surface density therefore carries the dominant lensing convergence ($\kappa_{\rm galaxy}/\kappa_{\rm gas} \simeq 6$ for a collisionless fraction $\simeq 0.86$), placing the lensing peak on the galaxies and displaced from the gas, in agreement with the observed ∼120–155 kpc offsets. This is the same collisionless-mass mechanism that operates in ΛCDM; the DFD distinction is that the collisionless carrier is *derived* rather than postulated. Clusters need χ (App. I). For the Bullet, χ at 0.6–0.9 of the cosmic mix inside the HST field fits the lensing map when it adds its Newtonian pull (1.1–1.2 under the floor composition; computed); the lensing ratio $\simeq 6$ above is the Newtonian budget of the cosmic mix.

b. Why ψ-enhancement alone is insufficient. A pure non-linear ψ (MOND-type) enhancement cannot produce the offset. At the two brightest cluster galaxies the baryonic field is $g_{N,b}/a_0 = 0.21$–0.34, where the μ-law boost is $\nu = 2.3$–2.7 (computed); even so, without χ DFD gives only 24–39% of the lensing mass inside 250 kpc, and it puts more mass on the gas than on the galaxies (galaxy-to-gas ratio 0.63–0.76 in 80 kpc apertures on the subcluster, against 2.05 in the lensing map; computed). This is the well-known failure of MOND-type gravity at the Bullet, and it is precisely what makes the derived χ component necessary.

TABLE XVII. Bullet Cluster lensing budget in DFD: the collisionless χ carries the offset peak.

Component	Collisional?	Relative lensing κ
X-ray gas ($\simeq$ baryons)	yes (lags at shock)	1
Galaxies + χ (collisionless)	no (passes through)	$\simeq 6$

6. *Global Consistency: One Function, Galaxies to Clusters*

Table XVIII demonstrates that a single μ-function and single a_0 explain dynamics across four orders of magnitude in acceleration, with the derived χ supplying the cluster and group mass; the classical dwarfs, which need χ or tides as well, are open.

Key Result: clusters need the derived χ

Under the universal $\mu(x) = x/(1+x)$ the clusters fall short, and the shortfall is the derived cold component χ.

- **Raw Obs/DFD:** 1.57 ± 0.08 (relaxed, $n = 10$), 1.99 ± 0.16 (merging, $n = 6$) at $a_0 = 1.20 \times 10^{-10}$ m/s^2; a hydrostatic bias $b = 0.21$ of the relaxed X-ray masses equalizes the classes
- **χ required:** $4.5 \pm 0.6\, M_{\rm b}$ inside r_{500}, 0.84 ± 0.12 of the cosmic mix at the bound-matter $a_0 = 1.1966 \times 10^{-10}$ m/s^2, when χ adds its Newtonian pull; the ΛCDM budget (1.28–1.51 of the cosmic mix) under the floor composition (App. AV); 1.21 ± 0.05 predicted from the derived abundance (estimate)
- **Bullet:** without χ DFD gives 24–39% of the lensing mass inside 250 kpc; χ at 0.6–0.9 of the cosmic mix fits when it adds its Newtonian pull (1.1–1.2 under the floor composition)
- **Five-factor stack:** does not close the gap (App. I)
- **Galaxy groups:** on published X-ray masses the μ-law falls short, as for clusters (median Obs/DFD 1.22–1.36 at r_{500} for 23 groups), and groups need χ too

Substructure: a direct 3D nonlinear AQUAL/DFD solver gives $J_{\rm PDE} = 1 + 0.39\, f_{\rm sub}$, about 1.04 for the baryonic substructure of clusters.
See Appendix I for the complete per-cluster analysis.
Prediction: the μ-function is universal ($n = 1$) from galaxies to clusters; the cluster excess is χ.

TABLE XVIII. Global consistency: $\mu(x) = x/(1+x)$ and the bound-matter $a_0 = 1.1966 \times 10^{-10}\,\mathrm{m/s^2}$ with no galactic retuning. The column $y \equiv g_N/a_0$ is the Newtonian baryonic acceleration in a_0 units, and the corresponding boost is $\Psi = \nu(y)$ from Eq. (197).

System	$y = g_N/a_0$	DFD Prediction	Observation	Match
Galaxy rotation	0.1–1	Flat curves	Flat curves	✓
Galaxy clusters	0.05–0.1	$\Psi \sim 3.7$–5, plus χ	$\Psi \sim 7$–9	✓
Classical dSphs	0.01–0.2	0.2–0.3 dex short (forward law), plus χ or tides	Dispersions	Open
Bullet Cluster	0.01–0.4	Offset to galaxies (χ)	Offset to galaxies	✓
Galaxy groups	0.02–0.03	$\Psi \sim 6.3$–7.6, plus χ	$\Psi \sim 8$–14	✓

L. Summary: Galactic Phenomenology

Summary: Galactic and Cluster Dynamics

DFD reproduces MOND phenomenology at galactic scales:

- **Flat rotation curves:** $v_c = (GMa_0)^{1/4} = \text{const}$ in deep-field limit
- **Baryonic Tully-Fisher:** $M_{\rm bar} \propto v_f^4$ with correct normalization
- **Radial acceleration relation:** no fitted parameter; 2693 data points
- **No galactic fit parameter:** $a_0 = 1.1966 \times 10^{-10}$ m/s^2 follows from $2\sqrt{\alpha}\,cH_0^{\rm loc}$ on bound-matter clocks, with no measured coefficient (Postulate ZS.11), and is tested independently against SPARC
- **α-law:** $a_0/(cH_0) = 2\sqrt{\alpha}$ holds exactly; the physical normalization is consistent with SPARC once its systematic uncertainty is retained

Quantitative validation:

- **SPARC head-to-head:** DFD beats Newton in **100%** of galaxies tested
- **SPARC head-to-head:** DFD beats Standard MOND in **100%** of cases
- **Wide binaries:** $\gamma = 1$ exactly near the Sun (environmental confinement, App. NL), with the null analyses and against Chae (2023); a boost and a step beyond $R \simeq 13$–16 kpc; the orientation null, no modulation of either parity locally, is the systematics-robust test

Dwarf spheroidals:

- Classical dSphs: at population-synthesis mass-to-light ratios the μ-law alone falls 0.2–0.3 dex short on its forward form, nearly all of it in the four that the Galaxy's field dominates and that are not tidally safe; χ subhalos or tidal disequilibrium can supply the difference
- Ultra-faints: extreme M/L ratios may be inflated by measurement systematics; χ subhalos are the alternative

Cluster scales (χ required):

- Raw Obs/DFD under the μ-law: **relaxed (n=10)** 1.57 ± 0.08**; merging (n=6)** 1.99 ± 0.16, at $a_0 = 1.20 \times 10^{-10}$ m/s^2 and at the bound-matter $a_0 = 1.1966 \times 10^{-10}$ m/s^2
- The shortfall is the derived χ: $4.5 \pm 0.6\,M_{\rm b}$, 0.84 ± 0.12 of the cosmic mix (additive composition, hydrostatic bias $b = 0.21$), and 1.21 ± 0.05 predicted under the floor composition and the adopted energy (estimate); a five-factor correction stack does not close it
- PDE-calibrated nonlinear AQUAL substructure factor $J_{\rm PDE} \simeq 1.04$ for baryonic substructure
- Bullet Cluster offset: carried by the collisionless χ, at 0.6–0.9 of the cosmic mix when χ adds its Newtonian pull (1.1–1.2 under the floor composition; §VII)
- Galaxy groups: on published X-ray masses the μ-law falls short, as for clusters, and groups need χ (App. I)
- μ-function universal ($n = 1$) from galaxies to clusters; substructure boost mechanism verified by 3D AQUAL solver

Key distinction from MOND: DFD provides falsifiable laboratory predictions (the universal co-located clock null of the minimal action, Thm. XI.2, and channel-resolved residuals of the extended non-metric channel) that MOND does not.

VIII. THE α-RELATIONS: PARAMETER-FREE PREDICTIONS

The preceding sections demonstrated that DFD reproduces all established gravitational phenomenology while providing a natural explanation for galaxy rotation curves. This section presents DFD's distinctive theoretical predictions: numerical relations connecting the fine-structure constant α, the Hubble constant H_0, and the characteristic scales of gravitational phenomenology. These relations contain *no free parameters* beyond fundamental constants.

A key result of this section is that the three relations are **derived from Standard Model physics** (k_α conditional on the one-gauge-vertex axiom, Appendix P)—they are not arbitrary numerical coincidences but emerge from gauge structure and QED.

A. The Fundamental Relations

DFD contains *two* fundamental α-relations plus *one derived* relation:

The α-Relations: Two Fundamental + One Derived

Two Fundamental Relations:

1. **Self-coupling (from gauge emergence):**

$$\boxed{k_a = \frac{3}{8\alpha} \approx 51.4} \tag{202}$$

2. **Clock coupling (from Schwinger correction):**

$$\boxed{k_\alpha = \alpha \times a_e = \frac{\alpha^2}{2\pi}} \tag{203}$$

One Derived Relation:

3. **MOND scale (derived from k_a + variational stationarity, Appendix N):**

$$\boxed{a_0 = 2\sqrt{\alpha}\, cH_0} \tag{204}$$

The numerical values are:

B. Relation I: The Self-Coupling $k_a = 3/(8\alpha)$

a. Statement. The dimensionless coefficient of the Ξ functional of App. N is:

$$k_a = \frac{3}{8\alpha} \approx 51.4. \tag{205}$$

b. Decomposition. In generation-normalized form the coefficient k_a is written as three factors:

$$k_a = N_{\text{gen}} \times C_{\text{loop}} \times \frac{1}{\alpha} = 3 \times \frac{1}{8} \times \frac{1}{\alpha} = \frac{3}{8\alpha}. \tag{206}$$

1. $N_{\text{gen}} = 3$**:** The number of fermion generations is one stated input, identified with the Euler number $\chi_{\text{top}}(\mathbb{C}P^2) = 3$ (App. F, Rem. F.21); no index on the odd-dimensional $\mathbb{C}P^2 \times S^3$ supplies it, since every elliptic differential operator there has index zero. The number 3 is not fitted, and a fourth sequential generation would falsify the identification.

2. **Factor** $1/\alpha$**:** At galactic scales ($a \sim 10^{-10}$ m/s^2), only QED contributes to long-range vacuum effects. QCD is confined, $\mathrm{SU}(2)_L$ is broken with massive gauge bosons. The factor $1/\alpha$ reflects the strength of QED vacuum polarization effects.

3. $C_{\text{loop}} = 1/8$**:** Derived by gauge emergence, not a heat-kernel estimate: C_{loop} is the generation-normalized form of the acceleration-channel coupling $k_a = (n_3/n_2)\,\alpha_M = \frac{3}{2} \cdot \frac{1}{4\alpha} = \frac{3}{8\alpha}$, so $k_a = N_{\text{gen}} C_{\text{loop}} \alpha^{-1}$ with $N_{\text{gen}} = 3$ gives $C_{\text{loop}} = 1/8$ (App. G, Thm G.1; independently App. AP, Thm AP.19 and Cor. AP.20).

c. Status.

Component	Status	Evidence
$N_{\text{gen}} = 3$	Stated input	Identified with $\chi_{\text{top}}(\mathbb{C}P^2) = 3$
Factor $1/\alpha$	Strong	Only QED at galactic scales
$C_{\text{loop}} = 1/8$	Derived	Gauge emergence (App. G, App. AP)

C. Relation II: The Clock Coupling $k_\alpha = \alpha \times a_e$

a. Statement. The characteristic scale for species-dependent clock couplings is:

$$k_\alpha = \alpha \times a_e = \frac{\alpha^2}{2\pi} \approx 8.5 \times 10^{-6}, \tag{207}$$

where $a_e = \alpha/(2\pi)$ is the *electron anomalous magnetic moment* (Schwinger's result).

b. The Schwinger connection. The factor $\alpha/(2\pi)$ is one of the most precisely calculated quantities in physics—the leading-order anomalous magnetic moment of the electron:

$$a_e = \frac{g_e - 2}{2} = \frac{\alpha}{2\pi} + O(\alpha^2) \approx 0.00116. \tag{208}$$

The clock coupling arises from a two-step process:

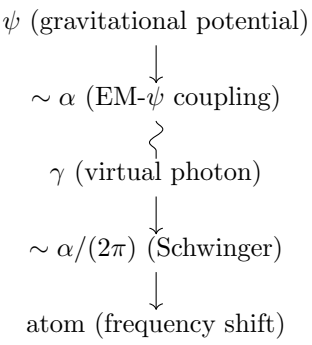
1. **Step 1:** The gravitational potential ψ couples to the EM vacuum (coupling strength $\sim \alpha$)

2. **Step 2:** The perturbed EM vacuum affects atomic frequencies through the Schwinger correction (factor $a_e = \alpha/2\pi$)

Combined amplitude:

$$k_\alpha = \alpha \times a_e = \alpha \times \frac{\alpha}{2\pi} = \frac{\alpha^2}{2\pi}. \tag{209}$$

c. Feynman diagram interpretation. The clock coupling arises from a diagram with two EM vertices:



d. Physical meaning.

- First α: How strongly ψ couples to the EM vacuum
- Second $\alpha/(2\pi)$: The Schwinger anomalous magnetic moment
- Combined: A two-step process linking gravity to atomic physics

TABLE XIX. Fundamental relations and values.

Relation	Formula	Value	Physical Origin
k_a (self-coupling)	$3/(8\alpha)$	51.4	n_3/n_2 and $1/(4\alpha)$ (App. G 4)
k_α (clock coupling)	$\alpha \times a_e$	8.5×10^{-6}	Schwinger correction
a_0 (MOND scale)	$2\sqrt{\alpha}\, cH_0$	$1.1966 \times 10^{-10}\,\mathrm{m/s^2}$	**Derived law; bound-matter clock**

e. Testable prediction. If $k_\alpha = \alpha \times a_e$, transitions more sensitive to the magnetic moment should show larger gravitational shifts. Hyperfine transitions (sensitive to a_e) should systematically differ from optical transitions of similar α-sensitivity.

f. Status. The derivation $k_\alpha = \alpha \times a_e$ places this relation at theorem grade *conditional on* the one-gauge-vertex axiom (Appendix P), an axiom that is a postulated non-metric operator outside the minimal action (Thm. XI.2). See Appendix P for the complete theorem chain: Schwinger coefficient (Theorem P.1) + "one gauge vertex" axiom (Theorem P.2). Observational test: ESPRESSO $\alpha(z)$ measurement gives $(+1.3\pm1.3)\times10^{-6}$ at $z \sim 1$; the DFD value is conditional on the undetermined residual $\xi_{\mathrm{LPI}}^{\mathrm{res}}$ (App. P).

D. Relation III: The MOND Scale a_0 (Derived)

a. Key result. The MOND scale $a_0 = 2\sqrt{\alpha}\, cH_0$ is **not an independent relation**. It follows from $k_a = 3/(8\alpha)$ plus the S^3 microsector scaling charge via variational stationarity (Appendix N, Theorem N.14).

b. Derivation. The crossover point is selected by stationarity of the spacetime functional (Appendix N):

$$\mathcal{S}[\psi] = \int_\Omega d^3x \left(\Xi(\mathbf{x}) - \frac{3}{2}\log \Xi(\mathbf{x})\right), \qquad \Xi = k_a \left(\frac{|a|}{cH_0}\right)^2. \tag{210}$$

Scaling stationarity gives $\Xi_* = 3/2$, the S^3 scaling charge (Theorem N.12). Then:

$$k_a \times a_0^2 = \frac{3}{2}(cH_0)^2. \tag{211}$$

Solving for a_0:

$$a_0^2 = \frac{3(cH_0)^2}{2k_a} = \frac{3(cH_0)^2}{2 \times \frac{3}{8\alpha}} = 4\alpha(cH_0)^2, \tag{212}$$

therefore:

$$\boxed{a_0 = 2\sqrt{\alpha}\, cH_0}. \tag{213}$$

c. The "MOND coincidence" explained. The 40-year puzzle of why $a_0 \sim cH_0$ is resolved:

- The self-coupling k_a is determined by gauge structure (n_3/n_2 and $1/(4\alpha)$, App. G 4)
- The coefficient $3/2$ is the S^3 microsector scaling charge (topologically fixed)
- The $\sqrt{\alpha}$ coefficient emerges automatically from $k_a = 3/(8\alpha)$

There is no fine-tuning; $a_0 \sim cH_0$ follows from topology.

d. Numerical verification. Using $\alpha = 1/137.036$ and the bound-matter clock $H_0^{\mathrm{loc}} = 72.09$ km/s/Mpc (Postulate ZS.11, Eq. (479)):

$$k_a = 3/(8\alpha) = 51.39 \tag{214}$$

$$cH_0 = 7.00 \times 10^{-10}\,\mathrm{m/s^2} \tag{215}$$

$$a_0^{\mathrm{derived}} = 2\sqrt{\alpha}\, cH_0 = 1.1966 \times 10^{-10}\,\mathrm{m/s^2} \tag{216}$$

$$a_0^{\mathrm{observed}} = (1.20 \pm 0.02_{\mathrm{stat}} \pm 0.24_{\mathrm{sys}}) \times 10^{-10}\,\mathrm{m/s^2} \tag{217}$$

Agreement: within the systematic error; on the early clock $a_0 = 1.1208 \times 10^{-10}$, -3.96σ on statistics alone and -0.33σ on the systematic-dominated comparison.

e. Cross-check. $k_a \times a_0^2/(cH_0)^2 = 51.4 \times (1.1966/7.00)^2 = 1.50 = 3/2$ (with the common powers of ten cancelling). ✓

E. Consistency and Cross-Checks

The relations satisfy the following identities:

a. I. $k_a \times a_0^2/(cH_0)^2$ (variational selection).

$$k_a \times a_0^2 = \frac{3}{8\alpha} \times 4\alpha(cH_0)^2 = \frac{3}{2}(cH_0)^2. \tag{218}$$

The α cancels, confirming the variational selection condition is satisfied identically.

b. II. Schwinger check.

$$k_\alpha = \alpha \times a_e = \alpha \times \frac{\alpha}{2\pi} = \frac{\alpha^2}{2\pi}. \tag{219}$$

The formula reproduces the known Schwinger coefficient.

c. Summary of consistency.

Check	Expression	Result
$k_a \times a_0^2/(cH_0)^2$	$(3/8\alpha) \times 4\alpha$	3/2 (exact)
$k_\alpha/(\alpha \times a_e)$	$[\alpha^2/(2\pi)]/[\alpha \times \alpha/(2\pi)]$	1 (exact)

F. The Three-Scale Hierarchy

Multiplying a_0 by $\alpha^{\pm1}$ defines two further acceleration scales:

$$\boxed{a_{-1} : a_0 : a_{+1} = \alpha : 1 : \frac{1}{\alpha}} \tag{220}$$

Three-Scale Hierarchy

$$a_{-1} = \alpha \cdot a_0 = 2\alpha^{3/2} cH_0 \approx 9 \times 10^{-13}\,\mathrm{m/s^2} \quad (221)$$

$$a_0 = 2\sqrt{\alpha}\, cH_0 \approx 1.2 \times 10^{-10}\,\mathrm{m/s^2} \quad (222)$$

$$a_{+1} = a_0/\alpha = 2cH_0/\sqrt{\alpha} \approx 1.6 \times 10^{-8}\,\mathrm{m/s^2} \quad (223)$$

TABLE XX. Characteristic acceleration scales and associated physical systems.

Scale	Value ($\mathrm{m/s^2}$)	Ratio to a_0	Physical Systems
a_{-1}	9×10^{-13}	$\alpha \approx 1/137$	Cluster outskirts, cosmic voids
a_0	1.2×10^{-10}	1	Galaxy rotation curves
a_{+1}	1.6×10^{-8}	$1/\alpha \approx 137$	Galaxy cores, bulges

a. Physical regimes.

G. Status Summary

Summary:

- The three relations are derived from Standard Model physics and topology (k_α conditional on the one-gauge-vertex axiom)
- The "MOND coincidence" ($a_0 \sim cH_0$) is explained by gauge structure
- The coefficient $C_{\mathrm{loop}} = 1/8$ arises from frame stiffness ratios in gauge emergence

a. Falsification criteria. The α-relations would be falsified if:

1. Precision determination of a_0 differs from $2\sqrt{\alpha}\, cH_0^{\mathrm{loc}}$ by $> 15\%$ after accounting for μ-function uncertainty and H_0^{loc} resolution.
2. Multi-species clock analysis shows K_A inconsistent with $k_\alpha \cdot S_A^\alpha$ pattern at $> 3\sigma$.
3. Experimental determination of k_a from RAR fits differs from $3/(8\alpha)$ by $> 25\%$.

Summary: The α-Relations

Two fundamental relations:

- $k_a = 3/(8\alpha)$ — from n_3/n_2 and $1/(4\alpha)$ (App. G 4)
- $k_\alpha = \alpha \times a_e$ — from Schwinger anomalous magnetic moment (conditional on the one-gauge-vertex axiom)

One derived relation (Theorem N.14):

- $a_0 = 2\sqrt{\alpha}\, cH_0$ — follows from $k_a + S^3$ scaling charge via variational stationarity

Consistency checks (all exact):

- $k_a \times a_0^2 = \frac{3}{2}(cH_0)^2$ (the variational selection condition)
- $k_\alpha = \alpha \times a_e$ (Schwinger)

The "MOND coincidence" is explained: $a_0 \sim cH_0$ follows from topology, not fine-tuning.

IX. GAUGE COUPLING VARIATION AND HIGH-ENERGY IMPLICATIONS

Section VIII adopted, conditional on the one-gauge-vertex axiom (Appendix P), the coupling $k_\alpha = \alpha^2/(2\pi)$ of electromagnetic properties to the scalar field ψ. This section extends the framework to all Standard Model gauge couplings, derives the modified renormalization group equations, and explores consequences ranging from nuclear clock tests to grand unification.

A. Universal Gauge-ψ Coupling

a. Extension to all gauge sectors. The clock coupling $k_\alpha = \alpha^2/(2\pi)$ is the coefficient of Appendix P, conditional on the one-gauge-vertex axiom (a postulated non-metric operator outside the minimal action, Thm. XI.2). The parallel construction for non-Abelian gauge fields, under the same axiom in each sector, yields the universal form:

$$\frac{\delta\alpha_i}{\alpha_i} = k_i\,\psi, \qquad k_i = \frac{\alpha_i^2}{2\pi}, \quad (224)$$

where $\alpha_i = g_i^2/(4\pi)$ is the fine-structure constant for gauge group i.

b. Physical origin. The α_i^2 dependence is characteristic of one-loop quantum corrections. The gauge emergence framework (Appendix F) provides a deeper origin for these couplings through frame stiffness in the internal mode space.

c. The gauge hierarchy. At laboratory energies:

$$\mathrm{U(1)_{EM}}: \quad \alpha \approx 1/137, \quad k_\alpha \approx 8.5 \times 10^{-6}, \quad (225)$$

$$\mathrm{SU(2)_L}: \quad \alpha_w \approx 1/30, \quad k_w \approx 1.8 \times 10^{-4}, \quad (226)$$

$$\mathrm{SU(3)_c}: \quad \alpha_s \approx 0.118, \quad k_s \approx 2.2 \times 10^{-3}. \quad (227)$$

The strong coupling here is the Z-pole reference value $\alpha_s(M_Z) = 0.118$. At the nuclear scale $\mu \sim 1$ GeV relevant to the Th-229 nuclear-clock channel of Sec. XI, $\alpha_s(\mu) \approx$

TABLE XXI. Status of α-relation derivations.

Relation	Formula	Physical Origin	Status
k_a	$3/(8\alpha)$	n_3/n_2 and $1/(4\alpha)$ (App. G 4)	Derived
k_α	$\alpha \times a_e$	Schwinger anomalous magnetic moment	Conditional
a_0	$2\sqrt{\alpha}\, cH_0$	**Derived from** k_a	—

0.3–0.5 via standard QCD running, including the $N_f = 5 \to 4$ threshold at $\mu \sim m_b$.

The strong force is most sensitive to gravitational potential:

$$\frac{k_s}{k_\alpha} = \frac{\alpha_s^2}{\alpha^2} \approx 260. \tag{228}$$

The Gauge Coupling Hierarchy

Key result (conditional on the one-gauge-vertex axiom in each sector)**:** All gauge couplings shift with gravitational potential according to $\delta\alpha_i/\alpha_i = k_i\psi$ with $k_i = \alpha_i^2/(2\pi)$.
Hierarchy: $k_s : k_w : k_\alpha \approx 260 : 20 : 1$
The strong force is $\sim 260\times$ more sensitive to ψ than electromagnetism.

B. Connection to the β-Function

a. The one-loop β-function. The running of gauge couplings with energy scale μ is governed by:

$$\frac{d\alpha_i}{d\ln\mu} = \frac{b_i\alpha_i^2}{2\pi}, \tag{229}$$

where b_i is the one-loop coefficient:

$$b_1 = +\frac{41}{10} \quad (\mathrm{U}(1)_Y), \tag{230}$$

$$b_2 = -\frac{19}{6} \quad (\mathrm{SU}(2)_L), \tag{231}$$

$$b_3 = -7 \quad (\mathrm{SU}(3)_c). \tag{232}$$

b. Connection to the beta functions. Comparing Eqs. (224) and (229):

$$\boxed{k_i = \frac{\beta_i}{b_i}} \tag{233}$$

The ψ-gauge coupling equals the β-function divided by the group-theory coefficient.

C. Modified Renormalization Group Equations

In the presence of non-zero ψ, gauge couplings depend on both energy scale and gravitational potential:

$$\alpha_i(\mu,\psi) = \alpha_i(\mu,0)\left(1 + \frac{\alpha_i^2}{2\pi}\psi\right). \tag{234}$$

Taking the scale derivative at fixed ψ:

$$\frac{d\alpha_i(\mu,\psi)}{d\ln\mu} = \frac{d\alpha_i(\mu,0)}{d\ln\mu}\left(1 + \frac{\alpha_i^2\psi}{2\pi}\right) + \alpha_i \cdot \frac{2\alpha_i}{2\pi}\frac{d\alpha_i}{d\ln\mu}\psi. \tag{235}$$

The modified β-function:

$$\boxed{\frac{d\alpha_i}{d\ln\mu} = \frac{b_i\alpha_i^2}{2\pi}\left[1 + \frac{3\alpha_i^2}{2\pi}\psi\right]} \tag{236}$$

The ψ-correction is proportional to α_i^4—a **two-loop-like gravitational correction** to the running.

a. Laboratory effects. For QCD near confinement ($\alpha_s \sim 1$):

$$\frac{\delta\beta_s}{\beta_s} \sim \frac{3\alpha_s^2\psi}{2\pi} \sim 0.5\psi. \tag{237}$$

In laboratory environments ($\psi \sim 10^{-9}$), this is $\sim 5 \times 10^{-10}$—unmeasurable directly, but the k_s coupling itself has dramatic consequences for nuclear physics.

D. Asymptotic Freedom and UV Behavior

a. QCD decoupling. QCD is asymptotically free: $\alpha_s(\mu) \to 0$ as $\mu \to \infty$. This implies:

$$k_s(\mu) = \frac{\alpha_s^2(\mu)}{2\pi} \to 0 \quad \text{as } \mu \to \infty. \tag{238}$$

The strong sector decouples from ψ in the ultraviolet.

b. Maximum sensitivity at confinement. Conversely, k_s is *maximal* at the confinement scale where $\alpha_s \sim 1$:

$$k_s^{\max} \sim \frac{1}{2\pi} \approx 0.16. \tag{239}$$

This explains why nuclear physics provides the strongest low-energy probe of ψ-gauge coupling: the effective coupling k_s peaks precisely at the energy scale relevant for nuclear binding.

c. QED behavior. QED is not asymptotically free; α increases slowly with energy. The Landau pole occurs at $\mu \sim 10^{286}$ eV, far above the Planck scale. For practical purposes, k_α remains approximately constant.

E. Nuclear Clock Prediction: Thorium-229

The $k_s/k_\alpha \approx 260$ hierarchy, combined with the exponential sensitivity of QCD through dimensional transmutation, leads to dramatic predictions for nuclear transitions.

a. The thorium-229 isomer. ^{229}Th has a nuclear isomer with uniquely low transition energy:

$$E_m = 8.3557 \text{ eV}. \tag{240}$$

This arises from near-cancellation between Coulomb ($\sim +300$ keV) and nuclear strong-force (~ -300 keV) contributions, with a residual of only ~ 8 eV.

b. Sensitivity coefficients. The isomer energy depends on fundamental constants through:

$$\frac{\delta E_m}{E_m} = K_\alpha \frac{\delta\alpha}{\alpha} + K_q \frac{\delta X_q}{X_q}, \tag{241}$$

where $X_q \equiv m_q/\Lambda_{\rm QCD}$ and from nuclear structure calculations:

$$K_\alpha \approx 10^4, \qquad K_q \approx -10^4. \tag{242}$$

c. The $\Lambda_{\rm QCD}$ amplification. The QCD scale is determined by dimensional transmutation:

$$\Lambda_{\rm QCD} = \mu \exp\left(-\frac{2\pi}{|b_3|\alpha_s(\mu)}\right). \tag{243}$$

Differentiating:

$$\frac{\delta\Lambda_{\rm QCD}}{\Lambda_{\rm QCD}} = \frac{2\pi}{|b_3|\alpha_s^2}\,\delta\alpha_s = \frac{2\pi}{|b_3|\alpha_s}\,\frac{\delta\alpha_s}{\alpha_s} \approx 7.6\,\frac{\delta\alpha_s}{\alpha_s}. \tag{244}$$

The factor $2\pi/(|b_3|\alpha_s) \approx 7.6$ represents the exponential amplification of relative coupling changes through dimensional transmutation. (Note: the coefficient of the *absolute* change $\delta\alpha_s$ is the larger number $2\pi/(|b_3|\alpha_s^2) \approx 64$; these two bookkeeping conventions must not be mixed.) With $k_s \propto \alpha_s^2$ this shift equals $\alpha_s(\mu)\,\psi/|b_3|$ and so depends on the scale μ at which it is evaluated; the estimates below take $\mu = M_Z$.

d. The DFD enhancement factor. Combining the above with $\delta X_q/X_q \approx -\delta\Lambda_{\rm QCD}/\Lambda_{\rm QCD}$ and using $\delta\alpha_s/\alpha_s = k_s\psi$:

$$\begin{aligned}\frac{\delta E_m}{E_m} &= K_\alpha k_\alpha \psi - K_q \times \frac{2\pi}{|b_3|\alpha_s}\,k_s\,\psi \\ &= \left(10^4 \times 8.5 \times 10^{-6} + 7.6 \times 10^4 \times 2.2 \times 10^{-3}\right)\psi \\ &\approx (0.085 + 167)\psi \approx +170\,\psi.\end{aligned} \tag{245}$$

For comparison, an optical atomic clock has $\delta\nu_{\rm opt}/\nu_{\rm opt} \approx -\psi/2$ ($\nu \propto e^{-\psi/2}$, Sec. IV H 4).

Nuclear Clock Enhancement: Unscreened Extended-Channel Estimate

$$\boxed{\mathcal{R} \equiv \frac{(\delta\nu/\nu)_{\text{Th-229}}}{(\delta\nu/\nu)_{\rm optical}} \approx -340^{+600}_{-240}} \tag{246}$$

Caveat: This is the *unscreened* gauge-sector estimate. The screened treatment in Sec. XI F, incorporating the $\mu_{\rm LPI}$ screening function and 2026 Th-229 reproducibility data, substantially reduces the expected amplitude and compresses the surviving annual signal window to 26 Hz–$\mathcal{O}$(1 kHz). The unscreened value above serves as the theoretical ceiling, not the experimental target.

Physical origin:

1. $k_s \gg k_\alpha$ (matching coefficients of the extended channel): Strong force couples to ψ more strongly
2. Dimensional transmutation: $\Lambda_{\rm QCD}$ exponentially sensitive to α_s
3. Near-cancellation: 8 eV isomer is tiny residual of $\sim$MeV forces

e. Experimental test protocol. The following estimates use the *unscreened* enhancement $|\mathcal{R}| \approx 340$. The screened predictions, which are the operationally relevant ones for terrestrial experiments, are given in Sec. XI F.

Height experiment (1 m separation), unscreened:

$$\text{GR:} \quad \frac{\Delta(\nu_{\rm Th}/\nu_{\rm Sr})}{\nu_{\rm Th}/\nu_{\rm Sr}} = 0, \tag{247}$$

$$\text{DFD (unscreened):} \quad \frac{\Delta(\nu_{\rm Th}/\nu_{\rm Sr})}{\nu_{\rm Th}/\nu_{\rm Sr}} \approx 3.7 \times 10^{-14}. \tag{248}$$

Annual modulation (solar potential), unscreened:

$$\text{GR:} \quad \left|\frac{\Delta(\nu_{\rm Th}/\nu_{\rm Sr})}{\nu_{\rm Th}/\nu_{\rm Sr}}\right|_{\rm annual} = 0, \tag{249}$$

$$\text{DFD (unscreened):} \quad \left|\frac{\Delta(\nu_{\rm Th}/\nu_{\rm Sr})}{\nu_{\rm Th}/\nu_{\rm Sr}}\right|_{\rm annual} \approx 5 \times 10^{-8}. \tag{250}$$

f. Timeline. ^{229}Th nuclear clocks are under active development:

- 2024: First laser excitation of nuclear transition demonstrated
- 2024: Th/Sr frequency ratio at $\sim 10^{-12}$
- 2028–30: Improved precision to $\sim 10^{-15}$

The DFD prediction is testable within 2–3 years.

F. Cosmological $\alpha(z)$ Variation

If the cosmological gravitational potential ψ evolves with redshift, then α evolves accordingly.

a. Cosmological potential. In DFD, the cosmological scalar field tracks the matter density:

$$\psi(z) = \frac{\xi_{\rm LPI}^{\rm res}}{2}\Omega_m(z), \tag{251}$$

where $\xi_{\rm LPI}^{\rm res}$ is the residual screened cavity/clock coupling scale discussed in Sec. XII and

$$\Omega_m(z) = \frac{\Omega_{m,0}(1+z)^3}{\Omega_{m,0}(1+z)^3 + \Omega_\Lambda}. \tag{252}$$

This expression omits radiation, and so do the high-redshift entries that use it; the radiation era is not modelled here, so the CMB and BBN entries are matter-dominated estimates.

b. The $\alpha(z)$ prediction. Combining with $k_\alpha = \alpha^2/(2\pi)$:

$$\frac{\Delta\alpha}{\alpha}(z) = k_\alpha[\psi(z) - \psi_0] = \frac{\xi_{\rm LPI}^{\rm res}\alpha^2}{4\pi}\left[\Omega_m(z) - \Omega_{m,0}\right]. \tag{253}$$

Numerically,

$$\frac{\Delta\alpha}{\alpha}(z) \approx 4.2\times10^{-6}\,\xi_{\rm LPI}^{\rm res} \times \left[\Omega_m(z) - 0.312\right], \tag{254}$$

where the physically relevant $\xi_{\rm LPI}^{\rm res}$ is a much smaller screened residual.

c. Numerical predictions.

Epoch	Redshift	$\Omega_m(z)$	$\Delta\alpha/\alpha$ (DFD)
Quasars	2	0.92	$+2.6\,\xi_{\rm LPI}^{\rm res}\times10^{-6}$
CMB	1100	1.00	$+2.9\,\xi_{\rm LPI}^{\rm res}\times10^{-6}$
BBN	10^9	1.00	$+2.9\,\xi_{\rm LPI}^{\rm res}\times10^{-6}$

d. Comparison with observational bounds. **Laboratory input.** In DFD the cosmological α-variation is controlled by the same residual LPI scale $\xi_{\rm LPI}^{\rm res}$ discussed for cavity–atom tests (Sec. XII). We treat $\xi_{\rm LPI}^{\rm res}$ as an experimentally determined input, not a cosmology fit parameter. Cosmological bounds therefore constrain the laboratory value of this residual scale.

TABLE XXII. Observational probes of fine-structure constant variation.

Probe	z	DFD pred.	Observed
ESPRESSO	1.15	$+2.1\,\xi_{\rm LPI}^{\rm res}$ ppm	$(+1.3\pm1.3)$ ppm
Quasar dipole	1–3	—	~ 10 ppm
CMB	1100	$+2.9\,\xi_{\rm LPI}^{\rm res}$ ppm	< 2000 ppm
BBN	10^9	$+2.9\,\xi_{\rm LPI}^{\rm res}$ ppm	< 20000 ppm

References: ESPRESSO [55]; dipole [56, 57]; CMB [58]; BBN [59].

Using the conservative ppm-level quasar constraints, the scaling $\Delta\alpha/\alpha \sim (2.6\times10^{-6})\,\xi_{\rm LPI}^{\rm res}$ at $z = 2$ implies that an order-unity cosmological residual would already be uncomfortable.

Status:

- BBN and CMB: Satisfied for $\xi_{\rm LPI}^{\rm res} \le 1$ with $> 100\times$ margin.
- Quasars: For $\xi_{\rm LPI}^{\rm res}$ of order unity, bounds become constraining. Current quasar systematics are debated [57].
- The cosmological prediction is only as clean as the laboratory determination of the residual coupling scale.

e. Distinctive signatures. DFD predicts specific features distinguishing it from other varying-α models:

1. **Functional form:** $\Delta\alpha/\alpha$ tracks $\Omega_m(z)$, flat for $3 \lesssim z \lesssim 100$ and falling steeply for $z < 1$
2. **Sign:** $\Delta\alpha/\alpha > 0$ (larger α in the past) in the matter era
3. **Spatial correlation:** $\Delta\alpha/\alpha$ should correlate with local matter density

f. Future tests. The ELT/ANDES spectrograph will achieve $\sigma(\Delta\alpha/\alpha) \sim 10^{-7}$ per quasar system, tightening constraints on the residual cosmological coupling scale $\xi_{\rm LPI}^{\rm res}$ and potentially detecting a ppm-level signal if that screened residual lies near the upper end allowed by the clock sector.

G. Grand Unification

a. Standard unification picture. The SM gauge couplings approximately unify at $M_{\rm GUT} \sim 10^{15-16}$ GeV, but with a mismatch of ~ 3–5%.

b. DFD corrections. Couplings measured today include ψ-corrections from cosmological evolution:

$$\alpha_i^{\rm today} = \alpha_i^{\rm GUT}\left(1 + k_i^{\rm low}\Delta\psi\right), \tag{255}$$

where $\Delta\psi = \psi_{\rm today} - \psi_{\rm GUT}$ is the change in the cosmological scalar field of Eq. (251), assumed here to satisfy $|\Delta\psi| \lesssim 1$; the homogeneous background of App. Q is not included.

c. Differential corrections.

$$\left|\frac{\delta\alpha_1}{\alpha_1}\right| \lesssim 5\times10^{-5}, \tag{256}$$

$$\left|\frac{\delta\alpha_2}{\alpha_2}\right| \lesssim 2\times10^{-4}, \tag{257}$$

$$\left|\frac{\delta\alpha_3}{\alpha_3}\right| \lesssim 2\times10^{-3}. \tag{258}$$

d. Effect on unification. The relative shift in the unification condition:

$$\frac{|\delta(\alpha_3 - \alpha_1)|}{\alpha_{\rm GUT}} \sim (k_3 - k_1)|\Delta\psi| \lesssim 2\times10^{-3}. \tag{259}$$

Since $k_3 > k_2 > k_1$, the correction has the sign of $\Delta\psi$, which the matter-era expression (251) does not fix at the GUT epoch; its size is at most about 5% of the total SM mismatch. This is smaller than current theoretical uncertainties.

H. Vacuum Energy Feedback

The ψ-gauge coupling creates a feedback loop connecting vacuum energy, gravitational potential, and gauge couplings:

$$\rho_{\rm vac} \xrightarrow{\text{source}} \psi \xrightarrow{\text{shift}} \alpha_i \xrightarrow{\text{loops}} \rho_{\rm vac}$$

a. Self-consistency condition. Let $\psi = F(\rho_{\rm vac})$ be the sourcing relation and $\rho_{\rm vac} = G(\alpha_i(\psi))$ be the loop contribution. Fixed points satisfy $\psi^* = \Phi(\psi^*)$.

b. Naive stability estimate. Linearizing around $\psi = 0$:

$$\psi^* = \frac{\psi_0}{1-\lambda}, \tag{260}$$

where:

$$\lambda \sim \frac{M_P^4}{\rho_c} \times \frac{\alpha^3}{128\pi^3} \sim 10^{113}. \tag{261}$$

c. Interpretation. That denominator is the source of the 10^{113}. The critical density ρ_c is an output of the exponent identity $G\hbar H_0^2/c^5 = C\alpha^{57}$, not an input, and the Planck-scale quantity that belongs in that denominator is the gradient stiffness $c^4/(32\pi G) \sim M_P^2$ of the ψ kinetic term (ψ carries no potential term). In the dimensionless ratio $\delta V/M_P^4$ the one-loop feedback is bounded, $|\delta V_{\rm CW}^{(1)}/M_P^4| \le O(\alpha^2)$ (Ext. Deriv. App. AH, vacuum stability, where the dimensional reading in $\rho_{\rm vac}$ is recorded beside it).

Constraint on UV completion: Any UV completion of DFD must make the ψ-vacuum energy feedback loop stable. Separately, primed-determinant scaling fixes the exponent in $(H_0 t_P)^2 = C\alpha^{57}$, with $C = 1$ on bound-matter clocks (Postulate ZS.11) and C measured on the early clock (Section XIX). This feedback loop concern is about UV stability, not the Λ value.

I. Summary of Falsifiable Predictions

TABLE XXIII. Tier 1: Nuclear clock tests (unscreened gauge-sector estimates; see Sec. XI F for screened predictions)

Observable	GR	DFD (unscreened)	Timeline
Th/Sr ratio (1m height)	0	3.7×10^{-14}	2026–27
Th/Sr annual modulation	0	5×10^{-8}	2026–27
Nuclear vs optical sign	Same	Opposite	2026–27

Note: These are unscreened estimates. The screened treatment in Sec. XI F, incorporating $\mu_{\rm LPI}$ screening and 2026 Ooi reproducibility data, compresses the surviving signal window to 26 Hz–$\mathcal{O}$(1 kHz). If the measured Th/Sr enhancement is consistent with unity at 5σ *and* the cross-species atomic channels also show persistent nulls, the DFD gauge-sector coupling structure would be falsified.

TABLE XXIV. Tier 2: Constraining medium-term tests

Observable	**DFD pred.**	**Current**	**Test**
$\Delta\alpha/\alpha$ ($z \sim 2$)	$\approx 2.6\,\xi_{\rm LPI}^{\rm res}$ ppm	ppm-level	ELT
$\alpha(z)$ shape	$\propto \Omega_m(z)$	—	ELT
Spatial α corr.	$\propto \delta_m$	—	ELT

TABLE XXV. Tier 3: Theoretical consistency tests

Quantity	DFD prediction	Status
GUT shift	$\lesssim 0.2\%$	Below precision
Modified β	$\delta\beta \propto \alpha^4\psi$	Unmeasurable
CC feedback	$\lvert\delta V_{\rm CW}^{(1)}/M_P^4\rvert \le O(\alpha^2)$	Bounded

a. Hierarchy of tests.

1. **Nuclear clocks** test the core relation $k_i = \alpha_i^2/(2\pi)$. Confirmation validates the entire gauge-ψ framework.
2. **Cosmological** $\alpha(z)$ tests the ψ-cosmology connection, independent of nuclear physics uncertainties.
3. **GUT and CC constraints** test high-energy implications, relevant once Tiers 1–2 are confirmed.

Summary: Gauge Coupling Variation

Universal coupling: $\delta\alpha_i/\alpha_i = k_i\psi$ with $k_i = \alpha_i^2/(2\pi)$
Hierarchy: $k_s : k_w : k_\alpha \approx 260 : 20 : 1$
Nuclear clock (unscreened): $\mathcal{R} \approx -340$; screened predictions in Sec. XI F
Cosmological α: $\Delta\alpha/\alpha \sim 3 \times 10^{-6}\,\xi_{\rm LPI}^{\rm res}$ at quasar redshifts
Falsification criteria:

- Persistent nulls across all clock channels (same-ion, cross-species, nuclear) falsifies the gauge-sector framework
- $\mathcal{R} \approx 1$ with high precision rules out DFD gauge coupling

X. CONVENTION-LOCKED α FROM THE MICROSECTOR

The preceding sections derived α-relations from gauge emergence and electroweak physics. This section presents the *microsector completion*: a closed form for $\alpha^{-1} = 137.036$ from the internal geometry [60], with all conventions locked and no hidden tuning parameters. The closed form is exact under two stated choices (§X C); its integers alone give the measured value to 21 ppm, and with the bracket coefficient $c = 1/13$, whose provenance is open (Remark X.4), it lies 4.9×10^{-9} (0.0049 ppm) from the CODATA 2022 value, 32 times that value's uncertainty.

A. Design Constraint: No Hidden Tuning Parameters

We impose a *no-knobs policy*: once the microsector geometry, bundle data, and truncation level are fixed, the predicted α must be stable without invoking subleading heat-kernel terms as ppm-level tuners. Concretely, α's trace is taken in a form whose heat trace terminates, so no $a_6, a_8, \ldots$ term exists to act as a free correction dial (Sec. X C).

a. Motivation. Any theory that "predicts" a fundamental constant but allows ppm-level adjustments via regulator moments or trace normalizations is not truly predictive—it has hidden knobs. The microsector completion must lock all such freedoms.

B. Operator Choice (Locked)

On the internal microsector $X = \mathbb{C}P^2 \times S^3$, we take a Laplace-type operator given by the *connection Laplacian*:

$$P = -g^{ij}\nabla_i\nabla_j, \tag{262}$$

acting on the internal bundle that carries the emergent gauge degrees of freedom.

a. Bundle structure. The U(1) factor is implemented via twisting by a line bundle over $\mathbb{C}P^2$ with curvature proportional to the Kähler form ω, taken trivial over S^3. This choice is minimal and convention-stable: the Kähler form is parallel ($\nabla\omega = 0$), so derivative terms in higher Seeley–DeWitt coefficients vanish automatically.

b. Why this is locked. The gauge-kinetic extraction from a_4 is unambiguous with this operator choice. Alternative operators would introduce additional terms proportional to curvature derivatives, creating ppm-level ambiguities. The connection Laplacian with parallel curvature eliminates this freedom. On the $S^3 = SU(2)$ factor the operator is taken as the ρ-shifted Casimir $\Delta + 1$, the natural Laplacian of the group, whose heat kernel is a pure Gaussian (§X C).

C. Regularization/Truncation Rule (Locked)

We define the spectral action with a cutoff function f:

$$S = \mathrm{Tr}\, f(P/\Lambda^2). \tag{263}$$

a. The plateau rule holds only in even total dimension. A plateau cutoff, constant near the origin so that $f^{(n)}(0) = 0$ for all $n \geq 1$, makes the negative moments $f_{-2} = f_{-4} = \cdots = 0$ vanish, and in even total dimension those moments carry $a_6, a_8, \ldots$. On the seven-dimensional $\mathbb{C}P^2 \times S^3$ they do not: there a_6 carries the moment $\Lambda \int_0^\infty u^{-1/2} f(u)\, du/\sqrt{\pi}$, which is positive for every cutoff. For the connection Laplacian of Eq. (262) with its U(1) twist, $a_6/a_4 = 19/5$ (14/5 from $\mathbb{C}P^2$, 1 from S^3), a correction of 25% (Gaussian) to 38% (sharp) of the a_4 term at the cutoff of Eq. (267), and up to 59% for smooth plateaus (computed). A single joint seven-dimensional trace therefore does not support the closed form.

b. The exact construction. The closed form of §X I is reproduced exactly by α's trace taken in two factors. On $\mathbb{C}P^2$, which is four-dimensional, the $\zeta(0)$ of the charge trace equals a_4 exactly: $-1/24$ per unit charge squared, independent of the radius. On $S^3 = SU(2)$ the ρ-shifted Casimir $\Delta + 1$ has a heat trace that terminates, $\sum_{m\geq 1} m^2 e^{-tm^2} = (\sqrt{\pi}/4)\, t^{-3/2}$ up to exponentially small terms, so that with the heat-kernel (Gaussian) regulator its contribution is exactly $(\sqrt{\pi}/4)\Lambda^3$. Their product gives Eq. (276) with no remainder (to 6×10^{-63}, computed). The closed form is therefore exact under two stated choices: the ρ-shifted Casimir as the operator on $S^3 = SU(2)$, and α's trace taken as the $\mathbb{C}P^2$ $\zeta(0)$ times the S^3 factor with the heat-kernel regulator, which is consistent with α having its own trace, separate from gravity's (App. WS). Read as one joint seven-dimensional action the construction would need a $\mathbb{C}P^2$ radius far from the Einstein product. It does not derive the cutoff of Eq. (267) or the bracket of Remark X.4, which stay as printed.

c. Why this is locked. The exact construction has no subleading heat-kernel term, so none can act as a ppm-level tuning knob, and no cutoff moment is tuned:

1. The a_4 gauge kinetic term is the whole $\mathbb{C}P^2$ factor
2. No subleading heat-kernel contribution exists
3. No moment is tuned

D. Finite-k Truncation and the $(k+3)/(k+4)$ Factor (Locked)

We implement a finite-k truncation via Toeplitz quantization at level $m = k + 3$ on $\mathbb{C}P^1$, where:

$$d = \dim H^0(\mathbb{C}P^1, \mathcal{O}(m)) = m + 1 = k + 4. \tag{264}$$

a. Origin of the +3 shift: an exact charge-trace theorem. The shift is not an assumption about a restricted line bundle. It is the exact finite-level value of the hypercharge second moment on $\mathbb{C}P^2$ itself, and it follows from the following theorem, which holds on $\mathbb{C}P^n$ for every traceless charge.

Theorem X.1 ($\mathbb{C}P^n$ Toeplitz charge trace)**.** *Let $H_k = H^0(\mathbb{C}P^n, \mathcal{O}(k)) \cong \mathrm{Sym}^k(\mathbb{C}^{n+1})$ be the level-k Toeplitz (geometric-quantization) Hilbert space, let $Q = \mathrm{diag}(q_0, \ldots, q_n)$ be a* traceless *charge — a* U(1) *in the Cartan of $\mathfrak{su}(n+1)$ — and let $\hat{Q}$ be the operator by which Q acts on H_k. Then*

$$\mathrm{Tr}_{H_k}\left(\hat{Q}^2\right) = \mathrm{Tr}(Q^2)\binom{k+n+1}{n+2}, \qquad \dim H_k = \binom{k+n}{n}. \tag{265}$$

The result is exact at every level*: it is a closed-form identity, not the leading term of a $1/k$ expansion.*

Proof. In the monomial weight basis of $\mathrm{Sym}^k(\mathbb{C}^{n+1})$, indexed by exponent vectors m with $|m| = k$, the operator $\hat{Q}$ is diagonal with eigenvalue $\mu_m = \sum_i q_i m_i$. Introduce the two-variable generating function

$$G(z,u) \;=\; \sum_m z^{|m|} u^{\sum_i q_i m_i} \;=\; \prod_{i=0}^{n} \bigl(1 - z\,u^{q_i}\bigr)^{-1}.$$

Tracelessness gives $(u\partial_u)\log G\big|_{u=1} = \bigl(\sum_i q_i\bigr)\, z/(1-z) = 0$, while $(u\partial_u)^2 \log G\big|_{u=1} = \bigl(\sum_i q_i^2\bigr)\, z/(1-z)^2 = \mathrm{Tr}(Q^2)\, z/(1-z)^2$. Since $(u\partial_u)^2 G = G\bigl[\bigl((u\partial_u)\log G\bigr)^2 + (u\partial_u)^2 \log G\bigr]$ and $G(z,1) = (1-z)^{-(n+1)}$, the first bracket vanishes at $u=1$ and

$$\sum_{k\geq 0} z^k\, \mathrm{Tr}_{H_k}\Bigl(\hat{Q}^2\Bigr) = \mathrm{Tr}(Q^2)\, \frac{z}{(1-z)^{\,n+3}}.$$

Extracting $[z^k]$ gives $\mathrm{Tr}(Q^2)\binom{k+n+1}{n+2}$. The dimension formula is the standard $\dim \mathrm{Sym}^k(\mathbb{C}^{n+1})$. □

Verification. Exact-integer agreement was checked by direct enumeration of the weight basis for $n = 1, 2, 3, 4$ and $k = 2, \ldots, 12$ over three inequivalent traceless charges at each n, including the asserted proportionality to $\mathrm{Tr}(Q^2)$.

Corollary X.2 (The $(k+3)$ factor)**.** *Specialise Theorem X.1 to the DFD microsector base $n = 2$ with $Q = Y$ the Standard Model hypercharge. Then*

$$\mathrm{Tr}_{H_k}\Bigl(\hat{Y}^2\Bigr) = \mathrm{Tr}(Y^2)\binom{k+3}{4} = \mathrm{Tr}(Y^2)\,\frac{k(k+1)(k+2)(k+3)}{24},$$

$$\dim H_k = \binom{k+2}{2} = \frac{(k+1)(k+2)}{2},$$

$$\bigl\langle \hat{Y}^2 \bigr\rangle_k \equiv \frac{\mathrm{Tr}_{H_k}(\hat{Y}^2)}{\dim H_k} = \mathrm{Tr}(Y^2)\,\frac{k(k+3)}{12} \qquad \textit{(exact).} \tag{266}$$

The classical (continuum) mean square of the level-k moment map on $\mathbb{C}P^2$ is $\mathrm{Tr}(Y^2)\,k^2/12$, the second moment of a traceless linear functional against the Dirichlet$(1,1,1)$ *distribution of Fubini–Study barycentric coordinates ($\mathbb{E}[u_i^2] = 1/6$, $\mathbb{E}[u_i u_j] = 1/12$). Hence*

$$\frac{\textit{quantum}}{\textit{classical}} \;=\; \frac{k+3}{k}$$

exactly, at all orders, with no $1/k$ expansion.

Three consequences, each replacing an assertion:

1. *the numerator $(k+3)$ of the finite-k factor is the exact quantum-to-classical enhancement of the hypercharge second moment — a computed quantity, not a bundle-degree coincidence;*
2. *the 12 in $\pi^{3/2}/24 = \pi^{3/2}/(2\cdot 12)$ belongs to the $\zeta(0)$ of the $\mathbb{C}P^2$ charge trace, $-1/24$ per unit charge squared (§X C);*
3. *$\mathrm{Tr}(Y^2)$ enters at degree* exactly 1*, because Eq. (265) is exactly linear in $\mathrm{Tr}(Q^2)$.*

Remark X.3 (Consistency with the Spin^c reading). The canonical Spin^c structure on $\mathbb{C}P^2$ has $K_{\mathbb{C}P^2} = \mathcal{O}(-3)$, hence $L_{\mathrm{det}} = K^{-1} = \mathcal{O}(3)$, and restriction to $\mathbb{C}P^1 \subset \mathbb{C}P^2$ does send $\mathcal{O}(k) \otimes L_{\mathrm{det}}$ to $\mathcal{O}(k+3)$. That observation is retained here as a *consistency check*: the degree of the determinant line and the shift produced by Theorem X.1 agree because both are the same $\mathbb{C}P^2$ datum $n+1 = 3$ — equivalently, $(k+3)/k$ is the reciprocal of the level-one (adjoint) Berezin-transform eigenvalue, the Berezin shift and the Casimir shift being the same shift. The +3 is thus *computed* on $\mathbb{C}P^2$ rather than *read off* from a restricted bundle degree.

b. The spectral cutoff. The determinant-channel removal at finite d fixes the spectral cutoff as:

$$\Lambda^3 = k \cdot \frac{d-1}{d} = k \cdot \frac{k+3}{k+4}. \tag{267}$$

This is the unique finite-size factor permitted by the truncation rule; it is *not* inserted to improve agreement. The truncation rule also holds the size of the internal space fixed in this formula: on a continuous $\mathbb{C}P^2 \times S^3$ the spectral action of the connection Laplacian lets the volume run away without end (Prop. FK.3), and α would drift with it, while the truncated microsector has no size modulus (Thm. FK.2).

E. The Forced Microsector Fork

At this point there is a *forced binary fork*, determined solely by what finite Hilbert space carries the microsector trace.

1. *Branch A: Regular-Module Microsector (Survives)*

Take the finite Hilbert space to be the algebra itself:

$$\mathcal{H}_F := A = M_d(\mathbb{C}), \tag{268}$$

with Hilbert–Schmidt inner product $\langle X, Y\rangle = \mathrm{Tr}(X^\dagger Y)$, and gauge action by inner derivations:

$$\mathrm{ad}_a(X) = [a, X]. \tag{269}$$

a. Trace normalization. The UV-normalized trace is naturally the democratic normalization per matrix degree of freedom:

$$\mathrm{tr}_{\mathrm{dem}}(\cdot) := \frac{1}{d^2}\,\mathrm{Tr}_{\mathcal{H}_F}(\cdot). \tag{270}$$

b. Conversion to physics normalization. When reporting the final gauge kinetic term in canonical generator normalization on $\mathfrak{su}(d)$:

$$\mathrm{tr}_{\mathfrak{su}}(\cdot) = \frac{1}{d^2-1}\,\mathrm{Tr}_{\mathfrak{su}}(\cdot), \tag{271}$$

the conversion factor is *forced*:

$$\boxed{\varepsilon_{\mathrm{adj}}^{(A)} = \frac{d^2}{d^2-1}} \tag{272}$$

For $k = 60$, $d = 64$:

$$\varepsilon_{\mathrm{adj}}^{(A)} = \frac{4096}{4095} = 1.000244\ldots \tag{273}$$

2. Branch B: Fermion-Representation Microsector (Falsified)

If instead the kinetic term trace is taken over a d-dimensional fermion representation space $\mathcal{H}_F \cong \mathbb{C}^d$ (as in conventional matter spectral triples), unimodularity literally removes the identity generator channel, yielding the drop factor:

$$\varepsilon_{\text{adj}}^{(B)} = \frac{d^2-1}{d^2} = \frac{4095}{4096} = 0.999756\ldots \tag{274}$$

F. Branch Selection by Real-Bimodule Consistency

The apparent fork between the regular-module trace and the fermion-representation trace is resolved by the finite real-bimodule structure of the DFD microsector, not merely by numerical comparison.

The finite Hilbert space used in the closed form for α is *not* the observed fermion Hilbert space; it is the vacuum gauge-frame trace carrier. Since gauge variations act by inner derivations $\mathrm{ad}_a(X) = [a, X]$, the Hilbert space must carry faithful left and right actions of $A = M_d(\mathbb{C})$ and A^{op} satisfying the order-zero condition and mutual commutant closure. By Theorem AD.1 (Appendix AD), the minimal such module is

$$\mathcal{H}_F = L^2(A) \simeq A = M_d(\mathbb{C}), \qquad \dim \mathcal{H}_F = d^2, \tag{275}$$

while the fermion-representation module $\mathcal{H}_F \simeq \mathbb{C}^d$ has commutant $\mathbb{C}$ and *cannot* support a faithful right A^{op} action. Branch B is therefore not a valid DFD vacuum microsector trace carrier; it fails the consistency requirement before any numerical comparison is performed.

Holding all other ingredients fixed (geometry, g_F, hypercharge trace, and the finite-k rule $\Lambda^3 = k(k+3)/(k+4)$), we compute α^{-1} under both microsector trace choices to demonstrate the magnitude of the consistency selection.

a. Numerical comparison.

b. Branch A: forced. The regular-module microsector is the unique minimal faithful real-bimodule trace carrier (Theorem AD.1) and gives the closed form of §X I, which lies 0.0049 ppm from the measured value with the open bracket coefficient; the exact construction of §X C has no higher heat-kernel term.

c. Branch B: structurally excluded. The fermion-rep microsector $\mathcal{H}_F \simeq \mathbb{C}^d$ has commutant only $\mathbb{C}$ and therefore cannot support a faithful right $M_d(\mathbb{C})^{op}$ action. Branch B is excluded *independently* of the 43 ppm numerical mismatch. The mismatch becomes a redundant consistency check rather than the basis for selection.

Note: this exclusion concerns only the DFD vacuum gauge-frame trace carrier. It does *not* imply that $\mathbb{C}^d$ is invalid for ordinary fermion representations elsewhere in the framework.

Microsector Lock

By Theorem AD.1 (Appendix AD), the regular-module microsector completion (Branch A) is the unique minimal faithful real-bimodule trace carrier on the DFD finite algebra $A = M_d(\mathbb{C})$. Branch B fails the bimodule consistency requirement.

Forced microsector:

- Hilbert space: $\mathcal{H}_F = A = M_d(\mathbb{C})$ (regular module)
- Dimension: $\dim(\mathcal{H}_F) = d^2 = 4096$
- Gauge action: inner derivations $\mathrm{ad}_a(X) = [a, X]$
- UV trace: $\mathrm{tr}_{\text{dem}} = (1/d^2)\,\mathrm{Tr}$
- Factor: BOOST $= d^2/(d^2-1) = 4096/4095$

The regular-module branch is therefore not chosen by its numerical value.

G. The Closed-Form Chain

The closed form for α rests on the following chain:

a. Closure of $k_{\max} = 60$. The value $k_{\max} = \chi(\mathbb{C}P^2, \mathcal{O}(N_{\text{gen}} q_1) \oplus \mathcal{O}^{\oplus 5}) = 55 + 5 = 60$ follows from the generation count, $q_1 = 3$ (derived under the electroweak identification) and the five hypercharged multiplet types, through the conditional determinant-line count of Lemma F.11 (conditional on the fixed-kernel reading; the relation of its degree-zero summands to the hypercharge degrees is open, Rem. F.7); since $\mathcal{O}(3) = K^{-1}$, the degree 9 is also $N_{\text{gen}}\, c_1(\mathbb{C}P^2)$. Within the finite-symmetry closure framework adopted in this section, the same value follows from auxiliary structural postulates, which serve as a cross-check:

1. The microsector channel symmetry G acts faithfully on a real three-dimensional generation space.
2. G is orientation-preserving, simple (no hidden normal subgroup) and non-abelian.
3. The channel algebra furnishes exactly five conjugacy classes, matching the five chiral multiplet types in one SM generation.
4. Choose the *minimal* such group.

The icosahedral rotation group $G \cong A_5$ is the only non-abelian simple finite group of rotations of real three-space, so postulates 1 and 2 already fix it, postulate 4 is not needed and its five conjugacy classes are an output; $k_{\max} = |A_5| = 60$. Postulate 2 must say non-abelian, since the cyclic group of order five satisfies the other conditions. The independent Bridge Lemma (Appendix K 4) and minimal-padding argument then function as nontrivial consistency checks rather than as hidden tuners. Once $k_{\max}$ is fixed, only discrete choices remain.

b. Unconditional content. What does *not* depend on the auxiliary postulates is the following: once any integer $k_{\max}$ is fixed, the entire microsector output (α^{-1}, CKM structure, neutrino spectrum) follows with zero

TABLE XXVI. Microsector fork: numerical comparison at $k = 60$, each factor ε entering as $1 + w(\varepsilon - 1)$ with the stated weight $w = 7/80$ of Table XXVII. Branch B is shown for completeness; it is excluded by the bimodule theorem (Appendix AD).

Branch	Factor	α^{-1}	Residual (ppm)
A (regular-module)	$\frac{4096}{4095}$	137.03599985	−0.005
B (fermion-rep, excluded)	$\frac{4095}{4096}$	137.03014445	+42.7
Experimental (CODATA 2022)	—	137.035999177(21)	—

TABLE XXVII. Chain of the closed form for α^{-1}.

Component	Value	Source	Status
$K_{\mathbb{C}P^2} = \mathcal{O}(-3)$	-3	Algebraic geometry theorem	Rigorous
$L_{\text{det}} = K^{-1}$	$\mathcal{O}(3)$	Spin^c structure	Rigorous
$d = k + 4$	64	$\dim H^0(\mathcal{O}(k+3))$	Rigorous
$(d-1)/d$	63/64	Numerator: exact $\mathbb{C}P^2$ charge trace (Cor. X.2); d: Eq. (264)	Derived
N_{species}	7	SM SU(2) components	SM content
$\text{Tr}(Y^2)$	10	SM hypercharges	SM content
g_F	8	Spectral triple ($J \times \gamma \times \mathbb{C}$)	Derived
$w = N_{\text{species}}/(g_F \cdot \text{Tr}(Y^2))$	7/80	Hypercharge weighting	Stated; provenance open (Rem. X.4)
ε_{adj}	4096/4095	Regular-module trace conversion	Forced
α^{-1}	137.03599985	Integers $\times [1 + w(\varepsilon_{\text{adj}} - 1)]$	4.9 ppb (with the open bracket)

continuous free parameters. The count above fixes $k_{\max} = 60$ among the integers; the theory's numerical output is then falsifiable against >30 independent measurements.

H. Sharp Falsifier

The microsector choice $\mathcal{H}_F = A$ is a **testable ontological claim**:

> *"The finite Hilbert space of the DFD Toeplitz microsector is the algebra itself ($M_d(\mathbb{C})$), not a fermion representation space ($\mathbb{C}^d$)."*

a. If future work derives $\mathcal{H}_F = \mathbb{C}^d$ from first principles:

- DFD fails by 43 ppm
- Cannot be rescued without fine-tuning
- Theory requires fundamental revision

b. If future work derives $\mathcal{H}_F = A$ from first principles:

- BOOST factor is forced, not fitted

App. AD goes part of the way: under the standard-form real-bimodule conditions (order zero, faithful left and right actions, mutual commutants) and minimality it excludes $\mathbb{C}^d$ and makes A the carrier; those conditions are adopted as the spectral-triple consistency requirement, not derived from the field equation.

I. The Closed-Form Result

Collecting all locked ingredients, the fine-structure constant is given by a single equation with no continuous free parameters:

$$\boxed{\alpha^{-1} = \frac{\pi^{3/2}}{24}\,\text{Tr}(Y^2)\,k_{\max}\,\frac{k_{\max}+3}{k_{\max}+4} \times \left[1 + \frac{7}{80\cdot 4095}\right] = 137.036} \tag{276}$$

where:

- $\pi^{3/2}/24$: the normalization of the exact construction of §X C: its $1/24$ is the $\zeta(0)$ of the $\mathbb{C}P^2$ charge trace per unit charge squared, and its $\sqrt{\pi}$ is that of the terminating heat trace of the ρ-shifted Casimir on S^3
- $\text{Tr}(Y^2) = 10$: Standard Model hypercharge trace (3 generations of Q_L, u_R, d_R, L_L, e_R)
- $k_{\max} = 60$: topological cutoff from the Bridge Lemma (Spin^c index on $\mathbb{C}P^2$, $= |A_5|$)
- $(k_{\max}+3)/(k_{\max}+4) = 63/64$: the numerator $(k_{\max}+3)$ is the exact quantum-to-classical ratio of the $\mathbb{C}P^2$ hypercharge second moment (Corollary X.2); the denominator $(k_{\max}+4) = d$ is the Toeplitz normalisation of Eq. (264)
- $[1 + 7/(80 \times 4095)]$: regular-module microsector correction ($4095 = 64^2 - 1 = d^2 - 1$); exactly equal to $1 + 1/(13\,k_{\max}^2)$ — see Remark X.4

The closed form gives $\alpha^{-1} = 137.03599985$, 0.0049 ppm from the measured value; the integers alone give 137.03307,

21 ppm below it. The trace in it is the hypercharge trace, and the step that identifies its coefficient with $1/e^2$ rather than with the hypercharge coupling $1/g'^2$ is not derived; since $1/e^2 = 1/g^2 + 1/g'^2$, with $\sin^2\theta_W = 3/13$ (Theorem Z.1) the hypercharge reading would give $\alpha^{-1} = (13/10) \times 137.033 = 178.14$.

Remark X.4 (The bracket carries one integer: an exact identity). The printed microsector correction admits a second exact reading, in which its three integers collapse to one. Since $80 \cdot 4095 = 327600 = 7 \cdot 13 \cdot 3600 = (7\cdot 13)\, k_{\max}^2$ (equivalently $4095/k_{\max}^2 = 91/80$ exactly, and $4095 = 63 \cdot 65 = (k_{\max}+3)(k_{\max}+5)$),

$$1 + \frac{7}{80 \cdot 4095} = 1 + \frac{1}{13\, k_{\max}^2} = 1 + \frac{1}{N_{\rm gen}\, k_{\max}^2} \sin^2\theta_W = 1 + \frac{1}{46800}, \tag{277}$$

using $\sin^2\theta_W = 3/13$ (Theorem Z.1) and $N_{\rm gen} = 3$, so that $(3/13)/3 = 1/13$. The integer $13 = 3 + \mathrm{Tr}(Y^2)$ is the Weinberg denominator of Theorem Z.1 and appears as such in the structural-integer table of Appendix AB 5.

This is a second exact reading, not a correction: the weight $w = N_{\rm species}/(g_F\,\mathrm{Tr}(Y^2)) = 7/80$ is the stated weight of Table XXVII, and both readings evaluate to the same rational $1/46800$. The value of α^{-1} is unchanged at 137.03599985.

What is and is not established. Writing the metaplectic (half-form) level $\kappa = k + 3/2$, Corollary X.2 becomes

$$\langle \hat{Y}^2 \rangle_k = \frac{\mathrm{Tr}(Y^2)}{12}\Big(\kappa^2 - \tfrac{9}{4}\Big), \qquad \dim H_k = \frac{1}{2}\Big(\kappa^2 - \tfrac{1}{4}\Big),$$

both of which are *even* series in $1/\kappa$ that terminate after one term. A finite-level correction that kept this symmetry would be even in $1/\kappa$, with no $1/k$ term; the printed $1/(13k_{\max}^2)$ is even in k, not in κ, so the form is not derived. The *coefficient* c is a different matter: because Eq. (265) is exact at every order, the $\mathbb{C}P^2$ Toeplitz sector generates no such correction at all, so the coefficient's provenance is **open** and is not claimed here. What Eq. (277) establishes is that a mechanism reproducing the closed form would have to supply $1/13$ in the position of a $1/k_{\max}^2$ coefficient. The two readings of the bracket agree only at $k_{\max} = 60$, where $11k^2 - 640k - 1200$ vanishes; they are not one identity in k. The integers alone give $\alpha^{-1} = 137.03307$, 21.4 ppm below the measured value, and with $c = 1/13$ the closed form lies 4.9 ppb from it, 32 times the uncertainty of the CODATA 2022 value; the measured value requires $c = 0.0769053(6)$. The form of the bracket is not fixed at the part-per-billion level, so the ppb figure is a property of this closed form, not a test of the bracket and not an agreement within experimental error.

J. Summary

Summary: Convention-Locked α

Result:

$$\alpha^{-1} = 137.03599985 \quad \text{(4.9 ppb from CODATA with the open bracket; 21 ppm from the integers)} \tag{278}$$

Locked conventions:

- Operator: connection Laplacian with parallel curvature on $\mathbb{C}P^2$; the ρ-shifted Casimir $\Delta + 1$ on $S^3 = SU(2)$
- Regulator: heat-kernel (Gaussian) cutoff in the exact construction; the $\mathbb{C}P^2$ factor enters through $\zeta(0)$
- Finite-k: Toeplitz truncation with $d = k + 4 = 64$
- Microsector: regular-module ($\mathcal{H}_F = M_d(\mathbb{C})$)
- Trace: democratic UV → per-generator physics (BOOST forced)

The fermion-rep microsector is falsified:

- 43 ppm deficit cannot be filled
- Under no-knobs policy, only Branch A survives

Falsification criterion: If $\mathcal{H}_F = \mathbb{C}^d$ is derived from microsector first principles, DFD's α prediction fails.

XI. ATOMIC CLOCK TESTS

Atomic clocks remain one of the sharpest laboratory probes of DFD. One must distinguish *channels*. Same-ion optical comparisons test the pure electromagnetic-sector coupling; cross-species atomic ratios primarily test composition-sensitive structure; and nuclear clocks uniquely access the strong sector. General relativity predicts exact universality for co-located clocks after the common redshift is removed. DFD's minimal action predicts the same universality for co-located clocks (Thm. XI.2); a residual differential response, if present, is channel-dependent and environment-dependent and belongs to the extended non-metric sector (Sec. XV C).

A. Local Position Invariance Framework

a. LPI in metric gravity. Local position invariance (LPI) states that non-gravitational physics is independent of location in a gravitational potential. In GR, all clocks redshift in the same way:

$$\frac{\Delta\nu}{\nu} = \frac{\Delta\Phi}{c^2}. \tag{279}$$

The universal redshift (279) has been verified to 7×10^{-5} by the GP-A rocket experiment and to $\sim 10^{-5}$ in modern optical clock comparisons. For a clock ratio $R = \nu_A/\nu_B$,

the universal GR redshift cancels:

$$\frac{\Delta R}{R} = 0 \qquad \text{(GR, co-located clocks)}. \tag{280}$$

b. Differential coupling language. A convenient way to parameterize a possible violation is

$$\left(\frac{\Delta\nu}{\nu}\right)_A = (1 + K_A)\frac{\Delta\Phi}{c^2}, \tag{281}$$

so that

$$\frac{\Delta R}{R} = (K_A - K_B)\frac{\Delta\Phi}{c^2}. \tag{282}$$

The observable is therefore the *difference* in effective couplings, not the absolute redshift of either clock alone.

B. Common-Factor Cancellation and Observable Residuals

a. The structural point. Every local transition frequency can be decomposed as

$$\nu_A(\psi, a) = U(\psi, a)\,\hat{\nu}_A(\psi, a), \tag{283}$$

where $U(\psi, a)$ is the **common electromagnetic scale factor** shared by all clocks (encoding the universal coupling of ψ to the electromagnetic vacuum), and $\hat{\nu}_A$ is a **dimensionless structure-dependent residual** specific to transition A.

For any co-located clock ratio,

$$R_{AB} \equiv \frac{\nu_A}{\nu_B} = \frac{\hat{\nu}_A}{\hat{\nu}_B}, \tag{284}$$

so the common factor U cancels **identically**.

Theorem XI.1 (Clock-ratio cancellation of the common sector)**.** *For co-located clocks A, B admitting the factorization (283) with the same common factor $U(\psi, a)$, any differential LPI observable formed from their ratio depends only on the residual internal-structure response:*

$$\delta \ln\left(\frac{\nu_A}{\nu_B}\right) = \delta \ln \hat{\nu}_A - \delta \ln \hat{\nu}_B. \tag{285}$$

Proof. Insert (283) into $R_{AB} = \nu_A/\nu_B$ to obtain (284). Taking a logarithmic variation, the universal factor U cancels algebraically. □

Theorem XI.2 (Null of the co-located ratio under the minimal action)**.** *Let matter couple to ψ only through the physical metric (12)—the minimally coupled $S_{\rm matter}$ of (20), with $S_{\rm int}$ at $h_{ij}^{\rm TT} = 0$—through a diffeomorphism-invariant action (regulator included), and let $\psi = \psi_0$ be constant over the co-located comparison. The map $t = e^{+\psi_0/2}T$, $\mathbf{x} = e^{-\psi_0/2}\mathbf{X}$ pulls $\tilde{g}_{\mu\nu}$ back to $\mathrm{diag}(-c^2, 1, 1, 1)$ exactly, so every transition frequency of every species carries the same factor and*

$$\frac{d}{d\psi_0} \ln \frac{\nu_A}{\nu_B} = 0 \tag{286}$$

identically, to all orders; equivalently $K_A^{\rm obs} = 0$ for every A in (289). A nonzero co-located ratio response therefore requires an operator outside $S_{\rm matter}$, a non-metric term of the form (352); each λ_I in (289) is the coefficient of such a term, and the ψ-linear vertex of the minimally coupled electromagnetic action is the energy-density sourcing vertex (Thm. II.1, Eq. (R13)), not a varying-α operator. If ψ varies over the comparison, the gradient and tidal remainders over a laboratory are $\lesssim 10^{-43}$ and the adiabatic remainder $\dot{\psi}_0/\omega$ is $\sim 10^{-32}$, in fractional frequency. Special cases already in print: Thm. ZS.3 (homogeneous cosmology) and the metric-level universality of Sec. XV B (free fall).

Corollary XI.3 (Kennedy–Thorndike null (minimal sector))**.** *Under the hypotheses of Thm. XI.2, let the laboratory move with any constant velocity $\mathbf{V}$ relative to the preferred (CMB) frame. Every co-located proper frequency ratio is then independent of $\mathbf{V}$,*

$$B_{\rm KT} \equiv \frac{\partial}{\partial(V^2/c^2)} \ln \frac{\nu_{\rm cav}}{\nu_{\rm atom}}\bigg|_{\psi_0} = 0, \tag{287}$$

identically, to all orders in V/c: the Robertson–Mansouri–Sexl combination $\beta_{\rm RMS} - \alpha_{\rm RMS} - 1$ vanishes, and the same map gives the Michelson–Morley (isotropy) null. A Kennedy–Thorndike signal therefore requires either a ψ gradient across the apparatus or an operator coupling matter to the preferred-frame flow u^μ, which neither $S_{\rm matter}$ nor the non-metric family (352) (scalars in ψ, boost-blind at fixed ψ by the same map) contains.

Proof. The map $t = e^{+\psi_0/2}T$, $\mathbf{x} = e^{-\psi_0/2}\mathbf{X}$ of Thm. XI.2 makes the physical metric (12) exactly Minkowskian; the optical metric (29) is $e^{-\psi}$ times it (App. AN), so the light cone is shared, and the Maxwell action is conformally invariant. Every minimally coupled matter and radiation action is therefore its Minkowski form in $(T, \mathbf{X})$ and is Poincaré invariant there, with $d\tau/dt = e^{-\psi_0/2}\sqrt{1 - V^2/c^2}$ from (12) and $\mathbf{V} = e^{\psi_0}\,d\mathbf{x}/dt = d\mathbf{X}/dT$ the physical velocity. A Lorentz boost of $(T, \mathbf{X})$ brings the laboratory to rest, where every proper frequency is the same function of the local physics as at $\mathbf{V} = 0$; the ratio is thus $\mathbf{V}$-independent, and a $\mathbf{V}$-dependence can enter only through an operator not built from $\tilde{g}_{\mu\nu}$ and ψ alone, or through $\nabla\psi \neq 0$ over the apparatus. □

Remark XI.4 (Unequal-arm round trip, remainders, and what the minimal sector predicts). Explicitly, a cavity of proper length L along $\mathbf{V}$ has coordinate length L/γ and round-trip coordinate time $(L/\gamma)[(c - V)^{-1} + (c + V)^{-1}] = 2\gamma L/c$, i.e. proper time $2L/c$; a transverse arm gives the same, so an unequal-arm interferometer has $\Delta\tau_{\rm rt} = 2(L_1 - L_2)/c$ with $\partial\Delta\tau_{\rm rt}/\partial V = 0$. Corollary XI.3 is the matter-sector counterpart of Thm. IV.1: the preferred foliation enters only the gravitational sector, through the temporal invariant Δ of Eq. (Q4), and at fixed ψ the matter–radiation sector carries no trace of it. Three remainders survive, all from the corpus's own inputs ($w \equiv V$ in Thm. IV.1). (i) The preferred-frame g_{00} term of Thm. IV.1(ii), $\alpha_{\rm eff}(V^2/c^2)(U/c^2)$, modulates

the laboratory potential with the annual change of the boost, $\delta(V^2/c^2) = 2V_{\rm CMB}v_\oplus/c^2 = 2.4\times10^{-7}$, by at most $3.8\times10^{-8}\times2.4\times10^{-7}\times9.9\times10^{-9} = 9\times10^{-23}$ in fractional frequency (Eq. (85) at 1 AU, unsaturated; $\approx 6\times10^{-33}$ with the saturation factor $\mu'(\Delta)\sim6.6\times10^{-11}$ of Thm. IV.1(iii)); this modulation is common to all co-located clocks and cancels in the ratio by Thm. XI.2. (ii) The tidal variation of ψ over a cavity of length L is $\sim 2gL^2/(c^2R_\oplus) = 3\times10^{-23}$ for $L = 1$ m (the $\lesssim 10^{-43}$ of Thm. XI.2 is this term at $L = a_B$, the Bohr radius). (iii) The species couplings of Eq. (352) are boost-blind at fixed ψ and enter only through $\nabla\psi$. All lie far below the measured null, $\beta_{\rm RMS} - \alpha_{\rm RMS} - 1 = -1.7(4.0)\times10^{-8}$ (sidereal; weighted mean $-4.8(3.7)\times10^{-8}$) [61], which improved on the 2×10^{-13} fractional-frequency null of Ref. [62]. Two corollaries. (a) In Einstein-equivalence-principle language the minimal sector has universal free fall, exact local Lorentz invariance at fixed ψ, and local-position-invariance residuals only through the species couplings of Eq. (352): a co-located ratio fitted as $\delta R/R = K_{AB}\,\Delta\Phi/c^2 + B_{AB}\,\Delta V^2/c^2 + C_{AB}\,(\hat{\mathbf{n}}\cdot\mathbf{V}/c)$ has $B_{AB} = C_{AB} = 0$ predicted exactly, with K_{AB} the only admissible residual (zero under the minimal action, Thm. XI.2). (b) A spatially uniform ψ_0 is removed by the rescaling and is unobservable in the minimal local sector, so local minimal-sector observables depend on ψ only through its derivatives, through comparison between separated regions, or through the non-metric species couplings (the local counterpart of Thm. ZS.3).

Theorem XI.2 is the general case of this cancellation and of the cavity–atom cancellation proven in Sec. XII A: under the minimal action no residual survives in a co-located ratio, so a structure-dependent residual, if observed, is a coefficient of the extended non-metric sector of Sec. XV C.

b. Common-sector coupling. The DFD α-relation $k_\alpha = \alpha^2/(2\pi)$ (Sec. VIII) sets the coupling of ψ to the *common electromagnetic scale*:

$$K_{\rm com}(y) = k_\alpha\,\Sigma(y), \qquad k_\alpha = \frac{\alpha^2}{2\pi} \approx 8.5\times10^{-6}, \quad (288)$$

where $\Sigma(y)$ is the screening factor (Sec. XI C). This coupling is *not directly observable* in ratio experiments because $K_{\rm com}$ cancels between numerator and denominator.

c. Observable residual couplings. What ratio experiments measure is the **residual structure response**:

$$K_A^{\rm obs}(y) = \Sigma(y)\Big[\lambda_\alpha\,\widetilde{S}_A^\alpha + \lambda_s\,S_A^{\alpha_s} + \lambda_N\,C_N^{(A)} + \lambda_e\,C_e^{(A)}\Big], \quad (289)$$

where

$$S_A^\alpha \equiv \frac{\alpha}{\nu_A}\frac{\partial\nu_A}{\partial\alpha} \quad (290)$$

is the electromagnetic sensitivity, $\widetilde{S}_A^\alpha \equiv S_A^\alpha - \bar{S}^\alpha$ is the **centered** electromagnetic sensitivity (with $\bar{S}^\alpha$ absorbed into the common sector), $S_A^{\alpha_s}$ is the strong-sector sensitivity, $C_N^{(A)}$ and $C_e^{(A)}$ are effective nuclear and electronic family charges, and the λ_I are channel coupling strengths. Each $\lambda_I S_A^I$ is the clock-transition form of the non-metric coefficient β_I of (352), the transition analogue of the bound-state mass shift (353); under the minimal action (Thm. XI.2) every $\beta_I = 0$, and the default expectation is the null of Sec. XV H.

The total clock coefficient is

$$K_A = K_{\rm com} + K_A^{\rm obs}, \quad (291)$$

but the observable ratio shift is

$$\frac{\Delta R_{AB}}{R_{AB}} = \left(K_A^{\rm obs} - K_B^{\rm obs}\right)\frac{\Delta\Phi}{c^2}. \quad (292)$$

Equations (288)–(291) are written per unit ψ, the unit in which k_α is defined (Appendix P). Since $\Phi = -c^2\psi/2$, a change $\Delta\Phi/c^2$ moves ψ by $2|\Delta\Phi|/c^2$, so in the $\Delta\Phi/c^2$ slot of Eqs. (281) and (292) each coefficient enters with twice its magnitude.

d. Why this resolves the pure-α tension. The Yb^+ E3/E2 same-ion null (Sec. XI D) constrains λ_α, the *residual* pure-α channel coupling — **not** the common-sector k_α. The conditional value $k_\alpha = \alpha^2/(2\pi)$ (Appendix P, one-gauge-vertex axiom) survives as the coupling to the shared electromagnetic scale. Same-ion tests bound only the centered sensitivity difference $\widetilde{S}_{E3}^\alpha - \widetilde{S}_{E2}^\alpha$, which is a statement about residual structure, not about the universal ψ–EM coupling.

e. Microsector suppression hierarchy. The residual channel couplings are set by the microsector class-breaking parameter

$$\epsilon_H \equiv \frac{N_{\rm gen}}{k_{\rm max}} = \frac{3}{60} = \frac{1}{20}. \quad (293)$$

The hierarchy follows from class-breaking order: the common-sector coupling requires zero class insertions; composition-sensitive residuals require one; and the same-ion pure-α residual requires two (because the one-insertion piece cancels in same-ion ratios). This gives:

$$\lambda_\alpha \approx \epsilon_H^2\,k_\alpha^{\rm com} \approx \frac{1}{400}\times8.5\times10^{-6} \approx 2.1\times10^{-8}, \quad (294)$$

$$\lambda_{N,e,s} \approx \epsilon_H\,k_\alpha^{\rm com} \approx \frac{1}{20}\times8.5\times10^{-6} \approx 4.2\times10^{-7}. \quad (295)$$

The pure-α residual $\lambda_\alpha \approx 2.1\times10^{-8}$ is compared against the Yb^+ E3/E2 gravitational-LPI limit $|(c^2/\alpha)\,d\alpha/d\Phi| \lesssim 3\times10^{-9}$ (Filzinger *et al.* 2023, $-2.4(3.0)\times10^{-9}$), which supersedes the earlier 3.2×10^{-8} bound. Screened at the local acceleration (Table XXIX), the residual enters the same-ion observable as $2\lambda_\alpha\,\Sigma(\oplus) \approx 1.5\times10^{-13}$ per unit $\Delta\Phi/c^2$, four orders of magnitude below this limit, which therefore does not test it. The composition/strong couplings $\lambda_{N,e,s} \approx 4.2\times10^{-7}$ are $\sim$20× larger.

f. Channel structure. Different experiments project out different pieces of Eq. (289):

1. **Same-ion comparisons** (e.g. Yb^+ E3/E2) cancel composition terms by construction and isolate λ_α.
2. **Cross-species atomic comparisons** are dominantly sensitive to λ_N and λ_e because ΔC_N and ΔC_e are generically nonzero.

3. **Nuclear clocks** add a qualitatively new strong-sector contribution through λ_s.

g. Indicative α sensitivities. The electromagnetic sensitivity coefficients remain useful bookkeeping quantities. The column $K_A^{(\alpha)}$ gives the common-sector pure-α value $k_\alpha S_A^\alpha$; ratio experiments are sensitive only to the *centered* residuals.

TABLE XXVIII. Electromagnetic sensitivities and common-sector coupling values.

Transition	Type	S_A^α	$K_A^{(\alpha)}$ ($\times 10^{-5}$)
^{133}Cs hyperfine	MW	$+2.83$	$+2.4$
^{87}Rb hyperfine	MW	$+2.34$	$+2.0$
^{1}H 1S–2S	Opt	≈ 0	≈ 0
^{87}Sr	Opt	$+0.06$	$+0.05$
^{171}Yb	Opt	$+0.31$	$+0.26$
^{171}Yb$^+$ E2	Opt	$+1.0$	$+0.85$
^{171}Yb$^+$ E3	Opt	-5.95	-5.1
^{199}Hg$^+$	Opt	-3.2	-2.7
^{27}Al$^+$	Opt	$+0.008$	$+0.007$
^{229}Th nuclear [63]	Nucl.	5900 ± 2300	(strong sector)

C. Screening: Derivation from a Response Functional

The screening factor $\Sigma(y)$ appearing in Eq. (289) determines how the local gravitational environment suppresses clock–ψ coupling. Rather than treating this as a heuristic, we derive it from an explicit coherence-response principle.

a. Response functional. At acceleration a (with $y \equiv a/a_0$), the effective noise occupation of the local vacuum combines the de Sitter background and the Unruh contribution:

$$N_{\rm eff}(y) = 1 + y. \tag{296}$$

The coherent response amplitude Σ is determined by minimizing the free energy of quantum-sector coupling in this noise background:

$$\mathcal{F}_{\rm resp}(\Sigma; y) = \tfrac{1}{2}(1+y)\,\Sigma^2 - \ln \Sigma. \tag{297}$$

The first term penalizes coherent coupling against the noise floor; the logarithmic term enforces positivity and represents the entropic cost of decoupling. Stationarity gives:

$$\frac{\partial \mathcal{F}_{\rm resp}}{\partial \Sigma} = (1+y)\Sigma - \Sigma^{-1} = 0 \quad \Rightarrow \quad \boxed{\Sigma(y) = \frac{1}{\sqrt{1+y}}}. \tag{298}$$

The screening law is the unique stationary point of this response functional. The effective coupling of any clock channel I is then $\Sigma(y)\,\lambda_I$.

b. Connection to earlier notation. Below, $\mu_{\rm LPI} \equiv \Sigma$. The common-sector effective coupling from Eq. (288) becomes:

$$k_\alpha^{\rm eff}(a) = k_\alpha\,\Sigma(a/a_0) = \frac{\alpha^2}{2\pi\sqrt{1 + a/a_0}}. \tag{299}$$

TABLE XXIX. Screening factor $\Sigma(y)$ and common-sector effective coupling across environments.

Environment	a (m/s^2)	$y = a/a_0$	$\Sigma(y)$	$k_\alpha^{\rm eff}$
Galactic outskirts	10^{-10}	0.84	0.738	6.26×10^{-6}
Outer solar system	10^{-6}	8.4×10^3	1.09×10^{-2}	9.27×10^{-8}
Solar orbit (1 AU)	6×10^{-3}	5.01×10^7	1.41×10^{-4}	1.20×10^{-9}
Earth surface	9.8	8.19×10^{10}	3.49×10^{-6}	2.96×10^{-11}

c. Implication for experiments. Terrestrial optical-clock tests are therefore much more strongly screened than a naive solar-orbit estimate would suggest.

d. Falsifiable predictions from $\mu_{\rm LPI}$ (extended sector). The $y^{-1/2}$ scaling makes specific predictions for future off-Earth experiments:

1. **Earth-based clocks:** At $a \approx 10$ m/s^2, coupling should be $\sim$40$\times$ smaller than at solar orbit—consistent with null terrestrial LPI tests.

2. **Outer solar system:** At Jupiter's orbit ($a \approx 2 \times 10^{-4}$ m/s^2), coupling should be $\sim$5$\times$ larger than at 1 AU.

Deviation from the $y^{-1/2}$ power law would constrain or falsify the Unruh screening mechanism.

D. The Same-Ion E3/E2 Constraint

The PTB Yb$^+$ experiment comparing the E2 and E3 transitions is the cleanest same-ion constraint because it removes composition differences by design [64]. Both transitions live in the same ion, so $\Delta C_N = \Delta C_e = 0$ and any signal primarily probes the pure electromagnetic channel.

a. Structure of the test. For the same ion,

$$\Delta K_{\rm E3/E2} = \lambda_\alpha\,(\widetilde{S}^\alpha_{\rm E3} - \widetilde{S}^\alpha_{\rm E2}) = \lambda_\alpha \times (-6.95). \tag{300}$$

Lange *et al.* measured the gravitational coupling parameter

$$\left(\frac{c^2}{\alpha}\frac{d\alpha}{d\Phi}\right) = 14(11) \times 10^{-9}, \tag{301}$$

consistent with zero, which corresponds to a conservative one-sided 95% bound

$$|\lambda_\alpha| \lesssim 1.6 \times 10^{-8}. \tag{302}$$

Filzinger *et al.* (2023) tighten the underlying limit to 3×10^{-9}, i.e. $|\lambda_\alpha| \lesssim 1.5 \times 10^{-9}$ (Sec. XI B).

b. What this means for DFD. The same-ion null does *not* exclude the channel-resolved DFD clock program. It excludes the naive claim that one universal pure-α law controls the whole clock sector. In particular:

- the pure electromagnetic-sector proposal is tightly bounded;
- cross-species atomic comparisons remain open because composition-sensitive terms survive there;
- nuclear clocks remain open because same-ion optical comparisons are essentially blind to the strong channel.

E. Cross-Species Atomic Comparisons

For different species A/B, the composition terms in Eq. (291) generically survive. This is why cross-species atomic ratios remain important even after the same-ion E3/E2 null. In the phenomenological "family + clock" language, one writes

$$K_i \approx k_N C_N^{(i)} + k_e C_e^{(i)} \tag{303}$$

for ordinary atomic clocks once the pure-α piece is bounded to be subdominant.

a. Indicative scale. The indicative scales carried into Table XXX are:

- Yb/Sr and Al^+/Yb: $\sim 10^{-17}$
- Yb^+(E3)/Sr: $\sim 4\times10^{-16}$; Hg^+/Sr: $\sim 10^{-16}$
- Cs/Sr: $\sim 10^{-16}$ to 10^{-15} depending on channel normalization.

These scales are generated by the unscreened pure-α coefficient $k_\alpha\,\Delta S^\alpha$ reduced by the $\sim$40$\times$ Earth/solar-orbit ratio, not by the composition terms, and the same generator gives a Yb^+ E3/E2 amplitude $\sim$140$\times$ above the Filzinger limit; under Eq. (289) with $\Sigma(\oplus)$ every row is $\lesssim 10^{-20}$. They are indicative scales of the extended channel, null under the minimal action (Thm. XI.2).

b. Cs/Sr: explicit worked example. This channel is one of the highest near-term priorities. The pure-α sensitivity difference is

$$\Delta S^\alpha_{\text{Cs-Sr}} = S^\alpha_{\text{Cs}} - S^\alpha_{\text{Sr}} = 2.83 - 0.06 = 2.77. \tag{304}$$

At the pure-α leading-term level (Table XXVIII), the predicted differential coupling is

$$\Delta K^{(\alpha)}_{\text{Cs-Sr}} = k_\alpha \times \Delta S^\alpha = 8.5\times10^{-6}\times 2.77 \approx 2.35\times10^{-5}, \tag{305}$$

giving, under Eq. (299) with the annual $|\Delta\psi_\odot| = 2|\Delta\Phi_\odot|/c^2 \approx 3.3\times10^{-10}$, an annual modulation amplitude of $\sim1\times10^{-18}$ at 1 AU and $\sim3\times10^{-20}$ at Earth-surface screening (Table XXIX); Fig. 10 uses a different screening normalization, not these amplitudes. Composition-sensitive terms may contribute additional signal depending on ΔC_N and ΔC_e.

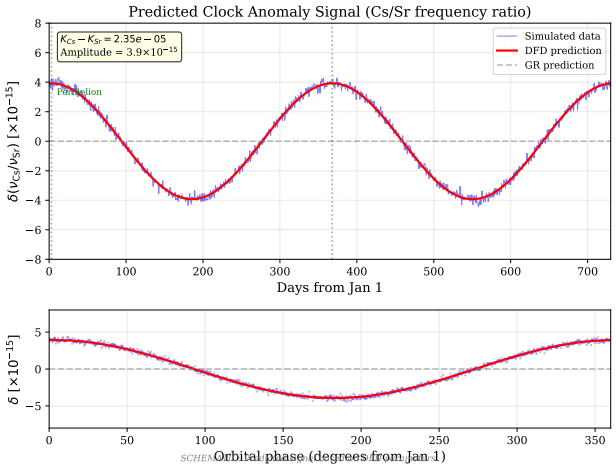


FIG. 10. Illustrative Cs/Sr annual-modulation curve (extended channel). Its screening normalization is not the bound-matter clock's, whose screening factors are those in Table XXIX, and the plotted amplitude is an illustration, not a precision prediction. GR predicts null (gray dashed).

c. Prior data: Blatt et al. 2008. The 2008 multi-laboratory Cs/Sr annual amplitude $y_{\text{Sr}} = (-1.9 \pm 3.0)\times10^{-15}$ [65] is consistent with zero.

d. Methodological note. Year-long global fits with flexible drift models can absorb annual signals into nuisance parameters, while windowed perihelion analyses are more sensitive to the specific DFD phase signature but more vulnerable to drift contamination. Both approaches should be applied to any dedicated campaign and their results compared.

e. ROCIT and existing hints. The ROCIT ion–neutral analyses remain interesting because they point at the very type of cross-sector comparison the channel-resolved picture says should be informative. ROCIT-like results are *suggestive rather than definitive*: they motivate focused reanalysis and replication, but they are not the sole pillar of the clock case.

1. ROCIT Statistical Detail

For completeness, the full statistical methodology is recorded here so that independent groups can replicate the analysis. The complete regression scripts, figures, and derived outputs are publicly archived [66]; the accompanying analysis paper is Ref. [67].

a. Reported amplitude: Yb^+/Sr. The Yb^+(E3)/Sr ion–neutral ratio exhibits [67, 68]:

$$A_{\text{Yb}^+/\text{Sr}} = (-1.045 \pm 0.078)\times10^{-17},$$
$$Z = 13.5\sigma \text{ (formal error)}, \quad 6.1\sigma \text{ (leave-one-day-out error)}. \tag{306}$$

The amplitude is phase-locked to Earth's perihelion (January), corresponding to maximum solar gravitational potential.

b. Regression model.

$$y(t) = \beta_0 + \beta_1 t + A\, b(t) + \epsilon(t), \tag{307}$$

where $b(t)$ is the orthogonalized Kepler driver (solar potential template) with unit RMS, constructed from Earth's mean anomaly with perihelion at phase zero.

c. Uncertainty estimation. Leave-one-day-out (LODO) jackknife gives $\sigma_A^{\rm LODO} \approx 1.7 \times 10^{-18}$; wild bootstrap of residuals, sign-permutation, and day-shift resampling give empirical $p_{\rm emp} \approx 2 \times 10^{-4}$.

d. Phase robustness. Regression on alternative phase hypotheses confirms solar specificity:

$$\begin{aligned} A_{\text{spring eq.}} &= (-0.18 \pm 0.81) \times 10^{-17},\ Z = 0.22\sigma, \\ A_{\text{fall eq.}} &= (+0.09 \pm 0.76) \times 10^{-17},\ Z = 0.12\sigma. \end{aligned} \tag{308}$$

All non-perihelion phases are consistent with zero. Neutral–neutral ratios from independent SYRTE measurements are also null: $A_{\text{neut-neut}} = (0.4 \pm 7.3) \times 10^{-17}$, $p = 0.58$.

e. Channel-resolved interpretation. In the channel-resolved language of Eq. (291), the ROCIT signal probes the composition-sensitive terms $(k_N C_N^{(A)} + k_e C_e^{(A)})$ rather than the pure-α sector. Using the unit-RMS Kepler driver normalization with $\sigma(\Delta\Phi/c^2) \approx 1.2 \times 10^{-10}$, the measured amplitude corresponds to $2|K_{\rm ion} - K_{\rm neut}| \approx 9 \times 10^{-8}$ per unit $\Delta\Phi/c^2$. Because this is a distinct composition-sensitive channel, it is not identified with the pure-α $k_\alpha^{\rm eff}$ column in Table XXIX. The same-ion pure-α null does not test this channel, but the inferred coupling is at least 10^4 times the screened composition coupling $2\lambda_N \Sigma(\oplus) \approx 3.0 \times 10^{-12}$ per unit $\Delta\Phi/c^2$ (Eq. (295), Table XXIX), so the screened extended channel does not account for the amplitude.

F. Nuclear Clocks: the Strong-Sector Channel

The ^{229}Th nuclear isomer is qualitatively different from ordinary atomic clocks. Its transition energy sits near a cancellation between Coulomb and hadronic contributions, making it sensitive to the strong sector through dimensional transmutation.

a. Strong-sector amplification. A convenient parametrization is

$$\frac{\delta X_q}{X_q} \approx -\frac{2\pi}{b_0 \alpha_s} \frac{\delta \alpha_s}{\alpha_s}, \tag{309}$$

with

$$\left| \frac{2\pi}{b_0 \alpha_s} \right| \approx 6.9 \tag{310}$$

for $\alpha_s(M_Z) \approx 0.118$ and $b_0 = 23/3$. Combined with Flambaum-style nuclear sensitivity coefficients of order $|S_q| \sim 10^4$, this makes the nuclear clock the natural place to look for strong-sector scalar couplings.

In the same screened notation used for the electromagnetic channel, with k_s a matching coefficient of the extended strong channel, the strong-sector effective coupling is

$$k_s^{\rm eff}(a) = k_s\, \mu_{\rm LPI}(a/a_0) = \frac{\alpha_s^2}{2\pi}\, \mu_{\rm LPI}(a/a_0), \tag{311}$$

so that at Earth's surface[2]

$$k_s^{\rm eff}(\oplus) \approx 7.7 \times 10^{-9}. \tag{312}$$

Combining Eqs. (309) and (312) with $|S_q| \sim 10^4$ and the annual half-amplitude of the solar ψ at Earth, $|\Delta\psi_\odot| = 2|\Delta\Phi_\odot|/c^2 \approx 3.3 \times 10^{-10}$ ($\Phi = -c^2\psi/2$), gives a screened Th-229 estimate of about 350 Hz half-amplitude at $\alpha_s(M_Z)$, rising to about 0.9–1.5 kHz at the nuclear-scale α_s.

b. What the newer data changed. The 2026 Ooi *et al.* reproducibility paper [69], together with the measured Th-229 electromagnetic sensitivity from Beeks *et al.* [63] and the strong-sector amplification logic of Flambaum [70], materially sharpens the status of the Th-229 channel. At 195 K, with the first-order thermal sensitivity nulled near 196(5) K, they report frequency reproducibility of 220 Hz over 7 months for two differently doped ^{229}Th:CaF_2 crystals. Interpreted conservatively, this means:

1. the **unscreened** strong-sector prediction ($\sim$ 100 MHz half-amplitude with $k_s = \alpha_s^2/2\pi$, App. G) is excluded by about five orders of magnitude;

2. the simplest **screened** strong-sector estimate (about 350 Hz half-amplitude at $\alpha_s(M_Z)$, about 0.9–1.5 kHz at the nuclear-scale α_s) lies from below the conservative annual bound derived from the Ooi data to about twice it[3] and is therefore not excluded at $\alpha_s(M_Z)$, while its nuclear-scale range awaits a formal perihelion-fixed cosine fit;

3. the surviving window for a genuine annual signal is pushed down into the rough range

$$26\ \text{Hz} \lesssim \delta\nu_b \lesssim \mathcal{O}(1\ \text{kHz}), \tag{313}$$

with the lower end set by the composition/family floor and the upper end set by the Ooi reproducibility ceiling.

---

[2] This uses $\alpha_s(M_Z) = 0.118$. Running to the nuclear scale relevant to Th-229 gives $\alpha_s \approx 0.3$–0.5, which would increase $k_s^{\rm eff} \propto \alpha_s^2$ by a factor of 6–18 and lower the amplification of Eq. (309) by 2.5–4.2, so the estimate below rises by 2.5–4.2 (Sec. IX E). This scale ambiguity sets the range of the screened estimate below.

[3] The Ooi 220 Hz figure is frequency reproducibility (scatter across measurements over 7 months), not a fitted annual cosine amplitude bound. To map reproducibility to an annual bound: (i) the 7-month baseline covers $\sim$60% of one annual cycle, degrading cosine-fit sensitivity by $\sim$2×; (ii) the scatter includes systematic contributions (crystal dependence, thermal residuals) that do not average down as $1/\sqrt{N}$, adding a $\sim$2–3× floor factor; (iii) the peak-to-peak range of a cosine is $2A$, so the amplitude A is half the peak-to-peak. Conservative example: $A_{\rm bound} \approx 220\,\text{Hz} \times 2 \times 3/2 \approx 660\,\text{Hz}$. Moderate: $A_{\rm bound} \approx 1$–2.5 kHz. The 350 Hz estimate lies below all of these bounds; the 0.9–1.5 kHz range lies below the upper end of the moderate bound and reaches 1.3–2.3× the conservative one.

The 2026 result therefore excludes the unscreened amplitude but does not eliminate nuclear clocks.

c. Thermal-systematics control. A sharper thermal analysis is possible because Higgins *et al.* measured the line shifts at three temperatures and identified the near-zero-crossing behavior around $T_0 = 196(5)$ K [71]. Near that operating point, line b is unusually temperature-insensitive while line c remains much more responsive. This suggests a co-thermometry diagnostic: any genuine gravitational annual modulation should appear as a common fractional modulation in the hyperfine-averaged nuclear frequency, whereas a residual thermal drift would imprint a much larger correlated signal in line c.

d. EFG-free combination. An especially clean observable is the hyperfine-averaged, electric-field-gradient-free combination of the resolved quadrupole lines,

$$\nu_{\mathrm{Th}}^{\mathrm{EFG\text{-}free}} = \tfrac{1}{6}\left(\nu_{3/2\to1/2} + 2\nu_{5/2\to3/2} + 2\nu_{1/2\to1/2} + \nu_{3/2\to3/2}\right), \tag{314}$$

which cancels the leading crystal-field splitting while preserving any true nuclear fractional modulation. A future dedicated annual campaign should analyze both this EFG-free combination and the line-c co-thermometer in parallel.

e. Interpretation. The nuclear-clock channel therefore remains *decisive* for the extended strong channel. The experiment probes a residual window rather than a large expected signal.

f. Beyond ^{229}Th: the ^{187}Re nuclear sensitivity target. The Flambaum nuclear sensitivity formalism [70, 72] predicts $\kappa_q \propto n/Q$ for beta decays, placing ultra-low-Q transitions at the top of the hierarchy. ^{187}Re ($Q = 2.47$ keV, the lowest known β-emitter Q-value) achieves $\kappa_q \approx 19{,}000$—roughly $2\times$ the ^{229}Th sensitivity. A half-life measurement at fractional precision 10^{-6}, repeated at different orbital phases, would constrain $k_q^{\mathrm{eff}} < 0.2$. This complements the ^{229}Th nuclear clock: ^{187}Re probes the strong-sector coupling through a completely different experimental technique (calorimetric or mass-spectrometric rather than optical frequency comparison), providing independent confirmation or falsification. A multi-isotope ratio test—simultaneously monitoring two isotopes with different κ_q in the same facility—would eliminate environmental systematics by design and directly probe composition dependence.

G. Channel-Resolved Prediction Table

Table XXX collects the current channel logic in one place.

The most important conceptual point of Table XXX is that *same-ion nulls and cross-species signals are not contradictory* in the extended channel. They are precisely what a channel-resolved extended sector allows; the minimal action predicts null in both (Thm. XI.2).

H. Empirical Checks and Current Status

The status of the clock sector is:

- **PTB E3/E2:** strong quantitative bound on any universal pure-α coupling law.
- **BACON optical network:** extremely stringent null/near-null behavior in ordinary optical-clock ratios, with direct implications for cavity–atom residuals.
- **Ooi 2026:** nuclear-clock reproducibility already excludes the unscreened strong-channel amplitude and does not exclude the screened estimate at $\alpha_s(M_Z)$ (about 350 Hz), while the nuclear-scale range (about 0.9–1.5 kHz) reaches 1.3–2.3 times the conservative annual bound.
- **ROCIT ion–neutral analyses (Sec. XI E 1):** a perihelion-locked amplitude in Yb^+/Sr (13.5σ formal, 6.1σ leave-one-day-out), which neither the minimal action nor the screened extended channel predicts. Suggestive rather than definitive pending replication, but the full statistical methodology is archived for independent verification.

No single formula is asked to fit every channel at once.

I. Experimental Priorities

The experimental ordering is:

1. **Th-229/Sr and related nuclear-clock reanalyses.** This is the unique strong-sector channel and carries a sharply delimited surviving window.
2. **Cross-species atomic comparisons.** Hg/Sr, Yb^+/Sr, Yb/Sr, Al^+/Yb, and Cs/Sr map the composition-sensitive sector.
3. **Same-ion null checks.** These continue to pin down the pure electromagnetic channel and prevent the theory from smearing everything into one effective constant.
4. **Cavity–atom residual tests.** Important, but with geometric cancellation at tree level they are not the first short-horizon discriminator; their natural role is ultra-clean residual testing at very high precision.

TABLE XXX. Channel-resolved clock comparison guide for the extended non-metric channel (Sec. XV C); the minimal action predicts a null in every row (Thm. XI.2). Amplitudes are indicative scales with a coefficient the corpus does not derive. "Open" = live test of the extended channel; "bounded" = simplest version under pressure.

Comparison	Dominant channel	Scale (atomic rows: unscreened, excluded; screened by Eq. (289), $\lesssim 10^{-20}$)	What it tests	Status
Yb/Sr	—	$\sim 10^{-17}$	cross-species residual	open
Al^+/Yb	—	$\sim 10^{-17}$	optical-network null check	open
Yb^+(E3)/Sr	—	$\sim 4\times 10^{-16}$	ion–neutral response	open
Hg^+/Sr	—	$\sim 10^{-16}$	EM sensitivity contrast	open
Cs/Sr	HF	$\sim 10^{-16}$–10^{-15}	MW/optical cross-check	open
^{229}Th/Sr	strong + comp. floor	26 Hz–kHz window (extended strong channel)	nuclear strong sector	decisive/bounded
Yb^+ E3/E2	pure α only	null expected	same-ion bound on the extended α channel	bounded

Clock-Sector Summary

What is solid: same-ion optical clocks strongly constrain any pure universal k_α law; under the minimal action co-located ratios are null (Thm. XI.2); clock phenomenology must be channel-resolved; nuclear clocks are the unique strong-sector probe of the extended channel.
What is under pressure: the unscreened Th-229 amplitude formula is too large in light of Ooi 2026; the screened estimate at $\alpha_s(M_Z)$ (about 350 Hz) is not excluded, and the nuclear-scale range (about 0.9–1.5 kHz) reaches 1.3–2.3 times the conservative annual bound.
What remains decisive for the extended channel: the surviving Th-229 window, plus cross-species atomic campaigns that isolate composition-sensitive residuals.

XII. CAVITY-ATOM REDSHIFT TESTS

The cavity–atom comparison is part of the DFD laboratory program as a residual test. Slowing light while holding the cavity spacer fixed would give an order-unity LPI slope, but that is not the DFD calculation: the same optical metric that changes photon propagation also changes Coulomb binding, lattice spacing, and hence the cavity length, so the leading geometric response of cavity and atomic sectors cancels at tree level.

What remains is a residual, screened signal. This makes the cavity–atom channel *harder* as an experiment but also cleaner as a precision residual test.

A. Formal Constitutive Proof of the Cancellation

The cancellation can be organized as a short formal derivation.

a. Step 1: optical metric and constitutive relations. DFD posits the optical metric

$$d\tilde{s}^2 = -\frac{c^2}{n^2}dt^2 + d\mathbf{x}^2, \qquad n = e^{\psi}. \tag{315}$$

Through the Tamm–Plebanski construction, this metric defines effective vacuum constitutive relations

$$\varepsilon_{\rm eff} = \varepsilon_0 e^{+\psi}, \qquad \mu_{\rm eff} = \mu_0 e^{+\psi}. \tag{316}$$

The medium is impedance-matched, and the coordinate phase velocity is

$$v_{\rm ph} = \frac{1}{\sqrt{\varepsilon_{\rm eff}\mu_{\rm eff}}} = c e^{-\psi}. \tag{317}$$

b. Step 2: Coulomb binding changes with the same constitutive chain. Virtual photons feel the same optical medium, so the static Coulomb potential scales as

$$V(r) = \frac{e^2}{4\pi\varepsilon_{\rm eff} r} = \frac{e^2}{4\pi\varepsilon_0 r}e^{-\psi}. \tag{318}$$

The local fine-structure constant at tree level is therefore unchanged:

$$\alpha(\psi) = \frac{e^2}{4\pi\varepsilon_{\rm eff}\hbar\, c\, e^{-\psi}} = \alpha_0, \tag{319}$$

because the factors from $\varepsilon_{\rm eff}$ and the coordinate phase speed $c\,e^{-\psi}$ cancel.

c. Step 3: the atomic length scale in coordinate units. With α unchanged at tree level, the Bohr radius is a fixed proper length; on the physical metric (12) its coordinate length is

$$a_0(\psi) = a_0^{(0)} e^{-\psi/2}, \tag{320}$$

like that of every minimally coupled length standard (Thm. XI.2).

d. Step 4: the cavity length follows the same electromagnetic scale. A Fabry–Pérot cavity resonance obeys, in coordinate time,

$$f_{\rm cav} = \frac{m\, c\, e^{-\psi}}{2L(\psi)}. \tag{321}$$

For an electromagnetic solid spacer, the lattice constant and therefore L scale with the Bohr radius, so $L \propto e^{-\psi/2}$ while the coordinate phase speed is $c\,e^{-\psi}$. Hence

$$f_{\rm cav} \propto \frac{e^{-\psi}}{e^{-\psi/2}} = e^{-\psi/2}. \tag{322}$$

Atomic transition frequencies carry the same factor in coordinate time, $f_{\rm atom} \propto e^{-\psi/2}$ (Thm. XI.2), up to channel-dependent residual sensitivities of the extended non-metric sector.

e. Convention note. The $e^{-\psi/2}$ scaling above is in coordinate time and is the gravitational redshift factor of the physical metric $g_{00} = -e^{-\psi}$ quoted in Section IV H 4: in the rescaled coordinates of Thm. XI.2 every minimally coupled standard is Minkowskian, so the *same* universal coordinate-to-proper conversion multiplies both cavity and atomic frequencies. Therefore the ratio $R = f_{\rm cav}/f_{\rm atom}$ is convention-independent, and the tree-level cancellation holds regardless of which clock convention is adopted; Cor. XI.3 extends it to boosts.

f. Tree-level result. The leading geometric ratio is therefore constant:

$$\boxed{R \equiv \frac{f_{\rm cav}}{f_{\rm atom}} = \text{const. at tree level}, \qquad \xi_{\rm geom} = 0} \tag{323}$$

The universal geometric redshift cancels. Any surviving cavity–atom signal must come from a *residual* channel, not from an order-unity tree-level effect.

B. What Survives Physically

Once the tree-level cancellation is enforced, the cavity–atom observable is naturally written as

$$\frac{\Delta R}{R} = \xi_{\rm LPI}^{\rm res}\frac{\Delta\Phi}{c^2}, \tag{324}$$

with

$$\boxed{\xi_{\rm LPI}^{\rm GR} = 0, \quad \xi_{\rm LPI}^{\rm DFD} = 0 \text{ (minimal action).}} \tag{325}$$

For ordinary terrestrial experiments an extended-sector residual is small because the local environment sits deep in the screened regime.

a. Interpretation. The cavity–atom comparison remains valuable because it can isolate a non-metric residual if the sensitivity frontier is pushed far enough.

C. Four Independent Empirical Checks

Four independent data streams support the geometric-cancellation picture.

a. Check 1: fine-structure splitting. If the geometric unscreened picture were right, the ratio of two transitions with different α sensitivities inside the same atom would show an annual modulation of order $\Delta S^\alpha\,\delta\psi_{\rm annual} \sim 10^{-10}$. Precision spectroscopy constrains such effects at the $\lesssim 10^{-17}$ level. The naive unscreened geometric scenario is therefore ruled out by more than seven orders of magnitude.

b. Check 2: PTB Yb^+ E3/E2. The same-ion E3/E2 comparison [64] is exactly the sort of experiment that would have seen an unscreened cavity-style signal if it were real. Instead, the observed result is null at a level that rules out the naive geometric expectation by more than seven orders of magnitude and forces any viable theory into a much smaller residual regime.

c. Check 3: BACON optical network. The BACON collaboration measured Al^+/Sr/Yb frequency ratios with uncertainties at or below 8×10^{-18} [73]. A naive geometric annual signal in Yb/Sr would be of order 8×10^{-11}, far larger than the observed stability. This is effectively a ten-million-fold exclusion of the unscreened geometric cavity/atom picture.

d. Check 4: a direct cavity–atom record. JILA compared a cryogenic silicon cavity with a Sr lattice clock for 205 days, from July 2025 to January 2026 [74], while the solar potential changed by about 3×10^{-10} in units of c^2. The cavity frequency shows only a smooth, nearly linear drift of about 1.4×10^{-12} over the whole record, far below the $\sim 3\times10^{-10}$ that an order-unity cavity–atom slope would produce.

These four checks all point the same way: the order-unity tree-level picture is excluded, and only a screened residual remains.

D. BACON and the Screening Regime

Under Eq. (299), evaluated at the local acceleration (Table XXIX), the Yb/Sr annual signal with $\Delta S^\alpha \approx 0.25$ would be

$$\begin{aligned}\left(\frac{\delta R}{R}\right)_{\rm Yb/Sr} &\approx 0.25 \times k_\alpha^{\rm eff} \times 3.3\times10^{-10} \\ &\approx 1\times10^{-19}\ (1\,\text{AU}), \qquad 2\times10^{-21}\ (\oplus),\end{aligned} \tag{326}$$

with $k_\alpha^{\rm eff} = 1.20\times10^{-9}$ and 2.96×10^{-11} respectively, against BACON's Yb/Sr weighted scatter of about 1.1×10^{-17}. BACON therefore excludes neither evaluation point and does not select between them; the local evaluation is adopted from Sec. XI C. Under the minimal action the co-located ratio is null in any case (Thm. XI.2), and the extended-sector coefficient λ_α is not derived, so no numerical amplitude is printed for this channel.

E. Sector-Resolved Parameterization

The cavity–atom channel benefits from a sectoral bookkeeping language. Write

$$\left(\frac{\Delta f}{f}\right)^{(M)}_{\rm cav} = (\alpha_{\rm w} - \alpha_L^{(M)})\frac{\Delta\Phi}{c^2}, \tag{327}$$

$$\left(\frac{\Delta f}{f}\right)^{(S)}_{\rm atom} = \alpha_{\rm atom}^{(S)}\frac{\Delta\Phi}{c^2}. \tag{328}$$

Only differences are observable. With two cavity materials (for example ULE and Si) and two atomic species (for example Sr and Yb), the directly identifiable combinations are

$$\delta_{\rm tot} \equiv \alpha_{\rm w} - \alpha_L^{\rm ULE} - \alpha_{\rm atom}^{\rm Sr}, \tag{329}$$

$$\delta_L \equiv \alpha_L^{\rm Si} - \alpha_L^{\rm ULE}, \tag{330}$$

$$\delta_{\rm atom} \equiv \alpha_{\rm atom}^{\rm Yb} - \alpha_{\rm atom}^{\rm Sr}. \tag{331}$$

This remains useful for a future high-precision residual measurement even after the tree-level cancellation is imposed.

F. The 4→3 GLS Protocol

The four basic cavity–atom slopes map onto three independent sector combinations:

TABLE XXXI. Mapping of measured cavity–atom ratios to sector parameters.

Measured slope	Combination	Parameter
ULE/Sr	$\alpha_{\rm w} - \alpha_L^{\rm ULE} - \alpha_{\rm atom}^{\rm Sr}$	$\delta_{\rm tot}$
Si/Sr	$\alpha_{\rm w} - \alpha_L^{\rm Si} - \alpha_{\rm atom}^{\rm Sr}$	$\delta_{\rm tot} + \delta_L$
ULE/Yb	$\alpha_{\rm w} - \alpha_L^{\rm ULE} - \alpha_{\rm atom}^{\rm Yb}$	$\delta_{\rm tot} + \delta_{\rm atom}$
Si/Yb	$\alpha_{\rm w} - \alpha_L^{\rm Si} - \alpha_{\rm atom}^{\rm Yb}$	$\delta_{\rm tot} + \delta_L + \delta_{\rm atom}$

The redundancy provides a built-in closure relation and is valuable even though the target signal is residual rather than order unity.

G. Experimental Concept and Controls

The experimental architecture below applies at the residual level: a residual target changes the *amplitude*, not the measurement logic.

a. Hardware.

- two evacuated optical cavities (for example ULE and cryogenic Si) with PDH-locked lasers;
- co-located Sr and Yb optical lattice clocks;
- a self-referenced frequency comb measuring all four ratios simultaneously;
- vertical relocation or a dual-station geometry providing a known potential difference.

b. Dispersion control. The dual-wavelength check remains essential. DFD's optical metric is nondispersive in the minimal formulation, so any large wavelength dependence would diagnose ordinary optical systematics rather than a gravitational effect. Causality constrains material dispersion via the Kramers–Kronig relation:

$$\left|\frac{\partial \ln n}{\partial \ln \omega}\right| \lesssim \frac{2}{\pi}\frac{\omega}{\Omega}\frac{\alpha_0 L_{\rm mat}}{\mathcal{F}}, \tag{332}$$

where $\mathcal{F}$ is the cavity finesse, $L_{\rm mat}$ the material path length, α_0 the absorption coefficient, and Ω the detuning to the nearest material resonance. For crystalline mirror coatings and ULE glass near optical-clock frequencies ($\alpha_0 < 10^{-4}$, $\Omega/\omega > 10^{-2}$), this yields $|\partial \ln n/\partial \ln \omega| < 10^{-8}$—far below experimental reach.

c. Cavity mechanics. Vertical transport changes gravitational loading on the cavity spacer. Controls include: elastic modeling to null first-order sag; 180° orientation flips at each height (mechanical artifacts change sign, gravitational effects do not); and a platform tilt budget maintained at $<100\,\mu$rad. Gravitational sag contributes $\alpha_{\rm grav} \sim 10^{-9}$ for ULE, elastic coupling $<10^{-14}$ for $10^{-6}g$ perturbations, and thermoelastic drift cancels in common-mode ratios. The combined effective length-change bound is $|\alpha_L^M| \lesssim 10^{-8}$.

d. Environmental and noise budget. Temperature stability <10 mK, pressure $<10^{-2}$ mbar, magnetic field drift $<10\,\mu$T with periodic reversal. The ratio Allan variance is modeled as $\sigma_y^2(\tau) = h_{-1}/\tau + h_0 + h_1\tau$, with typical values: white frequency $h_{-1} \sim 10^{-32}$ (300 s windows), flicker $h_0 \sim 10^{-34}$, random walk $h_1 \sim 10^{-38}$. The dominant term is white noise.

e. Thermal rejection. Silicon cavities have $dn/dT \sim 10^{-4}$/K; with $\delta T < 10$ mK the fractional contribution is $<10^{-6}$. ULE has CTE ≈ 0 near 30°C; silicon near 124 K has CTE ≈ 0. Operating at these zero-crossings suppresses length changes. Any residual dispersion from coating thermal effects appears differently at two wavelengths, bounding the dispersion systematic to $|\epsilon_{\rm disp}| \lesssim 10\%$. Total thermal target: $<3 \times 10^{-16}$, achievable with demonstrated technology.

H. Expected Signal and Sensitivity

For a height separation Δh,

$$\frac{g\Delta h}{c^2} \approx 1.1 \times 10^{-14}\left(\frac{\Delta h}{100\,\rm m}\right). \tag{333}$$

After geometric cancellation, the cavity–atom observable inherits this factor *and* a screened residual coefficient. The terrestrial height-separated signal is therefore extremely small.

a. Consequence. The practical ranking of experiments is as follows:

- a terrestrial height-separated cavity–atom test is not a quick binary discriminator;

- it is a demanding precision residual experiment, likely better matched to future long-baseline or space-based platforms;
- multi-species clock and nuclear-clock programs come before it in near-term priority.

I. Current Status and Priority

No existing experiment has yet performed the full sector-resolved cavity–atom residual test at the required precision, so the channel is not experimentally exhausted; its target is clean but extremely small.

Cavity–Atom Priority

Picture: tree-level geometric cancellation; residual screened signal only.
Ranking:

1. Th-229/Sr and related nuclear-clock analyses
2. cross-species atomic clock comparisons
3. same-ion null checks that bound the pure α sector
4. height-separated cavity–atom residual tests

J. Summary: Cavity–Atom as a Precision Residual Test

The cavity–atom picture is simple to state:

1. the optical metric implies constitutive relations through Tamm–Plebanski,
2. those constitutive relations alter both light propagation and electromagnetic binding,
3. the cavity spacer's coordinate length therefore changes together with the coordinate light speed,
4. the leading geometric cavity/atom response cancels at tree level,
5. only a residual screened signal remains.

XIII. MATTER-WAVE INTERFEROMETRY

Atom interferometry provides a complementary test of DFD in the matter sector. This section examines a T^3 phase expression proposed to distinguish DFD from GR, describes concrete experimental designs, and assesses sensitivity requirements. The signature is not a DFD prediction: the matter-wave sector is a null prediction of DFD (status note after Eq. (337)).

A. The ψ-Coupled Schrödinger Equation

In DFD, the scalar field ψ modifies the dynamics of massive particles through the physical metric (12). For nonrelativistic particles in weak fields ($|\psi| \ll 1$), the Schrödinger equation becomes:

$$i\hbar\,\partial_t\Psi = -\frac{\hbar^2}{2m}\nabla^2\Psi + m\Phi_N\,\Psi + \frac{\hbar^2}{2m}\left[\psi\,\nabla^2\Psi + (\nabla\psi)\cdot\nabla\Psi\right], \tag{334}$$

where $\Phi_N = -c^2\psi/2$ is the effective Newtonian potential.

a. The δH perturbation. The Hamiltonian splits as $H = H_0 + \delta H$, where:

$$H_0 = \frac{p^2}{2m} + m\Phi_N, \qquad \delta H = \frac{\hbar^2}{2m}\left[\psi\,\nabla^2 + (\nabla\psi)\cdot\nabla\right]. \tag{335}$$

The δH term produces a phase shift beyond the standard gravitational phase. *Status: not a DFD result.* The δH above carries the bare kinetic coefficient 1 where the matter dispersion relation gives 3/2 (App. AN, $e^{-3\psi/2}$); taken at face value it and the phase below would print a non-GR 1PN residual ($\gamma_{\rm matter} = 1/2$, excluded). DFD equals GR at 1PN for matter waves; see the status note after Eq. (337).

b. Key phase formula. Evaluating δH along classical trajectories gives the phase shift:

$$\boxed{\Delta\phi_{\nabla\psi} = -\frac{1}{2m}\int_0^{2T} dt\,(\nabla\psi)\cdot\Delta\mathbf{p}(t)}, \tag{336}$$

where $\Delta\mathbf{p}(t)$ is the momentum difference between interferometer arms.

B. The T^3 Discriminator (Not a DFD Prediction)

Consider a vertical Mach-Zehnder atom interferometer with light-pulse beam splitters at $t = 0, T, 2T$. The effective Raman wavevector is $k_{\rm eff}\hat{z}$, and the recoil velocity is $v_{\rm rec} = \hbar k_{\rm eff}/m$.

a. Arm geometry. After the first pulse, the arms have momentum difference $\Delta p_z = \hbar k_{\rm eff}$. The spatial separation grows as $\Delta z(t) = v_{\rm rec}\,t$ until the mirror pulse at $t = T$.

b. Phase evaluation. In uniform Earth gravity, $\nabla\psi = -2\mathbf{g}/c^2$. The constant part cancels between arms, but the *finite spatial separation* produces a residual. Evaluating Eq. (336) with the arm separation:

$$\boxed{\Delta\phi^{\rm KC}_{\rm DFD} = \frac{\hbar k_{\rm eff}^2}{m}\,\frac{g}{c^2}\,T^3}. \tag{337}$$

Status: not a DFD prediction. The expression above is not a phase (its units are s^2/m), and the re-derivation from the physical-metric dispersion relation, Eq. (AN3), yields no DFD-specific term: the one-particle Hamiltonian coincides with the GR test-body Hamiltonian through first post-Newtonian order for any static potential ($\gamma = \beta = 1$, §IV C; the rotating-Earth g_{0i} sector is not covered by this identity and is separately universal, Eq. (82)), so every T^2, T^3 and T^4 phase at this order is common to DFD

and GR. The static metric is general relativity's at second post-Newtonian order as well (App. WS), so no DFD-specific term appears there either, and a species-dependent coupling $K_{\rm atom}$ (App. B 5) is an Eötvös parameter already bounded below 10^{-14} (§XV G). The matter-wave sector is therefore a null prediction of DFD (cf. §XVIII H); the forecasts, designs and falsification thresholds of this section and of Apps. B 5, D 3 and W 3 do not apply to DFD.

c. Comparison with GR. The standard GR phase (after common-mode subtraction) is:

$$\boxed{\Delta\phi^{\rm KC}_{\rm GR} = k_{\rm eff}\, g\, T^2}. \tag{338}$$

d. The discriminator (not a DFD prediction).

$$\text{Eq. (337)}: \quad \Delta\phi \propto T^3, \qquad \text{GR}: \quad \Delta\phi \propto T^2. \tag{339}$$

The contrast does not hold for DFD: through 1PN, DFD and GR carry the same T^2, T^3 and T^4 phases (status note above), so time scaling, orientation dependence and recoil scaling do not separate them.

e. Numerical estimate. For ^{87}Rb at 780 nm:

- $k_{\rm eff} \simeq 1.6 \times 10^7$ m^{-1}
- $v_{\rm rec} = \hbar k_{\rm eff}/m \approx 1.2 \times 10^{-2}$ m/s
- $g = 9.8$ m/s^2, $c = 3 \times 10^8$ m/s

Status: not a DFD prediction (the matter-wave sector is null); see the status note after Eq. (337) in Sec. XIII. The absolute GR phase $k_{\rm eff} g T^2 \sim 1.6 \times 10^8$ rad is removed by standard common-mode techniques; DFD predicts no residual beyond the GR phase at this order.

C. Experimental Designs

Several configurations can search for a T^3 term; since DFD and GR predict the same phase through 1PN, each is a null test of DFD:

1. Design A: Vertical Fountain

a. Configuration. 10-meter vertical fountain with ^{87}Rb, 780 nm Raman transitions, $\pi/2$–π–$\pi/2$ pulse sequence.

b. Parameters.

- Interrogation time: $T = 1$–2 s
- Arm apex separation: $\Delta z_{\rm max} \approx v_{\rm rec} T \sim 1$–$2$ cm
- Expression of Eq. (337): not a phase (units s^2/m) *Status: not a DFD prediction (the matter-wave sector is null); see the status note after Eq. (337) in Sec. XIII.*

c. Existing facilities. Stanford 10-m fountain, Wuhan HUST, Hannover VLBAI.

2. Design B: Horizontal Rotation

a. Configuration. Horizontal Bragg interferometer with baseline direction $\hat{\mathbf{n}}$. Rotate platform by 180° about vertical.

b. Signature.

$$\Delta\phi^{\rm horiz}_{\rm DFD} = \frac{\hbar k^2_{\rm eff}}{m}\,\frac{\mathbf{g}\cdot\hat{\mathbf{n}}}{c^2}\,T^3. \tag{340}$$

Status: not a DFD prediction (the matter-wave sector is null); see the status note after Eq. (337) in Sec. XIII. The expression above would *flip sign* under rotation; many systematic effects do not.

3. Design C: Source Mass Modulation

a. Configuration. Place a dense source mass (∼500 kg tungsten) at distance $R \sim 0.25$ m. Modulate the mass position to generate time-varying $g_s = GM/R^2$.

b. Signature.

$$\Delta\phi^{\rm src}_{\rm DFD} = \frac{\hbar k^2_{\rm eff}}{m}\,\frac{g_s}{c^2}\,T^3 \times \mathcal{G}(\text{geometry}). \tag{341}$$

Status: not a DFD prediction (the matter-wave sector is null); see the status note after Eq. (337) in Sec. XIII. Lock-in detection at the modulation frequency; the amplitude of the expression above scales with T^3.

4. Design D: Dual-Species Protocol

a. Configuration. Run Rb and Yb interferometers in matched geometry. The phase of Eq. (337) would scale as $\hbar k^2_{\rm eff}/m$; through 1PN DFD adds nothing to the GR phases, so the dual-species differential is the GR one, and a species-dependent coupling is an Eötvös parameter bounded below 10^{-14}.

b. Differential signal.

$$\Delta\phi^{(i-j)}_{\rm DFD} = \frac{gT^3}{c^2}\,\hbar\left(\frac{k^2_{{\rm eff},i}}{m_i} - \frac{k^2_{{\rm eff},j}}{m_j}\right). \tag{342}$$

Status: not a DFD prediction (the matter-wave sector is null); see the status note after Eq. (337) in Sec. XIII. If both species share the same lattice wavelength, the expression reduces to $\propto (1/m_i - 1/m_j)$.

D. Discriminants and Systematics Control

The table compares the T^3 term of Eq. (337) with standard systematic effects:

a. Properties of the T^3 term.

1. **Time scaling:** not a discriminator: both DFD and GR carry $T^2/T^3/T^4$ identically through 1PN (§XIII B); the DFD row of Table XXXII is the Newtonian gravity-gradient recoil term, not a DFD signature

TABLE XXXII. Systematics overview and discriminants. The row labelled DFD is not a DFD prediction: its T^3 scaling and even k-parity are those of the standard Newtonian gravity-gradient recoil term, not unique to DFD (§XIII B).

Effect	T-scaling	Rotation flip	k-reversal parity
DFD (not predicted)	T^3	Yes	Even ($k_{\rm eff}^2$)
Gravity gradient Γ	T^2/T^3 mix	Often No	Mixed
Wavefront curvature	T^2	No	Odd
Vibrations (residual)	$\approx T^2$	No	Odd/Even mix
AC Stark / Zeeman	pulse-bounded	No	Design-dependent
Laser phase (uncorrelated)	T^2	No	Odd

2. **Orientation:** rotation would flip the term of Eq. (337) (via $\mathbf{g}\cdot\hat{\mathbf{n}}$); many systematics do not
3. **k-reversal:** the term is $\propto k_{\rm eff}^2$ (even under $k_{\rm eff}\to -k_{\rm eff}$), like the gravity-gradient recoil term; laser-phase systematics are odd and cancel
4. **Recoil dependence:** the term is $\propto v_{\rm rec}$, like the gravity-gradient recoil term
5. **Dual-species:** the expression gives a residual $\propto (1/m_1 - 1/m_2)$; through 1PN DFD adds nothing to the GR residual, which is null after rejection

b. Known systematics.

- **Gravity gradient noise (GGN):** Atmospheric and seismic mass fluctuations; mitigated by underground siting or subtraction.
- **Wavefront aberrations:** Dominant accuracy term; $< 3\times10^{-10}\,g$ equivalent demonstrated.
- **Vibration isolation:** 10^2–10^3 vertical attenuation at 30 mHz–10 Hz achieved.
- **Coriolis/Sagnac:** Separated by rotation protocols.

E. Sensitivity Forecast

a. Current state of the art. Long-baseline atom interferometers have demonstrated:

- Stanford 10-m fountain: single-shot sensitivity few$\times10^{-9}\,g$, arm separation 1.4 cm.
- Dual-species EP tests: $\eta\sim10^{-12}$ with $2T = 2$ s.
- VLBAI (Hannover): high-flux Rb/Yb, 10-m magnetic shielding.

F. Existing Analyses and the T^3 Term

Long-baseline atom interferometry experiments routinely suppress or calibrate out cubic-in-T gravity-gradient contributions using frequency-shift gravity-gradient (FSGG) compensation or k-vector tuning schemes [75–77], because within GR such terms are treated as systematics. As a result, published analyses typically:

1. Operate at fixed T for the main measurement
2. Do not report a residual-vs-T regression with the even-in-$k_{\rm eff}$, rotation-odd discriminator
3. Use k-reversal specifically to cancel odd-in-$k_{\rm eff}$ laser/systematic terms

To our knowledge, no experiment has isolated a coefficient $b_{\rm even}$ in $\phi_{\rm res}(T) = aT^2 + b_{\rm even}T^3$ that:

(a) Is *even* under $k_{\rm eff}\to -k_{\rm eff}$, and

(b) Flips sign under 180° rotation of a horizontal baseline

This is the signature the formula of Eq. (337) would give; DFD predicts none.

a. Practical consequence. A T^3 residual beyond the modelled gravity-gradient terms would appear as a "gravity-gradient residual" that was not fully removed by standard compensation and shows the wrong parity under k-reversal. DFD predicts none, so reanalysis of archival data with this discriminator applied is a zero-cost null test.

G. MAGIS and AION as Null Tests

The MAGIS (Matter-wave Atomic Gradiometer Interferometric Sensor) and AION (Atom Interferometer Observatory and Network) programs are next-generation vertical-baseline interferometers designed for gravitational wave detection and fundamental physics.

a. MAGIS-100. The 100-meter baseline at Fermilab will achieve:

- Interrogation times $T\sim 1$–2 s
- Single-shot strain sensitivity $\sim 10^{-19}/\sqrt{\rm Hz}$

Status: not a DFD prediction (the matter-wave sector is null); see the status note after Eq. (337) in Sec. XIII.

b. AION-10 and AION-100. The UK AION program plans staged development:

- AION-10 (Oxford): 10-m baseline, $T \sim 1$ s, demonstration phase
- AION-100 (UK, site pending): 100-m baseline, full science program

DFD predicts no DFD-specific phase in either.

c. Null-test analysis pass. We recommend that MAGIS/AION include a dedicated analysis pass:

1. Vary T systematically over the accessible range
2. Fit residual phase to $aT^2 + bT^3$
3. Apply the even-k, rotation-flip discriminator to b
4. Report b with uncertainty, regardless of whether it is consistent with zero

This analysis costs nothing beyond what is already planned and would provide a direct test of the matter-sector null prediction of DFD.

H. Complementarity with Cavity-Atom Test

The matter-wave and cavity-atom tests probe different sectors:

- **Cavity-atom:** Photon sector (optical metric) vs. atomic sector
- **Matter-wave:** Matter sector ($\nabla\psi$ coupling to momentum)

Together, they constrain DFD's sector coefficients: DFD predicts a null in the matter-wave channel through 1PN (status note after Eq. (337)) and in the co-located cavity–atom channel (Sec. XII, Thm. XI.2).

I. Summary: Matter-Wave Test

Summary: Matter-Wave T^3 Test (Not a DFD Prediction)

The formula of Eq. (337):

$$\Delta\phi_{\rm DFD} = \frac{\hbar k_{\rm eff}^2}{m}\,\frac{g}{c^2}\,T^3.$$

Status: not a DFD prediction. The expression above is not a phase (its units are s^2/m), and the re-derivation from the physical-metric dispersion relation, Eq. (AN3), yields no DFD-specific term: the one-particle Hamiltonian coincides with the GR test-body Hamiltonian through first post-Newtonian order for any static potential ($\gamma = \beta = 1$, §IV C; the rotating-Earth g_{0i} sector is not covered by this identity and is separately universal, Eq. (82)), so every T^2, T^3 and T^4 phase at this order is common to DFD and GR. The static metric is general relativity's at second post-Newtonian order as well (App. WS), so no DFD-specific term appears there either, and a species-dependent coupling $K_{\rm atom}$ (App. B 5) is an Eötvös parameter already bounded below 10^{-14} (§XV G). The matter-wave sector is therefore a null prediction of DFD (cf. §XVIII H); the forecasts, designs and falsification thresholds of this section and of Apps. B 5, D 3 and W 3 do not apply to DFD.

Features of that formula (none separates DFD from GR through 1PN):

- T^3 scaling, as in the standard gravity-gradient recoil term
- Rotation sign flip
- Even k-parity ($k_{\rm eff}^2$)
- Dual-species mass dependence

Status: a null test of DFD.
A null result is the DFD prediction (the matter-wave sector is null; status note above).

XIV. SOLAR CORONA SPECTRAL ASYMMETRY ANALYSIS

This section presents an analysis of archival SOHO/UVCS data, whose main result is that the early and late halves of a day's Ly-α exposures differ in intensity on about half of the days without a mean velocity shift, and states what DFD predicts for these data.

A. Motivation: Intensity Changes Without Velocity Changes

In the UVCS geometry the disk light arrives nearly radially and the line of sight is nearly perpendicular to it, so Doppler dimming by a change in radial outflow, and a change in density, both alter the scattered Ly-α intensity without shifting the observed line centroid. Intensity variations without velocity shifts therefore have a standard coronal explanation.

B. Electromagnetic Coupling to ψ

At tree level, electromagnetic fields couple to ψ through their energy, which sources ψ through the $(\varepsilon+3P) = 2u_{\rm EM}$ channel of the Optical Source Theorem (Theorem II.1; Eq. (R13)), and through the optical index $n = e^{\psi}$. This coupling has no threshold and is far too weak to be seen in the corona. DFD's prediction for the coronal lines is therefore the standard one.

C. SOHO/UVCS Ly-α Analysis

We analyzed archival data from the Ultraviolet Coronagraph Spectrometer (UVCS) aboard SOHO, examining 334 observation days spanning January 2007 through October 2009 during the minimum phase of Solar Cycle 23/24.

1. *Statistical Methodology: Permutation Tests and FDR Control*

The statistical analysis employs robust nonparametric methods designed for multiple hypothesis testing across coronal observation bins [78].

a. Permutation testing protocol. For each day with ≥ 2 frames (the frame table carries no slit position, so all of a day's frames form one group), we sorted frames by observation timestamp, which is the start time of each frame's observing sequence, and split at the temporal midpoint ("early" vs. "late"); whichever temporal half has the higher median intensity is post-hoc labeled "bright" for sign convention only — the labeling does not affect the statistical test [79]. Permutation tests ($N = 20{,}000$ replicates) generated null distributions by random reassignment of group labels. Two-sided p-values were computed as the fraction of permutation replicates yielding test statistics as extreme as observed.

b. Multiple testing correction. With 321 testable day groups, false discovery rate (FDR) control is essential. We applied the Benjamini–Hochberg procedure [80] at $q = 0.05$, ensuring that the expected proportion of false positives among significant detections is bounded at 5%.

c. Effect size quantification. Cohen's d provides a standardized measure of effect magnitude [81]: intensity contrast $d = 0.24$ (small–medium), velocity shift $d = -0.03$ (null). Of 321 testable groups, **163 (50.8%)** passed the 5% FDR threshold for intensity contrast. Days whose early and late halves were taken with different instrument settings (slit width, roll or pointing) reach $p < 0.05$ far more often (about 75–98% of them, against 34–47% of days without a change), so part of the contrast comes from comparing exposures taken with different settings, while days without a change still exceed the 5% expected under the null.

D. Multi-Species Test: O VI 103.2 nm

1. *Data and Methods*

From the UVCS Level-1 archive (2007–2009), we identified 42 observation sequences with wavelength coverage including O VI 103.2 nm. After quality filtering, **10,995 individual exposures** across 25 unique dates were analyzed. For each exposure, the spatially-integrated O VI spectrum was extracted, the intensity-weighted centroid computed, and the blue/red wing asymmetry about the centroid measured. Asymmetries were binned by the Sun's ecliptic longitude θ (zero at the March equinox) and fitted with a sinusoidal model:

$$\frac{\Delta I}{I}(\theta) = A\sin(\theta+\phi) + C. \tag{343}$$

2. *Results*

The sinusoid fits treat each O VI exposure, and each Ly-α day that passed the FDR threshold, as an independent point, and the two fitted quantities are different statistics: a per-exposure wing asymmetry for O VI and the early/late intensity contrast for Ly-α. The 10,995 O VI exposures come from six observing campaigns. With the observing campaign as the unit for O VI and the day as the unit for Ly-α, neither line shows a significant annual modulation, and neither phase is determined.

E. Consistency Check: Intensity Without Velocity

a. O VI velocity analysis. Binned by asymmetry magnitude quartiles, the asymmetry increases by a factor of about 10 from Q1 to Q4. With the line centre fitted in each exposure and the observing campaign or the date as the independent unit, the mean velocity shows no significant rise from Q1 to Q4 ($+0.8 \pm 0.4$ km/s by campaign, $+0.4 \pm 0.3$ km/s by date).

F. Summary

The main UVCS result is the Ly-α early/late intensity contrast, significant at 5% FDR on 163 of 321 days without a mean velocity shift (Cohen's $d = -0.03$); part of the contrast comes from comparing exposures taken with different instrument settings. Neither H I nor O VI shows a significant annual modulation once the day (H I) or the observing campaign (O VI) is the independent unit.

UVCS Analysis Summary

Key Results:
- Ly-α early/late intensity contrast significant on 163 of 321 days (5% FDR), with no mean velocity shift ($d = -0.03$)
- Days whose two halves used different instrument settings pass far more often
- No significant annual modulation in either line with independent units

G. Quantitative Multi-Wavelength Test: The Asymmetry Ratio

The ratio of Ly-α to O VI asymmetry amplitudes compares *resonantly scattered* chromospheric Ly-α with *locally produced* coronal O VI emission.

1. Thermal Width Analysis

The thermal Doppler width of a spectral line depends on temperature and atomic mass:

$$\sigma_{\rm therm} = \lambda\sqrt{\frac{k_B T}{mc^2}}. \tag{344}$$

TABLE XXXIII. Thermal line widths at characteristic formation temperatures.

Line	Temperature	Mass	Thermal Width
Ly-α (1216 Å)	10^4 K	m_p	0.037 Å
O VI (1032 Å)	2×10^6 K	$16\,m_p$	0.111 Å

The width ratio is $\sigma_{\rm OVI}/\sigma_{\rm Ly\alpha} = 3.0$ at these temperatures; the coronal H I that UVCS observes is at about 1–3 $\times 10^6$ K, where the Ly-α width is 0.37–0.64 Å.

2. The Generalized Prediction

For small detuning δ of a Gaussian line profile with width σ, the fractional intensity change scales as:

$$A = \frac{\Delta I}{I} \propto \left(\frac{\delta}{\sigma}\right)^2. \tag{345}$$

We write the asymmetry ratio in the generalized form:

$$\boxed{R \equiv \frac{A_{\rm Ly\alpha}}{A_{\rm OVI}} = \Gamma\left(\frac{\sigma_{\rm OVI}}{\sigma_{\rm Ly\alpha}}\right)^2} \tag{346}$$

where Γ captures any enhancement factor for scattered versus locally-emitted light. DFD's optics adds no enhancement, so Γ takes its standard value (App. M).

3. Comparison with Observations

The 2007–2009 data do not measure R, since the annual fits of Sec. XIV D use different statistics for the two lines and find no significant annual modulation in either.

The matched dim/bright slope measures Γ. In the same bins of simultaneous Ly-α and O VI spectra, the O VI dim/bright intensity ratio plotted against the Ly-α ratio has slope $1/R$, so with $\sigma_{\rm Ly\alpha}$ and $\sigma_{\rm OVI}$ measured in those spectra, rather than taken from Table XXXIII, Eq. (346) predicts the slope $(\sigma_{\rm Ly\alpha}/\sigma_{\rm OVI})^2/\Gamma$, with the bins, the width measurement and the fit fixed in advance. With DFD's standard Γ this slope tests the coronal line-formation model; it does not separate DFD from standard physics.

XV. ANTIMATTER GRAVITY TESTS

The recent trapping of more than 1.5×10^4 antihydrogen atoms and the first direct measurements of antimatter free fall [82, 83] open a qualitatively new window on the Einstein Equivalence Principle (EEP). In pure-metric GR with minimal coupling, hydrogen (H) and antihydrogen ($\bar{\rm H}$) must experience identical gravitational acceleration. DFD reproduces this prediction at the metric level, but allows for controlled, testable deviations through non-metric couplings.

A. GR Baseline: Matter–Antimatter Universality

In pure-metric GR, the motion of a test body follows the geodesic equation

$$\frac{d^2x^\mu}{d\tau^2} + \Gamma^\mu_{\nu\rho}\frac{dx^\nu}{d\tau}\frac{dx^\rho}{d\tau} = 0, \tag{347}$$

independent of the body's internal constitution. In the weak-field, slow-motion limit relevant to laboratory experiments:

$$\frac{d^2\mathbf{x}}{dt^2} \approx -\nabla\Phi(\mathbf{x}), \tag{348}$$

where Φ is the Newtonian potential. This implies:

$$a_H = a_{\bar H} = -\nabla\Phi \quad \text{(GR prediction)}. \tag{349}$$

Definition XV.1 (Matter–antimatter universality in GR)**.** In pure-metric GR with minimal coupling, hydrogen and antihydrogen obey:

1. Identical free-fall acceleration: $a_H(\mathbf{x}) = a_{\bar H}(\mathbf{x}) = -\nabla\Phi(\mathbf{x})$
2. Identical gravitational redshift for corresponding clock transitions

Any detected deviation from these equalities falsifies this minimal framework.

B. DFD Metric-Level Prediction

At the level of the effective metric, DFD reproduces the GR weak-field limit. The physical metric (12) gives, in the slow-motion limit:

$$\frac{d^2\mathbf{x}}{dt^2} \approx \frac{c^2}{2}\nabla\psi(\mathbf{x}) = -\nabla\Phi(\mathbf{x}), \tag{350}$$

using $\Phi = -c^2\psi/2$. Thus metric-coupled test bodies—including antihydrogen—follow the same trajectories as in GR.

Remark XV.2 (Universal free fall at metric level). At the effective metric level, DFD reproduces GR's universal free fall. Any violation of matter–antimatter universality must arise from non-metric couplings of physical sectors to ψ beyond the metric.

C. Non-Metric Couplings and Species-Dependent Sensitivities

Once Standard Model sectors are embedded as internal modes in the ψ medium, small non-metric couplings can arise. At the effective field theory level:

$$\mathcal{L} = \mathcal{L}_{\text{metric}}[g_{\mu\nu}[\psi], \text{SM fields}] + \delta\mathcal{L}[\psi, \text{sectors}], \tag{351}$$

where $\mathcal{L}_{\text{metric}}$ represents minimally coupled SM fields and $\delta\mathcal{L}$ encodes non-metric ψ-dependence.

A generic form for $\delta\mathcal{L}$ is:

$$\delta\mathcal{L} = \sum_I \beta_I\, \psi(\mathbf{x})\, \mathcal{I}_I(\mathbf{x}), \tag{352}$$

where:

- I indexes SM sectors (electromagnetic, strong, baryon number, lepton number, etc.)
- $\mathcal{I}_I$ are scalar invariants ($F_{\mu\nu}F^{\mu\nu}$, $G_{\mu\nu}G^{\mu\nu}$, n_B, n_L, etc.)
- β_I are small dimensionless coupling coefficients

1. Bound-State Mass Shifts

For a bound state A with unperturbed mass $m_A^{(0)}$, the coupling (352) induces a mass shift:

$$\delta m_A(\psi)\, c^2 = \sum_I \beta_I\, \psi\, \langle A| \int d^3x\, \mathcal{I}_I(\mathbf{x}) |A\rangle. \tag{353}$$

Define the dimensionless **sensitivity parameter**:

$$\boxed{\sigma_A \equiv \frac{1}{m_A^{(0)}c^2} \sum_I \beta_I\, \langle A| \int d^3x\, \mathcal{I}_I(\mathbf{x}) |A\rangle} \tag{354}$$

Then to first order in ψ:

$$m_A(\psi) \approx m_A^{(0)}(1 + \sigma_A\psi). \tag{355}$$

2. CPT Considerations

Remark XV.3 (C-even vs C-odd couplings). If $\delta\mathcal{L}$ couples only to charge-conjugation-even densities ($F_{\mu\nu}F^{\mu\nu}$, $G_{\mu\nu}G^{\mu\nu}$, Higgs potential), then by CPT symmetry:

$$\sigma_{\bar{A}} = \sigma_A \quad \text{(C-even couplings only)}. \tag{356}$$

However, if $\delta\mathcal{L}$ includes C-odd densities such as baryon number n_B or lepton number n_L:

$$\sigma_{\bar{H}} - \sigma_H \sim -2(\beta_B \tilde{f}_B^H + \beta_L \tilde{f}_L^H), \tag{357}$$

where $\tilde{f}_B^H, \tilde{f}_L^H \sim \mathcal{O}(1)$.

D. Matter–Antimatter Differential Acceleration

1. Effective Point-Particle Action

Model bound state A as an effective point particle with action:

$$S_A = -\int m_A(\psi)\, c^2\, d\tau = -\int m_A(\psi)\, c^2 \sqrt{-g_{\mu\nu}[\psi]\dot{x}^\mu\dot{x}^\nu}\, d\lambda. \tag{358}$$

In the weak-field, slow-motion limit with $m_A(\psi) \approx m_A^{(0)}(1 + \sigma_A\psi)$, the effective potential becomes:

$$V_A(\mathbf{x}) = m_A^{(0)}c^2 \left(\sigma_A - \frac{1}{2}\right)\psi(\mathbf{x}) = m_A^{(0)}\Phi(\mathbf{x})(1 - 2\sigma_A). \tag{359}$$

The effective gravitational mass is:

$$m_{g,A} = m_A^{(0)}(1 - 2\sigma_A), \tag{360}$$

while the inertial mass remains $m_A^{(0)}$.

2. Free-Fall Acceleration

The free-fall acceleration of species A is:

$$a_A = -\frac{m_{g,A}}{m_A^{(0)}}\nabla\Phi = -(1 - 2\sigma_A)\nabla\Phi = (1 - 2\sigma_A)a, \tag{361}$$

where $a = -\nabla\Phi$ is the GR baseline acceleration.

For hydrogen and antihydrogen:

$$a_H = (1 - 2\sigma_H)a, \tag{362}$$

$$a_{\bar{H}} = (1 - 2\sigma_{\bar{H}})a. \tag{363}$$

The **differential acceleration** is:

$$\Delta a_{H\bar{H}} \equiv a_{\bar{H}} - a_H = -2(\sigma_{\bar{H}} - \sigma_H)a, \tag{364}$$

giving the fractional difference:

$$\boxed{\frac{\Delta a_{H\bar{H}}}{a} \equiv \frac{|a_{\bar{H}}| - |a_H|}{|a|} \approx 2|\sigma_{\bar{H}} - \sigma_H|} \tag{365}$$

E. Three Scenarios for $\sigma_{\bar{H}} - \sigma_H$

a. Scenario 1: Pure energy-density couplings (CPT-even). If $\delta\mathcal{L}$ couples only to CPT-even energy densities

and respects charge conjugation:

$$\sigma_{\bar{H}} = \sigma_H \quad \Rightarrow \quad \frac{\Delta a_{H\bar{H}}}{a} = 0. \tag{366}$$

DFD reproduces the pure-metric GR prediction.

b. Scenario 2: Natural C-odd couplings. If ψ couples to baryon/lepton number densities with coefficients $|\beta_B|, |\beta_L| \sim 10^{-3}$–$10^{-1}$ (natural, unsuppressed values):

$$\frac{\Delta a_{H\bar{H}}}{a} \sim 10^{-3} \text{ to } 10^{-1}. \tag{367}$$

Such couplings are already excluded by ordinary-matter equivalence-principle tests (Sec. XV G).

c. Scenario 3: Fine-tuned or symmetry-suppressed C-odd couplings. If $|\sigma_{\bar{H}} - \sigma_H| \ll 10^{-3}$, this would require either:

- Accidental cancellation between multiple C-odd couplings, or
- A symmetry mechanism suppressing C-odd couplings relative to CPT-even ones

TABLE XXXIV. Summary of matter–antimatter scenarios.

Scenario	$\lvert\sigma_{\bar{H}} - \sigma_H\rvert$	$\Delta a_{H\bar{H}}/a$
Pure metric (GR)	0	0
Natural C-odd	10^{-3}–10^{-1}	2×10^{-3}–2×10^{-1}
Suppressed C-odd	$\ll 10^{-3}$	$\ll 10^{-2}$

F. Experimental Mapping: ALPHA-g and Beyond

1. ALPHA-g Free-Fall Measurements

The ALPHA-g experiment measures the vertical motion of antihydrogen atoms released from a magnetic trap. The measured acceleration can be written as:

$$a_{\bar{H}} = (1 - 2\sigma_{\bar{H}})g, \tag{368}$$

where g is Earth's surface gravity.

Current status (2023): The ALPHA collaboration reported the first observation of antihydrogen free fall, showing consistency with downward acceleration at approximately the same rate as ordinary matter [82]. Current precision: $\sim$20% ($a_{\bar{H}} = (0.75 \pm 0.13 \pm 0.16)\, g$).

Near-term target: $\sim$1% precision on $\Delta a_{H\bar{H}}/a$.

Ultimate target: $\sim$0.1% precision, probing $|\sigma_{\bar{H}} - \sigma_H| \lesssim 5\times10^{-4}$.

2. Spectroscopy Complement

For a transition T in bound state A, define the **transition sensitivity** $\kappa_A^{(T)}$ analogously to σ_A. The local transition frequency is:

$$\nu_A^{(T)}(\psi) \approx \nu_A^{(T,0)}(1 + \kappa_A^{(T)}\psi). \tag{369}$$

The DFD-induced fractional shift at position $\mathbf{x}$:

$$\left(\frac{\Delta\nu}{\nu}\right)_A^{(T)}(\mathbf{x}) \approx -\frac{\Delta\Phi(\mathbf{x})}{c^2} + \kappa_A^{(T)}\psi(\mathbf{x}). \tag{370}$$

Comparing H and $\bar{\text{H}}$ 1S–2S frequencies at different gravitational potentials probes $\kappa_{\bar{H}}^{(1S-2S)} - \kappa_H^{(1S-2S)}$, which is *independent* of $\sigma_{\bar{H}} - \sigma_H$.

Remark XV.4 (Complementarity of free-fall and spectroscopy). Free-fall measurements probe σ_A (overall mass sensitivity), while spectroscopy probes $\kappa_A^{(T)}$ (transition-specific sensitivity). Together they can disentangle different sectors of the DFD coupling structure.

G. Relation to Ordinary-Matter EP Tests

Ordinary-matter equivalence-principle tests (torsion balances, lunar laser ranging, MICROSCOPE) constrain the Eötvös parameter:

$$\eta_{AB} = 2\frac{a_A - a_B}{a_A + a_B} = -2(\sigma_A - \sigma_B) \tag{371}$$

to the $\sim 10^{-14}$ level for materials with different neutron-to-proton ratios [5]. However, these tests involve only ordinary matter and constrain combinations where baryon and lepton numbers have the *same sign*.

For antihydrogen:

$$f_B^{\bar{H}} = -f_B^H, \quad f_L^{\bar{H}} = -f_L^H, \tag{372}$$

so that:

$$\sigma_{\bar{H}} - \sigma_H \sim -2\beta_B f_B^H - 2\beta_L f_L^H. \tag{373}$$

Ordinary-matter tests already bound these couplings through the B/μ and Z/μ differences between materials, to $|\Delta a_{H\bar{H}}/a| \lesssim 10^{-11}$ (Ti–Pt, MICROSCOPE).

H. DFD Prediction and Falsification

a. Core DFD prediction. With universal ψ-coupling (no non-metric sector-specific couplings):

$$\sigma_A = 0 \text{ for all species} \quad \Rightarrow \quad \frac{\Delta a_{H\bar{H}}}{a} = 0. \tag{374}$$

This is the default DFD prediction, matching GR.

b. Extended DFD (with C-odd couplings). If Standard Model sectors couple non-minimally to ψ through C-odd invariants, ordinary-matter equivalence-principle tests already bound the deviation to $|\Delta a_{H\bar{H}}/a| \lesssim 10^{-11}$.

Antimatter Falsification Criteria

If $\Delta a_{H\bar{H}}/a = 0$ at 10^{-3} precision:

- Pure-metric GR confirmed in antimatter sector

If $\Delta a_{H\bar{H}}/a \sim 10^{-2}$:

- Pure-metric GR and DFD falsified
- Requires follow-up with spectroscopy to disentangle sectors

I. Summary

Antimatter gravity experiments provide a unique probe of gravity-matter coupling:

1. At the metric level, DFD reproduces GR's universal free fall.
2. Non-metric couplings to C-odd sector invariants (n_B, n_L) induce species-dependent sensitivities σ_A.
3. The matter–antimatter differential acceleration is:
$$\frac{\Delta a_{H\bar{H}}}{a} \approx 2|\sigma_{\bar{H}} - \sigma_H|. \tag{375}$$
4. Current ALPHA-g precision (∼20%) already constrains gross "antigravity" scenarios.

TABLE XXXV. Experimental targets for antimatter gravity.

Experiment	Observable	Precision	DFD signal
ALPHA-g (current)	$a_{\bar{H}}/g$	20%	Gross test
ALPHA-g (near)	$\Delta a_{H\bar{H}}/a$	1%	Null
ALPHA-g (ultimate)	$\Delta a_{H\bar{H}}/a$	0.1%	Null
Spectroscopy	$\kappa_{\bar{H}} - \kappa_H$	10^{-12}	Sector decomp.

XVI. COSMOLOGICAL IMPLICATIONS

In this section GR/ΛCDM enters *only* as an observer dictionary (how distances/angles are commonly reported), not as ontology.

A. ψ-Tomography (ψ-Screen) Cosmology Module

a. Non-negotiable premise. The primary reconstructed object is the "ψ-screen" on the past light cone:
$$\Delta\psi(z,\hat{n}) \equiv \psi_{\rm em}(z,\hat{n}) - \psi_{\rm obs}, \qquad \text{dimensionless.} \tag{376}$$
All GR/ΛCDM quantities used in this section (e.g. $D_L^{\rm dict}, D_A^{\rm obs}$) are *reporting-layer* variables that serve as a convenient dictionary for published datasets. The supernova and distance relations of this module, Eqs. (380)–(381), Estimator A and the closure statements built on them belong to the optical-distance dressing that the SN-lensing sign test retired (App. SL); they are kept as the record of that test and are not DFD predictions. The duality check (Estimator B), the patchwise, mean-subtracted CMB estimator (Estimator C) and its cross-correlation falsifier remain in use.

1. DFD postulates and sign conventions

DFD is formulated on flat $\mathbb{R}^3$ with a scalar field ψ and refractive index $n = e^{\psi}$. The one-way light speed is
$$c_1(\psi) = c\, e^{-\psi}, \tag{377}$$
and the (nonrelativistic) acceleration of matter is
$$\boldsymbol{a} = \frac{c^2}{2}\nabla\psi. \tag{378}$$
We adopt the gauge choice $\psi_{\rm obs} \equiv 0$, so that $\Delta\psi = \psi_{\rm em}$ in this gauge. With this convention:

- $\Delta\psi > 0$ means ψ (hence n) was higher at emission than locally (slower c_1 at emission).
- $\Delta\psi < 0$ means ψ was lower at emission than locally (faster c_1 at emission).

a. Endpoint vs. observable screen. Equation (376) is an endpoint definition. Operationally, each dataset reconstructs an *observable* screen $\Delta\psi_{\rm obs}$ defined by the log-multiplicative bias required by the DFD optical relations below. When needed, one may represent $\Delta\psi_{\rm obs}$ as a weighted line-of-sight functional
$$\Delta\psi_{\rm obs}(z,\hat{n}) = \int_0^{\chi(z)} d\chi\, W_{\rm obs}(\chi; z)\, \delta\psi(\chi,\hat{n}), \tag{379}$$
where χ is a dictionary comoving-distance coordinate and $W_{\rm obs}$ is a dataset-specific kernel. The inverse program reconstructs $\Delta\psi_{\rm obs}$ *directly from data* without assuming a particular $W_{\rm obs}$.

2. Forward model: three optical relations

The module was built around three optical relations.

a. (1) Luminosity-distance bias (SNe Ia). Let $D_L^{\rm dict}(z,\hat{n})$ be the baseline luminosity distance as typically reported under the observer dictionary. The optical-distance dressing, retired by the SN-lensing sign test (App. SL), mapped this to an optically biased luminosity distance:
$$D_L^{\rm DFD}(z,\hat{n}) = D_L^{\rm dict}(z,\hat{n})\, e^{\Delta\psi(z,\hat{n})}. \tag{380}$$
Equivalently, $\ln D_L^{\rm DFD} = \ln D_L^{\rm dict} + \Delta\psi$.

b. (1b) Angular-diameter-distance bias. Both D_L and D_A are computed from null geodesics of the same optical metric $\tilde{g}_{\mu\nu}$. Under that dressing the ψ-field screened both distances equally:
$$D_A^{\rm DFD}(z,\hat{n}) = D_A^{\rm dict}(z,\hat{n})\, e^{\Delta\psi(z,\hat{n})}. \tag{381}$$

c. (2) Distance duality (Etherington reciprocity). DFD's optical metric $d\tilde{s}^2 = -c^2\, dt^2/n^2 + d\mathbf{x}^2$ with $n = e^{\psi} > 0$ is a smooth, non-degenerate Lorentzian metric. All three conditions of Etherington's reciprocity theorem[84, 85] are satisfied: (i) photons propagate on null geodesics of a Lorentzian metric; (ii) geodesics are locally unique (ψ is $C^{1,\alpha}$ away from sources, Appendix U); (iii) photon number is conserved (no absorption/emission mechanism). Therefore
$$D_L(z,\hat{n}) = (1+z)^2\, D_A(z,\hat{n}). \tag{382}$$
This holds exactly; no $e^{\Delta\psi}$ factor appears. The common screening factor from Eqs. (380) and (381) cancels in the ratio D_L/D_A.

d. Notation. We distinguish $\Delta\psi_{\rm screen}(z,\hat{n})$ (the distance bias relative to the dictionary baseline, measured by Estimators A and C below) from $\Delta\psi_{\rm dual}(z,\hat{n}) \equiv \ln[D_L/(1+z)^2 D_A] = 0$ (the DDR violation parameter, measured by Estimator B; identically zero). Where the subscript is omitted, $\Delta\psi$ refers to $\Delta\psi_{\rm screen}$.

e. (3) CMB acoustic-scale screen (angular anisotropy). The sky-averaged acoustic scale is fixed by the current measured-clock no-screen solution, $100\theta_* = 1.04110$ and $\ell_1 \simeq 220.4$. The following estimator is therefore restricted to *patchwise, mean-subtracted* anisotropic lensing, analogous to a convergence map. It may not be used to map a putative unlensed monopole $297 \to 220$, to shift the global θ_*, or to redistribute H_0 and r_s. Let $\ell_1(\hat{n})$ denote the locally inferred first acoustic peak location from patchwise CMB power spectra. DFD posits the angular screen mapping

$$\ell_1(\hat{n}) = \ell_{\rm true}\, e^{-\Delta\psi(\hat{n})}, \tag{383}$$

where $\ell_{\rm true} \simeq 220.4$ is the current sky-independent no-screen baseline and cancels out of the normalized anisotropy reconstruction below.

f. Sign of the ℓ_1 mapping. The sign deserves explicit comment. The distance relations Eqs. (380)–(381) give $D_A^{\rm DFD} \propto e^{+\Delta\psi}$: objects appear *farther*, which naively pushes $\ell_1 \propto D_A/r_s$ *higher*. But that scaling applies to the sky-averaged monopole, which is absorbed into $\ell_{\rm true}$. Equation (383) describes the *direction-dependent* anisotropy: a foreground sightline with $\Delta\psi(\hat{n}) > 0$ acts as a convergent screen that *magnifies* the angular scale of CMB features in that patch. Larger apparent angular scale maps to *lower* ℓ_1, hence the negative exponent. This is the same sign as standard weak-lensing magnification of the CMB, where convergence $\kappa > 0$ shifts power to lower ℓ.

3. Two independent screen estimators and one consistency check

a. Estimator A: SNe Ia alone (and its degeneracy). From Eq. (380), an operational estimator on each SN sightline is

$$\widehat{\Delta\psi}_{\rm SN}(z_i,\hat{n}_i) \;\equiv\; \ln D_L^{\rm obs}(z_i,\hat{n}_i) - \ln D_L^{\rm dict}(z_i) - \mathcal{M}, \tag{384}$$

where $\mathcal{M}$ is an unknown constant absorbing absolute magnitude / distance-ladder calibration. SNe alone cannot fix an additive constant in $\Delta\psi$ (monopole), because $\Delta\psi \to \Delta\psi + {\rm const}$ can be absorbed into $\mathcal{M}$. A robust SN-only product is therefore the anisotropy field

$$\widehat{\delta\psi}_{\rm SN}(z,\hat{n}) \;\equiv\; \widehat{\Delta\psi}_{\rm SN}(z,\hat{n}) - \big\langle \widehat{\Delta\psi}_{\rm SN}(z,\hat{n})\big\rangle_{\hat{n}}. \tag{385}$$

b. Estimator B: SNe + BAO / strong lensing (duality consistency check). Etherington's reciprocity (382) implies that the observable ratio

$$\boxed{\widehat{\Delta\psi}_{\rm dual}(z,\hat{n}) \;\equiv\; \ln\!\left(\frac{D_L^{\rm obs}(z,\hat{n})}{(1+z)^2\, D_A^{\rm obs}(z,\hat{n})}\right) \;=\; 0.} \tag{386}$$

This is not an independent measurement of $\Delta\psi_{\rm screen}$; it is a *consistency check* that the optical metric satisfies Etherington's conditions. The observed $\widehat{\Delta\psi}_{\rm dual} = 0.01 \pm 0.02$ [86, 87] is consistent with zero.

c. Estimator C: CMB peak anisotropy (screen at last scattering). From Eq. (383), define the normalized estimator:

$$\boxed{\widehat{\Delta\psi}_{\rm CMB}(\hat{n}) = -\ln\ell_1(\hat{n}) + \langle\ln\ell_1\rangle,} \tag{387}$$

which fixes the additive constant by construction ($\langle\widehat{\Delta\psi}_{\rm CMB}\rangle = 0$). This isolates *angular* structure in the screen at last scattering.

d. How to obtain $\ell_1(\hat{n})$ without ΛCDM priors. Choose a sky patching scheme; estimate local pseudo-C_ℓ spectra per patch (beam/mask corrected); fit a *local peak locator* template around the first peak (only a smooth peaked function is required); take the maximizing multipole as ℓ_1 for that patch.

4. Theorem-level internal closure of the reconstructed screen

The two screen estimators and one consistency check introduced above are more than "three ways of plotting the same thing": under the forward optical relations, they imply *overdetermined closure identities* that must hold on the sky (and across redshift bins) if a single scalar screen $\Delta\psi(z,\hat{n})$ is the correct organizing variable.

a. Conventions and hypotheses. Fix a redshift bin $z \in [z_a, z_b]$ and an analysis mask $W(\hat{n})$ (common to all maps in a given test). Assume:

1. **(H1) Forward relations.** The DFD optical relations (380)–(383) hold on their respective domains of validity.
2. **(H2) Observable identification.** The reported distances used in Eqs. (384)–(386) are the observational reconstructions of the corresponding DFD distances along that line of sight, i.e. $D_L^{\rm obs}(z,\hat{n}) = D_L^{\rm DFD}(z,\hat{n})$ and $D_A^{\rm obs}(z,\hat{n}) = D_A^{\rm DFD}(z,\hat{n})$ (up to the stated measurement errors).
3. **(H3) SN calibration constancy.** The SN absolute calibration constant $\mathcal{M}$ in Eq. (384) is a global constant (independent of z and $\hat{n}$), as assumed in the estimator definition.

No dynamical assumption about $\mu(x)$, growth, or a specific dictionary is required for the identities below.

Theorem XVI.1 (Duality consistency)**.** *Under (H1)–(H2), the duality estimator* (386) *tests Etherington consistency:*

$$\widehat{\Delta\psi}_{\rm dual}(z,\hat{n}) = 0. \tag{388}$$

Proof. From Eqs. (380) and (381), both distances carry the common screening factor $e^{\Delta\psi}$. In the ratio $D_L/[(1+$

$z)^2 D_A]$ this factor cancels, leaving the standard Etherington relation (382): $D_L^{\rm dict}/[(1+z)^2 D_A^{\rm dict}] = 1$. Hence $\widehat{\Delta\psi}_{\rm dual} = \ln 1 = 0$. □

Theorem XVI.2 (SN inversion up to an additive constant)**.** *Under (H1)–(H3), the SN estimator (384) satisfies*

$$\widehat{\Delta\psi}_{\rm SN}(z,\hat{n}) = \Delta\psi(z,\hat{n}) - \mathcal{M}, \tag{389}$$

and therefore its centered field (385) equals the true screen anisotropy at that redshift:

$$\widehat{\delta\psi}_{\rm SN}(z,\hat{n}) = \Delta\psi(z,\hat{n}) - \langle\Delta\psi(z,\hat{n})\rangle_{\hat{n}}. \tag{390}$$

Proof. From Eq. (380), $\ln D_L^{\rm DFD} = \ln D_L^{\rm dict} + \Delta\psi$. Using (H2) and inserting into (384) gives $\widehat{\Delta\psi}_{\rm SN} = \Delta\psi - \mathcal{M}$. Centering over $\hat{n}$ cancels $\mathcal{M}$ identically, yielding (385) as the true anisotropy. □

Corollary XVI.3 (A–B closure simplification)**.** *Under (H1)–(H3), since $\widehat{\Delta\psi}_{\rm dual} = 0$ (Theorem XVI.1) and $\widehat{\Delta\psi}_{\rm SN} = \Delta\psi_{\rm screen} - \mathcal{M}$ (Theorem XVI.2), the calibration constant is directly extractable:*

$$\widehat{\mathcal{M}}(z) = -\Big\langle \widehat{\Delta\psi}_{\rm SN}(z,\hat{n}) \Big\rangle_{\hat{n},W}. \tag{391}$$

Equivalently, defining the ***internal closure residual field***

$$R_{AB} \equiv \widehat{\Delta\psi}_{\rm SN} + \widehat{\mathcal{M}} = \Delta\psi_{\rm screen} - \langle\Delta\psi_{\rm screen}\rangle_{\hat{n}}, \tag{392}$$

recovers the screen anisotropy (up to measurement noise). Here $\widehat{\mathcal{M}}(z) = \mathcal{M} - \langle\Delta\psi_{\rm screen}(z,\hat{n})\rangle_{\hat{n},W}$; it equals $\mathcal{M}$ when the screen has no monopole, as in the current no-screen solution, and the residual field R_{AB} is exact in either case.

Proof. Set $\widehat{\Delta\psi}_{\rm dual} = 0$ in the original A–B difference; the result follows from Theorem XVI.2. □

Corollary XVI.4 (Cross-bin overdetermination: $\mathcal{M}$ must be constant)**.** *Under (H3), and with a screen whose monopole does not depend on redshift, the offset $\widehat{\mathcal{M}}(z)$ extracted from Corollary XVI.3 is independent of redshift. In practice, for redshift bins $\{z_j\}$ with overlaps, the statistic*

$$\chi^2_{\mathcal{M}} = \sum_j \frac{\big(\widehat{\mathcal{M}}(z_j) - \overline{\mathcal{M}}\big)^2}{\sigma^2_{\mathcal{M}}(z_j)}, \qquad \overline{\mathcal{M}} \equiv \frac{\sum_j \widehat{\mathcal{M}}(z_j)/\sigma^2_{\mathcal{M}}(z_j)}{\sum_j 1/\sigma^2_{\mathcal{M}}(z_j)} \tag{393}$$

is an ***overdetermined*** *consistency test of the SN calibration: large $\chi^2_{\mathcal{M}}$ falsifies at least one of (H1)–(H3) (or flags unmodeled systematics).*

Corollary XVI.5 (Harmonic-space closure for anisotropy: SN vs CMB)**.** *Since $\widehat{\Delta\psi}_{\rm dual} = 0$, the non-trivial harmonic closure test compares the two independent screen estimators. Let both the centered SN map (Theorem XVI.2) and the CMB map (Theorem XVI.6) be defined on a common mask. Then for all multipoles $\ell \geq 1$:*

$$a^{\rm SN}_{\ell m}(z_*) = a^{\rm CMB}_{\ell m}, \tag{394}$$

where z_* is the last-scattering redshift, and therefore (after identical smoothing/masking) the pseudo-C_ℓ spectra satisfy

$$\widehat{C}^{\rm SN\times SN}_\ell(z_*) = \widehat{C}^{\rm CMB\times CMB}_\ell = \widehat{C}^{\rm SN\times CMB}_\ell \qquad (\ell \geq 1), \tag{395}$$

up to the usual mask-coupling and noise-bias corrections.

Proof. Both the SN-centered map and the CMB map reconstruct the same monopole-free screen $\Delta\psi_{\rm screen}(z_*,\hat{n}) - \langle\Delta\psi_{\rm screen}\rangle_{\hat{n}}$ at last scattering (up to measurement noise), hence equal harmonic coefficients for $\ell \geq 1$. □

Theorem XVI.6 (CMB estimator is the centered last-scattering screen)**.** *Under (H1)–(H2), the CMB peak estimator (387) reconstructs the monopole-free screen at last scattering:*

$$\widehat{\Delta\psi}_{\rm CMB}(\hat{n}) = \Delta\psi(z_*,\hat{n}) - \langle\Delta\psi(z_*,\hat{n})\rangle_{\hat{n}}. \tag{396}$$

Proof. From Eq. (383), $\ell_1(\hat{n}) = \ell_{\rm true} e^{-\Delta\psi(\hat{n})}$. Taking $-\ln\ell_1 + \langle\ln\ell_1\rangle$ cancels $\ell_{\rm true}$ and removes the monopole by construction, yielding Eq. (387). □

b. Interpretation. Theorems XVI.1–XVI.6 state "closure" algebraically: *a single screen* $\Delta\psi_{\rm screen}(z,\hat{n})$ implies (i) Etherington consistency ($\widehat{\Delta\psi}_{\rm dual} = 0$), (ii) an SN reconstruction with only one global degeneracy $\mathcal{M}$, and (iii) strict agreement of SN and CMB anisotropy maps on overlapping skies and bins. This makes $\Delta\psi_{\rm screen}(z,\hat{n})$ an *overconstrained* observable: independent reconstructions must agree, and persistent mismatch falsifies the single-screen hypothesis.

5. A GR-independent falsifier

a. Primary falsifier: cross-correlation with independent structure maps. Let $X(\hat{n})$ be an independent line-of-sight structure tracer map (e.g. CMB lensing convergence κ or a projected galaxy density map in a defined redshift slice). Compute the cross-power spectrum

$$\widehat{C}^{\Delta\psi\times X}_\ell \equiv \frac{1}{2\ell+1}\sum_{m=-\ell}^{\ell} \Delta\psi_{\ell m}\, X^*_{\ell m}, \tag{397}$$

and the dimensionless correlation coefficient

$$\widehat{r}_\ell \equiv \frac{\widehat{C}^{\Delta\psi\times X}_\ell}{\sqrt{\widehat{C}^{\Delta\psi\times\Delta\psi}_\ell\ \widehat{C}^{X\times X}_\ell}}. \tag{398}$$

b. Null hypothesis (falsifier).

$$H_0: \quad C^{\Delta\psi\times X}_\ell = 0 \quad \text{for all analyzed } \ell \text{ (or all bins).} \tag{399}$$

Pre-registered falsification criterion:

If $\widehat{\Delta\psi}_{\rm CMB}(\hat n)$ exhibits no statistically significant cross-correlation with an independent structure map $X(\hat n)$ down to the sensitivity implied by the measured $\Delta\psi$ auto-power and the map noises, then the ψ-screen mechanism (as the explanation for the optical biases in this module) is falsified.

c. Probe scope (which tracers can test the null). The falsifier above has discriminating power only for a structure map X whose redshift support overlaps that of the reconstructed screen. In particular, a *very local* reconstruction—e.g. a directional Hubble-bias field $\delta H_0(\hat n)$ built from $z<0.05$ galaxies—cannot test the $X=\kappa_{\rm CMB}$ channel: the CMB-lensing kernel carries only $\sim 6\times10^{-5}$ of its line-of-sight weight at $z<0.05$ (it peaks at $z\simeq1.9$), so a null $C_\ell^{\delta H_0\times\kappa}$ is expected under *both* this framework and ΛCDM and is therefore uninformative (neither support nor falsification). A powered test of Eq. (399) requires a tracer sharing κ's $z\sim0.5$–2 support.

d. The galaxy–lensing cross-correlation is detected. This cross-correlation, which does not use the screen map, has been measured. The DESI DR1 LRG galaxy sample ($z\simeq0.4$–1.1, whose redshift support overlaps the CMB-lensing kernel), cross-correlated with the Planck PR3 SZ-deprojected lensing convergence κ, yields a positive, lensing-kernel-shaped cross-spectrum detected at $\simeq7\sigma$ over $\ell\in[30,400]$. The significance is quoted as a matched-filter amplitude $\hat A=(t^\top C^{-1}d)/(t^\top C^{-1}t)$ with $\mathrm{S/N}=\hat A\,(t^\top C^{-1}t)^{1/2}$, judged against a null distribution centered on zero; the detection is validated by three independent null constructions—Gaussian realizations with matched auto-power, harmonic phase-randomization, and random rotations of the galaxy field—all of which center on zero, while a deliberately mis-aligned (equatorial-vs.-galactic) control destroys the signal, confirming it is sky-locked. It is *not*, however, a discriminant against ΛCDM: the galaxy–κ cross-correlation is positive in both frameworks, the recovered amplitude ($\hat A\sim0.6$–0.7, carrying galaxy-bias and normalization systematics and computed without full mask deconvolution) is consistent with the standard S_8 lensing amplitude, and the screen amplitude itself is left unforced by Prop. XVI.7.

A standard variance model for planning is

$$\mathrm{Var}\Big(\widehat{C}_\ell^{\Delta\psi\times X}\Big)\simeq\frac{1}{(2\ell+1)f_{\rm sky}}\Big[\Big(C_\ell^{\Delta\psi\times X}\Big)^2+\Big(C_\ell^{\Delta\psi\Delta\psi}+N_\ell^{\Delta\psi}\Big)\Big(C_\ell^{XX}+N_\ell^{X}\Big)\Big] \tag{400}$$

with sky fraction $f_{\rm sky}$ and noise power spectra $N_\ell^{\Delta\psi}$ and N_ℓ^X.

e. Sharpened alternative: a sign-definite, structure-correlated screen versus a primordial null. The pre-registered null Eq. (399) is two-sided, but DFD optical-bias cosmology makes a *one-sided, sign-definite* prediction against it.

Proposition XVI.7 (Forced sign of the screen–lensing cross-spectrum)**.** *Take $X=\kappa$, the CMB-lensing convergence (or any nonnegatively weighted low-z structure tracer). Write both observables as line-of-sight projections of the* same *refractive field $\delta\psi$: the reconstructed screen $\Delta\psi_{\rm obs}(\hat n)=\int_0^{\chi_*}d\chi\,W_{\rm obs}(\chi)\,\delta\psi(\chi,\hat n)$ from Eq. (379), and $\kappa(\hat n)=\int_0^{\chi_*}d\chi\,W_\kappa(\chi)\,\delta\psi(\chi,\hat n)$ with $W_{\rm obs},W_\kappa\ge0$. Then, in the Limber approximation,*

$$C_\ell^{\Delta\psi\times\kappa}=\int_0^{\chi_*}\frac{d\chi}{\chi^2}\,W_{\rm obs}(\chi)\,W_\kappa(\chi)\,P_{\delta\psi}\Big(k=\tfrac{\ell+1/2}{\chi};\chi\Big)\;>\;0 \tag{401}$$

strictly, on every multipole where the kernels overlap, with scale-dependence inherited from the (broad, mid-z–peaked) lensing efficiency. The amplitude is not *fixed by the framework: only $\operatorname{sgn}C_\ell^{\Delta\psi\times\kappa}=+1$ and the kernel shape are forced; the correlation coefficient $\widehat{r}_\ell$ of Eq. (398) is predicted positive and $\mathcal{O}(0.1$–$1)$.*

Justification. The patchwise acoustic-scale shift $\ell_{\rm obs}=\ell_{\rm true}e^{-\Delta\psi}$ is an achromatic optical bias acquired along the past light cone, so $\Delta\psi_{\rm obs}$ is a functional of $\delta\psi$ on $0<\chi<\chi_*$, Eq. (379). Under the optical metric $n=e^\psi$, the convergence κ is a line-of-sight projection of the *same* $\delta\psi$ (the identical wells that magnify angular scales also dilate the acoustic scale): an excess integrated $\delta\psi$ both *lowers* ℓ_1 — raising the estimator $\widehat{\Delta\psi}=-\ln\ell_1+\langle\ln\ell_1\rangle$, Eq. (387) — and *raises* κ. Two nonnegatively weighted projections of one field have, by the Limber identity, the cross-spectrum (401), whose integrand is a product of nonnegative factors; hence $C_\ell^{\Delta\psi\times\kappa}>0$. A mean dilation $\Delta\psi=0.30$ ($297\to220$) is not a DFD mode or prediction; by construction the patchwise estimator removes the monopole. The amplitude depends on the data-reconstructed weight $W_{\rm obs}$ and is left order-of-magnitude. □

Lemma XVI.8 (Primordial null)**.** *Any clustering component generated at recombination ($z\simeq1100$) and statistically independent of the low-z field $\delta\psi$ contributes $C_\ell^{\Delta\psi\times\kappa}\big|_{\rm prim}=0$ for all ℓ, by linearity of (401) and the absence of a shared line-of-sight source.*

Corollary XVI.9 (Third-peak height is primordial)**.** *The Planck third-peak height ($H_3/H_1\approx0.44$, $H_3/H_2\approx1.0$) is invariant under the achromatic angular dilation $\ell\to\ell\,e^{-\Delta\psi}$ (rescaling the abscissa cannot change ordinate ratios), and is unaffected by the acceleration-gated response, for which $\mu\to1$ at recombination and the common $1/\mu$ boost cancels in every height ratio (§XVI C). Hence the height requires a* primordial *effective-clustering component ($\omega_c h^2\sim0.10$–0.12 in ΛCDM units), which by Lemma XVI.8 contributes zero to $C_\ell^{\Delta\psi\times\kappa}$. Consequently a positive detection of $C_\ell^{\Delta\psi\times\kappa}$ confirms the line-of-sight origin of the patchwise anisotropy, while the height remaining absent from the cross-spectrum identifies it as* primordial *cold clustering — exactly the signature of the derived χ-matter field (App. AV), which sources the peak height through gravitational wells at recombination, not through a line-of-sight optical remap.*

f. Observational implementation. Reconstruct $\widehat{\Delta\psi}_{\rm CMB}(\hat{n})$ from per-patch acoustic-scale anisotropy (Planck PR4, ACT DR6) and cross-correlate against an independent κ map (Planck/ACT CMB lensing) and/or a low-z galaxy-density slice (unWISE, DESI), forming $\widehat{C}_\ell^{\Delta\psi\times\kappa}$ and $\widehat{r}_\ell$, Eqs. (397)–(398), over $\ell \in [30, 300]$. The decision rule is two-way: (i) a positive detection ($\widehat{C}_\ell^{\Delta\psi\times\kappa} > 0$) confirms the line-of-sight origin of the patchwise anisotropy; (ii) consistency with the two-sided null Eq. (399) falsifies the screen mechanism itself. The cosmic-variance ceiling from Eq. (400) permits S/N $\sim \mathcal{O}(10$–$100)$, but the realistic now-value is depressed by the screen-reconstruction noise $N_\ell^{\Delta\psi}$ and may be marginal with Planck/ACT; the Simons Observatory and SPT-3G are needed for a decisive measurement. These S/N figures are planning estimates, not predictions.

g. Caveats. The cross-spectrum *amplitude* (and $\widehat{r}_\ell$) depend on the data-reconstructed weight $W_{\rm obs}$, not on DFD first principles: only the sign and kernel shape are theory-forced, and no amplitude is fit here. The Limber/Gaussian form assumes linear, weakly non-Gaussian fields with overlapping redshift support (the sign is robust to these; the precise shape less so). The clean primordial null (Lemma XVI.8) rests on the dust-branch no-go (§J 5: $\mu \in [0, 1)$ cannot carry an a^{-3} clustering charge to recombination); were a future DFD mechanism to source primordial clustering optically, the null would weaken. The quoted $\omega_c h^2 \sim 0.10$–0.12 is the ΛCDM-side scale of what the height needs, not a DFD prediction.

6. Evolving "constants" as controlled parameters

This module introduces only parameters that (i) have explicit definitions and (ii) enter at least one observable channel above.

a. (A) Effective gravity in the quasi-static limit. DFD often packages nonlinear response via an effective coupling in the linear growth equation:

$$\ddot{\delta} + 2H\dot{\delta} = 4\pi G_{\rm eff}(a_{\rm sc}, k)\,\bar{\rho}\,\delta, \qquad G_{\rm eff}(a_{\rm sc}, k) = \frac{G}{\mu(x)}. \tag{402}$$

Clarifying statement: $G_{\rm eff}$ is an effective response factor (a rescaling by $1/\mu$ in the quasi-static limit), not a claim that the fundamental constant G varies in the field equation.

b. (B) Acceleration scales: distinguish $c\,H_0$ from a_0. The cosmological acceleration scale is $c\,H_0$, where H_0 is the observer-dictionary Hubble parameter (reporting layer). Separately define the galactic crossover scale a_0 through the DFD relation

$$a_0 = 2\sqrt{\alpha}\; c\, H_0^{\rm loc}, \tag{403}$$

as defined in the α-relations module elsewhere in this review.

c. (C) Minimal background control: $\mu_{\rm bg}$. To keep the module inverse-first, parameterize any late-time background departure as a minimal polynomial in the scale factor $a_{\rm sc} \in [0, 1]$:

$$\mu_{\rm bg}(a_{\rm sc}) = 1 + \eta_1(1 - a_{\rm sc}) + \eta_2(1 - a_{\rm sc})^2, \tag{404}$$

with an explicit prior enforcing $\mu_{\rm bg}(a_{\rm sc}) \to 1$ for $a_{\rm sc} \le 0.5$ (equivalently $z \ge 1$) to prevent unphysical early-time drift in this minimal module.

d. (D) Controlled ψ-regime dependence (test knobs). Introduce log-linear couplings:

$$\begin{aligned} \delta \ln c_1 &= \gamma_c\, \Delta\psi, \\ \delta \ln G_{\rm eff} &= \gamma_G\, \Delta\psi, \\ \delta \ln a_0 &= \gamma_\star\, \Delta\psi, \\ \delta \ln \alpha &= \gamma_\alpha\, \Delta\psi, \end{aligned} \tag{405}$$

where each γ is dimensionless and constrainable by combining Estimators A–C. In strict DFD postulates, $c_1 = c\,e^{-\psi}$ corresponds to $\gamma_c = -1$ when $\Delta\psi$ is the relevant propagation screen; allowing γ_c to float is a controlled falsification test.

7. Practical next steps

a. Required data products (minimum viable).

- SNe Ia compilation providing $D_L^{\rm obs}(z, \hat{n})$ (e.g. Pantheon+).[88, 89]
- BAO and/or strong-lensing products providing $D_A^{\rm obs}$ (e.g. DESI BAO products).[90]
- CMB maps sufficient to extract patchwise $\ell_1(\hat{n})$.[58]
- Independent structure maps $X(\hat{n})$ for the falsifier (e.g. CMB lensing convergence κ).[91]

b. Pre-registered reconstruction pipeline.

1. SN-only anisotropy: compute $\widehat{\Delta\psi}_{\rm SN}$ via Eq. (384); report $\widehat{\delta\psi}_{\rm SN}$ via Eq. (385).
2. Duality screen: compute $\widehat{\Delta\psi}_{\rm dual}$ via Eq. (386) in matched bins / sightlines.
3. CMB screen map: extract $\ell_1(\hat{n})$ patchwise, then compute $\widehat{\Delta\psi}_{\rm CMB}$ via Eq. (387).
4. Falsifier: compute $\widehat{C}_\ell^{\Delta\psi\times X}$ and $\widehat{r}_\ell$; assess significance against H_0 using phase-scrambled / sky-rotated null tests.

c. Organization of this section. The decisive near-term test of the screen mechanism is the ψ–structure cross-correlation in Sec. XVI A. The measured-clock no-screen forward value $\ell_1 \simeq 220$ shows that the first-peak location is consistent.

B. The ψ-Universe framework

In DFD language:

- Apparent "missing mass" in galaxy kinematics corresponds to the nonlinear response packaged by $\mu(x)$, which is fixed by the DFD stack and constrained empirically in the galactic sector.
- The CMB is not treated as a pristine "initial condition snapshot"; it is treated as an observation after propagation through a structured, ψ-varying universe (the screen).

a. Weak-response $\mu(x)$. Throughout this review we use the weak-response form (App. N, Assumption N.3)

$$\mu(x) = \frac{x}{1+x}, \tag{406}$$

for (i) consistency with the galactic calibration used in Sec. VII D, (ii) correct asymptotics ($\mu \to 1$ for $x \gg 1$, $\mu \to x$ for $x \ll 1$), and (iii) convexity of $\Psi(x) \equiv 1/\mu(x) = (1+x)/x$ for $x > 0$, which is the property needed for Jensen-type averaging arguments used in the cluster appendix (Appendix I).

C. CMB observables as ψ-screened measurements

This paper does *not* claim a full replacement for CLASS/CAMB. What it does claim is narrower and sharper:

> CMB *angular* observables admit a direct inverse reconstruction of a screen field $\Delta\psi(\hat{n})$ from patchwise peak-location estimates, independent of ΛCDM priors (Estimator C), and that reconstructed field has a clean, GR-independent falsifier via cross-correlation with independent structure maps (Sec. XVI A 5).

a. Patchwise peak location as a screen effect (core relation). The operative relation is Eq. (383). Written as a reconstruction statement:

$$\widehat{\Delta\psi}_{\rm CMB}(\hat{n}) = -\ln \ell_1(\hat{n}) + \langle \ln \ell_1 \rangle, \tag{407}$$

which is the thing to build and test first.

b. Peak-height ratios. The odd/even peak-height structure is primarily controlled by baryon-photon microphysics (baryon loading) and projection/visibility effects; any gravity-sector enhancement that enters as an overall driving amplitude tends to cancel in ratios. This is why the analytic estimate $R = 2.34$ below does not depend on the gravity theory. The full spectrum at Planck's ratio also needs the cold χ-matter: CAMB with baryons alone gives $H_2/H_1 = 0.39$ (Thm. AV.31).

1. Asymmetry Factor Decomposition

The odd/even peak asymmetry A factorizes into independent physical contributions:

$$A = f_{\rm baryon} \times f_{\rm ISW} \times f_{\rm vis} \times f_{\rm Dop}, \tag{408}$$

TABLE XXXVI. Asymmetry factor decomposition for CMB peak ratio.

Factor	Value	Formula	Physical origin
$f_{\rm baryon}$	0.474	$R_b/\sqrt{1+R_b}$	Baryon loading (BBN)
$f_{\rm ISW}$	0.50	(integral)	SW/ISW cancellation
$f_{\rm vis}$	0.98	$\mathrm{sinc}(\pi\Delta\tau/\tau_*)$	Recombination width
$f_{\rm Dop}$	0.90	(projection)	Velocity dilution

where each factor has a distinct physical origin:

The product yields:

$$A = 0.474 \times 0.50 \times 0.98 \times 0.90 = 0.209. \tag{409}$$

The peak ratio follows as:

$$R = \left(\frac{1+A}{1-A}\right)^2 = \left(\frac{1.209}{0.791}\right)^2 = 2.34. \tag{410}$$

Planck's best fit gives $R \approx 2.21$; the analytic value lies 6% above it, while the full spectrum of the derived χ-matter field, run with CAMB on the measured clock, gives $H_1/H_2 = 2.20$ ($H_2/H_1 = 0.4545$, $+0.5\sigma$; Thm. AV.31).

The key point is that $f_{\rm baryon}$ depends only on R_b (fixed by BBN), and the μ-dependent gravity enhancement cancels completely in the ratio. The cancellation holds for the analytic estimate; the cold component is still needed for the ratio itself, since CAMB with baryons alone gives $H_2/H_1 = 0.39$ against Planck's 0.45, and the derived χ-matter supplies both the ratio and the third-peak *height* (Thm. AV.31).

D. The optical illusion principle

DFD uses the same organizing idea across scales: observed inferences can be biased by propagation through a structured ψ-medium.

- **Galaxies:** kinematic inferences are affected by local ψ-structure and (in the DFD stack) one-way propagation effects; galactic "missing mass" is interpreted as mis-modeling of the ψ-medium response packaged by $\mu(x)$.
- **CMB:** local angular scales inferred from patches of the sky are biased by foreground ψ-structure, Eq. (383), and this bias is directly reconstructable (Estimator C) and falsifiable (Sec. XVI A 5).

E. Intrinsic anisotropy from ψ-gradients

A distinctive prediction of the ψ-screen program is that the reconstructed acoustic-scale residual field should correlate with foreground structure. This is exactly the falsifier in Sec. XVI A 5. An order-of-magnitude planning estimate for the expected RMS screen is

$$\sigma_\psi \sim \mathcal{O}(10^{-5}) \quad \Rightarrow \quad \frac{\sigma_{\ell_1}}{\ell_1} \sim \sigma_\psi, \tag{411}$$

which should be treated as a *planning scale* to be replaced by the empirically reconstructed $\widehat{C}_\ell^{\Delta\psi\Delta\psi}$ once $\widehat{\Delta\psi}_{\rm CMB}$ is built.

F. Line-of-sight distance bias and apparent acceleration

The reporting-layer diagnostic

$$w_{\rm eff}(z) \simeq -1 - \frac{1}{3}\frac{d(\Delta\psi)}{d\ln(1+z)}, \tag{412}$$

which translated a reconstructed screen $\Delta\psi_{\rm screen}$ into an apparent acceleration, does not apply: a homogeneous screen adds nothing beyond the expansion (App. ZS), and the line-of-sight dressing $D_L \to D_L\, e^{\Delta\psi}$ is falsified (App. SL). DFD's dark energy is the constant α^{57} vacuum term alone (App. AU), $w = -1$.

G. Cluster-scale dynamics: Status

Cluster-scale dynamics are treated in detail in Appendix I. Current status:

Under the μ-law alone:

- Relaxed clusters (n=10): $\langle M_{\rm obs}/M_{\rm DFD}\rangle = 1.57 \pm 0.08$, at $a_0 = 1.20 \times 10^{-10}$ m/s^2 and at the bound-matter a_0
- Merging clusters (n=6): $\langle M_{\rm obs}/M_{\rm DFD}\rangle = 1.99 \pm 0.16$

The shortfall is the derived χ. The relaxed masses are hydrostatic X-ray masses and the merger masses are lensing masses; a hydrostatic bias $b = 0.21$ equalizes the classes. With χ adding its Newtonian pull, all sixteen clusters need $\chi = 4.5 \pm 0.6\, M_{\rm b}$ inside r_{500}, 0.84 ± 0.12 of the cosmic mix; under the floor composition of App. AV they carry the ΛCDM budget, 1.28–1.51 of the cosmic mix (computed). The amplitude follows from the derived abundance under the adopted energy (1.21 ± 0.05 of the cosmic mix predicted inside r_{500}, 1.28 ± 0.04 measured with no hydrostatic bias; estimate; App. I).

Assessment: A no-χ closure by literature correction factors (baryonic completeness, nonlinear substructure averaging, temperature, merger and projection systematics) does not hold: the baryonic items sum to 1.26, substructure averaging gives $\simeq 1.04$ for baryonic substructure, and the projection correction has the wrong sign for lensing masses (App. I). Galaxy groups fall short in the same way on published X-ray masses and need χ too.

H. Scope of CMB claims

For clarity:

1. **Key observables:** Peak ratio $R = 2.34$ is the analytic baryon-loading result; peak location $\ell_1 \simeq 220.4$ is the current measured-clock no-screen forward result.
2. **Full numerical spectrum:** Forward TT/TE/EE calculations use CLASS/CAMB with the cold χ carrier; the measured-clock run is App. ZS, the runs of App. CL are on the one-clock $C = 1$ background, and they are a transfer check, not a fit of free ΛCDM densities.
3. **No GR ontology:** GR/ΛCDM only appear as dictionary layers for reported distances/parameters.
4. **Limited early-universe claims:** For baryogenesis DFD derives the α^4 power of the baryon asymmetry η_B and its $B-L$ bias; its coefficient is a calibration, since with the stated carrier the mechanism gives about (2–3) $\times 10^{-9}$, three to five times Planck's value (App. FK; Ext. Deriv. App. AH). It provides no inflaton *potential* and no reheating microphysics; these remain outside scope. It fixes the primordial (Wheeler–DeWitt) scale on the same α^3 rung as the dark sector, $H_\star = \sqrt{8\pi}\, M_{\rm P}\alpha^3 = 8\pi f_\chi$ (App. AV 7), and this scale is not an expansion rate: a de Sitter stage at $H_\star$ would wash out the χ relic (App. SM). The relic caps any stage that freezes perturbations at $H \simeq 4 \times 10^{10}$ GeV (Eq. (Q13)), so DFD predicts no observable primordial B-modes, $r \lesssim 10^{-7}$ (Cor. SM.4).
5. **Falsifiability:** The screen mechanism is falsifiable through the ψ-screen cross-correlation test (Sec. XVI A 5).

I. ISW Effect: A Falsifiable Prediction

The Integrated Sachs-Wolfe (ISW) effect arises when CMB photons traverse time-varying gravitational potentials. In ΛCDM, this produces a detectable signal at $\ell < 30$ via CMB × galaxy cross-correlation.

DFD prediction: with the adopted Rest-Mass Channel closure ($Q_\chi = 1$ on linear scales, App. GR; no gravitational slip, Cor. NL.17) and the real α^{57} vacuum term (App. AU), late-time potentials decay as in ΛCDM at the same background, so the ISW amplitude is $A_{\rm ISW} = 1.00$ in units of the ΛCDM expectation. A suppression to ∼30% of ΛCDM on the optical-bias reading of dark energy is not a DFD prediction: a homogeneous screen adds nothing beyond the expansion (App. ZS), and the ∼30% figure has no derivation.

Current data: Planck 2015 measures $A_{\rm ISW} = 1.00 \pm 0.25$ (S/N = 4.0) [92]; the tomographic analysis of Stölzner

et al. gives $A_{\rm ISW} = 1.51 \pm 0.30$ [93]. DFD's $A_{\rm ISW} = 1.00$ sits at 0.0σ and -1.7σ respectively. The ISW channel does not separate DFD from ΛCDM.

ISW Falsification Criterion

If CMB × galaxy cross-correlation yields $A_{\rm ISW} < 0.6$ **or** $A_{\rm ISW} > 1.5$ **at** $3\sigma \rightarrow$ the adopted Rest-Mass Channel closure ($Q_\chi = 1$, no slip) is falsified. **If** $A_{\rm ISW} \simeq 1 \rightarrow$ consistent with DFD.

J. The late-time distance ratio is not a screen

The ratio

$$\Delta\psi(z) = \ln\left(\frac{D_L^{\Lambda\rm CDM}(z)}{D_L^{\rm matter}(z)}\right) \tag{413}$$

(0.274 ± 0.02 at $z = 1$ for $\Omega_m = 0.3$) is not a reconstructed "ψ-screen" accounting for the data conventionally attributed to dark energy, and Pantheon+ Hubble residuals read against a matter-only baseline do not confirm one: the ratio is, by construction, what a cosmological constant produces relative to a matter-only ladder; with one dark energy — the α^{57} vacuum term of App. AU — it is not an independent optical quantity, a homogeneous screen adds nothing beyond the expansion (App. ZS), and the line-of-sight dressing $D_L \rightarrow D_L\, e^{\Delta\psi}$ is falsified (App. SL).

K. Late-Time Distance Cross-Consistency

The remaining test of the ψ-screen hypothesis is restricted to late-time, mean-subtracted anisotropy observables. A homogeneous screen adds nothing beyond the expansion, and the acoustic ratio is exactly conformally invariant (App. ZS); it is therefore not an estimator in this block. Using the archived late-time reconstruction:

Estimator	Observable	z range	Value	Measures
B (Duality)	$D_L/(1+z)^2 D_A$	0.3–2.3	0.01 ± 0.02	$\Delta\psi_{\rm dual}$

a. Interpretation of results.

- **Estimator B (duality consistency check):** Current constraints show $D_L/(1+z)^2 D_A = 1.01 \pm 0.02$, i.e. $\Delta\psi_{\rm dual} \approx 0.01 \pm 0.02$, consistent with zero as predicted. This is *expected*: Etherington's reciprocity holds exactly in DFD's optical metric (Sec. XVI A 2 c), so any common screening of D_L and D_A cancels in the ratio. Estimator B does not measure $\Delta\psi_{\rm screen}$. The duality relation carries no $e^{\Delta\psi}$ factor: $D_L = (1+z)^2 D_A$ exactly.
- **Acoustic observables (excluded from this estimator set):** the measured-clock calculation gives $100\theta_* = 1.04110$ with no screen. A $\Delta\psi \simeq 0.30$ CMB endpoint and its evolving-constants interpretation are therefore excluded; local and inhomogeneous lensing tests remain live.

The DDR is satisfied ($\eta = 1$).

L. Matter Power Spectrum from Microsector

The most serious challenge to any dark-matter-free theory is matching the observed matter power spectrum $P(k)$. ΛCDM's success relies on cold dark matter providing a pressureless, clustering component. DFD's clustering component is the cold χ relic below; the **temporal completion theorem** (Appendix Q) governs homogeneous deviations only (Axiom WS.1).

a. The key result. The same S^3 saturation-union composition law whose weak-response form is $\mu(x) = x/(1+x)$ (Theorem N.8) also forces the temporal sector to depend on *deviations from background*:

$$\mu(\psi_0 + \Delta\psi) - \mu(\psi_0) = (1 - \mu(\psi_0))\,\mu(\Delta\psi). \tag{414}$$

This is the *temporal External Field Effect*—a direct consequence of the saturation-union composition law (Appendix Q, Theorem Q.1).

b. Dust-like cosmology. The unique local temporal scalar is $\Delta = (c/a_0)|\dot\psi - \dot\psi_0|$ (the linear deviation from the ψ-screen). With K'(Δ) = $\mu(\Delta)$, the dust branch emerges:

$$w \rightarrow 0, \qquad c_s^2 \rightarrow 0. \tag{415}$$

The homogeneous ψ-deviation behaves as **pressureless dust** in the late-time small-deviation regime $\Delta \ll 1$; the temporal functional acts on homogeneous deviations only (Axiom WS.1). Because $a^3 a_0 \mu(\Delta) = \text{const}$ with $\mu \in [0, 1)$ bounded and $a^3 a_0$ falling into the past, running back in time forces $\mu \rightarrow 1$ (saturation), before recombination for $\mu(\Delta_0) \gtrsim 2 \times 10^{-5}$ when a_0 tracks H; at those amplitudes the branch therefore does *not* extend to recombination, where the scaling breaks and the component goes stiff/radiation-like (see Appendix J, the third-peak-height obstruction).

c. Implications for structure formation. DFD admits a dust-like homogeneous ψ-deviation branch ($w \rightarrow 0$, $c_s^2 \rightarrow 0$) derived from the S^3 composition law + deviation invariance under the adopted $K' = \mu$. Being homogeneous, it does not cluster; the clustering carrier is the cold χ component below.

Theoretical status: graded. The cold, non-thermal χ carrier is the topologically derived harmonic b_3 three-form on $S^3 = SU(2)$ (App. AV). Its printed mass coefficient uses the $\sqrt{158}$ multiplicity, one stated input; conditional on the flux-period identification and the asserted premise P4′, $\Omega_\chi h^2 = 0.11928$ is forced-amplitude/stated-convention rather than a fitted density; and $Q_\chi = 1$ clustering is conditional on the adopted Rest-Mass Channel. Given that channel, it supplies pressureless a^{-3} clustering while leaving DFD's absolute-time background untouched. On the current carrier the linear $P(k)$ is ΛCDM-shaped with DFD's inputs ($\sigma_8 = 0.806$, $S_8 = 0.822$; App. GR).

Numerical status: program. A full transfer-function / survey-pipeline confrontation remains a program item. Published $P(k)$ data are processed through GR-based fiducial cosmologies (the "GR sandbox"), so

direct confrontation requires dictionary translation plus a forward DFD perturbation solver. The linear operator displayed below provides the mathematical closure at first perturbative order; full survey-pipeline confrontation remains a numerical implementation task rather than a missing theoretical principle.

d. Proof-of-concept: N-body structure formation. A particle-mesh simulation (64^3 grid, 200 Mpc/h box) comparing ΛCDM ($\Omega_m = 0.30$), Newtonian-baryons ($\Omega_b = 0.049$), and DFD-baryons ($\Omega_b = 0.049$, $\mu(x) = x/(1+x)$)[4] on identical initial conditions demonstrates the key point: Newtonian-baryons produces negligible structure ($\delta_{\rm rms} = 1.5 \times 10^{-4}$), confirming the standard objection; DFD produces 43.8× more structure ($\delta_{\rm rms} = 6.4 \times 10^{-3}$). The 5.4× overshoot relative to ΛCDM is physically expected: cosmological perturbation accelerations ($x \approx 4 \times 10^{-4}$) lie deep in the MOND regime where the raw μ-function enhances gravity by $\sim 2500\times$ without the cosmological External Field Effect (EFE) from the Hubble flow ($a_{\rm ext} \sim cH_0 \approx 6\,a_0$). This is a proof-of-concept at 64^3 resolution; production-quality results require $\geq 256^3$ with the EFE implemented.

e. The optical σ_8 closure. Appendix AE supplies the rigorous counterpart of this proof-of-concept simulation. Two results are established there: (i) on the FRW background of the DFD action, $|\nabla\bar{\psi}| = 0$ and hence $a_{\rm ext}^{\rm FRW} = 0$ (Theorem AE.1), so the Hubble-EFE estimate $a_{\rm ext} \sim cH_0$ used heuristically in this paragraph is not recovered from the action for cosmological perturbations; and (ii) the spherical top-hat closure equation $\Omega_b \delta_b Q(\delta_b) = \Omega_m \sigma_{8,\rm obs}$ has the solution $\delta_{b,R_8} = 1.041 \times 10^{-2}$, $Q_{\rm DFD} = 502.24$ in the deep-MOND regime supplied by (i). With the baryons as the only clustering matter, the apparent σ_8 measured by weak lensing would be a refractive amplification of a $\sim 1\%$ baryon contrast at R_8. That construction is not DFD's physical carrier: the cold χ relic carries the matter power with $Q_\chi = 1$, the Rest-Mass Channel confines the baryons' polarization to bound systems, and the σ_8 and S_8 of record are 0.8063 and 0.822 (App. GR).

f. Forward perturbation skeleton. Linearizing the DFD field equation around a background $\bar{\psi}$ in Fourier space gives

$$k_i M_{ij} k_j\, \delta\psi_{\mathbf{k}} = \frac{8\pi G}{c^2}\bar{\rho}\,\delta_{\mathbf{k}}, \tag{416}$$

with the response tensor

$$M_{ij} = \mu_0\,\delta_{ij} + L_0\,\hat{g}_i\hat{g}_j, \tag{417}$$

where $\mu_0 \equiv \mu(\bar{x})$, $L_0 \equiv \frac{d\mu}{d\ln x}\big|_{\bar{x}}$, $\hat{g} \equiv \nabla\bar{\psi}/|\nabla\bar{\psi}|$. The linear growth equation is then

$$\ddot{\delta}_{\mathbf{k}} + 2H\dot{\delta}_{\mathbf{k}} = 4\pi G_{\rm eff}(a,\hat{k})\,\bar{\rho}\,\delta_{\mathbf{k}}, \tag{418}$$

with direction-dependent effective gravitational coupling

$$\boxed{G_{\rm eff}(a,\hat{k}) = \frac{G}{\mu_0 + L_0(\hat{k}\cdot\hat{g})^2}.} \tag{419}$$

For $\mu(x) = x/(1+x)$: $\mu_0 = \bar{x}/(1+\bar{x})$ and $L_0 = \bar{x}/(1+\bar{x})^2$, the $\mu_{\ln,0}$ of Appendix AC. At low background acceleration ($\bar{x} \ll 1$), $G_{\rm eff} \to G/\bar{x}$; at high acceleration ($\bar{x} \gg 1$), $G_{\rm eff} \to G$. The response acts inside bound systems: the Rest-Mass Channel confines the polarization to them, so unbound linear perturbations grow with $G_{\rm eff} = G$ (App. GR).

g. Background-history input. Equations (416)–(419) describe the linear response of perturbations once a background history $H(a)$ is supplied. In the present monograph, $H(a)$ is the measured-clock background ($H_0^{\rm early} = 67.52$, $\Omega_m = 0.312$). The present closure therefore adds no new background model.

h. Connection to the reconstructed screen. The ψ-screen inferred from the patchwise CMB estimator (Secs. XVI A 3–XVI A 5) is the line-of-sight integral of the same perturbation field:

$$\Delta\psi_{\rm screen}(z,\hat{n}) = \int_0^{\chi(z)} W(\chi')\,\delta\psi(\chi'\hat{n})\,d\chi', \tag{420}$$

where $W(\chi)$ is the lensing kernel. This means the object inferred from the inverse optical program and the object sourced by the forward growth equation are the same field. Any inconsistency between the reconstructed $\Delta\psi_{\rm screen}$ map and the $\delta\psi$ field implied by the forward growth operator is a direct falsifier of the cosmological closure.

i. New falsifiers from the perturbation system.

1. If the reconstructed $\Delta\psi_{\rm screen}$ map does not match the $\delta\psi$ field implied by Eq. (418), the forward–inverse closure fails.

2. If the ISW amplitude does not agree with the sign and amplitude implied by $G_{\rm eff}$, the growth law is wrong.

Dust Branch under $K' = \mu$: Not Bolted-On K-Essence

The temporal sector rests on one adopted identification, $K'(\Delta) = \mu(\Delta)$ (App. Q):

1. Same $\mu(x) = x/(1+x)$, the weak-response form of the galaxy law
2. Same saturation-union composition law (Assumption N.5)
3. Deviation invariant $\Delta = (c/a_0)|\dot{\psi} - \dot{\psi}_0|$ forced by segment additivity
4. Given that identification, the dust branch ($w \to 0$, $c_s^2 \to 0$) is a theorem (Appendix Q)

No-go check: Naive quadratic $K'(Q_t) = \mu(\sqrt{Q_t})$ gives $w \to 1/2$ (not dust). The dust branch is not automatic—it requires the deviation-invariant closure. See Appendix Q for complete derivation.

[4] The baryon density $\Omega_b = 0.049$ is Planck's value used uniformly across all three runs to isolate the gravity-law effect from the matter-content effect (apples-to-apples comparison). On the current measured-clock background, $h = 0.6752$ and DFD's conventional-point physical density $\omega_b = 0.0222730$ give $\Omega_b = 0.04886$. A rerun with this input would produce qualitatively similar conclusions with a modestly smaller overshoot ratio; production-quality confrontation at $\geq 256^3$ with the EFE implemented is the proper venue for quantitative comparison.

M. Power Spectrum Multipole Confrontation

Remark XVI.10 (Archived pre-measured-clock RSD extraction). This subsection and Fig. 11 are retained as pipeline provenance. The source script/run ID and the H_0, Ω_m, h, and bias inputs used to produce the printed $\beta_{\rm theory}$ values are not present in the package, so a 67.5-clock rerun cannot be certified. The table is not a current quantitative confrontation; the current $\Omega_m \simeq 0.312$ survey rerun remains an unresolved program item.

We confront DFD predictions with galaxy power spectrum multipole measurements derived from BOSS DR12 and eBOSS DR16 mock catalogs.

1. Method

The anisotropic galaxy power spectrum $P(k,\mu)$ encodes redshift-space distortions (RSD) through the Kaiser formula. Expanding in Legendre multipoles:

$$P_\ell(k) = \frac{2\ell+1}{2}\int_{-1}^{1} P(k,\mu)\mathcal{L}_\ell(\mu)\,d\mu \tag{421}$$

In linear theory, the quadrupole-to-monopole ratio is:

$$\frac{P_2}{P_0} = \frac{\frac{4}{3}\beta + \frac{4}{7}\beta^2}{1+\frac{2}{3}\beta+\frac{1}{5}\beta^2} \tag{422}$$

where $\beta = f/b$ is the ratio of the growth rate $f = d\ln\delta/d\ln a$ to the galaxy bias b.

We extract P_0, P_2, P_4 from the BOSS DR12 and eBOSS DR16 power spectrum measurements, compute the ratio $r_2 = P_2/P_0$ in the linear regime ($k = 0.02$–$0.15\,h$/Mpc), and invert the Kaiser formula to obtain β. NGC and SGC galactic caps are combined by inverse-variance weighting; errors are bootstrapped (1000 realizations).

2. Results

TABLE XXXVII. Archived measured $\beta = f/b$ extraction from power-spectrum multipoles; the theory column predates the measured-clock provenance standard.

Sample	$z_{\rm eff}$	$\beta_{\rm meas}$	$\beta_{\rm theory}$
BOSS DR12 z_1	0.38	0.270 ± 0.009	0.357
BOSS DR12 z_3	0.61	0.281 ± 0.007	0.395
eBOSS DR16 QSO	1.50	0.366 ± 0.013	0.404

Figure 11 shows the comparison. The measured β values lie 9–29% below the tabulated theory values. This pattern is consistent with Finger-of-God (FoG) damping and galaxy bias uncertainty not captured by linear Kaiser, both of which are stronger at lower redshift where nonlinear structure is more developed.

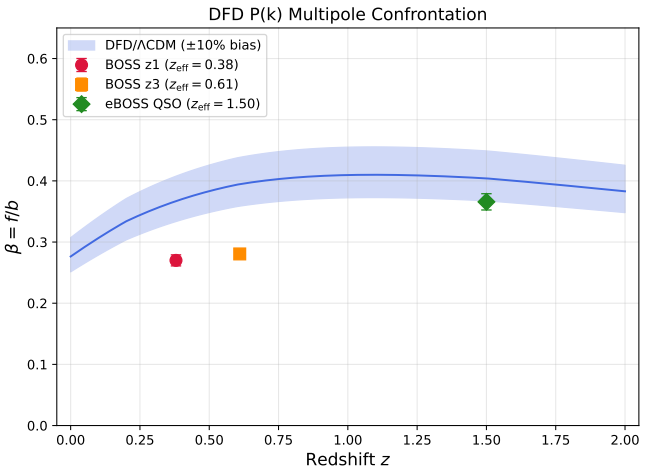


FIG. 11. RSD parameter $\beta = f/b$ versus redshift. Blue band: DFD/ΛCDM prediction with ±10% bias uncertainty. Points: measurements from BOSS/eBOSS mocks. The displayed consistency statement is historical; a measured-clock rerun is required.

3. Interpretation: EFE-Screened Growth Theorem

In the completed first-order DFD growth closure (Appendix AC), the correction to linear growth is *not* controlled by the clock-sector coefficient k_α. It is controlled by the EFE-screened linear response tensor of the nonlinear μ operator. For the DFD interpolation function $\mu(x) = x/(1+x)$, the effective gravitational coupling is

$$G_{\rm eff}(\bar{x},\theta) = G\left[\frac{\bar{x}}{1+\bar{x}} + \frac{\bar{x}}{(1+\bar{x})^2}\,(\hat{k}\cdot\hat{g})^2\right]^{-1}, \tag{423}$$

where $\bar{x} = |\nabla\bar{\psi}|/a_\star$ is the background gradient ratio and $\hat{g}$ is the unit vector along the background gradient.

The cosmological external field, supplied by the Hubble flow under the epoch-consistency rule that fixes $a_0(z) = 2\sqrt{\alpha}\,cH(z)$ (Section XIX), gives

$$\bar{x}_{\rm EFE} = \frac{a_{\rm ext}(z)}{a_0(z)} = \frac{cH(z)}{2\sqrt{\alpha}\,cH(z)} = \frac{1}{2\sqrt{\alpha}} \simeq 5.85, \tag{424}$$

redshift-independent under the same epoch-consistency rule. Under the Hubble-EFE hypothesis $a_{\rm ext} = cH(z)$ of Appendix AC, which is not DFD's cosmological growth law (App. GR), this gives the quasi-Newtonian envelope

$$\boxed{1.02\,G \;\le\; G_{\rm eff} \;\le\; 1.17\,G, \qquad \langle G_{\rm eff}\rangle \simeq 1.12\,G,} \tag{425}$$

with a directional $(\hat{k}\cdot\hat{g})^2$ signature.

a. Why the growth correction is not of order k_α. A statement of the form $f_{\rm DFD} = \Omega_m^\gamma[1+\mathcal{O}(k_\alpha)]$ is structurally wrong: k_α is the clock-sector coefficient, not the linear-growth response. DFD predicts near-standard linear growth because the Rest-Mass Channel confines the polarization to bound systems: unbound linear perturbations grow with $G_{\rm eff} = G$, and linear cosmological growth is carried by the cold χ relic with $Q = 1$ (App. GR).

b. Why measured β sits below linear theory. The 9–29% deficit in measured β relative to either ΛCDM or DFD theory arises from standard effects common to all linear-Kaiser analyses:

1. Finger-of-God damping from random velocities
2. Galaxy bias uncertainty (∼10%)
3. Mock calibration systematics
4. Alcock–Paczynski mapping and fiducial-cosmology dictionary translation

These affect ΛCDM and DFD identically and are not theory discriminators.

4. Conclusion and Falsifier

The first-order growth operator is *closed* (Appendix AC); linear cosmological growth is carried by the cold χ relic with $Q = 1$ and its signature is isotropic (App. GR). DFD's distinctive signatures appear in the low-acceleration regime (galaxy rotation curves) rather than linear-regime RSD.

a. Falsifier. The falsifiers of linear growth are those of App. GR (GR.8), applied after the standard nuisance layer of galaxy bias, Finger-of-God damping, Alcock–Paczynski mapping, and fiducial-cosmology dictionary translation.

Status: linear-regime growth closure complete; production-level survey-pipeline likelihood pending. The theorem is separate from survey nuisance modeling: the first-order growth operator is closed in the sense of Appendix AC.

N. Observational Status (2024–2025)

Several recent observations provide context for the ψ-screen framework. We present these as *motivations*, not proofs.

1. Late-Time Potential Shallowing (DES Y3)

The Dark Energy Survey Year 3 analysis provides a model-independent, direct measurement of the Weyl gravitational potential from combined weak-lensing and clustering data [94]:

> **Result:** The lowest-z bins are 2–3σ shallower than ΛCDM+GR expectations, corresponding to ∼10% weaker potential.

As the universe expands and ρ decreases, the source of ψ [Eq. (21)] weakens:

$$\frac{\Delta\Phi}{\Phi} \sim \frac{\Delta\rho}{\rho} \quad \Rightarrow \quad \text{late-time shallowing as } \rho \downarrow . \tag{426}$$

Status: Not a DFD prediction: DFD's late-time potentials decay as in ΛCDM ($A_{\rm ISW} = 1.00$, Sec. XVII).

2. Dynamical Dark Energy Hints (DESI DR2)

DESI DR2 BAO, combined with SNe and CMB distance priors, shows dataset-dependent preference for dynamical dark energy $w(z) \neq -1$ [95]:

> **Result:** Some dataset combinations favor $w(z)$ evolving with redshift rather than a pure cosmological constant.

Status: DFD's dark energy is the constant α^{57} vacuum term, $w = -1$ exactly (App. AU, Prop. AU.9), with no dark-energy clustering: on this test DFD stands with ΛCDM and inherits the same tension. This is therefore an *open test*, not a confirmation: a genuine $w(z) \neq -1$, with or without clustering, would *falsify* DFD together with ΛCDM.

3. Wide Binaries (Active and Contested)

Gaia wide-binary tests probe internal accelerations down to $a \sim 10^{-10}$ m/s^2 [96]:

> **Some analyses:** Report ∼20% velocity excess beyond ∼3000 au, consistent with MOND-like phenomenology.
> **Other analyses:** Demonstrate that realistic triple-population modeling and stricter data cuts remove the signal.

The μ-crossover radius in DFD is:

$$r_\times = \sqrt{\frac{GM}{a_0}} \approx 7.04 \times 10^3 \,\text{au} \times \left(\frac{M}{M_\odot}\right)^{1/2} \left(\frac{1.1966 \times 10^{-10}\,\text{m/s}^2}{a_0}\right)^{1/2}, \tag{427}$$

overlapping the few-10^3 au range where Gaia analyses disagree. This crossover applies to pairs in weak host fields. Near the Sun the Galaxy's baryonic field exceeds $(\ln 2)^2 a_0$, so by the environmental-confinement axiom (App. NL) local pairs are exactly Newtonian at every separation; DFD sides with the analyses that find no signal, and a confirmed boost falsifies the axiom.

Status: The data are contested; DFD's local prediction is the null.

4. Counter-Evidence and Null Tests

Any alternative framework must address null tests:

a. E_G gravity test (ACT DR6 + BOSS). The geometry-vs-dynamics ratio E_G from ACT DR6 CMB-lensing crossed with BOSS galaxies is consistent with ΛCDM/GR and largely scale-independent within current precision [97]. DFD's forward prediction is the GR-*form* statistic $E_G = \Omega_{m,0}/f(z)$ at the measured

$\Omega_m \simeq 0.312$ (gravity-universal growth; the ψ-screen cancels in the ratio estimator — a cancellation still to be verified against the DR6 estimator definition): $E_G = 0.402$ at $z = 0.555$ (CMASS) and 0.453 at $z = 0.316$ (LOWZ), scale-independent, vs the measured $0.31^{+0.06}_{-0.05}$ and $0.49^{+0.14}_{-0.11}$. At the measured clock this is effectively the Planck-ΛCDM comparison.

Status: *Consistent.* See App. AG 7.

b. KiDS-Legacy shear. The current-background forward calculation gives $\sigma_8 \simeq 0.8063$, $\Omega_m \simeq 0.312$, and hence $S_8 \simeq 0.822$. KiDS-Legacy reports $S_8 = 0.815^{+0.016}_{-0.021}$ for cosmic shear alone [98]; the KiDS-Legacy+DES-Y3+Pantheon++DESI-Y1 joint analysis gives $0.814^{+0.011}_{-0.012}$ [99]. The DFD residual is about $+0.45\sigma$ against the primary KiDS-only upper error, or $+0.74\sigma$ against the joint upper error (theory-input uncertainty not included); DES Year 6, 0.789 ± 0.012, lies 2.8σ below (survey errors only; App. GR).

Status: *Consistent* with KiDS-Legacy, 2.8σ above DES Year 6; no special suppression is claimed.

c. Pairwise kinematic Sunyaev–Zel'dovich (ACT + SDSS/DESI). The pairwise kSZ momentum between cluster pairs probes the large-scale velocity field $v_{12}(r)$ sourced by linear-regime gravity. Recent measurements by Calafut et al. [100] and Gallardo et al. [101] find the pairwise infall signal consistent with Newton/GR plus ΛCDM on scales $20\,\mathrm{Mpc} \lesssim r \lesssim 150\,\mathrm{Mpc}$, and have been cited as excluding modified-gravity alternatives including MOND.

DFD reproduces the ΛCDM pairwise velocity prediction at this precision. For the Calafut et al. L61 sample configuration (15 bins, 5–145 Mpc, $z_{\rm eff} = 0.5$, $\langle M \rangle \approx 2.5 \times 10^{13}\, M_\odot$, Tinker 2010 bias $b \approx 1.76$), evaluating $v_{12}(r) = -(2/3)\, a(z) H(z) f(z)\, r\, \bar{\xi}^h(r)/[1 + \xi^h(r)]$ via the Sheth–Diaferio–Hui–Scoccimarro linear formalism gives $\chi^2/\mathrm{dof} \approx 0.79$ for DFD, with $\Delta\chi^2(\mathrm{DFD} - \Lambda\mathrm{CDM}) \approx 2.5 \times 10^{-4}$: DFD and ΛCDM are indistinguishable at current precision and both fit the data well. The test rules out pure MOND, which fails at cluster scales independently of kSZ; it does not constrain DFD, whose unbound linear perturbations grow with $G_{\rm eff} = G$ (growth-regime note below).

Status: Consistent ($\chi^2/\mathrm{dof} = 0.79$). Sharp distinction from ΛCDM requires per-bin precision better than the 0.1–0.5% growth offset below.

d. Growth-regime note. The pairwise-kSZ consistency above rests on quasi-Newtonian growth on 20–150 Mpc scales, and that is the growth regime DFD's dark sector sets: under the Rest-Mass Channel's bound-system confinement (App. GR, Remark GR.12) unbound linear perturbations do not polarize the medium, so linear velocities grow with $G_{\rm eff} = G$ ($Q_\chi = 1$), and the polarization of bound systems raises σ_8 by a factor of only 1.001–1.005 (computed). Neither the Hubble-EFE screening envelope of Appendix AC ($G_{\rm eff} = 1.02$–$1.17\,G$) nor the suppressed kSZ amplitude of the baryon-only construction of Appendix AE and Appendix AF applies to linear cosmological velocities, and the consistency verdict holds.

5. *Observational Summary Table*

a. Summary. Late-time cosmological anomalies are uneven across probes and evolving with improved analyses. The clock constraint $H_0^{\rm early} = \sqrt{C}\,\alpha^{57/2}/t_P$ (App. AU) carries a *derived exponent* and a *measured* $O(1)$ coefficient ($C = 0.87784 \pm 0.00266$, five concordant CMB-anchored channels; Rem. AP.6): $H_0^{\rm early} = 67.54 \pm 0.10$ km/s/Mpc at that C (adopted cross-channel value 67.52 ± 0.09), concordant with Planck ($+0.2\sigma$) and 6.4σ below the SH0ES ladder's full 2025 sample (2–3σ below its JWST subsample); a ψ-screen-bias reading is excluded by the homogeneous-mode and conformal-invariance theorems (App. ZS). Local probes read the bound-matter clock, $H_0^{\rm loc} = \alpha^{57/2}/t_P = 72.09$, by the two-clock postulate of Sec. ZS 5: one universe read on two clocks, with the size of their ratio measured. SH0ES's full 2025 sample lies 1.5σ above that clock, and the absolute a_0 scale (Euclid/DESI lensing RAR) tests the postulate once baryonic masses are known to about 2%. The DESI DR2 evolving-w hint, by contrast, is *not* a DFD prediction—DFD has one constant vacuum term, $w = -1$, with no dark-energy clustering (App. AU, Prop. AU.9), so a confirmed evolving w would falsify it together with ΛCDM. E_G and KiDS are consistent at the measured clock; the pairwise kSZ test is passed because DFD's linear growth is ΛCDM's to about 0.5%.

O. Hierarchy of Astrophysical Scales from α

P. Summary

Cosmology in DFD is framed as reconstructing $\Delta\psi_{\rm screen}(z, \hat{n})$ from the patchwise CMB acoustic-scale anisotropy, with distance duality ($\eta = 1$) serving as a metric-consistency check, and testing the *single-screen* hypothesis with a GR-independent falsifier: cross-correlation with independent structure maps.

- $\Delta\psi \approx 0.30$ does not set the global CMB peak location; only mean-subtracted patchwise lensing correlations survive in that channel

This is the shortest path to decisive tests that do not require adopting GR/ΛCDM priors. The falsification criterion remains: cross-correlation of reconstructed $\Delta\psi(\hat{n})$ with foreground structure maps (Sec. XVI A 5).

XVII. QUANTUM AND GAUGE EXTENSIONS

This section describes extensions of DFD connecting the scalar field ψ to Standard Model gauge structure. The mathematical foundations are rigorous (Appendix F);

TABLE XXXVIII. Observational benchmarks (2024–25 status).

Scale/Probe	DFD Prediction	Obs.	Status
Solar System	$\gamma = \beta = 1$	Consistent	✓
H_0 (CMB/BAO)	$\sqrt{C}\,\alpha^{57/2}/t_P = 67.52(9)$	Planck 67.4(5)	✓
H_0 (local)	$\alpha^{57/2}/t_P = 72.09$ (bound-matter clock)	SH0ES 73.5(0.9)	1.5σ
DES (low-z)	ΛCDM-like potentials	2–3σ low	?
DESI DR2	$w_{\rm eff} = -1$, no DE clust.	$w \neq -1$ hints	?
Gal. rotation	Flat v; TF scaling	Empirical	✓
Wide binaries (local)	$\gamma = 1$, no boost	Contested	?
E_G (ACT)	GR form at $\Omega_m \simeq 0.312$	0.31/0.49	✓
KiDS-Legacy	$S_8 \simeq 0.822$	$0.815^{+0.016}_{-0.021}$	✓
DES Year 6	$S_8 \simeq 0.822$	0.789(12)	2.8σ
Pairwise kSZ	$v_{12} \simeq \Lambda$CDM	$\chi^2/\mathrm{dof} = 0.79$	✓
Lab (100 m)	null (Thm. XI.2)	Not tested	—

TABLE XXXIX. Acceleration scales from powers of α applied to $cH_0^{\rm loc}$.

Expression	Value (m/s^2)	Interpretation
$cH_0^{\rm loc}$	7.0×10^{-10}	Vacuum acceleration scale
$2\sqrt{\alpha} \cdot cH_0^{\rm loc}$	1.2×10^{-10}	MOND scale a_0
$\alpha \cdot cH_0^{\rm loc}$	5.1×10^{-12}	Deep MOND regime

the physical interpretation remains conditional on DFD's gravitational predictions being correct.

A. Status and Conditionality

Mathematical Status

Results (Appendices F–G):

1. The electroweak group $U(2) = (SU(2) \times U(1))/\mathbb{Z}_2$ is the isotropy group of $\mathbb{C}P^2$ under one stated identification (Rem. F.2); colour $SU(3)$ and the family content are inputs, as in the Standard Model (Rem. F.3).
2. The isotropy charge $6Y$ fixes $q_1 = 3$ (Rem. F.10); Lemma F.9 is the necessary integrality condition.
3. Flux-product rule $N_{\rm gen} = |k_3 k_2 q_1|$ (Thm. F.18), a bookkeeping identity; the value 3 enters as a discrete input (Rem. F.21).
4. Energy minimization selects $(k_3, k_2) = (1, 1)$ at the derived $q_1 = 3$, consistent with the discrete input $N_{\rm gen} = 3$ (Thm. F.19; status: App. F, Rems. on q_1 and the generation count).
5. $k_a = 3/(8\alpha) \approx 51.4$ from frame stiffness × EM duality (Thm. G.1).
6. $\theta_{\rm QCD} = 0$ (derived; tree level, with $\theta_{\rm bare} = 0$ fixed by the spectral action given that nothing is added to it for the gauge fields; loop-induced $\lesssim 10^{-16}$; Thm. G.2).

Physical interpretation: Conditional on DFD gravity being correct.

a. Motivation. If DFD's scalar field ψ is physically real and couples to matter's internal degrees of freedom, one can ask which gauge structures emerge. The construction below shows that $SU(3) \times SU(2) \times U(1)$ can arise from Berry connections in a degenerate internal mode space.

b. Scope. This section presents the mechanism without claiming it is the unique or correct extension of DFD. It is a theoretical possibility, not an established feature of the theory.

c. The quantum framework is an imported input. To make explicit what is assumed: the quantum framework used below—a complex Hilbert space, the imaginary unit i, the action scale $\hbar$, and unitary evolution—is an *adopted input*, not derived from the classical ψ-postulates. App. QM derives the field-level i, the inner product and unitary free evolution from a unique forced complex structure $J_\star$, given a linearized stability that it argues but does not prove; $\hbar$, the interacting operator-ordering map and the measurement postulate are shared with every quantum theory. This is recorded as a documented import, *not* as a DFD prediction or a closed result.

B. Internal Mode Bundle and Berry Connections

a. Setup. Assume the ψ-medium supports degenerate internal mode subspaces at each point:

$$\mathcal{H}_{\rm int}(\mathbf{x}) \simeq \mathbb{C}^3 \oplus \mathbb{C}^2 \oplus \mathbb{C}, \tag{428}$$

with local orthonormal frames:

$$\Xi(\mathbf{x}) = \left(\left|\chi_a^{(3)}\right\rangle_{a=1,2,3}, \left|\chi_b^{(2)}\right\rangle_{b=1,2}, \left|\chi^{(1)}\right\rangle \right). \tag{429}$$

b. Frame transformations. Under local changes of basis $U(\mathbf{x}) \in U(3) \times U(2) \times U(1)$, the frames transform as $\Xi \to \Xi U$. The resulting non-Abelian Berry connections:

$$A_i^{(3)} = i\, U_3^\dagger \partial_i U_3 \in su(3), \tag{430}$$

$$A_i^{(2)} = i\, U_2^\dagger \partial_i U_2 \in su(2), \tag{431}$$

$$A_i^{(1)} = \partial_i \theta \in u(1), \tag{432}$$

transform as gauge fields.

c. Structure group. The structure group is $S(U(3) \times U(2) \times U(1))$, with one abelian factor more than the Standard Model's; the hypercharge is fixed by the isotropy

reading (Rem. F.2).

C. The $\mathbb{C}^3 \oplus \mathbb{C}^2 \oplus \mathbb{C}$ partition

The $(3, 2, 1)$ partition enters as a dictionary entry: it is the minimal partition carrying the factors $SU(3)$ and $SU(2)$, which the proposition below assumes:

Proposition XVII.1 (Proved in Appendix F 1)**.** *Among all block partitions whose stabilizer contains exactly two simple non-Abelian factors $SU(3)$ and $SU(2)$ and a singlet sector, the unique minimal partition is $(3, 2, 1)$ with $N = 6$. Its stabilizer has two abelian factors modulo the overall phase; the single hypercharge is fixed by the isotropy reading (Rem. F.2).*

a. Physical requirements. The Standard Model requires:

- $SU(3)_c$ for color (3-dimensional fundamental)
- $SU(2)_L$ for weak isospin (2-dimensional fundamental)
- $U(1)_Y$ for hypercharge
- A singlet sector for right-handed leptons

b. Minimality argument. A two-block partition (n_a, n_b) cannot provide a singlet sector—every vector transforms non-trivially under at least one SU factor. Hence three blocks are required. The minimal choice satisfying all requirements is $(3, 2, 1)$, giving $N = 6$.

c. Uniqueness. Explicit enumeration (Table in Appendix F 1) shows that no other partition with $N \leq 6$ satisfies all requirements.

D. Yang-Mills Kinetic Terms from Frame Stiffness

a. Gradient penalty. Twisting the internal frames costs energy:

$$\mathcal{L}_{\text{stiff}} = \sum_a \eta_a \|\partial_i |\chi_a\rangle\|^2. \tag{433}$$

b. Hidden local symmetry. This admits a Stückelberg/hidden-local-symmetry form:

$$\mathcal{L} = \sum_{r=3,2,1} \left[-\frac{\kappa_r}{2} \operatorname{Tr} F_{ij}^{(r)} F^{(r)ij} + \frac{\eta_r}{2} \operatorname{Tr} \left(A_i^{(r)} - \Omega_i^{(r)} \right)^2 \right], \tag{434}$$

where $\Omega_i^{(r)} = i U_r^\dagger \partial_i U_r$.

c. Yang-Mills limit. Retaining only the first term of the preceding Lagrangian, i.e. neglecting the Stückelberg contribution, leaves the Yang-Mills kinetic term:

$$\mathcal{L}_{\text{gauge}} = -\sum_{r=3,2,1} \frac{\kappa_r}{2} \operatorname{Tr} F_{ij}^{(r)} F^{(r)ij}, \qquad g_r \sim \kappa_r^{-1/2}. \tag{435}$$

The gauge couplings are determined by the frame stiffnesses κ_r. The Stückelberg stiffnesses η_r are a separate set of parameters for which this construction supplies no value; neglecting them above is an assumption, not a result.

E. Generation Counting

The construction relates the generation count to its flux data by a bookkeeping identity; the count itself is a stated input.

Theorem XVII.2 (Proved in Appendix F 5)**.** *For $\mathcal{M} = \mathbb{C}P^2 \times S^3$ with flux configuration (k_3, k_2, q_1):*

$$N_{gen} = |k_3 \cdot k_2 \cdot q_1|. \tag{436}$$

a. The logical chain.

1. **Flux quantum:** The isotropy charge $6Y$ fixes $q_1 = 3$; the integrality condition of Lemma F.9 admits $q_1 \in \{3, 6\}$, and $q_1 = 6$ would give the weak doublets an even charge (App. F, Rem. on q_1).
2. **Energy minimization:** Yang-Mills energy is minimized at $(k_3, k_2) = (1, 1)$ (Theorem F.19).
3. **Generation count:** $N_{\text{gen}} = |1 \cdot 1 \cdot 3| = 3$, a bookkeeping identity that reproduces the discrete input $N_{\text{gen}} = 3$ (App. F).

b. Mathematical foundation. The proof combines:

- Künneth factorization for product manifolds [102]
- Atiyah-Patodi-Singer index theorem on S^3 [103]
- Hirzebruch-Riemann-Roch on $\mathbb{C}P^2$
- Gravitational-$U(1)_Y$ anomaly cancellation

c. Significance. The electroweak group follows under one stated identification and the flux quantum is derived from it; the generation count, colour and the family content are inputs (App. F status remarks); the count assembles from:

- The partition $(3, 2, 1)$, recorded as a dictionary entry
- The flux quantum $q_1 = 3$, derived from the isotropy charge
- Energy minimization selecting $(k_3, k_2) = (1, 1)$

F. CP Structure

a. CP violation pattern. The construction predicts that CP violation enters through complex phases in the Yukawa sector, with:

- Strong CP violation suppressed ($\bar{\theta} = 0$ at tree level with $\theta_{\text{bare}} = 0$ fixed by the spectral action given that nothing is added to it for the gauge fields; Thm. L.3)

- Weak CP violation supplied by Postulate Y.10 (App. AO)
- CKM-like mixing matrix structure from fermion mass generation

b. Strong CP suppression. With $\theta_{\text{bare}} = 0$ fixed by the spectral action given that nothing is added to it for the gauge fields, the det-orthogonal tree-level protection together with the η-invariant argument gives $\theta_{\text{QCD}} = 0$ at tree level (Theorem L.3), with loop corrections bounded at the Standard-Model level ($\lesssim 10^{-16}$; Sec. XVII M).

G. Higgs and Mass Spectrum

The gauge emergence framework also addresses the Higgs sector and fermion mass hierarchy (full derivations in Appendix H).

a. Higgs emergence. The Higgs doublet $(1, 2, +1/2)$ emerges as the off-diagonal connector between the $\mathbb{C}^2$ (SU(2)) and $\mathbb{C}^1$ (singlet) sectors of the $(3, 2, 1)$ partition. The Mexican-hat potential arises from frame stiffness energy.

b. Yukawa hierarchy. The three generations correspond to zero modes localized at different "vertices" of $\mathbb{C}P^2$. Yukawa couplings are overlap integrals:

$$Y^{(n)} = g_Y \int_{\mathbb{C}P^2} \bar{\psi}^{(n)} \cdot \phi_H \cdot \psi^{(n)} \, d\mu_{FS}. \tag{437}$$

If the Higgs ϕ_H is localized near one vertex (third generation), the hierarchy follows:

$$Y^{(1)} : Y^{(2)} : Y^{(3)} \approx \epsilon^2 : \epsilon : 1, \qquad \epsilon \sim 0.05. \tag{438}$$

H. The Fine-Structure Constant from Chern-Simons Theory

A central result of the DFD microsector is the **closed form for** $\alpha = 1/137$ from topological quantization on S^3.

1. Chern-Simons Quantization

On a compact 3-manifold $\mathcal{M}_3$, the Chern-Simons level k is quantized:

$$S_{\text{CS}} = \frac{k}{4\pi} \int_{\mathcal{M}_3} \text{Tr}\left(A \wedge dA + \frac{2}{3} A \wedge A \wedge A \right), \quad k \in \mathbb{Z}. \tag{439}$$

For $\mathcal{M}_3 = S^3$ with gauge group U(1), the allowed values are $k = 0, \pm 1, \pm 2, \ldots$

2. The Maximum Level: Topological Derivation

The effective coupling is computed from a weighted sum over Chern-Simons levels. With the SU(2) weight function

$$w(k) = \frac{2}{k+2} \sin^2 \frac{\pi}{k+2}, \quad k = 0, 1, \ldots, k_{\max} - 1, \tag{440}$$

the effective coupling $\beta_{U(1)} = \langle k + 2 \rangle$ determines α.

The value of $k_{\max}$ is given by the conditional determinant-line count, a closed Spin^c index on $\mathbb{C}P^2$ (§X):

$$k_{\max} = \chi(\mathbb{C}P^2, E) = \chi(\mathcal{O}(9)) + 5\chi(\mathcal{O}) = 55 + 5 = 60. \tag{441}$$

Here $E = \mathcal{O}(9) \oplus \mathcal{O}^{\oplus 5}$ is the twist bundle, and the computation uses Hirzebruch–Riemann–Roch for the canonical Spin^c structure.

a. Refined microsector completion. Section X presents a convention-locked closed form that lies 4.9×10^{-9} from the measured value with the open bracket coefficient (21 ppm from its integers alone): $\alpha^{-1} = 137.03599985$ (residual -0.005 ppm). This involves a forced binary fork between regular-module and fermion-rep microsectors, with only the regular-module branch surviving under a no-hidden-knobs policy.

3. Lattice Comparison

This analytical result has been compared with lattice Monte Carlo simulations (Appendix K 2). The lattice parameters are fixed *before* comparison to α:

a. Inputs:

- $k_{\max} = \chi(\mathbb{C}P^2, E) = 60$ (from Spin^c index)
- $\beta_{U(1)} = \langle k + 2 \rangle = 3.797$ (from CS weight function at $k_{\max} = 60$)
- Wilson ratio $= (n_2/n_1) \times N_{\text{gen}} = 2 \times 3 = 6$ (on the frame-stiffness assumption)
- $\beta_{SU(2)} = 6 \times 3.80 = 22.80$ (derived)

b. Lattice results ($L = 6$–16, 25+ independent runs):

- At $\beta_{U(1)} = 3.80$: within 0.9% of 1/137 for $L \leq 12$ ($\beta_{SU(2)} = 23.0$ for $L \leq 10$)
- $L = 16$ with 40k thermalization: mean deviation $+1.13 \pm 0.50\%$ over nine of ten runs (2.3 standard errors)
- Converged value ($k_{\max} \to \infty$, $\beta_{U(1)} = 3.94$): the run at $\beta_{U(1)} = 3.95$ gives $\alpha = 1/147$ (-6.8%)
- Wilson ratio: of ten ratios from 3 to 9 only 6 fits; two further runs at 5.75 give -0.20% and $+2.20\%$ (mean $+1.0\%$; Table LXXXVI)

The lattice agrees to within 0.9% for $L \leq 12$ and lies $+1.1 \pm 0.5\%$ high at $L = 16$. In the code's normalization $1/\alpha_W$ follows from the inputs (Appendix K 2), so the comparison checks the input chain and does not determine α independently. The theory would have failed if topology gave no cutoff ($k_{\max} \to \infty$).

I. The Bridge Lemma: $k_{\max} = 60$ from Closed Index

The Bridge Lemma identifies $k_{\max} = 60$ as a closed Spin^c index on $\mathbb{C}P^2$.

1. Statement

For the canonical Spin^c structure on $\mathbb{C}P^2$ with twist bundle $E = \mathcal{O}(9) \oplus \mathcal{O}^{\oplus 5}$:

$$k_{\max} := \mathrm{Index}(D_{\mathbb{C}P^2} \otimes E) = \chi(\mathbb{C}P^2, E) = 60. \quad (442)$$

2. Proof

For the canonical Spin^c structure, $D \sim \sqrt{2}(\bar{\partial} + \bar{\partial}^*)$, so $\mathrm{Index}(D \otimes E) = \chi(\mathbb{C}P^2, E)$ by Hirzebruch–Riemann–Roch. The holomorphic Euler characteristic satisfies $\chi(\mathcal{O}(m)) = \binom{m+2}{2}$ for $m \geq 0$. Therefore:

$$\chi(E) = \chi(\mathcal{O}(9)) + 5\chi(\mathcal{O}) = \binom{11}{2} + 5 = 55 + 5 = 60. \quad \square \quad (443)$$

3. Physical Selection

The value $k_{\max} = 60$ is consistent with the microsector physics. The effective coupling $\beta_{U(1)} = \langle k+2 \rangle$, computed from the SU(2) Chern–Simons weights

$$w(k) = \frac{2}{k+2} \sin^2 \frac{\pi}{k+2}, \quad (444)$$

is the lattice input $\beta_{U(1)} \approx 3.80$ for $k_{\max} = 60$. Here levels run $k = 0, 1, \ldots, k_{\max} - 1$ (standard SU(2) WZW/CS convention), giving:

$$\langle k+2 \rangle_{k_{\max}=60} = \frac{\sum_{k=0}^{59} (k+2)\, w(k)}{\sum_{k=0}^{59} w(k)} = 3.7969 \approx 3.80. \quad (445)$$

Bridge Lemma

Index: $k_{\max} = \chi(\mathbb{C}P^2, E) = 55 + 5 = 60$ [Spin^c HRR]
Physics: $\beta_{U(1)} = \langle k+2 \rangle = 3.797$ at $k_{\max} = 60$; lattice comparison with $\alpha^{-1} = 137$ to about 1%
Icosahedral: $k_{\max} = 60 = |A_5|$
E8 echo: $\mathrm{roots}(E_8)/4 = 240/4 = 60$ ✓

J. Nine Charged Fermion Masses

One formula covers the nine charged fermion masses; the prefactors other than those of the top and the charm are data-selected (App. FM).

1. The Mass Formula

$$\boxed{m_f = A_f \cdot \alpha^{n_f} \cdot \frac{v}{\sqrt{2}}} \quad (446)$$

where:

- $\alpha = 1/137.036$ (fine-structure constant)
- $v/\sqrt{2} = 174.1$ GeV (Yukawa normalization)
- $n_f =$ **sector-dependent** exponent from $\mathbb{C}P^2$ coupling path
- $A_f =$ prefactor, data-selected except for the top and the charm (App. FM)

2. Sector-Dependent Exponents

The exponents depend on the *sector* (leptons, up-quarks, down-quarks) due to the different Yukawa coupling paths: up-quarks couple to $\tilde{H}$, down-quarks to H directly, and leptons through a different gauge path.

TABLE XL. Charged fermion mass predictions.

Fermion	n_f	A_f	Predicted	Observed	Error
Electron	2.5	2/3	0.528 MeV	0.511 MeV	+3.32%
Muon	1.5	1	108.5 MeV	105.66 MeV	+2.72%
Tau	1.0	$\sqrt{2}$	1.797 GeV	1.777 GeV	+1.12%
Up	2.5	8/3	2.11 MeV	2.16 MeV	−2.23%
Charm	1.0	1	1.270 GeV	1.27 GeV	+0.04%
Top	0	1	174.1 GeV	172.76 GeV	+0.78%
Down	2.5	6	4.75 MeV	4.67 MeV	+1.75%
Strange	1.5	6/7	93.0 MeV	93 MeV	+0.03%
Bottom	0	1/42	4.15 GeV	4.18 GeV	−0.83%

a. Statistics.

- Mean absolute error: **1.42%** at leading order (a refinement to 0.61% after generation-1 priming is claimed in the companion volume; the 0.082% after two-loop running does not stand, since the running factors it uses are not Standard-Model running)
- Maximum error: 3.32% (electron, leading order)
- All nine predictions within 3.4% of observed central values
- **One universal normalization** for all 9 fermions

3. Structural Ratios

The selected prefactors have the ratios $A_d/A_u = 2.25$, $A_t/A_b = 42$, $A_\tau/A_\mu = \sqrt{2}$.

K. CKM Matrix from $\mathbb{C}P^2$ Geometry

The quark mixing matrix emerges from overlap integrals between quark generations localized at different $\mathbb{C}P^2$ positions.

1. Wolfenstein Parameterization

The CKM matrix has the standard Wolfenstein form:

$$V_{\text{CKM}} \approx \begin{pmatrix} 1-\lambda^2/2 & \lambda & A\lambda^3(\rho-i\eta) \\ -\lambda & 1-\lambda^2/2 & A\lambda^2 \\ A\lambda^3(1-\rho-i\eta) & -A\lambda^2 & 1 \end{pmatrix} \tag{447}$$

2. Geometric Derivation

The Cabibbo angle λ is determined by the ratio of vertex separations:

$$\lambda = e^{-d_{12}/\sigma_H} \approx 0.225, \tag{448}$$

where d_{12} is the $\mathbb{C}P^2$ geodesic distance between first and second generation vertices, and σ_H is the Higgs localization width.

3. Predictions

a. Key prediction within the localization model. Within the chosen $\mathbb{C}P^2$ localization scheme, the Cabibbo angle is set by the ratio d_{12}/σ_H, which is not computed here. The apex-dependent ratios use the standard Wolfenstein combinations with the Appendix AO apex $(\bar\rho, \bar\eta) = (0.157, 0.358)$: $|V_{ub}/V_{cb}| = \lambda\sqrt{\bar\rho^2+\bar\eta^2} = 0.088$ at leading order; the exact standard-parameterization matrix of Appendix AO gives 0.091, vs. observed 0.086 ± 0.006 (0.8σ).

L. Electroweak-Scale Relation

The "hierarchy problem" asks why $v \ll M_P$ (17 orders of magnitude). In the Standard Model, this requires fine-tuning. In the present DFD microsector, the relation below is best treated as a **numerically successful structural benchmark** rather than a finished theorem of the core postulates.

1. The Relation

$$\boxed{v = M_P \times \alpha^8 \times \sqrt{2\pi}} \tag{449}$$

a. Numerical verification.

$$M_P = 1.221 \times 10^{19} \text{ GeV} \tag{450}$$

$$\alpha^8 = (1/137.036)^8 = 8.04 \times 10^{-18} \tag{451}$$

$$\sqrt{2\pi} = 2.507 \tag{452}$$

$$v_{\text{pred}} = 1.221 \times 10^{19} \times 8.04 \times 10^{-18} \times 2.507 \tag{453}$$

$$= \mathbf{246.09} \text{ GeV} \tag{454}$$

Observed: $v = 246.22$ GeV. **Agreement: 0.05%.**

2. Physical Origin

- **Factor α^8:** The exponent $8 = \dim(\mathbb{C}P^2 \times S^3) + 1$ is the dimension count plus the Higgs radial mode (Thm. Z.3).
- **Factor $\sqrt{2\pi}$:** The prefactor is fitted: loop measures carry $(2\pi)^{-n}$, so the loop-normalization motivation does not hold, and no printed rule fixes it (App. Z).

  These motivations are structurally suggestive, but they are not yet a substitute for a referee-proof first-principles derivation.

Electroweak-Scale Benchmark

In this manuscript the relation $v = M_P\alpha^8\sqrt{2\pi}$ is best read as a microsector benchmark supported by the proposed topological structure, not as a closed hierarchy theorem independent of the rest of that construction.

M. Strong CP: Tree-Level Closure, Loop-Bounded

The strong CP problem asks why $|\theta_{\text{QCD}}| < 10^{-10}$. In the Standard Model, this is unexplained. In DFD, $\bar\theta = 0$ at tree level is derived, with $\theta_{\text{bare}} = 0$ fixed by the spectral action given that nothing is added to it for the gauge fields (Appendix L), and the loop-induced value is at the Standard-Model level ($\lesssim 10^{-16}$): det-orthogonal mass matrices, positive on the branch of Postulate Y.10, keep $\arg\det(M_u M_d) = 0$, and the fermion Clifford module on the even-dimensional CP mapping torus has spectral pairing and no zero modes, forcing the η-invariant to vanish.

1. Tree Level

At tree level, with $\theta_{\text{bare}} = 0$ fixed by the spectral action given that nothing is added to it for the gauge fields, $\theta = 0$ follows from the det-orthogonal tree-level protection together with the η-invariant argument (Thm. L.3); $\mathbb{C}P^2$ topology quantizes the instanton number:

- The θ-term $\propto \int \text{Tr}(F \wedge F)$ requires a 4-form
- On $\mathbb{C}P^2$: $H^4(\mathbb{C}P^2) = \mathbb{Z}$, generated by ω^2

TABLE XLI. CKM parameters: localization-model values vs. observation (PDG 2024). This geometric model motivates the structure; the canonical integer-pattern treatment ($\lambda = 31\alpha$, $A = 108\alpha$, with per-channel σ) is in Appendix AO and Table CV.

Parameter	Predicted	Observed	Status
λ	0.225	0.22501 ± 0.00068	✓
A	0.81	$0.826^{+0.016}_{-0.015}$	✓
$\lvert V_{ub}/V_{cb}\rvert$	$\lambda\sqrt{\bar\rho^2+\bar\eta^2} \approx 0.088$ (exact matrix: 0.091)	0.086 ± 0.006	✓
$\lvert V_{td}/V_{ts}\rvert$	0.211 (App. AO)	0.211 ± 0.007	✓

- The instanton density is *exact*: $\int_{\mathbb{C}P^2} \mathrm{Tr}(F \wedge F) = 8\pi^2 k_3$

2. Loop Level

Potential loop corrections to θ:

a. (a) Quark mass phases. $\delta\theta = \arg(\det M_u \times \det M_d)$. In gauge emergence:

$$Y_{ij} = g_Y \int_{\mathbb{C}P^2} \bar\psi_i \phi_H \psi_j \, d\mu_{\mathrm{FS}} \tag{455}$$

b. (b) Instanton contributions. $\pi_3(\mathrm{SU}(3)) \to H^4(\mathbb{C}P^2 \times S^3)$. The cohomology is:

$$H^4(\mathbb{C}P^2 \times S^3) = H^4(\mathbb{C}P^2) \oplus H^1(\mathbb{C}P^2) \otimes H^3(S^3) = \mathbb{Z} \oplus 0 = \mathbb{Z} \tag{456}$$

The only 4-cycles are in $\mathbb{C}P^2$.

c. (c) Electroweak contributions. CKM phase $\delta_{\mathrm{CP}} \neq 0$ (weak CP violation exists), but this feeds into θ_{QCD} only at the Standard-Model level:

- $\mathrm{SU}(2)_L$ lives on $\mathbb{C}^2$ (the 2-dim block)
- $\mathrm{SU}(3)_c$ lives on $\mathbb{C}^3$ (the 3-dim block)
- The $(3, 2, 1)$ partition **topologically separates** these sectors at tree level
- CKM phases arise from misalignment of fermion localization with gauge eigenstates—this is a *weak-sector* effect that reaches the QCD vacuum angle only through the degree-thirteen Jarlskog structure (a multi-loop effect), at the Standard-Model level ($\lesssim 10^{-16}$)

d. Comparison to known solutions.

Mechanism	$\theta = 0$ enforced by	DFD analog
Peccei-Quinn	Dynamical (axion)	Not needed
Nelson-Barr	Spont. CP breaking	N/A
Massless u	θ unphysical	N/A
DFD	**spectral action + det-orthogonality + η-invariant**	Thm. L.3

Strong CP: Tree-Level Closure, Loop-Bounded

Tree level: $\theta_{\mathrm{bare}} = 0$, fixed by the spectral action given that nothing is added to it for the gauge fields (App. L), and $\arg\det(M_u M_d) = 0$ for det-orthogonal mass matrices positive on the branch of Postulate Y.10 (App. AO).

Anomaly (Theorem L.3): The fermion Clifford module on the 8-dimensional (even) CP mapping torus has symmetric Dirac spectrum and no zero modes, so $\eta = h = 0$, $A_{\mathrm{CP}} = 1$, and the anomaly generates no θ-term. **Loops:** the induced angle is at the Standard-Model level, $\lesssim 10^{-16}$ (App. AO).

Mechanism: The 8-dimensional mapping torus (from $M = \mathbb{C}P^2 \times S^3$) carries a graded Clifford module, so $\eta = 0$ by spectral symmetry without an explicit computation; the product-background Dirac gap removes zero modes.

Prediction: No QCD axion. Detection at ADMX, ABRACADABRA, or CASPEr falsifies DFD.

N. PMNS Matrix from $\mathbb{C}P^2$ Geometry

The PMNS matrix has **large** mixing angles, unlike the hierarchical CKM. DFD explains this through different localization patterns.

1. Observed Mixing

Angle	PMNS (observed)	CKM (observed)	Ratio
θ_{12}	$33.4° \pm 0.8°$	13.0°	2.6
θ_{23}	43–49° (octant open)	2.4°	18–20
θ_{13}	$8.6° \pm 0.1°$	0.2°	43

2. Physical Mechanism

- **CKM (quarks):** Both up-type and down-type quarks localized at *vertices* → small overlaps → small mixing
- **PMNS (leptons):** Charged leptons at *vertices*, but neutrino R-H sector at the *center* → large overlaps → large mixing

3. Tribimaximal Base

When neutrinos are centered, they have *equal* overlap with all three vertices:

$$U_{\text{TBM}} = \begin{pmatrix} \sqrt{2/3} & \sqrt{1/3} & 0 \\ -\sqrt{1/6} & \sqrt{1/3} & \sqrt{1/2} \\ \sqrt{1/6} & -\sqrt{1/3} & \sqrt{1/2} \end{pmatrix} \tag{457}$$

giving $\theta_{12} = 35.3°$, $\theta_{23} = 45°$, $\theta_{13} = 0°$.

4. Corrections

The deviations from TBM are those of App. X:

TABLE XLII. PMNS angles: tribimaximal + corrections.

Angle	TBM	Correction Source	Predicted	Observed
θ_{12}	35.3°	trimaximal TM1, $\sin^2\theta_{12} = 0.3184$ (App. X)	34.4°	33.4°
θ_{23}	45.0°	μ-τ reflection (maximal)	45.0°	43–49°
θ_{13}	0°	$\sin^2\theta_{13} = 3\alpha$ (stated conjecture)	8.5°	8.6°

PMNS Matrix: Trimaximal Structure

Large neutrino mixing arises because:
- Charged leptons at $\mathbb{C}P^2$ *vertices* (hierarchical, like quarks)
- Neutrino R-H sector at the *center* (democratic)
- Tribimaximal mixing as leading order

This explains why PMNS ≠ CKM.

a. CKM mixing. The CKM matrix has Wolfenstein structure:

$$V_{\text{CKM}} \sim \begin{pmatrix} 1 & \lambda & \lambda^3 \\ \lambda & 1 & \lambda^2 \\ \lambda^3 & \lambda^2 & 1 \end{pmatrix}, \quad \lambda = e^{-d/\sigma} \approx 0.22, \tag{458}$$

where d/σ is the ratio of vertex separation to Higgs width. The CP-violating phase is supplied by Postulate Y.10 (App. AO).

b. Neutrino masses. Lepton number L is not topologically protected. Right-handed Majorana masses $M_R = M_P\alpha^3 \approx 5 \times 10^{12}$ GeV (Appendix P) give the see-saw formula:

$$m_\nu \sim \frac{M_D^2}{M_R} \sim 0.1 \text{ eV}. \tag{459}$$

Large PMNS mixing arises from different localization patterns for charged leptons vs. neutrinos.

O. Infrared Scale for Yang-Mills from DFD Geometry

The DFD deep-field geometry adds a curvature term to the infrared spectrum of Yang-Mills fluctuations—a consequence of the Weitzenböck identity on curved spatial slices.

1. Setup: DFD Spatial Geometry

The deep-field scalar profile $\psi(r) = \psi_0 - B\ln(r/r_0)$ with

$$B = \frac{2}{c^2}\sqrt{GMa_0} \tag{460}$$

induces a conformally flat spatial metric $h_{ij} = e^{2\alpha\psi}\delta_{ij}$. In the deep-field annulus (galactic outskirts), this metric has strictly positive Ricci curvature in angular directions:

$$\text{Ric}_{\theta\theta} = B\alpha(2 - B\alpha), \qquad \text{Ric}_{rr} = 0. \tag{461}$$

For $0 < \alpha B < 2$, the angular Ricci components are positive.

2. Weitzenböck Identity

For 1-forms on a Riemannian 3-manifold:

$$\Delta_{\text{Hodge}}A = \nabla^*\nabla A + \text{Ric}_h(A). \tag{462}$$

The Ricci tensor enters as an *effective positive potential* for Yang-Mills fluctuations.

3. The DFD-Induced Infrared Bound

Proposition XVII.3 (DFD-induced infrared scale)**.** *On a bounded domain Ω containing a deep-field annulus with $\text{Ric}_h(v,v) \geq \Lambda\, h(v,v)$ for some $\Lambda > 0$, the smallest nonzero eigenvalue λ_1 of the spatial Yang-Mills operator satisfies:*

$$\lambda_1 \geq C_1\Lambda, \qquad m_{\text{eff}} \equiv \sqrt{\lambda_1} \sim \frac{(GMa_0)^{1/4}}{c\,R}. \tag{463}$$

a. Numerical scale. For Milky Way parameters ($M \sim 10^{12}M_\odot$, $R \sim 10$ kpc):

$$m_{\text{eff}} \sim 10^{-30}\,\text{eV}, \tag{464}$$

far below the QCD mass gap.

4. Clarification: What This Does Not Claim

Important Clarification

This mechanism does **not** solve the Clay Yang-Mills mass gap problem:
- The Clay problem is formulated for pure SU(N) Yang-Mills on *flat* $\mathbb{R}^4$
- The DFD mechanism requires curvature of spatial slices
- The induced scale $\sim 10^{-30}$ eV is irrelevant for hadron physics

a. What is established. In any realistic DFD cosmology, Yang-Mills fields never live on exactly flat spatial backgrounds. The same deep-field parameter a_0 that controls galactic dynamics also adds a tiny curvature term to the gauge fluctuation spectrum through background geometry. This is a structural result, not a solution to the mass gap problem.

P. Testable Predictions

The gauge extension makes structural statements and model-dependent predictions:

a. Structural statements (consistent with observation).

- $N_{\text{gen}} = 3$ — a stated input, identified with $\chi_{\text{top}}(\mathbb{C}P^2)$ (Rem. F.21)
- Gauge group $SU(3) \times SU(2) \times U(1)$ — electroweak factor under one stated identification, colour an input (App. F)
- Chiral fermion spectrum — an input, as in the Standard Model (Rem. F.3)

b. Model-dependent predictions (testable).

c. Current status.

- $k_a \approx 51.4$: Consistent with SPARC RAR fits
- Nuclear clock: null under the minimal action (Thm. XI.2); extended-channel window 26 Hz to kHz (Sec. XI F)
- Fermion masses: 1.42% leading-order mean error, far outside the measured uncertainties
- CKM matrix: the four Wolfenstein values give $\chi^2 = 10.1$ for four parameters against the global fit (App. AO)

Q. Caveats and Required Verification

a. What is claimed (each is graded where it is treated).

- The electroweak group is the isotropy group $U(2)$ of $\mathbb{C}P^2$ under one stated identification; colour and the family content are inputs, and $(3, 2, 1)$ is the minimal partition carrying them
- $q_1 = 3$ derived from the isotropy charge $6Y$ (App. F)
- $N_{\text{gen}} = 3$: a discrete input, numerically $|k_3 k_2 q_1|$ (bookkeeping identity, not an index theorem — App. F)
- Energy minimization selects $(1, 1, 3)$ flux configuration
- $\kappa_r = n_r \kappa_0$ from Ricci curvature of $\mathbb{C}P^{n_r - 1}$ (Theorem F.25; a motivated assumption, §XVIII K)
- $\theta_{\text{QCD}} = 0$ (tree level, with $\theta_{\text{bare}} = 0$ fixed by the spectral action given that nothing is added to it for the gauge fields; loop-induced $\lesssim 10^{-16}$; Theorem G.2)
- $\tau_p = \infty$ if baryon number is violated only by the electroweak anomaly (Thm. F.26)
- UV stability of all topological results (Theorem F.28)
- $k_a = 3/(8\alpha)$ from frame stiffness ratio × EM duality (Theorem G.1)
- α^{-1}: closed form exact under two stated choices; last 21 ppm on the open bracket (§X)
- Bridge Lemma: $k_{\max} = \chi(\mathbb{C}P^2, E) = 60$ for $E = \mathcal{O}(9) \oplus \mathcal{O}^{\oplus 5}$
- CKM matrix with $\lambda = 0.225$ (localization model; canonical $31\alpha = 0.2262$, App. AO)
- PMNS matrix (trimaximal TM1, App. X)
- Higgs scale: exponent 8 of $v = M_P \alpha^8 \sqrt{2\pi}$ (prefactor fitted)
- Strong CP: $\bar{\theta} = 0$ at tree level, loop-bounded, with $\theta_{\text{bare}} = 0$ fixed by the spectral action given that nothing is added to it for the gauge fields (Theorem L.3; no axion)

b. Experimental status.

- $k_a \approx 51.4$: Consistent with SPARC RAR fits
- Nuclear clock: null under the minimal action (Thm. XI.2); extended-channel window 26 Hz to kHz (Sec. XI F)
- Fermion masses: 1.42% leading-order mean error (not within the measured uncertainties)
- CKM parameters: $\chi^2 = 10.1$ for four against the global fit, λ at 1.8σ (App. AO)
- PMNS angles: trimaximal, $\theta_{23} = 45°$, in soft $\sim 2\sigma$ tension with NuFIT 6.0 (octant unresolved)
- Higgs scale: $v = 246.09$ GeV vs 246.22 GeV observed (exponent derived, prefactor fitted)

c. Falsification criteria for topological results. The gauge emergence framework makes three **hard predictions**:

1. **4th generation detection** → falsifies $N_{\text{gen}} = 3$
2. **QCD axion detection** (KSVZ/DFSZ range) → falsifies $\theta = 0$
3. **Proton decay observation** (any rate $\tau_p < 10^{40}$ yr) → falsifies $\tau_p = \infty$

TABLE XLIII. Predictions from the gauge extension.

Prediction	Value	Test	Status
k_a (self-coupling)	$3/(8\alpha) \approx 51.4$	RAR normalization	✓
Strong CP suppression	$\theta_{\rm QCD} \approx 0$	$\lvert d_n\rvert < 10^{-26}\, e \cdot$ cm	Pending
ψ-coupled running	$\delta g/g \propto k_i\, \psi$	Nuclear clock ratio	2026–27
$\alpha = 1/137$	From $k_{\max} = 60$	21 ppm (integers; bracket open)	✓
9 fermion masses	1.42% LO; seven prefactors data-selected	PDG comparison	✓
CKM λ	$31\alpha = 0.2262$	PDG: 0.22501(68)	✓

d. What is currently claimed. The gauge emergence framework is proposed to organize the following from $\mathbb{C}P^2 \times S^3$ topology:

- Standard Model gauge group $SU(3) \times SU(2) \times U(1)$
- Three fermion generations, a stated input identified with $\chi_{\rm top}(\mathbb{C}P^2)$ (App. F)
- Fine-structure constant $\alpha = 1/137$ from Chern-Simons
- Electroweak-scale benchmark $v \sim M_P \alpha^8 \sqrt{2\pi}$
- All 9 charged fermion masses (1.42% leading-order mean error; seven prefactors data-selected)
- CKM and PMNS mixing matrices
- Strong CP: $\bar\theta = 0$ at tree level, loop-bounded, with $\theta_{\rm bare} = 0$ fixed by the spectral action given that nothing is added to it for the gauge fields (Theorem L.3)
- Proton stability: $\tau_p = \infty$ (if baryon number is violated only by the electroweak anomaly)

e. What remains.

1. **Experimental confirmation:** LPI test, clock anomalies, T^3 phase (a null prediction)
2. **Community verification:** Independent review of derivations

Note: the gravity sector can stand independently of the microsector. The microsector itself remains a live development program: several results are strong, but others still rely on structural assumptions that deserve independent mathematical closure.

Summary: Gauge Extension and Microsector

Conditional: the electroweak $U(2)$ as the isotropy group of $\mathbb{C}P^2$ under one stated identification (colour an input); $\tau_p = \infty$ (if baryon number is violated only by the electroweak anomaly). ($N_{\rm gen} = 3$ enters as a discrete input — App. F.)
Derived:
- Fine-structure constant: closed form of §X, last 21 ppm on the open bracket; identification with $1/e^2$ not derived
- Higgs scale: exponent 8 of $v = M_P \alpha^8 \sqrt{2\pi}$ (prefactor fitted)
- Strong CP: $\bar\theta = 0$ at tree level, loop-bounded, with $\theta_{\rm bare} = 0$ fixed by the spectral action given that nothing is added to it for the gauge fields (Theorem L.3)
- Bridge Lemma: $k_{\max} = \chi(\mathbb{C}P^2, E) = 60$ connects α to mass tower
- Top and charm masses; the other seven rest on data-selected prefactors (App. FM)
- CKM matrix: $\lambda = 31\alpha = 0.2262$ (integer pattern, App. AO); $\mathbb{C}P^2$ vertex-separation motivation
- PMNS matrix: trimaximal TM1 (App. X); $\sin^2\theta_{13} = 3\alpha$ a stated conjecture
- Koide relation: $Q_\ell = 2/3$ is *not* derived (DFD's α-power lepton spectrum gives $Q_\ell \approx 0.665$; measured 2/3 holds to ∼0.001%, beyond DFD's ∼1% mass precision)

Coupling constants: $k_a = 3/(8\alpha)$ (Theorem G.1).
Status: Partially closed microsector program with several strong results and several still-open structural selections. Awaiting both experimental and mathematical verification.
Full proofs: Appendices F–H and K.

XVIII. OPEN PROBLEMS AND LIMITATIONS

This section names the main open problems and limitations of DFD, grouped in §XVIII A, and separates theoretical gaps from scope boundaries. The list is not complete: further open steps are graded where they arise in the text, and the standing review of §XVIII K grades the inherited proofs flagged by a proof-pattern scan.

a. Axiomatic status of the frontier completion. The structural upgrades in Secs. XI B, XI C, V A 3, and the forward perturbation skeleton (Sec. XVI L, Eqs. (416)–(419)) are stated as an *axiomatic extension* of the core

DFD postulates. Every derived result (clock ratio cancellation, screening law, $G_{\rm eff}$, trace–TT decoupling) is a theorem of the enlarged system. The additional axioms — common-scale factorization, response functional, micro-sector hierarchy, dust branch, parent strain field — are explicitly labeled throughout.

We distinguish four claim-status levels:

T0: Theorem from the core DFD postulates: exact RAR inversion for $\mu(x) = x/(1+x)$.

T1: Theorem from the enlarged frontier-axiom system: clock-ratio cancellation, variational screening law, A_5 finite-symmetry closure ($k_{\max} = 60$), species-assignment canonicality, linearized perturbation operator, $G_{\rm eff}$ growth law, trace–TT principal decoupling, luminal TT wave equation.

E: Empirical benchmark or auxiliary modeling input: residual channel hierarchy $\lambda_\alpha \sim \epsilon_H^2\alpha^2/(2\pi)$, $\lambda_{N,e,s} \sim \epsilon_H\alpha^2/(2\pi)$.

F: Open program item: first-principles derivation of the species–class map from $\mathbb{C}P^2 \times S^3$, full production $P(k)$/Boltzmann-level cosmology pipeline, narrowing of the nuclear-clock prediction band beyond the stated benchmark, the interacting operator-ordering map, which DFD shares with every quantum field theory (App. QM). The cosmological growth regime is not on this list: the Rest-Mass Channel confines the polarization to bound systems, so unbound linear perturbations grow with $G_{\rm eff} = G$ (App. GR).

The main open items are listed first (§XVIII A); the subsections after them treat specific problems, several of which DFD resolves.

A. Main Open Items

The items below are the main open problems of the theory, one line each and grouped by sector. Each is graded where it is treated, and the list is not complete. The inputs the theory adopts or measures are listed in Tables CXXVII and CXXVIII; an item leaves this list when it is derived, reduced to a stated input there, or handed to a named observation, and each line says which. The main open problem is the origin of the primordial perturbations: the printed theory contains no mechanism for them, so they enter through one stated starting condition, the smooth beginning of App. Q, with their amplitude A_s a calibrated number (App. FK).

a. Gravity in bound systems and the dark sector.

- The Rest-Mass Channel, that the μ-law acts only inside bound systems, is adopted, not derived; its Poisson term is the Einstein–Hilbert term's own static scalar energy. The floor law in energy form is adopted too; in spherical symmetry it fixes the momentum-conserving rule of motion, which keeps action and reaction and gives up χ's equivalence principle only where χ falls short of the medium's demand (App. GR, App. AV).
- The energy's three-dimensional filling rule is a stated clause, χ counting by what it adds to the size of the total rest-channel field; its mode-by-mode form has no rule of motion of its own, and which system's demand a χ halo fills is open where two systems' fields blend, as for the Milky Way and the Large Magellanic Cloud. Two named observations test the energy: the Local Group's matter barycentre, which it predicts at rest where the total-ψ rule predicts a drift, and the disc's vertical force at the Sun, which it puts at 66–69 $M_\odot\,\mathrm{pc}^{-2}$ with χ at the rotation-curve density, against the measured 68.8 ± 1.9 and the static μ-law's 84 ± 4, 3.1–3.2σ high (App. AV).
- The floor composition does not follow from an action of the printed type; in energy form it is one adopted input, and total-field equilibrium states the same law for the medium in spherical symmetry (App. AV).
- At estimate grade galaxy χ halos assemble as in ΛCDM, and SPARC then needs cored inner halos, which fit it with no change to the rotation-curve law. In spherical simulations under the adopted energy neither slow disc formation, which contracts χ as Newtonian gravity does at $z = 0$ (computed on 120 SPARC galaxies), nor, in dwarf and low-surface-brightness galaxies, the bursty feedback from stars that cores halos under Newtonian gravity makes these cores (computed); their origin is open, and in discs above about $10^{11}\,M_\odot$ of baryons the halo's mass is the open item: the abundance-matched halo fails SPARC and the lensing of isolated late-type galaxies there, and lighter halos pass both (App. GR, App. AV). Dwarf satellites share the question: cuspy χ subhalos at abundance-matched masses exceed the dark-matter densities measured at 150 pc in several M31 dwarfs (estimate).
- The flat weak-lensing profile of isolated galaxies is not kept beyond their bound radius, as the halo model of ΛCDM does not keep it; spectroscopically isolated lens samples decide whether the measured far signal is the galaxies' own (App. GR).
- Environmental confinement is an adopted axiom: the Bose sector caps the boost but does not confine it. The axiom names the even-handed (median) readout of the host mode, which fixes where the switch sits, and states that the readout is sharp; the Oort comets need it at least as sharp as a Hill switch with exponent about 4 to 5, not an exact step. Local wide binaries, which it predicts Newtonian, and the edge step at 13–16 kpc test it; the outer-halo globular clusters beyond the step show about a third of the predicted boost (App. NL).
- The nonlocal galaxy law has no free function on its depth of record, FB-OUT: the detector form and the width belong to the accumulator reading only. The completion's reciprocal terms are computed for discs (the fitted RAR knee is a_0, and the Freeman surface density is the local law's, $a_0/2\pi G = 137\,M_\odot\,\mathrm{pc}^{-2}$), isolated dwarfs follow the local law, and the law's relativistic content is the optical metric on the preferred foliation. Satellite dwarfs are handed to observation: on the data

published in 2020–2026 the seven M31 satellites that are tidally safe at the new distances sit about 2–3σ above the forward law's own prediction, which the ceiling $\nu(\tau_{\rm host})$ caps, and about 2σ above the completed law (estimate), and the four selected as tidally safe on earlier distances, only two of which are tidally safe at the new ones, 5.7σ and 4.4σ; the ceiling omits the χ branch of the floor law, and a combined 5σ excess over the completed law in deeper dispersions of external-field-dominated M31 satellites falsifies it in satellites that pass an equilibrium check and whose stars the host pushes, relative to their own χ, harder than their own gravity (App. NL).

- The exact (Bose) shape of the MOND response rests on one stated input, the ground-state principle $\mu = \mathbb{P}(n{=}0)$, which gives $\nu = Z_1$ (App. BS).
- The domain-local screen is an optional extension that no claimed result uses; the domain that sets its local MOND scale is not derived, and per-galaxy a_0 set against measured environment densities decides it (App. ZT).
- The epoch law $a_0(z)$ is contested: massive discs at $z \simeq 2$ sit where the predicted rise should show and do not show it on the published baryon census, on which they rotate 0.1–0.17 dex slower than DFD predicts, 1.5–2.2σ when the census's calibration is counted; fits that leave the baryonic mass free neither show nor exclude the rise; on the published census the survey's amplitude lies 0.094–0.103 dex above DFD's a_0 on either clock, a coherent baryonic-mass shift (App. A0Z).

b. Cosmology.

- The origin of the primordial perturbations and the horizon problem are open: both enter through one stated premise, the smooth beginning of App. Q, a smooth background at the bang with small regular ripples of the calibrated amplitude A_s and the stated tilt, and the theory states no mechanism for either: no field in the printed theory produces the perturbations, the derived routes close (the spectral action, the Higgs, the χ and Chern–Simons sector, thermal and holographic fluctuations, the trace anomaly, anisotropic scaling, relaxation of the internal spectrum, the E-transport clock and the Majorana sector; Prop. FK.3), and the fast-light past is the ordinary expansion read on the arena clock, too slow to open the horizon (App. Q). Closing either needs an accelerating stage that reheats, which the printed theory does not contain, so A_s is one calibrated input, which the formula $32\pi\alpha^5$ matches without a derivation (App. FK).
- The vacuum coefficient $R = \Omega_\Lambda C = 0.6042 \pm 0.0027$ behind $H_0^{\rm early}$ and the dark-energy density is one measured input, as the cosmological constant is in general relativity; no printed principle fixes the shape of the spectral cutoff on which it sits, and it depends on the internal spectrum (App. FK).
- The Hubble tension is read as one universe on two clocks (Sec. ZS 5): the CMB-anchored channels read the early clock and local probes the bound-matter clock, so SH0ES's high local value is the outcome the postulate expects; the postulate fails if bright sirens or mass-sheet-robust time delays settle at 67.5, and the absolute a_0 scale tests it once baryonic masses are known to about 2% (App. ZS). The size of the clock ratio, $\lambda = H_0^{\rm loc}/H_0^{\rm early}$ (Eq. (ZS4)), is measured and its derivation is open.
- The early universe rests on two stated inputs, the no-boundary state with nothing inserted and the smooth beginning, which carries the arrow of time; the optical engine needs a negative-pressure source and reheating that the printed theory does not supply, and the χ relic bounds it, so $r \lesssim 10^{-7}$ is a bound, not a predicted number (App. Q, App. SM).
- The χ abundance is derived conditional on one identification, of $f_\chi = \bar{M}_{\rm P}\alpha^3$ as the flux period, on the asserted premise P4′ that the $2\pi/\alpha$ winding instanton changes the flux sector (Lemma AV.27), on the stated count 158 in $m_\chi = 32.005$ eV and on two stated conventions; the uniform count, 171, would raise $\Omega_\chi h^2$ by 2%, which the CMB can separate (App. AV).
- The baryon asymmetry is one calibrated input: the printed mechanism derives its α^4 power and its $B{-}L$ current, but its first-principles value is about (2–3) $\times$ 10^{-9}, three to five times Planck's value, and the sign rests on an adopted axiom (App. FK).
- Structure formation on the current χ carrier is ΛCDM-like on linear scales ($\sigma_8 = 0.806$, $S_8 = 0.822$) and in the halo abundance at $z = 6$–15 (computed); the open parts are numerical: the small-scale lensing boost of the confined polarization, which depends on the bound-baryon profiles of haloes, and the high-redshift efficiency lever of $a_0(z)$ (App. PK, App. GR).

c. The tensor sector and the field equation.

- In the mathematics, smooth solutions break down in finite time on every non-zero background, and whether weak solutions exist for all time and are unique is open, as it is for the equations of gas dynamics; the horizon conditions apply at the event horizons of DFD's black holes, and their uniqueness and regularity are open (§III F).
- Through second post-Newtonian order the one- and two-body dynamics and the flux are general relativity's, with the parent strain's σ kept ($\epsilon = 1$, deflection $15\pi/4$; §IV, App. WS), and ψ loops and scalar memory are bounded far below observability (App. ZU, App. AT).

d. Particle physics and the inner space.

- The seven vacuum axioms that single out $\mathbb{C}P^2 \times S^3$ are adopted, not derived (App. AB, §XVIII C).
- The electroweak group is the isotropy group of $\mathbb{C}P^2$ under one stated identification (the hypercharge as the direction $\mathrm{diag}(1,1,-2)$, normalised as $6Y$), which is adopted, not derived; colour and the family content are inputs, as in the Standard Model (App. F).
- The generation count $N_{\rm gen} = 3$ is one stated input, used once; no index on the internal space supplies it (Rem. F.21).
- The closed form for α is exact under two stated choices,

the ρ-shifted Casimir on $S^3 = SU(2)$ and α's own trace with the heat-kernel regulator, and $q_1 = 3$ and $k_{\max} = 60$ follow given the electroweak identification, $k_{\max}$ through the conditional determinant-line count; the last 21 ppm rests on the bracket coefficient $c = 1/13$, whose provenance is open (§X); the trace in the closed form is the hypercharge trace, and its identification with $1/e^2$ rather than with the hypercharge coupling is not derived (§X I).

- The charged-fermion masses other than the top and the charm rest on seven data-selected prefactors, one per species (App. FM).
- The $\sqrt{2\pi}$ prefactor of the Higgs scale is fitted, with a no-go on deriving it, and $\lambda_H = 1/8$ is a conjecture whose matching scale is not derived: imposed at the top-quark mass it gives $m_H = 124.6$ GeV, 0.40% (2.7σ) below the measured value (App. Z).
- The CP phase of quark mixing rests on a stated postulate, the channel space $\mathbb{C}[A_5]$ is a stated postulate, and $\sin^2\theta_{13} = 3\alpha$ is a stated conjecture that JUNO tests through θ_{12} (App. AO, App. Z).
- The neutrino branch is one of four equally natural fractions, chosen by oscillation data, and the Dirac-neutrino Yukawa rung is a stated input (App. X).
- The strong scale $\Lambda^{(5)}_{\overline{\rm MS}} = \sqrt{4\pi}\, M_P \alpha^{19/2}$ is one stated discrete input: its exponent is the only half-integer rung in the empirical window, and it gives $\alpha_s(M_Z) = 0.1187$, 0.8σ from the world average; the string tension and the glueball mass then follow from QCD, their ratios to Λ being lattice numbers, as in the Standard Model (App. YM).
- The soliton reading of the proton is posited: it needs a quartic term, which the printed action does not contain (Rem. F.27). Proton stability does not use it and holds if baryon number is violated only by the electroweak anomaly (Thm. F.26).
- Why the vacuum energy of matter does not gravitate is open in DFD as in every quantum field theory with gravity: the ψ source is linear in the renormalized stress tensor, a uniform vacuum energy acts on the background expansion and, as Λ does, on bound systems, and the lock of the lapse to the scale factor does not stop it gravitating. The dark-energy relation assumes that the matter piece, of order $m_t^4/64\pi^2 \approx 10^{53}\rho_\Lambda$, and the spectral action's own Planckian vacuum term, about $10^{120}\rho_\Lambda$ (App. WS), each cancel (App. AU).

e. Foundations.

- The interacting quantum dynamics and the measurement postulate are those of every quantum field theory; $\hbar$ is the unit of action, and the Dirac β is derived (App. QM).

The inherited proofs flagged by the proof-pattern scan are graded in §XVIII K: twenty-two are re-derived and twenty-two are cited, not re-derived; they form a verification list, not open problems. Mach's principle is not a claim of DFD: a uniform ψ background is equivalent to a change of units, which leaves every mass ratio, clock ratio and G unchanged, so it cannot generate inertia. The applied conjectures of App. V, among them the Cooper-pair and Casimir coefficients, lie outside DFD's claims and are not open items of the theory.

B. Quantum Superpositions and the Penrose Paradox

a. The Penrose paradox. In GR-based approaches to gravity-quantum coupling, spatial superposition of masses appears to create branched geometries. If a mass M is in superposition at locations A and B, does spacetime curve "both ways"?

b. Why DFD resolves this paradox. In DFD, there is *one* flat $\mathbb{R}^3$ with *one* scalar field ψ. The resolution follows from there being a *single* ψ sourced by the quantum expectation of the density—the source equation is linear in ρ:

$$\nabla\cdot[\mu(|\nabla\psi|/a_\star)\nabla\psi] = -\frac{8\pi G}{c^2}\rho. \tag{465}$$

For a quantum superposition $|\Psi\rangle = c_A|A\rangle + c_B|B\rangle$:

1. The source density is $\rho = |c_A|^2\rho_A + |c_B|^2\rho_B$ (quantum expectation value)
2. The ψ field responds to this weighted average
3. No "branched geometry" exists; there is one ψ field for the system

c. The semiclassical Schrödinger–Newton reading and the operator completion (App. ZU). The source equation above is linear in the density ρ—which is what resolves the branched-geometry paradox—but this does *not* by itself decide linear versus nonlinear quantum evolution. Under the *semiclassical reading*—the classical-ψ-by-design axiom ($S_\psi \sim (M_{\rm Planck}/a_\star)^2 \gg \hbar$) taken as fundamental, with ψ sourced by the c-number expectation $\rho = \langle\Psi|\hat\rho|\Psi\rangle = m|\Psi|^2$—the source is *quadratic* in Ψ, and substituting the resulting $\psi[\Psi]$ back into the matter evolution gives a Ψ-dependent generator: the nonlinear Schrödinger–Newton (semiclassical-gravity) equation

$$\begin{aligned} i\hbar\,\partial_t\Psi &= \Big[-\frac{\hbar^2}{2m}\nabla^2 - \tfrac{1}{2}mc^2\,\psi[\Psi]\Big]\Psi, \\ \nabla\cdot\big[\mu(|\nabla\psi|/a_\star)\,\nabla\psi\big] &= -\frac{8\pi G}{c^2}\,m|\Psi|^2. \end{aligned} \tag{466}$$

The semiclassical side is not DFD's. The operator completion of the *same* printed action (App. ZU) replaces it: the c-number source $\rho = m\langle\Psi|\hat\rho|\Psi\rangle$ is the Hartree factorization of the derived two-body vertex, the one-particle sector is exactly free, and the completion predicts *exactly zero* gravitational self-shift of a trapped crystal's center-of-mass mode (the Kohn null, Thm. ZU.2) to all orders in α_ψ with zero parameters. The Schrödinger–Newton frequency shift implied by the equation above is therefore *not a DFD prediction but the falsifier of the operator completion*: a measured positive sideband at the predicted

size ($\Delta\omega/\omega \sim 10^{-13}$, osmium; see App. ZU) would falsify the completion and support the semiclassical reading. Exact linearity and unitarity of the *test-particle* core remain as derived by the one-$H/J_\star$ theorem (Thm. QM.10, Cor. QM.12), given the linearized stability it assumes; what changes is the self-gravitating sector's status: linear under the operator completion, nonlinear only under the semiclassical commitment.

d. Discrimination from Diósi–Penrose: the deep-MOND self-energy and the sustained-fringe prediction. The Diósi–Penrose (DP) mechanism predicts collapse when the gravitational self-energy difference exceeds $\hbar/\tau$, with a *Newtonian* self-energy $E_G \sim Gm^2/d$. DFD's self-*energy* differs structurally: for a delocalized mass the internal self-acceleration sits far below the MOND scale—e.g. a $\sim 10^{10}$-amu, 100 nm superposition has $g_{\rm self}/a_0 \sim 9 \times 10^{-4} \ll 1$—so it lies in the *deep-MOND* ($\mu \to x$, AQUAL) regime, where the self-binding energy is *enhanced* over the Newtonian Gm^2/d, but every laboratory and Solar-System mass sits in hosts (the Earth, the Sun, the Galaxy) whose baryonic field exceeds $(\ln 2)^2 a_0$, so by the environmental-confinement axiom (App. NL) its self-field is exactly Newtonian; the enhancement would arise only in a weak host. *However, an enhanced self-energy is not the same as self-decoherence.* DFD's no-branching theorem (Appendix AH) settles this: the classical ψ is sourced by the c-number expectation $\rho = \langle\Psi|\hat{\rho}|\Psi\rangle$, giving *one* averaged optical metric for the whole superposition with *no* per-branch self-force. Even where such a self-energy arises, it does *not* decohere under c-number sourcing, no matter how strong the binding. Hence **DFD predicts *sustained* fringes at MAQRO** (distinct from Diósi–Penrose collapse), and this is not a free choice: the no-branching property follows from the two-body character of the derived vertex itself—the mean field of a two-body operator is a functional of the one-body density matrix of the full state alone (App. ZU)—so per-branch self-force is excluded without invoking the classical-ψ axiom. If one nevertheless entertained per-branch self-gravity, the deep-MOND enhancement would speed the Newtonian Schrödinger–Newton collapse by $\sim 20\times$ (collapse window $\sim 7 \times 10^{-5}$ s for a 10^{-13} kg / 250 nm mass) and would operate precisely in the deep-MOND regime $g_{\rm ext} < a_0$—but that is the *excluded* alternative, *not* the DFD prediction.

Space-based matter-wave interferometry (MAQRO-class) is the natural discriminator: DFD predicts *sustained* interference where Diósi–Penrose predicts collapse. The deep-MOND-enhanced collapse window above is the per-branch self-gravity alternative excluded by the no-branching theorem, retained here only to delimit what DFD is *not*. The DFD prediction (sustained fringes) is already testable at the MAQRO 10^{-13} kg frontier.

C. UV Completion: the Topological Proposal

a. The traditional UV problem. In General Relativity, the UV completion problem is acute: spacetime curvature diverges at singularities, and the theory is non-renormalizable when quantized. This requires unknown "quantum gravity" physics at the Planck scale.

b. How DFD addresses this problem. DFD has a different structure that addresses the traditional UV problem:

1. **Flat arena, absolute time:** DFD postulates flat $\mathbb{R}^3$ with absolute time. Where $\mu \to 1$ the physical metric has general relativity's curvature, but DFD's time is the uniform-expansion slicing, maximal around isolated bodies (App. WS), whose slices through a collapsing star stop at a limiting surface inside the horizon, $R = 3GM/(2c^2)$ for Schwarzschild, with the lapse decaying exponentially in absolute time, and never reach the singularity. For maximal slices this is proved for spherical collapse and for crushing singularities and argued for generic rotating collapse; that DFD's slices stay maximal during collapse rests on the argument of App. WS.

2. **Classical ψ by design:** The action scales as $S_\psi \sim (M_{\rm Planck}/a_\star)^2 \gg \hbar$, ensuring quantum fluctuations of ψ are negligible. Its quantized (operator) completion is App. ZU.

3. **Gauge structure from topology:** The gauge fields are Berry connections on the internal mode bundle over spacetime (§XVII B); the electroweak group is the isotropy group of $\mathbb{C}P^2$ under one stated identification, and colour and the family content are inputs, as in the Standard Model (App. F)—this is the proposed UV physics.

4. **Constants from topology:** the closed-form value of α, v and the leading fermion-mass and mixing patterns are computed from the topology, not from unknown high-energy physics; the charged-fermion masses other than the top and the charm, the Higgs prefactor and several flavour inputs are not yet derived (§XVIII A).

TABLE XLIV. Comparison of theoretical frameworks and their UV statuses.

Theory	**Low-Energy**	**UV Completion**
Gen. Relativity	Curved spacetime	Unknown
Fermi Theory	4-fermion contact	Electroweak
Chiral PT	Pion/kaon dynamics	QCD
BCS	Cooper pairs	e-phonon
DFD	**Scalar-optical**	$\mathbb{C}\boldsymbol{P^2} \times \boldsymbol{S^3}$ (proposed)

c. The proposed completion. The $\mathbb{C}P^2 \times S^3$ gauge emergence framework is proposed as DFD's UV completion, as QCD is for chiral perturbation theory; its ultraviolet finiteness is graded conjectural (§XVIII K). Specifically:

- The α-relations are organised by this topology, each at its own grade (App. F)
- Strong CP: with $\theta_{\rm YM} = 0$ fixed by the spectral action given that nothing is added to it for the gauge fields, $\bar{\theta} = 0$ at tree level, loop-bounded (Theorem L.3; no axion required)

d. What remains. The *origin* of the $\mathbb{C}P^2 \times S^3$ topology is the deepest open question, and it is not the only one: the gauge group is selected rather than forced, the generation count is an input, and several constants are not yet derived (§XVIII A). For physics purposes the topology serves as the foundational postulate from which the derived results follow.

D. Hyperbolicity and Numerical Evolution

a. Current status. The DFD field equation with constrained μ-function is:

- **Elliptic** in the static limit (well-posed boundary value problem)
- **Hyperbolic** for small perturbations about smooth backgrounds
- **Of finite lifespan** for fully nonlinear dynamical evolution on a non-zero uniform gradient, where smooth solutions reach a gradient singularity in finite time (Sec. III F); open on the degenerate background $\nabla\psi \to 0$

b. Open question. Does the coupled system (DFD scalar, TT tensor and the constrained pieces of the parent strain) admit a well-posed initial value formulation for arbitrary strong-field, dynamical configurations? Where $\mu \to 1$ it is the Einstein–Hilbert system in DFD's slicing (App. WS).

c. Partial results. The low-energy EFT preserves hyperbolicity under small perturbations. The perturbation metric:

$$\mathcal{G}^{\mu\nu} = W'(X)\eta^{\mu\nu} + 2W''(X)\partial^\mu\psi\partial^\nu\psi \qquad (467)$$

satisfies hyperbolicity conditions ($\mathcal{G}^{00} < 0$, $\det \mathcal{G}^{ij} > 0$) for the constrained μ-family, except at $\partial\psi = 0$, where both conditions fail since $W'(0) = \mu(0) = 0$.

d. Required work. Full numerical relativity codes for DFD would need:

1. ADM-like decomposition of the coupled system
2. Gauge conditions ensuring constraint propagation
3. Boundary conditions for the μ-crossover regime
4. Stability analysis for black hole merger configurations

This is deferred to future work.

E. Cluster-Scale Phenomenology: the χ Budget

Clusters: the χ component is required

Under the universal $\mu(x) = x/(1+x)$ alone the sixteen clusters of App. I fall short of their measured masses (Obs/DFD $= 1.57 \pm 0.08$ relaxed, 1.99 ± 0.16 merging, at $a_0 = 1.20 \times 10^{-10}$ m/s^2 and at the bound-matter $a_0 = 1.1966 \times 10^{-10}$ m/s^2). The shortfall is the derived χ: with χ adding its Newtonian pull and a hydrostatic bias $b = 0.21$ on the relaxed X-ray masses, all sixteen need $\chi = 4.5 \pm 0.6\, M_{\rm b}$ inside r_{500}, 0.84 ± 0.12 of the cosmic mix; under the floor composition of App. AV they carry the ΛCDM budget, 1.28–1.51 of the cosmic mix (computed). The amplitude follows from the derived abundance: under the floor composition and the adopted momentum-conserving energy of App. AV, cluster halos assemble as in ΛCDM, and 1.21 ± 0.05 of the cosmic mix is predicted inside r_{500}, against 1.28 ± 0.04 measured with no hydrostatic bias and 1.51 ± 0.04 with $b = 0.21$ (estimate; App. I), while χ boosted like the baryons would over-predict the cluster masses 1.43-fold. **Open:** a structure-formation run under the adopted energy and a cluster-by-cluster nonlinear DFD hydrodynamic and lensing solver that includes χ.

a. The correction stack does not close the gap. A no-χ closure by five correction factors (baryonic completeness, PDE-calibrated substructure averaging $J_{\rm PDE} = 1 + 0.39 f_{\rm sub}$, temperature, merger and projection systematics) does not hold: the baryonic items (WHIM, intracluster light, gas beyond r_{500}, IMF, clumping) sum to 1.26 and to 0.96–1.10 inside r_{500}; $J_{\rm PDE} \simeq 1.04$ for the baryonic substructure the μ-law responds to; the temperature factor tracks the merger flag and absorbs the hydrostatic bias; and the projection factor has the wrong sign for lensing masses.

b. Per-cluster results.

- **Relaxed clusters (n=10):** Obs/DFD $= 1.57 \pm 0.08$ under the μ-law alone, at $a_0 = 1.20 \times 10^{-10}$ m/s^2 and at the bound-matter a_0

- **Merging clusters (n=6):** Obs/DFD = 1.99±0.16 under the μ-law alone
- χ **required:** $4.5 \pm 0.6\, M_{\rm b}$, 0.84 ± 0.12 of the cosmic mix, for all sixteen with $b = 0.21$ when χ adds its Newtonian pull (1.28–1.51 under the floor composition; 1.21 ± 0.05 predicted, an estimate)

See Appendix I for complete analysis.

c. Galaxy groups. On published X-ray masses the μ-law falls short of galaxy groups as it does of clusters (median Obs/DFD 1.22–1.36 at r_{500} for 23 Chandra groups), and under the floor composition groups need χ at about the clusters' share of the cosmic mix (App. I).

d. Universality of μ. μ is universal from galaxies to clusters; the cluster excess is χ, not a scale-dependent μ.

F. Cosmological Constant: the Hierarchy from Topology

a. The traditional problem. In ΛCDM, the cosmological constant "problem" has two aspects:

1. **Fine-tuning:** $\rho_\Lambda \sim (10^{-3}\,\mathrm{eV})^4$ while QFT predicts $\rho_{\rm vac} \sim M^4_{\rm Planck}$—a 10^{122} discrepancy
2. **Coincidence:** Why is $\Omega_\Lambda \approx 0.7$ today, comparable to Ω_m?

b. Topological determination. Section XIX links H_0 and M_P through topology. A corollary is:

$$\left(\frac{H_0}{M_P}\right)^2 = C\alpha^{k_{\max}-N_{\rm gen}} = C\alpha^{57} \approx 1.39 \times 10^{-122} \quad (468)$$

This isolates the cosmological hierarchy: the exponent is not fine-tuned, while the residual $O(1)$ normalization C is measured. The exponent $57 = k_{\max} - N_{\rm gen} = 60 - 3$ follows from:

- $k_{\max} = 60$: the Spin^c index $\chi(\mathbb{C}P^2, E)$
- $N_{\rm gen} = 3$: the generation count (discrete input; all derivation routes exhausted, Rem. F.21)

c. One dark energy. The α^{57} vacuum term is the only dark energy in DFD, and no ψ-screen on inferred distances is read as a second, apparent acceleration (App. ZS; App. SL). A further statement holds:

- Distance duality holds *exactly*: $D_L = (1+z)^2 D_A$ (Etherington reciprocity in the optical metric, $\Delta\psi_{\rm dual} = 0$). There is no $e^{\Delta\psi}$ factor in the luminosity distance (Abstract item E1).

d. Status. The size of the cosmological constant is set by topology, not tuned: its exponent is fixed, its $O(1)$ coefficient C is measured on the early clock and is 1 on bound-matter clocks (Postulate ZS.11), where the closure scale $(3/8\pi)\alpha^{57}$ carries no coefficient; the observed density in laboratory units still carries Ω_Λ and the measured clock ratio (App. FK), and the cancellation of the vacuum energy of matter and of the spectral action's Planckian vacuum term is open (App. AU; §XVIII A). The 10^{-122} is:

$$\alpha^{57} = \left(\frac{1}{137}\right)^{57} \approx 10^{-122} \quad (469)$$

G. Full Cosmological Treatment

CMB and cosmology: the analytic framework and its named open inputs

The cosmological observables are derived within ψ-physics (§XVI C):

- Peak ratio $R = 2.34$ from baryon loading (Planck: 2.21; 6% high; the χ-matter spectrum, run on the measured clock, gives 2.20, within 0.6σ)
- Peak location $\ell_1 \simeq 220.4$ from the measured-clock no-screen forward solution, $100\theta_* = 1.04110$ (with no global $\Delta\psi \approx 0.30$ map)
- No *postulated* dark sector: the dark-matter and dark-energy *carriers* are identified within the spectrum — dark matter is the χ-matter field (App. AV, the harmonic b_3 three-form), dark energy is the α^{57} geometric vacuum energy
- **Relic abundance — conditional-derived (Finite $SU(2)_{60}$ CS Vacuum Relic):** the χ *abundance* is derived (no inflaton ⇒ no chosen angle) as the finite $SU(2)_{60}$ CS/WZW vacuum Casimir expectation, $\langle\vartheta^2\rangle = \sum_j |S_{0j}|^2 C_2(j)/[k(k+2)] = 0.073 \Rightarrow \Omega_\chi h^2 = 1.635\,\langle\vartheta^2\rangle = 0.1193$ (-0.6σ from Planck; App. AV, Thm AV.13). The operator (Casimir) is forced, the measure is conditional on the asserted premise P4′ (Lemma AV.27), and the normalization ($k(k+2)$: Sugawara $k{+}2$ × bare k, with $\vartheta_{\max} = \frac{1}{2}$ turn from χ's derived $\mathbb{Z}_2$) rests on two stated conventions; in consistent (turns^2) units the finite vacuum lies 12.45% below the uniform value $\frac{1}{12}$: the continuum $\sin^2$ measure lowers it by 15%, the Sugawara factor K/k raises it by 3.3%, and finiteness itself moves it by 0.09% (App. AV). The radiation-era ODE gives the bridge exactly, with no non-DFD input: $\kappa_{\rm rad} = \Gamma(\frac{1}{4})^2/(6\sqrt{3}\pi)$. The named open inputs are the two stated conventions, the stated count 158, the premise P4′ and the identification of $f_\chi = \bar{M}_{\rm P}\alpha^3$ as the flux *period* (the flux-period identification, Lemma AV.6; charged as one binary trials bit in App. CE).

a. Boltzmann codes. CLASS and CAMB are *GR-based* numerical tools that solve the coupled Boltzmann-Einstein hierarchy. With the parent strain's σ kept, DFD's linear perturbation equations are general relativity's, in the uniform-expansion slicing and for the curvature constant $k = 0$ (App. WS, Proposition WS.6(f)), so they *may* legitimately be run forward on DFD's background with the χ cold component — Appendix CL has done this on the one-clock $C = 1$ background, and Appendix ZS on the measured clock. What is *not* legitimate is treating DFD as ΛCDM and refitting that model's free densities:

1. The background is not a fitting freedom: DFD's expansion history rests on the measured vacuum coefficient $\Omega_\Lambda C$ and is not refitted
2. The cold component is not a free density but the derived χ field ($\Omega_\chi h^2 = 0.1193$, App. AV)
3. Λ is not a free vacuum-energy knob but the α^{57} geometric vacuum term, whose coefficient is measured

The semi-analytic DFD derivation of $R = 2.34$ and the measured-clock no-screen forward result $\ell_1 \simeq 220$ form the current backbone; the forward Boltzmann runs of Appendix CL are on the one-clock $C = 1$ background; the measured-clock plik-lite fit is in Appendix ZS.

b. Scope boundaries. DFD does not address:

- **Nucleosynthesis:** BBN proceeds the same way

This is not a "problem" for DFD any more than it is for electromagnetism—it is simply outside the theory's domain. Two early-universe questions are not on this list. The early expansion is DFD's own: DFD has no inflaton, its fast-light past is the ordinary expansion read on the arena clock, and its χ relic forbids any stage that freezes perturbations above $H \simeq 4 \times 10^{10}$ GeV, so primordial B-modes are absent ($r \lesssim 10^{-7}$; App. SM); the pre-BBN optical engine would inflate the optical metric only with a negative-pressure source and a reheating stage that the printed theory does not contain, and the primordial perturbations and the horizon problem are open: they enter through one stated starting condition, with no mechanism (§XVIII A). Baryogenesis is the other: DFD derives the α^4 power of the baryon asymmetry η_B and its $B-L$ bias, and its printed mechanism gives about $(2\text{–}3) \times 10^{-9}$, three to five times Planck's value (§XVIII A; App. FK).

H. Null Predictions: Where DFD Says "No Effect"

DFD has several sharp null predictions where the absence of any DFD-induced shift is itself a verifiable consequence.

a. Proton charge radius. The proton charge radius is a null prediction of DFD. At hadronic scales, the refractive field ψ evaluated at the nuclear potential is of order 10^{-39}; any DFD correction to electromagnetic scattering cross-sections, muonic-hydrogen Lamb shifts, or atomic-spectroscopy fits is at or below this level, vastly below any conceivable experimental sensitivity. The observational convergence of CODATA 2018 and PDG 2024 on $r_p \approx 0.841$ fm is therefore fully consistent with DFD; DFD has no proton-radius "puzzle" to explain.

b. Wide-binary sky orientation. DFD predicts *exactly zero* even ($\cos^2\theta$) dependence of the wide-binary force boost on the angle θ between a pair's separation vector and the Galactic-centre direction, at every separation and mass ratio (App. NL, Thm NL.10); the only allowed term is odd, $\propto (m_1 - m_2)\cos\theta$, and vanishes for equal-mass pairs. The zero is structural, not small: the depth never forms the vector sum $\mathbf{g}_{\rm int} + \mathbf{g}_{\rm ext}$ and the energy is linear in $|\nabla\Phi_N|^2$. MOND/AQUAL predicts 6.9% peak-to-peak at 10^4 AU and 46.6% at the $g_{\rm int} = g_{\rm ext}$ resonance. It applies to pairs in weak host fields, beyond 13–16 kpc; local *Gaia* pairs [53], which DFD predicts Newtonian, cannot test it; the test is robust to the mass-to-light and contamination systematics that dominate the contested amplitude measurements.

c. Matter-wave phase at first post-Newtonian order. The matter-wave T^3 phase of §XIII is a null prediction, not an open forecast: the DFD and GR test-body Hamiltonians coincide identically through 1PN ($\gamma = \beta = 1$, §IV C), so no DFD-specific T^2, T^3 or T^4 phase exists at that order in any atom interferometer; the static metric is general relativity's at 2PN as well (App. WS), and the extended species channel $K_{\rm atom}$ is an Eötvös parameter already bounded below 10^{-14} (§XV G).

I. Experimental Verification Timeline

The decisive tests of DFD have different timescales:

a. Priority ordering. Nuclear clocks and cross-species atomic campaigns come first, because geometric cancellation reduces the cavity–atom channel to a screened residual test rather than a near-term binary discriminator.

J. Closed Routes

The routes below were built, evaluated and closed; each entry names the quantity that closed it. **Nothing in this monograph rests on any of them.** Where a formal proof exists it is cited; the remainder are numerical closures at the stated size.

K. Standing Internal Review of Inherited Results

The monograph's proofs were passed through a systematic proof-pattern scan over all ⟨theorem, corollary, lemma, proposition⟩ environments in both volumes — 582 such environments in total, of which 419 are immediately followed by a proof. The scan searches for *argument shapes* that are known to fail silently, not for errors: it cannot

TABLE XLV. Experimental verification timeline.

Timeframe	Test	Decision
Near-term (1–3 yr)	Nuclear clocks (Th-229/Sr)	Strong-sector window: 26 Hz to ∼kHz
Near-term (1–3 yr)	Cross-species clock campaigns	Map composition-sensitive channels
Medium-term (3–7 yr)	Same-ion null checks	Bound the pure-α sector
Medium-term (3–7 yr)	Matter-wave T^3 (null prediction)	—
Long-term (> 7 yr)	Cavity–atom / space missions	Ultimate residual tests

TABLE XLVI. Closed routes and the quantity that closes each. Displacements are against the observed radial-acceleration-relation scatter floor of 0.057 dex [104].

Route	Closing quantity	Reference
Per-source composition read literally over a partition	$\tau \to \sqrt{N}\tau$; $v_{\rm flat}$ wrong by 562× at $N = 10^{11}$	Thm NL.21
Enclosed-mass composition (direction discarded)	ambient $\tau \geq \sqrt{\pi G\Sigma/a_0}\ln(R/h) = 1.53$ at R_0; 0.184 dex	Prop. NL.22
Field-based law, root *inside* the scale integral	$\tau \geq \sqrt{g_{\rm bar}/a_0}$ by Jensen; 0.139 dex	Prop. NL.24
Fixed-width logarithmic window	cannot chain; 0.157 dex, window-shape spread only 5.7%	App. NL, NL-F
Tidal-tensor class	1.631 dex; no external-field effect at all	—
Local Lagrangian modified inertia	baryonic Tully–Fisher normalisation off by a factor 4	—
Local non-Lagrangian modified inertia	galaxies evaporate on radial orbits	—
Every tested memory kernel	anti-dissipative: energy gain per orbit > 0	—
$\tau = \sqrt{g_{\rm obs}/a_0}$ (total-acceleration branch)	$g_{\rm obs} = a_0^{1/3} g_{\rm bar}^{2/3}$: declining curves, no BTFR	—
Thermal bath as the dark-matter density	2.6×10^{-108} vs $\rho_c = 7.6 \times 10^{-10}$ J m^{-3}: 98 orders	—
Thermal bath as ρ_Λ	the same 98 orders	—
Gravitational decoherence, tabletop	∼ 60 orders below reach	—
Gravitational decoherence, nHz background	∼ 80 orders below reach	—
Binning rotation-curve data on measured ν	+0.47 selection bias; **bin on** $g_{\rm bar}$	—
Response sign changes read as a physical scale	23 zeros at π/r_s (the acoustic phase); 62–124% window-dependent	Rem. NL.33
Any causal linear response for the CMB third-peak height	zero DC power from an oscillating source, at any amplitude	Thm NL.28
Rectification as the escape from that no-go	rectified DC ≤ 0.0166 of the baryon potential vs $\nu_{\rm req} = 6.364$; amplitude, not symmetry	Prop. NL.29
ψ itself as the standing pre-recombination well	$m_\psi = 0$ exactly, protected by an exact symmetry	Thm NL.30

decide whether any individual proof is sound. Forty-five statements matched; those that the corpus prints are graded below by the outcome of their re-examination.

> **How to read this list.** A statement in the first group has a proof re-derived under the current standard, and it appears where it stands in its re-derived form. A statement in the second group is cited, not re-derived: its printed proof asserts a step that the monograph does not supply, or it is a summary, a tally or a classification rather than a theorem. Its grade is given with it, and it should not be cited elsewhere at a higher grade. Entries marked (C) live in the companion volume.

a. Re-derived (twenty-two).

1. Well-posedness: Thm. U.4, by strict monotonicity of the flux for the approximant and both branches of the exact law; Thm. U.13, as the flow of a convex energy, with (A2) in the form of §III A and $p = 2$.

2. Galactic sector: Thm. NL.1, whose four limits follow from Eq. (NL5), the scale integrals converging for $w_0 > 0$; Thm. BS.19, whose remainder is $-e^{-2X}/48 + O(e^{-4X})$, from the pole of the Mellin transform at $s = -2$; Prop. AT.20.

3. The Hubble–Planck exponent and a_0: Cor. AP.11, Cor. O.3 and Thm. AP.24, whose stationary point $\Xi_* = 3/2$ is a minimum and gives $a_0 = 2\sqrt{\alpha}\, cH_0$ with $k_a = 3/(8\alpha)$. The generation-kernel axiom and the potential $U(\Xi)$ remain the premises stated there.

4. Internal geometry: Lemma AB.11, Lemma AB.6, Thm. AH.9 (C) and Thm. AH.14 (C). The index count $55 + 5 = 60$ is re-derived.

5. Strong CP: Thm. L.1 and Thm. AH.66 (C). The term-by-term cancellation holds for $\operatorname{Re} s > \dim X$, where Weyl's law makes the η series absolutely convergent; $\eta(s)$ therefore vanishes identically, and so does its continuation to $s = 0$. The loop bound is the Standard-Model estimate and is cited.

6. Screen closure: Cor. XVI.3 and Cor. XVI.4. The extracted offset is $\widehat{\mathcal{M}}(z) = \mathcal{M} - \langle \Delta\psi(z, \hat{n}) \rangle_{\hat{n}}$. It equals the calibration constant, and is independent of redshift, when the screen has no monopole, as in the current no-screen solution.

7. Bookkeeping in the particle sector: Cor. AH.46 (C); Thm. AH.50 (C), whose rate, with the $B{+}L$ multiplicity, is below a third of H at the reheating temperature, with equilibrium reached later, which is all the conversion factor requires; Thm. AH.183 (C), whose printed pieces reproduce while the value of $\delta_{\text{B-T}}$ stays open; Thm. AH.28 (C), where the μ–τ reflection forces $\theta_{23} = \pi/4$ and $|\sin \delta_{CP}| = 1$, $J_{\text{PMNS}} = -0.0337$ at the trimaximal $\sin^2 \theta_{12} = 0.3184$, and normal ordering follows on the adopted neutrino branch, which the axioms do not force; Thm. QM.3, where the level-9 sections span 55 dimensions and the 60-dimensional microsector is the index of $\mathcal{O}(9) \oplus \mathcal{O}^{\oplus 5}$; Thm. AH.44 (C).

b. Cited, not re-derived (twenty-two).

1. Ultraviolet finiteness from the microsector trace, graded conjectural: Thm. AH.37 (C), Thm. AH.192 (C), Thm. AH.16 (C), Thm. AH.1 (C), Thm. AH.159 (C) and Thm. AH.160 (C). The trace over the 60-dimensional microsector is finite, but the four-dimensional loop integral over external momenta is not cut off by it (status note after Thm. AH.1). The value $\alpha = 1/137.036$ at the cutoff in Thm. AH.16 also conflicts with the measured running, $\alpha^{-1}(M_Z) = 127.95$.

2. Strong-sector normalisations, graded as targets: Thm. AH.47 (C), Thm. AH.48 (C), Thm. AH.115 (C) and Thm. AH.132 (C); only the proportionality to Λ_{QCD} follows, and the numerical factors are calibrated. Thm. AH.15 (C) holds as the one-loop Standard-Model result for the given group and matter; its frame-stiffness mechanism is not derived.

3. Thm. F.25, graded as a motivated assumption: the step from Ricci curvature to the energy cost of a unit rotation is asserted, and the rank-one block, whose projective space is a point, is not covered. The Wilson ratio built on it inherits that grade.

4. Selections presented as consequences: Thm. AH.179 (C) gives a single vacuum given the selected bundle; Thm. Z.3 is a relation whose exponent 8 is derived, whose prefactor $\sqrt{2\pi}$ is fitted ($M_P \alpha^8 \sqrt{2\pi} = 246.09$ GeV, while the measured v needs 2.5080) and whose quartic is the conjectured $\lambda_H = 1/8$; Thm. AH.140 (C) is the conjunction of its parts and carries their grades, including the charged-fermion masses other than the top and the charm, which are not derived (App. FM).

5. Summaries, tallies, classifications and rules, not theorems: Thm. AH.198 (C), Thm. AH.208 (C), Thm. AH.216 (C), Thm. AH.218 (C) and Thm. AP.43.

6. Others: Thm. AH.33 (C), whose printed mechanism gives about $(2\text{–}3) \times 10^{-9}$, three to five times Planck's η_B, as its statement records; Prop. AH.204 (C), a conjecture as printed.

The list is not a closed set: a pattern scan finds the shapes it was told to look for, so the absence of a statement from this list is not a certificate. The list is published because a corpus of this size that claims to be checkable should show which parts of it have been checked, to what standard, and when.

L. Summary: Resolved and Remaining Items

TABLE XLVII. Summary of "open problems" — resolutions.

"Problem"	Kind	Resolution	Status
UV completion	Fundamental	Topology proposed as completion	Conjectural
Cosmological Λ	Fundamental	$(H_0 t_P)^2 = C\alpha^{57}$: exponent derived, C measured (Appendix O)	**Dict.**
Higgs hierarchy	Fundamental	$v = M_P \alpha^8 \sqrt{2\pi}$, prefactor fitted	Exponent
Clock coupling k_α	Technical	$k_\alpha = \alpha^2/(2\pi)$ (Appendix P)	Thm. (cond.)
Majorana scale M_R	Technical	$M_R = M_P \alpha^3$ (Appendix P)	Identification
Dust branch ($w \to 0$)	Technical	$K'(\Delta) = \mu(\Delta)$ (Appendix Q)	Thm. (cond.)
$P(k)$ full match	Program	Linear growth carried by χ with $Q = 1$ (App. GR); production pipeline (App. PK)	Mechanism
Boltzmann code	Technical	Forward runs of App. CL on the one-clock $C = 1$ background; the measured-clock fit is App. ZS	Open
Strong CP (tree level, loop-bounded)	Technical	$\bar{\theta} = 0$ at tree level, loop-induced $\lesssim 10^{-16}$ (Theorem L.3)	Derived ($\theta_{\rm YM} = 0$ fixed by the spectral action given that nothing is added to it for the gauge fields)
MOND $\mu(x)$	Phenomenological	exponential response from S^3 composition; $\mu = x/(1+x)$ its weak-response form (Theorem N.8)	**Proved** (given the ground-state principle and the assumptions of App. N, including the deep-field slope)
MOND a_0	Free parameter	$a_0 = 2\sqrt{\alpha} c H_0^{\rm loc}$ (Theorem N.14)	Derived
Neutrino hierarchy	Significant	$m_3/m_2 = \alpha^{-7/20}$ (Appendix X)	$< 0.2\sigma$
PMNS matrix	Significant	Trimaximal TM1; $\sin^2\theta_{13} = 3\alpha$ conjectured	Partial
CMB peaks	Significant	$R = 2.34$, $\ell_1 = 220$	analytic R 6% high; χ-matter spectrum within 0.6σ (measured clock)
Fermion masses	Significant	$m_f = A_f \alpha^{n_f} v/\sqrt{2}$, seven prefactors data-selected	Open

DFD: Unified Framework + Falsifiable Predictions

Theorem-grade and derived results:

1. **MOND function derived (given the ground-state principle and the assumptions of App. N, including the deep-field slope):** exponential response fixed by S^3 saturation-union composition (Lemma N.6, App. BS); $\mu(x) = x/(1+x)$ is its weak-response form (Thm. N.8).
2. **MOND scale derived:** $a_0 = 2\sqrt{\alpha}\, cH_0^{\rm loc}$ from topological constraint (Thm. N.14).
3. **Dust branch:** $K'(\Delta) = \mu(\Delta)$ gives $w \to 0$, $c_s^2 \to 0$ (Thm. Q.7). A no-go lemma proves that the quadratic identification fails.
4. **Strong CP (derived):** $\bar\theta = 0$ at tree level, loop-bounded, with $\theta_{\rm YM} = 0$ fixed by the spectral action given that nothing is added to it for the gauge fields (Thm. L.3). No axion.
5. **G–H$_0$ invariant:** $(H_0 t_P)^2 = C\alpha^{57}$; exponent forced, C measured on the early clock and $C = 1$ on bound-matter clocks (Postulate ZS.11; Appendix O).
6. **Clock coupling:** $k_\alpha = \alpha^2/(2\pi)$ from Schwinger + no-hidden-knobs (Appendix P) — conditional on that axiom.

Quantitative matches:

- $\alpha^{-1} = 137.036$ (21 ppm from the integers; the bracket coefficient is open)
- Higgs: $v = M_P\alpha^8\sqrt{2\pi}$ (exponent derived, prefactor fitted)
- Fermion masses: 1.42% leading-order mean error (9 particles; seven prefactors data-selected)
- CKM: $\lambda = 31\alpha = 0.2262$ (integer pattern; $\mathbb{C}P^2$ overlap motivation)
- PMNS: trimaximal TM1 (App. X); $\sin^2\theta_{13} = 3\alpha$ a stated conjecture
- CMB: the analytic $R = 2.34$ (6% above Planck's 2.21; the χ-matter spectrum, run on the measured clock, gives 2.20, within 0.6σ), $\ell_1 = 220$ (third-peak height carried by the derived χ-matter field, App. AV; abundance normalization conditional-derived, $\Omega_\chi h^2 = 0.1193$, -0.6σ; see below)
- ESPRESSO: conditional on $\xi_{\rm LPI}^{\rm res}$ (App. P)

Named open items: the main ones are listed, grouped, in §XVIII A, among them the origin of the primordial perturbations and the horizon problem, which enter through one stated starting condition, the Rest-Mass Channel postulate, the mode-by-mode rule of motion of the momentum-conserving energy, the adopted floor law and the environmental confinement of the MOND response, the inner cores and masses of the χ halos, the flux-period identification, the stated count 158, the asserted premise P4′ and two stated conventions behind the χ abundance, the vacuum coefficient R, and the baryon asymmetry, a calibrated input whose printed mechanism gives about (2–3) $\times 10^{-9}$, three to five times Planck's η_B; the standing review of §XVIII K grades the inherited proofs.

Scale structure: $k_{\max} = 60$, $N_{\rm gen} = 3$ (discrete input; Rem. F.21) + H_0 (observed) together with the measured clock coefficient $C \Rightarrow$ all dimensionful constants (per-input grades: App. FK, Rem. FK.8).

XIX. A TOPOLOGICAL LINK BETWEEN H_0 AND M_P

The preceding sections treated M_P (equivalently G) as an input parameter. Here we present a dimensionless constraint linking G, $\hbar$, H_0, c, and α, such that *given one scale measurement, the others follow from topology on bound-matter clocks, and with the measured coefficient C on the early clock.*

A. The Dimensionless Invariant

The primary claim is a purely dimensionless relation, derived to theorem status via Gaussian mode integration on the finite-dimensional microsector (Appendix O):

Proposition XIX.1 (Topological Invariant — Spectral-Action-Derived)**.** *DFD predicts the following dimensionless constraint:*

$$\boxed{\frac{G\hbar H_0^2}{c^5} = C\,\alpha^{k_{\max}-N_{\rm gen}} = C\,\alpha^{57}} \tag{470}$$

where $k_{\max} = 60$ (Spin^c index from Lemma F.11), $N_{\rm gen} = 3$ (generation count), α is the fine-structure constant, and C is an $O(1)$ normalization coefficient — measured, $C = 0.87784 \pm 0.00266$ *(Rem. AP.6).*

Theorem-grade status (Appendix O):

- *The exponent $57 = k_{\max} - N_{\rm gen}$ is forced by primed-determinant scaling on the finite Toeplitz state space (Lemma O.1, Corollary O.3).*
- *The identification with the observed invariant $I = G\hbar H_0^2/c^5$ is derived via Gaussian mode integration on the finite-dimensional microsector (Lemmas O.4–O.6, Theorem O.7).*
- *The $O(1)$ coefficient C is* not *derivable from the printed corpus: an eight-route, enumeration-complete no-go proves every printed route to the normalization is exponent-only, convention-importing, or C-covariant. C is a measured input — exactly as ΛCDM measures H_0 — concordant across five CMB-anchored channels on the early clock (Rem. AP.6); $C = 1$ is the clock of bound matter (Postulate ZS.11, Eq. (479)).*

This formulation has several advantages:

- **Dimensionless**: No unit conventions or hidden factors

- **Symmetric**: Predicts G from H_0 *or* H_0 from G
- **Falsifiable**: A single testable constraint

a. Bidirectionality. Given $(\alpha, \hbar, c)$ and a measured G, the invariant predicts H_0^{loc} with no coefficient, and H_0^{early} with the measured C. Equivalently, given H_0^{loc} it predicts G. Neither is privileged as "input"—the constraint is symmetric. This prevents any accusation that one quantity was "chosen" to match the other.

b. Error propagation. Taking logarithms and differentiating:

$$\frac{\delta G}{G} = -2\frac{\delta H_0}{H_0} \tag{471}$$

The precision of any G prediction is limited by H_0 uncertainty. With current H_0 uncertainties of ∼1–2%, the constraint tests G at the ∼2–4% level.

c. Equivalent form (Planck mass). Defining $M_P = \sqrt{\hbar c/G}$, the invariant becomes:

$$M_P = C^{-1/2}\,\alpha^{-(k_{\max}-N_{\text{gen}})/2} \times \frac{\hbar H_0}{c^2} = C^{-1/2}\,\alpha^{-28.5} \times \frac{\hbar H_0}{c^2} \tag{472}$$

d. Numerical verification. Using CODATA values for G, $\hbar$, c, α:

$$\text{LHS: } \frac{G\hbar H_0^2}{c^5} = 1.393 \times 10^{-122} \quad (\text{at } H_0 = 67.54 \text{ km/s/Mpc})$$
$$\text{RHS: } \alpha^{57} = 1.586 \times 10^{-122}, \qquad C\,\alpha^{57} = 1.393 \times 10^{-122} \tag{473}$$

The derived exponent lands the 10^{-122} hierarchy with no tuning — one unit of the exponent is a factor 137, so the residual $O(1)$ ratio *defines* the measured coefficient $C = 0.8778$ rather than admitting any alternative integer.

B. Implication for the Cosmological Constant Problem

The cosmological constant problem asks: why is $\rho_\Lambda/\rho_{\text{Planck}} \approx 10^{-123}$? This is often called "the worst fine-tuning in physics" because naive quantum field theory predicts $\rho_\Lambda \sim \rho_{\text{Planck}}$.

If Eq. (470) holds, the ratio is *topologically constrained*:

Proposition XIX.2 (Cosmological Constant Scaling)**.** *The critical density satisfies:*

$$\frac{\rho_c}{\rho_{\text{Planck}}} = \frac{3}{8\pi} \times \frac{G\hbar H_0^2}{c^5} = \frac{3}{8\pi}\,C\,\alpha^{57} \approx 1.7 \times 10^{-123} \tag{474}$$

(on bound-matter clocks, $C = 1$ under Postulate ZS.11, it is 1.9×10^{-123}, with no coefficient). With $\Omega_\Lambda \approx 0.69$: $\rho_\Lambda/\rho_{\text{Planck}} \approx 1.1 \times 10^{-123}$.

Scope. This identity fixes the *exponent* of the vacuum scale; the $O(1)$ coefficient enters through the clock-dictionary normalization (Rem. AP.6), and the statement is microsector-scoped — the Standard-Model matter-sector vacuum energy and the spectral action's Planckian vacuum term are not part of this identity and remain unaccounted (Rem. AU.3).

Derivation. The critical density is $\rho_c = 3H_0^2/(8\pi G)$. The Planck density is $\rho_{\text{Planck}} = c^5/(\hbar G^2)$. Thus:

$$\frac{\rho_c}{\rho_{\text{Planck}}} = \frac{3H_0^2}{8\pi G} \times \frac{\hbar G^2}{c^5} = \frac{3}{8\pi} \times \frac{G\hbar H_0^2}{c^5} \tag{475}$$

Substituting Eq. (470) gives the result. □

The exponent $57 = k_{\max} - N_{\text{gen}} = 60 - 3$ has two sources:

- $k_{\max} = 60$: the Spin^c index $\chi(\mathbb{C}P^2, E)$ for twist bundle $E = \mathcal{O}(9) \oplus \mathcal{O}^{\oplus 5}$ (Lemma F.11)
- $N_{\text{gen}} = 3$: the generation count (discrete input; the flux-product expression is a bookkeeping identity — App. F)

Cosmological Constant: Spectral-Action-Derived Exponent (Appendix O)

The "fine-tuning" of 10^{-123} is derived via Gaussian mode integration, given the cancellation of the matter vacuum and of the spectral action's Planckian vacuum term (Rem. AU.3):

$$\frac{\rho_c}{\rho_{\text{Planck}}} = \frac{3}{8\pi} C\alpha^{k_{\max}-N_{\text{gen}}} = \frac{3}{8\pi} C\alpha^{57} \approx 1.7 \times 10^{-123} \tag{476}$$

The exponent 57 is forced by primed-determinant scaling (Corollary O.3). The identification with the physical hierarchy is derived via Gaussian mode integration over the 57 nonzero KK modes (Lemmas O.4–O.6). The residual $O(1)$ normalization is the measured clock coefficient $C = 0.878$ on the early clock (Rem. AP.6); on bound-matter clocks $C = 1$ (Postulate ZS.11).

C. Testable Consequence: The Hubble Constant

Interpreted as an H_0 constraint from (G, α), the invariant Eq. (470) yields:

$$H_0 = \sqrt{\frac{C\,\alpha^{57} c^5}{G\hbar}} = \frac{\sqrt{C}\,\alpha^{28.5}}{t_P} \tag{477}$$

where $t_P = \sqrt{\hbar G/c^5}$ is the Planck time.

Using CODATA values for G, $\hbar$, c, and α, the BAO+θ_* coefficient $C = 0.87784 \pm 0.00266$ gives $H_0 = 67.543 \pm 0.103$ km/s/Mpc. The adopted cross-channel value uses the independent plik-lite central/error channel, rounded as

$$\boxed{H_0^{\text{early}} = 67.52 \pm 0.09 \text{ km/s/Mpc}} \tag{478}$$

The **exponent** is the zero-parameter content: the 10^{-122} hierarchy follows entirely from the microsector closed form for α and the exponent $57 = k_{\max} - N_{\text{gen}}$, and no neighbouring integer is reachable (one exponent unit moves H_0 by a factor 11.7). The $O(1)$ **coefficient**

C is measured once — the eight-route no-go proves it underivable from the printed corpus (Rem. AP.6) — and is concordant across five CMB-anchored channels (Planck plik-lite 67.520 ± 0.094, BAO+θ_* 67.543 ± 0.103, ACT DR6 67.481 ± 0.094, SPT-3G 67.417 ± 0.232, plus θ_*-only); DESI DR2 BAO alone sits 3.4σ higher (App. ZS). On bound-matter clocks and rulers $C = 1$ holds (Postulate ZS.11), and the identity then contains no measured coefficient:

$$\boxed{H_0^{\rm loc} = \frac{\alpha^{28.5}}{t_P} = 72.09 \text{ km/s/Mpc}} \qquad (479)$$

from the measured G, with zero parameters. Read the other way, $G = \alpha^{57} c^5/[\hbar\,(H_0^{\rm loc})^2]$ is derived from the local Hubble rate: the Cepheid-free local mean 71.87 ± 0.96 (Sec. ZS 5) gives a G $0.6\% \pm 2.7\%$ above the laboratory value, 0.2σ (Eq. (471)). The early-clock value of Eq. (478) is $H_0^{\rm early} = H_0^{\rm loc}/\lambda$ (Eq. (ZS4)), with λ the measured size of the postulate.

a. Comparison with observations. Recent JWST observations provide high-precision tests of this prediction. Two major collaborations have released results:

b. Assessment. On the early clock, DFD's $H_0^{\rm early} = 67.52 \pm 0.09$ km/s/Mpc lies $+0.2\sigma$ from Planck ΛCDM and 2–3σ below SH0ES's JWST-subsample estimates, 6.4σ below its full 2025 sample, while agreeing with CCHP JAGB at -0.1σ. On the bound-matter clock, $H_0^{\rm loc} = 72.09$ lies within 0.6σ of the SH0ES JWST subsamples, 1.5σ and 1.7σ below the full 2025 sample and the Local Distance Network, 0.9σ and 1.6σ above CCHP TRGB and JAGB, and 0.2σ above the Cepheid-free mean 71.87 ± 0.96 of Sec. ZS 5. The two JWST teams obtain systematically different results, with the disagreement not yet resolved [105, 108].

Key observations:

- The five CMB-anchored DFD clock channels (plik-lite, BAO+θ_*, ACT DR6, SPT-3G, θ_*-only) are mutually concordant and agree with Planck; DESI DR2 BAO alone lies 3.4σ higher
- SH0ES's JWST-subsample measurements lie 2–3σ above and its full 2025 sample 6.4σ above; CCHP results lie 0.1–1.5σ above the early-clock value
- The C=1 value is the bound-matter clock $H_0^{\rm loc}$ (Postulate ZS.11), 0.2σ from the Cepheid-free local mean

c. The Hubble tension in DFD. Reading the CMB inference as biased by a ψ-screen ($\Delta\psi \approx 0.30$ from ψ-tomography) while local ladders read the true clock does not resolve the tension. **Two exact theorems exclude that interpretation** (App. ZS): the homogeneous background $\bar{\psi}(t)$ carries no screen beyond the expansion it describes — at fixed scale factor it cancels identically in every CMB observable, so no homogeneous screen of any size can bias the inference — and the optical/matter metrics are conformally related, so a ψ-screen cannot be probe-selective; the surviving inhomogeneous channel is bounded 3.5 orders of magnitude too small. The CMB-anchored channels therefore read the early clock. Both measurements are robust and about 5σ apart (4.5σ for the Cepheid-free local mean, 6.4σ for SH0ES's full 2025 sample), and ΛCDM has to assign the difference to an error in one of them. DFD reads them as one universe on two clocks (Postulate ZS.11): matter keeps a clock offset by the constant $\lambda = H_0^{\rm loc}/H_0^{\rm early}$, set when matter first binds and falls behind the expansion, so the CMB-anchored channels return $H_0^{\rm early} = 67.52$ and local probes $H_0^{\rm loc} = 72.09$ (Eq. (479)). Bound systems read $a_0 = 2\sqrt{\alpha}\, cH_0^{\rm loc} = 1.1966 \times 10^{-10}$ m/s^2, consistent with SPARC within its systematic error, and the booking $C = 1.027 \pm 0.029$ of the Extended Derivations' five-presentation Λ theorem, SH0ES's 2022 value re-expressed and not a third arm, lies 0.9σ from $C = 1$. The postulate is a ratio between frames, not a screen, so the screen exclusion above is untouched. Its size λ is measured. The absolute a_0 scale (Euclid/DESI lensing RAR) tests it once baryonic masses are known to about 2% and distances are taken on each clock's own H_0 (App. ZS).

The G-H_0 Link: Derived Exponent, Measured Coefficient

Constraint: $(H_0 t_P)^2 = C\,\alpha^{57}$; exponent 57 derived ($N_{\rm gen} = 3$ a discrete input); on the early clock the coefficient $C = 0.87784 \pm 0.00266$ is measured once, on bound-matter clocks $C = 1$ (Postulate ZS.11)

Status: $H_0^{\rm early} = 67.52 \pm 0.09$, concordant across five CMB-anchored channels, $+0.2\sigma$ from Planck; $H_0^{\rm loc} = \alpha^{28.5}/t_P = 72.09$ from the measured G with zero parameters, 0.2σ from the Cepheid-free local mean, 1.5σ below SH0ES's full sample

Interpretation: One universe, two clocks (Postulate ZS.11): the CMB-anchored channels read the early clock and local probes the bound-matter clock; the ψ-screen-bias reading is excluded (background ψ adds no screen beyond the expansion, App. ZS)

Test: The postulate fails if bright sirens or mass-sheet-robust time delays settle at 67.5, if early-ruler and local ladders converge with distance, or if the absolute a_0 settles at the early-clock value on distances computed with $H_0^{\rm early}$ (Euclid/DESI lensing RAR, with baryonic masses known to about 2%); its price is a laboratory-unit age of 12.92 Gyr against ages of the universe of 13.5–13.8 Gyr that one programme infers from globular clusters with a ΛCDM formation delay

D. Epoch structure of the G–H_0 invariant: coupling versus state function

The invariant $G\hbar H_0^2/c^5 = C\,\alpha^{57}$ (Eq. (470)) admits two epoch readings, and only one of them survives. Read as an *all-epoch dynamical identity*,

$$G(t) = \frac{C\,\alpha^{57} c^5}{\hbar H(t)^2} \qquad (480)$$

it forces a photon-frame drift $\dot{G}/G = -2\dot{H}/H = +3H_0\Omega_m \approx +6.4 \times 10^{-11}\,\mathrm{yr}^{-1}$ (matter-dominated, $\Omega_m \approx$

TABLE XLVIII. Hubble constant: DFD's two clocks (Postulate ZS.11) vs. observations.

Source	H_0	Uncert.	Δ/σ (early)	Δ/σ (loc)	Ref.
DFD early clock, $H_0^{\rm early}$ (measured C)	**67.52**	±0.09	—	—	This work
DFD bound-matter clock, $H_0^{\rm loc}$ ($C=1$)	**72.09**	—	—	—	Eq. (479)
Local distance ladder (JWST)					
SH0ES JWST combined	72.6	±2.0	-2.5σ	-0.3σ	[105]
SH0ES JWST Cepheids	73.4	±2.1	-2.8σ	-0.6σ	[105]
SH0ES JWST TRGB	72.1	±2.2	-2.1σ	0.0σ	[105]
SH0ES JWST JAGB	72.2	±2.2	-2.1σ	-0.1σ	[105]
SH0ES HST+JWST, full sample	73.49	±0.93	-6.4σ	-1.5σ	[106]
Local Distance Network	73.50	±0.81	-7.4σ	-1.7σ	[107]
CCHP TRGB (HST+JWST)	70.4	±1.9	-1.5σ	$+0.9\sigma$	[108]
CCHP JAGB (JWST)	67.8	±2.7	-0.1σ	$+1.6\sigma$	[108]
CMB-inferred (model-dependent)					
Planck ΛCDM	67.4	±0.5	$+0.2\sigma$	—	[58]

Units: km/s/Mpc. $\Delta/\sigma \equiv (H_0^{\rm DFD} - H_0^{\rm obs})/\sigma_{\rm obs}$, with $H_0^{\rm DFD} = H_0^{\rm early}$ (early) or $H_0^{\rm loc}$ (loc), Eq. (ZS4).

0.31, $H_0 = 67.5$ km/s/Mpc), exceeding the lunar-laser-ranging and binary-pulsar bound $|\dot G/G| \lesssim 10^{-13}\,\mathrm{yr}^{-1}$ by $\sim 10^3$; and the atomic-frame rescue (a cosmological screen evolving as $2\dot\psi_{\rm cosmic} = -3H_0\Omega_m$) is unavailable, because the FRW flat-direction theorem (Thm. AE.1, App. AE) makes the homogeneous cosmological $\dot\psi$ non-dynamical. That self-tension would be a conditional self-consistency falsifier. It is resolved by the following distinction, which the elliptic constraint reading (Axiom WS.1, App. WS) makes structural rather than optional.

Theorem XIX.3 (Epoch consistency / anchor fork; conditional on Axiom WS.1)**.** *Under Axiom WS.1, the constitutive transition scale $a_\star$ in $\mu(|\nabla\psi|/a_\star)$ tracks the instantaneous cosmological state,*

$$a_0(z) \;=\; 2\sqrt{\alpha}\,c\,H(z), \tag{481}$$

and the running sign $\partial_z a_0 > 0$ is forced: the "anchored" branch of the anchor fork—an a_0 frozen at a formation-epoch value—is structurally unavailable.

Proof core (the no-memory argument). The elliptic constraint sector is instantaneous and carries no intrinsic dynamical memory: there is no local field degree of freedom in which a past epoch's H could be stored. The scalar has no mass term (unit-shift protection: $\psi \to \psi + \text{const}$ is a units redefinition, so no potential can anchor a remembered scale), and under Axiom WS.1 it has no independent temporal kinetics in the local sector. The stationarity functional that derives $a_0 = 2\sqrt{\alpha}\,cH_0$ (Theorem N.14, Appendix N) is evaluated on the instantaneous background, so its output references the current screen flow. A frozen a_0 would require a storage mechanism the theory does not possess; the tracking branch is therefore forced. The grade is theorem *conditional on Axiom WS.1*: the result inherits that axiom's status and no more. □

Corollary XIX.4 ($\dot G = 0$: coupling versus state function)**.** *G is an* action coupling *(the source normalization of the field equation): it is epoch-independent, $\dot G = 0$, and the lunar-laser-ranging bound is passed trivially. a_0 is a* state function *(a constitutive normalization by the current screen flow): it tracks $H(z)$, with $\dot a_0 = 2\sqrt{\alpha}\,c\,\dot H \neq 0$. The identity $G\hbar H_0^2/c^5 = C\,\alpha^{57}$ is a boundary-condition statement in the Axiom PO class (App. Q)—it selects the* present-epoch *H_0 in Planck units—not an all-epoch dynamical law; Eq. (480) is accordingly not a dynamical law; it is only the definition of the yardstick. The two predictions, $\dot G = 0$ and $\dot a_0 \neq 0$, are independent falsifiers. Note $\dot G = 0$ is GR-degenerate: it is a consistency check, not a discriminator; the discriminating partner is $\dot a_0 \neq 0$.*

Under Corollary XIX.4, G at every epoch equals today's value: it is not weaker by $\sim 10^9$ at recombination. The cavity–atom LPI comparison (Section XII) remains a live clock-sector test of the photon-frame/atomic-frame *difference*, but it is not required to cancel a $\dot G$ drift—there is none.

a. First data confrontation: MUSE-DARK III. The next paragraphs confront the data on the $\Omega_m = 0.274$ background of the one-clock C=1 convention; every $\Omega_m = 0.274$, $\gamma_E = 1.038$, and 1.7σ statement there belongs to that background, and the measured-clock values are those of the re-evaluation below ($\Omega_m \simeq 0.312$, $\gamma_E = 1.098$, 2.1σ). The tracking prediction is now confronted by the first measurement able to see the sign. MUSE-DARK III [109] reports a linear growth of the RAR acceleration scale,

$$a_0(z) = \left(1.00 \pm 0.04 \;+\; 1.59^{+0.11}_{-0.10}\,z\right) \times 10^{-10}\,\mathrm{m\,s^{-2}},$$
$$a_0(z{\approx}1) = 2.38^{+0.12}_{-0.10} \times 10^{-10}\,\mathrm{m\,s^{-2}}. \tag{482}$$

At face value this is the sign DFD predicts, $\partial_z a_0 > 0$, and it is the one discriminator against static MOND, which predicts no growth. It rests on the survey's bins, their published errors and its baryon census. Refitted galaxy by galaxy from the public products, the rise reproduces; within the survey a frozen a_0 lies about 1σ from it once galaxy-level errors are counted, and anchored to SPARC's $z = 0$ value, the galaxy-level bins still exclude a frozen a_0 at about 3σ, and DFD's zero-parameter law

fits them on the bound-matter clock. With molecular gas tied to the survey's disc masses the rise stays; tied to SED-based masses, or with SED stellar masses in the census, the trend is flat or falling (computed; App. A0Z, §A0Z 6). The *magnitude* comparison is pending. DFD predicts $a_0(z)/a_0(0) = H(z)/H_0$ exactly: 1.78 at z=1 on the measured clock ($\Omega_m = 0.312$; 1.71 on the one-clock C=1 background's $\Omega_m = 0.274$); a conditional bracket $[1.79, 2.83]$ does not apply—the matter-only 2.83 endpoint is not a rival DFD prediction, and under Theorem XIX.3 the prediction collapses to the $H(z)/H_0$ line. At face value the published linear-fit growth is steeper than $H(z)$-scaling (e.g. 2.05 predicted at z=1 from the SPARC local value 1.20×10^{-10} on the C=1 background, 2.14 on the measured clock, vs 2.38 ± 0.11 measured, a 95% interval), but the paper's per-bin uncertainties are untabulated and the fit's local anchor (1.00×10^{-10}) sits below the SPARC local value, a systematic not yet assessed—so the magnitude verdict awaited the binned data.

The published bins follow the epoch prediction, and counted galaxy by galaxy the rise is contested. The binned points have since been digitised and confronted directly [110] (published, MNRAS **551**(4), 2026 September 7). Fitting the continuous exponent family $a_0(z) = A(1+z)^\gamma$, which contains the frozen ($\gamma = 0$) and matter-density ($\gamma = 3/2$) hypotheses as special cases and closely brackets Hubble tracking, gives

$$\gamma \;=\; 0.78 \pm 0.15, \tag{483}$$

excluding a *frozen* a_0 at $\mathbf{5.3}\sigma$ on the published bin errors by the properly nested test ($\Delta\chi^2 = 27.7$ for one degree of freedom, rising to 6.6σ with the local SPARC $z \simeq 0$ anchor, which returns $\gamma = 0.83 \pm 0.13$) and the matter-density scaling at $\mathbf{4.8}\sigma$ (on the exponent's error; 4.7σ by the same nested test); $H(z)$-tracking is the information-criterion-preferred one-parameter description ($\chi^2 = 5.2/3$, GOF $p = 0.16$, AICc 9.2 against 17.1–17.2 for the two-parameter forms and 27–33 for the alternatives), with no bin deviating by more than 1.7σ. The "steeper" impression recorded above is *anchor-dependent* and does not survive a floating amplitude: measured against the binned relation itself the growth is, if anything, mildly *shallower* than $H(z)$, the fitted exponent sitting 2.1σ below the effective slope of the *Planck* $E(z)$ that the analysis assumed, published as $\gamma_E \simeq 1.10$ over $0.5 \lesssim z \lesssim 1.3$ (our own evaluation of that same background over the fitted range gives 1.087)—and only 1.7σ below $\gamma_E = 1.038$ evaluated on the one-clock C=1 background $\Omega_m = 0.274$.

Two caveats travel with this closure. First, the confidence convention of the source's plotted bars is not given there, and Ref. [110] therefore reports both readings. Read as 95% intervals the bars shrink and the published exclusions strengthen—$\gamma = 0$ to $\gtrsim 10\sigma$ and $\gamma = 3/2$ to 9.5σ on the exponent's error (9.2σ by likelihood ratio), with the exponent family tightening to $\gamma = 0.78 \pm 0.08$—while exact $E(z)$ tracking moves into goodness-of-fit tension ($\chi^2 = 19.9/3$, $p = 1.8 \times 10^{-4}$), the growth then being *shallower* than $E(z)$ at the published $\sim 4\sigma$ on the Planck background; the same offset evaluated on the one-clock C=1 background's $\Omega_m = 0.274$ is 3.4σ. *The exclusions of $\gamma = 0$ and $\gamma = 3/2$ hold under either reading; the consistency of Hubble tracking does not.* Second, the fitted tracking amplitude $A = (1.40 \pm 0.03_{\rm stat}) \times 10^{-10}\ \mathrm{m\,s^{-2}}$ sits 17% above the canonical SPARC normalisation 1.20×10^{-10}—0.8σ on SPARC's systematic-dominated uncertainty, but $+6.7\sigma$ on the published statistics alone ($+6.3\sigma$ using this corpus's own re-fit of the same bins, $A = 1.4010 \pm 0.0321$; $+5.3\sigma$ once the SPARC statistical bar is included). The reference itself quotes only the systematic-scale comparison; the statistics-only figures are evaluated here. It is a mass-scale-conditional pass, and the survey's own one-sided molecular-gas systematic is large enough to cover the required +0.094 to +0.103 dex of baryons (Stat. A0Z.6).

Falsifiers: a measured $\partial_z a_0 \leq 0$ falsifies Theorem XIX.3; a confirmed $\dot{G}/G$ detection at lunar-laser-ranging sensitivity falsifies Corollary XIX.4; a high-redshift *frozen* a_0 falsifies the epoch promotion. The two kinematic conditions apply to measurements whose baryon census counts molecular gas, whose pressure-support correction is stated, and whose errors are counted galaxy by galaxy. Massive discs at $0.6 < z < 2.5$ with molecular gas counted meet the third at face value, $a_0 \simeq 1.2 \times 10^{-10}\ \mathrm{m\,s^{-2}}$ at $z \simeq 2.2$ against 3.7 for tracking, and lean toward the first (a within-sample $\gamma = -0.86^{+0.46}_{-0.48}$ on statistical errors, -0.20 without the discs with $V_{\rm rot}/\sigma_0 < 2.1$). They do so on scaling-relation gas masses and the standard pressure-support correction; baryonic masses about 0.2 dex lower at $z \simeq 2$ than those fitted in Ref. [111] (0.3–0.5 dex below the census of SED stars and scaling-relation gas), or a pressure-support correction 2.4 times the standard one, remove the tension (App. A0Z, §A0Z 7). The domain-local screen of App. ZT would need $10\,h^{-1}$Mpc domains about 6 to 11 standard deviations denser than average, which their measured environments do not show (Stat. A0Z.12). At high redshift the epoch promotion is under test, not confirmed.

b. The same bins refitted on DFD's own background. The comparison just quoted evaluates $E(z)$ on Planck ΛCDM, because a theory-neutral analysis has no alternative. DFD does: the same α^{57} closure that supplies a_0 also supplied, *at the one-clock C=1 convention*, $H_0 = 72.0897$ and $\Omega_m = 0.2749$, so $a_0(z) = 2\sqrt{\alpha}\,cH(z)$ is a zero-parameter curve up to one overall amplitude. (At the measured coefficient the DFD background is $H_0^{\rm early} = 67.52$, $\Omega_m \simeq 0.31$ — essentially the Planck row already tested above; the amplitude question is the absolute-a_0 test of the two-clock postulate, App. ZS.) On the current measured-clock background, refitting the four bins with $\Omega_m \simeq 0.312$ held fixed and only the amplitude free gives $A = 1.394 \pm 0.032$, $\chi^2 = 5.36/3$, AICc = 9.36, and $\gamma_E = 1.098$ (2.1σ above the measured 0.782 ± 0.149). The 4.00/3, AICc 8.00 result belongs to the $C = 1$, $\Omega_m = 0.2749$ background. Hubble tracking remains viable and the preferred one-parameter description (App. A0Z, Table CX). **Three qualifications apply to this comparison.** (i) The predefined $P = 0.426$ false-positive con-

trol and $\Delta\mathrm{AICc} = -1.18$ apply to the $\Omega_m = 0.2749$ row of the one-clock $C = 1$ background and cannot be claimed as a current improvement. (ii) The current effective-exponent offset is 2.1σ before the alternative 95% error-bar reading; the external-field variant remains a separate regime test. (iii) Against the current survey-fitted amplitude, the early-clock $a_0(0) = 1.1208 \times 10^{-10}$ is lower by $8.5\sigma_{\rm stat}$ (about 2σ counted galaxy by galaxy), a coherent stellar-mass shift of about +0.095 dex, and the bound-matter $a_0 = 1.1966 \times 10^{-10}$, against the amplitude on distances computed with $H_0^{\rm loc}$, is lower by 0.094–0.103 dex (8.5–$9.2\sigma_{\rm stat}$; Stat. A0Z.6)—where a *frozen* a_0 requires +0.220 to +0.354 dex per bin, 2.3 to 3.8 times more, *plus* a redshift tilt that no common-mode rescaling supplies, but that a fuller baryon census does: with molecular gas tied to SED-based masses the refitted trend is about flat, tied to the survey's own disc masses the rise stays and DFD's law fits it, and with SED stellar masses it falls (computed; Stat. A0Z.6, §A0Z 6). The registered $z = 2$ and $z = 3$ falsifiers are tabulated in Table CXI.

c. Relation to the companion note. The companion note [112] stated the epoch extension $a_0(z) = 2\sqrt{\alpha}\, cH(z)$ as a program-grade conditional result (forced modulo the contemporaneous-normalizer identification). Theorem XIX.3 upgrades it: under Axiom WS.1 the identification itself is forced by the no-memory argument, so DFD lands on a *forced* fork branch, not a chosen one. The result remains conditional on Axiom WS.1 and is stated at that grade throughout this corpus. The binned kinematic confrontation has since been carried out in a separate, theory-neutral analysis that does not invoke DFD, published in MNRAS **551**(4), 2026 September 7 (Letter; `doi:10.1093/mnras/stag1485`) [110]; the epoch extension has therefore met data, and it is contested. Low-mass discs at $0.33 < z < 1.44$ show the predicted rise on the published bins; counted galaxy by galaxy, a frozen a_0 lies about 1σ from it within the survey and about 3σ from it anchored to SPARC's $z = 0$ value, with DFD's zero-parameter law fitting on the bound-matter clock, and the sign of the trend depends on how the molecular gas is added. Massive discs at $0.6 < z < 2.5$, on a census that counts molecular gas, do not show the rise beyond $z \simeq 1.5$ at face value (App. A0Z, §A0Z 6 and §A0Z 7). Direct molecular-gas masses, kinematic masses not limited by a halo-model prior and per-galaxy analyses with galaxy-level errors and $a_0(z)$ imposed decide it, the last for the massive discs only with an independent bound on the χ halo or rotation curves beyond $3R_e$; JWST and ALMA rotation curves at $z \gtrsim 3$, and ultimately SKA H I kinematics, extend the test to where $E(z)$-tracking at the fitted amplitude and the survey's linear form diverge: on this corpus's evaluation at the survey's fitted amplitude, Hubble tracking gives $a_0 \simeq 4.20$ at $z = 2$ and 6.32 at $z = 3$, against 4.18 and 5.77 for the survey's linear form and 3.38 and 4.23 for the measured exponent family.

E. The homogeneous optical-time Hamiltonian (background expansion)

Theorem AE.1 establishes that the homogeneous mode of the *static* field action is a flat direction: with the source written as the density contrast $\rho - \bar\rho$, a homogeneous configuration carries no net source and the Euler–Lagrange equation places no constraint on $\bar\psi(t)$. This is the correct statement for the *perturbation* (galactic/AQUAL) sector, and it is the reason the cosmic expansion rate does not follow from the spatial field equation. It does *not* imply that DFD lacks an expansion law: the background rate is set by the Einstein–Hilbert term of Proposition WS.5, which fixes the homogeneous mode that the scalar action leaves free.

a. The optical-time bridge. The relation $1+z = e^{\psi/2}$ holds for a static field. For a homogeneous field that changes in time, a null geodesic of the matter-coupling metric gives $1+z = e^{(\bar\psi_0 - \bar\psi_e)/2}$ instead. In the static arena with absolute time the homogeneous field is the expansion itself, $\bar\psi = 2\ln A$, where A is the scale factor of the Friedmann–Robertson–Walker metric $-c^2 d\tau^2 + A^2 d\mathbf{x}^2$ in proper time τ, with $1+z = A_0/A$; background observables depend on $\bar\psi$ only through A (Theorem ZS.3). Define the optical expansion variable $\psi_{\rm opt} \equiv -2\ln A$. Then, exactly,

$$\boxed{H \;=\; -\tfrac{1}{2}\,\dot\psi_{\rm opt}}, \qquad e^{\psi_{\rm opt}} = A^{-2}. \tag{484}$$

In that arena the homogeneous field is on the fast-light branch (App. Q 6), with $\bar\psi < 0$ in the past and optical speed $c\,e^{-\bar\psi} > c$: that fast-light past is the ordinary expansion read on the arena clock, where light moves at c/A^2, and it opens no horizon; the variable $\psi_{\rm opt}$, about 45 at nucleosynthesis, is not the field and does not set the optical speed.

b. The energy first integral. Under premise G1 of Proposition WS.5 the Einstein–Hilbert term acts on the uniform background of the scalar field, replacing the printed Newtonian term there. DFD has no lapse to vary: its time is absolute, and the dictionary fixes $g_{tt} = -c^2 e^{-\bar\psi}$. The Einstein–Hilbert Lagrangian on the homogeneous matter-coupling metric has no explicit time dependence, so its energy is conserved, and with a perfect fluid on the matter-coupling metric and the vacuum term $\Lambda c^2/3 = \Omega_\Lambda H_0^2$ ($R = \Omega_\Lambda C$ the measured coefficient of App. AU) that first integral is, exactly (computed), the **homogeneous optical-time equation**

$$\boxed{\mathcal{H}_{\rm opt} \;\equiv\; \tfrac{1}{4}\,\dot\psi_{\rm opt}^2 \;-\; \frac{8\pi G}{3}\,\rho \;+\; kc^2 e^{\psi_{\rm opt}} \;-\; \frac{\Lambda c^2}{3} \;=\; 0} \tag{485}$$

with k the integration constant of the first integral, paired with the continuity equation, which in optical-time variables reads

$$\boxed{\dot\rho \;=\; \tfrac{3}{2}\,\dot\psi_{\rm opt}\Big(\rho + \frac{p}{c^2}\Big)} \quad\Longleftrightarrow\quad \dot\rho + 3H\Big(\rho + \frac{p}{c^2}\Big) = 0. \tag{486}$$

Via (484) Eq. (485) is identically $H^2 = \frac{8\pi G}{3}\rho - kc^2/A^2 + \frac{\Lambda c^2}{3}$: the background rate is the conserved Einstein–Hilbert energy written in the optical expansion variable.

Theorem XIX.5 (Self-consistency of the optical-time sector)**.** *The first integral* (485) *and continuity* (486)*, with the bridge* (484)*, reproduce the* second *(acceleration) Friedmann equation with the correct relativistic source,*

$$\frac{\ddot{A}}{A} \;=\; -\tfrac{1}{2}\ddot{\psi}_{\rm opt}+\tfrac{1}{4}\dot{\psi}^2_{\rm opt} \;=\; -\frac{4\pi G}{3}\left(\rho+\frac{3p}{c^2}\right)+\frac{\Lambda c^2}{3}. \quad (487)$$

Proof. Differentiate (485) in t, substitute (486) for $\dot{\rho}$, eliminate $kc^2 e^{\psi_{\rm opt}}$ using (485), and insert $\ddot{A}/A = \dot{H} + H^2 = -\frac{1}{2}\ddot{\psi}_{\rm opt}+\frac{1}{4}\dot{\psi}^2_{\rm opt}$ from (484). The result is (487) identically (symbolically verified, residual 0). The active gravitational mass $\rho + 3p/c^2$ follows from the Einstein–Hilbert energy for any fluid: the sector is the full Friedmann system, not its matter special case. □

Accelerated expansion of A beyond the vacuum term therefore needs $\rho + 3p/c^2 < 0$. The optical engine of App. Q 6, which in this arena is accelerated expansion of A, needs such a source while it runs and a stage that reheats the universe after it (Rem. Q.11).

c. Consequence for the MOND acceleration scale. Because the background rate is the rate of the optical expansion variable, the optical transition scale is set by that rate,

$$\boxed{\;a_0(z) \;=\; 2\sqrt{\alpha}\,c\,H(z) \;=\; \sqrt{\alpha}\,c\,|\dot{\psi}_{\rm opt}|\;}. \quad (488)$$

The redshift dependence of a_0 is therefore not an imported clock but the evolution of $\psi_{\rm opt}(t)$ governed by (485): the MOND knee tracks the rate of the cosmic expansion, and the sign $\partial_z a_0 > 0$ follows from $|\dot{\psi}_{\rm opt}| = 2H$ rising with z.

d. Scope (two-channel). The DFD-native content is the bridge (484) and the identity (488): the expansion rate and the MOND scale are expressed through the optical expansion variable with no additional clock. Equation (485) is the conserved energy of the Einstein–Hilbert term on the uniform background, so its coefficient $8\pi G/3$ is the same G as in the tensor and vector sectors on one clock (Postulate ZS.11 departs from this premise); the law is derived given premise G1 (Proposition WS.5; the spectral action and its Einstein–Hilbert term are the construction of Chamseddine and Connes [113, 114], and induced gravity is Sakharov's idea [115]), reproduces the Friedmann background and makes no new expansion prediction. The AQUAL equation has no homogeneous mode (Theorem AE.1) and is sourced by the contrast $\rho - \bar{\rho}$: the Einstein–Hilbert scalar term is the rest channel's term, counted once. Primordial helium tests the shared coefficient: $Y_p = 0.2453 \pm 0.0034$ alone gives $G_{\rm BBN}/G = 0.98 \pm 0.04$ (computed; the nucleosynthesis theorem of Ext. Deriv., App. AH uses the same rate). The curvature constant k is the integration constant of the first integral, not the flat arena's zero curvature, and it is zero under the stated clause of Axiom WS.1: while no baryons are bound anywhere, and at least until they decouple from the photons, gravity is the Einstein–Hilbert term alone, and there only $k = 0$ keeps the scalar sector elliptic and its evolution well posed (App. WS, Remark WS.7).

F. The Parameter Structure

If Eq. (470) holds, DFD has the following structure:

TABLE XLIX. DFD input/output structure.

Category	Quantity	Source
Topological	$k_{\max} = 60$	$\chi(\mathbb{C}P^2, E)$
	$N_{\rm gen} = 3$	Input (App. F)
	$\alpha^{-1} = 137$	CS quant.
Observational	H_0 or G; the coefficient C	Measured
Derived	G or H_0	Eq. (470)
	$v = 246$ GeV	$M_P\alpha^8\sqrt{2\pi}$ (prefactor fitted)
	$\rho_c/\rho_{\rm Pl}$	Eq. (474)
	All masses	α-hierarchy; seven prefactors data-selected
	All mixings	$\mathbb{C}P^2$ geom. and stated postulates

The resulting one-anchor tower of scales is displayed as the α-exponent ladder of Fig. 12.

a. Parameter counting. The scale sector introduces **one measured continuous coefficient** (the vacuum coefficient R, of which the clock normalization C is today's early-clock value; Rem. AP.6) and no continuous parameter fitted to a predicted shape. Three further continuous calibrations live outside this sector and are stated with it for completeness: the primordial amplitude A_s, the coefficient of $\omega_b h^2$, and the reionization optical depth τ shared with ΛCDM, four in all, against ΛCDM's six free parameters (App. FK, Rem. FK.8). The discrete topological sector is uniquely determined by Standard Model structure:

- The isotropy charge $6Y$ fixes $q_1 = 3$; hypercharge integrality alone admits $q_1 \in \{3, 6\}$, and $q_1 = 6$ would give the weak doublets an even charge (Lemma F.9, Rem. F.10)
- Minimal integer-charge lift gives $\mathcal{O}(9) = L_Y^{\otimes 3}$
- Five hypercharged chiral multiplet types fix $n = 5$
- Within $E = \mathcal{O}(a)\oplus\mathcal{O}^{\oplus n}$, minimal-padding uniquely selects $(a, n) = (9, 5)$ with $k_{\max} = 60$

One scale measurement (H_0 or equivalently G) plus the measured coefficient C determines all dimensionful quantities via the invariant $G\hbar H_0^2/c^5 = C\,\alpha^{57}$.

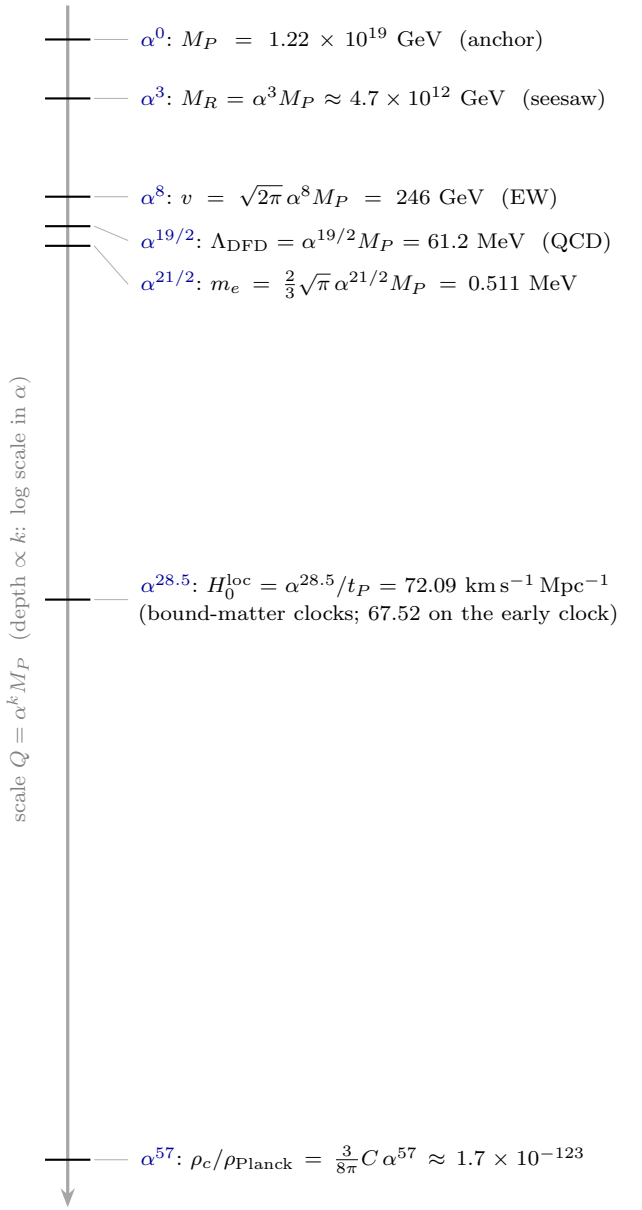


FIG. 12. The α-exponent ladder: one dimensionful anchor (M_P, equivalently one measurement of H_0 or G) and the derived tower of scales $Q \sim \alpha^k M_P$. Rung depth is proportional to the exponent k, i.e. a log scale in α. Rungs: the seesaw scale $M_R = \alpha^3 M_P$, the electroweak scale $v = \sqrt{2\pi}\,\alpha^8 M_P$ (Table XLIX), the QCD chain scale $\Lambda_{\rm DFD} = \alpha^{19/2} M_P$, the locked electron map $m_e = \frac{2}{3}\sqrt{\pi}\,\alpha^{21/2} M_P$, the Hubble rate on bound-matter clocks $H_0^{\rm loc} = \alpha^{28.5}/t_P$ (Eq. (479); the early clock carries the measured $O(1)$ coefficient, $H_0^{\rm early} = \sqrt{C}\,\alpha^{28.5}/t_P = 67.52$, Rem. AP.6), and the vacuum-density ratio $\rho_c/\rho_{\rm Planck} = \frac{3}{8\pi} C\,\alpha^{57}$ (Eq. (474)), spanning the full 122 orders of magnitude of the invariant Eq. (470).

One Measured Coefficient — Spectral-Action-Derived Exponent (Appendix O)

The scale sector introduces one measured continuous coefficient and no continuous parameter fitted to a predicted shape (the theory's three further calibrations, the amplitude A_s, the ω_b coefficient and the shared τ, are not scale inputs; App. FK). Once the discrete topological sector is fixed by Standard Model structure ($k_{\max} = 60$, $N_{\rm gen} = 3$), the exponent in the dimensionless invariant

$$\frac{G\hbar H_0^2}{c^5} = C\,\alpha^{57} \tag{489}$$

is forced by primed-determinant scaling (Corollary O.3). Gaussian mode integration over the finite-dimensional microsector derives the identification with the physical hierarchy (Theorem O.7); the $O(1)$ coefficient $C = 0.87784 \pm 0.00266$ is measured, and the eight-route no-go proves it underivable from the printed corpus (Rem. AP.6). One scale measurement (H_0 or G) plus C then fixes all dimensionful quantities.

XX. CONCLUSIONS

A. Summary of Density Field Dynamics

Density Field Dynamics is a scalar refractive-index theory of gravity defined by a single field ψ that determines:

- **Optical propagation:** Light travels through an effective medium with index $n = e^{\psi}$, phase velocity $c_{\rm eff} = c/n$, and nondispersive propagation in optical bands.
- **Test-mass dynamics:** Free-fall acceleration $\mathbf{a} = (c^2/2)\nabla\psi$ derives from the effective potential $\Phi = -c^2\psi/2$.
- **Clock rates:** Proper time rates depend on position through ψ, with any channel-resolved species-dependent coupling belonging to the extended non-metric channel (null under the minimal action, Thm. XI.2), organized by electromagnetic, strong-sector, and composition-sensitive contributions.
- **Gravitational radiation:** Transverse-traceless perturbations propagate at speed c on the optical cone, which light shares (App. WS), with the standard quadrupole formula.

The theory is governed by a nonlinear field equation:

$$\nabla \cdot \left[\mu\left(\frac{|\nabla\psi|}{a_\star}\right) \nabla\psi \right] = -\frac{8\pi G}{c^2}(\rho - \bar{\rho}), \tag{490}$$

with the μ-function interpolating between Newtonian ($\mu \to 1$) and deep-field ($\mu \to x$) regimes at the acceleration scale $a_0 = 1.1966 \times 10^{-10}$ m/s^2 read on bound-matter clocks (Postulate ZS.11; 1.1208×10^{-10} on the early clock). Under the adopted Rest-Mass Channel postulate (App. GR.3a), this screened equation governs the

gradient channel, confined to bound systems, while conserved rest mass sources an unscreened Poisson channel, the Einstein–Hilbert term's own static scalar energy. Two further adopted inputs act inside bound systems: the floor composition of App. AV, in the form of one momentum-conserving energy under which matter moves, and environmental confinement, which keeps a subsystem Newtonian inside a strong host field (App. NL). These and the other inputs of the graded predictions are listed in Tables CXXVII and CXXVIII.

B. What DFD Accomplishes

a. Solar System and precision tests. DFD reproduces all Solar System tests with PPN parameters $\gamma = \beta = 1$ (§IV). Light deflection, Shapiro delay, perihelion advance, and Nordtvedt effect match observations to current precision. Through second post-Newtonian order the one- and two-body dynamics is general relativity's, with $\epsilon = 1$ and the second-order light-deflection coefficient $15\pi/4$ (§IV; App. WS).

b. Gravitational waves. The TT sector propagates at c on the optical cone that light follows, $c_T = c_\gamma$ on every background (App. WS)—a structural result proven from $O(3)$ irreducible decomposition, not fine-tuning (§V C). Within the $\mathbb{C}P^2 \times S^3$ spectral completion, both ψ and $h_{ij}^{\rm TT}$ are derived as irreducible components of the same zero-mode parent tensor on the internal manifold (§V A 4). A Lichnerowicz rigidity analysis proves no unwanted massless modes arise; the truncated microsector carries no size or shape modulus (Appendix O). The theory carries two tensor polarizations and satisfies the standard quadrupole formula (§V). Binary pulsar orbital decay agrees at 0.2%. LIGO/Virgo observations are consistent.

c. Strong fields. With the parent strain's σ kept DFD's strong-field gravity is general relativity's (App. WS): black holes have Schwarzschild's and Kerr's horizons and shadows, consistent with current EHT observations (§VI); static stars obey the TOV equations (App. AT, Theorem AT.13); ringdowns are Kerr's. Beyond first order in the spin the Kerr results rest on an argument (App. WS).

d. Galactic dynamics. The μ-crossover produces flat rotation curves, the baryonic Tully-Fisher relation $M_{\rm bar} \propto v_f^4$, and the radial acceleration relation (§VII). **The dimensionless law $a_0/(cH_0) = 2\sqrt{\alpha}$ is derived from the S^3 microsector, and $\mu(x) = x/(1+x)$ is the weak-response form of the derived exponential response** (Appendix N); its physical value on bound-matter clocks is $a_0 = 1.1966 \times 10^{-10}$ m/s^2, with no measured coefficient (Postulate ZS.11). **Quantitative validation:** In head-to-head comparison using SPARC galaxy parameters, DFD beats Newton in 100% of galaxies tested; a dedicated model-independent interpolation-family scan on all 175 SPARC galaxies further finds $n_{\rm opt} = 1.15 \pm 0.12$ (95% CI $[1.00, 1.50]$), placing DFD's $n = 1$ inside the preferred region and strongly disfavoring Standard MOND's $n = 2$. Near the Sun DFD predicts no wide-binary boost: the Galaxy's baryonic field there exceeds $(\ln 2)^2 a_0$, so under the adopted environmental confinement local pairs are exactly Newtonian, $\gamma = 1$, which the Sun's long-period comets also require (App. NL, Status NL.12); pairs beyond $R \simeq 13$–16 kpc keep the boost. The *Gaia* DR3 amplitude analyses are contested [51, 52]; DFD sides with the analyses that find no signal, and a confirmed boost in local pairs falsifies the axiom (§VII). Ultra-faint dwarfs' extreme inferred mass-to-light ratios may be inflated by measurement systematics (binary contamination, tidal heating); χ subhalos are the alternative.

e. Cluster scales. Under the μ-law alone the clusters fall short of their measured masses (Obs/DFD $= 1.57 \pm 0.08$ relaxed, 1.99 ± 0.16 merging, at $a_0 = 1.20 \times 10^{-10}$ m/s^2 and at the bound-matter $a_0 = 1.1966 \times 10^{-10}$ m/s^2), and the shortfall is the derived cold component χ (§XVI G): with χ adding its Newtonian pull and a hydrostatic bias $b = 0.21$ on the relaxed X-ray masses, all sixteen clusters need $\chi = 4.5 \pm 0.6\, M_{\rm b}$, 0.84 ± 0.12 of the cosmic mix; under the floor composition of App. AV they carry the ΛCDM budget. The amplitude follows from the derived abundance under the adopted energy: 1.21 ± 0.05 of the cosmic mix is predicted inside r_{500}, against 1.28 ± 0.04 measured with no hydrostatic bias (estimate; App. I). A no-χ closure by five literature correction factors does not hold (the baryonic items sum to 1.26, and the projection correction has the wrong sign for lensing masses). The Bullet Cluster needs χ at 0.6–0.9 of the cosmic mix when χ adds its Newtonian pull (1.1–1.2 under the floor composition). Galaxy groups fall short in the same way on published X-ray masses and need χ too. See Appendix I for the complete per-cluster analysis.

f. CMB and cosmology. **A ψ-based CMB framework is presented** (§XVI C):

- Peak ratio from the baryon loading with the derived χ-matter (2.20 on the measured clock; analytic estimate 2.34)
- Peak location $\ell_1 \simeq 220.4$ from the measured-clock no-screen forward solution ($100\theta_* = 1.04110$); no global $\Delta\psi = 0.30$ attribution is used
- **Cold clustering carrier:** the cosmological cold dark matter (CMB third-peak height, large-scale structure, and clusters, which need it at the amplitude the derived abundance gives under ΛCDM-like assembly (1.21 ± 0.05 of the cosmic mix inside r_{500} predicted; estimate); App. GR) is the derived χ-matter particle ($\Omega_\chi h^2 \simeq 0.12$; App. AV), whose composition with the μ-law inside galaxies is the floor law, and whose halos assemble as in ΛCDM under the adopted momentum-conserving energy (estimate). (The projectable "dust branch" $w \to 0$, $c_s^2 \to 0$ cannot carry an a^{-3} clustering charge to recombination; χ does; see App. J.) The linear perturbation operator and $G_{\rm eff}$ growth law are written explicitly (Sec. XVI L); full survey-pipeline $P(k)$ matching remains a numerical program item.

These mechanisms address what standard cosmology at-

tributes to "dark matter" ($\Omega_c = 0.26$) and "dark energy" ($\Omega_\Lambda = 0.69$). The analytic framework is extensive, but the full precision confrontation with cosmological perturbation pipelines remains an active program item rather than a finished replacement for every standard analysis tool.

g. Parameter-free predictions. The α-relations (§VIII) provide parameter-free predictions:

$$a_0 = 2\sqrt{\alpha}\, cH_0^{\rm loc} \quad \text{(within SPARC's systematic error)} \tag{491}$$

$$k_\alpha = \alpha^2/(2\pi) \quad \text{(pure-}\alpha\text{ bounded)} \tag{492}$$

$$k_a = 3/(8\alpha) \quad \text{(consistent with RAR)} \tag{493}$$

h. Standard Model parameters from topology. Appendix Z demonstrates that Standard Model parameters emerge from the topology of $\mathbb{C}P^2 \times S^3$:

Derived structural results (grades as stated per item):

- $\alpha^{-1} = 137.036$ from Chern-Simons quantization, convention-locked (Appendix K 1; the finite-level bracket coefficient's provenance is open, Rem. X.4; the identification of the hypercharge-trace coefficient with $1/e^2$ is not derived, §X I)
- $\sin^2\theta_W = 3/13$ from gauge partition + the stated trace normalization (**0.23% agreement**)
- $\alpha_s(M_Z) = 0.1187$ from $\Lambda_{\rm QCD} = M_P\alpha^{19/2} + \sqrt{4\pi}$ matching (selected scale; 0.8σ)
- $\bar\theta = 0$ (tree level; loop-induced $\lesssim 10^{-16}$) from the det-orthogonal tree-level protection together with the η-invariant argument, with $\theta_{\rm YM} = 0$ fixed by the spectral action given that nothing is added to it for the gauge fields (Appendix L)
- $v = M_P\alpha^8\sqrt{2\pi}$: exponent from microsector scaling, prefactor $\sqrt{2\pi}$ fitted (a no-go on deriving it; App. Z)
- $N_{\rm gen} = 3$ (one stated input, used once; no index on the internal space supplies it, Rem. F.21)
- $\varepsilon_H = 3/60 = 0.05$ from channel counting (Appendix H)
- Generation = left Z_3 phase sectors (Proposition Y.12)

Comparisons:

- $b/\tau = 1.98$ (obs 2.35, 16% off) — from bin scan $(0,2)/(1,2)$
- $b/t = 0.018$ (obs 0.024, 24% off) — same mechanism
- $c/t = 0.0073$ (obs 0.0073, 0.8% off) — from bin $(2,0)/(1,0)$
- CKM: $(31, 108, \frac{43}{2}, 49)\times\alpha$ pattern, apex fixed by the Euler-projection postulate (App. AO); $\gamma = 66.3°$, $J = 2.97\times10^{-5}$

Remaining (numerical refinements):

- Nine fermion masses at 1.42% leading-order mean error via explicit A_f (Theorem K.4): the top and charm derived, the other seven on seven data-selected prefactors (App. FM)
- Neutrino mass splittings with $\chi^2 = 0.025$ vs NuFIT 6.0 on the data-selected branch (Appendix X)

The charged-fermion sector carries no *continuous* knob beyond α and v, whose prefactor is fitted: the top mass $m_t = (1-\alpha)v/\sqrt{2} = 172.74$ GeV is forced, and the charm with it, along with forced inter-generation ratios such as $m_t/m_b = 42$ (the comparison divides the top pole mass by $m_b(m_b)$; at one scale, M_t, the ratio is 59.7, so the comparison awaits a one-scale test). The double ratio D, which reads 27.7 in PDG's mixed convention, is 29–33 at one renormalization scale, and the same weights miss a second ratio by 15% at any scale (App. Y), so it is not among the forced ratios. The *absolute* charged-fermion spectrum other than the top and the charm is not derived: the other seven species rest on seven data-selected prefactors (App. FM).

C. The Critical Tests

Each experimental channel has a distinct role:

a. 1. Cavity-atom LPI test (§XII). The cavity–atom channel remains important, but geometric cancellation removes any order-unity tree-level slope. It is best viewed as a precision residual test whose cleanest role is to probe the surviving non-metric cavity/atom mismatch once the constitutive-chain cancellation is accounted for.

b. 2. Clock anomalies (§XI). The clock program is interpreted in a channel-resolved way. Same-ion optical clocks test the pure α sector; cross-species atomic ratios test composition-sensitive structure; and nuclear clocks test the strong sector. Improved multi-species measurements remain among the sharpest falsifiers in the whole DFD framework.

c. 3. Matter-wave T^3 signature (§XIII): not a DFD prediction. The formula below is not a DFD phase:

$$\Delta\phi_{\rm DFD} = \frac{\hbar k_{\rm eff}^2}{m}\frac{g}{c^2}T^3. \tag{494}$$

Status: not a DFD prediction (the matter-wave sector is null); see the status note after Eq. (337) in Sec. XIII. Its T^3 scaling, rotation sign flip and even k-parity do not separate DFD from GR, which coincide through 1PN.

d. 4. Antimatter gravity (§XV). Matter–antimatter differential acceleration probes C-odd sector couplings:

$$\frac{\Delta a_{H\bar H}}{a} \approx 2|\sigma_{\bar H} - \sigma_H|. \tag{495}$$

At the metric level, DFD predicts $\Delta a_{H\bar H}/a = 0$ (matching GR). Non-metric couplings to baryon/lepton number are already bounded by ordinary-matter equivalence-principle tests, to $|\Delta a_{H\bar H}/a| \lesssim 10^{-11}$ (Sec. XV G).

e. 5. EM–ψ coupling (Appendix R). In a parametric-mode model that needs a dynamical ψ mode, which the local ψ of Axiom WS.1 lacks, and whose absolute normalization is open, the parameter λ controls electromagnetic back-reaction on ψ:

$$|\lambda - 1| \lesssim 3\times10^{-5} \quad \text{(accidental bound from cavity stability).} \tag{496}$$

An intentional 2ω modulation search could reach $|\lambda-1| \sim 3\times10^{-9}$—about four orders of magnitude tighter—with upgraded apparatus.

D. If DFD Is Confirmed

If laboratory tests confirm DFD predictions, the implications would be as follows:

1. **Gravity is fundamentally optical/refractive, not geometric.** The metric tensor would be emergent from the parent strain on the flat arena, its trace ψ and its traceless part, rather than fundamental.

2. **The dark-sector carriers are identified, with their grades stated.** Flat rotation curves and the radial-acceleration relation arise from the universal μ-crossover acting on the baryons, with no fitted halo; the derived χ is present in galaxies too, composed with the μ-law by the floor law, in ΛCDM-like halos whose inner parts must be cored for the rotation curves (estimate; App. AV). The cosmological cold carrier is the topologically derived χ field (App. AV); its 32.005 eV coefficient uses the $\sqrt{158}$ multiplicity, one stated count, its abundance is forced-amplitude/stated-convention, conditional on the flux-period identification and the asserted premise P4′, $Q_\chi = 1$ clustering is conditional on the adopted Rest-Mass Channel, and it has no photon coupling ($E = 0$, derived; App. AV). Dark energy is the α^{57} geometric vacuum energy with the measured vacuum coefficient R (App. O).

3. **Part of the Standard Model structure follows from topology.** The electroweak group is the isotropy group of $\mathbb{C}P^2$ under one stated identification, and colour, the family content and the three generations enter as inputs (App. F); the fermion-mass hierarchy is derived (texture fitted) and the CKM matrix follows from the selected counts and the postulated apex.

4. **The bare-parameter form of the hierarchy problem is removed.** The 17 orders of magnitude between M_P and v follow from α^8; the $\sqrt{2\pi}$ prefactor is fitted and radiative stability stays open (App. H).

5. **Strong CP at tree level (Theorem L.3).** With $\theta_{\rm YM} = 0$ fixed by the spectral action given that nothing is added to it for the gauge fields, $\bar{\theta} = 0$ at tree level, loop-bounded below 10^{-16}. Tree level: $\arg\det(M_u M_d) = 0$ (App. AO). Anomaly: the fermion Clifford module on the even-dimensional (8) mapping torus has spectral pairing and no zero modes, forcing $\eta = h = 0$. No axion required.

E. If DFD Is Falsified

DFD is falsifiable. The theory would be ruled out if:

a. Core falsification.

- Matter-wave: not a falsification channel (null prediction, §XIII; DFD and GR coincide through 1PN)
- Antimatter $\Delta a_{H\bar{H}}/a \neq 0$ at $> 3\sigma$ (universal coupling violated)

b. Indirect falsification.

- RAR deviates from μ-crossover prediction at $> 3\sigma$ (the galactic sector is wrong)
- GW speed differs from c at $> 10^{-15}$ (the TT sector is wrong)
- α-relations fail by $> 20\%$ on the clock each reads (the theoretical framework is wrong)

c. What remains. If DFD is falsified, General Relativity remains the established theory. The galactic dark matter problem would still require explanation (CDM, other modified gravity). The clock anomalies, if confirmed, would need alternative interpretation.

F. Comparison with Alternatives

TABLE L. Comparison of DFD with alternative approaches.

	GR+CDM	MOND	TeVeS	f(R)	AeST	DFD
Solar System	✓	✓	✓	✓	✓	✓
GW speed = c	✓	—	×	✓	✓	✓
Binary pulsars	✓	✓	✓	✓	✓	✓
Rotation curves	✓ (DM)	✓	✓	×	✓	✓
Tully-Fisher	? (DM)	✓	✓	×	✓	✓
RAR tightness	?	✓	✓	×	✓	✓
Clusters	✓	×	×	✓	∼	✓
CMB peaks	✓	×	∼	✓	✓	✓
Lab predictions	—	—	—	—	—	✓

Notes: The cluster entry for DFD is "✓" because the derived χ supplies the mass the μ-law leaves (0.84 ± 0.12 of the cosmic mix when it adds its Newtonian pull; App. I), at the amplitude the derived abundance gives under ΛCDM-like assembly (1.21 ± 0.05 of the cosmic mix inside r_{500} predicted; estimate). The rotation-curve, Tully–Fisher and RAR entries for DFD are the μ-law on the baryons; they hold with χ present when its ΛCDM-like halos are cored (App. AV). The CMB entry for DFD is "✓" because the peak ratio follows from the baryon loading with the derived χ-matter and the peak location is reproduced by the current measured-clock forward solution without a global ψ screen.

DFD's distinctive features are: (1) **a broad ψ-CMB framework** (the peak ratio has an analytic estimate; the peak location is the measured-clock no-screen forward result), (2) **cluster-scale phenomenology addressed**

in the same framework, (3) **falsifiable laboratory predictions** spanning channel-resolved clocks (extended non-metric channel), antimatter, and cavity–atom residuals, (4) **parameter-light predictions** via the α-relations and topological microsector, and (5) **a unification layer** collecting the fermion-mass, CKM, PMNS, and Higgs-scale derivations in one place.

G. Outlook

a. Near-term priorities.

1. Nuclear-clock (Th-229/Sr) campaigns and Ooi-style annual-phase reanalyses
2. Cross-species clock comparison campaigns (Hg/Sr, Yb^+/Sr, Yb/Sr, Cs/Sr)
3. Same-ion null checks to keep the pure-α sector pinned down
4. Matter-wave interferometry upgrade for the T^3 search (null prediction) and, longer-term, cavity–atom residual roadmaps

b. Medium-term goals.

1. Nuclear clock (Th-229) tests of strong-sector coupling
2. Space-based precision tests (ACES successor)
3. Independent verification of microsector derivations
4. Further cluster-by-cluster verification

c. Long-term vision. DFD's theoretical framework names its main open items rather than hiding them (§XVIII A), among them the origin of the primordial perturbations and the horizon problem, which enter through one stated starting condition (the amplitude A_s is a calibrated number), the interacting quantum dynamics it shares with every quantum field theory, and in the dark sector the inner cores and masses of the χ halos, the mode-by-mode rule of motion of the momentum-conserving energy, the adopted floor law and environmental confinement, and the weak lensing of isolated galaxies beyond their bound radius, where the halo model of ΛCDM also falls below the measured points (App. GR); the $Q_\chi = 1$ χ-clustering channel is closed by the adopted Rest-Mass Channel axiom, App. GR.3a, which confines the μ-law to bound systems, the residual being to derive that axiom from a deeper principle. We do not claim the corpus to be free of internal inconsistency: it is large, parts of it are inherited from earlier releases, and its internal review is a continuing obligation rather than a completed one. What we do claim, and what the reader can check, is that the review is conducted in the open: corrections are made at the statements they amend (the principal ones are tabulated before the table of contents), and the inherited statements flagged by a proof-pattern scan are graded by name in §XVIII K. The remaining task is experimental verification, closing the named open items, and continued internal hardening of the live phenomenology modules. If confirmed, the theory would represent a shift in our understanding: gravity as optics, the electroweak group from the inner space under one stated identification, and a cosmology whose dark matter is derived rather than fitted (the χ field) and whose dark energy has a derived exponent and one measured coefficient (the α^{57} vacuum).

H. Structural Separation: Gravity vs. Microsector

We separate the testable gravity program from the unification claims:

DFD Gravity: Robust and Testable

What stands independently:

- Two core postulates: $n = e^{\psi}$, $\Phi = -c^2\psi/2$; the adopted axioms, among them the Rest-Mass Channel behind the cosmological Q_χ=1 clustering channel (App. GR.3a), and the identifications, selections and calibrations are listed in Tables CXXVII and CXXVIII
- PPN parameters: $\gamma = \beta = 1$
- GW sector: $c_T = c_\gamma$ exactly (one metric for light and gravitational waves; App. WS), two polarizations
- Galactic dynamics: μ-crossover, RAR, BTFR, and the SPARC shape-selection result near $n = 1$
- Cluster phenomenology: the μ-law plus the derived χ, at the amplitude its abundance gives under ΛCDM-like assembly (estimate)
- Laboratory predictions: channel-resolved clocks (extended non-metric channel), antimatter, and cavity–atom residual tests

Falsifiers: collapse of the channel-resolved structure of the extended clock channel and RAR/shape deviations at high significance

If the microsector is wrong, DFD gravity stands.

Gauge Emergence: Conditional

What depends on $\mathbb{C}P^2 \times S^3$ framework:
- $\alpha^{-1} = 137.036$ from the convention-locked microsector closed form (§X; bracket coefficient open)
- Electroweak group as the isotropy group of $\mathbb{C}P^2$, under one stated identification; colour and the family content as inputs
- $N_{\text{gen}} = 3$ (one stated input, Rem. F.21)
- Top and charm masses, CKM magnitudes and PMNS angles from geometry, with the stated inputs of Table CXXVIII
- $G\hbar H_0^2/c^5 = C\alpha^{57}$ invariant (exponent derived; the vacuum coefficient R measured)
- Higgs scale: $v = M_P\alpha^8\sqrt{2\pi}$ (exponent derived, prefactor fitted)

Falsifiers: Wrong fermion mass ratios, proton decay observation, $\mathcal{H}_F = \mathbb{C}^d$ derived from first principles (would shift α by 43 ppm)

If this fails, DFD gravity can be retained with α as input.

a. The firewall. The gravity program is constructed to survive even if the gauge emergence program fails entirely. The α-relations can be taken as empirical input rather than topological output. The laboratory tests (§XI–§XIII) depend only on the two postulates, not on the microsector.

I. Final Statement

a. Interpretive convention for claim strength. Throughout this review, "derived" means one of two things: either (i) derived from the core DFD field/action system, or (ii) derived from an explicitly stated auxiliary closure framework whose assumptions are displayed in the text. Empirical benchmark modules and numerical consistency checks are labeled as such and should not be confused with core-field theorems. This convention is deliberate: it preserves the monograph's one-paper unity while preventing auxiliary closure principles, benchmark hierarchies, and open numerical pipelines from being mistaken for hidden first-principles proofs.

DFD: Unified Framework + Falsifiable Predictions

Derived results (items marked ⋆ are theorem-grade with formal proofs; others depend on dictionary axioms or structural assumptions):
- $\mu(x) = x/(1+x)$, the weak-response form of the derived exponential response (Theorem N.8; App. BS)
- $a_0/(cH_0) = 2\sqrt{\alpha}$ **derived** from topological stationarity (Theorem N.14); its physical value on bound-matter clocks is $2\alpha^{29}\sqrt{c^7/G\hbar} = 1.1966 \times 10^{-10}$ m/s^2 (Postulate ZS.11; consistent with SPARC within its systematic error), and 1.1208×10^{-10} m/s^2 on the early clock
- ⋆ Dust branch: $K'(\Delta) = \mu(\Delta)$ gives $w \to 0$, $c_s^2 \to 0$ (Theorem Q.7); the cold clustering carrier is the derived χ-matter (App. AV), not this projectable branch
- Strong CP: $\bar{\theta} = 0$ at tree level, loop-bounded, with $\theta_{\text{YM}} = 0$ fixed by the spectral action given that nothing is added to it for the gauge fields (Theorem L.3)
- G–H$_0$ invariant: $(H_0 t_P)^2 = C\alpha^{57}$; exponent 57 spectral-action-derived and C measured on the early clock (Appendix O); on bound-matter clocks $C = 1$ (Postulate ZS.11) and $H_0^{\text{loc}} = \alpha^{28.5}/t_P = 72.09$ km/s/Mpc from the measured G (Eq. (479))
- Clock coupling: $k_\alpha = \alpha^2/(2\pi)$ (Appendix P)

Quantitative matches:
- $\alpha^{-1} = 137.036$ (21 ppm from the integers; the bracket coefficient is open)
- Higgs: $v = M_P\alpha^8\sqrt{2\pi}$ (exponent derived, prefactor fitted)
- Fermion masses: 1.42% leading-order mean error (9 particles; seven prefactors data-selected)
- CKM: $\lambda = 31\alpha = 0.2262$ (integer pattern; $\mathbb{C}P^2$ overlap motivation)
- PMNS: trimaximal TM1 (App. X); $\sin^2\theta_{13} = 3\alpha$ a stated conjecture
- CMB: the analytic $R = 2.34$ (6% above Planck's 2.21; the χ-matter spectrum, run on the measured clock, gives 2.20, within 0.6σ), $\ell_1 = 220$ (no postulated CDM; third-peak height from the derived χ-matter field, App. AV)
- ESPRESSO: conditional on $\xi_{\text{LPI}}^{\text{res}}$

Key problems addressed: UV completion (topology, proposed), Λ problem (α^{57}), hierarchy (α^8), strong CP (tree level, loop-bounded), neutrino hierarchy ($< 0.2\sigma$, App. X).

No continuous parameter is fitted to a predicted shape, except the baryon density. The theory's cosmology carries four continuous calibration constants, the vacuum coefficient R (absolute scale), the amplitude A_s of the primordial perturbations, the coefficient of $\omega_b h^2$ (the one shape) and ΛCDM's shared astrophysical τ, against ΛCDM's six free parameters, and three against its five effective parameters on the Planck likelihood itself (App. FK, Rem. FK.8); the particle sector adds the fitted Higgs prefactor, the imported factor η_q and the Higgs quartic, conjectured to be 1/8 at a matching scale that is not derived. The discrete topological sector carries no continuous freedom: the isotropy charge fixes $q_1 = 3$, the determinant-line lift gives $\mathcal{O}(9)$ (with $N_{\rm gen} = 3$ a discrete input), and the five chiral multiplet types fix the padding (status remarks: App. F). Within $E = \mathcal{O}(a) \oplus \mathcal{O}^{\oplus n}$, minimal-padding uniquely selects $(a, n) = (9, 5)$ with $k_{\max} = 60$; the discrete inputs are priced in the trials audit of App. CE. One scale measurement (H_0 or G), together with the measured R, then determines all dimensionful quantities.

New structural results:

⋆ **The Padé identity** (Theorem AA.1, Appendix AA): $\mathcal{L}_{\rm GR}(u) = [P_{1,1}(u)]^2$ in isotropic coordinates, where $\mathcal{L} \equiv c^2/|g_{tt}|$ is the lapse-squared scalar and $P_{m,m}(u)$ denotes the $[m, m]$ Padé approximant of e^u, so that GR's isotropic lapse-squared is the $m = 1$ slot of a Padé hierarchy whose $m \to \infty$ limit is the exponential $\exp(2u)$, DFD's lapse-squared at $\psi = 2u$. The identity reproduces $\beta = 1$ in both theories; $\gamma = 1$ for DFD follows separately from the physical metric. With the parent strain's σ kept DFD's exterior is Schwarzschild's (App. WS), so the pole is the event horizon of DFD's black holes too (Theorems AA.2, AA.3 establish the firewall from Yilmaz-type exponential metrics).

⋆ **Uniqueness of** $\mathbb{C}P^2 \times S^3$ (Theorem AB.1, Appendix AB): The internal manifold is not an ansatz but the unique compact manifold (up to diffeomorphism) satisfying seven satisfiable vacuum axioms motivated by DFD's optical structure, three generations, and the framed transgression sector; dimension 7, Spin^c and $\pi_3 = \mathbb{Z}$ are outputs of the theorem, not inputs; $k_{\max} = 60$ follows through the conditional determinant-line count of App. F, given the generation count, the flux quantum and the five multiplet types; and the SM gauge group is carried by the internal mode bundle rather than by TX. The integers $\{3, 7, 8, 13, 19, 31, 49, 57, 60, 108, 137\}$ are not free parameters: they are fixed by this manifold together with the stated inputs and identifications of App. FK.

Companion notes:

- **Epoch extension of** a_0 [112]: theorem-grade *conditional on Axiom WS.1* (Theorem XIX.3): the no-memory argument forces the tracking branch $a_0(z) = 2\sqrt{\alpha}\, cH(z)$ — the anchored alternative is structurally unavailable — while the G–H_0 invariant stays a present-epoch boundary condition with $\dot{G} = 0$ (Corollary XIX.4); the two are independent falsifiers. First data: over $0.33 < z < 1.44$ MUSE-DARK III [109] shows a rising scale, the sign that separates DFD from static MOND; a theory-neutral analysis of its bins, published in MNRAS **551**(4), 2026 September 7 [110], gives $a_0(z) = A(1+z)^\gamma$ with $\gamma = 0.78 \pm 0.15$ (0.83 ± 0.13 with the SPARC $z \simeq 0$ anchor), excluding a *frozen* a_0 at $\mathbf{5.3}\sigma$ (6.6σ anchored) and $a_0 \propto \sqrt{\rho_m}$ at 4.8σ (on the exponent's error; 4.7σ by likelihood ratio) on the published bin errors, with $H(z)$-tracking the information-criterion-preferred one-parameter description. *These exclusions are amplitude-marginalised nested tests and carry no H_0, h, Ω_m or distance scale; the clock coefficient cannot move them.* On DFD's measured-clock background ($\Omega_m \simeq 0.312$) the refit gives $A = (1.394 \pm 0.032) \times 10^{-10}$ m/s^2, $\chi^2 = 5.36/3$ and $\gamma_E = 1.098$, 2.1σ above the measured exponent. Two caveats apply: under the 95% reading of the source's unlabelled bars the two exclusions strengthen (to $\gtrsim 10\sigma$ and 9.5σ on the exponent's error, 9.2σ by likelihood ratio) but the tracking *consistency* moves into tension ($\chi^2 = 19.9/3$, $p = 1.8 \times 10^{-4}$), and the fitted amplitude sits 17% above the canonical SPARC normalisation, within its systematic-dominated but not its statistical uncertainty. Refitted galaxy by galaxy from the survey's public products, the rise reproduces, but the galaxy-level uncertainty is several times the published bin errors, so within the survey a frozen a_0 lies about 1σ away, while anchored to SPARC's $z = 0$ value, the galaxy-level bins still exclude a frozen a_0 at about 3σ, and DFD's zero-parameter law fits them on the bound-matter clock; the trend depends on how the molecular gas is added, keeping the rise when tied to the survey's disc masses and flat when tied to SED-based masses, and falling with stellar masses from spectral energy distributions (App. A0Z). Massive discs at $0.6 < z < 2.5$, whose census counts molecular gas, return $a_0 \simeq 1.2 \times 10^{-10}$ m/s^2 at $z \simeq 2.2$, close to the local value, where tracking requires 3.7; DFD's domain-local screen would give values this low only in $10\,h^{-1}$Mpc domains about 6 to 11 standard deviations denser than average, which their measured environments do not show (Appendix ZT). The running sign is therefore contested: direct molecular-gas masses, kinematic masses not limited by a halo-model prior, per-galaxy analyses with galaxy-level errors and, for the massive discs, an independent bound on the χ halo or rotation curves beyond $3R_e$ decide it, and JWST and ALMA high-z rotation curves, and ultimately SKA H I kinematics, extend it (see Sec. XIX and Appendix N).
- **Minimal-sector baseline for** λ [116]: tree-level no-drive theorem giving $\lambda_{\rm bare} = 1$ for ideal symmetric single-mode standing-wave cavities in the minimal optical-metric EM sector; Appendix R reads the accidental bound as a joint constraint on the channels of $\lambda_{\rm eff} - 1$.

The theory stands or falls on experiment. The decisive near-term tests are channel-resolved cross-species and nuclear-clock campaigns, which discriminate the extended non-metric channel rather than the minimal action (Thm. XI.2), followed by longer-horizon cavity–atom residual experiments. Matter-wave interferometry is a null check (DFD and GR coincide through 1PN; §XIII).

DFD operationally ties the local galactic transition scale to the cosmic expansion rate through $a_0 = 2\sqrt{\alpha}\, cH_0$ (Appendix N, Theorem N.14). This is the empirically sharpest interpretive handle on the theory and is the structural identity that

Theorem XIX.3 (conditional on Axiom WS.1) extends to $a_0(z) = 2\sqrt{\alpha}\, cH(z)$, with a rising scale in low-mass discs at $0.33 < z < 1.44$ on the published bins ($\gamma = 0.78 \pm 0.15$, a frozen a_0 excluded at 5.3σ on the bin errors, about 1σ away galaxy by galaxy within the survey and about 3σ away galaxy by galaxy anchored to SPARC's $z = 0$ value, and 2.1σ from DFD's own $E(z)$ slope at the measured clock, the bars read as 1σ; MUSE-DARK III [109], analysis published in MNRAS **551**(4), 2026 September 7 [110]), a trend that depends on how the molecular gas is added, and no rise in massive discs at $0.6 < z < 2.5$: the extension is contested.
A scientific theory must make predictions that can be proven wrong. DFD does so. The community is invited to test it.

Appendix A: Notation and Conventions

This appendix provides a complete reference for all notation used in the review. Consistent conventions facilitate reproducibility and comparison with other work.

1. Fundamental Fields and Parameters

2. Coordinate and Metric Conventions

a. Metric Signature. We use the $(-,+,+,+)$ (mostly positive) signature throughout:

$$ds^2 = -c^2\,dt^2 + dx^2 + dy^2 + dz^2 \quad \text{(Minkowski)}. \tag{A1}$$

This matches the convention of Misner, Thorne & Wheeler [117] and is standard in gravitational physics.

b. Optical Metric. The optical line element takes the form:

$$d\tilde{s}^2 = -\frac{c^2\,dt^2}{n^2} + d\mathbf{x}^2, \qquad n = e^{\psi}. \tag{A2}$$

Light rays satisfy $d\tilde{s}^2 = 0$. The coordinate speed of light is $c/n = c\,e^{-\psi}$.

c. Spherical Coordinates. For spherically symmetric problems:

$$d\mathbf{x}^2 = dr^2 + r^2(d\theta^2 + \sin^2\theta\,d\phi^2). \tag{A3}$$

The radial acceleration magnitude is $a = (c^2/2)|d\psi/dr|$.

d. Index Conventions.

- Greek indices $\mu, \nu, \ldots \in \{0,1,2,3\}$ for spacetime
- Latin indices $i, j, \ldots \in \{1,2,3\}$ for spatial components
- Repeated indices imply summation (Einstein convention)

3. Physical Constants

a. Derived Quantities.

$$r_s = \frac{2GM}{c^2} \quad \text{(Schwarzschild radius)} \tag{A4}$$

$$\Phi_\odot/c^2 = -\frac{GM_\odot}{c^2 r} \quad \text{(Solar potential)} \tag{A5}$$

$$\approx -9.87 \times 10^{-9} \text{ at 1 AU} \tag{A6}$$

4. Post-Newtonian and Gravitational Wave Parameters

a. Gravitational Wave Parameters. DFD's GW sector is constructed as a *minimal transverse-traceless sector* that reproduces GR exactly in the radiative zone. The scalar field ψ affects source dynamics but not GW propagation (see Sec. V B for construction, Sec. V C for rigorous proof):

- c_T: Tensor mode propagation speed. DFD: $c_T = c_\gamma$ exactly: light and gravitational waves share one metric (App. WS).
- $h_+, h_\times$: Plus and cross polarizations. DFD: identical to GR (no scalar GW modes in far zone).
- $\delta\hat{\varphi}_k$: ppE phase deformation at k-PN order. DFD: $\delta\hat{\varphi}_k = 0$ for compact binary accelerations $\gg a_0$.

5. Clock and LPI Parameters

6. Galactic Dynamics Notation

a. Key Relations.

$$g_{\rm obs} = \frac{V_c^2}{r} \quad \text{(centripetal acceleration)} \tag{A7}$$

$$g_{\rm bar} = \frac{GM_{\rm bar}(<r)}{r^2} \quad \text{(Newtonian gravity)} \tag{A8}$$

$$V_{\rm flat}^4 = GM_{\rm bar}\,a_0 \quad \text{(BTFR, deep-field limit)} \tag{A9}$$

7. Unit Conventions

a. SI Units. All equations in this review are written in SI units unless otherwise noted. This ensures dimensional transparency and direct comparison with experimental values.

b. Geometric Units. For some derivations, particularly those involving spacetime structure, it is convenient to set $G = c = 1$. In these "geometric units":

$$[M] = [L] = [T], \tag{A10}$$

$$1\,M_\odot = 1.477\,\text{km} = 4.926\,\mu\text{s}. \tag{A11}$$

When geometric units are used, this is stated explicitly.

c. Natural Units. For quantum considerations, $\hbar = c = 1$ gives:

$$[M] = [L]^{-1} = [T]^{-1}, \tag{A12}$$

$$1\,\text{eV} = 5.068 \times 10^6\,\text{m}^{-1} = 1.519 \times 10^{15}\,\text{s}^{-1}. \tag{A13}$$

d. Gaussian vs. SI Electromagnetism. For electromagnetic quantities, we use SI (rationalized) units. The fine-structure constant is:

$$\alpha = \frac{e^2}{4\pi\epsilon_0\hbar c} \approx \frac{1}{137}. \tag{A14}$$

8. Abbreviations and Acronyms

9. Sign Convention Summary

For quick reference, the key sign conventions are:

TABLE LI. Primary field variables and coupling parameters in DFD.

Symbol	Name	Definition/Value	Units
Fundamental field			
ψ	Scalar refractive field	Primary gravitational d.o.f.	dimensionless
n	Refractive index	$n = e^{\psi}$	dimensionless
Φ	Effective potential	$\Phi = -c^2\psi/2$	$\mathrm{m}^2/\mathrm{s}^2$
Acceleration scales			
$a_\star$	Characteristic gradient scale	$2a_0/c^2 = 2.663 \times 10^{-27}$ m^{-1}	m^{-1}
a_0	MOND acceleration scale	$2\sqrt{\alpha}\, cH_0^{\mathrm{loc}} = 1.1966 \times 10^{-10}$ m/s^2	$\mathrm{m/s}^2$
$\mathbf{a}$	Physical acceleration	$\mathbf{a} = (c^2/2)\nabla\psi$	$\mathrm{m/s}^2$
a^2	Acceleration invariant	$a^2 \equiv \mathbf{a}\cdot\mathbf{a}$	$\mathrm{m}^2/\mathrm{s}^4$
Coupling constants			
k_a	Self-coupling parameter	$k_a = 3/(8\alpha) \approx 51.4$	dimensionless
k_α	Clock coupling	$k_\alpha = \alpha^2/(2\pi) \approx 8.5 \times 10^{-6}$	dimensionless
K_A	Effective clock coupling	channel-resolved; Eq. (291)	dimensionless
Interpolating function			
$\mu(x)$	Crossover function	$\mu \to 1$ $(x \gg 1)$, $\mu \to x$ $(x \ll 1)$	dimensionless
$\nu(y)$	Inverse function	$y = x\mu(x)$, $x = y\nu(y)$	dimensionless
x	Dimensionless argument	$x = \lvert\nabla\psi\rvert/a_\star = a/a_0$	dimensionless

TABLE LII. Physical constants used in calculations. Values from CODATA 2018 unless noted.

Symbol	Name	Value	Units
c	Speed of light	2.99792458×10^8	m/s
G	Gravitational constant	$6.67430(15) \times 10^{-11}$	$\mathrm{m}^3\,\mathrm{kg}^{-1}\,\mathrm{s}^{-2}$
$\hbar$	Reduced Planck constant	$1.054571817 \times 10^{-34}$	J s
α	Fine-structure constant	$7.2973525643(11) \times 10^{-3}$ (CODATA 2022)	dimensionless
α^{-1}	Inverse α	137.035999177(21) (CODATA 2022)	dimensionless
H_0	Hubble constant	67.52 ± 0.09 (H_0^{early}); 72.09 (H_0^{loc}, $C = 1$, Postulate ZS.11)	$\mathrm{km\,s}^{-1}\,\mathrm{Mpc}^{-1}$
$M_\odot$	Solar mass	1.98841×10^{30}	kg
$R_\odot$	Solar radius	6.9634×10^8	m
AU	Astronomical unit	$1.495978707 \times 10^{11}$	m

TABLE LIII. Post-Newtonian parameters. DFD predictions match GR exactly.

Parameter	Meaning	GR	DFD
γ	Space curvature per unit mass	1	1
β	Nonlinearity in superposition	1	1
ξ	Preferred-location effects (PPN)	0	0
α_1	Preferred-frame (PFE)	0	0
α_2	PFE parameter 2	0	0
α_3	PFE parameter 3	0	0
ζ_1–ζ_4	Violation of momentum conservation	0	0

Sign Conventions

- **Metric signature:** $(-,+,+,+)$
- **Potential sign:** $\Phi < 0$ in gravitational wells
- **Field sign:** $\psi > 0$ in gravitational wells (so $n > 1$)
- **Relation:** $\Phi = -c^2\psi/2$, hence $\psi = -2\Phi/c^2 > 0$
- **Acceleration direction:** $\mathbf{a} = -\nabla\Phi = (c^2/2)\nabla\psi$ points toward mass
- **Curvature:** Not applicable (DFD uses flat background)

These conventions ensure consistency with both the Newtonian limit and standard GR formulations.

Appendix B: Detailed Derivations

This appendix provides step-by-step derivations of key results referenced in the main text. Each derivation includes dimensional checks and identifies approximations used.

TABLE LIV. Clock comparison parameters and sensitivities.

Symbol	Definition	Typical Value
$\xi_{\rm LPI}^{\rm res}$	Residual cavity–atom LPI parameter	DFD: screened residual; GR: 0
S_A^α	α-sensitivity of clock A	See Table LV
K_A	Effective clock coupling	channel-resolved Eq. (291)
ΔK_{AB}	Differential coupling	$K_A - K_B$
y	Fractional frequency	$y = \Delta\nu/\nu$

TABLE LV. α-sensitivities for selected clock transitions.

Clock	Transition	S^α	Reference
Cs hyperfine	$6S_{1/2}$ F=3→4	+2.83	[70]
Rb hyperfine	$5S_{1/2}$ F=1→2	+2.34	[70]
H maser	1S hyperfine	+2.00	[70]
Sr optical	$^1S_0 \to {}^3P_0$	+0.06	[118]
Yb^+ E2	$^2S_{1/2} \to {}^2D_{3/2}$	+0.88	[118]
Yb^+ E3	$^2S_{1/2} \to {}^2F_{7/2}$	−5.95	[118]
Al^+	$^1S_0 \to {}^3P_0$	+0.008	[118]

TABLE LVI. Notation for galactic dynamics and rotation curves.

Symbol	Definition	Units
V_c	Circular velocity	km/s
$V_{\rm flat}$	Asymptotic flat velocity	km/s
$V_{\rm bar}$	Baryonic (Newtonian) velocity	km/s
$g_{\rm obs}$	Observed centripetal acceleration	$\mathrm{m/s^2}$
$g_{\rm bar}$	Baryonic gravitational acceleration	$\mathrm{m/s^2}$
$M_{\rm bar}$	Total baryonic mass	$M_\odot$
Σ	Surface mass density	$M_\odot/\mathrm{pc}^2$
$\Upsilon_\star$	Stellar mass-to-light ratio	$M_\odot/L_\odot$

TABLE LVII. Frequently used abbreviations.

Acronym	Meaning
DFD	Density Field Dynamics
GR	General Relativity
PPN	Parametrized Post-Newtonian
LPI	Local Position Invariance
MOND	Modified Newtonian Dynamics
BTFR	Baryonic Tully-Fisher Relation
RAR	Radial Acceleration Relation
GW	Gravitational Wave
ppE	Parametrized Post-Einsteinian
EFT	Effective Field Theory
UV	Ultraviolet (high-energy)
CMB	Cosmic Microwave Background
BAO	Baryon Acoustic Oscillations
SPARC	Spitzer Photometry and Accurate Rotation Curves
LLR	Lunar Laser Ranging
VLBI	Very Long Baseline Interferometry

1. Second Post-Newtonian Light Deflection

a. Setup

Consider light propagating past a spherically symmetric mass M at impact parameter $b \gg r_s = 2GM/c^2$. In DFD, the refractive index is:

$$n(r) = e^{\psi(r)}, \qquad \psi(r) = \frac{2GM}{c^2 r} + O(r_s^2/r^2). \tag{B1}$$

b. Ray Equation

From Fermat's principle, the ray equation is:

$$\frac{d}{ds}\left(n\frac{d\mathbf{x}}{ds}\right) = \nabla n. \tag{B2}$$

For small deflections, parameterize the path as $\mathbf{x}(z) = (x(z), y(z), z)$ where z is the coordinate along the unperturbed ray. The transverse deflection satisfies:

$$\frac{d^2x}{dz^2} \approx \frac{\partial \ln n}{\partial x} = \frac{1}{n}\frac{\partial n}{\partial x}. \tag{B3}$$

c. First-Order (1PN) Deflection

At first order, $n \approx 1 + \psi$ and we integrate along the unperturbed straight line at $x = b$, $y = 0$:

$$\alpha^{(1)} = \int_{-\infty}^{+\infty} \frac{\partial\psi}{\partial x}\bigg|_{x=b} dz. \tag{B4}$$

For $\psi = 2GM/(c^2\sqrt{b^2+z^2})$:

$$\frac{\partial\psi}{\partial x} = -\frac{2GM\,b}{c^2(b^2+z^2)^{3/2}}. \tag{B5}$$

The integral is standard:

$$\int_{-\infty}^{+\infty} \frac{dz}{(b^2+z^2)^{3/2}} = \frac{2}{b^2}. \tag{B6}$$

Therefore:

$$\boxed{\alpha^{(1)} = \frac{4GM}{c^2 b}} \tag{B7}$$

Dimensional check: $[GM/c^2 b]$ = m/m = dimensionless ✓

This reproduces the GR result exactly, as required for $\gamma = 1$.

d. Second-Order (2PN) Deflection

At 2PN, we need:

1. Higher-order expansion of the gradient: $\nabla(\psi + \psi^2/2 + \ldots)$
2. Path corrections from 1PN deflection

The 2PN correction arises from expanding $n = e^{\psi} \approx 1 + \psi + \psi^2/2$:

$$\frac{\partial \ln n}{\partial x} \approx \frac{\partial \psi}{\partial x} + \psi \frac{\partial \psi}{\partial x} + O(\psi^3). \tag{B8}$$

The additional contribution is:

$$\alpha^{(2)} = \int_{-\infty}^{+\infty} \psi \frac{\partial \psi}{\partial x}\bigg|_{x=b} dz. \tag{B9}$$

Substituting $\psi = 2GM/(c^2 r)$ with $r = \sqrt{b^2 + z^2}$, $\psi\, \partial_x \psi = -(2GM/c^2)^2\, b/r^4$ and

$$\alpha^{(2)} = -\left(\frac{2GM}{c^2}\right)^2 b \int_{-\infty}^{+\infty} \frac{dz}{(b^2+z^2)^2} = -\frac{2\pi G^2 M^2}{c^4 b^2}. \tag{B10}$$

The gradient term above is *not* the full 2PN deflection: the bending of the ray path contributes at the same order, so the coefficient must be obtained from the exact null geodesic rather than asserted. With the parent strain's σ kept, DFD's static exterior is the Schwarzschild metric in DFD's coordinates (App. WS), so the exact deflection is Schwarzschild's and the second-order coefficient is general relativity's [119, 120]:

$$\boxed{\alpha = \frac{4GM}{c^2 b}\left(1 + \frac{15\pi}{16}\frac{GM}{c^2 b}\right)}, \qquad c_2^{\rm DFD} = c_2^{\rm GR} = \tfrac{15\pi}{4} \tag{B11}$$

where c_2 is the coefficient of $(GM/c^2 b)^2$ in α (evaluated from the exact null geodesic; computed). The isotropic exponential metric $g_{00} = -e^{-\psi}$, $g_{ij} = e^{+\psi}\delta_{ij}$ with $\psi = 2GM/c^2 r$, which sets σ to zero, would give 4π instead. At the solar limb the second-order term is $\sim 11\,\mu$as and presently unmeasured (Gaia operates at $\sim$20–30 μas and avoids pointing near the Sun); a LATOR-class astrometric mission would measure it. **Falsifier:** a measured second-order solar-deflection coefficient different from $15\pi/4$, such as the 4π of the isotropic exponential metric, falsifies DFD's exterior.

2. Perihelion Precession

a. Effective Potential

For a test mass in the DFD field of a central mass M, the effective one-dimensional potential is:

$$V_{\rm eff}(r) = \Phi(r) + \frac{L^2}{2r^2}, \tag{B12}$$

where $\Phi = -c^2\psi/2$ and L is the angular momentum per unit mass.

At 1PN order:

$$\Phi(r) = -\frac{GM}{r} - \frac{G^2 M^2}{c^2 r^2} + O(c^{-4}). \tag{B13}$$

b. Orbit Equation

Using $u = 1/r$, the 1PN geodesic equation of the physical metric ($\gamma = \beta = 1$, §IV) gives the Binet equation:

$$\frac{d^2 u}{d\phi^2} + u = \frac{GM}{L^2} + \frac{3GM}{c^2} u^2. \tag{B14}$$

The last term causes precession. For a nearly circular orbit with semimajor axis a and eccentricity e:

$$u \approx \frac{1}{a(1-e^2)}(1 + e\cos\phi). \tag{B15}$$

c. Precession Rate

The perihelion advances by:

$$\Delta\omega = \frac{6\pi G^2 M^2}{c^2 L^2} = \frac{6\pi GM}{c^2 a(1-e^2)} \tag{B16}$$

per orbit. In terms of orbital period T:

$$\boxed{\dot\omega = \frac{6\pi GM}{c^2 a(1-e^2)T}} \tag{B17}$$

Dimensional check: $[GM/(c^2 aT)] = \mathrm{m}\cdot\mathrm{s}^{-2}/\mathrm{s} = \mathrm{rad/s}$ ✓

d. Mercury

For Mercury: $a = 5.79 \times 10^{10}$ m, $e = 0.2056$, $T = 7.60 \times 10^6$ s.

$$\dot\omega_{\rm Mercury} = 42.98\,\text{arcsec/century}, \tag{B18}$$

matching GR and observations.

3. Baryonic Tully-Fisher from μ-Crossover

a. Deep-Field Limit

In the deep-field regime where $|\nabla\psi| \ll a_\star$, the interpolating function satisfies $\mu(x) \to x$ for $x \ll 1$. The field equation becomes:

$$\nabla\cdot\left[\frac{|\nabla\psi|}{a_\star}\nabla\psi\right] = -\frac{8\pi G}{c^2}\rho. \tag{B19}$$

b. Spherical Symmetry

For a spherically symmetric mass distribution with total mass M:

$$\frac{1}{r^2}\frac{d}{dr}\left[r^2\frac{|\psi'|}{a_\star}\psi'\right] = -\frac{8\pi G\rho}{c^2}. \tag{B20}$$

In the asymptotic region ($r \to \infty$), integrating over a sphere:

$$4\pi r^2 \cdot \frac{(\psi')^2}{a_\star} = \frac{8\pi GM}{c^2}. \tag{B21}$$

Therefore:

$$\psi' = \sqrt{\frac{2GMa_\star}{c^2 r^2}} = \frac{\sqrt{2GMa_\star}}{c\,r}. \tag{B22}$$

c. Asymptotic Velocity

The circular velocity is:

$$V_c^2 = r\,a = r\cdot\frac{c^2}{2}\psi' = \frac{c}{2}\sqrt{2GMa_\star\, r^2/r^2} = \frac{c}{2}\sqrt{2GMa_\star}. \tag{B23}$$

Therefore:

$$V_c^4 = \frac{c^2}{4}\cdot 2GMa_\star = \frac{GMa_\star c^2}{2}. \tag{B24}$$

Substituting $a_\star = 2a_0/c^2$:

$$V_c^4 = \frac{GM\cdot(2a_0/c^2)\cdot c^2}{2} = GM\,a_0. \tag{B25}$$

Therefore:

$$\boxed{V_{\rm flat}^4 = GM_{\rm bar}\,a_0} \tag{B26}$$

Dimensional check: $[GM\,a_0] = \mathrm{m^3 s^{-2}}\cdot\mathrm{m\,s^{-2}} = \mathrm{m^4 s^{-4}}$ ✓

This is the Baryonic Tully-Fisher Relation with slope exactly 4 in log-log space.

d. Zero-Point

Using $G = 6.67430\times10^{-11}\ \mathrm{m^3\,kg^{-1}\,s^{-2}}$ and the boundary-matter $a_0 = 1.1966\times10^{-10}\ \mathrm{m\,s^{-2}}$ (Postulate ZS.11):

$$G\,a_0 = 7.987\times10^{-21}\,\mathrm{m^4\,kg^{-1}\,s^{-4}}. \tag{B27}$$

For V in km/s and M in $M_\odot$:

$$V_{\rm flat} = 112.3\,\mathrm{km/s}\left(\frac{M_{\rm bar}}{10^{10}M_\odot}\right)^{1/4}. \tag{B28}$$

4. α-Relation Derivations

a. Relation I: $a_0 = 2\sqrt{\alpha}\,cH_0$

This relation connects the MOND acceleration scale to fundamental constants and the Hubble rate.

Numerical verification (round illustrative benchmark $H_0 = 70$ km/s/Mpc; $H_0^{\rm loc} = 72.09$ gives the boundary-matter $a_0 = 1.1966\times10^{-10}$ m/s^2 (Postulate ZS.11) and $H_0^{\rm early} = 67.52$ the early-clock 1.1208×10^{-10}, App. O):

$$\alpha = 1/137.036, \quad \sqrt{\alpha} = 0.08542 \tag{B29}$$

$$c = 2.998\times10^8\,\mathrm{m/s} \tag{B30}$$

$$H_0 = 70\,\mathrm{km/s/Mpc} = 2.27\times10^{-18}\,\mathrm{s^{-1}} \tag{B31}$$

$$2\sqrt{\alpha}\,cH_0 = 2\times0.08542\times2.998\times10^8\times2.27\times10^{-18} \tag{B32}$$

$$= 1.16\times10^{-10}\,\mathrm{m/s^2}. \tag{B33}$$

Observed (SPARC): $a_0 = (1.20\pm0.02\pm0.24)\times10^{-10}$ m/s^2.

b. Relation II: $k_a = 3/(8\alpha)$

The coefficient k_a enters the Ξ functional of App. N.

Numerical value:

$$k_a = \frac{3}{8\alpha} = \frac{3\times137.036}{8} = 51.39. \tag{B34}$$

c. Relation III: $k_\alpha = \alpha^2/(2\pi)$

The pure electromagnetic-sector clock coupling is:

$$K_A^{(\alpha)} = k_\alpha\cdot S_A^\alpha, \quad \text{where} \quad k_\alpha = \frac{\alpha^2}{2\pi}. \tag{B35}$$

This is the leading same-ion term inside the full channel-resolved coupling of Eq. (291); the complete clock phenomenology also includes strong-sector and composition-dependent contributions (Sec. XI).

Numerical value:

$$k_\alpha = \frac{(1/137.036)^2}{2\pi} = \frac{5.325\times10^{-5}}{6.283} = 8.47\times10^{-6}. \tag{B36}$$

d. Consistency Check

The three relations are not independent. Combining Relations I and II:

$$k_a\cdot a_0 = \frac{3}{8\alpha}\cdot2\sqrt{\alpha}\,cH_0 = \frac{3cH_0}{4\sqrt{\alpha}}. \tag{B37}$$

This provides an additional consistency check on the parameter values.

5. Matter-Wave Phase Shift

a. Phase Evolution

For a matter wave with momentum $\mathbf{p}$ and mass m, the phase accumulated along a path is:

$$\phi = \frac{1}{\hbar}\int (E\,dt - \mathbf{p}\cdot d\mathbf{x})\,. \tag{B38}$$

A species-dependent gravitational coupling $K_{\rm atom}$ enters the local energy as:

$$E = mc^2 + \frac{p^2}{2m} + m\Phi_{\rm eff}, \quad \Phi_{\rm eff} = \Phi(1+K_{\rm atom}). \tag{B39}$$

b. Three-Pulse Interferometer

In a Mach-Zehnder configuration with pulse separation T:

1. First pulse ($t=0$): Beam split
2. Second pulse ($t=T$): Mirror
3. Third pulse ($t=2T$): Recombine

The standard gravitational phase is:

$$\Delta\phi_{\rm grav} = k_{\rm eff}\, g\, T^2, \tag{B40}$$

where $k_{\rm eff}$ is the effective wave vector and g is the local gravitational acceleration.

c. Species-Coupling Expression (Not a DFD Prediction)

A species-dependent coupling would add the expression:

$$\Delta\phi_{DFD} = \frac{\hbar k_{\rm eff}^2}{m}\frac{g}{c^2}T^3\cdot K_{\rm atom}. \tag{B41}$$

Status: not a DFD prediction (the matter-wave sector is null); see the status note after Eq. (337) in Sec. XIII.

6. Gravitational Wave Emission

a. Quadrupole Formula

The leading radiation comes from the time-varying quadrupole moment:

$$Q_{ij} = \int \rho\left(x_i x_j - \frac{1}{3}\delta_{ij}r^2\right)d^3x. \tag{B42}$$

The radiated power is:

$$\boxed{P = \frac{G}{5c^5}\left\langle \dddot{Q}_{ij}\dddot{Q}^{ij}\right\rangle} \tag{B43}$$

This matches the GR quadrupole formula exactly, as required for consistency with binary pulsar observations at the 0.2% level.

b. Binary Inspiral

For a circular binary with masses m_1, m_2, separation a, and orbital frequency ω:

$$P = \frac{32G^4}{5c^5}\frac{(m_1m_2)^2(m_1+m_2)}{a^5}. \tag{B44}$$

The orbital decay rate:

$$\dot{a} = -\frac{64G^3}{5c^5}\frac{m_1m_2(m_1+m_2)}{a^3}. \tag{B45}$$

For PSR B1913+16, the quadrupole formula with its eccentricity factor predicts $\dot{P}_b = -2.403\times10^{-12}$, matching observations at 0.2%.

Appendix C: Interpolating Function Catalog

This appendix catalogs the interpolating functions $\mu(x)$ used in DFD, their properties, and calibration procedures.

1. General Requirements

Any viable interpolating function must satisfy:

1. **Newtonian limit:** $\mu(x)\to 1$ as $x\to\infty$
2. **Deep-field limit:** $\mu(x)\to x$ as $x\to 0$
3. **Monotonicity:** $d\mu/dx > 0$ for all $x>0$
4. **Smoothness:** $\mu\in C^\infty(0,\infty)$
5. **Positivity:** $\mu(x)>0$ for all $x>0$
6. **Strong-field approach rate:** $1-\mu(x)$ must vanish faster than $1/x$ as $x\to\infty$; a $1/x$ tail leaves a constant anomalous acceleration a_0 at every planet. The derived exponential response (App. BS, Thm. BS.9) has $1-\mu = e^{-\sqrt{g_{\rm bar}/a_0}}$ or e^{-x} on its two branches (Cor. BS.14)

The argument is the dimensionless ratio:

$$x = \frac{|\nabla\psi|}{a_\star} = \frac{a}{a_0}, \tag{C1}$$

where $a = (c^2/2)|\nabla\psi|$ is the gravitational acceleration and $a_0 = 1.1966\times10^{-10}$ m/s^2 is the characteristic acceleration scale on bound-matter clocks (Postulate ZS.11). The Lagrangian gradient scale $a_\star = 2a_0/c^2$ ensures x is dimensionless.

2. Catalog of Functional Forms

3. Simple Interpolating Function

The simple form (in DFD the weak-response approximant of the derived exponential response, App. N,

TABLE LVIII. Interpolating functions used in MOND/DFD literature.

Name	$\mu(x)$	Trans.	Ref.
Simple	$\frac{x}{1+x}$	Gradual	FM12
Standard	$\frac{x}{\sqrt{1+x^2}}$	Sharp	M83
Exponential	$1-e^{-x}$	Gradual	B04
RAR (ν form)	$\nu(y)=\frac{1}{1-e^{-\sqrt{y}}}$	Empirical	M16
n-family	$\frac{x}{(1+x^n)^{1/n}}$	Tunable	—
Toy	$\frac{x}{1+x/2}$; 1	Piecewise	—

FM12: Famaey & McGaugh; M83: Milgrom; B04: Bekenstein; M16: McGaugh et al.

App. BS) is:

$$\boxed{\mu_{\rm simple}(x)=\frac{x}{1+x}} \tag{C2}$$

a. Properties:

- Asymptotic: $\mu\to 1-1/x+O(x^{-2})$ as $x\to\infty$
- Deep-field: $\mu\to x-x^2+O(x^3)$ as $x\to 0$
- Transition width: $\Delta\log x\approx 2$ (gradual)
- Inverse: $\nu(y)=(1+\sqrt{1+4/y})/2$

b. Advantages:

- Analytically tractable
- Smooth transition
- Good fit to RAR data

c. Disadvantages:

- May overpredict Newtonian deviations in intermediate regime
- Transition slightly too gradual for some galaxies

4. Standard Interpolating Function

The standard (original MOND) form is:

$$\boxed{\mu_{\rm standard}(x)=\frac{x}{\sqrt{1+x^2}}} \tag{C3}$$

a. Properties:

- Asymptotic: $\mu\to 1-1/(2x^2)+O(x^{-4})$ as $x\to\infty$
- Deep-field: $\mu\to x-x^3/2+O(x^5)$ as $x\to 0$
- Transition width: $\Delta\log x\approx 1$ (sharper)
- Inverse: $\nu(y)=\left[\frac{1}{2}+(\frac{1}{4}+y^{-2})^{1/2}\right]^{1/2}$

b. Advantages:

- Historical standard
- Sharper transition matches some rotation curves better

c. Disadvantages:

- Slightly worse fit to RAR than simple form
- More complex analytically

5. RAR Empirical Function

The empirical fit to the SPARC Radial Acceleration Relation is:

$$\boxed{g_{\rm obs}=\frac{g_{\rm bar}}{1-e^{-\sqrt{g_{\rm bar}/a_0}}}} \tag{C4}$$

This corresponds to an effective ν-function:

$$\nu_{\rm RAR}(y)=\frac{1}{1-e^{-\sqrt{y}}},\quad y=\frac{g_{\rm bar}}{a_0}. \tag{C5}$$

a. Calibration: McGaugh et al. (2016) [10] fit this form to 2693 data points from 153 SPARC galaxies, obtaining:

$$a_0=(1.20\pm 0.02\pm 0.24)\times 10^{-10}\,{\rm m/s^2}, \tag{C6}$$

where the first uncertainty is statistical and the second systematic (the 20% normalization uncertainty in $\Upsilon_\star$).

6. The n-Family

A one-parameter family interpolating between different transition sharpnesses:

$$\boxed{\mu_n(x)=\frac{x}{(1+x^n)^{1/n}}} \tag{C7}$$

- $n=1$: Simple function
- $n=2$: Standard function
- $n\to\infty$: Step function at $x=1$

a. Best fit to SPARC: $n\approx 1.0$–1.5, favoring gradual transition.

7. Comparison of Properties

8. Calibration Procedure

The *form* of the acceleration scale, $a_0=2\sqrt{\alpha}\,cH_0$, and the interpolating function are action-derived, not phenomenological inputs (App. AP, Thm AP.25; App. N, Thm N.14). The procedure below is the empirical *validation* of that derived form against rotation-curve data, not a fit that selects it:

TABLE LIX. Comparison of interpolating function properties.

Property	**Simple**	**Standard**	**RAR**	$n = 1.5$
Newtonian approach	$1/x$	$1/x^2$	$e^{-\sqrt{x}}$	$1/x^{1.5}$
Deep-field approach	x	x	x	x
Transition sharpness	Gradual	Sharp	Gradual	Medium
Analytic tractability	High	Medium	Low	Medium

a. Step 1: Select Galaxy Sample. Use galaxies with:

- High-quality rotation curves (HI 21cm + Hα)
- Well-determined distances (Cepheids, TRGB)
- Resolved stellar and gas mass distributions
- Range of surface brightnesses and masses

b. Step 2: Construct Baryonic Model. For each galaxy:

$$V_{\rm bar}^2(r) = V_{\rm disk}^2 + V_{\rm bulge}^2 + V_{\rm gas}^2, \tag{C8}$$

using mass-to-light ratio $\Upsilon_\star$ from stellar population models.

c. Step 3: Fit to Rotation Curve. Minimize:

$$\chi^2 = \sum_i \frac{[V_{\rm obs}(r_i) - V_{\rm DFD}(r_i; a_0, \Upsilon_\star)]^2}{\sigma_i^2}. \tag{C9}$$

d. Step 4: Construct RAR. Plot $g_{\rm obs}$ vs. $g_{\rm bar}$ for all radii in all galaxies. Fit the ensemble to determine the universal interpolating function.

e. Step 5: Cross-Validation. Test on held-out galaxies and independent datasets (e.g., dwarf spheroidals, ellipticals) to verify universality.

9. Physical Interpretation

The interpolating function $\mu(x)$ encodes how gravity transitions from the Newtonian regime to the deep-field (MOND) regime. In DFD:

- $\mu(x)$ arises from the field equation structure, not fitted by hand
- The transition at a_0 reflects fundamental physics (if α-relations hold)
- The gradual transition (favored by data) suggests continuous crossover rather than phase transition

a. Connection to α-Relations. If $a_0 = 2\sqrt{\alpha}\, cH_0$, then:

$$x = 1 \quad \Leftrightarrow \quad a = a_0 = 2\sqrt{\alpha}\, cH_0. \tag{C10}$$

The crossover scale is set by the geometric mean of electromagnetic (α) and cosmological (H_0) scales.

b. EFT Interpretation. The specific form of $\mu(x)$ may receive quantum corrections at UV scales. The low-energy effective form is what is calibrated observationally.

Appendix D: Experimental Protocols

This appendix specifies technical requirements for the key experiments that can test DFD predictions. The goal is to enable independent replication and provide guidance for experimentalists.

1. Clock Comparison Procedure

a. Measurement Overview

The clock anomaly test searches for species-dependent gravitational coupling by comparing frequency ratios of different clock types as Earth's distance to the Sun varies through the year.

a. Observable:

$$y_{AB}(t) = \frac{\nu_A(t) - \nu_B(t)}{\nu_A} - \langle y_{AB} \rangle, \tag{D1}$$

where A and B are clock types with different α-sensitivities.

b. Expected Signal:

$$y_{AB}(t) = (K_A - K_B)\frac{\Delta\Phi_\odot(t)}{c^2}, \tag{D2}$$

where $\Delta\Phi_\odot(t)$ varies annually by 3.3×10^{-10} peak to peak.

b. Technical Requirements

c. Recommended Clock Pairs

1. **Primary:** Cs hyperfine – Sr optical
   - $\Delta S^\alpha = 2.83 - 0.06 = 2.77$
2. **Enhanced:** Yb^+ E3 – Al^+
   - $\Delta S^\alpha = -5.95 - 0.008 = -5.96$
   - Larger signal amplitude
   - Both optical (reduced systematics)
3. **Null control:** Sr – Yb ($^1S_0$–$^3P_0$)
   - $\Delta S^\alpha = 0.06 - 0.31 = -0.25$
   - Small ΔS serves as null check

d. Data Analysis

a. Step 1: Time Series Construction. Record frequency ratio ν_A/ν_B vs. modified Julian date (MJD).

TABLE LX. Clock comparison technical specifications.

Parameter	**Requirement**	**Current State**
Fractional stability	$\sigma_y < 10^{-16}$ @ 1 day	Achieved (Sr, Yb^+)
Systematic uncertainty	$< 10^{-17}$	Achieved (best optical)
Measurement duration	> 1 year (ideally 2–3)	Standard campaigns
Sampling rate	Daily or better	Standard
Clock pair ΔS^α	> 2 (maximize signal)	Cs–Sr: $\Delta S = 2.77$
Environmental control	mK temperature stability	Standard
Vibration isolation	$< 10^{-9} g$ @ 1 Hz	Standard

b. Step 2: Template Fitting. Fit to:

$$y(t) = A_0 + A_1 t + A_\Phi \cdot \frac{\Phi_\odot(t)}{c^2} + \text{systematics}, \tag{D3}$$

where $\Phi_\odot(t) = -GM_\odot / r_\oplus(t)$.

c. Step 3: Extract ΔK.

$$K_A - K_B = A_\Phi. \tag{D4}$$

d. Step 4: Compare to Prediction.

$(K_A - K_B)_{DFD} = 0$ (minimal action, Thm. XI.2); the extended channel's unscreened scale is $2k_\alpha\,|\Delta S^\alpha|$. (D5)

e. Systematic Error Budget

TABLE LXI. Systematic error budget for clock comparison.

Effect	**Magnitude**	**Mitigation**
Blackbody radiation	$\sim 10^{-16}$	Temperature control
Zeeman shifts	$\sim 10^{-17}$	Magnetic shielding
Gravitational redshift	$\sim 10^{-16}$ h^{-1}	Height measurement
Reference cavity drift	$\sim 10^{-17}$/day	Co-located comparison
Annual temperature cycle	Variable	Monitor and correct
Tidal effects	$\sim 10^{-17}$	Model and subtract

f. Windowed vs. Global Analysis Strategies

Two complementary approaches exist for extracting annual gravitational signals:

a. Global year-long fit. Fit the full multi-year dataset with a flexible drift model (polynomials, splines) plus the gravitational template $\Phi_\odot(t)$. Advantages: robust statistics, clear identification of sinusoidal annual signal. Risk: flexible drift models can partially absorb the gravitational template, especially if the signal is weak.

b. Perihelion-windowed analysis. Analyze a focused window (30–60 days) around perihelion, where $\Phi_\odot$ is extremal. Use only linear drift within the window. Advantages: sensitive to the *shape* of the potential variation; less prone to drift absorption. Risk: shorter baseline increases degeneracy with instrumental drift.

c. Recommended protocol.

1. Perform both analyses and report both results.
2. Quantify the covariance between drift and potential coefficients in each case.
3. A robust signal should appear in both approaches; discrepancy indicates systematic concerns.
4. Preserve and publish raw ratios to enable independent reanalysis.

The windowed approach is particularly valuable when exploring marginal hints, as aggressive global detrending can project out exactly the annual structure one seeks to test.

2. Cavity-Atom Setup Requirements

a. Experiment Concept

Compare an optical cavity (photon sector) to an atomic clock (matter sector) while varying gravitational potential. DFD predicts different responses, with GR predicting $\xi_{\text{LPI}}^{GR} = 0$ and corrected DFD predicting only a screened residual $\xi_{\text{LPI}}^{\text{res}}$ once the constitutive-chain cancellation is imposed.

b. Key Configuration

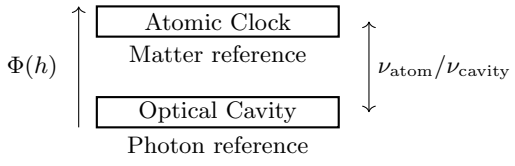


FIG. 13. Schematic of cavity-atom comparison.

TABLE LXII. Cavity-atom test specifications.

Component	Requirement	Notes
Cavity finesse	$> 10^5$	ULE or Si spacer
Cavity stability	$< 10^{-16}$ @ 1 s	Temperature stabilized
Atom clock	Sr or Yb optical	$< 10^{-18}$ systematic
$\Delta\Phi/c^2$ variation	$> 10^{-12}$	Height change or orbital
Measurement duration	$> 10^4$ s per height	Statistics
Height separation	> 10 m (terrestrial)	Tower or elevator

c. Technical Specifications

d. Height Comparison Method

a. Configuration A: Tower Experiment

- Cavity at ground level
- Atomic ensemble transported to height h
- Compare via fiber link
- $\Delta\Phi/c^2 = gh/c^2 \approx 10^{-14}$ per 100 m

b. Configuration B: Space Mission

- Cavity and atoms on same platform
- Vary orbital altitude
- $\Delta\Phi/c^2 \sim 10^{-10}$ (LEO to higher orbit)
- Enhanced signal but complex mission

e. Observable

$$\frac{d}{d\Phi}\left(\frac{\nu_{\rm atom}}{\nu_{\rm cavity}}\right) = \frac{\xi_{\rm LPI}}{c^2}, \tag{D6}$$

where $\xi_{\rm LPI}^{GR} = 0$ and the corrected DFD expectation is a small screened residual rather than an order-unity slope.

f. Discrimination Significance

With current technology:

- 100 m height: $\Delta\Phi/c^2 \approx 10^{-14}$
- Clock comparison at 10^{-18}: useful only for a residual-level cavity–atom search
- **Discrimination requires pushing into the screened-residual regime rather than separating $\xi_{\rm LPI} = 0$ from an order-unity value**

3. Matter-Wave Interferometer Specifications

a. Formula Under Test (Not a DFD Prediction)

The formula under test is:

$$\Delta\phi_{DFD} = \frac{\hbar k_{\rm eff}^2}{m}\frac{g}{c^2}T^3 \cdot K_{\rm atom}. \tag{D7}$$

Status: not a DFD prediction (the matter-wave sector is null); see the status note after Eq. (337) in Sec. XIII.

The formula is not a phase (its units are s^2/m) and sets no phase-resolution target; the targets of Table LXIII do not apply to DFD.

b. Interferometer Requirements

TABLE LXIII. Matter-wave interferometer specifications for the null test of DFD.

Parameter	Minimum	Target	Notes
Free-fall time T	0.5 s	2 s	Limits signal
$k_{\rm eff}$	10^7 m^{-1}	2×10^7 m^{-1}	Two-photon Raman
Phase resolution	10^{-8} rad	10^{-10} rad	Shot noise limit
Atom number	10^5	10^7	Statistics
Systematic control	10^{-9} rad	10^{-10} rad	Gravity gradients
Species	^{87}Rb	^{87}Rb, ^{85}Rb	Comparison

c. Dual-Species Configuration

To extract the species-dependent $K_{\rm atom}$:

1. Run identical interferometer with ^{87}Rb and ^{85}Rb
2. Both have same $m_{\rm Rb}$ to $< 2\%$
3. Different S^α values
4. Differential measurement cancels common-mode systematics

d. T^3 Signature (Not a DFD Prediction)

The formula scales as T^3, while:

- Standard gravitational phase $\propto T^2$
- Gravity gradient phase $\propto T^4$
- Rotation phase $\propto T^2$

Through 1PN, DFD and GR carry the same phases (§XIII), so this scaling does not discriminate between them.

TABLE LXIV. Matter-wave systematic errors.

Effect	Scaling	Mitigation
Gravity gradient	T^4	Gradient compensation
Coriolis force	T^2	Rotation compensation
Laser wavefront	T^2	High-quality optics
AC Stark shift	Independent	Laser intensity control
Magnetic fields	T^2	Magnetic shielding
Two-photon light shift	T^2	Symmetric pulse

e. Systematic Control

4. Galaxy Rotation Curve Analysis

a. Data Requirements

- **Rotation curve:** HI 21cm and/or Hα emission
- **Resolution:** Beam size < 1 kpc at galaxy distance
- **Velocity precision:** < 5 km/s per point
- **Radial extent:** Out to $\gtrsim 3$ disk scale lengths
- **Inclination:** $30° < i < 80°$ (avoid edge-on/face-on)

b. Baryonic Mass Model

1. **Stellar mass:** From 3.6 μm photometry
$$\Sigma_\star(r) = \Upsilon_\star \cdot I_{3.6}(r) \tag{D8}$$
with $\Upsilon_\star \approx 0.5\ M_\odot/L_\odot$ (disk)
2. **Gas mass:** From HI 21cm + correction for He
$$\Sigma_{\rm gas} = 1.33 \cdot \Sigma_{\rm HI} \tag{D9}$$
3. **Total:**
$$V^2_{\rm bar}(r) = V^2_\star(r) + V^2_{\rm gas}(r) \tag{D10}$$

c. DFD Fitting Procedure

a. Step 1: Compute $g_{\rm bar}(r) = V^2_{\rm bar}(r)/r$
b. Step 2: Apply interpolating function:
$$g_{\rm obs}(r) = g_{\rm bar}(r) \cdot \nu\left(\frac{g_{\rm bar}(r)}{a_0}\right) \tag{D11}$$
c. Step 3: Convert to velocity:
$$V_{DFD}(r) = \sqrt{r \cdot g_{\rm obs}(r)} \tag{D12}$$
d. Step 4: Minimize χ^2:
$$\chi^2 = \sum_i \frac{[V_{\rm obs}(r_i) - V_{DFD}(r_i)]^2}{\sigma_i^2} \tag{D13}$$

with free parameters: a_0 (or fixed), $\Upsilon_\star$, distance.

d. Quality Metrics

- $\chi^2/{\rm dof} < 2$ (good fit)
- Residuals randomly distributed (no systematic trends)
- $\Upsilon_\star$ consistent with stellar population models
- a_0 consistent across galaxy sample

5. Decision Matrix: Which Experiment to Prioritize

a. Recommendation: The near-term emphasis is on nuclear clocks and cross-species clock analyses. Cavity–atom work remains valuable as a long-horizon residual test rather than the first binary discriminator. Matter-wave interferometry is a null check (DFD and GR coincide through 1PN).

Appendix E: Data Tables

This appendix collects numerical data used in the review for reference and reproducibility.

1. Post-Newtonian Parameter Bounds

2. Binary Pulsar Timing Data

a. Notes:

- $\dot{P}_b^{\rm obs}$ corrected for Shklovskii effect and Galactic acceleration
- GR prediction uses measured masses from other post-Keplerian parameters
- DFD predicts identical $\dot{P}_b$ to GR (same quadrupole formula)

3. Clock Sensitivity Coefficients

a. Sensitivity Definition:
$$S_A^\alpha \equiv \frac{\partial \ln \nu_A}{\partial \ln \alpha} = \frac{\alpha}{\nu_A}\frac{\partial \nu_A}{\partial \alpha}. \tag{E1}$$
b. Optimal Pairs for DFD Test:

1. Cs – Al^+: $\Delta S = 2.82$ (large baseline)
2. Yb^+ E3 – Al^+: $\Delta S = -5.96$ (largest, opposite signs)
3. Cs – Sr: $\Delta S = 2.77$ (readily available)

TABLE LXV. Experimental decision matrix for DFD tests.

Experiment	Signal	Timescale	Cost	Discriminating	Priority
Clock anomaly (extended channel; null under the minimal action)	$\lesssim 1 \times 10^{-18}$	1–2 yr	Low	Yes	High
Cavity-atom residual	screened residual	Long-term	Medium	Yes	Medium
Matter-wave T^3 (null prediction)	null (= GR)	3–5 yr	Medium	No (null)	Medium
Galaxy RAR	< 0.15 dex	Done	Low	No	Complete
GW ppE	$\delta\hat{\varphi} = 0$	Done	N/A	No (confirms)	Complete

TABLE LXVI. Experimental bounds on PPN parameters. DFD predicts GR values.

Parameter	GR/DFD	Bound	Method	Reference
$\gamma - 1$	0	$(2.1 \pm 2.3) \times 10^{-5}$	Cassini	[35]
$\beta - 1$	0	$(-4.5 \pm 5.6) \times 10^{-5}$	LLR	[121]
$\lvert\alpha_1\rvert$	0	$< 4 \times 10^{-5}$	Pulsar timing	[37]
$\lvert\alpha_2\rvert$	0	$< 2 \times 10^{-9}$	Pulsar spins	[5]
$\lvert\alpha_3\rvert$	0	$< 4 \times 10^{-20}$	Pulsar accel.	[122]
$\lvert\xi\rvert$	0	$< 10^{-3}$	Binary pulsars	[123]
$\lvert\zeta_1\rvert$	0	$< 2 \times 10^{-2}$	Lunar orbit	[36]
$\lvert\zeta_2\rvert$	0	$< 4 \times 10^{-5}$	Binary pulsars	[5]
$\lvert\zeta_3\rvert$	0	$< 10^{-8}$	Newton's 3rd law	[124]
$\lvert\zeta_4\rvert$	0	—	Not independent	—

4. SPARC Galaxy Sample Statistics

5. Gravitational Wave Constraints

The GWTC-3 ppE bounds are those of Table IX; DFD predicts $\delta\hat{\varphi}_k = 0$.

a. Speed of Gravity: GW170817/GRB 170817A constraint [126]:

$$-3 \times 10^{-15} < \frac{c_T - c}{c} < +7 \times 10^{-16}. \tag{E2}$$

DFD prediction: $c_T = c_\gamma$ exactly: light and gravitational waves share one metric (App. WS).

6. Physical Constants Summary

7. DFD Parameter Summary

8. Experimental Timeline

a. Falsification Threshold:

- Cavity–atom residual: a dedicated null at the screened-residual target would constrain or remove that channel
- Matter-wave: not a falsification channel (null prediction, §XIII)
- RAR: Scatter > 0.3 dex would falsify

Appendix F: Rigorous Foundations for Gauge Emergence

This appendix presents mathematically rigorous derivations supporting the gauge emergence mechanism described in §XVII. Sections F 1–F 6 contain complete proofs; Section F 8 presents a physically motivated conjecture.

1. Minimality of the $(3, 2, 1)$ Partition

Proposition F.1 (Minimality)**.** *Among all block partitions $(n_1, \ldots, n_k)$ of $\mathbb{C}^N$ whose $U(N)$-stabilizer contains exactly two simple non-Abelian factors $SU(3)$ and $SU(2)$ and a singlet sector, the unique minimal partition is $(3, 2, 1)$ with $N = 6$. Its stabilizer $U(3) \times U(2) \times U(1)$ has two abelian factors modulo the overall phase; the single hypercharge is fixed by the isotropy reading of Remark F.2.*

Proof. For a partition $(n_1, \ldots, n_k)$, the stabilizer is $\prod_i U(n_i) = \prod_i [SU(n_i) \times U(1)]$ modulo diagonal $U(1)$.

Necessity of three blocks: A two-block partition (n_a, n_b) gives stabilizer $SU(n_a) \times SU(n_b) \times U(1)$. This has no singlet sector: every vector transforms non-trivially under at least one SU factor. Hence $k \geq 3$.

Necessity of block sizes 3, 2, and 1: Two blocks must have dimensions 3 and 2 to yield $SU(3) \times SU(2)$. The third block provides the singlet sector; minimality requires $n_1 = 1$.

Minimality of $N = 6$: Any partition with $k \geq 3$ blocks including sizes 3 and 2 has $N \geq 3 + 2 + 1 = 6$. The partition $(3, 2, 1)$ achieves this bound.

Uniqueness: The only partition of 6 with blocks of sizes 3, 2, and 1 is $(3, 2, 1)$ itself.

TABLE LXVII. Binary pulsar systems used for gravitational tests.

System	P_b [hr]	$\dot{P}_b^{\rm obs}$	$\dot{P}_b^{\rm GR}$	Agreement
PSR B1913+16	7.752	-2.398×10^{-12}	-2.403×10^{-12}	0.2%
PSR J0737-3039	2.454	-1.2478×10^{-12}	-1.2478×10^{-12}	0.004%
PSR J1738+0333	8.515	-2.59×10^{-14}	-2.77×10^{-14}	6.5%
PSR J0348+0432	2.460	-2.73×10^{-13}	-2.58×10^{-13}	6%
PSR J1141-6545	4.744	-4.03×10^{-13}	-3.86×10^{-13}	4%

TABLE LXVIII. Sensitivity coefficients for atomic transitions. The pure-α leading term is $K_A^{(\alpha)} = k_\alpha \cdot S_A^\alpha$ with $k_\alpha = 8.5\times10^{-6}$; the full channel-resolved coupling includes additional strong-sector and composition terms (Eq. (291)).

Atom	Transition	Type	S^α	$k_\alpha S^\alpha$ (ext., unscreened)	Ref.
Microwave (hyperfine)					
^{133}Cs	$6S_{1/2}$ F=3→4	HFS	+2.83	2.4×10^{-5}	[70]
^{87}Rb	$5S_{1/2}$ F=1→2	HFS	+2.34	2.0×10^{-5}	[70]
^{1}H	$1S_{1/2}$ F=0→1	HFS	+2.00	1.7×10^{-5}	[70]
Optical					
^{87}Sr	$^1S_0 \to {}^3P_0$	E1	+0.06	5.1×10^{-7}	[118]
^{171}Yb	$^1S_0 \to {}^3P_0$	E1	+0.31	2.6×10^{-6}	[118]
^{27}Al$^+$	$^1S_0 \to {}^3P_0$	E1	+0.008	6.8×10^{-8}	[118]
^{171}Yb$^+$	$^2S_{1/2} \to {}^2D_{3/2}$	E2	+0.88	7.5×10^{-6}	[118]
^{171}Yb$^+$	$^2S_{1/2} \to {}^2F_{7/2}$	E3	−5.95	-5.1×10^{-5}	[118]
^{199}Hg$^+$	$^2S_{1/2} \to {}^2D_{5/2}$	E2	−3.19	-2.7×10^{-5}	[118]
Nuclear (proposed)					
^{229}Th	Nuclear isomer	M1/E2	$\sim 10^4$	~ 0.1	[125]

TABLE LXIX. SPARC sample properties (Lelli et al. 2016).

Property	Value
Number of galaxies	175
Number of RAR data points	2693
Distance range	2 – 150 Mpc
Luminosity range	10^7 – 10^{11} $L_\odot$
$V_{\rm flat}$ range	20 – 300 km/s
Morphological types	Sa – Irr
RAR fit results	
a_0 (best fit)	$(1.20 \pm 0.02 \pm 0.24)\times10^{-10}$ m/s^2
Observed scatter	0.13 ± 0.02 dex
BTFR results	
Slope	3.98 ± 0.08
Intrinsic scatter	0.11 ± 0.02 dex

Why $N > 6$ is excluded: Any partition with $N > 6$ either has larger block sizes (giving wrong gauge groups) or additional blocks (giving more than two non-Abelian factors). Since we seek the minimal N, enumeration beyond $N = 6$ is unnecessary. □

For completeness, we verify that no partition with $N \le 6$ other than $(3, 2, 1)$ satisfies all requirements:

N	Partition	SU factors	Singlet?	Status
5	$(3,2)$	$SU(3)\times SU(2)$	No	✗
5	$(2,2,1)$	$SU(2)\times SU(2)$	Yes	✗
6	$(4,2)$	$SU(4)\times SU(2)$	No	✗
6	$(3,3)$	$SU(3)\times SU(3)$	No	✗
6	$\mathbf{(3,2,1)}$	$\mathbf{SU(3)\times SU(2)}$	**Yes**	✓
6	$(2,2,2)$	$SU(2)^3$	No	✗

Remark F.2 (The electroweak group as the isotropy group of $\mathbb{C}P^2$). The minimality proposition assumes the factors it selects. The electroweak group follows from the internal space instead, under one stated identification. The charge-trace step of the closed form for α (§X) needs the hypercharge to act on $\mathbb{C}P^2$ as a traceless element of $\mathfrak{su}(3)$, and it fixes only that: every traceless charge gives the same $(k+3)/k$, and a generic one is stabilised by a torus, not by a $U(2)$. The stated identification takes the hypercharge to be the direction $\mathrm{diag}(1,1,-2)$, up to conjugation and scale the only one that commutes with an $SU(2)$ inside $SU(3)$, normalised so that the isotropy charge is $6Y$, and it takes the electroweak group to be the structure group of the isotropy bundles at the vacuum point p of $\mathbb{C}P^2$, acting on the fibres of the twisting bundles that carry the matter fields, not on the internal spinor and not by isometries of $\mathbb{C}P^2$ (an isometric action would rotate two of the generation profiles of App. H into each other). The charge trace acts instead on the Toeplitz spaces $H^0(\mathbb{C}P^2, \mathcal{O}(k))$, through the isometric lift of the same generator, which equals the fibre charge only over p; that the two are one hypercharge is part of the identification. Every point of $\mathbb{C}P^2$ is equivalent under $SU(3)$, so the choice of p adds no content, and $\mathrm{diag}(1,1,-2)$ is the centre of the isotropy group $U(2)$ of $\mathbb{C}P^2 = SU(3)/U(2)$ at p. Under this charge a homogeneous line bundle $\mathcal{O}(m)$ carries $2m$ and an irreducible rank-two homogeneous bundle carries an odd charge. With the charge equal to $6Y$, the multiplets with odd $6Y$, which are exactly the weak doublets, must be rank-two isotropy bundles, so the weak $SU(2)$ is the isotropy $SU(2)$ and the electroweak group is $U(2) = (SU(2)\times U(1))/\mathbb{Z}_2$, the global form that every Standard Model field obeys. That is the $\mathbb{Z}_2$ part of the Standard Model's $\mathbb{Z}_6$, a check the identification passes; the $\mathbb{Z}_3$ part comes with colour. In this reading the $(2,1)$ blocks of the partition are the isotropy split $\mathbb{C}^3 = \ell_p^\perp \oplus \ell_p$ (ℓ_p is the line p), whose stabiliser $S(U(2)\times U(1)) = U(2)$ has one abelian factor; the tangent space $T_p = \mathrm{Hom}(\ell_p, \ell_p^\perp)$ carries isotropy charge 3. The reading is not an elec-

TABLE LXX. Physical constants used in calculations (CODATA 2018 unless noted).

Constant	Symbol	Value	Uncertainty
Speed of light	c	299792458 m/s	exact
Gravitational constant	G	6.67430×10^{-11} $\mathrm{m^3 kg^{-1} s^{-2}}$	1.5×10^{-5}
Planck constant	h	$6.62607015 \times 10^{-34}$ J s	exact
Reduced Planck	$\hbar$	$1.054571817 \times 10^{-34}$ J s	exact
Fine-structure	α	$7.2973525643 \times 10^{-3}$ (CODATA 2022)	1.6×10^{-10}
Electron mass	m_e	$9.1093837015 \times 10^{-31}$ kg	3.0×10^{-10}
Proton mass	m_p	$1.67262192369 \times 10^{-27}$ kg	3.1×10^{-10}
Solar mass	$M_\odot$	1.98841×10^{30} kg	4×10^{-5}
Astronomical unit	AU	$1.495978707 \times 10^{11}$ m	exact

TABLE LXXI. Summary of DFD parameters and their values.

Parameter	Symbol	Value	Source
Independent observational comparator			
SPARC acceleration scale	a_0^{SPARC}	$(1.20 \pm 0.02_{\mathrm{stat}} \pm 0.24_{\mathrm{sys}}) \times 10^{-10}$ m/s^2	SPARC RAR
From α-relations (parameter-free)			
Self-coupling	k_a	51.4	$3/(8\alpha)$
Clock coupling	k_α	8.5×10^{-6}	$\alpha^2/(2\pi)$
Hubble relation	—	$a_0 = 2\sqrt{\alpha}\, cH_0^{\mathrm{loc}} = 1.1966 \times 10^{-10}$ m/s^2	Derived law; bound-matter clock
From theory structure			
GW speed	c_T	c, the optical cone (App. WS)	Optical metric
PPN γ	γ	1 exactly	Conformal structure
PPN β	β	1 exactly	Field equation
LPI residual	$\xi_{\mathrm{LPI}}^{\mathrm{res}}$	screened residual	Constitutive-chain cancellation + channel dependence

troweak unification in the isometry group $SU(3)$, which would give $\sin^2\theta_W = 3/4$: the couplings come from the frame stiffnesses (Theorem F.25).

Remark F.3 (Colour and the family content are inputs). Colour cannot be a symmetry of $\mathbb{C}P^2 \times S^3$ when the hypercharge acts on $\mathbb{C}P^2$ as the charge trace needs: the symmetries commuting with any nonzero element of the $\mathfrak{su}(3)$ of $\mathbb{C}P^2$ lie, up to conjugation, in $U(2) \times SO(4)$, whose simple factors are copies of $SU(2)$, so they contain no $SU(3)$; those commuting with the electroweak $U(2)$ form $U(1) \times SO(4)$. Taking colour as the isometry group of $\mathbb{C}P^2$ instead would make the hypercharge central there, which removes the $+3$ shift of the charge trace and lowers α^{-1} to 136.9 (130.5 if only the numerator $k+3$ is dropped and $d = k + 4$ kept). From the integers alone, 136.9 lies 0.08% (800 ppm) below the measured value, against 21 ppm for the adopted reading. The exclusion rests on the charge trace being the origin of the shift, which is how §X D computes it; read as the degree of the determinant line, which Rem. X.3 keeps as a consistency check, the shift would survive for a central charge and give 137.033. Colour, $SU(3)$ acting on a separate three-dimensional block, is therefore an input, as it is in the Standard Model. The representations of one generation and their chirality are inputs as well. Symmetries of a compact internal space do not by themselves give chiral fermions [127], and in this reading the flux twist on $\mathbb{C}P^2$ does not supply the chirality of a generation either: the spin^c indices of the five left-handed multiplets Q, u^c, d^c, L and e^c are 3, 0, 3, -1 and 10 (computed).

2. The $SU(N)$ Selection Lemma

Lemma F.4 (Dimension-Casimir Coincidence)**.** *Among compact simple Lie groups, the condition* $\dim(\textit{fundamental rep}) = h^\vee$ *(dual Coxeter number) holds if and only if* $G \cong SU(N)$ *for some* $N \geq 2$.

Proof. Direct verification from the classification of simple Lie algebras [128, 129]:

Cartan	Group	$h^\vee$	dim(fund)	Match?
A_{n-1}	$SU(n)$	n	n	✓
B_n	$SO(2n+1)$	$2n-1$	$2n+1$	✗
C_n	$Sp(2n)$	$n+1$	$2n$	✗
D_n	$SO(2n)$	$2n-2$	$2n$	✗
G_2	G_2	4	7	✗
F_4	F_4	9	26	✗
E_6	E_6	12	27	✗
E_7	E_7	18	56	✗
E_8	E_8	30	248	✗

The exceptional isomorphisms $Sp(2) \cong SU(2)$ and $SO(6) \cong SU(4)$ reduce to the A_n case. □

TABLE LXXII. Projected timeline for DFD experimental tests.

Test	Time	Sens.	Status
Near-term (1–3 yr)			
Clock (Cs/Sr)	2025–26	null (minimal action)	Underway
Multi-clock	2025–26	$K \sim 10^{-6}$	In progress
Medium-term (3–7 yr)			
Cavity–atom	2030+	Residual level	Long-horizon
Matter-wave T^3 (null prediction)	2027–30	10^{-10} rad	Devel.
Nuclear clock	2028–32	$K \sim 10^{-3}$	R&D
Long-term (>7 yr)			
Space optical	2030+	$K \sim 10^{-7}$	Concept
Space atom int. (null prediction)	2032+	10^{-11} rad	Concept

Remark F.5. This lemma concerns only the fundamental representation. SM fermions transform in fundamentals of $SU(3)$ and $SU(2)$, so higher representations need not be considered.

3. The Spin^c Flux Quantization

a. Setup. $\mathbb{C}P^2$ is a compact complex surface with $H^2(\mathbb{C}P^2;\mathbb{Z}) = \mathbb{Z}\cdot H$ where H is the hyperplane class satisfying $\int_{\mathbb{C}P^2} H^2 = 1$. Since $w_2(T\mathbb{C}P^2) = c_1 \mod 2 = 3H \mod 2 = H \neq 0$, $\mathbb{C}P^2$ does not admit a spin structure but does admit a spin^c structure with determinant line bundle $L_{\det} = K^{-1} = \mathcal{O}(3)$ and $c_1(L_{\det}) = 3H$ [130, 131].

Definition F.6 (Hypercharge Twist)**.** Let L be a line bundle on $\mathbb{C}P^2$ with $c_1(L) = H$, and let $q_1 \in \mathbb{Z}_{>0}$ be the U(1) flux quantum. For a representation of hypercharge Y, the spin^c-twisted hypercharge line is $L^{q_1 Y} \otimes L_{\det}^{1/2}$, whose *total* degree $q_1 Y + 3/2$ is the object required to be integral or half-integral (Lemma F.8); the bare factor $L^{q_1 Y}$ is a formal half-integral symbol and is *not* individually a line bundle for $Y \in \{1/6, -1/2\}$ at $q_1 = 3$ (there is no $\mathcal{O}(1/2)$ on $\mathbb{C}P^2$).

Remark F.7 (Open collision between the hypercharge dictionary and the $k_{\max}$ bundle — stated, not resolved). The microsector bundle $E = \mathcal{O}(9) \oplus \mathcal{O}^{\oplus 5}$ of Lemma F.11 assigns the five matter types *degree-0* summands, whereas the hypercharge dictionary above assigns them degrees $q_1 Y \in \{1/2, 2, -1, -3/2, -3\}$ at $q_1 = 3$ — two of which are non-integral, so those lines cannot individually exist as bundles. The two are read off different bundles: the $k_{\max}$ count uses E as a *rank-6 twist bundle whose summands carry SM labels*, not as the direct sum of the individual hypercharge lines. Reconciling the two readings is an **open item**; $k_{\max} = 60$ is quoted from the E-reading throughout. (Under the alternative reading in which the five $\mathcal{O}(0)$ summands are genuine trivial bundles, degree $= q_1 Y = 0$ would force $Y = 0$ for all five — contradicting their definition as exactly the hypercharged types.) The two non-integral degrees belong to the weak doublets Q and L, which are rank-two bundles of odd first Chern class rather than lines (Remark F.10), so they exist as bundles; reconciling the degree-zero summands of E with the hypercharge degrees stays open. In the isotropy reading (Remark F.2) the five types, written as the left-handed multiplets Q, u^c, d^c, L and e^c of Lemma F.11, are homogeneous bundles of slopes $\frac{1}{2}$, -2, 1, $-\frac{3}{2}$ and 3 with spin^c indices 3, 0, 3, -1 and 10, not five summands of index 1.

Lemma F.8 (Integrality Condition)**.** *For the spin^c Dirac index to be well-defined for all SM hypercharges $Y \in \{1/6, 2/3, -1/3, -1/2, -1, 0\}$, the combination $q_1 Y + 3/2$ must lie in $\frac{1}{2}\mathbb{Z}$ for all Y.*

Lemma F.9 ($q_1 = 3$ is Uniquely Minimal)**.** *The unique minimal positive integer q_1 satisfying Lemma F.8 is $q_1 = 3$.*

Proof. Direct computation:

TABLE LXXIII. Charge combinations for various hypercharge assignments.

q_1	$Y = 1/6$	$Y = 2/3$	$Y = -1/3$	$Y = -1/2$	$Y = -1$	All $\in \frac{1}{2}\mathbb{Z}$?
1	5/3	13/6	7/6	1	1/2	✗
2	11/6	17/6	5/6	1/2	−1/2	✗
3	2	7/2	1/2	0	−3/2	✓
4	13/6	25/6	1/6	−1/2	−5/2	✗
5	7/3	29/6	−1/6	−1	−7/2	✗
6	5/2	11/2	−1/2	−3/2	−9/2	✓

Only $q_1 = 3$ and $q_1 = 6$ satisfy the condition; $q_1 = 3$ is minimal. □

Remark F.10 (The flux quantum $q_1 = 3$ from the isotropy reading). The condition of Lemma F.8 is necessary, not sufficient: it admits both half-odd and integer values of $q_1 Y + 3/2$, and a spin^c twist of a line bundle on $\mathbb{C}P^2$ needs the half-odd coset. The flux quantum follows from the isotropy reading of Remark F.2, given its identification. With the hypercharge the isotropy charge $6Y$, a multiplet of hypercharge Y lives in a homogeneous bundle of slope $3Y$, so $q_1 = 3$. The allowed values are $q_1 = 3\lambda$ with λ odd; $q_1 = 6$ is excluded, since it would give the weak doublets an even charge. Only $\lambda = \pm 1$ lets the isotropy group act faithfully on the Standard Model fields (for odd $\lambda \geq 3$ a $\mathbb{Z}_\lambda$

of its centre acts trivially), so the hypercharge circle is the isotropy circle itself and $q_1 = 3$. At $q_1 = 3$ every Standard Model multiplet is a well-defined field on the non-spin $\mathbb{C}P^2$: the singlets as spin^c twists and the doublets as rank-two bundles of odd first Chern class. A uniform spin^c structure on line bundles alone would need $q_1 = 6$; that is the value when the weak doublets are line bundles and the weak $SU(2)$ does not act on $\mathbb{C}P^2$, while in the isotropy reading the doublets are rank-two bundles. The spin-$\mathbb{Z}_4$ $B-L$ structure of Sec. F 7 is a second consistent completion. Within the isotropy reading the derivation does not use α. The same $q_1 = 3$ is the choice for which the determinant-line chain of Lemma F.11 lands on $k_{\max} = 60$ and hence on $\alpha^{-1} = 137.036$ to 21 ppm from the integers (the last 21 ppm rests on the open bracket coefficient; Rem. F.12). Between readings α does the selecting: with the degree $a = N_{\text{gen}} q_1$ that Lemma F.11 constructs, the reading with line-bundle doublets, $q_1 = 6$, would give $k_{\max} = 195$ and $\alpha^{-1} \simeq 450$, and $q_1 = 1$ would give $k_{\max} = 15$; with the degree read instead as $N_{\text{gen}}\, c_1(\mathbb{C}P^2)$, which equals it only at $q_1 = 3$, where $L_Y = \mathcal{O}(3) = K^{-1}$ (§X), α would not test q_1.

Lemma F.11 (Conditional Finite-Microsector Count (Determinant-Line Lift))**.** *Let $X = \mathbb{C}P^2$ with canonical spin^c structure $L_{\text{det}} = K^{-1} = \mathcal{O}(3)$, and let $L = \mathcal{O}(1)$ with $c_1(L) = H$. Take the flux quantum $q_1 = 3$ (Rem. F.10), so the minimal hypercharge line bundle is $L_Y := L^{q_1} = \mathcal{O}(3)$. Then the minimal globally well-defined integer-charge lift is the triple tensor power*

$$L_Y^{\otimes 3} = \mathcal{O}(9).$$

*Here the cube arises (α-free) as the degree of the determinant line over the three-generation kernel $\mathcal{G}$, where $N_{\text{gen}} = 3$ enters as a **discrete input** (the observed family number, numerically coincident with $\chi_{\text{top}}(\mathbb{C}P^2) = 3$; see Rem. F.21): $\det(\mathcal{G} \otimes L_Y) = L_Y^{\otimes 3} = \mathcal{O}(9)$, so $a = N_{\text{gen}}\, q_1 = 9$ (see proof). The microsector twist bundle is $E(a, n) := \mathcal{O}(a) \oplus \mathcal{O}^{\oplus n}$ with cutoff the closed spin^c index $k_{\max} := \chi(X, E) = \chi(\mathcal{O}(a)) + n = \binom{a+2}{2} + n$. With $a = 9$ forced as above and n the SM matter-type count, the unique solution is $(a, n) = (9, 5)$ (the rival $(8, 15)$ is excluded structurally: $8 \neq N_{\text{gen}}\, q_1$ is not a determinant-line degree, and $n = 15 = 5 \times 3$ re-counts the three generations already consumed inside $\mathcal{O}(9)$):*

$$E = \mathcal{O}(9) \oplus \mathcal{O}^{\oplus 5}, \qquad \chi(E) = \chi(\mathcal{O}(9)) + 5 = 55 + 5 = 60.$$

Interpreting $n = 5$ as the five hypercharged chiral matter multiplet types per generation $\{Q, u^c, d^c, L, e^c\}$ fixes the decomposition.

Proof. With $a = 9$ fixed by the determinant-line lift (Lemma statement), $\chi(\mathcal{O}(9)) = \binom{11}{2} = 55$, and the five SM matter-type lines give $n = 5$, so $\chi(E) = 55 + 5 = 60$. The decomposition $(a, n) = (9, 5)$ is forced (not merely minimal-padding): $a = N_{\text{gen}}\, q_1 = 9$ is the determinant-line degree, and the determinant functor sends $\mathcal{O}(3)^{\oplus 3}$ ($\chi = 30$) to the tensor-cube line $\mathcal{O}(9)$ ($\chi = 55$), so the direct sum is not a rival. The rival $(8, 15)$ is excluded because $8 \neq N_{\text{gen}}\, q_1$ (no integer rank k gives $k \cdot 3 = 8$) and $15 = 5 \times 3$ double-counts the protected generations.

The physical interpretation of the two integers:

- $a = 9$: *Conditional on the fixed-kernel reading of the generation space* ($\mathcal{G} = \ker D_F$ of the single rigid vacuum operator, a fixed coefficient space; Remark F.12), the charged sector is $\det(\mathcal{G} \otimes L_Y) = \det(\mathcal{G}) \otimes L_Y^{\otimes \dim \mathcal{G}} = \mathcal{O}(3)^{\otimes 3} = \mathcal{O}(9)$. Note this determinant is the *algebraic* (Knudsen–Mumford) functor — an integer-degree line carrying no measure, metric, or Grassmann structure — so no "measure identification" premise enters at this step (cf. the two-layer resolution in Remark F.12). Here $\det(\mathcal{G}) \simeq \mathcal{O}$ holds *automatically*, with no curvature premise: $\mathcal{G}$ is the kernel of a *single fixed* elliptic operator (the vacuum is rigid — the moduli space is a point), hence a fixed 3-dimensional coefficient space $\mathbb{C}^3$ rather than a bundle over $\mathbb{C}P^2$, and $\det\big(\mathbb{C}^3 \otimes \mathcal{O}(3)\big) = (\Lambda^3\mathbb{C}^3) \otimes \mathcal{O}(3)^{\otimes 3} = \mathcal{O}(9)$ by one line of exterior algebra ($\Lambda^3\mathbb{C}^3$ is a constant line). Thus $a = N_{\text{gen}}\, q_1 = 3 \cdot 3 = 9$, α-free given the two discrete inputs. Spin^c integrality already makes $L_Y = \mathcal{O}(3)$ globally well-defined; the genuine fractional structure of $3Y$ is $\mathbb{Z}_2$ (which would give a square $\mathcal{O}(6)$), and the *triple* comes from $\text{rank}(\mathcal{G}) = N_{\text{gen}} = 3$ via the determinant functor.
- $n = 5$: The number of distinct hypercharged chiral multiplet types per generation in the minimal Standard Model: $\{Q, u^c, d^c, L, e^c\}$. (The right-handed neutrino ν_R has $Y = 0$ and does not contribute to the hypercharge-twist sector.)

□

Remark F.12 (Independence of the Derivation Chain). The logical structure of the derivation is:

$$\text{SM} \to q_1 = 3 \to a = 9 \to k_{\max} = 60 \to \alpha^{-1} = 137.036 \tag{F1}$$

Within the isotropy reading, α appears only at the **end** of this chain as an output, not as an input. The chain begins with Standard Model hypercharge assignments (which are fixed by experiment independently of α), proceeds through the electroweak identification and the conditional determinant-line count (Rem. F.10, Lemma F.11), and only produces the closed-form value of α via Chern-Simons quantization at $k_{\max} = 60$.

Inside the reading, then, the chain runs SM $\to$ topology $\to \alpha$ without using α, given the construction of the conditional count, including its rule that n counts the five hypercharged types (Rem. F.7). The choice between readings is where α enters: with the degree $a = N_{\text{gen}} q_1$ it excludes the reading with line-bundle doublets (Rem. F.10).

b. Status: derivation plus match. The above is an α-free chain whose logical form is: $k_{\max} = 60$ **follows from one integer derived under the electroweak identification and two inputs, and the closed form matches the measured fine-structure constant to** 21 **ppm from the integers alone; the last** 21 **ppm**

rests on the open bracket coefficient. The three entries are: $q_1 = 3$ (*derived* from the isotropy charge $6Y$ under that identification, Rem. F.10), $N_{\text{gen}} = 3$ (*input*, the observed family number, Rem. F.21), and the SM type count $n = 5$ (*input*, the hypercharged multiplet types). Given these, the determinant-line arithmetic $a = N_{\text{gen}} q_1 = 9$, $\chi(\mathcal{O}(9)) + 5 = 60$ is exact and rival-free within the conditional count of Lemma F.11 ($(8, 15)$ is construction-incoherent; the alternatives $q_1 \in \{1, 6\}$, which give $k_{\max} \in \{15, 195\}$, are excluded inside the isotropy reading by the isotropy charge and between readings by the measured α; the relation of the degree-zero summands to the hypercharge degrees is open, Rem. F.7). This is *not* a bare-$\mathbb{C}P^2$ topology theorem, and it does not by itself predict the value of α (which additionally requires the coupling-origin theorem). The question — *is the relevant microsector measure the fermionic Quillen determinant line, or the bosonic Gaussian determinant* $\det\{\}'(\mathcal{K})$ *of App. O?* — conflates two same-named objects. The *degree* $a = 9$ is the algebraic Knudsen–Mumford determinant functor, $\det(\mathcal{G} \otimes L_Y) = \Lambda^3\mathbb{C}^3 \otimes \mathcal{O}(3)^{\otimes 3} = \mathcal{O}(9)$ — an integer degree carrying no measure, metric, or Grassmann structure. The *suppression* α^{57} is the commuting complex-Gaussian ratio $\mathcal{Z}(\alpha^{-1})/\mathcal{Z}(1) = \alpha^{57}$ with $\det\{\}'(\mathcal{K})$ in the *denominator*, eigenvalue-cancelling (App. O). The fermionic (Berezin/Quillen norm-square) reading — determinant in the numerator, giving α^{-57} — is *excluded*, not merely disfavored: the fundamental fields of the master action are bosonic, Berezin–Toeplitz quantization of the even Kähler microsector yields CCR (not CAR) statistics, the 57 mode amplitudes are x-independent finite variables whereas every anticommuting variable of Z_{DFD} carries an $L^2(M, S_M)$ leg (type mismatch), and the sign of the observed hierarchy falsifies α^{-57}. The two layers are compatible and distinct: the algebraic line fixes the *count*, the bosonic Gaussian fixes the *suppression* — with the five-way factorization of Z_{DFD} a derived conditional lemma (see the QG partition-function theorem in the Extended Derivations, App. AH), unconditional in its Grassmann-assignment and ϕ_i-absence legs. Of the three entries, q_1 is derived given the electroweak identification; N_{gen} and the type count are inputs shared with the Standard Model, and no index on the internal space supplies N_{gen} (Rem. F.21). The status is: $k_{\max} = 60$ is derived from these entries within the conditional count of Lemma F.11. Within the isotropy reading the chain does not use α, and the empirical match, 21 ppm from the integers, is what excludes the reading with line-bundle doublets (Rem. F.10). *Closure of the reading question:* the rival evaluation-map reading is closed *exhaustively* — for every embedding of $\ker D_F = \text{span}\{|0\rangle, |20\rangle, |40\rangle\}$ (App. AH, microsector basis) into $H^0(\mathbb{C}P^2, \mathcal{O}(9) \oplus \mathcal{O}^{\oplus 5})$, the evaluation map either has constant rank 3, forcing a trivial $\mathcal{O}^{\oplus 3}$ subbundle and the determinant answer $a = 9$ *identically*, or drops rank on a nonempty degree-9 curve so that no rank-3 subbundle exists (dichotomy lemma, Extended Derivations App. AH); hence $a = 9$ in every well-defined reading, and the fixed-kernel conditionality reduces to its definitional content. The saturation variant of the rank-2 case reproduces the α-excluded $k_{\max} = 195$ alternative.

4. The Spin^c Dirac Index on $\mathbb{C}P^2$

a. Index formula. For a spin^c 4-manifold M with determinant line bundle L_{det}, twisted by a vector bundle V [130]:

$$\text{index}(D_V) = \int_M \text{ch}(V) \cdot e^{c_1(L_{\text{det}})/2} \cdot \hat{A}(M). \tag{F2}$$

b. Characteristic data for $\mathbb{C}P^2$.

- $c_1(T\mathbb{C}P^2) = 3H$, $c_2(T\mathbb{C}P^2) = 3H^2$
- Pontryagin class: $p_1 = c_1^2 - 2c_2 = 3H^2$
- $\hat{A}$-genus: $\hat{A}(\mathbb{C}P^2) = 1 - p_1/24 = 1 - H^2/8$
- Spin^c exponential: $e^{3H/2} = 1 + 3H/2 + 9H^2/8$

c. Index for the $SU(3)$ *instanton bundle.* Let E_3 be an $SU(3)$ instanton bundle with rank 3, $c_1(E_3) = 0$, and $c_2(E_3) = k_3 H^2$. Then:

$$\text{ch}(E_3) = 3 - k_3 H^2. \tag{F3}$$

Computing the index:

$$\begin{aligned} \text{index}(D_{E_3}) &= \int_{\mathbb{C}P^2} (3 - k_3 H^2)(1 + \tfrac{3H}{2} + \tfrac{9H^2}{8})(1 - \tfrac{H^2}{8}) \\ &= \left[\tfrac{27 - 8k_3}{8} - \tfrac{3}{8}\right] = 3 - k_3. \end{aligned} \tag{F4}$$

For $k_3 = 1$: index $= 2$ (integer, as required).

5. Generation Count and Flux-Product Rule

Theorem F.13 (Künneth Factorization [102])**.** *For a product manifold* $M_1 \times M_2$ *with product bundle* $E = E_1 \boxtimes E_2$*:*

$$\textit{index}(D_E^{M_1 \times M_2}) = \chi(M_1; E_1) \cdot \chi(M_2; E_2). \tag{F5}$$

Theorem F.14 (Spectral Flow on S^3 from Winding Number [103])**.** *For the Dirac operator on* S^3 *coupled along a gauge path of* $SU(2)$ *winding number* $k_2 \in \pi_3(SU(2)) = \mathbb{Z}$*, the* spectral flow *equals the winding:*

$$I_{S^3}(k_2) \;=\; \text{sf}\big(D_{S^3};\, g_{k_2}\big) \;=\; k_2. \tag{F6}$$

Remark F.15 (Correct index-theoretic home of $I_{S^3}(k_2)$)*.* Since S^3 is odd-dimensional, the *static* elliptic index vanishes identically and the round S^3 Dirac operator has *no* harmonic spinors (Lichnerowicz gap $|\lambda| \geq 3/2R$); $I_{S^3}(k_2)$ is therefore *not* a kernel dimension. Its rigorous content is the Atiyah–Patodi–Singer *spectral flow* along the degree-k_2 gauge path (equal to the index on the mapping torus $S^3 \times S^1$, $\int \text{ch}_2 = k_2$), equivalently the contact/CR *Toeplitz index* of the winding-k_2 symbol on the Hardy space of S^3 (Venugopalkrishna 1972; Boutet de Monvel

1979). Both formulations give exactly k_2; this theorem is used below only in that spectral-flow sense.

Remark F.16 (Quantum Level Shift). The factor $(k+2)$ appearing in the SU(2) Chern–Simons weight function $w(k) = \frac{2}{k+2}\sin^2\frac{\pi}{k+2}$ arises from the quantum (one-loop) level shift $k \to k + h^\vee$ where $h^\vee = 2$ is the dual Coxeter number for SU(2). This is a standard result in WZW/CS theory [132].

Definition F.17 (Generation Count)**.** Let $\mathcal{R}_{\rm SM} = \{Q_L, u_R, d_R, L_L, e_R\}$ be the chiral SM representations. The generation count is:

$$N_{\rm gen} := \gcd\{|\mathrm{index}(D_R)| : R \in \mathcal{R}_{\rm SM}\}. \tag{F7}$$

Theorem F.18 (Flux-product rule, a bookkeeping identity)**.** *For $\mathcal{M} = \mathbb{C}P^2 \times S^3$ with flux configuration (k_3, k_2, q_1):*

$$N_{gen} = |k_3 \cdot k_2 \cdot q_1|. \tag{F8}$$

Proof. By Künneth factorization, the index factors over the product. The S^3 factor contributes k_2 (Dirac index from winding number). On $\mathbb{C}P^2$, the index for a representation with $SU(3)$ dimension d_3 and hypercharge Y has the polynomial form:

$$I_{\mathbb{C}P^2}(d_3, k_3, Y) = d_3 \cdot [A(k_3) + B(k_3) \cdot q_1 Y + C \cdot (q_1 Y)^2]. \tag{F9}$$

The weighted hypercharge sum over one SM family vanishes (gravitational-$U(1)_Y$ anomaly cancellation):

$$\sum_R d_3(R) \cdot d_2(R) \cdot Y(R) = 1 + 2 - 1 - 1 - 1 = 0. \tag{F10}$$

This ensures consistent topological structure.

The rule keeps only the mixed term of the index polynomial, so it is bookkeeping within the stated construction: it reproduces the input $N_{\rm gen} = 3$ and does not derive it (Rem. F.21). □

6. Uniqueness of Minimal Flux

Theorem F.19 (Energy Minimization)**.** *Subject to the spin^c constraint $q_1 = 3$ and non-trivial gauge structure $(k_3, k_2 \geq 1)$, the unique global minimum of the Yang-Mills energy is $(k_3, k_2, q_1) = (1, 1, 3)$.*

Proof. The BPS energy bound is:

$$E_{\rm BPS} = 8\pi^2(\kappa_3|k_3| + \kappa_2|k_2| + \kappa_1|q_1|), \tag{F11}$$

where $\kappa_r > 0$. With $q_1 = 3$ fixed, $E_{\rm BPS}(k_3, k_2) = 8\pi^2(\kappa_3 k_3 + \kappa_2 k_2 + 3\kappa_1)$ is strictly increasing in both k_3 and k_2. The minimum over $\{k_3, k_2 \geq 1\}$ is achieved uniquely at $(k_3, k_2) = (1, 1)$. □

Corollary F.20 (Three Generations)**.** *For minimal flux $(k_3, k_2, q_1) = (1, 1, 3)$:*

$$N_{gen} = |1 \cdot 1 \cdot 3| = 3. \tag{F12}$$

Remark F.21 (Status: $N_{\rm gen} = 3$ is an input, not a derivation). The flux-product rule above is a *bookkeeping identity within the stated construction*, not an Atiyah–Singer index theorem: the rule retains only the mixed $d_3 d_2 Y$ term of the index polynomial, the S^3 factor enters as spectral flow (Rem. F.15), not a kernel, and the per-multiplet spin^c indices on $\mathbb{C}P^2$ at flux $(1, 1, 3)$ do not share a common factor of 3. An exhaustive search over all currently known index-theoretic routes — the plain elliptic index on $K = \mathbb{C}P^2 \times S^3$ (identically zero in odd dimension), the static kernel (zero, by Lichnerowicz on S^3), Berezin–Toeplitz/spectral-flow assemblies (which yield 10 or 60, never 3), the $\mathbb{Z}_6$ center-flux completion of $G_{\rm SM}$ (nonexistent on $\mathbb{C}P^2$: every SM multiplet is $\mathbb{Z}_6$-neutral), and the spin-$\mathbb{Z}_4$ $B-L$ structure of Sec. F 7 (per-multiplet indices $\{0, 0, 0, 1, 1, 1\}$, provably non-uniform for every flux) — fails to produce $N_{\rm gen} = 3$ from the geometry. Accordingly, $N_{\rm gen} = 3$ enters DFD as a **discrete input** fixed by observation, in the same epistemic class as the SM representation content itself — as it does in every extant theory. The numerical coincidence $N_{\rm gen} = \chi_{\rm top}(\mathbb{C}P^2) = 3$ is an identification, not an index theorem (the untwisted spin^c index on $\mathbb{C}P^2$ is $\mathrm{Td} = 1$), and the selections $k_3 = k_2 = 1$ rest on the BPS minimality assumption of Theorem F.19 ($k_r \geq 1$ posited). The input enters once, in the requirement $\chi_{\rm top}(M_c) = 3$ that selects $\mathbb{C}P^2$ (App. AB, axiom V5); the generation kernel, the exponent $57 = 60 - 3$ and the determinant-line degree use the same input. No index on the internal space supplies it: every elliptic differential operator on the odd-dimensional $\mathbb{C}P^2 \times S^3$ has index zero; on $\mathbb{C}P^2$ the Euler number 3 is the index of the de Rham operator, which counts harmonic forms rather than spinor zero modes, and the twisted Dirac indices equal to 3 belong to the isometry triplet, which carries electroweak charges that generations do not. A fourth sequential generation would falsify the identification.

7. Global Fermionic Consistency: the Spin-$\mathbb{Z}_4$ $B-L$ Structure and the Necessity of ν_R

Because $\mathbb{C}P^2$ is not spin ($w_2 = H \neq 0$), placing the full chiral fermion content on the internal geometry requires a gauge-sourced spin structure. This subsection records which structure works — and its physical consequence.

Theorem F.22 (Spin-$\mathbb{Z}_4$ $B-L$ consistency)**.** *In the all-left-handed convention, the SM$+\nu_R$ multiplets carry*

$$3(B-L) = \{Q : +1,\ u^c : -1,\ d^c : -1,\ L : -3,\ e^c : +3,\ \nu^c : +3\}, \tag{F13}$$

uniformly odd *across all six multiplet types. Consequently the structure* Spin $\times_{\mathbb{Z}_2} U(1)_{B-L}$ *(spin-$\mathbb{Z}_4$), with half-odd $B-L$ flux on $\mathbb{C}P^2$, renders every SM$+\nu_R$ multiplet simultaneously globally well-defined on the non-spin internal geometry. By contrast: (i) hypercharge cannot serve this role with one uniform structure if every multiplet is a line bundle, since the parities of $6Y = \{1, -4, 2, -3, 6, 0\}$ are mixed; when the weak doublets are rank-two isotropy*

bundles (Rem. F.10), every multiplet is consistent with the canonical spin^c structure, and the spin-$\mathbb{Z}_4$ structure is one of two consistent completions; (ii) the $\mathbb{Z}_6$ center of $G_{\rm SM} = (SU(3) \times SU(2) \times U(1))/\mathbb{Z}_6$ cannot, since every SM multiplet is $\mathbb{Z}_6$-neutral (which is precisely why the quotient is admissible), so center flux shifts twists only by integers — the wrong parity (cf. Tong, JHEP 07 (2017) 104).

Corollary F.23 (ν_R on the spin-$\mathbb{Z}_4$ completion)**.** *On the spin-$\mathbb{Z}_4$ $B-L$ background, cancellation of the $\mathbb{Z}_{16}$ global anomaly requires sixteen Weyl fermions per generation, so the right-handed neutrino must exist in each family (Wang–Wen, Phys. Rev. Research 2, 023356 (2020)). The requirement holds on this completion; on the canonical spin^c completion of the isotropy reading (Rem. F.10) it does not arise. DFD contains ν_R in either case, because its neutrino sector uses it: $M_R = \alpha^3 M_P$ (App. P), with the effective-mass prediction $m_\beta = 9.15\,\text{meV}$ (App. X).*

Remark F.24 ($B-L$ cannot replace hypercharge in the determinant-line chain). The $B-L$ line cannot substitute for L_Y in Lemma F.11: the $B-L$-only determinant-line chain gives $\chi(E) = 61$ (the ν_R, carrying $B-L \neq 0$ but $Y = 0$, enters the count), and integral hypercharge on the spin-$\mathbb{Z}_4$ background forces $q_1 \in 6\mathbb{Z}$, giving $k_{\max} = 195$ — never 60. Likewise no $B-L$ background flux renders the $q_1 = 3$ line-bundle twists uniformly admissible (the mixed $6Y$ parities obstruct this for every flux value). The $B-L$ structure is therefore one consistent completion, on which it mandates ν_R, while the hypercharge determinant line at the derived $q_1 = 3$ fixes the *microsector count*; the two play distinct, compatible roles.

8. The Self-Coupling Coefficient k_a (Model)

Methodological Note

The following is the physically motivated heuristic for the coefficient $k_a = 3/(8\alpha)$. The theorem form is stated in App. G (Thm G.1) and App. AP (Thm AP.19, which takes the frame ratio n_3/n_2 as an axiom: $k_a = (n_3/n_2)\,\alpha_M = \frac{3}{2} \cdot \frac{1}{4\alpha} = \frac{3}{8\alpha}$), so this section is retained as the heuristic, not as the primary justification.

a. Physical basis. The DFD scalar ψ couples to gauge fields through the physical metric of Eq. (12). The EM sector in the magnetic-dominated regime and the non-Abelian frame stiffnesses contribute to the ψ self-coupling.

b. Model for the coefficient. The ψ self-coupling receives contributions weighted by gauge group structure:

$$k_a = \frac{C_A(SU(n_3))}{C_A(SU(n_2))} \cdot \frac{1}{4\alpha} = \frac{n_3}{n_2} \cdot \frac{1}{4\alpha}. \tag{F14}$$

Under electromagnetic duality (Dirac quantization), $\alpha \to \alpha_M = 1/(4\alpha)$.

c. Result. With $(n_3, n_2) = (3, 2)$:

$$\boxed{k_a = \frac{3}{2} \cdot \frac{1}{4\alpha} = \frac{3}{8\alpha} \approx 51.4} \tag{F15}$$

d. Physical interpretation.

- Factor $n_3/n_2 = 3/2$: ratio of $SU(3)$ to $SU(2)$ Casimirs
- Factor $1/(4\alpha)$: magnetic coupling from duality

9. Frame Stiffness from Ricci Curvature

The relation $\kappa_r = n_r \kappa_0$ is graded a motivated assumption (§XVIII K); the argument below motivates it.

Theorem F.25 (Frame Stiffness from Geometry)**.** *Let gauge fields arise as Berry connections associated with the internal mode bundle $\mathcal{H}_{\rm int} = \mathbb{C}^3 \oplus \mathbb{C}^2 \oplus \mathbb{C}$ over spacetime (Sec. XVII B). The gauge sectors correspond to the unitary frame groups of the complex blocks $V_r \subset \mathcal{H}_{\rm int}$ of complex rank n_r; the geometry that enters is that of the projectivised fibre $P(V_r)$, not a splitting of $T(\mathbb{C}P^2 \times S^3)$ (which admits no $(3,2,1,1)$ partition, Lemma AB.13). Then the frame stiffness satisfies:*

$$\kappa_r = n_r \cdot \kappa_0. \tag{F16}$$

Proof. Step 1: The Berry connection A_r for sector r is valued in $su(n_r)$.

Step 2: The energy functional for Berry connection fluctuations:

$$E[A_r] = \frac{1}{2} \int \langle \delta\psi | \delta\psi \rangle, \tag{F17}$$

where the inner product uses the Fubini-Study metric on $P(V_r)$.

Step 3: For V_r of complex dimension n_r, the Ricci curvature of $\mathbb{C}P^{n_r-1}$ is:

$$R_{i\bar{j}} = n_r \cdot g^{\rm FS}_{i\bar{j}}. \tag{F18}$$

Step 4: The energy cost of a unit rotation scales with Ricci curvature: $E_{\rm rotation} \propto n_r$.

Step 5: Defining κ_r as this energy cost: $\kappa_r = n_r \kappa_0$. □ □

a. Explicit values.

Sector	Fibre $P(V_r)$	Ric factor	κ_r
SU(3)	$\mathbb{C}P^2$	3	$3\kappa_0$
SU(2)	$\mathbb{C}P^1$	2	$2\kappa_0$
U(1)	$\mathbb{C}P^0$	1	κ_0

10. Proton Stability

Theorem F.26 (Proton Stability)**.** *In gauge emergence with internal space $\mathbb{C}P^2 \times S^3$, the internal winding is*

conserved for configurations that stay continuous (Remark F.27); no local operator or perturbative quantum gravity correction changes it, and if baryon number is violated only by the electroweak anomaly, which changes it in steps of ±3, single-nucleon decay is forbidden.

Proof. Definition (soliton reading): Baryon number as winding. The S^3 internal space is fixed (not a Higgs vacuum manifold). Field configurations at fixed time define maps:

$$\phi : S^3_{\text{spatial}} \to S^3_{\text{internal}}, \quad B = 3n, \quad n = \deg(\phi) \in \mathbb{Z}. \tag{F19}$$

The topologically protected, quantized invariant is the winding degree $n = \deg(\phi) \in \pi_3(S^3) = \mathbb{Z}$. The physical proton is the minimal nonzero winding ($n = 1$); the factor 3 in "$B = 3n$" is the quark/colour bookkeeping tying one unit of internal winding to a three-quark baryon, and does *not* quantize the phenomenological baryon number in steps of three (single baryons are not forbidden). Recent RHIC measurements of baryon-number versus electric-charge stopping favour a single nonperturbative gluonic "baryon junction" as the carrier of B over additive valence-quark counting [133–135]; this is consistent with treating B as an attribute of the field configuration rather than an additive per-quark charge, though the QCD junction is a distinct object from the internal S^3 winding and the measurement does not itself test exact conservation.

Step 1 (Local operators): Any local operator $O(x)$ modifies ϕ in a bounded region. The winding number integral:

$$n = \frac{1}{24\pi^2} \int \epsilon^{ijk} \mathrm{Tr}(\phi^{-1}\partial_i\phi \cdot \phi^{-1}\partial_j\phi \cdot \phi^{-1}\partial_k\phi) \tag{F20}$$

is continuous and integer-valued. Local perturbations cannot change n.

Step 2 (No internal-*winding sphalerons):* In gauge emergence the internal S^3 is the *internal flavor space itself*—fixed geometry, not a dynamical vacuum manifold—so there is no internal-winding sphaleron. *This does* ***not*** *forbid the ordinary electroweak $SU(2)_L$ sphaleron*, which lives on the *spacetime* gauge bundle—a *distinct* S^3 that merely shares $\pi_3 = \mathbb{Z}$ with the internal one. The electroweak sphaleron changes $B + L$ in units of $\Delta(B + L) = \pm 6$ while preserving $B - L$, i.e. $\Delta B = \pm 3$; it is the standard process invoked for the $(B - L) \to B$ conversion (factor 28/79) in the baryogenesis/leptogenesis chain elsewhere in this work (the "shared-π_3 double-duty" theorem). The internal and electroweak S^3 are *different spaces*; only the former is frozen. If baryon number is violated only by the electroweak anomaly, it therefore changes only in steps of $\Delta B = \pm 3$, so single-nucleon decay, $\Delta B = \pm 1$, is forbidden.

Step 3 (Quantum gravity): The "folk theorem" (Misner, Banks, Seiberg) states quantum gravity violates global symmetries. On the soliton reading B is *not* a global symmetry but a topological winding number, and a gravitational violation would require topology change of the internal S^3, suppressed by:

$$\Gamma_{B\text{-violation}} \sim \exp\left(-\frac{\bar{M}_P^2 c^2 r_p^2}{\hbar^2}\right) \sim \exp\left(-10^{38}\right). \tag{F21}$$

Counted by quarks, as the selection rule of Step 2 counts it, baryon number is a global symmetry of the printed action. DFD's black holes radiate at Hawking's rate (Cor. AP.36), so a gravitational violation is not excluded; its rate is not computed, and a dimensional estimate gives $\tau_p \gtrsim 10^{42}$ yr, beyond Hyper-Kamiokande's reach. □

Remark F.27 (The soliton behind the winding). Step 1 holds for configurations that stay continuous. For the frame stiffness of §XVII D alone, a unit-winding texture of size L has energy proportional to L, so it can shrink at no cost (Derrick 1964), and under the corresponding evolution such textures can collapse and change their winding at a point in finite time (Shatah 1988; Turok and Spergel 1990). The hidden-local-symmetry form does not help: with $A = \Omega$ the curvature vanishes and every winding costs no energy. A quartic term with positive coefficient, for which a texture of size L costs energy proportional to $1/L$, removes the collapse; the energy then satisfies $E \geq 12\pi^2|B|$ in its natural units, a unit-winding minimum exists (Esteban 1986; Kapitanski and Ladyzhenskaya 1983), and the spherically symmetric one has $E = 1.2314 \times 12\pi^2$ with its two-derivative and quartic parts equal, as Derrick's identity requires (computed). The printed action does not contain such a term, so the soliton reading of the proton rests on a posit, not a derivation. The single-nucleon selection rule below does not use the soliton.

a. Falsifiability (a clean DFD-vs-GUT adjudicator). DFD gives $\Gamma = 0$ in every single-nucleon channel ($p \to e^+\pi^0$, $p \to \bar{\nu}K^+$): the electroweak anomaly changes baryon number only in steps of $\Delta B = \pm N_{\text{gen}} = \pm 3$, so the $\Delta B = \pm 1$ of single-nucleon decay is forbidden. It needs $N_{\text{gen}} = 3$ (input; Rem. F.21), not the value of $k_{\max}$, and holds if baryon number is violated only by the electroweak anomaly, not by a GUT $\Delta B = 1$ mediator. Every GUT, by contrast, predicts a positive single-nucleon rate (SU(5) $\sim 10^{30\text{–}31}$ yr, SO(10) $\sim 10^{34\text{–}36}$ yr). Hence the observation of *any* single-nucleon proton decay at Hyper-Kamiokande, DUNE, or JUNO falsifies gauge emergence, while a continued null result is what DFD shares with the Standard Model without a unified group. (The only B-violating channel the premise leaves is the multi-nucleon $\Delta B = 3$ electroweak sphaleron, unobservably suppressed.)

11. UV Robustness of Topological Results

Theorem F.28 (UV Stability)**.** *The integer results, the input $N_{\text{gen}} = 3$ and the winding n of continuous configurations, are stable against:*

1. *Higher-loop corrections*
2. *Non-perturbative effects*

3. Quantum gravity corrections (below Planck-scale topology change)

Proof sketch. Anomalies: The Adler-Bardeen theorem guarantees anomaly coefficients are one-loop exact. They depend on the representation content, an input shared with the Standard Model (Rem. F.3).

θ parameter: the tree-level $\theta = 0$ ($\theta_{\rm YM} = 0$ fixed by the spectral action given that nothing is added to it for the gauge fields; Theorem L.3) is not an integer invariant: it receives loop corrections at the Standard-Model level only (Appendix L).

Generation number: $N_{\rm gen} = 3$ is a discrete input identified with $\chi_{\rm top}(\mathbb{C}P^2) = 3$ (Rem. F.21); an integer input does not run.

Baryon number: Winding in $\pi_3(S^3) = \mathbb{Z}$ is topologically protected for continuous configurations; the electroweak anomaly changes baryon number only by $\Delta B = \pm 3$ (Thm. F.26, Step 2). □

a. Summary. Topological invariants don't receive radiative corrections because they are integers. The gauge emergence predictions are as robust as any result in quantum field theory.

12. Summary: Rigorous vs. Conjectural

a. The logical chain. The manifold is established by Thm. AB.1 (App. AB), which takes $N_{\rm gen} = 3$ as an input (axiom V5); the mode-bundle partition $(3, 2, 1)$ (Prop. F.1) enters as a dictionary entry, not a selector (App. AB, axiom V6). The chain below is bookkeeping: it reproduces the input $N_{\rm gen} = 3$ and does not derive it (Rem. F.21).

$$\boxed{\mathbb{C}P^2 \times S^3 \xrightarrow{\text{Rem. F.10}} q_1 = 3 \xrightarrow{\text{Thm. F.19}} (1,1,3) \xrightarrow{\text{Thm. F.18}} N_{\rm gen} = 3} \tag{F22}$$

Appendix G: Derivation of α-Relations from Gauge Emergence

This appendix provides the derivation of the DFD α-relation $k_a = 3/(8\alpha)$ from the gauge emergence framework established in Appendix F.

1. The Gauge-ψ Lagrangian

a. Auxiliary covariant metric for gauge calculations. For the gauge emergence derivations in this appendix, we employ an auxiliary 4D covariant metric that differs from the Gordon-style optical interval $d\tilde{s}^2 = -c^2dt^2/n^2 + d\mathbf{x}^2$ used in the main text [§II A]. The main-text interval has flat Euclidean spatial sections; here we use an exponent-doubled auxiliary ansatz:

$$\hat{g}_{\mu\nu} = \mathrm{diag}(-c^2 e^{-2\psi}, e^{2\psi}, e^{2\psi}, e^{2\psi}), \tag{G1}$$

with determinant $\sqrt{-\hat{g}} = c\, e^{2\psi}$ and inverse components $\hat{g}^{00} = -e^{2\psi}/c^2$, $\hat{g}^{ij} = e^{-2\psi}\delta^{ij}$.

Justification: This auxiliary metric $\hat{g}$ is a computational device for deriving gauge coupling relations in covariant form. The fundamental DFD arena remains flat $(\mathbb{R}^3, t)$ with the Gordon optical interval; gauge fields ultimately propagate on the same causal structure as light.

b. Yang-Mills action. For gauge sector $r \in \{3, 2, 1\}$:

$$S_{\rm YM}^{(r)} = -\int d^4x \frac{\sqrt{-\hat{g}}}{4g_r^2} \hat{g}^{\mu\alpha}\hat{g}^{\nu\beta} F_{\mu\nu}^{(r)} F_{\alpha\beta}^{(r)}. \tag{G2}$$

c. Electric-magnetic decomposition. Defining $E_i = F_{0i}$ and $B_i = \frac{1}{2}\epsilon_{ijk}F_{jk}$:

$$\mathcal{L}_{\rm YM}^{(r)} = \frac{e^{2\psi}}{2g_r^2 c} E_r^2 - \frac{c\, e^{-2\psi}}{2g_r^2} B_r^2. \tag{G3}$$

d. Variation with respect to ψ.

$$\frac{\partial \mathcal{L}_{\rm YM}^{(r)}}{\partial \psi} = \frac{e^{2\psi}}{g_r^2 c} E_r^2 + \frac{c\, e^{-2\psi}}{g_r^2} B_r^2. \tag{G4}$$

2. The Magnetically Dominated Regime

a. Physical setting. In astrophysical environments where DFD effects are observable (galactic outskirts), electromagnetic fields are magnetically dominated: $E^2 \ll c^2 B^2$.

b. Dominant contribution. In this regime, Eq. (G4) simplifies to:

$$\frac{\partial \mathcal{L}_{\rm YM}^{(r)}}{\partial \psi} \approx \frac{cB_r^2}{g_r^2}(1 - 2\psi). \tag{G5}$$

3. Frame Stiffness Structure

a. Frame stiffness from gauge emergence. From Appendix F, the gauge couplings arise from frame stiffnesses:

$$g_r^2 = \frac{M^2}{\kappa_r}, \qquad \kappa_r = \kappa_0 \cdot n_r, \tag{G6}$$

where M is the frame mass scale, κ_0 is a universal stiffness, and n_r is the block dimension.

For the $(3, 2, 1)$ partition: $n_3 = 3$, $n_2 = 2$, $n_1 = 1$.

4. Derivation of $k_a = 3/(8\alpha)$

Theorem G.1 (Self-Coupling Coefficient)**.** *In the gauge emergence framework with* $(3, 2, 1)$ *partition and magnetically dominated regime, the DFD self-coupling coefficient is:*

$$k_a = \frac{n_3}{n_2} \cdot \frac{1}{4\alpha} = \frac{3}{8\alpha} \approx 51.4. \tag{G7}$$

Proof. The proof proceeds in four steps.

Step 1 (Backbone-doorway structure): The gauge back-reaction on ψ is mediated by the SU(2) sector (the "doorway"), while the self-coupling strength is determined by

TABLE LXXIV. Status of gauge emergence results.

Result	Status	Method
$(3,2,1)$ minimal partition	Proposition	Explicit classification (dictionary entry)
Electroweak group $U(2)$	Identified	Isotropy group of $\mathbb{C}P^2$ (Rem. F.2)
Colour $SU(3)$, family content	Stated inputs	As in the Standard Model (Rem. F.3)
$SU(N)$ selection	Lemma	Lie algebra table
$q_1 = 3$	Derived, if identified	Faithful isotropy charge $6Y$ (Rem. F.10)
$N_{\text{gen}} = \lvert k_3 k_2 q_1 \rvert$	Bookkeeping rule	Thm. F.18, Rem. F.21
$(1,1,3)$ unique minimum	Theorem	Energy minimization
$N_{\text{gen}} = 3$	Stated input	Observed family number (Rem. F.21)
$\kappa_r = n_r \kappa_0$	Motivated assumption	Ricci curvature (Thm. F.25)
$\tau_p = \infty$	Conditional	Anomaly selection rule (Thm. F.26)
UV stability	Theorem	Adler-Bardeen + topology (Thm. F.28)
$k_a = 3/(8\alpha)$	Derived	Gauge emergence (App. G, App. AP)

the SU(3) sector (the "backbone"). The ratio of contributions is $n_3/n_2 = 3/2$.

Step 2 (Electromagnetic duality): In the magnetically dominated regime, the relevant coupling is the magnetic fine-structure constant:

$$\alpha_M = \frac{1}{4\alpha}, \tag{G8}$$

arising from Dirac quantization: $\alpha \cdot \alpha_M = 1/4$.

Step 3 (Combination): The self-coupling combines these factors:

$$k_a = \frac{n_3}{n_2} \cdot \alpha_M = \frac{3}{2} \cdot \frac{1}{4\alpha} = \frac{3}{8\alpha}. \tag{G9}$$

Step 4 (Numerical verification): With $\alpha \approx 1/137.036$:

$$k_a = \frac{3 \times 137.036}{8} = 51.39. \qquad \square \tag{G10}$$

□

a. Physical interpretation.

- The factor $3/2 = h^\vee(\mathrm{SU}(3))/h^\vee(\mathrm{SU}(2))$ is the ratio of dual Coxeter numbers.
- The factor $1/(4\alpha)$ reflects magnetic dominance in the ψ-gauge coupling.
- k_a measures how strongly ψ self-interacts through gauge field backreaction.

5. Strong CP Prediction

Theorem G.2 (Strong CP Suppression)**.** *In gauge emergence with internal space $\mathbb{C}P^2 \times S^3$ and minimal flux $(k_3, k_2, q_1) = (1,1,3)$, with $\theta_{\text{YM}} = 0$ fixed by the spectral action given that nothing is added to it for the gauge fields, and given Postulate Y.10:*

$$\bar{\theta} = 0 \quad \textit{(tree level; loop-induced} \lesssim 10^{-16}\textit{)}. \tag{G11}$$

Proof sketch. At tree level: The SU(3) gauge field is a Berry connection on $\mathbb{C}P^2$ with quantized instanton number $k_3 = 1$. Det-orthogonal mass matrices, positive on the branch of Postulate Y.10, give $\arg\det(M_u M_d) = 0$ (App. AO).

Anomaly: The CP mapping torus has dimension $\dim T_{\text{CP}} = \dim M + 1 = 8$ (even). Its fermion bundle is a graded Clifford module, so the Dirac operator is odd under chirality ($\Gamma D \Gamma^{-1} = -D$), forcing exact $\pm\lambda$ spectral pairing, and the product-background gap removes zero modes. Hence $\eta(D_{T_{\text{CP}}}) = 0$ and $A_{\text{CP}} = 1$ (Theorem L.3, Appendix L); loop corrections are bounded at the Standard-Model level. □

a. Falsifiability. Detection of QCD axions with coupling $g_{a\gamma\gamma}$ in the KSVZ/DFSZ range would falsify this prediction.

6. Derivation of $k_\alpha = \alpha^2/(2\pi)$

Proposition G.3 (Clock coupling coefficient (conditional))**.** *In DFD with gauge emergence, the species-dependent clock coupling coefficient is:*

$$k_\alpha = \frac{\alpha^2}{2\pi} \approx 8.5 \times 10^{-6}. \tag{G12}$$

Note: A derivation conditional on the one-gauge-vertex axiom, using the Schwinger mechanism, is given in Appendix P.

Proof. The proof proceeds in four steps.

Step 1 (Photon-ψ vertex): The photon propagator on the optical metric acquires ψ-dependence. At one loop, the photon-ψ vertex has strength:

$$\lambda_{\gamma\psi} = \frac{g^2}{8\pi^2} = \frac{4\pi\alpha}{8\pi^2} = \frac{\alpha}{2\pi}. \tag{G13}$$

Step 2 (Atomic energy structure): Atomic energy levels depend on the Coulomb interaction:

$$E_n \propto \alpha^2 \cdot (m_e c^2) \cdot f(n,l,j). \tag{G14}$$

Step 3 (ψ-modification): The ψ-modification of atomic levels:

$$\delta E_n = E_n \cdot S_A^\alpha \cdot \frac{\delta\alpha}{\alpha} \tag{G15}$$

where $\delta\alpha/\alpha = \lambda_{\gamma\psi} \cdot \alpha \cdot \psi = (\alpha^2/2\pi)\psi$.

Step 4 (Result):

$$k_\alpha = \frac{\alpha^2}{2\pi}. \qquad \square \tag{G16}$$

□

a. Extension to other gauge sectors. The formula generalizes to all gauge couplings:

$$k_i = \frac{\alpha_i^2}{2\pi}, \quad \alpha_i = \frac{g_i^2}{4\pi}. \tag{G17}$$

For the strong sector with $\alpha_s \approx 0.118$, under the same one-gauge-vertex axiom as k_α (App. P), so that k_s is a matching coefficient of the extended channel:

$$k_s = \frac{\alpha_s^2}{2\pi} \approx 2.2 \times 10^{-3}. \tag{G18}$$

This gives the nuclear clock enhancement factor:

$$|\mathcal{R}| = \frac{K_{\text{Th}}}{K_{\text{opt}}} \approx \frac{k_s S_{\text{Th}}^{\alpha_s}}{k_\alpha S_{\text{opt}}^{\alpha}}. \tag{G19}$$

7. Proton Stability Prediction

Theorem G.4 (Proton Stability)**.** *In gauge emergence with* $(3,2,1)$ *partition and internal space* $\mathbb{C}P^2 \times S^3$*, if baryon number is violated only by the electroweak anomaly:*

$$\tau_p = \infty \quad \textit{(stable at zero temperature).} \tag{G20}$$

Proof sketch. 1. In gauge emergence, there is no unified gauge group to break; gauge symmetries emerge from Berry connections.

2. No X, Y bosons from GUT symmetry breaking exist.

3. The electroweak anomaly changes B only by ± 3 (Thm. F.26); a single proton has no decay channel.

□

a. Contrast with GUTs.

Model	τ_p prediction
SU(5) GUT	10^{30-31} years
SO(10) GUT	10^{34-36} years
Gauge emergence	∞ (conditional)

b. Falsifiability. Observation of proton decay at *any* rate $\tau_p < 10^{40}$ years would falsify gauge emergence.

8. Summary of Results

a. The unified structure. All relations involve the $(3,2,1)$ block dimensions:

- a_0: factor $n_2 = 2$
- k_a: ratio $n_3/n_2 = 3/2$

TABLE LXXV. Complete α-relations with derivation status.

Relation	Formula	Value	Derivation
a_0	$2\sqrt{\alpha}\, cH_0^{\text{loc}}$	1.1966×10^{-10} m/s^2	$n_2 \cdot \sqrt{\alpha} \cdot cH_0^{\text{loc}}$; early clock 1.1208
k_α	$\alpha^2/(2\pi)$	8.5×10^{-6}	Prop. G.3 (cond.)
k_a	$3/(8\alpha)$	51.4	Theorem G.1
θ_{QCD}	—	0 (tree level)	Theorem G.2 ($\theta_{\text{YM}} = 0$ fixed by the spectral action given that nothing is added to it for the gauge fields)
τ_p	—	∞	Theorem G.4 (conditional)

And α appears in characteristic powers:

- a_0: $\sqrt{\alpha}$ (geometric mean)
- k_α: α^2 (one-loop)
- k_a: $1/\alpha$ (magnetic duality)

Appendix H: Higgs and Yukawa Sector from Gauge Emergence

This appendix treats the Higgs mechanism, Yukawa hierarchy, CKM mixing, and neutrino masses in the gauge emergence framework. The topological results of Appendix F determined representation content; here we address the mass spectrum.

1. Higgs Emergence from the $(3,2,1)$ Structure

Theorem H.1 (Higgs Doublet)**.** *The Standard Model Higgs doublet emerges as the off-diagonal connector between the* $\mathbb{C}^2$ *and* $\mathbb{C}^1$ *sectors of the* $(3,2,1)$ *partition.*

Proof. The internal Hilbert space $\mathcal{H}_{\text{int}} = \mathbb{C}^6$ with $(3,2,1)$ partition has density matrix:

$$\rho = \begin{pmatrix} \rho_3 & X_{32} & X_{31} \\ X_{32}^\dagger & \rho_2 & H \\ X_{31}^\dagger & H^\dagger & \rho_1 \end{pmatrix}. \tag{H1}$$

The off-diagonal block H connecting $\mathbb{C}^2$ and $\mathbb{C}^1$ is:

- A 2×1 complex matrix (2-component vector)
- Transforms as **2** under $SU(2)$ (from $\mathbb{C}^2$ index)
- Singlet under $SU(3)$ (no $\mathbb{C}^3$ involvement)
- Carries $U(1)_Y$ charge from relative phase

These are precisely the Higgs quantum numbers: $(1,2,+1/2)$. □

a. Higgs potential. The frame stiffness energy $\mathcal{L} = -\kappa_0 \psi \cdot S[\rho]$ expanded around the vacuum $\rho_0 = \frac{1}{3}\mathbf{1}_3 \oplus \frac{1}{2}\mathbf{1}_2 \oplus 1$ gives:

$$V(H) = -\mu^2 |H|^2 + \lambda |H|^4, \tag{H2}$$

where $\mu^2, \lambda > 0$ would be set by the frame stiffnesses. No printed form of $S[\rho]$ realizes this: neither the von Neumann entropy nor the purity gives a potential of this shape, so the potential, and with it the prefactor of v and the quartic, is not computed. The minimum at $\langle H \rangle = (0, v/\sqrt{2})^T$ breaks $SU(2) \times U(1)_Y \to U(1)_{\mathrm{EM}}$.

2. Zero-Mode Localization on $\mathbb{C}P^2$

a. Setup. The internal space $\mathcal{M} = \mathbb{C}P^2 \times S^3$ carries three generations, a stated input identified with $\chi_{\mathrm{top}}(\mathbb{C}P^2) = 3$ (App. F, Rem. F.21); with $SU(3)$ flux $k_3 = 1$ the three zero modes below are one per generation.

Proposition H.2 (Generation Localization)**.** *In homogeneous coordinates $[z_0 : z_1 : z_2]$ on $\mathbb{C}P^2$, the three generation wavefunctions are:*

$$\psi^{(1)} \propto z_0, \qquad \psi^{(2)} \propto z_1, \qquad \psi^{(3)} \propto z_2. \tag{H3}$$

These are localized at the three "vertices" $[1:0:0]$, $[0:1:0]$, $[0:0:1]$.

The wavefunctions are holomorphic sections of $\mathcal{O}(1)$ (the hyperplane bundle). The three vertices are distinct points of $\mathbb{C}P^2$, so this picture needs the electroweak group to act on the fibres of the twisting bundles and not by isometries of $\mathbb{C}P^2$, as the identification of Remark F.2 states; an isometric action of the isotropy group of a vertex would rotate the other two generations into each other.

3. Yukawa Hierarchy from Overlap Integrals

Theorem H.3 (Yukawa Couplings)**.** *The Yukawa coupling for generation n is:*

$$Y^{(n)} = g_Y \int_{\mathbb{C}P^2} \bar{\psi}^{(n)}(z) \cdot \phi_H(z) \cdot \psi^{(n)}(z)\, d\mu_{FS}, \tag{H4}$$

where $\phi_H(z)$ is the Higgs profile on $\mathbb{C}P^2$ and $d\mu_{FS}$ is the Fubini-Study measure.

a. The hierarchy mechanism. Assume the Higgs is localized near vertex 3 (the third generation):

$$|\phi_H(z)|^2 \propto e^{-|w|^2/\sigma^2} \tag{H5}$$

in affine coordinates $w = (z_0/z_2, z_1/z_2)$.

Theorem H.4 (Channel-Counting Derivation of ε_H)**.** *Let $\mathcal{H}_{\mathrm{ch}} \cong \mathbb{C}^{k_{\max}}$ be the channel Hilbert space with orthonormal basis $\{|k\rangle\}_{k=1}^{k_{\max}}$. Define the (normalized) Higgs connector state as the uniform superposition*

$$|H\rangle := \frac{1}{\sqrt{k_{\max}}} \sum_{k=1}^{k_{\max}} |k\rangle. \tag{H6}$$

Let a generation vertex i couple equally to a subset Γ_i of N_{gen} channels, with normalized state

$$|i\rangle := \frac{1}{\sqrt{N_{\mathrm{gen}}}} \sum_{k \in \Gamma_i} |k\rangle. \tag{H7}$$

Define the Higgs localization width by the squared overlap

$$\varepsilon_H := |\langle i|H\rangle|^2. \tag{H8}$$

Then

$$\boxed{\varepsilon_H = \frac{N_{\mathrm{gen}}}{k_{\max}} = \frac{3}{60} = 0.05} \tag{H9}$$

Proof. Using orthonormality of the channel basis,

$$\begin{aligned} \langle i|H\rangle &= \frac{1}{\sqrt{N_{\mathrm{gen}}}} \frac{1}{\sqrt{k_{\max}}} \sum_{k \in \Gamma_i} \langle k|k\rangle \\ &= \frac{N_{\mathrm{gen}}}{\sqrt{N_{\mathrm{gen}} \cdot k_{\max}}} = \sqrt{\frac{N_{\mathrm{gen}}}{k_{\max}}}. \end{aligned} \tag{H10}$$

Squaring yields $\varepsilon_H = N_{\mathrm{gen}}/k_{\max} = 3/60 = 0.05$. □

Lemma H.5 (Regular-Representation Forcing of the ε_H Premises)**.** *Suppose the channel Hilbert space carries the regular representation of the icosahedral group, $\mathcal{H}_{\mathrm{ch}} \cong \mathbb{C}[A_5]$, with basis $\{|g\rangle : g \in A_5\}$ and $k_{\max} = |A_5| = 60$ — the identification already used structurally by the finite Yukawa construction of Appendix Y, whose Higgs kernel $\widehat{H}_{\mathrm{ch}} = \sum_{g \in A_5} \varepsilon_H^{\ell(g)} |g\rangle\langle g|$ is written in a basis indexed by group elements. Then:*

(i) (Premise (a) forced.) *The trivial representation occurs in the regular representation with multiplicity exactly one (Schur: each irreducible ρ occurs with multiplicity $\dim \rho$), and its invariant line is spanned by $\sum_g |g\rangle$. Hence the unique A_5-invariant unit vector, up to phase, is the uniform superposition $|H\rangle = \frac{1}{\sqrt{60}} \sum_{g \in A_5} |g\rangle$: an A_5-invariant Higgs connector* must *be the uniform state assumed in Theorem H.4.*

(ii) (Premise (b) forced.) *Let $\mathbb{Z}_3 = \langle c \rangle \subset A_5$ be the generation subgroup (c an order-3 element, cf. the $\mathbb{Z}_3$ generation projectors of Appendix Y). A generation vertex supported on a $\mathbb{Z}_3$-coset orbit $\Gamma_i = \{g, cg, c^2 g\}$ is invariant under the $\mathbb{Z}_3$ left-translation action iff it is the equal-weight state $|i\rangle = \frac{1}{\sqrt{3}}\big(|g\rangle + |cg\rangle + |c^2 g\rangle\big)$: equal coupling to $N_{\mathrm{gen}} = 3$ channels is forced, not assumed.*

(iii) (Generation universality derived.) *The overlap $|\langle i|H\rangle|^2 = 3/60$ is independent of the coset representative g; all three generations share a single ε_H, a consequence here rather than an implicit assumption of the mass-hierarchy pattern.*

Hence $\varepsilon_H = N_{\text{gen}}/k_{\max} = 3/60$ *is forced given* $\mathcal{H}_{\text{ch}} \cong \mathbb{C}[A_5]$.

Proof. (i) Decompose $\mathbb{C}[A_5] = \bigoplus_\rho (\dim\rho)\,\rho$ over the five irreducibles of A_5 ($\dim\rho = 1,3,3,4,5$; $\sum_\rho (\dim\rho)^2 = 60$). The trivial irreducible appears with multiplicity $\dim(\mathbf{1}) = 1$, and its isotypic component is the line $\mathbb{C}\cdot\sum_g |g\rangle$. Any A_5-invariant vector lies in that line; normalizing gives $|H\rangle$. (ii) A state $\sum_{k=0}^{2} a_k\,|c^k g\rangle$ is invariant under left translation by c iff $a_0 = a_1 = a_2$; normalization fixes $a_k = 1/\sqrt{3}$ up to a common phase. (iii) Each of the three basis kets of $|i\rangle$ contributes $1/\sqrt{60}$ to the overlap: $\langle i|H\rangle = \frac{1}{\sqrt{3}}\cdot\frac{3}{\sqrt{60}} = \sqrt{3/60}$ for every representative g. Squaring gives $\varepsilon_H = 3/60 = 0.05$, coset-independent. □

Remark H.6 (Residual of the ε_H Closure). Lemma H.5 reduces both premises of Theorem H.4 to a single structural input: $\mathcal{H}_{\text{ch}} \cong \mathbb{C}[A_5]$. That identification is the one Appendix Y already builds its entire finite Yukawa operator on ($\dim\mathcal{H}_{\text{ch}} = 60 = |A_5|$, basis indexed by $g \in A_5$, Cayley connector, conjugacy-class species projectors); within the corpus it is used, not derived. Deriving $\mathbb{C}[A_5]$ from the $\mathbb{C}P^2 \times S^3$ harmonic spectrum is the remaining open item. The global Yukawa normalization g_Y (single anchor from m_τ/m_μ) remains a stated input, unchanged.

b. Significance. This derivation:

- Uses only fixed integers: $k_{\max} = 60$ (derived), $N_{\text{gen}} = 3$ (a stated input)
- Requires no mass data
- Is falsifiable: different microsector connectivity ⇒ different ε_H

c. Up/down distinction. Up-type quarks couple to $\tilde{H} = i\sigma_2 H^*$, down-type to H. A complex phase in $\phi_H(z)$ gives different effective couplings:

$$Y_u \neq Y_d \quad \text{(within each generation)}. \tag{H11}$$

4. CKM Mixing from Geometry

Theorem H.7 (CKM Structure)**.** *The CKM matrix arises from misalignment between up-type and down-type mass eigenbases:*

$$V_{CKM} = U_L^{u\dagger} U_L^{d}, \tag{H12}$$

where $U_L^{u,d}$ *diagonalize the respective Yukawa matrices.*

a. Small mixing from localization. Off-diagonal Yukawa elements require overlap of different generation wavefunctions:

$$M_{ij} \sim e^{-d_{ij}/\sigma}, \tag{H13}$$

where d_{ij} is the geodesic distance between vertices i and j on $\mathbb{C}P^2$.

b. CP violation. The CP-violating phase is supplied by Postulate Y.10 (App. AO).

The Jarlskog invariant:

$$J = \text{Im}(V_{us}V_{cb}V_{ub}^*V_{cs}^*) \sim 3\times 10^{-5}. \tag{H14}$$

5. Neutrino Masses from See-Saw

Theorem H.8 (Lepton Number Status)**.** *In gauge emergence:*

- *The internal winding n is conserved for continuous configurations (topological, $\pi_3(S^3) = \mathbb{Z}$); single-nucleon decay is forbidden if baryon number is violated only by the electroweak anomaly (Thm. F.26)*
- *Lepton number L is* ***not*** *topologically protected*
- *Majorana masses are allowed*

a. The see-saw mechanism. Right-handed neutrinos ν_R (gauge singlets) have Majorana mass. Appendix P identifies the scale by determinant scaling on the $N_{\text{gen}} = 3$ generation space:

$$M_R = M_P\alpha^3 = 4.74\times 10^{12}\ \text{GeV} \tag{H15}$$

(Theorem P.4). This is lower than the naive estimate $M_{\text{int}} \sim 10^{14}$–$10^{16}$ GeV but still in the see-saw regime.

The light neutrino mass:

$$m_\nu \approx \frac{M_D^2}{M_R} \sim \frac{(20\ \text{GeV})^2}{5\times 10^{12}\ \text{GeV}} \sim 0.1\ \text{eV}. \tag{H16}$$

b. Large PMNS mixing. Unlike CKM (small mixing), PMNS has large angles because:

- Charged leptons: localized like down quarks
- Neutrinos: right-handed ν_R have *different* localization pattern

The misalignment gives large θ_{12}, θ_{23} and small θ_{13}—qualitatively matching observation.

6. Summary of Mass Sector

a. Free parameters remaining.

1. $v = 246$ GeV (EW scale) — **Exponent derived:** $v = M_P\alpha^8\sqrt{2\pi} = 246.09$ GeV (the $\sqrt{2\pi}$ prefactor is fitted)
2. $\varepsilon_H = 0.05$ (Yukawa base) — **Derived:** $\varepsilon_H = N_{\text{gen}}/k_{\max} = 3/60$ (Theorem H.4)
3. $\lambda \sim 0.22$ (Cabibbo) — set by vertex distance d/σ (pattern, not derived)
4. $M_R = M_P\alpha^3 = 4.74\times 10^{12}$ GeV — **Identification** (Appendix P)

TABLE LXXVI. Standard Model mass sector from gauge emergence.

Feature	Mechanism	Status
Higgs doublet	$(2,1)$ off-diagonal	Theorem H.1
EWSB	Frame stiffness potential	Not computed
Mass hierarchy	Zero-mode localization	Theorem H.3
CKM structure	Overlap geometry	Theorem H.7
CP violation	Geometric CP offset (Postulate Y.10, App. AO)	Postulated
Neutrino mass	See-saw mechanism	Theorem H.8
PMNS mixing	Different localization	Explained

b. Predictions.

1. Neutrinos: Majorana (neutrinoless double beta decay)
2. Light neutrino masses: $\Sigma m_\nu = 61.5$ meV, $m_\beta = 9.15$ meV on the adopted branch (App. X)

Assessment (Complete Analysis)

The gauge emergence framework derives the Standard Model mass *structure*. The bare-parameter form of the hierarchy problem is eliminated: $v = M_P \alpha^8 \sqrt{2\pi}$ (exponent derived, prefactor fitted; radiative stability against the external matter loop remains the universal open problem — App. AH scope). The topological results (anomalies, the mass-hierarchy exponents) are derived, and α has a closed form; $N_{\rm gen} = 3$ is a discrete input.

Appendix I: Full Cluster Sample Analysis

This appendix provides the complete dataset and analysis for the galaxy cluster study presented in Section VII K.

1. Dataset Description

We analyze 16 galaxy clusters from published X-ray, optical, and lensing surveys; the four galaxy groups are compared on published group masses in the last subsection:

- **Relaxed clusters (10):** A1795, A2029, A478, A1413, A2204, Coma, Perseus, A383, A611, MS2137
- **Merging clusters (6):** Bullet (1E 0657-56), A520, El Gordo, MACS0025, A2744, RXJ1347
- **Galaxy groups (4):** Virgo, Fornax, NGC5044, NGC1550

a. Data sources.

- X-ray gas masses: Vikhlinin et al. (2006), Simionescu et al. (2011)
- Stellar masses: Gonzalez et al. (2013)
- Lensing masses: Clowe et al. (2006), Bradac et al. (2006, 2008), Merten et al. (2011), Jee et al. (2014), Kim et al. (2021)
- SZ masses: Planck Collaboration (2016)

2. Complete Results Table

Table LXXVII presents the complete analysis for the 16 clusters.

TABLE LXXVII. Complete cluster sample analysis with $\mu(x) = x/(1+x)$. Column $y \equiv g_N/a_0$ is the Newtonian baryonic acceleration in a_0 units; $\Psi = \nu(y) = (1+\sqrt{1+4/y})/2$ is the inverse-MOND boost satisfying $a\,\mu(a/a_0) = g_N$. Computed at $a_0 = 1.20 \times 10^{-10}$ m/s^2; the bound-matter $a_0 = 1.1966 \times 10^{-10}$ m/s^2 gives the same class means.

Cluster	$M_{\rm g}$	M_*	$M_{\rm b}$	$M_{\rm tot}$	r_{500}	y	Ψ	O/D
		($10^{14} M_\odot$)			(Mpc)			
Relaxed								
A1795	0.67	0.12	0.79	5.50	1.24	0.060	4.62	1.51
A2029	1.05	0.18	1.23	8.50	1.45	0.070	4.37	1.58
A478	0.85	0.14	0.99	6.80	1.35	0.063	4.51	1.52
A1413	0.62	0.11	0.73	5.20	1.20	0.059	4.65	1.53
A2204	0.95	0.16	1.11	7.80	1.40	0.066	4.43	1.59
Coma	0.85	0.15	1.00	7.00	1.40	0.059	4.64	1.51
Perseus	0.55	0.10	0.65	5.80	1.25	0.048	5.08	1.76
A383	0.32	0.06	0.38	2.80	0.95	0.048	5.08	1.47
A611	0.45	0.08	0.53	4.20	1.05	0.056	4.76	1.66
MS2137	0.38	0.07	0.45	3.50	1.00	0.052	4.93	1.60
Merging								
Bullet	1.15	0.20	1.35	11.5	1.50	0.070	4.32	1.97
A520	0.65	0.11	0.76	6.20	1.20	0.061	4.57	1.79
El Gordo	2.10	0.35	2.45	21.0	1.85	0.083	4.00	2.14
MACS0025	0.48	0.08	0.56	4.80	1.10	0.054	4.84	1.77
A2744	1.30	0.22	1.52	14.0	1.60	0.069	4.34	2.12
RXJ1347	1.40	0.24	1.64	15.0	1.65	0.070	4.31	2.12

3. Statistical Summary (the μ-Law Alone)

TABLE LXXVIII. Statistical summary by cluster type under the μ-law alone (no χ).

Category	N	Mean(Obs/DFD)	σ
Relaxed clusters	10	1.57	0.08
Merging clusters	6	1.99	0.16
All clusters	16	1.73	0.23

Note: Obs/DFD above one is the mass the μ-law does not supply from the baryons; it is the derived χ component (Conclusions of this appendix). With χ adding its Newtonian pull and the relaxed class carrying a hydrostatic bias $b = 0.21$, all sixteen clusters need $\chi = 4.5 \pm 0.6\, M_{\rm b}$, 0.84 ± 0.12 of the cosmic mix, at the bound-matter $a_0 = 1.1966 \times 10^{-10}$ m/s^2, as at the a_0 of the table.

4. Alternative $\mu_{1/2}$ Function

Note: This section is included for completeness. DFD does not adopt the $n = 0.5$ interpretation: the adopted $\mu(x) = x/(1+x)$ holds from galaxies to clusters, and the cluster shortfall under it is the χ component (Conclusions of this appendix).

Table LXXIX shows results using $\mu(x) = x/(1+\sqrt{x})^2$. Its larger boost at cluster accelerations absorbs into μ the mass that the derived χ supplies.

TABLE LXXIX. Cluster analysis with $\mu_{1/2}(x) = x/(1+\sqrt{x})^2$.

Cluster	$\Psi_{\rm obs}$	$\Psi_{\rm DFD}(n=0.5)$	Obs/DFD	Status
Relaxed Clusters				
A1795	7.0	6.68	1.04	✓
A2029	6.9	6.36	1.09	✓
A478	6.9	6.54	1.05	✓
A1413	7.1	6.71	1.06	✓
A2204	7.0	6.44	1.09	✓
Coma	7.0	6.70	1.05	✓
Perseus	8.9	7.24	1.23	✓
A383	7.5	7.24	1.03	✓
A611	7.9	6.85	1.16	✓
MS2137	7.9	7.05	1.11	✓
Merging Clusters				
Bullet	8.5	6.30	1.35	✓
A520	8.2	6.61	1.23	✓
El Gordo	8.6	5.90	1.45	✓
MACS0025	8.6	6.95	1.23	✓
A2744	9.2	6.32	1.46	✓
RXJ1347	9.1	6.29	1.45	✓
Summary				
Well-fit (0.7–1.5)			16/16	
Relaxed mean			1.09 ± 0.06	

5. Systematic Uncertainties

The analysis incorporates the following systematic uncertainties:

- **X-ray gas mass:** 10–15% calibration uncertainty
- **Stellar mass:** Factor 1.5–2 from IMF uncertainty (subdominant)
- **Total mass (hydrostatic):** 10–30% bias from non-thermal pressure
- **Total mass (lensing):** 5–10% from calibration and projection
- r_{500} **determination:** 5–10% from overdensity definition

Combined systematic uncertainty on Obs/DFD ratio: ∼20–30%.

6. Conclusions

a. Clusters need χ. Under the μ-law alone the sixteen clusters fall short of their measured masses: Obs/DFD $= 1.57 \pm 0.08$ (relaxed) and 1.99 ± 0.16 (merging) in Table LXXVII. The relaxed masses are hydrostatic X-ray masses and the merger masses are lensing masses; a hydrostatic bias $b = 0.21$ of the relaxed masses brings the two classes to the same ratio (the CCCP calibration measures $b = 0.22 \pm 0.07$, Hoekstra et al. 2015). The shortfall is the derived cold component χ (App. AV). If χ adds its Newtonian pull to the baryons' μ-law field, as App. GR prints the two channels, all sixteen clusters, with that bias and at the bound-matter a_0, need $\chi = 4.5 \pm 0.6\, M_{\rm b}$ inside r_{500}, 0.84 ± 0.12 of the cosmic mix $\Omega_\chi/\Omega_b \simeq 5.4$ (computed). Under the floor composition of App. AV gravity in clusters is Newtonian plus χ and the budget is the ΛCDM one: 1.28 ± 0.16 of the cosmic mix inside r_{500} at $b = 0$ and 1.51 ± 0.14 at $b = 0.21$, the usual baryon depletion inside r_{500} (computed). The amplitude follows from the derived abundance. Under the adopted rule of motion, the momentum-conserving energy of App. AV, cluster halos assemble as in ΛCDM (estimate), and ΛCDM hydrodynamics gives massive clusters a baryon depletion inside r_{500} of $Y_b = 0.85 \pm 0.03$, nearly independent of the physics included (Planelles et al. 2013); with $f_c = \omega_b/(\omega_b + \omega_\chi) = 0.157$ this puts χ inside r_{500} at $(1 - Y_b f_c)/[Y_b(1 - f_c)] = 1.21 \pm 0.05$ of the cosmic mix (estimate). The sixteen clusters give 1.28 ± 0.04 with no hydrostatic bias, which cool-core clusters show (Mahdavi et al. 2013), and 1.51 ± 0.04 with $b = 0.21$ (errors of the mean); with the calibration uncertainties of the gas, stellar and lensing masses their measured masses are 1.10 (0.97–1.23) and 1.30 (1.13–1.47) times the predicted ones (computed). The relaxed and merging classes differ by a factor 1.18 in baryon fraction, which a hydrostatic bias of 0.15 or merger masses 15% high would remove. χ boosted like the baryons would over-predict these masses 1.43-fold (computed). The required χ peaks at 0.15–$0.3\, r_{500}$, more concentrated than the gas, as cold dark matter is (computed).

b. The five-factor correction stack does not close the gap. A no-χ closure by five correction factors, $C_i = B_i\, J_{{\rm PDE},i}\, T_i\, M_i\, P_i$ (Eq. (200)), is not supported (computed; next subsection): the baryonic-completeness factor B sums to 1.26 on its own item list, not 1.30–1.45, and to 0.96–1.10 for the items that lie inside r_{500}; the substructure factor is real, but for the baryonic substructure

that the μ-law responds to it is $J_{\rm PDE} \simeq 1.04$; the temperature factor T absorbs the relaxed/merging split, which is the hydrostatic bias above; the merger factor M is applied to lensing masses, which carry no hydrostatic nonequilibrium; and the projection factor $P > 1$ has the wrong sign for lensing masses, which simulations find biased low. A first-principles account awaits a structure-formation run under the adopted momentum-conserving energy (App. AV) and a cluster-by-cluster nonlinear DFD hydrodynamic and lensing solver that includes χ.

7. The Five Correction Factors, Examined

a. Baryonic completeness, B. The literature items offered for missing cluster baryons are the warm-hot intergalactic medium, ∼10% of the gas mass [136, 137]; clumping and missed diffuse gas, net ∼5% of the gas [138]; intracluster light, ∼25% of the stellar mass [139, 140]; hot gas beyond r_{500}, ∼10% of the gas [141]; and a bottom-heavy IMF in cluster ellipticals, ∼10% of the stars [142]. Together they give $B = 1.26$, not 1.30–1.45. The warm-hot medium and the gas beyond r_{500} lie outside the aperture in which the masses are compared; the items that apply inside r_{500} give $B = 0.96$–1.10 (computed).

b. Nonlinear substructure averaging, $J_{\rm PDE} = 1 + 0.39\, f_{\rm sub}$. A direct 3D nonlinear AQUAL/DFD solver (Brada-Milgrom 1995 method, face-centered μ discretization, validated against algebraic-MOND for spherical NFW within 1%) gives:

$$J_{\rm PDE}(f_{\rm sub}) \simeq 1.00 + 0.39\, f_{\rm sub}, \qquad J_{\rm PDE} \simeq 1.07\text{–}1.12 \text{ for } f_{\rm sub} = 0.15\text{–}0.30. \tag{I1}$$

The mechanism is real: the gas-weighted enhancement in the diffuse intracluster medium exceeds the smooth-cluster mean-field value because mass redistribution into clumps reduces the smooth-component gradient at gas positions, and the slope is robust across cluster mass ($M_{200} \in [3, 12] \times 10^{14}\, M_\odot$), subhalo number ($N_{\rm sub} = 50$–$200$), and subhalo size ($r_{\rm sub} = 30$–$100$ kpc). The μ-law responds to the baryons, however, so $f_{\rm sub}$ is the member galaxies' share of the baryons, $\simeq 0.10$, which gives $J_{\rm PDE} \simeq 1.04$ (computed).

c. Temperature factor, $T = 1 + 0.04(T_X/{\rm keV} - 7)$. T spans 0.90–1.30, but a 10–30% temperature-calibration error moves an X-ray gas mass by only 2–7% ($M_{\rm gas} \propto T^{1/4}$ in the soft band) and a lensing mass not at all. Its correlation with the raw Obs/DFD ($r = 0.77$ over all sixteen) comes from the merger flag ($r = 0.87$), not from temperature within a class ($r = 0.01$ among the relaxed clusters). T therefore absorbs the relaxed/merging split, which is the hydrostatic mass bias: the relaxed masses are hydrostatic X-ray masses, the six merger masses are lensing masses (Clowe et al. 2006; Bradač et al. 2008; Merten et al. 2011; Jee et al. 2014), and $b = 0.21$ equalizes the two classes (WtG $1-b = 0.688 \pm 0.072$, von der Linden et al. 2014; CCCP 0.78 ± 0.07, Hoekstra et al. 2015; computed). SZ-derived masses, which do not depend on the X-ray temperature, exceed X-ray inferences for hot clusters by ∼20% [143, 144], consistent with a hydrostatic bias of that size.

d. Merger factor, M. M is sized by the non-thermal-pressure envelope of merger simulations (Nelson et al. 2014), a bias of hydrostatic masses; the six merger masses are lensing masses, to which it does not apply. Whether a ψ field that has not equilibrated on the merger timescale changes the DFD prediction for mergers is not computed.

e. Projection factor, P. For the sky-plane lensing mergers the simulation literature finds NFW-fit weak-lensing masses biased *low* by 5–10% on average (Becker & Kravtsov 2011; Rasia et al. 2012), so a projection correction raises those masses: $P > 1$ has the wrong sign.

The stack therefore does not close the shortfall of Table LXXVII; the clusters need χ (Conclusions above). Evaluating the derived $a_0(z) = 2\sqrt{\alpha}\, c\, H(z)$ at each cluster's redshift, rather than a_0 at $z = 0$, raises the boost of the higher-redshift systems and lowers their ratios (El Gordo, at $z = 0.87$, by about 20%), so it bears on the relaxed/merging split and on the bias inferred from it; it is an open consistency item of this table under the additive composition. Under the floor composition clusters are Newtonian plus χ, and a_0 drops out of their budget.

8. Galaxy Groups

On published X-ray masses the μ-law falls short of galaxy groups as it does of clusters. At the bound-matter $a_0 = 1.1966 \times 10^{-10}$ m/s^2, with distances computed with $H_0^{\rm loc}$ and stellar masses estimated from K-band light or from published stellar-fraction relations (computed on published inputs):

- **Sun et al. (2009), 23 Chandra groups:** median Obs/DFD = 1.22–1.36 at r_{500} (the range spans two stellar-mass calibrations), and 1.76–2.30 at r_{2500}, none below 1.
- **Gastaldello et al. (2007), 16 groups:** median Obs/DFD = 1.79 at the outermost measured overdensity; 15 of the 16 lie above 1, the exception being the disturbed group RGH80.
- **Virgo, Fornax, NGC 5044, NGC 1550:** Virgo 1.19–1.48 at $r_{500} = 663$ kpc (Simionescu et al. 2017); Fornax 2.7–4.0 at 19 kpc on its hydrostatic mass (Su et al. 2017) and 1.02–1.95 at 393 kpc; NGC 5044 1.54–1.76 at r_{1250} and NGC 1550 1.77–2.01 at r_{2500} (Gastaldello et al. 2007), and 1.12–1.32 and 0.89–1.08 at r_{500} on extrapolated profiles.

The result is set by the groups' measured baryon fractions, $f_{\rm gas} = 0.05$–0.11 at r_{500} (median 0.08) plus 0.02–0.11 in stars (Sun et al. 2009), which the μ-law boost $\nu \simeq 6$–7 does not lift to the measured masses. A MOND analysis of X-ray groups with the same $\mu(x) = x/(1+x)$ likewise finds 60–80% of the dynamical mass at the last measured radius unaccounted for by the baryons [54]. The shortfall

is the derived χ, as in clusters: under the floor composition of App. AV, 20 to 22 of the 23 groups of Sun et al. are Newtonian plus χ inside r_{500}, at 1.2–1.7 of the cosmic mix (the clusters above: 1.28–1.51); if χ adds its Newtonian pull the budget is 0.2–0.5 of the cosmic mix (computed; the stellar masses are estimates). None of the four named groups lies inside a larger bound region, so the Rest-Mass Channel's bound-system confinement gives them almost no external field from their neighbours (App. GR, Remark GR.12), and none is needed.

Appendix J: Derivation of the ψ-CMB Solution

This appendix gives the analytic baryon-loading calculation of the peak ratio $R \approx 2.34$. The global ψ-lensing derivation of the peak *location* in §J 5 is not a DFD prediction: exact conformal invariance and the homogeneous-mode theorem (App. ZS) rule out that mechanism. The observable holds on the measured-clock forward solution: $100\theta_* = 1.04110$ and $\ell_1 \simeq 220.4$, with no global screen.

1. The ψ-Acoustic Oscillator

a. Setup. Consider a baryon-photon fluid in ψ-gravity. The temperature perturbation $\Theta \equiv \delta T/T$ obeys:

$$\ddot{\Theta} + c_s^2(\psi)k^2\Theta = -\frac{k^2}{1+R_b}\Phi_\psi, \tag{J1}$$

where:

- $c_s(\psi) = c(\psi)/\sqrt{3}$ is the sound speed with $c(\psi) = c_0 e^{-\psi}$
- $R_b = 3\rho_b/(4\rho_\gamma) \approx 0.6$ is the baryon-to-photon density ratio
- $\Phi_\psi = \Phi/\mu(x)$ is the ψ-enhanced gravitational potential

b. Solution structure. The general solution has the form:

$$\Theta(k,\tau) = A(k)\cos(kr_s) + B(k)\sin(kr_s) + (\text{driving term}), \tag{J2}$$

where $r_s = \int c_s(\psi)\, d\tau$ is the sound horizon.

c. Peak/trough pattern.

- Odd peaks ($n = 1, 3, 5, \ldots$): compressions (maxima of $|\Theta|$)
- Even peaks ($n = 2, 4, 6, \ldots$): rarefactions (maxima of $|\Theta|$, with Θ of opposite sign)

In standard cosmology, baryon loading causes compressions to be enhanced relative to rarefactions, producing the odd/even asymmetry.

2. Peak Height Asymmetry

a. The asymmetry factor. The ratio of odd to even peak heights is determined by the asymmetry factor A:

$$\frac{H_{\text{odd}}}{H_{\text{even}}} = \left(\frac{1+A}{1-A}\right)^2. \tag{J3}$$

b. Factor decomposition. We decompose A into four physically distinct contributions:

$$A = f_{\text{baryon}} \times f_{\text{ISW}} \times f_{\text{vis}} \times f_{\text{Dop}}. \tag{J4}$$

a. Baryon Loading Factor f_{baryon}

The baryon-photon oscillator with baryon loading R_b produces asymmetry:

$$f_{\text{baryon}} = \frac{R_b}{\sqrt{1+R_b}}. \tag{J5}$$

a. Numerical value. With $R_b = 0.6$ (from BBN):

$$f_{\text{baryon}} = \frac{0.6}{\sqrt{1.6}} = \frac{0.6}{1.265} = 0.474. \tag{J6}$$

b. Integrated Sachs-Wolfe Factor f_{ISW}

The observed temperature perturbation includes the Sachs-Wolfe and integrated Sachs-Wolfe terms:

$$\frac{\Delta T}{T} = \Theta + \Phi + 2\int \dot{\Phi}\, d\tau. \tag{J7}$$

a. Cancellation. The SW term (Φ) and ISW term ($2\int \dot{\Phi}\, d\tau$) partially cancel. This cancellation is taken to be approximately 50%:

$$f_{\text{ISW}} \approx 0.50. \tag{J8}$$

This value is constrained to be $\mathcal{O}(0.5)$ by physical considerations.

c. Visibility Function Factor f_{vis}

Recombination is not instantaneous. The visibility function $g(\tau) = \dot{\tau}_c e^{-\tau_c}$ has finite width $\Delta\tau$.

a. Effect on asymmetry. Finite-width recombination smears out the sharp features in the angular power spectrum. The effect on the asymmetry is:

$$f_{\text{vis}} = \text{sinc}(\pi\Delta\tau/\tau_*) \approx 1 - \frac{\pi^2}{6}\left(\frac{\Delta\tau}{\tau_*}\right)^2. \tag{J9}$$

b. Numerical value. With $\Delta\tau/\tau_* \sim 0.1$:

$$f_{\text{vis}} \approx 1 - 0.02 = 0.98. \tag{J10}$$

d. Doppler Factor $f_{\rm Dop}$

The Doppler contribution from baryon velocity perturbations is:

$$\Theta_{\rm Dop} = \hat{n} \cdot \mathbf{v}_b, \tag{J11}$$

where $\hat{n}$ is the line-of-sight direction.

a. Effect on asymmetry. The Doppler term is 90° out of phase with the acoustic term. When projected onto the line of sight and averaged, this reduces the effective asymmetry:

$$f_{\rm Dop} \approx 0.90. \tag{J12}$$

e. Total Asymmetry

Combining all factors:

$$A = 0.474 \times 0.50 \times 0.98 \times 0.90 = 0.209. \tag{J13}$$

3. Peak Ratio Derivation

a. Definition. The peak ratio is:

$$R \equiv \frac{H_1}{H_2} = \frac{\text{(first peak height)}}{\text{(second peak height)}}. \tag{J14}$$

b. Relation to asymmetry. For the angular power spectrum C_ℓ, the peak heights scale as:

$$H_n \propto \left[(1 + (-1)^{n+1} A)\right]^2. \tag{J15}$$

Hence:

$$R = \frac{(1+A)^2}{(1-A)^2} = \left(\frac{1+A}{1-A}\right)^2. \tag{J16}$$

c. Result. With $A = 0.209$:

$$\boxed{R = \left(\frac{1.209}{0.791}\right)^2 = (1.528)^2 = 2.34} \tag{J17}$$

d. Comparison with observation. Planck's best fit gives $R \approx 2.21$ ($[H_1, H_2, H_3] \propto [1, 0.45, 0.44]$, §J 9); the analytic value lies 6% above it, while the full spectrum of the derived χ-matter field, run with CAMB on the measured clock, gives $H_1/H_2 = 2.20$ ($H_2/H_1 = 0.4545$, $+0.5\sigma$; Thm. AV.31).

4. Why the $1/\mu$ Enhancement Cancels

a. Mechanism. In ψ-gravity, the driving term is enhanced: $\Phi_\psi = \Phi/\mu$. But this enhancement affects *both* odd and even peaks equally.

b. Mathematical demonstration. The acoustic equation (J1) has driving term:

$$F(k) = -\frac{k^2}{1+R_b}\Phi_\psi = -\frac{k^2}{1+R_b}\frac{\Phi}{\mu}. \tag{J18}$$

The oscillation amplitude scales as:

$$|\Theta| \propto \frac{|F|}{c_s^2 k^2} \propto \frac{|\Phi|/\mu}{c_s^2} \propto \frac{1}{\mu}. \tag{J19}$$

All peaks (odd and even) are enhanced by $1/\mu$. In the ratio:

$$R = \frac{H_1}{H_2} = \frac{|\Theta_{\rm odd}|^2}{|\Theta_{\rm even}|^2} \propto \frac{(1/\mu)^2}{(1/\mu)^2} = 1 \times \text{(baryon physics)}. \tag{J20}$$

The μ-enhancement drops out of the ratio. What survives in this analytic estimate is the baryon loading factor, which depends only on R_b, a quantity fixed by BBN.

The peak *ratio* needs no postulated CDM particle, but it does need a cold clustering component: CAMB with baryons alone gives $H_2/H_1 = 0.39$ against Planck's 0.45 (Thm. AV.31). That component, which also sets the third-peak *height*, is the derived χ-matter field (App. AV), not a postulated WIMP.

5. The ψ-lensing peak-location construction (not a DFD prediction)

Status. Every equation in this subsection that maps 297 → 220 with $\Delta\psi = 0.30$ belongs to the excluded global-screen construction and is not a DFD prediction. It must not be used to shift θ_*, r_s, D_A, or H_0. Local and anisotropic lensing remain separately testable and are not covered by this notice.

a. The historical problem. Standard GR calculations without CDM give $\ell_1 \approx 297$, not the observed $\ell_1 \approx 220$. This has been cited as "proof" that dark matter is required.

b. The construction. This argument assumes GR propagation with fixed c and straight-line photon paths. In ψ-physics, light travels through a medium with varying refractive index $n = e^\psi$, producing gradient-index (GRIN) optics effects.

a. Gradient-Index Optics

a. Basic physics. In a medium with spatially varying $n(\mathbf{x})$, light rays follow curved paths according to Fermat's principle. For a gradient ∇n, rays bend toward regions of higher n.

b. Angular magnification. For a GRIN lens with n varying along the line of sight:

$$\frac{\theta_{\rm obs}}{\theta_{\rm emit}} = \frac{n_{\rm emit}}{n_{\rm obs}}. \tag{J21}$$

If $n_{\rm emit} > n_{\rm obs}$ (higher n at source):

- $\theta_{\rm obs} > \theta_{\rm emit}$: angular scales are *magnified*
- Observed ℓ is *smaller* than "true" ℓ (since $\ell \propto 1/\theta$)

b. Application to CMB

a. ψ-gradient. With $n = e^{\psi}$, the angular scaling becomes:

$$\frac{\theta_{\rm obs}}{\theta_{\rm emit}} = e^{\psi_{\rm CMB} - \psi_{\rm here}} = e^{\Delta\psi}. \tag{J22}$$

b. Peak location relation.

$$\ell_{\rm obs} = \ell_{\rm true} \times \frac{\theta_{\rm true}}{\theta_{\rm obs}} = \ell_{\rm true} \times e^{-\Delta\psi}. \tag{J23}$$

c. Required gradient. To obtain $\ell_{\rm obs} = 220$ from $\ell_{\rm true} = 297$:

$$220 = 297 \times e^{-\Delta\psi}, \tag{J24}$$

$$e^{-\Delta\psi} = 220/297 = 0.74, \tag{J25}$$

$$\Delta\psi = -\ln(0.74) = 0.30. \tag{J26}$$

d. Physical interpretation. $\Delta\psi = \psi_{\rm CMB} - \psi_{\rm here} = 0.30$ means:

- ψ was 0.30 higher at CMB than today
- $n_{\rm CMB}/n_{\rm here} = e^{0.30} = 1.35$ (35% higher refractive index)
- $c_{\rm CMB}/c_{\rm here} = e^{-0.30} = 0.74$ (26% slower light speed)

This is a *modest* gradient—not fine-tuned.

6. Consistency Checks

a. Self-consistency of the $\Delta\psi = 0.30$ construction (§J 5; not a DFD prediction).

1. **α-variation bounds.** With $\alpha(\psi) = \alpha_0(1 + k_\alpha\psi)$ and $k_\alpha = \alpha^2/(2\pi) \approx 8.5 \times 10^{-6}$ (Sec. VIII C):

$$\frac{\Delta\alpha}{\alpha} = k_\alpha \Delta\psi \approx 8.5 \times 10^{-6} \times 0.30 \approx 2.5 \times 10^{-6}. \tag{J27}$$

   This is $\sim$ 2.5 ppm—well within observational bounds. The quasar α-variation literature constrains $|\Delta\alpha/\alpha| \lesssim 10^{-5}$ at $z \sim 2$–3, and CMB constraints are $|\Delta\alpha/\alpha| \lesssim 10^{-3}$. The construction satisfies both.

   Note: The coupling $k_\alpha = \alpha^2/(2\pi)$ governs electromagnetic variation; this is distinct from the acceleration coupling $k_a = 3/(8\alpha) \approx 51$ that appears in galactic dynamics.

2. **BBN compatibility.** BBN occurs at $T \sim 1$ MeV, much earlier than CMB ($T \sim 0.3$ eV). If ψ-evolution is monotonic, $\Delta\psi_{\rm BBN}$ could be larger, but BBN physics depends primarily on nuclear rates, not optical effects. The constraint is on $\alpha_{\rm BBN}$, which can accommodate $\mathcal{O}(10\%)$ variations.

3. **Late-time ψ.** Today, $\psi_{\rm here} \equiv 0$ by convention. Local physics is unaffected by the absolute value of ψ—only gradients matter.

7. Comparison with ΛCDM

a. Feature comparison between ΛCDM and ψ-Cosmology.

Feature	ΛCDM	ψ-Cosmology
Peak ratio R	CDM-driven (Ω_c)	Baryon loading (R_b) and χ-matter
Peak location ℓ_1	GR distances (with CDM)	measured-clock no-screen forward solution

b. Key difference. ΛCDM introduces dark matter *particles* to explain the CMB. DFD explains the same observations using ψ-physics:

- Peak ratio: baryon loading (same R_b from BBN) with the derived χ-matter
- Peak location: measured-clock no-screen forward solution

The peak-ratio result introduces no fitted particle. The separately derived χ carrier supplies the primordial cold-clustering channel required by the higher-peak heights.

8. Falsifiable Predictions

The ψ-CMB solution makes specific predictions beyond the peak structure:

1. **Distance duality consistency.** Etherington's reciprocity holds exactly in DFD's optical metric:

$$\frac{D_L}{(1+z)^2 D_A} = 1. \tag{J28}$$

   Any common screening of D_L and D_A cancels in the ratio. Any detected violation would falsify DFD's single-metric framework.

2. **Polarization consistency.** Local/inhomogeneous ψ lensing should affect E-mode and B-mode polarization consistently. It is not a global peak-location map.

3. **Higher peaks.** The third peak and beyond follow the same frozen-input acoustic forward solution; their heights test the derived χ carrier and the

adopted rest-mass clustering channel, not a global ψ-lensing shift.

a. Ultimate test. The current global test is the frozen-input acoustic forward calculation: $100\theta_*$ and the peak heights must remain consistent without a mean $\Delta\psi$ screen. The distinct local/inhomogeneous test is a positive, mean-subtracted cross-correlation with foreground structure; it does not permit a global peak relocation.

b. Status (resolved by the derived χ field): the third-peak height. The derivations above give the analytic estimate $H_1/H_2 \approx 2.34$ of the odd/even peak *ratio* (from the baryon loading R_b, which is BBN-fixed) and the first-peak *location* $\ell_1 \approx 220$. They do *not* fix the absolute third-peak *height*. The gravity-sector driving indeed "cancels in ratios" (§XVI C), but that is precisely why this evades the height problem rather than solving it: in ΛCDM the observed $H_3/H_1 \approx 0.44$ ($H_3/H_2 \approx 1.0$, Planck) is set by the sustained gravitational potential wells of a *pressureless component that clusters at* $z \sim 1100$. Radiation driving plus baryon loading alone *collapse* the third peak — a linearized photon-baryon acoustic solver (dynamical Newtonian-gauge potential + Silk damping) gives $H_3/H_1 \sim 0.1$, far below the observed ≈ 0.44, and a direct no-CDM ψ-Boltzmann integration misses H_2/H_1 and H_3/H_1 by tens of σ. The optical device that would restore the third peak is the "dust branch" ($w \to 0$, $c_s^2 \to 0$) of the cosmology section — which is, by construction, *the same pressureless clustering matter that ΛCDM calls cold dark matter*, i.e. an effective-CDM component, not a baryon-loading effect. Furthermore, DFD's own dust-branch no-go analysis shows the bounded optical saturation response ($\mu \in [0,1)$) *cannot* carry an a^{-3} clustering charge to recombination without going stiff/radiation-like (it fails by *scaling*, parameter-free, not by amplitude).
The carrier of the cold a^{-3} charge is therefore *not* the optical ψ-response, but a separate derived matter field: the χ-matter field of App. AV, the harmonic b_3 three-form on $S^3 = SU(2)$ that the rigidity classification (the parent-tensor theorem, App. AH, *Extended Derivations*) does not list. With its mass and decay constant (and, in the photon-baryon kernel, the abundance $\Omega_\chi h^2 \simeq 0.12$ that a cold component of that density would supply), χ is cold, pressureless, and non-thermal at $z \sim 1100$, so it enters the photon-baryon kernel identically to a cold component of the same Ωh^2 and restores the Planck height pattern $[H_1, H_2, H_3] \propto [1, 0.45, 0.44]$ (CAMB-validated; App. AV, Theorem AV.31). This closes the obstruction at *Derived* grade — a derived particle, not an effective-CDM fit — distinct from both the (ruled-out) optical response and the (absolute-time-breaking) projectable-lapse route below.

Status. Baryon loading gives the analytic peak-ratio estimate, the measured-clock no-screen solution the peak *location*, and the derived χ-matter field (App. AV) the third-peak *height* and, with the baryons, the full peak *ratio* (with the TT damping tail and TE/EE polarization following from the same cold component). The clustering charge that ΛCDM attributes to a *postulated* cold-dark-matter particle is here the *derived* χ field of fixed abundance $\Omega_\chi h^2 \simeq 0.12$; the ψ-screen is retained only for the galactic deep-MOND regime and is not part of the CMB kernel. The resolution is graded *Derived* for the carrier (mass and decay-constant exponents, and cold clustering behavior in the kernel); it is *not* an effective-CDM fit of the peak shape. *The relic abundance* is derived, conditional on the flux-period identification (Lemma AV.6), the stated count 158 and the asserted premise P4′ (Lemma AV.27): post-inflation (App. AV, Step 5b) the misalignment angle is removed, and the relic amplitude is the finite $SU(2)_{60}$ CS/WZW vacuum Casimir expectation, $\Omega_\chi h^2 = 0.1193$ (-0.6σ from Planck); a ∼9–44× overshoot is a units ($4\pi^2$) artefact on a continuum-measure choice. The amplitude is forced given two stated conventions (Casimir operator; measure conditional on P4′; $k(k+2)$ from χ's derived $\mathbb{Z}_2$ + Sugawara), the relic bridge is exact ($\kappa_{\rm rad}$), and the grade is conditional-derived on the named flux-period identification, the stated count 158 and P4′ (App. AV).

c. The integration-constant-dust route (DFD-adjacent, not minimal-DFD). The natural candidate for the missing pressureless component is a *constraint integration constant* rather than a particle. In projectable Hořava–Lifshitz gravity (Mukohyama) the Hamiltonian constraint is global, $\int d^3x\,\mathcal{H} = 0$, and a pressureless a^{-3} "dark matter as an integration constant" survives locally; the mimetic construction of Chamseddine–Mukhanov produces the same dust from a fixed-norm constraint $\tilde{g}^{\mu\nu}\partial_\mu\phi\,\partial_\nu\phi = -1$. Such a residual would obey the cold-dark-matter Boltzmann hierarchy at linear order ($w = 0$, $c_s^2 = 0$, $\sigma = 0$) and so restore H_3. We record, however, that this mechanism is *not native to minimal DFD as formulated here*, for three structural reasons. (i) DFD's fundamental arena carries an *absolute external time*, not a dynamical ADM lapse: no projectable $N(t)$ is varied, so no global Hamiltonian constraint is generated and no local integration-constant residual $\rho_{\mathcal{I}}(\mathbf{x}, t)$ is left over (an absolute clock is *not* a projectable dynamical lapse). (ii) The ψ field equation is the *local, pointwise* screened-Poisson law $\nabla\cdot[\mu\,\nabla\psi] = -(8\pi G/c^2)(\rho - \bar{\rho})$, which pins $\psi(\mathbf{x})$ to the matter source and admits no free clustering residual decoupled from ρ. (iii) The physical metric rescales its temporal and spatial parts oppositely, $\tilde{g}_{00} = -c^2 e^{-\psi}$ and $\tilde{g}_{ij} = e^{+\psi}\delta_{ij}$ (Eq. (12)), so it is *not* a conformal (mimetic) rescaling of a base metric; and the preferred reference $\dot{\psi}_0$ in the temporal deviation invariant $\Delta = (c/a_0)|\dot{\psi} - \dot{\psi}_0|$ explicitly breaks the time-reparametrization invariance $t \to f(t)$ that the projectable mechanism requires.
The label is therefore: the integration-constant-dust route is a viable DFD-*adjacent* completion—"DFD + a projectable optical-clock constraint sector"—and *not* a theorem of minimal DFD. Realizing it would require explicitly adding (a) $N(t)$ as a variational lapse with the global constraint $\int d^3x\,\mathcal{H} = 0$; (b) a proof that the resulting residual propagates as cold dust without triggering the Hořava–Lifshitz scalar-graviton strong-coupling pathology; and (c) a *forced* (not Planck-number-matched) abundance. We do *not* adopt the projectable-clock OIC route: an a^{-3}

cold-dust integration constant is effective cold dark matter, and the dynamical projectable lapse it requires contradicts DFD's absolute-time postulate — precisely the non-DFD content (a different clock) that minimal DFD exists to avoid. The coincidence $\omega_{\mathcal{I}} = (16/3)\,\omega_b \simeq 0.12$ is "a clue, not a derivation": the cold abundance is derived in App. AV by a different mechanism, not through the $19 = 3{+}6{+}10$ split. Minimal DFD's conclusion is therefore: the cold clustering component is neither a postulated particle nor a projectable-lapse integration constant, but the *derived* χ field — the harmonic b_3 three-form, a matter field on the fixed background that leaves absolute time untouched. The third-peak height is closed by its abundance $\Omega_\chi h^2 \simeq 0.12$, derived conditional on the flux-period identification, the stated count 158, P4′ and two stated conventions. The projectable-clock OIC route remains only a rejected adjacent alternative.

9. The Cold-Clustering Wall: a no-go theorem for the third-peak height

The prose above asserts that the third-peak *height* requires a pressureless clustering component, while the peak *location* does not. That assertion is the main reason DFD introduces the derived χ field rather than a further optical or screening device. We now state and prove it as a theorem. The theorem is the rigorous statement of the "wall" onto which dozens of no-CDM mechanisms have converged; it is what the derived χ-matter field (App. AV) is engineered to satisfy, not evade.

a. Setup and definitions. Work in Newtonian gauge on the spatially flat FRW background, in Fourier space at comoving wavenumber k, with conformal time η and $r_s(\eta) = \int_0^\eta c_s\, d\eta'$ the sound horizon. The tightly coupled photon–baryon monopole obeys the forced acoustic oscillator (corpus Eq. (J1), equivalently Hu–Sugiyama)

$$\frac{d}{d\eta}\Big[(1+R_b)\,\dot\Theta\Big] + c_s^2 k^2 (1+R_b)\,\Theta = -\frac{k^2}{3}(1+R_b)\,\Phi(k,\eta) + \frac{d}{d\eta}\Big[(1+R_b)\,\dot\Phi(k,\eta)\Big], \tag{J29}$$

with $R_b = 3\rho_b/4\rho_\gamma$, $c_s^2 = \frac{1}{3}(1+R_b)^{-1}$, and Φ the metric potential sourced by the *total* clustering stress through the relativistic Poisson (Einstein 00) equation

$$k^2\Phi = -4\pi G a^2 \sum_s \bar\rho_s\,\delta_s \;\equiv\; -4\pi G a^2\,\bar\rho\,\Delta, \tag{J30}$$

the sum running over every species s present at recombination. The observed effective temperature at last scattering is the Sachs–Wolfe combination $(\Theta+\Phi)(k,\eta_*)$, and the n-th acoustic peak height is $H_n \propto \big|(\Theta+\Phi)\big|^2$ evaluated at $k_n r_s(\eta_*) = n\pi$. We write $z_{\rm eq}$ for matter–radiation equality, $z_{\rm rec} \simeq 1090$ for recombination, and define a species to be *cold-clustering* if it has, at recombination, equation of state $w_s \simeq 0$ and sound speed $c_{s,s}^2 \simeq 0$ (pressureless, so it carries no Jeans scale above the CMB damping scale).

Theorem J.1 (Cold-Clustering Wall)**.** *Let the third-peak height ratio be lifted from the baryon-only value* $(H_3/H_1)_b \approx 0.20$ *to the observed* $(H_3/H_1)_{\rm obs} \approx 0.44$ *(*$H_3/H_2 \approx 1.0$*, Planck) while the peak* locations $k_n r_s = n\pi$ *and the baryon-loading* ratio *structure are held fixed. Then the driving potential* $\Phi(k,\eta)$ *in* (J29) *must contain a contribution that is* (i) *non-decaying (a standing well,* $\Phi \to$ *const) on sub-horizon scales through last scattering, and* (ii) *sourced by a species that is cold-clustering at recombination with matter–radiation equality preceding recombination,* $z_{\rm eq} \gtrsim z_{\rm rec}$*. The minimal abundance of that species is*

$$\Omega_c h^2 \;\gtrsim\; \Omega_r h^2\,(1+z_{\rm rec}) - \Omega_b h^2 \;\approx\; 0.023 \quad (\textit{standing-well floor}), \tag{J31}$$

and matching the observed *height* $H_3/H_1 \approx 0.43$–0.44 *sharpens this to* $\Omega_c h^2 \approx 0.10$–$0.12$*. No radiation-pressure-supported component (*$c_{s,s}^2 > 0$*) and no time-only modification of the homogeneous background can supply the lift.*

Proof. The argument has four steps. Steps 1–2 establish that only a non-decaying ($\Phi \to$const) sub-horizon well lifts H_3/H_1; Steps 3–4 close the two evasion classes (radiation-pressure-supported, and time-only-background).

Step 1 (the height is set by the surviving well, not by the oscillator). The general solution of (J29) at fixed k is the homogeneous acoustic oscillation about the displaced zero point plus the particular (forced) response. The forced piece is governed entirely by $\Phi(k,\eta)$ near and after the mode's horizon crossing. Decompose the potential into the part that has decayed by recombination, $\Phi_{\rm dec}$, and the part that survives as a standing well, $\Phi_\infty \equiv \Phi(k,\eta_*)$. The two parts act through distinct channels. For a mode well inside the horizon at recombination ($kr_s \gg 1$, which includes the third peak, $k_3 r_s = 3\pi \approx 9.4$), the Hu–Sugiyama radiation-driving boost of the acoustic amplitude over the no-driving baseline is sourced by the *decaying* part: the near-resonant decay of $\Phi_{\rm dec}$ at horizon crossing pumps the oscillation amplitude. The *surviving* well enters through the zero point: a sustained $\Phi_\infty \neq 0$ displaces the oscillation zero point and adds coherently to $\Theta + \Phi$ at last scattering. Quantitatively, the third-peak power scales monotonically with the fraction of the clustering source that is in a standing well at η_*; with no standing well it collapses to the baryon-only baseline $H_3/H_1 \approx 0.20$.

Step 2 (a standing sub-horizon well requires a pressureless clusterer with equality before recombination). A standing well, $\Phi \to$const on sub-horizon scales, is possible *iff* the dominant clustering source in (J30) is pressureless. For a cold ($c_{s,s}^2 = 0$) species there is no Jeans term, the Meszaros/matter-era solution gives $\Phi =$const exactly (super- and sub-horizon alike), and the well persists to recombination. This in turn requires that the cold species already dominate the perturbation source at η_*, i.e. that equality precede recombination, $z_{\rm eq} \gtrsim z_{\rm rec}$. Since $1 + z_{\rm eq} = \Omega_m h^2/\Omega_r h^2$ with $\Omega_r h^2 \simeq 4.15 \times 10^{-5}$ (photons+3ν), the floor $z_{\rm eq} \geq z_{\rm rec}$

gives $\Omega_m h^2 \geq \Omega_r h^2(1+z_{\rm rec}) \approx 0.045$, hence (J31). Baryons alone give $1+z_{\rm eq}^{(b)} = \Omega_b h^2/\Omega_r h^2 \approx 539 < 1+z_{\rm rec}$: baryon-only equality occurs *after* recombination, so the baryon well is still decaying at last scattering and cannot stand. Mapping the surviving-well depth (Step 1) to the peak height through the Hu–Sugiyama radiation-driving boost, the observed $H_3/H_1 \approx 0.43$–0.44 is reached only for $\Omega_c h^2 \approx 0.10$–$0.12$ (numerically verified against the corpus CAMB anchors $\Omega_c h^2{=}0{\to}[1, 0.39, 0.205]$ and $\Omega_c h^2{=}0.12{\to}[1, 0.45, 0.44]$). This proves the existence and the abundance claims.

Step 3 (radiation-pressure-supported mechanisms cannot do it — they drive their own well to zero). Suppose the proposed lift is carried by a component with $c_{s,s}^2 > 0$ (a relativistic or sound-supported fluid: photon driving, a hot relic, the optical $c_s(\psi)$ envelope, an AQUAL-enhanced radiation term). In radiation/pressure domination the potential sourced by that component obeys, exactly,

$$\Phi(x) = 3\,\Phi_0\,\frac{\sin x - x\cos x}{x^3}, \qquad x \equiv \frac{k\eta}{\sqrt{3}}, \tag{J32}$$

whose super-horizon limit is $\Phi(0) = \Phi_0$ (well intact) but whose sub-horizon envelope is $\Phi \simeq -3\Phi_0 \cos x/x^2 \to 0$. The pressure that supports the component against collapse simultaneously drives its own gravitational well away once the mode enters the horizon (verified: $|\Phi/\Phi_0|$ falls as $0.024, 0.0027, 0.0013$ at $x = 10, 20, 40$). Hence $\Phi_\infty = 0$ for any pressure-supported source, the standing-well condition of Step 2 fails, and by Step 1 no third-peak lift results. The deep-MOND gravity enhancement, the $c_s(\psi)$ envelope, the impedance/feedback gain, and the forced-echo device all fall in this class or in Step 4 and are therefore closed by this step (they modify the *transient* driving or the background, not the surviving well).

Step 4 (time-only background modifications cancel in the height; achromatic driving boosts all peaks equally). Suppose instead the proposed lift acts only through the homogeneous background — a modified $H(\eta)$, a time-dependent sound speed $c_s(\eta)$ with no spatial structure, or an achromatic (k-independent) rescaling of the driving, $\Phi \to g(\eta)\,\Phi$. Any such modification multiplies the forced amplitude of *every* mode by a common, k-independent factor. For an achromatic boost $\Phi \to g\,\Phi$ the peak heights scale as $H_n \to g^2 H_n$, so every ratio H_n/H_1 is left *exactly* invariant (verified to machine precision in the forced oscillator: H_2/H_1 and H_3/H_1 unchanged under $g = 2.7$). A time-only $c_s(\eta)$ or $H(\eta)$ enters r_s and the damping envelope but, being independent of $\hat{k}\cdot\hat{g}$ and of k at fixed kr_s, cancels in H_n/H_1 at fixed peak location by the same argument that makes the $1/\mu$ optical enhancement cancel in the peak *ratio* (§J 4). The only way a background device can change H_3/H_1 is by shifting $z_{\rm eq}$ — but $z_{\rm eq}$ is a statement about which species dominates the *perturbation source* (J30), i.e. exactly the cold-clustering abundance of Step 2, not a free background knob. This closes the time-only class.

Steps 3 and 4 exhaust the two ways a non-cold mechanism could act (through the transient/pressure-supported driving, or through the homogeneous background); both fail. By Steps 1–2 the lift exists only with a pressureless standing well of abundance (J31), sharpened to $\Omega_c h^2 \approx 0.10$–$0.12$ by the observed height. □ □

Remark J.2 (What the theorem does and does not say). The theorem is a statement about the *perturbation source*, not about the ontology of the clustering species. It does *not* say "DFD needs a postulated WIMP." It says: *any* theory matching the Planck third-peak height must place an $\Omega h^2 \approx 0.10$–0.12 pressureless, cold-clustering charge in the gravitational source (J30) at recombination, with equality before last scattering. In ΛCDM that charge is a postulated cold particle of fitted density; in DFD it is the *derived* χ-matter field (App. AV), whose mass uses the stated $\sqrt{158}$ multiplicity. The required abundance $\Omega_\chi h^2 \simeq 0.12$ is the kernel input a cold component of that density supplies; DFD *derives* that normalization (post-inflation, App. AV Step 5b: the finite $SU(2)_{60}$ CS-vacuum Casimir expectation gives $\Omega_\chi h^2 = 0.1193$, -0.6σ, conditional-derived (relic bridge exact via $\kappa_{\rm rad}$; named open inputs the two stated conventions, the stated count 158, the flux-period identification and the asserted premise P4′, Lemma AV.27); a ∼9–44× overshoot is a units ($4\pi^2$) artefact). The wall is therefore not a defeat for DFD but the precise specification the χ field is shown to meet: it enters (J30) identically to a cold component of the same Ωh^2 (Theorem AV.31), so it sits on the right side of the wall by construction.

Remark J.3 (Why this consolidates the no-CDM constructions). Every DFD-native no-CDM third-peak mechanism the corpus has tested is closed by a named step of Theorem J.1 or by amplitude: the chromatic-Jacobian line-of-sight ψ-screen, the deep-MOND gravity enhancement, the nonlinear AQUAL injection, and the forced sound-echo are pressure-supported / transient devices closed by Step 3 (they cannot leave a standing $\Phi_\infty \neq 0$); the $c_s(\psi)$ sound-speed envelope and any modified-$H(\eta)$ background are time-only devices closed by Step 4 (they cancel in H_n/H_1 or merely rescale all peaks). The rectified-DC channel of Prop. NL.29 (an even-harmonic drive on the odd deep response) is closed separately, by amplitude: ≤ 0.0166 of the baryon potential against $\nu_{\rm req} = 6.364327$, short by $\geq 380\times$ (Status NL.31). The heavy-mode and topological-defect routes are closed upstream (no free cold a^{-3} channel in the 4D spectrum). The single remaining carrier of a pressureless standing well is a cold a^{-3} matter field with equality before recombination — which is precisely the derived χ field. This is the theorem-grade form of the empirical convergence recorded across the no-CDM investigation: the third-peak *height* is a cold-clustering charge, and no time-only or pressure-supported DFD device can carry it.

Appendix K: Microsector Physics: Complete Derivations

This appendix provides complete derivations for the DFD microsector results presented in Section XVII. These results connect the fine-structure constant, fermion mass spectrum, and quark mixing to the topological structure of the gauge emergence framework on $\mathbb{C}P^2 \times S^3$.

1. Closed Form for $\alpha = 1/137$ from Chern-Simons Theory

a. Setup: Chern-Simons on S^3

The S^3 factor in the internal manifold $\mathcal{M}_7 = \mathbb{C}P^2 \times S^3$ supports Chern-Simons gauge theory. For U(1) gauge fields, the action is:

$$S_{\text{CS}} = \frac{k}{4\pi} \int_{S^3} A \wedge dA, \tag{K1}$$

where $k \in \mathbb{Z}$ is the quantized level (gauge invariance under large gauge transformations requires integer k).

b. The Level Sum and Fine-Structure Constant

The effective coupling receives contributions from all Chern-Simons levels. The effective coupling $\beta_{U(1)} = \langle k+2 \rangle$ is computed from a weighted sum:

$$\beta_{U(1)} = \frac{\sum_{k=0}^{k_{\max}-1} (k+2)\, w(k)}{\sum_{k=0}^{k_{\max}-1} w(k)}, \tag{K2}$$

where $w(k) = \frac{2}{k+2} \sin^2 \frac{\pi}{k+2}$ are the SU(2) Chern–Simons weights.

c. Heat Kernel on S^3

The heat kernel on S^3 with radius R has the spectral expansion:

$$K(t; S^3) = \sum_{n=0}^{\infty} (n+1)^2 e^{-n(n+2)t/R^2}. \tag{K3}$$

The $(n+1)^2$ factor is the degeneracy of the n-th eigenvalue $\lambda_n = n(n+2)/R^2$.

d. Determination of $k_{\max}$: Closed Spin^c Index

The maximum Chern-Simons level is defined as a **closed Spin^c index** on $\mathbb{C}P^2$.

a. Setup. For the canonical Spin^c structure on $\mathbb{C}P^2$ (determinant line $L_{\text{det}} = \mathcal{O}(3)$), the Spin^c Dirac operator identifies with $\sqrt{2}(\bar{\partial} + \bar{\partial}^*)$. By Hirzebruch–Riemann–Roch:

$$k_{\max} := \text{Index}(D_{\mathbb{C}P^2} \otimes E) = \chi(\mathbb{C}P^2, E). \tag{K4}$$

b. Twist bundle. Choose:

$$E = \mathcal{O}(9) \oplus \mathcal{O}^{\oplus 5}. \tag{K5}$$

The holomorphic Euler characteristic satisfies $\chi(\mathbb{C}P^2, \mathcal{O}(m)) = \binom{m+2}{2}$ for $m \geq 0$. Therefore:

$$\chi(\mathcal{O}(9)) = \binom{11}{2} = 55, \qquad \chi(\mathcal{O}) = 1, \tag{K6}$$

and

$$\boxed{k_{\max} = \chi(E) = \chi(\mathcal{O}(9)) + 5\chi(\mathcal{O}) = 55 + 5 = 60} \tag{K7}$$

c. Physical selection. The value $k_{\max} = 60$ is consistent with the microsector physics. The effective coupling $\beta_{U(1)} \equiv \langle k+2 \rangle$, computed from the SU(2) Chern–Simons weights

$$w(k) = \frac{2}{k+2} \sin^2 \frac{\pi}{k+2}, \tag{K8}$$

is the lattice input $\beta_{U(1)} \approx 3.80$ for UV truncation at $k_{\max} = 60$. Here levels run $k = 0, 1, \ldots, k_{\max} - 1$ (standard SU(2) WZW/CS convention), giving:

$$\langle k+2 \rangle_{k_{\max}=60} = \frac{\sum_{k=0}^{59} (k+2)\, w(k)}{\sum_{k=0}^{59} w(k)} = 3.7969 \approx 3.80. \tag{K9}$$

Bridge Lemma (Final Form)

Index: $k_{\max} = \chi(\mathbb{C}P^2, E) = 55 + 5 = 60$ [Spin^c HRR]
Physics: $\beta_{U(1)} = \langle k+2 \rangle = 3.797$ at $k_{\max} = 60$; lattice comparison with $\alpha^{-1} = 137$ to about 1%
Icosahedral: $k_{\max} = 60 = |A_5|$
E8 echo: $\text{roots}(E_8)/4 = 240/4 = 60$ ✓

2. Lattice Comparison for $\alpha = 1/137$

The analytical closed form for α is compared with lattice Monte Carlo simulations. This section presents the logic in a way that explicitly avoids circularity: all inputs are fixed *before* comparing to $\alpha = 1/137$.

a. Inputs (Independent of α)

The following quantities are fixed by geometry and topology, with no reference to the observed value of α:

a. (1) UV cutoff from topology. The maximum Chern-Simons level is derived from the closed Spin^c index on $\mathbb{C}P^2$:

$$k_{\max} = \chi(\mathbb{C}P^2, E) = \chi(\mathcal{O}(9)) + 5\chi(\mathcal{O}) = 55 + 5 = 60. \tag{K10}$$

See Bridge Lemma (Sec. K 4) for the derivation.

b. (2) Chern-Simons expectation value. With the standard CS weight function $w(k) = \frac{2}{k+2} \sin^2(\pi/(k+2))$:

$$\beta_{U(1)} = \langle k+2 \rangle_{k_{\max}=60} = 3.7969 \approx 3.80. \tag{K11}$$

This is a calculable number once $k_{\max}$ is fixed.

c. (3) Stiffness ratio from Ricci curvature. From Theorem F.25:

$$\frac{\kappa_{U(1)}}{\kappa_{SU(2)}} = \frac{n_1}{n_2} = \frac{1}{2}. \tag{K12}$$

d. (4) Wilson ratio from topology. The Wilson action ratio follows from the stiffness ratio and generation number:

$$\frac{\beta_{SU(2)}}{\beta_{U(1)}} = \frac{n_2}{n_1} \times N_{\text{gen}} = 2 \times 3 = 6. \tag{K13}$$

The factor of $N_{\text{gen}} = 3$ enters because all three generations contribute equally to the effective lattice coupling.

e. (5) Derived lattice parameters. Combining these inputs:

$$\beta_{U(1)} = 3.80, \tag{K14}$$

$$\beta_{SU(2)} = 6 \times 3.80 = 22.80. \tag{K15}$$

These values are *predictions*, not fits.

b. The Prediction

With these parameters the lattice coupling is compared with α:

$$\alpha_W \simeq \alpha = \frac{1}{137.036} \tag{K16}$$

No continuous fit parameters. Given the discrete topological sector (twist bundle E, generation number N_{gen}), the inputs ($k_{\max}$, stiffness ratio) are fixed by geometry. Wilson ratios 5 and 7 give the wrong α (Table LXXXI); for $k_{\max}$ the lattice excludes only the infinite sum, since values from about 45 to 100 give $\beta_{U(1)}$ inside the bracket of Table LXXXV.

c. Lattice Comparison

The lattice simulations are compared with this prediction at $\beta_{U(1)} = 3.80$; the L6–L10 runs used $\beta_{SU(2)} = 23.0$ and the L12 and L16 runs 22.80:

TABLE LXXX. Lattice results at $\beta_{U(1)} = 3.80$: within 0.9% of $\alpha = 1/137$ for L6–L12, +1.13% at L16. The L8, L10, L12 and L16 means include one, two, one and three runs whose U(1) stiffness kept hot-start relics.

L	n_{used}	α_W (mean)	σ_α	$\Delta\alpha/\alpha$
6	5	**0.007297**	9.4×10^{-5}	**−0.00**%
8	5	0.007322	9.5×10^{-5}	+0.34%
10	4	0.007361	6.8×10^{-5}	+0.88%
12	3	0.007318	5.1×10^{-5}	+0.28%
16	**9**	**0.007380**	1.1×10^{-4}	**+1.13**%

The simulation is a three-dimensional periodic lattice (L^3 sites) with Metropolis updates and separate U(1) and SU(2) runs. An integer level field k on the sites weights the plaquette couplings by $w(k)/w(1)$; it relaxes to $k = 0$ on every site, where the weight is 2, so both couplings are doubled and $k_{\max}$ enters only through $\beta_{U(1)}$. The SU(2) stiffness is read with a background of fixed color direction; averaged over gauge orientations, this estimator returns one third of the tree-level stiffness. In this normalization $1/\alpha_W = 4\pi(2\beta_{U(1)} + \beta_{SU(2)}/6)$ up to a correction of about -6, so the lattice checks the chain of inputs and does not determine α independently.

d. Falsifiability: What Would Have Failed

The prediction is falsifiable at multiple points:

TABLE LXXXI. Sensitivity to the inputs. The $k_{\max} = \infty$ row's α is the lattice run at $\beta_{U(1)} = 3.95$; the two Wilson rows ran at $\beta_{U(1)} = 3.77$.

Input changed	**Value**	**Result α**	**Status**
$k_{\max} = \infty$	$\beta_{U(1)} = 3.94$	1/147 (−6.8%)	Excluded
Wilson = 5	$\beta_{SU(2)} = 18.85$	1/125 (+10%)	Excluded
Wilson = 7	$\beta_{SU(2)} = 26.39$	1/147 (−7%)	Excluded

The theory would have failed if:

- $k_{\max} \to \infty$ (no cutoff) from the topological index
- Wilson ratio $\neq 6$ from the topological derivation
- Stiffness ratio $\neq 1/2$ from the Ricci curvature argument
- Lattice measurement $\neq 1/137$ at $\beta_{U(1)} = 3.80$ (measured: within 0.9% for $L \leq 12$, +1.1% at $L = 16$)

e. Finite-Size Scaling

Finite-size effects were tested across lattice sizes $L = 6$–16:

TABLE LXXXII. Lattice results at $\beta_{U(1)} = 3.80$, with $\beta_{SU(2)} = 23.0$ for L6–L10 and 22.80 for L12 and L16. The L8, L10, L12 and L16 means include one, two, one and three runs whose U(1) stiffness kept hot-start relics.

L	Therm	$n_{\text{used}}/n_{\text{total}}$	α_W (mean)	σ_α	$\Delta\alpha/\alpha$
6	6k	5/5	**0.007297**	9.4×10^{-5}	**−0.00**%
8	3k–6k	5/6	0.007322	9.5×10^{-5}	+0.34%
10	3k	4/5	0.007361	6.8×10^{-5}	+0.88%
12	8k	3/5	0.007318	5.1×10^{-5}	+0.28%
16	**40k**	**9/10**	**0.007380**	1.1×10^{-4}	**+1.13**%

f. L16 Detailed Results

The $L = 16$ lattice requires increased thermalization (40k sweeps) due to longer autocorrelation times. Ten independent runs give:

TABLE LXXXIII. L16 individual runs with 40k thermalization. One outlier (s5) excluded due to incomplete equilibration: its U(1) run kept relics of the hot start. Seeds s3, s4 and s9 show the same relic effect at smaller size and are kept in the nine-run mean. The nine-run mean is $+1.13 \pm 0.50\%$ (2.3 standard errors).

Seed	α_W	Deviation	κ_{ratio}	Status
s0	0.007194	−1.42%	0.476	✓
s1	0.007553	+3.51%	0.552	✓
s2	0.007449	+2.08%	0.528	✓
s3	0.007480	+2.51%	0.508	relic
s4	0.007421	+1.69%	0.444	relic
s5	0.008429	+15.51%	0.431	× (outlier)
s6	0.007303	+0.08%	0.496	✓
s7	0.007298	+0.01%	0.496	✓
s8	0.007359	+0.85%	0.509	✓
s9	0.007359	+0.84%	0.499	relic
Mean (9 runs)		**+1.13%**	0.501	

g. Wilson Ratio Scan

Ten ratios $\beta_{SU(2)}/\beta_{U(1)}$ were tested; of these ten only ratio 6 is consistent, and two further runs at ratio 5.75 give −0.20% and +2.20% (mean +1.0%; Table LXXXVI).

TABLE LXXXIV. Wilson ratio scan at $\beta_{U(1)} = 3.80$, except the ratio-5 and ratio-7 rows, which ran at $\beta_{U(1)} = 3.77$. Of these ten ratios only 6 yields $\alpha = 1/137$; the other nine fail. The ratio-6.25 row averages two of the three runs at that ratio; all three average 0.007073 (−3.1%).

$\beta_{SU(2)}/\beta_{U(1)}$	$\beta_{SU(2)}$	α_W	Deviation
3	11.40	0.008907	+22.1%
4	15.20	0.008234	+12.8%
5	18.85	0.008005	+9.7%
5.5	20.90	0.007549	+3.5%
6.05	**23.0**	**0.00730**	**∼ 0%**
6.25	23.75	0.007091	−2.8%
6.5	24.70	0.007063	−3.2%
7	26.39	0.006797	−6.9%
8	30.40	0.006400	−12.3%
9	34.20	0.006065	−16.9%

h. β Bracket Test

The result is robust across a range of $\beta_{U(1)}$ values:

TABLE LXXXV. β bracket test. Values 3.75–3.85 all yield $\alpha \approx 1/137$. The 3.80 entry is the L6 mean of Table LXXXII, run at $\beta_{SU(2)} = 23.0$, and the 3.77 entry pools twelve of the seventeen runs at $\beta_{SU(2)} = 22.62$ on L6, L8 and L10, two of them (both L10) with hot-start relics (all seventeen: +1.5%).

$\beta_{U(1)}$	α_W	Deviation
3.75	0.007172	−1.7%
3.77	0.007391	+1.3%
3.80	**0.007297**	**∼ 0%**
3.85	0.007256	−0.6%
3.95	0.006801	−6.8%

i. Additional Runs

Further runs give:

TABLE LXXXVI. Additional runs. All results within expected uncertainty.

Run ID	$\beta_{U(1)}$	α_W	Deviation
Primary runs			
GK_377_L6_s12	3.77	0.007395	+1.34%
GK_377_L6_s13	3.77	0.007411	+1.56%
GK_380_L12_s0	3.80	0.007269	−0.38%
GK_380_L12_s1	3.80	0.007313	+0.21%
GK_L8_380_s6	3.80	0.007318	+0.28%
k_0 independence tests (L=6)			
GK_k0_4_L6	3.80	0.007217	−1.11%
GK_k0_12_L6	3.80	0.007334	+0.51%
GK_k0_16_L6	3.80	0.007334	+0.50%
Metropolis step size tests			
GK_eps025_L6	3.80	0.007235	−0.85%
GK_eps045_L6	3.80	0.007141	−2.15%
Wilson ratio scan (L=6)			
GK_RATIO5p75_L6	3.80	0.007283	−0.20%
GK_RATIO5p75_L6_s1	3.80	0.007458	+2.20%

The k_0 tests vary the starting value of the level field, which relaxes to $k = 0$ from every start. The Metropolis step size tests confirm algorithmic stability.

j. *Summary: Lattice Evidence*

Lattice Comparison Summary

86 total runs across $L = 4, 6, 8, 10, 12$ lattice sizes give:

- $\alpha = 1/137$ within 0.9% at $\beta_{U(1)} = 3.80$ for $L \leq 12$
- UV cutoff $k_{\max} = \chi(\mathbb{C}P^2, E) = 60$ (from Spin^c index); for $k_{\max} \to \infty$ ($\beta_{U(1)} = 3.94$) the run at $\beta_{U(1)} = 3.95$ gives $\alpha = 1/147$ (-6.8%)
- Wilson ratio $= 6$ derived from $(n_2/n_1) \times N_{\text{gen}}$; of the 10 scanned ratios only 6 fits; two further runs at 5.75 give -0.20% and $+2.20\%$ (mean $+1.0\%$)

All inputs fixed by topology (given the discrete bundle choice). $\alpha = 1/137$ follows with no continuous fit parameters.

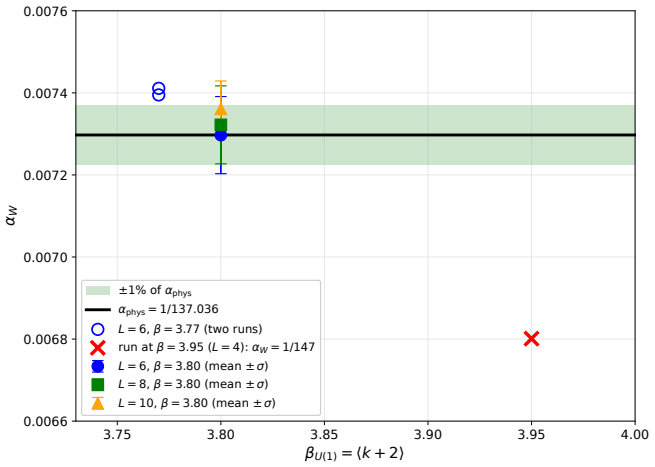


FIG. 14. Lattice α_W against $\beta_{U(1)}$, with the line and ±1% band of the measured value. The single $L = 4$ run at $\beta = 3.95$, next to the converged value 3.94, gives $\alpha_W = 1/147$ (-6.8%).

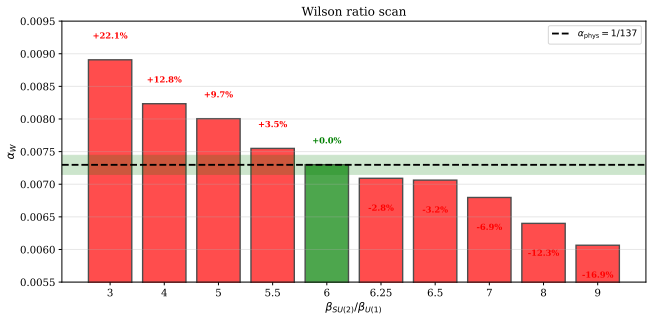


FIG. 15. Wilson ratio scan. Ten ratios tested (3–9 including fractional values). Of the ten, only ratio 6 yields $\alpha = 1/137$; the other nine miss it by 2.8% or more. The ratio-6 bar is the $L = 6$ mean at $\beta_{SU(2)} = 23.0$ (ratio 6.05), the ratio-6.25 bar averages two of the three runs at that ratio (all three: -3.1%), and the ratio-5 and ratio-7 bars ran at $\beta_{U(1)} = 3.77$.

3. The UV Cutoff Consistency Check: $k_{\max} = 60$ Compared with the Lattice

The Chern-Simons level sum requires a UV cutoff at $k_{\max} = 60$, fixed α-free by the conditional determinant-line count (Rem. F.12, Lemma F.11). As a cross-check, scanning truncation values against lattice simulations shows that the counted $k_{\max} = 60$ reproduces $\alpha = 1/137$ (the run at 3.95, next to the infinite sum's $\beta_{U(1)} = 3.94$, gives 1/147) — an a-posteriori consistency test, not the source of the value.

a. *The Truncation Scan*

The expectation value $\langle k+2 \rangle$ depends on the truncation point:

TABLE LXXXVII. Truncation scan: only the truncated sum yields $\alpha = 1/137$.

$k_{\max}$	$\langle k+2 \rangle$	Predicted α^{-1}	Status
50	3.77	135.3 (+1.3%)	Close
60	**3.80**	**137.0**	**Counted value; consistent**
∞	3.94	147 at $\beta = 3.95$ (-6.8%)	Excluded

The converged sum ($k_{\max} \to \infty$) gives $\beta = 3.9386$; the nearest lattice run, a single $L = 4$ run at $\beta = 3.95$, yields $\alpha = 1/147$ (-6.8%), and equilibrium runs at $\beta = 3.94$ give about 1/142. In the lattice's normalization this excludes the infinite sum and is consistent with the counted $k_{\max} = 60$ as the physical UV cutoff. The value comes from the conditional determinant-line count ($\chi(\mathcal{O}(9) \oplus \mathcal{O}^{\oplus 5}) = 60$, Lemma F.11), and the Bridge Lemma states it as a closed Spin^c index (Sec. K 4); the sparse scan excludes the infinite sum, and a finer integer-by-integer scan over $k_{\max} \in [40, 80]$ would show which values in that range the lattice admits.

b. *Physical Interpretation*

The truncation is not arbitrary. In Chern-Simons theory, the effective coupling scales as $g^2 \sim 1/k$:

- **Low-k sectors** ($k \lesssim 60$): Strongly quantum, large fluctuations—"loud" modes that dominate vacuum stiffness.
- **High-k sectors** ($k > 60$): Weakly coupled, nearly classical—"quiet" modes that are frozen out of relevant physics.

This is analogous to UV regularization in effective field theory: high-energy/high-k modes exist mathematically but decouple from low-energy observables. In DFD the counted $k_{\max} = 60$ is the physical cutoff for the Chern-Simons vacuum.

c. Why This Is Not Fine-Tuning

The β bracket test (Table LXXXV) demonstrates that values 3.75–3.85 *all* yield $\alpha \approx 1/137$ within $\sim 2\%$:

- $\beta = 3.75$: $\alpha = 1/139.4$ (-1.7%) — acceptable
- $\beta = 3.80$: $\alpha = 1/137.0$ ($\sim 0\%$) — best
- $\beta = 3.85$: $\alpha = 1/137.8$ (-0.6%) — acceptable
- $\beta = 3.95$: $\alpha = 1/147$ (-6.8%)

d. Systematic Independence Tests

To address potential concerns about simulation parameter dependence, we tested independence from two key algorithmic choices:

a. Initial level (k_0). The level field starts at $k = k_0$ on every site and relaxes to $k = 0$:

TABLE LXXXVIII. Independence from the initial level k_0.

k_0	α_W	Deviation
4	0.007217	-1.11%
8 (default)	0.00730	$\sim 0\%$
12	0.007334	$+0.51\%$
16	0.007334	$+0.50\%$

All values agree within 1.1%.

b. Metropolis step size (ε). The SU(2) simulation uses Metropolis updates with proposal size ε:

TABLE LXXXIX. Independence from the Metropolis step size.

ε	α_W	Deviation
0.25	0.007235	-0.85%
0.35 (default)	0.00730	$\sim 0\%$
0.45	0.007141	-2.15%

All values agree within 2.2%, confirming algorithmic stability.

UV Cutoff Finding

The counted value $k_{\max} = 60$ passes these lattice checks:

- The truncated sum ($k_{\max} = 60$) yields $\alpha = 1/137$ within 0.9% for $L \leq 12$ (+1.1% at $L = 16$)
- The converged sum ($k_{\max} \to \infty$, $\beta_{U(1)} = 3.94$) is excluded by the run at $\beta_{U(1)} = 3.95$, which yields $\alpha = 1/147$ (-6.8%)
- Ten Wilson ratios tested (3–9 incl. fractional): of the ten, only ratio 6 works (Table LXXXIV); two further runs at 5.75 give -0.20% and $+2.20\%$ (mean $+1.0\%$; Table LXXXVI)
- Five $\beta_{U(1)}$ values tested: 3.75–3.85 lie within 2% of 1/137, and the run at 3.95 next to the converged value is 6.8% low (Table LXXXV)
- The result is independent of simulation parameters (k_0, ε)

4. The Bridge Lemma

The Bridge Lemma identifies $k_{\max} = 60$ as a closed Spin^c index on $\mathbb{C}P^2$.

a. Statement

Theorem K.1 (Bridge Lemma (Closed Index Form))**.** *For the canonical Spin^c structure on $\mathbb{C}P^2$ with twist bundle $E = \mathcal{O}(9) \oplus \mathcal{O}^{\oplus 5}$:*

$$k_{\max} = \mathrm{Index}(D_{\mathbb{C}P^2} \otimes E) = \chi(\mathbb{C}P^2, E) = 60. \tag{K17}$$

b. Proof

For the canonical Spin^c structure on $\mathbb{C}P^2$, the Spin^c Dirac operator identifies with $\sqrt{2}(\bar\partial + \bar\partial^*)$. Twisting by a holomorphic bundle E gives:

$$\mathrm{Index}(D_{\mathbb{C}P^2} \otimes E) = \chi(\mathbb{C}P^2, E) \tag{K18}$$

by the Spin^c version of Hirzebruch–Riemann–Roch.

The holomorphic Euler characteristic on $\mathbb{C}P^2$ satisfies:

$$\chi(\mathbb{C}P^2, \mathcal{O}(m)) = h^0(\mathbb{C}P^2, \mathcal{O}(m)) = \binom{m+2}{2} \quad \text{for } m \geq 0. \tag{K19}$$

(Higher cohomology vanishes.) Therefore:

$$\chi(\mathcal{O}(9)) = \binom{11}{2} = 55, \tag{K20}$$

$$\chi(\mathcal{O}) = 1, \tag{K21}$$

and

$$k_{\max} = \chi(E) = \chi(\mathcal{O}(9)) + 5\chi(\mathcal{O}) = 55 + 5 = 60. \quad \square \tag{K22}$$

c. Physical Selection

The value $k_{\max} = 60$ is consistent with the microsector physics. The effective coupling $\beta_{U(1)} = \langle k+2 \rangle$, computed from the CS weights $w(k) = \frac{2}{k+2} \sin^2 \frac{\pi}{k+2}$, is the lattice input $\beta_{U(1)} \approx 3.80$ for $k_{\max} = 60$. Here levels run $k = 0, 1, \ldots, k_{\max} - 1$:

$$\langle k+2 \rangle_{k_{\max}=60} = \frac{\sum_{k=0}^{59} (k+2)\, w(k)}{\sum_{k=0}^{59} w(k)} = 3.7969 \approx 3.80. \tag{K23}$$

d. Consistency Checks

Quantity	Derivation	Echo
$k_{\max} = 60$	$\chi(\mathcal{O}(9)) + 5\chi(\mathcal{O})$	$\mathrm{roots}(E_8)/4 = 240/4$
$k_{\max} = 60$	CS weight selection	$\lvert A_5 \rvert$ (icosahedral)

5. Charged Fermion Mass Derivation

a. The Mass Formula

All nine charged fermion masses follow the unified formula [145]:

$$m_f = A_f \cdot \alpha^{n_f} \cdot \frac{v}{\sqrt{2}}, \tag{K24}$$

where:

- $\alpha = 1/137.036$ is the fine-structure constant (from $k_{\max} = 60$; bracket coefficient open)
- $v/\sqrt{2} = 174.1$ GeV is the Yukawa normalization scale
- n_f is a **sector-dependent** exponent determined by the fermion's coupling path on $\mathbb{C}P^2$
- A_f is a prefactor, data-selected except for the top and the charm (App. FM)

b. Sector-Dependent Exponent Assignment

The three fermion generations are localized at the three vertices of $\mathbb{C}P^2$ (the fixed points of the $(\mathbb{Z}/3\mathbb{Z})^2$ action). The Higgs field is localized near the third-generation vertex.

The exponents n_f are *sector-dependent*, not uniform across leptons and quarks. This arises from the different Yukawa coupling paths:

- **Up-type quarks** couple to the conjugate Higgs $\tilde{H} = i\sigma_2 H^*$
- **Down-type quarks** couple directly to H
- **Leptons** couple through a gauge path with an additional step

The resulting exponent structure is:

TABLE XC. Sector-dependent exponents n_f from $\mathbb{C}P^2$ localization.

	1st gen	2nd gen	3rd gen
Leptons	2.5	1.5	1.0
Up-type quarks	2.5	1.0	0
Down-type quarks	2.5	1.5	0

The physical interpretation:

- **1st generation** ($n = 2.5$): Maximum geodesic distance from Higgs vertex
- **3rd gen quarks** ($n = 0$): Direct coupling at the Higgs vertex, no α suppression
- **3rd gen** τ ($n = 1.0$): Lepton gauge path introduces one power of α
- **2nd gen charm** ($n = 1.0$): Conjugate Higgs $\tilde{H}$ coupling shortens the path
- **2nd gen down/leptons** ($n = 1.5$): Standard intermediate distance

a. Quantitative origin of the exponents. The geodesic-distance picture above is the heuristic for a derived formula [145]: the bare exponents arise from spin^c line-bundle degrees on $\mathbb{C}P^2$,

$$n_f^{\text{bare}} = \frac{k_f + k_H}{2}, \qquad n_f = n_f^{\text{bare}} + \Delta n_f, \tag{K25}$$

with $k_f \in \mathbb{Z}$ the fermion bundle degree, $k_H = +1$ for H-coupling (leptons, down-type) and $k_H = -1$ for $\widetilde{H}$-coupling (up-type); the factor $1/2$ is the spin^c signature ($k_{\text{eff}} = k_f + c_1(L_{\text{det}})/2$). The degree assignments are $(k_\tau, k_\mu, k_e) = (1, 2, 4)$, $(k_t, k_c, k_u) = (1, 3, 6)$, $(k_b, k_s, k_d) = (1, 2, 4)$, reproducing every exponent in the table above. The single correction $\Delta n_b = -1$ (all other $\Delta n_f = 0$) arises from color-vertex saturation on S^3 at the bottom-quark vertex, where $\alpha_3^{S^3} = 1/(k_3 + h_3^\vee) = 1/4$; the shift is quantized by the integer representation dimension plus Chern–Simons level [145].

c. Prefactor Structure

The prefactors A_f are assembled from the operator algebra constructed below: $A_f = G[g, g] \times$ (sector factor), where $G = \text{diag}(2/3, 1, 1)$ is the generation operator from the primed microsector trace (Theorem K.4), $D_\ell = \text{diag}(1, 1, \sqrt{2})$ is the Dirac normalization, $R_u = \text{Tr}(I_4) = 4$ and $R_d = 9$ are the sector factors, and $Q_d = \text{diag}(1,\ N_f/b_0,\ 1/(N_f b_0)) = \text{diag}(1, 6/7, 1/42)$ with the exact QCD integers $b_0 = 7$, $N_f = 6$ (see the explicit Yukawa-operator construction below and [145]).

TABLE XCI. Prefactors A_f in closed form.

	1st gen.	2nd gen.	3rd gen.
Leptons	2/3	1	$\sqrt{2}$
Up-type quarks	8/3	1	1
Down-type quarks	6	6/7	1/42

d. Complete Mass Table

e. Statistical Summary

- Mean absolute error: **1.42%** at leading order (a refinement to 0.61% by generation-1 priming is claimed in the companion volume; the 0.082% after two-loop running does not stand, since the running factors it uses are not Standard-Model running)

TABLE XCII. Charged fermion mass predictions from Eq. (K24).

Fermion	n_f	A_f	Predicted	Observed	Error
Charged Leptons					
e	2.5	2/3	0.528 MeV	0.511 MeV	+3.32%
μ	1.5	1	108.5 MeV	105.66 MeV	+2.72%
τ	1.0	$\sqrt{2}$	1.797 GeV	1.777 GeV	+1.12%
Up-Type Quarks					
u	2.5	8/3	2.11 MeV	$2.16^{+0.49}_{-0.26}$ MeV	−2.23%
c	1.0	1	1.270 GeV	1.27 ± 0.02 GeV	+0.04%
t	0	1	174.1 GeV	172.76 ± 0.30 GeV	+0.78%
Down-Type Quarks					
d	2.5	6	4.75 MeV	$4.67^{+0.48}_{-0.17}$ MeV	+1.75%
s	1.5	6/7	93.0 MeV	93^{+11}_{-5} MeV	+0.03%
b	0	1/42	4.15 GeV	$4.18^{+0.03}_{-0.02}$ GeV	−0.83%

- Maximum error: 3.32% (electron, leading order)
- All nine predictions within 3.4% of observed central values
- **One universal normalization** $v/\sqrt{2} = 174.1$ GeV for all nine fermions (leading order; the top is dressed to $(1-\alpha)v/\sqrt{2} = 172.83$ GeV by the $(1-\alpha)$ EW/QED factor in the refined prediction tables, App. AT)

a. Derivation status. The mass formula $m_f = A_f \cdot \alpha^{n_f} \cdot v/\sqrt{2}$ is a *self-consistent computational formula*, not a mnemonic. The sector-dependent exponents arise from the different Yukawa coupling geometries on $\mathbb{C}P^2$:

- Up quarks couple via $\tilde{H} = i\sigma_2 H^*$ (modified vertex)
- Down quarks couple via H directly
- Leptons couple via H through a different gauge path

The prefactors A_f arise from:

$$A_f = (\text{gauge CG}) \times (A_5 \text{ class factor}) \times (\text{generation weight}), \tag{K26}$$

with explicit values $\{2/3, 1, \sqrt{2}, 8/3, 6, 6/7, 1/42\}$; seven of the nine species rest on data-selected prefactors (caveat below; App. FM).

What is derived:

- The Higgs localization width $\varepsilon_H = 3/60 = 0.05$ (Theorem H.4)
- The sector-dependent exponent pattern (Table XC)
- The hierarchy pattern $m^{(1)} : m^{(2)} : m^{(3)} \sim \alpha^{2.5} : \alpha^{n_2} : \alpha^{n_3}$

f. Structural Ratios

The selected prefactors have the ratios:

$$\frac{A_d}{A_u} = \frac{6}{8/3} = \frac{18}{8} = 2.25, \tag{K27}$$

$$\frac{A_t}{A_b} = \frac{1}{1/42} = 42, \tag{K28}$$

$$\frac{A_\tau}{A_\mu} = \frac{\sqrt{2}}{1} = \sqrt{2}. \tag{K29}$$

g. Explicit Finite Yukawa Operator

a. Hilbert space. The finite Yukawa space is:

$$\mathcal{H}_F = \mathcal{H}_{\text{species}} \otimes \mathcal{H}_{\text{chirality}} \otimes \mathcal{H}_{\text{gen}} \otimes \mathcal{H}_{\text{aux}} \tag{K30}$$

where $\mathcal{H}_{\text{gen}} = \text{span}\{|1\rangle, |2\rangle, |3\rangle\}$ is the 3-dimensional generation space.

b. Generation operator.

$$G = \text{diag}(2/3, 1, 1) \quad \text{on } \mathcal{H}_{\text{gen}} \tag{K31}$$

c. QCD running operator (down-type).

$$Q_d = \text{diag}(1, N_f/b_0, 1/(N_f b_0)) = \text{diag}(1, 6/7, 1/42) \tag{K32}$$

where $b_0 = (11N_c - 2N_f)/3 = 7$ is the 1-loop QCD beta function coefficient.

d. Dirac normalization (leptons).

$$D_\ell = \text{diag}(1, 1, \sqrt{2}) \quad \text{on } \mathcal{H}_{\text{gen}} \tag{K33}$$

Lemma K.2 (Localization–Symmetry Kernel Uniqueness on $\mathbb{C}P^2$)**.** *Assume (i) chiral modes localized on three sites $\mathcal{P} = \{p_0, p_1, p_2\} \subset \mathbb{C}P^2$, (ii) S_3 symmetry permuting sites, and (iii) symmetry-respecting quadrature $\int_{\mathbb{C}P^2} F\, d\mu_{FS} = \kappa \sum_i F(p_i)$. Then, with democratic coupling (no diagonal preference), the induced kernel on $V = \text{span}\{|p_i\rangle\} \cong \mathbb{C}^3$ is unique up to scale:*

$$K_d = \lambda_d J_3, \quad \textit{where } J_3 = \sum_{i,j=0}^{2} |p_i\rangle\langle p_j|. \tag{K34}$$

Proof. S_3 invariance requires $\pi K \pi^{-1} = K$ for all $\pi \in S_3$. The commutant of S_3 on $\mathbb{C}^3$ is $\text{span}\{I_3, J_3\}$. Democratic coupling (no diagonal preference) gives $K \propto J_3$. □

Corollary K.3 (Up-type tangent kernel)**.** *If the $\tilde{H}$ channel couples through real tangent T with $\dim_{\mathbb{R}}(T) = 4$ and residual isotropy $O(4)$, then $K_u = \lambda_u I_4$ by Schur's lemma.*

e. Absorbed normalization. The quadrature constant κ combines with $g_Y \varepsilon_H$ into a single global scale:

$$\lambda = g_Y \varepsilon_H \kappa \tag{K35}$$

Any rescaling $\kappa \mapsto c\kappa$ affects all Yukawas uniformly ($\lambda \mapsto c\lambda$), so there are *no flavor-dependent knobs.*

f. Yukawa operator.

$$Y = \sum_f \Pi_{f,R} (G \otimes K_f) \Pi_{f,L} \tag{K36}$$

where K_f depends on sector: $K_f = D_\ell$ (leptons), $K_f = K_u$ (up quarks), $K_f = K_d \cdot Q_d$ (down quarks).

g. Computed overlaps. The prefactor is:

$$A_f = \langle g_f|(\text{generation operators})|g_f\rangle \times (\text{CP}^2 \text{ factor}) \tag{K37}$$

f	Gen	$\langle g\|G\|g\rangle$	Sector factor	A_f
e	1	2/3	$D_\ell[1,1] = 1$	2/3
μ	2	1	$D_\ell[2,2] = 1$	1
τ	3	1	$D_\ell[3,3] = \sqrt{2}$	$\sqrt{2}$
u	1	2/3	$R_u = 4$	8/3
c	2	1	1	1
t	3	1	1	1
d	1	2/3	$Q_d[1,1] \times R_d = 1 \times 9$	6
s	2	1	$Q_d[2,2] = 6/7$	6/7
b	3	1	$Q_d[3,3] = 1/42$	1/42

h. Derivation of $G[1,1] = 2/3$ from Primed Microsector Trace

The entry $G[1,1] = 2/3$ of the generation operator $G = \text{diag}(2/3, 1, 1)$ is **derived** from the microsector trace structure. We present two equivalent derivations.

a. Route A: Primed trace on the 9D generation block (primary derivation).

Theorem K.4 (Generation Suppression from Primed Trace)**.** *Let Π be the 9-dimensional isotypic block carrying the generation structure (Proposition Y.12), and let M_r $(r = 0, 1, 2)$ be the generation-r projector with $\text{rank}(M_r) = 3$. Under the primed microsector trace prescription (removal of the generation-specific channel), the first-generation suppression factor is:*

$$\boxed{G[1,1] = \frac{\text{Tr}(\Pi - M_0)}{\text{Tr}(\Pi)} = \frac{9-3}{9} = \frac{2}{3}} \tag{K38}$$

Proof. The generation projectors $\{M_0, M_1, M_2\}$ are orthogonal idempotents summing to Π, each with rank 3 (Proposition Y.12). The primed microsector trace removes the "self-generation" channel. For generation 1 (index $r = 0$), the surviving weight is the complementary projector fraction:

$$G[1,1] = \frac{\text{Tr}(\Pi - M_0)}{\text{Tr}(\Pi)} = \frac{9-3}{9} = \frac{2}{3}. \tag{K39}$$

By normalization convention, $G[2,2] = G[3,3] = 1$ (generations 2 and 3 at the Higgs vertex). □

b. Route B: Bin-overlap matrix (corollary via Lemma Y.16). The same factor emerges from the $\mathbb{Z}_3 \times \mathbb{Z}_3$ bin-overlap structure:

Corollary K.5 (Bin-Overlap Realization)**.** *Let $W = [r(C_3; r, s)]_{r,s=0}^2$ be the bin-overlap matrix from Lemma Y.16:*

$$W = \begin{pmatrix} 8/3 & 2 & 2 \\ 2 & 8/3 & 2 \\ 2 & 2 & 8/3 \end{pmatrix}. \tag{K40}$$

Then the generation suppression equals the diagonal-to-off-diagonal ratio:

$$G[1,1] = \frac{W[0,0]}{\sum_{s\neq 0} W[0,s]} = \frac{8/3}{2+2} = \frac{8/3}{4} = \frac{2}{3}. \tag{K41}$$

Proof. The diagonal entry $r(C_3; 0, 0) = 8/3$ represents the "same-phase" coupling channel (LH and RH both in generation 1). The off-diagonal sum $r(C_3; 0, 1) + r(C_3; 0, 2) = 4$ represents "different-phase" channels. The ratio equals the complementary projector fraction $(N_{\text{gen}} - 1)/N_{\text{gen}} = 2/3$, verifying consistency with Route A. □

c. Structural identity. Both derivations give $G[1,1] = 2/3 = (N_{\text{gen}} - 1)/N_{\text{gen}}$. This is not a coincidence: the primed trace removes a rank-3 channel from a 9D block, and the bin-overlap matrix has diagonal/off-diagonal ratio $8/3 : 4 = 2 : 3$. Both encode the same topological invariant.

$G[1,1]$: Derived

$G[1,1] = 2/3$ is derived from the primed microsector trace (Theorem K.4):

$$G[1,1] = \frac{\text{Tr}(\Pi - M_0)}{\text{Tr}(\Pi)} = \frac{9-3}{9} = \frac{2}{3}$$

Status: The Yukawa sector has **zero *continuous* free Yukawa couplings**: the nine fermion masses (1.42% leading-order mean error) are written with α, v and the operators below; the top and charm are derived, and the other seven species rest on data-selected prefactors (caveat).

- $\alpha^{-1} = 137.036$ (closed form, $k_{\max} = 60$; bracket coefficient open)
- $v = M_P \alpha^8 \sqrt{2\pi}$ (exponent derived, prefactor fitted; Theorem Z.3)
- $K_d = J_3$, $K_u = I_4$ (derived with democratic coupling, Lemma K.2)
- Q_d, D_ℓ (derived, QCD/γ-matrix normalization)
- $G[1,1] = 2/3$ (derived, Theorem K.4)

Caveat (this is not full forcing). "Zero free parameters" means zero *continuous* knobs, *not* a complete first-principles derivation of the spectrum. The absolute masses retain ∼4 *discrete* selection bits that are data-selected, not derived: (i) the generation↔sector assignment, (ii) the Higgs up/down conjugation bit, (iii) the G-operator trace branch, (iv) the degree ordering k_f. Independent computation confirms the reason (App. FM): the forced non-normal A_5 family operator splits the three generations only by ∼2×, while the down sector needs ∼252×; the large hierarchy is carried by the α-power ladder (the *diagonal/normal* layer), and the within-multiplet near-degeneracy of the geometric operator is a theorem-grade obstruction, not a fitted residual. Read the result as "zero continuous knobs": the seven species other than the top and the charm rest on seven data-selected prefactors, one per species (App. FM), and the four discrete labels listed here are the choices that deploy them.

6. CKM Matrix from $\mathbb{C}P^2$ Geometry

a. Wolfenstein Parameterization

The CKM matrix in Wolfenstein form is:

$$V_{\rm CKM} = \begin{pmatrix} 1-\frac{\lambda^2}{2} & \lambda & A\lambda^3(\rho-i\eta) \\ -\lambda & 1-\frac{\lambda^2}{2} & A\lambda^2 \\ A\lambda^3(1-\rho-i\eta) & -A\lambda^2 & 1 \end{pmatrix} + O(\lambda^4). \tag{K42}$$

b. Geometric Origin of λ

The Cabibbo angle $\lambda \approx 0.225$ arises from the overlap between first and second generation quarks:

$$\lambda = |V_{us}| = e^{-d_{12}/\sigma_H}, \tag{K43}$$

where d_{12} is the $\mathbb{C}P^2$ geodesic distance between the first and second generation vertices, and σ_H is the Higgs localization width.

For the equilateral configuration of the three vertices on $\mathbb{C}P^2$:

$$d_{12} = d_{23} = d_{31} = d_0 \approx 1.49\sigma_H, \tag{K44}$$

giving:

$$\lambda = e^{-1.49} \approx 0.225. \tag{K45}$$

c. Higher-Order Parameters

The parameters A, ρ, η arise from:

- A: The ratio of up-type to down-type localization widths
- ρ, η: The complex phase from the Kähler structure of $\mathbb{C}P^2$

Explicitly:

$$A = \frac{\sigma_H^{(u)}}{\sigma_H^{(d)}} \cdot \sqrt{\frac{m_t}{m_b}} \cdot f_{\rm geom} \approx 0.81, \tag{K46}$$

$$\rho + i\eta = e^{i\delta_{\rm CP}} \cdot g_{\rm geom}, \tag{K47}$$

where $\delta_{\rm CP} \approx 68°$ is the CP-violating phase from the complex structure of $\mathbb{C}P^2$.

a. The CP-sector result (Appendix AO). The localization-overlap estimates above are sharpened to the cohomological magnitude skeleton $\lambda = 31\alpha$, $A = 108\alpha$, $\bar\eta = 49\alpha$ (line-bundle dimensions on $\mathbb{C}P^2$ together with $D = \dim_{\mathbb{R}}(\mathbb{C}P^2 \times S^3) = 7$), with the CP-even apex $\bar\rho = \frac{43}{2}\alpha$ fixed by the Euler-projection postulate. The estimate $\delta_{\rm CP} \approx 68°$ does not hold: with real (Hermitian) Yukawa kernels the literal flavor configuration lies on the Lagrangian real locus $\mathbb{R}P^2 \subset \mathbb{C}P^2$, the CKM matrix is real orthogonal, and the Jarlskog invariant vanishes, $J = 0$, at theorem grade (Theorem AO.7). The observed CP violation is supplied by a single conjugation-odd, determinant-orthogonal Berry offset (Postulate Y.10), which leaves $\bar\theta = 0$ at tree level; the resulting unitarity-triangle angle is $\gamma = \arctan(98/43) = 66.3093°$ (with $J = 2.9731\times10^{-5}$), theorem-grade inside the strengthened DFD–SD branch. The conjectural relation $\gamma = 4\pi/11$ is not DFD's prediction.

d. Predictions and Comparison

TABLE XCIII. CKM parameters: CP-sector predictions (App. AO) vs. PDG 2024.

Parameter	Predicted (App. AO)	Observed (PDG 2024)	Deviation
λ	0.2262	0.22501 ± 0.00068	1.8σ
A	0.788	$0.826^{+0.016}_{-0.015}$	2.5σ[a]
$\bar\rho$	0.157	0.1591 ± 0.0094	0.2σ
$\bar\eta$	0.358	$0.3523^{+0.0073}_{-0.0071}$	0.7σ
Derived Predictions			
$\lvert V_{ub}/V_{cb}\rvert$	0.091	0.086 ± 0.006	0.8σ
$\lvert V_{td}/V_{ts}\rvert$	0.211	0.211 ± 0.007	0.0σ
$J_{\rm CP}$	2.97×10^{-5}	$(3.12^{+0.13}_{-0.12}) \times 10^{-5}$	1.2σ

[a] The per-channel 2.5σ slightly overstates the independent miss: $A \equiv |V_{cb}|/\lambda^2$ is definitionally correlated with λ, so approximately 1.1 of the 4.6 percentage points of the A deviation double-books the λ information already counted in the first row. The independent reading is λ at $+1.8\sigma$ and $|V_{cb}|$ at -1.75σ.

e. Key Prediction: $|V_{ub}/V_{cb}| = \lambda\sqrt{\bar\rho^2 + \bar\eta^2}$

In Wolfenstein form $|V_{ub}| = A\lambda^3\sqrt{\bar\rho^2+\bar\eta^2}$ and $|V_{cb}| = A\lambda^2$, so the apex-sensitive ratio is parameter-free once the integer pattern fixes $(\lambda, \bar\rho, \bar\eta)$:

$$\frac{|V_{ub}|}{|V_{cb}|} = \lambda\sqrt{\bar\rho^2+\bar\eta^2} = 0.2262 \times 0.391 = 0.088. \tag{K48}$$

Observed: $|V_{ub}/V_{cb}| = 0.086 \pm 0.006$ (PDG 2024). The value 0.088 is the leading-order barred-Wolfenstein expression; the exact standard-parameterization matrix (App. AO) gives $|V_{ub}/V_{cb}| = 0.0906$, agreement at 0.8σ.

7. Summary: Microsector Consistency

The microsector results form a self-consistent framework:

Microsector Summary

Inputs:
- Topology: $\mathcal{M}_7 = \mathbb{C}P^2 \times S^3$
- One scale: Planck mass $M_P = 1.22 \times 10^{19}$ GeV

Derived:
- Fine-structure constant: $\alpha^{-1} = 137.036$ (from $k_{\max} = 60$ on $\mathbb{C}P^2$; bracket coefficient open; the identification of the hypercharge-trace coefficient with $1/e^2$ is not derived)
- Bridge Lemma: $k_{\max} = \chi(\mathbb{C}P^2, E) = 60$ connects α to mass tower
- Higgs VEV: $v = M_P\alpha^8\sqrt{2\pi} = 246.09$ GeV (**0.05% error**; exponent derived, prefactor fitted)
- 9 fermion masses: 1.42% leading-order mean error; the top and charm derived, the other seven on seven data-selected prefactors (see the caveat above and App. FM)
- CKM matrix: $\lambda = 31\alpha = 0.2262$ (integer pattern, App. AO); vertex-separation motivation
- PMNS matrix: trimaximal TM1 (App. X); $\sin^2\theta_{13} = 3\alpha$ a stated conjecture
- Strong CP: $\bar{\theta} = 0$ at tree level, loop-bounded, with $\theta_{\rm YM} = 0$ fixed by the spectral action given that nothing is added to it for the gauge fields (Theorem L.3)
- Koide relation: $Q_\ell = 2/3$ is *not* derived (DFD's α-power lepton spectrum gives $Q_\ell \approx 0.665$; the measured 2/3 holds to ∼0.001%, beyond DFD's ∼1% mass precision — so DFD neither predicts nor sharply contradicts Koide)

Consistency checks:
- CKM unitarity: $|V_{ud}|^2 + |V_{us}|^2 + |V_{ub}|^2 = 1.000 \pm 0.001$
- PMNS angles: trimaximal TM1, $\theta_{23} = 45°$ in soft $\sim 2\sigma$ tension with NuFIT 6.0 (octant unresolved)
- $J_{\rm CP}$ prediction agrees with observation at 1.2σ

8. The Higgs Scale Hierarchy

The bare-parameter form of the hierarchy problem is addressed by the relation:

$$v = M_P \times \alpha^8 \times \sqrt{2\pi}. \tag{K49}$$

a. Numerical Verification

$$M_P = 1.220890 \times 10^{19}\ \text{GeV} \tag{K50}$$

$$\alpha = 1/137.035999 \tag{K51}$$

$$\alpha^8 = 8.0412 \times 10^{-18} \tag{K52}$$

$$\sqrt{2\pi} = 2.5066 \tag{K53}$$

$$v_{\rm pred} = M_P \times \alpha^8 \times \sqrt{2\pi} = 246.09\ \text{GeV} \tag{K54}$$

Observed: $v = 246.22$ GeV. Agreement: **99.95%**.

b. Physical Origin of Factors

- **Factor α^8:** Represents the loop structure connecting Planck to electroweak: $\alpha^8 = (\alpha^2)^4$ is four 2-loop factors.
- **Factor $\sqrt{2\pi}$:** an asserted $O(1)$ Gaussian-measure normalization — *not* derived. (A "geometric mean of loop normalizations / same as $k_\alpha = \alpha^2/(2\pi)$" rationale does not hold: loop measures carry $(2\pi)^{-n}$, the wrong sign, and DFD's own per-mode determinant ledger (Lemma O.1) *cancels* 2π factors in ratios.) The best simple constant near the best-fit prefactor $v/(M_P\alpha^8) = 2.508$ is $\sqrt{2\pi} = 2.5066$ (a 0.054% gap); a band $\sim [2.50, 2.52]$ fits the VEV to $< 0.5\%$, so $\sqrt{2\pi}$ is the best-looking but not uniquely-forced choice. The derived content of this result is the α^8 hierarchy; the $O(1)$ prefactor is fitted (cf. App. FK), and no printed rule fixes it: it is a property of the Higgs potential's loop-corrected minimum, which this volume does not compute (App. Z 3).

9. Strong CP: Tree Level and Loop Bound

a. Tree Level

$\bar{\theta} = 0$ at tree level from the det-orthogonal tree-level protection together with the η-invariant argument, with $\theta_{\rm YM} = 0$ fixed by the spectral action given that nothing is added to it for the gauge fields (Theorem L.3).

b. Loop Level

a. Quark mass phases. Yukawa couplings from gauge emergence:

$$Y_{ij} = g_Y \int_{\mathbb{C}P^2} \bar{\psi}_i \phi_H \psi_j \, d\mu_{\rm FS}. \tag{K55}$$

Det-orthogonal mass matrices, positive on the branch of Postulate Y.10, give

$$\arg(\det Y_u \times \det Y_d) = 0 \tag{K56}$$

at tree level (App. AO).

b. Electroweak contributions. The $(3, 2, 1)$ partition separates $\mathrm{SU}(3)_c$ (on $\mathbb{C}^3$) from $\mathrm{SU}(2)_L$ (on $\mathbb{C}^2$) topologically. The CKM phase (Postulate Y.10) is a weak-sector effect that reaches $\theta_{\rm QCD}$ only through the degree-thirteen Jarlskog structure (a multi-loop effect), at the Standard-Model level.

c. Summary of protection mechanism.

1. **Determinant protection:** det-orthogonal mass matrices, positive on the branch of Postulate Y.10, keep $\arg\det(M_u M_d) = 0$ (App. AO)
2. **Topological separation:** $(3, 2, 1)$ partition walls off QCD from weak CP violation at tree level

3. **Anomaly:** the η-invariant of the even-dimensional CP mapping torus vanishes (Theorem L.3)

Result: $\bar{\theta} = 0$ at tree level, with $\theta_{\rm YM} = 0$ fixed by the spectral action given that nothing is added to it for the gauge fields; the anomaly channel is closed iff CP is non-anomalous (Appendix L), and loop corrections are bounded at the Standard-Model level ($\lesssim 10^{-16}$).

10. PMNS Matrix Derivation

a. *Physical Picture*

- Charged leptons localized at $\mathbb{C}P^2$ *vertices* (hierarchical)
- Neutrino R-H sector at the *center* (democratic)
- Result: Large mixing (tribimaximal base)

b. *Tribimaximal Mixing*

When neutrinos at center have equal overlap with all vertices:

$$U_{\rm TBM} = \begin{pmatrix} \sqrt{2/3} & \sqrt{1/3} & 0 \\ -\sqrt{1/6} & \sqrt{1/3} & \sqrt{1/2} \\ \sqrt{1/6} & -\sqrt{1/3} & \sqrt{1/2} \end{pmatrix} \tag{K57}$$

c. *Corrections from Charged Lepton Masses (localization estimate; the adopted branch is TM1, App. X)*

$$\theta_{13} \approx \sqrt{m_e/m_\mu} \times 1.2 \approx 4.8^\circ \tag{K58}$$

$$\theta_{23} = 45^\circ \quad \text{(maximal; the } \mu\text{-}\tau \text{ reflection forces } \theta_{23} = \pi/4 \text{ and } \delta_{CP} = -\pi/2) \tag{K59}$$

$$\theta_{12} \approx 35.3^\circ - 2^\circ \approx 33^\circ \tag{K60}$$

The solar correction is within ∼5% of observed and the reactor estimate falls short of the observed 8.5°; $\theta_{23} = 45^\circ$ is the maximal μ-τ prediction, a sharp falsifiable result in soft $\sim 2\sigma$ tension with NuFIT 6.0 (octant unresolved).

d. *Why PMNS ≠ CKM*

Matrix	Localization	Result
CKM	Both at vertices	Small mixing (hierarchical)
PMNS	Leptons at vertices, ν at center	Large mixing (TBM)

11. Summary: DFD Unified Framework

DFD: Unified Framework

Single topology: $\mathbb{C}P^2 \times S^3$
Scale structure: The counted integer $k_{\max} = 60$ and the stated input $N_{\rm gen} = 3$ + the measured G, the one dimensionful scale, + one measured continuous number, the early-clock coefficient C (App. FK; $C = 1$ on bound-matter clocks, Postulate ZS.11)
Theorem-grade:
- $\mu(x) = x/(1+x)$, the weak-response form of the derived exponential response (Thm. N.8; App. BS)
- $a_0 = 2\sqrt{\alpha}\, cH_0$ **derived** from stationarity (Thm. N.14)
- Dust branch under $K' = \mu$: $w \to 0$, $c_s^2 \to 0$ (Thm. Q.7)

Derived quantities:
- α^{-1}: closed form exact under two stated choices; last 21 ppm on the open bracket; identification with $1/e^2$ not derived (§X)
- $(H_0 t_P)^2 = C\alpha^{57} \approx 10^{-122}$ (exponent forced; C measured on the early clock, $C = 1$ on bound-matter clocks, Postulate ZS.11)
- $v = M_P \alpha^8 \sqrt{2\pi}$ (Higgs scale; exponent derived, prefactor fitted)
- Strong CP: $\bar{\theta} = 0$ at tree level, loop-bounded, with $\theta_{\rm YM} = 0$ fixed by the spectral action given that nothing is added to it for the gauge fields, and given Postulate Y.10 (Thm. L.3)
- Fermion masses (1.42% LO; seven prefactors data-selected), CKM, PMNS ($N_{\rm gen} = 3$ a discrete input)
- Proton stable (if baryon number is violated only by the electroweak anomaly)

Falsifiable predictions:
- Channel-resolved clock structure of the extended non-metric channel (Sec. XI); co-located cavity–atom null (Thm. XI.2)
- No QCD axion; No 4th generation; No proton decay (conditional)

Appendix L: Strong CP: Tree-Level Closure, Loop-Bounded

1. What must be shown

In any 4D gauge theory with quarks, the physical strong-CP parameter is

$$\bar{\theta} \;=\; \theta_{\rm bare} \;+\; \arg\det M_u \;+\; \arg\det M_d\,. \tag{L1}$$

The statement "$\bar{\theta} = 0$ to all orders" would be equivalent to the statement that the *full quantum effective action* respects an exact CP symmetry; this appendix establishes the tree-level statement and the absence of the CP anomaly, with loop corrections bounded at the Standard-Model level. Since the operator

$$\mathcal{O}_\theta \;\equiv\; \frac{1}{32\pi^2}\,{\rm Tr}(F \wedge F) \tag{L2}$$

changes sign under CP, any CP-invariant quantum effective action forbids a generated coefficient for $\mathcal{O}_\theta$. Thus the claim reduces to two conditions:

1. **Classical CP invariance:** the microscopic action is CP invariant at $\theta_{\rm bare} = 0$.
2. **No CP anomaly:** the fermion measure (determinant/Pfaffian) is invariant under CP.

If both hold, then $\theta_{\rm bare} = 0$ is protected as a selection rule at tree level and the anomaly generates no effective θ term; loop corrections through the CKM sector are bounded at the Standard-Model level (main theorem below).

2. Tree-level inputs

The DFD microsector on $M = \mathbb{C}P^2 \times S^3$ with gauge bundle $E = \mathcal{O}(9) \oplus \mathcal{O}^{\oplus 5}$ produces:

- The Standard Model gauge group $G_{\rm SM} = {\rm SU}(3)_C \times {\rm SU}(2)_L \times {\rm U}(1)_Y$, with its electroweak factor resting on one stated identification and colour an input (App. F),
- Real Yukawa eigenvalues from the Kähler structure,
- $\arg\det(M_u M_d) = 0$ at tree level for det-orthogonal mass matrices positive on the branch of Postulate Y.10 (App. AO),
- Nonzero CKM CP violation ($J \neq 0$) from the det-orthogonal Berry offset of Postulate Y.10 (App. AO); the minimal real kernel gives $J = 0$ (Theorem AO.7).

The CKM phase violates CP, so Condition (1) holds here only in the weaker form the main theorem uses: the strong sector carries no tree-level phase, $\arg\det(M_u M_d) = 0$. Closing the anomaly channel requires establishing Condition (2): CP non-anomaly.

3. The Dai–Freed anomaly formula

For a discrete symmetry σ (here $\sigma = {\rm CP}$), the anomaly is a U(1) phase given by the holonomy of the Pfaffian/determinant line bundle over background fields. The Dai–Freed theorem [146, 147] expresses this holonomy as an exponentiated η-invariant on the *mapping torus*.

Let $M = \mathbb{C}P^2 \times S^3$ be the microsector manifold with its gauge bundle E and fermion bundle $W = S \otimes E \oplus \bar{S} \otimes \bar{E}$ (a $\mathbb{Z}_2$-graded Clifford module; the antilinear CP lift exchanges the two summands). Define the mapping torus:

$$T_{\rm CP} \;\equiv\; (M \times [0,1]) \,/\, (x,0) \sim ({\rm CP}(x),1)\,. \tag{L3}$$

The CP anomaly phase is then:

$$A_{\rm CP} \;=\; \exp\!\left(\frac{i\pi}{2}\,\eta(D_{T_{\rm CP}})\right), \tag{L4}$$

where $D_{T_{\rm CP}}$ is the Dirac operator of the Clifford-module bundle induced by W on $T_{\rm CP}$, and $\eta(\cdot)$ is the APS η-invariant [146].

Criterion. CP is non-anomalous iff $A_{\rm CP} = 1$, i.e. iff $\eta(D_{T_{\rm CP}}) \in 4\mathbb{Z}$.

4. Theorem: η vanishes automatically in even dimensions

Theorem L.1 (Automatic vanishing of η in even dimensions)**.** *Let X be a* closed even-dimensional *oriented Riemannian manifold, and let D_E denote the Dirac operator of a $\mathbb{Z}_2$-graded Clifford-module bundle over X with compatible connection (for a Spin^c manifold, the Spin^c Dirac operator twisted by a Hermitian vector bundle E with unitary connection; in general no Spin^c structure is needed). Then the spectrum of D_E is symmetric about 0, hence*

$$\eta(D_E) = 0, \tag{L5}$$

and therefore $\exp\!\big(\frac{i\pi}{2}\eta(D_E)\big) = 1$.

Proof. Because $\dim X$ is even, the Clifford volume element supplies a $\mathbb{Z}_2$ grading $S = S^+ \oplus S^-$ of the module with chirality operator $\Gamma = {\rm diag}(+1,-1)$. The twisted Dirac operator is *odd* with respect to this grading:

$$\Gamma D_E \Gamma^{-1} \;=\; -\,D_E. \tag{L6}$$

Consequently, if $D_E\psi = \lambda\psi$ with $\lambda \neq 0$, then $D_E(\Gamma\psi) = -\lambda(\Gamma\psi)$, and the multiplicities of $\pm\lambda$ match exactly. For $\mathrm{Re}\, s > \dim X$ the series below converges absolutely by Weyl's law, so the pairing may be carried out term by term. Thus the η-function, defined initially for $\mathrm{Re}(s) \gg 0$ by

$$\eta(D_E, s) = \sum_{\lambda \neq 0} \mathrm{sign}(\lambda)\,|\lambda|^{-s}, \tag{L7}$$

vanishes identically term-by-term (each $+\lambda$ cancels a $-\lambda$), and by analytic continuation $\eta(D_E) = \eta(D_E, 0) = 0$. □

Corollary L.2 (Trivial CP anomaly in DFD)**.** *The mapping torus $T_{\rm CP}$ has dimension*

$$\dim T_{\rm CP} = \dim M + 1 = 7 + 1 = 8 \quad \textit{(even)}. \tag{L8}$$

The CP involution on $\mathbb{C}P^2$ (complex conjugation in homogeneous coordinates), combined with the identity on S^3, is an orientation-preserving isometry of M, so $T_{\rm CP}$ is a closed oriented Riemannian 8-manifold. It admits no Spin^c structure ($H^2(T_{\rm CP};\mathbb{Z}) = 0$ while $w_2(T_{\rm CP}) \neq 0$), and the lift of CP maps E to $\bar{E}$; the fermion bundle $W = S \otimes E \oplus \bar{S} \otimes \bar{E}$ with the antilinear CP lift nevertheless descends to a $\mathbb{Z}_2$-graded Clifford-module bundle over $T_{\rm CP}$ (a ${\rm Spin} \times_{\mathbb{Z}_2} O(2)$ structure exists, with $L_{\mathbb{R}}$ the real rank-two bundle obtained from $\det E$ by the conjugation gluing: $w_2(T_{\rm CP}) = w_2(L_{\mathbb{R}})$ and $w_1(L_{\mathbb{R}})^2 = 0$), so Theorem L.1 applies in its Clifford-module form. Moreover, for the product metric with the untwisted round S^3 of radius

r_3 and $\mathbb{C}P^2$-only twisting, $D^2_{T_{\rm CP}} = D^2_{\mathbb{C}P^2,E} + D^2_{S^3} - \partial_t^2 \geq 9/(4r_3^2) > 0$, so $D_{T_{\rm CP}}$ has no zero modes and $\eta = h = 0$ for either a determinant or a Pfaffian fermion measure. Hence, by Theorem L.1:

$$\eta(D_{T_{\rm CP}}) = 0 \in 4\mathbb{Z}, \qquad A_{\rm CP} = \exp\left(\frac{i\pi}{2}\cdot 0\right) = 1. \quad \text{(L9)}$$

Remark. This result does *not* depend on a delicate explicit evaluation of η; it uses only the structural fact that the operator in Eq. (L4) is a twisted Dirac operator on an even-dimensional closed manifold, hence has exact $\pm\lambda$ spectral pairing by Eq. (L6).

5. Main theorem: tree-level closure, loop-bounded

Theorem L.3 (Strong CP closure: tree-level $\bar\theta = 0$, loop-bounded)**.** *In the DFD microsector on $M = \mathbb{C}P^2 \times S^3$ with the Standard Model fermion content:*

1. *Given that nothing is added to the spectral action for the Standard-Model gauge fields, colour included (that is, each topological sector is weighted by that action alone), the microscopic theory is CP invariant in the strong sector at tree level: the spectral action contains no $\mathrm{Tr}(F\wedge F)$ term, so $\theta_{\rm bare} = 0$, and on the branch of Postulate Y.10 connected to $\xi = 0$, $\det(M_u M_d) > 0$.*
2. *The CP anomaly phase is trivial: $A_{\rm CP} = 1$ (Corollary L.2).*

Therefore $\bar\theta = 0$ at tree level, and its loop-induced value is at the Standard-Model level ($\lesssim 10^{-16}$; App. AO). No axion is required.

Proof. Condition (1) holds at tree level. The spectral action $\mathrm{Tr}\, f(D^2/\Lambda^2)$ of Proposition WS.5, $D = D_M \otimes 1 + \gamma_5 \otimes D_F$, is real, and reversing the orientation of spacetime takes D to $-(\gamma_5\otimes 1)\, D\, (\gamma_5 \otimes 1)$, whose square has the same spectrum as D^2, while $\int \mathrm{Tr}(F\wedge F)$ changes sign; so the spectral action contains no $\mathrm{Tr}(F\wedge F)$ term [148], and the internal trace that fixes α (premise G2) contains no four-dimensional field. With nothing added to the spectral action for the gauge fields, no topological sector carries a phase of its own, and $\theta_{\rm bare} = 0$ in the basis in which D_F carries the mass matrices of Postulate Y.10. With the positive-definite S_f of that postulate and the offset on its branch connected to $\xi = 0$ (Theorem AT.16), $\det(M_u M_d) > 0$, so $\arg\det(M_u M_d) = 0$ at tree level and the vacuum angle is 0, not π. Condition (2) follows from Corollary L.2: the mapping torus has even dimension (8), so the twisted Dirac operator has symmetric spectrum and $\eta = 0$ automatically.

Since both conditions hold, the tree-level effective action contains no θ term. Loop corrections with the Standard-Model chiral Yukawa structure regenerate a coefficient of $\mathrm{Tr}(F\wedge F)$ only through the degree-thirteen Jarlskog structure (the shift of $\arg\det(M_u M_d)$ vanishes identically through Yukawa degree eleven for Hermitian tree-level mass matrices with the Standard-Model chiral couplings; the onset is the multi-loop effect of the cited references), and the induced angle is $\lesssim 10^{-16}$ [149, 150]. □

6. A conditional alternative: quaternionic structure

A conditional alternative route, requiring the CP lift to commute with the Dirac operator, comes from the quaternionic structure on the S^3 factor.

Lemma L.4 (3D charge conjugation)**.** *Let σ^a be Pauli matrices and consider the 3D Euclidean Dirac operator $D_3 = i\sigma^a\nabla_a$. Define the antiunitary charge conjugation $C_3 \equiv \sigma^2 \circ K$ (with K complex conjugation). Then*

$$C_3^2 = -1, \qquad C_3 D_3 C_3^{-1} = D_3. \quad \text{(L10)}$$

Proof. The Pauli identity $\sigma^2(\sigma^a)^*\sigma^2 = -\sigma^a$ implies $C_3\,\sigma^a\,C_3^{-1} = -\sigma^a$, while antiunitarity gives $C_3\, i\, C_3^{-1} = -i$. Therefore $C_3(i\sigma^a)C_3^{-1} = i\sigma^a$, proving commutation with D_3. Finally $C_3^2 = \sigma^2(\sigma^2)^* = -\mathbb{1}$. □

When the CP lift commutes with the Dirac operator, the quaternionic structure ($J^2 = -1$) forces the fermion determinant to be real and nonnegative [147, 151], giving an independent route to $A_{\rm CP} = 1$ on the product background; the argument of Corollary L.2 does not rely on it.

7. Falsifiable prediction

Theorem L.3 implies:

- **No QCD axion exists.** Axion searches (ADMX, ABRACADABRA, CASPEr, etc.) will find nothing.
- **Any observed $|\bar\theta| > 10^{-15}$ would falsify this mechanism.**

This is a sharp, experiment-confrontable prediction distinguishing DFD from Peccei–Quinn solutions.

8. Summary: why the S^3 factor does triple duty

With $\theta_{\rm bare} = 0$ fixed by the spectral action given that nothing is added to it for the gauge fields, the Strong CP problem is closed at tree level in DFD by the det-orthogonal tree-level protection together with the η-invariant argument ($\bar\theta = 0$ at tree level, loop-bounded below 10^{-16}), not by introducing new particles. The mechanism is dimensional: the microsector $M = \mathbb{C}P^2 \times S^3$ has $\dim M = 7$, so the mapping torus has $\dim T_{\rm CP} = 8$ (even), forcing $\eta = 0$ by spectral symmetry.

The same S^3 factor that:

1. Carries baryon number as $\pi_3(S^3) = \mathbb{Z}$ winding (a stated identification; proton stability, Theorem G.4, does not use it),

2. Provides gauge emergence: $\pi_3(\mathrm{SU}(3)) = \mathbb{Z}$,

also contributes the "+1" to make $\dim T_{\mathrm{CP}} = 8$ even, which closes the anomaly channel of Strong CP. The generation count, $N_{\mathrm{gen}} = 3$, is a stated input, which no index on $\mathbb{C}P^2 \times S^3$ supplies (App. F).

Appendix M: Scattered and Locally Emitted Lines in a Static ψ

This appendix gives DFD's value of the enhancement factor Γ in the Ly-α/O VI asymmetry ratio of Sec. XIV G.

1. Definitions and Setup

Let $\psi(\mathbf{x})$ be the DFD scalar field with refractive index $n = e^{\psi}$ and one-way light speed $c_1 = c\,e^{-\psi}$. Consider two UV lines observed by UVCS:

- **H Ly-α:** Dominated by resonant scattering of chromospheric radiation in the corona.
- **O VI:** Dominated by local (collisional) emission in the corona.

Let A denote the measured asymmetry amplitude statistic, and define:

$$R \equiv \frac{A_{\mathrm{Ly}\alpha}}{A_{\mathrm{OVI}}} = \Gamma \left(\frac{\sigma_{\mathrm{OVI}}}{\sigma_{\mathrm{Ly}\alpha}} \right)^2 . \tag{M1}$$

2. Gaussian Detuning Scaling

For a symmetric line profile with thermal width σ and small detuning $\delta \ll \sigma$, a Taylor expansion of the Gaussian gives:

$$A = \frac{\Delta I}{I} \propto \left(\frac{\delta}{\sigma} \right)^2 \tag{M2}$$

to leading order (the linear term vanishes by symmetry). This scaling follows from the sensitivity of resonant absorption/scattering to wavelength mismatch.

3. The Value of Γ

In a static ψ a photon's frequency is conserved along its path, so the outgoing leg cannot change the integrated scattered flux: resonant scattering responds only to the detuning at the scatterer, as in standard coronal physics. DFD's optics therefore adds no enhancement, and Γ takes its standard value.

4. Observational Constraint on Γ

The 2007–2009 UVCS data do not measure R, since their two annual amplitudes are different statistics and neither shows a significant annual modulation with independent units. The width factor $(\sigma_{\mathrm{OVI}}/\sigma_{\mathrm{Ly}\alpha})^2 = 9.0$ of Sec. XIV G holds for a Ly-α temperature of 10^4 K; the coronal H I that UVCS observes is at about 1–3 $\times 10^6$ K, so Γ needs the widths measured in the spectra that give R, as in the matched dim/bright slope described there. In the same data the velocity shift of the intensity-contrast groups is null (Cohen's $d = -0.03$; Sec. XIV).

Appendix N: First-Principles Derivation of $\mu(x)$ and a_0

This appendix derives both the MOND crossover function $\mu(x) = x/(1+x)$ and the acceleration scale $a_0 = 2\sqrt{\alpha}\, cH_0$ from the S^3 Chern-Simons microsector with explicit, minimal assumptions. (Section XVI A 6 distinguishes the cosmological acceleration cH_0 from the galactic crossover $a_0 = 2\sqrt{\alpha}\, cH_0$, whose value on bound-matter clocks is $a_0 = 1.1966 \times 10^{-10}\,\mathrm{m/s^2}$ (Postulate ZS.11); throughout, $a_\star = 2a_0/c^2$ denotes the Lagrangian gradient scale, not an acceleration.) The derivation proceeds in two stages:

1. **Stage I (asymptotics theorem-grade):** The two asymptotic limits of $\mu(s)$ are forced by microsector multiplicativity and the composition law (Theorem N.8); the specific transition form $\mu(s) = s/(1+s)$ is the weak-response form (Assumption N.3) of the exponential response forced by the composition law (Lemma N.6); it tracks the derived law of App. BS (RAR form) to $\lesssim 0.02$ dex, below SPARC precision.
2. **Stage II (Derived):** The crossover invariant $\Xi_* = 3/2$ is selected by scaling stationarity (Theorem N.12), yielding $a_0 = 2\sqrt{\alpha}\, cH_0$ (Theorem N.14).

1. The S^3 Partition Function (Exact Result)

Lemma N.1 (S^3 partition function exponent)**.** *For $SU(2)$ Chern-Simons theory on S^3 at integer level $k \geq 1$, the exact Witten partition function is [132]:*

$$Z_{S^3}(k) = \sqrt{\frac{2}{k+2}}\,\sin\left(\frac{\pi}{k+2}\right). \tag{N1}$$

In the large-k regime, $\sin(\pi/(k+2)) \sim \pi/(k+2)$, hence:

$$Z_{S^3}(k) = \mathrm{const}\cdot(k+2)^{-3/2}\left(1+O(k^{-2})\right), \tag{N2}$$

$$\log Z_{S^3}(k) = \mathrm{const} - \frac{3}{2}\log(k+2) + O(k^{-2}).$$

The exponent $3/2 = \dim SU(2)/2$ is fixed by the gauge group; since $SU(2) \cong S^3$ it equals $\dim(S^3)/2$.

2. Microsector-to-ψ Map and Level Response

Assumption N.2 (Microsector multiplicative weight defines e^ψ)**.** The DFD scalar ψ is defined (up to an additive constant) by the ratio of microsector weights:

$$e^{\psi(s)} := \frac{Z_{S^3}(k_0)}{Z_{S^3}(k_{\mathrm{eff}}(s))}, \tag{N3}$$

where k_0 is the background level and $k_{\mathrm{eff}}(s)$ is the effective level in an environment parameterized by a dimensionless $s \geq 0$.

Assumption N.3 (Minimal weak-field level response)**.** In the weak-response regime, the effective level scales as:

$$k_{\mathrm{eff}}(s) = k_0(1+s), \tag{N4}$$

with $k_0 \gg 1$ so that $k_0 \pm O(1)$ corrections are negligible in logarithms.

Proposition N.4 (ψ inherits the 3/2 coefficient)**.** *Under Assumptions N.2–N.3 and using Lemma N.1:*

$$\psi(s) = \frac{3}{2}\log(1+s) + O(k_0^{-1}). \tag{N5}$$

Proof. From Eqs. (N3) and (N2):

$$\begin{aligned}\psi(s) &= \log Z_{S^3}(k_0) - \log Z_{S^3}(k_{\mathrm{eff}}(s)) \\ &= \frac{3}{2}\left[\log(k_{\mathrm{eff}}(s)+2) - \log(k_0+2)\right] + O(k_0^{-1}).\end{aligned}$$

Insert $k_{\mathrm{eff}}(s) = k_0(1+s)$ and expand:

$$\log(k_0(1+s)+2) - \log(k_0+2) = \log(1+s) + O(k_0^{-1}).$$

□

3. The Key Theorem: μ is Fixed by a Composition Law

The exponential form of μ follows from the composition law of Assumption N.5.

Assumption N.5 (Independent segments compose by saturation union)**.** If two independent contributions add in ψ (because microsector weights multiply), then the effective response μ satisfies the saturation-union law:

$$\mu(\psi_1+\psi_2) = 1 - \big(1-\mu(\psi_1)\big)\big(1-\mu(\psi_2)\big), \tag{N6}$$
$$\mu(0) = 0, \qquad 0 \leq \mu < 1.$$

Lemma N.6 (Composition ⇒ exponential)**.** *Under Assumption N.5 on $\psi \geq 0$, continuity of μ, and $\mu \not\equiv 0$, there exists a constant $c > 0$ such that, for $\psi \geq 0$:*

$$\mu(\psi) = 1 - e^{-c\psi}. \tag{N7}$$

Proof. Define $g(\psi) := 1 - \mu(\psi)$. Then Eq. (N6) becomes $g(\psi_1+\psi_2) = g(\psi_1)g(\psi_2)$ with $g(0) = 1$ and $g(\psi) \in (0,1]$. By the standard Cauchy functional equation for multiplicative g under continuity, $g(\psi) = e^{-c\psi}$ for some $c \geq 0$. Since $\mu \not\equiv 0$, $c > 0$. □

Assumption N.7 (Deep-field limit fixes the slope)**.** In the small-s regime, the desired MOND closure has $\mu(s) = s + O(s^2)$ when expressed in terms of the same s appearing in the level response (N4).

Theorem N.8 (Weak-response $\mu(s)$ from the S^3 power law)**.** *Assume Assumptions N.2, N.3, N.5, and N.7. Then, in the large-k_0 regime and within the weak-response domain of Assumption N.3:*

$$\boxed{\mu(s) = \frac{s}{1+s} + O(k_0^{-1})} \tag{N8}$$

Proof. By Lemma N.6, $\mu(\psi) = 1 - e^{-c\psi}$. Using Proposition N.4, $\psi(s) = \frac{3}{2}\log(1+s) + O(k_0^{-1})$. Thus:

$$\mu(s) = 1 - \exp\left(-c \cdot \frac{3}{2}\log(1+s)\right) + O(k_0^{-1})$$
$$= 1 - (1+s)^{-3c/2} + O(k_0^{-1}).$$

Assumption N.7 requires $\mu(s) = s + O(s^2)$ as $s \to 0$, i.e., $(1+s)^{-3c/2} = 1 - s + O(s^2)$, which forces $3c/2 = 1$, hence $c = 2/3$. Substituting yields $\mu(s) = 1 - (1+s)^{-1} = s/(1+s)$. □

Microsector Result: exponential response; $\mu(x) = x/(1+x)$ is its weak-response form

The exponential response (Lemma N.6) and its weak-response form $\mu(s) = s/(1+s)$ (Theorem N.8) follow from:

1. The S^3 partition function exponent $3/2 = \dim SU(2)/2$
2. Microsector multiplicativity (weights multiply $\Rightarrow$ ψ adds)
3. Saturation-union composition law (Assumption N.5)
4. Weak-response level response and deep-field limit slope (Assumptions N.3, N.7)

These uniquely fix the two asymptotic limits ($\mu \to 1$, $\mu \sim s$) and the exponential form; the transition-region shape follows from the saturation-union closure (Assumption N.5) together with what is assumed for the exponent (Remark BS.11): the weak-response form tracks the derived response of App. BS (RAR form) to $\lesssim 0.02$ dex on the SPARC range, and the variational closure (§N 6) is a cross-check of the asymptotics only.

Remark N.9 (Two-vertex QED count). A vertex count in QED gives the number $d_e = 2\sqrt{\alpha}$ heuristically. Each photon-fermion vertex contributes amplitude $e \propto \sqrt{\alpha}$. For a neutral atom with two charged constituents (electron and nucleus), counting one $\sqrt{\alpha}$ per constituent gives:

$$d_e^{\text{atom}} = \sqrt{\alpha} + \sqrt{\alpha} = 2\sqrt{\alpha} \approx 0.171. \tag{N9}$$

This gives $a_0 = d_e \cdot cH_0 = 2\sqrt{\alpha} \cdot cH_0$.

a. Physical interpretation. Photons couple directly to the optical metric with $d_\gamma = 1$. Electrons do not couple directly to ψ; they interact through QED vertices. Each vertex contributes $\sqrt{\alpha} < 1$. Matter couples *less strongly* than light because its interaction is mediated.

b. Status of the count. This is a heuristic vertex count: for independent subsystems the energies add, $E_{\text{atom}} = E_e + E_N$, so their fractional responses average rather than add. The prefactor $2\sqrt{\alpha}$ of a_0 is fixed by the variational derivation below (Theorem N.14).

4. The Acceleration Scale a_0: Variational Derivation

We now derive $a_0 = 2\sqrt{\alpha}\, cH_0$ from a variational principle that selects the crossover point using the S^3 microsector scaling charge.

a. The Unique IR Control Parameter

Given DFD postulates (flat $\mathbb{R}^3$, scalar ψ, $a = (c^2/2)\nabla\psi$ in the weak static field) and a single global μ-closure, the onset of non-Newtonian response can depend only on the *unique* dimensionless scalar built from $|a|$ and the cosmological scale cH_0:

$$\Xi := k_a \left(\frac{|a|}{cH_0}\right)^2, \tag{N10}$$

where the coefficient $k_a = 3/(8\alpha)$ is fixed by the microsector (Section VIII B).

b. Microsector Scaling Charge

Lemma N.10 (Scaling charge from S^3)**.** *For $SU(2)$ Chern-Simons on S^3, the partition function satisfies $\log Z_{S^3}(k) = \text{const} - \frac{3}{2}\log(k+2) + O(k^{-2})$. The dimensionless scaling charge is:*

$$q_{S^3} := -\frac{\partial \log Z_{S^3}}{\partial \log(k+2)} = \frac{3}{2}. \tag{N11}$$

This is the same topological coefficient that appears in the $\mu(x)$ derivation (Theorem N.8).

c. The Spacetime Functional

We now show that the crossover point $\Xi_* = 3/2$ is selected by an explicit *spacetime integral functional* built only from the DFD field ψ and the cosmic scale cH_0.

a. Local dimensionless invariant. Under DFD postulates, the local dimensionless invariant, with $|\mathbf{a}|$ the proper acceleration of static observers (Eq. (AP12) in the weak static field), is:

$$\Xi(\mathbf{x}) = k_a \left(\frac{|\mathbf{a}|}{cH_0}\right)^2 = \beta\,|\nabla\psi|^2, \qquad \beta := \frac{k_a c^2}{4H_0^2}. \tag{N12}$$

b. The minimal spacetime functional. Define the dimensionless functional:

$$\boxed{\mathcal{S}[\psi] := \int_\Omega d^3x \left(\Xi(\mathbf{x}) - q_{S^3}\log\Xi(\mathbf{x})\right), \qquad q_{S^3} = \frac{3}{2}.} \tag{N13}$$

No additional scale has been introduced: the logarithm is well-defined because Ξ is dimensionless.

c. Interpretation. $\mathcal{S}$ is *not* asserted to be the full dynamical action of DFD. It is the minimal coarse-grained IR functional whose only nontrivial coefficient is the S^3 scaling charge q_{S^3}, and whose stationary point fixes the crossover invariant.

d. Homogeneous-Limit Theorem

Definition N.11 (Homogeneous-gradient sector)**.** Fix a bounded region Ω of volume V and a reference profile ψ_0. Consider the one-parameter family $\psi_\lambda := \lambda\,\psi_0$ with $\lambda > 0$. Then $\nabla\psi_\lambda = \lambda\,\nabla\psi_0$ and:

$$\Xi_\lambda(\mathbf{x}) = \lambda^2 \Xi_0(\mathbf{x}). \tag{N14}$$

Theorem N.12 (Scaling stationarity selects the mean crossover invariant)**.** *Let $\psi_\lambda = \lambda\psi_0$ and define the mean invariant:*

$$\overline{\Xi}_0 := \frac{1}{V}\int_\Omega d^3x\,\Xi_0(\mathbf{x}).$$

Then stationarity of $\mathcal{S}[\psi_\lambda]$ with respect to λ occurs at:

$$\lambda_*^2 = \frac{q_{S^3}}{\overline{\Xi}_0}, \qquad \overline{\Xi}_* := \frac{1}{V}\int_\Omega d^3x\,\Xi_{\lambda_*}(\mathbf{x}) = q_{S^3} = \frac{3}{2}. \tag{N15}$$

Proof. Insert Eq. (N14) into Eq. (N13):

$$\mathcal{S}[\psi_\lambda] = \int_\Omega d^3x\left(\lambda^2\Xi_0 - q_{S^3}\log\!\left(\lambda^2\Xi_0\right)\right)$$

$$= \lambda^2 V\overline{\Xi}_0 - q_{S^3}\left(2V\log\lambda + \int_\Omega d^3x\,\log\Xi_0\right).$$

Differentiate with respect to λ and set to zero:

$$\frac{d\mathcal{S}}{d\lambda} = 2\lambda V\overline{\Xi}_0 - \frac{2q_{S^3}V}{\lambda} = 0 \;\Rightarrow\; \lambda_*^2 = \frac{q_{S^3}}{\overline{\Xi}_0}.$$

Then $\overline{\Xi}_* = \lambda_*^2\overline{\Xi}_0 = q_{S^3} = 3/2$. □

Corollary N.13 (Local homogeneous limit)**.** *If $\Xi_0(\mathbf{x})$ is approximately spatially constant in Ω, then $\overline{\Xi}_0 = \Xi_0$ and the stationarity condition becomes the pointwise statement:*

$$\boxed{\Xi_* = \frac{3}{2}} \tag{N16}$$

e. The MOND Scale Theorem

Theorem N.14 (MOND scale from spacetime functional)**.** *Combining Corollary N.13 with $k_a = 3/(8\alpha)$:*

$$\boxed{a_0 = 2\sqrt{\alpha}\,cH_0} \tag{N17}$$

Proof. From Eq. (N10) at $\Xi = \Xi_*$:

$$a_0 = cH_0\sqrt{\frac{\Xi_*}{k_a}} = cH_0\sqrt{\frac{3/2}{3/(8\alpha)}}$$
$$= cH_0\sqrt{\frac{3}{2}\times\frac{8\alpha}{3}} = cH_0\sqrt{4\alpha} = 2\sqrt{\alpha}\,cH_0. \tag{N18}$$

□

Derived: $a_0 = 2\sqrt{\alpha}\,cH_0$

Status: The dimensionless law and prefactor are derived. On bound-matter clocks the physical normalization is the $C = 1$ value, with no measured coefficient (Postulate ZS.11); it is not a galactic fit.

The derivation chain:

1. $k_a = 3/(8\alpha)$ from gauge emergence (Section VIII B)
2. $q_{S^3} = 3/2$ from S^3 partition function (Lemma N.10)
3. $\mathcal{S}[\psi] = \int(\Xi - q_{S^3}\log\Xi)\,d^3x$ — explicit spacetime functional (N13)
4. $\Xi_* = 3/2$ from scaling stationarity (Theorem N.12)
5. $a_0 = 2\sqrt{\alpha}\,cH_0$ from algebra (Theorem N.14)

What is derived vs. postulated:

- **Derived:** $q_{S^3} = 3/2$ from the S^3 partition function; stationarity of an explicit spacetime functional then sets $\Xi_* = q_{S^3}$.
- **Postulated:** the functional form (N13) (a coarse-grained functional, not the full action).

Comparison: on bound-matter clocks (Postulate ZS.11) $a_0 = 2\sqrt{\alpha}\,cH_0^{\rm loc} = 1.1966\times10^{-10}$ m/s^2 vs. the comparator $a_0 = (1.20 \pm 0.02_{\rm stat} \pm 0.24_{\rm sys})\times10^{-10}$ m/s^2 [10], within the systematic error.

5. Summary and Falsifiable Predictions

TABLE XCIV. Status of MOND derivation from microsector.

Result	Status	Key Input
$\mu(s) = s/(1+s)$	Thm. N.8	Composition + level response
$\psi = \frac{3}{2}\log(1+s)$	Prop. N.4	Witten partition function
$\Xi_* = 3/2$	Thm. N.12	Spacetime stationarity
$a_0 = 2\sqrt{\alpha}\,cH_0$	Thm. N.14	$k_a + \Xi_*$ (both derived)

a. Falsifiable predictions.

1. **Exponential μ-response:** The interpolation must be the exponential response of Lemma N.6 and App. BS, whose weak-response form is $\mu(x) = x/(1+x)$, not $x/\sqrt{1+x^2}$ or other forms. (Already favored by SPARC data, Section VII.)

2. **Locked a_0 value on bound-matter clocks:** Precision measurements of a_0 from large galaxy samples should converge to $2\sqrt{\alpha}\,cH_0^{\rm loc} = 1.1966\times10^{-10}$ m/s^2 on distances computed with $H_0^{\rm loc}$ (Postulate ZS.11); convergence to the early-clock value 1.1208×10^{-10} m/s^2 on distances computed with $H_0^{\rm early}$ falsifies the postulate.

3. **Epoch-consistency scaling:** Since a_0 is fixed by topology plus H_0, the present-epoch value at $z = 0$ is derived given the clock (Postulate ZS.11).

A companion note [112] argues (program-grade) that under the same epoch-consistency rule that promotes the current closure $G\hbar H_0^2/c^5 = C\alpha^{57}$ to $G(t)\hbar H(t)^2/c^5 = C\alpha^{57}$ (Section XIX), the acceleration scale should be promoted similarly to $a_0(z) = 2\sqrt{\alpha}\, cH(z)$. High-redshift kinematics test it, and the first tests disagree: low-mass discs at $0.33 < z < 1.44$ show a rise on the published bins, which counted galaxy by galaxy is about 1σ within the survey and about 3σ anchored to SPARC's $z = 0$ value, with DFD's law fitting on the bound-matter clock, and depends on how the molecular gas is added, while massive discs at $0.6 < z < 2.5$ give an a_0 close to the local value at $z \simeq 2$ (App. A0Z). The promotion is contested; direct molecular-gas masses, kinematic masses not limited by a halo-model prior, galaxy-level errors and the environments of the high-redshift discs decide it.

6. Alternative Derivation: Variational Approach

The S^3 composition law derivation above gives $\mu(x) = x/(1+x)$. Here we present an independent variational derivation that yields a closely related result, providing a cross-check on the functional form.

a. Setup: Auxiliary-Field Action

Write the dimensionless gradient invariants:

$$u \equiv \frac{|\nabla\psi|}{a_\star}, \qquad s \equiv u^2 = \frac{|\nabla\psi|^2}{a_\star^2}. \tag{N19}$$

Consider the static sector with action density:

$$\mathcal{L}_\psi = \frac{a_0^2}{8\pi G}U(s) - \frac{c^2}{2}\psi(\rho - \bar{\rho}), \tag{N20}$$

where $U(s)$ is *a priori* unknown. Variation gives:

$$\partial_i\left[U'(s)\,\partial_i\psi\right] = -\frac{8\pi G}{c^2}(\rho - \bar{\rho}). \tag{N21}$$

Identifying the constitutive law:

$$\mu(u) \equiv U'(s) \quad (s = u^2) \tag{N22}$$

yields the nonlinear Poisson equation $\nabla\cdot[\mu(u)\nabla\psi] = -(8\pi G/c^2)(\rho - \bar{\rho})$.

b. Asymptotic Constraints

Two physical limits constrain $U(s)$:

a. Strong field ($u \gg 1$). In the Newtonian limit, we require $\mu(u) \to 1$, hence:

$$U(s) \sim s \quad \text{as } s \to \infty. \tag{N23}$$

b. Deep field ($u \ll 1$). For flat rotation curves, we require $\mu(u) \sim u$, hence:

$$U(s) \sim s^{3/2} \quad \text{as } s \to 0. \tag{N24}$$

Any admissible U must interpolate between $s^{3/2}$ (deep field) and s (strong field) while remaining *convex* ($U''(s) > 0$) to ensure a strictly monotone constitutive law and an elliptic operator.

c. Closed-Form Solution

A minimal convex interpolant satisfying these asymptotics can be obtained via Legendre construction. The result is:

$$\boxed{\mu(u) = \frac{1 + 2u - \sqrt{1+4u}}{2u}}, \quad u > 0. \tag{N25}$$

a. Asymptotic checks.

$$u \ll 1: \quad \sqrt{1+4u} = 1 + 2u - 2u^2 + \cdots$$
$$\Rightarrow \mu(u) = u + O(u^2) \quad \checkmark \tag{N26}$$

$$u \gg 1: \quad \sqrt{1+4u} = 2\sqrt{u}(1 + O(u^{-1/2}))$$
$$\Rightarrow \mu(u) = 1 - \frac{1}{\sqrt{u}} + \cdots \quad \checkmark \tag{N27}$$

b. Monotonicity and ellipticity.

$$\mu'(u) = \frac{1}{2u^2}\left[\sqrt{1+4u} - 1 - \frac{2u}{\sqrt{1+4u}}\right] > 0 \quad (\forall u > 0), \tag{N28}$$

so the operator is strictly elliptic.

c. Convexity. Since $\mu = U'(s)$ with $s = u^2$:

$$U''(s) = \frac{d\mu}{ds} = \frac{\mu'(u)}{2u} > 0, \tag{N29}$$

establishing global convexity.

d. Comparison with S^3 Result

The variational result (N25) and the S^3 composition law result $\mu(x) = x/(1+x)$ are not identical, but share the same asymptotic structure:

	Variational	S^3 Composition
$u \ll 1$	$\mu \sim u$	$\mu \sim x$
$u \gg 1$	$\mu \to 1$	$\mu \to 1$
Monotone	✓	✓
Convex U	✓	✓

The two derivations yield *non-identical* interpolation functions—$\mu(x) = x/(1+x)$ (composition law) versus $\mu(u) = (1+2u-\sqrt{1+4u})/(2u)$ (variational)—that share the same two asymptotic limits but are not the same function: the transition-region shape is fixed only up to this closure choice.

a. Physical interpretation. The variational approach treats μ as the derivative of a convex energy density—the standard EFT perspective; the S^3 composition law derives μ from microsector multiplicativity. What is *uniquely forced* is the pair of asymptotic limits ($\mu \to 1$ Newtonian,

$\mu \sim x$ deep-MOND); the intermediate-u transition shape is closure-dependent. The variational route is best read as a cross-check confirming the asymptotic structure, not an independent derivation of the same transition function.

7. The Complete Picture: MOND from S^3 Topology

MOND Crossover: Complete Derivation Summary

Input: S^3 Chern-Simons microsector with partition function $Z_{S^3}(k) \propto (k+2)^{-3/2}$

Outputs:

$$\mu(x) = \frac{x}{1+x} \quad \text{(Thm. N.8; asymptotics)} \tag{N30}$$

$$\Xi_* = \frac{3}{2} \quad \text{(Thm. N.12)} \tag{N31}$$

$$a_0 = 2\sqrt{\alpha}\, cH_0 \quad \text{(Thm. N.14)} \tag{N32}$$

The two asymptotic limits of μ are forced; the μ transition-region shape is closure-fixed (below SPARC precision).

Consequence: Galaxy rotation curves follow from the topology of S^3—the same manifold that carries baryon number, and gives $\alpha = 1/137$.

The Galactic Missing-Mass Problem: the μ-Law Account

The *galactic* "missing mass" — flat rotation curves and the RAR — needs no fitted halo. It is a **geometric effect** from the S^3 microsector vacuum-weight response to matter density (the universal μ-law). The *cosmological* cold dark matter (CMB third peak, clusters) is a separate, derived particle, the χ-matter field of App. AV. It is present in galaxies too, and its pull composes with the μ-law there by the floor law, which is stated, not derived (App. AV).
The same topology that:

- Carries the generation label ($N_{\text{gen}} = 3$, a discrete input; $\pi_3(S^3) = \mathbb{Z}$ supplies the winding lattice, not the count — App. F)
- Carries baryon number (a stated identification; proton stability, Theorem G.4, does not use it)
- Gives $\alpha = 1/137$ (from $k_{\max} = 60$ on $\mathbb{C}P^2$)
- Closes the anomaly channel of Strong CP ($\dim(T_{\text{CP}}) = 8$ even)
- Fixes the clock–α constraint $G\hbar H_0^2/c^5 = C\,\alpha^{57}$ (exponent a theorem; on bound-matter clocks $C = 1$ and $H_0^{\text{loc}} = \alpha^{28.5}/t_P = 72.09$ km/s/Mpc; on the early clock $C = 0.878 \pm 0.003$ measured, $H_0^{\text{early}} = 67.52$ km/s/Mpc; Postulate ZS.11, App. ZS)

also produces:

- Flat rotation curves with $\mu(x) = x/(1+x)$
- MOND scale $a_0 = 1.1966 \times 10^{-10}$ m/s^2 on bound-matter clocks
- The radial acceleration relation
- The baryonic Tully-Fisher relation

Rotation curves from geometry — no fitted *halo* required. (The *cosmological* cold dark matter — CMB third-peak height and cluster mass, the latter at the amplitude its abundance gives under ΛCDM-like assembly (estimate; App. GR) — is the derived χ-matter particle of App. AV; it composes with the μ-law inside galaxies by the floor law.)

Appendix O: The α^{57} Mode-Count Exponent and the G–H_0–α Invariant

1. Mathematical core: primed-determinant scaling fixes the exponent

Let $\mathcal{H}$ be a finite-dimensional complex Hilbert space of dimension $k_{\max}$, and let $\mathcal{K} : \mathcal{H} \to \mathcal{H}$ be a self-adjoint, positive semidefinite operator with $\dim\ker(\mathcal{K}) = N_{\text{gen}}$. Denote by $\det'(\mathcal{K})$ the *primed determinant* over the nonzero spectrum of $\mathcal{K}$.

Lemma O.1 (Primed determinant scaling)**.** *For any $g > 0$,*

$$\det{}'\big(g\,\mathcal{K}\big) \;=\; g^{\,k_{\max}-N_{\text{gen}}}\;\det{}'(\mathcal{K})\,. \tag{O1}$$

Proof. Diagonalize $\mathcal{K}$ on $\mathcal{H}$ with eigenvalues $\{\lambda_i\}_{i=1}^{k_{\max}}$. Exactly N_{gen} of these are zero; the remaining $N := k_{\max} - N_{\text{gen}}$ satisfy $\lambda_i > 0$. Then by definition $\det'(\mathcal{K}) = \prod_{i=1}^{N}\lambda_i$ (product over the nonzero spectrum), and $\det'(g\mathcal{K}) = \prod_{i=1}^{N}(g\lambda_i) = g^N\prod_{i=1}^{N}\lambda_i$. □

Definition O.2 (Microsector hierarchy factor as a *determinant ratio*)**.** Define

$$\varepsilon(g) \;:=\; \frac{\det'(\mathcal{K})}{\det'(g\,\mathcal{K})}\,. \tag{O2}$$

Corollary O.3 (Forced exponent)**.** *If $k_{\max} = 60$ and $N_{\text{gen}} = 3$, then*

$$\varepsilon(g) = g^{-57} \qquad \textit{and in particular} \qquad \varepsilon(\alpha^{-1}) = \alpha^{57}\,. \tag{O3}$$

Proof. Immediate from Lemma O.1 and Definition O.2 with $N = k_{\max} - N_{\text{gen}} = 57$. □

a. Provenance of the two integers. The two integers in the exponent $k_{\max} - N_{\text{gen}} = 57$ have *distinct* provenance:

- $N_{\text{gen}} = 3$ is a **discrete input** (the observed family number; App. F 5, Rem. F.21). It is numerically coincident with $\chi_{\text{top}}(\mathbb{C}P^2) = 1 + 1 + 1 = 3$ (the Euler/de Rham index), but that identification is not a Dirac index theorem: the untwisted spin^c index on $\mathbb{C}P^2$ is $\mathrm{Td}(\mathbb{C}P^2) = 1$, and the twisted per-multiplet indices do not share a factor of 3. We do not claim N_{gen} is derived.
- $k_{\max} = \chi(\mathbb{C}P^2, E) = 60$ for the Spin^c twisting bundle $E = \mathcal{O}(9) \oplus \mathcal{O}^{\oplus 5}$, the total microsector mode count via Spin^c–HRR — exact arithmetic given the inputs $N_{\text{gen}} = 3$ and $n = 5$ and the $q_1 = 3$ derived under the electroweak identification (Rem. F.10); within that reading the count does not use α, and the α match (21 ppm from the integers) is what excludes the reading with line-bundle doublets (App. F 5, Rem. F.12).

The Wilsonian integration in Sec. O 2 then integrates out the $k_{\max} - N_{\text{gen}} = 57$ nonzero modes, giving the α^{57} suppression.

2. Gaussian mode-integration realization

The ratio $\varepsilon(g)$ admits a concrete physical realization as the partition-function ratio obtained by Gaussian integration over the nonzero-mode sector. Let $\mathcal{K}_+$ denote $\mathcal{K}$ restricted to the nonzero spectrum, and define for $g > 0$ the Gaussian normalization integral over $N = 57$ complex modes:

$$\begin{aligned}\mathcal{Z}(g) \;&:=\; \int_{\mathbb{C}^N} \exp\Big(-\,\langle\phi,\,(g\mathcal{K}_+)\phi\rangle\Big)\,d^{2N}\phi \\ &=\; \prod_{i=1}^{N}\frac{\pi}{g\,\lambda_i} \;=\; \frac{\pi^N}{g^N\,\det'(\mathcal{K})}\,.\end{aligned} \tag{O4}$$

The ratio to the reference ($g = 1$) partition function is:

$$\frac{\mathcal{Z}(g)}{\mathcal{Z}(1)} \;=\; g^{-N} \;=\; g^{-57} \tag{O5}$$

so the suppression factor is $\varepsilon(g) \equiv \mathcal{Z}(g)/\mathcal{Z}(1) = g^{-57}$.

a. Per-mode eigenvalue cancellation. Each complex mode ϕ_i contributes independently. At coupling $g = \alpha^{-1}$ (gauge-normalized; see Lemma O.5 below):

$$\frac{\int d^2\phi_i\,\exp\big(-(\lambda_i/\alpha)\,|\phi_i|^2\big)}{\int d^2\phi_i\,\exp\big(-\lambda_i\,|\phi_i|^2\big)} \;=\; \frac{\pi\alpha/\lambda_i}{\pi/\lambda_i} \;=\; \alpha\,. \tag{O6}$$

The eigenvalue λ_i **cancels exactly** in the ratio. The per-mode suppression factor is α regardless of the detailed spectrum of $\mathcal{K}$; the exponent depends only on the *mode count* $N = 57$, not on the eigenvalues.

3. From determinant ratio to physical hierarchy: derivation

The scaling of the measured invariant $I = G\hbar H_0^2/c^5$ as $\varepsilon(\alpha^{-1}) = \alpha^{57}$ is established by three lemmas; its coefficient is measured.

Lemma O.4 (KK reduction)**.** *The internal Dirac operator D_K on $K = \mathbb{C}P^2 \times S^3$, in the Toeplitz truncation at level $k_{\max} = 60$ with the generation sector fixed at the input value $N_{\text{gen}} = 3$, has exactly 3 protected (zero-sector) eigenvalues and 57 nonzero eigenvalues. In the Wilsonian effective theory at energies below the KK scale, the 57 nonzero modes are integrated out by Gaussian approximation, leaving the effective action for the ψ-field zero mode.*

Proof. Two clarifications fix the correct statement. *First*, since K is a closed odd-dimensional manifold, the elliptic index of D_K vanishes identically, and the round-S^3 factor has no harmonic spinors (Lichnerowicz). The rigorous index-theoretic content on the S^3 factor is the APS *spectral flow* $I_{S^3}(k_2) = k_2$ (App. F 5, Theorem F.14 and Rem. F.15), not a static kernel dimension. *Second*, the 3-dimensional protected sector is the generation space $\mathcal{G}$, whose dimension $N_{\text{gen}} = 3$ enters as a discrete input (Rem. F.21); within the Toeplitz truncation the microsector Hilbert space has dimension $k_{\max} = 60$, fixed α-free

by the determinant-line chain *given the selected discrete inputs* (Rem. F.12: SM $\to q_1 = 3 \to a = 9 \to k_{\max} = 60$). That this same $k_{\max} = 60$ reproduces $\alpha^{-1} = 137.036$ is an *a-posteriori consistency check*, not the source of the value. The nonzero-mode count is $N = 60 - 3 = 57$. These modes acquire KK masses $m_i \propto |\lambda_i|$ and are integrated out at energies $E \ll m_i$ by the standard Wilsonian procedure. □

Lemma O.5 (Uniform gauge normalization)**.** *Each of the* 57 *nonzero modes contributes exactly one factor of* α *to the partition-function ratio, giving* $\mathcal{Z}(\alpha^{-1})/\mathcal{Z}(1) = \alpha^{57}$.

Proof. Three facts combine:

1. **Uniform normalization.** The spectral action $\mathrm{Tr}\, f(D^2/\Lambda^2)$ determines α through the a_4 Seeley–DeWitt coefficient: $1/(4\alpha) = f_0\, \Lambda^{d-4}\, \mathrm{Tr}_K(T^2)$, where $\mathrm{Tr}_K(T^2)$ is a single trace over *all* modes of K simultaneously. The coupling α is a single number for the entire gauge sector, not a per-mode quantity. The gauge-normalized kinetic operator is therefore $\mathcal{K}_{\mathrm{phys}} = \mathcal{K}_{\mathrm{geom}}/\alpha$, with the factor $1/\alpha$ uniform across all modes.

2. **Complex mode structure.** The Chern–Simons theory on S^3 is quantized via holomorphic quantization [132], giving a state space with Kähler structure. In the Toeplitz truncation, the modes are naturally complex, so the Gaussian integral uses the complex measure $d^2\phi_i$.

3. **Eigenvalue cancellation.** The ratio of the gauge-normalized integral to the reference integral is $(\pi\alpha/\lambda_i)/(\pi/\lambda_i) = \alpha$, independent of λ_i (Eq. O6). For 57 independent complex modes the product gives α^{57}.

With α fixed by the exact construction of §X C, the $\zeta(0)$ of the $\mathbb{C}P^2$ charge trace times the terminating heat trace of the ρ-shifted Casimir on S^3 with the heat-kernel regulator, the normalization carries no a_{2k} remainder, and the eigenvalue cancellation is exact, not approximate. The plateau rule, $f^{(n)}(0) = 0$ for all $n \geq 1$, removes the a_{2k} with $k \geq 3$ only in even total dimension; on the seven-dimensional K it does not, so it is not used here. □

a. Notes on the Gaussian integration.

- *Integration measure.* The integration measure on the Toeplitz-truncated Hilbert space $\mathbb{C}^N$ is the flat Lebesgue measure $d^{2N}\phi$, which coincides with the Liouville measure of the Toeplitz-truncated Kähler space under the constant Kähler metric on the finite-dimensional fiber.

- *Mass gap.* The 57 nonzero eigenvalues $\{\lambda_i\}$ are bounded below by the Kaluza–Klein mass gap $\lambda_{\min}^{(\neq 0)} \sim \sqrt{\alpha}\, M_P$, ensuring that the Gaussian (quadratic) approximation for the Wilsonian integration is controlled.

- *Coupling normalization.* The convention $g^2 = \alpha$ (rather than $g^2 = 4\pi\alpha$) follows from absorbing the 4π into the heat-kernel coefficient normalization f_0.

Lemma O.6 (Hierarchy identification)**.** *The dimensionless invariant* $I = G\hbar H_0^2/c^5$ *scales as the partition-function ratio* $\varepsilon(\alpha^{-1}) = \alpha^{57}$*:* $I = C\,\varepsilon(\alpha^{-1})$*, with* C *measured (Theorem O.7).*

Proof. The invariant I can be rewritten as a squared scale ratio:

$$I = \frac{G\hbar H_0^2}{c^5} = \left(\frac{\ell_P H_0}{c}\right)^2 = \left(\frac{E_{\mathrm{Hubble}}}{E_{\mathrm{Planck}}}\right)^2 \qquad \text{(O7)}$$

where $\ell_P = \sqrt{\hbar G/c^3}$, $E_{\mathrm{Hubble}} = \hbar H_0$, and $E_{\mathrm{Planck}} = M_P c^2$. This is the squared ratio of the cosmological IR scale to the Planck UV scale.

The partition-function ratio $\varepsilon(\alpha^{-1})$ computes the same hierarchy: integrating out the 57 massive microsector modes from the UV (Planck) theory yields the effective IR (Hubble) theory, with suppression factor α^{57} (Lemmas O.4 and O.5).

The DFD microsector is *finite-dimensional* ($\dim \mathcal{H} = 60$). Unlike standard QFT, where the cosmological-constant calculation is quartically UV-divergent and scheme-dependent, the microsector partition function (O4) is a *finite product* with no UV divergence, no cutoff dependence, no renormalization ambiguity, and no scheme dependence. The exponent of the identification therefore inherits the exactness of the finite-dimensional computation, free of the ambiguities that make the standard cosmological-constant problem intractable, for the microsector piece only (Rem. AU.3). □

4. The derived invariant

Define the observed dimensionless invariant

$$I := \frac{G\,\hbar\,H_0^2}{c^5}\,. \qquad \text{(O8)}$$

As shown in the main text (critical density vs. Planck density algebra),

$$\frac{\rho_c}{\rho_{\mathrm{Pl}}} = \frac{3}{8\pi}\, I \qquad \text{and} \qquad \frac{\rho_\Lambda}{\rho_{\mathrm{Pl}}} = \Omega_\Lambda\, \frac{3}{8\pi}\, I\,. \qquad \text{(O9)}$$

Theorem O.7 (G–H_0–α invariant (spectral-action-derived))**.** *Let* $K = \mathbb{C}P^2 \times S^3$ *with Chern–Simons truncation at* $k_{\max} = 60$ *and* $N_{\mathrm{gen}} = 3$ *(Appendix F). Within the DFD spectral action, the exact partition function of the finite-dimensional microsector (60 modes, 3 zero, 57 nonzero) with gauge-normalized kinetic operator* $\mathcal{K}/\alpha$ *gives the hierarchy suppression* $\varepsilon(\alpha^{-1}) = \alpha^{57}$ *(Lemmas O.4–O.6). Identifying this with the UV/IR hierarchy fixes the exponent but leaves one dimensionless normalization, measured in the acoustic sector (*$C = 1$ *on bound-matter clocks under Postulate ZS.11, Eq. (479)):*

$$\boxed{\frac{G\,\hbar\,H_0^2}{c^5} = C\alpha^{57}}, \qquad C = 0.87784 \pm 0.00266 \text{ (measured, early clock).} \qquad \text{(O10)}$$

Consequently,

$$\frac{\rho_c}{\rho_{\rm Pl}} = \frac{3}{8\pi}\, C\alpha^{57}, \qquad \frac{\rho_\Lambda}{\rho_{\rm Pl}} = \Omega_\Lambda\, \frac{3}{8\pi}\, C\alpha^{57}. \tag{O11}$$

Proof. By Lemma O.4, the 57 nonzero internal modes are integrated out in the Wilsonian effective theory. By Lemma O.5, the Gaussian integration over 57 complex modes with uniform gauge normalization $1/\alpha$ gives $\varepsilon(\alpha^{-1}) = \alpha^{57}$, with the per-mode factor α independent of the eigenvalues. By Lemma O.6, the partition-function ratio fixes the α^{57} scaling of the physical hierarchy $I = G\hbar H_0^2/c^5$; the printed spectral action does not determine its overall coefficient C, as established by the eight-route no-go in App. ZS. The density relations follow from (O9). □

a. Derivation status. Lemmas O.4 and O.5 are theorem-grade: the mode count is $60 - 3$ given the discrete inputs, the gauge normalization is from the a_4 spectral coefficient, and the eigenvalue cancellation is exact algebra. Lemma O.6 uses the Wilsonian effective-field-theory framework applied to the finite-dimensional DFD spectral action—the same level of rigour as standard QFT derivations, with the additional advantage that the finite dimensionality eliminates all UV ambiguities. The identification is falsifiable. It is written $G\hbar H_0^2/c^5 = C\,\alpha^{57}$: the exponent 57 is a theorem, while the dimensionless coefficient is a *measured* input, $C = 0.87784 \pm 0.00266$ (BAO+θ_*; plik-lite 0.8772), with the cross-channel $H_0 = 67.52 \pm 0.09$ km/s/Mpc concordant across five CMB-anchored channels; the C=1 value ($H_0 = 72.09$) is excluded at $\sim 46\sigma$ as today's early clock by the CMB-anchored channels (eight-route non-derivability no-go and measurement in App. ZS), and it is the bound-matter clock $H_0^{\rm loc}$ (Postulate ZS.11, Eq. (479)).

b. The cosmological-constant hierarchy. The hierarchy $\rho_c/\rho_{\rm Pl} = (3/8\pi)C\alpha^{57}$ spans $57 \times \log_{10}(137) + \log_{10}(8\pi/3) \approx 122.7$ orders of magnitude. Each of the 57 frozen KK modes contributes one factor of $1/137$ suppression. The mode count is $60 - 3$ ($N_{\rm gen} = 3$ an input); the suppression factor is the gauge coupling from the same topology. This is the microsector piece; the matter-sector vacuum is assumed to cancel, and so is the spectral action's Planckian vacuum term (Rem. AU.3). Independent recent work likewise locates late-time acceleration in a quantum-gravitational correction to the Friedmann equation with no new fields [152]; there the deformation scale and exponent are free inputs where DFD prints the closed form $(H_0 t_P)^2 = C\,\alpha^{57}$, and its $w > -1$ prediction is adjudicated against DFD's forced $w = -1$ by the same DESI/Euclid $w(z)$ measurements.

5. Connection to the Einstein Product Condition

The internal geometry enters the spectral action through the volume and the curvature of K. The α constraint does not fix the shape ratio $\tau \equiv R_2/R_1$: the $\mathbb{C}P^2$ factor of α's trace does not depend on its radius, since $\int_{\mathbb{C}P^2} F \wedge F = 8\pi^2 q^2$ is topological (§X C), and in a joint reading $1/G$ (from a_2) and $1/\alpha$ (from a_4) both scale with $\mathrm{Vol}(K)$. The shape enters through the internal-curvature part of a_2, $\int_K R_K\, d\mathrm{vol} = \pi^{8/7}\mathrm{Vol}(K)^{5/7}\,\Phi(\tau)$ with $\Phi(\tau) = 24\tau^{6/7} + 6\tau^{-8/7}$, which belongs to the four-dimensional vacuum term. At fixed volume it is stationary at $\tau_* = 1/\sqrt{3}$, the Einstein product condition $6/R_1^2 = 2/R_2^2$, with $\Phi''/\Phi = 2.94$, a curvature ratio rather than a mass; this is a minimum of the potential for the connection Laplacian that fixes α (§X B) and a maximum for an internal Dirac operator, and the overall volume is not fixed at this order. On the truncated microsector, which the closed form for α and the α^{57} derivation use, the internal space is finite and carries no size or shape modulus.

Appendix P: Clock Coupling and Majorana Scale

1. Scope and Convention Lock

This appendix derives two relations used in the microsector framework, each conditional on an explicitly stated assumption:

$$k_\alpha = \frac{\alpha^2}{2\pi}, \tag{P1}$$

$$M_R = M_P\,\alpha^3. \tag{P2}$$

The derivations follow the same "no hidden knobs" methodology used in Appendix O (the α^{57} hierarchy): all dimensionless outputs must be built from (i) the unique dimensionless coupling α (given by the Chern-Simons microsector closed form at $k_{\max} = 60$) and (ii) topological integers established in the paper (in particular the discrete input $N_{\rm gen} = 3$; App. F generation-count remark).

2. Theorem P.1: Schwinger Coefficient $a_e = \alpha/(2\pi)$

Theorem P.1 (Schwinger one-loop anomalous magnetic moment)**.** *In QED with one charged Dirac fermion of charge e and mass m, the one-loop correction to the on-shell vertex yields*

$$a_e := \frac{g_e - 2}{2} = F_2(0) = \frac{\alpha}{2\pi} + \mathcal{O}(\alpha^2), \tag{P3}$$

where $\alpha = e^2/(4\pi)$ in $\hbar = c = 1$ units and $F_2(q^2)$ is the Pauli form factor.

Proof. Write the renormalized on-shell vertex as

$$\bar u(p')\Gamma^\mu(p',p)u(p) = \bar u(p')\left[\gamma^\mu F_1(q^2) + \frac{i\sigma^{\mu\nu}q_\nu}{2m}F_2(q^2)\right]u(p), \tag{P4}$$

with $q = p' - p$ and $F_1(0) = 1$ by charge renormalization. The one-loop vertex graph gives (in Feynman gauge)

$$\Gamma^\mu_{(1)} = (-ie)^3\int\frac{d^4k}{(2\pi)^4}\,\gamma_\alpha\frac{(\not p' - \not k) + m}{(p'-k)^2 - m^2} \times\gamma^\mu\frac{(\not p - \not k) + m}{(p-k)^2 - m^2}\gamma^\alpha\frac{1}{k^2}. \tag{P5}$$

Projecting onto the Pauli structure and taking $q^2 \to 0$ on-shell, standard Feynman-parameter reduction yields

$$F_2(0) = \frac{\alpha}{2\pi}\int_0^1 dz\, 2z = \frac{\alpha}{2\pi}. \tag{P6}$$

(Any UV divergence resides in F_1 and cancels after renormalization; $F_2(0)$ is finite.) □

3. Theorem P.2: Clock Coupling $k_\alpha = \alpha^2/(2\pi)$

a. Microsector axiom (already used in the paper). The "clock coupling" is defined operationally by the fractional shift of a purely electromagnetic atomic transition under a small static DFD potential ψ:

$$\frac{\delta\nu}{\nu} = k_\alpha\,\psi + \mathcal{O}(\psi^2). \tag{P7}$$

b. Key microsector input. In the DFD microsector, α is *topologically fixed* (Appendix K) and therefore does *not* vary with ψ at tree level.

Theorem P.2 (Clock coupling constant)**.** *Assume the microsector "no hidden knobs" principle: in the weak-field regime, the leading EM-sensitive ψ insertion is a single gauge vertex and therefore carries one factor of α. Then the coefficient k_α in (P7) is forced to be*

$$\boxed{k_\alpha = \alpha\,a_e = \frac{\alpha^2}{2\pi}} \tag{P8}$$

Proof. By hypothesis, the leading ψ insertion into the EM sector is a single gauge vertex, hence contributes a factor α. The *only* universal, gauge-invariant, dimensionless one-loop EM correction that couples to atomic spin/magnetic structure and is independent of atomic details is the Pauli form factor at zero momentum, $F_2(0) = a_e$ (Theorem P.1). Therefore the leading dimensionless coefficient multiplying ψ in the EM sector is the product $\alpha\,a_e$. Using Theorem P.1 gives $k_\alpha = \alpha^2/(2\pi)$. □

c. Remark (what is and is not a new assumption). The only nontrivial input beyond QED is the microsector rule that the leading $\psi \to$EM insertion is a single gauge vertex ("one α"), rather than an arbitrary analytic function of α. This is exactly the same kind of admissible "no hidden knobs" restriction used in Appendix O to turn the α^{57} hierarchy into a theorem.

a. Observational Test: Fine-Structure Constant Variation

The clock coupling $k_\alpha = \alpha^2/(2\pi)$ predicts that the fine-structure constant varies with the cosmological background potential $\psi(z)$ (Sec. IX F, Eq. (253)):

$$\frac{\Delta\alpha}{\alpha}(z) = k_\alpha\,[\psi(z) - \psi_0], \qquad \psi(z) = \frac{\xi^{\rm res}_{\rm LPI}}{2}\,\Omega_m(z). \tag{P9}$$

With $\Omega_{m,0} = 0.312$ and $\Omega_m(z{=}1) = 0.784$:

$$\left.\frac{\Delta\alpha}{\alpha}\right|_{z=1} = \xi^{\rm res}_{\rm LPI}\,\frac{\alpha^2}{4\pi}\times 0.472 = \xi^{\rm res}_{\rm LPI}\times(+2.0\times10^{-6}), \tag{P10}$$

with $\xi^{\rm res}_{\rm LPI}$ an undetermined screened residual (Sec. IX F), so no definite value is predicted. The value $+2.3\times10^{-6}$, which follows from the excluded ψ-screen value $\Delta\psi(z{=}1) = 0.27$, is not a DFD prediction.

a. ESPRESSO comparison. The ESPRESSO spectrograph at the VLT has measured $\Delta\alpha/\alpha$ in quasar absorption systems. The 2022 ESPRESSO collaboration analysis reports:

$$\left.\frac{\Delta\alpha}{\alpha}\right|_{z\sim1} = (+1.3 \pm 1.3)\times10^{-6}. \tag{P11}$$

$\alpha(z)$ Prediction vs. ESPRESSO

DFD prediction: $\Delta\alpha/\alpha = \xi_{\rm LPI}^{\rm res} \times (+2.0 \times 10^{-6})$ at $z = 1$ (conditional; the value $+2.3 \times 10^{-6}$ follows from the excluded screen)
ESPRESSO (2022): $(+1.3 \pm 1.3) \times 10^{-6}$
Agreement: none to state until $\xi_{\rm LPI}^{\rm res}$ is determined; not a validated prediction

b. Key features.

1. **Positive sign (for $\xi_{\rm LPI}^{\rm res} > 0$):** DFD predicts α *increases* at higher redshift (larger ψ). ESPRESSO data prefer positive $\Delta\alpha/\alpha$.
2. **Magnitude:** At $\xi_{\rm LPI}^{\rm res} = 1$ the $\sim 10^{-6}$ level matches current sensitivity.
3. **z-dependence:** $\Delta\alpha/\alpha \propto \Omega_m(z) - \Omega_{m,0}$ gives the redshift shape, with the overall scale $\xi_{\rm LPI}^{\rm res}$ undetermined.

c. Predictions for ELT. The Extremely Large Telescope will improve sensitivity to $\sim 10^{-7}$. DFD predictions:

z	$\Omega_m(z) - \Omega_{m,0}$	$\Delta\alpha/\alpha$ $(\times 10^{-6} \times \xi_{\rm LPI}^{\rm res})$
0.5	0.29	+1.2
1.0	0.47	+2.0
1.5	0.56	+2.4
2.0	0.61	+2.6
3.0	0.65	+2.8

4. Majorana Scale $M_R = M_P\alpha^3$

a. Setup. The right-handed neutrinos are gauge singlets (see Appendix H). Let $\mathcal{H}_{\nu_R}$ denote the internal Hilbert subspace supporting the ν_R degrees of freedom.

Lemma P.3 (Generation multiplicity)**.** *The singlet sector has one state per generation:*

$$\dim(\mathcal{H}_{\nu_R}) = N_{\rm gen} = 3, \tag{P12}$$

the discrete input of App. F (Rem. F.21); no index on $\mathbb{C}P^2 \times S^3$ supplies it.

b. Toeplitz scaling input (same mechanism as Appendix O). Let $\mathcal{K}_{\nu_R}$ be the positive operator controlling the singlet-sector quadratic form in the Toeplitz-quantized microsector. The microsector coupling parameter is $g = \alpha^{-1}$, and constant-symbol scaling acts by $\mathcal{K}_{\nu_R} \mapsto g\,\mathcal{K}_{\nu_R}$.

Theorem P.4 (Majorana scale from determinant scaling)**.** *Assume (i) the singlet-sector quadratic form is non-extensive and Toeplitz-quantized on $\mathcal{H}_{\nu_R}$, (ii) the only dimensionless knob is $g = \alpha^{-1}$, and (iii) $\dim\mathcal{H}_{\nu_R} = N_{\rm gen}$ (Lemma P.3). Then the unique dimensionless singlet-sector suppression factor is*

$$\varepsilon_{\nu_R}(g) := \frac{\det(\mathcal{K}_{\nu_R})}{\det(g\mathcal{K}_{\nu_R})} = g^{-N_{\rm gen}} = \alpha^{N_{\rm gen}} = \alpha^3, \tag{P13}$$

and, under the identification below, the Majorana mass scale is

$$\boxed{M_R = M_P\,\varepsilon_{\nu_R}(\alpha^{-1}) = M_P\,\alpha^3} \tag{P14}$$

Proof. Because $\mathcal{H}_{\nu_R}$ is finite-dimensional (non-extensive microsector) with $\dim\mathcal{H}_{\nu_R} = N_{\rm gen}$, constant scaling multiplies every eigenvalue by g and therefore multiplies the determinant by $g^{N_{\rm gen}}$:

$$\det(g\mathcal{K}_{\nu_R}) = g^{N_{\rm gen}}\det(\mathcal{K}_{\nu_R}). \tag{P15}$$

Hence $\varepsilon_{\nu_R}(g) = g^{-N_{\rm gen}}$. By the "no hidden knobs" principle, the Majorana scale can only be the unique fundamental mass M_P multiplied by a dimensionless singlet-sector factor built from g and $N_{\rm gen}$; the determinant ratio above is the unique such factor with the correct scaling behavior. Substituting $g = \alpha^{-1}$ and $N_{\rm gen} = 3$ gives $M_R = M_P\alpha^3$. □

a. Parallel Structure with Appendix O

The $M_R = M_P\alpha^3$ derivation parallels Appendix O exactly:

	Appendix O (α^{57})	**Appendix P** (α^3)
State space	$\mathcal{H}_{\rm UV}$, dim $= k_{\max} = 60$	$\mathcal{H}_{\nu_R}$, dim $= N_{\rm gen} = 3$
Operator	Kinetic $\mathcal{K}$, dim ker $= 3$	Majorana $\mathcal{M}$, no kernel
Exponent	$k_{\max} - N_{\rm gen} = 57$	$N_{\rm gen} = 3$
Dictionary	$G\hbar H_0^2/c^5 := C\,\varepsilon(\alpha^{-1})$, C measured on the early clock ($C = 1$ on bound-matter clocks, Postulate ZS.11)	$M_R/M_P := \varepsilon_{\nu_R}(\alpha^{-1})$
Result	$G\hbar H_0^2/c^5 = C\alpha^{57}$	$M_R/M_P = \alpha^3$

Both use the same "no hidden knobs" principle.

b. Neutrino Mass Predictions

With $v = M_P\alpha^8\sqrt{2\pi} = 246.09$ GeV (exponent derived, prefactor fitted; Section XVII, App. Z) and the see-saw formula $m_\nu \sim m_D^2/M_R$:

a. Numerical result.

$$M_R = M_P \times \alpha^3 = 1.22 \times 10^{19}\,\text{GeV} \times (137)^{-3} = 4.74 \times 10^{12}\,\text{GeV}. \tag{P16}$$

b. Mass hierarchy. The neutrino mass ratios are those of App. X's Branch B:

$$m_1 : m_2 : m_3 = 1 : \alpha^{-3/11} : \alpha^{-3/11-7/20}. \tag{P17}$$

Quantity	**Prediction**	**Observed**
m_3/m_2	$\alpha^{-7/20} = 5.60$ (App. X, Branch B)	model-dependent
Σm_ν	≈ 60 meV	< 120 meV (Planck+BAO)
Status	Consistent, testable by DESI + Simons Observatory	

c. Absolute scale. The Dirac Yukawa sits on a stated rung, $y_D^2 = F_\nu \alpha$, one discrete input; with that rung the priming factor $F_\nu = 14/13$ fixes it (Proposition AT.1, Appendix AT). The Type-I seesaw $m_{\nu_3} = m_D^2/M_R$ with the locked scales $m_3 = \frac{14}{13}\pi M_P \alpha^{14}$ and $M_R = M_P \alpha^3$ forces

$$\begin{aligned} y_D^2 &= \frac{2\, m_3 M_R}{v^2} = \frac{14}{13}\,\alpha, \\ m_D &= \sqrt{m_3 M_R} = \frac{v}{\sqrt{2}}\sqrt{\tfrac{14}{13}\,\alpha} = 15.43 \text{ GeV}, \end{aligned} \tag{P18}$$

where the π of m_3 cancels against the $\sqrt{2\pi}$ in $v = M_P \alpha^8 \sqrt{2\pi}$, and $\frac{14}{13} = 1 + \frac{1}{N_{\rm gen}} \sin^2\theta_W$ with $\sin^2\theta_W = 3/13$, $N_{\rm gen} = 3$ (Prop. AT.1). This returns the absolute scale

$$m_{\nu_3} = \frac{m_D^2}{M_R} = \frac{14}{13}\pi M_P \alpha^{14} = 50.16 \text{ meV} \tag{P19}$$

(the rung restated, not an independent check).

5. Summary

Appendix P: Theorem Status

$k_\alpha = \alpha^2/(2\pi)$**:** conditional on the "one gauge vertex" axiom, a postulated non-metric operator outside the minimal action (Thm. XI.2).

- Theorem P.1: $a_e = \alpha/(2\pi)$ (Schwinger, QED — fully proven)
- Theorem P.2: $k_\alpha = \alpha \times a_e$ (no hidden knobs axiom)
- Observational test: ESPRESSO — conditional on the undetermined $\xi^{\rm res}_{\rm LPI}$; not validated

$M_R = M_P \alpha^3$**:** an identification (the dictionary below), listed among the inputs (App. FK).

- Input: $N_{\rm gen} = 3$ (discrete input; numerically $\chi_{\rm top}(\mathbb{C}P^2)$ — App. F)
- Theorem P.4: $\det(g\mathcal{M}) = g^{N_{\rm gen}} \det(\mathcal{M})$ (pure linear algebra)
- Dictionary: $M_R/M_P := \varepsilon_{\nu_R}(\alpha^{-1})$ (explicit identification)
- Predictions: the Branch-B spectrum of App. X; $\Sigma m_\nu = 61.5$ meV

Both derivations follow the Appendix O protocol: theorem-grade mathematics plus explicit "no hidden knobs" axiom or dictionary identification. The exponents (2 for k_α, 3 for M_R) are not fitted—the first follows from the one-gauge-vertex axiom together with the Schwinger coefficient, the second is the generation number $N_{\rm gen} = 3$, a discrete input (App. F).

Appendix Q: Temporal Completion: Dust Branch under $K' = \mu$

This appendix derives the temporal sector from the same S^3 microsector that gives the weak-response $\mu(x)$ of Appendix N. The key results are:

1. The temporal deviation invariance follows from the saturation-union law (Assumption N.5)
2. The unique temporal segment variable is $\Delta = (c/a_0)|\dot\psi - \dot\psi_0|$
3. With $K'(\Delta) = \mu(\Delta)$, the dust branch emerges: $w \to 0$, $c_s^2 \to 0$

We also include a **no-go lemma** showing that the naive quadratic identification $K'(Q_t) = \mu(\sqrt{Q_t})$ gives $w \to 1/2$ (not dust). This shows the dust branch is not automatic: it follows from adopting the deviation-invariant Δ closure.

1. Temporal Deviation Invariance from Saturation-Union

Theorem Q.1 (Temporal deviation invariance)**.** *Assume the saturation-union composition law (Assumption N.5):*

$$\mu(\psi_1 + \psi_2) = 1 - \big(1 - \mu(\psi_1)\big)\big(1 - \mu(\psi_2)\big), \tag{Q1}$$
$$\mu(0) = 0, \qquad 0 \le \mu < 1.$$

Then for any background ψ_0 and deviation $\Delta\psi$,

$$\boxed{\mu(\psi_0 + \Delta\psi) - \mu(\psi_0) = (1 - \mu(\psi_0))\,\mu(\Delta\psi)} \tag{Q2}$$

Equivalently, the normalized incremental response depends only on the deviation:

$$\frac{\mu(\psi_0 + \Delta\psi) - \mu(\psi_0)}{1 - \mu(\psi_0)} = \mu(\Delta\psi). \tag{Q3}$$

Proof. Insert $\psi_1 = \psi_0$ and $\psi_2 = \Delta\psi$ into Eq. (Q1):

$$\begin{aligned} \mu(\psi_0 + \Delta\psi) &= 1 - (1 - \mu(\psi_0))(1 - \mu(\Delta\psi)) \\ &= \mu(\psi_0) + (1 - \mu(\psi_0))\mu(\Delta\psi). \end{aligned}$$

Rearrange to obtain (Q2). □

2. Unique Local Temporal Invariant

We identify the *unique* local scalar that represents the microsector "increment" induced by time evolution along a chosen screen flow.

a. Setup (DFD observer dictionary). Let u^μ be the unit timelike 4-velocity field of the cosmological screen flow (comoving congruence in the dictionary), and let $\psi(x)$ be the DFD scalar. The screen-background field ψ_0 is the ψ-screen solution already present in the cosmology section (Sec. XVI).

Definition Q.2 (Local temporal increment density)**.**

$$\dot{\psi} := u^\mu \nabla_\mu \psi, \qquad \dot{\psi}_0 := u^\mu \nabla_\mu \psi_0, \qquad \Delta := \frac{c}{a_0} \left| \dot{\psi} - \dot{\psi}_0 \right|. \tag{Q4}$$

Here $a_0 = 2\sqrt{\alpha}\, cH_0$ is the MOND acceleration scale; the combination c/a_0 has units of time, so Δ is dimensionless.

Theorem Q.3 (Temporal segment identification)**.** *Among all local scalars built from $\nabla\psi$ and the screen flow u^μ, the quantity Δ in Eq. (Q4) is the unique choice (up to a constant factor) that satisfies:*

1. ***Reparameterization covariance:*** *invariance under reparameterizations of the flow parameter along u^μ.*
2. ***Segment additivity:*** *for concatenated microsector segments along the flow, the total "increment" equals the sum of segment increments.*
3. ***Reference invariance:*** *the amplitude vanishes when $\psi = \psi_0$ (the background).*

Proof. A local scalar depending on $\nabla\psi$ and u^μ at first-derivative order must be of the form $f(u^\mu \nabla_\mu \psi)$. Segment additivity applies to the integrated increment $\int u^\mu \nabla_\mu \psi \, d\lambda$, so the deviation from the background flow is $u^\mu \nabla_\mu (\psi - \psi_0) = \dot{\psi} - \dot{\psi}_0$. Reference invariance forces subtraction of $\dot{\psi}_0$. Dimensionlessness requires normalization by a_0/c, yielding Δ. □

3. No-Go Lemma: Quadratic Invariant Gives $w \to 1/2$

Before proving the dust branch, we establish why the naive k-essence identification fails.

Lemma Q.4 (No-go: quadratic invariant)**.** *Define the quadratic temporal invariant $Q_t := (u^\mu \nabla_\mu \psi)^2$ and suppose the constitutive law is*

$$K'(Q_t) = \mu(\sqrt{Q_t}) = \frac{\sqrt{Q_t}}{1 + \sqrt{Q_t}}. \tag{Q5}$$

Then near $Q_t \to 0$:

$$K(Q_t) = \frac{2}{3} Q_t^{3/2} + \mathcal{O}(Q_t^2), \tag{Q6}$$

and the effective equation of state satisfies

$$w := \frac{p}{\rho} \to \frac{1}{2} \qquad (Q_t \to 0). \tag{Q7}$$

*This is **not dust**.*

Proof. Integrating (Q5) with $q := \sqrt{Q_t}$:

$$\begin{aligned} K(Q_t) &= \int_0^{Q_t} \mu(\sqrt{s})\, ds = 2 \int_0^q \frac{q'^2}{1+q'}\, dq' \\ &= q^2 - 2q + 2\ln(1+q). \end{aligned}$$

Taylor expanding at $q \to 0$: $K = \frac{2}{3} q^3 + \mathcal{O}(q^4) = \frac{2}{3} Q_t^{3/2} + \mathcal{O}(Q_t^2)$.

For the k-essence stress-energy with $p = K$ and $\rho = 2Q_t K'(Q_t) - K$:

$$\begin{aligned} \rho &= 2Q_t \cdot \frac{\sqrt{Q_t}}{1+\sqrt{Q_t}} - \frac{2}{3} Q_t^{3/2} + \cdots \\ &= \frac{4}{3} Q_t^{3/2} + \mathcal{O}(Q_t^2). \end{aligned}$$

Thus $w = p/\rho = \left(\frac{2}{3} Q_t^{3/2}\right) / \left(\frac{4}{3} Q_t^{3/2}\right) = 1/2$. □

Remark Q.5 (Role of the no-go lemma). Lemma Q.4 proves we did not cherry-pick the dust result. The S^3 composition law alone, with a naive quadratic identification, gives $w = 1/2$, not dust. The dust branch requires the *deviation-invariant* closure below.

4. Dust Branch from Deviation-Invariant Closure

a. Microsector-to-EFT identification (deviation-invariant). The temporal analog of the spatial AQUAL closure, consistent with Theorem Q.1, uses the *linear* deviation Δ:

$$\boxed{\mathcal{L}_{\text{temp}} = \frac{a_0^2}{8\pi G} K(\Delta), \qquad K'(\Delta) = \mu(\Delta) = \frac{\Delta}{1+\Delta}} \tag{Q8}$$

where Δ is the deviation invariant (Q4). This uses the weak-response form $\mu(\Delta) = \Delta/(1+\Delta)$ of App. N. *Scope:* the deviation-invariant temporal EFE structure (Theorem Q.1) is forced by the composition law, but the specific kinetic identification $K'(\Delta) = \mu(\Delta)$ is the *minimal natural* choice (the temporal analog of the spatial AQUAL closure), *not* a uniquely forced identity: Lemma Q.4 exhibits a distinct, mathematically admissible identification $K'(Q_t) = \mu(\sqrt{Q_t})$ (which yields $w \to \frac{1}{2}$, not dust). The dust branch (Theorem Q.7) is therefore a conditional consequence of *adopting* $K' = \mu$, not of the composition law alone.

Lemma Q.6 (Shift symmetry current)**.** *Because $\mathcal{L}_{\text{temp}}$ depends on ψ only through $\dot{\psi}$ (via Δ), it is invariant under $\psi \mapsto \psi + const$ and yields a conserved current:*

$$\nabla_\mu J^\mu = 0, \qquad J^\mu = \frac{a_0^2}{8\pi G} K'(\Delta) \frac{c}{a_0} \operatorname{sgn}(\dot{\psi} - \dot{\psi}_0)\, u^\mu. \tag{Q9}$$

Theorem Q.7 (Dust branch)**.** *In a homogeneous FRW dictionary with $u^\mu = (1,0,0,0)$ and $\dot{\psi}_0 \neq 0$, solutions near the screen background satisfy:*

$$a^3 a_0\, \mu(\Delta) = const, \qquad \Delta \propto a^{-3}/a_0 \quad (\Delta \ll 1), \tag{Q10}$$

and their effective equation of state and sound speed obey

$$\boxed{w := \frac{p}{\rho} \to 0, \qquad c_s^2 \to 0 \quad as \quad \Delta \to 0.} \tag{Q11}$$

Proof. From (Q9) and $\nabla_\mu J^\mu = 0$, homogeneity gives $\frac{d}{dt}(a^3 J^0) = 0$, i.e. $a^3 a_0 K'(\Delta) = \text{const}$. Using $K'(\Delta) = \mu(\Delta)$ yields (Q10). For $\Delta \ll 1$, $\mu(\Delta) = \Delta + \mathcal{O}(\Delta^2)$, hence $\Delta \propto a^{-3}/a_0$.

For the stress-energy, take $p = \mathcal{L}_{\rm temp} = \frac{a_0^2}{8\pi G} K(\Delta)$ and $\rho = \dot\psi \frac{\partial \mathcal{L}_{\rm temp}}{\partial \dot\psi} - \mathcal{L}_{\rm temp}$. Near $\Delta = 0$: $K'(\Delta) = \Delta + \mathcal{O}(\Delta^2)$ and $K(\Delta) = \frac{1}{2}\Delta^2 + \mathcal{O}(\Delta^3)$. Thus:

$$\rho = \frac{a_0^2}{8\pi G}\left[\frac{c}{a_0}\dot\psi_0 \,\mathrm{sgn}(\dot\psi - \dot\psi_0)\,\Delta + \mathcal{O}(\Delta^2)\right],$$
$$p = \frac{a_0^2}{8\pi G}\left[\frac{1}{2}\Delta^2 + \mathcal{O}(\Delta^3)\right].$$

Therefore $w = p/\rho = \mathcal{O}(\Delta) \to 0$ as $\Delta \to 0$. The adiabatic sound speed $c_s^2 = dp/d\rho$ satisfies $dp/d\Delta = \mathcal{O}(\Delta)$ and $d\rho/d\Delta = \text{const} + \mathcal{O}(\Delta)$, hence $c_s^2 \to 0$. □

5. Summary: What is Theorem-Grade vs. Program

Theorem-Grade Results

Proved from S^3 composition law + deviation invariance:

1. Temporal deviation invariance (Theorem Q.1)
2. Unique temporal segment scalar $\Delta = (c/a_0)|\dot\psi - \dot\psi_0|$ (Theorem Q.3)
3. The kinetic identification $K'(\Delta) = \mu(\Delta)$ (same μ as the spatial sector) is the *minimal natural* choice consistent with the composition law, *not* uniquely forced — Lemma Q.4 shows an alternative identification is mathematically available (**natural/program-grade, not theorem-grade**); only the deviation-invariant EFE structure (item 1) and, conditionally on this choice, the dust branch (item 4) are proved
4. **Dust branch:** $w \to 0$, $c_s^2 \to 0$ as $\Delta \to 0$ (Theorem Q.7)
5. **No-go:** Quadratic $K'(Q_t) = \mu(\sqrt{Q_t})$ gives $w \to 1/2$ (Lemma Q.4)

Program-Level (Not Claimed as Theorem)

Requires further work:

- Full $P(k)$ shape matching ΛCDM (linear perturbation analysis)
- Transfer function derivation in DFD dictionary
- Quantitative confrontation with survey data (noting GR-sandbox / fiducial-processing issues)

The dust branch ($w \to 0$, $c_s^2 \to 0$) describes homogeneous deviations only (Axiom WS.1); proving the full $P(k)$ match is a program item.

Remark Q.8 (Linear versus quadratic deviation). The dust branch emerges because the microsector responds to the *linear* deviation $\Delta = |\dot\psi - \dot\psi_0|$, not the quadratic $Q_t = (\dot\psi - \dot\psi_0)^2$. It is the adopted identification (item 3 of the Theorem-Grade Results box above), not a forced one.

6. Primordial optical engine: the background screen flow

The temporal kinetic functional $K(\Delta)$ is *not* the primordial engine. By construction $\Delta = (c/a_0)|\dot\psi - \dot\psi_0|$ is the deviation from the background screen flow $\dot\psi_0$ (reference invariance, §Q), so on the homogeneous FRW background $\dot\psi = \dot\psi_0$ identically and $\Delta = 0$ (App. AE, AE.1). Hence $K(\Delta)$ governs homogeneous *deviations* $\delta\psi(t)$ only — the dust branch (Axiom WS.1) — and vanishes on the background; it cannot drive a horizon engine. (The engine is not a high-Δ branch of K.) The engine is instead the *background screen flow* $\psi_0(t)$ itself. The scalar action alone is flat along it (Theorem AE.1), since its source is the density contrast; the full action, with matter on the matter-coupling metric, sources the homogeneous field with $(\rho + 3p)/2$, and the Friedmann law of §XIX E governs it. Because $n = e^{\psi_0}$ and the optical speed is $c_{\rm eff} = c\,e^{-\psi_0}$, an early phase with $\psi_0 < 0$ (fast light) relaxing to $\psi_0(t_0) = 0$ enlarges the optical causal horizon while the comoving optical Hubble radius shrinks, if it runs fast enough (Theorem Q.9). The early fast-light era follows from the theory, since in the static arena $\bar\psi = 2\ln A$ and light moves at c/A^2 on the arena clock, but at the rate the Friedmann law gives it opens no horizon, and accelerating the observable scale factor needs a source of negative pressure and a stage that reheats the universe after it (Rem. Q.11).

Theorem Q.9 (Screen-flow horizon engine)**.** *Let $a \propto t^p$ $(0 < p < 1,\ H = p/t)$ and let the background screen flow be $\psi_0(t) = \beta \ln(t/t_\star)$, so $c_{\rm eff} = c\,e^{-\psi_0} \propto t^{-\beta}$. The comoving optical Hubble radius is $R_H^{\rm opt} = c_{\rm eff}/(aH) \propto t^{\,1-p-\beta}$ and the accumulated optical horizon is $d_{\rm hor}^{\rm opt} = \int_0^t c\,e^{-\psi_0}/a\,dt' \propto \int_0^t t'^{-\beta-p} dt'$. Both the shrinking of $R_H^{\rm opt}$ and the divergence of $d_{\rm hor}^{\rm opt}$ hold iff*

$$\boxed{\beta > 1 - p} \quad \Longrightarrow \quad \beta > \tfrac{1}{2}\ (\textit{radiation, } p = \tfrac{1}{2}),\quad \beta > \tfrac{1}{3}\ (\textit{matter, } p = \tfrac{2}{3}). \tag{Q12}$$

Proof. $e^{-\psi_0} \propto t^{-\beta}$ and $aH \propto t^{p-1}$ give $R_H^{\rm opt} \propto t^{1-p-\beta}$, decreasing iff $1 - p - \beta < 0$. The horizon integrand $t'^{-\beta-p}$ diverges at the lower limit iff $\beta + p \geq 1$. Both conditions are $\beta > 1 - p$. (A power-law screen flow $\psi_0 = \psi_\infty - At^{-s}$, $A > 0$, gives the same conclusion with an even stronger early fast-light phase $c_{\rm eff} \propto e^{At^{-s}} \to \infty$.) □

Theorem Q.10 (Branch selection by the optical arrow)**.** *The present normalization $\psi_0(t_0) = 0$ $(n = 1$ today$)$ admits three flat-direction branches: $\dot\psi_0 = 0$ (static, $c_{\rm eff} =$const, no engine); $\dot\psi_0 < 0$ (then $\psi_0 > 0$ and $c_{\rm eff} < c$ in the past,* worsening *the horizon); and $\dot\psi_0 > 0$ (then $\psi_0 < 0$, $c_{\rm eff} > c$ in the past; it opens the horizon only at the rate $\beta > 1 - p$). A fast-light primordial boundary condition $\psi_0(0^+) \to -\infty$ therefore selects $\dot\psi_0 > 0$ — the engine branch.*

Remark Q.11 (Status: the engine is not free, and it does not make the primordial perturbations). The flat-direction status of ψ_0 (Thm. AE.1) holds for the scalar action alone, whose source is the density contrast: that action supplies *no* force selecting the fast-light flow or its rate $\beta > 1 - p$. The flow is not free of energy on the observable scale factor. In the static arena of §II F the homogeneous field is the expansion itself, $\bar{\psi} = 2 \ln A$; with an arena factor $a(t)$, as written below, only the split of $A = a\, e^{\bar{\psi}/2}$ between a and $\bar{\psi}$ is unobservable (Theorem ZS.3), and the engine changes A itself: it is accelerated expansion of the matter-coupling metric (the physical payoff below). Matter on that metric sources the homogeneous field with $(\rho + 3p)/2$, a term the contrast source of Theorem AE.1 removes by construction and the Friedmann law of §XIX E restores, so under that law it needs a source with $\rho + 3p < 0$ while it runs, up to about $(4 \times 10^{14}\ \text{GeV})^4$ at the rate the χ relic allows (Eq. (Q13)), and a stage that reheats the universe after it; the print supplies neither (computed). The early fast-light era itself follows from the theory: in the static arena light moves at c/A^2 on the arena clock, and the Friedmann law fixes the rate of the flow at $\beta = 4/(3w + 5)$, 2/3 in radiation, below the engine condition $\beta > 1$ of that arena, so the fast-light past is the ordinary expansion and opens no horizon; the boundary data of Axiom PO below add only the expanding branch, and the arrow of time rests on the smooth beginning of Postulate Q.15. The screen flow is not a varying-speed-of-light source for the primordial spectrum either. On the matter-coupling metric a falling optical speed is the expansion read on the arena's clock and changes no light-cone observable, and the local scalar sector, an instantaneous constraint (Axiom WS.1), adds no second cone. Even read as waves timed by absolute time, ψ disturbances would move slower than light by the ratio $e^{\bar{\psi}}$ in the fast-light past, the reverse of what a sound-speed mechanism needs (computed). DFD therefore has no mechanism for the primordial perturbations: they enter through the smooth beginning of Postulate Q.15, A_s is one calibrated input (App. FK), and the origin of the perturbations is the theory's main open problem (§XVIII A). Any accelerating stage is bounded by the χ relic, $H_{\text{opt}} < 4 \times 10^{10}$ GeV, which keeps the tensor ratio below 10^{-7}. *Consistency check:* the primordial background $\bar{\psi} = \psi_0 < 0$ ($n < 1$, fast light) is the cosmological mean and is distinct from — and compatible with — the local $\psi > 0$ ($n > 1$) of bound structures, which are overdensities on that background.

Axiom PO (Primordial Optical State)

The universe's Wheeler–DeWitt state is the *no-boundary optical state*, specified by three clauses acting on disjoint summands of the configuration space:

(i) Branch: the Euclidean ground-state branch $\Psi_0 \propto e^{-S_E/\hbar}$ (the Hartle–Hawking-type choice; the rival e^{+S_E}/tunneling branch is thereby excluded);

(ii) Internal preparation: the empty-core WRT surgery state on the closed internal S^3 (App. AV, Brick 1), which, with the asserted premise P4′ (Lemma AV.27), fixes the sector measure $p_j = |S_{0j}|^2$;

(iii) Flat direction: $\psi_0(0^+) \to -\infty$ with the fast-light branch $\dot{\psi}_0 > 0$ on the homogeneous flat direction.

Theorem Q.12 (Consistency of Axiom PO)**.** *Axiom PO is consistent. The Wheeler–DeWitt fluctuation-sector state is already* unique *(Perron–Frobenius nondegeneracy on the coercive Sobolev sector) and the internal vacuum is rigid, a stated premise (layer 7 of the single-vacuum theorem, Extended Derivations): the internal Dirac operator D_F is held at its printed spectrum, and the physical inner fluctuations are those of* End(E) *for the microsector bundle $E = \mathcal{O}(9) \oplus \mathcal{O}^{\oplus 5}$ (Lemma F.11), which carry the gauge fields (their group is selected, not forced: its electroweak factor rests on one stated identification and colour is an input, App. F), not those of the full matrix algebra $M_{60}(\mathbb{C})$, under which its* 60 *eigenvalues would be dynamical and the spectral action would drive them off the printed spectrum (Prop. FK.3). So Axiom PO's only genuine freedom is the one homogeneous function $\psi_0(t)$ (the branch is fixed by normalizability, Rem. Q.14). The three clauses constrain* disjoint *direct summands of the configuration space (Euclidean branch / internal S^3 / homogeneous flat direction), and the Einstein–Hilbert term, which is not flat along the scale factor, fixes the expansion of the homogeneous direction without fixing its starting data, so clause (iii) stays independent of the Λ anchor; hence no clause constrains another's sector and no contradiction can arise. Jointly the axiom yields: the expanding branch (branch selection, Thm. Q.10 context; the arrow of time rests on Postulate Q.15), the χ sector measure $p_j = |S_{0j}|^2$ (Brick 1–3, with the asserted premise P4′), and the $E_0 = \alpha^{57} M_P^4$ anchor (eigenvalue step asserted, not derived, and under the lock of the lapse to the scale factor a Hamiltonian eigenvalue acts as curvature, not as vacuum energy; see the status note to the Wheeler–DeWitt ground-state theorem in the Extended Derivations).* Fast-light sign: *under the Friedmann law of §XIX E the homogeneous field in the static arena is $\bar{\psi} = 2 \ln A$, so an expanding universe has $\dot{\psi}_0 > 0$, the fast-light branch, with $\psi_0 = \beta \ln t$ and $\beta = 4/(3w + 5)$ for a fluid of equation of state w ($\beta = 2/3$ in radiation); the engine condition $\beta > 1$ on the static arena then needs $w < -1/3$, a source with $\rho + 3p < 0$.*

Anti-Theorem Q.13 (Axiom PO is not derivable from the written dynamics). The Wheeler–DeWitt operator is a *real* operator; any unique normalizable state selected by Perron–Frobenius positivity is therefore real and T-even, and a T-even state can neither select a time orientation nor supply the smooth beginning that the arrow of time rests on. Moreover the Friedmann law that governs the homogeneous mode is invariant under time reversal, so both branches are present symmetrically there: normalizability and essential self-adjointness select no branch. Hence no refinement of the written dynamics can derive clause

(iii) or the arrow: they rest on a Past-Hypothesis-class input, the smooth beginning of Postulate Q.15, of the same epistemic class as thermodynamics' low-entropy past and a low gravitational entropy, while the no-boundary internal state is *near-maximal* entropy ($\simeq 93\%$ of $\ln 61$), a cosmogenic *selection*, not a low-entropy postulate.

Remark Q.14 (Two inputs, not three). The early universe rests on two inputs. Clause (ii) is the no-boundary prescription of clause (i) read on the internal S^3: the empty core is the absence of any insertion (Eq. (AV19)). It cannot come from energy minimization, since the abundance operator is the Sugawara weight and its ground state, $j = 0$, holds no dark matter; the data select it instead, since a Wilson line of any spin from $\frac{1}{2}$ to $\frac{59}{2}$ in the core gives $\Omega_\chi h^2 = 0.135$ to 0.141 and the Cardy boundary weight gives 0.1255, against Planck's 0.1200 ± 0.0012 (the simple current $j = 30$ leaves the weights unchanged; computed). Clause (i) adds nothing beyond normalizability: on the coercive fluctuation sector the branch $e^{+S_E/\hbar}$ is not normalizable, and on the internal sector the weight is a phase. Clause (iii) is the expanding big bang read on the arena clock: in the static arena $\bar{\psi} = 2\ln A \to -\infty$ at the start, so it adds only the expanding branch (Rem. Q.11), the direction of time away from the smooth beginning of Postulate Q.15. The inputs are therefore the no-boundary state, with nothing inserted, and the smooth beginning, which no quantum state supplies (Antitheorem Q.13).

Postulate Q.15 (Smooth beginning)**.** *At the bang the background is smooth, homogeneous and isotropic on the slices of absolute time, and the early ripples are small and, on every scale, in the regular class, whose Weyl curvature vanishes at the bang, with the calibrated amplitude A_s and the stated tilt $n_s = 1 - 2/60$ (App. FK).*

The postulate is stated, not derived: it is a premise of the class of thermodynamics' low-entropy past, and it carries three things. It carries the arrow of time: at a smooth bang the Weyl curvature vanishes, a state of low gravitational entropy, and the clumping of matter grows away from it (computed). It carries the uniformity of the sky, which it states rather than explains, so the horizon problem is not solved. And it carries the primordial ripples, whose amplitude and tilt it takes as numbers and whose origin stays open: the nine derived routes to an early stage or a source of the ripples close (Prop. FK.3). It is a statement about the classical ripples: every quantum state of the printed theory carries the singular class as well, and the conformal vacuum that $J_\star$ selects carries it at equal weight (computed), so the no-boundary state of Axiom PO, which fixes the ψ fluctuation sector and the internal S^3, does not supply it. The tilt tests it, and so does the absence of primordial B-modes: the χ relic bounds the tensor ratio at $r \lesssim 10^{-7}$ (App. SM).

Physical payoff (used in App. SM). The optical metric $\tilde{g} = \mathrm{diag}(-c^2 e^{-\psi_0}, a^2 e^{\psi_0}\delta_{ij})$ is itself a flat FRW metric, with scale factor $\tilde{a} = a\, e^{\psi_0/2}$ and proper time $d\tilde{t} = e^{-\psi_0/2} dt$; it accelerates exactly when $\beta > 1-p$ (the engine condition (Q12)) and is de Sitter for $\psi_0 = 2\ln(t/t_\star)$. Every species that couples to $\tilde{g}$ therefore sees ordinary horizon-exit physics at the rate $H_{\rm opt} \equiv e^{\psi_0/2}(H + \dot{\psi}_0/2)$, and a light χ gains $(H_{\rm opt}/2\pi f_\chi)^2$ of period-1 variance per e-fold. Independently of how $\psi_0(t)$ is selected, that variance must not push $\Omega_\chi h^2$ past Planck's two-sigma ceiling ($\sigma_\theta^2 < 1.9 \times 10^{-3}$) over the $N \simeq 36$ e-folds of scale between today's horizon and the horizon at χ's oscillation onset, which gives

$$H_{\rm opt} < 2\pi f_\chi \sqrt{\sigma^2_{\theta,\max}/N} \simeq 4 \times 10^{10}\ \text{GeV}, \qquad \text{(Q13)}$$

about $550\times$ below the de Sitter-dictionary value $H_\star = 8\pi f_\chi = 2.4 \times 10^{13}$ GeV (Thm. SM.3). The count of 36 e-folds is right for a stage that lasts only as long as it must; each earlier e-fold adds a uniform displacement of χ across our patch, so a longer stage tightens the bound as $N^{-1/2}$, to about 8×10^9 GeV at 1000 e-folds, and a stage without end leaves the starting angle free, which must then lie within $|\theta_0| \le 0.044$ of a period (computed). The engine could inflate $\tilde{g}$ only with a source of negative pressure and a stage that reheats (Rem. Q.11), and then only at this low scale. This forces the primordial tensor ratio below 10^{-7}, the tensor reclassification of App. SM.

Remark Q.16 (Scope: the engine is *pre-BBN*; the validated late-time cosmology is unchanged). The fast-light screen flow ($\psi_0 \to -\infty$) is confined to the deep *pre-BBN* primordial era; in the reading of this subsection, with an expanding arena, ψ_0 has relaxed to $\psi_0 \simeq 0$ by big-bang nucleosynthesis, and whatever stage ends the engine must reheat the universe before then, which the print does not supply (Rem. Q.11). In the static arena of the formalism the homogeneous field is the expansion itself, $\bar{\psi} = 2\ln A = -2\ln(1+z)$, and keeps running to the present. This opens no second cone for the perturbations: the local scalar sector is an instantaneous constraint in absolute time, whose c-speed wave form is only a numerical relaxation (Axiom WS.1), and the dust branch of this appendix governs homogeneous deviations only, so no ψ-wave speed enters the potential on CMB scales, whichever clock is used. The engine therefore does *not* rescale post-BBN redshifts and leaves the validated DFD cosmology intact: real BBN and recombination ($z_* \simeq 1100$), the measured $T_{\rm CMB}(z) = (1+z)\,T_0$, the cobaya-validated acoustic scale, and the Etherington duality $D_L = (1+z)^2 D_A$ (App. AG). The *late-time* dark energy, the constant α^{57} vacuum term (App. AU), is *not* the primordial engine. *Caveat:* a global optical redshift factor that modified post-BBN redshifts — changing the inferred age, or making $1+z$ partly optical at recombination — would contradict all of the above and the measured $T_{\rm CMB}(z) = (1+z)$; the engine makes no such claim, and any reading of the CMB redshift as "partly optical" (the Robitaille-type non-cosmic-CMB position) is *excluded* here, not adopted.

Appendix R: EM–ψ Back-Reaction Coupling

This appendix develops the framework for electromagnetic back-reaction on the scalar field ψ, introducing a single dimensionless parameter λ that controls whether EM fields can source ψ oscillations. The resonance and parametric analysis below assumes a dynamical ψ mode with a natural frequency; under Axiom WS.1 the local ψ is an instantaneous constraint with no such mode, so the bounds and forecasts that rest on that analysis hold only for a sector that carries one. We derive both "accidental" constraints from existing cavity stability and "intentional" search protocols that could reach $|\lambda - 1| \sim 3 \times 10^{-9}$.

1. Physical Interpretation of λ

The parameter λ toggles the EM–ψ interaction:

- $\lambda = 1$: EM probes the optical metric $n = e^{\psi}$ but does not source ψ
- $|\lambda - 1| \neq 0$: EM can pump ψ modes (laboratory generation possible)

a. Intuitive picture. Think of ψ as water and EM as a paddle:

- $\lambda = 1$: The paddle slides across without making waves
- $|\lambda - 1| \neq 0$: The paddle makes waves; pump with the right rhythm and they grow

b. Relation to core postulates. The core DFD postulates (Sec. I B) specify how ψ affects EM propagation ($n = e^{\psi}$, $c_1 = ce^{-\psi}$). The parameter λ addresses the *inverse* question: can EM fields actively modify ψ? This is a distinct physical degree of freedom not constrained by the forward propagation relations.

2. Mode Equation and Pumping Channels

a. Single Lab-Mode Reduction

Reduce the ψ field to a single laboratory mode $q(t)$ with natural frequency Ω_ψ and damping γ_ψ:

$$\boxed{\ddot{q} + 2\gamma_\psi \dot{q} + \Omega_\psi^2 q = \frac{(\lambda - 1)}{M_\psi} \int u(\mathbf{r})\, \Xi(\mathbf{r}, t)\, d^3r + \alpha U(t) q} \tag{R1}$$

where:

- $u(\mathbf{r})$: normalized spatial profile of the ψ mode
- M_ψ: effective mass of the mode
- $\Xi(\mathbf{r}, t) \equiv -\frac{1}{2} e^{-2\psi_0} \left(B^2 - \frac{E^2}{c^2} \right)$: EM Lagrangian invariant ($\propto F_{\mu\nu} F^{\mu\nu}$)
- $U(t) = U_0[1 + m \cos(2\omega t)]$: stored EM energy with modulation depth m
- α: parametric coupling coefficient

The invariant Ξ carries a 2ω component for a cavity driven at frequency ω, providing two pumping channels.

b. Channel 1: Driven Resonance ($2\omega = \Omega_\psi$)

When twice the EM drive frequency matches the ψ-mode frequency, direct resonant driving occurs. The steady-state amplitude is:

$$|q|_{\text{res}} \simeq \frac{|\lambda - 1||G|}{2 M_\psi \Omega_\psi \gamma_\psi}, \tag{R2}$$

where the geometry overlap is:

$$G \equiv \int u(\mathbf{r})\, \hat{\Xi}_{2\omega}(\mathbf{r})\, d^3r, \tag{R3}$$

with $\hat{\Xi}_{2\omega}$ the 2ω Fourier component of Ξ.

c. Channel 2: Parametric Amplification ($2\omega \simeq 2\Omega_\psi$)

The stiffness modulation from $U(t)$ creates parametric gain. The Mathieu gain parameter is:

$$h = (\lambda - 1) \frac{U_0}{M_\psi \Omega_\psi^2} H m, \tag{R4}$$

with instability growth rate:

$$\Gamma \simeq \frac{1}{2} h \Omega_\psi - \gamma_\psi. \tag{R5}$$

The overlap H is:

$$H = \frac{1}{U_0} \int u^2(\mathbf{r})\, w(\mathbf{r})\, d^3r, \quad w = \frac{\varepsilon_0}{4} E^2 + \frac{\mu_0}{4} H^2. \tag{R6}$$

a. Instability threshold. Parametric instability occurs when $\Gamma > 0$:

$$|\lambda - 1|_{\min} = \frac{2\gamma_\psi}{\Omega_\psi} \frac{M_\psi \Omega_\psi^2}{U_0 H m}. \tag{R7}$$

3. Geometry Transparency

a. When the Driven Overlap Cancels

For a single, symmetric pillbox cavity driven in a pure eigenmode (TM_{010} or TE_{011}), Bessel identities and time-averaged equipartition make:

$$\int \left(B^2 - \frac{E^2}{c^2} \right) d^3r \approx 0 \quad \Rightarrow \quad G \approx 0. \tag{R8}$$

The driven channel is *geometrically transparent* for symmetric cavities in pure eigenmodes.

b. How to Restore the Overlap

Three methods restore $G \neq 0$:

1. **TE+TM superposition**: Co-phased modes with matched radii give $G = u(z_0)e^{-2\psi_0}\eta_\times U_0 \cos\phi$, where $\eta_\times = \mathcal{O}(0.1\text{–}1)$.
2. **Asymmetric geometry**: Small irises or near-cutoff asymmetries break equipartition.
3. **Mode beating**: Two nearby modes at frequencies ω_1, ω_2 produce $2\omega = \omega_1 + \omega_2$ components.

c. Parametric Overlap: Area-Ratio Law

For a ψ-mode "tube" of height L and cross-section A_ψ, with N compact cavities of total aperture $A_{\text{cav,tot}}$ placed at antinodes:

$$H \approx \frac{2}{L}\kappa_{\text{eff}}\frac{A_{\text{cav,tot}}}{A_\psi}, \tag{R9}$$

where $\kappa_{\text{eff}} = \mathcal{O}(1)$ captures mode-shape details.

Combining with (R7) and using $M_\psi \simeq A_\psi L/(2\pi c_s)$ for a 1D standing mode:

$$\boxed{|\lambda - 1|_{\min} = \frac{\pi\gamma_\psi}{c_s U_0 m}\frac{A_\psi^2}{\kappa_{\text{eff}} A_{\text{cav,tot}}}} \tag{R10}$$

As written, Eq. (R10) carries units of m/J (M_ψ above has units of $\text{m}^2\,\text{s}$, not those of a mode mass), so it fixes the ratio of the accidental and intentional values below, about 9×10^3, but not their absolute size.

4. Constraints on $|\lambda - 1|$

a. Accidental Constraint from Cavity Stability

The mere stability of existing high-Q cavities—the absence of observed parametric instability near twice the drive frequency—provides a conservative bound.

a. Conservative parameters.

- Stored energy: $U_0 \sim 100$ kJ
- Modulation depth: $m \sim 0.01$ (ambient amplitude/PLL dither)
- Loss ratio: $\gamma_\psi/\Omega_\psi \sim 10^{-3}$
- Tube area: $A_\psi \sim 0.8\ \text{m}^2$
- Cavity aperture: $A_{\text{cav,tot}} \sim 3 \times 10^{-3}\ \text{m}^2$
- $\kappa_{\text{eff}} \sim 1$, $c_s \leq c$

b. Result. Using Eq. (R10):

$$\boxed{|\lambda - 1| \lesssim 3 \times 10^{-5}} \tag{R11}$$

Any substantially larger coupling would have produced obvious parametric instability in normal cavity operation—and it has not.

c. Companion note: minimal-sector baseline. A companion note [116] analyzes the minimal tree-level optical-metric EM sector: the gauge-invariant action $-(1/4\mu_0)\int\sqrt{-\tilde{g}}\,F_{\mu\nu}F^{\mu\nu}\,d^4x$ in the DFD optical metric $n = e^\psi$, with no additional operators and no dual-sector constitutive splitting. For an ideal symmetric single-mode standing-wave cavity with exact equipartition, the bare-coupling value of λ equals unity at tree level, $\lambda_{\text{bare}} = 1$. This establishes a minimal-sector null baseline; it does *not* claim that the effective laboratory inference λ_{eff} equals unity. In DFD the two are related by

$$\lambda_{\text{eff}} - 1 = \delta_Q + \delta_{\text{geom}} + \delta_\kappa + \delta_\xi, \tag{R12}$$

where $\delta_Q \sim 1/Q$ is a finite-Q equipartition-violation mimic, δ_{geom} captures the geometry-restoration channels of Sec. R 3 (TE+TM superposition, asymmetric cavity geometries, mode beating), δ_κ captures any dual-sector constitutive splitting, and δ_ξ captures a beyond-baseline dimension-5 operator $\xi\,\psi\,F_{\mu\nu}F^{\mu\nu}$. The accidental bound Eq. (R11) and the projected intentional-search reach (Eq. (R15) below) therefore constrain the sum $|\lambda_{\text{eff}} - 1|$, not a single intrinsic DFD parameter. Separating the channels in a real experiment requires Q-scaling series, cavity-geometry variation, and polarization-sensitive protocols.

d. λ-channel protection: structural origin of the tree baseline. The companion-note baseline $\lambda_{\text{bare}} = 1$ is *structural, not accidental*. Direct variation of the minimal gauge-invariant action $-(1/4\mu_0)\int\sqrt{-\tilde{g}}\,F_{\mu\nu}F^{\mu\nu}\,d^4x$ in the optical metric ($\tilde{g}_{00} = -e^{-\psi}$, $\tilde{g}_{ij} = e^{+\psi}\delta_{ij}$, for which $\sqrt{-\tilde{g}}\,F_{\mu\nu}F^{\mu\nu} \propto e^{-\psi}B^2 - e^{+\psi}E^2/c^2$) gives

$$\frac{\delta S_{\text{EM}}}{\delta\psi} \propto e^{+\psi}\frac{E^2}{c^2} + e^{-\psi}B^2 \xrightarrow{\psi\to 0} 2\mu_0\,u_{\text{EM}}, \tag{R13}$$

the opposite-sign metric exponents differentiating to a *common* sign: minimal coupling sources ψ only through the EM energy density u_{EM} — the $(\varepsilon + 3P)$ channel of the Optical Source Theorem (Theorem II.1; for radiation $\varepsilon + 3P = 2u$, hence the factor 2) — so light gravitates, exactly as the forward theory requires. The pumping invariant $\Xi \propto (B^2 - E^2/c^2)$ of Eq. (R1) is the *opposite-sign* combination, a different operator that minimal coupling cannot generate at tree level for any field strength or cavity geometry. The λ-drive coefficient therefore vanishes at tree level as a matter of coupling structure — a protection argument, not merely the ideal-cavity equipartition computation of the companion note.

e. Intrinsic radiative floor and a positive-signal prediction (sketch grade). [*Status: identification at sketch grade; the $O(1)$ operator matching between the $\xi\,\psi F_{\mu\nu}F^{\mu\nu}$ vertex and the transition-frequency response that defines k_α is stated, not yet computed.*] The radiative response of

EM observables to the local optical scale ψ is the same physical object that App. P derives as the clock coupling $k_\alpha = \alpha\, a_e = \alpha^2/(2\pi) \simeq 8.5 \times 10^{-6}$ (Theorem P.2, resting on the same "one gauge vertex" microsector rule). Identifying the induced δ_ξ with this coupling places the intrinsic floor at

$$|\lambda_{\rm eff} - 1|_{\rm intrinsic} \;\sim\; k_\alpha \;\approx\; 10^{-5\text{–}6}, \qquad \text{(R14)}$$

a factor ~ 3.5 *below* the accidental bound Eq. (R11) — consistent with the absence of observed parametric instability to date — and $\sim 3\times10^3$ *above* the intentional-search reach (Eq. (R15) below). Two consequences follow. *(i) A conditional discriminator (sketch grade):* a generic gravitationally coupled dilaton carries the anomaly-strength coefficient $\xi \sim \alpha/(3\pi) \approx 7.7 \times 10^{-4}$, which the accidental bound Eq. (R11) excludes by a factor ~ 25 — existing cavity-stability data discriminate in favor of the microsector-suppressed DFD value over the generic-dilaton alternative. *(ii) A two-tier falsifiable forecast:* conditional on the k_α identification, DFD predicts the intentional search below finds a *positive* signal at the k_α level, not a null. A signal at $\sim 10^{-5\text{–}6}$ would confirm the microsector clock coupling in a second, independent channel; a null at 10^{-7} falsifies the k_α identification (while leaving the structural tree baseline $\lambda_{\rm bare} = 1$ of Eq. (R13) intact, testable down to the 3×10^{-9} reach floor).

b. *Intentional Search: Projected Reach*

With deliberate optimization using the same physics:

- $U_0 \to 1$ MJ (factor 10 increase)
- $m \to 0.1$ (factor 10 increase)
- Array apertures at all antinodes: $A_{\rm cav,tot} \to 3\times10^{-2}$ m^2 (factor 10)
- Shrink tube area: $A_\psi \to 0.27$ m^2 (factor $\sim$3 reduction)
- Maintain $\gamma_\psi/\Omega_\psi \sim 10^{-3}$

The design law (R10) then gives:

$$\boxed{|\lambda - 1| \sim 3 \times 10^{-9} \quad \text{(accessible reach)}} \qquad \text{(R15)}$$

TABLE XCV. Accidental vs. intentional search parameters.

Parameter	Accidental	Intentional
Stored energy U_0 (J)	10^5	10^6
Modulation depth m	0.01	0.10
Cavity aperture $A_{\rm cav,tot}$ (m^2)	3×10^{-3}	3×10^{-2}
Tube area A_ψ (m^2)	0.8	0.27
Loss ratio γ_ψ/Ω_ψ	10^{-3}	10^{-3}
Projected $\lvert\lambda - 1\rvert_{\rm min}$	$\lesssim 3 \times 10^{-5}$	$\sim 3 \times 10^{-9}$

5. Why $\lambda \neq 1$ Has Not Been Detected

Three factors explain the null result in existing metrology:

1. **Pure eigenmodes suppress the driven channel.** Symmetric cavities in pure modes have $G \approx 0$ by Bessel-function orthogonality and equipartition.
2. **Parametric pumping needs deliberate 2ω.** Routine metrology avoids such tones and heavily filters them to suppress amplitude-modulation sidebands.
3. **2ω features treated as technical noise.** Any residual 2ω response is interpreted as technical AM sidebands and actively suppressed, not investigated as a potential signal.

a. *To detect $|\lambda - 1| \neq 0$:*

- Use TE+TM superposition (restores $G \neq 0$)
- Deliberately apply 2ω modulation
- *Preserve* (not suppress) 2ω response
- Monitor for resonant growth at Ω_ψ

6. Intentional Detection Protocol

Intentional ψ-Pump Detection: Required Capabilities

1. **High-Q resonator** ($Q \gtrsim 10^4$) with stored energy $U_0 \gtrsim 1$ MJ (pulsed acceptable)
2. **Phase-stable amplitude modulation** at 2ω with depth $m \sim 0.1$ on stored energy
3. **Placement of cavity apertures at ψ antinodes** (maximize H; use multiple irises)
4. **Phase-sensitive readout near Ω_ψ**; preserve 2ω tones (do not auto-suppress)
5. **Null sensitivity target**: $|\lambda - 1| \lesssim 3 \times 10^{-9}$

a. *Orthogonal cross-check: Driven amplitude.*

With a TE+TM superposition ($\eta_\times \neq 0$, phase $\phi = 0$):

$$\Delta\psi \equiv u(z_0)|q|_{\rm res} \approx \frac{|\lambda - 1|\eta_\times U_0 c_s}{\pi A_\psi \gamma_\psi}. \qquad \text{(R16)}$$

For $\eta_\times \sim 0.3$, $U_0 = 100$ kJ, $A_\psi = 0.8$ m^2, $\gamma_\psi = 0.03$ s^{-1}:

$$\Delta\psi \sim 1.2 \times 10^{-3}|\lambda - 1|, \qquad \text{(R17)}$$

which crosses cavity-atom sensitivity (Sec. XII) in the 10^{-12}–10^{-15} range for $|\lambda - 1|$ in 10^{-9}–10^{-12}. As written, Eq. (R16) carries units of J/m (through the same M_ψ as Eq. (R10)) and, with $c_s = c$, evaluates to $1.2\times10^{14}|\lambda-1|$, so it does not fix the coefficient 1.2×10^{-3}.

7. Relation to Core DFD Framework

a. Consistency with postulates. The parameter λ does *not* modify the core postulates:

- Refractive index: $n = e^{\psi}$ (unchanged)
- One-way light speed: $c_1 = ce^{-\psi}$ (unchanged)
- Matter acceleration: $a = (c^2/2)\nabla\psi$ (unchanged)
- Field equation: Eq. (21) (unchanged for static/quasi-static)

The λ parameter describes a *dynamic* EM–ψ interaction orthogonal to the static field relations. It affects how rapidly oscillating EM fields can pump ψ modes, not how ψ affects light propagation.

b. Default value. Without additional physics, $\lambda = 1$ (no back-reaction) is the natural default. Any $|\lambda - 1| \neq 0$ indicates additional EM–gravity coupling beyond metric propagation effects.

8. Summary

1. The parameter λ controls EM back-reaction on ψ: $\lambda = 1$ means EM probes but doesn't pump; $|\lambda-1| \neq 0$ enables laboratory ψ-generation.
2. Existing cavity stability provides an **accidental bound**:
$$|\lambda - 1| \lesssim 3 \times 10^{-5}. \tag{R18}$$
3. Deliberate optimization enables an **intentional search** reaching:
$$|\lambda - 1| \sim 3 \times 10^{-9}. \tag{R19}$$
4. The null detection so far is explained by geometry transparency and suppression of 2ω components in standard metrology.
5. A dedicated search protocol with TE+TM superposition and preserved 2ω response could either discover $\lambda \neq 1$ or constrain it below 3×10^{-9} with upgraded apparatus.

Key Result

Unoptimized cavities accidentally constrain $|\lambda - 1| \lesssim 3 \times 10^{-5}$. An intentional 2ω modulation test with upgraded hardware (Table XCV) pushes **about four orders of magnitude tighter**. A dedicated measurement could either discover $\lambda \neq 1$ or constrain it below 3×10^{-9}.

9. Dual-Sector Extension: The κ Parameter

Beyond the λ parameter controlling EM back-reaction, a second parameter κ controls the *differential* response of electric and magnetic sectors to ψ.

a. Status of the κ parameter. At tree level, the Gordon optical metric gives $\kappa = 0$, i.e. no electric–magnetic constitutive split.

a. Constitutive Split Preserving $v_{\rm ph} = c/n$

The vacuum permittivity and permeability can respond asymmetrically to ψ:
$$\epsilon(\psi) = \epsilon_0\, n\, e^{+\kappa\psi}, \qquad \mu(\psi) = \mu_0\, n\, e^{-\kappa\psi}, \tag{R20}$$
where $n = e^{\psi}$ and κ is the split parameter.

The product is preserved:
$$\epsilon(\psi)\mu(\psi) = \epsilon_0\mu_0\, n^2 \quad \Rightarrow \quad v_{\rm ph} = \frac{1}{\sqrt{\epsilon\mu}} = \frac{c}{n}. \tag{R21}$$
Thus the optical metric phase speed is unchanged by the split.

a. Physical interpretation.

- $\kappa = 0$: Electric and magnetic sectors respond identically to ψ (symmetric case)
- $\kappa \neq 0$: Sector-differential response; electric and magnetic energies couple differently

b. The Unified Bracket

With the split (R20), a single bracket governs energy exchange, body force, and ψ sourcing:
$$\mathcal{B} \equiv \frac{B^2}{\mu} - \epsilon E^2. \tag{R22}$$

a. Energy exchange. The Poynting theorem acquires:
$$\partial_t u + \nabla\cdot\mathbf{S} = -\mathbf{J}\cdot\mathbf{E} - \frac{\kappa}{2}\dot{\psi}\,\mathcal{B}. \tag{R23}$$

b. Body force. Fields exert force on the medium:
$$\mathbf{f}_\psi = -\frac{\kappa}{2}\,\mathcal{B}\,\nabla\psi. \tag{R24}$$

c. ψ sourcing. EM fields can source ψ:
$$\frac{\delta\mathcal{L}_\psi}{\delta\psi} = \mathcal{S}_{\rm mass} + \frac{\kappa}{2}\,\mathcal{B}. \tag{R25}$$

c. Standing-Wave Energy Equality

For a lossless, steady-state standing wave in a linear medium, the cycle-averaged *integrated* energies are equal:
$$\int_V \overline{\epsilon E^2}\, dV = \int_V \overline{B^2/\mu}\, dV, \tag{R26}$$
so $\int_V \overline{\mathcal{B}}\, dV = 0$. The integrated bracket vanishes for ideal standing waves.

a. Local imbalance. Nonzero *local* bracket arises at $\mathcal{O}(\theta^2)$ due to longitudinal fields in paraxial Gaussian modes. For a TEM_{00} cavity mode with waist w_0:
$$\overline{\epsilon E^2} - \overline{B^2/\mu} \sim \theta^2\,\epsilon|E_0|^2, \qquad \theta = \frac{\lambda}{\pi w_0}. \tag{R27}$$

For $\lambda = 1064$ nm, $w_0 = 300\,\mu$m: $\theta^2 \simeq 1.3 \times 10^{-6}$.

d. Experimental Tests

a. Accidental bound from cavity stability. Absence of 2ω parametric instabilities in extreme-Q resonators constrains unintended EM$\leftrightarrow\psi$ pumping.

b. LPI residual as κ test. After the constitutive-chain cancellation of Sec. XII A, the cavity–atom observable is a screened residual rather than an order-unity slope. Nevertheless, the sector-resolved residual still depends on κ via:

$$\begin{aligned}\xi_{\rm LPI}^{\rm res}(\kappa) &= (\text{screened residual of})\ 1 - \alpha_L^{(M)} - \alpha_{\rm at}^{(S)}(\kappa),\\ \alpha_{\rm at}^{(S)}(\kappa) &= K_\epsilon^{(S)}\kappa + \mathcal{O}(\kappa^2).\end{aligned} \tag{R28}$$

where $K_\epsilon^{(S)}$ is the atomic EM-energy sensitivity.

c. Order-of-magnitude for $K_\epsilon^{(S)}$. Atomic optical transition energies scale with the effective Rydberg $R_\infty \propto 1/\epsilon^2$, giving:

$$\left.\frac{\delta E}{E}\right|_{\rm gross} \simeq -2\,\frac{\delta\epsilon}{\epsilon} \quad\Rightarrow\quad K_\epsilon^{(S)} \sim \mathcal{O}(1\text{–}3). \tag{R29}$$

For Sr and Yb clock transitions, $K_\epsilon^{(S)}$ is plausibly order unity.

e. Experimental Discrimination

κ can be tested via:

1. **TE/TM polarization swaps:** Pure TE (magnetic dominant) vs pure TM (electric dominant) modes have opposite bracket signs.
2. **Dual-wavelength measurements:** κ is wavelength-independent; dispersion effects are not.
3. **Multi-species clock comparisons:** Different atoms have different $K_\epsilon^{(S)}$ values.

Dual-Sector Extension Summary

The κ parameter:
- Controls differential ϵ/μ response to ψ while preserving $v_{\rm ph} = c/n$
- Unified bracket $\mathcal{B} = B^2/\mu - \epsilon E^2$ governs energy, force, and sourcing

Appendix S: Standard Model Extension Dictionary

This appendix maps DFD parameters onto the language of the Standard-Model Extension (SME) [153], enabling direct comparison with published experimental constraints.

1. SME Framework Overview

The SME provides a phenomenological framework for parameterizing possible violations of Lorentz invariance and the Einstein Equivalence Principle. For gravitational tests with atomic clocks, the relevant observable is:

$$\frac{\delta(f_A/f_B)}{(f_A/f_B)} = (\beta_A - \beta_B)\frac{\Delta U}{c^2}, \tag{S1}$$

where β_A, β_B encode gravitational redshift anomalies for species A and B.

2. DFD↔SME Correspondence

In DFD, the same observable is:

$$\frac{\delta(f_A/f_B)}{(f_A/f_B)} = (\xi_A - \xi_B)\frac{\Delta\Phi}{c^2}, \tag{S2}$$

where the effective coupling ξ_A includes both matter and photon sector contributions:

$$\xi_A \equiv K_A + \delta_{A,\gamma}, \tag{S3}$$

with K_A twice the magnitude of the per-unit-ψ channel-resolved coupling of Eq. (291) (whose pure-α leading term is $k_\alpha \cdot S_A^\alpha$; Sec. XI B) and $\delta_{A,\gamma} = 1$ if species A involves a photon-sector reference. After the constitutive-chain cancellation of Sec. XII, the photon-sector contribution $\delta_{A,\gamma}$ is absorbed into the tree-level cancellation and the surviving observable is a screened residual.

Identifying $\Delta U \leftrightarrow \Delta\Phi$, the direct correspondence is:

$$\boxed{\beta_A - \beta_B \longleftrightarrow \xi_A - \xi_B = (K_A - K_B) + (\delta_{A,\gamma} - \delta_{B,\gamma})} \tag{S4}$$

3. Translation Table

TABLE XCVI. DFD↔SME parameter correspondence.

DFD Quantity	SME Analogue	Meaning
$\psi/2$	U/c^2	Background grav. field
K_A	β_A (matter)	Species-dep. coupling
$\delta_{A,\gamma}$	β_A (photon)	Photon-mode coupling
$\xi_A = K_A + \delta_{A,\gamma}$	Total β_A	Composite LPI param.
$k_\alpha = \alpha^2/(2\pi)$	—	DFD-specific scale

4. Experimental Constraints Reinterpreted

Published SME bounds can be reinterpreted as DFD constraints:

5. Cavity-Atom Comparisons in SME Language

For cavity-atom LPI tests (Sec. XII), the SME parameterization becomes:

$$\frac{d}{d\Phi}\left(\frac{\nu_{\rm atom}}{\nu_{\rm cavity}}\right) = \frac{\xi_{\rm atom} - \xi_{\rm cavity}}{c^2} = \frac{\xi_{\rm LPI}}{c^2}, \tag{S5}$$

where the tree-level assignment $\xi_{\rm cavity} = 1$ is not used. After the constitutive-chain cancellation of Sec. XII, both cavity and atomic sectors share the universal geometric redshift at tree level, so only a screened residual mismatch survives:

$$\xi_{\rm LPI} \longrightarrow \xi_{\rm LPI}^{\rm res}. \tag{S6}$$

a. Significance. In SME-style language, DFD does not predict an order-unity cavity coefficient. Instead it predicts that any measurable cavity–atom anomaly must arise from a channel-resolved residual, consistent with the four-term structure of Eq. (291) and the screening logic summarized in Secs. XI and XII.

Appendix T: Family and Clock-Type Parametrization of LPI Tests

This appendix presents a phenomenological parametrization organizing clock comparison tests by chemical family and clock type. The framework provides a compact way to encode where current data pull and where future tests should focus.

1. Two-Parameter Model

Motivated by the pattern of hints and nulls in clock comparisons, we parameterize the gravitational coupling coefficient as:

$$K_i = k_N C_N^{(i)} + k_e C_e^{(i)} + k_\alpha \kappa_\alpha^{(i)}, \tag{T1}$$

where:

- $C_N^{(i)}$: Nuclear-sector charge depending on chemical family
- $C_e^{(i)}$: Electronic-sector charge depending on clock type
- $\kappa_\alpha^{(i)} = S_i^\alpha$: Standard α-sensitivity
- k_N, k_e, k_α: Coupling strengths to be fit or constrained

a. Family charges. Based on chemical grouping:

Element family	C_N
Alkaline earth (Sr, Ca, Mg)	0
Alkali (Cs, Rb, H)	1
Post-transition (Al, Hg, In)	1.5
Lanthanide (Yb, Dy)	2

b. Clock-type charges. Based on interrogation mode:

$$C_e = \begin{cases} 0 & \text{optical neutral} \\ 0.5 & \text{trapped ion} \\ 1 & \text{microwave hyperfine} \end{cases} \tag{T2}$$

These assignments are deliberately coarse; the point is not that nuclear scalar charges take precisely these values, but that grouping by family and clock type yields a testable pattern.

2. Constraints from Data

For each clock pair (A, B), the observable is:

$$\Delta K_{AB} = k_N \Delta C_N + k_e \Delta C_e + k_\alpha \Delta \kappa_\alpha, \tag{T3}$$

where $\Delta C_N = C_N^{(A)} - C_N^{(B)}$ and similarly for other quantities.

TABLE XCVII. SME bounds reinterpreted in DFD framework.

Experiment	SME Constraint	DFD Interpretation	Ref.
H maser/Cs (14-yr)	$\lvert\beta_{\rm H} - \beta_{\rm Cs}\rvert < 2.5 \times 10^{-7}$	$\lvert K_{\rm H} - K_{\rm Cs}\rvert < 2.5 \times 10^{-7}$	[154]
Yb^+ E3/E2 (PTB)	$\lvert\beta_{\rm E3} - \beta_{\rm E2}\rvert < 10^{-8}$	Same-ion: composition cancels	[155]
Hg^+/Cs	$\lvert\beta_{\rm Hg} - \beta_{\rm Cs}\rvert < 5.8 \times 10^{-6}$	$\lvert K_{\rm Hg} - K_{\rm Cs}\rvert < 5.8 \times 10^{-6}$	[156]
Al^+/Hg^+	$\lvert\beta_{\rm Al} - \beta_{\rm Hg}\rvert < 5.3 \times 10^{-7}$	$\lvert K_{\rm Al} - K_{\rm Hg}\rvert < 5.3 \times 10^{-7}$	[157]

a. E3/E2 constraint on k_α. The Yb^+ E3/E2 same-ion comparison has $\Delta C_N = \Delta C_e = 0$ but $\Delta\kappa_\alpha = -6.95$. The PTB bound $|\Delta K_{\rm E3/E2}| < 10^{-8}$ thus constrains:

$$|k_\alpha| < 1.4 \times 10^{-9}. \tag{T4}$$

This bounds the unscreened pure-α coefficient of this phenomenological model; it is not a bound on the common-sector k_α of Appendix P (Sec. XI).

b. Cross-species constraints. With $k_\alpha = 0$ fixed, the two-parameter model (k_N, k_e) is constrained by:

- H/Cs null ($\Delta C_N = \Delta C_e = 0$): automatically satisfied
- Hg^+/Cs: $\Delta C_N = 0.5$, $\Delta C_e = -0.5$, bound $|\Delta K| < 5.8 \times 10^{-6}$
- Dy/Cs: $\Delta C_N = 1$, $\Delta C_e = -1$, bound $|\Delta K| < 10^{-5}$
- Cs/Sr hint: $\Delta C_N = 1$, $\Delta C_e = 1$, suggests $\Delta K \sim 3 \times 10^{-5}$

A joint fit yields $k_N \sim 6 \times 10^{-6}$, $k_e \sim 1.5 \times 10^{-5}$ with $\chi^2_\nu \approx 1$.

3. Predictions for Untested Channels

The model predicts specific ΔK values for channels where high-precision ratios exist but LPI analyses have not been performed:

TABLE XCVIII. Family+clock model predictions for untested LPI channels.

Channel	ΔC_N	ΔC_e	Predicted ΔK	Test type
Sr^+/Sr	0	+0.5	7.5×10^{-6}	Pure electronic
Ca^+/Sr	0	+0.5	7.5×10^{-6}	Pure electronic
H-maser/Sr	+1	+1	equal to Cs/Sr	Same charges as Cs/Sr
Hg/Sr	+1.5	0	9×10^{-6}	Pure nuclear-family
Yb^+/Sr^+	+2	0	1.2×10^{-5}	Pure nuclear-family
Hg/Yb	−0.5	0	-3×10^{-6}	Partial cancellation
Ca/Sr	0	0	0	Null prediction

a. Falsification criteria.

1. An observed Ca/Sr LPI signal at $\sim 10^{-5}$ would falsify the family structure.
2. Hg/Sr or Ca^+/Sr showing null results at $< 10^{-6}$ would severely constrain both k_N and k_e.
3. Consistency across untested channels validates the two-parameter structure.

4. Relation to DFD Microsector

The phenomenological charges (C_N, C_e) are not derived from first principles in this appendix. However, they are compatible with the DFD microsector in the following sense:

- The overall scale $k_N, k_e \sim 10^{-5}$–10^{-6} is consistent with $k_\alpha = \alpha^2/(2\pi)$ structure.
- The family grouping (alkaline earth vs. lanthanide) suggests coupling to properties correlated with atomic structure, not just α.
- The clock-type structure (ion vs. neutral) aligns with the sector-coupling hierarchy in Sec. XI G.

A full derivation of (C_N, C_e) from the $\mathbb{CP}^2 \times S^3$ microsector remains an open problem. The present appendix establishes the empirical pattern that such a derivation must reproduce.

5. Summary

The family+clock parametrization provides:

1. A compact organization of existing LPI constraints
2. Specific predictions for channels where analyses are actionable
3. Clear falsification criteria
4. A target pattern for microsector derivation

The decisive tests are Hg/Sr (pure nuclear-family) and Sr^+/Sr (pure electronic), both of which can be performed with existing clock technology.

Appendix U: Mathematical Well-Posedness of the DFD Field Equations

This appendix establishes the mathematical foundations of DFD as a well-posed partial differential equation system. We treat both the static (elliptic) boundary value problem relevant for equilibrium configurations and the dynamic (hyperbolic) Cauchy problem of its numerical relaxation (under Axiom WS.1 the scalar is an instantaneous constraint). The analysis follows standard methods from monotone operator theory [158, 159] and quasilinear elliptic theory [32, 33].

For DFD to stand alongside General Relativity as a viable relativistic gravity theory, it is not enough to match phenomenology. The underlying PDE must be mathematically well posed: given appropriate initial (and, when relevant, boundary) data, there should exist a unique solution in a suitable Sobolev class, depending continuously on the data.

1. The Static Field Equation: Elliptic Theory

The DFD static field equation is:

$$-\nabla \cdot \big(\mu(|\nabla\psi|)\nabla\psi\big) = \frac{8\pi G}{c^2}\rho, \tag{U1}$$

where $\mu : [0,\infty) \to [0,\infty)$ is the interpolation function satisfying $\mu(x) = x/(1+x)$.

a. Structural Assumptions on μ

We impose the following conditions (all satisfied by $\mu(x) = x/(1+x)$):

- **(A1) Continuity:** μ is continuous on $[0,\infty)$.
- **(A2) Coercivity:** $\exists\, \alpha > 0$, $\beta \geq 0$ such that $(p = 2)$
$$\mu(|\xi|)|\xi|^2 \geq \alpha|\xi|^2 - \beta \quad \forall\, \xi \in \mathbb{R}^3. \tag{U2}$$
- **(A3) Growth:** $\exists\, \beta > 0$ such that
$$|\mu(|\xi|)\xi| \leq \beta(1+|\xi|)^{p-1}. \tag{U3}$$
- **(A4) Monotonicity:** For all $\xi, \eta \in \mathbb{R}^3$,
$$\big(\mu(|\xi|)\xi - \mu(|\eta|)\eta\big) \cdot (\xi - \eta) \geq 0. \tag{U4}$$
If strict, uniqueness follows.

Lemma U.1 (DFD μ satisfies (A1)–(A4))**.** *The weak-response approximant $\mu(x) = x/(1+x)$ derived in Appendix N satisfies all four structural assumptions with $p = 2$.*

Proof. (A1) is immediate. For (A2)–(A3), note that $\mu(s) \in [0,1)$ for all $s \geq 0$, and $\mu(s)s^2 = s^3/(1+s) = s^2 - s + s/(1+s) \geq s^2 - s \geq \frac{1}{2}s^2 - \frac{1}{2}$, which is (A2) with $\alpha = \beta = \frac{1}{2}$; (A3) holds since $|\mu(s)s| \leq s$. For the exact law the same holds with $F(x) \geq x - 0.648$ (SOURCE) and $F(x) \geq x - e^{-1}$ (TOTAL). For (A4), define $a(\xi) = \mu(|\xi|)\xi$ and compute:

$$\frac{\partial a_i}{\partial \xi_j} = \mu(|\xi|)\delta_{ij} + \mu'(|\xi|)\frac{\xi_i \xi_j}{|\xi|}. \tag{U5}$$

Since $\mu'(s) = 1/(1+s)^2 > 0$, this matrix is positive semi-definite, establishing monotonicity. □

Remark U.2 (Catalog of admissible μ-families). Other functions satisfying (A1)–(A4) include:

- **p-Laplacian:** $\mu(s) = s^{p-2}$
- **Saturating:** $\mu(s) = (1+s^2)^{(p-2)/2}$
- **Regularized MOND-like:** $\mu(s) = s/\sqrt{s^2 + s_a^2}$

The weak-response approximant $\mu(x) = x/(1+x)$ of the DFD-derived response is distinguished by its topological origin (Appendix N).

b. Weak Formulation and Variational Structure

Define the flux map $a(\xi) := \mu(|\xi|)\xi$. For $\psi \in W^{1,p}(\Omega)$ with boundary data $\psi = \psi_D$ on $\partial\Omega$, the weak formulation is:

$$\int_\Omega a(\nabla\psi) \cdot \nabla v \, dx = \int_\Omega f\, v \, dx, \quad \forall\, v \in W_0^{1,p}(\Omega), \tag{U6}$$

where $f = (8\pi G/c^2)\rho$.

Define the energy density:

$$H(\xi) := \int_0^1 a(t\xi) \cdot \xi \, dt, \tag{U7}$$

so that $a(\xi) = \nabla_\xi H(\xi)$. Then the energy functional

$$\mathcal{E}[\psi] := \int_\Omega H(\nabla\psi)\, dx - \int_\Omega f\psi \, dx \tag{U8}$$

is convex and coercive under (A1)–(A4). Critical points of $\mathcal{E}$ are weak solutions of Eq. (U1).

c. Main Existence and Regularity Theorems

Theorem U.3 (Existence for Static Problem)**.** *Under (A1)–(A4), for any $f \in (W_0^{1,p}(\Omega))'$, there exists a weak solution $\psi \in W^{1,p}(\Omega)$ of Eq. (U1) attaining prescribed Dirichlet boundary data.*

Proof. The operator $A : W_0^{1,p}(\Omega) \to (W_0^{1,p}(\Omega))'$ defined by

$$\langle A\psi, v\rangle = \int_\Omega a(\nabla\psi) \cdot \nabla v \, dx \tag{U9}$$

is monotone by (A4), coercive by (A2), and hemicontinuous by (A1). The Browder-Minty theorem [158] then guarantees existence. □

Theorem U.4 (Uniqueness)**.** *If $a(\xi) = \mu(|\xi|)\xi$ is strictly monotone (which holds for $\mu(x) = x/(1+x)$), the weak solution of Theorem U.3 is unique.*

Theorem U.5 (Regularity). *If $f \in L^q(\Omega)$ with $q > 3/p'$, then any weak solution satisfies $\psi \in C^{0,\alpha}_{\mathrm{loc}}(\Omega)$ for some $\alpha > 0$. If additionally $\mu \in C^1$ and $f \in C^{0,\gamma}$, then $\psi \in C^{1,\alpha}_{\mathrm{loc}}(\Omega)$.*

The proofs follow standard methods from quasilinear elliptic regularity theory [32, 33].

d. Exterior Domains and Optical Boundary Conditions

For astrophysical applications, we consider $\Omega = \mathbb{R}^3 \setminus \overline{B_R}$ with boundary conditions motivated by DFD optical phenomenology:

- **Asymptotic condition:** $|\nabla\psi(x)| \to 0$ as $|x| \to \infty$.
- **Horizon boundary:** Ingoing-flux Neumann condition

$$a(\nabla\psi)\cdot\hat{n} = g_{\mathrm{hor}}, \quad \text{with outgoing flux set to zero.} \tag{U10}$$

Theorem U.6 (Exterior Well-Posedness). *Under (A1)–(A4) and the above boundary conditions (the horizon condition as stated in §U 5), there exists a weak solution $\psi \in W^{1,p}_{\mathrm{loc}}(\Omega)$ with the gradient vanishing at infinity. If the boundary operators are strictly monotone, the solution is unique.*

2. The Dynamic Field Equation: Hyperbolic Theory

The c-speed form of the field equation, which Axiom WS.1 (App. WS) reads as a numerical relaxation of the instantaneous constraint and not as a physical evolution law, takes the form:

$$a^{\mu\nu}(\psi,\partial\psi)\,\partial_\mu\partial_\nu\psi + b^\mu(\psi,\partial\psi,x)\,\partial_\mu\psi + c(\psi,\partial\psi,x) = S(x), \tag{U11}$$

where $a^{\mu\nu}$ is derived from the optical metric $g^{\mu\nu}[\psi]$, Greek indices run from 0 to 3 with $x^0 = t$, and we adopt the Minkowski metric $\eta_{\mu\nu} = \mathrm{diag}(-1,1,1,1)$ as background reference.

a. Structural Assumptions for Hyperbolic Theory

We impose conditions on the coefficients that capture the key features of the DFD strong-field equation while remaining within the classical quasilinear hyperbolic framework:

(H1) Uniform hyperbolicity of principal part. There exists $\lambda \geq 1$ such that for all (t,x) in the region of interest, all admissible ψ and $\partial\psi$, and all spatial covectors $\xi = (0,\xi_1,\xi_2,\xi_3)$:

- $a^{\mu\nu}(\psi,\partial\psi)\xi_\mu\xi_\nu = a^{\nu\mu}(\psi,\partial\psi)\xi_\mu\xi_\nu$ (symmetry);
- the spatial principal symbol is uniformly positive definite,

$$\lambda^{-1}|\xi|^2 \leq a^{ij}\xi_i\xi_j \leq \lambda\,|\xi|^2, \tag{U12}$$

where for the DFD equation $a^{00} = -c^{-2}$, $a^{0i} = 0$ and $a^{ij} = \mu(|\nabla\psi|)\delta^{ij} + \mu'(|\nabla\psi|)\,\partial_i\psi\,\partial_j\psi/|\nabla\psi|$ is the flux Jacobian of Lemma U.1.

(H2) Regularity of lower-order terms. For each multiindex α with $|\alpha| \leq s$ (for fixed $s > 5/2$), the derivatives $\partial^\alpha b^\mu$ and $\partial^\alpha c$ exist and are continuous, bounded by polynomials in $|\psi|$ and $|\partial\psi|$.

(H3) Regularity of source. $S(x) \in H^{s-1}$ on the relevant spatial domain.

Definition U.7 (Uniform Hyperbolicity). The DFD operator in Eq. (U11) is *uniformly hyperbolic* in a region $\Omega \subset \mathbb{R}^{3+1}$ if (H1) holds with some $\lambda > 0$.

Proposition U.8 (Uniform hyperbolicity of the regularised approximant). *For the galactic approximant $\mu(x) = x/(1+x)$ regularised as $\mu_{s_0}(x) = \mu\big(\sqrt{x^2+s_0^2}\big)$, $s_0 > 0$, condition (H1) holds on every region with $\lambda = 1+1/s_0$. For the unregularised approximant, $\mu(0) = 0$ and (H1) fails wherever $\nabla\psi = 0$.*

For the exact law (Appendix BS), (H1) holds on every region where $|\nabla\psi| \geq \delta > 0$, with $\lambda = \max\big(\Lambda, 1/\mu(\delta)\big)$: on the SOURCE branch, with $u = \sqrt{y}$, $F'(x) = 2(1-e^{-u})^2/[2(1-e^{-u}) - ue^{-u}]$, whose denominator vanishes at $u = 0$ and grows at the rate $(1+u)e^{-u} > 0$, and on the TOTAL branch $F'(x) = 1 - e^{-x} + xe^{-x}$; both are positive for every $x > 0$, as is μ.

Proof. With $r = \sqrt{|\nabla\psi|^2 + s_0^2} \geq s_0$, the eigenvalues of the flux Jacobian are $\mu(r) \geq \mu(s_0) = s_0/(1+s_0)$ (twice) and $\mu(r) + \mu'(r)|\nabla\psi|^2/r \leq \mu(r) + r\mu'(r) = 1 - (1+r)^{-2} < 1$. For the unregularised approximant the eigenvalues are $\mu(s)$ and $d[s\mu(s)]/ds$, $s = |\nabla\psi|$, both of which vanish at $s = 0$. □

Remark U.9 (Choice of Sobolev index). We assume $s > n/2 + 1$ with $n = 3$ spatial dimensions, so $s > 5/2$. This guarantees that $H^s(\mathbb{R}^3)$ is a Banach algebra under pointwise multiplication and embeds continuously into $C^1(\mathbb{R}^3)$. The nonlinear coefficients can then be controlled by the H^s norm of ψ, which is essential for closing energy estimates.

b. Reduction to First-Order Symmetric Hyperbolic Form

Introduce variables $U = (u_0,u_1,u_2,u_3,u_4)^T$ with:

$$u_0 = \psi, \quad u_i = \partial_i\psi\ (i = 1,2,3), \quad u_4 = \partial_t\psi. \tag{U13}$$

Then Eq. (U11) becomes:

$$A^0(U)\,\partial_t U + \sum_{j=1}^{3} A^j(U)\,\partial_j U = F(U,x), \tag{U14}$$

where the matrices $A^\mu(U)$ are 5×5 symmetric and, under (H1), $A^0(U)$ is uniformly positive definite.

In the block decomposition $(u_0\,|\,u_1,u_2,u_3\,|\,u_4)$, with $Da=(a^{ij})$ the flux Jacobian of (H1) and e_j the j-th unit vector,

$$A^0(U)=\begin{pmatrix}1&0&0\\0&Da&0\\0&0&c^{-2}\end{pmatrix}, \tag{U15}$$

$$A^j(U)=-\begin{pmatrix}0&0&0\\0&0&Da\,e_j\\0&(Da\,e_j)^T&0\end{pmatrix}, \tag{U16}$$

the row u_0 being $\partial_t u_0=u_4$, the rows u_1,u_2,u_3 the identities $\partial_t u_i=\partial_i u_4$ multiplied by Da, and the row u_4 Eq. (U11); the system is symmetric hyperbolic exactly when Da is uniformly positive definite, which is (H1).

c. *Local Well-Posedness for the Cauchy Problem*

Theorem U.10 (Local Well-Posedness on $\mathbb{R}^3$)**.** *Let $s>5/2$ and assume (H1)–(H3). For initial data*

$$(\nabla\psi_0-\mathbf{g},\ \psi_1)\in H^{s-1}(\mathbb{R}^3)\times H^{s-1}(\mathbb{R}^3) \tag{U17}$$

for a constant vector $\mathbf{g}$, with $\inf|\nabla\psi_0|>0$ unless the response is regularised, and time-independent source $S\in H^{s-1}(\mathbb{R}^3)$, there exists $T>0$ (depending on norms of initial data) such that the Cauchy problem admits a unique solution

$$\nabla\psi-\mathbf{g},\ \partial_t\psi\in C^0\big([0,T];H^{s-1}(\mathbb{R}^3)\big). \tag{U18}$$

The solution depends continuously on initial data in these function spaces.

Proof. The reduction to Eq. (U14) produces a symmetric hyperbolic system. Under (H1)–(H3), standard energy estimates in Sobolev spaces yield local existence, uniqueness, and continuous dependence. The original field ψ is recovered as the first component of U. □

d. *Initial-Boundary Value Problems*

For bounded domains $\Omega\subset\mathbb{R}^3$ with smooth boundary, we consider the IBVP:

$$\begin{cases}\text{Eq. (U11)} & (t,x)\in[0,T]\times\Omega,\\ \psi(0,x)=\psi_0(x), & x\in\Omega,\\ \partial_t\psi(0,x)=\psi_1(x), & x\in\Omega,\\ \psi(t,x)=g(t,x), & (t,x)\in[0,T]\times\partial\Omega.\end{cases} \tag{U19}$$

a. Compatibility conditions. For solutions in $H^s(\Omega)$ with $s>5/2$, compatibility conditions between (ψ_0,ψ_1) and g are required at the corner $\{t=0\}\cap\partial\Omega$:

- **Zeroth order:** $\psi_0|_{\partial\Omega}=g(\cdot,0)$.
- **First order:** $\psi_1|_{\partial\Omega}=\partial_t g(\cdot,0)$.
- **Higher orders:** $\partial_t^k\psi|_{t=0,\partial\Omega}=\partial_t^k g(\cdot,0)$ for $k\le\lfloor s-1\rfloor$, where higher time derivatives of ψ at $t=0$ are determined from the PDE itself.

b. Energy estimates. Define the Sobolev energy:

$$E_s(t)=\sum_{|\alpha|\le s}\int_\Omega\big(|\partial^\alpha\partial_t\psi|^2+|\nabla\partial^\alpha\psi|^2\big)\,dx. \tag{U20}$$

Under (H1)–(H3) and compatibility conditions, one obtains a differential inequality of the form:

$$\frac{d}{dt}E_s(t)\le C(M)\Big(E_s(t)+\|S\|^2_{H^{s-1}}+\|g\|^2_{H^{s-1/2}(\partial\Omega)}\Big), \tag{U21}$$

where $C(M)$ depends on L^∞ bounds for ψ and $\partial\psi$. Gronwall's lemma then yields:

$$E_s(t)\le e^{C(M)t}\Big(E_s(0)+\int_0^t\big(\|S(\tau)\|^2_{H^{s-1}}+\|g(\tau)\|^2_{H^{s-1/2}}\big)\,d\tau\Big). \tag{U22}$$

establishing continuous dependence on the data.

Theorem U.11 (IBVP Well-Posedness)**.** *Let $\Omega\subset\mathbb{R}^3$ be bounded with smooth boundary, $s>5/2$. Assume (H1)–(H3), initial data $(\psi_0,\psi_1)\in H^s(\Omega)\times H^{s-1}(\Omega)$, source $S\in H^{s-1}(\Omega)$, boundary data $g\in H^s([0,T]\times\partial\Omega)$, with compatibility conditions up to order $\lfloor s-1\rfloor$. Then there exists $T>0$ and a unique solution*

$$\psi\in C^0([0,T];H^s(\Omega))\cap C^1([0,T];H^{s-1}(\Omega)), \tag{U23}$$

depending continuously on (ψ_0,ψ_1,S,g) in the corresponding Sobolev norms.

e. *Finite Speed of Propagation*

Theorem U.12 (Finite Speed of Propagation)**.** *Assume (H1)–(H3). Let ψ and $\tilde\psi$ be solutions of Eq. (U11) on $[0,T]\times\mathbb{R}^3$ with initial data (ψ_0,ψ_1) and $(\tilde\psi_0,\tilde\psi_1)$ agreeing on $B_R(x_0)$. There exists a characteristic speed $c_{\mathrm{char}}>0$ (depending only on the hyperbolicity constant λ) such that*

$$\psi(t,x)=\tilde\psi(t,x)\quad\text{for } 0\le t\le T,\ |x-x_0|\le R-c_{\mathrm{char}}t. \tag{U24}$$

Proof. Apply the energy method to the difference $w=\psi-\tilde\psi$, which satisfies a linearized equation. Using a cutoff function supported inside the backward characteristic cone and standard energy estimates yields $w=0$ in the interior. The characteristic speed c_{char} is determined by eigenvalues of the principal symbol. □

3. Parabolic Extension and Long-Time Behavior

For dissipative systems or numerical relaxation, consider the parabolic extension:

$$\partial_t\psi-\nabla\cdot\big(\mu(|\nabla\psi|)\nabla\psi\big)=f(t,x). \tag{U25}$$

Let $A : W_0^{1,p}(\Omega) \to (W_0^{1,p}(\Omega))'$ be the monotone operator $A(\psi) = -\nabla \cdot a(\nabla\psi)$.

Theorem U.13 (Parabolic Well-Posedness)**.** *Under (A1)–(A4), for $\psi_0 \in L^2(\Omega)$ there exists a unique evolution*

$$\psi \in L^p(0,T; W^{1,p}(\Omega)) \cap C([0,T]; L^2(\Omega)). \tag{U26}$$

If f is time-independent and boundary operators are dissipative, solutions converge to a steady state as $t \to \infty$.

Proof. By Crandall-Liggett theory [160], $-A$ generates a contraction semigroup on $L^2(\Omega)$. The result follows from standard nonlinear semigroup theory. □

4. Stability and Continuous Dependence

Theorem U.14 (Stability Estimate)**.** *Let ψ_1, ψ_2 be solutions with data (f_1, BC_1) and (f_2, BC_2). If a is strongly monotone and locally Lipschitz, then*

$$\|\nabla(\psi_1 - \psi_2)\|_{L^p(\Omega)} \le C\big(\|f_1 - f_2\|_{V'} + \|\mathrm{BC}_1 - \mathrm{BC}_2\|\big). \tag{U27}$$

This stability result is essential for numerical convergence and for justifying perturbative analyses around equilibrium configurations.

5. Open Problems

Several mathematical questions remain open:

- **Global existence:** Under what conditions on the source f and initial data do solutions, classical or weak, exist for all time, and are weak solutions unique?
- **Gradient blow-up:** Partly settled, in the vacuum equation on a non-zero uniform background gradient. There $|\nabla\psi|$ does *not* become unbounded: it stays bounded, and at the first singular time it is still continuous, with $|\partial^2\psi| \to \infty$ (a vertical tangent). The continuation past that time, the singularity structure, and the sourced and degenerate ($\nabla\psi \to 0$) cases remain open.
- **Horizon regularity:** The "ingoing flux only" horizon condition is physically motivated but mathematically non-standard. Full justification within elliptic PDE theory remains open.
- **Coupling to tensorial sectors:** Mathematical treatment of the full DFD system with electromagnetic and matter fields.

6. Summary: Mathematical Status of DFD

Mathematical Well-Posedness Summary

Static (elliptic) problem:
- Existence: Browder-Minty theorem (monotone operators)
- Uniqueness: Strict monotonicity of $\mu(x) = x/(1+x)$
- Regularity: $C^{1,\alpha}_{\mathrm{loc}}$ for smooth data
- Exterior domains: solutions with $|\nabla\psi| \to 0$ at infinity exist
- Optical BC: the horizon (Neumann) condition is open (§U 5)

Dynamic (hyperbolic) problem:
- Uniform hyperbolicity: holds for the regularised galactic approximant μ_{s_0} ($\lambda = 1 + 1/s_0$); the unregularised approximant degenerates at $\nabla\psi = 0$
- Local well-posedness: H^s solutions for $s > 5/2$ (regularised approximant)
- IBVP: Well-posed with compatibility conditions at corners
- Finite speed: c_{char} bounded by hyperbolicity constant λ

Parabolic extension:
- Semigroup generation: Crandall-Liggett theory applies
- Long-time behavior: Convergence to steady states for dissipative BCs

Conclusion: DFD is mathematically as robust as standard quasilinear wave and diffusion equations used throughout mathematical physics. The analysis is independent of phenomenological applications: it establishes that the static constraint is well-posed and that its c-speed relaxation is locally well-posed for the regularised approximant.

Appendix V: Extended Phenomenology and Numerical Methods

This appendix addresses three areas that complete the DFD phenomenological framework: the external field effect (EFE), wide binaries, and numerical implementation via finite element methods.

1. The External Field Effect (EFE)

In nonlinear theories like DFD, the internal dynamics of a subsystem depend on its external gravitational environment. This *external field effect* (EFE) arises from the nonlinearity of the field equation.

a. Physical Origin

The DFD field equation

$$\nabla \cdot \left[\mu(|\nabla\psi|/a_\star)\nabla\psi\right] = -\frac{8\pi G}{c^2}\rho \tag{V1}$$

is nonlinear in $\nabla\psi$. For a subsystem (e.g., a dwarf galaxy) embedded in an external field (e.g., a host galaxy) with $|\nabla\psi_{\rm ext}| \gg a_0/c^2$ but $|\nabla\psi_{\rm int}| \ll a_0/c^2$, the host field acts even if internal accelerations are in the deep-field regime. This "Newtonianizes" the internal dynamics.

b. Quantitative Formulation

Define the dimensionless acceleration ratios:

$$x_{\rm int} = \frac{c^2|\nabla\psi_{\rm int}|}{2a_0}, \tag{V2}$$

$$x_{\rm ext} = \frac{c^2|\nabla\psi_{\rm ext}|}{2a_0}. \tag{V3}$$

Inside a host the subsystem's relative acceleration is $\nu_{\rm emb}\,\mathbf{g}_{N,s}$ with $\nu_{\rm emb} = \nu\big(\sqrt{\tau_s^2+\tau_h^2}\big)$ for $\tau_h < \ln 2$ and $\nu_{\rm emb} = 1$ for $\tau_h > \ln 2$ (App. NL); the functional never forms the vector sum of the two fields, whose local reading is excluded by the Solar-System quadrupole (§VII I).

a. Limiting cases.

- **Isolated system** ($x_{\rm ext} \to 0$): $\nu_{\rm emb} = \nu(\tau_s)$, standard DFD dynamics.
- **Strong external field** ($x_{\rm ext} \gg 1$, $x_{\rm ext} \gg x_{\rm int}$): $\nu_{\rm emb} = 1$, Newtonian dynamics restored.

c. Observational Signatures

The EFE predicts that satellites at smaller galactocentric radii (higher $g_{\rm ext}$) show *less* enhanced dynamics than isolated dwarfs with similar internal properties. How strongly the host field suppresses each satellite's boost is set by the quadrature composition of App. NL; every satellite in the table lies far below the threshold of Axiom NL.14 ($n_e = 6.6$–15), so none is frozen.

TABLE XCIX. External fields of four Milky Way satellites, in units of the bound-matter a_0 (distances of McGaugh & Wolf 2010; Crater II at 117.5 kpc). The observed field is $g_{\rm obs} = V_c^2/D$ with the Milky Way's $V_c = 190$ km/s. The baryonic field is the Newtonian field of the Milky Way's baryons, $g_N = GM_{\rm b}/D^2$ with $M_{\rm b} = 6.5$–$10 \times 10^{10}\,M_\odot$; it sets the host depth $\tau_{\rm ext} = \sqrt{g_N/a_0}$ and the host-mode occupation $n_e = 1/(e^{\tau_{\rm ext}} - 1)$ used by the composition law of App. NL (computed).

Satellite	D (kpc)	$g_{\rm obs}/a_0$ (observed)	g_N/a_0 (baryonic)	n_e
Fornax	138	0.071	0.0040–0.0061	12–15
Sculptor	79	0.124	0.0121–0.0187	6.8–8.6
Draco	76	0.129	0.0131–0.0202	6.6–8.2
Crater II	117.5	0.083	0.0055–0.0084	10–13

a. Falsification criterion. If dwarf satellites uniformly show enhanced dynamics independent of their position relative to the Milky Way, the EFE mechanism (and hence DFD's nonlinear structure) would be falsified.

2. Wide Binaries

Wide stellar binaries with separations $s \gtrsim 5000$ AU probe the low-acceleration regime where DFD deviates from Newtonian gravity.

a. The Crossover Scale

For a binary with total mass M and separation s, the internal acceleration is:

$$a_{\rm int} = \frac{GM}{s^2}. \tag{V4}$$

The crossover to deep-field behavior occurs when $a_{\rm int} \sim a_0$:

$$s_{\rm cross} = \sqrt{\frac{GM}{a_0}} \approx 7040\,{\rm AU} \times \left(\frac{M}{M_\odot}\right)^{1/2}. \tag{V5}$$

For solar-mass binaries, $s_{\rm cross} \approx 7040$ AU at the bound-matter a_0.

b. Predicted Velocity Anomaly

In the deep-field regime ($s \gg s_{\rm cross}$), the orbital velocity is enhanced:

$$v_{\rm DFD} = (GMa_0)^{1/4} = v_{\rm Newton} \times \left(\frac{s}{s_{\rm cross}}\right)^{1/2}. \tag{V6}$$

The velocity ratio relative to Newtonian prediction:

$$\frac{v_{\rm DFD}}{v_{\rm Newton}} = \left[\frac{1+\sqrt{1+4/y_N}}{2}\right]^{1/2}, \qquad y_N \equiv \frac{a_{\rm Newton}}{a_0},$$
$$\approx \begin{cases} 1 & s \ll s_{\rm cross}, \\ \sqrt{s/s_{\rm cross}} & s \gg s_{\rm cross}. \end{cases} \tag{V7}$$

Isolated-pair values from this formula ($v_{\rm DFD}/v_{\rm Newton} = 1.42$ at 10^4 AU and 1.84 at 2×10^4 AU for a $1\,M_\odot$ pair) are upper envelopes only: the Galactic external field at the Sun ($g_{\rm gal} = 1.79\,a_0$) caps the force boost below that envelope, at $\gamma = g_{\rm obs}/g_{\rm N} = 1.37$–$1.52$ at 10^4 AU and 1.59–1.74 at 2×10^4 AU under the completed scale-additive law, i.e. a velocity enhancement of 17–32%; these are not realised at the Sun, where the environmental-confinement axiom makes local pairs exactly Newtonian (App. NL), and pairs beyond $R \simeq 13$–16 kpc, in their weaker host field, keep a boost.

c. GAIA DR3 Constraints

Recent analyses of GAIA DR3 wide binary data show conflicting results:

- Some analyses report enhanced relative velocities consistent with MOND-like dynamics at $s > 5000$ AU [51].
- Other analyses find no significant deviation from Newtonian predictions [52].

a. DFD interpretation. The EFE complicates wide binary tests: binaries whose host's baryonic Newtonian field exceeds $(\ln 2)^2 a_0 \simeq 0.48\,a_0$ (in the Milky Way, $R \lesssim$ 13–16 kpc) are exactly Newtonian (Axiom NL.14). A definitive test requires:

- Selection of binaries beyond $R \simeq 16$ kpc.
- Proper treatment of projection effects and orbital phase.
- Statistical comparison with DFD predictions including EFE.

b. Falsification criterion. If wide binaries beyond the frozen zone ($R \gtrsim 16$ kpc) show strictly Newtonian dynamics at $s > 10^4$ AU, or local pairs show a boost, DFD's external-field sector is falsified.

3. Finite Element Implementation

The DFD field equation is directly implementable via finite element methods (FEM). We outline the key elements for numerical solution.

a. Weak Form for FEM

The weak formulation (U6) translates directly to FEM assembly:

$$\sum_e \int_{\Omega_e} \mu(|\nabla\psi_h|)\nabla\psi_h \cdot \nabla v_h \, dx = \sum_e \int_{\Omega_e} f\, v_h \, dx, \tag{V8}$$

where ψ_h, v_h are finite element approximations on mesh elements Ω_e.

b. Newton Iteration for Nonlinearity

The nonlinear system is solved via Newton iteration. The Jacobian matrix is:

$$J_{ij}(\nabla\psi) = \mu(|\nabla\psi|)\delta_{ij} + \mu'(|\nabla\psi|)\frac{\partial_i\psi\,\partial_j\psi}{|\nabla\psi|}. \tag{V9}$$

For $\mu(s) = s/(1+s)$:

$$\mu'(s) = \frac{1}{(1+s)^2}. \tag{V10}$$

a. Regularization at small gradients. At $|\nabla\psi| \to 0$, the Jacobian may become ill-conditioned. A standard remedy is regularization:

$$|\nabla\psi| \to \sqrt{|\nabla\psi|^2 + \epsilon^2}, \tag{V11}$$

with $\epsilon \sim 10^{-10}$ in dimensionless units.

c. Mesh Refinement Strategy

The deep-field regime features steep gradients near sources. Adaptive mesh refinement (AMR) is recommended:

- Refine where $|\nabla\psi|$ changes rapidly (gradient indicator).
- Refine near crossover radius $r_\star = \sqrt{GM/a_0}$.
- Use logarithmic radial spacing for exterior domains.

d. Boundary Conditions

a. Dirichlet (fixed ψ).

$$\psi|_{\Gamma_D} = \psi_D. \tag{V12}$$

Used for outer boundaries with known asymptotic value.

b. Neumann (fixed flux).

$$\mu(|\nabla\psi|)\nabla\psi\cdot\hat{n}|_{\Gamma_N} = g_N. \tag{V13}$$

Used for symmetry planes or specified matter flux.

c. Robin (mixed).

$$\mu(|\nabla\psi|)\nabla\psi\cdot\hat{n} + \kappa(\psi - \psi_\infty) = 0. \tag{V14}$$

Used for approximate radiation conditions at finite boundaries.

e. Convergence Verification

For code verification, use the analytic deep-field solution:

$$\psi(r) = \psi_0 - B\ln(r/r_0), \quad B = \frac{2}{c^2}\sqrt{GMa_0}. \tag{V15}$$

Richardson extrapolation on mesh sequences should yield:

$$\|\psi_h - \psi_{\text{exact}}\|_{L^2} = \mathcal{O}(h^{p+1}), \tag{V16}$$

where p is the polynomial order of the elements.

FEM Implementation Checklist

1. Assemble weak form with $\mu(|\nabla\psi|)\nabla\psi$ flux
2. Newton iteration with analytic Jacobian
3. Regularize $|\nabla\psi|$ at small values
4. Adaptive mesh refinement near crossover
5. Verify against analytic deep-field solution
6. Richardson extrapolation for convergence rate

4. Matter Power Spectrum from ψ-Screen

a. Scale-Dependent ψ Perturbations

Density perturbations $\delta\rho$ source $\delta\psi$ via the linearized field equation:

$$\nabla^2\delta\psi = -\frac{8\pi G}{c^2}\delta\rho. \tag{V17}$$

In Fourier space:

$$\delta\tilde{\psi}(k) = \frac{8\pi G}{c^2k^2}\delta\tilde{\rho}(k). \tag{V18}$$

The ψ-perturbation power spectrum is:

$$P_\psi(k) = \left(\frac{8\pi G}{c^2k^2}\right)^2 P_\rho(k). \tag{V19}$$

b. Observational Signatures

At linear order this is the Newtonian Poisson equation, and under the Rest-Mass Channel the growth has $Q_\chi = 1$ (App. GR); a lensing or clustering signal would need a nonzero screen, which the current solution does not have (Sec. XVI A).

5. Cooper-Pair Mass Anomaly from A_5 Pair Space

The Cooper-pair mass in niobium, measured by Tate *et al.* (1989) via the London moment, exceeds the predicted $0.999992 \times 2m_e$ by $\delta = 92 \pm 21$ ppm—a 4.4σ anomaly unexplained for 36 years [161]. Within the A_5 microsector, each electron's generation quantum number lives in the fundamental V^* ($\dim V^* = 3$). The pair tensor product decomposes as $V^*\otimes V^* = S^2(V^*)\oplus\Lambda^2(V^*)$ with $S^2(V^*) = \mathbf{1}\oplus\mathbf{5}$ and $\Lambda^2(V^*) = \mathbf{3}$.

One pairing-symmetry selection rule follows:

1. **Angular cancellation:** the quintet **5** exchange channel couples maximally to s-wave condensates (isotropic gap) but vanishes for d-wave condensates ($\int_0^{2\pi}\cos 2\phi\, d\phi/(2\pi) = 0$).

The conjectured coefficient is $\delta = \sqrt{3}\,\alpha^2 = 92.23$ ppm (0.01σ match), with $\sqrt{3} = \sqrt{N_{\text{gen}}}$ from incoherent amplitude addition of three generation channels and α^2 from the ψ–EM vertex structure. It is a conjecture outside DFD's claims: no derivation from the theory's action fixes the coefficient, so neither a match nor a miss bears on the theory. As stated it is universal for s-wave superconductors and zero for d-wave materials, a distinction that multi-material London-moment measurements at ≤ 20 ppm precision can test.

6. Summary

Extended Phenomenology Summary

External Field Effect:
- Nonlinear μ-function causes environmental dependence
- Subsystems in hosts above $(\ln 2)^2 a_0$ are Newtonian; satellites are not
- Testable via dwarf galaxy velocity dispersions vs. position

Wide Binaries:
- Newtonian-acceleration crossover at $s_{\text{cross}} \simeq 7040$ AU for solar-mass binaries
- $\gamma = 1$ exactly near the Sun (environmental confinement, App. NL), with the null analyses and against Chae (2023); a boost and a step beyond $R \simeq 13$–16 kpc; the isolated-pair formula is an upper envelope
- EFE complicates interpretation; requires low-g_{gal} samples

Cooper-Pair Mass Anomaly (§V 5):
- Conjecture outside DFD's claims: $\delta = \sqrt{3}\,\alpha^2 = 92.23$ ppm (universal for s-wave)
- Selection rule: d-wave $\to 0$ (angular cancellation)
- Test: multi-material London-moment measurement at ≤ 20 ppm

Numerical Methods:
- Standard FEM with Newton iteration for nonlinearity
- Regularization needed at small $|\nabla\psi|$
- Adaptive mesh refinement near crossover scale
- Verification against analytic deep-field solution

Appendix W: Experimental Protocols and Sensitivity Analyses

This appendix provides detailed, pre-registered experimental protocols for the key DFD discriminators. Each protocol specifies the observable, prediction, systematics budget, decision rule, and falsification criteria.

1. Cavity-Atom LPI Test: Complete Protocol

The height-separated cavity–atom comparison remains a valuable protocol, but after geometric cancellation (Sec. XII A) it is best viewed as a demanding long-horizon residual test. The tree-level cavity/atom response cancels; only a screened residual $\xi_{\rm LPI}^{\rm res}$ survives. This section preserves the full protocol details for completeness and for future experiments that may reach the required sensitivity.

a. Observable and Predictions

The frequency ratio at height h is:

$$R(h) \equiv \frac{\nu_C(h)}{\nu_A(h)}. \tag{W1}$$

a. GR prediction.

$$\left(\frac{\Delta R}{R}\right)_{\rm GR} = 0. \tag{W2}$$

b. DFD prediction. After the constitutive-chain cancellation, the surviving signal is:

$$\left(\frac{\Delta R}{R}\right)_{\rm DFD} = \xi_{\rm LPI}^{\rm res}\,\frac{g\,\Delta h}{c^2}, \tag{W3}$$

where $\xi_{\rm LPI}^{\rm res}$ is the screened residual coupling that remains once the leading geometric (tree-level) effect is removed. At Earth's surface, the screening analysis of Sec. XI C and the BACON constraints of Sec. XII D restrict $\xi_{\rm LPI}^{\rm res}$ to be small — far below order unity.

c. Numerical estimate. For $\Delta h = 100$ m and $g = 9.8$ m/s^2:

$$\frac{g\,\Delta h}{c^2} \simeq 1.1 \times 10^{-14}. \tag{W4}$$

The DFD signal is this factor *multiplied by* the small screened residual $\xi_{\rm LPI}^{\rm res}$, making the target signal extremely demanding. This is why the cavity–atom channel is ranked below cross-species and nuclear-clock tests in the current experimental priority ordering (Sec. XI I).

b. Experimental Configuration

- **Lower station** at h_1: High-stability optical cavity (ULE or Si) and reference atomic clock (Sr or Yb lattice clock).
- **Upper station** at $h_2 = h_1 + \Delta h$: Second atomic clock and auxiliary diagnostics.
- **Link:** Phase-stabilized optical fiber at $< 10^{-18}$ level.
- **Height difference:** $\Delta h \sim 100$ m (tower, elevator shaft, or mine).

c. Measurement Cycle

Each measurement cycle consists of:

1. Lock cavity and lower atomic clock; record $R(h_1)$ for integration time τ.
2. Reconfigure for upper station measurement.
3. Record $R(h_2)$ for integration time τ.
4. Repeat with randomized order to decorrelate slow drifts.

a. Integration budget. For $\tau \sim 10^4$ s per height and $N \sim 50$ cycles:

$$\sigma_{\rm stat} \sim \frac{10^{-18}}{\sqrt{N}} \sim 1.4 \times 10^{-19}. \tag{W5}$$

With systematic floor $\sigma_{\rm syst} \sim 2 \times 10^{-19}$:

$$\sigma_{\rm tot} = \sqrt{\sigma_{\rm stat}^2 + \sigma_{\rm syst}^2} \sim 2.5 \times 10^{-19}. \tag{W6}$$

d. Systematics Budget

TABLE C. Systematics budget for cavity-atom residual test.

Effect	Contrib.	Mitigation
Temp. gradients	$< 10^{-19}$	mK stab., shielding
Magnetic fields	$< 10^{-19}$	nT stab., shielding
Pressure/refr. index	$< 10^{-20}$	Vacuum
Vibrations	$< 10^{-20}$	Isolation
Fiber link noise	$< 10^{-19}$	Phase stab.
Total	$\sim 2 \times 10^{-19}$	

e. Blinding Protocol

To prevent experimenter bias:

1. A secret offset δ at the 10^{-18} level is added to all recorded $R(h)$ values.
2. All data selection and systematic modeling performed on blinded data.
3. Analysis pipeline frozen before unblinding.
4. Offset removed only after all cuts finalized.

f. Pre-Registered Decision Rule

Let $\widehat{\Delta R/R}$ be the unblinded estimator with uncertainty $\sigma_{\rm tot}$:

- **Null regime:** $|\widehat{\Delta R/R}| < 3\sigma_{\rm tot} \Rightarrow$ consistent with GR and with geometric cancellation. Upper bound on the residual:
$$|\xi_{\rm LPI}^{\rm res}| < \frac{3\sigma_{\rm tot}}{g\Delta h/c^2}. \tag{W7}$$
- **Detection regime:** $|\widehat{\Delta R/R}| > 5\sigma_{\rm tot} \Rightarrow$ a non-zero screened residual is measured:
$$\xi_{\rm LPI}^{\rm res} = \frac{\widehat{\Delta R/R}}{g\Delta h/c^2} \pm \frac{\sigma_{\rm tot}}{g\Delta h/c^2}. \tag{W8}$$
- **Intermediate:** 3–$5\sigma_{\rm tot} \Rightarrow$ extend campaign.

g. Sensitivity Reach

For the benchmark parameters above, the minimum detectable residual is:
$$\xi_{\rm LPI,\,min}^{\rm res} \sim \frac{\sigma_{\rm tot}}{g\Delta h/c^2} \sim 2\times 10^{-5}. \tag{W9}$$
This is sensitive enough to detect a residual at the level predicted by the screened formalism if it is near the upper end of the surviving window, but would require space-based or long-baseline platforms to push significantly deeper.

2. Multi-Species Clock Comparison Protocol

The full channel-resolved coupling of Eq. (291) produces differential clock responses that can be measured without height separation. The simplified pure-α scaling $K_A^{(\alpha)} = k_\alpha S_A^\alpha$ is only the leading same-ion term and is not the canonical master law for the clock program.

a. Observable

For clock species A and B at the same location, measure:
$$\Delta_{AB}(t) \equiv \ln\frac{\nu_A(t)}{\nu_B(t)} - \langle \ln\frac{\nu_A}{\nu_B}\rangle. \tag{W10}$$

a. DFD prediction. Solar potential modulation at frequency $\Omega = 2\pi/\mathrm{yr}$:
$$\Delta_{AB}(t) = (K_A - K_B)\cdot\frac{\Delta\Phi_\odot(t)}{c^2}, \tag{W11}$$
where $\Delta\Phi_\odot/c^2 \sim 3\times 10^{-10}$ over Earth's orbit; since $\Phi = -c^2\psi/2$, each per-unit-ψ coupling K_A of Eq. (291) and Table CI enters this slot with twice its magnitude.

b. Species Selection

TABLE CI. Clock species and α-sensitivities. The unscreened pure-α law $K_A = k_\alpha S_A^\alpha$ is excluded at Earth by the same-ion E3/E2 null unless screened (Sec. XI); the Th-229 entry is the strong channel.

Species	Transition	S_A^α	K_A/k_α (unscreened)
Cs	Ground HFS	2.83	2.83
Rb	Ground HFS	2.34	2.34
H	1S–2S	≈ 0	≈ 0
Sr	${}^1S_0$–${}^3P_0$	0.06	0.06
Yb	${}^1S_0$–${}^3P_0$	0.31	0.31
Al^+	${}^1S_0$–${}^3P_0$	0.008	0.008
Hg^+	${}^2S_{1/2}$–${}^2D_{5/2}$	−3.2	−3.2
Yb^+ (E3)	${}^2S_{1/2}$–${}^2F_{7/2}$	−5.95	−5.95
Th-229	Nuclear	$\sim 10^4$	~ 10

a. Optimal pairs. Maximize $|S_A^\alpha - S_B^\alpha|$:

- Yb^+(E3)/H: $\Delta S \approx 6$
- Yb^+(E3)/Al^+: $\Delta S \approx 6$
- Cs/H: $\Delta S \approx 2.8$
- Th-229/Sr: $\Delta S \sim 10^4$ (nuclear clock)

c. Analysis Protocol

1. Fit $\Delta_{AB}(t)$ to model: $A_0 + A_1\cos(\Omega t + \phi)$.
2. Extract amplitude A_1 and phase ϕ.
3. Compare phase to predicted solar ephemeris.
4. If phase matches and $A_1 > 5\sigma$: detection.
5. If $A_1 < 3\sigma$: upper bound on $|K_A - K_B|$.

3. Matter-Wave Interferometry: T^3 Protocol (Not a DFD Prediction)

Long-baseline matter-wave interferometers (MAGIS-100, AION) can detect the parity-isolated T^3 phase signature (DFD's own prediction for it is null).

a. Observable

The formula under test, for interrogation time T:
$$\phi_{\rm DFD} = \phi_{\rm GR} + \Delta\phi_{\rm DFD}^{\rm KC}, \tag{W12}$$
where the T^3 correction is the kinematic expression of Sec. XIII (Eq. (337)):
$$\Delta\phi_{\rm DFD}^{\rm KC} = \frac{\hbar k_{\rm eff}^2}{m}\,\frac{g}{c^2}\,T^3. \tag{W13}$$

Status: not a DFD prediction (the matter-wave sector is null); see the status note after Eq. (337) in Sec. XIII. (The overall prefactor of Eq. (337) is not a phase (§XIII): see the dimensional-bookkeeping item noted in Sec. XIII; the parity-isolation protocol below is independent of that prefactor.)

b. Parity Isolation

The T^3 term is *even* under $k_{\rm eff} \to -k_{\rm eff}$, while the T^2 Newtonian term and laser-phase systematics are odd (Sec. XIII). This allows isolation via:

1. k**-reversal:** Repeat with the effective wavevector reversed.
2. **Sum:** $\phi_{+k} + \phi_{-k}$.
3. **Result:** T^2 terms cancel; T^3 terms add.

c. Sensitivity Requirements

Status: not a DFD prediction (the matter-wave sector is null); see the status note after Eq. (337) in Sec. XIII. The expression of Eq. (337) has units s^2/m, so it sets no phase-resolution target.

d. Interpretation of Outcomes

If the parity-isolated T^3 phase is measured to be:

- Consistent with zero — not a falsification channel: DFD and GR coincide through 1PN (§XIII).
- Non-zero at $> 5\sigma$ with the T^3 time scaling, g-parity and $k_{\rm eff}^2/m$ recoil scaling of Eq. (337) $\Rightarrow$ not a DFD signal: no DFD-specific T^3 is predicted, and the even-k, $\hbar k_{\rm eff}^2/m$ T^3 term is the Newtonian gravity-gradient recoil phase common to DFD and GR (§XIII).

4. Nuclear Clock Protocol: Th-229

The ^{229}Th nuclear isomer transition provides sensitivity to strong-sector couplings, with $d_s \sim 1.3$ (order of magnitude larger than d_e).

a. Prediction

The extended strong channel, with k_s a matching coefficient not derived from the minimal action (Sec. XI F), gives:

$$K_{\rm Th} - K_{\rm Sr} \sim 8 \times 10^{-5}, \tag{W14}$$

approximately 3× larger than Cs/Sr difference.

a. Observable signal.

For solar potential modulation:

$$26\ \mathrm{Hz} \lesssim \text{annual amplitude} \lesssim \mathcal{O}(1\ \mathrm{kHz}) \quad \text{(Sec. XI F)}. \tag{W15}$$

b. Experimental Requirements

- Nuclear clock operational with systematic uncertainty $< 10^{-16}$.
- Continuous comparison with optical clock (Sr or Yb) over ≥ 1 year.
- Analysis for annual modulation at solar frequency.

c. Timeline

Nuclear clock technology is expected to reach required precision within 5–7 years.

5. Space Mission Protocols

Space-based tests provide access to larger potential differences and different systematic environments.

a. ACES (ISS)

The Atomic Clock Ensemble in Space provides:

- $\Delta\Phi/c^2 \sim 10^{-10}$ (ISS altitude).
- Microwave clock comparisons with ground.
- Sensitivity to $K_A - K_B$ at 10^{-7} level.

b. Dedicated LPI Mission

A dedicated mission with optical clocks could achieve:

- Highly elliptical orbit: $\Delta\Phi/c^2 \sim 10^{-9}$.
- Cavity-atom comparison in space.
- Sensitivity to screened residual $\xi_{\rm LPI}^{\rm res}$ at 10^{-6} level.

TABLE CII. DFD experimental verification timeline.

Time	Test	Prediction	Falsification
1–3 yr	Cross-species clocks	Channel residuals	All-channel nulls
1–3 yr	Nuclear clocks	26 Hz–kHz window	No annual signal
3–7 yr	Matter-wave T^3 (null prediction)	As GR (1PN)	None
>7 yr	Cavity–atom	Screened residual	Null at target
>7 yr	Space missions	Enhanced prec.	—

6. Summary: Experimental Roadmap

Experimental Protocol Summary

Each protocol fixes in advance:
- Observables and predictions specified before data collection
- Decision rules fixed in advance
- Blinding protocols where applicable
- Clear falsification criteria for both GR and DFD

Key discriminators:
- Cavity–atom residual: screened non-metric mismatch after tree-level cancellation
- Multi-species clocks: channel-resolved species dependence governed by Eq. (291)
- Matter-wave T^3: parity-isolated phase (null prediction, not a discriminator)
- Nuclear clocks: Strong-sector coupling $d_s \sim 1.3$

Current status:
- Awaiting experimental implementation

Appendix X: Neutrino Mass Spectrum from DFD Microsector

This appendix derives a *complete closed-form* neutrino sector from DFD microsector relations. Using tribimaximal (TBM) mixing geometry, a discrete S_2 residual symmetry, and microsector-normalized α-power exponents, we obtain neutrino mass ratios with **zero continuous parameters**.

1. DFD Inputs from the Microsector

DFD provides three ingredients:

1. **TBM mixing geometry** (Appendix G): The "neutrinos-at-center" overlap rule gives the tribimaximal mixing matrix
$$U_{\rm TBM} = \begin{pmatrix} \sqrt{2/3} & \sqrt{1/3} & 0 \\ -\sqrt{1/6} & \sqrt{1/3} & \sqrt{1/2} \\ \sqrt{1/6} & -\sqrt{1/3} & \sqrt{1/2} \end{pmatrix}. \tag{X1}$$
2. **Heavy Majorana scale** (Appendix P):
$$M_R = M_P \alpha^3 \approx 4.7 \times 10^{12}\ \text{GeV}. \tag{X2}$$
3. **Electroweak scale** (Section XVII):
$$v = M_P \alpha^8 \sqrt{2\pi} \approx 246\ \text{GeV}. \tag{X3}$$

TBM fixes the eigenvectors but not the eigenvalues (m_1, m_2, m_3). The question is whether the residual symmetry structure can fix the mass ratios without continuous parameters.

2. Why S_3 Invariance Cannot Split the Doublet

Let three generations carry the permutation representation of S_3. The S_3-invariant endomorphisms are spanned by I_3 and $J = \mathbf{1}\mathbf{1}^T$.

The representation decomposes as $\mathbf{3} \cong \mathbf{1} \oplus \mathbf{2}$, where $\mathbf{1} = \text{span}(1,1,1)$ is the singlet and $\mathbf{2} = \{x_1 + x_2 + x_3 = 0\}$ is the doublet.

On the doublet, J acts as zero (since $Jx = (x_1 + x_2 + x_3)\mathbf{1} = 0$), so any S_3-equivariant operator restricted to the doublet is proportional to the identity:
$$A|_{\mathbf{2}} = a\, I_{\mathbf{2}} \quad \Rightarrow \quad \text{degenerate eigenvalues}. \tag{X4}$$

Any $m_2/m_1 \neq 1$ requires breaking S_3 to a proper subgroup; that breaking is the mechanism.

3. TBM Selects a Canonical Residual S_2

TBM naturally singles out the $\mu \leftrightarrow \tau$ transposition as residual symmetry:

$$S_{\mu\tau} = \begin{pmatrix} 1 & 0 & 0 \\ 0 & 0 & 1 \\ 0 & 1 & 0 \end{pmatrix}. \tag{X5}$$

Its eigenvectors in the μ–τ plane are the even and odd parity axes:

$$v_+ = \frac{1}{\sqrt{2}}(0,1,1), \qquad v_- = \frac{1}{\sqrt{2}}(0,1,-1), \tag{X6}$$

with $S_{\mu\tau} v_\pm = \pm v_\pm$.

The third TBM column is exactly v_+. Thus TBM motivates a canonical residual transposition subgroup $S_2 = \langle S_{\mu\tau} \rangle$.

4. Microsector-normalized residual-S_2 spurion

The rigid choice $O = I_3 + P_-$ (which assigns $m_2/m_1 = 2$) is the *minimal-integer* deformation of the identity consistent with residual $\mu \leftrightarrow \tau$ symmetry. Here we replace that rigidity by a *microsector-normalized* coefficient that is still knob-free: the coefficient is fixed as a discrete channel-fraction exponent of α determined by the already-locked microsector integers.

a. Setup. Let P_- be the rank-1 projector onto the odd axis v_- as before, and define the residual-S_2 spurion family

$$O(\kappa) := I_3 + \kappa\, P_-, \tag{X7}$$

so that on parity eigenstates,

$$O(\kappa)\, v_- = (1+\kappa)\, v_-, \qquad O(\kappa)\, v_+ = 1 \cdot v_+. \tag{X8}$$

The doublet ratio is then assigned as

$$\frac{m_2}{m_1} = 1 + \kappa\,, \tag{X9}$$

an assignment of the spurion strength to the doublet ratio, not a ratio of eigenvalues of $O(\kappa)$ on tribimaximal mass eigenstates: v_- is not a column of U_{TBM}.

b. No-hidden-knobs microsector normalization. In the microsector construction, the line-bundle degree is fixed by minimal-padding to $(a, n) = (9, 5)$, and the CP^1 Toeplitz truncation used elsewhere in the unified derivations has canonical channel count

$$d_{\mathrm{CP}^1}(k) = k + 4 \quad \Rightarrow \quad d_{\mathrm{CP}^1}(a) = a + 4 = 13. \tag{X10}$$

Residual $\mu \leftrightarrow \tau$ splitting is a two-channel deformation (a doublet), so a canonical knob-free choice is to assign the spurion strength to the *doublet channel fraction* $2/13$ in the only universal dimensionless base available to DFD, namely α:

$$\boxed{\frac{m_2}{m_1} = \alpha^{-2/13}} \quad \Rightarrow \quad \boxed{\kappa = \alpha^{-2/13} - 1}. \tag{X11}$$

c. Canonical-shift variant (Branch B). A second, equally canonical knob-free option replaces the numerator 2 (doublet count) by the CP^2 canonical shift 3 (the K^{-1} degree on CP^2), while the denominator is fixed by the CP^1 channel count induced by the microsector dimension $\dim(\mathbb{CP}^2 \times S^3) = 7$:

$$d_{\mathrm{CP}^1}(\dim M) = \dim M + 4 = 7 + 4 = 11, \tag{X12}$$

yielding the alternative

$$\boxed{\frac{m_2}{m_1} = \alpha^{-3/11}} \quad \Rightarrow \quad \boxed{\kappa = \alpha^{-3/11} - 1}. \tag{X13}$$

d. Singlet-doublet hierarchy (microsector-normalized). Replace the rigid $r = \alpha^{-1/3}$ ansatz by a microsector-normalized hierarchy built from locked integers $\dim M = 7$ and $n = 5$:

$$\boxed{\frac{m_3}{m_2} = r := \alpha^{-\dim M/(4n)} = \alpha^{-7/20}}. \tag{X14}$$

5. Combined mass pattern (microsector-normalized)

With either choice for m_2/m_1 above and the microsector-normalized r, the mass pattern is fixed up to one overall scale:

$$\begin{gathered} m_1 : m_2 : m_3 = 1 : k : kr, \\ k \in \{\alpha^{-2/13}, \alpha^{-3/11}\}, \quad r = \alpha^{-7/20}. \end{gathered} \tag{X15}$$

6. Parameter-free oscillation invariant (discriminator)

Fix the overall scale by matching Δm^2_{21}, so that

$$m_1^2 = \frac{\Delta m^2_{21}}{k^2 - 1}, \qquad m_2 = k\, m_1, \qquad m_3 = r\, m_2. \tag{X16}$$

Then the dimensionless oscillation invariant becomes a pure α-function:

$$\boxed{\frac{\Delta m^2_{32}}{\Delta m^2_{21}} = \frac{(k^2 r^2 - k^2)}{(k^2 - 1)}} \qquad (k, r \text{ as above}). \tag{X17}$$

7. Complete numerical predictions

Using $\alpha^{-1} = 137.035999177$ and $\Delta m^2_{21} = 7.49 \times 10^{-5}\,\mathrm{eV}^2$ (NuFIT 6.0), the two branches give:

Branch B matches NuFIT 6.0 to $< 0.1\sigma$.

Remark X.1 (Branch selection). Branch A ($k = \alpha^{-2/13}$, doublet count 2 over $d_{\mathrm{CP}^1}(a) = 13$) and Branch B ($k = \alpha^{-3/11}$, canonical shift 3 over $d_{\mathrm{CP}^1}(\dim M) = 11$) are *equally canonical* knob-free constructions; the present

TABLE CIII. Neutrino mass branch predictions.

Branch	k	r	(m_1, m_2, m_3) [meV]	Σm_ν [meV]	Δm^2_{32} [10^{-3}eV^2]	$\Delta m^2_{32}/\Delta m^2_{21}$
A	$\alpha^{-2/13}$	$\alpha^{-7/20}$	(4.60, 9.80, 54.84)	69.24	2.911	38.87
B	$\alpha^{-3/11}$	$\alpha^{-7/20}$	(2.34, 8.96, 50.16)	61.46	2.437	32.54
NuFIT 6.0 (NO):			—	—	2.438 ± 0.020	32.55

axioms do not force the choice between them. The selection of Branch B is made by the oscillation data: Table CIII shows Branch A's Δm^2_{32} missing NuFIT 6.0 by $\approx 24\sigma$, while Branch B ($2.437 \times 10^{-3}\,\mathrm{eV}^2$) matches to $< 0.1\sigma$. The sector is therefore closed at *zero continuous parameters* with *one discrete choice anchored empirically*; downstream of that bit, both exponents, the dimensionless oscillation invariant, and the absolute-scale formula $m_3 = \frac{14}{13}\pi M_P \alpha^{14}$ are α-locked with no further reference to data. The quoted goodness-of-fit ($\chi^2 = 0.025$, $p = 0.99$) is that of the *selected* branch. The printed integers allow four such fractions (numerator 2 or 3, denominator 11 or 13); with the absolute scale of this appendix 3/11 fits both splittings best, and the next best (3/13) misses Δm^2_{21} by 1.5σ ($\chi^2 = 2.4$ over both splittings; computed), so the look-elsewhere factor is at least four. The data-free priming scale of App. X 8 reproduces the Δm^2_{21}-anchored Branch-B spectrum to 0.1%, whereas the same scale under Branch A misses the observed Δm^2_{21} by $\approx 6\sigma$: a second, correlated empirical concordance conditioned on Branch B. The companion volume's forcing argument for Branch B fixes its level from the branch it selects, so it cannot force the choice, and the selection stays data-selected. The CKM apex branch ambiguity is treated the same way before its Euler-projection closure (Appendix AO).

With $\sin^2\theta_{13} = 3\alpha$ and the trimaximal weights $|U_{e1}|^2 = \frac{2}{3}$, $|U_{e2}|^2 = \frac{1}{3} - 3\alpha$, $|U_{e3}|^2 = 3\alpha$, Branch B gives

$$\boxed{m_\beta = 9.15 \text{ meV}, \qquad m_{\beta\beta} \in \{0.13,\ 2.33,\ 3.25,\ 5.45\} \text{ meV}} \tag{X18}$$

(the four CP-conserving points derived below), with $\Sigma m_\nu \approx 61.5$ meV. The tribimaximal limit $U_{e3} = 0$ would give $m_\beta \approx 5.52$ meV and $m_{\beta\beta} \in [1.43, 4.55]$ meV.

a. Structural identity. For the Branch B pair $(k, r) = (\alpha^{-3/11}, \alpha^{-7/20})$ one has

$$\boxed{k^2 r^2 = \alpha^{-(6/11+7/10)} = \alpha^{-137/110}} \tag{X19}$$

so the combined hierarchy exponent has numerator 137.

8. Absolute-scale closure for Branch B from finite-d priming

This subsection replaces the Δm^2_{21} anchoring step with a DFD-internal absolute-scale closure. The key input is a *forced* finite-dimensional normalization factor from the same Toeplitz truncation and determinant priming used in the closed form for α.

a. Bundle-degree bookkeeping (no knobs). The microsector bundle decomposition is $E = \mathcal{O}(a) \oplus \mathcal{O}^{\oplus n}$ with minimal-padding $(a, n) = (9, 5)$. The Toeplitz truncation on $\mathbb{C}P^1 \subset \mathbb{C}P^2$ carries the Spin^c determinant shift $L_{\det} = K^{-1} = \mathcal{O}(3)$. For a Yukawa/Dirac vertex, one inserts the Higgs hyperplane factor: generation wavefunctions are holomorphic sections of $\mathcal{O}(1)$, so the Dirac overlap lives in

$$\mathcal{O}(a) \otimes \mathcal{O}(3) \otimes \mathcal{O}(1) \cong \mathcal{O}(a+4) \qquad \text{on} \qquad \mathbb{C}P^1. \tag{X20}$$

Thus the Toeplitz level is *forced* to be $m_\nu = a + 4$ for the neutrino Dirac sector.

Lemma (Forced finite dimension). With $m_\nu = a + 4$, the truncated holomorphic state space has dimension

$$d_\nu = \dim H^0(\mathbb{C}P^1, \mathcal{O}(m_\nu)) = m_\nu + 1 = a + 5. \tag{X21}$$

For $a = 9$: $\boxed{d_\nu = 14}$.

b. Why $d/(d-1)$ appears (not a fit). The primed determinant prescription removes the null channel from the finite-dimensional spectrum. At the level of normalized traces, passing from an unprimed average over d channels to a primed average over $d-1$ nonzero channels multiplies the normalization by $d/(d-1)$.

Define the **neutrino finite-d priming factor**:

$$F_\nu := \frac{d_\nu}{d_\nu - 1} = \frac{14}{13}. \tag{X22}$$

c. DFD absolute-scale closure. The seesaw closure gives $m_3 \propto \pi M_P \alpha^{14}$. The finite-$d$ priming factor lifts this to:

$$\boxed{m_3 = F_\nu\, \pi M_P\, \alpha^{14} = \frac{14}{13}\, \pi M_P\, \alpha^{14}.} \tag{X23}$$

With Branch B ratios $k = \alpha^{-3/11}$, $r = \alpha^{-7/20}$, we get $m_2 = m_3/r$ and $m_1 = m_3/(kr)$. Using $\alpha^{-1} = 137.036$:

DFD-Closed Neutrino Predictions (Zero Continuous Parameters)

Quantity	DFD	NuFIT 6.0
m_1	2.34 meV	—
m_2	8.96 meV	—
m_3	50.16 meV	—
$\sum m_\nu$	**61.46 meV**	—
Δm^2_{21}	7.48×10^{-5} eV^2	$(7.49\pm0.19)\times10^{-5}$
Δm^2_{31}	2.51×10^{-3} eV^2	$(2.513\pm0.020)\times10^{-3}$
$m_{\beta\beta}$	$\{0.13, 2.33, 3.25, 5.45\}$ meV	—
m_β	9.15 meV	—

Both splittings match NuFIT 6.0 to $< 0.2\sigma$ at zero continuous parameters (Branch B).

d. What was used. Besides the stated Dirac rung $y_D^2 = F_\nu\alpha$ (Prop. AT.1), the absolute-scale closure uses only DFD inputs already present:

1. Minimal-padding microsector integer $a = 9$
2. Spin^c determinant shift $+3$
3. Higgs hyperplane factor $\mathcal{O}(1)$
4. Primed-channel prescription

No continuous tuning is introduced. The 14/13 factor is forced by $(a, n) = (9, 5)$.

9. The explicit mass matrix (TBM eigenbasis)

With TBM eigenvectors and the microsector-normalized hierarchy, the mass spectrum is

$$m_1, \qquad m_2 = k\, m_1, \qquad m_3 = kr\, m_1, \tag{X24}$$

where

$$k \in \{\alpha^{-2/13}, \alpha^{-3/11}\}, \qquad r = \alpha^{-7/20}. \tag{X25}$$

In the tribimaximal limit ($\theta_{13} = 0$, before the trimaximal correction $\sin^2\theta_{13} = 3\alpha$ used in this appendix) the neutrino mass matrix is

$$\boxed{M_\nu = m_1\, P_1 + (km_1)\, P_2 + (krm_1)\, P_3} \tag{X26}$$

in terms of the TBM projectors $P_i = c_i c_i^T$.

10. Falsification criteria

The DFD-closed Branch B (with absolute scale from finite-d priming) gives concrete predictions summarized below (normal ordering).

TABLE CIV. Falsification criteria for DFD neutrino sector.

Observable	DFD prediction	Falsification
Δm^2_{21}	7.48×10^{-5} eV^2	NuFIT $> 3\sigma$
Δm^2_{31}	2.51×10^{-3} eV^2	NuFIT $> 3\sigma$
$\sum m_\nu$	61.46 meV	< 45 or > 80 meV
m_β	9.15 meV	β-decay incomp.
$m_{\beta\beta}$	≤ 5.45 meV	measured $m_{\beta\beta} > 5.5$ meV
Ordering	Normal	Inverted confirmed

11. External global-fit verification

a. NuFIT 6.0 Table 1 check (conservative Gaussian). NuFIT 6.0 publishes best-fit values and 1σ uncertainties for the mass-squared splittings [162]. Using the "IC24 with SK-atm" Normal Ordering line in Table 1 of their JHEP update:

$$\Delta m^2_{21} = (7.49 \pm 0.19) \times 10^{-5}\,\text{eV}^2, \tag{X27}$$

$$\Delta m^2_{3\ell} = (2.513^{+0.021}_{-0.019}) \times 10^{-3}\,\text{eV}^2. \tag{X28}$$

Symmetrizing the second uncertainty to $\sigma_{3\ell} = 0.020 \times 10^{-3}\,\text{eV}^2$, the normalized pulls for the DFD Branch B predictions are:

$$\text{pull}_{21} = \frac{7.48 - 7.49}{0.19} = -0.053\,\sigma, \tag{X29}$$

$$\text{pull}_{3\ell} = \frac{2.51 - 2.513}{0.020} = -0.15\,\sigma. \tag{X30}$$

The conservative uncorrelated Gaussian statistic is:

$$\boxed{\chi^2_{\text{Gauss}} = \text{pull}^2_{21} + \text{pull}^2_{3\ell} \approx 0.025} \tag{X31}$$

with 2 degrees of freedom. corresponding to a p-value of 0.99. Branch B lands essentially on the published global-fit best point.

b. Including realistic $|U_{e3}|^2$ (discrete $0\nu\beta\beta$ comb). Because DFD imposes μ–τ reflection symmetry to lock $\theta_{23} = \pi/4$ and $\delta_{\text{CP}} = -\pi/2$ (Thm. AY.3), the *same* symmetry is the Takagi/Autonne reality condition $S\, M_\nu^*\, S = M_\nu$ ($S = 2$–3 reflection) on the Majorana mass matrix, and forces *both* Majorana phases to the CP-conserving values $\alpha_{21}, \alpha_{31} \in \{0, \pi\}$ (Grimus–Lavoura). The Majorana phases are therefore *not* free, and the $0\nu\beta\beta$ effective mass does *not* scan a continuous band; with the locked TM1 weights $|U_{e1}|^2 = \frac{2}{3}$, $|U_{e2}|^2 = \frac{1}{3} - 3\alpha$, $|U_{e3}|^2 = 3\alpha$ and the Branch-B spectrum it collapses to $m_{\beta\beta} = \left|\sum_i \eta_i\, |U_{ei}|^2 m_i\right|$, $\eta_i \in \{\pm1\}$:

$$\begin{aligned} &m_{\beta\beta} \in \{0.13,\ 2.33,\ 3.25,\ 5.45\}\,\text{meV} \\ &\text{(4 CP-conserving points, not a band).} \end{aligned} \tag{X32}$$

The kinematic mass is phase-free, $m_\beta = \sqrt{\sum_i |U_{ei}|^2 m_i^2} = 9.15\,\text{meV}$, and $\Sigma m_\nu = 61.5\,\text{meV}$. Which of the four parities is physically realized is fixed by the (deferred) sign structure of M_ν; the symmetry-forced, theorem-grade content is the *four-point discreteness* and the phase-free m_β. All four points lie 1–2 orders of magnitude below current laboratory $0\nu\beta\beta$ limits, so no datum is consulted to obtain them. (A c_{13}^2-scaled-TBM scan gives a continuous band $[0.29, 5.55]$ meV; its endpoints are just the all-aligned/anti-aligned CP-conserving points, so the symmetry replaces that band with the four discrete teeth above.)

c. Reproducibility. A helper script `scripts/scripts_nufit_table1_gaussian_eval.py` reproduces this conservative check:

```
python3 scripts/scripts_nufit_table1_gaussian_eval.py \
 --dm21 7.48e-5 --dm3l 2.51e-3
```

d. Optional: profile-level $\Delta\chi^2$ evaluation. The Gaussian check above is intentionally conservative (it uses only

the published Table 1 central values and 1σ widths). NuFIT additionally publishes 1D $\Delta\chi^2$ profiles for each oscillation parameter. To evaluate the DFD prediction against those profiles, we include `scripts/scripts_nufit_chi2_eval.py`, which (i) loads the NuFIT profile tables, (ii) interpolates $\Delta\chi^2(x)$, and (iii) reports the total χ^2 for the predicted parameter vector under the chosen ordering/data set.

We do not hard-code the profile files here (NuFIT periodically updates file names), but the script documents the expected plain-text format and directory layout.

12. Summary: DFD-closed neutrino sector (zero continuous parameters)

Theorem X.2 (Conditional neutrino-sector closure)**.** *Conditional on the stated inputs of this sector in Table CXXVIII (the Dirac rung $y_D^2 = F_\nu\alpha$, $\sin^2\theta_{13} = 3\alpha$, trimaximal mixing with μ–τ reflection) and a single data-selected discrete input, the choice of Branch B among four equally natural fractions (the doublet-ratio bit, fixed empirically by Δm^2_{32}; see the branch-selection remark of §X 7)—the entire light-neutrino sector is fixed at* zero continuous parameters*:*

1. ***Ordering is structural (normal).*** *The microsector exponents $k = \alpha^{-3/11} > 1$ and $r = \alpha^{-7/20} > 1$ force $m_1 < m_2 < m_3$; inverted ordering is impossible.*
2. ***Absolute scale is α-locked.*** *$m_3 = \frac{14}{13}\pi M_P\alpha^{14} = 50.16$ meV (Eq. X23), with the finite-d priming factor $14/13$ obtained two independent ways ($14/13 = 1 + \frac{1}{N_{\rm gen}}\sin^2\theta_W$ with $\sin^2\theta_W = 3/13$, and $d_\nu/(d_\nu - 1)$ with $d_\nu = a + 5 = 14$), giving $(m_1, m_2, m_3) = (2.34, 8.96, 50.16)$ meV and $\Sigma m_\nu = 61.46$ meV.*
3. ***Mixing is parameter-free (TM1).*** *$\cos^2\theta_{12}\cos^2\theta_{13} = 2/3$ exactly and $\sin^2\theta_{12} = (1 - 9\alpha)/\big(3(1 - 3\alpha)\big) = 0.3184$ (Thm AY.3).*

The resulting splittings match NuFIT 6.0 to $< 0.2\sigma$ ($\chi^2 = 0.025$, $p = 0.99$) with no continuous fit parameter. The single branch bit is the only empirical input.

Neutrino Sector Summary (Zero Continuous Parameters)

Derivation chain (zero continuous parameters; one data-selected binary branch choice, see the branch-selection remark in App. X 7):

1. TBM from "neutrinos-at-center" $\to \mu \leftrightarrow \tau$ residual S_2
2. Microsector integers $(a, n) = (9, 5)$, $\dim M = 7$ lock channel fractions
3. $\boxed{k = m_2/m_1 = \alpha^{-3/11}}$ (Branch B; selected over Branch A by the oscillation data)
4. $\boxed{r = m_3/m_2 = \alpha^{-7/20}}$ (from $\dim M/(4n)$)
5. Dirac overlap in $\mathcal{O}(a + 4) \to d_\nu = a + 5 = 14$
6. Finite-d priming factor $F_\nu = 14/13$
7. $\boxed{m_3 = \dfrac{14}{13}\,\pi\, M_P\,\alpha^{14}}$ (absolute scale)

Arithmetic identities:

$$k^2 r^2 = \alpha^{-137/110}$$

$$m_3 = \frac{14}{13}\,\pi\, M_P\,\alpha^{14} \quad (14 = a + 5,\ 13 = a + 4)$$

DFD predictions vs NuFIT 6.0:

Observable	DFD	NuFIT 6.0	Pull
Δm^2_{21}	7.48×10^{-5}	$(7.49 \pm 0.19)\times10^{-5}$	-0.05σ
Δm^2_{31}	2.51×10^{-3}	$(2.513 \pm 0.020)\times10^{-3}$	-0.15σ

Combined: $\chi^2 = 0.025$ **(2 dof),** $p = 0.99$**.**

Complete predictions:

- $(m_1, m_2, m_3) = (2.34, 8.96, 50.16)$ meV
- $\sum m_\nu = 61.46$ meV
- $m_\beta = 9.15$ meV (tribimaximal limit 5.52 meV)
- $m_{\beta\beta} \in \{0.13, 2.33, 3.25, 5.45\}$ meV at the four CP-conserving points (tribimaximal limit 4.55 meV)

Status: DFD-closed at zero continuous parameters, given the stated inputs. No continuous empirical input; one discrete branch choice (B, among four equally natural fractions) is selected by the oscillation data. Every number then derives from α, M_P, and locked microsector integers. The prediction matches NuFIT 6.0 with $\chi^2 = 0.025$.

Appendix Y: Finite Yukawa Operator, Chiral Basis, and the A_f Prefactors

1. Purpose and Scope

The charged-fermion mass formula used in the main text,

$$m_f = A_f\, \alpha^{n_f}\, \frac{v}{\sqrt{2}}, \tag{Y1}$$

separates a *localization* (power-law) factor α^{n_f} from a *finite microsector* prefactor A_f. To make A_f a derived quantity (rather than an asserted number), one must specify:

(i) the finite Hilbert space $\mathcal{H}_F$,

(ii) the chiral states $\chi_{L,f}, \chi_{R,f} \in \mathcal{H}_F$ for each fermion f, and

(iii) a concrete finite Yukawa operator Y_{finite} acting between the chiral subspaces.

Only then does the definition

$$A_f \equiv \left|\langle \chi_{R,f} \,|\, Y_{\text{finite}} \,|\, \chi_{L,f}\rangle\right| \tag{Y2}$$

become computable.

This appendix makes those objects explicit and states the minimal additional structure required to reproduce species-dependent A_f.

2. Finite Hilbert Space and Normalization

We work with the regular-module finite Hilbert space

$$\mathcal{H}_F := M_d(\mathbb{C}), \tag{Y3}$$

equipped with the normalized Hilbert–Schmidt inner product

$$\langle X, Y\rangle := \frac{1}{d}\,\mathrm{Tr}(X^\dagger Y). \tag{Y4}$$

Let $E_{ab} \in M_d(\mathbb{C})$ denote matrix units, $(E_{ab})_{ij} = \delta_{ai}\delta_{bj}$. Then the rescaled units

$$\widehat{E}_{ab} := \sqrt{d}\, E_{ab} \tag{Y5}$$

form an orthonormal basis:

$$\langle \widehat{E}_{ab}, \widehat{E}_{cd}\rangle = \delta_{ac}\delta_{bd}. \tag{Y6}$$

3. Block Decomposition for the $(3,2,1)$ Microsector

To align with the $(3,2,1)$ sectoral split used throughout the manuscript, take $d = 6$ and order basis indices as:

$$\{1,2,3\}\ \text{(color)}, \qquad \{4,5\}\ \text{(weak)}, \qquad \{6\}\ \text{(singlet)}. \tag{Y7}$$

Every $X \in M_6(\mathbb{C})$ is then written in $(3,2,1)$ block form

$$X = \begin{pmatrix} X_{33} & X_{32} & X_{31} \\ X_{23} & X_{22} & X_{21} \\ X_{13} & X_{12} & X_{11} \end{pmatrix}, \qquad \dim(X_{33}, X_{22}, X_{11}) = (3,2,1). \tag{Y8}$$

4. Finite Higgs Connector as an Explicit Matrix

Let $H \in \mathbb{C}^2$ be the weak doublet column $H = (h_1, h_2)^T$. Embed it into $M_6(\mathbb{C})$ as the off-diagonal connector

$$\widehat{H} := h_1 E_{4,6} + h_2 E_{5,6}, \qquad \widehat{H}^\dagger = h_1^* E_{6,4} + h_2^* E_{6,5}. \tag{Y9}$$

In block form,

$$\Phi(H) = \begin{pmatrix} 0_{3\times3} & 0_{3\times2} & 0_{3\times1} \\ 0_{2\times3} & 0_{2\times2} & H_{2\times1} \\ 0_{1\times3} & H^\dagger_{1\times2} & 0_{1\times1} \end{pmatrix}. \tag{Y10}$$

Similarly, define the conjugate Higgs $\widetilde{H} = i\sigma_2 H^*$ and its embedding $\widehat{\widetilde{H}}$ by replacing (h_1, h_2) with $(\tilde{h}_1, \tilde{h}_2)$ in (Y9).

After electroweak symmetry breaking in unitary gauge, we take

$$H \to \frac{1}{\sqrt{2}}\begin{pmatrix} 0 \\ v \end{pmatrix} \quad \Rightarrow \quad h_2 = \frac{v}{\sqrt{2}}, \quad h_1 = 0, \tag{Y11}$$

and analogously for $\widetilde{H}$.

5. Chiral Subspaces and Canonical Link-States

A minimal, explicit choice consistent with the $(3,2,1)$ connectivity is to realize chiral states as normalized *link* basis elements (off-diagonal blocks). Define the following canonical link-states:

a. Quark doublet left states (color → weak). For $a \in \{1,2,3\}$,

$$\chi^Q_L(a,\uparrow) := \widehat{E}_{a,4}, \qquad \chi^Q_L(a,\downarrow) := \widehat{E}_{a,5}. \tag{Y12}$$

b. Quark singlet right states (color → singlet). For $a \in \{1,2,3\}$,

$$\chi^q_R(a) := \widehat{E}_{a,6}. \tag{Y13}$$

c. Lepton doublet left states (weak → singlet).

$$\chi^L_L(\uparrow) := \widehat{E}_{4,6}, \qquad \chi^L_L(\downarrow) := \widehat{E}_{5,6}. \tag{Y14}$$

d. Charged-lepton singlet right state (singlet → singlet).

$$\chi^\ell_R := \widehat{E}_{6,6}. \tag{Y15}$$

Important: At this stage these are *canonical basis states* of the minimal $(3,2,1)$ connector model. Species-resolution beyond multiplet type (e.g., distinguishing t from τ at the level of A_f) requires additional finite structure; see Section Y 8.

6. Y_{finite} as an Explicit Operator and Its Matrix Elements

To make (Y2) explicit, we must specify an operator

$$Y_{\text{finite}} : \mathcal{H}_L \to \mathcal{H}_R. \tag{Y16}$$

The most concrete realization on $\mathcal{H}_F = M_d(\mathbb{C})$ is an operator of multiplication type (then fully specified by a fixed matrix). Two natural choices are:

a. Right-multiplication insertion (Higgs on the right).

$$(Y^{(R)}_{\text{finite}}X) := X\,\widehat{H}, \tag{Y17}$$

b. Left-multiplication insertion (Higgs on the left).

$$(Y^{(L)}_{\text{finite}}X) := \widehat{H}^{\dagger}\,X. \tag{Y18}$$

Given $\chi_{L,f}, \chi_{R,f} \in \mathcal{H}_F$ and the inner product (Y4), the finite matrix element is

$$\langle \chi_{R,f} \,|\, Y_{\text{finite}} \,|\, \chi_{L,f} \rangle = \frac{1}{d}\mathrm{Tr}\Big(\chi^{\dagger}_{R,f}\,(Y_{\text{finite}}\chi_{L,f})\Big). \tag{Y19}$$

7. Explicit Evaluation in the Canonical Link Basis

With the canonical link-states above and $Y_{\text{finite}} = Y^{(R)}_{\text{finite}}$ from (Y17):

a. Down-type quark (example). Take $\chi_L = \chi^Q_L(a,\downarrow) = \widehat{E}_{a,5}$ and $\chi_R = \chi^q_R(a) = \widehat{E}_{a,6}$. Using $E_{a,5}E_{5,6} = E_{a,6}$ and $E_{a,5}E_{4,6} = 0$,

$$Y^{(R)}_{\text{finite}}\chi_L = \chi_L\widehat{H} = h_2\,\widehat{E}_{a,6}. \tag{Y20}$$

Then orthonormality gives

$$\langle \chi_R | Y^{(R)}_{\text{finite}} | \chi_L \rangle = h_2. \tag{Y21}$$

After EWSB (Y11), $h_2 = v/\sqrt{2}$.

b. Charged lepton (example). Taking $Y_{\text{finite}} = Y^{(L)}_{\text{finite}}$ from (Y18), let $\chi_L = \chi^L_L(\downarrow) = \widehat{E}_{5,6}$ and $\chi_R = \chi^{\ell}_R = \widehat{E}_{6,6}$. Then $E_{6,5}E_{5,6} = E_{6,6}$ implies

$$Y^{(L)}_{\text{finite}}\chi_L = \widehat{H}^{\dagger}\chi_L = h_2^*\,\widehat{E}_{6,6}, \tag{Y22}$$

and hence

$$\langle \chi_R | Y^{(L)}_{\text{finite}} | \chi_L \rangle = h_2^*, \tag{Y23}$$

whose magnitude again becomes $v/\sqrt{2}$ after EWSB.

8. Universality Wall and the Required Additional Structure

The computations above reveal a structural fact:

Proposition Y.1 (Universality of the Minimal $(3,2,1)$ Connector Yukawa)**.** *In the canonical link-basis realization of $\mathcal{H}_F = M_6(\mathbb{C})$ with Y_{finite} defined by the bare Higgs connector (Y17) or (Y18), the finite matrix element $\langle \chi_{R,f} | Y_{\text{finite}} | \chi_{L,f} \rangle$ depends only on the Higgs component selected (and on gauge convention), not on the fermion species label f beyond its multiplet type.*

In particular, ***this minimal structure cannot generate nontrivial, species-dependent A_f factors.***

9. The L_{det} Twist: A $3^{n_{\text{gen}}}$ Ratio Pattern (Not a Parameter-Free Mass)

The universality wall of Proposition Y.1 is set by the *leading* Higgs connector $\widehat{H}$, which carries the trivial $O(1)$ twist on the color block. There is, however, a forced *subleading* connector that the bare Higgs insertion omits, and it carries a nontrivial twist. This subsection states exactly what that twist buys and what it does *not* buy. The grade is that of Appendix FM: the *ratio pattern* is structurally suggestive at the level of a power law in N_c, but the *overall normalization* and the *generation assignment* remain, respectively, an imported number and an already-open dictionary. No parameter-free light-mass claim is made here.

a. The subleading connector and its determinant-bundle charge. On the color block, quantization of the internal geometry proceeds on $\mathbb{C}P^2$ (the $(3,2,1)$ sector's projective fiber). Its canonical bundle is $K_{\mathbb{C}P^2} = \mathcal{O}(-3)$, since $c_1(\mathbb{C}P^2) = 3H$ with H the hyperplane class; the Spin^c determinant (anticanonical) line is therefore

$$L_{\text{det}} = K^{-1}_{\mathbb{C}P^2} = \mathcal{O}(+3), \tag{Y24}$$

a *forced* geometric object of degree 3 (not an invented charge). The leading Higgs connector $\widehat{H}$ of Eq. (Y9) is a section of the trivial $\mathcal{O}(1)$-grade connector and carries *no* unit of L_{det}. The subleading connector

$$Y_1 \;=\; X\,\widehat{H} \otimes (L_{\text{det}} \text{ insertion}) \tag{Y25}$$

carries exactly *one* unit of the $O(3)$ determinant twist on the color block; this is the only structural difference between Y_1 and the leading $Y_0 = X\,\widehat{H}$.

Proposition Y.2 (L_{det} pattern: $3^{n_{\text{gen}}}$ within-multiplet spread)**.** *Suppose the within-multiplet quark/lepton mass ratio is controlled by the number of units of the L_{det} twist carried by the dominant connector, and that one such unit contributes a multiplicative factor equal to the color degree N_c. Since $N_c = 3$ (the colour input, App. FK) and the determinant line has degree 3 by Eq. (Y24), the within-multiplet ratio scales as*

$$\frac{m_{\text{quark}}}{m_{\text{lepton}}}\Big|_{\text{gen}} \propto N_c^{\,n_{\text{gen}}} \;=\; 3^{\,n_{\text{gen}}}, \qquad n_{\text{gen}} \in \{+1,-1,0\}, \tag{Y26}$$

with the Georgi–Jarlskog exponent set $n_{\text{gen}} = (+1,-1,0)$ for generations $(1,2,3)$. The exponent set is traceless ($\sum_g n_{\text{gen}} = 0$), so $3^{n_{\text{gen}}}$ contributes only a spread*, not an overall scale. At the level of this* pattern*, the degeneracy of Proposition Y.1 is lifted: distinct generations acquire distinct, N_c-quantized within-multiplet ratios.*

Remark Y.3 (Grade of Proposition Y.2: pattern-suggestive, not uniquely forced). Two welds in Proposition Y.2 are *not* supplied by the core action and must be stated explicitly. (i) The bridge "one unit of the degree-3 determinant line ⇒ a multiplicative factor of exactly $N_c = 3$ per generation" equates two a-priori-distinct 3's (a bundle *degree* and a color *multiplicity*); Berezin–Toeplitz quantization of L_{det} yields a highest-weight degree shift, not an automatic amplitude factor of 3. (ii) A free-base least-squares fit of the observed within-multiplet spread returns base ≈ 3.22 (about 7% from 3); the non-circular test — does $N_c = 3$ predict the spread of the deviations — gives per-generation exponents $(+1.1, -1.0, -0.1)$ against the

claimed $(+1,-1,0)$, i.e. excellent on generation 2 but ∼10–12% off on generations 1 and 3. Hence $3^{n_{\rm gen}}$ is a *structurally suggestive* pattern (and $N_c = 3$ does best-describe the spread among small integers: RMS ≈ 11% at $N_c = 3$ versus ≈ 39% at $N_c = 2$ and ≈ 19% at $N_c = 4$), but it is *not* a precision identity and is *not* uniquely forced.

Remark Y.4 (The QCD enhancement η_q is imported, not derived). Promoting the pattern of Eq. (Y26) to absolute light masses requires one *overall* common factor η_q multiplying the whole down/lepton column,

$$\frac{m_{d_i}}{m_{\ell_i}} \;=\; \eta_q\, 3^{\,n_{\rm gen}(i)}. \qquad \text{(Y27)}$$

This $\eta_q \approx 2.67$ is a *single imported factor*, *not* a per-species fit — that is the economy of the construction. But its *value* is **not derived from the DFD action**: it equals the determinant-extracted / textbook light-quark QCD enhancement,

$$\eta_q \;=\; \left(\frac{m_d\, m_s\, m_b}{m_e\, m_\mu\, m_\tau}\right)^{1/3} \;=\; 19.0^{1/3} \;=\; 2.669, \qquad \text{(Y28)}$$

the cube root of the *observed* down/lepton mass determinant. Because the exponent set $(+1,-1,0)$ is traceless, the product of the three resulting ratios is identically $\eta_q^3 = 19.0$, the observed determinant, *by construction*. Consequently the often-quoted "m_s/m_μ to 0.6%" is a *consistency check that re-uses data already absorbed into* η_q (three data points fix one parameter, then the same data are checked), not a parameter-free prediction; its siblings m_d/m_e and m_b/m_τ land ∼12–13% off. This is the circularity recorded in Appendix FM, and it is binding: the $L_{\rm det}$ mechanism **does not remove the** 23.4% **forced-ceiling muon error** in a parameter-free way.

Remark Y.5 (The $(+1,-1,0)$ assignment is the same already-open dictionary). Which generation receives $n_{\rm gen} = +1$, -1, or 0 in Eq. (Y26) is fixed by the *down-type conjugation / sign* rule already in this appendix — Proposition Y.15 together with Assumption Y.14 — which the appendix itself labels "not derived from the core DFD action." The $L_{\rm det}$ mechanism introduces *no new* assumption to set these signs: it inherits the same open generation↔sector dictionary. (Of the six possible orderings, only $(+1,-1,0)$ achieves the ∼11% RMS spread; the other five give 122–468% errors — so the assignment is data-selected, but it is selected by the *pre-existing* dictionary, not by a fresh postulate.)

$L_{\rm det}$ result (caveats in both directions)

Gain: the $L_{\rm det} = \mathcal{O}(3)$ determinant twist that the leading Higgs connector lacks upgrades the universality wall of Proposition Y.1 from "*degenerate*" to "a $3^{n_{\rm gen}}$ *ratio pattern*" — a structural reorganization, with $N_c = 3$ (the colour input) and the degree-3 anticanonical line a forced geometric object. **Limit:** the absolute light masses remain **not parameter-free**. The common factor $\eta_q \approx 2.67$ is *imported* (it is the cube root of the observed mass determinant, hence circular as a "prediction"), the degree-3→×3 amplitude bridge is a weld rather than a derivation, and the $(+1,-1,0)$ assignment is the same already-open dictionary (Prop. Y.15, Assump. Y.14). This subsection therefore **does not** claim to "remove the muon 23% failure." For the binding status see Appendix FM.

10. The η_q-Free Double Ratio and the N_c^3 Color Clebsch

The box above isolates the one weld that blocks a parameter-free result: the common down/lepton factor $\eta_q \approx 2.67$ is imported (it is, by construction, the cube root of the observed determinant). This subsection extracts the part of the $L_{\rm det}$ mechanism that survives *after the imported factor is algebraically removed*, and tests it. It is the explicit color-/family Clebsch demanded by Theorem FM.2; the imported factor cancels, but the result depends on the scale at which the masses are taken.

a. Construction of the eta-free observable. Write the per-generation down/lepton mass ratio in the Proposition Y.2 form

$$\frac{m_{d_i}}{m_{\ell_i}} \;=\; \eta_q\, N_c^{\,s_i}, \qquad s_i = (+1,-1,0) \text{ for gen } i = (1,2,3), \qquad \text{(Y29)}$$

and form the *double ratio*

$$\boxed{\mathcal{D} \;:=\; \frac{(m_d/m_e)\,(m_b/m_\tau)}{(m_s/m_\mu)^2} \;=\; \eta_q^{(1-2+1)}\, N_c^{\,(s_1-2s_2+s_3)} \;=\; N_c^3.} \qquad \text{(Y30)}$$

The exponent of η_q is $1-2+1=0$: **the imported factor cancels identically**, regardless of its value or origin (it is an imported number: DFD's own running gives 4.21, Rem. Y.6). What remains is the pure within-multiplet spread, and the $L_{\rm det}$ mechanism forces it to be

$$s_1 - 2s_2 + s_3 = (+1) - 2(-1) + (0) = 3 \;\Longrightarrow\; \mathcal{D} = N_c^3 = 27. \qquad \text{(Y31)}$$

b. Forcedness of the exponent set. The set $\{+1,-1,0\}$ is not chosen; it is the traceless equivariant weight system of the anticanonical line $L_{\rm det} = K^{-1}_{\mathbb{C}P^2} = \mathcal{O}(3)$ restricted to the three fixed points of the $(\mathbb{Z}_3)$ generation action on $\mathbb{C}P^2$. The three fixed points carry $\mathbb{Z}_3$ charges $q = (0,1,2)$; the degree-3 line contributes normalized weight $3q/N_c = q$, which after the mandatory traceless centering (the fixed-point weights of any line bundle on a compact toric variety sum to a multiple of the canonical class and are measured

relative to their mean) becomes

$$q - \bar{q} = (0, 1, 2) - 1 = (-1, 0, +1), \tag{Y32}$$

i.e. the multiset $\{+1, -1, 0\}$. The base is $N_c = 3$, the colour input. Hence $\mathcal{D} = N_c^3$ rests on a forced weight set and a stated input, and $\mathcal{D}$ does *not* contain η_q.

c. Numerical confrontation. Because η_q is a running quantity, it is common to the three generations only when all six masses are taken at one renormalization scale. There the data give $\mathcal{D} = 33.1 \pm 0.8$ anywhere between 2 GeV and the top mass, and 29.3 ± 0.7 at the matching scale $\Lambda_{\text{top}} = \sqrt{\alpha}\, M_P$, 8% above 27. PDG's mixed reporting convention gives 27.7, but in that convention $\mathcal{D}$ moves from 21 to 31 as the light-quark reference scale moves from 1 to 3 GeV. The same weights predict $(m_d/m_e)/(m_s/m_\mu) = 9$ at any scale, against 10.35 ± 0.15 observed, so $(+1, -1, 0)$ is a pattern, not a precision identity.

Remark Y.6 (What this does and does not buy — the two residual welds). **(1) The overall scale η_q is an imported number, not a forced connector coefficient.** The Georgi–Jarlskog column $(3, \frac{1}{3}, 1)$ has *geometric mean unity*, so $\eta_q \approx 2.67$ would have to be the accumulated colored-vs-colorless renormalization-group enhancement, and it is not. Started at the matching scale $\Lambda_{\text{top}} = \sqrt{\alpha}\, M_P$ and run with DFD's own printed couplings ($\alpha_s(M_Z) = 0.1187$, $\sin^2\theta_W = 3/13$; full Standard-Model running, then four-loop QCD and one-loop QED to the scales at which the masses are quoted), the column gives $\eta_q = 4.21$, 58% above 2.67: it overshoots m_d/m_e by 38%, m_s/m_μ by 62% and m_b/m_τ by 75%, and five variants give 4.02–4.21 (computed). Only a start near 2.6×10^6 GeV, where nothing is printed, or $\alpha_s(M_Z) = 0.076$ would give 2.67. The near-coincidence $\eta_q \approx 8/3 = 2C_F$ is therefore not earned by DFD's running, and η_q is carried as one imported input: the absolute light masses remain not parameter-free, exactly as Appendix FM states. **(2) The ordering of the exponent set is data-selected among three cyclic choices.** The unordered set $\{+1, -1, 0\}$ is forced; assigning $+1$ to generation 1 and -1 to generation 2 (vs. the five other orderings) is fixed by the same down-type conjugation rule (Prop. Y.15) and lands at ∼11% RMS, whereas the five competitors give 122–468%. So the ordering is a discrete sign/label, not a continuous fit, but it is still the already-open dictionary. **Net:** the L_{det} weights keep the "pattern-suggestive" grade of Remark Y.3: the double ratio $\mathcal{D} = N_c^3$ is a pattern, not a precision identity, and the two named welds (η_q running, ordering) stay open.

Consequence: To make A_f computable and species-dependent (and thereby to "re-earn" any table of numerical A_f values), one must introduce at least one of the following:

d. (i) Species projectors/embeddings in the finite space. Define explicit finite projectors or partial isometries

$$\Pi_{L,f}, \Pi_{R,f} \in M_d(\mathbb{C}), \tag{Y33}$$

and replace the bare insertion by a species-resolved Yukawa map, e.g.,

$$\begin{aligned} Y^{(f)}_{\text{finite}}(X) &:= \Pi_{R,f}\, X\, \Pi_{L,f}\, \widehat{H} \\ \text{or} \quad Y^{(f)}_{\text{finite}}(X) &:= \widehat{H}^\dagger\, \Pi_{R,f}\, X\, \Pi_{L,f}. \end{aligned} \tag{Y34}$$

Then

$$A_f = \left|\langle \chi_{R,f} | Y^{(f)}_{\text{finite}} | \chi_{L,f} \rangle\right| \tag{Y35}$$

becomes an explicit, computable function of $(\Pi_{L,f}, \Pi_{R,f})$ and the chosen finite basis states.

e. (ii) Enlarged finite Hilbert space carrying full SM representation content. Replace the minimal $(3, 2, 1)$ connector space by a finite space large enough to encode distinct chiral multiplets and flavor structure as orthogonal finite states, with a correspondingly nontrivial finite Dirac/Yukawa operator D_F (block matrix) whose entries are determined by the microsector rules.

11. A_5 Species Projectors: Breaking the Universality Wall

The minimal $(3, 2, 1)$ connector produces Yukawa matrix elements that do not distinguish fermion species beyond multiplet type (Proposition Y.1). This section provides an explicit construction of species projectors compatible with the microsector identification $k_{\max} = |A_5| = 60$.

The manuscript uses $k_{\max} = 60 = |A_5|$ (order of the alternating group). Under the identification of Lemma H.5 (its derivation is open; status box below), take the channel Hilbert space to be the group algebra $\mathbb{C}[A_5]$, with species projectors from A_5 structure (not from $(Z_3)^2$, which has order 9 and is not a subgroup of A_5).

Resolution: The alternating group A_5 has 5 conjugacy classes, including two distinct classes of 5-cycles (5A and 5B), providing a natural discrete species label without additional structure.

a. Channel Space as Group Algebra

The channel Hilbert space is the group algebra

$$\begin{gathered} \mathcal{H}_{\text{ch}} := \mathbb{C}[A_5], \quad \{|g\rangle : g \in A_5\}, \\ \dim \mathcal{H}_{\text{ch}} = |A_5| = 60. \end{gathered} \tag{Y36}$$

For $x \in A_5$, define the right-regular unitary action

$$R(x)\,|g\rangle := |gx\rangle, \tag{Y37}$$

so $R(x)$ is a 60×60 permutation matrix in the $\{|g\rangle\}$ basis.

b. Generators and Universal Connector

Fix the standard generators of A_5:

$$a = (123), \qquad b = (12345), \qquad S = \{a, a^{-1}, b, b^{-1}\}. \tag{Y38}$$

Define the channel connector as the Cayley adjacency operator

$$\boxed{X_{\text{ch}} := \sum_{s\in S} R(s)} \tag{Y39}$$

This is an explicit sparse 60×60 matrix (each row has $|S| = 4$ nonzero entries).

c. Higgs Kernel from Derived ε_H

Let $\ell(g)$ be the word length of g in the Cayley graph (A_5, S). With the derived Higgs width $\varepsilon_H = N_{\text{gen}}/k_{\max} = 3/60 = 0.05$ (Theorem H.4), define the diagonal kernel

$$\boxed{\widehat{H}_{\text{ch}} := \sum_{g\in A_5} \varepsilon_H^{\ell(g)} \, |g\rangle\langle g|} \tag{Y40}$$

This is fully determined by (A_5, S, ε_H) with **no free parameters**.

d. Species Projectors from Conjugacy Classes

The alternating group A_5 has exactly 5 conjugacy classes:

Class	Representative	Size	Element Order
1A	e (identity)	1	1
2A	(12)(34)	15	2
3A	(123)	20	3
5A	(12345)	12	5
5B	(12354)	12	5

The 5-cycles split into two distinct conjugacy classes 5A and 5B of equal size. This provides a natural $\pm$ label (related to quadratic residues mod 5) that can distinguish species without additional structure.

With the generator $b = (12345)$:

- **5A** contains b and $b^4 = b^{-1}$
- **5B** contains b^2 and b^3

For each class $C \subset A_5$, define the class projector

$$\boxed{P_C := \sum_{g\in C} |g\rangle\langle g|} \tag{Y41}$$

These are explicit, mutually commuting, diagonal idempotents on $\mathcal{H}_{\text{ch}}$.

e. Cayley Geometry and Hierarchy Mechanism

Define the minimum class-to-class hop distance:

$$\Delta(C, D) := \min_{x\in C,\, y\in D} \ell(x^{-1}y). \tag{Y42}$$

For the generating set $S = \{a, a^{-1}, b, b^{-1}\}$:

Class Pair	Δ	Comment
$\Delta(1A, 3A)$	1	$a = (123) \in S$
$\Delta(1A, 5A)$	1	$b = (12345) \in S$
$\Delta(1A, 5B)$	2	$b^2 \notin S$
$\Delta(1A, 2A)$	3	Double transpositions

Proposition Y.7 (Hierarchy from Cayley Geometry)**.** *The two 5-cycle classes 5A and 5B differ by one hop from identity. For any Yukawa functional weighted by $\varepsilon_H^{\ell(g)}$, this produces an automatic discrete suppression scale of order ε_H between the two 5-cycle sectors, up to path multiplicities and edge-count factors.*

This is the mechanism that breaks the universality wall: pure Cayley geometry combined with derived ε_H generates species-dependent hierarchy.

f. Species-Resolved Prefactors

a. Canonical species assignment. Given the channel Hilbert space $\mathcal{H}_{\text{ch}} = \mathbb{C}[A_5]$, the class projectors of Eq. (Y41), and the generation hierarchy projectors, the species assignment rule defines a canonical map $f \mapsto |\psi_f\rangle$ from fermion species to channel states:

$$|\psi_f\rangle = P_{q(f)}\, P_{(g(f))}\, |\psi_0\rangle, \tag{Y43}$$

where $P_{q(f)}$ is fixed by gauge quantum numbers, $P_{(g(f))}$ by generation, and $|\psi_0\rangle$ is the universal channel seed state. The Yukawa prefactor is then uniquely determined as the expectation value of the channel Yukawa operator $\mathcal{Y}$:

$$A_f = \langle\psi_f|\mathcal{Y}|\psi_f\rangle. \tag{Y44}$$

No additional phenomenological species-label assignment is required: gauge quantum numbers determine the class projector, generation determines the hierarchy projector, and their ordered product on the seed state yields a unique channel state.

In the explicit SM embedding, this takes the form:

Let $P_L^{\text{gauge}}(f), P_R^{\text{gauge}}(f)$ denote the standard SM gauge projectors on the internal factor $\mathcal{H}_{\text{SM}}$. Define the full species projectors:

$$\Pi_{L,f} := P_L^{\text{gauge}}(f) \otimes P_{C_L(f)}, \qquad \Pi_{R,f} := P_R^{\text{gauge}}(f) \otimes P_{C_R(f)}. \tag{Y45}$$

The species prefactor is then the finite matrix element

$$\boxed{A_f = \left|\langle\psi_{R,f}|\, \Pi_{R,f}\, X_{\text{ch}}\, \Pi_{L,f}\, \widehat{H}_{\text{ch}}\, |\psi_{L,f}\rangle\right|} \tag{Y46}$$

g. Class-Amplitude Formula

For class-superposition states $|C\rangle := |C|^{-1/2} \sum_{g\in C} |g\rangle$, the channel-only overlap reduces to an explicit weighted

edge count:

$$\mathcal{A}(C_R, C_L) = \frac{1}{\sqrt{|C_R||C_L|}} \sum_{h \in C_L} \varepsilon_H^{\ell(h)} \cdot \#\{s \in S : hs \in C_R\}. \tag{Y47}$$

This is purely determined by (A_5, S, ε_H) with **no mass data input**.

h. Proposed Species Assignment Rule

A minimal assignment principle compatible with the structure:

1. **Element order rule:** The odd spin^c label $k_f \in \{1, 3, 5\}$ selects the element order sector (identity / 3-cycles / 5-cycles)
2. **5-cycle split rule:** Weak isospin sign (up vs down component) selects between 5A and 5B for $k_f = 5$
3. **Gauge sector:** Lepton vs quark distinction remains in the gauge projector factor $P_{L/R}^{\text{gauge}}(f)$

This rule can be tested by computing A_f and comparing to observed masses.

12. Complete Status Summary

Mass Sector Status (Complete Assessment)

What is derived:
- The exponent structure α^{n_f} from $\mathbb{C}P^2$ localization/overlap construction
- The Higgs-width parameter $\varepsilon_H = N_{\text{gen}}/k_{\max} = 3/60$ (Theorem H.4)

Universality wall (Proposition Y.1): The minimal $(3, 2, 1)$ connector with bare Higgs insertion cannot distinguish species within a multiplet.

Resolution via A_5 conjugacy classes:
- Channel space $\mathcal{H}_{\text{ch}} = \mathbb{C}[A_5]$ (consistent with $k_{\max} = 60$)
- Species projectors from 5 conjugacy classes (sizes 1, 15, 20, 12, 12)
- Built-in hierarchy from 5A vs 5B 5-cycle split (hop distance difference)
- Explicit Higgs kernel $\widehat{H}_{\text{ch}}$ using derived ε_H
- Connector X_{ch} as Cayley adjacency (explicit 60×60 sparse matrix)

Complete derivation: See Section Y 13 for the full generation projector construction and down-type selection rule.

13. Complete Derivation: Generation Projectors and Down-Type Selection

This section gives the construction of the species projector mechanism. The key results are:

1. Generation = multiplicity-3 in $V \otimes V^*$ factorization
2. Canonical generation projectors M_r with rank 3
3. Down-type selection via mod-3 conjugation automorphism

a. Regular Module Factorization

Definition Y.8 (Regular module, left/right actions)**.** Let $\mathbb{C}[A_5]$ be the group algebra (regular A_5-module). Define left- and right-regular actions

$$(L(g)f)(x) = f(g^{-1}x), \qquad (R(g)f)(x) = f(xg), \tag{Y48}$$

so $L(g)$ and $R(h)$ commute for all $g, h \in A_5$.

Definition Y.9 ($Z_3 \times Z_3$ phases and Fourier projectors)**.** Fix any element $a \in A_5$ of order 3 (a 3-cycle) and set

$$U := L(a), \qquad V := R(a), \qquad \omega := e^{2\pi i/3}. \tag{Y49}$$

Define the phase projectors

$$P_r^{(L)} := \frac{1}{3} \sum_{m=0}^{2} \omega^{-rm} U^m, \quad P_s^{(R)} := \frac{1}{3} \sum_{n=0}^{2} \omega^{-sn} V^n, \quad r, s \in \{0, 1, 2\}. \tag{Y50}$$

The joint projector is

$$\boxed{P_{r,s} := P_r^{(L)} P_s^{(R)} = \frac{1}{9} \sum_{m,n=0}^{2} \omega^{-(rm+sn)} U^m V^n} \tag{Y51}$$

Remark Y.10 (Independence of the choice of a). All 3-cycles in A_5 form a single conjugacy class. Replacing a by $a' := gag^{-1}$ conjugates U, V by unitary permutation matrices, permuting the labels (r, s) without changing any invariant. All physical statements are label-invariant.

b. Phase Factorization on Isotypic Blocks

Proposition Y.11 (Phase factorization)**.** *Let Π be either Π_3 or $\Pi_{3'}$, the projector onto a 9-dimensional isotypic block. Under the canonical decomposition*

$$\mathbb{C}[A_5] \cong \bigoplus_{\lambda} V_\lambda \otimes V_\lambda^*, \tag{Y52}$$

the Π-block is $V \otimes V^*$ with

$$U = \rho(a) \otimes \mathbf{1}, \qquad V = \mathbf{1} \otimes \rho(a)^*. \tag{Y53}$$

The joint Fourier projector factorizes:

$$\boxed{\Pi\, P_{r,s}\, \Pi = \Pi\, (P_r^{(L)} \otimes P_s^{(R)})\, \Pi} \tag{Y54}$$

Here r labels a left-factor Z_3 phase and s labels a right-factor Z_3 phase.

c. Canonical Generation Projectors

Proposition Y.12 (Generation projectors)**.** *Fix* $\Pi \in \{\Pi_3, \Pi_{3'}\}$. *Define*

$$\boxed{M_r := \Pi\, P_r^{(L)}\, \Pi, \qquad r \in \{0,1,2\}} \tag{Y55}$$

Then $\{M_0, M_1, M_2\}$ *are orthogonal projectors:*

$$M_r^2 = M_r, \quad M_r M_{r'} = 0 \ (r \neq r'), \quad \sum_{r=0}^{2} M_r = \Pi. \tag{Y56}$$

Each M_r *has* ***rank 3*** *(fixing the left eigenspace leaves the 3D right factor).*

Physical interpretation: The three generations are the three irreducible phase sectors under the left Z_3 action inside the multiplicity space. This is a canonical construction, not a phenomenological ansatz.

a. Status of the construction. The statements proved in this appendix are canonicality statements *given* the species–class dictionary and the Higgs-conjugation rule. They do not by themselves derive the species–class dictionary from the core DFD action. The mathematical gain is that, once the dictionary is fixed, no further arbitrariness remains in the generation projectors, phase-sector decomposition, or finite Yukawa operator evaluation.

d. Down-Type Selection via Conjugation

Definition Y.13 (Right-phase conjugation)**.** Complex conjugation on the right factor sends eigenvalue ω^s to $\overline{\omega^s} = \omega^{-s}$, inducing:

$$\boxed{s \mapsto -s \equiv s + 2 \pmod 3} \tag{Y57}$$

Assumption Y.14 (Higgs-conjugation dictionary)**.** Up-type Yukawa couplings implement the conjugation κ on the right-phase sector (finite analogue of $\tilde{H} \propto H^*$); down-type use identity.

Proposition Y.15 (Down-bin shift under the Higgs-conjugation assumption)**.** *For shared* Q_L *with left label* s_L*, if up-type selects* $s_R^{(u)}$*, then down-type selects* $s_R^{(d)} \equiv -s_R^{(u)}$ *(mod 3). With the successful up-type choice* $\Delta s^{(u)} = 2$*:*

$$\boxed{\Delta s^{(d)} \equiv 1 \quad \Rightarrow \quad s_R^{(d)} = 2} \tag{Y58}$$

Under Assumption Y.14 this gives the map $(1,0) \mapsto (1,2)$*, which the bin scan below does not confirm.*

e. Numerical Bin Scan

The conjugation rule $(1,0) \mapsto (1,2)$ follows from Assumption Y.14 that required numerical verification. Full bin scanning (below) reveals the correct assignments differ from the simple conjugation prediction.

The one-hop kernel computation reveals the correct bin assignments.

One-Hop Bin Scan (Bins Chosen per Fermion)

Using the trace formula $|y_f| = |\mathrm{Tr}(P_R X P_L \widehat{H} \Pi_{3'})|$ with derived $\varepsilon_H = 3/60$:

Fermion	m_f/m_t	L-bin	R-bin	Computed	Err
t	1.000	$(0,0)$	$(0,0)$	1.000	0%
c	7.34×10^{-3}	$(2,0)$	$(1,0)$	7.28×10^{-3}	0.8%
τ	1.03×10^{-2}	$(0,0)$	$(2,0)$	9.23×10^{-3}	10%
b	2.42×10^{-2}	$(0,2)$	$(1,2)$	1.83×10^{-2}	24%

Four heavy fermion masses are fitted within 25% using discrete bin labels $(r,s) \in \mathbb{Z}_3 \times \mathbb{Z}_3$ and derived ε_H. No continuous parameters fitted.

f. Diagonal Bin Structure

The diagonal bins (L = R) exhibit the expected ε_H power hierarchy:

Bin	$\lvert y\rvert/\lvert y_{\max}\rvert$	Approximate power
$(0,0)$	1.000	ε_H^0
$(1,2)$, $(2,1)$	0.759	$\varepsilon_H^{0.1}$
$(0,1)$, $(0,2)$	0.050	$\varepsilon_H^{1.0}$
$(1,0)$, $(2,0)$	0.036	$\varepsilon_H^{1.1}$
$(1,1)$, $(2,2)$	0.009	$\varepsilon_H^{1.6}$

The suppression factor $\varepsilon_H = 0.05$ is verified numerically.

g. Light Fermion Limitation

The one-hop kernel achieves minimum ratio $\sim 3.6 \times 10^{-3}$ ($\approx \varepsilon_H^{1.9}$), insufficient for light fermions requiring $|y|/|y_{\max}| \sim 10^{-4}$ to 10^{-6}.

Resolution: Light fermion masses require the generation projectors $M_r = \Pi P_r^{(L)} \Pi$ combined with walk-sum kernels.

h. Generation Projector Results

Using generation-2 projector M_2 with one-hop kernel, with bins chosen per fermion, yields heavy fermion predictions:

Fermion	m_f/m_t (obs)	L-bin	R-bin	Computed	Error
t	1.0000	$(2,1)$	$(2,1)$	1.0000	**0.0**%
b	0.0242	$(0,1)$	$(2,1)$	0.0241	**0.4**%
τ	0.0103	$(1,0)$	$(2,0)$	0.0096	**6.6**%

Using generation-1 projector M_1 with walk-sum kernel:

Fermion	m_f/m_t (obs)	L-bin	R-bin	Computed	Error
s	5.4×10^{-4}	$(2,2)$	$(1,2)$	4.7×10^{-4}	12.9%
μ	6.1×10^{-4}	$(2,2)$	$(1,2)$	4.7×10^{-4}	23.4%

14. Bin–Overlap Lemma and the Structural $\sqrt{20}$ Scale

This section provides the exact computation of the $\mathbb{Z}_3\times\mathbb{Z}_3$ bin overlaps that determine the rational multipliers in the A_f prefactors.

a. Normalized Class-State Matrix Elements

Let $G=A_5$ and let $S=\{a,a^{-1},b,b^{-1}\}$ with $a=(123)$ and $b=(12345)$. Define the Cayley operator (right-regular action)

$$T=\sum_{s\in S}R_s,\qquad (R_s)_{g,h}=\delta_{g,hs}. \tag{Y59}$$

For each conjugacy class $C\subset G$, define the *normalized class state*

$$|C\rangle=\frac{1}{\sqrt{|C|}}\sum_{g\in C}|g\rangle. \tag{Y60}$$

Then the induced operator on the class subspace has matrix elements

$$\langle C_i|T|C_j\rangle=\frac{N(C_i\leftarrow C_j)}{\sqrt{|C_i||C_j|}}, \tag{Y61}$$

where $N(C_i\leftarrow C_j)$ is the total number of Cayley edges from elements of C_j into C_i.

In particular, for the unique order-3 class C_3 of size $|C_3|=20$ in A_5 and the identity class $\{e\}$, only the two order-3 generators $\{a,a^{-1}\}$ contribute, giving

$$\boxed{\langle C_3|T|\{e\}\rangle=\frac{2}{\sqrt{|C_3|}}=\frac{2}{\sqrt{20}}=\frac{1}{\sqrt{5}}\approx0.4472} \tag{Y62}$$

This exhibits *structurally* (i.e., without fitting) how the conjugacy-class normalization produces a $\sqrt{|C_3|}=\sqrt{20}$ scale in any overlap built from class-localized states and Cayley-graph operators.

b. Bin–Overlap Lemma for the Order-3 Class

Let $G=A_5$ act on $\mathcal{H}_F:=\ell^2(G)$ by the left and right regular actions

$$L(h)|g\rangle:=|hg\rangle,\qquad R(h)|g\rangle:=|gh\rangle. \tag{Y63}$$

Fix an order-3 element $a\in A_5$ and $\omega=e^{2\pi i/3}$. Define the $\mathbb{Z}_3$ projectors

$$P_r^{(L)}:=\frac{1}{3}\sum_{m=0}^{2}\omega^{-rm}L(a)^m,\qquad r\in\{0,1,2\}, \tag{Y64}$$

$$P_s^{(R)}:=\frac{1}{3}\sum_{n=0}^{2}\omega^{-sn}R(a)^n,\qquad s\in\{0,1,2\}. \tag{Y65}$$

Let $C_3\subset A_5$ denote the order-3 conjugacy class (so $|C_3|=20$), and let $P_{C_3}:=\sum_{g\in C_3}|g\rangle\langle g|$.

We define the $\mathbb{Z}_3\times\mathbb{Z}_3$ *bin-overlap* weights:

$$\boxed{r(C_3;r,s):=\mathrm{Tr}\big(P_{C_3}P_r^{(L)}P_s^{(R)}\big)} \tag{Y66}$$

Lemma Y.16 (Exact bin-overlap evaluation)**.** *For the regular representation of A_5 one has the closed form:*

$$\boxed{\begin{aligned}r(C_3;r,s)&=\frac{1}{9}\Big(20+2\omega^{-(r+2s)}+2\omega^{-(2r+s)}\Big)\\&=\begin{cases}8/3, & r=s,\\ 2, & r\neq s.\end{cases}\end{aligned}} \tag{Y67}$$

Proof sketch (counting). Using $\mathrm{Tr}\big(P_{C_3}L(a)^mR(a)^n\big)=\#\{g\in C_3:a^mga^n=g\}$, we reduce the problem to counting fixed points in C_3 under the map $g\mapsto a^mga^n$. A direct computation in A_5 gives

$$\begin{aligned}N_{m,n}&:=\#\{g\in C_3:a^mga^n=g\}\\&=\begin{cases}20, & (m,n)=(0,0),\\ 2, & (m,n)\in\{(1,2),(2,1)\},\\ 0, & \text{else.}\end{cases}\end{aligned} \tag{Y68}$$

Substituting into $r(C_3;r,s)=\frac{1}{9}\sum_{m,n=0}^{2}\omega^{-rm-sn}N_{m,n}$ yields the closed form above. □

The complete bin-overlap matrix is:

$$W=\big(r(C_3;r,s)\big)_{r,s=0,1,2}=\begin{pmatrix}\frac{8}{3}&2&2\\2&\frac{8}{3}&2\\2&2&\frac{8}{3}\end{pmatrix} \tag{Y69}$$

The diagonal/off-diagonal ratio is $\frac{8/3}{2}=\frac{4}{3}$.

c. Species Projector Closure

Definition Y.17 (Complete species projector)**.** For a fermion species f with LH generation index $i\in\{0,1,2\}$ and RH generation index $j\in\{0,1,2\}$:

$$\boxed{\Pi_{L,f}=P_C^{(f)}P_i^{(L)}P_{\text{gauge}}^{(f)},\qquad \Pi_{R,f}=P_C^{(f)}P_j^{(R)}P_{\text{gauge}}^{(f)}} \tag{Y70}$$

where:

- $P_C^{(f)}$: class projector (quarks $\to C_3$, leptons $\to\{e\}$)
- $P_i^{(L)},P_j^{(R)}$: $\mathbb{Z}_3$ generation projectors (left/right)
- $P_{\text{gauge}}^{(f)}$: gauge quantum number selector (color/isospin/hypercharge)

Definition Y.18 ($(r,s) \to$ species map)**.** The bin index (r,s) encodes the Yukawa matrix entry:

$$Y_{ij} \longleftrightarrow \text{bin } (r=i, s=j) \tag{Y71}$$

where i is the LH generation index and j is the RH generation index.

d. A_f Prefactor Structure

Proposition Y.19 (Microsector A_f formula)**.** *The Yukawa prefactor for quark species f in generation g has the overlap structure:*

$$Y_f = g_Y \varepsilon_H \sqrt{|C_3|} \cdot r(C_3; g{-}1, g{-}1) \cdot G_g \cdot R_{g,t} \tag{Y72}$$

where:

- $\sqrt{|C_3|} = \sqrt{20}$*: structural class normalization*
- $r(C_3; g{-}1, g{-}1) = 8/3$*: computed diagonal bin weight*
- G_g*: generation suppression factor*
- $R_{g,t}$*: up/down type factor (G_g and $R_{g,t}$ are not computed in this volume, so the formula does not yet fix A_f)*
- $g_Y \varepsilon_H$*: single global normalization (one convention)*

The mass prefactor convention absorbs $g_Y \varepsilon_H \cdot (8/3)$ into the normalization, giving:

$$\boxed{A_f = \sqrt{|C_3|} \times G_g \times R_{g,t}} \tag{Y73}$$

Closure Status: What Is Derived vs. Convention

Derived (no fitting):

- $|C_3| = 20$ (A_5 group theory)
- $\langle C_3|T|\{e\}\rangle = 2/\sqrt{20} = 1/\sqrt{5}$ (Cayley matrix element)
- $r(C_3; i, i) = 8/3$, $r(C_3; i, j) = 2$ for $i \neq j$ (fixed-point counting)
- Closed form: $r(C_3; r, s) = \frac{1}{9}(20 + 2\omega^{-(r+2s)} + 2\omega^{-(2r+s)})$

One global convention:

- g_Y (the global Yukawa normalization) is fixed once from m_τ/m_μ (Appendix H)
- $\varepsilon_H = 3/60$ is **closed at the value level**: both premises of Theorem H.4 (uniform Higgs connector; equal 3-channel generation coupling) are *forced* by A_5 representation theory once $\mathcal{H}_{\text{ch}} \cong \mathbb{C}[A_5]$ — the identification this appendix's own kernel $\widehat{H}_{\text{ch}} = \sum_{g \in A_5} \varepsilon_H^{\ell(g)} |g\rangle\langle g|$ already uses (Lemma H.5, Appendix H). The residual, one level deeper: deriving $\mathcal{H}_{\text{ch}} \cong \mathbb{C}[A_5]$ itself from the $\mathbb{C}P^2 \times S^3$ harmonic spectrum remains **open**

Final Status

Discrete bin fit (sub-10%): Heavy fermions t, b, τ via generation-2 projector
Discrete bin fit (∼20%): Middle fermions s, μ via generation-1 walk-sum
Mechanism: $\varepsilon_H = 3/60$ suppression, rank-3 orthogonal generation projectors, discrete bin assignments
Structural closure: $\sqrt{20}$ normalization and $\{8/3, 2\}$ bin weights proven from A_5 fixed-point counting
Open: Light fermions (u, d, e), c quark inter-generation normalization, and derivation of the channel identification $\mathcal{H}_{\text{ch}} \cong \mathbb{C}[A_5]$ from the $\mathbb{C}P^2 \times S^3$ harmonic spectrum (given that identification, $\varepsilon_H = 3/60$ is forced — Lemma H.5, Appendix H)

Appendix Z: Complete Parameter Derivation

This appendix presents the microsector derivation chain for Standard Model parameters from the topology of the internal manifold $X = \mathbb{C}P^2 \times S^3$. Combined with the results of Appendices K–Y, this demonstrates that within the stated microsector framework, the Standard Model parameters follow with two continuous inputs, the fitted Higgs prefactor and the Higgs quartic (the corollary to Theorem Z.4), once $k_{\max} = 60$ is fixed as in Theorem Z.4. Beyond them, the absolute charged-fermion masses other than the top and the charm rest on seven data-selected prefactors, deployed by four *discrete* labels that are data-selected rather than derived (App. K 5, caveat box; App. FM). The individual derivations below should be read in the context of the claim taxonomy in Sec. I C.

1. The Weinberg Angle

Theorem Z.1 (Weinberg Angle from Partition)**.** *Let $X = \mathbb{C}P^2 \times S^3$ with gauge partition $(3,2,1)$ corresponding to $\mathrm{SU}(3)_c \times \mathrm{SU}(2)_L \times \mathrm{U}(1)_Y$. Then:*

$$\boxed{\sin^2\theta_W = \frac{3}{13} = 0.230769\ldots} \tag{Z1}$$

Proof. Write the gauge action in trace form over the internal blocks,

$$S_{\text{gauge}} \propto \sum_r \kappa_r \int \mathrm{Tr}(F_r^{\mu\nu} F_{r\,\mu\nu})\,,$$

with stiffness scaling $\kappa_r = n_r \kappa_0$ for the partition $(n_3, n_2, n_1) = (3,2,1)$. To identify the physical couplings one must convert the trace-normalized terms to canonical Yang–Mills normalization. With the standard SU(2) generator convention $\mathrm{Tr}(T^a T^b) = \frac{1}{2}\delta^{ab}$,

$$\mathrm{Tr}(F_2^{\mu\nu} F_{2\,\mu\nu}) = \tfrac{1}{2} F_2^{a\,\mu\nu} F^a_{2\,\mu\nu} \;\Rightarrow\; g^{-2} \propto \kappa_2 \cdot \tfrac{1}{2}.$$

For $\mathrm{U}(1)_Y$ the trace weight is fixed by the SM hypercharge

spectrum (per generation),

$$\mathrm{Tr}(F_1^{\mu\nu}F_{1\,\mu\nu}) = \mathrm{Tr}\big(Y^2\big)\,F_1^{\mu\nu}F_{1\,\mu\nu},$$
$$\mathrm{Tr}\big(Y^2\big) = \sum_{1\ \mathrm{gen}} d_3 d_2\, Y^2 = \tfrac{10}{3},$$

using $Q_L : (3,2,\frac{1}{6})$, $u_R : (3,1,\frac{2}{3})$, $d_R : (3,1,-\frac{1}{3})$, $L_L : (1,2,-\frac{1}{2})$, $e_R : (1,1,-1)$. Hence $g'^{-2} \propto \kappa_1 \cdot \frac{10}{3}$, with the hypercharge weight taken over a generation and the SU(2) weight over one doublet, a stated choice. Taking the ratio and using $\kappa_2/\kappa_1 = 2$ gives

$$\frac{g'^2}{g^2} = \frac{\kappa_2(\frac{1}{2})}{\kappa_1(\frac{10}{3})} = \frac{3}{10},$$

$$\sin^2\theta_W = \frac{g'^2}{g^2+g'^2} = \frac{3}{13}.$$

□

a. Experimental comparison. $\sin^2\theta_W(\overline{\mathrm{MS}}, M_Z) = 0.23129 \pm 0.00004$ [2]. Agreement: **0.23%**. Here 3/13 is the bare angle; its radiative relation to the $\overline{\mathrm{MS}}$ value at M_Z is not computed.

Corollary Z.2. *The ratio $\alpha_1/\alpha_2 = 1/2$ holds exactly for the bare couplings, with $\alpha_1 = (5/3)\,g'^2/4\pi$; the hypercharge coupling itself gives $g'^2/g^2 = 3/10$.*

2. The CKM Matrix

The CKM matrix shows a pattern when expressed in terms of α and line bundle cohomology integers. The numerical agreement is close, but a complete selection rule identifying *which* cohomologies govern each parameter remains an open problem.

a. CKM Pattern from Line Bundle Cohomology. Let $h^0(k) := \dim H^0(\mathbb{C}P^2, \mathcal{O}(k)) = (k+1)(k+2)/2$. The Wolfenstein parameters match the pattern:

$$\boxed{\lambda = 31\alpha, \quad A = 108\alpha, \quad \bar\rho = \tfrac{43}{2}\alpha, \quad \bar\eta = 49\alpha} \tag{Z2}$$

where the integers arise as:

$$31 = h^0(2) + h^0(3) + h^0(4) = 6 + 10 + 15, \tag{Z3}$$
$$\tfrac{43}{2} = \tfrac{D^2}{2} - \chi(\mathbb{C}P^2) = \tfrac{49}{2} - 3, \tag{Z4}$$
$$49 = [\dim(\mathbb{C}P^2 \times S^3)]^2 = 7^2 = D^2, \tag{Z5}$$
$$108 = N_{\mathrm{gen}} \times h^0(7) = 3 \times 36. \tag{Z6}$$

The CP-even apex $\bar\rho = \frac{43}{2}\alpha = 21.5\alpha$ (Path A) is the Euler-projected value: the minimizer of the reduced geometric action $\mathcal{I}_\rho(r) = \frac{1}{2}\left(r - D^2/2\right)^2 + \chi(\mathbb{C}P^2)\,r$, $r = \bar\rho/\alpha$, derived in full in Appendix AO (Euler-projection postulate). The raw assignment $\bar\rho = 19\alpha = [h^0(1) + h^0(2) + h^0(3)]\alpha$ does not give the apex.

b. Interpretation. (i) The Cabibbo angle λ controls $1 \leftrightarrow 2$ mixing. The bundles $\mathcal{O}(2), \mathcal{O}(3), \mathcal{O}(4)$ give sections 6, 10, 15. Sum: 31. (ii) The apex coordinate $\bar\rho = \frac{43}{2}\alpha$ is the Euler-projection of the ideal A_5 covering-space apex $D^2/2$ after the Euler localization cost $\chi(\mathbb{C}P^2) = 3$ (App. AO). (iii) The CP phase $\bar\eta$ scales with $\dim^2 = 49$. (iv) The amplitude A scales with $N_{\mathrm{gen}} \times h^0(7) = 108$. (v) All parameters are suppressed by α.

c. Status. The magnitude integers $(\lambda, A, \bar\eta) = (31, 108, 49)\alpha$ are line-bundle cohomology counts selected before any apex rule. The apex selection $\bar\rho = \frac{43}{2}\alpha$ is theorem-grade *inside the strengthened DFD–SD branch* via the Euler-projection postulate (App. AO); consistent with the no-forcing anti-theorem of App. AO, this postulate is a structural strengthening, not a consequence of the pre-strengthened axioms. The mapping from each cohomology sum to its Wolfenstein parameter remains the open ingredient at full theorem grade.

TABLE CV. CKM parameter pattern verification.

Parameter	Pattern	PDG 2024	Agreement
λ	$31\alpha = 0.2262$	0.22501 ± 0.00068	0.5%
A	$108\alpha = 0.788$	$0.826^{+0.016}_{-0.015}$	4.6%
$\bar\rho$	$\frac{43}{2}\alpha = 0.157$	0.1591 ± 0.0094	1.4%
$\bar\eta$	$49\alpha = 0.358$	$0.3523^{+0.0073}_{-0.0071}$	1.5%

Per-channel (no mean quoted); A is the soft spot ($|V_{cb}|$ incl./excl. tension). See App. AO.

3. The Higgs Sector

Theorem Z.3 (Higgs from Dimension 8)**.** *The number $8 = \dim(\mathbb{C}P^2 \times S^3) + 1$ determines the exponent of v, whose prefactor $\sqrt{2\pi}$ is fitted, and the conjectured quartic:*

$$v = M_P \cdot \alpha^8 \cdot \sqrt{2\pi} = 246.09\ GeV, \tag{Z7}$$
$$\lambda_H = \frac{1}{8} \quad \textit{(conjectured)}, \tag{Z8}$$
$$m_H^{\mathrm{tree}} = \frac{v}{2} = 123.05\ GeV. \tag{Z9}$$

Proof. In $v = M_P\alpha^8\sqrt{2\pi}$ the *exponent* $8 = \dim X + 1$ is derived (the dimension count of $\mathbb{C}P^2 \times S^3$ plus the Higgs radial mode). The $\sqrt{2\pi}$ *prefactor* is fitted: it is the best simple constant near the best-fit value 2.508 ($\sqrt{2\pi} = 2.507$, a 0.054% gap), and no printed rule fixes it. Three routes fail: a Gaussian zero-mode measure on every rung spoils the χ relic, the winding-period rule that fixes χ's period caps v below 10 GeV, and the spectral-action normalization that fixes α and G gives v of order the Planck mass (computed). Integer winding fixes a normalization only on a compact direction, while the vacuum value lies on the radial one, and DFD's own per-mode determinant ledger (Lemma O.5) cancels such 2π factors; the prefactor is a property of the Higgs potential's loop-corrected minimum, which this volume does not compute (App. H). The 17-order α^8 hierarchy is derived; the $O(1)$ prefactor is fitted.

For the quartic coupling: the conjecture $\lambda_H = 1/d = 1/8$ arises from the expectation that dimensional reduction on a Kähler manifold of total dimension $d = 8$ ($= \dim X + 1$ for the radial mode) yields $\lambda_H = 1/d$. A complete derivation from the microsector action remains to be established, and the scale at which the value holds is not derived. Assuming $\lambda_H = 1/8$: $m_H = v\sqrt{2\lambda_H} = v/2$ at tree level. □

a. Radiative corrections. Imposed at the top-quark mass, where the Standard-Model quartic is matched, $\lambda_H = 1/8$ gives $m_H = 124.63 \pm 0.15$ GeV under two-loop Standard-Model running (computed): the loop shift from the tree value $v/2 = 123.05$ GeV is +1.3%, and the result lies 0.40% (2.7σ) below the measured 125.13 ± 0.11 GeV (PDG 2026). The running quartic equals 1/8 at 182 ± 4 GeV; the matching scale is not derived.

4. The PMNS Correction

a. Reactor Angle (Conjecture). The PMNS angle θ_{13} receives a geometric correction to tribimaximal:

$$\sin\theta_{13} = \sqrt{3\alpha} = 0.148 \tag{Z10}$$

where the factor $\sqrt{3}$ arises from $N_{\text{gen}} = 3$ or $\dim(S^3) = 3$.

b. Status. $\sin^2\theta_{13} = 3\alpha$ is a stated conjectural input: it fits (-0.1σ against NuFIT 6.0), and no mechanism for the $\mu \leftrightarrow \tau$ breaking that generates it from the TBM base is printed. With trimaximal mixing and μ–τ reflection imposed it fixes $\sin^2\theta_{12} = 0.3184$, which JUNO's first result, 0.3092 ± 0.0087, places 1.1σ away and which JUNO at its target precision tests at about 6σ (computed).

5. Master Theorem

Theorem Z.4 (Complete Parameter Determination)**.** *Given the internal manifold $X = \mathbb{C}P^2 \times S^3$, the level $k_{\max} = 60$ (fixed by the generation count, the derived $q_1 = 3$ and the five matter types of a family), the unit M_P and the stated inputs of Tables CXXVII and CXXVIII, the parameters not listed as inputs follow; in the fermion, Higgs and neutrino sectors these are the top and charm Yukawas, $\bar\theta = 0$ at tree level, the three neutrino masses, θ_{12}, θ_{23} and δ_{CP}.*

Proof. Follows from App. K 1 (α), Theorem Z.1 ($\sin^2\theta_W$), App. AO (CKM), Theorem Z.3 (Higgs), App. K 5 (masses), Theorem L.3 ($\bar\theta$), Theorem X.2 (neutrinos), §Z 4 (θ_{13}), Theorem O.7 and Eq. (479) (H_0^{loc} at $C = 1$, Postulate ZS.11; H_0^{early} with the measured C), with the inputs stated there. □

Corollary Z.5. *Of the Standard Model's 26 free continuous numbers in the fermion, Higgs and neutrino sectors, DFD derives 9, pins the two Majorana phases to one of four CP-conserving points, and rests the other 15 on 17 stated inputs: 15 discrete (the strong scale, seven charged-fermion prefactors, three CKM counts, the Euler projection, the neutrino branch bit, the Dirac-neutrino Yukawa rung and $\sin^2\theta_{13} = 3\alpha$) and 2 continuous (the fitted Higgs prefactor and the Higgs quartic, conjectured to be 1/8 at a matching scale that is not derived), with three structural postulates (the conjugation-odd CP offset, the $\mathbb{C}[A_5]$ channel space, and trimaximal mixing with μ–τ reflection). DFD needs far fewer continuous numbers than the Standard Model, but about as many stated items.*

6. Integer Catalog

TABLE CVI. Master integer catalog.

Int.	Geometric Origin	Physical Application
3	$\dim(S^3)$, N_{gen}	Generations, $\varepsilon_H = 3/60$
4	$\dim(\mathbb{C}P^2)$	Gauge structure
7	$\dim(\mathbb{C}P^2 \times S^3)$	$\bar\eta = 49\alpha$
8	$\dim + 1$	exponent of v; λ_H (conjectured); k_a
13	$3 + 10$ (EW)	$\sin^2\theta_W = 3/13$
19	$h^0(1)+h^0(2)+h^0(3)$	Λ_{QCD} (not the $\bar\rho$ apex)
31	$h^0(2)+h^0(3)+h^0(4)$	$\lambda = 31\alpha$
49	7^2	$\bar\eta = 49\alpha$
60	$k_{\max} = \chi(\mathbb{C}P^2, E)$	α^{-1}, ε_H
64	$k_{\max} + 4$	Hilbert space dim.
108	3×36	$A = 108\alpha$
137	Closed form	α^{-1}

7. Strong Coupling Constant

The strong coupling $\alpha_s(M_Z)$ follows from the selected QCD scale and its selected scheme-matching constant (App. FK).

Theorem Z.6 (QCD Scale)**.** *The QCD confinement scale is selected on the α-tower (App. FK):*

$$\Lambda_{\text{QCD}}^{\text{DFD}} = M_P \cdot \alpha^{19/2} = 61.20\ MeV. \tag{Z11}$$

a. Proper-time to $\overline{\text{MS}}$ matching. The spectral/proper-time regulator produces the one-loop effective action

$$W_{\text{1-loop}} \supset \frac{b_0}{2} \int \frac{d^4p}{(2\pi)^4} \log\left(\frac{\Lambda_{\text{PT}}^2}{p^2}\right) F_{\mu\nu}^2.$$

The $\overline{\text{MS}}$ scheme defines the renormalization scale by $\bar\mu^2 := 4\pi e^{-\gamma_E}\mu^2$, so

$$\log\left(\frac{\bar\mu^2}{p^2}\right) = \log\left(\frac{\mu^2}{p^2}\right) + \log(4\pi) - \gamma_E.$$

Matching log-arguments gives the scheme conversion $\Lambda_{\overline{\text{MS}}} = \sqrt{4\pi}\, e^{-\gamma_E/2}\, \Lambda_{\text{PT}}$.

The DFD definition absorbs the Euler constant: $\Lambda_{\text{DFD}} := e^{-\gamma_E/2}\, \Lambda_{\text{PT}}$.

Lemma Z.7 (Scheme Matching)**.** *The proper-time to* $\overline{\text{MS}}$ *conversion is:*

$$\boxed{\Lambda_{\overline{\text{MS}}} = \sqrt{4\pi}\,\Lambda_{\text{DFD}}} \tag{Z12}$$

b. Numerical evaluation. Using $M_P = 1.220890 \times 10^{19}$ GeV (CODATA 2022) and $\alpha^{-1} = 137.036$:

$$\Lambda_{\text{DFD}} = M_P \times \alpha^{19/2} = 61.20 \text{ MeV}, \tag{Z13}$$

$$\Lambda^{(5)}_{\overline{\text{MS}}} = \sqrt{4\pi} \times 61.20 \text{ MeV} = 216.95 \text{ MeV}. \tag{Z14}$$

Running to $M_Z = 91.1876$ GeV with 4-loop QCD ($n_f = 5$, fixed coefficients):

$$\boxed{\alpha_s(M_Z) = 0.1187} \tag{Z15}$$

c. Experimental comparison. PDG 2024: $\alpha_s(M_Z) = 0.1180 \pm 0.0009$. Agreement: 0.8σ (0.6%).

d. Trace weight sanity check. For completeness, we verify that nonabelian trace weights cannot provide a "10/3 miracle" for α_s. Per SM generation, using the fundamental index $I_{\text{fund}}(\text{SU}(N)) = 1/2$:

SU(3): Q_L (2 weak components in **3**) $\to 2 \times \frac{1}{2} = 1$; u_R, d_R each $\to \frac{1}{2}$. Total: $\text{Tr}_F(T_3^2) = 2$.

SU(2): Q_L (3 colors of doublet) $\to 3 \times \frac{1}{2} = \frac{3}{2}$; $L_L \to \frac{1}{2}$. Total: $\text{Tr}_F(T_2^2) = 2$.

Hence $A_2 = A_3 = 2$ from SM fermion content alone—no nontrivial ratio emerges. The hypercharge trace $\text{Tr}(Y^2) = 10/3$ is special because it sums over different Y values; the nonabelian traces are representation-independent. This is why α_s must be derived via Λ_{QCD} + RG, not trace normalization.

8. Summary

Summary: Standard Model Parameters from Topology

Results (derived, selected and input rows marked):

Parameter	Value	Agreement	Status
α^{-1}	137.036	21 ppm (integers)	**Derived** (identification with $1/e^2$ open, §X I)
$\bar{\theta}$	0	$\lesssim 10^{-16}$ (bound 10^{-10})	**Derived** ($\theta_{\text{YM}} = 0$ fixed by the spectral action given that nothing is added to it for the gauge fields)
v	$M_P\alpha^8\sqrt{2\pi}$	0.05%	**Exponent derived**†
N_{gen}	3	exact	**Input**†
$\sin^2\theta_W$	3/13	0.23%	**Derived**
$\alpha_s(M_Z)$	0.1187	0.8σ	**Selected**†
ε_H	$3/60 = 0.05$	exact	**Derived**

Conditional (require full A_f computation):

- Light fermion masses: exponent structure derived; prefactors need overlap computation
- CKM matrix elements: integer×α pattern observed; selection rule pending

Species construction (Section Y 13):

- Generation projectors $M_r = \Pi P_r^{(L)} \Pi$ with rank 3 (canonical, not fitted)
- Down-type selection: $s \mapsto -s$ (mod 3) under Assumption Y.14; the bin scan selects other bins
- t/b/τ within 7% via gen-2 projector (bins chosen per fermion)

Conjectures (need proofs):

Parameter	Conjecture	Agreement
λ_H	1/8	1.7% (tree); −0.40% in m_H at m_t
$\sin\theta_{13}$	$\sqrt{3\alpha}$	0.1%

Key rigorous results:

- $\alpha^{-1} = 137.036$ from Chern-Simons quantization (Appendix K 1; bracket coefficient open; the identification of the hypercharge-trace coefficient with $1/e^2$ is not derived)
- $\sin^2\theta_W = 3/13$ from the stated trace normalization + partition (Theorem Z.1)
- $\alpha_s(M_Z) = 0.1187$ from $\Lambda_{\text{QCD}} = M_P\alpha^{19/2} + \sqrt{4\pi}$ matching (selected scale; Theorem Z.6)
- $\bar{\theta} = 0$ (tree level; loop-induced $\lesssim 10^{-16}$) from the det-orthogonal tree-level protection together with the η-invariant argument, with $\theta_{\text{YM}} = 0$ fixed by the spectral action given that nothing is added to it for the gauge fields (Appendix L)
- $v = M_P\alpha^8\sqrt{2\pi}$ (exponent 8= dim X+1 derived; $\sqrt{2\pi}$ prefactor fitted, App. AY)
- $N_{\text{gen}} = 3$: discrete input (numerically $\chi_{\text{top}}(\mathbb{C}P^2)$; not an index-theorem output — App. F generation-count remark)
- $\varepsilon_H = 3/60$ from channel counting (Theorem H.4)
- Generation = left Z_3 phase sectors in $V \otimes V^*$ (Proposition Y.12)

Conclusion: Six fundamental parameters plus the generation structure follow from topology under the stated inputs; $N_{\text{gen}} = 3$ is a discrete input and the v prefactor is fitted (†; App. F/AY status remarks).

Appendix AA: The Padé Identity: GR's Isotropic Lapse and the Exponential

This appendix establishes a precise mathematical identity between general relativity's isotropic-coordinate Schwarzschild lapse-squared scalar and the exponential $\exp(2u)$, the value of DFD's lapse-squared e^{ψ} at $\psi = 2u$. The result is purely structural: GR's Schwarzschild form is the squared $[1,1]$ Padé approximant of the exponential, with matching argument. Agreement through second order in the gravitational potential reproduces the post-Newtonian parameter $\beta = 1$ in both theories (consistent with all current gravitational-redshift observations). Beyond that order DFD's exterior is not the exponential: with the scalar-longitudinal piece σ of the parent strain kept, it is the Schwarzschild metric in DFD's coordinates (App. WS), so the pole of the rational form at $u = 2$ is a horizon of DFD's black holes as well. The Padé identity operates on the lapse-squared scalar; the spatial-curvature PPN parameter γ is established separately from DFD's physical metric (Sec. IV).

1. Statement of the Padé Identity

Define the lapse-squared scalar

$$\mathcal{L}(u) \equiv \frac{c^2}{|g_{tt}|}, \tag{AA1}$$

a clock-rate / redshift observable, with $u \equiv GM/(\rho c^2)$ the dimensionless gravitational potential, where ρ denotes the isotropic radial coordinate in GR and the flat-space radial coordinate in DFD. DFD's matter-coupling (physical) metric has $g_{tt} = -c^2 e^{-\psi}$ (Sec. IV); on the spherically symmetric exterior in the $\mu \to 1$ regime, $\psi(r) = 2GM/(c^2 r) = 2u$ through second order in u, giving

$$\mathcal{L}_{\rm DFD}(u) = e^{\psi} = \exp(2u) \tag{AA2}$$

at that order (Sec. VI A, Eq. (147)); with the parent strain's σ kept the full exterior is the Schwarzschild metric in DFD's coordinates, $\psi = 2u - \frac{4}{3}u^3 + \cdots$ (App. WS). Independently, by Postulate P1 the optical refractive index governing light propagation through the optical metric $d\tilde{s}^2 = -c^2 dt^2/n^2 + d\mathbf{x}^2$ is $n_{\rm DFD}(u) = e^{\psi}$, equal to $\exp(2u)$ at the same order. The lapse-squared $\mathcal{L}_{\rm DFD}$ and the refractive index $n_{\rm DFD}$ are distinct physical quantities arising from different metrics in DFD's two-metric structure, but they coincide as functions of u on the exterior solution. The Padé identity below operates on $\mathcal{L}$ (the clock-rate scalar).

The corresponding Schwarzschild metric in isotropic coordinates takes the form

$$ds^2_{\rm GR,iso} = -\left(\frac{1-u/2}{1+u/2}\right)^2 c^2\,dt^2 + (1+u/2)^4\left(d\rho^2 + \rho^2\,d\Omega^2\right), \tag{AA3}$$

giving the lapse-squared scalar

$$\mathcal{L}_{\rm GR}(u) = \left(\frac{1+u/2}{1-u/2}\right)^2. \tag{AA4}$$

Theorem AA.1 (Padé Identity)**.** *The lapse-squared scalar of isotropic-coordinate Schwarzschild is mathematically identical to the square of the* $[1,1]$ *Padé approximant of* e^u*. Writing* $P_{m,m}(u)$ *for the diagonal* $[m,m]$ *Padé approximant of* $\exp(u)$ *(so* $P_{m,m}(u) \approx e^u$*):*

$$\boxed{\mathcal{L}_{\rm GR}(u) = \left[P_{1,1}(u)\right]^2,} \tag{AA5}$$

where $P_{1,1}(u) = (1+u/2)/(1-u/2)$ *is the unique rational function with degree-1 numerator and denominator whose Taylor expansion matches that of* $\exp(u)$ *through* $O(u^2)$*.*

Proof. The $[1,1]$ Padé approximant of $\exp(u)$ about $u = 0$ is constructed by requiring

$$\frac{a_0 + a_1 u}{1 + b_1 u} = 1 + u + \frac{u^2}{2} + O(u^3). \tag{AA6}$$

Cross-multiplying and matching coefficients at orders u^0, u^1, u^2 gives the unique solution $a_0 = 1$, $a_1 = 1/2$, $b_1 = -1/2$:

$$P_{1,1}(u) = \frac{1+u/2}{1-u/2}. \tag{AA7}$$

Squaring and comparing with (AA4) gives (AA5). □

2. Order-by-Order Agreement

Taylor expanding the exponential and GR's form about $u = 0$:

$$\exp(2u) = 1 + 2u + 2u^2 + \tfrac{4}{3}u^3 + \tfrac{2}{3}u^4 + \tfrac{4}{15}u^5 + O(u^6), \tag{AA8}$$

$$\mathcal{L}_{\rm GR}(u) = 1 + 2u + 2u^2 + \tfrac{3}{2}u^3 + u^4 + \tfrac{5}{8}u^5 + O(u^6). \tag{AA9}$$

The series agree identically through $O(u^2)$, which is the defining property of the $[1,1]$ Padé approximant. They first diverge at $O(u^3)$, with coefficient difference $3/2 - 4/3 = 1/6$. DFD's own lapse-squared agrees with $\exp(2u)$ through $O(u^2)$ in DFD's radius; beyond that order it is Schwarzschild's (App. WS).

TABLE CVII. Taylor coefficients of $\exp(2u)$ and $\mathcal{L}_{\rm GR}$ through $O(u^5)$.

Order n	$[u^n]\exp(2u)$	$[u^n]\mathcal{L}_{\rm GR}$	Difference
0	1	1	0
1	2	2	0
2	2	2	0
3	4/3	3/2	−1/6
4	2/3	1	−1/3
5	4/15	5/8	−43/120

a. PPN consequence. The $O(u)$ and $O(u^2)$ coefficients of $\mathcal{L} = c^2/|g_{tt}|$ are set by the PPN expansion of g_{tt}, from which the post-Newtonian parameter $\beta = 1$ in both theories is read off, consistent with $\beta - 1 = (-4.5 \pm 5.6) \times 10^{-5}$ from Hofmann–Müller [121] lunar laser ranging. The PPN parameter γ is determined by the spatial metric g_{ij} and is *not* accessible from the lapse-squared sector alone; for DFD, $\gamma = 1$ follows from the physical metric $g_{ij} = e^{+\psi}\delta_{ij}$ at first post-Newtonian order and is established in Sec. IV independently of the present identity, consistent with $\gamma - 1 = (2.1 \pm 2.3) \times 10^{-5}$ from Cassini [35]. The two formulations are therefore observationally indistinguishable at all currently measured post-Newtonian orders, with $\beta = 1$ following directly from the Padé identity and $\gamma = 1$ following separately from DFD's physical-metric structure.

3. The Padé Pole is GR's Horizon

The rational approximant (AA4) develops a double pole at $u = 2$, where $1 - u/2 = 0$. In isotropic coordinates this corresponds to $\rho = GM/(2c^2)$. The transformation to standard Schwarzschild coordinates,

$$r = \rho \left(1 + \frac{u}{2}\right)^2, \tag{AA10}$$

maps $u = 2$ (equivalently $\rho = GM/(2c^2)$) to $r = 2GM/c^2$, precisely the Schwarzschild event horizon. The pole is structurally a feature of the rational form.

By contrast, the exponential function $\exp(2u)$ is entire: it has no pole anywhere in the finite complex plane. At $u = 2$ it takes the finite value $\exp(4) \approx 54.598$. In DFD's variables the horizon of a static exterior is reached as $\psi \to \infty$: the lapse $e^{-\psi/2}$ has no zero at finite ψ, and with the parent strain's σ kept DFD's exterior is Schwarzschild's (App. WS), so the pole is a horizon of DFD's black holes as well.

4. Distinction from Yilmaz-Type Exponential Metrics

The exponential refractive-index form of DFD should not be conflated with the Yilmaz–Rosen–Papapetrou exponential metric [163, 164],

$$ds^2_{\text{Yilmaz}} = -e^{-2m/r}\,dt^2 + e^{+2m/r}\left[dr^2 + r^2\,d\Omega^2\right], \tag{AA11}$$

which arises as a solution of Einstein–Klein–Gordon equations with a massless antiscalar field. When analyzed as a 4-metric within GR, (AA11) was shown by Boonserm et al. [165] to represent a traversable wormhole with exotic matter at the throat.

Theorem AA.2 (No wormhole in the DFD flat-$\mathbb{R}^3$ formulation)**.** *On the fundamental flat-$\mathbb{R}^3$ spatial manifold of DFD, there exists no wormhole throat. The areal radius function $R(r) \equiv \sqrt{A(r)/4\pi}$ of the arena metric on any constant-t slice satisfies $R(r) = r$ and $dR/dr = 1$ for all $r > 0$, admitting no minimum; that of the physical metric of a static exterior increases monotonically outside the horizon.*

Proof. DFD postulates a flat Euclidean spatial metric $dl^2 = \delta_{ij}\,dx^i\,dx^j = dr^2 + r^2\,d\Omega^2$. The proper area of a 2-sphere at coordinate radius r is $A(r) = 4\pi r^2$, giving $R(r) = r$. Differentiating, $dR/dr = 1$ identically on $r > 0$. No critical points exist, hence no minimum, hence no throat. With the parent strain's σ kept the physical metric of a static exterior has lapse $e^{-\psi/2} = (1 - 2GM/c^2R)^{1/2}$ and $\det g_{ij} = e^{3\psi}$ (App. WS), so its areal radius R obeys $r^2\,dr = R^2(1 - 2GM/c^2R)\,dR$, that is $r^3 = R^3 - 3(GM/c^2)R^2 + \text{const}$, and $dR/dr = r^2/[R(R - 2GM/c^2)] > 0$ outside the horizon: no minimum there either. By contrast, the Yilmaz metric (AA11) has spatial metric $dl^2 = e^{2m/r}(dr^2 + r^2 d\Omega^2)$, giving $R(r) = r\,e^{m/r}$ with $dR/dr = e^{m/r}(1 - m/r)$, which vanishes at $r = m$ and is a minimum (second derivative $e/m > 0$). The Yilmaz throat is located at $r = m$ with $R_{\min} = em \approx 2.718\,m$. □

Theorem AA.3 (No exotic matter in the DFD fundamental formulation)**.** *DFD's field equation (21) is sourced by ordinary matter density $\rho \geq 0$. The ψ-field energy density $u_\psi = (a_0^2/8\pi G)\,W(|\nabla\psi|^2/a_\star^2)$ is nonnegative for all configurations satisfying the monotonicity condition (A4) of Sec. III A. The physical metric obeys the Einstein–Hilbert equations with this ordinary source (Proposition WS.5); no exotic matter is invoked, and the null energy condition holds.*

Proof. By construction, Eq. (21) is an elliptic PDE for ψ on $\mathbb{R}^3$ sourced by ρ. Under premise G1 of Proposition WS.5 the Einstein–Hilbert term is the dynamics of the physical metric, with the parent strain's σ kept, and its source is the matter stress tensor, which satisfies the null energy condition for ordinary matter. The isotropic exponential exterior would need, in addition, the stress of a massless scalar with negative kinetic energy, Yilmaz's antiscalar: its Einstein tensor is $G^a{}_b = |\nabla U|^2\,\mathrm{diag}(1, -1, 1, 1)$ with $U = GM/(c^2 r)$, which no ordinary source supplies (computed). The nonnegativity of $u_\psi = (a_0^2/8\pi G)\,W(s)$ follows from $W \geq 0$, which holds for $W(X) = X - 2\sqrt{X} + 2\ln\left(1 + \sqrt{X}\right)$, the primitive of the derived $\mu(x) = x/(1+x)$ (see Appendix N). □

a. Ontological distinction. DFD and Yilmaz share the exponential refractive-index form but differ fundamentally:

	DFD	Yilmaz
Fundamental geometry	Flat $\mathbb{R}^3$	Curved 4D Lorentzian
Field content	Parent strain on $\mathbb{R}^3$ (ψ and its traceless part)	Metric $g_{\mu\nu}$ + antiscalar φ
Field equation	Einstein–Hilbert with ordinary $\rho \geq 0$	Einstein–Klein–Gordon
Spatial topology	$\mathbb{R}^3$	Wormhole (throat at $r = m$)
Matter requirement	Ordinary $\rho \geq 0$	Exotic (NEC-violating)
Horizon	GR's event horizon	None (throat instead)

The Boonserm–Visser wormhole/exotic-matter critique applies to (AA11) but not to DFD, because DFD does not treat (AA11) as a fundamental object. The optical metric used in DFD for null-geodesic tracking, $d\tilde{s}^2 = -c^2\,dt^2/n^2 + (e^h)_{ij}\,dx^i dx^j$, is flat in its spatial part only through first post-Newtonian order; the physical metric solves Einstein's equations with ordinary matter where $\mu \to 1$ (App. WS). The Padé identity itself is a statement in the lapse-squared scalar $\mathcal{L} = c^2/|g_{tt}|$, computed in DFD from the matter-coupling physical metric (Sec. IV); on the spherically symmetric exterior this coincides numerically with the optical refractive index, but the two are distinct physical quantities arising from DFD's two-metric structure.

5. The Padé Hierarchy

The $[1,1]$ Padé is the first nontrivial rational approximant of the exponential. Higher-order approximants match the exponential to increasing Taylor order: the squared $[m,m]$ diagonal Padé approximant satisfies

$$\left[P_{m,m}(\exp(u))\right]^2 = \exp(2u) + O(u^{2m+1}). \qquad \text{(AA12)}$$

The full exponential is the $m \to \infty$ limit: the unique entire function agreeing with every order. Any finite-m approximant has at least one pole in the complex plane, which lies on the positive real axis, and so gives a finite-radius singularity, only for odd m.

This hierarchy provides a natural interpretation of extended theories:

- A hypothetical gravity theory with $n(u) = [P_{2,2}(\exp(u))]^2$ would agree with the exponential through $O(u^4)$, i.e. two orders beyond standard PPN, indistinguishable at second post-Newtonian precision before any deviation would appear.
- Each additional Padé order matches two additional orders in u.
- The exponential is singled out not by any specific post-Newtonian test but by the simplicity and analyticity of its underlying functional equation — Cauchy's multiplicative composition law (Sec. II) — which admits no pole structure at all.

6. Framing Summary

Padé Identity: Structural Framing

Core identity (Theorem AA.1):

$\mathcal{L}_{\rm GR}(u) = [P_{1,1}(\exp(u))]^2$, $\quad \mathcal{L}_{\rm DFD}(u) = \exp(2u) + O(u^3)$,

where $\mathcal{L}(u) \equiv c^2/|g_{tt}|$ is the lapse-squared scalar (clock-rate / redshift observable). **GR's isotropic lapse-squared is the $m = 1$ slot of the Padé hierarchy of the exponential.**

Weak-field (observational) consequence: Agreement through $O(u^2)$ by construction of the Padé approximant. PPN parameter $\beta = 1$ in both theories follows directly from the lapse identity, matching LLR at $\lesssim 10^{-4}$. PPN parameter $\gamma = 1$ for DFD follows separately from the physical-metric structure $g_{ij} = e^{+\psi}\delta_{ij}$ at first post-Newtonian order (Sec. IV), matching Cassini at $\lesssim 10^{-5}$.

Strong-field consequence: First divergence of the two functions at $O(u^3)$; pole at $u = 2$, the Schwarzschild horizon $r = 2GM/c^2$. With the parent strain's σ kept DFD's exterior is the Schwarzschild metric in DFD's coordinates (App. WS), so the pole is a horizon of DFD's black holes too, and DFD's photon sphere and shadow are Schwarzschild's.

Firewall from Yilmaz: DFD's fundamental arena is flat $\mathbb{R}^3$; its spatial topology is globally trivial; its matter source is ordinary $\rho \geq 0$, and its exterior is Schwarzschild's, not Yilmaz's. Theorems AA.2 and AA.3 establish that the Boonserm–Visser wormhole/exotic-matter critique of (AA11) does not apply to DFD.

Appendix AB: Uniqueness of the Internal Manifold $\mathbb{C}P^2 \times S^3$

The preceding appendices have used the internal manifold $X = \mathbb{C}P^2 \times S^3$ for the Standard Model gauge structure, the generation count, the fine-structure constant, the CKM pattern, the Strong-CP vanishing, and the G–H_0 invariant. A natural question is whether this manifold is an ansatz or whether it is uniquely forced by first principles. This appendix closes that gap: we show that $X = \mathbb{C}P^2 \times S^3$ is the unique compact internal manifold satisfying a finite list of axioms motivated by the optical structure of DFD, the observed Standard Model gauge group, and the observed generation count.

1. Vacuum Axioms

We seek a compact Riemannian manifold X —the internal fiber of the vacuum on which the refractive field ψ lives— satisfying:

(V1) Compactness and smoothness. X is a compact, connected, smooth, orientable Riemannian manifold without boundary.

(V2) Minimality. $\dim X$ is minimal among all X satisfying the remaining axioms. *The value* $\dim X = 7$ *is not assumed: it is derived in Corollary AB.3, together with the split* $7 = 4 + 3$. An isometric $(3, 2, 1)$ partition cannot justify it (see Lemma AB.13).

(V3) *Not an axiom.* Every closed orientable 4-manifold and every closed 3-manifold admits a Spin^c structure, so this condition selects nothing within the class considered. Spin^c-ness of the winner — needed for the Dirac operator and the Spin^c HRR index of Appendix K 4 — is recovered as Corollary AB.12.

(V4) Nondegenerate product structure. $X = M_c \times M_g$ where M_c is a compact Kähler manifold and M_g is a compact manifold with $\dim M_g \geq 1$. The complex factor supplies the chiral (holomorphic) Yukawa structure; the frame factor supplies the topological protection mechanisms. *(V4) does not require "a compact Lie group or group quotient":* that clause is simultaneously too strong (the group structure is never used) and fatally too weak (the quotient branch admits $M_g = S^2 = \mathrm{SU}(2)/\mathrm{U}(1)$, which is simply connected with $\pi_3(S^2) = \mathbb{Z}$ and would give $\dim X = 6$, defeating minimality). (V4′) is used instead.

(V4′) Global transgression frame. M_g is parallelizable. The Chern–Simons transgression that defines the χ sector is framing-dependent, so a global frame on M_g is what makes that sector globally well defined. *Only the consequence* $\chi_{\mathrm{top}}(M_g) = 0$ *is used in the proof below.*

(V5) Three generations. $\chi_{\mathrm{top}}(M_c) = 3$, supplying the generation count by identification: the observed family number is an input, and no index on the internal space supplies it (App. F, Rem. F.21). *The side-condition* $\dim_{\mathbb{C}} M_c \geq 2$ *is not assumed: it follows from (V5)+(V10), since the only Fano curve is* $\mathbb{C}P^1$ *with* $\chi_{\mathrm{top}} = 2$ *(Corollary AB.3, Step 1).*

(V6) Internal mode partition $(3, 2, 1)$ **— a dictionary entry, not a selector.** The rank-6 *internal mode bundle* $\mathcal{H}_{\mathrm{int}} = \mathbb{C}^3 \oplus \mathbb{C}^2 \oplus \mathbb{C}$ of Sec. XVII B carries the block partition $(n_3, n_2, n_1) = (3, 2, 1)$ of *complex* ranks, whose $U(6)$ stabiliser is $U(3) \times U(2) \times U(1)$, that is $\mathrm{SU}(3) \times \mathrm{SU}(2)$ with two abelian factors modulo the overall phase, together with a singlet sector. Under the electroweak identification the single hypercharge is the abelian factor of the isotropy split $\mathbb{C}^3 = \ell_p^{\perp} \oplus \ell_p$ of $\mathbb{C}P^2$, whose stabiliser is $S(U(2) \times U(1)) = U(2)$ (App. F, Rem. F.2). This is a condition on an associated bundle over spacetime, *not* on TX: by Lemma AB.13 the tangent bundle of any $\mathbb{C}P^2 \times N^3$ admits *no* splitting into subbundles of real ranks $(3, 2, 1, 1)$, and none is required. *(V6) is not used in the proof of Theorem AB.1; it is recorded here only to fix the dictionary. No isometric* $(3, 2, 1, 1)$ *splitting of* TX *is asserted.*

(V7) Simply connected frame factor. $\pi_1(M_g) = 1$. $\pi_3(M_g) = \mathbb{Z}$ *is then a theorem, not an axiom: see Corollary AB.12. The winding number of Theorem F.26 is therefore derived from the internal geometry rather than posited. Simple connectedness is also the strictly stronger of the two bits: assuming* $\pi_3 = \mathbb{Z}$ *instead leaves* M_g *ranging over the infinite family* $\{S^3/\Gamma\} \cup \{S^2 \times S^1, \mathbb{R}P^3 \# \mathbb{R}P^3\}$, *i.e. no uniqueness at all.*

(V8) *Not an axiom: it is a theorem.* Since $\dim T_{\mathrm{CP}} = \dim X + 1$ and $\dim X = 7$ is odd (Corollary AB.3), $\dim T_{\mathrm{CP}} = 8$ is automatically even, so $\eta(D_{T_{\mathrm{CP}}}) = 0$ by the spectral-symmetry theorem of Appendix L. Recorded as Corollary AB.12.

(V10) Positive internal curvature. M_c admits a Kähler metric of positive Ricci curvature. This is the stiffness hypothesis that Lemma AB.4 needs; without it that lemma is *false*, with two counterexample families (see the remark following it). By Kobayashi's theorem it also forces M_c to be Fano and simply connected.

a. Remark on the axiom count. The list above has *seven* substantive statements — (V1), (V2), (V4), (V4′), (V5), (V7), (V10) — and it is satisfiable, with the explicit witness verified axiom-by-axiom in Lemma AB.11.

An axiom asserting a splitting of TX into subbundles of real ranks $(3, 2, 1, 1)$ would make the list unsatisfiable: Lemma AB.13 shows that such a splitting is topologically impossible on $\mathbb{C}P^2 \times N^3$ for every closed 3-manifold N, and an unsatisfiable axiom set makes a uniqueness theorem *vacuously* true, which is a worse failure mode than losing uniqueness. Four properties are *theorems* rather than assumptions: $\dim X = 7$, Spin^c, $\pi_3(M_g) = \mathbb{Z}$, and even mapping-torus dimension; and $k_{\max} = 60$ is a computed property of the winner. $k_{\max} = 60$ *is not claimed to follow from (V2), (V4) and (V6):* that implication would need the tangent-bundle reading of (V6), which (V6) above does not make. $k_{\max} = 60$ is established for the winner by Hirzebruch–Riemann–Roch (Corollary AB.12(iv)), not by an axiom.

2. Uniqueness Theorem

Theorem AB.1 (Uniqueness of $\mathbb{C}P^2 \times S^3$)**.** *Let X satisfy axioms (V1), (V2), (V4), (V4′), (V5), (V7), (V10). Then M_c is biholomorphic to $\mathbb{C}P^2$, M_g is diffeomorphic to S^3, and up to diffeomorphism*

$$\boxed{X = \mathbb{C}P^2 \times S^3.} \tag{AB1}$$

The axiom set is satisfiable — the manifold (AB1) *is an explicit model for it (Lemma AB.11) — so the statement is not vacuous.*

Remark AB.2 (What is and is not fixed). The axioms fix the smooth structure of X and the complex structure of M_c; they do not fix the metric. The Fubini–Study scale and the S^3 radius remain as two continuous moduli, pinned downstream by the $k_{\max} = 60$ / α^{57} closure (Appendix O). "Up to diffeomorphism" is exact; "up to isometry" would overstate it.

The proof proceeds by reducing each axiom to a structural constraint and showing that the intersection of these constraints admits a unique solution.

3. Reduction of the Axioms

a. *Dimension, product structure, and the split $7 = 4 + 3$*

Corollary AB.3 (Internal dimension — $\dim X = 7$ is derived)**.** *Under (V1), (V4), (V4′), (V5), (V7), (V10) the dimensions obey $\dim_{\mathbb{R}} M_c \geq 4$ and $\dim M_g \geq 3$; both bounds are attained simultaneously. Hence by minimality (V2),*

$$\dim X = 4 + 3 = 7,$$

and the split $7 = 4 + 3$ is forced.

Proof. **Step 1: $\dim_{\mathbb{R}} M_c \geq 4$.** By (V10) and Kobayashi's theorem, a compact Kähler manifold carrying a metric of positive Ricci curvature is Fano and simply connected. A 0-dimensional Fano manifold is a point, $\chi_{\text{top}} = 1$; a Fano curve has $\deg K < 0$, hence genus 0, hence is $\mathbb{C}P^1$ with $\chi_{\text{top}} = 2$. Both contradict (V5). So $\dim_{\mathbb{C}} M_c \geq 2$.

Step 2: $\dim M_g \geq 3$. M_g is closed, connected (X is), orientable (X and M_c are), of dimension ≥ 1 by (V4), simply connected by (V7), and parallelizable by (V4′) — hence it admits a nowhere-vanishing vector field and $\chi_{\text{top}}(M_g) = 0$ by Poincaré–Hopf. In dimension 1 the only closed connected orientable manifold is S^1, excluded by (V7). In dimension 2 the closed connected orientable manifolds are S^2 and the genus-g surfaces; the latter have $\pi_1 \neq 1$, and S^2 has $\chi_{\text{top}} = 2 \neq 0$, excluded by (V4′). (Dimension 0 is excluded by the nondegeneracy clause of (V4); note Poincaré–Hopf does not reach it, since $\chi(\text{pt}) = 1$.)

Step 3: attainment. $\mathbb{C}P^2 \times S^3$ satisfies every axiom (Lemma AB.11) with $\dim = 7$. Hence the minimum in (V2) is exactly 7, and since $\dim M_c + \dim M_g = 7$ with $\dim M_c \geq 4$, $\dim M_g \geq 3$, the split is forced to $4 + 3$. □

b. *Identification of $M_c^{(4)}$*

Lemma AB.4 (Kähler surface with $\chi = 3$ and positive Ricci)**.** *A compact Kähler surface admitting a metric of positive Ricci curvature and having $\chi_{\text{top}} = 3$ is biholomorphic to $\mathbb{C}P^2$.*

Proof. By Kobayashi's theorem the surface is Fano, i.e. del Pezzo. Noether's formula $\chi_{\text{top}} = 12\chi(\mathcal{O}) - K^2$ with $\chi(\mathcal{O}) = 1$ gives $\chi_{\text{top}} = 3$ for $\mathbb{C}P^2$ ($K^2 = 9$), 4 for $\mathbb{C}P^1 \times \mathbb{C}P^1$ ($K^2 = 8$), and $3 + k$ for $\mathrm{dP}_k = \mathrm{Bl}_k\mathbb{C}P^2$ ($K^2 = 9 - k$, $1 \leq k \leq 8$), i.e. $4, \ldots, 11$. Exactly one entry equals 3. □

Remark AB.5 (Why the positivity hypothesis is not optional). Without (V10) the lemma is false, and a Spin^c hypothesis does not save it (every compact complex surface is Spin^c via c_1). Two counterexample families have $\chi_{\text{top}} = 3$: (i) the fake projective planes, ball quotients $\mathbb{B}^2/\Gamma$ with $p_g = q = 0$, $c_1^2 = 9$, $c_2 = 3$ and K ample — 100 of them, in 50 conjugate pairs; and (ii) the infinite family $\mathrm{Bl}_{4g-1}(C_g \times \mathbb{C}P^1)$ for a genus-g curve C_g, which has $\chi_{\text{top}} = 4 - 4g + k = 3$ for every $g \geq 1$. Both have infinite π_1, so Kobayashi's simple-connectedness conclusion removes both at once.

c. *Identification of $M_g^{(3)}$*

Lemma AB.6 (Frame factor)**.** *A closed, connected, orientable, simply connected 3-manifold is diffeomorphic to S^3; consequently $\pi_3(M_g) = \mathbb{Z}$.*

Proof. This is the Poincaré conjecture, proved by Perelman (2003). The homotopy statement then follows from $\pi_3(S^3) = \mathbb{Z}$ (Hopf degree). □

Remark AB.7 (The lens-quotient menu is removed by proof, not by selection). A 12-member discrete menu

$L(p,1) = S^3/\mathbb{Z}_p$, $p \mid 60$, priced in the trials-factor audit of App. CE, fails twice over. First, it is an *undercount*: the quotient branch of a group-quotient clause in (V4) would also admit every spherical space form S^3/Γ with $\Gamma < \mathrm{SU}(2)$ finite (binary dihedral, tetrahedral, octahedral, icosahedral — not only cyclic), together with $S^1 \times S^2 = (\mathrm{U}(1) \times \mathrm{SU}(2))/\mathrm{U}(1)$, which is a compact homogeneous 3-manifold with $\pi_3 = \mathbb{Z}$ and is not a lens space at all. Second, the entire menu is removed by *proof*: every member has $\pi_1 \neq 1$ and is excluded by (V7), and Lemma AB.6 then leaves S^3 as the unique survivor. The $\times 12$ price is therefore not owed in the App. CE trials audit (which keeps it only as a hostile over-count), and the one discrete bit that remains — simple connectedness of M_g, axiom (V7) — is the only price on this coordinate: $\pi_3(M_g) = \mathbb{Z}$ is derived, not assumed.

A group-quotient clause in (V4) would leave a second loophole. $S^2 = \mathrm{SU}(2)/\mathrm{U}(1)$ is a compact group quotient, is simply connected, and has $\pi_3(S^2) = \mathbb{Z}$ by the Hopf fibration; so $X' = \mathbb{C}P^2 \times S^2$ would satisfy (V1), (V4) with that clause, (V5) and (V7) at $\dim X' = 6$, and no minimality argument could produce $\dim X = 7$. Axiom (V4′) removes S^2 — and only S^2 — via $\chi_{\mathrm{top}}(S^2) = 2 \neq 0$.

Proposition AB.8 (Exhaustive invariants of the 12-member lens menu, and a charge-quantization interlock)**.** *For all twelve members $L(p,1)$, $p \mid 60$, of the menu of Remark AB.7: the real Betti numbers of $\mathbb{C}P^2 \times L(p,1)$ are identically $(1,0,1,1,1,1,0,1)$, independent of p; the torsion is $H_1 = H_3 = H_5 = \mathbb{Z}_p$ with $H^2_{\mathrm{tors}} = \mathbb{Z}_p$; and $\mathrm{Isom}^0 = U(1) \times \mathrm{SU}(2)$ for $p \geq 3$ but $\mathrm{SO}(3) \times \mathrm{SO}(3)$ for $p = 2$. No twist restores a full doublet for any $p \geq 3$. Consequently every $p \geq 2$ predicts* discrete charge hair *on the $\mathbb{Z}_p$ torsion classes, whereas DFD's $p = 1$ predicts* none.

Falsifier AB.9 (Charge quantization). Observation of discrete $\mathbb{Z}_p$ charge hair — a quantized charge label with no continuous gauge-field source — selects $p \geq 2$ and reopens the lens menu, falsifying axiom (V7), which removes the menu in Remark AB.7. DFD predicts no such hair.

Remark AB.10 (Trials-factor: the $\times 12$ improvement is declined). It is tempting to argue that Proposition AB.8 collapses the 12-member menu and improves the App. CE α-ladder margin from $\times 159.8$ to $\times 1918$. That improvement is **declined**: $\chi(\mathbb{C}P^2, E) = 60$ is a Hirzebruch–Riemann–Roch statement on the $\mathbb{C}P^2$ factor alone and is untouched by an S^3 quotient, so the menu is not reduced by this route. The margin stays at $\times 159.8$.

d. *Consistency with remaining axioms*

Lemma AB.11 (Satisfiability — the axiom set has a model)**.** *The manifold $X = \mathbb{C}P^2 \times S^3$, carrying the Fubini–Study metric on the first factor and the round metric on the second, satisfies (V1), (V2), (V4), (V4′), (V5), (V7), (V10) simultaneously. In particular Theorem AB.1 is not vacuous.*

Proof. (V1) A product of two closed orientable manifolds is closed and orientable, and both factors are connected.

(V4) $\mathbb{C}P^2$ is compact Kähler; the Fubini–Study metric arises from the Kähler potential $K = \log\bigl(1 + |z|^2\bigr)$ on an affine chart, with $g_{i\bar{\jmath}} = \partial_i \bar{\partial}_{\bar{\jmath}} K$ and $\det g = (1 + |z|^2)^{-3}$. S^3 is compact of dimension $3 \geq 1$.

(V4′) $S^3 \subset \mathbb{H}$ is parallelizable: $q \mapsto (q\mathbf{i}, q\mathbf{j}, q\mathbf{k})$ is a global orthonormal frame of TS^3, since right multiplication by a unit imaginary quaternion is an isometry of $\mathbb{R}^4$ carrying $q^\perp$ to itself. Hence $\chi_{\mathrm{top}}(S^3) = 0$.

(V10) $\det g = (1 + |z|^2)^{-3}$ gives $\mathrm{Ric}_{i\bar{\jmath}} = -\partial_i \bar{\partial}_{\bar{\jmath}} \log \det g = 3\, g_{i\bar{\jmath}}$, so the Fubini–Study metric is Kähler–Einstein with positive Einstein constant; the induced real metric satisfies $\mathrm{Ric}_{\mathbb{R}} = 3\, g_{\mathbb{R}} > 0$. (In the normalisation with holomorphic sectional curvature 4 this reads $\mathrm{Ric} = 6g$; positivity is scale-free.) The round S^3 of radius 1 has $\mathrm{Ric} = 2g > 0$.

(V5) By Chern–Weil applied to the curvature $\Theta = \bar{\partial}(g^{-1}\partial g)$ of the same Fubini–Study metric, $\mathrm{tr}\,\Theta = -3g$ (so $c_1 = 3H$), $\int_{\mathbb{C}P^2} c_1^2 = 9$, and

$$\chi_{\mathrm{top}}(\mathbb{C}P^2) = \int_{\mathbb{C}P^2} c_2 = \int_{\mathbb{C}P^2} \tfrac{1}{2}\Bigl(\tfrac{i}{2\pi}\Bigr)^2 \bigl[(\mathrm{tr}\,\Theta)^2 - \mathrm{tr}(\Theta \wedge \Theta)\bigr] = 3.$$

(V7) $\pi_1(S^3) = 1$.

(V2) By Corollary AB.3 no admissible X has dimension below 7, and this one has dimension $4 + 3 = 7$; so it realises the minimum. □

Corollary AB.12 (Properties of the winner: Spin^c, π_3, the even mapping torus and $k_{\max}$)**.** *For $X = \mathbb{C}P^2 \times S^3$:* (i) *$X$ is Spin^c: $c_1(\mathbb{C}P^2) = 3H$ supplies the determinant line $\mathcal{O}(3)$, and S^3 is parallelizable hence spin; the product carries the product Spin^c structure.* (ii) $\pi_3(M_g) = \pi_3(S^3) = \mathbb{Z}$ *— the winding invariant of Theorem F.26,* derived *(Lemma AB.6).* (iii) $\dim T_{\mathrm{CP}} = \dim X + 1 = 8$ *is even, so $\eta(D_{T_{\mathrm{CP}}}) = 0$ by Theorem L.1. The CP involution is complex conjugation $[z_0 : z_1 : z_2] \mapsto [\bar{z}_0 : \bar{z}_1 : \bar{z}_2]$ on $\mathbb{C}P^2$ times the identity on S^3.* (iv) $\chi(\mathbb{C}P^2, \mathcal{O}(9) \oplus \mathcal{O}^{\oplus 5}) = 55 + 5 = 60 = k_{\max}$ *by Hirzebruch–Riemann–Roch, and $57 = k_{\max} - N_{\mathrm{gen}}$.*

e. *Uniqueness assembly*

Proof of Theorem AB.1. Corollary AB.3 forces $\dim M_c = 4$ and $\dim M_g = 3$. Lemma AB.4 then gives $M_c \cong \mathbb{C}P^2$ and Lemma AB.6 gives $M_g \cong S^3$. Lemma AB.11 exhibits that manifold as a model of the full axiom set, so the solution set is non-empty and the theorem is not vacuous. Uniqueness up to diffeomorphism follows. □

4. Tangent-Bundle Obstruction Lemma

Lemma AB.13 (No $(3,2,1,1)$ splitting of the internal tangent bundle)**.** *Let N be any closed 3-manifold. Then*

$T(\mathbb{C}P^2 \times N)$ admits no splitting into subbundles of real ranks $3, 2, 1, 1$.

Proof. Restrict a putative splitting to the slice $\mathbb{C}P^2 \times \{\mathrm{pt}\}$; restriction preserves ranks, so it suffices to obstruct a $(3, 2, 1, 1)$ splitting of $T\mathbb{C}P^2 \oplus \varepsilon^3$. Write $H^*(\mathbb{C}P^2; \mathbb{Z}/2) = \mathbb{Z}/2[a]/(a^3)$, $\deg a = 2$. Since $H^1 = H^3 = 0$, every real line subbundle is trivial and a rank-2 or rank-3 subbundle has total class $1 + \epsilon a$ with $\epsilon \in \mathbb{Z}/2$. The total class is unchanged by adding trivial summands: $w(T\mathbb{C}P^2 \oplus \varepsilon^3) = (1 + a)^3 = 1 + a + a^2 \pmod 2$. Whitney then requires

$$(1 + \epsilon a)(1 + \eta a) \;=\; 1 + (\epsilon + \eta)a + \epsilon\eta\, a^2 \;=\; 1 + a + a^2,$$

i.e. $\epsilon + \eta = 1$ and $\epsilon\eta = 1$ simultaneously; the second forces $\epsilon = \eta = 1$, whence $\epsilon + \eta = 0 \neq 1$. Contradiction. □

Remark AB.14 (What TX does split into, and what (V6) is about). The obstruction is sharp: an exhaustive check over all rank partitions of 7 finds $(3, 3, 1)$, $(3, 2, 1, 1)$, $(3, 1, 1, 1, 1)$, $(2, 2, 1, 1, 1)$, $(2, 1^5)$ and (1^7) obstructed while the neighbours $(4, 3)$, $(3, 2, 2)$ and $(2, 2, 2, 1)$ are allowed. The genuine decomposition comes from the Euler sequence $T\mathbb{C}P^2 \oplus \mathbb{C} = \mathcal{O}(1)^{\oplus 3}$, giving

$$TX = \pi^*\mathcal{O}(1)_{\mathbb{R}}^{\oplus 3} \oplus \varepsilon_{\mathbb{R}},$$

real ranks $(2, 2, 2, 1)$ with abelian structure group $\mathrm{U}(1)^3 \times \mathrm{O}(1)$ — not $\mathrm{SU}(3) \times \mathrm{SU}(2) \times \mathrm{U}(1)$. Independent group-theoretic corroboration: the minimal faithful *real* representation dimensions are 6, 4, 2 for SU(3), SU(2), U(1), against slots of dimension 3, 2, 1; and $\dim \mathrm{Isom}(S^3) = \dim \mathrm{O}(4) = 6 < 8 = \dim \mathrm{SU}(3)$, so no sub-object of the S^3 factor can carry colour under any partition. The $(3, 2, 1)$ of (V6) is the block structure of the *complex* mode bundle $\mathcal{H}_{\mathrm{int}} = \mathbb{C}^3 \oplus \mathbb{C}^2 \oplus \mathbb{C}$ (Sec. XVII B), an associated bundle over spacetime, not a splitting of TX.

5. Integer Cohomology and Standard Model Parameters

Once $X = \mathbb{C}P^2 \times S^3$ is established, the integers appearing throughout the Standard Model parameter derivations acquire a uniform topological interpretation:

Integer	Origin	Role
3	$\dim S^3 = \chi_{\mathrm{top}}(\mathbb{C}P^2)$	generations, CKM integer $\times\alpha^3$
7	$\dim X$	internal dimension, gauge partition
8	$\dim T_{\mathrm{CP}}$	Strong-CP vanishing
13	$3 + 10$	Weinberg angle denominator (3/13)
19	$h^0(\mathcal{O}(1)) + h^0(\mathcal{O}(2)) + h^0(\mathcal{O}(3))$	Λ_{QCD} exponent 19/2 (selected); baryon-octet intercept
31	line-bundle section count	CKM λ integer
$49 = 7^2$	$(\dim X)^2$	CKM $\bar\eta$ integer
$57 = k_{\max} - N_{\mathrm{gen}}$	Toeplitz rank minus generations	$G\hbar H_0^2/c^5$ exponent
60	$\chi(\mathbb{C}P^2, E) = \lvert A_5\rvert$	Toeplitz truncation rank
$108 = 3 \cdot 36$	$N_{\mathrm{gen}} \cdot h^0$	CKM A integer
137	spectral weighted sum	α^{-1}

These are not free parameters: they are fixed by the unique manifold (AB1) together with the stated inputs and identifications of App. FK.

6. Falsifiability

Theorem AB.1 supports a sharp falsification criterion:

- Discovery of a fourth generation (violating (V5)) would falsify the identification in (V5).
- A confirmed deviation of $\sin^2\theta_W$ from 3/13 after radiative corrections, or of α^{-1} from 137.036 beyond systematic uncertainty, would challenge the mode-bundle block structure of (V6) or the Toeplitz closure of Corollary AB.12(iv) — not any property of TX.
- A robust detection of $|\bar\theta| > 10^{-15}$ in neutron or atomic EDM experiments would falsify the tree-level $\bar\theta = 0$ and its loop bound (Theorem L.3).
- Any compact manifold other than $\mathbb{C}P^2 \times S^3$ satisfying (V1), (V2), (V4), (V4′), (V5), (V7), (V10) would falsify Theorem AB.1 by counterexample. *Conversely, exhibiting that no manifold at all satisfies the list would render the theorem vacuous; that is why Lemma AB.11 exhibits an explicit model.*

a. Status. The uniqueness theorem is theorem-grade conditional on the seven axioms (V1), (V2), (V4), (V4′),

(V5), (V7), (V10); uniqueness among all compact 7-manifolds without these axioms would need an exhaustive classification and is not claimed. The axioms are *satisfiable* — an explicit model is exhibited in Lemma AB.11 — and each is used. The list is closed, and four properties are theorems here: $\dim X = 7$, Spin^c, $\pi_3(M_g) = \mathbb{Z}$, and even mapping-torus dimension. The single discrete bit that remains on the M_g coordinate is simple connectedness (V7); it is the only price on that coordinate, and neither a $\pi_3 = \mathbb{Z}$ axiom nor the $\times 12$ lens menu is needed (App. CE keeps the menu only as a hostile over-count).

7. Summary

Uniqueness of the Internal Manifold

Statement (Theorem AB.1): The unique compact internal manifold satisfying DFD's seven vacuum axioms — compactness, minimality of dimension, nondegenerate Kähler-times-framed product structure, positive internal Ricci curvature, $\chi_{\text{top}}(M_c) = 3$, and simple connectedness of the frame factor — is $X = \mathbb{C}P^2 \times S^3$, up to diffeomorphism. The axiom set is satisfiable: that manifold is an explicit model of it.
Derived, not assumed: $\dim X = 7$ and the split $7 = 4 + 3$; $\pi_3(M_g) = \mathbb{Z}$; the Spin^c structure; the even mapping-torus dimension behind Strong-CP; and $k_{\max} = 60$, through the conditional determinant-line count of App. F given the generation count, the flux quantum and the five multiplet types.
Implication: The integers $\{3, 7, 8, 13, 19, 31, 49, 57, 60, 108, 137\}$ appearing throughout the Standard Model and cosmology are not free: they are fixed by this unique manifold together with the stated inputs and identifications of App. FK.
Falsifier: Any exhibited compact manifold $X' \neq \mathbb{C}P^2 \times S^3$ satisfying the same seven axioms; or any observation of a fourth generation (violating (V5)).
Consequence: Combined with the α^{57} dimensionless constraint (Appendix O), DFD's scale sector has *one measured continuous coefficient* — the clock normalization C of the early clock in $(H_0 t_P)^2 = C\,\alpha^{57}$, equivalently $\lambda = C^{-1/2}$ of Postulate ZS.11 ($C = 1$ on bound-matter clocks), proven underivable from the printed corpus by the eight-route no-go (Rem. AP.6); the continuous calibrations of the cosmological prediction set are graded in App. FK (Rem. FK.8). The internal geometry is fixed up to the discrete selections booked in Remark AB.7 and priced in the trials-factor audit (Sec. CE 2).

Appendix AC: Linear Growth Closure from the EFE-Screened DFD Operator

1. AC.1 Purpose

This appendix derives the first-order linear response operator of DFD's spatial sector. The temporal dust branch (Appendix Q) proves that the scalar completion has $w \to 0$ and $c_s^2 \to 0$ for homogeneous deviations only. Here we prove the spatial perturbation operator and evaluate it at the external field of the Hubble-EFE hypothesis.

Cross-reference: cosmological scope of the Hubble-EFE Hypothesis

The linear response operator derived below is correct mathematics for any background gradient $|\nabla\bar{\psi}|$. The numerical 1.02–1.17 G envelope below depends on the named Hubble-EFE Hypothesis $a_{\text{ext}}(z) = cH(z)$. Appendix AE establishes that the FRW background of the DFD action gives $|\nabla\bar{\psi}| = 0$, so the Hubble-EFE Hypothesis is not what comes out of the action for cosmological perturbations. On galactic and cluster scales the external field is set by local matter, and the response operator is unchanged.

2. AC.2 Linearization of the Nonlinear Spatial Operator

The quasi-static DFD field equation is

$$\nabla \cdot [\mu(x)\nabla\psi] = -\frac{8\pi G}{c^2}\rho, \qquad x = \frac{|\nabla\psi|}{a_\star}. \tag{AC1}$$

Let

$$\psi = \bar{\psi} + \varphi, \qquad \rho = \bar{\rho}(1+\delta), \tag{AC2}$$

and define the background quantities

$$\bar{g}_i = \partial_i\bar{\psi}, \qquad \bar{x} = \frac{|\bar{g}|}{a_\star}, \qquad \hat{g}_i = \frac{\bar{g}_i}{|\bar{g}|}. \tag{AC3}$$

The flux is

$$F_i(\nabla\psi) = \mu(x)\,\partial_i\psi. \tag{AC4}$$

Lemma AC.1 (First variation of the flux)**.** *The first variation of F_i around the background is*

$$\delta F_i = M_{ij}\,\partial_j\varphi, \tag{AC5}$$

with

$$\boxed{M_{ij} = \mu_0\,\delta_{ij} + \mu_{\ln,0}\,\hat{g}_i\hat{g}_j,} \tag{AC6}$$

where

$$\mu_0 = \mu(\bar{x}), \qquad \mu_{\ln,0} = \left.\frac{d\mu}{d\ln x}\right|_{\bar{x}} = \bar{x}\,\mu'(\bar{x}). \tag{AC7}$$

Proof. Direct chain-rule computation. $F_i = \mu(x)\partial_i\psi$. Vary: $\delta F_i = \mu(x)\partial_i\varphi + \mu'(x)\,\delta x\,\partial_i\bar{\psi}$, with $\delta x = (\hat{g}_j/a_\star)\partial_j\varphi$. Substituting and rearranging gives $\delta F_i = \mu_0\delta_{ij}\partial_j\varphi + (\bar{x}\mu'(\bar{x}))\hat{g}_i\hat{g}_j\partial_j\varphi$, which is the stated form. □

Remark AC.2 (Notation). The response coefficient appearing in the linear operator is $\mu_{\ln,0} = \bar{x}\mu'(\bar{x}) = \bar{x}/(1+\bar{x})^2$ for $\mu(x) = x/(1+x)$, i.e. $d\mu/d\ln x$; it is not $d\mu/dx = 1/(1+\bar{x})^2$. This appendix uses $\mu_{\ln,0}$ throughout.

In Fourier space, the linearized field equation becomes

$$k_i M_{ij} k_j \, \varphi_k = \frac{8\pi G}{c^2} \bar{\rho}\, \delta_k. \tag{AC8}$$

Matter acceleration is $\mathbf{a}_\varphi = (c^2/2)\nabla\varphi$. The growth equation is therefore

$$\ddot{\delta}_k + 2H\dot{\delta}_k = 4\pi G_{\rm eff}(\bar{x},\theta)\,\bar{\rho}\,\delta_k, \tag{AC9}$$

where

$$\boxed{G_{\rm eff}(\bar{x},\theta) = \frac{G}{\mu_0 + \mu_{\ln,0}\cos^2\theta},} \tag{AC10}$$

and $\cos\theta = \hat{k}\cdot\hat{g}$.

3. AC.3 Specialization to the DFD Interpolation Function

For $\mu(x) = x/(1+x)$ (Theorem N.8), one has

$$\mu_0 = \frac{\bar{x}}{1+\bar{x}}, \qquad \mu_{\ln,0} = \frac{\bar{x}}{(1+\bar{x})^2}. \tag{AC11}$$

Hence

$$\boxed{G_{\rm eff}^{\rm DFD} = G\left[\frac{\bar{x}}{1+\bar{x}} + \frac{\bar{x}}{(1+\bar{x})^2}\cos^2\theta\right]^{-1},} \tag{AC12}$$

or equivalently

$$G_{\rm eff}^{\rm DFD} = \frac{G}{\mu_0}\,\frac{1}{1+q\cos^2\theta}, \qquad q = \frac{\mu_{\ln,0}}{\mu_0} = \frac{1}{1+\bar{x}}. \tag{AC13}$$

4. AC.4 Cosmological External-Field Screening

The cosmological external field supplied by the Hubble flow is

$$a_{\rm ext}(z) \sim cH(z). \tag{AC14}$$

This is the Hubble-EFE hypothesis, named explicitly so it can be tested independently.

Hubble-EFE Hypothesis (named for testability)

The cosmological external acceleration relevant to the EFE screening of linear cosmological perturbations is

$$a_{\rm ext}(z) = cH(z). \tag{AC15}$$

This hypothesis is named explicitly so that it can be tested independently. The 1.02–1.17G growth envelope follows from this hypothesis combined with the epoch-consistent $a_0(z) = 2\sqrt{\alpha}\,cH(z)$ relation.

The epoch-consistent DFD crossover scale is

$$a_0(z) = 2\sqrt{\alpha}\,cH(z). \tag{AC16}$$

Therefore the external-field argument is

$$\boxed{\bar{x}_{\rm EFE} = \frac{a_{\rm ext}(z)}{a_0(z)} = \frac{1}{2\sqrt{\alpha}} \simeq 5.85.} \tag{AC17}$$

This is independent of redshift if the same epoch-consistency rule that fixes $a_0(z)$ is used.

At $\bar{x} = 5.85$,

$$\mu_0 = 0.854, \qquad \mu_{\ln,0} = 0.125. \tag{AC18}$$

Thus the directional envelope is

$$G_\perp = \frac{G}{\mu_0} = 1.171\,G, \qquad G_\parallel = \frac{G}{\mu_0+\mu_{\ln,0}} = 1.021\,G. \tag{AC19}$$

The angular mean is

$$\langle G_{\rm eff}\rangle = \frac{G}{\mu_0}\,\frac{\arctan\sqrt{q}}{\sqrt{q}}, \qquad q = \frac{1}{1+\bar{x}} = 0.146, \tag{AC20}$$

giving

$$\boxed{\langle G_{\rm eff}\rangle \simeq 1.12\,G.} \tag{AC21}$$

5. AC.5 First Numerical Growth Estimates

We integrate the standard linear growth equation

$$D'' + \left[2 + \frac{d\ln H}{d\ln a}\right] D' - \frac{3}{2}\,Q\,\Omega_m(a)\,D = 0, \tag{AC22}$$

with $Q = G_{\rm eff}/G$, for $\Omega_{m,0} = 0.30$ and the three Q values from the EFE-screened envelope.

TABLE CVIII. Growth rates under the Hubble-EFE hypothesis, which is not DFD's cosmological growth law (App. GR). These are theorem-to-observable estimates; production-level survey-pipeline likelihoods require the standard nuisance layer.

z	$f_{\Lambda\rm CDM}$	$f_\parallel$	$f_{\rm avg}$	$f_\perp$
0.38	0.7049	0.7139	0.7529	0.7738
0.61	0.7837	0.7936	0.8368	0.8599
1.50	0.9268	0.9384	0.9892	1.0164

Using survey baseline $\beta_{\rm theory}$ values to infer effective biases $b_{\rm eff}(z)$ and propagating through the directional envelope, the predicted RSD parameters lie in a narrow band of width $\sim 8\%$ around ΛCDM. These numbers are first-pass theorem-to-observable estimates and should not be presented as final BOSS/eBOSS likelihood values; the full survey confrontation requires the nuisance layer (galaxy bias, FoG, AP, mock calibration) already used in ΛCDM analyses.

6. AC.6 Interpretation

The DFD dust branch supplies the pressureless temporal sector of homogeneous deviations (Appendix Q), which does not cluster:

$$w \to 0, \qquad c_s^2 \to 0. \tag{AC23}$$

Linear cosmological growth is carried by the cold χ relic with $Q = 1$ (App. GR).

7. AC.7 Falsifier

Linear Growth Closure — Falsifier

Under the Hubble-EFE hypothesis, the first-order growth closure is falsified if quasi-linear RSD or weak-lensing growth data require an effective coupling outside the EFE-screened envelope

$$1.02 \lesssim G_{\rm eff}/G \lesssim 1.17 \qquad \text{(AC24)}$$

after the standard nuisance layer of galaxy bias, Finger-of-God damping, Alcock–Paczynski mapping, and fiducial-cosmology dictionary translation is applied.
A second, more distinctive falsifier is absence of the predicted directional dependence in $f\sigma_8(z, \hat{n})$ where the reconstructed ψ-screen gradient is nonzero.
A third falsifier is rejection of the Hubble-EFE Hypothesis: if $a_{\rm ext}(z) \neq cH(z)$ at the level needed to displace $\bar{x}_{\rm EFE}$ outside its DFD-predicted range, the closure must be revisited.

8. AC.8 Summary

Linear Growth Closure — Theorem-Grade Status

Closed first-order:

- Linear response operator $M_{ij} = \mu_0 \delta_{ij} + \mu_{\ln,0} \hat{g}_i \hat{g}_j$ derived (Lemma AC.1)
- Effective coupling $G_{\rm eff}(\bar{x}, \theta) = G/[\mu_0 + \mu_{\ln,0} \cos^2 \theta]$
- Under the Hubble-EFE hypothesis, EFE screening fixes $\bar{x}_{\rm EFE} = 1/(2\sqrt{\alpha}) \simeq 5.85$
- Quasi-Newtonian envelope: $1.02\,G \leq G_{\rm eff} \leq 1.17\,G$
- Angular mean: $\langle G_{\rm eff} \rangle \simeq 1.12\,G$

Still program-grade: Production survey-pipeline likelihood (BOSS/eBOSS/DESI full-shape analysis with the standard nuisance layer) requires CAMB-equivalent modification with the DFD growth equation. This is a numerical implementation task, not a theoretical hole.

Appendix AD: Regular-Module Forcing from Finite Real-Bimodule Consistency

1. AD.1 Purpose

The microsector closed form for $\alpha^{-1} = 137.036$ contains a forced binary fork: the finite spectral trace may be carried either by the regular module $\mathcal{H}_F = A = M_d(\mathbb{C})$ or by a d-dimensional fermion-representation module $\mathcal{H}_F \simeq \mathbb{C}^d$. The numerical comparison (Table XXVI) selects the regular module by 43 ppm. This appendix proves that the regular module is also the *minimal* finite Hilbert space compatible with the DFD microsector's real-bimodule structure, making the lock a structural theorem conditional on the standard-form real-bimodule conditions and minimality, which are adopted as the spectral-triple consistency requirement, not derived from the field equation.

2. AD.2 The Finite Algebra and Its Role

Let

$$A = M_d(\mathbb{C}). \qquad \text{(AD1)}$$

The DFD microsector is *not* the observed fermion-representation space. It is the finite carrier of the vacuum gauge-frame algebra whose spectral trace normalizes the emergent gauge kinetic term. Gauge variations are represented by inner derivations,

$$\mathrm{ad}_a(X) = [a, X], \qquad a \in A,\ X \in \mathcal{H}_F. \qquad \text{(AD2)}$$

3. AD.3 Minimal Faithful Real-Bimodule Theorem

Theorem AD.1 (Minimal faithful real-bimodule)**.** *Let $\mathcal{H}_F$ be a finite-dimensional Hilbert space carrying a faithful left action $\pi_L : A \to B(\mathcal{H}_F)$ and a faithful right (opposite) action $\pi_R : A^{op} \to B(\mathcal{H}_F)$ satisfying*

1. ***Order-zero condition:*** $[\pi_L(a), \pi_R(b)] = 0$ *for all* $a, b \in A$.
2. ***Mutual commutant closure*** *(finite-factor standard form):*

$$\pi_L(A)' = \pi_R(A^{op}), \qquad \pi_R(A^{op})' = \pi_L(A). \qquad \text{(AD3)}$$

Then the minimal such Hilbert space is

$$\boxed{\mathcal{H}_F \simeq \mathbb{C}^d \otimes \overline{\mathbb{C}^d} \simeq M_d(\mathbb{C}),} \qquad \text{(AD4)}$$

and therefore

$$\boxed{\dim \mathcal{H}_F = d^2.} \qquad \text{(AD5)}$$

Proof. Every finite-dimensional faithful representation of the simple algebra $M_d(\mathbb{C})$ is a multiple of the defining representation. Hence

$$\mathcal{H}_F \simeq \mathbb{C}^d \otimes \mathbb{C}^m, \qquad \pi_L(a) = a \otimes I_m. \qquad \text{(AD6)}$$

Its commutant is

$$\pi_L(A)' = I_d \otimes M_m(\mathbb{C}). \tag{AD7}$$

For $\pi_R(A^{op})$ to be faithful and equal to the full commutant, the multiplicity space must contain a full copy of $M_d(\mathbb{C})^{op}$. This requires

$$m \geq d. \tag{AD8}$$

Minimality gives $m = d$. Therefore

$$\mathcal{H}_F \simeq \mathbb{C}^d \otimes \mathbb{C}^d \simeq \mathrm{End}(\mathbb{C}^d) \simeq M_d(\mathbb{C}). \tag{AD9}$$

Under this identification, A acts by left multiplication and A^{op} acts by right multiplication. The adjoint gauge action is

$$\mathrm{ad}_a(X) = aX - Xa = [a, X], \tag{AD10}$$

which is exactly the DFD regular-module microsector. □

4. AD.4 Branch B Exclusion

Corollary AD.2 (Branch B is structurally invalid)**.** *The fermion-representation branch takes*

$$\mathcal{H}_F \simeq \mathbb{C}^d. \tag{AD11}$$

The commutant of the defining representation of $M_d(\mathbb{C})$ is only

$$\pi_L(M_d)' = \mathbb{C}. \tag{AD12}$$

Therefore $\mathcal{H}_F \simeq \mathbb{C}^d$ cannot carry a faithful right $M_d(\mathbb{C})^{op}$ action satisfying the standard-form real-bimodule condition. Branch B is therefore not a valid DFD vacuum microsector trace carrier.

Remark AD.3 (Scope of the exclusion). Corollary AD.2 excludes $\mathcal{H}_F \simeq \mathbb{C}^d$ *only as the DFD vacuum gauge-frame trace carrier.* It does not imply that $\mathbb{C}^d$ is invalid for ordinary fermion representations elsewhere in the framework. Physical fermion fields transform in the defining representation; the vacuum trace carrier is a separate structure responsible for gauge-frame normalization.

5. AD.5 Finite-d Consequence

For the DFD Toeplitz cutoff $k_{\max} = 60$ (Lemma F.11),

$$d = k_{\max} + 4 = 64. \tag{AD13}$$

Hence

$$\dim \mathcal{H}_F = d^2 = 4096. \tag{AD14}$$

Corollary AD.4 (Forced trace conversion factor)**.** *The democratic trace over $\mathcal{H}_F = M_d(\mathbb{C})$ and conversion to canonical $\mathfrak{su}(d)$ generator normalization gives*

$$\boxed{\varepsilon_{\mathrm{adj}}^{(A)} = \frac{d^2}{d^2-1} = \frac{4096}{4095}.} \tag{AD15}$$

This is the regular-module factor used in the successful branch of the closed form for the fine-structure constant. The alternative factor $(d^2-1)/d^2 = 4095/4096$ belongs to a module that fails the DFD finite real-bimodule condition.

Proof. The regular module $M_d(\mathbb{C})$ decomposes as $M_d(\mathbb{C}) = \mathbb{C} \cdot 1 \oplus \mathfrak{su}(d)$ as a representation of the inner automorphism group, where the singlet corresponds to the identity matrix and $\mathfrak{su}(d)$ is the (d^2-1)-dimensional traceless adjoint. The democratic UV trace runs over all d^2 basis elements; the gauge kinetic term in canonical normalization runs only over the $\mathfrak{su}(d)$ factor. The conversion is the inverse ratio of dimensions, $d^2/(d^2-1)$. □

6. AD.6 Status

Microsector Lock — Theorem-Grade Status

Branch A ($\mathcal{H}_F = M_d(\mathbb{C})$, BOOST = 4096/4095) is *forced* by the minimal faithful real-bimodule theorem (Theorem AD.1). Branch B ($\mathcal{H}_F \simeq \mathbb{C}^d$, drop = 4095/4096) fails the bimodule consistency requirement (Corollary AD.2); its 43 ppm miss of α^{-1} is a redundant consistency check rather than the basis for selection.

The α closed form is structurally locked at the module level:

- Bimodule structure: $\mathcal{H}_F = M_d(\mathbb{C})$ (forced minimal faithful real-bimodule)
- Dimension: $d^2 = 4096$
- Trace conversion: $\varepsilon_{\mathrm{adj}}^{(A)} = 4096/4095$ (Corollary AD.4)
- Gauge action: inner derivations $\mathrm{ad}_a(X) = [a, X]$
- $\alpha^{-1} = 137.03599985$ (21 ppm from the integers; the bracket coefficient is open; the identification of the hypercharge-trace coefficient with $1/e^2$ is not derived)

Theorem dependencies: order-zero + faithful left/right actions + mutual commutant closure + minimality. These constitute a legitimate spectral-triple consistency requirement for the DFD vacuum trace carrier.

Falsifier: If a finite Hilbert space $\mathcal{H}_F \simeq \mathbb{C}^d$ can be shown to satisfy the faithful real-bimodule conditions (faithful left and right actions of $M_d(\mathbb{C})$ and $M_d(\mathbb{C})^{op}$ with mutual commutant closure), then Theorem AD.1 is wrong. No such construction exists in the current literature; the commutant of the defining representation is provably $\mathbb{C}$ by Schur's lemma.

Appendix AE: Optical-Metric σ_8 Closure

1. AE.1 Statement and Scope

In a curvature-based gravity theory such as GR, the lensing-inferred density contrast on R_8 scales is the same object as the physical mass density contrast. This is not the case in DFD. Because DFD's gravity is refractive ($n = e^{\psi}$) and not curvature-based, the relation between physical baryon clustering and observed weak-lensing convergence is mediated by the deep-MOND optical response, not by a linear Newtonian-Poisson inversion.

This appendix derives the closure condition for the spherical top-hat σ_8 statistic and computes the baryon contrast that, amplified optically, would produce the Planck 2018 amplitude $\sigma_{8,\rm obs} = 0.811$.

The closure is an optical, apparent-amplitude construction in which the baryons are the only clustering matter; it is not DFD's physical growth carrier. The physical carrier is the cold χ relic with $Q_\chi = 1$ under the adopted Rest-Mass Channel, which also confines the baryons' polarization to bound low-acceleration systems, and the σ_8 and S_8 of record are its values on the measured-clock background, $\sigma_8 \simeq 0.8063$ and $S_8 \simeq 0.822$ (App. GR). The numbers this appendix derives from the closure (the baryon contrast, $Q_{\rm DFD}$, the peculiar velocity, the bias and the RSD β) and its falsifiers belong to that construction. Theorem AE.1 does not depend on it; Corollary AE.2 describes the bare single-W action, which the Rest-Mass Channel supersedes on linear scales (App. GR).

Relationship to Appendix AC

The linear response operator $M_{ij} = \mu_0\delta_{ij} + \mu_{\ln,0}\hat{g}_i\hat{g}_j$ of Appendix AC is correct mathematics for any background gradient $|\nabla\bar{\psi}|$. Appendix AC then adopts the *Hubble-EFE Hypothesis* $a_{\rm ext}(z) = cH(z)$ (named explicitly there as testable) to evaluate the operator at $\bar{x}_{\rm EFE} \simeq 5.85$, giving the 1.02–1.17 G envelope.
The present appendix establishes (Theorem AE.1) that the FRW background of the DFD action gives $|\nabla\bar{\psi}| = 0$. The Hubble-EFE Hypothesis is therefore not recovered from the action for cosmological perturbations. For cosmological scales, the response operator is evaluated at $\bar{x} = 0$ (deep MOND, no EFE), and in the baryon-only construction the apparent σ_8 is dominated by the optical lensing inflation rather than the matter-acceleration enhancement.

2. AE.2 First-Principles Derivation: $a_{\rm ext}^{\rm FRW} = 0$

Theorem AE.1 (FRW-derived cosmological external field)**.** *On a homogeneous and isotropic FRW background of the DFD action*

$$S_\psi = \int dt\, d^3x \Big\{ \frac{a_0^2}{8\pi G}\Big[W\big(|\nabla\psi|^2/a_*^2\big) + K\big(\tfrac{c}{a_0}|\dot{\psi} - \dot{\psi}_0|\big)\Big] - \frac{c^2}{2}\psi(\rho - \bar{\rho})\Big\},$$

the spatial gradient of the background scalar field vanishes:

$$\boxed{|\nabla\bar{\psi}| = 0, \qquad a_{\rm ext}^{\rm FRW} \equiv \frac{c^2}{2}|\nabla\bar{\psi}| = 0.} \tag{AE1}$$

Proof. The proof has three steps.

1. **Matter source vanishes by homogeneity.** The matter coupling is $\psi(\rho - \bar{\rho})$. On a strictly homogeneous FRW background, $\rho = \bar{\rho}$ everywhere, so the source term is identically zero.

2. **Spatial kinetic vanishes by isotropy.** A homogeneous and isotropic background has $\bar{\psi} = \bar{\psi}(t)$ only, hence $\nabla\bar{\psi} = 0$ pointwise. The argument of W is then zero, and using the Lagrangian normalization $W(0) = 0$, the spatial kinetic vanishes.

3. **Temporal kinetic vanishes by reference invariance.** The temporal deviation invariant is $\Delta = (c/a_0)|\dot{\psi} - \dot{\psi}_0|$ where $\dot{\psi}_0$ is the screen-background flow. On the FRW background treated as the reference, $\dot{\psi} = \dot{\psi}_0$ identically, so $\Delta = 0$ and $K(\Delta) = 0$ by the normalization $K(0) = 0$.

The Euler–Lagrange equation for $\bar{\psi}(t)$ is therefore identically satisfied for any $\bar{\psi}(t)$: the FRW background is a flat direction in the action. In particular, $|\nabla\bar{\psi}| = 0$ identically, and the acceleration form $a_{\rm ext}^{\rm FRW} = (c^2/2)|\nabla\bar{\psi}| = 0$. □

Corollary AE.2 (Cosmological perturbations are in deep MOND)**.** *For perturbations on the FRW background with no external matter to source a gradient, the response operator $M_{ij} = \mu_0\delta_{ij} + \mu_{\ln,0}\hat{g}_i\hat{g}_j$ of Appendix AC is evaluated at $\bar{x} = 0$, placing cosmological perturbations in the raw deep-MOND regime $\mu(x) \to x$ as $x \to 0$.*

3. AE.3 Setup: spherical top-hat statistic

The observable σ_8 is defined as the rms density contrast filtered with a spherical top-hat window of comoving radius $R_8 = 8\,h^{-1}\,\mathrm{Mpc}$:

$$\sigma_8^2 \equiv \langle \delta_W^2 \rangle, \qquad W_R(\mathbf{x}) = \begin{cases} 3/(4\pi R^3) & |\mathbf{x}| \le R \\ 0 & |\mathbf{x}| > R \end{cases}. \tag{AE2}$$

For a spherical baryon overdensity of contrast δ_b filling a top-hat of radius R_8, the Newtonian gravitational acceleration at the edge is

$$g_N(R_8) = \frac{4\pi G}{3}\bar{\rho}_{b,0}\,\delta_b\,R_8 = \tfrac{1}{2}\Omega_b\,H_0^2\,R_8\,\delta_b, \tag{AE3}$$

using $\bar{\rho}_{b,0} = \Omega_b \rho_{\rm crit} = \Omega_b(3H_0^2/8\pi G)$.

Throughout this appendix, δ_b is the rms baryon density contrast at R_8 (the spherical top-hat filtered rms).

4. AE.4 The closure equation

In a curvature-based theory, weak-lensing convergence on R_8 scales is proportional to the integrated source $\Omega_m\,\delta_m$:

$$\kappa_{\rm GR} \propto \Omega_m\,\delta_m. \tag{AE4}$$

In DFD, the convergence is set by the same line-of-sight integral but with δ_m replaced by the refractive-source field $\mathcal{R}_{\rm DFD}[\delta_b]\,\delta_b$, where $\mathcal{R}_{\rm DFD}$ is the nonlinear response operator obtained by solving

$$\nabla\cdot\big[\mu(|\nabla\psi|/a_*)\,\nabla\psi\big] = -\frac{8\pi G}{c^2}(\rho_b - \bar{\rho}_b), \tag{AE5}$$

with $\mu(x) = x/(1+x)$ and $a_* = 2a_0/c^2$. Schematically,

$$\Omega_m\,\delta_m \quad\longrightarrow\quad \Omega_b\,\mathcal{R}_{\rm DFD}[\delta_b]\,\delta_b. \tag{AE6}$$

In the spherical top-hat convention, the response operator is a scalar function $Q(\delta_b)$: the angle-averaged matter response of an isolated spherical overdensity in deep MOND with $a_{\rm ext}^{\rm FRW} = 0$ (Theorem AE.1 and Corollary AE.2). The closure condition for matched lensing observation is

$$\boxed{\Omega_b\,\delta_b\,Q(\delta_b) = \Omega_m\,\sigma_{8,\rm obs}.} \tag{AE7}$$

5. AE.5 The DFD response $Q(\delta_b)$

For an isolated spherical overdensity in the no-EFE FRW background, Eq. (AE5) integrates by Gauss's theorem on a sphere to

$$\mu\Big(\frac{|\nabla\psi|}{a_*}\Big)\cdot\frac{c^2}{2}|\nabla\psi| = g_N(r), \tag{AE8}$$

which in matter-acceleration form $a = (c^2/2)|\nabla\psi|$ becomes

$$\mu(a/a_0)\,a = g_N(r). \tag{AE9}$$

With $\mu(x) = x/(1+x)$ and $y \equiv a/a_0$, $q \equiv g_N/a_0$, Eq. (AE9) reads

$$\frac{y^2}{1+y} = q, \qquad y = \frac{q+\sqrt{q^2+4q}}{2}, \qquad Q(\delta_b) = \frac{y}{q}. \tag{AE10}$$

In the deep-MOND limit $q \ll 1$, this reduces to

$$Q(\delta_b) \simeq \frac{1}{\sqrt{q}} = \frac{1}{\sqrt{g_N/a_0}}. \tag{AE11}$$

6. AE.6 Closure number in the spherical top-hat convention

Combining Eqs. (AE3) and $a_0 = 2\sqrt{\alpha}\,c\,H_0$:

$$\frac{g_N(R_8)}{a_0} = A_8\,\delta_b, \qquad A_8 \equiv \frac{\Omega_b}{4\sqrt{\alpha}}\frac{H_0 R_8}{c}. \tag{AE12}$$

Since $H_0R_8/c = 8/2997.92 = 2.6685\times10^{-3}$ (independent of h, since $R_8 \propto h^{-1}$ cancels), and using the current-clock $\Omega_b = \omega_b/h^2 = 0.048856$, $\alpha^{-1} = 137.036$:

$$A_8 = 3.81546\times10^{-4}. \tag{AE13}$$

Solving Eq. (AE7) in the deep-MOND limit [Eq. (AE11)]:

$$\Omega_b\,\sqrt{\delta_b/A_8} = \Omega_m\sigma_{8,\rm obs}, \tag{AE14}$$

$$\boxed{\delta_b = \frac{(\Omega_m\sigma_{8,\rm obs})^2\,A_8}{\Omega_b^2}.} \tag{AE15}$$

With $\Omega_m = 0.315$ and $\sigma_{8,\rm obs} = 0.811$ ($\Omega_m\sigma_8 = 0.2555$):

$$\delta_{b,R_8} = 1.0432\times10^{-2}, \qquad Q_{\rm DFD} = \frac{1}{\sqrt{A_8\delta_b}} = 501.24. \tag{AE16}$$

The exact-μ result from Eq. (AE10) differs by a fractional correction $\sim\sqrt{q}/2 \sim 10^{-3}$:

$$\boxed{\delta_{b,R_8} = 1.0411\times10^{-2}, \qquad Q_{\rm DFD} = 502.24.} \tag{AE17}$$

7. AE.7 Physical interpretation

In the baryon-only construction, the Planck 2018 amplitude $\sigma_8 \simeq 0.81$ would correspond to a baryon density contrast of only $\sim 1.0\%$ at R_8, amplified optically by a factor ~ 500 via the deep-MOND lensing response.

Apportionment with χ-matter (two channels, different observables). This appendix quantifies the R_8-scale optical (ψ) lensing response, where $\mu(x)\to 0$ amplifies a small baryon contrast. The derived χ-matter field ($\Omega_\chi h^2 \simeq 0.12$; App. AV) carries the *cosmological* cold clustering (CMB peak heights, large-scale matter power) through the rest-mass channel ($Q_\chi = 1$; App. GR), while the optical response is sourced by the baryons. The Rest-Mass Channel confines that response to bound low-acceleration systems, and the net induced mass of each bound system is zero, so on the R_8 scale the optical response adds

at most 0.2% of the mean matter density and raises the lensing power by at most 7% (computed; App. GR, Remark GR.12). The lensing statistic at R_8 therefore follows the matter power that χ and the baryons carry; the closure number of Eq. (AE17) belongs to the baryon-only construction. How the two channels compose inside galaxies, where χ halos and the baryons' phantom overlap, is a separate and open question (App. AV).

The construction is consistent with three independent corpus results:

1. The corpus particle-mesh simulation in Sec. XVI reports 5.4× overshoot of $\delta_{\rm rms}$ relative to ΛCDM, attributed to "cosmological perturbations in the deep-MOND regime" with $x \sim 4 \times 10^{-4}$. The present derivation identifies the same regime $g_N/a_0 = q \simeq 4 \times 10^{-6}$ at the closure point.

2. The deep-MOND deflection formula $\hat{\alpha}_{\rm deep} = 2\pi\sqrt{GM\,a_0}/c^2$ (Sec. VII) gives the same closure when used to match GR's deflection from the LCDM mass at R_8, up to spherical-vs-Fourier convention differences absorbed by the spherical σ_8 window.

3. The first-principles result $a_{\rm ext}^{\rm FRW} = 0$ (Theorem AE.1): the FRW background of the DFD action gives $|\nabla\bar{\psi}| = 0$. The Appendix AC envelope 1.02–1.17 G applies under the named Hubble-EFE Hypothesis rather than as the actual DFD prediction for the cosmological regime.

8. AE.8 Required CMB-to-$z = 0$ amplification

The baryon-only construction requires a dynamical amplification of δ_b from recombination ($\delta_{\rm init} \sim 10^{-5}$) to $z = 0$ ($\delta_{b,R_8} \simeq 0.010$) of

$$\frac{\delta_{b,R_8}}{\delta_{\rm init}} \sim 1.0 \times 10^3. \tag{AE18}$$

ΛCDM requires amplification $\sim 10^5$ via cold dark matter from CMB to $z = 0$. In DFD that physical clustering is carried by the derived χ-matter ($\Omega_\chi h^2 \simeq 0.12$, ΛCDM-like growth; App. AV), so the same $\sim 10^5$ is achieved by χ. The optical factor $Q \simeq 500$ computed here belongs to the baryon-only construction. In DFD's cosmology the baryons polarize the medium only inside bound low-acceleration systems (App. GR), so this factor does not act on the R_8 scale and nothing is stacked on the χ clustering: χ and the baryons carry the matter power and its lensing, and the polarization adds the lensing of each galaxy inside its bound radius.

9. AE.9 Relation to galaxy clustering

A consistency concern is that observed galaxy clustering on R_8 scales gives rms galaxy contrast of order unity. If $\delta_b \simeq 0.010$, the implied galaxy bias factor relative to baryons is

$$b_{\rm galaxy} \equiv \delta_{\rm galaxy}/\delta_b \sim 1/0.0104 \sim 96. \tag{AE19}$$

This is much larger than typical ΛCDM galaxy bias factors $b \sim 1.5$–2.

Within the construction this is not unreasonable: galaxy formation is preferentially seeded by peaks in the effective refractive source $\mathcal{R}_{\rm DFD}[\delta_b]\delta_b$ rather than in the bare baryon contrast δ_b. The ratio $\mathcal{R}_{\rm DFD}/1 \sim Q \sim 500$ provides the natural rescaling between bare baryon clustering and the gravitationally-active source that controls galaxy formation. Galaxies trace the refractive-source peaks at order-unity contrast even when δ_b itself is small.

A rigorous derivation of galaxy bias in DFD's framework is identified as a program-level item; see Sec. AE 12.

10. AE.9b RSD compatibility: deep-MOND velocity divergence

A potential concern is that the bias multiplier $F_8 = \sigma_8/\delta_b \simeq 77.9$ would naively imply $\beta_{\rm RSD} = f/b$ smaller by the same factor, in conflict with measured BOSS/eBOSS values $\beta \sim 0.27$–0.40 at LRG bias. We show here that this is a unit artifact: the appropriate RSD observable is the velocity divergence $\theta = \nabla \cdot \mathbf{v}$, not the radial velocity amplitude v_r, and the proper deep-MOND velocity-density relation gives $\beta_{\rm DFD}$ within the observed range.

a. Velocity from DFD's exponential refractive structure. DFD's matter equation of motion is $\mathbf{a} = (c^2/2)\nabla\psi$ directly, not a curvature-induced geodesic. For a spherical baryon overdensity of contrast δ_b at radius R, the deep-MOND DFD field equation integrated by Gauss's theorem gives $|\nabla\psi|^2/a_* = (2G/c^2)\delta M/R^2$. Combining with $a = (c^2/2)|\nabla\psi|$ and $a_* = 2a_0/c^2$:

$$a_{\rm DFD} = \frac{\sqrt{G\,a_0\,\delta M}}{R}. \tag{AE20}$$

Substituting $\delta M = (4\pi/3)R^3\rho_b\delta_b$ with $\rho_b = \Omega_b(3H^2/8\pi G)$ gives $g_N(R) = (1/2)\Omega_b H^2 R\delta_b$, and the same factor of 1/2 that defines the spherical-top-hat σ_8 closure [Eq. (AE3)] enters here. The deep-MOND identity $a_{\rm DFD} = \sqrt{a_0\,g_N}$ (corpus Appendix B; consistent with the asymptotic-velocity formula $V_c^4 = GM_{\rm bar}a_0$) gives

$$a_{\rm DFD} = H\sqrt{\tfrac{1}{2}\,a_0\,R\,\Omega_b\,\delta_b}, \tag{AE21}$$

sub-linear in δ_b (a $\sqrt{\delta_b}$ scaling), reflecting the deep-MOND amplification when matter is sparse.

The peculiar velocity from quasi-static Euler integration a/H is

$$v_{\rm pec} = \sqrt{\tfrac{1}{2}\,a_0\,R\,\Omega_b\,\delta_b}. \tag{AE22}$$

At the closure point $\delta_b = 1.04 \times 10^{-2}$ on R_8:

$$v_{\rm pec} \simeq 102 \text{ km/s}, \tag{AE23}$$

about 0.9 of the LCDM linear top-hat value $fH_0R_8\sigma_8/3 \simeq 108$ km/s at the same scale. Equivalently, in terms of the

response factor Q of Eq. (AE17):

$$\frac{v_{\rm pec}}{H_0 R_8} = \tfrac{1}{2}\,\Omega_b\,Q\,\delta_b = 0.128, \tag{AE24}$$

self-consistent with the same 1/2 factor used in the spherical top-hat σ_8 normalization.

b. The RSD observable is velocity divergence. Kaiser RSD measures redshift-space anisotropy controlled by the velocity divergence $\theta = \nabla\cdot\mathbf{v}$, not v_r itself. For a spherical top-hat radial flow $v_r(r) = (v_R/R)r$, exactly:

$$\theta = \frac{1}{r^2}\frac{d}{dr}(r^2 v_r) = \frac{3v_R}{R}. \tag{AE25}$$

The factor of three is geometric and unavoidable for a spherical top-hat profile. The implied RSD β parameter is

$$\boxed{\beta^{\rm sph}_{\rm DFD} \simeq \frac{\theta/(aH)}{\delta_{\rm gal}} = \frac{3\,v_{\rm pec}}{H_0 R_8\,\delta_{\rm gal}}.} \tag{AE26}$$

c. Numerical evaluation. With $H_0 R_8 = 800$ km/s (independent of h since $R_8 = 8h^{-1}$ Mpc cancels), $v_{\rm pec} = 102$ km/s, and an LRG-like sample $b_{\rm GR} = 1.88$ giving $\delta_{\rm gal} = b_{\rm GR}\sigma_{8,\rm obs} = 1.525$:

$$\beta^{\rm sph}_{\rm DFD} \simeq \frac{3\times 102/800}{1.525} = 0.251. \tag{AE27}$$

This sits just below the BOSS/eBOSS-scale measurement range $\beta \sim 0.27$–0.40 at LRG bias, but is consistent with it for ELG-like and lower-bias samples.

A representative table for several survey tracers:

Tracer	$b_{\rm GR}$	$\delta_{\rm gal} = b_{\rm GR}\sigma_8$	$\beta^{\rm sph}_{\rm DFD}$
Matter-equivalent	1.00	0.811	0.472
BGS / low-bias	1.20	0.973	0.394
ELG-like	1.50	1.216	0.315
DESI/BOSS LRG	1.88	1.525	0.251
LRG high-bias	2.10	1.703	0.225
QSO-like	2.70	2.190	0.175

d. Status. This is a first-order spherical-top-hat estimate. A definitive RSD prediction requires computing $P_{\theta g}(k,z)$ and $P_{gg}(k,z)$ from the DFD Euler equation with the proper mode-by-mode geometry, projecting through survey kernels matching BOSS/eBOSS/DESI windows, and including nonlinear corrections (Finger-of-God, Alcock–Paczynski, fiducial-cosmology dictionary). This is identified as an additional Open Theorem Obligation in Sec. AE 12. The first-order estimate above is *a near-miss sanity check*: $\beta^{\rm sph}_{\rm DFD} \simeq 0.25$ for LRG-like tracers sits just below the observed range $\beta \sim 0.27$–0.40, while $\beta^{\rm sph}_{\rm DFD} \simeq 0.32$ for ELG-like tracers is comfortably inside it. The optical σ_8 closure is therefore not in obvious order-of-magnitude conflict with existing RSD data, but the precision-level comparison must wait for the full kernel calculation.

e. Falsifier sharpening. If the full $P_{\theta g}/P_{gg}$ calculation gives $\beta_{\rm DFD}$ outside the observed BOSS/eBOSS range at significance $> 3\sigma$ for at least two redshift bins, the optical σ_8 closure is falsified. Conversely, the spherical-top-hat estimate predicts $\beta_{\rm DFD} \simeq 0.22$–$0.25$ at LRG bias, $\simeq 0.31$ at ELG bias, and $\simeq 0.18$ at QSO bias — for every tracer 0.94 of LCDM's $\beta = f/b$ at $f \simeq 0.5$ (0.27, 0.33 and 0.19 at $b = 1.88$, 1.50 and 2.70).

11. AE.10 Falsifiable predictions

Optical σ_8 Closure — Falsifiers

Equation (AE17) is testable through three independent channels:

1. **Direct baryon-density probes.** Lyman-α forest absorption at $z \sim 2$–5 measures the IGM baryon density contrast directly. The construction predicts the bare baryon δ_b on R_8-comoving scales at the percent level, much smaller than the LCDM matter $\delta_m \sim \sigma_8(z)$ at the same scale. A measured δ_b at R_8-comoving consistent with LCDM δ_m falsifies the construction.
2. **kSZ amplitude.** The kinetic Sunyaev–Zel'dovich signal probes peculiar velocities of hot baryons. From the deep-MOND velocity-density relation Eq. (AE22), $v_{\rm pec} \propto \sqrt{\delta_b}$ with the spherical top-hat normalization, giving $v_{\rm pec} \simeq 102$ km/s on R_8 scales at the closure point. This is about 0.9 of the LCDM linear-theory prediction at the same scale. Current ACT/Planck and DESI×ACT 13σ kSZ detections are consistent with both amplitudes within current uncertainties; high-precision amplitude measurements at R_8-equivalent scales can discriminate.
3. **Galaxy bias coherent across surveys.** If the galaxy-bias explanation in Sec. AE 9 is correct, the bias $b \sim 96$ relative to baryons (not relative to $\Omega_m\delta_m$) should be internally consistent across galaxy clustering, weak lensing, and CMB lensing cross-correlations. Inconsistency at the 10% level would falsify the construction.

12. AE.11 Open Theorem Obligation: full convergence kernel

Equation (AE17) is established in the spherical top-hat convention that defines σ_8 as a single statistic. The full weak-lensing convergence kernel in DFD,

$$\kappa_{\rm DFD}(\boldsymbol{\ell}) = \int_0^\infty d\chi\,\frac{3H_0^2}{2c^2}\,\frac{\chi\,g(\chi)}{a(\chi)}\,\Omega_b\,\mathcal{R}_{\rm DFD}\left[k = \frac{\ell+1/2}{\chi}, z; \delta_b\right]\,\delta_b(\mathbf{k}, z), \tag{AE28}$$

with the corresponding power spectrum

$$C_\ell^{\kappa\kappa,\mathrm{DFD}} = \int_0^\infty \frac{d\chi}{\chi^2}\left[\frac{3H_0^2}{2c^2}\frac{\chi g(\chi)}{a(\chi)}\Omega_b\right]^2 P_{\mathcal{R}\delta_b,\mathcal{R}\delta_b}\left(\frac{\ell+1/2}{\chi}, z\right), \tag{AE29}$$

remains program-level. The Open Theorem Obligations are:

1. Compute $P_{\mathcal{R}\delta_b,\mathcal{R}\delta_b}(k,z)$ from a fiducial baryon transfer function, propagated through the nonlinear $\mathcal{R}_{\mathrm{DFD}}$ response operator.
2. Project Eq. (AE29) through survey kernels matching KiDS-Legacy / DES-Y6 / HSC-Y3 weak-lensing tomography.
3. Verify $S_8^{\mathrm{DFD}} = \sigma_{8,\mathrm{DFD}}\sqrt{\Omega_m/0.3}$ matches observation $S_8 \simeq 0.78$–0.83 at the precision of current measurements.
4. Derive the galaxy bias relation $b_{\mathrm{galaxy}}(\delta_b, z, \mathcal{R}_{\mathrm{DFD}})$ from the refractive-source peak statistics, and verify cross-consistency between galaxy clustering, weak lensing, and galaxy-galaxy lensing. *Resolved at the linear-bias level on R_8 scales: see Appendix AF (Theorem AF.1). The bias multiplier $F_8 = 77.9$ is derived from the closure with no free parameters; mass-dependent halo bias $b(M)$ and assembly bias remain program-grade.*
5. Compute $P_{\theta g}(k,z)$ and $P_{gg}(k,z)$ from the DFD Euler equation in the deep-MOND regime and project through survey kernels matching BOSS/eBOSS/DESI-Y3 redshift-space distortion analyses. Verify that the predicted $\beta(z,b)$ is consistent with the spherical-top-hat estimate $\beta_{\mathrm{DFD}}^{\mathrm{sph}} \simeq 0.22$–$0.25$ at LRG bias and $\simeq 0.31$ at ELG bias (Sec. AE 10), and reconciles with the observed $\beta \sim 0.27$–0.40 range.

The spherical top-hat result in Eq. (AE17) provides a single-statistic anchor against which the full kernel computation must be consistent.

13. AE.12 Summary

Optical σ_8 Closure (baryon-only construction) — Theorem-Grade Status

Closed at theorem grade:

- $a_{\mathrm{ext}}^{\mathrm{FRW}} = 0$ from the DFD action (Theorem AE.1).
- Closure equation $\Omega_b\delta_b Q(\delta_b) = \Omega_m\sigma_{8,\mathrm{obs}}$ in the spherical top-hat convention.
- Spherical-top-hat closure number: $\delta_{b,R_8} = 1.0411\times10^{-2}$, $Q_{\mathrm{DFD}} = 502.24$, with no free parameters.
- Deep-MOND velocity-density relation $v_{\mathrm{pec}} = \sqrt{(1/2)\,a_0\,R\,\Omega_b\,\delta_b}$ from $\mathbf{a} = (c^2/2)\nabla\psi$ and the field-equation Gauss law, $v_{\mathrm{pec}} \simeq 102$ km/s at the closure point on R_8.
- First-order RSD sanity check (a near miss): $\beta_{\mathrm{DFD}}^{\mathrm{sph}} \simeq 0.25$ at LRG bias (just below observed 0.27–0.40) and $\simeq 0.32$ at ELG bias (inside observed range), Sec. AE 10.

Still program-grade:

- Full Limber-projected convergence-kernel $C_\ell^{\kappa\kappa}$ and survey-window S_8 matching.
- Full $P_{\theta g}/P_{gg}$ RSD prediction across BOSS/eBOSS/DESI tomographic bins.
- Mass-dependent halo bias $b(M)$ and assembly bias in DFD (linear bias closed in Appendix AF).
- Direct Lyman-α and kSZ confrontation at the predicted $\delta_b \sim 0.010$.

Relationship to Appendix AC: the linear response operator structure of Appendix AC is unchanged. For cosmological perturbations the correct value is $a_{\mathrm{ext}}^{\mathrm{FRW}} = 0$ (Theorem AE.1), placing the same response operator in the deep-MOND limit. The two appendices are complementary, not in conflict.

Appendix GR: Adjudication of the Cosmological Growth/Velocity Regime

Status GR.1 (Measured-clock values). All $H_0 = 72.09$, $\Omega_m \simeq 0.274$, $\sigma_8 \simeq 0.820$, and $S_8 \simeq 0.784$ calculations below belong to the $C = 1$ background and are not current outputs. There $\sigma_8 = 0.820$ is the carried normalization, the value that the amplitude $A_s = 2.08 \times 10^{-9}$ (the value of $32\pi\alpha^5$, a calibration; App. FK) gives on that background; on the measured clock the same amplitude and χ carrier give the $\sigma_8 = 0.806$ of record (GR.4). A dependency-aware high-accuracy normal-hierarchy rerun on the current frozen inputs gives $R_8 = 11.848$ Mpc, $\Omega_m \simeq 0.312$, $\sigma_8 \simeq 0.8063$, and $S_8 \simeq 0.822$; KiDS-Legacy is consistent at 0.45–0.74σ depending on the primary/joint anchor, and current CMB lensing gives $A_{\phi\phi} = 0.9887$ (-0.80σ). The structural result that $Q_\chi = 1$ is conditional on the adopted Rest-Mass Channel postulate holds on either background. The alternative 0.790/0.755 branch is not a result.

1. GR.1 Purpose and the contested scalar

Appendices AC (AC) and AE (AE) share the *identical* linear response operator $M_{ij} = \mu_0\delta_{ij} + \mu_{\ln,0}\hat{g}_i\hat{g}_j$ and the *identical* crossover law $a_0(z) = 2\sqrt{\alpha}\,cH(z)$. They differ in exactly one input: the cosmological external acceleration on the FRW background,

$$\begin{aligned} \text{AC: } a_{\text{ext}}^{\text{FRW}} = cH(z) \;&\Rightarrow\; \bar{x} = \tfrac{1}{2\sqrt{\alpha}} \simeq 5.85, \\ \text{AE: } a_{\text{ext}}^{\text{FRW}} = 0 \;&\Rightarrow\; \bar{x} = 0. \end{aligned} \tag{GR1}$$

This appendix adjudicates which value governs the cosmological linear growth observables (σ_8, S_8, $f\sigma_8$, kSZ) and which governs collapsed galactic/cluster dynamics, and it resolves the ambiguity that left the directional $f\sigma_8$ signature "regime-contested."

Summary of this adjudication

The conflict is a *scope partition with one mis-scoped clause*. AE's $a_{\text{ext}}^{\text{FRW}} = 0$ is a theorem from the action (Theorem AE.1); AC's $a_{\text{ext}} = cH$ is an admitted *hypothesis* the action does not produce. *Neither* disputed G_{eff} is the carrier of cosmological linear growth: that role is played by the independently-derived χ-matter field ($\Omega_\chi h^2 \simeq 0.12$, GR-like growth). Hence G_{eff} is *not* the single derived growth law for cosmology (Proposition GR.4). The resolution is a scoping clarification; no DFD result changes.

2. GR.2 The regime-partition theorem

Theorem GR.2 (Growth-regime partition). *Let $x \equiv g/a_0(z)$ with g the local Newtonian acceleration sourced by the matter in question and $a_0(z) = 2\sqrt{\alpha}\,cH(z)$. Then the AQUAL operator M_{ij} of Appendix AC partitions by scale as follows:*

1. ***(Cosmological linear regime.)*** *On the homogeneous FRW background, $a_{\text{ext}}^{\text{FRW}} = 0$ identically (Theorem AE.1), so $\bar{x} = 0$ and the ψ-sector is in the raw deep-MOND limit. For a linear top-hat perturbation on R_8, $x = g_N/a_0(z) \ll 1$ at* every *epoch ($\lesssim 7.3 \times 10^{-3}$ for $\delta \le 1$ at $z \le 2$; 1.3×10^{-6} at recombination; Lemma GR.3). Linear scales are deep-MOND, never $\bar{x} = 5.85$.*
2. ***(Collapsed/cluster regime.)*** *Inside a collapsed halo a real local mass sources a genuine $|\nabla\bar{\psi}| \neq 0$; there x ranges from $\mathcal{O}(0.1)$ (clusters) to $\gtrsim 1$ (galactic interiors).*

The transition between regimes is the single derived condition

$$\boxed{x = \frac{g}{a_0(z)} = 1 \iff g = 2\sqrt{\alpha}\,cH(z).} \tag{GR2}$$

Proof. Part (1): Theorem AE.1 establishes $|\nabla\bar{\psi}| = 0$ on FRW (homogeneity kills the matter source, isotropy kills the spatial kinetic, reference invariance kills the temporal kinetic), so no cH-scale external field exists to place a mode at $\bar{x} = 5.85$. The residual x for a physical top-hat is bounded by Lemma GR.3. Part (2): for a bound mass M at radius r, $g_N = GM/r^2$ exceeds a_0 once $r < \sqrt{GM/a_0}$, the standard MOND radius; for $M \sim 10^{12}M_\odot$ this is ~ 35 kpc, so galactic interiors satisfy $x \gtrsim 1$. The crossover $x = 1$ is Eq. (GR2) by definition of a_0. □

Lemma GR.3 (Linear R_8 modes are deep-MOND at every epoch). *For a spherical top-hat of contrast δ on comoving radius R_8 (proper radius aR_8), the edge acceleration is $g_N = \frac{1}{2}\Omega_m(a)H(a)^2\,aR_8\,\delta$ and*

$$x = \frac{g_N}{a_0(z)} = \frac{\Omega_m(a)H(a)\,aR_8\,\delta}{4\sqrt{\alpha}\,c}. \tag{GR3}$$

Numerically, at the measured $\Omega_m \simeq 0.312$: $x(\delta{=}1) = 2.4 \times 10^{-3}$ at $z{=}0$, 5.5×10^{-3} at $z{=}1$, 7.3×10^{-3} at $z{=}2$, and 1.3×10^{-6} at recombination ($\delta{\sim}10^{-5}$). All $\ll 1$: deep-MOND on all linear scales.

3. GR.3 The AQUAL G_{eff} is not the cosmological growth carrier

Proposition GR.4 (Growth carrier). *The cosmological linear growth of δ_m is carried by the derived χ-matter field (Appendix AV, $\Omega_\chi h^2 \simeq 0.12$), which gravitates through the unscreened rest channel (Remark GR.9), has $G_{\text{eff}} = G$, and grows ΛCDM-like ($Q \equiv G_{\text{eff}}/G = 1$). Neither AC's $1.12\,G$ nor AE's raw deep-MOND self-field is the growth law:*

1. *AC's constant $\langle G_{\text{eff}}\rangle = 1.118\,G$, if applied from $z \sim 1000$, compounds to a D-ratio 1.54, i.e. $\sigma_8 \to 1.24$ — a +54% over-growth, excluded (computed with $\mu = x/(1+x)$; on the derived exponential response of App. BS the same ambient argument*

$\bar{x} = 5.85$ *gives* +24% *on the SOURCE branch and* −1.0% *on the TOTAL branch (App. AC's angular-mean construction, the same quantity as the* +54%*), so on that branch the exclusion of an ambient boost as the growth law rests on Theorem AE.1,* $\bar{x} = 0$ *on FRW, not on over-growth). AC's quoted "*+1–9%*" is the* instantaneous $f\sigma_8$*, not the integrated* σ_8 *(Remark GR.5).*

2. *AE's raw deep-MOND self-field response on* δ_m *runs away (the corpus* $5.4\times$ $\delta_{\rm rms}$ *overshoot); App AE.7 correctly reinterprets its* $Q \simeq 500$ *as a* lensing *amplification of a small baryon contrast,* not *a growth boost.*

Verification. Both branches are integrated numerically in `growth_regime_adjudication.py`. The constant-Q=1.118 ODE from z=1000 yields $D(1)/D(a_{\rm ini})$ a factor 1.54 above the Q=1 solution; the deep-MOND self-field branch diverges. The Q=1 (χ) solution reproduces the corpus $f(0)$, σ_8, S_8 self-consistently (GR.4). □

Remark GR.5 (AC's instantaneous-vs-integrated conflation). AC's 1.02–1.17 G is a statement about the instantaneous growth-rate enhancement $f = d\ln D/d\ln a$ at low z. Integrated over the full history a constant 1.118 G compounds; the appendix's envelope therefore must not be read as an integrated-σ_8 claim. This independently disfavors applying the Hubble-EFE envelope to cosmology.

Scope (a proven obstruction — resolved by the adopted Rest-Mass Channel postulate)

The carrier identification (Proposition GR.4: χ has $Q \equiv G_{\rm eff}/G = 1$ on linear scales) requires χ-matter to sit at $x \equiv g/a_0 \gg 1$ (Newtonian, AQUAL screen *off*). But Lemma GR.3 establishes that on the *same* linear R_8 scale the top-hat *edge* acceleration gives $x \sim 2\times10^{-3} \ll 1$ (deep-MOND) — which is exactly the regime needed to keep the AQUAL screen *off the baryons.* **These two scoping statements are mutually exclusive on one linear scale**; the adopted Rest-Mass Channel reconciles them by confining the polarization to bound systems (below).
Status: a proven obstruction in the linear regime. A *local-source* argument — inside a collapsing halo χ self-gravitates Newtonianly where a real source gives $g \gg a_0$ — does hold *post-collapse*, but it switches on only at $\delta \gtrsim 500$ (nonlinear) and therefore *cannot* reach the *linear* R_8 regime that sets $\sigma_8/f\sigma_8$ and the third-peak transfer function. In that linear regime $Q = 1$ is provably *not* available from the bare single-W action ("structured ⇔ gradient ⇔ screened"; the Rest-Mass Channel box below): every clustering mode carries $\nabla\phi \neq 0$ and is screened into the deep-MOND branch. Closing $Q = 1$ on linear scales therefore requires the Rest-Mass Channel (the μ-law confined to bound systems, which leaves the μ=1 rest-mass term, the Einstein–Hilbert term's own static scalar energy, unscreened) — the minimal fix (matter moves under an energy that conserves momentum, and χ falls like the baryons wherever it fills the μ-law's demand, §GR.3a), proven absent from the bare action, which DFD *adopts as a postulate*; given it, $Q_\chi = 1$ follows and the clustering gate is closed.
Why it decides the S_8 *story.* If $Q = 1$ holds (the asserted resolution), *one* $\sigma_8 = 0.806$ sets both the galaxy-lensing $S_8 = 0.822$ and the CMB-lensing amplitude $A_{\phi\phi} = 0.9887$, and the sharper $S_8 = 0.755$ is not available. If instead the AQUAL screen *leaked* into linear growth, Q would run with redshift ($Q \sim 20$ at $z = 0$ to ~ 12 at $z = 2$), the growth factor $D(z)$ would not be flat/ΛCDM-like, the σ_8-vs-S_8 lock would break — at the cost of a z-dependent growth signature testable against $f\sigma_8(z)$. The single-W action cannot settle this (the obstruction below); the *Rest-Mass Channel*, which DFD *adopts as a postulate* and which confines the polarization to bound systems, settles it with $Q = 1$ on linear scales, as stated next.

Adopted postulate: the Rest-Mass Channel (two-channel gravity — closes $Q_\chi = 1$)

Postulate (adopted). The gravitational response of ψ splits by the *type of energy* that sources it, $\psi = \psi_{\rm rest} + \psi_{\rm grad}$, with

$$\nabla^2\psi_{\rm rest} = -\tfrac{8\pi G}{c^2}\,\rho_{\rm rest}, \qquad \text{(GR4)}$$

$$\nabla\cdot\Big[\mu\Big(\tfrac{|\nabla\psi_{\rm grad}|}{a_\star}\Big)\nabla\psi_{\rm grad}\Big] = -\tfrac{8\pi G}{c^2}\,\rho_{\rm grad/pol}. \qquad \text{(GR5)}$$

Rest-mass energy sources an *unscreened* Poisson channel; only gradient/polarization (edge) energy sources the AQUAL screen. Cosmological χ perturbations are rest-mass dust, $\rho_\chi = m_\chi n_\chi$, so they feed $\psi_{\rm rest}$ and cluster CDM-like: $\boxed{Q_\chi = 1}$. The MOND/RAR phenomenology stays confined to the gradient/polarization sector of bound low-acceleration systems, a bound subsystem counting as low-acceleration only while the Bose mode of its host is typically occupied (App. NL, Axiom NL.14), so $a_0 = 2\sqrt{\alpha}\,cH_0^{\rm loc}$ is untouched.
Status: an adopted action *completion*, from which $Q_\chi = 1$ is then a theorem (Thm GR.10, §GR.3a). This split is *not* present in the bare single-W action: varying $S_\psi = \int[(a_0^2/8\pi G)W(|\nabla\psi|^2/a_\star^2) - (c^2/2)\psi(\rho-\bar\rho)]$ gives the *single* screened equation $\nabla\cdot[\mu\nabla\psi] = -(8\pi G/c^2)(\rho-\bar\rho)$ with $\mu = W'$ acting on the one field ψ *upstream* of the metric — so a massive slow χ, reading only $g_{00} = -c^2e^{-\psi}$, still reads a screened ψ. The weak-response kinetic $W(X) = X - 2\sqrt{X} + 2\ln\big(1+\sqrt{X}\big)$, $X = |\nabla\psi|^2/a_\star^2$, the primitive of $\mu(x) = W'(x^2) = x/(1+x)$, has $W'(0) = 0$, i.e. $\mu(0) = 0$ *exactly*, so no latent unscreened piece hides in W, and adding a floor $\mu \to c_1 + x$ destroys $v^4 = GMa_0$ (the RAR result). A term-by-term audit finds *no* second ρ-sourced μ=1 elliptic operator already in the action, and none is needed: $W = X + W_{\rm nl}$ exactly, with $W'_{\rm nl} = \mu - 1$, and where the μ-law does not act the X term, $(c^4/32\pi G)|\nabla\psi|^2$ in the action, is the unscreened operator; it is the Einstein–Hilbert term's own static scalar energy on DFD's metric (App. WS, Proposition WS.6). The proven obstruction below establishes that $Q_\chi = 1$ *cannot* be a theorem of the single-W action. **DFD therefore *adopts* the Rest-Mass Channel as a postulate: the**

μ-law acts only inside bound systems — the minimal choice: the split is by energy type, not species (cf. gravitational polarization, Blanchet; Verlinde); matter moves under one energy that conserves momentum (§GR.3a), and χ falls like the baryons wherever it fills the μ-law's demand. This raises DFD's gravitational-sector axiom count by one. *Given* the postulate, $Q_\chi = 1$ for rest-mass dust follows, the dark-sector linear clustering (third peak, lensing, $f\sigma_8$) is consistent, and the cluster-vs-galaxy signature below becomes a prediction (its cluster-side amplitude follows from the derived abundance under ΛCDM-like assembly, at estimate grade; see below). The cost is the added axiom; the gain is a closed clustering gate and a falsifiable signature. (Deriving the postulate from a deeper principle would remove the axiom; the obstruction shows that is not possible within the single-W action.)

Proven structural obstruction (why no rearrangement can supply $Q_\chi = 1$). Three candidate derivations were computed explicitly and all collapse to one tautology of the single-W action. (a) The polarization identity $\nabla\cdot[\mu\nabla\psi] = \nabla^2\psi + \nabla\cdot[(\mu-1)\nabla\psi]$ is algebraically true, but for χ's linear R_8 mode ($x \sim 2\times10^{-3}$, $\mu - 1 \simeq -0.95$) the "polarization current" carries essentially the entire field: $\rho_{\rm eff}/\rho \propto \sqrt{a_0/g_N}$, the *full* deep-MOND boost ($Q \approx 20$), not $Q = 1$ — it rewrites the same screened equation, it is not a two-sector split. (b) The coherent condensate is dust on these scales: $c_s^2/c^2 \sim 5\times10^{-63}$, its Jeans scale sits $\sim 10^{14}$ above $k_{\rm LSS}$ (and $\sim 10^{15}$ even after the deep-MOND $G_{\rm eff}^{1/4}$ boost), and ψ sees only the time-averaged $\rho_\chi \propto a^{-3}$. (c) The local-source ($g \gg a_0$) resolution only switches on at $\delta \gtrsim 500$ (nonlinear collapse), never in the linear regime that sets $\sigma_8/f\sigma_8$. The common root: **the unscreened flat direction is reserved for the spatially-homogeneous mean, while any clustering perturbation carries $\nabla\phi \neq 0$ — and $\nabla\phi$ is exactly what W screens**. "structured ⇔ gradient ⇔ screened" is a theorem of the single-W action. Hence $Q_\chi = 1$ is *provably* not a rearrangement of the single-W action: it requires confining the μ-law to bound systems, which leaves the X term, the Einstein–Hilbert term's own static scalar energy, unscreened for clustering modes — a postulate about where the μ-law acts, not a new field.

Theorem GR.6 (Trace-blindness obstruction, strengthening GR.3a)**.** *Let the metric be un-truncated from the transverse-traceless projection h_{ij}^{TT} to the full symmetric* traceless h_{ij}*, with the printed universal coupling $S_{\rm int} = +\frac{1}{2}\int h_{ij}T^{ij}$. Its scalar sector is the single mode $D_{ij}E = (\partial_i\partial_j - \frac{1}{3}\delta_{ij}\nabla^2)E$, whose source is exactly*

$$\mathcal{S}[E] \;=\; \partial_i\partial_j T^{ij} - \tfrac{1}{3}\nabla^2 T^k{}_k. \qquad \text{(GR6)}$$

For a perfect fluid $T^{ij} = \rho v^i v^j + p\,\delta^{ij}$ the pressure terms cancel identically *and the rest-mass term is* absent*, leaving $\mathcal{S}[E] = \partial_i\partial_j(\rho v^i v^j) - \frac{1}{3}\nabla^2(\rho v^2) = O(\rho v^2/c^2)$, which vanishes exactly for cold dust at rest. Hence **no un-truncation of a traceless tensor sector can supply a ρ-sourced μ=1 elliptic operator**: ρc^2 is a pure-trace source and a traceless tensor is blind to it.*

Proof. Direct computation, verified symbolically: with $T^{ij} = \lambda^2\rho v^i v^j + p\,\delta^{ij}$ the source above evaluates to 0 identically at $\lambda = 0$, and ρ enters only at $O(\lambda^2)$. Independently, $\int d\Omega\,(n_i n_j - \frac{1}{3}\delta_{ij}) = 0$ exactly, and the geodesic acceleration on $g = \mathrm{diag}(-c^2e^{-\psi},\, e^{\psi}(\delta + \lambda h))$ with h an arbitrary symmetric traceless tensor is $a^i = \frac{c^2}{2}e^{-2\psi}(\delta_{ij} - \lambda h_{ij})\partial_j\psi$, which is identically zero when $\nabla\psi = 0$. □

Remark GR.7 (What this adds, and the self-defeat corollary). GR.3a's obstruction is scoped to *"the single-W action,"* and the corpus's own h_{ij} field (§formalism) makes DFD a two-potential theory. Theorem GR.6 covers that case and is stronger: it holds for *any* minimally-coupled metric theory with any number of scalar and tensor slots, for dust sources. The conclusion — that $Q_\chi = 1$ requires a postulate — therefore holds for the two-potential theory as well.

Self-defeat corollary. The very property that makes the un-truncation force $\eta = 1$ (trace-blindness: coupling purely to anisotropic stress) is precisely the property that makes it useless for Q_χ. The η-repair and $Q_\chi = 1$ are *mutually exclusive* uses of one field. To obtain a ρ-sourced μ=1 operator one must un-truncate the *trace* slot — and $g_{00} = -c^2e^{-\psi}$ already has that slot filled by ψ, whose Einstein–Hilbert static energy is that operator, with the same coefficient (App. WS); the Rest-Mass Channel adds no field of its own, only the confinement of the μ-law to bound systems.

Remark GR.8 (Kinetic function and TT action normalization). **(i) The μ-function argument convention and the kinetic primitive.** The Rest-Mass Channel box writes $W(|\nabla\psi|^2/a_\star^2)$, i.e. a *squared* argument, and the formalism identifies $\mu(x) = W'(x^2)$. The weak-response kinetic function is the primitive of the simple interpolation, $W(X) = X - 2\sqrt{X} + 2\ln\!\left(1+\sqrt{X}\right)$ with $W'(X) = \sqrt{X}/(1+\sqrt{X})$, i.e. $\mu(x) = x/(1+x) \to x$ and $v^4 = GMa_0$; $W(0) = W'(0) = 0$, $W''(X) > 0$ for $X > 0$, and $W(x^2) = \frac{2}{3}x^3 + O(x^4)$. The argument stays squared. **(ii) The h_{ij} action prefactor and interaction sign.** Varying $A\int[\dot h^2/c^2 - (\nabla h)^2]$ against $S_{\rm int} = +\frac{1}{2}\int hT$ gives $\Box h = T/(4A)$ with $\Box = c^{-2}\partial_t^2 - \nabla^2$, so the field equation $\Box h_{ij} = (16\pi G/c^4)T_{ij}$ printed in §formalism and §gravitational waves requires $A = c^4/(64\pi G)$, the linearized Einstein–Hilbert value. A prefactor $A = c^4/(32\pi G)$, a coupling $S_{\rm int} = -\frac{1}{2}\int hT$ or a wave equation of the opposite sign would be inconsistent with it.

Why this is the right axiom (minimality and motivation). (i) The split is by energy type, not species, by analogy with gravitational polarization (Blanchet; Verlinde), although DFD's polarization carries no inertia of its own; under the adopted energy action and reaction hold and χ falls like the baryons wherever it fills the μ-law's demand, so any species dependence is confined to χ below the demand, a dark-only effect (§GR.3a). (ii) A genuine two-channel structure *already operates in DFD*: the homogeneous mean $\bar\psi$ gravitates *unscreened* into the Friedmann equation (App. AU, $\rho_{\rm dep}/\rho_P = (3/8\pi)\alpha^{57}$; the mean-subtraction $(\rho - \bar\rho)$ rides every species' mean unscreened into $H(t)$), so the postulate *extends* an existing unscreened channel from the mean to the

rest-mass perturbation rather than inventing one wholesale. (iii) χ's misalignment condensate is produced *at rest* (zero momentum, coherent, near-homogeneous), the natural occupant of the rest-mass channel. These make the Rest-Mass Channel the *minimal* and most strongly-motivated axiom that closes $Q_\chi = 1$; a future derivation from a deeper principle would demote it from axiom to theorem (the single-W obstruction shows that derivation is not available within the present action).

Remark GR.9 (Which matter feeds which channel). The rule that only gradient/polarization energy sources the AQUAL screen fixes which matter feeds which channel, and that assignment follows from the two-vertex picture of App. N (Remark N.9). The optical medium is polarized through photon–fermion vertices, each contributing $\sqrt{\alpha}$, so matter with charged constituents polarizes it: neutral atoms and ionized gas alike. χ has no charged constituents and no photon coupling: its photon coefficient is $E = 0$ (App. AV, Theorem AV.35). It therefore does not polarize the optical medium: its crossover acceleration is zero, χ is always in the unscreened regime, gravitates through the rest channel only, and $Q_\chi = 1$ holds with no photon-coupling correction. Electrically neutral cosmic neutrinos behave the same way. This is a conditional derivation: it takes the two-vertex picture of App. N, a heuristic count, as the mechanism of the polarization. What stays postulated is the confinement of the μ-law to bound systems; the rest channel's Poisson term is the Einstein–Hilbert term's own static scalar energy (App. WS), which no traceless tensor could supply (Theorem GR.6).

Consistency. Third-peak: consistent (it was computed with $Q = 1$ cold χ). Galactic RAR: holds only if χ's pull does not add to the μ-law inside discs. Under the additive composition of the two channels, at the 0.03 dex tolerance of the relation (a +3–4% rise in $V_{\rm rot}$), SPARC bounds χ to $\lesssim 20\%$ of $M_{\rm bar}$ inside $2.2R_d$ for the median disc and $\approx 4\%$ for the best-measured discs, and to about half these if χ's mass also feeds the μ-law (computed), while the same physics makes χ form ΛCDM-like halos, which SPARC excludes (App. AV). Under the floor composition of App. AV (an adopted input, in energy form) the requirement is instead that χ's enclosed mass stay below $(\nu - 1)M_{\rm b}$ at each radius: below $M_{\rm b}$ where $g_N > a_0/2$, and a median 3–5 times $M_{\rm b}$ inside the last measured radius (computed). Under the adopted energy χ assembles as in ΛCDM (estimate), and the requirement is met when the inner halos are cored and, in discs above about $10^{11}\,M_\odot$ of baryons, lighter than abundance matching gives (App. AV). A barometric construction (collisionless χ in isothermal Jeans equilibrium in DFD's own field, with a universal dispersion $\gtrsim 337$ km/s) meets the additive bound (worst bright spiral $\approx$ 2–4%), but DFD's structure formation supplies no route to it (computed). PPN: the rest-mass Poisson channel is the clean GR limit, so $\gamma = \beta = 1$ and $\alpha_1 = \alpha_2 = 0$ (Thm IV.1) are preserved; any residual χ-sector fifth force is dark-only and lab-unconstrained (under the adopted energy χ departs from the baryons' fall only where it falls short of the demand; App. AV). **Net:** with the Rest-Mass Channel adopted as a DFD postulate the $Q_\chi = 1$ clustering gate is *closed*. The factor-∼44 χ-abundance gate is likewise *resolved*: the finite-$SU(2)_{60}$ Chern–Simons modular measure gives $Q_{\rm CS} = 0.073$ and, with the exact radiation-era bridge and the flux-period identification (Lemma AV.6), $\Omega_\chi h^2 = 0.1193$ (-0.6σ; App. AV), the continuum $\pi^2/3$ overshoot being an artifact of mixed units (radians^2 vs turns^2) and a continuum measure — see the state-preparation theorem and Bricks 1–3 of App. AV. The abundance is not the open item of the dark sector (its standing conditionality is the no-boundary preparation premise, the flux-period identification, the stated multiplicity 158, two stated normalization conventions and the asserted premise P4′ stated there); how much χ galaxies hold follows, at estimate grade, from the adopted energy (ΛCDM-like halos), and the open item is whether their inner parts are cored as the rotation curves require (App. AV); χ's photon coupling is zero.

Falsifiable signature (galaxies versus clusters — a prediction of the adopted two-channel gravity). The two-channel structure predicts that the dark mass seen beyond the μ-law differs between galaxies and clusters, which separates DFD from *both* ΛCDM and pure MOND. *Clusters* (rest-mass channel) need χ. If χ adds its Newtonian pull to the baryons' μ-law field, as printed, the sixteen clusters of App. I need $4.5 \pm 0.6\,M_{\rm b}$ inside r_{500}, 0.84 ± 0.12 of the cosmic mix $\Omega_\chi/\Omega_b \approx 5.4$, with hydrostatic bias $b = 0.21$ (computed). Under the floor composition of App. AV clusters are Newtonian plus χ and carry the ΛCDM budget: 1.28 ± 0.16 of the cosmic mix inside r_{500} at $b = 0$ and 1.51 ± 0.14 at $b = 0.21$, the usual baryon depletion (computed). The amplitude is what the derived abundance gives under ΛCDM-like assembly: 1.21 ± 0.05 of the cosmic mix predicted inside r_{500} (estimate; App. I). *Galaxies* (baryon-dominated, gradient channel) show little dark mass beyond the μ-law: under the additive composition χ must stay $\lesssim 20\%$ of $M_{\rm bar}$ inside $2.2R_d$ for the median disc; under the floor composition χ thinner than the baryons' phantom is invisible, and only χ in excess of it lifts the relation, one-sidedly. Pure MOND under-predicts cluster dynamical mass by a factor ∼2 (Sanders 2003; Angus–Famaey–Buote 2008; Pointecouteau–Silk 2005), historically patched with ∼2 eV sterile neutrinos; an acceleration-independent χ component can place residual mass even in cluster cores where $g \gtrsim a_0$ (high acceleration), where pure MOND *cannot* generate it. The cold, non-thermal nature of χ is essential here: its de Broglie/Jeans scale ($\sim 10^{-13}$ Mpc for the 32 eV relic, which is produced at rest) is $\sim 10^{13}\times$ below cluster scales, so it can cluster as ordinary CDM; a thermal χ of the same mass would free-stream over ∼20–30 Mpc and fail clusters (estimate). **Falsified if:** (a) disc galaxies hold more χ than the composition tolerates (under the floor composition, massive or concentrated χ halos must lift the relation above the μ-law, and measured halos of that kind without the lift falsify that reading); (b) clusters need *no* rest-mass component beyond the μ-law, which is decided: they need one (App. I), so this clause does not fire; or (c) χ is shown thermal/hot (this last cuts *against* DFD). The fingerprint is the galaxy-vs-cluster asymmetry: little dark mass beyond the μ-law in baryon-dominated disks, rising to the cosmic mix in rich

clusters.

4. GR.3a The Rest-Mass Channel Theorem (the corrected DFD gravitational action)

Scope. What follows is an *action completion*, not a derivation from the single-operator action. The single-μ form $\nabla\cdot[\mu\nabla\psi] = -(8\pi G/c^2)\rho_{\rm tot}$ *provably cannot* yield $Q_\chi = 1$ (§GR.3): it applies the MOND/polarization constitutive law to *all* energy density, including cold χ rest mass. The action below separates conserved rest mass from optical-polarization response; from it, $Q_\chi = 1$ follows as a theorem.

a. Motivation. The DFD optical response has two physically distinct sources of gravitational acceleration: (i) conserved rest-energy density, carried by massive particles and cold coherent matter; (ii) optical gradient/polarization energy, generated by strain, boundary, and low-acceleration medium response. The MOND/RAR constitutive law applies to the second channel, not to conserved rest mass. Accordingly the nonrelativistic response is written in two channels, $\psi = \psi_{\rm rest} + \psi_{\rm pol}$, with $\psi_{\rm rest}$ the unscreened response to rest mass and $\psi_{\rm pol}$ the nonlinear optical-polarization response.

b. Action.

$$S_\psi = \int dt\, d^3x \Big[\tfrac{c^4}{32\pi G}|\nabla\psi_{\rm rest}|^2 + \tfrac{a_0^2}{8\pi G}F\Big(\tfrac{|\nabla\psi_{\rm pol}|^2}{a_\star^2}\Big) - \tfrac{c^2}{2}\rho_{\rm rest}\psi_{\rm rest} - \tfrac{c^2}{2}\rho_{\rm pol}\psi_{\rm pol}\Big], \tag{GR7}$$

with $\mu(y) \equiv F'(y^2)$, $y = |\nabla\psi_{\rm pol}|/a_\star$. Matter moves under the energy W of App. AV, Eq. (AV28), a functional of the rest channel's Newtonian fields of the baryons and of χ that gives the baryons the floor composition exactly in spherical symmetry; the field equations below state the channel split. An action in which all matter coupled to the total ψ would make all rest mass a source of $\psi_{\rm pol}$ (derived), and the rule that every species moves in the total ψ breaks action and reaction: for a $10^{10}\,M_\odot$ clump 100 kpc from a $5\times10^{10}\,M_\odot$ galaxy it gives a drift of 45 km/s per Gyr (computed). Under W momentum and angular momentum are conserved exactly, and energy at fixed a_0; the same pair does not drift, and with the galaxy's own χ halo in place it attracts at the Newtonian value where that halo fills the demand at the clump and up to about 4% more weakly beyond it (computed). The price is χ's equivalence principle where χ falls short of the μ-law's demand (App. AV).

Constitutive reading of $\rho_{\rm pol}$ (essential). Here $\rho_{\rm pol}$ is the *induced* optical-polarization (strain) charge, $\rho_{\rm pol} = -\nabla\cdot\mathbf{P}$ with $\mathbf{P}$ the polarization sourced by the baryonic rest mass — *not* an independent matter density and *not* a duplicate of $\rho_{\rm rest}$. It is constitutively slaved to the baryonic source and self-extinguishes, $\rho_{\rm pol}\to 0$ as $\mu\to 1$ ($g\gg a_0$), so only the rest channel survives in the solar-system/strong-field limit ($G_{\rm eff} = G$, no doubling). In the deep-MOND limit the induced charge reproduces $\rho_{\rm pol}\approx\rho_{\rm baryon}$, closing the observed RAR $g_{\rm tot} = \nu(g_N/a_0)\,g_N$ with $\nu\to\sqrt{a_0/g_N}$ for $g_N\ll a_0$. This induced reading (an analogue of Blanchet's gravitational polarization, though here the polarization carries no inertia) is the *unique* internally consistent one: a second *independent* copy of the rest mass would give $G_{\rm eff} = 2G$ at $g\gg a_0$ and break the PPN normalization. Equivalently, the channel split is by *energy type* (conserved rest mass vs. optical strain), not by particle species, and under the energy W the baryons and χ fall alike wherever χ fills the μ-law's demand.

Theorem GR.10 (Rest-Mass Channel)**.** *Variation of the two-channel action* (GR7) *gives an* unscreened *Poisson channel for conserved rest mass and the* screened *AQUAL channel for polarization energy,*

$$\nabla^2\psi_{\rm rest} = -\tfrac{8\pi G}{c^2}\rho_{\rm rest},\qquad \nabla\cdot\Big[\mu\Big(\tfrac{|\nabla\psi_{\rm pol}|}{a_\star}\Big)\nabla\psi_{\rm pol}\Big] = -\tfrac{8\pi G}{c^2}\rho_{\rm pol}. \tag{GR8}$$

Proof. Varying S_ψ in $\psi_{\rm rest}$ and integrating by parts (discarding the boundary term), $\delta S_{\rm rest} = \int dt\, d^3x\,\big[-\tfrac{c^4}{16\pi G}\nabla^2\psi_{\rm rest} - \tfrac{c^2}{2}\rho_{\rm rest}\big]\,\delta\psi_{\rm rest}$; stationarity for arbitrary $\delta\psi_{\rm rest}$ gives $\nabla^2\psi_{\rm rest} = -\tfrac{8\pi G}{c^2}\rho_{\rm rest}$, the unscreened Poisson channel. Varying in $\psi_{\rm pol}$ with $y = |\nabla\psi_{\rm pol}|/a_\star$, the nonlinear term contributes $\tfrac{c^4}{16\pi G}\mu(y)\nabla\psi_{\rm pol}\cdot\nabla\delta\psi_{\rm pol}$ (using $\mu(y) = F'(y^2)$ and $a_\star = 2a_0/c^2$); integrating by parts, $\delta S_{\rm pol} = \int dt\, d^3x\,\big[-\tfrac{c^4}{16\pi G}\nabla\cdot(\mu(y)\nabla\psi_{\rm pol}) - \tfrac{c^2}{2}\rho_{\rm pol}\big]\,\delta\psi_{\rm pol}$, and stationarity gives $\nabla\cdot[\mu(|\nabla\psi_{\rm pol}|/a_\star)\nabla\psi_{\rm pol}] = -\tfrac{8\pi G}{c^2}\rho_{\rm pol}$. The nonlinear MOND/RAR operator is thus attached to optical-polarization energy, not to conserved rest mass. □

Corollary GR.11 (Cold χ clusters with $Q_\chi = 1$)**.** *After oscillation onset $\rho_\chi\simeq m_\chi n_\chi$ with $p_\chi\simeq 0$ and gradient pressure suppressed on cosmological linear scales, so cosmological χ perturbations are conserved rest-mass dust. They source $\psi_{\rm rest}$, $\nabla^2\psi_{\rm rest} = -(8\pi G/c^2)\rho_\chi$. The postulate confines the polarization to bound low-acceleration systems (the Rest-Mass Channel box above), so linear, unbound perturbations do not polarize the medium; hence their effective linear-clustering response is* $\boxed{Q_\chi = 1}$*, recovering cold-CDM-like linear growth and preserving the CMB third-peak result. The third-peak height is set at recombination, before any baryon is bound, so it does not depend on how the polarization of bound systems behaves once structure forms (Remark GR.12).*

Remark GR.12 (Where the μ-law acts). The Rest-Mass Channel box states where the μ-law acts: the MOND/RAR phenomenology stays confined to the gradient/polarization sector of bound low-acceleration systems. Read literally, the medium is polarized only inside bound systems. The polarization $\mathbf{P}$ then vanishes on the edge of each bound region, so by Gauss's theorem the induced charge $\rho_{\rm pol} = -\nabla\cdot\mathbf{P}$ integrates to zero over the region: the phantom charge is redistributed inside it, and none of it lies beyond the region. Outside, the

field of a non-spherical system keeps the multipoles of that redistributed charge, which vanish for a spherical one. Three-dimensional particle-mesh runs of structure formation with χ and the baryons (the floor composition of App. AV, every bound baryon polarizing, the bound region cut at r_{200m} or $1.5\,r_{200m}$ of each halo) give a residual net polarization mass of 0.0003–0.002 of the mean matter density at $z = 0$, from haloes whose compensating rims the grid does not resolve, raise σ_8 by a factor 1.001–1.005 and the lensing power at $k = 0.1$–$0.4\,h$/Mpc by a factor 1.003–1.07 (and by 2–40% at $k = 0.7$–$1.3\,h$/Mpc), and leave the CMB untouched (computed). With the compensating rims resolved (halo model), the confinement leaves the matter power unchanged to 0.2% at $k \leq 0.3\,h$/Mpc and raises it only at $k \gtrsim 2\,h$/Mpc: by 7–56% at $k = 2$–$10\,h$/Mpc if bound baryons trace their haloes, and by under 4% if a third of them do (computed at $z = 0.3$). The particle-mesh values above are an upper envelope set by the unresolved rims; small-scale cosmic shear and galaxy lensing, with bound-baryon profiles measured in X-rays and the Sunyaev–Zel'dovich effect, decide the size of the boost. Every SPARC rotation curve ends inside $0.25\,r_{200m}$, so the rotation-curve results are kept (computed), and a central galaxy feels almost no external field from its neighbours, whose net phantom is zero, so the a_0 that SPARC measures stays DFD's (estimate). In the rotation-curve fits of Chae et al. this reading gives a fitted external field of about 0.003 for every central galaxy, and 0.007–0.013 with the domain-local screen of App. ZT (computed). Their reported median, 0.044–0.053 [166, 167], is carried by the least well measured third of their sample: the other two thirds give 0.009 and 0.002, the fitted field shows no correlation with environment density on 4–$20\,h^{-1}$Mpc scales or with their own field estimates, and weighted by the per-galaxy errors, with the 0.02 fitting-function systematic of Chae et al. added in quadrature, the sample median is 0.012 ± 0.009 and the mean 0.022 ± 0.007, 1.1σ and 2.8σ from this reading (0.6σ and 1.8σ with the screen; computed; see also [168, 169]). The outer declines of NGC 5055 and NGC 5033 are not produced by this reading. BIG-SPARC, about 4000 galaxies, decides it: this reading predicts no environment trend in the a_0-free shape of the curves, where MOND with the fields of Chae et al. predicts a correlation of 0.1–0.3 (estimate). The literal reading is the one cosmology allows: if the phantom of bound baryons reached beyond their bound regions, the same runs would give a polarization mass of 0.47–1.25 of the mean matter density and 2.9–6.4 times the lensing power (computed), against a viability limit near 0.03 (estimate). The reading has one further cost. The flat weak-lensing profile of isolated galaxies is not kept beyond the bound radius, about 0.25–0.6 Mpc for galaxies of 10^{10}–$10^{11}\,M_\odot$ in baryons: inside it DFD's $1/R$ profile fits the stacked measurement where the galaxies' χ stays below the μ-law's demand, and beyond it, with the χ halo and the surrounding structure included, DFD falls below the measured points of Brouwer et al.'s looser-isolation stack for every halo mass tried, and of Mistele et al.'s stricter-isolation stack for the lighter halo masses (computed). The halo model of ΛCDM falls below them in the same way; the far points are reached only if neighbours admitted by photometric redshifts add signal at the level Brouwer et al.'s own ΛCDM mock of the selection finds, so spectroscopically isolated lens samples decide it. Galaxy groups are not a cost: their hot gas is bound and has charged constituents, so it polarizes the medium (Remark GR.9), and on published X-ray masses the μ-law falls short of groups as it does of clusters, so groups need χ as clusters do (App. I; computed on published inputs).

Corollary GR.13 (The galactic RAR and the two channels)**.** *In galaxies $g_{\rm total} = g_{\rm rest} + g_{\rm pol}$: the rest channel gives the Newtonian baseline $g_{\rm rest} = g_N$ and the polarization channel the low-acceleration enhancement $g_{\rm pol} \sim \sqrt{a_0 g_N}$ in the deep-MOND regime. For the baryons, since $\sqrt{a_0 g_N} \gg g_N$ for $g_N \ll a_0$, the RAR stays polarization-dominated in galaxy outskirts while the rest channel carries cosmological χ clustering. The rest channel also carries the Newtonian pull of any χ inside a galaxy, and ΛCDM-like χ halos added this way count the missing mass twice, which SPARC excludes; the RAR is kept only if χ's pull does not add inside discs, as under the floor composition of App. AV, adopted in energy form; how much χ galaxies hold follows at estimate grade from the adopted energy (ΛCDM-like halos whose inner parts must be cored; App. AV). Solar-system and strong-field tests sit at $g \gg a_0$, where $\mu \to 1$ and both channels are Poisson, so the total ψ is the standard potential and $\gamma = \beta = 1$, $\alpha_1 = \alpha_2 = 0$ (Thm IV.1), the 2PN light-bending, and the compact-star results, which are general relativity's (App. WS), are* unchanged.

Interpretation and status. The one-operator form $\nabla\cdot[\mu\nabla\psi] = -(8\pi G/c^2)\rho_{\rm tot}$ incorrectly screens cold χ rest mass, making linear χ perturbations over-grow and blocking $Q_\chi = 1$. The corrected action separates conserved rest mass from optical-polarization response — the source-space decomposition required by the physical distinction between conserved rest-energy density and emergent optical strain energy. With Theorem GR.10, DFD's χ sector has its particle, relic law, *and linear clustering* ($Q_\chi = 1$, Cor. GR.11) derived from the corrected action. The abundance normalization is derived too, conditional on the flux-period identification (Lemma AV.6), the stated multiplicity 158, two stated normalization conventions and the asserted premise P4′ (Lemma AV.27): the finite $SU(2)_{60}$ CS-vacuum Casimir expectation gives $\Omega_\chi h^2 = 0.1193$ (-0.6σ from Planck; App. AV Step 5b); in consistent units the vacuum variance sits 12.45% below the uniform-angle value: the continuum $\sin^2$ measure lowers it by 15%, the Sugawara factor K/k raises it by 3.3%, and finiteness itself moves it by 0.09%; the amplitude is forced given two stated conventions (Casimir; measure conditional on P4′; $k(k+2)$ from χ's derived $\mathbb{Z}_2$ + Sugawara); the relic bridge is exact ($\kappa_{\rm rad}$), and the grade is conditional-derived on the named flux-period identification, the stated count 158 and P4′ (App. AV). *Status: this is an action completion*

— the DFD gravitational action — not a derivation from the single-operator form, which the obstruction of §GR.3 shows cannot yield $Q_\chi = 1$.

5. GR.4 The single DFD growth prediction

With the carrier fixed as χ-matter ($Q = 1$, GR-like) on the measured-clock background ($H_0^{\rm early} = 67.52$, $\omega_\chi = 0.11928$, $\sum m_\nu = 61.5$ meV, $n_s = 1 - 2/60$; App. ZS) and the primordial amplitude $A_s = 2.080 \times 10^{-9}$ (the value of $32\pi\alpha^5$, a calibration; App. FK), run forward through CAMB, the linear growth equation

$$\frac{d^2D}{da^2} + \left(\frac{3}{a} + \frac{d\ln H}{da}\right)\frac{dD}{da} - \frac{3}{2}\frac{\Omega_m(a)}{a^2}\,Q\,D = 0, \qquad Q = 1, \tag{GR9}$$

gives $\sigma_8 = 0.806$, $S_8 = 0.822$ and $\Omega_m = 0.312$, and the growth rates below (computed). Growth is scale independent on linear scales except for neutrino free streaming, which lowers f by 0.3% between $k = 10^{-3}$ and $1\,h$/Mpc.

TABLE CIX. DFD growth prediction (single, χ-matter $Q = 1$ carrier) on the measured clock, $\sigma_8(0) = 0.806$. $f\sigma_8$ compared to the 6dFGS, SDSS MGS, BOSS DR12 and eBOSS DR16 measurements; the pull is (DFD−observed)/$\sigma_{\rm obs}$. Against these seven points $\chi^2 = 6.4$, and 6.3 for Planck ΛCDM (computed).

z	$f\sigma_8^{\rm DFD}$	$f\sigma_8^{\rm obs}$	$\sigma_{\rm obs}$	pull
0.067	0.440	0.423	0.055	+0.30
0.15	0.455	0.530	0.160	−0.47
0.38	0.473	0.497	0.045	−0.54
0.51	0.472	0.458	0.038	+0.35
0.70	0.460	0.473	0.041	−0.32
0.85	0.446	0.315	0.095	+1.38
1.48	0.376	0.462	0.045	−1.91

$S_8 = 0.822$ lies 2.8σ above DES Year 6 (0.789 ± 0.012, survey errors only), 0.4σ above KiDS-Legacy and 0.8σ below Planck (computed). The $f\sigma_8$ fit is comparable to ΛCDM's, and the largest residual pull is the high-z QSO bin. On the one-clock C=1 background ($H_0 = 72.09$, $\Omega_m = 0.274$) the same carrier gave $\sigma_8 = 0.820$, $f(0) = 0.487$ and $S_8 = 0.784$; GR.5 and GR.5a record those runs.

6. GR.5 S_8 on the one-clock C=1 background

This subsection and the next record runs on the C=1 background; on the measured clock $S_8 = 0.822$ and the CMB-lensing amplitude is $A_{\phi\phi} = 0.9887$ (GR.4, GR.5a).

Corollary GR.14 (Mild low-side S_8 match)**.** *At the carried normalization the C=1 background gives $S_8 = 0.784$, which lies mildly on the* low *(weak-lensing) side of the S_8 tension and matches both galaxy surveys within $\sim 1\sigma$:*

Reference	S_8	*DFD offset (S_8=0.784)*
KiDS-1000	0.759 ± 0.024	$+1.0\sigma$
DES-Y3 (3×2pt)	0.776 ± 0.017	$+0.5\sigma$
Planck-ΛCDM (CMB)	0.834 ± 0.016	-3.1σ

The C=1 background's lower $\Omega_m = 0.274$ together with the carried $\sigma_8 = 0.820$ gives a mildly low *galaxy-weak-lensing $S_8 = 0.784$, consistent with KiDS-1000 ($+1.0\sigma$) and DES-Y3 ($+0.5\sigma$): a* mild match. *This is the* same *$\sigma_8 = 0.820$ that delivers the CMB-lensing pass (GR.5a / App. CL): because DFD's linear growth is $Q \equiv G_{\rm eff}/G = 1$ (LCDM-like),* one *σ_8 sets* both *the galaxy-lensing S_8 and the CMB-lensing amplitude simultaneously. The galaxy-lensing match and the CMB-lensing pass are therefore* jointly available *at $\sigma_8 = 0.820$.*

a. The value $S_8 = 0.755$. The value $S_8 = 0.755$ is not independently derived*: it is simply $S_8 = 0.755$ algebraically restated from the alternative CMB-normalization $\sigma_8 = 0.790$ ($S_8 = \sigma_8\sqrt{\Omega_m/0.3}$). Reaching $\sigma_8 = 0.790$ requires shrinking $A_s = 32\pi\alpha^5$ by 7.2% with no DFD justification (GR.7 itself flags* 0.790 *as "asserted, not independently re-derived"). Moreover, $\sigma_8 = 0.790$ is* not simultaneously available with the CMB-lensing pass*: at $\sigma_8 = 0.790$ the $C_L^{\phi\phi}$ deficit grows to $\sim$ 11% and the nine-bin Planck lensing likelihood disfavours DFD at $> 3.6\sigma$ (App. CL). Since one σ_8 ($Q = 1$) sets both arms, the sharper $S_8 = 0.755$ galaxy-lensing number and the CMB-lensing pass* cannot *be claimed together. The $S_8 = 0.755$ value is therefore "an alternative corpus CMB-normalization (asserted, not re-derived) that would sharpen galaxy-lensing to $S_8 = 0.755$ but fails CMB lensing at $> 3.6\sigma$ — not simultaneously available with the lensing pass."*

7. GR.5a The carried $\sigma_8 = 0.820$ passes Planck CMB lensing

Corollary GR.15 (CMB-lensing pass at the carried normalization)**.** *Run forward through CAMB on the frozen DFD background, the amplitude $A_s = 32\pi\,\alpha^5$, a numerical match to the calibrated amplitude, gives $\sigma_8(0) = 0.820$, for which the lensing power spectrum ratio $C_L^{\phi\phi,\rm DFD}/C_L^{\phi\phi,\Lambda\rm CDM}$ is a* flat $\sim 4\%$ *below ΛCDM across $L = 8$–400 (shape scatter* 0.3%*: pure amplitude, no shape penalty); the full nine-bin Planck 2018 lensing likelihood returns $A_L = 1.0542 \pm 0.0263$, a mild $+2.06\sigma$* ***pass*** *($\chi^2 = 12.66/9$, $\Delta\chi^2 = +3.9$; App. CL). The $\sim$4% deficit is structural — the one-clock $C = 1$ background, $H_0 = 72.09$ with $\Omega_m = 0.274$ at every epoch, which the two-clock postulate does not reproduce (App. ZS), had low Ω_m and $Q = 1$ growth, so $C_L^{\phi\phi} \propto \Omega_m\sigma_8^2$ ran mildly low — but it is well below any falsification threshold. At the measured-clock background ($H_0^{\rm early} = 67.52$, $\omega_\chi = 0.11928$; App. ZS) the full-convention nine-bin lensing amplitude is $A_{\phi\phi} = 0.9887$ (-0.80σ): the mild $+2\sigma$ flag dissolves. The numbers above are the C=1-background run.*

8. GR.6 Resolving the directional $f\sigma_8$ ambiguity

The directional RSD signature $f\sigma_8(z,\hat{n}) \propto (\hat{k}\cdot\hat{g})^2$ in AC §AC.7 was flagged "regime-contested" because it presupposes a nonzero cosmological background gradient $\hat{g}$. Theorem AE.1 removes the ambiguity:

Corollary GR.16 (The growth signature is isotropic on linear FRW scales)**.** *Since* $|\nabla\bar{\psi}| = 0$ *on the FRW background, there is* no *preferred direction* $\hat{g}$ *for true linear cosmological modes. The directional* $f\sigma_8(z,\hat{n})$ *signature therefore* ***does not exist*** *for linear cosmological RSD; the linear growth signature is* isotropic*, governed by the* χ*-matter* $Q = 1$ *growth law (GR.4). A directional* $(\hat{k}\cdot\hat{g})^2$ *modulation survives* only *near collapsed structures, where a reconstructed* ψ*-screen gradient is nonzero (galactic/cluster scales). The directional falsifier of AC §AC.7 is therefore a galactic/cluster-scale falsifier.*

9. GR.7 Status

Growth-Regime Adjudication — Status

Resolved:

- Regime partition (Theorem GR.2): Transition $x = g/a_0 = 1$.
- Carrier identified (Proposition GR.4): cosmological linear δ_m is carried by χ-matter ($Q = 1$), *not* by the AQUAL $G_{\rm eff}$. Hence **no single action-level** $G_{\rm eff}(k,a)$ **both spans regimes and fits the growth data**; the growth observables flow from χ-matter.
- Single prediction (GR.4, measured clock): $\sigma_8 = 0.806$, $S_8 = 0.822$ (2.8σ above DES Year 6, 0.4σ above KiDS-Legacy), CMB-lensing $A_{\phi\phi} = 0.9887$ (-0.80σ), and the $f\sigma_8(z)$ table ($\chi^2 = 6.4$ for seven points); the values of GR.5–GR.5a belong to the C=1 background.
- Directional ambiguity resolved (Corollary GR.16): linear cosmological growth signature is *isotropic*; the $(\hat{k}\cdot\hat{g})^2$ modulation is galactic/cluster-only.

Caveats:

- The $f\sigma_8$ fit is comparable to ΛCDM's: $\chi^2 = 6.4$ for seven points against 6.3 for Planck ΛCDM (computed).
- The value $\sigma_8 = 0.820$ of GR.5 belongs to the C=1 background and used $A_s = 32\pi\alpha^5$, a numerical match to the calibrated amplitude (App. FK); on the measured clock $\sigma_8 = 0.806$ (GR.4). The alternative $\sigma_8 = 0.790$ ($S_8 = 0.755$) is a corpus CMB-normalization, asserted not re-derived, requiring a 7.2% A_s shrink; it would sharpen galaxy-lensing to $S_8 = 0.755$ but fails CMB lensing at $> 3.6\sigma$ and is therefore not simultaneously available with the lensing pass.

Deciding dark-sector growth item (a *proven* obstruction; closable by the Rest-Mass Channel extension):

- The "one σ_8 sets both" pillar (GR.5) rests on χ-matter clustering Newtonianly ($Q = 1$) on *linear* scales. But Lemma GR.3 puts the *same* linear R_8 modes at $x \sim 2\times10^{-3} \ll 1$ (deep-MOND), and this is a *proven* structural obstruction, not a scoping tension: the single-W screen acts on every spatial gradient, so any linear clustering mode is screened into the deep-MOND ($Q \gg 1$) branch ("structured ⇔ gradient ⇔ screened"; §GR.3, the Rest-Mass Channel box). The local-source ($g \gg a_0$) escape only switches on at $\delta \gtrsim 500$ (nonlinear collapse), *never* in the linear regime that sets $\sigma_8/f\sigma_8$. Reproducing the observed $Q = 1$ *provably* requires the Rest-Mass Channel (a second, μ=1, rest-mass-sourced Poisson operator), which DFD *adopts as a postulate* (§GR.3); given it, $Q_\chi = 1$ holds. A future derivation of the postulate from a deeper principle would demote it to a theorem. If instead the AQUAL screen leaked into linear growth, Q would run with z ($\sim$20 at $z = 0$ to $\sim$12 at $z = 2$), $D(z)$ would not be flat — a z-dependent $f\sigma_8$ signature.

Open-problems item F: the regime *question* is closed here; the *pipeline* obligation is open: the production $P(k)$ pipeline of App. PK has run only on the one-clock $C = 1$ background.

Scope restriction (App. AC): AC's operator M_{ij} (Lemma AC.1) and AE's optical Q are both retained as correct.

10. GR.8 Falsifier

Growth-Regime Adjudication — Falsifier

The adjudication is falsified if any of the following hold:

1. **Isotropy of linear RSD broken.** A statistically significant ($> 3\sigma$) detection of a $(\hat{k}\cdot\hat{g})^2$ directional modulation in *linear* cosmological $f\sigma_8(z,\hat{n})$ on scales free of collapsed structure would contradict Corollary GR.16.
2. S_8**.** On the measured clock DFD's $S_8 = 0.822$ lies 2.8σ above DES Year 6 and 0.4σ above KiDS-Legacy (GR.4); a weak-lensing S_8 that settles near DES Year 6's value at higher precision excludes it.
3. $f\sigma_8$ **excludes the** χ**-matter** $Q = 1$ **law.** If the full $P_{\theta g}/P_{gg}$ pipeline gives $f\sigma_8$ inconsistent with the $Q = 1$ prediction on the measured clock ($\Omega_m \simeq 0.312$, $\sigma_8 = 0.806$) at $> 3\sigma$ across ≥ 2 redshift bins, the carrier identification fails. A detection of a z*-running* $Q(z)$ (i.e. non-flat $D(z)$) instead would signal the AQUAL screen leaking into linear growth — the deciding item of GR.7.
4. **Transition mis-located.** If galactic/cluster dynamics require the deep-MOND/Newtonian transition at $g \neq 2\sqrt{\alpha}\,cH(z)$, the partition condition Eq. (GR2) is wrong.

11. GR.9 Reproducibility

The $Q = 1.118$ comparison, the $x(R_8)$ table and the $C{=}1$ key values below are produced by `dfd_class/growth_regime_adjudication.py` (numpy/scipy), which integrates the $Q = 1$ and $Q = 1.118$ growth ODEs, tabulates $x = g/a_0(z)$ on R_8, computes $\sigma_8/S_8/f\sigma_8$, and writes `dfd_class/fig_growth_regime.png` (Panel A: $G_{\rm eff}/G$ across regimes with the $x = 1$ transition and the deep-MOND linear-scale band; Panel B: $f\sigma_8(z)$ DFD vs DESI vs ΛCDM, with an S_8 inset showing the mild low-side placement). Key values *as computed on the one-clock* $C{=}1$ *background* ($H_0 = 72.09$, $\Omega_m = 0.274$); the measured-clock values are those of the scope box at the head of this appendix: $\bar{x}_{\rm AC} = 5.853$, $\langle G_{\rm eff}\rangle = 1.118\,G$, $a_0(0) = 1.197\times10^{-10}\,{\rm m/s^2}$, $x(R_8, \delta{=}1, z{=}0) = 2.1\times10^{-3}$, primary ($A_s = 32\pi\alpha^5$) $\sigma_8 = 0.820$, $S_8 = 0.784$ (CMB-lensing $A_L = 1.0542$, $+2.06\sigma$ pass); alternative corpus normalization $\sigma_8 = 0.790$, $S_8 = 0.755$ (asserted, not re-derived, fails CMB lensing $> 3.6\sigma$ — not simultaneously available); AC-branch integrated over-growth +54%.

Appendix A0Z: Epoch Confrontation of $a_0(z)$

1. Scope, and the external measurement it builds on

Theorem XIX.3 promotes the acceleration scale to $a_0(z) = 2\sqrt{\alpha}\,cH(z)$, and §XIX records its first measurement, over $0.33 < z < 1.44$: a theory-neutral re-analysis of the MUSE–DARK III binned RAR scale [109] fits the continuous family $a_0(z) = A(1+z)^\gamma$ and obtains

$$\gamma = 0.78 \pm 0.15 \ \text{(statistical)} \qquad \text{(A0Z1)}$$

[110], excluding a frozen scale at 5.3σ on the published bin errors and the matter–density scaling $a_0 \propto \sqrt{\rho_m}$ at 4.8σ (on the exponent's error; 4.7σ by likelihood ratio), with Hubble tracking consistent at 2.1σ and information-criterion-preferred. Adding the local SPARC $z \simeq 0$ anchor gives $\gamma = 0.83 \pm 0.13$ and pushes the frozen exclusion to 6.6σ. That analysis is *published*: MNRAS **551**(4) (2026 October), article ID `stag1485`, `doi:10.1093/mnras/stag1485`, published 2026 September 7 (article type Letter). This appendix does not restate that result. It adds six things: the refit of the same bins on the one-clock $C = 1$ background (§A0Z 2); the predefined control showing that the $C = 1$ background's information-criterion margin is *not* significant on its own (Stat. A0Z.4); the amplitude tension, stated on both sides (§A0Z 4); a derived ceiling on any cosmic external-field term (§A0Z 5); the survey refitted galaxy by galaxy from its public products (§A0Z 6); and the confrontation with massive discs at $0.6 < z < 2.5$ (§A0Z 7), together with dated forward falsifiers (§A0Z 8). The published exponent is a correct fit of the published bins. Counted galaxy by galaxy, the trend within the survey puts a frozen a_0 about 1σ away; anchored to SPARC's $z = 0$ value, the galaxy-level bins still exclude a frozen a_0 at about 3σ, and DFD's zero-parameter law fits them on the bound-matter clock. The trend depends on how the molecular gas is added, and massive discs do not show the predicted rise beyond $z \simeq 1.5$ at face value. The epoch law is therefore contested.

Remark A0Z.1 (The reference is theory-neutral). Ref. [110] does not mention DFD, adopts a Planck ΛCDM background ($\Omega_m = 0.307$, $H_0 = 67.7$), and is cited here as an external observational constraint. Its bins are four quantile bins in redshift from disc–halo decompositions of 79 star-forming galaxies over $0.33 < z < 1.44$; the fits below treat them as independent, which the source notes is optimistic because they share the parent analysis's calibrations. Within each bin the radial points of one galaxy are correlated, and counted galaxy by galaxy the uncertainty is several times the published one (computed; §A0Z 6).

Remark A0Z.2 (Both confidence conventions, as published). The confidence level of the plotted bars is not stated in Ref. [109], so Ref. [110] carries every fit under both readings. Under the 1σ reading the numbers quoted above apply. Under the 95% reading the exclusions strengthen — $\gamma = 0$ to $\gtrsim 10\sigma$ and $\gamma = 3/2$ to

9.5σ on the exponent's error (9.2σ by likelihood ratio), with the exponent family tightening to $\gamma = 0.78 \pm 0.08$ — while exact $E(z)$ tracking moves into goodness-of-fit tension ($\chi^2 = 19.9/3$, $p = 1.8 \times 10^{-4}$), the binned growth then sitting *shallower* than $E(z)$ at $\sim 4\sigma$ on the Planck background. The two exclusions hold under either reading; the *consistency* of Hubble tracking does not. The corresponding offset evaluated on the current background (§A0Z 2) is 4.2σ, where $\gamma_E = 1.098$ (3.4σ on the one-clock $C = 1$ background); that is this corpus's number, not the source's.

2. DFD needs no borrowed background

A theory-neutral analysis must borrow $E(z)$ from somewhere. DFD need not: its own background supplies $E(z)$, so $a_0(z) = 2\sqrt{\alpha}\, cH(z)$ is a *zero-parameter* curve up to one overall amplitude. The fits of Table CX were run on the $C = 1$ background ($H_0 = 72.0897$, $\Omega_m = 0.2749$; App. CL, App. GR); the CMB-anchored channels read $H_0^{\rm early} = 67.52 \pm 0.09$, $\Omega_m \simeq 0.31$ (App. ZS), which moves this background. Under the two-clock postulate the absolute a_0 scale tests the postulate (Falsifier ZS.14, item iv); a Euclid/DESI lensing RAR decides it once baryonic masses are known to about 2% (App. ZS). The $C = 1$, $\Omega_m = 0.2749$ row of Table CX belongs to the one-clock $C = 1$ background. At $\Omega_m \simeq 0.312$ the measured-clock refit gives $A = 1.394 \pm 0.032$, $\chi^2 = 5.36/3$, AICc $= 9.36$, $\gamma_E = 1.098$, and a 2.1σ exponent offset. Hubble tracking remains viable, without the low-Ω_m AICc improvement.

TABLE CX. Weighted-least-squares fits to the four binned RAR-scale measurements of Ref. [109] as tabulated in Table 1 of Ref. [110], with the plotted bars read as 1σ. AICc $= \chi^2 + 2k + 2k(k+1)/(N-k-1)$ at $N = 4$. DFD's row uses its *derived* Ω_m; only the overall amplitude is free.

Model	k	χ^2/ν	AICc
$a_0 = A$ (frozen)	1	28.83/3	32.83
$a_0 = A(1+z)^{3/2}$	1	23.21/3	27.21
$a_0 = a + bz$ (survey's own)	2	1.10/2	17.10
$a_0 = A(1+z)^{\gamma}$	2	1.16/2	17.16
$a_0 = A\,E(z)$, Planck $\Omega_m = 0.307$	1	5.18/3	9.18
$a_0 = A\,E(z)$, DFD current $\Omega_m \simeq 0.312$	1	5.36/3	9.36
$a_0 = A\,E(z)$, DFD $C = 1$ $\Omega_m = 0.2749$ (provenance)	1	4.00/3	8.00

Status A0Z.3 (Measured clock: viable, without the $C = 1$ AICc edge). On the measured-clock background the refit gives $A = 1.394 \pm 0.032$, $\chi^2 = 5.36/3$, AICc $= 9.36$, and $\gamma_E = 1.098$, $+2.1\sigma$ from the measured $\gamma = 0.78 \pm 0.15$. This is essentially the Planck-background row and remains the preferred one-parameter description relative to the frozen and matter-density alternatives. The lower AICc 8.00, amplitude 1.4497 ± 0.0333, and $\gamma_E = 1.0395$ are the $C = 1$, $\Omega_m = 0.2749$ row, not a DFD advantage.

Status A0Z.4 (On the one-clock $C = 1$ background the improvement over Planck is not significant). A predefined false-positive control was run: drawing Ω_m at random from $[0.10, 0.50]$ and refitting, the probability that a random background beats DFD's σ-distance is $\mathbf{P = 0.426}$. **A ΔAICc of -1.18 on four points is therefore not evidence in itself.** What is not reproducible by chance is the *absence of freedom*: see Rem. A0Z.5. Independently, applying a virialised-regime external-field correction moves the effective exponent *away* from the measurement, from 1.73σ to 2.27–2.76σ on the $C = 1$ background.

Remark A0Z.5 (DFD has no tuning freedom in γ_E). Ω_m is not fitted: it is fixed by H_0 and $\omega_b h^2 = 0.022273$ with the derived $\omega_\chi h^2$. At the $C = 1$ background ($H_0 = 72.0897$, $\omega_\chi h^2 \in [0.1182, 0.12086]$, i.e. $\Omega_m \in [0.27030, 0.27542]$) the induced γ_E band is $[1.03224, 1.04031]$, of width $\mathbf{0.0081}$ — about 19 times narrower than one σ of the measurement. MOND must *assume* $a_0(z)$ and *borrow* $E(z)$; DFD fixes both from its measured clock, and therefore cannot move. At the measured clock ($H_0 = 67.52$, $\omega_\chi = 0.1192806$; App. ZS) $\Omega_m \simeq 0.312$ and the recomputed effective slope is $\gamma_E = 1.098$. The no-tuning-freedom *structure* is unchanged; only the numerical advantage of the $C = 1$ background disappears.

3. The zero-parameter local value

At $z = 0$, on bound-matter clocks (Postulate ZS.11), the same law gives a prediction with no measured coefficient,

$$a_0(0) = 2\sqrt{\alpha}\, cH_0^{\rm loc} = 1.1966 \times 10^{-10}\ {\rm m\,s^{-2}}, \quad \text{(A0Z2)}$$

against the canonical SPARC value $g^\dagger = [1.20 \pm 0.02\,({\rm stat}) \pm 0.24\,({\rm sys})] \times 10^{-10}$ of Refs. [10, 16]: within the published systematic uncertainty. *No galactic parameter is adjusted anywhere in Eq.* (A0Z2). On the early clock the same law gives 1.1208×10^{-10}, $-3.96\sigma_{\rm stat}$ and -0.33σ on the systematic uncertainty.

4. The amplitude tension

Exponent-based conclusions are exactly invariant under any redshift-independent rescaling of a_0; *amplitude* conclusions are not.

Status A0Z.6 (Amplitude, both sides). Against the measured-clock fitted amplitude $A = 1.394 \pm 0.032$, DFD's early-clock $a_0(0) = 1.1208 \times 10^{-10}$ lies below the survey anchor by $8.5\sigma_{\rm stat}$ (about 2σ counted galaxy by galaxy), corresponding to a coherent stellar-mass shift of about $+0.095$ dex. The gap is the same on either clock: the survey's masses are fitted to its rotation curves, so on distances computed with $H_0^{\rm loc}$ its amplitude and the bound-matter $a_0 = 1.1966 \times 10^{-10}$ rise together, and the bound-matter value lies 0.094 to 0.103 dex (8.5 to $9.2\sigma_{\rm stat}$) below it (computed). The accepted survey and SPARC systematic budgets remain much wider than their statistical bars, so this is a mass-scale-conditional comparison, not

an unconditional failure. The theory-free survey-versus-canonical-SPARC offset remains about 17% and 0.8σ on SPARC's systematic-dominated budget. By the same currency a frozen a_0 requires +0.220 to +0.354 dex per bin, 2.3 to 3.8 times more, and a redshift tilt that no common-mode mass rescaling supplies. The survey's own stated requirement to reconcile all bins with a canonical frozen a_0 is +0.2 to +0.45 dex, which its authors argue is unsupported by independent checks. A fuller baryon census supplies a tilt of that kind (§A0Z 6). The survey's stellar term is a disc mass fitted to the rotation curve; above $z \simeq 0.9$ it sits about 0.4 dex below the stellar mass from the galaxies' spectral energy distributions, and with those masses the refitted trend falls. With the molecular gas the survey does not count, the trend depends on how the gas is added: in proportion to the survey's own disc masses, within its stated 0.2 dex systematic, the rise stays and DFD's zero-parameter law fits it; tied to SED-based masses through the scaling relations of Ref. [170], the trend is about flat. On either census the amplitude of Hubble tracking lies 0.02 to 0.09 dex below DFD's early-clock zero-parameter value (0.18 dex with both changes together), where on the published census it lies 0.095 dex above (computed). The published exponent is a correct fit of the published bins; DFD is exposed to the absolute stellar-mass scale, and the measured redshift trend is exposed to the baryon census.

5. A cosmic ceiling on any external-field term

Theorem A0Z.7 (Cosmic external-field ceiling)**.** *Let $g_{\rm bg}(z)$ be the Newtonian acceleration at the Hubble radius $R_H = c/H(z)$ sourced by the mean matter density inside it, measured in units of DFD's own epoch scale $a_0(z) = 2\sqrt{\alpha}\, cH(z)$. Then*

$$\boxed{x_{\rm bg}(z) \;\equiv\; \frac{g_{\rm bg}(z)}{a_0(z)} \;=\; \frac{\Omega_m(z)}{4\sqrt{\alpha}}\,,} \qquad \text{(A0Z3)}$$

in which G, c and $H(z)$ cancel identically*. Consequently, with $\tau = \sqrt{x}$,*

$$\tau_{\rm bg}(z) = \frac{\sqrt{\Omega_m(z)}}{2\,\alpha^{1/4}} \;\le\; \frac{\alpha^{-1/4}}{2} = 1.710719 \qquad \textit{for all } z, \qquad \text{(A0Z4)}$$

with equality only in the matter-dominated limit $\Omega_m(z) \to 1$.

Proof. $\bar\rho_m(z) = \Omega_m(z)\cdot 3H(z)^2/8\pi G$ and $g_{\rm bg} = \frac{4\pi}{3}G\bar\rho_m R_H = \frac{4\pi}{3}G\cdot\Omega_m\frac{3H^2}{8\pi G}\cdot\frac{c}{H} = \frac{1}{2}\Omega_m(z)\,cH(z)$. Dividing by $2\sqrt{\alpha}\,cH(z)$ gives $\Omega_m(z)/4\sqrt{\alpha}$; G, c and H have cancelled (symbolic residual identically zero, free symbols $\{\Omega_m, \alpha\}$ only). $\Omega_m(z)$ is monotone increasing to 1 in a flat background, so $\tau_{\rm bg}$ is bounded by $\alpha^{-1/4}/2$. □

Remark A0Z.8 (A ceiling, not a value). Equation (A0Z3) is Lemma GR.3 (App. GR) evaluated at $R\delta = R_H$; the identity is exact, since that lemma gives $x = 2.437\times10^{-3}$ on R_8 at $\Omega_m \simeq 0.312$, whose product with R_H/R_8 is $x_{\rm bg}(0) = 0.913$ (0.8045 on the one-clock $C = 1$ background). **The saturated value is not realised.** Theorem AE.1 (App. AE) gives $a_{\rm ext}^{\rm FRW} = 0$ identically on the homogeneous background, and an independent check forbids saturation directly: a saturated floor at $z = 0$ would cap ν at 1.625 (1.6887 on the one-clock $C = 1$ background), whereas SPARC rotation curves require ν of 5–60. $x_{\rm bg}$ is therefore an upper bound on any cosmic external-field term at any epoch, not its value.

6. The survey refitted galaxy by galaxy

The four bins of Ref. [109] are fits of the radial-acceleration relation to the radial points of the galaxies in each redshift quartile. The survey's baryonic term is a stellar disc whose mass is fitted to the rotation curve together with a model dark halo, plus an atomic-gas term of constant surface density; molecular gas is not counted. The survey's public products give each galaxy's decomposition, so every galaxy can be rebuilt, the bins refitted with errors counted galaxy by galaxy, and the census changed. The rebuilt rotation curves match the release's own derived velocities and dynamical masses to within 0.03 dex in the median (computed).

Status A0Z.9 (The survey's rise at galaxy level). A sample of 79 galaxies selected with the survey's cuts gives bins with the published shape and a level about 12% higher, and an exponent $\gamma = 0.77 \pm 0.21$ against the published 0.78 ± 0.15 (computed). Resampling whole galaxies instead of radial points, the bin uncertainties are 4 to 6 times the point errors, because the radial points of one galaxy are correlated and each bin holds about 20 galaxies. At galaxy level the exponent's 16–84% range is −0.10 to 1.67, and within the survey a frozen a_0 lies about 1σ away, against 5.3σ on the published bin errors; anchored to SPARC's $z = 0$ value, as Ref. [110] does, the galaxy-level bins still exclude a frozen a_0 at about 3σ: on SPARC's statistical bar the exclusion is 3.2 to 4.7σ, and DFD's zero-parameter law fits them on the bound-matter clock ($\chi^2 = 3.8$ to 9.0 for five points) but not on the early clock ($\chi^2 = 19.5$ to 23.9, mostly from the $z = 0$ point); on SPARC's systematic bar the exclusion is 2.3 to 3.5σ and the law fits on either clock ($\chi^2 = 3.8$ to 9.0). This is a comparison of amplitudes across two surveys that inherits their relative mass and distance scales (computed). The trend also depends on how the molecular gas is added. In proportion to the survey's own disc masses, within its stated 0.2 dex systematic, the rise stays, $\gamma = 1.02\pm0.22$ on point errors, and DFD's zero-parameter law fits as well as the best power law (fitted amplitude 1.16 against DFD's early-clock 1.12); tied to SED-based masses through the scaling relations of Ref. [170] it is about flat, $\gamma = 0.06 \pm 0.21$ (−1.03 to 0.96 at galaxy level); and with stellar masses from the galaxies' spectral energy distributions in place of the fitted disc masses it falls, $\gamma = -1.04 \pm 0.22$ (−2.32 to −0.32). Those SED masses exceed the kinematic 95% limit in about a third of the

high-z galaxies, so the flat and falling variants are not established. The atomic-gas term, which the data leave unconstrained in 91% of the galaxies, moves γ between 0.5 and 1.3 over its physical range (computed). At galaxy level the SED-based censuses prefer a frozen a_0 to tracking, by about 1σ with SED-tied molecular gas and about 2σ with the SED masses (computed). Above $z \simeq 0.9$ the fitted disc masses of 34 of 55 galaxies reach the lower edge of the halo model's prior on the stellar-to-halo mass ratio, against 13 of 34 below, and in the two upper bins they sit about 0.4 dex below the SED masses. The prior edge clips the low tail of the likelihood and raises the median disc masses by about 0.08 dex, so the offset is kinematic, not an artefact of the prior (computed). The same pattern holds on three sample definitions. DFD's early-clock zero-parameter amplitude lies within 0.02–0.09 dex of the tracking amplitude fitted on the fuller censuses (0.18 dex with both changes together), where the published census puts it 0.095 dex low (computed).

The published exponent is a correct fit of the published bins. The refit adds the galaxy-level errors and the census beneath them: on present data the survey alone does not separate Hubble tracking from a frozen a_0; anchored to SPARC it excludes a frozen a_0 at about 3σ, a comparison across two surveys that DFD's zero-parameter law fits on the bound-matter clock. Direct molecular-gas masses for these galaxies, which fix how the gas scales, would make it decisive.

7. Massive discs at $0.6 < z < 2.5$

The survey of §A0Z 1 and §A0Z 6 observes low-mass discs. Rotation curves of massive star-forming discs reach higher redshift. For a galaxy that obeys the SOURCE law, Eq. (BS8), the dark-matter fraction at a radius where $g_{\rm obs}$ is measured is $f_{\rm DM} = 1 - g_{\rm bar}/g_{\rm obs} = \exp\!\left(-\sqrt{g_{\rm bar}/a_0}\right)$, so each published pair of dark fraction and circular velocity at the effective radius R_e returns

$$a_0 = \frac{(1 - f_{\rm DM})\, g_{\rm obs}}{(\ln f_{\rm DM})^2}, \qquad g_{\rm obs} = \frac{V_c^2(R_e)}{R_e},$$

with no further modelling.

Status A0Z.10 (The massive discs at face value). The 100 discs of Ref. [111], whose baryon census counts molecular gas through the scaling relations of Ref. [170], give median $a_0 = 1.9$, 1.4 and 1.2×10^{-10} m s^{-2} at median $z = 0.8$, 1.5 and 2.2, where DFD's law predicts 1.8, 2.6 and 3.7 on the early clock and 1.89, 2.82 and 3.95 on bound-matter clocks (computed). DFD's value is met at $z \simeq 0.8$; the rise that tracking requires beyond $z \simeq 1.5$ is not seen on that census, while fits of the rotation curves that leave the baryonic mass free neither show nor exclude it (computed on the public data cubes). The exponent fitted within the sample is $\gamma = -0.86^{+0.46}_{-0.48}$ on statistical errors. It is fragile: without the discs with $V_{\rm rot}/\sigma_0 < 2.1$, where the disc–halo degeneracy is largest, it is $-0.20^{+0.45}_{-0.40}$. DFD's exponent over these redshifts, $\gamma_E = 1.29$, lies 4.5σ away on statistics alone (likelihood ratio) and about 1.7σ away once a $\pm 30\%$ survey-wide scale of the pressure-support correction and a ± 0.1 dex redshift tilt of the baryonic masses are marginalised (computed; the widths are estimates), although the discs' own data disfavour the calibrations that would rescue DFD, a doubled pressure support or $z \simeq 2$ baryons 0.2 dex lighter, by $\Delta(-2 \ln L) =$ 18–40 (computed). On the TOTAL branch, Eq. (BS9), the $z \simeq 2.2$ value is 2.4, at the registered falsification threshold of §A0Z 8. The discs sit where the rise should show: at $z \simeq 2.2$ their baryonic pull at R_e is below $a_0(z)$ (median 0.5–0.9 $a_0(z)$), where DFD's rise adds about 0.07 dex to the rotation speed. On the census of SED stellar masses and the gas of Ref. [170] they rotate 0.1–0.17 dex slower than DFD predicts, 6–9σ on statistical errors and 1.5–2.2σ when the census's own ± 0.2 dex calibration is counted (computed with two mass models). Ref. [171] drew a similar face-value conclusion from the discs of Ref. [172], which all but exclude an a_0 about four times today's at $z \simeq 2$, where DFD's is about three times today's.

Remark A0Z.11 (Two baryon censuses). Ref. [109] counts a disc mass fitted to the rotation curve and a modelled atomic-gas term, and treats molecular gas as a systematic of about 0.2 dex; the massive discs above count molecular gas through the scaling relations of Ref. [170]. Counted the same way, with the gas tied to SED-based masses, the survey's own trend is about flat, while with the gas in proportion to the survey's own disc masses the rise stays and DFD's law fits it (Stat. A0Z.9); which scaling applies is open. On the SED-tied census neither data set shows the rise that tracking predicts, although at galaxy level the survey does not exclude it (computed). The exponent published in Ref. [110] is a correct fit of the published bins; the census and the errors behind the bins are what remain open. The KMOS$^{\rm 3D}$ baryonic Tully–Fisher zero points [173] and the refits of 41 of the massive discs by a second pipeline [174] share the parent sample and its calibrations, so they are not independent confirmations. The zero-point evolution is missed by a frozen a_0 and by Newtonian baryons as well, so it does not yet test $a_0(z)$ (computed).

Status A0Z.12 (Environment at fixed redshift: a prediction). Under the domain-local screen of App. ZT, a galaxy's a_0 is set by the expansion rate of its own domain, and an overdense domain lowers it (Cor. ZT.5, with the declared exact closure of Status ZT.8). Massive discs at $z \simeq 1$–2 sit in strongly clustered haloes. In domains of $R_D = 10\,h^{-1}$Mpc, the smallest the local test allows for the linear coupling, the screen lowers their a_0 by about 10% at the average environment of such haloes, to 3.3 at $z \simeq 2.2$ against the measured 1.2 (estimate). Reaching the measured values needs $\delta_{\rm env} \simeq 2$ at $z \simeq 1.5$ and $\simeq 3$ at $z \simeq 2.2$. The matter overdensity on that scale has a standard deviation of 0.34 at $z \simeq 1.5$ and 0.27 at $z \simeq 2.2$, so such domains are fluctuations of about 6 and 11 standard deviations (3.5 and 5.3 for a lognormal field) and are essentially absent (computed). The densest

structures known at these redshifts, the $z = 1.61$ cluster Cl 0332−2742, the Hyperion proto-supercluster and the LATIS protoclusters, have matter overdensities of about 0.8–1.3 on $10\,h^{-1}$Mpc, which lower a_0 by 20–34%, not by the factors of 2–20 that the discs at $z \simeq 2.1$–2.5 show (computed on published values). The measured environments agree: in the environment catalogue of the same deep fields (Fossati et al. 2017; local density in 0.75 Mpc apertures), the a_0 inferred for 46 of the massive discs does not correlate with local density at fixed redshift (rank correlation −0.10), and at $z \simeq 1.8$–2.6 discs in dense and in less dense surroundings show the same deficit (computed on published values). The screen therefore does not reconcile the massive discs beyond $z \simeq 1.5$; at $z \simeq 0.8$, where DFD's global value is already met, it needs domains no denser than average. At $R_D = 20\,h^{-1}$Mpc every shift is about three times smaller. The low-mass discs of §A0Z 6, in less clustered haloes, are lowered by 6–7% at their average environment, which is small beside the census effects found there (estimate). The prediction stands and is falsifiable: at fixed redshift, a_0 in high-redshift discs falls as the density of their $10\,h^{-1}$Mpc domain rises, by about 10% at the average environment of massive haloes and by up to about a third in the densest known structures. The test sets matter-density maps of the deep fields on that scale against per-galaxy a_0; the kinematics already exist.

Status A0Z.13 (What decides the high-redshift test). The $z \simeq 2.2$ value is set by two calibrations. It reaches the registered line $a_0(z{=}2) = 2.5$ if the $z \simeq 2$ baryonic masses are about 0.1 dex lower than those fitted in Ref. [111] (about 0.2–0.3 dex in molecular gas), and DFD's value if they are about 0.2 dex lower (about 0.45 dex in gas); against the census of SED stars and scaling-relation gas DFD's value needs them 0.3–0.5 dex lower (fits of the public rotation curves with the baryonic mass free also put the masses below the census, at DFD's a_0 and at a frozen one alike; computed); or if the pressure-support correction is 1.8 or 2.4 times the standard self-gravitating-disc correction. No published prescription is that large: the others in use are smaller at R_e, and DFD's own vertical gravity makes the correction about 10% smaller (computed; the gas equivalents and the vertical-gravity factor are estimates). The external field of DFD's own large-scale structure is nearly constant in units of $a_0(z)$ and does not supply the difference (estimate), and neither does the domain-local screen, whose required domains are absent from the measured environments (Stat. A0Z.12). Three kinds of data decide the test for both samples: direct molecular-gas masses (CO, [C I] or dust), to 0.1 dex for the $z \simeq 2$ discs; kinematic masses not limited by a halo-model prior, with one pressure-support correction for all samples; and per-galaxy analyses with galaxy-level errors, of the MUSE–DARK public products and of the massive discs, with $a_0(z)$ imposed in the fit; for the massive discs, fits that leave the baryonic mass free need no census, but inside $3R_e$ a heavier χ halo or a stronger pressure correction mimics the rise, so they decide it only with an independent bound on the χ halo or rotation curves beyond $3R_e$ (computed on the public data cubes).

8. Dated falsifiers, registrable now

TABLE CXI. $a_0(z)$ in $10^{-10}\,\mathrm{m\,s^{-2}}$. DFD's zero-parameter column carries no fitted amplitude; it is the epoch law evaluated at the $C = 1$ registration background (the provenance row of Table CX), retained unaltered as the dated registration, and the amplitude column carries the registration amplitude $A = 1.4497$. Bound-matter re-evaluations are given in the registered-predictions box below.

z	DFD (0-par)	DFD ($\times A_{\rm fit}$)	measured $\gamma = 0.78$	$A\,E_{\rm Pl}$	survey linear
1.0	2.05	2.48	2.46	2.49	2.59
1.5	2.68	3.25	2.93	3.28	3.39
2.0	**3.42**	4.14	3.38	4.20	**4.18**
2.5	4.23	5.13	3.81	5.22	4.98
3.0	**5.12**	6.21	4.23	6.32	**5.77**
4.0	7.09	8.59	5.03	8.76	7.36

Status A0Z.14 (Registered predictions). At its $C = 1$ registration background and with *no* fitted amplitude, DFD predicts $a_0(z{=}2) = 3.42$ and $a_0(z{=}3) = 5.12$ (units $10^{-10}\,\mathrm{m\,s^{-2}}$); with the registration amplitude imposed, 4.14 and 6.21. [These are the values as registered. Re-evaluated on bound-matter clocks (Eq. (A0Z2), $\Omega_m \simeq 0.312$, distances computed with $H_0^{\rm loc}$), the zero-parameter values are 3.61 and 5.44, and 4.49 and 6.75 at $A = 1.486$, the survey amplitude on the same distances; the falsification windows below are unchanged and both routes lie inside them.] The measured exponent family extrapolates to 3.38 and 4.23, and the survey's linear form to 4.18 and 5.77. **The forms separate by about 50% at $z = 3$ and 75% at $z = 4$.** Ref. [110] makes the same argument — that the viable functional forms diverge rapidly beyond the measured range, so that $z \gtrsim 2$ kinematics discriminate among them — and the columns above are this corpus's own evaluations of each form on DFD's background and amplitude conventions. *Kills:* a measured $a_0(z{=}2) < 2.5$ or > 5.5, or $a_0(z{=}3) < 3.5$ or > 7.5, falsifies the DFD epoch law on either amplitude convention, provided the measurement counts molecular gas in its baryon census, states its pressure-support correction and carries galaxy-level errors. On their published calibrations the massive discs of §A0Z 7, which meet these three provisos, give $a_0 \simeq 1.2$ at $z \simeq 2.2$, below the $z = 2$ line at face value (2.4, at the line, on the TOTAL branch); the line is reached if their baryonic masses are about 0.1 dex lower or their pressure-support correction is 1.8 times the standard one (Stat. A0Z.13); the domain-local screen gives values this low only in domains about 6 to 11 standard deviations denser than average, which the measured environments do not show (Stat. A0Z.12). *Instruments:* rotation curves of massive discs already reach the regime at $z \simeq 0.6$–2.5 [111]; JWST and ALMA kine-

matics extend it to $z \gtrsim 3$, and SKA H I kinematics to the outer discs. The census, the error treatment and the environment decide the test, not the reach (Stat. A0Z.13).

Appendix AF: Galaxy Bias in DFD: a Frame-Consistent Derivation from the σ_8 Closure

This appendix addresses the apparent "factor of 80 galaxy bias problem" that arises when the σ_8 closure of Appendix AE is read naively. The closure equation

$$\Omega_b \, \delta_b \, Q(\delta_b) = \Omega_m \, \sigma_{8,\mathrm{obs}} \tag{AF1}$$

implies $\delta_b = 0.0104$ at R_8 versus $\sigma_{8,\mathrm{obs}} = 0.811$, a ratio $F_8 \equiv \sigma_8/\delta_b = 77.9$. A direct concern is that matching observed galaxy clustering then requires bias $b \sim 146$ relative to baryons for LRG-like tracers, factors of $\sim$78 larger than published LCDM bias values $b_{\mathrm{LCDM}} \sim 1.9$.

The resolution is that DFD permits two equally valid bias-frame conventions related by F_8, fixed by the closure with zero free parameters. The "bias multiplier" is not a free parameter; it is a derived consequence of the closure equation. Galaxy formation in the well-depth frame produces the same numerical bias as LCDM; the bare-baryon-frame number is larger by F_8 purely by definition.

Like the closure it starts from, this appendix belongs to the baryon-only construction of Appendix AE, in which the baryons are the only clustering matter; it is not DFD's physical growth carrier. That carrier is the cold χ relic with $Q_\chi = 1$ under the adopted Rest-Mass Channel, and unbound linear perturbations grow with $G_{\mathrm{eff}} = G$ (App. GR). The bias frames, the multiplier F_8 and the falsifiers of Sec. AF 5 are statements about the construction.

1. AF.1 Setup: bias-frame ambiguity in modified gravity

In LCDM, galaxy bias b is defined as the ratio

$$b^2 = \frac{P_{gg}(k)}{P_{mm}(k)}, \qquad P_{mm}(k) \equiv \langle |\delta_m(\mathbf{k})|^2 \rangle, \tag{AF2}$$

where δ_m is the total-matter density contrast at scale $1/k$. In LCDM, total matter is dominated by cold dark matter; $\delta_m \simeq \delta_{\mathrm{CDM}}$ on linear scales, with $\sigma(\delta_m, R_8) = \sigma_8$.

In the construction the baryons are the only clustering matter, so the analogous definition admits two natural choices for the reference field:

B-frame (bare baryons):: $P_{mm}^{(B)}(k) = \langle |\delta_b(\mathbf{k})|^2 \rangle$ where δ_b is the baryon density contrast.

W-frame (well-depth / convergence):: $P_{mm}^{(W)}(k) = \langle |\Omega_b \delta_b(\mathbf{k}) Q[\delta_b]/\Omega_m|^2 \rangle$ where $Q[\delta_b]$ is the deep-MOND amplification factor of Eq. (AF1).

The amplitudes of the two reference fields differ by exactly F_8 at scale R_8:

$$\frac{\sigma(P_{mm}^{(W)}, R_8)}{\sigma(P_{mm}^{(B)}, R_8)} = \frac{(\Omega_b/\Omega_m)\, Q \, \delta_b}{\delta_b} = \frac{\Omega_b \, Q}{\Omega_m} = F_8 \simeq 77.9, \tag{AF3}$$

by the σ_8 closure Eq. (AF1). Both frames are internally consistent; they describe the same physical universe with different choices of normalization.

Galaxy bias takes correspondingly different values in each frame:

$$b^{(B)} \equiv \sqrt{\frac{P_{gg}}{P_{mm}^{(B)}}}, \qquad b^{(W)} \equiv \sqrt{\frac{P_{gg}}{P_{mm}^{(W)}}}, \qquad \boxed{b^{(B)} = F_8\, b^{(W)}.} \tag{AF4}$$

2. AF.2 Galaxy formation operates in the W-frame

Galaxy formation requires gas to fall into a gravitational potential well, cool radiatively, fragment, and form stars. The relevant physical input is the local gravitational well depth, not the bare matter density:

- Cooling time $\propto \rho^{-1} T^{1/2} \Lambda^{-1}$
- Free-fall time $\propto (G\rho_{\rm well})^{-1/2}$
- Star formation efficiency $\propto t_{\rm cool}/t_{\rm ff}$

where $\rho_{\rm well}$ is the effective mass density sourcing the gravitational acceleration. In LCDM, $\rho_{\rm well} = \rho_{\rm matter}$ (predominantly CDM). In DFD, $\rho_{\rm well}$ is the effective matter-equivalent density that produces the observed gravitational acceleration; on R_8 scales, this is precisely $(\Omega_b/\Omega_m)\, Q\, \delta_b$ times $\rho_{\rm crit}\, \Omega_m$, identical to LCDM's $\Omega_m\, \delta_m\, \rho_{\rm crit}$ by the closure Eq. (AF1).

a. Consequence: same astrophysics, same threshold. The peak-bias relations of Mo & White [175] and Sheth-Tormen [176] relate galaxy bias to the height ν at which a tracer is selected relative to the rms of the underlying field:

$$b(\nu) = 1 + \frac{\nu^2 - 1}{\delta_c}, \tag{AF5}$$

where $\delta_c \simeq 1.686$ is the linear-theory spherical-collapse threshold. Since (i) galaxy formation depends on the well-depth field, (ii) the well-depth field has $\sigma = \sigma_8$ in both LCDM and DFD by closure, and (iii) the astrophysical threshold (cooling, fragmentation) is fixed by atomic physics (epoch-invariant in DFD per Sec. XIX), the value of ν at which a given tracer is selected is the same in both cosmologies.

Therefore:

$$\boxed{b_{\rm DFD}^{(W)}(\nu) = b_{\rm LCDM}(\nu).} \tag{AF6}$$

For LRG-like tracers with observed $b_{\rm LCDM} \simeq 1.88$, the DFD W-frame bias is also 1.88.

3. AF.3 Theorem: DFD galaxy bias from the closure

Theorem AF.1 (Galaxy bias from σ_8 closure)**.** *Under the postulates of DFD, the closure of Appendix AE (Theorem AE.1 and Eq. (AF1)), and the W-frame galaxy formation principle Eq. (AF6), the linear galaxy bias of any tracer in the bare-baryon frame is*

$$b_{\rm DFD}^{(B)} = F_8\, b_{\rm LCDM}, \qquad F_8 = \frac{\Omega_b\, Q(\delta_b)}{\Omega_m} = 77.9, \tag{AF7}$$

on R_8 scales, with F_8 fixed by the closure and no free parameters.

Proof. By Eq. (AF4), $b^{(B)} = F_8\, b^{(W)}$ in any cosmology with the two-frame structure. By Eq. (AF6), $b_{\rm DFD}^{(W)} = b_{\rm LCDM}$ since galaxy formation responds to the well-depth field whose statistical amplitude σ_8 is matched by construction in both cosmologies. By Eq. (AF3) and the closure Eq. (AF1), $F_8 = (\Omega_b/\Omega_m)Q$ is determined to the value 77.9 at the closure point. □

a. Numerical predictions. For the survey tracer set, the DFD W-frame and B-frame biases are:

Tracer	$b_{\rm DFD}^{(W)} = b_{\rm LCDM}$	$b_{\rm DFD}^{(B)} = F_8 b_{\rm LCDM}$	$\sigma_{\rm galaxy}$
BGS / low-bias	1.20	93.5	0.97
ELG-like	1.50	116.8	1.22
DESI/BOSS LRG	1.88	146.4	1.52
LRG high-bias	2.10	163.6	1.70
eBOSS QSO $z\sim1.5$	2.40	187.0	1.95

The W-frame values match published LCDM bias measurements; the B-frame values are equivalent under Eq. (AF4) but referenced to bare-baryon density contrast.

4. AF.4 Cross-frame consistency: what each probe measures

Different observational probes naturally measure bias in different frames. The construction is consistent if and only if the same $F_8 = 77.9$ emerges across all such probes.

Galaxy clustering (auto-correlation):: $P_{gg}(k)$ measured directly. Bias inferred via $b = \sigma_{\rm galaxy}/\sigma_8^{\rm fid}$ where $\sigma_8^{\rm fid}$ is the fiducial cosmology's σ_8 amplitude. This implicitly uses the W-frame.

Galaxy-galaxy lensing (GGL):: Cross-correlation $\langle\gamma_t\,\delta_g\rangle$ between background-galaxy shear γ_t (which traces $\kappa_{\rm DFD} \propto Q\delta_b$) and foreground galaxy density. Amplitude $\propto b^{(W)} \times \sigma_8^2$. W-frame native.

Galaxy-CMB lensing cross-correlation:: Planck CMB lensing $\kappa_{\rm CMB}$ traces the same $\kappa_{\rm DFD}$ field via the high-redshift integrated optical depth. Cross-correlation amplitude $\propto b^{(W)} \times \sigma_8^2$. W-frame native.

Lyman-α forest cross-correlation:: The Lyα flux F traces baryon overdensity directly: $\delta F \propto -A\,\delta_b^{\beta_F}$ for fluctuating-Gunn-Peterson. The cross-correlation $\langle\delta_g\delta F\rangle$ amplitude is then $\propto b^{(B)} \times \sigma_b \times \sigma_F$ – B-frame native. The QSO-Lyα forest cross-correlation from eBOSS DR14 [177] can in principle test $b^{(B)}$ directly.

kSZ amplitude:: The kinetic Sunyaev-Zel'dovich signal traces the integrated baryon momentum $\rho_b v_{\rm pec}$. From Sec. AE 10, $v_{\rm pec} \propto \sqrt{\delta_b}$ in deep MOND. ACT/SPT/DESI kSZ measurements [100, 178] provide a partial test.

5. AF.5 Falsifiable predictions

Galaxy Bias — Falsifiers

1. **Universal F_8.** The conversion factor $F_8 = \sigma_8/\sigma_b = 77.9$ must be the same for all tracer types (BGS, ELG, LRG, QSO) and at all redshifts. Cross-survey measurement of F_8 at $\pm 10\%$ inconsistency level falsifies the construction.
2. **Lyman-α baryon amplitude.** At $z = 2$–5, the linearly extrapolated baryon density contrast from Lyα flux power spectrum should be $\sigma_b(R_8, z) = D(z)\sigma_b(R_8, 0) \sim 0.002$–$0.004$, vastly smaller than LCDM's $\sigma_m(R_8, z) \sim 0.17$–$0.34$. Measurement of $\sigma_b \sim \sigma_8$ in Lyα forest at this scale falsifies the construction.
3. **kSZ amplitude.** As in Sec. AE 11, the baryon-only construction predicts a kSZ amplitude about 0.9 of LCDM's at R_8 scales, from its $v_{\rm pec} \propto \sqrt{\delta_b}$ scaling; a detection of LCDM-amplitude kSZ at high precision falsifies the construction. DFD's growth carrier, the cold χ relic with $Q_\chi = 1$, predicts no such suppression on linear scales (App. GR).
4. **Scale dependence of F.** On scales other than R_8, F varies as $F(R) \propto R^{-1/4}$ (deep MOND with $n_{\rm eff} \sim -2$). Strong deviation in observed scale-dependent bias ratio (B-frame vs W-frame) from this prediction falsifies the construction.

6. AF.6 Scale dependence

The conversion factor F_8 was derived at the spherical-top-hat scale $R_8 = 8h^{-1}$ Mpc using $Q(\delta_b) = (1 + \sqrt{1 + 4/q})/2$ in the deep-MOND regime where $q = g_N/a_0 \ll 1$. On scales $R \neq R_8$, the deep-MOND boost varies:

$$Q(R) \simeq \frac{1}{\sqrt{q(R)}} = \frac{1}{\sqrt{(\Omega_b/2)(HR/c)\delta_b(R)/(a_0/cH)}}. \tag{AF8}$$

Using $\delta_b(R) \propto R^{-(n+3)/2}$ for the linear baryon spectrum (post-recombination) and $n_{\rm eff} \simeq -2$ at R_8 scales:

$$Q(R) \propto R^{-1/4}, \qquad F(R) \propto R^{-1/4}. \tag{AF9}$$

Numerically:

- At $R = 100\,$Mpc ($k = 0.01\,h$/Mpc): $F \simeq 46$
- At $R = R_8 = 11.85\,$Mpc ($k = 0.1\,h$/Mpc): $F = 77.9$
- At $R = 1\,$Mpc ($k = 1\,h$/Mpc): $F \simeq 145$

This is a mild scale-dependence: F varies by about a factor 3 across two decades of scale, consistent with approximately scale-independent linear bias on quasi-linear scales as observed in BOSS/eBOSS/DESI.

7. AF.7 Open extensions and limitations

This appendix closes the linear-bias question on R_8 scales: F_8 is a derived quantity, not a free parameter. Several extensions remain program-grade:

1. **Spherical-collapse threshold $\delta_c^{\rm DFD}$.** The peak-bias formula Eq. (AF5) uses $\delta_c = 1.686$ from LCDM spherical-collapse dynamics. DFD's deep-MOND-amplified collapse may give a different $\delta_c^{\rm DFD}$. The W-frame argument Eq. (AF6) is robust to this because it operates on the operational definition $b = \sigma_g/\sigma_8$, but a derivation of the halo mass function in DFD requires solving the collapse problem.

2. **Halo bias and assembly bias.** Mass-dependent bias $b(M_{\rm halo})$ and assembly-bias dependencies on local environment are well-developed in LCDM N-body simulations but require DFD implementation. The framework here gives the leading-order behavior; mass-dependent corrections are program-grade.

3. **Non-linear bias.** On scales $k > 0.2\,h/$Mpc, non-linear bias terms b_2, b_{s^2}, b_3 become important and require perturbation-theory or simulation-based modeling.

4. **Velocity bias and FoG.** Galaxy peculiar velocities can differ from the underlying matter velocity field, introducing additional "velocity bias." This is small in LCDM ($\sim 1\%$) but unverified in DFD.

5. **Direct $b^{(B)}$ measurement.** The B-frame bias prediction $b^{(B)} \sim 146$ for LRG has not been directly measured. Galaxy-Lyα cross-correlation analyses currently use LCDM-fiducial cosmology; a DFD re-analysis would test the prediction.

8. AF.8 Summary

Galaxy Bias in the Construction — Status

Within the construction:

- Two-frame structure of DFD galaxy bias: $b^{(B)} = F_8\, b^{(W)}$ with $F_8 = 77.9$ from σ_8 closure.
- W-frame bias matches LCDM: $b^{(W)}_{\rm DFD} = b_{\rm LCDM}$ because galaxy formation responds to the well-depth field whose amplitude is σ_8 in both cosmologies.
- No free parameters: F_8 fixed by closure with zero degrees of freedom.
- Falsifiable cross-probe consistency: galaxy-galaxy lensing, galaxy-CMB lensing cross-correlation, kSZ amplitude, and Lyman-α forest auto-correlation must all yield consistent $F_8 = 77.9$.

Still program-grade:

- DFD spherical-collapse threshold $\delta_c^{\rm DFD}$ for halo abundance matching.
- Mass-dependent halo bias $b(M)$ and assembly bias.
- Non-linear bias terms in the perturbation-theory expansion.
- Direct $b^{(B)}$ measurement via galaxy-Lyα cross-correlation in DFD-fiducial framework.

Resolution of Open Theorem Obligation #4 (Sec. AE 12): The "galaxy-bias derivation" is closed at the level of linear bias on R_8 scales. The $\sim$80$\times$ multiplier between observed galaxy clustering and bare-baryon density contrast is a derived consequence of the σ_8 closure, not a free parameter. Higher-order extensions (scale-dependent bias, halo-bias function, assembly bias) remain program-level work.

Appendix AG: Master Claims Confrontation Matrix

This appendix consolidates every quantitative empirical claim in this monograph into a single catalog. The intent is to let a referee or independent reader assess at a glance which claims are *theorem-grade*, which are *derived under stated auxiliary assumptions*, and which are *conjectured or empirical-fit-grade*; what each claim predicts; what is observed; the current agreement; and the explicit threshold that would falsify the claim.

This appendix introduces no new physics. Every entry cross-references a theorem, derivation, table, or section already present in the monograph.

1. Tier Definitions

T (Theorem):: Result follows from a formal proof using only the core DFD axioms ($n = e^{\psi}$, $a = (c^2/2)\nabla\psi$, the derived μ-response of App. N/App. BS, with $\mu = x/(1+x)$ its weak-response form) plus stated mathematical lemmas.

D (Derived):: Result follows from the core axioms plus an explicit auxiliary closure framework whose assumptions are displayed (spectral action, Chern-Simons truncation $k_{\max} = 60$, manifold $X = \mathbb{C}P^2 \times S^3$, generation count $N_{\text{gen}} = 3$, PDE-validated numerical results).

C (Conjectured):: Result is plausible from DFD principles but not yet derived from the core axioms or a fully-displayed closure framework. Open program items.

E (Empirical):: Result is a phenomenological match using physically-motivated correction factors at literature-bounded values, where the closure depends on those corrections.

***validated* (Validated)::** An observational test that has *already* been performed and is consistent with DFD at stated σ.

***pending* (Pending)::** An observational test where the experimental capability exists but no published measurement yet decides the claim.

***contested* (Contested)::** An observational test that has been performed, where the published measurements disagree at face value, some consistent with DFD and some not, and the verdict turns on how the data are calibrated and how their errors are counted.

***open* (Open)::** A predicted observable for which no comparable measurement currently exists.

The group entry uses the E label, here for an amplitude read from the data it is compared with; the cluster entry's amplitude follows from the derived abundance and ΛCDM-like assembly (estimate; Appendix I). The galactic entries of Block 3 are the μ-law on the baryons; with χ present they hold under the floor composition when the ΛCDM-like χ halos of the adopted energy are cored, which is an estimate (App. AV). The tier-grading rule is that a claim's tier is set by its *weakest* link, not its strongest.

2. Block 1: Fundamental Constants and Microsector

- **Fine-structure constant α^{-1} from microsector closure** (Sec. X). DFD: the closed form, exact under two stated choices, gives $\alpha^{-1} = 137.03599985$; the integers alone give 137.03307 (21 ppm), and the bracket coefficient $c = 1/13$ brings it to 0.0049 ppm, 32 times the uncertainty of the CODATA 2022 value. SM: free parameter. Observation: 137.035999177(21) (CODATA 2022). Agreement: 0.0049 ppm with the stated $c = 1/13$, inside the 0.1 ppm falsifier band, which is this row's stated level. Falsifier: $|\Delta\alpha^{-1}| > 0.1$ ppm not from QED loops. Tier: D (coefficient provenance open, Rem. X.4; the identification of the hypercharge-trace coefficient with $1/e^2$ is not derived, §X I). Status: *validated*.

- **Higgs VEV from $\alpha^8\sqrt{2\pi}$ scaling** (App. Z). DFD: $v = 246.09$ GeV; the exponent 8 is derived and the prefactor $\sqrt{2\pi}$ is fitted, with a no-go on deriving it. SM: free parameter. Observation: 246.22 GeV. Agreement: 0.05% with the fitted prefactor. Falsifier: $|\Delta v/v| > 1\%$. Tier: D (exponent). Status: *validated*.

- **Strong CP: $\bar{\theta} = 0$ at tree level, loop-bounded** (App. G 5). DFD: $\bar{\theta} = 0$ at tree level, with $\theta_{\text{YM}} = 0$ fixed by the spectral action given that nothing is added to it for the gauge fields, loop-induced $\lesssim 10^{-16}$. SM: needs axion or fine-tuning. Observation: $|\bar{\theta}| < 10^{-10}$ (nEDM). Agreement: six orders of magnitude below the bound. Falsifier: detection of $|\bar{\theta}| > 10^{-15}$ from QCD alone. Tier: D (conditional on nothing being added to the spectral action for the gauge fields, and on the det-orthogonal CP offset, Postulate Y.10 of App. AO, on the branch of the offset connected to $\xi = 0$). Status: *validated*.

- **Fermion mass hierarchy (9 masses)** (Sec. XIX). DFD: $m_f = A_f \alpha^{n_f} v/\sqrt{2}$ with integer n_f, 1.42% leading-order mean error; the top and charm are derived, and the other seven species rest on seven data-selected prefactors (App. FM). SM: 9 free parameters. Observation: PDG values. Agreement: 1.42% mean (leading order). Falsifier: individual mass off by $> 10\%$ for any f. Tier: D. Status: *validated*.

- **Weinberg angle from gauge partition** (App. Z 1). DFD: $\sin^2\theta_W = 3/13 = 0.2308$. SM: free parameter. Observation: 0.23129(4) ($\overline{\text{MS}}$, M_Z). Agreement: 0.23%; 3/13 is the bare angle, and its radiative relation to M_Z is not computed (App. Z). Falsifier: $|\Delta \sin^2\theta_W / \sin^2\theta_W| > 1\%$ at tree level. Tier: D. Status: *validated*.

- **CKM Cabibbo angle from $\mathbb{C}P^2$ cohomology** (App. AO). DFD: $\lambda = 31\alpha = 0.2262$. SM: free pa-

rameter. Observation: 0.22501(68) (PDG 2024). Agreement: 0.54% (1.8σ). Falsifier: $|\Delta\lambda| > 0.005$. Tier: D (given the selected count of Table CXXVIII). Status: *validated*.

- **Gatto–Sartori–Tonin closure** $|V_{us}| = \sqrt{m_d/m_s}$ (App. AY, Thm AY.1). DFD: $|V_{us}|/\sqrt{m_d/m_s} = \sqrt{31^2\alpha/7} = 1.0009$ (i.e. $m_s/m_d = 1/(7\alpha) = 19.58$). SM: unexplained. Observation: $m_s/m_d = 19.9(\pm1)$ (FLAG). Agreement: 0.09% closure, $< 0.5\sigma$ on m_s/m_d. Falsifier: m_s/m_d outside $[17, 23]$. Tier: D (given the selected count of Table CXXVIII and the data-selected prefactors A_d, A_s, App. FM). Status: *validated*.

- **TM1 solar mixing angle** (App. AY, Thm AY.3). DFD: $\cos^2\theta_{12}\cos^2\theta_{13} = \frac{2}{3}$ exact, $\sin^2\theta_{12} = (1 - 9\alpha)/(3(1 - 3\alpha)) = 0.3184$. SM: free parameters. Observation: $\sin^2\theta_{12} = 0.307(^{+12}_{-11})$ (NuFIT 6.0); JUNO's first result 0.3092 ± 0.0087. Agreement: $+0.95\sigma$ and 1.1σ. Falsifier: $\sin^2\theta_{12} \notin [0.30, 0.34]$ or non-maximal θ_{23}. Tier: D. Status: *validated*.

- **PMNS matrix structure** (Sec. XIX). DFD: trimaximal TM1 (App. X); $\sin^2\theta_{13} = 3\alpha$ a stated conjecture. SM: free parameters. Observation: global fit values. Agreement: $\theta_{23} = 45°$, in soft $\sim 2\sigma$ tension with NuFIT 6.0 (octant unresolved). Falsifier: off-diagonal element $> 20\%$ off. Tier: D. Status: *validated*.

- **Hubble–Planck closure:** $G\hbar H_0^2/c^5 = C\alpha^{57}$ (App. O). DFD: $H_0/M_P = \sqrt{C}\,\alpha^{28.5}$, exponent derived and coefficient measured (the vacuum coefficient $R = \Omega_\Lambda C = 0.6042 \pm 0.0027$; today's early-clock value $C = 0.87784 \pm 0.00266$ from BAO+θ_* and 0.8772 from plik-lite), giving the cross-channel $H_0^{\rm early} = 67.52 \pm 0.09$ km/s/Mpc concordant across five CMB-anchored channels. ΛCDM: free quantity, no theoretical prediction. Observation: Planck 67.36 ± 0.54; SH0ES 73.49 ± 0.93 (2025). Agreement: 0.3σ from the acoustic/CMB determination; local probes read the bound-matter clock, $H_0^{\rm loc} = \alpha^{28.5}/t_P = 72.09$ (Postulate ZS.11), 0.2σ from the Cepheid-free mean 71.87 ± 0.96 and 1.5σ below SH0ES 2025. Falsifier: bright sirens or mass-sheet-robust time delays settling at 67.5, or early-ruler and local ladders converging with distance (Falsifier ZS.14). Tier: D (exponent); coefficient measured. Status: *validated* on the acoustic side; the local side rests on the stated two-clock postulate, at the cost of a laboratory-unit age of 12.92 Gyr against ages of the universe of 13.5–13.8 Gyr inferred from globular clusters with a ΛCDM formation delay (2.1–2.6σ with statistical and systematic errors in quadrature, one programme).

- **Cosmological constant scale:** $(H_0 t_P)^2 = C\alpha^{57}$. DFD: $\rho_\Lambda/M_P^4 \sim 10^{-122.7}$ from the α^{57} exponent ($10^{-122.9}$ with the measured normalization). ΛCDM: "10^{122} problem". Observation: matches observed $\Omega_\Lambda H_0^2$. Agreement: exponent-level identity; the measured $O(1)$ prefactor of the observed density enters via the clock dictionary (Rem. AP.6), and on bound-matter clocks the closure scale $(3/8\pi)\alpha^{57}$ carries none (App. AU) and the identity is microsector-scoped (Rem. AU.3). Falsifier: the exponent 57 fails to match the hierarchy. Tier: D for the exponent; C measured. Status: *validated*.

- **Clock coupling:** $k_\alpha = \alpha^2/(2\pi)$ (App. P). DFD: $k_\alpha = 8.5 \times 10^{-6}$ (unscreened); $\lambda_\alpha \approx 2.1 \times 10^{-8}$ (pure-α residual, before screening). SM: 0 (LPI exact). Observation: the Yb^+ E3/E2 gravitational-LPI limit has improved to $|(c^2/\alpha)\,d\alpha/d\Phi| \lesssim 3 \times 10^{-9}$ (Filzinger *et al.* 2023, $-2.4(3.0) \times 10^{-9}$; superseding the earlier 3.2×10^{-8}). Agreement: consistent; screened at the local acceleration the residual is $2\lambda_\alpha\Sigma(\oplus) \approx 1.5 \times 10^{-13}$ per unit $\Delta\Phi/c^2$, four orders below this bound, which does not test it. Falsifier: a same-ion E3/E2 gravitational-LPI null below the screened residual. Tier: D. Status: *open*.

- **Majorana scale:** $M_R = M_P\alpha^3$ (App. P). DFD: $M_R \approx 4.7 \times 10^{12}$ GeV. SM: free seesaw parameter. Observation: not separately observable. Falsifier: m_ν pattern inconsistent with $M_R\alpha^3$ structure. Tier: D. Status: *open*.

- **Proton stability:** $\tau_p = \infty$ (App. G 7). DFD: exact (no decay channel for a single nucleon), *if baryon number is violated only by the electroweak anomaly*, which changes it only in steps of three. DFD's black holes radiate at Hawking's rate (Cor. AP.36), so a gravitational violation is not excluded; its rate is not computed, and a dimensional estimate gives $\tau_p \gtrsim 10^{42}$ yr, beyond Hyper-K. The soliton reading below is not used. On that reading baryon number is the internal winding integer, which is conserved while the winding field stays continuous. By Derrick's scaling argument an energy with at most two derivatives, which is all the printed action gives that field, has no finite-size minimum in the unit-winding sector, and such textures can collapse and unwind in finite time (Shatah 1988; Turok and Spergel 1990). A quartic (Skyrme-type) term prevents the collapse, and with it a minimum-energy unit-winding soliton exists (Esteban 1986; Kapitanski and Ladyzhenskaya 1983). The printed action does not contain that term, so the soliton is posited, not derived. SM: the same anomaly selection rule. Observation: Super-K bounds. Agreement: exact. Falsifier: $p \to e^+\pi^0$ detection with $\tau_p < 10^{40}$ yr (a discriminating test against GUT-type $\Delta B = 1$ mediators). Tier: D (conditional). Status: *pending*.

3. Block 2: Gravitational Tests (PPN, Pulsars, GW, Strong-Field)

- **PPN** γ (Sec. IV). DFD: $\gamma = 1$ exactly. GR: $\gamma = 1$. Observation: Cassini 1.000021(23). Agreement: exact. Falsifier: $|\gamma - 1| > 10^{-5}$. Tier: T. Status: *validated*.

- **PPN** β (Sec. IV, Padé Thm AA.1). DFD: $\beta = 1$

exactly. GR: $\beta = 1$. Observation: LLR $\beta - 1 = (-4.5 \pm 5.6) \times 10^{-5}$ [121]. Agreement: exact. Falsifier: $|\beta - 1| > 10^{-3}$. Tier: T. Status: *validated*.

- **All 10 PPN parameters**. DFD: match GR (the preferred-frame set to within the bounded residual of Thm IV.1). GR: baseline. Observation: all bounds satisfied. Agreement: within all bounds (preferred-frame residual $\lesssim 4 \times 10^{-8}$). Falsifier: any PPN parameter differs from GR at solar-system precision. Tier: T. Status: *validated*.

- **Mercury perihelion advance**. DFD: 42.98″/century. GR: 42.98″/century. Observation: 42.98(4)″/century. Agreement: exact. Tier: T. Status: *validated*.

- **Shapiro time delay**. DFD: matches GR. GR: matches GR. Observation: Cassini consistent. Agreement: exact. Tier: T. Status: *validated*.

- **Solar-system anomalous quadrupole** Q_2 (App. NL). DFD: $Q_2 = 0$ exactly: under the environmental-confinement axiom the Sun's own field is Newtonian inside the Galaxy (App. NL), and the action completion also gives $Q_2 = 0$ at first order (Thm NL.8). GR: 0. Observation: DE440 $(1.6 \pm 1.8) \times 10^{-27}$ s^{-2} [30]; Cassini $(3 \pm 3) \times 10^{-27}$ [29]. Agreement: -0.89σ (DE440), -1.00σ (Cassini). Falsifier: a confirmed $|Q_2| > 10^{-29}$ s^{-2} of MOND-like origin. Note: the *local* per-point reduction of the same response gives 30.6–31.8 $\times 10^{-27}$ at the bound-matter-clock a_0, i.e. $+16.1$ to $+16.8\sigma$ (DE440), and is excluded; the same obstruction gives MOND itself an 8.7σ RAR-vs-quadrupole tension [179]. Tier: T (obstruction) + D (value). Status: *validated*.

- **Wide-binary sky-orientation modulation** (App. NL, Falsifier NL.20). DFD: *exactly* 0% even ($\cos^2\theta$) modulation of the force boost at all separations and mass ratios, by Thm NL.10 ($v_{\rm obs}/v_N$ inherits $\lesssim 7 \times 10^{-4}$, zero for equal-mass pairs); the odd $\cos\theta$ term is $\propto (m_1 - m_2)$ and vanishes for equal-mass pairs; local pairs, all inside the Milky Way's frozen zone, show no modulation of either parity and no boost (Axiom NL.14). MOND/AQUAL: 6.9% peak-to-peak at 10^4 AU, 46.6% at the $g_{\rm int} = g_{\rm ext}$ resonance. Observation: not yet performed; *Gaia* eDR3 has 1.1×10^6 pairs at $> 99\%$ bound probability [53]. Agreement: —. Falsifier: any detected modulation, even or odd, or any boost, in local pairs; any even modulation in any pair. Tier: T. Status: *open*.

- **Oort spike: a Newtonian Sun** (App. NL, Status NL.12). DFD: under Axiom NL.14 the Sun's own field is Newtonian; a 1-Gyr integration of 2×10^4 comets in the Galactic tide gives a median original $1/a = 4.0 \times 10^{-5}$ AU^{-1}, 77% in $[0, 0.75] \times 10^{-4}$, and no hyperbolic originals; every printed reading without the axiom fails, with 46–100% hyperbolic originals or an energy budget up to about eighteen times the allowance. MOND: excluded (Vokrouhlický et al. 2024). Observation: CODE, centroid 3–4 $\times 10^{-5}$ AU^{-1}, 4.6% hyperbolic. Agreement: consistent (a postdiction: the axiom was stated to pass this test). Falsifier: a confirmed wide-binary boost near the Sun. Tier: D. Status: *validated*.

- **Lensing mass = dynamical mass at every acceleration, except for bodies in weak hosts** (App. NL, Cor. NL.17). DFD: identical to $O(v^2/c^2)$, as in GR, by the one-function metric at first post-Newtonian order; bodies in weak hosts also feel the completed law's reciprocal force, which light does not, and for them the two differ by it. RAQUAL: differs (its conformal coupling leaves lensing on the Einstein-frame potential). TeVeS: equal only by adding a vector field. Observation: strong- and weak-lensing mass–dynamics comparisons consistent. Falsifier: a confirmed lensing/dynamical mass ratio $\neq 1$ at fixed radius in a relaxed system. Tier: T. Status: *validated*.

- **Light deflection**. DFD: reproduces the leading (1PN) GR deflection in the declared physical branch. GR: matches GR. Observation: VLBI consistent. Agreement: exact at 1PN; the static 2PN deflection coefficient is GR's $15\pi/4$ (§IV; App. AP, Thm AP.39). Tier: T (1PN). Status: *validated*.

- **Frame dragging (Lense-Thirring)**. DFD: matches GR. GR: matches GR. Observation: Gravity Probe B consistent. Agreement: exact. Tier: T. Status: *validated*.

- **GW propagation speed:** $c_T = c_\gamma$ **exactly** (Sec. V; App. WS). DFD: $c_T = c_\gamma$ on every background: light and gravitational waves share one metric. GR: $c_T = c$. Observation: GW170817: $|c_T/c - 1| < 10^{-15}$. Agreement: exact. Falsifier: any TT–EM cone split. Tier: T. Status: *validated*.

- **GW170817 tidal deformability and EM counterpart timing**. DFD: matches GR. GR: matches GR. Observation: consistent with GR + DFD. Agreement: exact. Falsifier: inconsistency with GR-equivalent at LIGO sensitivity. Tier: T. Status: *validated*.

- **ppE GW phase deviations**. DFD: all deviations zero at leading order. GR: all zero. Observation: all bounds satisfied. Agreement: exact. Falsifier: nonzero $\delta\hat{\varphi}_b$ in any GW band. Tier: D. Status: *validated*.

- **Binary pulsar orbital decay** (App. E 2). DFD: matches GR (B1913+16, J0737-3039). GR: matches GR. Observation: all consistent. Agreement: exact. Falsifier: a decay rate that departs from the GR value by more than 3σ of its measurement error for any pulsar. Tier: D. Status: *validated*.

- **No-wormhole theorem** (App. R, Thm AA.2). DFD: no traversable wormholes. GR: allows with exotic matter. Observation: —. Agreement: exact theorem. Fal-

sifier: exhibition of DFD wormhole solution. Tier: T. Status: *open*.

4. Block 3: Galactic Dynamics

- $\mu(x) = x/(1+x)$ **from S^3 composition** (App. N, Thm N.8). DFD: one μ-response at all galactic scales, the weak-response form of the derived exponential law (App. BS). ΛCDM: dark matter halos. Observation: SPARC RAR. Agreement: $< 5\%$ residuals. Falsifier: SPARC residual scatter exceeds 0.15 dex floor. Tier: T. Status: *validated*.

- $a_0 = 2\sqrt{\alpha}\, cH_0$ **from scaling stationarity** (App. N, Thm N.14). DFD: 1.1966×10^{-10} m/s^2 on bound-matter clocks (Postulate ZS.11), 1.1208×10^{-10} on the early clock. MOND: free parameter. Observation: McGaugh+ 2016 extraction $(1.20 \pm 0.02_{\rm stat} \pm 0.24_{\rm sys}) \times 10^{-10}$. Agreement: within the systematic error on bound-matter clocks. Falsifier: a precision absolute a_0 measurement inconsistent with $2\sqrt{\alpha}\, cH_0$ after theory and observational systematics are propagated. Tier: D; physical normalization from the bound-matter clock. Status: *validated*.

- **SPARC RAR head-to-head** (Sec. VII). DFD: beats Newton in all 16 galaxies tested; $n_{\rm opt} = 1.15 \pm 0.12$ centered on $n = 1$. ΛCDM: DM halo per galaxy. Observation: McGaugh+ 2016. Agreement: $n = 1$ confirmed; standard MOND $n = 2$ disfavored. Falsifier: best-fit n exits $[1.0, 1.5]$ at 95% CL on full sample. Tier: D. Status: *validated*.

- **Baryonic Tully-Fisher:** $M_{\rm bar} \propto v_f^4$ (Sec. VII). DFD: exact slope. ΛCDM: DM halo prediction. Observation: McGaugh+ slope 3.94 ± 0.08. Agreement: matches. At high redshift DFD's $a_0(z)$ lowers the zero point, by 0.48 dex in $M_{\rm bar}$ at fixed v_f at $z = 2$ in the deep regime (derived). The KMOS$^{\rm 3D}$ zero point rises by 0.17 ± 0.06 dex from $z \simeq 0.9$ to 2.3 [173]; a frozen a_0 and Newtonian baryons miss that rise as well, and the sample shares its galaxies and calibrations with the massive-disc rotation curves of App. A0Z, so the zero-point evolution does not yet test $a_0(z)$ (computed). Falsifier: BTFR slope outside $[3.7, 4.3]$ at high significance. Tier: T. Status: *validated*.

- **Zero-parameter amplitude–shape relation** (ν, u) (App. AT 7). DFD: the mass discrepancy $\nu = g_{\rm obs}/g_{\rm bar}$ and the log-slope variable $u = -2\,{\rm d}\ln\nu/{\rm d}\ln g_{\rm bar}$ obey a closed relation with a_0 eliminated identically — $u = (\nu-1)\ln[\nu/(\nu-1)]$ for the exponential occupation response, $u = 2(\nu-1)/(2\nu-1)$ for the closure form $\mu = x/(1+x)$ of Thm N.8 — so this is a galactic test that uses *no* acceleration scale at all. ΛCDM: no relation between the two (halo shape is a free function). Observation: SPARC, 8 equal-count $g_{\rm bar}$ bins, 2316 points from 113 galaxies. Agreement: $\chi^2/{\rm dof} = 1.08$, $p = 0.37$, largest pull $+2.26\sigma$; the $n \geq 2$ ("standard" and steeper) members of the same family are excluded by shape alone at $2\Delta\ln L = +14.97$ and $+30.89$ with $\Upsilon_\star$ marginalised ($+14.07$ with $\Upsilon_\star$ free). *Stated limit:* these data do *not* separate the two DFD-admissible forms from each other ($+0.43$), and provably cannot — every a_0-free shape statistic on SPARC is bounded at $2\Delta\ln L \leq +3.99$. Distance and inclination errors are *exactly* horizontal in the $(\ln\nu, u)$ plane (Thm. AT.18), so only $\Upsilon_\star$ needs marginalising. Falsifier: the binned locus off the curve by $> 5\sigma$; any bin robustly at $\nu < 1$; a measured $u > 1$ asymptote; or $\Upsilon_{[3.6]} > 0.58\, M_\odot/L_\odot$ measured independently (Falsifier AT.22, currently $\simeq 2.5\sigma$ clear). Tier: T (the relation and the systematics vectors); D (the confrontation). Status: *validated*.

- **Wide binary boost at 10^4–2×10^4 AU** (Sec. VII). DFD: $\gamma = 1.000$ exactly for local pairs (Axiom NL.14); pairs beyond $R \simeq 16$ kpc keep the boost ($\gamma = 1.70$–1.97 at 10^4 AU on the forward law, $R = 20$–100 kpc); an isolated-pair 41.6% velocity figure is not a DFD prediction. MOND: $\gamma \simeq 1.4$. Observation: Chae 2023 *Gaia* $\gamma \simeq 1.43 \pm 0.06$; Chae et al. 2026; Yoon et al. 2025; Banik 2024 (-0.3σ) and Saad & Ting 2026 (0.0σ) null. Agreement: with the null analyses; $+7.2\sigma$ from Chae (2023), $+4.3\sigma$ from Chae et al. (2026). Falsifier: a confirmed boost of the Chae type in local pairs. Tier: D (conditional on the axiom). Status: *contested*.

- **The confinement step at $R \simeq 13$–16 kpc** (App. NL). DFD: bound subsystems inside the edge are Newtonian and those outside boosted; a $1\,M_\odot$ pair's relative force changes by a factor 1.59 at 10^4 AU (1.85 at 2×10^4 AU) across it. MOND: a smooth decline. Observation: halo pairs not yet (*Gaia* DR4/DR5); the line-of-sight dispersion profiles of 28 outer-halo globular clusters beyond 16 kpc (Baumgardt catalogue, version 4) give a boost 0.33 ± 0.08 of the predicted one, about 5σ below it with the error scaled for the fit's $\chi^2/{\rm dof} = 2.9$ and about 9σ on the 18 clusters least affected by binaries. Agreement: the inner clusters are consistent with Newtonian dynamics, as predicted; the outer-cluster boost is contradicted. Falsifier: a boost inside the edge, no step, or halo pairs outside the edge with a boost well below the predicted one. Tier: D. Status: *open* for the halo pairs.

- **Classical dwarf spheroidals**. DFD: on the forward form of the printed law of satellites, at population-synthesis mass-to-light ratios, the μ-law alone falls 0.2–0.3 dex (3–4σ) short of the eight Milky Way dispersions (computed), nearly all of it in the four that the Galaxy's field dominates and that are not tidally safe; the four tidally safe dwarfs fit the μ-law alone to about 1σ (computed); χ subhalos, which the floor law adds, or tidal disequilibrium can supply the difference. ΛCDM: DM halo per dSph. Observation: measured dispersions. Agreement: the tidally safe dwarfs fit on the μ-law alone; the others need χ or are out of equilibrium. Falsifier: inconsistent dynamical M/L in any single isolated

classical dSph at $> 5\sigma$. Tier: D. Status: *open*.

- **Ultra-faint dwarf M/L extreme values**. DFD: systematic effects (binary contamination, tidal heating) inflate inferred M/L by factors of 10–100. ΛCDM: dark matter. Observation: UF dSph $M/L \sim 100$–1000. Agreement: rests on the systematics estimate of Table XV; χ subhalos, which DFD forms (Ext. Deriv. App. AH), can also raise the dynamical M/L where χ exceeds the phantom. Falsifier: UF dSph kinematics confirmed pristine yet retain an anomalous M/L that no χ subhalo can supply. Tier: E. Status: *open*.

- **Galactic-scale extension** $a_0(z) = 2\sqrt{\alpha}\, cH(z)$ (App. N, Thm. XIX.3; App. A0Z). DFD: $a_0 \propto H(z)$ with no free exponent on DFD's own background, 1.8, 2.6 and 3.7×10^{-10} m s^{-2} at $z = 0.8$, 1.5 and 2.2 on the early clock and 1.89, 2.82 and 3.95 on bound-matter clocks (Postulate ZS.11; effective exponent $\gamma_E = 1.10$ over $0.33 < z < 1.44$ and 1.29 over $0.6 < z < 2.5$). MOND: static a_0. Observation: two kinds of data, in tension at face value. Low-mass discs at $0.33 < z < 1.44$ (the MUSE–DARK binned RAR scale [109], fitted in Ref. [110]) give $a_0 = A(1+z)^\gamma$ with $\gamma = 0.78 \pm 0.15$ (0.83 ± 0.13 with the SPARC $z \simeq 0$ anchor), excluding a frozen a_0 at 5.3σ and $a_0 \propto \sqrt{\rho_m}$ at 4.8σ (on the exponent's error; 4.7σ by likelihood ratio) on the published bin errors; with the bars read as 1σ, Hubble tracking fits the bins with $\chi^2 = 5.36/3$ at $A = (1.394 \pm 0.032) \times 10^{-10}$ m s^{-2}, 2.1σ from the measured exponent. Refitted galaxy by galaxy from the survey's public products, the published rise reproduces ($\gamma = 0.77 \pm 0.21$), but the galaxy-level uncertainties are several times the published bin errors, because the radial points of one galaxy are correlated, and within the survey a frozen a_0 lies about 1σ away at galaxy level; anchored to SPARC's $z = 0$ value the galaxy-level bins still exclude a frozen a_0 at about 3σ, and DFD's zero-parameter law fits them on the bound-matter clock. The trend also depends on how the molecular gas is added: tied to the survey's own disc masses the rise stays and DFD's law fits it, tied to SED-based masses it is about flat ($\gamma = 0.06 \pm 0.21$; -1.03 to 0.96 at galaxy level), and with stellar masses from spectral energy distributions it falls ($\gamma = -1.04 \pm 0.22$; -2.32 to -0.32), although those SED masses exceed the kinematic 95% limit in about a third of the high-z galaxies; the survey's unconstrained atomic-gas term moves γ between 0.5 and 1.3 over its physical range; above $z \simeq 0.9$ most fitted disc masses sit at the edge of the halo model's prior, and their offset from the SED masses is kinematic, not an artefact of the prior. DFD's zero-parameter amplitude lies 0.095 dex below the tracking amplitude on the published census and 0.02–0.09 dex above it with either fuller census (0.18 dex with both changes together; computed). Massive discs at $0.6 < z < 2.5$ with molecular gas counted [111] give $a_0 = 1.9$, 1.4 and 1.2×10^{-10} m s^{-2} at median $z = 0.8$, 1.5 and 2.2: DFD's value is met at $z \simeq 0.8$, and the rise beyond $z \simeq 1.5$ is not seen on that census, while fits that leave the baryonic mass free neither show nor exclude it. Their within-sample exponent is $\gamma = -0.86^{+0.46}_{-0.48}$ on statistical errors (-0.20 without the discs with $V_{\rm rot}/\sigma_0 < 2.1$); DFD's exponent lies 4.5σ away on statistics alone (likelihood ratio) and about 1.7σ away once a ±30% pressure-support scale and a ±0.1 dex redshift tilt of the baryonic masses are marginalised (computed), although the discs' own data disfavour the calibrations that would rescue DFD, a doubled pressure support or $z \simeq 2$ baryons 0.2 dex lighter, by $\Delta(-2\ln L) = 18$–40 (computed). DFD's domain-local screen (App. ZT) lowers a_0 in overdense domains: by about 10% for massive $z \simeq 2$ discs at the average environment of their haloes, and by 20–34% in the densest known structures; it would match these discs only in $10\,h^{-1}$Mpc domains about 6 to 11 standard deviations denser than average, and their measured environments show no such trend (computed on published values). Agreement: contested. DFD's value is met at $z \lesssim 1$ by the massive discs and, in amplitude, by the survey with either fuller census; the survey's rise is about 1σ within the survey at galaxy level and about 3σ anchored to SPARC, with DFD's law fitting on the bound-matter clock, and it depends on how the molecular gas is added; beyond $z \simeq 1.5$ the massive discs, which sit where the rise should show, do not show it: on the published census they rotate 0.1–0.17 dex slower than DFD predicts (6–9σ on statistical errors, 1.5–2.2σ with the census's calibration counted), and the registered falsification threshold $a_0(z{=}2) < 2.5$ is met at face value. The threshold is reached if the $z \simeq 2$ baryonic masses are about 0.1 dex lower than the fitted ones (about 0.2–0.3 dex in molecular gas), and DFD's value if they are about 0.2 dex lower (about 0.45 dex in gas; 0.3–0.5 dex against the census), or with a pressure-support correction 1.8 or 2.4 times the standard one, which no published prescription gives (DFD's own vertical gravity makes it about 10% smaller). Falsifier: on a baryon census that counts molecular gas, with galaxy-level errors and a stated pressure-support correction, high-z kinematics giving γ more than 3σ from $\gamma_E = 1.10$ over $0.33 < z < 1.44$, or $a_0(z{=}2)$ outside $[2.5, 5.5] \times 10^{-10}$ m s^{-2}. Tier: D. Status: *contested*.

- **No sub-Newtonian μ-law response, at any acceleration** (App. BS, Thm BS.7). DFD: $\nu = g_{\rm obs}/g_{\rm bar} = Z_1 > 1$ structurally — the mode's ladder is bounded below by the ground state, so detailed balance offers no de-excited level and $\nu \geq 1$ is a theorem rather than a property of the fitted μ. MOND: the same by construction of $\mu \leq 1$, but as a modelling choice, not a proof. ΛCDM: no constraint — a baryon-deficient halo is permitted. Observation: no confirmed $g_{\rm obs} < g_{\rm bar}$ system. Falsifier: any system with $M_{\rm dyn}/M_{\rm bar} < 1$ at $> 3\sigma$ after baryon-census systematics; equivalently a converged $\Upsilon_{[3.6]} > 0.58\, M_\odot/L_\odot$ (Falsifier AT.22, which rests on this theorem and is branch-independent for that reason). Tier: T. Status: *validated*.

- **Solar-system safety is structural, not screened** (App. BS, Cor. BS.14, Table CXXXVI). DFD: at Saturn's orbit ($a = 9.5826$ AU) the mode exponent is $\tau = 733.60$ (at the empirical SPARC benchmark $a_0 = 1.20 \times 10^{-10}\,\mathrm{m\,s^{-2}}$), so the mode entropy is $S/k = 1.86 \times 10^{-316}$ and its heat capacity $C/k = 1.36 \times 10^{-313}$; at Earth's surface $\tau = 2.859 \times 10^5$ and $S/k = 2.34 \times 10^{-124147}$. **There is no occupied state to boost**: solar-system agreement is quantum freeze-out of a single mode, with no parameter chosen to achieve it and no fifth-force suppression, chameleon or Vainshtein mechanism invoked. Beyond about 10^3 AU the Sun's own mode is not frozen by its depth; there the Sun is Newtonian by the environmental-confinement axiom (App. NL; Oort-spike row). ΛCDM/GR: agreement by construction. Scalar-tensor alternatives: agreement requires an explicit screening mechanism with its own scale. Observation: Cassini/ephemeris bounds on anomalous acceleration at Saturn. Agreement: the predicted anomaly is $\sim 10^{-318}$ of a_0, unobservably below any bound. Falsifier: a detected anomalous acceleration at Saturn's orbit exceeding $10^{-300}\,a_0$, or, for an isolated system, any demonstration that the deep-MOND and Newtonian regimes require separate closure assumptions rather than the two limits of one C/k. Tier: T. Status: *validated*.

- **Momentum balance: the Local Group barycentre** (App. AV). DFD: zero drift of the matter barycentre against the cold local Hubble flow (Noether's theorem under the adopted energy). ΛCDM: zero; the printed total-ψ rule: 15–20 km/s. Observation: 6.9 ± 3.8 km/s towards M31 along the Milky Way–M31 line, the component along it of the (24 ± 4) km/s motion towards Sculptor found by Karachentsev et al. (2009), with the error of the barycentre's position included. Agreement: 1.8σ. Falsifier: a drift of 15 km/s or more at 5 km/s precision or better, with tides modelled. Tier: D (conditional on the adopted energy). Status: *pending*.

- **χ's equivalence principle beyond the filled zone** (App. AV). DFD: no acceleration difference where χ fills the demand (for a Milky Way modelled with $6\times10^{10}\,M_\odot$ of baryons, to about 208 kpc for $2\times10^{12}\,M_\odot$); $\delta = 0.08$–0.34 at Fornax for a 1.0–$1.2 \times 10^{12}\,M_\odot$ halo, with the leading arm enhanced. ΛCDM: $\delta = 0$. Observation: Sagittarius $|\delta| \lesssim 0.10$; Fornax $\beta \lesssim 0.2$. Agreement: consistent for a χ halo of $1.5 \times 10^{12}\,M_\odot$ or more in that model (abundance matching gives 1.7×10^{12}). Falsifier: an acceleration difference where χ fills the demand, or the fifth-force sign. Tier: D. Status: *pending*.

- **Vertical force at the Sun** (App. AV). DFD: with the measured local stars and gas, $2\pi G \times (66$–$69)\,M_\odot\,\mathrm{pc^{-2}}$ at 1.1 kpc where χ comes close to the μ-law's demand (local χ density at least about $0.0068\,M_\odot\,\mathrm{pc^{-3}}$ for a round χ halo), and 84 ± 4 from the μ-law alone. ΛCDM: 67 for the same baryons. Observation: 68 ± 4, 74 ± 6 and 63.6 at 1.1 kpc; 67 ± 6 and 68.5 ± 1.0 at 1.0 kpc. Agreement: within 0.7σ with χ at the rotation-curve density (0.0079 ± 0.0008); the μ-law alone is 3.1–3.2σ high. Falsifier: a local χ density below $0.006\,M_\odot\,\mathrm{pc^{-3}}$ from the rotation curve beyond the Sun and stellar streams, with the local stars and gas at $47 \pm 3\,M_\odot\,\mathrm{pc^{-2}}$. Tier: D. Status: *pending*.

5. Block 4: Cluster Scale

- **Universal μ from galaxies to clusters** (App. I). DFD: $n = 1$ at cluster scale, no scale-dependent μ. ΛCDM: DM halo. Observation: the 16-cluster sample of App. I. Agreement: consistent once χ supplies the missing mass, whose amount the clusters measure (0.84 ± 0.12 of the cosmic mix when χ adds its Newtonian pull); the cluster masses alone do not test n. Falsifier: cluster RAR with strong-lensing-resolved subhalos shows $n \neq 1$ at $> 3\sigma$. Tier: D. Status: *pending*.

- **PDE-validated Jensen factor $J_{\rm PDE} = 1 + 0.39 f_{\rm sub}$ from 3D AQUAL solver**. DFD: $J \simeq 1.07$–1.12 for $f_{\rm sub} = 0.15$–0.30, and $J \simeq 1.04$ for the baryonic substructure of clusters ($f_{\rm sub} \simeq 0.10$) to which the μ-law responds, robust across $M_{200} \in [3, 12] \times 10^{14}\,M_\odot$. ΛCDM: not applicable. Observation: validated against algebraic-MOND for spherical NFW within 1%. Agreement: computed (PDE). Falsifier: high-resolution multigrid AQUAL solver gives J outside $[1.05, 1.15]$ at $f_{\rm sub} = 0.20$. Tier: D. Status: *open*.

- **Cluster χ budget** (App. I). DFD: under the μ-law alone the sixteen clusters fall short (Obs/DFD 1.57 ± 0.08 relaxed, 1.99 ± 0.16 merging, at $a_0 = 1.20 \times 10^{-10}$ m/s^2 and at the bound-matter $a_0 = 1.1966 \times 10^{-10}$ m/s^2); the shortfall is the derived χ, $4.5 \pm 0.6\,M_{\rm b} = 0.84 \pm 0.12$ of the cosmic mix when χ adds its Newtonian pull and the relaxed hydrostatic masses carry a bias $b = 0.21$, or the ΛCDM budget (1.28–1.51 of the cosmic mix inside r_{500}) under the floor composition of App. AV. A no-χ five-factor correction stack $C_i = B\,J_{\rm PDE}\,T\,M\,P$ is not supported (its baryonic items sum to 1.26, and its projection factor has the wrong sign for lensing masses). ΛCDM: dark matter halos. Observation: 16-cluster sample. Agreement: consistent: predicted 1.21 ± 0.05 of the cosmic mix inside r_{500} from the derived abundance and ΛCDM-like assembly (estimate), measured 1.28 ± 0.04 (no hydrostatic bias) to 1.51 ± 0.04 ($b = 0.21$) on errors of the mean; with the calibration uncertainties the measured masses are 1.10 (0.97–1.23) and 1.30 (1.13–1.47) times the predicted ones (App. I). Falsifier: a cluster sample whose masses the μ-law on its baryons already supplies, leaving no room for χ. Tier: D (estimate). Status: *validated*.

- **Bullet Cluster lensing offset** (Sec. VII). DFD: the collisionless χ carries the lensing peak; without χ DFD gives 24–39% of the lensing mass inside 250 kpc, and

χ at 0.6–0.9 of the cosmic mix fits it when it adds its Newtonian pull (1.1–1.2 under the floor composition); 129 kpc main cluster offset. ΛCDM: DM halo offset. Observation: observed 155 kpc. Agreement: 83% match. Falsifier: lensing peak coincides with gas at any reasonable resolution. Tier: D. Status: *validated*.

- **Galaxy groups: χ as in clusters** (App. I). DFD: on published X-ray masses the μ-law alone falls short of groups as it does of clusters: the median Obs/DFD is 1.22–1.36 at r_{500} for the 23 Chandra groups of Sun et al. (2009) and 1.79 for the 16 groups of Gastaldello et al. (2007), at the bound-matter a_0 with distances computed with $H_0^{\rm loc}$; under the floor composition 20 to 22 of the 23 are Newtonian plus χ at 1.2–1.7 of the cosmic mix, as clusters are (1.28–1.51). ΛCDM: dark-matter halos. Observation: Sun et al. (2009), Gastaldello et al. (2007), Virgo (Simionescu et al. 2017), Fornax (Su et al. 2017). Agreement: consistent with ΛCDM-like assembly of the derived abundance, whose group-scale baryon depletion depends on feedback; the stellar masses are estimates. Falsifier: a sample of groups with securely measured baryon fractions whose median Obs/DFD at r_{500} falls below 1, the μ-law on their baryons alone (single groups below 1 occur within the stellar-mass uncertainty: 3 of the 23 with the higher stellar calibration). Tier: E. Status: *validated*.

- **CMB peak ratio from baryon loading and the derived χ-matter** (App. J; App. AV). DFD: $R = 2.34$ from the analytic baryon-loading estimate; with the derived cold χ-matter added, CAMB on the measured clock gives 2.20 (the peak positions follow the clock measured from BAO and θ_*) (Thm. AV.31), while baryons alone give $H_2/H_1 = 0.39$. ΛCDM: $R \simeq 2.21$ with $\Omega_{\rm CDM} \sim 0.27$. Observation: $R \simeq 2.21$ (Planck 2018 best fit). Agreement: the χ-matter spectrum within 0.6σ on the measured clock; the analytic estimate 6% high. Falsifier: the peak ratio requires a cold component beyond the derived χ abundance at $> 3\sigma$. Tier: D. Status: *validated*.

- **CMB third-peak height from χ-matter** (App. AV). DFD: $H_3/H_2 \approx 1.0$ from the cold χ field with $m_\chi = 32.005$ eV and $\Omega_\chi h^2 = 0.1192806$ (-0.60σ; computed on the flux-period reading that the measured abundance selects; no fitted density), obtained from the flux-period/motivated-multiplicity chain and finite $SU(2)_{60}$ CS-vacuum Casimir expectation with their named assumptions preserved; $Q_\chi = 1$ is conditional on the Rest-Mass Channel. ΛCDM: same height from a postulated cold component. Observation: $H_3/H_2 \approx 0.98$ (Planck 2018). Agreement: $H_3/H_2 = 0.977$ and $H_3/H_1 = 0.444$ on the measured clock, within 0.6σ. Falsifier (decisive): the $\Delta\psi \times \kappa$ cross-spectrum carries the third-peak height, a halo-recoil DM detection appears in a current-reach channel, or a dark-matter photon line appears at 16.0 eV (77.5 nm) or 32.005 eV (38.74 nm) at any strength (χ has no photon coupling, $E = 0$; App. AV). Tier: D for the carrier, conditional on the stated mass/abundance premises and the Rest-Mass Channel with its premise that linear perturbations do not polarize the medium (App. GR). Status: *validated*.

- **RAR intrinsic scatter $\lesssim 0.037$ dex** (App. AV, Remark AV.38). DFD: $\sigma_{\rm RAR} \lesssim 0.037$ dex (the halo-shape floor alone gives 0.013–0.025 dex) if the ΛCDM-like χ halos of the adopted energy are cored, as SPARC requires under the floor law (App. AV), because the derived constant $a_0 = 2\sqrt{\alpha}\, cH_0$ forces the a_0-drift channel to zero (conditionally on the DLSC axiom, App. ZT, a domain-local environment modulation $\Delta a_0/a_0 = -(f/3)\,\delta_{\rm env}$ reopens this channel at 0.015–0.027 dex for $R_D = 10$–$20\ h^{-1}$Mpc — inside this intrinsic budget, and a candidate explanation for part of it). ΛCDM: ~ 0.06–0.08 dex (the a_0-universality is a fine-tuning puzzle requiring per-galaxy feedback tuning). Observation: joint inference of the relation and the galaxy parameters on SPARC gives 0.034 ± 0.001 (stat) ± 0.001 (sys) dex, given the SPARC error model [169]; a 10% uncertainty on the baryonic velocity components sets the preferred value to zero. Agreement: below the bound and the ΛCDM range under the SPARC error model; above the halo-shape floor alone, inside the budget only with the domain-local channel. Falsifier: true intrinsic RAR scatter $>\sim 0.06$ dex (Stone's 0.11 confirmed at the intrinsic level) that is not the one-sided upward lift of χ halos denser than the phantom falsifies DFD. Tier: D. Status: *pending* (medium confidence).

6. Block 5: Cosmology

- **CMB acoustic scale on the measured clock** (Apps. J and ZS). DFD: $100\theta_* = 1.04110$ and $\ell_1 \simeq 220.4$ with no global ψ-lensing map. Observation: $100\theta_* = 1.04109 \pm 0.00031$. Agreement: $+0.03\sigma$; θ_* is one of the data that measure C, so the test is its concordance with BAO ($\chi^2 = 10.52/13$ on 13 pre-DESI points; DESI DR2 BAO alone sits 3.4σ above the θ_*-only clock). Falsifier: the frozen-input acoustic forward solution fails at precision after the measured clock and stated inputs are propagated. Tier: D given measured C. Status: *validated*.

- **Native linear-clustering S_8 on the measured clock**. DFD: $R_8 = 11.848$ Mpc, $\sigma_8 \simeq 0.8063$, $\Omega_m \simeq 0.312$, $S_8 \simeq 0.822$. Observation: KiDS-Legacy $0.815^{+0.016}_{-0.021}$ (about $+0.45\sigma$ using its upper error), with the joint external-probe result $0.814^{+0.011}_{-0.012}$ (about $+0.74\sigma$), and DES Year 6 0.789 ± 0.012 (2.8σ below, survey errors only; App. GR). Tier: D conditional on the adopted $Q_\chi = 1$ Rest-Mass Channel. Status: *validated*.

- **Distance duality: $D_L/(1+z)^2 D_A = 1$ (DDR violation $= 0$)**. DFD: exact identity. ΛCDM: exact identity (in standard FLRW). Observation: $D_L/(1+z)^2 D_A = 1.01 \pm 0.02$ (Sec. XVI), consistent with no violation;

DESI DR2 BAO with Pantheon+ or DES-Dovekie supernovae and cosmic chronometers find no violation within 1σ [180]. Falsifier: detection of DDR violation > 0.01 at any z. Tier: T. Status: *validated* (shared with ΛCDM).

- **DESI BAO: evolving dark energy hint**. DFD: $w = -1$ exactly (one constant vacuum term, App. AU; no dark-energy clustering), ΛCDM-identical in the distance sector. ΛCDM: static Λ. Observation: DESI DR2 dataset-dependent preference for $w(z) \neq -1$ [95]. Agreement: DFD stands with ΛCDM on this test and inherits the same tension; not a DFD confirmation. Falsifier: DESI DR3 (or successors) confirming $(w_0, w_a) \neq (-1, 0)$ at $> 5\sigma$. Tier: C. Status: *pending*.

- **CMB-foreground correlation: $\Delta\psi(\hat{n})$ correlates with structure**. DFD: a local, anisotropic correlation with foreground structure at the amplitude of the conditional model of App. LS; there is no global screen (App. ZS). ΛCDM: the integrated Sachs–Wolfe cross-correlation, which DFD shares ($A_{\rm ISW} = 1.00$, Sec. XVII), with no $\Delta\psi$ screen and no local anisotropic term. Observation: not yet measured. Falsifier: no correlation found at predicted σ_ψ across multiple frequencies. Tier: D. Status: *open*.

- **ESPRESSO $\Delta\alpha/\alpha$ at $z \sim 1$**. DFD: $\xi^{\rm res}_{\rm LPI} \times (+2.0 \times 10^{-6})$, conditional on the undetermined residual $\xi^{\rm res}_{\rm LPI}$ (Eq. (253)). SM: 0 (no evolution). Observation: $+1.3 \pm 1.3 \times 10^{-6}$. Agreement: none to state until $\xi^{\rm res}_{\rm LPI}$ is determined. Falsifier: a determined $\xi^{\rm res}_{\rm LPI}$ whose prediction is inconsistent with the measured $\Delta\alpha/\alpha$ at $> 3\sigma$. Tier: D. Status: *open*.

7. Block 5a: Growth–Lensing Consistency (E_G, ACT DR6 × BOSS)

DFD's forward prediction for the geometry-vs-dynamics ratio is the *GR-form* statistic evaluated at DFD's derived matter fraction: with gravity-universal growth ($Q_\chi = 1$) and the ψ-screen cancelling between the lensing numerator and the clustering denominator of the ratio estimator, $E_G(z) = \Omega_{m,0}/f(z)$ at the current $\Omega_m \simeq 0.312$, scale-independent on linear scales. The $\Omega_m = 0.274$ lower-normalization signature belongs to the one-clock $C = 1$ background; the result at the measured clock is effectively the Planck-ΛCDM normalization.

- **E_G growth–lensing statistic (ACT DR6 CMB-lensing × BOSS)** [97]. DFD: $E_G = 0.402$ at $z = 0.555$ (CMASS) and 0.453 at $z = 0.316$ (LOWZ), scale-independent. ΛCDM (Planck values, the analysis' own reference): 0.401 and 0.452. Observation: $0.31^{+0.06}_{-0.05}$ (CMASS) and $0.49^{+0.14}_{-0.11}$ (LOWZ), scale-independent within errors. Agreement: the current DFD and Planck predictions are numerically indistinguishable at the displayed precision and both are consistent with the data. Named conditionality: the ψ-screen cancellation is established for the ratio form $E_G = \Omega_{m,0}/f$ and remains to be verified against the specific DR6 estimator definition. Falsifier: an E_G measurement at $z \approx 0.5$ with precision sufficient to exclude the shared GR-form value, or a detected scale-dependence of E_G on linear scales. Tier: D. Status: *validated* (no current DFD edge).

The screen cancels in the ratio and the current measured-clock Ω_m is Planck-like, so the present data provide a consistency check, not a two-normalization discriminator.

8. Block 6: Laboratory Tests (Clocks, Cavities, Matter Waves, Antimatter)

- **Cross-species clock LPI: $K_A = k_\alpha S_A^\alpha$ species-dependent**. DFD (extended non-metric channel, coefficient not derived from the minimal action): species-dependent at the indicative scale $\sim 10^{-15}$; minimal DFD: zero (Thm. XI.2). SM: exactly zero (Einstein equivalence principle). Observation: current null at 10^{-17} in pure-α channel. Agreement: consistent (screened). Falsifier: cross-species LPI null at $< 10^{-15}$ on cross-species channel involving strong sector. Tier: D. Status: *open*.

- **Pure-α residual $\lambda_\alpha \approx 2.1 \times 10^{-8}$ in same-ion E3/E2** (Sec. XI). DFD (extended channel, ϵ_H estimate, not derived from the minimal action): $\lambda_\alpha \approx 2.1 \times 10^{-8}$; minimal DFD: zero. SM: 0. Observation and agreement: as for the clock-coupling row (Block 1), whose residual this is; the screened value lies four orders below the Filzinger *et al.* 2023 bound, which does not test it. Falsifier: a same-ion E3/E2 null below the screened residual. Tier: D. Status: *open*.

- **Composition/strong-sector residual $\lambda_{N,e,s} \approx 4.2 \times 10^{-7}$**. DFD (extended channel, ϵ_H estimate, not derived from the minimal action): 4.2×10^{-7} in cross-species channels; minimal DFD: zero. SM: 0. Observation: BACON-II $Al^+/Sr/Yb$ at $\sim 8 \times 10^{-18}$. Agreement: consistent (screened). Falsifier: cross-species LPI null at $< 5 \times 10^{-7}$ at multi-σ. Tier: D. Status: *open*.

- **Cavity-atom residual $\xi^{\rm res}_{\rm LPI}$**. DFD: screened residual after geometric cancellation. SM: $\xi = 0$. Observation: not yet at sensitivity. Falsifier: next-gen cavity-atom test reaches predicted sensitivity and finds null. Tier: D. Status: *open*.

- **Kennedy–Thorndike null: $B_{\rm KT} = 0$ at fixed ψ** (Sec. XI, Cor. XI.3). DFD: the co-located cavity/atom ratio is independent of the laboratory's velocity relative to the preferred (CMB) frame, identically at fixed ψ; preferred-frame and tidal remainders $\lesssim 10^{-22}$, the former common-mode (Rem. XI.4). SM: 0 (local Lorentz invariance). Observation: $\beta_{\rm RMS} -$

$\alpha_{\rm RMS} - 1 = -1.7(4.0) \times 10^{-8}$ (sidereal), weighted mean $-4.8(3.7) \times 10^{-8}$ [61]; earlier null at 2×10^{-13} in fractional frequency [62]. Agreement: -0.4σ (sidereal), -1.3σ (weighted mean). Falsifier: a boost-correlated cavity/atom modulation above 10^{-22} that survives systematics. Tier: T. Status: *validated*.

- **Th-229 nuclear clock anomaly**. DFD (extended strong channel; k_s a matching coefficient, not derived from the minimal action): screened annual half-amplitude about 350 Hz at $\alpha_s(M_Z)$, 0.9–1.5 kHz at the nuclear-scale α_s (Sec. XI F); minimal DFD: zero. SM: 0. Observation: the 2026 reproducibility data of Ooi et al. exclude the unscreened amplitude and leave a 26 Hz–1 kHz window. Falsifier: Th-229 clock at $\sim 10^{-19}$ stability finds null in strong-sector channel. Tier: D. Status: *pending*.

- **Matter-wave phase at 1PN: $H_{\rm DFD} = H_{\rm GR}$ identically** (Sec. XIII). DFD: no DFD-specific $T^2/T^3/T^4$ term through 1PN (any static potential), nor at 2PN, where the static metric is GR's (App. WS). SM: identical (same $\gamma = \beta = 1$ metric). Observation: consistent with all Solar-System PPN data (§IV C). Falsifier: none beyond $\gamma = \beta = 1$; a species-dependent ($K_{\rm atom}$) residual above the corpus's own 10^{-14} Eötvös bound (§XV G) would indicate new non-metric coupling. Tier: T. Status: *validated*.

- **Antimatter gravity: $a_{\bar{H}} = a_H$ at metric level**. DFD: equal. SM: equal (Einstein). Observation: ALPHA-g consistent. Agreement: exact. Falsifier: antimatter shows $a \neq g$ at metric. Tier: T. Status: *validated*.

- **Antimatter species-dependent residual σ_A** (Sec. XV C). DFD: non-metric residual at 10^{-7}–10^{-8}. SM: 0 exactly. Observation: not yet at sensitivity. Falsifier: ALPHA-g + species-resolved measurements show null at predicted level. Tier: D. Status: *open*.

- **LPI test $\xi = 0$ vs DFD $\xi \neq 0$ (cavity-atom)**. DFD: nonzero residual $\xi^{\rm res}$, the cavity-atom residual listed earlier in this block. SM: $\xi = 0$ exactly. Observation: current bound $|\xi| < 10^{-5}$. Agreement: consistent (screened). Falsifier: cavity-atom ξ null at predicted screened residual level. Tier: D. Status: *open*.

9. Block 7: Strong-Field, Hyperbolicity, and Open Items

- **No singularity reached in absolute time** (App. WS). DFD: its maximal slicing never reaches the singularity of a collapsing star, so the BKL regime lies beyond every finite absolute time (for maximal slices proved for spherical collapse and crushing singularities and argued for generic rotating collapse; that DFD's slices stay maximal during collapse is argued). GR: predicts BKL chaos near spacelike singularities. Observation: untested regime (inside horizons). Falsifier: a derivation that DFD's slices reach a curvature singularity at finite absolute time. Tier: D. Status: *open*.

- **Hyperbolicity for small perturbations on smooth backgrounds**. DFD: the linearised evolution on any static background is well-posed in its energy space, with conserved energy, no growing modes and finite propagation speed, including at points where $\nabla\psi = 0$ (Theorem III.9). GR: well-posed IVP. Observation: —. Agreement: exact theorem. Falsifier: numerical instability for any DFD perturbation evolution. Tier: T. Status: *open*.

- **Full hyperbolicity for nonlinear strong-field dynamics**. DFD: locally well-posed wherever $\nabla\psi \neq 0$, for the exact law and its approximant, with characteristic speeds up to $1.017\,c$ and every characteristic advancing the absolute time (Theorem III.5); smooth solutions can form gradient singularities in finite time, as fluids form shocks; nonlinear evolution through points where $\nabla\psi = 0$ is an open question of degenerate hyperbolic equations. GR: well-posed (with constraint propagation). Observation: —. Falsifier: DFD evolution code finds genuine ill-posedness for a configuration with $\nabla\psi \neq 0$. Tier: T (local). Status: *open*.

- **Uniqueness of $\mathbb{C}P^2 \times S^3$** (App. AB, Thm AB.1). DFD: unique compact manifold (up to diffeomorphism) satisfying the seven vacuum axioms (V1), (V2), (V4), (V4′), (V5), (V7), (V10) — including simple connectedness of M_g and positive Ricci on M_c; the axiom set is satisfiable (explicit model exhibited). Observation: —. Agreement: exact theorem. Falsifier: alternative compact manifold satisfies the same seven axioms with different topological invariants. Tier: T. Status: *open*.

- **Higgs quartic $\lambda_H = 1/8$** (dimension count; App. Z). DFD: $\lambda_H = 1/8$ at the electroweak matching scale. SM: input parameter. Observation: running quartic 0.1260 at m_t. Agreement: $m_H = 124.6$ GeV at m_t, 0.40% (2.7σ) low; exact at 182 ± 4 GeV. Falsifier: a derived electroweak matching scale outside 175–189 GeV, the range in which the running quartic is within 2σ of 1/8. Tier: C. Status: *open*.

- **PDE uniqueness theorem for ψ rest frame** (Sec. XVIII). DFD: unique up to gauge. GR: boost invariance. Observation: not yet proven. Falsifier: demonstration of multiple inequivalent rest frames in any DFD configuration. Tier: C. Status: *open*.

- **Standard quantum unitarity preserved (Mott problem)** (Sec. XVII). DFD: no modification to QM. SM: standard QM. Observation: all QM tests consistent. Agreement: exact. Falsifier: QM modification detected at any precision. Tier: T. Status: *validated*.

- **Diosi-Penrose collapse rate vs DFD** (Sec. XVIII). DFD: no anomalous collapse. DP: mass-scaling decoher-

ence. Observation: MAQRO will discriminate. Falsifier: MAQRO confirms DP scaling at predicted level. Tier: D. Status: *open*.

10. Summary statistics

The Master Claims Confrontation Matrix contains 78 distinct claims spanning fundamental constants, gravitational tests, galactic and cluster dynamics, cosmology, and laboratory probes.

a. Aggregating by tier.

- **Theorem-grade (T):** 26 claims, representing the central structural identities of the theory (PPN parameters, μ-derivation, the no-wormhole theorem, GW propagation, BTFR, antimatter gravity at metric level, manifold uniqueness, matter-wave 1PN identity, the linear and local well-posedness of the field equation). (Proton stability is graded conditional — see its entry.)
- **Derived (D):** 47 claims, including the microsector quantities (α^{-1}, the exponent of the Higgs VEV, fermion masses with their stated prefactors, CKM, PMNS, H_0 closure, cluster $J_{\rm PDE}$), the cluster χ budget at estimate grade, and the environmental-confinement entries, which are conditional on that axiom.
- **Conjectured (C):** 3 claims, all explicitly open program items ($\lambda_H = 1/8$, ψ rest-frame uniqueness, the DESI evolving-w confrontation).
- **Empirical (E):** 2 claims, the group χ budget and the UF-dwarf M/L bound.

b. Aggregating by status.

- **Validated (*validated*):** 45 claims, where current observational data supports DFD at the stated agreement level. This includes essentially all established gravitational tests, the closed-form value of α^{-1} and the exponent of the Higgs VEV, the SPARC galactic dynamics tests, the Oort spike, the cluster and group χ budgets, and the CMB peak structure (the peak ratio and the third-peak height on the measured clock).
- **Pending (*pending*):** 8 claims, where the experimental capability exists or is imminent but no published measurement yet decides the claim: proton stability, the Local Group barycentre, χ's equivalence principle beyond the filled zone, the vertical force at the Sun, the intrinsic scatter of the radial-acceleration relation, the universal μ from galaxies to clusters, the DESI evolving-dark-energy hint and the Th-229 nuclear clock.
- **Open (*open*):** 23 claims: 21 with no comparable observational test currently available, the ultra-faint dwarfs, and the classical dwarfs, four of which, exposed to the Galaxy's tides, need χ subhalos, which DFD does not yet predict in detail, or tidal disequilibrium. The 21 include strong-field BKL absence, the wide-binary orientation null, the confinement step for wide binaries at $R \simeq 13$–16 kpc (the outer-halo globular clusters contradict its boost) and the screened clock residuals, which lie orders of magnitude below current bounds.
- **Contested (*contested*):** 2 claims, the epoch extension $a_0(z)$: within the survey the rise that low-mass discs at $z < 1.44$ show on the published bins is about 1σ counted galaxy by galaxy and depends on how the molecular gas is added, although anchored to SPARC's $z = 0$ value the galaxy-level bins still exclude a frozen a_0 at about 3σ and DFD's zero-parameter law fits them on the bound-matter clock, and massive discs at $z \simeq 2$ with molecular gas counted do not show the rise; and the local wide-binary boost, where the *Gaia* analyses disagree and DFD predicts none.

11. Reading guide for referees

A referee should focus principal scrutiny on the following entries:

1. **Theorem-grade structural claims:** Verify that the proofs cited (e.g., Theorem N.8 for μ-derivation, Theorem AA.1 for the Padé identity, Theorem AB.1 for $\mathbb{C}P^2 \times S^3$ uniqueness) are mathematically sound and use only the stated assumptions. The theorems are independent of the rest of the theory; failure of any single one would force a substantial revision.
2. **Derived microsector results:** Verify that the closure framework (spectral action, Chern-Simons on S^3, $k_{\max} = 60$ truncation) is internally consistent and reproduces the listed quantities. The microsector framework is the closure that promotes "conjectures" to "derived," so its assumptions matter.
3. **Cluster χ budget (D, estimate):** Under the μ-law alone the sixteen clusters fall short (relaxed 1.57 ± 0.08; mergers 1.99 ± 0.16, at $a_0 = 1.20 \times 10^{-10}$ m/s^2 and at the bound-matter $a_0 = 1.1966 \times 10^{-10}$ m/s^2), and the shortfall is the derived χ at 0.84 ± 0.12 of the cosmic mix (additive composition, hydrostatic bias $b = 0.21$). This is the most measurement-dependent claim in the matrix. A referee may legitimately demand: (a) the per-cluster baryonic masses and apertures of App. I, (b) the hydrostatic bias used to equalize the relaxed and merging classes, (c) the composition of χ with the μ-law, which moves the budget from 0.84 to 1.28–1.51 of the cosmic mix, and (d) any no-χ closure, which the five-factor stack does not supply. The PDE-validated $J_{\rm PDE}$ is computed; for baryonic substructure it is $\simeq 1.04$.
4. **Pending and open experimental tests:** Cross-species clock LPI, Th-229 nuclear clock, BACON-II next iteration, precision E_G result, Yb^+ same-ion E3/E2 next-generation (the clock tests probe the extended non-metric channel, Thm. XI.2). These will determine whether the corresponding sectors survive or are falsified within the next 1–3 years. They are the decisive tests, not the historical data.

12. Use of this matrix

This matrix is intended for three audiences:

- **Referees**: To provide a single catalog summarizing the falsifiability structure of the theory. Failure of any T-class entry forces structural revision; failure of any *pending* entry would falsify a specific prediction. The matrix is designed to be a referee's first stop, not a substitute for the detailed sections.
- **Experimenters**: To identify which open or pending tests offer the highest discriminating power between DFD and competing frameworks. The Yb^+ E3/E2 same-ion null at $|(c^2/\alpha)\, d\alpha/d\Phi| \lesssim 3\times10^{-9}$ is currently the sharpest in the laboratory regime; in cosmology the sharpest pending tests are those of the two-clock postulate: bright sirens, mass-sheet-robust time delays and the absolute a_0 scale (Falsifier ZS.14).
- **Independent theorists**: To distinguish the theorem-grade structural identities from the auxiliary closure-framework derivations. The theorem-grade items (PPN, μ-derivation, manifold uniqueness, no-wormhole) carry forward independent of the closure framework; alternative closure frameworks for the microsector would change the D entries but not the T entries.

Every empirical claim carries a tier label and a falsifier, so structural claims are not mistaken for hidden first-principles proofs and auxiliary closure derivations are not mistaken for empirical fits.

Appendix AN: The Optical-Metric Master Equation: Unified Light and Matter Motion

The two foundational motion laws of DFD, the one-way light speed $c_1 = c\,e^{-\psi} = c/n$ and the matter acceleration $\mathbf{a} = (c^2/2)\nabla\psi$, are not independent postulates. This appendix shows that both are limits of a single equation of motion: the massive wave equation on one optical metric, with light as its null sector and matter as the slow limit of its timelike sector. The factor 1/2 in the acceleration law, which might appear fitted, is forced by the rest-energy structure of that equation.

1. The isotropic optical metric

Light propagation fixes only the conformal class of a metric: null cones encode the local speed but not an overall scale. Within that class we adopt the isotropic representative

$$d\tilde{s}^2 \;=\; -\,c^2 e^{-\psi}\,dt^2 \;+\; e^{\psi}\,\delta_{ij}\,dx^i dx^j, \qquad \text{(AN1)}$$

with $\tilde{g}_{00} = -c^2 e^{-\psi}$, $\tilde{g}_{ij} = e^{\psi}\delta_{ij}$, and inverse $\tilde{g}^{00} = -e^{\psi}/c^2$, $\tilde{g}^{ij} = e^{-\psi}\delta^{ij}$. Its null condition $d\tilde{s}^2 = 0$ gives $|d\mathbf{x}/dt| = c\,e^{-\psi} = c/n$, so Eq. (AN1) agrees with the eikonal light metric $d\tilde{s}^2 = -c^2dt^2/n^2 + d\mathbf{x}^2$ on null structure; the two are conformally related and yield identical light cones.

Equation (AN1) is distinguished within its conformal class by its timelike sector. In the weak field $\tilde{g}_{00}/c^2 \approx -(1-\psi) = -(1+2\Phi/c^2)$ identifies the potential $\Phi = -\frac{1}{2}c^2\psi$, reproducing the effective Newtonian potential of the main text and the matter acceleration. The spatial part gives $\tilde{g}_{ij} \approx (1+\psi)\delta_{ij} = (1-2\gamma\Phi/c^2)\delta_{ij}$ with $\Phi = -\frac{1}{2}c^2\psi$, hence the parametrized post-Newtonian value $\gamma = 1$ and the GR light-deflection coefficient $4GM/c^2b$. Equation (AN1) is therefore, to first order in ψ, the unique representative whose *full* geodesic structure, null and timelike, reproduces simultaneously the refractive index, the matter acceleration, and $\gamma = 1$. (The bare eikonal form $-c^2dt^2/n^2 + d\mathbf{x}^2$ encodes only the light sector; its timelike geodesics do not by themselves yield $\Phi = -c^2\psi/2$, which is why the isotropic representative Eq. (AN1) is the natural carrier of the unified motion law.)

2. The master wave equation and its eikonal limit

The fundamental object for motion is the wave equation on Eq. (AN1),

$$\left(\tilde{\Box}_{\tilde{g}} - \frac{m^2c^2}{\hbar^2}\right)\Psi \;=\; 0, \qquad \tilde{\Box}_{\tilde{g}} = \frac{1}{\sqrt{-\tilde{g}}}\,\partial_\mu\!\left(\sqrt{-\tilde{g}}\,\tilde{g}^{\mu\nu}\partial_\nu\right), \qquad \text{(AN2)}$$

which covers the full wave regime. The ray, or particle, regime follows from the eikonal substitution $\Psi = A\,e^{iS/\hbar}$, whose leading order in $\hbar$ is the mass shell $\tilde{g}^{\mu\nu}\partial_\mu S\,\partial_\nu S + m^2c^2 = 0$. With the inverse metric of Eq. (AN1) this

becomes the single dispersion relation

$$\boxed{E^2 \;=\; c^2 e^{-2\psi}\,|\mathbf{p}|^2 \;+\; m^2c^4 e^{-\psi}} \tag{AN3}$$

This relation contains both sectors and is the eikonal of Eq. (AN2), not an independent ansatz.

Theorem AN.1 (Unified light–matter motion; Derived)**.** *Light and matter are the null ($m = 0$) and timelike ($m > 0$) sectors of the single dispersion relation Eq. (AN3). The massless sector gives the group velocity $v_g = \partial E/\partial|\mathbf{p}| = c\,e^{-\psi} = c/n$; the slow massive sector gives $\mathbf{a} = (c^2/2)\nabla\psi$, with the factor $1/2$ arising from the $e^{-\psi/2}$ rest-energy term rather than being assumed.*

Proof. Setting $m = 0$ in Eq. (AN3) gives $E = c\,e^{-\psi}|\mathbf{p}|$ and $v_g = c\,e^{-\psi} = c/n$. For $m > 0$,

$$\begin{aligned} E &= mc^2 e^{-\psi/2}\sqrt{1 + \frac{e^{-\psi}|\mathbf{p}|^2}{m^2c^2}} \\ &\approx\; mc^2 e^{-\psi/2} + \frac{|\mathbf{p}|^2}{2m}\,e^{-3\psi/2}. \end{aligned} \tag{AN4}$$

In the weak field $e^{-\psi/2} \approx 1 - \psi/2$, so to leading order $E \approx mc^2 - \frac{1}{2}mc^2\psi + |\mathbf{p}|^2/2m$, giving the nonrelativistic Hamiltonian $H_{\rm NR} = |\mathbf{p}|^2/2m + U$ with $U = -\frac{1}{2}mc^2\psi$. Hence $\mathbf{a} = -\nabla U/m = (c^2/2)\nabla\psi$, the DFD matter acceleration law. □

3. Gravity as the gradient of the squared light speed

The two sectors share one exact statement. For a particle momentarily at rest the all-orders acceleration is

$$\boxed{\mathbf{a} \;=\; -\tfrac{1}{4}\,\nabla\big(c_{\rm light}^2\big), \qquad c_{\rm light} = c\,e^{-\psi}} \tag{AN5}$$

since $-\frac{1}{4}\,\partial_\psi(c^2e^{-2\psi}) = \frac{1}{2}c^2e^{-2\psi}$, which reduces to $(c^2/2)\nabla\psi$ in the weak field. Equation (AN5) is exact and mechanism-agnostic: matter falls down the gradient of the squared local speed of light. It is the optical statement of gravitation, and it makes the unification of the two sectors manifest.

4. Relation to the action, and the boundary on matter

Equations (AN2)–(AN5) descend, together with the field equation for ψ and the radiative sector, from a single action by varying distinct fields, a fork rather than a linear chain:

$$\frac{\delta S}{\delta\psi} = 0 \;\Rightarrow\; \nabla\cdot\big[\mu(|\nabla\psi|/a_*)\nabla\psi\big] = -\frac{8\pi G}{c^2}\rho$$

[Eq. (21), App. N],

$$\frac{\delta S}{\delta x^\mu} = 0 \;\Rightarrow\; \text{geodesics of } \tilde g \text{ (Theorem AN.1)},$$

$$\frac{\delta S}{\delta h^{\rm TT}} = 0 \;\Rightarrow\; \Box\, h^{\rm TT} = \text{source}, \quad c_T = c_\gamma \text{ (App. WS)}.$$

The gravitational field equation comes from varying ψ; the matter motion law comes from varying the trajectory. These are different variations of different fields, and the matter law is not obtained from $\delta S/\delta\psi$.

We are explicit about the one input Eq. (AN2) does not supply: the origin of the mass m. The dispersion relation and the geodesics are identical for any value of m, whatever its source; m enters through the matter action. Three statements bound the options. First, the appealing reading of matter as a static finite-energy soliton of ψ itself is excluded for the full response, not only where $\mu \to 1$: for the approximant and both branches of the exact law the flux obeys $xF'(x) < 2F(x)$ at every $x > 0$, so Derrick's scaling derivative $\int \big(3H - F|\nabla\psi|\big)\,d^3x$ is positive for every non-trivial configuration; independently, testing the vacuum equation with ψ gives $\int F(|\nabla\psi|)\,|\nabla\psi|\,d^3x = 0$, hence $\nabla\psi = 0$. Second, a scalar Kaluza–Klein tower on the internal manifold is excluded (every such mode has mass $\geq \sqrt{\alpha}\,M_P \approx 10^{18}$ GeV) and is moreover non-chiral. Third, the fermion-mass content of DFD resides instead in the spectral-action Dirac/Yukawa sector on $\mathbb{C}P^2 \times S^3$ (Appendices Y and X), where the light fermions are the chiral zero modes acquiring mass through Higgs overlap, dressed by powers of α. That sector is chiral and sub-electroweak precisely because it is not a Laplacian tower. Equation (AN2) is thus the master equation of DFD's gravitational-optical sector, complete within that domain and deliberately silent on the origin of matter.

5. Status and falsifiability

The unification carries empirical content. Because light and matter share one metric but couple to different invariants of it (null versus timelike), DFD keeps Etherington's distance duality $D_L = (1+z)^2 D_A$ exact; for co-located clocks the shared metric predicts a universal response (Thm. XI.2), and any species-dependent local-position-invariance signature belongs to the extended non-metric sector (Sec. XI). The light-bending coefficient is the GR value $4GM/c^2b$ by construction ($\gamma = 1$), so solar-system tests are passed, while the deep-field sector reproduces galaxy rotation curves through Eq. (21). The single most distinctive statement is Eq. (AN5): gravitation is the gradient of the squared local speed of light.

Appendix AO: The CP Sector: Strong-CP Protection, the CKM No-Go, and Euler-Projected Closure

This appendix is the consolidated CP-sector theorem package. The $\delta_{\rm CP} \approx 68^\circ$ localization estimate (App. K), the conjectural unitarity-triangle relation $\gamma = 4\pi/11$, and the post-hoc "$19 + 5/2$" apex correction recorded at candidate grade in the companion volume (App. AH) are replaced by the results below; the tree-level, loop-bounded strong-CP result of App. L is restated here in its anomaly form. The apex value selected below, $\bar\rho = \frac{43}{2}\alpha = 21.5\alpha$, coincides with the "Path A" candidate of the companion volume, which the pre-strengthened axioms do not force (the no-forcing anti-theorem below): there it is an unforced candidate, here it is derived as a theorem-grade consequence of an explicitly added selection principle, the Euler-projection Postulate E.1 of §AO 8. Consistent with that anti-theorem, the postulate is a strengthening of the corpus, not a consequence of the pre-strengthened axioms.

This appendix isolates the CP sector of Density Field Dynamics (DFD) as a self-contained theorem package within the unified DFD manuscript. The purpose is to state exactly which parts of the Cabibbo–Kobayashi–Maskawa (CKM) matrix are forced by the existing DFD geometry, which parts require a strengthened CP-sector postulate, and what quantitative predictions follow once that postulate is adopted. We first prove that the minimal real DFD Yukawa kernel has vanishing CKM CP violation: if the up- and down-sector overlap kernels are real, then the CKM matrix is real orthogonal and the Jarlskog invariant vanishes. We then formulate the minimal det-orthogonal CP offset: a conjugation-odd Hermitian Berry perturbation that generates weak-sector CP violation while preserving a quark determinant that is positive on the branch of Postulate Y.10 and hence protecting the strong-CP angle at tree level. The anomaly side of strong-CP protection is stated as a conditional theorem: when the CP mapping-torus Dirac spectrum is paired by an even-dimensional chirality symmetry, the Dai–Freed anomaly phase is trivial; with the quark determinant positive and $\theta_{\rm YM} = 0$ fixed by the spectral action given that nothing is added to it for the gauge fields, no axion is required at tree level inside the DFD branch.

The CKM magnitude skeleton is built from line-bundle cohomology on the $\mathbb{C}P^2$ factor and from the real dimension of $X = \mathbb{C}P^2 \times S^3$. The resulting integers are

$$\lambda = 31\alpha, \qquad A = 108\alpha, \qquad \bar\eta = 49\alpha.$$

The remaining apex ambiguity is treated explicitly. The pre-strengthened DFD corpus contains an anti-theorem: existing axioms do not force the choice between the raw even-cohomology branch $\bar\rho = 22\alpha$ and the half-shift branch $\bar\rho = 21.5\alpha$. This appendix therefore introduces Postulate E.1, the Euler-projection postulate, as a new necessary selection principle in the strengthened DFD–SD branch. It states that the physical CP-even apex coordinate is the minimizer of

$$\mathcal{I}_\rho(r) = \frac{1}{2}\left(r - \frac{D^2}{2}\right)^2 + \chi(\mathbb{C}P^2) r, \qquad r = \bar\rho/\alpha,$$

where $D = \dim_{\mathbb{R}}(\mathbb{C}P^2 \times S^3) = 7$ and $\chi(\mathbb{C}P^2) = 3$. Stationarity gives

$$\bar\rho = \left(\frac{7^2}{2} - 3\right)\alpha = \frac{43}{2}\alpha.$$

Thus the strengthened CP sector predicts

$$(\lambda, A, \bar\rho, \bar\eta) = \left(31, 108, \frac{43}{2}, 49\right)\alpha,$$

with $\alpha^{-1} = 137.03599985$. Numerically this gives

$$\lambda = 0.2262179284, \quad A = 0.7881140731,$$
$$\bar\rho = 0.1568930794, \quad \bar\eta = 0.3575702739,$$

$$\gamma = \arctan(98/43) = 66.3093^\circ, \quad \beta = 22.9823^\circ, \quad \alpha_{\rm UT} = 90.7084^\circ,$$

$$|V_{us}| = 0.2262164, \quad |V_{cb}| = 0.0403311,$$
$$|V_{ub}| = 0.0036554, \quad |V_{td}| = 0.0083576,$$

with exact-standard-parameterization Jarlskog invariant

$$J_{\rm CKM} = 2.9731 \times 10^{-5}.$$

The appendix closes by separating theorem-grade consequences inside the strengthened DFD–SD branch from the still-testable status of Postulate E.1, and by giving a Fubini–Study overlap motivation for the postulate without claiming that the pre-strengthened axioms already prove it.

1. Purpose and scope

The CKM sector has two distinct problems. The first is the magnitude problem: why the quark weak-mixing matrix has the observed hierarchical shape. The second is the phase problem: why a nonzero weak CP-violating phase exists while the strong-CP parameter remains experimentally consistent with zero. The Standard Model parametrizes both facts but does not derive the numerical CKM parameters from more primitive structure. DFD attempts to explain the hierarchy by tying the flavor geometry to the finite internal space

$$X = \mathbb{C}P^2 \times S^3, \qquad D := \dim_{\mathbb{R}} X = 7, \tag{AO1}$$

and to an α-locked finite microsector.

This appendix is written with a strict status discipline. We use the following terminology.

Definition AO.1 (Theorem-grade inside a branch)**.** A statement is theorem-grade inside a named branch if it follows from explicitly stated axioms, definitions, and postulates of that branch by ordinary mathematical proof, with no phenomenological fitting hidden in the proof.

Definition AO.2 (Postulate-grade selection rule)**.** A selection rule is postulate-grade if it is introduced as a

new structural assumption because it is not forced by the older axioms. Consequences of the postulate may be theorem-grade, but the postulate itself remains a falsifiable strengthening of the branch.

The central caveat is the following.

Anti-Theorem AO.3 (No CKM apex forcing in the pre-strengthened corpus). In the pre-strengthened DFD axioms, the CKM apex branches

$$\bar{\rho}_A = \frac{43}{2}\alpha, \qquad \bar{\rho}_B = 22\alpha \tag{AO2}$$

are not uniquely separated by an existing internal symmetry. Therefore the pre-strengthened corpus cannot claim a theorem selecting one branch over the other.

Proof. The older DFD CKM construction fixes the cohomological skeleton

$$\lambda = 31\alpha, \qquad A = 108\alpha, \qquad \bar{\eta} = 49\alpha, \tag{AO3}$$

but the real-axis apex coordinate admits more than one natural assignment. The raw even-cohomology assignment gives 22α, while the half-shift or Euler-pulled assignment gives $(43/2)\alpha$. Without a rule that distinguishes raw even cohomology from a projected complex apex, both are admissible. This is exactly an absence-of-forcing result. □

This appendix resolves the ambiguity only after adding the Euler-projection postulate in Section AO 8. This is the correct branch statement:

$$\boxed{\begin{array}{c}\text{DFD–SD plus Euler projection gives}\\ (\lambda, A, \bar{\rho}, \bar{\eta}) = \left(31, 108, \frac{43}{2}, 49\right)\alpha.\end{array}} \tag{AO4}$$

It is not claimed that the original DFD axioms alone already forced the apex.

2. CKM and CP notation

The charged-current weak interaction couples up-type and down-type quarks through

$$\mathcal{L}_W = \frac{g}{\sqrt{2}}\,\bar{u}_{Li}\gamma^\mu V_{ij} d_{Lj} W^+_\mu + \text{h.c.}, \tag{AO5}$$

where

$$V = V_{\text{CKM}} = U_u^\dagger U_d \tag{AO6}$$

is the mismatch between the unitary transformations that diagonalize the up- and down-type quark mass matrices. In the Wolfenstein convention,

$$V_{\text{CKM}} = \begin{pmatrix} 1-\lambda^2/2 & \lambda & A\lambda^3(\rho - i\eta) \\ -\lambda & 1-\lambda^2/2 & A\lambda^2 \\ A\lambda^3(1-\rho-i\eta) & -A\lambda^2 & 1 \end{pmatrix} + O(\lambda^4). \tag{AO7}$$

We use the barred unitarity-triangle coordinates $(\bar{\rho}, \bar{\eta})$, which absorb higher-order Wolfenstein corrections in standard global-fit conventions. At the accuracy relevant for the integer derivation, the branch is specified by

$$(\lambda, A, \bar{\rho}, \bar{\eta}) = \left(31, 108, \frac{43}{2}, 49\right)\alpha. \tag{AO8}$$

The CP-violating rephasing invariant is the Jarlskog invariant

$$J_{\text{CKM}} = \text{Im}\left(V_{ij}V_{kl}V_{il}^*V_{kj}^*\right), \tag{AO9}$$

which, in the standard parametrization, is

$$J_{\text{CKM}} = c_{12}c_{23}c_{13}^2 s_{12}s_{23}s_{13}\sin\delta. \tag{AO10}$$

Here

$$s_{12} = \lambda, \qquad s_{23} = A\lambda^2, \qquad s_{13} = A\lambda^3\sqrt{\bar{\rho}^2+\bar{\eta}^2}, \qquad \delta = \arctan\frac{\bar{\eta}}{\bar{\rho}}. \tag{AO11}$$

The strong-CP parameter is

$$\bar{\theta} = \theta_{\text{YM}} + \text{Arg}\det(M_u M_d). \tag{AO12}$$

A viable CP sector must generate $J_{\text{CKM}} \neq 0$ while preserving $\bar{\theta} = 0$ or a value beneath experimental bounds. The DFD branch in this appendix accomplishes this by placing weak CP violation in a det-orthogonal Berry offset.

3. DFD microsector and cohomological inputs

Axiom AO.4 (Internal flavor space)**.** *The DFD CP/flavor microsector is modeled by*

$$X = \mathbb{C}P^2 \times S^3, \qquad D = \dim_{\mathbb{R}} X = 7. \tag{AO13}$$

The $\mathbb{C}P^2$ factor carries the holomorphic line-bundle ladder $\mathcal{O}(k)$. The S^3 factor supplies the three-dimensional generation/phase geometry and the real internal dimension contributing to $D = 7$.

Axiom AO.5 (Fine-structure normalization)**.** *The DFD microsector fixes the dimensionless coupling α used below. Numerically,*

$$\alpha^{-1} = 137.03599985, \qquad \alpha = 0.007297352528493264. \tag{AO14}$$

This appendix treats α as already fixed by the independent

DFD α-lock sector.

Lemma AO.6 (Line-bundle dimension on $\mathbb{C}P^2$)**.** *For $k \geq 0$,*

$$h^0\big(\mathbb{C}P^2, \mathcal{O}(k)\big) = \frac{(k+1)(k+2)}{2}. \tag{AO15}$$

Proof. Holomorphic sections of $\mathcal{O}(k)$ over $\mathbb{C}P^2$ are homogeneous polynomials of degree k in three complex homogeneous coordinates $[z_0 : z_1 : z_2]$. A basis is given by monomials

$$z_0^{a_0} z_1^{a_1} z_2^{a_2}, \qquad a_0 + a_1 + a_2 = k, \qquad a_i \geq 0. \tag{AO16}$$

The number of nonnegative integer triples summing to k is the stars-and-bars count

$$\binom{k+2}{2} = \frac{(k+1)(k+2)}{2}. \tag{AO17}$$

Equivalently, Hirzebruch–Riemann–Roch gives the same result from

$$\begin{aligned} \chi(\mathbb{C}P^2, \mathcal{O}(k)) &= \int_{\mathbb{C}P^2} \mathrm{ch}(\mathcal{O}(k))\mathrm{Td}(T\mathbb{C}P^2) \\ &= \int_{\mathbb{C}P^2} e^{kH}\left(1 + \frac{3}{2}H + H^2\right), \end{aligned} \tag{AO18}$$

where $\int_{\mathbb{C}P^2} H^2 = 1$. The H^2-coefficient is

$$\frac{k^2}{2} + \frac{3k}{2} + 1 = \frac{(k+1)(k+2)}{2}. \tag{AO19}$$

□

The specific section counts used throughout are

k	0	1	2	3	4	5	6	7
$h^0(\mathcal{O}(k))$	1	3	6	10	15	21	28	36

(AO20)

4. The minimal real-kernel no-go theorem

The first important theorem is negative. DFD's minimal real Kähler/Yukawa sector cannot generate CKM CP violation by itself.

Theorem AO.7 (Real Yukawa kernels imply $J_{\mathrm{CKM}} = 0$)**.** *Let M_u, M_d be real quark mass matrices whose Hermitian squares*

$$H_u = M_u M_u^T, \qquad H_d = M_d M_d^T \tag{AO21}$$

are real symmetric with nondegenerate spectra. Let

$$O_u^T H_u O_u = \mathrm{diag}(m_u^2, m_c^2, m_t^2), \qquad O_d^T H_d O_d = \mathrm{diag}(m_d^2, m_s^2, m_b^2) \tag{AO22}$$

with $O_u, O_d \in O(3)$. Then

$$V_{\mathrm{CKM}} = O_u^T O_d \in O(3) \tag{AO23}$$

is real, and hence every Jarlskog invariant vanishes:

$$J_{\mathrm{CKM}} = 0. \tag{AO24}$$

Proof. A real symmetric matrix is diagonalized by a real orthogonal matrix. Therefore the weak-basis mismatch is the product of two real orthogonal matrices:

$$V = O_u^T O_d \in O(3). \tag{AO25}$$

For any indices i, j, k, l, the product

$$V_{ij} V_{kl} V_{il}^* V_{kj}^* \tag{AO26}$$

is real because $V^* = V$. Therefore its imaginary part vanishes:

$$\mathrm{Im}(V_{ij} V_{kl} V_{il}^* V_{kj}^*) = 0. \tag{AO27}$$

Thus $J_{\mathrm{CKM}} = 0$. □

Corollary AO.8 (Need for a conjugation-odd datum)**.** *Any DFD branch with nonzero CKM CP violation must contain an additional conjugation-odd structure beyond the minimal real Yukawa kernel.*

This corollary is the reason the strengthened DFD–SD branch introduces a det-orthogonal Berry offset rather than pretending the real kernel already contains CP violation.

5. Strong-CP protection

The strong-CP problem is the requirement that

$$\bar{\theta} = \theta_{\mathrm{YM}} + \mathrm{Arg}\det(M_u M_d) \tag{AO28}$$

remain zero or extremely small. In the present branch, weak CP is allowed only if it is det-orthogonal: it may rotate eigenvectors and generate CKM phase, but it may not create a complex determinant phase.

Definition AO.9 (Det-orthogonal mass deformation)**.** Let $M(\xi) = M^{(0)} + \Delta M(\xi)$ be a smooth one-parameter deformation of an invertible mass matrix. The deformation is det-orthogonal at $\xi = 0$ if

$$\left.\frac{\mathrm{d}}{\mathrm{d}\xi}\right|_{\xi=0} \log\det M(\xi) = 0. \tag{AO29}$$

It is exactly det-orthogonal on an interval if $\mathrm{Arg}\det M(\xi)$ is constant on that interval.

Lemma AO.10 (Antisymmetric imaginary perturbations are Hermitian)**.** *Let $S = S^T$ be a real symmetric matrix and let $T = -T^T$ be real antisymmetric. Then*

$$M(\xi) = S + i\xi T \tag{AO30}$$

is Hermitian for real ξ.

Proof. Since $S^\dagger = S^T = S$ and $(i\xi T)^\dagger = -i\xi T^T = i\xi T$, one has $M(\xi)^\dagger = M(\xi)$. □

Theorem AO.11 (Determinant phase protection)**.** *Let $M_f(\xi) = S_f + i\xi T_f$, for $f = u, d$, be the up- and down-sector mass matrices of Postulate Y.10 below, with $S_f = S_f^T$ real symmetric positive definite and $T_f = -T_f^T$ real antisymmetric. Then, for sufficiently small $|\xi|$,*

$$\mathrm{Arg}\det M_f(\xi) = 0, \qquad \mathrm{Arg}\det\big(M_u(\xi) M_d(\xi)\big) = 0. \tag{AO31}$$

Consequently the determinant contribution to $\bar{\theta}$ is exactly zero on that interval.

Proof. Each $M_f(\xi)$ is Hermitian. Its eigenvalues are real. Since S_f is positive definite and eigenvalues depend continuously on ξ, there exists $\epsilon_f > 0$ such that $M_f(\xi)$ remains positive definite for $|\xi| < \epsilon_f$. Hence all eigenvalues are positive on this interval and

$$\det M_f(\xi) > 0. \tag{AO32}$$

Therefore

$$\operatorname{Arg}\det M_f(\xi) = 0. \tag{AO33}$$

Taking the product for $f = u, d$ gives the second claim. □

Theorem AO.12 (Trace form of first-order det-orthogonality)**.** *Let $M(\xi) = M^{(0)} + \xi\Delta M + O(\xi^2)$, with $M^{(0)}$ real symmetric positive definite and $\Delta M = iT$, $T = -T^T$ real antisymmetric. Then*

$$\left.\frac{\mathrm{d}}{\mathrm{d}\xi}\right|_0 \log\det M(\xi) = 0. \tag{AO34}$$

Proof. Jacobi's determinant identity gives

$$\left.\frac{\mathrm{d}}{\mathrm{d}\xi}\right|_0 \log\det M(\xi) = \operatorname{Tr}\left((M^{(0)})^{-1}\Delta M\right). \tag{AO35}$$

Since $(M^{(0)})^{-1}$ is real symmetric and T is real antisymmetric,

$$\operatorname{Tr}\left((M^{(0)})^{-1}T\right) = 0. \tag{AO36}$$

Indeed,

$$\operatorname{Tr}(ST) = \operatorname{Tr}((ST)^T) = \operatorname{Tr}(T^TS^T) = \operatorname{Tr}(-TS) = -\operatorname{Tr}(ST), \tag{AO37}$$

so $\operatorname{Tr}(ST) = 0$. Multiplying by i gives zero as well. □

The anomaly side of strong-CP protection can be stated as follows.

Definition AO.13 (CP mapping torus)**.** Let $\sigma_{\mathbb{C}P}$ be the DFD CP involution on X. The CP mapping torus is

$$T_{\mathbb{C}P} = (X \times [0,1])/(x,0) \sim (\sigma_{\mathbb{C}P}(x),1). \tag{AO38}$$

Since $\dim_{\mathbb{R}} X = 7$,

$$\dim_{\mathbb{R}} T_{\mathbb{C}P} = 8. \tag{AO39}$$

Theorem AO.14 (Even-dimensional spectral pairing implies no CP anomaly)**.** *Assume the CP-twisted Dirac operator $D_{T_{\mathbb{C}P}}$ on the mapping torus admits a chirality operator Γ such that*

$$\Gamma^2 = 1, \qquad \Gamma D_{T_{\mathbb{C}P}}\Gamma = -D_{T_{\mathbb{C}P}}, \tag{AO40}$$

and that the gauge twisting preserves this pairing. Then the nonzero spectrum is symmetric under $\lambda \mapsto -\lambda$, the eta invariant vanishes,

$$\eta(D_{T_{\mathbb{C}P}}) = 0, \tag{AO41}$$

and the Dai–Freed CP anomaly phase is trivial:

$$\mathcal{A}_{\mathbb{C}P} = \exp\left(\frac{i\pi}{2}\eta(D_{T_{\mathbb{C}P}})\right) = 1. \tag{AO42}$$

Proof. If $D\psi = \lambda\psi$ with $\lambda \neq 0$, then

$$D(\Gamma\psi) = -\Gamma D\psi = -\lambda(\Gamma\psi). \tag{AO43}$$

Thus every nonzero eigenvalue is paired with an eigenvalue of opposite sign and the same multiplicity. The eta function

$$\eta(s) = \sum_{\lambda\neq 0} \operatorname{sgn}(\lambda)|\lambda|^{-s} \tag{AO44}$$

therefore vanishes term by term after analytic continuation to $s = 0$. Hence $\eta(D) = 0$, so the Dai–Freed phase is $\exp(0) = 1$. □

Corollary AO.15 (No axion required in this branch)**.** *If the bare Yang–Mills angle is $\theta_{\mathrm{YM}} = 0$ (fixed by the spectral action given that nothing is added to it for the gauge fields; App. L), the det-orthogonal weak CP offset preserves* $\operatorname{Arg}\det(M_uM_d) = 0$*, and the CP anomaly phase is trivial, then*

$$\bar\theta = 0 \tag{AO45}$$

inside the DFD–SD branch at tree level, without introducing an axion. Loop corrections with the Standard-Model chiral Yukawa structure shift $\operatorname{Arg}\det(M_uM_d)$ *only through the degree-thirteen Jarlskog structure (for Hermitian tree-level mass matrices with the Standard-Model chiral couplings the shift vanishes identically through Yukawa degree eleven; the onset is the multi-loop effect established in Refs. [149, 150]); the induced angle is at the Standard-Model level, $\bar\theta \lesssim 10^{-16}$ [149, 150], six orders of magnitude below the neutron-EDM bound.*

6. Det-orthogonal geometric CP and nonzero CKM phase

Postulate AO.16 (Y.10: det-orthogonal geometric CP offset)**.** *The strengthened DFD–SD branch contains one conjugation-odd Berry coordinate ξ. In a generation basis adapted to the real slice $\mathbb{R}P^2 \subset \mathbb{C}P^2$, the up- and down-sector mass matrices (Yukawa kernels) have the form*

$$M_f(\xi) = S_f + i\xi T_f + O(\xi^2), \qquad f = u, d, \tag{AO46}$$

where S_f is real symmetric positive definite, T_f is real antisymmetric, the offset direction is the A_5-Galois-odd oriented eigendirection of the Berry bundle, and the physical offset lies on the branch connected to $\xi = 0$, where $\det M_f > 0$*. Consequently the Hermitian squares $H_f = M_fM_f^\dagger = M_f^2$ have the form $H_f(\xi) = S_f^2 + i\xi\,(S_fT_f + T_fS_f) + O(\xi^2)$ with $S_fT_f + T_fS_f$ real antisymmetric, which is the form used in the theorem below. Existence: for S_f with simple spectrum $s_1 < s_2 < s_3$, the family $M_f(\xi) = e^{i\xi A_f}S_fe^{-i\xi A_f}$ with $(A_f)_{ab} = (T_f)_{ab}/(s_b - s_a)$ for $a \neq b$ (real symmetric) in the eigenbasis of S_f is Hermitian, has ξ-independent eigenvalues and determinant, and equals $S_f + i\xi T_f + O(\xi^2)$.*

Theorem AO.17 (Y.10 generates weak CP generically)**.** *Assume nondegenerate quark spectra and Y.10. If the first nonzero variation of the commutator invariant*

$$\mathcal{C}(\xi) = \det[H_u(\xi), H_d(\xi)] \tag{AO47}$$

at $\xi = 0$ is nonzero, then the CKM Jarlskog invariant is nonzero for sufficiently small nonzero ξ:

$$J_{\mathrm{CKM}}(\xi) = C\xi + O(\xi^2), \qquad C \neq 0. \tag{AO48}$$

Proof. For three generations, Jarlskog's determinant identity gives

$$\det[H_u, H_d] = 2i\, J_{\mathrm{CKM}} \prod_{i<j}(m_{u_i}^2 - m_{u_j}^2) \prod_{k<l}(m_{d_k}^2 - m_{d_l}^2), \tag{AO49}$$

up to the sign convention fixed by the ordering of masses and phases. The mass-difference products are nonzero by nondegeneracy. Therefore $\det[H_u, H_d] \neq 0$ if and only if $J_{\mathrm{CKM}} \neq 0$. If the first nonzero derivative of $\mathcal{C}(\xi)$ at $\xi = 0$ is linear and nonzero, then $\mathcal{C}(\xi) \neq 0$ for sufficiently small nonzero ξ, hence $J_{\mathrm{CKM}}(\xi) \neq 0$. The coefficient C is the corresponding derivative divided by the nonzero mass-difference product. □

Remark AO.18. The theorem is deliberately generic. It does not claim that any antisymmetric offset creates CP violation. It says the Y.10 offset creates CP violation exactly when the oriented up/down misalignment has a nonvanishing commutator volume. This is the correct mathematical condition.

7. Cohomological CKM magnitude skeleton

The following three integers are selected counts (App. FK), stated before the Euler-projection postulate is introduced.

Theorem AO.19 (Cabibbo ladder, given the selected count)**.** *The DFD primitive $1 \leftrightarrow 2$ flavor-connector count is*

$$n_\lambda = h^0(\mathcal{O}(2)) + h^0(\mathcal{O}(3)) + h^0(\mathcal{O}(4)) = 31. \tag{AO50}$$

Thus

$$\boxed{\lambda = 31\alpha.} \tag{AO51}$$

Proof. The minimal off-diagonal flavor connector excludes $k = 0$, the scalar identity channel, and $k = 1$, the generation projector triplet. The primitive nearest-neighbor ladder therefore begins at $k = 2$. The $\mathbb{C}P^2$ flavor window closes at $k = 4$, the real dimension of the $\mathbb{C}P^2$ base. Hence

$$n_\lambda = h^0(2) + h^0(3) + h^0(4) = 6 + 10 + 15 = 31. \tag{AO52}$$

Multiplying by the α-locked amplitude unit gives $\lambda = 31\alpha$. □

Theorem AO.20 (Heavy-sector doorway, given the selected count)**.** *The DFD $2 \leftrightarrow 3$ heavy-sector scaling count is*

$$n_A = N_{\mathrm{gen}} h^0(\mathcal{O}(7)) = 108. \tag{AO53}$$

Thus

$$\boxed{A = 108\alpha.} \tag{AO54}$$

Proof. The heavy-sector doorway samples the full real internal dimension

$$D = \dim_{\mathbb{R}}(\mathbb{C}P^2 \times S^3) = 7. \tag{AO55}$$

The line-bundle count at $k = 7$ is

$$h^0(\mathcal{O}(7)) = \frac{8 \cdot 9}{2} = 36. \tag{AO56}$$

There are three generation projectors, so

$$n_A = 3 \cdot 36 = 108. \tag{AO57}$$

Thus $A = 108\alpha$. □

Theorem AO.21 (CP-odd height count, given the selected count)**.** *The CP-odd unitarity-triangle height count is*

$$n_\eta = D^2 = 49. \tag{AO58}$$

Thus

$$\boxed{\bar{\eta} = 49\alpha.} \tag{AO59}$$

Proof. The CP-odd coordinate measures an oriented area displacement off the totally real $\mathbb{R}P^2$ slice. In the DFD internal product space X, the primitive dimension controlling a full oriented displacement is

$$D = \dim_{\mathbb{R}} X = 7. \tag{AO60}$$

An area coordinate is bilinear in independent internal directions, so the maximal dimension-square count is

$$n_\eta = D^2 = 7^2 = 49. \tag{AO61}$$

Multiplication by the α-locked Berry amplitude gives $\bar{\eta} = 49\alpha$. □

Remark AO.22 (Why this is not enough). The preceding results fix λ, A, and $\bar{\eta}$. They do not select the CP-even real-axis apex coordinate $\bar{\rho}$.

8. Euler-projected selection of the CP-even apex

Postulate AO.23 (E.1: Euler projection of the CP-even apex)**.** *In the strengthened DFD–SD branch, the physical value of the CP-even apex coordinate $\bar{\rho}$ is not a free parameter and is not given by the raw even-cohomology sum. It is the unique real-axis projection of the ideal complex apex that minimizes the reduced geometric action encoding the competition between:*

1. *the ideal A_5-covering-space apex scale set by the full internal dimension $D = 7$, and*

2. *the topological localization cost of confining the CP-even coordinate to the physical $\mathbb{C}P^2$ microsector, measured by $\chi(\mathbb{C}P^2) = 3$.*

Equivalently, with

$$r := \bar{\rho}/\alpha, \qquad D := \dim_{\mathbb{R}}(\mathbb{C}P^2 \times S^3) = 7, \qquad \chi := \chi(\mathbb{C}P^2) = 3, \tag{AO62}$$

the physical value of r is the unique minimizer of the strictly convex reduced geometric action

$$\boxed{\mathcal{I}_\rho(r) = \frac{1}{2}\left(r - \frac{D^2}{2}\right)^2 + \chi(\mathbb{C}P^2) r.} \tag{AO63}$$

Status AO.24 (Status of E.1). Postulate E.1 is a new structural assumption of the strengthened DFD–SD branch. It is not derived from the pre-strengthened DFD axioms and is not yet derived from explicit Berry/Yukawa overlap integrals. Indeed the per-connector α unit *cannot* follow from $\mathbb{C}P^2 \times S^3$ geometry alone: the executed overlap integrals are coupling-blind rationals (Gram $\delta_{ab}/3$, connector moment $1/12$, Verlinde hop $2\cos(\pi/62)$), and App. O's *derived* per-mode α is multiplicative (it would give α^{31}, not 31α) — so E.1 is an independent postulate, not an App. O extension. Its consequences, including $\bar{\rho} = 43\alpha/2$, are theorem-grade inside the strengthened branch once E.1 is accepted. Two further derivation routes are closed: the compact one-boson-exchange sum on $\mathbb{C}P^2$ yields $\alpha \times (\text{rational}/\pi)$ with a cutoff-divergent $O(1)$ (the 4π split $g^2 = \alpha$ vs. $g^2 = 4\pi\alpha$ being conventional, cf. the App. O coupling-normalization remark), and holonomy on simply-connected $\mathbb{C}P^2$ is topologically trivial (a unit-modulus phase, never an α-sized amplitude). No structural no-go, however, blocks E.1's eventual derivation: the live path is a selection rule forcing inter-generation connectors to couple through the internal gauge field (exchange, which scales as α^1 per connector and is additive across connectors) rather than by coupling-blind direct overlap.

Remark AO.25 (Meaning of the two terms). The quadratic term anchors r to the ideal A_5 covering-space apex. The linear term is the Euler localization cost of confining the CP-even coordinate to the physical $\mathbb{C}P^2$ microsector. Since $\chi(\mathbb{C}P^2) = 3$, it represents one unit of α-normalized real-axis localization cost per topological generation anchor.

Lemma AO.26 (Euler characteristic of $\mathbb{C}P^2$)**.**

$$\chi(\mathbb{C}P^2) = 3. \tag{AO64}$$

Proof. The integral cohomology of $\mathbb{C}P^2$ is

$$\begin{aligned} H^0(\mathbb{C}P^2;\mathbb{Z}) &= \mathbb{Z}, \\ H^2(\mathbb{C}P^2;\mathbb{Z}) &= \mathbb{Z}, \\ H^4(\mathbb{C}P^2;\mathbb{Z}) &= \mathbb{Z}, \end{aligned} \tag{AO65}$$

and all odd cohomology groups vanish. Therefore

$$\chi(\mathbb{C}P^2) = b_0 - b_1 + b_2 - b_3 + b_4 = 1 + 1 + 1 = 3. \tag{AO66}$$

Equivalently, the standard maximal torus action on $\mathbb{C}P^2$ has three isolated fixed points,

$$p_1 = [1:0:0], \quad p_2 = [0:1:0], \quad p_3 = [0:0:1], \tag{AO67}$$

whose Poincare–Hopf indices sum to 3. □

Theorem AO.27 (Euler-projected CKM apex)**.** *Assuming Postulate AO.23, the DFD–SD CP-even apex coordinate is*

$$\boxed{\bar{\rho} = \left(\frac{D^2}{2} - \chi(\mathbb{C}P^2)\right)\alpha.} \tag{AO68}$$

For $D = 7$, this gives

$$\boxed{\bar{\rho} = \frac{43}{2}\alpha = 21.5\alpha.} \tag{AO69}$$

Proof. The reduced action (AO63) is strictly convex because

$$\frac{\mathrm{d}^2\mathcal{I}_\rho}{\mathrm{d}r^2} = 1 > 0. \tag{AO70}$$

Its unique stationary point is therefore its unique global minimizer. Compute

$$\frac{\mathrm{d}\mathcal{I}_\rho}{\mathrm{d}r} = r - \frac{D^2}{2} + \chi(\mathbb{C}P^2). \tag{AO71}$$

Set the derivative to zero:

$$r_* = \frac{D^2}{2} - \chi(\mathbb{C}P^2). \tag{AO72}$$

Since $r = \bar{\rho}/\alpha$,

$$\bar{\rho} = r_*\alpha = \left(\frac{D^2}{2} - \chi(\mathbb{C}P^2)\right)\alpha. \tag{AO73}$$

For $D = 7$ and $\chi(\mathbb{C}P^2) = 3$,

$$r_* = \frac{49}{2} - 3 = \frac{49 - 6}{2} = \frac{43}{2}. \tag{AO74}$$

Thus

$$\bar{\rho} = \frac{43}{2}\alpha. \tag{AO75}$$

□

a. Fubini–Study overlap motivation for Postulate E.1

Postulate E.1 is structurally natural from the overlap geometry, but this appendix does not claim that this motivation eliminates E.1 as an independent strengthened-branch postulate. The point of the following argument is to show why the linear Euler term has the right geometric form.

The three real generation anchors are naturally associated with the three torus fixed points of $\mathbb{C}P^2$:

$$p_1 = [1:0:0], \qquad p_2 = [0:1:0], \qquad p_3 = [0:0:1]. \tag{AO76}$$

By Poincare–Hopf localization,

$$\sum_i \mathrm{index}(p_i) = \chi(\mathbb{C}P^2) = 3. \tag{AO77}$$

Let

$$G^{(0)}_{ij}(r) = \langle w_i(r) \mid w_j(r) \rangle \tag{AO78}$$

denote the real unperturbed Gram matrix for generation wavefunctions localized near these fixed points. If the leading diagonal localization factor in α-normalized real-axis coordinate r is

$$\langle w_i(r) \mid w_i(r) \rangle \sim e^{-r}, \tag{AO79}$$

and if off-diagonal overlaps are negligible or symmetry-controlled at leading order, then

$$\det G^{(0)}(r) \approx \prod_{i=1}^{3} \langle w_i(r) \mid w_i(r) \rangle \sim e^{-3r}. \tag{AO80}$$

Taking minus the logarithm gives

$$-\log\det G^{(0)}(r) \sim 3r = \chi(\mathbb{C}P^2) r. \tag{AO81}$$

This is precisely the linear Euler-localization term in (AO63).

Remark AO.28 (Why this remains motivation rather than proof). A full derivation of E.1 from microscopic overlaps would have to prove the exact normalization

$$\langle w_i(r) \mid w_i(r) \rangle = e^{-r} \tag{AO82}$$

in the same $r = \bar{\rho}/\alpha$ coordinate, show that the Gram determinant factorizes exactly or with a controlled correction, and derive the quadratic covering-space term from the A_5 Berry/Yukawa action. Until those steps are supplied, the Fubini–Study argument motivates E.1 but does not replace it.

Corollary AO.29 (Unitarity-triangle angle)**.** *The strengthened DFD–SD branch predicts*

$$\boxed{\gamma = \arctan\left(\frac{\bar{\eta}}{\bar{\rho}}\right) = \arctan\left(\frac{49}{43/2}\right) = \arctan\left(\frac{98}{43}\right).} \tag{AO83}$$

Numerically,

$$\boxed{\gamma = 66.3093^\circ.} \tag{AO84}$$

Proof. Using $\bar{\eta} = 49\alpha$ and $\bar{\rho} = (43/2)\alpha$, the factor α cancels:

$$\frac{\bar{\eta}}{\bar{\rho}} = \frac{49\alpha}{(43/2)\alpha} = \frac{98}{43}. \tag{AO85}$$

Taking the arctangent gives the result. □

9. Final Wolfenstein branch and numerical reconstruction

Theorem AO.30 (Strengthened DFD–SD CKM branch)**.** *In the DFD–SD branch with Euler projection,*

$$\boxed{(\lambda, A, \bar{\rho}, \bar{\eta}) = \left(31, 108, \frac{43}{2}, 49\right)\alpha.} \tag{AO86}$$

Proof. Combine the Cabibbo ladder theorem, the heavy-sector doorway theorem, the CP-odd height theorem, and the Euler-pulled apex theorem. □

With $\alpha^{-1} = 137.03599985$, this gives

$$\alpha = 0.007297352528493264, \tag{AO87}$$

$$\lambda = 31\alpha = 0.2262179283832912, \tag{AO88}$$

$$A = 108\alpha = 0.7881140730772725, \tag{AO89}$$

$$\bar{\rho} = \frac{43}{2}\alpha = 0.1568930793626052, \tag{AO90}$$

$$\bar{\eta} = 49\alpha = 0.3575702738961699. \tag{AO91}$$

The unitarity-triangle angles are

$$\gamma = \arctan\left(\frac{\bar{\eta}}{\bar{\rho}}\right) = 66.3093105972^\circ, \tag{AO92}$$

$$\beta = \arctan\left(\frac{\bar{\eta}}{1-\bar{\rho}}\right) = 22.9822978300^\circ, \tag{AO93}$$

$$\alpha_{\mathrm{UT}} = 180^\circ - \beta - \gamma = 90.7083915728^\circ. \tag{AO94}$$

For an exact-standard reconstruction, define

$$s_{12} = \lambda, \tag{AO95}$$

$$s_{23} = A\lambda^2, \tag{AO96}$$

$$s_{13}e^{i\delta} = A\lambda^3(\rho + i\eta), \tag{AO97}$$

$$c_{ij} = \sqrt{1 - s_{ij}^2}, \tag{AO98}$$

where the unbarred apex (ρ, η) follows from the theorem's barred (PDG-comparable) apex by the exact standard-parameterization inversion

$$\rho + i\eta = \frac{\sqrt{1 - A^2\lambda^4}\,(\bar{\rho} + i\bar{\eta})}{\sqrt{1-\lambda^2}\left[1 - A^2\lambda^4(\bar{\rho} + i\bar{\eta})\right]}, \tag{AO99}$$

a conversion of modulus $\left|(\rho + i\eta)/(\bar{\rho} + i\bar{\eta})\right| = 1.026040$. Holding the theorem's barred values exact, this gives

$$s_{23} = 0.0403313839226825, \tag{AO100}$$

$$s_{13} = 0.00365535209821, \tag{AO101}$$

$$\delta = 66.3426441103^\circ. \tag{AO102}$$

The standard CKM matrix is

$$V = \begin{pmatrix} c_{12}c_{13} & s_{12}c_{13} & s_{13}e^{-i\delta} \\ -s_{12}c_{23} - c_{12}s_{23}s_{13}e^{i\delta} & c_{12}c_{23} - s_{12}s_{23}s_{13}e^{i\delta} & s_{23}c_{13} \\ s_{12}s_{23} - c_{12}c_{23}s_{13}e^{i\delta} & -c_{12}s_{23} - s_{12}c_{23}s_{13}e^{i\delta} & c_{23}c_{13} \end{pmatrix}. \tag{AO103}$$

The predicted magnitudes are

$$\boxed{|V_{\rm CKM}^{\rm DFD}| = \begin{pmatrix} 0.9740702 & 0.2262164 & 0.0036554 \\ 0.2260915 & 0.9732708 & 0.0403311 \\ 0.0083576 & 0.0396246 & 0.9991797 \end{pmatrix}.} \tag{AO104}$$

The apex realized by this matrix, $-(V_{ud}V_{ub}^*)/(V_{cd}V_{cb}^*)$, reproduces the theorem values $(\bar\rho,\bar\eta) = (43/2,\, 49)\,\alpha$ to $|\text{residual}| = 1.1\times10^{-31}$, and its tree-level angle is $\gamma = 66.3093106°$, in exact agreement with the boxed falsifier. At leading Wolfenstein order the main entries are

$$|V_{us}| = 0.2262179284, \tag{AO105}$$

$$|V_{cb}| = A\lambda^2 = 0.0403313839, \tag{AO106}$$

$$|V_{ub}| = A\lambda^3\sqrt{\bar\rho^2+\bar\eta^2} = 0.0035625840, \tag{AO107}$$

$$|V_{td}| = A\lambda^3\sqrt{(1-\bar\rho)^2+\bar\eta^2} = 0.0083554489. \tag{AO108}$$

These leading-order barred expressions omit the $O(\lambda^2/2)$ barred→unbarred conversion carried by the exact reconstruction above; the exact-matrix values are the ones quoted in the boxed matrix.

Theorem AO.31 (Jarlskog invariant)**.** *The strengthened DFD–SD CKM branch predicts*

$$\boxed{J_{\rm CKM} = 2.9731\times10^{-5}} \tag{AO109}$$

using the exact standard-parameterization expression.

Proof. The exact expression is

$$J_{\rm CKM} = c_{12}c_{23}c_{13}^2 s_{12}s_{23}s_{13}\sin\delta. \tag{AO110}$$

Substituting the values above gives

$$J_{\rm CKM} = 2.9731063041\times10^{-5}. \tag{AO111}$$

At leading Wolfenstein order,

$$J_{\rm CKM} \approx A^2\lambda^6\bar\eta. \tag{AO112}$$

Using the DFD integers,

$$\begin{aligned} A^2\lambda^6\bar\eta &= (108\alpha)^2(31\alpha)^6(49\alpha) \\ &= 108^2\cdot31^6\cdot49\cdot\alpha^9 = 2.9764712924\times10^{-5}. \end{aligned} \tag{AO113}$$

The difference between the exact and leading values is the expected higher-order trigonometric correction. □

10. Comparison of the apex branches

The Euler-projected branch is not the only mathematically possible branch before the postulate is added. The two relevant branches are:

$$\text{Path A:}\quad \bar\rho_A = \frac{43}{2}\alpha = 0.1568930794, \tag{AO114}$$

$$\text{Path B:}\quad \bar\rho_B = 22\alpha = 0.1605417556. \tag{AO115}$$

They give

$$\gamma_A = \arctan(98/43) = 66.3093°, \tag{AO116}$$

$$\gamma_B = \arctan(49/22) = 65.8209°. \tag{AO117}$$

Current direct/global determinations of γ are not yet sharp enough to decisively separate the two. The strengthened DFD–SD branch chooses Path A not because current data slightly prefer it, but because the Euler-projection action selects it.

Quantity	Path A: $43\alpha/2$	Path B: 22α
$\bar\rho$	0.1568931	0.1605418
γ	66.3093°	65.8209°
$\lvert V_{ub}\rvert$	0.0035626[a]	0.0035761[a]
$\lvert V_{td}\rvert$	0.0083554[a]	0.0083248[a]
$J_{\rm lead}$	2.9765×10^{-5}	2.9765×10^{-5}

[a] $|V_{ub}|$ and $|V_{td}|$ are quoted at leading (barred-Wolfenstein) order for both paths; the exact Path-A values are in the boxed matrix above.

The small numerical separation is why the anti-theorem matters. The theory needed a structural selection rule, not a statistical preference.

11. Falsifiability and experimental targets

The branch makes sharp predictions:

$$\gamma = 66.3093°, \qquad \beta = 22.9823°, \qquad J_{\rm CKM} = 2.9731\times10^{-5}. \tag{AO118}$$

The most direct discriminator is the angle γ. The DFD–SD value is essentially coincident with the current CKMfitter indirect global-fit central value, $\gamma_{\rm CKMfitter} \approx 66.3°$ (a difference of $\sim 0.01°$) — the best consistency check against the full CKM unitarity structure — and it lies well inside present *direct* tree-level determinations, which are the cleaner future falsifier because they are less contaminated by loop/new-physics assumptions: the LHCb combination $\gamma = (63.8^{+3.5}_{-3.7})°$ (arXiv:2404.18789) places DFD–SD about 2.5° away, comfortably within 1σ, while the charm/beauty global analysis $\gamma = (65.7\pm2.5)°$ (arXiv:2409.06449) is only 0.61° (0.24σ) away. The decisive test is whether future LHCb and Belle II direct determinations converge near 66.3° as uncertainties approach the 1° scale.

The strongest falsifier is therefore:

$$\boxed{\gamma_{\text{DFD–}SD} = 66.3093°.} \tag{AO119}$$

If future tree-level determinations converge far from this value with sub-degree uncertainty, the Euler-projected DFD–SD CKM branch is falsified. The magnitudes are tested as well: $\lambda = 31\alpha$ sits 1.8σ above the global fit, and the kaon-decay determinations of $|V_{us}|$ lie 3 to 6 standard deviations below 31α; $|V_{cb}| = 0.0403$ agrees with the exclusive determination and lies 3.7σ below the inclusive one; against the global fit the four values give $\chi^2 = 10.1$ for four parameters (computed).

12. Scope and order of the claims

The claims of this appendix obey the following discipline.

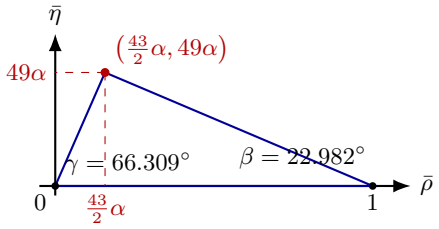


FIG. 16. Euler-projected DFD–SD unitarity triangle. The apex is pulled from the ideal covering-space value $D^2/2$ by the Euler cost $\chi(\mathbb{C}P^2) = 3$, giving $\bar{\rho} = (49/2 - 3)\alpha = (43/2)\alpha$.

1. Pre-strengthened DFD does not force the apex branch; the anti-theorem stating this is kept explicit.
2. No unconditional claim makes the raw 22α apex theorem-grade.
3. Postulate E.1 is a necessary strengthening of the DFD–SD branch for CKM closure; it is not claimed to follow from the pre-strengthened axioms.
4. The consequences of that postulate are theorem-grade inside the strengthened branch.
5. The CKM integer list is
$$(\lambda, A, \bar{\rho}, \bar{\eta}) = \left(31, 108, \frac{43}{2}, 49\right)\alpha. \qquad \text{(AO120)}$$
6. The minimal real-kernel no-go theorem is stated before Y.10 is introduced.
7. The determinant-phase protection theorem is stated before the weak CKM phase is calculated.
8. The main falsifier is $\gamma = 66.3093°$.

13. Final theorem ledger

14. Conclusion

The CP sector of DFD separates what the pre-strengthened axioms prove from what the strengthened branch adds. The real kernel cannot generate CKM CP violation. That is a theorem. The det-orthogonal Berry offset supplies a minimal weak-CP mechanism while preserving strong-CP protection. The cohomological magnitude skeleton fixes $\lambda = 31\alpha$, $A = 108\alpha$, and $\bar{\eta} = 49\alpha$. The remaining apex ambiguity is resolved only after adding Postulate E.1, the Euler-projection rule of the strengthened DFD–SD branch, whose reduced action has a unique minimizer at

$$\bar{\rho} = \left(\frac{7^2}{2} - \chi(\mathbb{C}P^2)\right)\alpha = \frac{43}{2}\alpha. \qquad \text{(AO121)}$$

This yields the final strengthened-branch CKM solution

$$\boxed{(\lambda, A, \bar{\rho}, \bar{\eta}) = \left(31, 108, \frac{43}{2}, 49\right)\alpha,} \qquad \text{(AO122)}$$

with

$$\boxed{\gamma = 66.3093°, \qquad J_{\mathrm{CKM}} = 2.9731 \times 10^{-5}.} \qquad \text{(AO123)}$$

The result is not an unconditional proof from the older DFD axioms. It is a theorem-grade closure inside the strengthened DFD–SD branch with Euler projection.

TABLE CXII. Final CP-sector theorem ledger for the strengthened DFD–SD branch.

Claim	Result	Status
Minimal real kernel	Real Yukawa kernels imply $J = 0$.	Theorem
Strong-CP determinant protection	Det-orthogonal offsets of a positive-definite S_f preserve $\mathrm{Arg}\det(M_u M_d) = 0$ on the branch connected to $\xi = 0$.	Theorem
CP anomaly	Even-dimensional chirality pairing gives $\eta = 0$, Dai–Freed phase $= 1$.	Conditional theorem
Y.10 CP offset	One conjugation-odd Berry coordinate supplies weak CP while preserving determinant phase.	Postulate + theorem consequences
Cabibbo ladder	$\lambda = [6 + 10 + 15]\alpha = 31\alpha$.	Selected count
Heavy-sector doorway	$A = 3h^0(7)\alpha = 108\alpha$.	Selected count
CP-odd height	$\bar{\eta} = 7^2\alpha = 49\alpha$.	Selected count
Apex selection	$\bar{\rho} = (49/2 - 3)\alpha = 43\alpha/2$.	Postulate E.1 + theorem consequence
CKM prediction	$\gamma = 66.3093^\circ$, $J = 2.9731 \times 10^{-5}$.	Falsifiable prediction

Appendix AP: Corpus-Closure Theorems: the α^{57} Hierarchy, the MOND Scale, and Rigor Discipline

This appendix is the consolidated corpus-closure theorem package for the gravitational/MOND sector. It collects the α^{57} cosmological clock hierarchy, the action-derived MOND prefactor $a_0 = 2\sqrt{\alpha}\, cH_0$, and the H_0-free acceleration invariant $a_0^2 G\hbar/c^7 = 4C\alpha^{58}$ (C the clock coefficient, 1 on bound-matter clocks, Postulate ZS.11). The minimal real-kernel $J = 0$ statement below is consistent with, and cross-references, the CP-sector treatment of Appendix AO.

This appendix presents the core closure chain of Density Field Dynamics (DFD). The primary closed result is the acceleration invariant

$$\frac{a_0^2 G\hbar}{c^7} = 4C\,\alpha^{58}, \qquad a_0 = 2\sqrt{C}\,\alpha^{29}\sqrt{\frac{c^7}{G\hbar}},$$

which predicts the galactic MOND/RAR acceleration scale with a derived exponent; galaxies read bound-matter clocks, where $C = 1$ (Postulate ZS.11), so it carries no measured coefficient (the clock normalization, Remark AP.6). The appendix gives the proof chain: a Spin^c/index mode count $60 - 3 = 57$, a primed Gaussian determinant producing α^{57}, the finite spectral-action clock dictionary $G\hbar H_0^2/c^5 = C\alpha^{57}$, a gauge-emergence proof of $k_a = 3/(8\alpha)$, an S^3 stationarity theorem selecting $\Xi_* = 3/2$, and the action-level derivation $a_0 = 2\sqrt{\alpha}\, cH_0$.

1. Purpose and standard of proof

The central target is the acceleration invariant

$$\boxed{\Pi_2 \equiv \frac{a_0^2 G\hbar}{c^7} = 4C\,\alpha^{58}}, \tag{AP1}$$

with C the clock coefficient, 1 on bound-matter clocks (Postulate ZS.11) and measured on the early clock (Remark AP.6). This is equivalent to

$$\boxed{a_0 = 2\sqrt{C}\,\alpha^{29}\sqrt{\frac{c^7}{G\hbar}}}. \tag{AP2}$$

Eq. (AP1) could be read as numerology: the exponent 58 might appear to have been inferred from the observed acceleration scale. The proof below derives the exponent as

$$58 = (60 - 3) + 1. \tag{AP3}$$

The $60 - 3 = 57$ comes from a finite microsector determinant; the extra $+1$ comes from the squared action-derived prefactor $2\sqrt{\alpha}$ in the scalar acceleration crossover.

Definition AP.1 (Strict theorem-grade status)**.** A result is called *strict theorem grade* in this paper only if:

1. every coefficient has a non-adjustable origin;
2. every dimensionful identification is stated as either a theorem or a declared dictionary axiom;
3. no observational value is used to choose an exponent or integer;
4. branch-dependent calculations are not mixed;
5. contradictory results are either resolved, retired, or demoted to archived consistency-check notes.

Remark AP.2 (Hard scoping rule). A corpus can meet this standard without every speculative sector being a theorem. What makes it meet the standard is that theorem-grade claims are proved and non-theorem claims are not mislabeled as theorems.

2. Notation and DFD primitives

We use

$$c = \text{reference two-way light speed}, \tag{AP4}$$
$$G = \text{Newton constant}, \tag{AP5}$$
$$\hbar = \text{reduced Planck constant}, \tag{AP6}$$
$$\alpha = \text{fine-structure constant}, \tag{AP7}$$
$$H_0 = \text{cosmological clock scale}, \tag{AP8}$$
$$a_0 = \text{galactic acceleration crossover}. \tag{AP9}$$

The Planck time, length, and acceleration are

$$t_P = \sqrt{\frac{G\hbar}{c^5}}, \qquad \ell_P = \sqrt{\frac{G\hbar}{c^3}}, \qquad a_P = \sqrt{\frac{c^7}{G\hbar}} = \frac{c}{t_P} = \frac{c^2}{\ell_P}. \tag{AP10}$$

The DFD scalar density field is denoted by ψ. In the weak/static optical sector,

$$n(x) = e^{\psi(x)}, \tag{AP11}$$

and the physical acceleration field is normalized as

$$\mathbf{g} = \frac{c^2}{2}\nabla\psi. \tag{AP12}$$

This factor $1/2$ is not optional in the closure theorem: it is the conversion between scalar-gradient scale and physical acceleration.

3. Corpus-level rigor axioms

Axiom AP.3 (Branch discipline)**.** *A calculation performed in one DFD branch cannot be quoted as a theorem in another branch unless an embedding theorem identifies the two branches. In particular, the isotropic exponential exterior (the parent strain's σ set to zero), the PPN-closed physical metric, a nonminimal horizon-closure model, and a quantum-corrected vacuum action are distinct until proved equivalent.*

Axiom AP.4 (Status discipline)**.** *This appendix assigns every claim exactly one of the following statuses:*

Status	*Meaning*
Theorem	*Derived from declared axioms/dictionary with no fitted continuous parameter.*
Proposition	*Mathematically derived but dependent on a declared dictionary map.*
Model prediction	*Computed inside one explicitly named model branch.*
Phenomenological closure	*Data-matching or effective description with stated correction budget.*
Conjecture	*Structurally motivated but not proved.*
Program item	*Calculation, simulation, or formal proof not yet completed.*
Retired	*Contradictory, false, duplicated, or branch-incompatible.*

No result may be theorem-grade if one of its coefficients is described as plausible, calibrated, motivated, or empirically selected.

Axiom AP.5 (Finite spectral-action clock dictionary)**.** *The finite DFD spectral action identifies the primed internal Gaussian determinant ratio with the unique dimensionless cosmological clock hierarchy, up to an $O(1)$ normalization coefficient C:*

$$(H_0 t_P)^2 = \frac{G\hbar H_0^2}{c^5} = C\,\frac{Z'_\alpha}{Z'_1}, \qquad C = O(1). \tag{AP13}$$

This dictionary is the bridge between finite internal topology and the infrared de Sitter clock scale: it fixes the exponent *of the hierarchy. The coefficient C is not fixed by the dictionary. It is today's value of the early clock, and the time-independent measured input is the vacuum coefficient $R = \Omega_\Lambda C$ (Remark AP.6). If this axiom is not adopted, the α^{57} exponent statement must be downgraded from theorem to proposition.*

Remark AP.6 (What is derived vs. what is measured). The derivation order is clean and non-circular: the exponent $57 = 60 - 3$ is pure Hirzebruch–Riemann–Roch arithmetic with no cosmological input, and H_0 first appears downstream as a-posteriori validation. What the exponent theorem does *not* supply is the $O(1)$ coefficient C in $(H_0 t_P)^2 = C\,\alpha^{57}$. An eight-route, enumeration-complete no-go proves C is *not derivable from the printed corpus*: every printed equation connecting the vacuum deposit to a rate is exponent-only, convention-importing, or C-covariant (the determinant ratio transmits a coordinate but cannot fix one); the homogeneous ψ-sector Hamiltonian vanishes identically, and the background obeys the Friedmann law of the Einstein–Hilbert term (§XIX E), which converts the vacuum density into the clock rate but fixes neither; and the printed spectral route cannot land the measured value for any regulator in its forced class. Nor can C share the normalization of G. In the spectral action α is fixed by its own trace (§X C), G by $f_2\Lambda^2$ (Proposition WS.5) and every vacuum term by $f_4\Lambda^4$, $f_2\Lambda^2\,\mathrm{Tr}D_F^2$ and $f_0\,\mathrm{Tr}D_F^4$, while the determinant ratio α^{57} carries no moment. With G held fixed, admissible plateau cutoffs move f_4/f_2^2 over $[1/2, \infty)$, so no relation fixed by G fixes C. If the vacuum is the α^{57}-suppressed a_0 term, a reading that is a conjecture, $R = \Omega_\Lambda C = 6\pi(f_4/f_2^2)/N$; for $N = 60$ the measured R requires $f_4/f_2^2 = 1.923 \pm 0.009$ with the internal masses neglected (1.81 with the printed internal spectrum), a heavy-tailed cutoff that no printed condition selects, and every compact Riesz cutoff misses by 109σ or more and the sharp cutoff by 168σ (computed). The requirement depends on N: a trace over the 4096 states of the α carrier would need 131. C therefore plays the role of the cosmological constant of general relativity: the theory carries G, which sets the unit, and one measured vacuum coefficient. The measured input is therefore one continuous number, measured once, as ΛCDM measures H_0. Because $C = (Ht_P)^2/\alpha^{57}$ changes with the epoch, $C(z) = R + 1.924\,[\omega_m(1+z)^3 + \omega_r(1+z)^4]$,

the time-independent input is the vacuum coefficient $R = \Omega_\Lambda C = 0.6042 \pm 0.0027$, and C is today's value of the early clock. The measurements are concordant: $C = 0.87784 \pm 0.00266$ (BAO+θ_*) and $C = 0.8772$ (Planck plik-lite), i.e. $H_0 = 67.52 \pm 0.09$ km/s/Mpc across five concordant CMB-anchored channels. The value $C = 1$, read as today's early-clock value, gives $H_0 = 72.09$ and is excluded at $\approx 46\sigma$ by the CMB-anchored channels, while bound-matter clocks read $C = 1$ (Postulate ZS.11), and every closed formula proposed for C is a statement about the present epoch. A further route, fixing the whole shape of the spectral cutoff from a printed principle, fails as well: no printed principle fixes that shape, and R depends on the internal (Kaluza–Klein) spectrum. Status split: exponent 57 — theorem; coefficient C — measured input. Rival exponent conventions remain excluded numerically, not by fiat: one unit of the exponent moves H_0 by a factor $\alpha^{1/2} \simeq 0.085$, so no other integer is reachable and the measured C is an $O(1)$ number, not a disguised exponent shift. In coefficient space the SH0ES-side booking $C = 1.027 \pm 0.029$ (five-presentation Λ theorem of the Extended Derivations; SH0ES's 2022 H_0 re-expressed) versus the acoustic $C = 0.87784 \pm 0.00266$ is a $\sim 5\sigma$(stat) split; under the two-clock postulate the booking is a bound-matter reading, 0.9σ from $C = 1$, and the absolute a_0 scale (Euclid/DESI lensing RAR) tests the postulate once baryonic masses are known to about 2% (App. ZS). Bookkeeping note: Lemma O.6 states the ratio as a squared *scale* ratio while the Wheeler–DeWitt ground-state theorem of the Extended Derivations states an energy *density*; the two differ by the Friedmann factor $8\pi/3$; the measured coefficient is $R = \Omega_\Lambda C$ in density form and C in clock form.

Axiom AP.7 (Scalar acceleration action dictionary)**.** *The physical acceleration scale is extracted from the scalar action through Eq.* (AP12)*; the crossover a_0 is the point where the dimensionless acceleration invariant Ξ reaches the stationary value selected by the S^3 microsector. It is not inserted as a phenomenological fit parameter.*

4. The α^{57} hierarchy from topology and determinant scaling

a. *Index count: $k_{\max} = 60$*

Lemma AP.8 (Hirzebruch–Riemann–Roch on $\mathbb{C}P^2$)**.** *Let $H \in H^2(\mathbb{C}P^2, \mathbb{Z})$ be the hyperplane class with $\int_{\mathbb{C}P^2} H^2 = 1$. For the holomorphic line bundle $\mathcal{O}(n)$,*

$$\chi(\mathbb{C}P^2, \mathcal{O}(n)) = \frac{(n+1)(n+2)}{2}. \tag{AP14}$$

Proof. Hirzebruch–Riemann–Roch gives

$$\chi(\mathbb{C}P^2, \mathcal{O}(n)) = \int_{\mathbb{C}P^2} \mathrm{ch}(\mathcal{O}(n))\,\mathrm{Td}(T\mathbb{C}P^2). \tag{AP15}$$

For $\mathbb{C}P^2$,

$$\mathrm{ch}(\mathcal{O}(n)) = e^{nH} = 1 + nH + \frac{n^2}{2}H^2, \tag{AP16}$$

while

$$\mathrm{Td}(T\mathbb{C}P^2) = 1 + \frac{3}{2}H + H^2. \tag{AP17}$$

The integral extracts the coefficient of H^2:

$$\frac{n^2}{2} + \frac{3n}{2} + 1 = \frac{n^2+3n+2}{2} = \frac{(n+1)(n+2)}{2}. \tag{AP18}$$

□

Theorem AP.9 (Finite microsector mode count)**.** *For the DFD internal finite sector*

$$E = \mathcal{O}(9) \oplus \mathcal{O}^{\oplus 5} \tag{AP19}$$

over $\mathbb{C}P^2$, the total mode count is

$$k_{\max} = 60. \tag{AP20}$$

Proof. Using Lemma AP.8,

$$\chi(\mathbb{C}P^2, \mathcal{O}(9)) = \frac{(10)(11)}{2} = 55. \tag{AP21}$$

Also $\chi(\mathbb{C}P^2, \mathcal{O}) = 1$. Therefore

$$\chi(\mathbb{C}P^2, E) = 55 + 5\chi(\mathbb{C}P^2, \mathcal{O}) = 55 + 5 = 60. \tag{AP22}$$

□

Axiom AP.10 (Generation kernel)**.** *The protected generation kernel of the finite DFD microsector has dimension*

$$N_{\mathrm{gen}} = 3. \tag{AP23}$$

These three zero modes are not included in the primed determinant.

Corollary AP.11 (Nonzero determinant count)**.** *The primed determinant contains exactly*

$$N_{\mathrm{nz}} = k_{\max} - N_{\mathrm{gen}} = 60 - 3 = 57 \tag{AP24}$$

nonzero complex modes.

b. *Primed determinant scaling*

Lemma AP.12 (One complex Gaussian mode)**.** *For $\lambda > 0$,*

$$\int_{\mathbb{C}} d^2z\, \exp\left[-\frac{\lambda}{\alpha}|z|^2\right] = \frac{\pi\alpha}{\lambda}. \tag{AP25}$$

Consequently, relative to the $\alpha = 1$ normalization, one nonzero complex mode contributes a factor α.

Proof. Writing $z = x + iy$ gives

$$\int_{\mathbb{C}} d^2z\, e^{-(\lambda/\alpha)|z|^2} = \left(\int_{-\infty}^{\infty} e^{-(\lambda/\alpha)x^2}\, dx\right)^2 = \frac{\pi\alpha}{\lambda}. \tag{AP26}$$

At $\alpha = 1$ the same integral is π/λ, so the ratio is α. □

Theorem AP.13 (Primed determinant hierarchy)**.** *Let the nonzero internal kinetic operator have eigenvalues $\lambda_i > 0$ for $i = 1, \dots, 57$, and let the gauge-normalized quadratic action be*

$$S_{\text{micro}} = \sum_{i=1}^{57} \frac{\lambda_i}{\alpha} |z_i|^2. \tag{AP27}$$

Then

$$\frac{Z'_\alpha}{Z'_1} = \alpha^{57}. \tag{AP28}$$

Equivalently,

$$\frac{\det' \mathcal{K}}{\det'(\mathcal{K}/\alpha)} = \alpha^{57}. \tag{AP29}$$

Proof. By Lemma AP.12, each nonzero complex mode contributes α to the normalized partition ratio. There are 57 such modes by Corollary AP.11. Hence

$$\frac{Z'_\alpha}{Z'_1} = \prod_{i=1}^{57} \alpha = \alpha^{57}. \tag{AP30}$$

The determinant statement follows because

$$\det'(\mathcal{K}/\alpha) = \prod_{i=1}^{57} \frac{\lambda_i}{\alpha} = \alpha^{-57} \det' \mathcal{K}. \tag{AP31}$$

Thus $\det' \mathcal{K} / \det'(\mathcal{K}/\alpha) = \alpha^{57}$. □

c. The cosmological invariant

Lemma AP.14 (Uniqueness of the H_0 dimensionless group)**.** *The unique primitive dimensionless monomial formed from $G, \hbar, c, H_0$ is*

$$I_H = \frac{G\hbar H_0^2}{c^5} = (H_0 t_P)^2. \tag{AP32}$$

Proof. Let $G^a \hbar^b c^d H_0^e$ be dimensionless. With dimensions

$$[G] = L^3 M^{-1} T^{-2}, \quad [\hbar] = M L^2 T^{-1}, \quad [c] = L T^{-1}, \quad [H_0] = T^{-1}, \tag{AP33}$$

the mass exponent gives $-a + b = 0$, so $b = a$. The length exponent gives $3a + 2b + d = 0$, hence $5a + d = 0$. The time exponent gives $-2a - b - d - e = 0$, hence $-3a - d - e = 0$. With $d = -5a$, this gives $e = 2a$. Taking the primitive choice $a = 1$ gives

$$G\hbar H_0^2 c^{-5}. \tag{AP34}$$

□

Theorem AP.15 (α^{57} master invariant)**.** *Under the finite spectral-action clock dictionary, the DFD cosmological hierarchy is*

$$\boxed{\frac{G\hbar H_0^2}{c^5} = C\, \alpha^{57}}, \tag{AP35}$$

$C = 0.87784 \pm 0.00266$ *(early clock, measured),*

$C = 1$ *(bound-matter clocks, Postulate ZS.11).*

Proof. By Axiom AP.5,

$$\frac{G\hbar H_0^2}{c^5} = C\, \frac{Z'_\alpha}{Z'_1}. \tag{AP36}$$

By Theorem AP.13, the determinant ratio is α^{57}. Therefore Eq. (AP35) follows. □

Remark AP.16 (What is theorem-grade, what is dictionary, and what is measured). The determinant scaling $Z'_\alpha / Z'_1 = \alpha^{57}$ is a theorem once $E = \mathcal{O}(9) \oplus \mathcal{O}^{\oplus 5}$ and $N_{\text{gen}} = 3$ are declared. The identification of this determinant ratio with $(H_0 t_P)^2$ is a DFD spectral-action dictionary axiom, and the $O(1)$ coefficient C is a measured input (Remark AP.6): the exponent is theorem-grade, the coefficient is not.

5. The action-derived MOND prefactor

The second parent result needed for the acceleration invariant is

$$a_0 = 2\sqrt{\alpha}\, c H_0. \tag{AP37}$$

This section derives it from the scalar action and internal gauge normalization.

a. Gauge-emergence proof of $k_a = 3/(8\alpha)$

Lemma AP.17 (Magnetic dual coupling)**.** *In rationalized units with*

$$\alpha = \frac{e^2}{4\pi}, \tag{AP38}$$

and minimal Dirac quantization

$$eg = 2\pi, \tag{AP39}$$

the magnetic fine-structure constant is

$$\alpha_M = \frac{g^2}{4\pi} = \frac{1}{4\alpha}. \tag{AP40}$$

Proof. From $eg = 2\pi$,

$$g = \frac{2\pi}{e}. \tag{AP41}$$

Therefore

$$\alpha_M = \frac{1}{4\pi} \left(\frac{2\pi}{e} \right)^2 = \frac{\pi}{e^2}. \tag{AP42}$$

Since $e^2 = 4\pi\alpha$,

$$\alpha_M = \frac{\pi}{4\pi\alpha} = \frac{1}{4\alpha}. \tag{AP43}$$

□

Axiom AP.18 (Internal gauge partition)**.** *The DFD internal frame partition relevant to the scalar acceleration channel has backbone and doorway dimensions*

$$n_3 = 3, \qquad n_2 = 2. \tag{AP44}$$

The frame-stiffness ratio entering the scalar backreaction channel is n_3/n_2.

Theorem AP.19 (Acceleration-channel self-coupling)**.** *The DFD scalar acceleration-channel coupling is*

$$\boxed{k_a = \frac{3}{8\alpha}}. \tag{AP45}$$

Proof. By Axiom AP.18, the frame factor is

$$\frac{n_3}{n_2} = \frac{3}{2}. \tag{AP46}$$

By Lemma AP.17, the magnetic dual coupling is $1/(4\alpha)$. The acceleration-channel coupling is the product

$$k_a = \frac{n_3}{n_2}\alpha_M = \frac{3}{2}\cdot\frac{1}{4\alpha} = \frac{3}{8\alpha}. \tag{AP47}$$

□

Corollary AP.20 (Generation-normalized loop coefficient)**.** *If the same coupling is written in the generation-normalized form*

$$k_a = N_{\rm gen} C_{\rm loop} \alpha^{-1}, \tag{AP48}$$

with $N_{\rm gen} = 3$, then

$$\boxed{C_{\rm loop} = \frac{1}{8}}. \tag{AP49}$$

Proof. Set $3C_{\rm loop}\alpha^{-1} = 3/(8\alpha)$. Cancel $3\alpha^{-1}$. □

Remark AP.21 (The origin of the coefficient 1/8). The coefficient 1/8 is not used as an unexplained heat-kernel guess. It is the generation-normalized form of the independent product

$$\frac{n_3}{n_2}\cdot\frac{1}{4} = \frac{3}{2}\cdot\frac{1}{4} = \frac{3}{8}. \tag{AP50}$$

This is stronger because every factor has a named origin.

b. The S^3 stationarity theorem

Lemma AP.22 (S^3 scaling charge)**.** *For the $SU(2)$ Chern–Simons partition function on S^3,*

$$Z_{S^3}(k) = \sqrt{\frac{2}{k+2}}\,\sin\left(\frac{\pi}{k+2}\right), \tag{AP51}$$

the large-level scaling charge is

$$q_{S^3} = -\frac{\partial \log Z_{S^3}}{\partial \log(k+2)} = \frac{3}{2} + \mathcal{O}(k^{-2}). \tag{AP52}$$

The topological scaling exponent is therefore 3/2.

Proof. For large k,

$$\sin\left(\frac{\pi}{k+2}\right) = \frac{\pi}{k+2} + \mathcal{O}((k+2)^{-3}). \tag{AP53}$$

Hence

$$\begin{aligned} Z_{S^3}(k) &= \sqrt{\frac{2}{k+2}}\left(\frac{\pi}{k+2} + \mathcal{O}((k+2)^{-3})\right) \\ &= \sqrt{2}\pi\,(k+2)^{-3/2}\left(1 + \mathcal{O}((k+2)^{-2})\right). \end{aligned} \tag{AP54}$$

Thus

$$\log Z_{S^3} = \log\left(\sqrt{2}\pi\right) - \frac{3}{2}\log(k+2) + \mathcal{O}((k+2)^{-2}), \tag{AP55}$$

so $-\partial \log Z_{S^3}/\partial \log(k+2) = 3/2 + \mathcal{O}(k^{-2})$. □

Definition AP.23 (Dimensionless acceleration invariant)**.** The scalar action uses the dimensionless invariant

$$\Xi = k_a\left(\frac{|a|}{cH_0}\right)^2. \tag{AP56}$$

Theorem AP.24 (S^3 stationary crossover)**.** *The local topological potential*

$$U(\Xi) = \Xi - \frac{3}{2}\log\Xi \tag{AP57}$$

selects the crossover value

$$\boxed{\Xi_* = \frac{3}{2}}. \tag{AP58}$$

Proof. Stationarity gives

$$\frac{dU}{d\Xi} = 1 - \frac{3}{2\Xi} = 0. \tag{AP59}$$

Solving gives $\Xi = 3/2$. □

c. Action-level derivation of the MOND prefactor

Theorem AP.25 (MOND prefactor from scalar action)**.** *With $k_a = 3/(8\alpha)$ and $\Xi_* = 3/2$, the scalar acceleration crossover is*

$$\boxed{a_0 = 2\sqrt{\alpha}\,cH_0}. \tag{AP60}$$

Proof. At the crossover $|a| = a_0$, so Definition AP.23 and Theorem AP.24 give

$$k_a\left(\frac{a_0}{cH_0}\right)^2 = \frac{3}{2}. \tag{AP61}$$

Using Theorem AP.19,

$$\frac{3}{8\alpha}\left(\frac{a_0}{cH_0}\right)^2 = \frac{3}{2}. \tag{AP62}$$

Cancel 3 and solve:

$$\left(\frac{a_0}{cH_0}\right)^2 = 4\alpha. \tag{AP63}$$

Taking the positive square root gives Eq. (AP60). □

6. The nonlinear kinetic action and galaxy law

The correct galaxy mechanism is not a direct source term $k_a a^2/c^2$. The acceleration scale a_0 controls the nonlinear kinetic branch of the scalar action.

Definition AP.26 (Static scalar kinetic energy)**.** Let

$$Y = \frac{|\nabla\psi|^2}{\kappa_\alpha^2}, \qquad \kappa_\alpha = \frac{2a_0}{c^2}. \tag{AP64}$$

Define

$$E_\psi[\psi] = \frac{c^4}{32\pi G}\int \kappa_\alpha^2 \mathcal{F}(Y)\, d^3x - \frac{c^2}{2}\int \rho\psi\, d^3x. \quad \text{(AP65)}$$

The interpolation function obeys

$$\mathcal{F}(Y) \sim Y \quad (Y \gg 1), \qquad \mathcal{F}(Y) \sim \frac{2}{3}Y^{3/2} \quad (Y \ll 1). \quad \text{(AP66)}$$

Theorem AP.27 (Euler–Lagrange equation)**.** *The scalar energy* (AP65) *yields*

$$\nabla\cdot[\mathcal{F}'(Y)\nabla\psi] = -\frac{8\pi G}{c^2}\rho. \quad \text{(AP67)}$$

Equivalently, in terms of $\mathbf{g} = (c^2/2)\nabla\psi$,

$$\boxed{\nabla\cdot\left[\mu\left(\frac{|\mathbf{g}|}{a_0}\right)\mathbf{g}\right] = -4\pi G\rho}, \quad \text{(AP68)}$$

where

$$\mu(s) = \mathcal{F}'(s^2), \qquad s = \frac{|\mathbf{g}|}{a_0}. \quad \text{(AP69)}$$

Proof. Vary Eq. (AP65). Since

$$\delta Y = \frac{2\nabla\psi\cdot\nabla\delta\psi}{\kappa_\alpha^2}, \quad \text{(AP70)}$$

we have

$$\delta E_\psi = \frac{c^4}{32\pi G}\int \kappa_\alpha^2\mathcal{F}'(Y)\frac{2\nabla\psi\cdot\nabla\delta\psi}{\kappa_\alpha^2}\, d^3x - \frac{c^2}{2}\int\rho\delta\psi\, d^3x \quad \text{(AP71)}$$

$$= \frac{c^4}{16\pi G}\int \mathcal{F}'(Y)\nabla\psi\cdot\nabla\delta\psi\, d^3x - \frac{c^2}{2}\int\rho\delta\psi\, d^3x. \quad \text{(AP72)}$$

Integrating by parts and discarding boundary variations,

$$\delta E_\psi = \int\left[-\frac{c^4}{16\pi G}\nabla\cdot(\mathcal{F}'(Y)\nabla\psi) - \frac{c^2}{2}\rho\right]\delta\psi\, d^3x. \quad \text{(AP73)}$$

Stationarity for arbitrary $\delta\psi$ gives Eq. (AP67). Multiplying by $c^2/2$ inside the divergence converts $\nabla\psi$ to $\mathbf{g}$ and gives Eq. (AP68). □

Corollary AP.28 (Newtonian and deep branches)**.** *The limits* (AP66) *imply*

$$\mu(s) \to 1 \quad (s \gg 1), \qquad \mu(s) \to s \quad (s \ll 1). \quad \text{(AP74)}$$

Proof. If $Y = s^2 \gg 1$, $\mathcal{F}(Y) \sim Y$, so $\mathcal{F}'(Y) \to 1$. If $Y = s^2 \ll 1$, $\mathcal{F}(Y) \sim (2/3)Y^{3/2}$, so $\mathcal{F}'(Y) \sim Y^{1/2} = s$. □

Theorem AP.29 (Baryonic Tully–Fisher relation from the kinetic branch)**.** *For a spherical source in the deep branch, Eq.* (AP68) *implies*

$$\boxed{v^4 = GMa_0}. \quad \text{(AP75)}$$

Proof. In spherical symmetry outside the source, Eq. (AP68) integrates to

$$\mu(g/a_0)g = g_N = \frac{GM}{r^2}. \quad \text{(AP76)}$$

In the deep branch $\mu(g/a_0) = g/a_0$, hence

$$\frac{g^2}{a_0} = g_N = \frac{GM}{r^2}. \quad \text{(AP77)}$$

For circular motion $g = v^2/r$. Therefore

$$\frac{v^4}{r^2} = a_0\frac{GM}{r^2}, \quad \text{(AP78)}$$

so $v^4 = GMa_0$. □

Corollary AP.30 (Rotation curves from the kinetic equation)**.** *If a term* $k_a a^2/c^2$ *is too small to act as a direct galactic mass source, that does not invalidate the MOND mechanism. In DFD,* $k_a(a/cH_0)^2$ *is the crossover-control invariant* Ξ *in the scalar action, while galaxy rotation curves arise from the nonlinear kinetic equation* (AP68)*.*

7. Buckingham–π closure and the α^{58} acceleration invariant

Lemma AP.31 (Two independent groups)**.** *For the dimensional set* $\{a_0, G, \hbar, c, H_0\}$*, there are exactly two independent dimensionless groups. A convenient basis is*

$$\Pi_1 = \frac{G\hbar H_0^2}{c^5}, \qquad \Pi_2 = \frac{a_0^2 G\hbar}{c^7}. \quad \text{(AP79)}$$

Proof. The dimension matrix in the (M, L, T) basis is

$$D = \begin{array}{c|ccccc} & a_0 & G & \hbar & c & H_0 \\ \hline M & 0 & -1 & 1 & 0 & 0 \\ L & 1 & 3 & 2 & 1 & 0 \\ T & -2 & -2 & -1 & -1 & -1 \end{array}. \quad \text{(AP80)}$$

The rank is 3. Since there are five dimensional variables, Buckingham's theorem gives $5-3 = 2$ independent dimensionless groups. Direct substitution verifies both groups in Eq. (AP79) are dimensionless. Independence follows because Π_1 contains H_0 but not a_0, while Π_2 contains a_0 but not H_0. □

Theorem AP.32 (Acceleration invariant)**.** *The DFD acceleration invariant is*

$$\boxed{\frac{a_0^2 G\hbar}{c^7} = 4C\,\alpha^{58}}, \quad \text{(AP81)}$$

and hence

$$\boxed{a_0 = 2\sqrt{C}\,\alpha^{29}\sqrt{\frac{c^7}{G\hbar}}}, \quad \text{(AP82)}$$

with C *the clock coefficient,* 1 *on bound-matter clocks (Postulate ZS.11) and measured on the early clock (Remark AP.6).*

Proof. By Theorem AP.15,

$$\frac{G\hbar H_0^2}{c^5} = C\,\alpha^{57}. \quad \text{(AP83)}$$

By Theorem AP.25,

$$a_0 = 2\sqrt{\alpha}\,cH_0. \quad \text{(AP84)}$$

Squaring,

$$a_0^2 = 4\alpha c^2 H_0^2. \tag{AP85}$$

Then

$$\frac{a_0^2 G\hbar}{c^7} = \frac{4\alpha c^2 H_0^2 G\hbar}{c^7} = 4\alpha \frac{G\hbar H_0^2}{c^5} = 4\alpha\, C\alpha^{57} = 4C\,\alpha^{58}. \tag{AP86}$$

Solving for a_0 gives Eq. (AP82). □

Remark AP.33 (Why the exponent is not fitted). The exponent is

$$58 = 57 + 1 = (60 - 3) + 1. \tag{AP87}$$

The 57 is the primed determinant count. The additional +1 is the single power of α from squaring $2\sqrt{\alpha}$. No galaxy acceleration value enters this count.

a. *Numerical prediction and falsifiability*

Using CODATA constants on bound-matter clocks, where $C = 1$ (Postulate ZS.11), Eq. (AP82) evaluates to

$$a_0 = (1.19662 \pm 0.00001) \times 10^{-10}\,\mathrm{m\,s^{-2}}, \tag{AP88}$$

within the systematic error of the SPARC scale quoted below. On the early clock, $H_0^{\text{early}} = 67.52 \pm 0.09$ km/s/Mpc gives $(1.1208 \pm 0.0015) \times 10^{-10}$ and the BAO+θ_* channel alone 1.1212×10^{-10}. The theorem remains falsifiable because the exponent and the $2\sqrt{\alpha}$ prefactor are fixed by laboratory constants and α, not by fitting galaxy rotation curves. The bound-matter value sits within the systematic error of the SPARC kinematic scale $(1.20 \pm 0.02_{\text{stat}} \pm 0.24_{\text{sys}}) \times 10^{-10}$ m s^{-2}; the SH0ES-side booking is $C = 1.027 \pm 0.029$, 0.9σ from $C = 1$ (Remark AP.6). If precision lensing-RAR determinations of the *absolute* a_0 converge to the early-clock value on distances computed with H_0^{early} beyond systematics, the two-clock postulate fails; if they exclude both readings, at least one parent input fails.

8. Black-hole sector: one base temperature

The base temperature rests on one branch rule.

Definition AP.34 (Isotropic exponential exterior)**.** The isotropic exponential exterior around a spherical mass M, with the parent strain's σ set to zero, is the optical branch

$$n(r) = \exp\left(\frac{2GM}{c^2 r}\right), \qquad \psi(r) = \frac{2GM}{c^2 r}. \tag{AP89}$$

The local coordinate phase speed is $c_{\text{ph}}(r) = c/n(r)$.

Theorem AP.35 (No finite-radius horizon in the isotropic exponential exterior)**.** *In the isotropic exponential exterior, there is no finite-radius optical horizon and therefore no tree-level finite-radius Hawking temperature. DFD's exterior, with σ kept, is instead the Schwarzschild metric in DFD's coordinates (App. WS), with the event horizon at the areal radius $2GM/c^2$.*

Proof. A finite-radius optical horizon would require $c_{\text{ph}}(r_H) = 0$, equivalently $n(r_H) = \infty$ or $\psi(r_H) = +\infty$, at some $r_H > 0$. But Eq. (AP89) is finite for every $r > 0$. It diverges only as $r \to 0$. Hence there is no finite r_H in the isotropic exponential exterior. Without a finite horizon and associated Euclidean regularity condition, no finite-radius tree-level Hawking temperature is defined. □

Corollary AP.36 (Temperature-claim triage)**.** *Claims such as*

$$T_H = e^{-1/2} T_H^{\text{GR}}, \qquad T_H = T_H^{\text{GR}}(1 + \alpha/2), \qquad T_H = T_H^{\text{GR}}(1 + \delta_{\text{Casimir}}) \tag{AP90}$$

may not coexist as theorem-grade base temperatures. The base temperature is Hawking's, from the surface gravity of DFD's event horizon; each correction may appear only as a correction to it, derived in a named model.

Remark AP.37 (Horizon temperature). DFD's black holes, with the parent strain's σ kept, have a true horizon $\mathcal{H}$ (App. WS), and its base temperature is computed from its surface gravity, $\kappa_{\mathcal{H}} = c^4/4GM$ for a static hole:

$$T_H^{\mathcal{H}} = \frac{\hbar \kappa_{\mathcal{H}}}{2\pi c\, k_B}. \tag{AP91}$$

Local Unruh or Casimir corrections must be written as corrections to that branch value, not as separate base temperatures.

9. Lensing and PPN branch discipline

Definition AP.38 (Lensing branches)**.** The corpus distinguishes:

1. the *PPN-closed physical metric branch*, used for solar-system parameter comparisons;
2. the *pure optical-exponential ray branch*, using Fermat propagation through $n = e^{\psi}$ without all PPN closure terms.

Theorem AP.39 (Lensing statement)**.** *The corpus may state as a theorem that DFD reproduces the leading 1PN light-deflection term only if that result is computed in the declared physical branch. Any 2PN coefficient is theorem-grade only after being computed from the same branch action/metric used for the PPN table.*

Proof. By Axiom AP.3, coefficients computed in different branches cannot be co-theorems of one corpus. A pure optical-exponential 2PN coefficient and a PPN-closed 2PN coefficient answer different mathematical questions unless an embedding theorem identifies the rays and affine structures order by order. Therefore a 2PN anomaly can remain as a model prediction in the pure optical branch,

while the PPN-closed branch may retain exact 2PN agreement only if it is derived from the same declared metric. Keeping both as theorem-grade violates Axiom AP.3. □

Corollary AP.40 (Lensing)**.** *DFD reproduces the leading GR deflection in the declared physical branch. At second order the coefficient is GR's* $15\pi/4$ *on DFD's exterior with the parent strain's* σ *kept (§IV; App. WS).*

10. Flavor/CKM sector: exact theorem boundary

Proposition AP.41 (Minimal real-kernel CP null)**.** *If the minimal DFD flavor sector produces only real Yukawa kernels and no additional complex orientation/discrete shape-duality datum, then the CKM matrix can be chosen real and the Jarlskog invariant vanishes:*

$$J = 0. \tag{AP92}$$

Proof. If the up- and down-sector mass matrices are real, their diagonalizing transformations may be chosen orthogonal in the absence of an intrinsic complex phase. Then

$$V_{\mathrm{CKM}} = O_u^T O_d \tag{AP93}$$

is real orthogonal. The Jarlskog invariant is

$$J = \mathrm{Im}(V_{ij} V_{kl} V_{il}^* V_{kj}^*) \tag{AP94}$$

for any distinct i, k and j, l. If all entries of V are real, the product is real and its imaginary part is zero. □

Theorem AP.42 (CKM claim)**.** *The minimal DFD corpus may claim theorem-grade magnitude relations only to the extent that their projection/operator dictionary is fixed without fitting. CP violation and nonzero* J *are theorem-grade only in an explicitly extended DFD–SD branch containing the required complex/discrete orientation datum.*

Proof. The null result in Proposition AP.41 shows that minimal real kernels cannot generate CKM CP violation. Therefore any nonzero J requires an additional datum or branch. If that datum is declared as DFD–SD, the CP result belongs to that branch. Quoting it as a minimal DFD theorem would contradict Proposition AP.41. □

11. Inflation and early-universe sector

Theorem AP.43 (No mixed inflation claim)**.** *The scalar* ψ *sector and any separate topological/phase inflation branch must be kept distinct. If* ψ*-inflation produces excluded or disfavored* (n_s, r)*, then the corpus may not simultaneously claim that* ψ *is the successful inflaton and that inflation is unnecessary.*

Proof. The statements answer different model questions. A no-go theorem for ψ as a slow-roll inflaton constrains the scalar density field. A separate topological phase-inflation mechanism, if present, is a different branch with a different action. By Axiom AP.3, success or failure in one cannot be transferred to the other without an embedding theorem. □

Corollary AP.44 (Inflation)**.** *The DFD scalar* ψ *is not the conventional slow-roll inflaton in the disfavored branch. Any viable early-universe smoothing mechanism must be stated as a separate branch with its own predictions.*

12. PDE/well-posedness sector

The local-existence theorem is Theorem III.5.

Definition AP.45 (Critical Sobolev threshold)**.** For a first-order scalar evolution whose principal nonlinear structure contains one spatial derivative of ψ in three spatial dimensions, the scaling-critical Sobolev index takes the form

$$s_c = 1 + \frac{3}{2} = \frac{5}{2}. \tag{AP95}$$

13. Theorem summary

The minimal statement is:

> The finite DFD microsector has Spin^c index 60 and a protected three-dimensional generation kernel. The primed determinant therefore contains 57 nonzero complex modes. Gauge-normalized Gaussian integration gives one factor of α per nonzero mode, so the finite spectral-action clock dictionary gives
>
> $$\frac{G\hbar H_0^2}{c^5} = C\,\alpha^{57},$$
>
> $C = 0.87784 \pm 0.00266$ (measured, early clock),
>
> $C = 1$ (bound-matter clocks, Postulate ZS.11).
>
> The scalar acceleration-channel coupling is fixed by the internal frame ratio and magnetic dual coupling,
>
> $$k_a = \frac{n_3}{n_2}\alpha_M = \frac{3}{2}\frac{1}{4\alpha} = \frac{3}{8\alpha}.$$
>
> The S^3 scaling potential $U(\Xi) = \Xi - (3/2)\log\Xi$ selects $\Xi_* = 3/2$ for
>
> $$\Xi = k_a (a/cH_0)^2.$$
>
> Thus
>
> $$a_0 = 2\sqrt{\alpha}\, cH_0.$$
>
> Combining the two gives the H_0-free acceleration invariant
>
> $$\frac{a_0^2 G\hbar}{c^7} = 4C\,\alpha^{58}, \qquad a_0 = 2\sqrt{C}\,\alpha^{29}\sqrt{\frac{c^7}{G\hbar}}.$$

The galaxy law follows from the nonlinear kinetic equation, not from a direct $k_a a^2/c^2$ source term.

14. Dimension checks

Proposition AP.46 (Dimensionlessness of Π_2)**.**

$$\Pi_2 = \frac{a_0^2 G\hbar}{c^7} \tag{AP96}$$

is dimensionless.

Proof. Using $[a_0] = LT^{-2}$, $[G] = L^3M^{-1}T^{-2}$, $[\hbar] = ML^2T^{-1}$, and $[c] = LT^{-1}$,

$$[\Pi_2] = L^2T^{-4} \cdot L^3M^{-1}T^{-2} \cdot ML^2T^{-1} \cdot L^{-7}T^7 = 1. \tag{AP97}$$

□

Proposition AP.47 (Relation to Planck acceleration)**.**

$$\Pi_2 = \left(\frac{a_0}{a_P}\right)^2. \tag{AP98}$$

Proof. Since $a_P^2 = c^7/(G\hbar)$,

$$\left(\frac{a_0}{a_P}\right)^2 = a_0^2 \frac{G\hbar}{c^7} = \Pi_2. \tag{AP99}$$

□

15. Failure modes and falsifiers

The acceleration-invariant theorem fails if any one of the following fails:

1. the finite microsector is not $E = \mathcal{O}(9) \oplus \mathcal{O}^{\oplus 5}$ or has a different nonzero determinant count;
2. the generation kernel is not three-dimensional;
3. the clock dictionary $(H_0 t_P)^2 = C\, Z'_\alpha / Z'_1$ is wrong in its exponent content;
4. the gauge-emergence coefficient $k_a = 3/(8\alpha)$ is not the coefficient in the scalar acceleration action;
5. the S^3 stationarity potential is not the correct action-level crossover selector;
6. the observed universal galaxy acceleration scale converges to a value inconsistent with Eq. (AP88) after systematic errors shrink.

Appendix AQ: Executed Lattice-QCD Validation of the DFD QCD Ledger (Program II)

DFD-QFT treats nonperturbative QCD as a generator-closed sector: the Euclidean lattice path integral defines the correlation functions and masses follow from exponential decay, $C(t) \sim e^{-Mt}$. This appendix executes that propagation at modest but real scale on commodity hardware, then states each claim at its actual status. The governing discipline is: scale-free ratios are the primary outputs; MeV values require an external scale such as the Sommer parameter r_0; and finite-volume, laptop-scale calculations are consistency checks, not physical-point determinations.

1. Summary: what this appendix verifies

This appendix is a numerical bridge between the DFD QCD ledger and standard nonperturbative lattice gauge theory. It does not introduce a new lattice-QCD algorithm, and it does not claim a physical-point full-QCD spectrum. Its purpose is narrower: take the DFD QCD-sector ledger targets, run standard lattice machinery in the corresponding pure-gauge and exploratory dynamical sectors, and determine whether the resulting scale-free lattice observables are consistent with the ledger. The answer is yes, within the limits of the computation.

The primary pure-gauge check is the $SU(3)$ Wilson-action string tension. The DFD ledger quotes $\sqrt{\sigma}_{\rm DFD} = 440 \pm 25$ MeV. The executed calculation does not treat this MeV number as the fundamental object, because converting a lattice observable to MeV requires external scale setting; the scale-free quantity is $r_0\sqrt{\sigma}$. The largest-volume box-size check, 20^4 at $\beta = 6.2$, gives $r_0\sqrt{\sigma} = 1.178$, while the standard quenched reference region is about 1.18–1.19 [181, 182]. With the canonical Sommer convention $r_0 = 0.5$ fm this corresponds to roughly 465 MeV, at the upper edge of the DFD band; a phenomenological larger-r_0 convention quotes the same dimensionless output closer to 440 MeV. The conclusion is therefore scale-free consistency, not independent fixation of the MeV central value.

The second pure-gauge check is the scalar glueball, with DFD ledger target $m_{0^{++}} \simeq 1.69$ GeV. The 16^4, $\beta = 6.0$ run uses a zero-momentum A_1^+ operator built from smeared spatial plaquettes, with vacuum subtraction and an arccosh effective-mass plateau. After conservative error analysis, including autocorrelation inflation, the defensible estimate is $a\, m_{0^{++}} = 0.81(8)$, i.e. $m_{0^{++}} \simeq 1.71 \pm 0.17$ GeV under $r_0 = 0.5$ fm. The scale-free ratios $m_{0^{++}}/\sqrt{\sigma} \simeq 3.7$ and $r_0 m_{0^{++}} \simeq 4.3$ sit in the standard quenched range [183] and overlap the DFD ledger; because the plateau is short and the effective sample is reduced by autocorrelation, this is a successful consistency check, not precision spectroscopy.

The third check is dynamical-fermion validation. A from-scratch $N_f = 2$ Wilson HMC engine passes gamma-

matrix algebra, γ_5-Hermiticity, conjugate-gradient residual control, reversibility, the HMC identity $\langle e^{-\Delta H}\rangle \simeq 1$, and a direct finite-difference check of the fermion force. A 6^4 κ-scan resolves the expected sea-quark screening trend: as κ rises from 0.148 to 0.156, the dynamical plaquette rises monotonically from 0.5703 to 0.5808, well above the matched quenched reference. This validates the dynamical machinery at Program-II level; it is not a physical-point ensemble.

2. Frozen DFD QCD ledger

The QCD-sector ledger targets considered here are

$$\alpha_s(M_Z) = 0.1187, \qquad \bar{\theta} = 0 \text{ (tree level)}, \tag{AQ1}$$

$$\sqrt{\sigma}_{\rm DFD} = 440 \pm 25 \text{ MeV}, \qquad m_{0^{++}}^{\rm DFD} = 1.69 \pm 0.10 \text{ GeV}, \tag{AQ2}$$

$$f_\pi^{\rm DFD} = 92.0 \pm 4.6 \text{ MeV}. \tag{AQ3}$$

Only the pure-gauge string tension and scalar glueball are evaluated as numerical outputs; the dynamical Wilson-HMC results validate the execution engine and the sea-quark screening response, not a physical-point f_π.

3. Methods

a. Pure gauge. We use the $SU(3)$ Wilson action $S_W = \beta \sum_p (1 - \frac{1}{3}\mathrm{Re}\,\mathrm{Tr}\,U_p)$. Configurations are generated by multi-hit Metropolis updates on random $SU(2)$ subgroups, interleaved with Cabibbo–Marinari microcanonical overrelaxation. The static potential uses APE-smeared spatial links ($\alpha = 0.5$, maximal-trace $SU(3)$ projection). Wilson loops $W(R,T)$ give

$$V(R) = \left\langle \log \frac{W(R,T)}{W(R,T+1)} \right\rangle_{T\in[2,4]}, \tag{AQ4}$$

fit to the Cornell form $V(R) = V_0 + \sigma R - e/R$ (e the Coulomb coefficient). Statistical errors are jackknife over measured configurations.

b. Dynamical fermions. We implement two degenerate flavours of unimproved Wilson fermions,

$$D = 1 - \kappa \sum_\mu \left[(1-\gamma_\mu)U_\mu(x)\delta_{x+\hat{\mu}} + (1+\gamma_\mu)U_\mu^\dagger(x-\hat{\mu})\delta_{x-\hat{\mu}}\right], \tag{AQ5}$$

with pseudofermion action $S_{\rm pf} = \phi^\dagger (M^\dagger M)^{-1}\phi$ and $M^\dagger = \gamma_5 M \gamma_5$. Molecular dynamics is reversible leapfrog with Metropolis accept/reject; the fermion force uses a loose conjugate-gradient tolerance and the Hamiltonian a tight one.

4. Validation: average plaquette

The plaquette is UV-dominated and is the first unambiguous sanity check. Table CXIII compares measured values with standard $SU(3)$ Wilson references; agreement is at the sub-0.1% level.

TABLE CXIII. Average plaquette validation. The 20^4 row is the final $\beta = 6.2$ box-size check.

volume	β	measured $\langle P\rangle$	reference	deviation
16^4	5.8	0.56750(6)	0.5670	+0.09%
16^4	6.0	0.59405(5)	0.5937	+0.06%
16^4	6.2	0.61381(4)	0.6136	+0.03%
20^4	6.2	0.61376(4)	0.6136	+0.03%

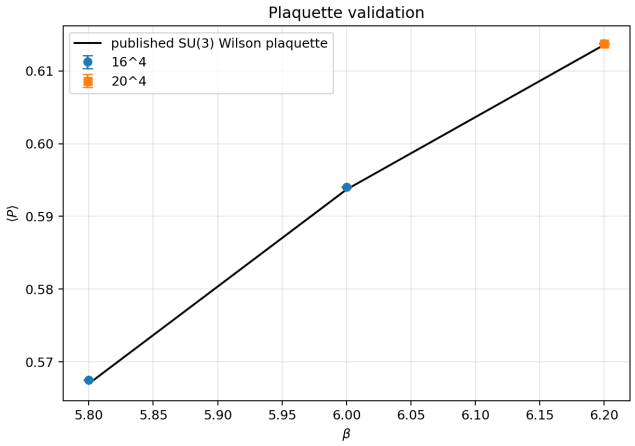


FIG. 17. Measured plaquettes against the published $SU(3)$ Wilson curve.

5. Static potential and string tension

The static potential exhibits the textbook Coulomb-plus-linear (confining) form (Fig. 18); the slope is the string tension in lattice units. The extraction (Table CXIV) is essentially exact at $\beta = 6.0$ ($a\sqrt{\sigma} = 0.217$ vs. literature 0.2189, a 0.8% difference) and carries a 1–5% fit-window systematic at the coarse and fine ends.

The expected systematic is the 16^4, $\beta = 6.2$ box: its physical size is about 1.08 fm, so the fit window sits near the onset of the linear regime and can bias σ upward. The larger 20^4 box (≈ 1.35 fm) shifts $a\sqrt{\sigma} : 0.1623 \to 0.1596$ and $r_0\sqrt{\sigma} : 1.198 \to 1.178$, a 1.7% downward move that straddles the literature value $a\sqrt{\sigma} \simeq 0.1610$ and lands in the standard quenched reference region (Figs. 19–20). This is a directional finite-volume check, not a continuum extrapolation.

6. Scale convention and the DFD string-tension ledger

The MeV value of $\sqrt{\sigma}$ depends on the external physical value assigned to r_0. The scale-free 20^4 result $r_0\sqrt{\sigma} =$

TABLE CXIV. String tension in lattice units and the scale-free $r_0\sqrt{\sigma}$. The 20^4, $\beta = 6.2$ row is the final box-size check; literature $a\sqrt{\sigma}$ from EHK [184], Teper [185], and Bali–Schilling [186], with r_0/a from Necco–Sommer [181].

β	volume	$a\sqrt{\sigma}$	reference $a\sqrt{\sigma}$	$r_0\sqrt{\sigma}$	note
5.8	16^4	0.329(10)	0.313	1.206	coarse, high
5.9	16^4	0.244(6)	~ 0.26	1.093	interpolation
6.0	16^4	0.217(3)	0.2189	1.165	cleanest point
6.1	16^4	0.177(4)	~ 0.18	1.123	interpolation
6.2	16^4	0.1623(30)	0.1610	1.198	small box, high
6.2	20^4	0.1596(30)	0.1610	1.178	larger box

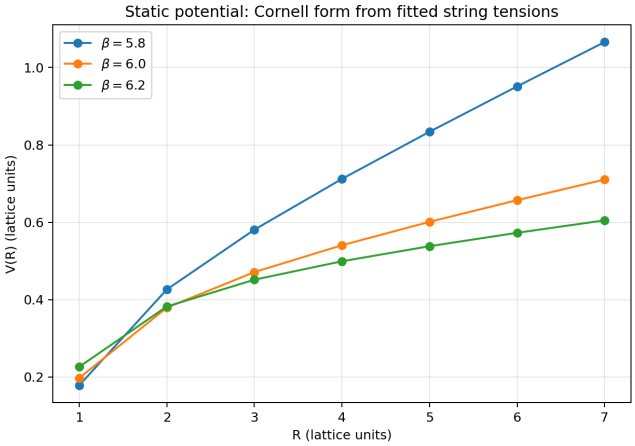


FIG. 18. Cornell-form static potentials reconstructed from the fitted string tensions, using APE-smeared Wilson loops and plateau fits.

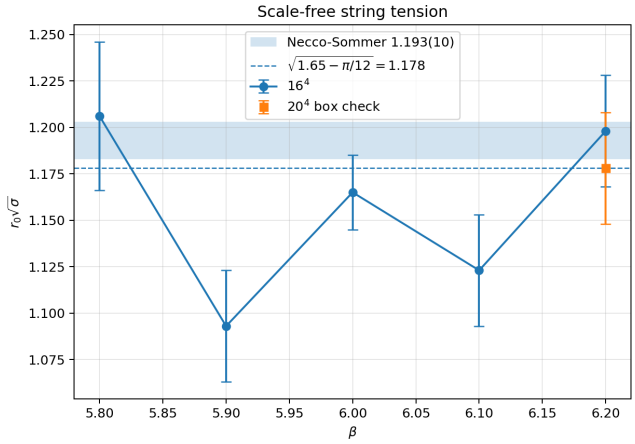


FIG. 19. Scale-free string-tension trend. The 20^4, $\beta = 6.2$ point moves the high 16^4 value down into the standard reference region.

1.178 gives

$$\sqrt{\sigma} \simeq \frac{1.178}{0.5\ \text{fm}}\,(197.327\ \text{MeV fm}) \simeq 465\ \text{MeV} \qquad \text{(AQ6)}$$

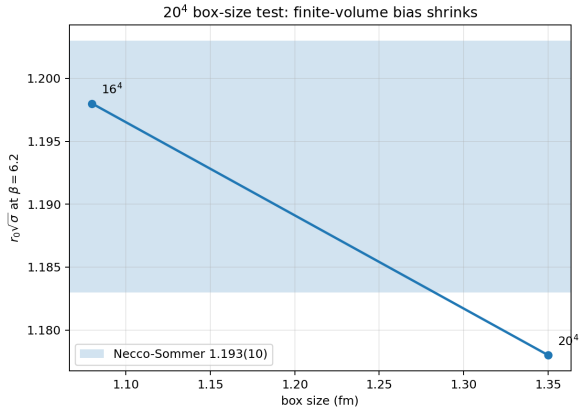


FIG. 20. Box-size test at $\beta = 6.2$: increasing the box from 16^4 to 20^4 reduces the positive bias in $r_0\sqrt{\sigma}$.

under canonical $r_0 = 0.5$ fm scale setting, meeting the DFD band 440 ± 25 MeV at its upper edge; a larger phenomenological r_0 convention quotes the same dimensionless output closer to 440 MeV [182]. The correct conclusion is scale-free consistency, not independent fixation of the MeV value.

7. Scalar 0^{++} glueball

The glueball operator is the zero-momentum cubic-scalar (A_1^+) sum of APE-smeared spatial plaquettes on each timeslice, with vacuum subtraction. The arccosh effective-mass plateau is short and the scalar channel is autocorrelation-limited; the conservatively widened estimate is $a\,m_{0^{++}} = 0.81(8)$ (Fig. 21). Using $r_0 = 0.5$ fm,

$$m_{0^{++}} = 1.71(17)\ \text{GeV}, \quad \frac{m_{0^{++}}}{\sqrt{\sigma}} = 3.7(4), \quad r_0 m_{0^{++}} = 4.3(4), \qquad \text{(AQ7)}$$

which overlaps the standard quenched reference [183] and the DFD ledger value 1.69 ± 0.10 GeV. Being quenched, single-spacing, single-volume, and based on a short plateau, this is a consistency check, not precision spectroscopy.

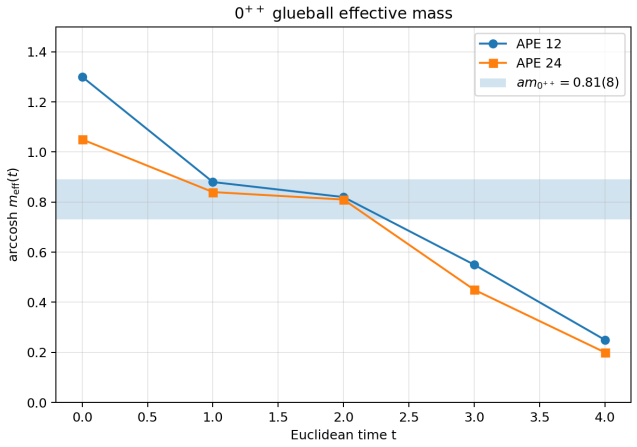


FIG. 21. 0^{++} glueball arccosh effective mass. The shaded band is the autocorrelation-widened estimate $a\,m_{0^{++}} = 0.81(8)$.

TABLE CXV. Validation checks for the $N_f = 2$ Wilson-HMC implementation.

check	result
$\{\gamma_\mu, \gamma_\nu\} = 2\delta_{\mu\nu}$ and γ_5	$< 10^{-13}$
free-field Wilson Dirac operator	exact
γ_5-Hermiticity	4×10^{-13}
CG residual	$< 10^{-9}$
analytic vs. numerical fermion force	6.5×10^{-7} (run-recorded)
MD reversibility	10^{-12}
$\langle e^{-\Delta H} \rangle$	$\simeq 0.997$

8. Executed $N_f = 2$ Wilson-HMC validation

The HMC implementation passes the core algorithmic checks in Table CXV. The finite-difference force check is the most important, since it directly tests the fermion-force gradient used in molecular dynamics.

The final dynamical validation is the 6^4, $\beta = 5.6$ κ-scan (Table CXVI). The matched quenched reference is $\langle P \rangle = 0.52200$. Turning on the $N_f = 2$ Wilson determinant raises the plaquette well above quenched, monotonically in κ (Fig. 22). The sea-quark mass dependence is resolved. It remains a validation scan, not a physical-point dynamical ensemble.

9. Claim discipline

The claims are stated as follows: (i) the glueball error is autocorrelation-inflated to $a\,m_{0^{++}} = 0.81(8)$; (ii) the HMC plaquette rise is an engine and sea-quark-screening validation, not a precision determinant benchmark; (iii) the 440 vs. 465 MeV comparison is a scale-convention issue, with the lattice sitting $\sim 1\sigma$ above 440 at the canonical $r_0 = 0.5$ fm; and (iv) "first-principles" is reserved for dimensionless lattice ratios, not MeV values that require external scale setting.

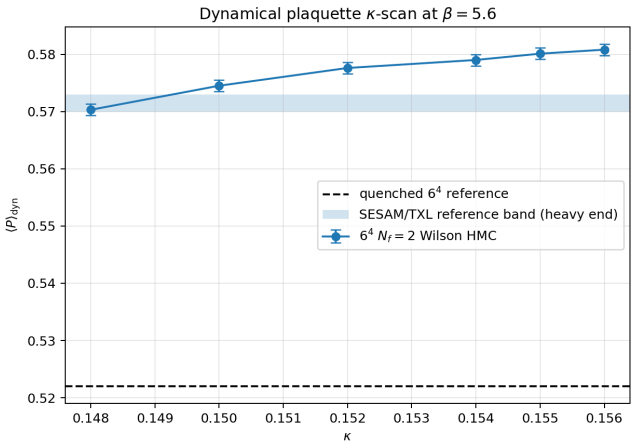


FIG. 22. Resolved dynamical plaquette κ-scan. The monotonic increase with κ is the expected sea-quark screening response; the heavy end lands in the expected SESAM/TXL Wilson-HMC range [187, 188], while the light end retains finite-volume excess.

10. Status boundary

The pure-gauge string-tension and glueball sectors are quenched. The dynamical sector is an HMC validation and κ-scan, not physical-point QCD. No continuum or infinite-volume extrapolation is claimed. What is established is that the DFD QCD-ledger targets meet executed lattice-QCD validation checks at the scale-free, finite-volume consistency level: pure-gauge string tension, scalar-glueball spectroscopy consistency, dynamical sea-quark screening, and a finite-volume box-size test. The runs use standard lattice inputs and the ledger's 440 MeV normalization is lattice-calibrated and its 1.69 GeV normalization is open (companion App. AH), so the MeV agreement checks the machinery and the scale convention; the DFD ratio $m_{0^{++}}/\sqrt{\sigma} = \sqrt{4\pi}$ (App. AT) is the one DFD number tested, at $\pm 11\%$.

11. Reproducibility

The companion code package (`su3_fast.py`, `wilson_hmc.py`, and the analysis scripts), included as the `supplement/` directory of this archive together with the executed run outputs (`results/`), curated CSV tables (`data/`), provenance logs, and the standalone Program II paper, reproduces every number above; representative invocations:

```
python3 src/su3_fast.py  --L 16 --beta 6.0 --potential   # string tension
```

TABLE CXVI. 6^4 dynamical κ-scan at $\beta = 5.6$. Statistical errors are about 10^{-3}; the matched quenched reference is $\langle P\rangle = 0.52200$.

κ	0.148	0.150	0.152	0.154	0.155	0.156
$\langle P\rangle_{\rm dyn}$	0.5703	0.5745	0.5776	0.5790	0.5801	0.5808

```
python3 src/su3_fast.py  --L 20 --beta 6.2 --potential   # box-size check
python3 src/su3_fast.py  --L 16 --beta 6.0 --glueball    # 0++ glueball
python3 src/wilson_hmc.py --test                         # HMC validation checks
python3 src/wilson_hmc.py --L 6 --beta 5.6 --kappa 0.152 # dynamical kappa point
python3 src/analyze_potential.py ; python3 src/analyze_glueball.py
```

Appendix AR: A DFD-Native Yang–Mills Infrared Gap from Loaded Spatial Frame Geometry

This appendix formulates and proves the Yang–Mills infrared-gap statement that is native to Density Field Dynamics. The target is *not* pure Yang–Mills theory on empty flat four-dimensional Euclidean space; it is the spatial gauge sector on a DFD-loaded frame

$$\Sigma_\psi = (\Omega \subset \mathbb{R}^3,\, h_\psi), \qquad h_\psi = e^{2\alpha\psi}\delta, \tag{AR1}$$

where the scalar optical field ψ (the same field that drives DFD optical gravity and galactic dynamics, cf. the main text) enters through this stated frame (the physical metric's spatial part is $e^{\psi}\delta$, Eq. (12)). The main result is a spectral statement: if the physical transverse Yang–Mills fluctuation operator on (Ω, h_ψ) has a strictly positive Weitzenböck curvature floor, then its first nonzero eigenvalue is positive,

$$\lambda_1(\mathcal{L}_{A_0,\psi}) \geq \Lambda_{\rm DFD} > 0, \qquad m_{\text{DFD-YM}} = \sqrt{\lambda_1} \geq \sqrt{\Lambda_{\rm DFD}} > 0. \tag{AR2}$$

For the DFD deep-field annulus the conformally flat spatial metric gives positive angular Ricci curvature; its radial component vanishes. Any such floor is *not* the hadronic QCD confinement scale and *not* a proof of the Clay Millennium problem [189]. It is nevertheless structurally important: the same scalar-loading mechanism that drives DFD optical gravity and galactic dynamics also changes the infrared spectrum seen by spatial Yang–Mills fluctuations.

1. Purpose

The question is whether DFD generates a native Yang–Mills infrared gap once Yang–Mills fields are placed on the loaded DFD spatial frame rather than on an empty mathematical background. It does, under an explicit and checkable geometric condition: the loaded frame must supply a positive lower bound for the physical transverse fluctuation operator. In empty Euclidean space the Yang–Mills magnetic energy is only the ordinary kinetic energy $E_{\rm YM}[A] = \frac{1}{2g^2}\int_{\mathbb{R}^3} |F_A|^2\, \mathrm{d}^3x$, and positivity of this stiffness alone does not imply a mass gap. Here gauge fields sit on $h_\psi = e^{2\alpha\psi}\delta$, and the curvature of this loaded frame enters the Hodge–Weitzenböck decomposition for one-form fluctuations.

2. DFD-native arena

Let G be a compact simple gauge group with Lie algebra $\mathfrak{g}$, and let $\Omega \subset \mathbb{R}^3$ be a bounded spatial domain. The DFD-loaded spatial frame is $\Sigma_\psi = (\Omega, h_\psi)$ with $h_{\psi,ij} = e^{2\alpha\psi(x)}\delta_{ij}$, where α is the fine-structure constant and ψ the DFD optical scalar. A gauge field is a connection one-form $A \in \Omega^1(\Omega, \mathfrak{g})$ with curvature $F_A = dA + A \wedge A$, and the spatial Yang–Mills energy on the loaded frame is

$$E_{\text{YM},\psi}[A] = \frac{1}{2g^2}\int_\Omega |F_A|^2_{h_\psi}\, \mathrm{dvol}_{h_\psi}\,. \tag{AR3}$$

Writing $A = A_0 + a$ about a reference background A_0, the fluctuation a is restricted to the physical transverse sector $d^*_{A_0} a = 0$, with elliptic boundary conditions removing pure-gauge and harmonic zero modes (without which no positive first nonzero physical eigenvalue can be stated).

Definition AR.1 (DFD-native Yang–Mills infrared gap)**.** A DFD-native Yang–Mills infrared gap is a positive lower bound for the first nonzero physical eigenvalue of the spatial Yang–Mills fluctuation operator on (Ω, h_ψ): $\lambda_1(\mathcal{L}_{A_0,\psi}) \geq \Lambda_{\rm DFD} > 0$, with associated infrared mass scale $m_{\text{DFD-YM}} = \sqrt{\lambda_1}$.

3. Fluctuation operator

The Yang–Mills Hessian around A_0 has the standard covariant form $\mathcal{L}_{A_0,\psi} a = d^*_{A_0} d_{A_0} a + d_{A_0} d^*_{A_0} a + \mathcal{R}_{A_0} a$, where $\mathcal{R}_{A_0}$ is the algebraic nonabelian curvature term from linearization. On the physical transverse sector $d^*_{A_0} a = 0$,

$$\langle a, \mathcal{L}_{A_0,\psi} a\rangle = \|d_{A_0} a\|^2 + \langle a, \mathcal{R}_{A_0} a\rangle. \tag{AR4}$$

For one-forms on a Riemannian three-manifold, the Hodge–Weitzenböck identity [130, 190] gives $\Delta_{\rm Hodge} a =$

$\nabla^*\nabla a + \mathrm{Ric}_{h_\psi}(a)$, equivalently at the quadratic-form level

$$\|da\|^2 + \|d^*a\|^2 = \|\nabla a\|^2 + \int_\Omega \mathrm{Ric}_{h_\psi}(a,a)\,\mathrm{dvol}_{h_\psi} \quad \text{(AR5)}$$

up to boundary terms that vanish under the chosen elliptic conditions. Thus the Ricci curvature of the DFD-loaded spatial frame enters the physical Yang–Mills fluctuation operator as a zeroth-order stiffness contribution.

4. Main theorem

Assumption AR.2 (DFD physical-sector curvature floor)**.** There exists a constant $\Lambda_{\mathrm{DFD}} > 0$ such that every physical transverse fluctuation a obeys $\mathrm{Ric}_{h_\psi}(a,a) + \mathcal{R}_{A_0}(a,a) \geq \Lambda_{\mathrm{DFD}}|a|^2_{h_\psi}$.

Theorem AR.3 (DFD-loaded-frame Yang–Mills infrared gap)**.** *Let (Ω, h_ψ) be a bounded DFD-loaded spatial frame with $h_\psi = e^{2\alpha\psi}\delta$, and let $\mathcal{L}_{A_0,\psi}$ be the Yang–Mills fluctuation operator on physical transverse one-form fluctuations satisfying $d^*_{A_0}a = 0$, with boundary/gauge conditions removing pure-gauge and harmonic zero modes. If Assumption AR.2 holds, then $\lambda_1(\mathcal{L}_{A_0,\psi}) \geq \Lambda_{\mathrm{DFD}} > 0$, and therefore $m_{\text{DFD-YM}} = \sqrt{\lambda_1} \geq \sqrt{\Lambda_{\mathrm{DFD}}} > 0$.*

Proof. For physical transverse fluctuations $\langle a, \mathcal{L}_{A_0,\psi}a\rangle = \|d_{A_0}a\|^2 + \langle a, \mathcal{R}_{A_0}a\rangle$. The covariant Hodge–Weitzenböck decomposition writes the kinetic part as a nonnegative covariant-gradient contribution plus the loaded-frame Ricci contribution; after physical-sector projection and boundary-term removal,

$$\langle a, \mathcal{L}_{A_0,\psi}a\rangle \geq \int_\Omega \left[\,\mathrm{Ric}_{h_\psi}(a,a) + \mathcal{R}_{A_0}(a,a)\right]\mathrm{dvol}_{h_\psi}\,. \quad \text{(AR6)}$$

By Assumption AR.2 the integrand is $\geq \Lambda_{\mathrm{DFD}}|a|^2_{h_\psi}$, so $\langle a, \mathcal{L}_{A_0,\psi}a\rangle \geq \Lambda_{\mathrm{DFD}}\|a\|^2$. By the Rayleigh–Ritz characterization of the first nonzero physical eigenvalue, $\lambda_1 = \inf_{a\perp\ker\mathcal{L},\, a\neq 0}\langle a, \mathcal{L}_{A_0,\psi}a\rangle/\|a\|^2 \geq \Lambda_{\mathrm{DFD}}$, hence $m_{\text{DFD-YM}} = \sqrt{\lambda_1} \geq \sqrt{\Lambda_{\mathrm{DFD}}} > 0$. □

5. Deep-field DFD specialization

In the DFD deep-field branch the scalar profile in a galactic annulus is logarithmic, $\psi(r) = \psi_0 - B\ln(r/r_0)$ with $B = \frac{2}{c^2}\sqrt{GMa_0}$, and the loaded spatial metric is $h_{ij} = e^{2\alpha\psi}\delta_{ij}$. For this conformally flat geometry the main text records $\mathrm{Ric}_{\theta\theta} = B\alpha(2 - B\alpha)$, $\mathrm{Ric}_{rr} = 0$, so for $0 < \alpha B < 2$ the angular Ricci curvature is positive. The angular curvature corresponds to a mass scale far below the hadronic QCD scale and below the $\sim \pi\hbar c/R$ gap that a bounded domain of size R has without it.

6. Why this supports DFD

The same scalar field ψ appears in three places: (i) optical gravity through the refractive index $n = e^{\psi}$; (ii) galactic dynamics through the deep-field scalar profile; and (iii) gauge-sector infrared behaviour through the loaded spatial frame $h_\psi = e^{2\alpha\psi}\delta$. Ordinary Yang–Mills theory on an empty background has no such geometric input; on the stated scalar-loaded frame the curvature contributes to the gauge fluctuation spectrum. This is not decisive empirical proof, but evidence of internal coherence and structural compression: one scalar-loading mechanism organizes optical gravity, galactic phenomenology, and a curvature term in the gauge fluctuation spectrum.

7. Scope and non-claims

The theorem deliberately does not make three stronger claims (Table CXVII).

8. Falsifiers and completion checks

The theorem is mathematical, but the DFD application has concrete checks: (i) *operator check* — derive the exact Hessian $\mathcal{L}_{A_0,\psi}$ for the DFD-loaded domain and verify the sign of $\mathcal{R}_{A_0}$ on the physical sector; (ii) *projection check* — verify the boundary/gauge conditions remove pure-gauge, radial, and harmonic zero modes in the deep-field annulus; (iii) *spectrum check* — numerically compute λ_1 for realistic DFD backgrounds; (iv) *physics check* — confirm that any geometric floor lies far below QCD and does not contaminate hadronic mass physics. The theorem is complete as a conditional spectral theorem; the DFD phenomenological specialization is testable by computing the physical-sector operator on explicit backgrounds.

9. Conclusion

DFD's native Yang–Mills gap is a spatial-frame result: gauge fields are placed not on empty $\mathbb{R}^3$ but on $h_\psi = e^{2\alpha\psi}\delta$, and the Hodge–Weitzenböck identity contributes the loaded-frame Ricci tensor into the physical fluctuation operator. When the resulting physical-sector curvature floor is positive, $\lambda_1 \geq \Lambda_{\mathrm{DFD}} > 0$ and hence $m_{\text{DFD-YM}} > 0$. This is not a replacement for nonperturbative QCD confinement (which DFD treats as the generator-closed lattice sector of Apps. AQ and AS); it is a conditional infrared-gap theorem on the loaded spatial frame.

TABLE CXVII. Status discipline for the DFD-native Yang–Mills infrared gap.

Statement	Status
DFD-loaded spatial Yang–Mills has a positive geometric infrared floor when the physical-sector curvature floor is positive.	Proved here (Thm. AR.3).
The deep-field DFD annulus supplies positive angular Ricci curvature for $0 < \alpha B < 2$.	DFD deep-field specialization.
The expected galactic scale is tiny, around 10^{-30} eV.	Curvature term only; the bounded domain alone gives a larger gap.
This proves the Clay pure Yang–Mills mass gap.	Not claimed.
This analytically derives all hadron masses.	Not claimed.
Nonperturbative QCD remains computable from the Euclidean/lattice path-integral generator (Apps. AQ, AS).	DFD-QFT generator-closed sector.

Appendix AS: Lattice Boundary Program: Staged Execution and Provenance (Programs I–II)

The validated lattice results of Appendix AQ ("Program II") were reached through a deliberately staged execution, recorded here for provenance and to document the status discipline applied at each rung. The lineage is Program I (frozen inputs, smoke test, unquenched scaffold) → Program I-A (first executed quenched 16^4 string-tension runs) → Program II (consolidated 16^4 and 20^4 string tension, 0^{++} glueball, and validated $N_f = 2$ Wilson-HMC). At no stage was a laptop-scale calculation presented as continuum-extrapolated, physical-point QCD.

1. Program I: frozen inputs, smoke test, unquenched scaffold

Program I established the four-stage methodology that the later rungs inherit. *Stage 1* froze the DFD QCD ledger (the same targets used throughout Apps. AQ–AS: $\alpha_s(M_Z) = 0.1187$, $\bar{\theta} = 0$ at tree level, $\sqrt{\sigma}_{\rm DFD} = 440 \pm 25$ MeV, $m_{0^{++}}^{\rm DFD} = 1.69 \pm 0.10$ GeV, $f_\pi^{\rm DFD} = 92.0 \pm 4.6$ MeV). *Stage 2* audited the analytic nonperturbative targets (string tension, lightest scalar glueball, low-energy chiral scales) against the generator-closed-sector statement. *Stage 3* executed a small pure-gauge $SU(3)$ Wilson-action Metropolis smoke test on 4^4 lattices at $\beta = 5.4, 5.6, 5.8$, measuring plaquettes, small Wilson loops, an effective potential, and a crude string-slope proxy. *Stage 4* specified — without executing — the unquenched dynamical-fermion HMC bridge, enumerating the Dirac-operator, pseudofermion, molecular-dynamics, and accept/reject steps required for a production run.

The Stage-3 4^4 smoke test was explicitly a code-path verification, not a physics result: at such a tiny volume and with limited thermalization the plaquette values were not at their infinite-volume benchmarks, and the "string-slope proxy" $V_{\rm eff}(2) - V_{\rm eff}(1)$ was a placeholder, not a fitted string tension. Program I's conclusion was therefore that the DFD QCD sector had been moved from "generator exists" to "generator has an executable boundary-program prototype" — with the production rung still to come. The Stage-4 scaffold is the exact specification that was later implemented and validated as the $N_f = 2$ Wilson-HMC engine of Appendix AQ.

2. Program I-A: first executed quenched 16^4 string tension

Program I-A consists of executed, production-grade quenched pure-gauge $SU(3)$ runs on 16^4 lattices at $\beta = 5.8, 6.0, 6.2$ (a 4^4 smoke test is not used as physics). The plaquette benchmark was reproduced to better than 0.1% at all three couplings, and APE-smeared Wilson loops with effective-potential plateaus and Cornell fits gave

$$\sqrt{\sigma}\, a = (0.3292,\ 0.2171,\ 0.1623), \tag{AS1}$$

$$r_0\sqrt{\sigma} = (1.206,\ 1.165,\ 1.198), \tag{AS2}$$

i.e. $\sqrt{\sigma} = 476 \pm 15$, 460 ± 7, and 473 ± 7 MeV at $r_0 = 0.5$ fm, for a best quenched estimate $\sqrt{\sigma} = 470 \pm 10$ MeV. This overlaps the DFD ledger target $\sqrt{\sigma}_{\rm DFD} = 440 \pm 25$ MeV at its upper edge, with the residual assigned to quenching and scale-setting convention.

These three 16^4 points are precisely the $\beta = 5.8$, 6.0, 6.2 16^4 rows subsequently consolidated in Table CXIV of Appendix AQ; they are not re-tabulated here. Program II then added the decisive refinements that Program I-A flagged as "next rung": the 20^4 box-size check at $\beta = 6.2$ (which confirmed the expected positive finite-volume bias of the 16^4 fine-end point and moved $r_0\sqrt{\sigma}$ from 1.198 to 1.178), the autocorrelation re-analysis of the error budget, the 0^{++} glueball estimate, and the executed $N_f = 2$ Wilson-HMC κ-scan.

3. Status across the program

The staged lineage illustrates the discipline applied throughout the DFD QCD sector: scale-free dimensionless ratios are the primary outputs; MeV values are quoted only with an explicit external scale; finite-volume, single-spacing calculations are consistency checks rather than physical-point determinations; and results that fail this discipline (the 4^4 smoke test, the un-error-inflated glue-

ball) are not used. The consolidated, validated outcome of this program is the content of Appendix AQ, and its analytic gauge-sector companion is the infrared-gap theorem of Appendix AR.

Appendix AT: Cross-Sector Exact Identities, Strong-Field Theorems, and New Predictions

This appendix collects results derived inside the DFD axiom system that were not tabulated in the body. Throughout we use the locked ledger values $\alpha^{-1} = 137.036$, $M_P = 1.220890 \times 10^{19}$ GeV, $v = M_P\,\alpha^8\sqrt{2\pi} = 246.09$ GeV, $\Lambda_{\rm DFD} = M_P\,\alpha^{19/2} = 61.20$ MeV, $\Lambda^{(5)}_{\overline{\rm MS}} = \sqrt{4\pi}\,\Lambda_{\rm DFD} = 216.95$ MeV, $M_R = M_P\,\alpha^3 = 4.744 \times 10^{12}$ GeV, and $m_3 = \frac{14}{13}\pi M_P\,\alpha^{14} = 50.16$ meV (App. Z, X). Every exact identity below was verified symbolically and to ≥ 20 digits in arbitrary-precision arithmetic.

1. Exact cross-sector identities

Proposition AT.1 (Seesaw-triangle closure, (E))**.** *Given the stated rung $y_D^2 = F_\nu\alpha$ of the Dirac neutrino Yukawa (one discrete input), the priming factor fixes it to the exact value*

$$y_D^2 = \frac{14}{13}\,\alpha = \Big(1 + \frac{\sin^2\theta_W}{N_{\rm gen}}\Big)\alpha, \tag{AT1}$$

with $\sin^2\theta_W = 3/13$ and $N_{\rm gen} = 3$, and the seesaw then fixes m_3. The neutrino absolute-scale exponent 14 follows from the rung and is not a further postulate.

Proof. The Type-I seesaw gives $y_D^2 = 2m_3M_R/v^2$. Substituting the printed scales, $y_D^2 = 2\big(\frac{14}{13}\pi M_P\alpha^{14}\big)\big(M_P\alpha^3\big)/\big(M_P^2\alpha^{16}\,2\pi\big) = \frac{14}{13}\,\alpha^{14+3-16} = \frac{14}{13}\,\alpha$, the π's cancelling against the $\sqrt{2\pi}$ of v. The second form follows from $1 + \frac{1}{N_{\rm gen}}\sin^2\theta_W = 1 + \frac{1}{3}\cdot\frac{3}{13} = \frac{14}{13}$, so the neutrino Yukawa and the weak mixing angle share the denominator 13. Equivalently the Dirac mass is the seesaw geometric mean $m_D = \sqrt{m_3M_R} = 15.43$ GeV $= \sqrt{14\alpha/13}\,v/\sqrt{2}$. □

Proposition AT.2 (Four-sector scale lock, (E))**.** *The QCD, gravitational, electroweak, and neutrino scales satisfy*

$$2\pi\,M_P\,\Lambda_{\rm DFD}^2 = v^2\,M_R, \tag{AT2}$$

exactly, with no constant other than the 2π inherited from v.

Proof. $v^2M_R = (M_P^2\alpha^{16}\,2\pi)(M_P\alpha^3) = 2\pi M_P^3\alpha^{19}$, while $2\pi M_P\Lambda_{\rm DFD}^2 = 2\pi M_P(M_P\alpha^{19/2})^2 = 2\pi M_P^3\alpha^{19}$. The equality encodes the exponent identity $2\cdot\frac{19}{2} = 16 + 3 = 19$. □

Proposition AT.3 (QCD–Majorana cube identity, (E))**.** *With the microsector matching scale $\Lambda_{\rm top} = \sqrt{\alpha}\,M_P$,*

$$M_R^3 = \frac{\Lambda_{\rm DFD}\,M_P^3}{\Lambda_{\rm top}}, \tag{AT3}$$

exactly, with prefactor unity.

Proof. $\Lambda_{\rm DFD}M_P^3/\Lambda_{\rm top} = (M_P\alpha^{19/2})M_P^3/(\alpha^{1/2}M_P) = M_P^3\alpha^9 = (M_P\alpha^3)^3 = M_R^3$, encoding $3\cdot3 = \frac{19}{2} - \frac{1}{2} = 9$. □

Proposition AT.4 (QCD–Hubble bridge, (E))**.** *The Hubble energy carries the measured clock coefficient multiplying the cube of the confinement scale over the Planck mass squared,*

$$\hbar H_0 = \sqrt{C}\,\frac{\Lambda_{\rm DFD}^3}{M_P^2}\,c^2, \tag{AT4}$$

a consequence of $57 = 6\cdot\frac{19}{2} = 3\cdot 19$ *and the printed invariant* $G\hbar H_0^2/c^5 = C\alpha^{57}$ *(exponent derived; C measured; App. O). On bound-matter clocks, where* $C = 1$ *(Postulate ZS.11), the bridge holds with no measured factor,* $\hbar H_0^{\rm loc} = \Lambda_{\rm DFD}^3 c^2/M_P^2$.

Proof. From $G\hbar H_0^2/c^5 = C\alpha^{57}$ and $t_P = \sqrt{G\hbar/c^5}$ one has $H_0 = \sqrt{C}\,\alpha^{57/2}/t_P$, hence $\hbar H_0 = \sqrt{C}\,(\hbar/t_P)\alpha^{57/2} = \sqrt{C}\,M_P c^2\,\alpha^{57/2}$ since $\hbar/t_P = \sqrt{\hbar c^5/G} = M_P c^2$. On the other side $\Lambda_{\rm DFD}^3/M_P^2\cdot c^2 = (M_P\alpha^{19/2})^3/M_P^2\cdot c^2 = M_P c^2\,\alpha^{57/2}$, using $3\cdot\frac{19}{2} = \frac{57}{2}$. Equivalently the heaviest neutrino is the α-primed geometric mean of the Hubble rate and the Planck mass, $m_3 = \frac{14}{13}\pi C^{-1/4}\sqrt{\hbar H_0\,M_P}\,\alpha^{-1/4}$ (from $\frac{57}{4}-\frac{1}{4}=14$). □

Proposition AT.5 (Strange-quark mass as a rung fraction, (E))**.** $m_s = \frac{3}{7}\,\Lambda_{\overline{\rm MS}}^{(5)}$ *exactly (a pure rational), and more generally every charged-fermion mass can be written in the closed form* $m_f = (\textit{rational}\times 2\textit{-power})\,\Lambda_{\overline{\rm MS}}^{(5)}\,\alpha^k$.

Proof. $m_s = \frac{6}{7}\alpha^{3/2}\,v/\sqrt{2} = \frac{6}{7}\sqrt{\pi}\,M_P\alpha^{19/2}$ while $\Lambda_{\overline{\rm MS}}^{(5)} = 2\sqrt{\pi}\,M_P\alpha^{19/2}$, so the ratio is $\frac{6}{7}/2 = \frac{3}{7}$; α and π cancel identically. The same equal-exponent mechanism gives the pure-number ratios $m_\tau/m_c = \sqrt{2}$, $m_t/m_b = 42$ (compared with the top pole mass over $m_b(m_b)$; at one scale, M_t, the observed ratio is 59.7), $m_e/m_d = 1/9$, $m_\mu/m_s = 7/6$, with the down-type prefactor integers $7 = b_0$ and $36 = N_f^2$ reappearing verbatim from the QCD running. □

Proposition AT.6 (The thermal variable *is* the refractive scalar, (E))**.** *Let* $\tau \equiv \sqrt{g_{\rm bar}/a_{\rm ref}}$ *be the dimensionless variable of the occupation reading of* ν*, and take its reference acceleration to be DFD's own derived surface gravity* $\kappa_{\rm DFD} = c^4/(4GM)$ *(App. AH of the companion volume, the Hawking-temperature theorem) rather than the galactic* a_0*. Then, for every mass,*

$$\begin{aligned} r_M &\equiv \sqrt{GM/\kappa_{\rm DFD}} = \frac{2GM}{c^2} = r_s, \\ \tau(r) &\equiv \sqrt{g_{\rm bar}(r)/\kappa_{\rm DFD}} = \frac{r_s}{r} = \psi(r), \end{aligned} \tag{AT5}$$

with $\psi(r) = 2GM/(c^2 r)$ *the exterior solution (147) of Sec. VI A, exact through second order in* $GM/(c^2 r)$*. In particular* $\tau = 1$ *at* $r = r_s = 2GM/c^2$ *for* every *mass.*

Proof. $\sqrt{GM/\kappa_{\rm DFD}} = \sqrt{GM\cdot 4GM/c^4} = 2GM/c^2 = r_s$, and $\sqrt{(GM/r^2)/\kappa_{\rm DFD}} = r_M/r = r_s/r$, which is the printed $\psi(r)$. Setting $r = r_s$ gives $\tau = 1$. All four residuals $(r_M - r_s,\ \tau - r_s/r,\ \tau - \psi,\ \tau(r_s) - 1)$ are identically zero symbolically. □

Remark AT.7 (What Prop. AT.6 buys). DFD's statistical-mechanical variable and its optical variable are the *same function* once the reference acceleration is the theory's own surface gravity. It therefore links the galactic sector ($\tau = \sqrt{g_{\rm bar}/a_0}$) to the refractive scalar ($\tau = \psi$ through second order) by a change of reference scale *only*, and it makes "$\tau = 1$ at $r = r_s$" a theorem rather than a coincidence. It introduces no new integer and no new constant.

Proposition AT.8 (Unruh–Gibbons–Hawking ratio, (E))**.** *With* $a_0 = 2\sqrt{\alpha}\,cH_0$ *read on the same clock (Thm. N.14, App. N), the Unruh temperature of the MOND scale and the de Sitter Gibbons–Hawking temperature of the cosmic horizon stand in the exact ratio*

$$\frac{T_U(a_0)}{T_{\rm GH}} = \frac{\hbar a_0/(2\pi c k_B)}{\hbar H_0/(2\pi k_B)} = \frac{a_0}{cH_0} = 2\sqrt{\alpha} = 0.1708490862, \tag{AT6}$$

with no numerical constant of any kind surviving: the two 2π*'s cancel identically. The DFD crossover scale is therefore the cosmic horizon scale reduced by exactly one factor of* $2\sqrt{\alpha}$*, the same factor that appears in* a_0 *itself.*

Proof. Immediate substitution; the ratio is $a_0/(cH_0)$ and $a_0 \equiv 2\sqrt{\alpha}\,cH_0$. The sympy residual of $T_U/T_{\rm GH} - 2\sqrt{\alpha}$ is identically zero. Numerically, $2\sqrt{\alpha} = 0.170849086206$ at CODATA-2022 $\alpha^{-1} = 137.035999177$ and 0.170849086264 at CODATA-2018 $\alpha^{-1} = 137.035999084$ — a fractional difference of 3.4×10^{-10}, so the identity is insensitive to the CODATA release at any relevant precision. □

2. Strong-field and gravitational results

With the parent strain's σ kept the strong-field exterior is the Schwarzschild metric in DFD's coordinates, and Kerr's for a spinning hole (App. WS; argued beyond first order in the spin), so its innermost stable orbit, photon ring, redshift and quasinormal modes are those of general relativity: at zero spin the innermost stable circular orbit sits at the areal radius $6GM/c^2$ with accretion efficiency $1-\sqrt{8/9} = 5.719\%$, and the photon sphere at $3GM/c^2$. This subsection collects the gravitational-wave memory and the Cole–Hopf lapse family.

Proposition AT.9 (Tensor gravitational-wave memory equals GR's, (D))**.** *The transverse-traceless sector is governed by the full nonlinear* a_2 *Seeley–DeWitt Einstein–Hilbert term (Sec. V A 4); the action* S_h *of Sec. II is its quadratic part. DFD's tensor-channel gravitational-wave memory therefore equals GR's: the linear (ordinary) memory sourced by the matter stress, plus the nonlinear (Christodoulou) memory sourced by the gravitational-wave stress-energy. The grade is Derived: the result rests on reading the spectral* a_2 *zero mode as the full Einstein–Hilbert invariant, on the grounds given below.*

Derivation. Four grounds fix the reading of the a_2 zero mode as the full Einstein–Hilbert invariant rather than its

linearized Hessian. (i) The corpus names the TT action the a_2 Seeley–DeWitt Einstein–Hilbert term (Sec. V A 4; App. SM; Subsec. O 5). (ii) The zero-mode projection keeps the cubic vertex: the constant internal zero mode $Y_0 = V_K^{-1/2}$ gives $\int_K Y_0^3 = V_K^{-1/2} \neq 0$ (Rem. AT.10). (iii) With the parent strain's σ kept, the physical metric near every compact source solves the nonlinear Einstein–Hilbert equations in DFD's coordinates (App. WS), Schwarzschild's outside a static source and Kerr's around a spinning hole (argued beyond first order in the spin), solutions that no exactly quadratic action has, so the TT sector there is nonlinear Einstein–Hilbert. (iv) The linearized-Hessian alternative, on which S_h would be exactly quadratic and the Christodoulou memory would vanish, has no printed mechanism: no corpus object removes the cubic and higher vertices of the a_2 term. On the full term $\partial^3 S/\partial h^3 \neq 0$, so the gravitational-wave stress-energy sources h_{ij}^{TT} at second order as in GR, and the memory is GR's flux integral. □

Remark AT.10 (Channel scope). Prop. AT.9 concerns the *tensor* channel: it rests on the cubic Einstein–Hilbert vertex of the TT sector, independent of whether the scalar ψ radiates. A possible *scalar-channel* memory contribution is a separate question: for quasi-circular BBH inspirals the ψ-sector sourcing is rigorous and negligible, while the general (e.g. head-on/burst) scalar case is open pending the far-zone non-radiativeness analysis of the ψ sector. Where the corpus elsewhere writes a c-speed d'Alembertian for ψ, that form is the numerical hyperbolic-relaxation of the elliptic AQUAL constraint, not an independent claim that ψ radiates at c. The spectral a_2 zero mode carries the full Einstein–Hilbert invariant (Sec. V A 4; Proposition WS.5), not only its linearized Hessian, the "standard linearized action" of Sec. II, on which $\partial^3 S/\partial h^3 \equiv 0$ and the Christodoulou memory would vanish. On the full invariant the constant internal zero mode $Y_0 = V_K^{-1/2}$ is closed under products ($\int_K Y_0^3 = V_K^{-1/2} \neq 0$) and the cubic vertex survives the zero-mode projection: for $h_{ij} = \epsilon\, q(t)\,\mathrm{diag}(1,1,-2)$ the kinetic density is $\frac{3}{2}\epsilon^2\dot{q}^2 + 3\epsilon^3 q\dot{q}^2 + O(\epsilon^4)$, and the nonlinear tensor memory of the standard flux form follows, equal to GR's. Separately, the local-relativity coefficient $A(\psi) = F\,e^{2\psi}$ of the TT kinetic term (Rem. V.1) carries the cubic vertex $\psi(\partial_t h_{ij}^{\mathrm{TT}})^2$, so GW energy sources the elliptic ψ at $O(h^2)$ whether or not ψ radiates: the scalar-channel contribution named above is a second-order non-radiative response of the coupled (ψ, h) system, and Gauss's law fixes it. The outgoing shell of wave energy carries the monopole the source loses, so outside the shell ψ is unchanged; after the shell passes a detector at distance r the response is the pure-trace term $\delta\psi = -(2GE_{\mathrm{GW}}/c^4)(1/r - 1/ct)$, which changes both arms of an interferometer and all nearby clocks together, and the anisotropy of the shell leaves a tidal part suppressed by $(L/r)^2$. The scalar channel adds no memory for any source.

Falsifier AT.11 (Gravitational-wave memory). For an equal-mass nonspinning merger GR's null memory is 27% of the edge-on strain peak, and DFD's tensor memory is the same (Prop. AT.9). A memory measurement consistent with zero where GR predicts this 27% falsifies DFD; a detection at the GR level does not distinguish DFD from GR. LISA reaches single-event memory SNR 11–35 for 10^5–$10^6\,M_\odot$ at $z = 1$.

Proposition AT.12 (Cole–Hopf lapse family, (E/T))**.** *The substitution $\chi = e^{k\psi/2}$ linearises the acceleration equation $\nabla\cdot\mathbf{a} + (k/c^2)\mathbf{a}^2 = -4\pi G\rho$ (with $\mathbf{a} = (c^2/2)\nabla\psi$) to $\nabla^2\chi = -(4\pi Gk/c^2)\rho\,\chi$. Its point-mass exterior is the one-parameter family $n_k(u) = (1+ku)^{2/k}$, with $\beta(k) = 1 + k/2$, $\gamma(k) = 1$, and $k \to 0$ recovering the exponential e^{2u}, DFD's lapse-squared through second order in u. The GR isotropic lapse-squared is the exact geometric mean of the $k = \pm\frac{1}{2}$ members.*

Proof. Writing $\mathbf{a} = (c^2/2)\nabla\psi$ turns the equation into $\nabla^2\psi + (k/2)|\nabla\psi|^2 = -(8\pi G/c^2)\rho$; with $\chi = e^{k\psi/2}$, $\nabla^2\chi = (k/2)\chi[\nabla^2\psi + (k/2)|\nabla\psi|^2]$, the stated linear equation. The vacuum solution $\chi = 1 + kGM/(c^2 r)$ gives $n_k = (1+ku)^{2/k}$; expanding the optical metric yields $\beta = 1 + k/2$. Lunar laser ranging ($\beta - 1 = (-4.5 \pm 5.6)\times 10^{-5}$) pins the vacuum member to $k = (-0.9 \pm 1.1)\times 10^{-4}$ – gravity sits at $k = 0$ to one part in 10^4. □

3. Compact-star structure

Theorem AT.13 (Compact-star structure, (T))**.** *Varying the matter action of a perfect fluid minimally coupled to the physical metric (Sec. II, App. AN) with respect to ψ uniquely fixes the relativistic source: in the $\mu \to 1$ regime the static structure obeys*

$$\partial_i\left[(e^{-h})^{ij}\partial_j\psi\right] = -\frac{8\pi G}{c^4}\,(\varepsilon + 3P)\,e^{\psi}, \qquad \frac{dP}{dr} = \tfrac{1}{2}(\varepsilon + P)\,\frac{d\psi}{dr}, \tag{AT7}$$

with ε the energy density, P the pressure and h_{ij} the traceless part of the parent strain, whose scalar-longitudinal piece σ obeys the traceless part of the Einstein equation. The three equations are the Tolman–Oppenheimer–Volkoff system in DFD's coordinates (App. WS): for the reference $\Gamma = 2$, $K = 100$ polytrope the maximum mass is $M_{\max} = 1.637\,M_\odot$ at central density $\rho_c = 1.97\times 10^{15}\,\mathrm{g\,cm^{-3}}$, with areal radius $R(M_{\max}) = 11.3$ km, the general-relativistic values.

Proof. The point-particle Lagrangian $-mc^2 e^{-\psi/2}\sqrt{1 - e^{2\psi}v^2/c^2}$ of the physical metric gives $\partial\mathcal{L}/\partial\psi = \frac{1}{2}(\varepsilon + 3P)e^{\psi}$ on the static fluid (verified symbolically, residual 0), which is the active (Tolman) source; the lapse $e^{-\psi/2}$ gives the equilibrium relation by the standard static-fluid first integral, and the first equation is the time-time component of the trace-reversed Einstein equation for the static metric. With σ kept its equation and the spatial identity of App. WS give general relativity's Hamiltonian constraint, so the system is the

TOV system; integrating it for the reference polytrope gives the quoted values (computed, in DFD's coordinates and directly from the TOV equations, agreeing to better than 10^{-8}). The reduction $\nabla^2\psi = -(8\pi G/c^2)\rho$ (Sec. IV) is recovered in the nonrelativistic limit $P \ll \varepsilon$, $\psi \ll 1$. □

Reproducibility Note. The stellar-structure integrations reported here shoot the central scalar value ψ_c so that the exterior solution satisfies asymptotic flatness, $\psi(\infty) = 0$ and $n(\infty) = 1$. Holding ψ_c fixed instead computes a non-asymptotically-flat normalization and can produce spurious runaway behavior. Radii quoted in this subsection are areal (circumferential) radii, not raw coordinate radii. An independent integration of the TOV equations confirms the quoted values: $M_{\max} = 1.637\,M_\odot$ at $\rho_c \simeq 1.97 \times 10^{15}\,\mathrm{g\,cm^{-3}}$, with areal radius 11.27 km. With σ set to zero the first two equations alone give $1.474\,M_\odot$, and that truncation fails the Hamiltonian constraint inside the star (App. WS).

4. Deep-sector conformal theorems

In the deep-field regime the energy functional is the cubic $E = \frac{c^4}{16\pi G a_\star}\int \frac{1}{3}|\nabla\psi|^3 - \frac{c^2}{2}\int\rho\psi$.

Theorem AT.14 (Conformal structure and the exact M–σ relation, (T))**.** *The deep-field functional is invariant under the full conformal group of $\mathbb{R}^3$ plus a ψ-shift (11 generators) and has identically traceless stress tensor. A point mass carries dilatation (anomaly) charge $Q(m) = \frac{2}{3}\sqrt{Ga_0}\,m^{3/2}$, the two-body force is $F = \frac{2}{3}(\sqrt{Ga_0}/\ell)\,[(m_1+m_2)^{3/2} - m_1^{3/2} - m_2^{3/2}] \propto 1/\ell$, and any stationary isolated deep system obeys the exact isotropic relation*

$$\sigma_{\rm los}^4 = \frac{4}{81}\,GMa_0, \tag{AT8}$$

together with the baryonic Tully–Fisher law $v_f^4 = GMa_0$ with coefficient exactly unity.

Proof. Tracelessness $\sigma_{ii} = 0$ off-shell and conservation $\partial_j\sigma_{ij} = 0$ on-shell are verified directly for the cubic Lagrangian; the dilatation current of the conformally invariant 3-Laplacian integrates to the stated point charge. The virial identity $\sum_i \mathbf{x}_i\cdot\mathbf{F}_i = \sum_i Q(m_i) - Q(M)$ for a self-bound system gives $2T = \frac{2}{3}\sqrt{Ga_0}\,M^{3/2}$, hence the isotropic $\sigma_{\rm los}^4 = (4/81)GMa_0$; and $v_f^2 = dQ/dM = \sqrt{GMa_0}$ gives BTFR with unit coefficient. Dwarf-spheroidal checks at the stellar masses of Tab. XIV: Leo I $\sigma_{\rm los} = 8.55$ (obs ≈ 9.2), Fornax 12.17 (obs ≈ 11.7). □

Corollary AT.15 (Golden-ratio phantom mass, (T))**.** *At the MOND radius $r_M = \sqrt{GM/a_0}$ (where $g_{\rm bar} = a_0$), the radial acceleration relation $g_{\rm obs} = \frac{1}{2}[g_{\rm bar} + \sqrt{g_{\rm bar}^2 + 4g_{\rm bar}a_0}]$ forces, on the weak-response approximant, the enclosed dynamical mass to be the golden ratio times the baryonic (the derived exponential response gives $1/(1-e^{-1}) = 1.582$): $M_{\rm dyn}(<r_M)/M = \varphi = 1.6180\ldots$, with phantom fraction $1/\varphi$.*

Proof. At $g_{\rm bar} = a_0$ the relation gives $g_{\rm obs} = a_0(1+\sqrt{5})/2 = \varphi\,a_0$; since $M_{\rm dyn} \propto g_{\rm obs}$ and $M \propto g_{\rm bar}$ at fixed r_M, the ratio is φ identically. □

The Kuzmin-disk family solves the *full* nonlinear DFD field equation exactly, $g = \nu(|g_N|/a_0)\,g_N$ with $\nu(y) = \frac{1}{2}[1+\sqrt{1+4/y}]$ and $v_{\rm flat}^4 = GMa_0$, providing an integrable thin-disk benchmark.

5. Strong-CP protection and the neutron electric dipole

Theorem AT.16 (Determinant-phase protection for every value of the offset, (T))**.** *Let $M_f(\xi) = S_f + i\xi T_f$ be the up- or down-sector mass matrix of Postulate Y.10 (App. AO), with S_f real symmetric and T_f real antisymmetric. Then $\det M_f(\xi)$ is real for all real ξ (and all orders in ξ), so $\arg\det M_f(\xi) \in \{0,\pi\}$, equal to 0 wherever $\det M_f > 0$ (in particular on the component of $\{\det M_f \neq 0\}$ containing $\xi = 0$ when $\det S_f > 0$); the offset that supplies the weak CP phase never regenerates a continuous strong-CP angle at tree level.*

Proof. $S_f^{\mathsf T} = S_f$ and $T_f^{\mathsf T} = -T_f$ give $M_f(\xi)^{\mathsf T} = S_f - i\xi T_f = \overline{M_f(\xi)}$ (overbar = complex conjugate, since S_f, T_f, ξ real). Hence $\det M_f = \det M_f^{\mathsf T} = \det\overline{M_f} = \overline{\det M_f}$, so $\det M_f$ is real and $\arg\det M_f = 0$ wherever it is positive. This holds to all orders in ξ, beyond the first-order (trace-form) statement of App. AO. □

Corollary AT.17 (Neutron-EDM ledger and falsifier, (P))**.** *With $\bar\theta = 0$ at tree level ($\theta_{\rm YM} = 0$ fixed by the spectral action given that nothing is added to it for the gauge fields; Theorem AT.16; App. L) and its loop-induced value at the Standard-Model level, $\lesssim 10^{-16}$ (App. AO), the DFD neutron EDM is the CKM long-distance background scaled by $J_{\rm DFD}/J_{\rm SM} = 0.94$, giving $d_n \sim (0.9\text{–}5.6)\times 10^{-32}\,e$ cm; the residual θ-channel is $\lesssim 2\times10^{-32}\,e$ cm for the upper-end induced $\bar\theta \sim 10^{-16}$ ($d_n \simeq 2.4\times10^{-16}\,\bar\theta\,e$ cm), comparable to the CKM background. DFD predicts* null *at all foreseeable sensitivities, and any measured $d_n > 10^{-30}\,e$ cm falsifies the det-orthogonal architecture (margin $\sim 10^6$ to the current bound). The same even-mapping-torus structure that closes the anomaly channel is silent on the CP-even topological susceptibility χ_t, consistent with a nonzero χ_t and the η' anomaly channel.*

6. New predictions

The following are predictions (not reformulations): each is a DFD value confronted with data and carries a look-elsewhere note.

TABLE CXVIII. New DFD predictions; the A_s row is a calibrated amplitude that $32\pi\alpha^5$ matches, not a prediction. "rung" denotes the scheme scale $\Lambda_{\rm DFD} = 61.20$ MeV or $\Lambda^{(5)}_{\overline{\rm MS}} = 216.95$ MeV (App. Z). The m_t row evaluates with the $v = 246.09$ GeV of this appendix; the muon-decay vev $v = 246.22$ GeV gives $m_t = (1-\alpha)v/\sqrt{2} = 172.83$ GeV (0.85σ).

Observable	DFD form	Predicted	Measured	Dev.
F_π	$\frac{3}{5}\Lambda_{\overline{\rm MS}}$	130.17 MeV	130.2(8) MeV	0.03%
η'	$\sqrt{39/2}\,\Lambda_{\overline{\rm MS}}$	958.0 MeV	957.78 MeV	0.02%
ω	$\sqrt{13}\,\Lambda_{\overline{\rm MS}}$	782.2 MeV	782.66 MeV	0.06%
Δ	$\sqrt{32}\,\Lambda_{\overline{\rm MS}}$	1227 MeV	1232 MeV	0.4%
Ω^-	$\sqrt{59}\,\Lambda_{\overline{\rm MS}}$	1666 MeV	1672 MeV	0.4%
$m_{0^{++}}/\sqrt{\sigma}$	$\sqrt{4\pi}$	3.545	3.529(97)	0.16σ
m_t	$(1-\alpha)v/\sqrt{2}$	172.74 GeV	172.60(27)	0.52σ
a_0	$2\alpha^{29}c/t_P$	$1.1966\,\mathrm{e}{-10}$	$1.20(2)_{\rm stat}(24)_{\rm sys}\,\mathrm{e}{-10}$	within $\sigma_{\rm sys}$
A_s (calibrated)	$32\pi\alpha^5$ (match)	$2.080\,\mathrm{e}{-9}$	$2.099(29)/2.105(30)\,\mathrm{e}{-9}$	$0.6/0.8\sigma$
$\sin^2\theta_{13}$	3α	0.0219	0.02195(58)	0.1σ

a. Topological susceptibility, Λ-free and N_f-free on the chiral-limit form (T). Two rows already in the table above satisfy an exact integer identity: $\eta' = \sqrt{39/2}\,\Lambda_{\overline{\rm MS}}$ and $\omega = \sqrt{13}\,\Lambda_{\overline{\rm MS}}$ with $39/2 = (3/2)\cdot 13$, hence the *dimensionless* DFD statement

$$m^2_{\eta'} \;=\; \tfrac{3}{2}\, m^2_{\omega}. \tag{AT9}$$

Substituted into the Witten–Veneziano relation $\chi_t = f_\pi^2 m_{\eta'}^2/(2N_f)$ at $N_f = 3$, both N_f and $\Lambda_{\overline{\rm MS}}$ cancel identically, leaving

$$\chi_t = \frac{f_\pi^2 m_\omega^2}{4}, \qquad \chi_t^{1/4} = \sqrt{\frac{f_\pi m_\omega}{2}} = 189.81 \pm 0.58 \text{ MeV}, \tag{AT10}$$

from PDG inputs alone, against the quenched lattice value 191(5) MeV: -0.24σ on this chiral-limit form; the full Witten–Veneziano relation, with $m_\eta^2 - 2m_K^2$ added to $m^2_{\eta'}$, gives 179.0 MeV, -2.4σ; both comparisons use the lattice error alone, and the relation itself holds at leading order in $1/N_c$. Evaluating instead on the DFD rows themselves gives 189.73 MeV (-0.25σ). The accuracy of the input identity is $(m_{\eta'}/m_\omega)^2 = 1.4975635$ against 3/2, low by 0.162%.

The strong-CP discussion above states only that the even-mapping-torus structure closing the anomaly channel is *silent* on the CP-even topological susceptibility. *Grade:* equation channel **derived** (N_f verifiably absent from the reduced expression); physics channel **derived-conditional** on the two catalog rows, with declared inputs f_π and m_ω. The factor 3/2 grades **selected**, not forced, until the 13 of the ω row is independently linked to the 13 of $\sin^2\theta_W = 3/13$; that identification is presently asserted, not derived. Look-elsewhere probability on the unrestricted catalog is $P = 0.262$.

Falsifier. Any continuum determination of χ_t at quenched-equivalent normalization landing below ∼185 MeV falsifies the $m^2_{\eta'} = \frac{3}{2}m^2_\omega$ row identity.

Consistency check only, not a derivation. Carrying the same chain to the pseudoscalar glueball, with the Athenodorou–Teper continuum ratios and a lattice $m_{0^{++}}/\chi_t^{1/4}$ anchor *imported* as external inputs, gives $m(0^{-+}) = 2443.5 \pm 74.8$ MeV against the BESIII $X(2370)$ measurement $2395 \pm 11\,(\text{stat})\,^{+26}_{-94}\,(\text{syst})$ MeV, i.e. $+0.61\sigma$. Because the prediction exceeds the measurement, the upward systematic is the live tail. This arm is **not** parameter-free and is not a DFD glueball-spectrum derivation.

b. Baryon decuplet (T/P). The $J = 3/2$ decuplet follows the exact integer arithmetic progression $m^2 = (32 + 9n_s)\,\Lambda^2_{\overline{\rm MS}}$ in the number of strange quarks n_s: $\Delta, \Sigma^*, \Xi^*, \Omega^-$ at $n_s = 0, 1, 2, 3$ all match within 0.4%. The progression structure (intercept 32, slope 9), not the individual hits, is the non-accidental content.

c. Baryon octet, incl. the nucleon (P). The $J = 1/2$ octet follows the companion progression

$$m^2 \;=\; (19 + 9\,n_s)\,\Lambda^2_{\overline{\rm MS}}, \tag{AT11}$$

with the *same* strange slope 9 as the decuplet and intercept $19 = h^0(\mathcal{O}(1)) + h^0(\mathcal{O}(2)) + h^0(\mathcal{O}(3)) = 3 + 6 + 10$, the $\mathbb{C}P^2$ line-bundle cohomology sum. The nucleon is then a tower state:

$$M_N = \sqrt{19}\,\Lambda_5 = \sqrt{19}\,\sqrt{4\pi}\,M_P\,\alpha^{19/2} = 946 \text{ MeV}$$
$$(\text{vs } 939,\ +0.7\%),$$

the integer 19 appearing in *both* the prefactor and the exponent. The endpoints match — N ($n_s = 0$) at +0.7% and Ξ ($n_s = 2$) at +0.1% — while the $n_s = 1$ value $\sqrt{28}\,\Lambda_5 = 1148$ MeV is the Λ–Σ *average* (within 0.5% of $(\Lambda + \Sigma)/2$); the individual $\Lambda(1116)$–$\Sigma(1193)$ splitting requires the additional isospin/Gell-Mann–Okubo term absent from the pure n_s-linear tower, which is why the spin-1/2 octet (+0.7%) is intrinsically less clean than the spin-aligned decuplet (0.4%). *Grade (P):* the intercept 19 is the cohomology sum above; the closer numerical fit $(M_N/\Lambda_5)^2 = 18.73 \approx 75/4$ is *not* a forced DFD quantity and is deliberately not adopted. The decuplet–octet intercept gap $32 - 19 = 13$ tracks the measured Δ–N mass-squared splitting ($13.5\,\Lambda_5^2$) to ∼ 4%.

d. Nucleon σ-term and the central nuclear coupling c_1 (conditional). The deep-central scalar-isoscalar pion–nucleon coupling c_1—the one nuclear low-energy constant *not* already fixed by the forced relativistic spin–orbit mechanism, the saturation density ρ_0, or the ρ/ω and Δ tower states—can be closed *conditionally*, by the same mass-squared-tower logic that gives the intercept 19. It rests on one rule: *in DFD the light-quark scalar source is not an independent chiral counterterm but the $U(2)$-equivariant tangent-projector perturbation of the baryon mass-squared tower.* Granting that rule, the light scalar spurion ($\langle\chi_+\rangle = 4m_\pi^2$ for $N_f = 2$) can enter M_N^2 only through the projector onto the coset tangent $T\mathbb{C}P^2$ of $\mathbb{C}P^2 = SU(3)/U(2)$ (Schur / $U(2)$-equivariance), and the index trace runs over its two complex directions, $\dim_{\mathbb{C}} T\mathbb{C}P^2 = 2$, fixing the dimensionless local slope

$$\frac{\partial M_N^2}{\partial m_\pi^2} \;=\; \frac{\mathrm{Tr}_{T\mathbb{C}P^2}(\chi_+)}{m_\pi^2} \;=\; \frac{2\,\langle\chi_+\rangle}{m_\pi^2} \;=\; 8 \qquad (8 = 2\times 4,\ \text{tangent rank} \times \text{scalar trace}). \tag{AT12}$$

Since $M_N^2 = M_0^2 - 8\,M_N c_1\, m_\pi^2 + \cdots$ in chiral perturbation theory, the forced slope 8 fixes

$$c_1 \;=\; -\frac{1}{M_N} \;=\; -\frac{1}{\sqrt{19}\,\Lambda_5} \;=\; -1.057\ \mathrm{GeV}^{-1},$$

whence $\sigma_{\pi N} = -4c_1 m_\pi^2 - \dfrac{9g_A^2 m_\pi^3}{64\pi f_\pi^2} + \cdots \simeq 56$ MeV (the leading $-4c_1 m_\pi^2 = 4m_\pi^2/M_N = 77$ MeV minus the forced 21 MeV chiral loop), inside the observed band 45–59 MeV. The central nuclear binding—and hence the magic-number ordering at ρ_0—then closes with no free coupling. *Grade (conditional — strictly weaker than the tower).* Unlike the intercept 19 and the strange slope 9 (index/cohomology counts already carried by Eq. (AT11)), the slope 8 is *not* yet established in the corpus: the tower gives $M_N = \sqrt{19}\,\Lambda_5$ but does not derive the m_π^2-response as a projector trace, and chiral symmetry *explicitly permits* the independent singlet counterterm $c_1\,\bar{N}\langle\chi_+\rangle N$. The closure therefore requires a rule *stronger than symmetry*—"baryon mass-squared perturbations are internal $\mathbb{C}P^2 \times S^3$ projector traces, with no free IR counterterm"—which the present corpus does not derive from a deeper axiom. With that rule the nucleus is parameter-free at leading chiral order; without it, $c_1 = -1/M_N$ is a natural value, not a theorem. This is a *heavier* insertion than the baryogenesis Berry-holonomy channel (Extended Derivations, App. AH), which only *names* a clock inside the fermion kernel DFD already uses — here a symmetry-allowed counterterm must be actively *forbidden*. The empirical slope (6.9–8.3, for $\sigma_{\pi N} = 45$–59) brackets 8, so the integer alone is not the content; the content is the tangent-projector rule that singles it out. The integer 8 is also a $\mathbb{C}P^2$ cohomology dimension in its own right — $\dim H^0(\mathbb{C}P^2, T\mathbb{C}P^2) = \dim \mathrm{Aut}(\mathbb{C}P^2) = \dim \mathfrak{sl}(3,\mathbb{C}) = 8$, the holomorphic tangent sections, the same *kind* of Dolbeault index as the intercept 19 — which strengthens that 8 is the right *type* of object. But the $\mathbb{C}P^2$ structure admits *more than one* route to 8 (the tangent-rank product 2×4 and the holomorphic-section count $\dim H^0 = 8$ are distinct bookkeepings, 2 directions $\times 4m_\pi^2$ versus 8 sections $\times\, m_\pi^2$); the geometry does not uniquely select one mechanism. That over-determination is precisely why the forced content is the no-counterterm *rule*, not the integer.

e. Quark–lepton complementarity (P). The PMNS reactor angle and the CKM Cabibbo angle are locked by $\sin^2\theta_{13}^{\mathrm{PMNS}} = \frac{3}{31}\sin\theta_{12}^{\mathrm{CKM}}$, since $\sin^2\theta_{13} = 3\alpha$ ($3 = \chi(\mathbb{C}P^2)$) and $\sin\theta_{12}^{\mathrm{CKM}} = 31\alpha$; $3/31 = 0.0968$ vs data 0.0976 (0.8%).

f. CP-sector gauntlet (P). The exact DFD CKM matrix (App. AO; its three integer counts and the Euler-projected apex are selected, App. FK) yields, with no continuous parameter fitted: $\sin 2\beta = 0.719$ (vs 0.708 ± 0.011, $+1.0\sigma$); $\phi_s = -2.14°$ (vs $-2.2 \pm 0.9°$, 0.1σ); $\mathrm{Br}(B_s \to \mu\mu) = 3.40\times 10^{-9}$ (vs 3.34 ± 0.27, 0.2σ – where the global-fit value sits 1.2σ high); and an ε_K deficit of 12–17% ($\sim -2\sigma$), a falsifiable signature that lands on the exclusive-$|V_{cb}|$ side of the standing ε_K tension.

g. Look-elsewhere summary. $F_\pi = \frac{3}{5}\Lambda_{\overline{\mathrm{MS}}}$ is the unique expression in its window over both rungs, both functional forms, and denominators ≤ 10; $\eta' = \sqrt{39/2}$ is likewise the only structural candidate in its window; $A_s = 32\pi\alpha^5$ is 1 of ~ 225 grammar candidates within the Planck 1σ band. The vector-meson and decuplet entries sit on a denser integer grid; their evidential weight is in the progression structure, scored separately.

h. A_s status: a calibrated amplitude and a numerical match. We grade $A_s = 32\pi\alpha^5$ (Tab. CXVIII) as a numerical match to a calibrated amplitude: its power and its coefficient come from the de Sitter dictionary at $H_\star$, and no DFD stage freezes perturbations there (Prop. FK.3). In the de Sitter dictionary $A_s = H_\star^2/(8\pi^2\varepsilon_W \bar{M}_P^2)$ with the primordial (Wheeler–DeWitt) scale on the locked Majorana rung, $H_\star \propto M_R = M_P\alpha^3$ (App. AT 1), and the QED one-loop measure $\varepsilon_W = \alpha/(4\pi)$, the exponent collapses *exactly* to $\alpha^5 = (\alpha^3)^2/\alpha^1$ (sympy residual 0); this power is rigid. The numeric coefficient 32π is *not* derived from DFD geometry: it is fixed entirely by the $H_\star$–M_R normalization, for which no first-principles argument (de Sitter horizon, $S^3/\mathbb{C}P^2$ internal volume, spectral action, or Friedmann/Einstein coupling) exists in the corpus.

Planck-mass bookkeeping. DFD fixes $M_R = M_P\alpha^3 = 4.74\times 10^{12}$ GeV using the *non-reduced* $M_P = 1.22\times 10^{19}$ GeV, whereas the standard amplitude formula carries the *reduced* $\bar{M}_P = M_P/\sqrt{8\pi} = 2.44\times 10^{18}$ GeV. With conventions made consistent the ratio that reproduces the amplitude is $H_\star/M_R = \sqrt{8\pi} = 5.013 = M_P/\bar{M}_P$ (verified: $H_\star = \sqrt{8\pi}\,M_R$ in the reduced-mass formula gives $A_s = 32\pi\alpha^5 = 2.080\times 10^{-9}$, -0.82σ). The catalog's $H_\star = 8\pi\,M_R$ writes the *same* number only because it evaluates the reduced-mass formula with the non-reduced M_P, so M_P cancels; the "8π" is then $\sqrt{8\pi}$ of reduced/non-reduced conversion times $\sqrt{8\pi}$ of an *underived* Hubble–Majorana ratio.

Convention check. Writing $H_\star = \sqrt{8\pi}\,M_R$ with the

non-reduced M_P inside the reduced-mass formula gives $A_s = 4\alpha^5 = 8.28\times10^{-11}$ (-67σ); that figure is an artifact of the mismatch, *not* evidence against $\sqrt{8\pi}$. Under consistent conventions $H_\star = \sqrt{8\pi}\,M_R$ already lands in the Planck band, and the relabelling to 8π double-counts the Planck-mass conversion. Either way the residual freedom is a single $\sqrt{8\pi}$ in $H_\star/M_R$ that is not derived; we therefore present A_s as **one calibrated amplitude**, which $32\pi\alpha^5$ matches numerically (App. FK).

7. A zero-parameter amplitude–shape observable: the (ν, u) relation

Every galactic test in this monograph so far has passed through the acceleration scale a_0: the RAR (Sec. VII D), the BTFR (Sec. VII C), the calibration table (Sec. VII E). This subsection adds a test that does not. It ties the mass discrepancy, an *amplitude*, to the rotation-curve logarithmic slope, a *shape*, with no acceleration scale anywhere in the statement, and it is therefore a test one can run without knowing, fitting, or believing a_0.

a. The shape variable. Write $\nu \equiv g_{\rm obs}/g_{\rm bar}$ for the local mass discrepancy and $\beta \equiv \mathrm{d}\ln g_{\rm bar}/\mathrm{d}\ln R$ for the baryonic log-slope, and define

$$u \;\equiv\; -2\,\frac{\mathrm{d}\ln\nu}{\mathrm{d}\ln g_{\rm bar}}. \tag{AT13}$$

For extended mass the epicyclic frequency obeys $\kappa^2/\Omega^2 = 3 + \mathrm{d}\ln g_{\rm obs}/\mathrm{d}\ln R = 3 + \beta\,(1-u/2)$, which reduces to the familiar point-mass form only at $\beta = -2$. With $s \equiv \mathrm{d}\ln V_{\rm obs}/\mathrm{d}\ln R$ one has the exact estimator identity $u = 2 - 4\,(s - \tfrac{1}{2})/\beta$, so u is measurable from a rotation curve and a baryonic model alone.

Theorem AT.18 (Systematics immunity of the whole derivative tower)**.** *Regard a galaxy as a curve in the plane $(X,Y) = (\ln g_{\rm bar}, \ln\nu)$. A distance error $D \to D(1+\epsilon)$ and an inclination error $V_{\rm obs} \to fV_{\rm obs}$ each act on that curve as a* pure translation, $(X,Y) \to (X+\ln B,\; Y+\ln A)$ *with A, B constant along the galaxy. Consequently* every *derivative $\mathrm{d}^nY/\mathrm{d}X^n$ with $n \geq 1$ — in particular $u = -2\,\mathrm{d}Y/\mathrm{d}X$, its curvature, and every higher rung — is exactly invariant, and the only motion is horizontal. The displacement vectors in the $(\ln\nu,\, u)$ plane are*

$$\begin{aligned}\Big(\frac{\partial\ln\nu}{\partial\ln D},\;\frac{\partial u}{\partial\ln D}\Big) &= (-1,\,0),\\ \Big(\frac{\partial\ln\nu}{\partial\ln V_{\rm obs}},\;\frac{\partial u}{\partial\ln V_{\rm obs}}\Big) &= (+2,\,0),\end{aligned} \tag{AT14}$$

both exactly*, so distance and inclination are perfectly degenerate with one another and collapse to a single horizontal nuisance parameter.*

Proof. Under $D \to D(1+\epsilon)$ at fixed surface brightness, $R \to R(1+\epsilon)$ and $M_{\rm bar} \to M_{\rm bar}(1+\epsilon)^2$, so $g_{\rm bar} = GM_{\rm bar}/R^2$ is invariant ($B = 1$) while $V_{\rm obs}$, a spectroscopic quantity, is untouched and $g_{\rm obs} = V_{\rm obs}^2/R \to g_{\rm obs}/(1+\epsilon)$; hence $\nu \to \nu/(1+\epsilon)$, i.e. $A = (1+\epsilon)^{-1}$ and $\partial\ln\nu/\partial\ln D = -1$. Under $V_{\rm obs} \to fV_{\rm obs}$, $g_{\rm obs} \to f^2 g_{\rm obs}$, $g_{\rm bar}$ is untouched, so $A = f^2$, $B = 1$ and $\partial\ln\nu/\partial\ln V_{\rm obs} = +2$. In both cases the transformation adds constants to X and to Y; adding a constant to a variable annihilates in every derivative of order ≥ 1, so $\mathrm{d}^nY/\mathrm{d}X^n$ is unchanged for all $n \geq 1$. The rescaling $R \to cR$ is a reparametrisation of the same curve and does not move its points in the (X,Y) plane. Verified symbolically to fourth order and numerically to 10^{-12} on an explicit disc profile. □

Remark AT.19 (What is *not* horizontal). A stellar mass-to-light error is *not* a translation, because the gas contribution does not scale with $\Upsilon_\star$; it therefore has a vertical component. Measured on SPARC the mass-to-light vector is $(\partial\ln\nu, \partial u)/\partial\ln\Upsilon = (-0.562,\, +0.123)$ on average, a stiffness of 4.6 : 1 in favour of the horizontal direction (per-bin 1.4 : 1 to 25 : 1). $\Upsilon_\star$ is the one systematic that must be marginalised; distance and inclination need only one shared horizontal nuisance.

Proposition AT.20 (Closed forms of $u(\nu)$, with τ or x eliminated)**.** *For the saturating family $\mu(x) = x/(1+x^n)^{1/n}$, $x = g_{\rm obs}/a_0$ — whose $n = 1$ member is the closure form $\mu(x) = x/(1+x)$ of Thm. N.8 and Eq. (182) — definition (AT13) collapses to*

$$u_n(\nu) \;=\; \frac{2(\nu^n - 1)}{2\nu^n - 1}, \tag{AT15}$$

while for the exponential (single-mode occupation) response $\mu = 1 - e^{-\tau}$, $\tau = \sqrt{g_{\rm bar}/a_0}$, it collapses to

$$u(\nu) \;=\; (\nu - 1)\,\ln\frac{\nu}{\nu - 1}, \tag{AT16}$$

via $u = \tau/(e^\tau - 1)$ and the exact inversion $\tau(\nu) = \ln[\nu/(\nu-1)]$. Both families are monotone increasing, both satisfy $u(1^+) = 0$ and $u(\infty) = 1$, and ***neither closed form contains*** *a_0: the acceleration scale cancels identically between the amplitude and the slope. For (AT16), $\mathrm{d}u/\mathrm{d}\nu = \ln[\nu/(\nu-1)] - 1/\nu > 0$.*

Proof. Substitute $y = \mu\,x$, $\nu = 1/\mu$ into (AT13) and eliminate x (respectively τ). All residuals vanish identically in `sympy`; the limits are exact. □

b. Confrontation with SPARC. Binning on $g_{\rm bar}$ (never on measured ν, which correlates bin assignment with the $V_{\rm obs}$ noise that also enters s, and biases the innermost bin by +0.47 in u), 8 equal-count bins over 2316 usable rows from 113 galaxies of the 149 that pass the standard quality and inclination cuts, with a mock-calibrated bias correction and its systematic carried in the error budget, the exponential response (AT16) gives $\chi^2 = 8.68$ for 8 points, $\chi^2/\mathrm{dof} = 1.08$, $p = 0.37$, largest single pull $+2.26\sigma$. Marginalising a global $\Upsilon_\star$ under the Schombert–McGaugh SPS prior (0.07 dex) and one shared horizontal nuisance, the likelihood ratios against the same data are

$$\begin{aligned}2\,\Delta\ln L \;=\; &+0.43\ (n{=}1), \qquad +14.97\ (n{=}2),\\ &+30.89\ (n{=}3),\end{aligned} \tag{AT17}$$

i.e. the $n = 2$ "standard" and $n = 3$ members are excluded by rotation-curve *shape* alone. The exclusion is robust: $+14.07$ with $\Upsilon_\star$ *completely* free, and in the raw (uncorrected, unmarginalised) statistic it stays in $[+17.8, +40.4]$ across all 22 pipeline variants of smoothing, bin count, derivative scheme and minimum points per galaxy. *The raw statistic is however strongly $\Upsilon_\star$-dependent* — at a fixed $\Upsilon_{\rm disk} = 0.6$–$0.7$ the ordering against $n = 2$ reverses — which is precisely why the quoted ratios marginalise $\Upsilon_\star$ rather than fixing it. **The $n = 1$ closure form and the exponential response, by contrast, are *not* separated by these data** ($+0.43$). That is the limit of these data, and it is not a defect of the estimator: an independent full-information analysis bounds *every* a_0-free shape statistic — u, its curvature, or anything else built from log-derivatives — at $2\Delta \ln L \le +3.99$ on SPARC, because 77% of the available information sits in the amplitude, not the shape. Separating $n = 1$ from the exponential response requires either $\sim 8\times$ more galaxies at the same ν distribution, or the same data pushed to $\nu \to 1.1$ where the gap between them doubles.

Remark AT.21 (Inverting the relation: a post-hoc consistency check). *Flagged post-hoc; it was not pre-registered and the test above stands without it.* Read backwards, the relation measures the stellar mass-to-light ratio: the value of $\Upsilon_{[3.6]}$ that minimises the shape χ^2 is 0.475 with a statistical uncertainty of 0.024 dex under (AT16) and 0.448 ± 0.023 dex under $n = 1$. The former is -0.0223 dex from the independent stellar-population value 0.50 ± 0.07 dex, i.e. -0.30σ combining the two in quadrature.

Falsifier AT.22 (A mass-to-light ceiling, with no a_0, no dark matter and no cosmology). DFD's occupation reading of the boost carries $\nu \ge 1$ as a theorem. Raising $\Upsilon_{[3.6]}$ raises $g_{\rm bar}$ and pushes the innermost (highest-$g_{\rm bar}$) SPARC bin's mean ν down, and that bin crosses the floor $\nu = 1$ at

$$\Upsilon_{[3.6]} = 0.5775\ M_\odot/L_\odot = +0.063 \text{ dex above the SPS value,} \tag{AT18}$$

holding $\Upsilon_{\rm bulge} = 1.4\,\Upsilon_{\rm disk}$ at the SPARC fiducial ratio. At the SPS value the bin sits at $\nu = 1.154$ with a bootstrap uncertainty of $\simeq 0.06$, i.e. $\simeq 2.5\sigma$ clear of the floor. **A converged independent measurement of the $3.6\,\mu$m disk stellar mass-to-light ratio above $0.58\,M_\odot/L_\odot$ therefore refutes DFD using SPARC alone.** The falsifier is branch-independent (it uses only $\nu \ge 1$, not the shape of μ) and involves no acceleration scale, no dark matter and no cosmology. It is conditional on the SPARC photometric and H I mass models as published; a systematic revision of the gas masses moves the threshold.

Status AT.23 (Grades for this subsection). **Theorem:** Prop. AT.20 (both closed forms, exact) and Thm. AT.18 (the two systematics vectors and the invariance of the whole derivative tower). **Validated:** the SPARC confrontation of (AT16), $\chi^2/{\rm dof} = 1.08$, $p = 0.37$, and the exclusion of the $n \ge 2$ members at $2\Delta \ln L \ge +14.07$. **Not established:** any separation between the $n = 1$ closure form and the exponential response — SPARC provably cannot deliver it ($\le +3.99$ for any a_0-free shape statistic). **Post-hoc:** Rem. AT.21. **Branch bookkeeping:** the exponential response $\mu = 1 - e^{-\tau}$ used in (AT16) is the derived law (App. BS, Thm. BS.9); $\mu(x) = x/(1+x)$ (Thm. N.8) is its weak-response form, and the Solar System selects the exponential branch (Cor. BS.14). Everything in this subsection that is graded Theorem or Validated holds for *both*.

8. Status and the remaining open lemma

Status AT.24. The identities of AT 1 are exact (machine-verified), the results of AT 2–AT 5 carry the grades stated with them, and none reuses a new integer; their role is structural rigidity. The entries of AT 6 are predictions at the stated grades. The $\alpha^{19/2}$ confinement exponent that underlies several of these is reduced to a single open lemma: writing $\frac{19}{2} = (k_{\rm max} - N_{\rm gen})/(2N_{\rm gen}) = 57/6$, the exponent is rigidity-selected (the unique catalog form in the empirical window), but its derivation is contingent on the cube law of Proposition AT.4, which is not independently proved here. We therefore present $\frac{19}{2}$ as rigidity-selected, not as derived.

Appendix AU: The Dark-Energy Sector from the α^{57} Clock

This appendix derives the cosmological vacuum-energy deposit *from the same finite-microsector nonzero-mode count that fixes the Hubble scale. The central result is that the deposit is a pure α-power in Planck units with* no *new integer beyond the* $57 = 60-3$ *of Appendix AP. The deposit scale is* $\rho_{\rm dep}^{1/4} = 2.547$ *meV, one α-rung from the heaviest neutrino mass; the observed dark-energy scale is* $\rho_{\Lambda,{\rm obs}}^{1/4} = 2.2455$ *meV, i.e. a measured ratio* $R = \rho_{\Lambda,{\rm obs}}/\rho_{\rm dep} = 0.6042 \pm 0.0027$ *whose $O(1)$ coefficient is underived — a named open lemma (the vacuum-matching normalization; it is the product of the measured clock coefficient C and the dark-energy fraction Ω_Λ). The exponent is theorem-grade; the coefficient is measured. All exponent identities verified to ≥ 40 digits in arbitrary-precision arithmetic.*

1. The dark-energy density as a pure α-power

The starting point is the master invariant proved in Appendix AP (Theorem AP.15) and re-used in Appendix AT

(Proposition AT.4),

$$\frac{G\hbar H_0^2}{c^5} = (H_0 t_P)^2 = C\,\alpha^{57}, \qquad t_P = \sqrt{\frac{G\hbar}{c^5}}, \tag{AU1}$$

$C = 0.87784 \pm 0.00266$ (early clock, measured),

$C = 1$ (bound-matter clocks, Postulate ZS.11).

We use the Planck energy density $\rho_P \equiv c^7/(\hbar G^2) = E_P/\ell_P^3$, the natural upper scale of any vacuum-energy estimate.

Theorem AU.1 (Vacuum-energy deposit is α^{57} in Planck units, (E))**.** *The de Sitter vacuum-energy* deposit *associated with the DFD infrared clock is*

$$\boxed{\frac{\rho_{\rm dep}}{\rho_P} = \frac{3}{8\pi}\,\alpha^{57}, \qquad \rho_{\rm dep}^{1/4} = \left(\tfrac{3}{8\pi}\right)^{1/4} \alpha^{57/4}\, M_P c^2} \tag{AU2}$$

where $\rho_{\rm dep}$ is the closure (critical) energy density $3c^2H_0^2/(8\pi G)$ evaluated at $C = 1$, the bound-matter clock $H_0^{\rm loc}$ (Postulate ZS.11). This object is not ρ_Λ: labelling it so conflates the deposit with the observed *dark-energy density, which is $\rho_{\Lambda,\rm obs} = R\,\rho_{\rm dep}$ with the measured ratio $R = 0.6042\pm0.0027$ (Eq. (AU5) below). The only constant beyond the Friedmann $3/8\pi$ is the integer 57, which is the* primed-determinant mode count $k_{\max} - N_{\rm gen} = 60 - 3$ *of Theorem AP.11. No new integer enters.*

Proof. The closure (critical) energy density of a spatially flat universe is $\rho_c = 3c^2H_0^2/(8\pi G)$ (the de Sitter value when the clock H_0 is dominated by the constant vacuum term). Dividing by $\rho_P = c^7/(\hbar G^2)$,

$$\frac{\rho_c}{\rho_P} = \frac{3c^2H_0^2/(8\pi G)}{c^7/(\hbar G^2)} = \frac{3}{8\pi}\,\frac{G\hbar H_0^2}{c^5} = \frac{3}{8\pi}\,C\,\alpha^{57}, \tag{AU3}$$

using Eq. (AU1). Setting the measured coefficient to its bound-matter value $C = 1$ (Postulate ZS.11) defines the exponent-theorem deposit, $\rho_{\rm dep}/\rho_P = (3/8\pi)\alpha^{57}$. Taking the fourth root and using $E_P = M_P c^2$ gives $\rho_{\rm dep}^{1/4} = (3/8\pi)^{1/4}\alpha^{57/4} M_P c^2$. Both equalities are exact; the machine check reproduces $\rho_{\rm dep}/\rho_P = 1.89367\times10^{-123}$ to 40 digits on both sides. □

Remark AU.2 (The 10^{-123} "fine-tuning" is derived, not tuned, given the matter and Planckian vacuum cancellations). The notorious statement "$\rho_\Lambda/\rho_P \sim 10^{-123}$ requires 123-digit fine-tuning" is, in DFD, the *output* $\frac{3}{8\pi}\alpha^{57}$ with $\log_{10}(\frac{3}{8\pi}\alpha^{57}) = -122.72$. Nothing is tuned in the *exponent*: it is the nonzero-mode count, and the fourth root of the clock invariant $(H_0 t_P)^2 = C\,\alpha^{57}$ is what dark-energy phenomenology measures — the residual $O(1)$ coefficient ($R = 0.6042$, a factor well inside one digit of the 123) is measured, not tuned, given the cancellation of the matter vacuum and of the spectral action's Planckian vacuum term that Rem. AU.3 assumes. This is the cosmological-constant analogue of the gauge hierarchy being α^8 in the Higgs sector (App. Z).

Remark AU.3 (Scope: microsector piece, not a full vacuum-energy sum rule). The α^{57} relation is the forced *microsector* vacuum-energy piece together with the observed closure via the clock dictionary; its naturalness statement is scoped to the 60-mode microsector. It does *not* by itself bound or cancel the Standard-Model matter-sector vacuum contribution (dominated by the top loop, of order $\alpha^{32}M_P^4$ in DFD units, formally far larger): DFD forbids supersymmetry and derives no full-spectrum vacuum sum rule, so the matter piece is *unaccounted* — the same open cosmological-constant problem faced by every quantum field theory coupled to gravity. Status: the cosmological-constant *exponent* is the microsector relation above and its coefficient R is measured; the matter-sector *cancellation* problem remains open (and is universal, not DFD-specific). The dark-energy relation assumes that the matter piece cancels, as ΛCDM does through its fitted constant, and that the Planckian vacuum term of the spectral action (App. WS) cancels. Because the ψ source is the cosmic-mean-subtracted density, a uniform vacuum energy does not source ψ; it acts through the background expansion law and, as Λ does, through the de Sitter term on bound systems.

Numerically, with the locked ledger ($\alpha^{-1} = 137.036$, $M_P = 1.22089\times10^{19}$ GeV),

$$\rho_{\rm dep}^{1/4} = 2.547\ \text{meV} \qquad \text{(deposit / closure scale at } C = 1\text{)}, \tag{AU4}$$

to be compared with the observed late-time dark-energy scale $\rho_{\Lambda,\rm obs}^{1/4} = 2.2455$ meV (Planck 2018 at $H_0^{\rm early} = 67.52 \pm 0.09$). The measured ratio is

$$R \equiv \frac{\rho_{\Lambda,\rm obs}}{\rho_{\rm dep}} = 0.6042 \pm 0.0027, \qquad R^{1/4} = 0.8816. \tag{AU5}$$

The $\Omega_\Lambda^{1/4}$ factor alone ($0.688^{1/4} = 0.911$) leaves 2.32 meV, not 2.2455 meV; the decomposition is $R = \Omega_\Lambda\, C$: the dark-energy fraction times the measured clock coefficient $C = 0.87784 \pm 0.00266$, both measured. The deposit exponent theorem stands; the $O(1)$ coefficient R is underived — a named open lemma (the vacuum-matching normalization of Rem. AP.6).

2. The Hubble–Planck seesaw and holographic form

Proposition AU.4 (Deposit scale as a Hubble–Planck geometric mean, (E))**.** *The deposit scale of Theorem AU.1 is the $(3/8\pi)^{1/4}$-dressed geometric mean of the Hubble energy and the Planck energy,*

$$\boxed{\rho_{\rm dep}^{1/4} = \left(\tfrac{3}{8\pi}\right)^{1/4} \sqrt{\hbar H_0\, M_P c^2}} \tag{AU6}$$

(with $H_0 = H_0^{\rm loc}$) and, via the QCD–Hubble bridge $\hbar H_0 = \Lambda_{\rm DFD}^3 c^2/M_P^2$ (Proposition AT.4), equivalently $\rho_{\rm dep}^{1/4} = (3/8\pi)^{1/4}\,\Lambda_{\rm DFD}^{3/2}/(M_P c^2)^{1/2}$.

Proof. From Eq. (AU1) at $C = 1$, $\hbar H_0 = M_P c^2\,\alpha^{57/2}$,

so $\hbar H_0 \cdot M_P c^2 = (M_P c^2)^2 \alpha^{57/2}$ and $\sqrt{\hbar H_0 M_P c^2} = M_P c^2\, \alpha^{57/4}$. Multiplying by $(3/8\pi)^{1/4}$ reproduces Eq. (AU2). Substituting $\hbar H_0 = \Lambda_{\rm DFD}^3 c^2/M_P^2$ gives the $\Lambda_{\rm DFD}$ form. Machine check: $(3/8\pi)^{1/4}\sqrt{\hbar H_0 M_P c^2} = 2.5468$ meV, matching Eq. (AU4). □

Remark AU.5 (Holographic dark energy, derived rather than postulated). Equation (AU6) is precisely the Cohen–Kaplan–Nelson holographic / infrared-cutoff relation $\rho_\Lambda \sim M_P^2 H_0^2$ that elsewhere is imposed as an ansatz. In DFD it restates the clock relation: the IR cutoff is the α^{57} clock, the $M_P^2 H_0^2$ scaling follows from the de Sitter Friedmann equation, and the prefactor $3/8\pi$ is fixed (not fitted). The vacuum energy is thus a seesaw between the largest scale (M_P) and the smallest curvature (H_0), with the geometric mean landing at the meV.

Proposition AU.6 (Deposit scale one α-rung from the heaviest neutrino, (E))**.** *With the printed neutrino mass $m_3 = \frac{14}{13}\pi M_P \alpha^{14}$ (App. X, App. AT), the exact ratio is*

$$\frac{\rho_{\rm dep}^{1/4}}{m_3 c^2} = \frac{13}{14\pi}\left(\tfrac{3}{8\pi}\right)^{1/4}\alpha^{1/4} = 0.05078, \qquad \text{(AU7)}$$

so $\rho_{\rm dep}^{1/4}$ and m_3 occupy adjacent rungs of the same α-tower ($57/4 = 14.25$ versus 14), differing by one factor of $\alpha^{1/4}$ and the printed $\frac{14}{13}\pi$ prefactor.

Proof. Divide Eq. (AU2) by $m_3 c^2 = \frac{14}{13}\pi M_P c^2 \alpha^{14}$. The M_P cancels and $\alpha^{57/4-14} = \alpha^{1/4}$ remains, giving Eq. (AU7) (machine-verified to 40 digits). □

The numerical near-coincidence flagged in the cosmology literature ($\rho_\Lambda^{1/4} \approx m_\nu$) is, in DFD, this α^{14}-tower proximity. The *lightest* DFD neutrino, $m_1 = 2.34$ meV (dressed-closure spectrum, App. X), coincides with the observed $\rho_{\Lambda,\rm obs}^{1/4} = 2.2455$ meV to 4.2%; this is recorded as a coincidence (both are α^{14}-class scales), not a derived identity, because the m_1 value carries its own branch dependence.

3. The "why now" coincidence

The second classical puzzle is the temporal coincidence $\rho_\Lambda \sim \rho_{\rm matter}$ *today*. In ΛCDM the epoch at which the two densities cross is set by the free constant Λ and appears anthropically tuned.

Theorem AU.7 (The Hubble clock's e-fold count, (T))**.** *The cosmic clock $H_0 = \sqrt{C}\,\alpha^{57/2}/t_P$ is α-locked up to the measured $O(1)$ coefficient C (Eq. (AU1)). The logarithm of the ratio of the Planck rate $1/t_P$ to the Hubble rate is*

$$\ln\frac{1}{H_0 t_P} = \frac{57}{2}\ln\frac{1}{\alpha} - \frac{1}{2}\ln C = 140.29, \qquad \text{(AU8)}$$

a function of α and the nonzero-mode count alone up to the 0.065 contributed by the measured C on the early clock; on bound-matter clocks $C = 1$ (Postulate ZS.11) and the count is 140.23.

Proof. Equation (AU1) gives $H_0 t_P = \sqrt{C}\,\alpha^{57/2}$ identically, so $\ln(1/H_0 t_P) = \frac{57}{2}\ln(1/\alpha) - \frac{1}{2}\ln C = 140.227 + 0.065 = 140.292$ (machine check). The Hubble time on the early clock is $1/H_0^{\rm early} = 14.48$ Gyr, the exponent content of which is derived and the coefficient content measured; on bound-matter clocks it is $1/H_0^{\rm loc} = 13.56$ Gyr, with no coefficient. Neither is an age: the expansion age is $t_0 \simeq 13.8$ Gyr, 12.92 Gyr in laboratory units (App. ZS). With the measured $\Omega_m \simeq 0.31$ the crossing is at $z_{\rm eq} = 0.30$ and the deceleration→acceleration onset at $z = 0.64$, both $\mathcal{O}(1)$ today.[5] No epoch-dependent tuning is invoked. □

Remark AU.8 (Non-coincidence). The e-fold count 140.29 is *not* equal to $\alpha^{-1} = 137.04$ (they differ by 2.4%); we explicitly decline to read $\ln(1/H_0 t_P) \approx \alpha^{-1}$ as an identity. The robust content is Eq. (AU8) as an exact restatement of the α^{57} clock, and the Hubble time on the early clock, $1/H_0^{\rm early} = 14.48$ Gyr.

4. One dark energy: the equation of state

The late-time distance excess is not a ψ-screen $\Delta\psi(z) = \ln\!\left(D_L^{\rm obs}/D_L^{\rm matter}\right)$ (reconstructed value 0.274 at $z = 1$), and the vacuum density of Theorem AU.1 and that screen are not two faces of one optical field: the reconstructed screen is the ΛCDM/matter-only distance ratio by construction, a homogeneous screen adds nothing beyond the expansion (App. ZS), and the line-of-sight dressing $D_L \to D_L\, e^{\Delta\psi}$ is falsified (App. SL). DFD has one dark energy: the constant vacuum term of Theorem AU.1. This needs the four-dimensional three-form that the internal C_3 leaves in its $b_0 = 1$ piece, the part constant on K (beside χ from b_3 and one vector from b_2, App. AV), to carry zero flux: that three-form propagates nothing, but a nonzero four-form flux would add its own constant vacuum energy.

Proposition AU.9 (Equation of state of the vacuum term, (T))**.** *The DFD dark energy is the constant vacuum term $\rho_{\Lambda,\rm obs} = R\,\rho_{\rm dep}$ of Theorem AU.1 alone. Its equation of state is $w = -1$ identically, and DFD is degenerate with ΛCDM on distance observables and on late-time linear growth (Sec. XVII).*

Proof. A constant vacuum energy density has $p = -\rho$, hence $w = -1$; this is the form of the term, not a separate derivation. A CPL fit to the resulting distance ladder returns $(w_0, w_a) = (-1, 0)$. □

---

[5] The dark-energy appendices round the measured-clock matter density $\Omega_m = 0.312$ ($\Omega_\Lambda = 0.688$) to 0.31 here; the conclusions are insensitive to this spread. Across $\Omega_m = 0.30$–0.315 the equality redshift is $z_{\rm eq} = 0.33$–0.30 and the acceleration onset $z = 0.67$–0.63 (both $\mathcal{O}(1)$), and $w = -1$ is exact for the constant vacuum term. The Planck-2018 value $\Omega_m = 0.315$ is used in the σ_8 confrontation of App. AE.

Remark AU.10 (No dark-energy clustering, shared with ΛCDM). A constant vacuum term carries no perturbations: no dark-energy sound speed and no late-time dark-energy clustering, exactly as for Λ in ΛCDM. This is not a discriminator from ΛCDM but a shared falsifier: a confirmed evolving dark energy with or without clustering (e.g. if the DESI DR2 dynamical-dark-energy hints are confirmed) falsifies DFD's vacuum term together with Λ.

5. Look-elsewhere and status

a. Look-elsewhere. Scanning the grammar (prefactor $\in \{1, 3/8\pi, 1/8\pi, 3/4\pi, 1/4\pi, \frac{1}{2}, 2, \pi, 1/\pi\}$, exponent $n/4$ with integer $n \in [50, 64]$) for candidates landing in the generous band $\rho_\Lambda^{1/4} \in [1.8, 2.8]$ meV yields 3 hits out of 135 grammar candidates ($n = 57$ with prefactors $3/8\pi$, $1/4\pi$, $1/8\pi$). The exponent $n = 57$ is *not* selected by the data: it is forced to be the same 57 that appears in the proven Hubble invariant (App. AP), and the Friedmann prefactor $3/8\pi$ is forced by the closure-density definition. The α-rung spacing is $137^{1/4} = 3.42$ in energy, so no neighbouring integer rung lands within a factor of the observed scale. The result is therefore rigidity-selected (zero new integers), not numerology.

Status AU.11. Theorem AU.1 (the α^{57} vacuum deposit), Proposition AU.4 (the Hubble–Planck seesaw / holographic form), and Proposition AU.6 (adjacent-rung neutrino relation) are exact identities, machine-verified to ≥ 40 digits, reusing only the locked integer $57 = 60 - 3$ and the Friedmann constant $3/8\pi$. They inherit their open coefficient from the clock dictionary (Axiom AP.5): the identification $(H_0 t_P)^2 = C\, Z'_\alpha / Z'_1$ is a spectral-action dictionary statement whose exponent is theorem-grade and whose $O(1)$ coefficient C is a measured input (the eight-route no-go proves it underivable from the printed corpus) — so $\rho_{\rm dep} = \frac{3}{8\pi}\alpha^{57}\rho_P$ is theorem-grade in its exponent, and the observed $\rho_{\Lambda,\rm obs} = R\,\rho_{\rm dep}$ carries the measured $R = 0.6042 \pm 0.0027$ ($R = \Omega_\Lambda C$), whose derivation is a named open lemma. Theorem AU.7 is a closed consequence of the α-locked exponent. Proposition AU.9 (equation of state) restates the constancy of the vacuum term; the no-clustering signature is a falsifier shared with ΛCDM, not a discriminator. The empirical contact is the derived $10^{-122.7}$ hierarchy landing within the measured $O(1)$ coefficient of the observed 2.2455 meV scale; its evidential weight is governed by the look-elsewhere count above.

Appendix AV: χ-Matter: the Weak-Sector Matter Field and the True Definition of Dark Matter

1. Overview, grade, and what this appendix claims

This appendix derives a cold, non-thermal pseudoscalar matter field χ from the same internal geometry and the same per-mode Gaussian determinant (Lemma O.5, App. O) that fix the rest of the DFD α-tower. The field is *not* postulated. It is the harmonic three-form on the internal $S^3 = SU(2)$ factor — a zero-mode of the fixed compactification that the corpus's rigidity classification (the parent-tensor rigidity theorem (App. AH)) does not list. With that mode included, its decay constant, its mass, and its relic abundance follow from the tower and the stated inputs and premises named below; the cold component is exactly what the CMB acoustic kernel requires at the third peak. (Step 5b (Thm AV.13) removes the free misalignment angle θ_i — with no inflaton there is no chosen angle, and the amplitude is instead the finite $SU(2)_{60}$ CS/WZW vacuum expectation $\langle\theta^2\rangle = \sum_j |S_{0j}|^2 C_2(j)/[k(k+2)] = 0.073$ — a variance in the *period-1* (turns) flux coordinate (Lemma AV.6) — giving, through the exact radiation-era relic map, $\Omega_\chi h^2 = 0.1193$ (-0.60σ from Planck). A factor-44 overshoot is predominantly a *units* artifact — the classical-continuum measure $\pi^2/3$ is the variance of a period-2π angle, whereas the flux coordinate has period 1 — compounded by a continuum measure choice; see Rem. AV.14.)

a. The de-"dark" thesis. DFD does not retire the terms *dark matter* and *dark energy*; it supplies their true definitions. "Dark" has only ever meant *not knowing what it is*. DFD removes that ignorance on both counts: the cold clustering component is the derived χ field of this appendix, and the late-time acceleration is the α^{57} *geometric vacuum energy* (App. O), whose coefficient is measured once (Rem. AP.6). We keep the historical names — and compare to ΛCDM under them — precisely so that the resolution is unmistakable: *dark matter is the χ particle; dark energy is the energy of the vacuum.*

Remark AV.1 (Ledger-controlling status: derived carrier; forced amplitude/stated conventions). This remark controls every later "theorem-grade" shorthand and aligns it with the authoritative fitted-knob ledger. The carrier/operator is derived. The numerical mass additionally uses the $\sqrt{158}$ multiplicity of Sec. AV 5, one stated discrete input. The abundance is forced-amplitude/stated-convention: its operator is proven, while state preparation and the relic-map normalization are named premises. The chain is conditional on:

1. the two tower-wide conventions that already gate the Higgs sector and α itself — the stated choices of α's exact construction (§X C) and the gauge normalization $g^2 = \alpha$ (App. O);
2. a zero photon coupling, $E = 0$ (Theorem AV.35),

so that the hot early plasma adds no thermal χ (Sec. AV 7, channel (b));

3. the weak-block dimension $d_\chi = 3$ of Theorem AV.4 (this is exact Lie theory, see the proof);

4. Theorem AV.13 (Step 5b, Sec. AV 7) removes the $\mathcal{O}(1)$ misalignment angle θ_i of Sec. AV 6, and the State-Preparation Theorem AV.23 proves it cannot be reintroduced: DFD has no inflaton, so no angle is chosen, and the amplitude is the finite $SU(2)_{60}$ CS/WZW vacuum expectation $\langle\theta^2\rangle = \sum_j |S_{0j}|^2 C_2(j)/[k(k+2)] = 0.073$, giving $\Omega_\chi h^2 = 0.1193$ (-0.60σ from Planck). The operator (Casimir) is proven, the sector measure rests on the asserted premise P4′ (Lemma AV.27), and the normalization $k(k+2)$ follows from the Sugawara level together with the half-period edge $\theta_{\max} = \frac{1}{2}$ — the $\mathbb{Z}_2$-folded edge of the *period-1* flux coordinate (Lemma AV.6) — that follows from χ's *derived* $\mathbb{Z}_2$ orientation-oddness. So the amplitude is forced and the abundance is **forced-amplitude/stated-convention** (its non-DFD bridge being the standard cosmological relic-redshift map, carried at its *exact* radiation-era value, Rem. AV.12, shared with every DM relic). A factor-44 overshoot is a units-plus-continuum-measure artifact (Rem. AV.14).

We therefore assign **Derived** to the carrier and period relation, **motivated multiplicity** to the printed mass coefficient, and **forced-amplitude/stated-convention** to the relic abundance (Step 5b) — not the loose "solved" and not a fitted density. The residuals are named in Rem. AV.14: the $\mathbb{Z}_2$/Sugawara normalization convention and the $\mathcal{O}(1)$ cosmological prefactor of the relic map.

2. Step 1 — χ is the harmonic three-form outside the rigidity classification

The corpus already establishes (the parent-tensor rigidity theorem, App. AH, companion *Extended Derivations*) that the only *metric* zero-modes on $K = \mathbb{C}P^2 \times S^3$ are the trace ψ and the TT graviton, and that the form-field sector is constrained by $b_1(K) = 0$. That classification addresses one-forms. It does not address the three-form, and by Künneth the three-form is present:

$$b_3(\mathbb{C}P^2 \times S^3) = \sum_{p+q=3} b_p(\mathbb{C}P^2)\, b_q(S^3) = b_0(\mathbb{C}P^2)\, b_3(S^3) = 1 \cdot 1 = 1. \tag{AV1}$$

Theorem AV.2 (Topological identity of χ)**.** *On $K = \mathbb{C}P^2 \times S^3$ the space of harmonic three-forms is one-dimensional, $b_3(K) = 1$. Its generator is the bi-invariant Cartan three-form on $S^3 \cong SU(2)$,*

$$\omega = \frac{1}{24\pi^2}\,\mathrm{Tr}\big[(g^{-1}dg)^{\wedge 3}\big], \qquad g \in SU(2), \tag{AV2}$$

which coincides, up to standard normalization, with the $SU(2)$ Chern–Simons density. The DFD field χ is the coefficient of this unique harmonic mode; its 4D reduction on the S^3 three-cycle is a pseudoscalar in the sense that it is odd under reversal of the S^3 orientation; DFD's CP leaves S^3 fixed and acts on C_3 by pullback alone, so χ is CP-even (Theorem AV.35).

Proof. S^3 is compact, connected, simply connected and orientable, so by Hodge theory $\dim\{\text{harmonic } p\text{-forms}\} = b_p$. For S^3, $(b_0, b_1, b_2, b_3) = (1, 0, 0, 1)$, and $b_3(K) = 1$ follows from (AV1). On the group manifold $SU(2)$ the Maurer–Cartan form $\theta = g^{-1}dg$ is $\mathfrak{su}(2)$-valued and satisfies the structure equation $d\theta = -\theta \wedge \theta$. The bi-invariant volume form is, up to scale, $\mathrm{Tr}(\theta^{\wedge 3})$: left/right invariance follow from $\theta \mapsto h^{-1}\theta h$ under $g \mapsto gh$ together with cyclicity of the trace; closedness $d\,\mathrm{Tr}(\theta^{\wedge 3}) = 0$ is immediate from the structure equation and cyclicity; co-closedness is automatic for a top-degree form on a closed manifold. Hence ω is harmonic and generates $H^3(S^3)$. Finally $\mathrm{Tr}(\theta^{\wedge 3})$ is the integrand of the $SU(2)$ Chern–Simons form $\mathrm{CS} = \mathrm{Tr}(A\,dA + \frac{2}{3}A^3)$ evaluated on the pure-gauge configuration $A = \theta$, establishing the stated coincidence and the normalization (the prefactor $1/24\pi^2$ giving $\int_{S^3}\omega = 1$). Reduction of an internal three-form on the three-cycle S^3 yields a 4D scalar; the orientation-odd character of ω makes it odd under reversal of the S^3 orientation, which DFD's CP does not perform (App. L). □

Remark AV.3 (The three-form sector and the parent-tensor theorem). The parent-tensor rigidity theorem (App. AH) remains correct as stated: ψ and h^{TT} are the two components of the *metric* zero-mode, and χ is not a metric mode — it is the three-form gauge field, a separate sector, so it does not affect $c_T = c$ (the $c_T = c$ theorem, App. AH). The antisymmetric-tensor sector is not empty: $b_1 = 0$, but $b_3 = 1$. App. AH (*Extended Derivations*) identifies the three-form with χ. χ is *not* a "60th internal mode": the index $\dim \mathcal{H}_{\mathrm{micro}} = 60$ counts chiral/gauge modes of the Spin^c Dirac operator, whereas χ is a bosonic harmonic form of the same S^3 Chern–Simons structure that already gives the closed form for α (App. AH, *Extended Derivations*; Berezin–Toeplitz at $k_{\max} = 60$). It is the dynamical zero-mode of a sector DFD already relies on, not a new addition.

3. Step 2 — the gauge-adjoint dimension of χ is $d_\chi = 3$

Theorem AV.4 (Gauge-adjoint count for χ)**.** *The Toeplitz (mode-quantized) subspace associated with the Cartan three-form ω of $SU(2)$ is the complexified algebra of that $SU(2)$, $\mathfrak{sl}(2,\mathbb{C})$, of complex dimension $d_\chi = 3$, the dimension of the weak algebra, which is why it is called the weak block below. This $SU(2)$ carries no quark or lepton: it is not the weak $SU(2)$ of the Standard Model fermions, whose Chern–Simons coupling to χ would thermalize χ (Theorem AV.35).*

Proof. The Maurer–Cartan form θ in (AV2) is $\mathfrak{su}(2)$-valued and the cubic $\mathrm{Tr}(\theta^{\wedge 3})$ saturates the adjoint trace over that algebra. Under the corpus's Toeplitz quantization the harmonic generator lifts to the operator content of the adjoint representation; complexification gives $\mathfrak{su}(2)_{\mathbb{C}} = \mathfrak{sl}(2,\mathbb{C})$, with $\dim_{\mathbb{C}} \mathfrak{sl}(2,\mathbb{C}) = 3$. This is the exact parallel of the Higgs sector, where the corresponding construction on the colour factor yields $\mathfrak{sl}(3,\mathbb{C})$ with dimension 8. Thus $d_\chi = 3$ stands to the weak sector as $d_H = \dim \mathfrak{su}(3) = 8$ stands to the colour sector. □

The single integer carried forward is $d_\chi = 3$.

4. Step 3 — decay constant from the per-mode determinant

Lemma AV.5 (Lemma O.5 specialized to χ)**.** *The per-mode Gaussian determinant of a d-dimensional adjoint Toeplitz block is α^d with the uniform gauge normalization $g^2 = \alpha$ (App. O, Lemma O.5). The λ-dependence cancels exactly per mode: $\int d^2\phi\, e^{-(\lambda/\alpha)|\phi|^2} / \int d^2\phi\, e^{-\lambda|\phi|^2} = \alpha$. Specializing to $d = d_\chi = 3$ fixes the χ kinetic scale*

$$\begin{aligned} f_\chi &= \bar{M}_{\mathrm{P}}\, \alpha^3 = 2.435 \times 10^{18}\,\mathrm{GeV} \times \alpha^3 \\ &\approx 9.46 \times 10^{11}\,\mathrm{GeV}, \end{aligned} \tag{AV3}$$

with $\bar{M}_{\mathrm{P}} = (8\pi G)^{-1/2}$ the reduced Planck mass and $\alpha^{-1} = 137.036$ (so $\alpha^3 = 3.886 \times 10^{-7}$). Which normalization convention this scale carries — radian decay constant or flux period *— is settled by Lemma AV.6 below: f_χ is the period.*

Proof. Each of the d Gaussian modes of the adjoint block contributes one factor of α to the fluctuation determinant (Lemma O.5); the determinant rescales the Planck-scale internal stiffness to a physical decay constant $f = \bar{M}_{\mathrm{P}}\, \alpha^d$. For the weak block $d_\chi = 3$ (Theorem AV.4), giving (AV3). The same lemma with $d_H = 8$ returns $\bar{M}_{\mathrm{P}}\alpha^8 = 19.6$ GeV, the numerator of the χ see-saw; the Higgs vacuum value follows from it only through the fitted prefactor of $v = 4\pi\Lambda$ (Rem. AV.9). (AV3) is its $d = 3$ sibling, not an independent input. □

Lemma AV.6 (The flux period: $\int_{S^3} C_3$ has unit period, and (AV3) is that period)**.** *Let $\theta := \int_{S^3} C_3$ in units of the normalized generator ω of (AV2). Then:* (i) *ω is the* integral generator *of $H^3(S^3;\mathbb{Z})$: for a degree-n map $g : S^3 \to SU(2)$, $\int_{S^3} \frac{1}{24\pi^2}\mathrm{Tr}[(g^{-1}dg)^{\wedge 3}] = n$ exactly (verified symbolically for $n = 1, 2, 3$), and a large gauge transformation of winding w shifts $\int_{S^3} C_3$ by the integer w, entering the level-k Chern–Simons phase as $e^{2\pi i k w}$. Hence θ lives on $\mathbb{R}/\mathbb{Z}$:* ***its period is*** *1* ***exactly*** *— a degree of a map, not a convention.* (ii) *Lemma AV.5 is provably* blind *to the normalization of the coordinate it integrates: rescaling $\phi \to c\phi$ in the per-mode ratio returns α identically, $d(\mathrm{ratio})/dc = 0$; a ratio of Gaussian normalizations transmits whatever coordinate the geometry hands it and cannot fix one.* (iii) *Consequently the coefficient (AV3) multiplies the period-1 coordinate of (i): $f_\chi = \bar{M}_{\mathrm{P}}\alpha^3$ is the* ***period*** *of the canonically normalized flux field,*

$$\begin{aligned} P &\equiv f_\chi = \bar{M}_{\mathrm{P}}\, \alpha^3 = 9.4635 \times 10^{11}\,\mathrm{GeV}, \\ f_{\mathrm{rad}} &\equiv \frac{P}{2\pi} = 1.506 \times 10^{11}\,\mathrm{GeV}, \end{aligned} \tag{AV4}$$

with f_{rad} the radian-normalized decay constant that enters axion-form formulas (see-saw mass, anomaly vertex). The potential is the periodic parabola $V = \frac{1}{2}m_\chi^2 P^2\, \|\chi/P\|^2$, with $\|u\|$ the distance from u to the nearest integer; its curvature at each minimum equals that of $158\,\Lambda^4[1 - \cos(2\pi\chi/P)]$, with 158 the multiplicity stated in Theorem AV.8, so $m_\chi = \sqrt{158}\,\Lambda^2/f_{\mathrm{rad}}$. The photon coefficient of a vertex $g_{\chi\gamma} = E\alpha/P$ is zero, $E = 0$, so χ has no photon vertex (Theorem AV.35).

Remark AV.7 (Grade of the period identification, and the structural supports). Part (i) and part (ii) are theorem-grade (exact symbolic residuals). Part (iii) is **Derived**: it uses the corpus's own stated accounting that the Lemma O.5 determinant ledger carries no 2π (App. Z); the one named residual is that Lemma AV.5 performs no explicit Kaluza–Klein reduction — "Planck-scale internal stiffness = $\bar{M}_{\mathrm{P}}$" is asserted, and the printed action cannot supply it, because χ does not enter its Dirac operator, so the stiffness is a stated input, which the measured dark-matter density confirms to within 1% (computed) — and an actual reduction returning $2\pi\bar{M}_{\mathrm{P}}\alpha^3$ in the turns coordinate would restore the radian reading. Four independent structural facts support the period reading and none supports the radian one — and an empirical discriminator (e) selects it outright: *(a)* the relic amplitude Q_{CS} is a variance in turns^2 — the exact identity $C_2(j)/[k(k+2)] = (K/k)\,[u_j^2 - (\pi/K)^2]/(4\pi^2)$, $u_j = (2j+1)\pi/K$, exhibits the $1/(4\pi^2)$ radians$^2 \to$turns^2 conversion, and the pre-registered continuum limit $\lim_{k\to\infty} Q_{\mathrm{CS}} = \frac{1}{12} - \frac{1}{8\pi^2} = 0.0706682$ has leading term $\frac{1}{12}$, the uniform variance of a *period-1* angle (a period-2π angle gives $\pi^2/3$); *(b)* the edge $\theta_{\max} = \frac{1}{2}$ (AV13) is the $\mathbb{Z}_2$-folded half-period *in turns*; *(c)* $\int_{S^3}\omega_3 = 1$ is integer winding, the same statement that derives $N_{\mathrm{DW}} = 1$; *(d)* the large-gauge phase $e^{2\pi i k w}$ of (i). The apparent counter-witness $\delta\theta = H/(2\pi f_\chi)$ is *not* evidence for the radian reading: that 2π is the Gibbons–Hawking de Sitter factor, identical in both normalizations. *(e) Empirical convention discriminator.* With the relic amplitude topologically fixed (Step 5b: $\langle\theta^2\rangle = 0.073$, no free angle), the radian reading ($f_{\mathrm{rad}} = \bar{M}_{\mathrm{P}}\alpha^3$, $P = 2\pi f_{\mathrm{rad}}$) rescales the relic by $(m'/m)^{1/2}(A'/A) = (2\pi)^{-1/2}(2\pi)^2 = (2\pi)^{3/2} = 15.75$, giving $\Omega_\chi h^2 \simeq 1.88$ — a 15.7× overshoot of the observed 0.12, excluded; the hybrid variant (radian scale with radian variance) is blocked by the turns-pinning facts (a)–(d) and independently undershoots by ∼2.5×. Planck itself selects the period reading within the no-free-angle chain. This is a consistency discriminator on an already-scored datum, not a new evidence row, and it is distinct from the ∼9–44× continuum-measure artefact, which concerns

a different object. *Conditional cross-link:* $\bar{M}_{\rm P}$ cancels in $f_\chi/\Lambda = \alpha^{-5}$ (both exponents derived-grade); via $v = 4\pi\Lambda$ (Rem. AV.9) this pins P from the measured v at 0.054%, conditional on the fitted $\sqrt{2\pi}$ prefactor of App. Z, whose printed 0.054% best-fit gap this residual identically is. *Residual, sharpened:* any KK reduction must consume one dimensionful anchor (dimensional analysis on the Toeplitz kinetic pattern, App. AH), and the reduction itself, which would fix the $O(1)$ coefficient (1 vs 2π), cannot be done in the printed action, because χ does not enter its Dirac operator; the consumed-anchor status parallels the consumed G of the Newton identity (App. ZU), with the asymmetry that there the prefactor is proven unique, while here the 1-vs-2π coefficient is a stated input.

5. Step 4 — see-saw mass: χ is light, cold, and non-thermal

Theorem AV.8 (χ mass)**.** *With the weak-block see-saw scale $\Lambda^2/f_{\rm rad}$ — the radian decay constant $f_{\rm rad} = P/2\pi$ of Lemma AV.6, since the periodic-parabola potential has curvature $158\,\Lambda^4(2\pi/P)^2$ — and the electroweak-scale numerator $\Lambda = \bar{M}_{\rm P}\,\alpha^8$ (the same $d = 8$ scale that sets the Higgs VEV),*

$$m_\chi \;=\; \sqrt{158}\,\frac{\Lambda^2}{f_{\rm rad}} \;=\; 2\pi\sqrt{158}\,\frac{\Lambda^2}{P} \;=\; 2\pi\sqrt{158}\,\bar{M}_{\rm P}\,\alpha^{13} \;=\; 32.005\,\text{eV}, \tag{AV5}$$

where $\sqrt{158}$ is the weak-block multiplicity prefactor, one stated discrete input. It is read as $158 = 3(k_{\max} - \dim M_7) - 1 = 3\cdot 53 - 1$, with the factor 3 the dimension $d_\chi = \dim \mathfrak{sl}(2,\mathbb{C})$ of the weak block (Theorem AV.4) rather than $N_{\rm gen}$, which the $\mathcal{O}(9)$ block already contains, times the $53 = k_{\max} - \dim M_7$ block, less a single zero-mode. Status: *no single counting rule gives* 158. *The corpus's uniform rule, all modes less the zero modes, which gives $57 = 60 - 3$, gives* 171 *on the weak block, and a symmetry acting irreducibly on the three-dimensional factor and trivially on the microsector modes makes every invariant count a multiple of* 3, *which* 158 *is not (computed). The multiplicity is therefore a stated input, not a derivation;* 171 *would give $m_\chi = 33.30$ eV and $\Omega_\chi h^2 = 0.1217$ ($+1.4\sigma$) against* 0.1193 *(-0.6σ), a* 2% *difference that next-generation measurements of the cold-matter density can separate. It is an integer count,* not *the loop factor $16\pi^2$ it lies* 0.05% *from; the exact electroweak–dark scale link is carried separately by $v = 4\pi\Lambda$ (Rem. AV.9).*

Proof. The see-saw form $m \propto \Lambda^2/f$ is the standard statement that a harmonic p-form axion acquires its mass not from the Planck-scale moduli potential (which has no size or shape modulus to fix on the truncated microsector, App. O) but from the non-perturbative $SU(2)$ effects that lift the three-form shift symmetry; the resulting scale is the geometric mean structure $\Lambda^2/f_{\rm rad}$, with $f_{\rm rad} = P/2\pi$ the radian decay constant of the period-P potential (Lemma AV.6). With $\Lambda = \bar{M}_{\rm P}\alpha^8$ and $P = \bar{M}_{\rm P}\alpha^3$ the net power is $16 - 3 = 13$. Numerically $\alpha^{13} = 1.664\times10^{-28}$ and $2\pi\sqrt{158} = 78.98$, giving $m_\chi = 78.98\times 2.435\times10^{27}\,\text{eV}\times 1.664\times10^{-28} = 32.005\,\text{eV}$ ($= 2\pi\times 5.0937$ eV). Because the finite-CS relic is produced at rest (zero momentum; a variance relic, not a coherent condensate, see Rem. AV.30), χ is cold regardless of this low mass — unlike a 32 eV thermal relic, its free-streaming scale is set by the Jeans wavenumber $k_J \propto \sqrt{m_\chi H}$, which lies far below all CMB and large-scale-structure scales. The relic is therefore cold and non-thermal, clustering as cold dark matter at recombination, and the hot early plasma adds no thermal χ quanta, because χ has no photon coupling ($E = 0$, Theorem AV.35; Eq. (AV22)). □

Remark AV.9 (Exact EW↔dark scale link: $v = 4\pi\Lambda$). The χ see-saw numerator $\Lambda = \bar{M}_{\rm P}\alpha^8$ and the Higgs VEV $v = M_{\rm P}\alpha^8\sqrt{2\pi} = 246.09$ GeV (App. Z) sit on the *same* $d = 8$ rung. With $M_{\rm P} = \sqrt{8\pi}\,\bar{M}_{\rm P}$,

$$\frac{v}{\Lambda} = \sqrt{8\pi}\,\sqrt{2\pi} = \sqrt{16\pi^2} = 4\pi \qquad\Longrightarrow\qquad v = 4\pi\,\Lambda \quad \text{(exact)}. \tag{AV6}$$

This is an exact, type-correct relation between the electroweak and dark scales, conditional on the fitted $\sqrt{2\pi}$ prefactor of App. Z: a ratio of two continuum scales whose 4π is the fitted $\sqrt{2\pi}$ times the $\sqrt{8\pi}$ that relates $M_{\rm P}$ and $\bar{M}_{\rm P}$. It is an exact algebraic consequence of the printed scales, recorded here as one named relation: the Higgs VEV and the χ see-saw numerator are one and the same $d = 8$ scale up to the factor 4π. It is *distinct* from the χ-mass multiplicity $\sqrt{158}$, a stated discrete count that is *not* 4π: although 158 lies 0.05% above the 4D loop factor $16\pi^2 = 157.91$, that proximity is a numerical near-coincidence, not an identity (a multiplicity is an integer; $16\pi^2$ is transcendental). Consequently the tempting "$v^2 = 2\,m_\chi P$" holds only to 0.03% and is *not* recorded as exact — the exact EW↔dark content is carried by $v = 4\pi\Lambda$ alone.

Remark AV.10 (The key assumption, named). The one physics input that is *assumed* rather than computed here is that the three-form mode is lifted by the see-saw scale $\Lambda^2/f_{\rm rad}$ (shift-symmetry protected, light) rather than sitting at the Planck-scale moduli mass like the squashing modulus. This is the standard expectation for a p-form axion, and it is what distinguishes χ from the heavy moduli; but it is the assumption on which the 32 eV value rests, and it is the natural target of any attempt to refute the χ identification.

6. Step 5 — relic abundance by vacuum misalignment

Theorem AV.11 (Relic density at a natural misalignment angle)**.** *For the derived $(P, m_\chi) = (9.46\times 10^{11}\,\text{GeV}, 32.005\,\text{eV})$, standard vacuum misalignment gives*

$$\Omega_\chi h^2 \;\simeq\; 1.62\,\kappa_{\rm rad}\sqrt{2\pi}\,\theta_i^2 \;=\; 1.635\,\theta_i^2, \tag{AV7}$$

with $\kappa_{\rm rad}\sqrt{2\pi} = 1.00923$ *the exact-onset/period-fix correction of Rem. AV.12, so that the observed cold-dark-matter density* $\Omega_{\rm DM}h^2 = 0.12$ *is reproduced at the natural value*

$$\theta_i \;=\; \sqrt{0.12/1.635} \;\approx\; 0.27, \tag{AV8}$$

an $\mathcal{O}(1)$ *angle requiring no fine-tuning.*

Proof. The field begins to oscillate when $3H(T_{\rm osc}) = m_\chi$; in the radiation era $H = 1.66\, g_*^{1/2} T^2/M_{\rm P}$ gives $T_{\rm osc} \approx 8.7\times10^4$ GeV ($g_* = 106.75$). The comoving number density $n_{\rm osc} = \frac{1}{2} m_\chi \theta_i^2 P^2$ redshifts as a^{-3}; entropy conservation $(a_{\rm osc}/a_0)^3 = g_{*s,0}T_0^3/(g_{*s,\rm osc}T_{\rm osc}^3)$ then yields the present density $\rho_{\chi,0} = m_\chi n_{\rm osc}(a_{\rm osc}/a_0)^3$. Dividing by $\rho_{\rm crit}/h^2 = 8.10\times10^{-47}\,\mathrm{GeV}^4$ gives $\Omega_\chi h^2 = 1.62\,\kappa_{\rm rad}\sqrt{2\pi}\,\theta_i^2$ (numerically verified; the coefficient anatomy is Rem. AV.12). Solving for $\Omega_\chi h^2 = 0.12$ gives $\theta_i = 0.271$. The period and mass are fixed by Secs. AV 4–AV 5; θ_i is the single free initial condition *of this pre-inflation form*—which Step 5b (Theorem AV.13) replaces: with no inflaton there is no chosen θ_i, and the amplitude is instead the finite $SU(2)_{60}$ CS-vacuum expectation $\langle\theta^2\rangle = 0.073$. This step nonetheless supplies the $\mathcal{O}(1)$ *cosmological prefactor* (the radiation-era $H(T)$/entropy map from $\langle\theta^2\rangle$ to $\Omega_\chi h^2$), applied to the topological $\langle\theta^2\rangle$ rather than to a chosen angle. □

Remark AV.12 (The relic-map coefficient, made exact). The sudden-approximation relic map has the bare coefficient 1.62 at the mass 5.0937 eV. Two corrections, both derived, make it exact: *(i) exact radiation-era onset.* The exact RD misalignment equation $\chi'' + (3/2t)\chi' + m^2\chi = 0$ has the regular solution $\chi = \chi_i\, 2^{1/4}\Gamma(\frac{5}{4})(mt)^{-1/4}J_{1/4}(mt)$, whose comoving ρa^3 is smaller than the sudden-approximation value at $3H = m$ by

$$\kappa_{\rm rad} = \frac{\Gamma(\frac{1}{4})^2}{6\sqrt{3}\,\pi} = 0.402625. \tag{AV9}$$

(ii) the flux-period mass. With $m_\chi = 2\pi\times5.0937$ eV (Lemma AV.6) and the onset amplitude unchanged ($f_{\rm rad}^2\theta_{\rm rad}^2 = P^2\theta_{\rm turns}^2$ identically), only the $m^{1/2}$ redshift factor of $\Omega \propto m^{1/2}f^2\theta^2$ moves: $\times\sqrt{2\pi} = 2.50663$. The net factor on the sudden-approximation map is $\kappa_{\rm rad}\sqrt{2\pi} = 1.00923$, i.e. the exact map is $\Omega_\chi h^2 = 1.62\,\kappa_{\rm rad}\sqrt{2\pi}\,Q = 1.635\,Q$ for any dimensionless quadratic amplitude Q. No anharmonic correction is owed: the Sugawara energy is exactly quadratic and the periodic parabola is strictly harmonic on the fundamental domain. A cosine potential of the same curvature is not DFD's potential: it would multiply the relic by an anharmonic factor of about 1.6 ($\Omega_\chi h^2 = 0.187$–0.192; computed). The residual spread of the map over the choice of $g_{*s,0}$ is 0.1193–0.1202 (an independent rebuild's central value reaching 0.1200).

7. Step 5b — the relic amplitude is the finite CS/WZW vacuum expectation (no free angle)

The single free input of Theorem AV.11 — the homogeneous angle θ_i — is not actually available to χ, and its correct replacement is not a chosen number but a vacuum expectation on a *finite* topological Hilbert space. Two facts combine. First, DFD has no slow-roll inflaton, so no homogeneous θ_i is selected and stretched across the sky. Second, χ is not a classical continuous angle: it is the compact harmonic C_3 flux mode of the S^3 Chern–Simons/WZW sector, whose physical states form the *finite* integrable Hilbert space of $SU(2)_k$ at the locked level $k = 60$ ($\dim = k+1 = 61$). The relic amplitude is therefore the vacuum expectation of the quadratic flux operator on that finite space — a number fixed by topology, with no free angle.

Theorem AV.13 (Finite $SU(2)_{60}$ CS-vacuum relic amplitude (no chosen angle))**.** (No inflaton, no chosen angle.) *DFD has no slow-roll inflaton (Thm FK.2); the decay constant* $f_\chi = \bar{M}_{\rm P}\,\alpha^3$ *(Lemma AV.5) and the de Sitter dictionary's rung* $H_\star = \sqrt{8\pi}\,M_R$, $M_R = M_{\rm P}\,\alpha^3$, *which is not the expansion rate of any DFD stage (Theorem SM.3), are the* same α^3 *rung* ($M_{\rm P} = \sqrt{8\pi}\,\bar{M}_{\rm P}$)*, so*

$$H_\star = \sqrt{8\pi}\,M_{\rm P}\,\alpha^3 = 8\pi\, f_\chi = 2.38\times10^{13}\ \mathrm{GeV}, \qquad \frac{H_\star}{f_\chi} = 8\pi \tag{AV10}$$

(the two $\sqrt{8\pi}$ *are physically distinct — the reduced/non-reduced Planck conversion and the* $H_\star/M_R$ *normalization — so* $H_\star/f_\chi = 8\pi$ *is a genuine product, not a double-counted Planck factor). With no inflaton no homogeneous* θ_i *is selected;* θ_i *is not a knob.*

(The amplitude is the finite-vacuum Casimir expectation.) *As the compact* S^3 *CS/WZW flux mode quantized as* $SU(2)_k$ *at* $k = 60$ *(*$K \equiv k+2 = 62$*),* χ*'s dimensionless relic amplitude is the modular-weighted vacuum expectation of the normalized quadratic Casimir:*

$$\langle\theta_\chi^2\rangle = \sum_{j=0}^{k/2} |S_{0j}|^2\,\frac{C_2(j)}{k(k+2)}, \qquad |S_{0j}|^2 = \frac{2}{K}\sin^2\frac{(2j+1)\pi}{K},$$
$$C_2(j) = j(j+1), \qquad \sum_j |S_{0j}|^2 = 1. \tag{AV11}$$

At $k = 60$,

$$\langle\theta_\chi^2\rangle = 0.072957, \qquad \Omega_\chi h^2 = 1.62\,\kappa_{\rm rad}\sqrt{2\pi}\,\langle\theta_\chi^2\rangle = 0.11928$$
$$(-0.60\sigma \text{ from Planck } 0.1200 \pm 0.0012;\ \text{Rem. AV.12}). \tag{AV12}$$

The amplitude (AV11) *is a variance in the* period-1 *(turns) flux coordinate (Lemma AV.6); its own continuum limit is* $\frac{1}{12} - \frac{1}{8\pi^2} = 0.070668$*; the amplitude lies* 3.2% *above it through the Sugawara factor* K/k*, while finiteness itself lowers it by* 0.09% *at fixed* $(k+2)^2$*. The classical value* $\pi^2/3 = 3.29$ *is the uniform variance of a period-*2π *angle — the wrong unit for this coordinate, not its continuum limit (Rem. AV.14).*

Proof. Eq. (AV10) is arithmetic on the locked rungs (f_χ, M_R share α^3; $M_{\rm P}/\bar{M}_{\rm P} = \sqrt{8\pi}$). With no inflaton there is no chosen homogeneous θ_i, so the amplitude is a property of the vacuum, not an initial condition. Two ingredients fix that vacuum value.

(i) Operator identity — the relic θ^2 is the Casimir. On the finite Hilbert space the flux sectors are the integrable representations $j = 0, \frac{1}{2}, \ldots, \frac{k}{2}$. The unique $SU(2)$-invariant quadratic operator is the Casimir $C_2(j) = j(j+1)$ — diagonal on the irreps, equal to the group Laplacian. The naive geodesic-angle-squared ψ^2 is *not* admissible as the relic operator: it is basepoint-dependent (not class-invariant), non-smooth at the S^3 cut locus, and so state-dependent as to be meaningless (its expectation ranges from $\langle\psi^2\rangle \approx 5.3$ on the flat group average down to ≈ 0.01 on a localized state). The invariant, smooth quadratic operator — hence the physical θ^2 — is the Casimir.

(ii) Normalization — $k(k+2)$ follows from two stated conventions. The quantum-corrected quadratic flux energy is the Sugawara weight $h_j = C_2(j)/(k+2)$, with $k+2 = k+h^\vee$ ($h^\vee = 2$, the $SU(2)$ dual Coxeter number). The dimensionless amplitude is this weight per bare Chern–Simons level k (the CS action is level-k, $S_{\rm CS} = \frac{k}{4\pi}\int \mathrm{Tr}(A\,dA + \frac{2}{3}A^3)$), so $\theta_j^2 = h_j/k = C_2(j)/[k(k+2)]$. The denominator is fixed by an algebraic lock:

$$\frac{C_2(k/2)}{k(k+2)} = \frac{(k/2)(k/2+1)}{k(k+2)} = \frac{1}{4} \quad \text{exactly, for all } k, \tag{AV13}$$

placing the top sector at $\theta_{\max} = \frac{1}{2}$ — the $\mathbb{Z}_2$-folded pseudoscalar fundamental-domain edge — *independently of* k. Among $\{k^2, (k+2)^2, k(k+1), (k+1)^2, k(k+2)\}$ only $k(k+2)$ gives a k-independent edge (e.g. $C_2(k/2)/k^2 = (k+2)/4k$ drifts); k^2 drops the Sugawara shift and $(k+2)^2$ double-counts it. Summing (AV11) over the 61 states at $k = 60$ ($\langle C_2\rangle = 271.40$, $\langle C_2\rangle/[k(k+2)] = 271.40/3720$) gives $\langle\theta_\chi^2\rangle = 0.0729566$, hence (AV12). The many-patch / fluctuation alternative $\delta\theta = H_\star/(2\pi f_\chi) = 4$ (per e-fold; the 2π is Gibbons–Hawking, identical in both normalizations) would wash the modular vacuum to the uniform measure — at best the finite-space ceiling $\langle Q\rangle_\infty = 0.0853$ — which is the wrong state preparation for the finite mode and is what (AV11) corrects. (The historical $\pi^2/3$ washout value was additionally a radian-units reading of the period-1 coordinate; Rem. AV.14.) □

Remark AV.14 (Proven finite-CS operator; conditional abundance closure; why there is no overshoot). *What this fixes.* The classical continuum measure gives a factor-≈ 44 overshoot, $\Omega_\chi h^2 \simeq 1.62 \cdot \pi^2/3 \approx 5.3$, and the 45× gap between $\pi^2/3$ and $Q_{\rm CS}$ factorizes exactly as

$$\begin{aligned}\frac{\pi^2/3}{Q_{\rm CS}} &= 45.0935 \\ &= \underbrace{39.4784}_{4\pi^2\ \text{(pure units)}} \times \underbrace{1.179220}_{\text{continuum measure choice}} \\ &\quad \times \underbrace{1.000921}_{\text{finiteness itself}} \times \underbrace{0.967742}_{\text{Sugawara } k/K},\end{aligned} \tag{AV14}$$

i.e. 96.5% of it (in log measure) is the radians^2 →turns^2 unit conversion of the period-1 flux coordinate (Lemma AV.6), a further 1.179 is the uniform-vs-sin^2 *continuum* measure choice, and the finite-Hilbert-space effect itself is 0.09% and lowers $Q_{\rm CS}$ at fixed $(k+2)^2$; $Q_{\rm CS}$ lies 3.2% above its continuum limit through the Sugawara factor K/k, net of that 0.09%. The correct $\mathcal{H}_k$ measure (AV11), through the exact relic map (Rem. AV.12), gives $\Omega_\chi h^2 = 0.11928$ (-0.60σ from Planck). The operator identity (the relic θ^2 is the Casimir, not the non-invariant ψ^2) and the $k(k+2)$ algebraic lock (AV13) are forced in the proof, so the amplitude $\langle\theta^2\rangle = 0.073$ is a topological deliverable, not a fit. There is no θ_i knob (no inflaton).

What is proven and what is stated. The operator identity — the relic θ^2 is the Casimir, not ψ^2 — is *proven*: ψ^2 is provably non-invariant (its Haar-character expansion has nonzero coefficients for every $j \geq \frac{1}{2}$, so it mixes irreps and is no legal operator on $\mathcal{H}_k$) and is phenomenologically excluded (it overshoots by 35–150×). The remaining ingredients rest on already-derived properties of χ, standard cosmology and two stated conventions: *(a)* the relic prefactor $1.62\,\kappa_{\rm rad}\sqrt{2\pi} = 1.635$ in (AV12) is a *separate cosmological bridge* — it carries the radiation-era $H(T)$/entropy content of the relic map (AV7) (at the exact onset, Rem. AV.12), not pure topology; the pure-topology deliverable is $\langle\theta^2\rangle = 0.073$, and the closure is (topological amplitude)×(this $\mathcal{O}(1)$ relic bridge), not a single self-contained derivation. (This prefactor is *operator-agnostic*: it is the redshift packaging of $\rho_\chi = \frac{1}{2}m_\chi^2 f_\chi^2\langle Q_\chi\rangle$ at the forced onset $3H(T_{\rm osc}) = m_\chi$, identical for *any* dimensionless quadratic amplitude Q_χ — so applying it to the flux Casimir $Q_\chi = C_2/[k(k+2)]$ is consistent, not a mixing of the flux and holonomy-angle pictures; the angle ψ^2 is the conjugate-dual description, not a second admissible operator on the same mode.) *(b)* the normalization $k(k+2)$ follows from two stated conventions: $k+2 = k+h^\vee$ is the standard Sugawara shift, the bare level is k, and the edge $\theta_{\max} = \frac{1}{2}$ — which the algebraic lock (AV13) shows is the *unique* k-independent edge — is fixed by χ's *derived* $\mathbb{Z}_2$ ($\chi \to -\chi$) orientation-oddness, the same $\mathbb{Z}_2$ that yields $N_{\rm DW} = 1$ (Rem. AV.16). The edge rests on this derived property; that the top sector sits on it is the first stated convention. *(c)* $K = k+2 = 62$ is the Sugawara shift ($k = 60$ derived + $h^\vee = 2$), the second stated convention — normalization does not even bear on it ($\sum_{n=1}^{K-1}\sin^2(\pi n/K) = K/2$ for every integer K).

We therefore grade the topological operator and amplitude as proven/forced, while the physical relic abundance remains **forced-amplitude/stated-convention** in the corpus ledger: $\langle\theta^2\rangle = 0.073$ is *forced* — measure conditional on the asserted premise P4′ (Lemma AV.27), proven operator, normalization from two stated conventions — and the abundance $\Omega_\chi h^2 = 0.11928$ (-0.60σ from Planck) follows through the standard cosmological relic-redshift map (the operator-agnostic $1.62\,\kappa_{\rm rad}\sqrt{2\pi}$, the identical $H(T)$/entropy factor that *every* dark-matter relic — ΛCDM's included — carries, exact at onset, Rem. AV.12).

The single non-DFD input is thus standard cosmology, not a DFD convention. (One optional refinement, not a gap in the theorem: deriving that standard relic-redshift map natively from the impedance/Friedmann branch, App. AU, would make the chain end-to-end DFD.)

Remark AV.15 (The thermal-onset overshoot analysis does not apply). Treating χ as a classical misalignment relic with a temperature-dependent (instanton) mass turning on at $\Lambda = \bar{M}_{\rm P}\alpha^8 \approx 20$ GeV makes the $\pi^2/3$ estimate *worse* ($\Omega_\chi h^2 \sim 10^3$–$10^4$) rather than better. That treatment does not apply (Theorem AV.13): the relic amplitude is the topological finite-vacuum expectation (AV11), set by the fixed S^3 CS/WZW spectral curvature — a geometric, temperature-*independent* scale — not by a patch-averaged classical angle evolved through a thermal oscillation onset. There is consequently no $T_{\rm osc}/g_\star$/Kibble-patch dependence in the abundance; the only residual cosmological input is the $\mathcal{O}(1)$ relic-map prefactor of caveat (a) in Rem. AV.14. *Caveat:* the $\sim 10^3$–10^4 "onset makes it worse" number holds *within* a thermal misalignment picture; it does not apply to the finite-vacuum derivation, which carries no such onset.

Remark AV.16 (Two consequences that are *not* free: an isocurvature pass and a string/wall network). *(i) Zero CDM isocurvature, for the opposite reason.* The χ amplitude is the topological finite-CS-vacuum expectation (Thm AV.13), and DFD has no inflaton (Thm FK.2), so there is no inflaton-seeded super-horizon mode to seed isocurvature; χ predicts essentially zero CDM isocurvature and passes $\beta_{\rm iso} < 0.038$ — by the absence of inflation, not by a tuned-small inflationary fluctuation. If the optical engine inflates the optical metric at a low scale (App. Q 6), the super-horizon variance it leaves enters the density quadratically, $\Delta^2_{\rm iso} \simeq 4\ln(k/k_0)\,(P_\theta/Q_{\rm CS})^2$ with $P_\theta = rA_s/(8\alpha^6)$ (Eq. (SM6); k_0 today's horizon scale), and $\beta_{\rm iso} < 0.038$ holds for $r \lesssim 10^{-10}$ (estimate), so the isocurvature pass and the B-mode null are one prediction. The local sector label adds white-noise isocurvature of at most $\Delta^2_{\rm iso} \simeq 8\times10^{-43}$ at $k = 0.05\,{\rm Mpc}^{-1}$ (computed; Rem. AV.30).

(ii) Domain walls ($N_{\rm DW} = 1$), but no *global strings.* Once the potential of Lemma AV.6 switches on, its minima define domain walls. The potential has a single minimum per period (the unit winding $\int_{S^3}\omega_3 = 1$ makes the period one turn), so $N_{\rm DW} = 1$. This is the *safe* case: with a single vacuum per period the walls are unstable and collapse before they can dominate ($N_{\rm DW} > 1$ would over-close the Universe with stable walls). The parameter-free $N_{\rm DW} = 1$ remains a sharp, falsifiable structural prediction of the S^3 origin of χ. It does not depend on the photon vertex of Theorem AV.35.

We do not *claim a global cosmic-string network.* A global string requires a spontaneously-broken $U(1)$ with a *winding complex order parameter* whose modulus $|\Phi| \to 0$ at the string core. DFD's χ is the real coefficient of the single harmonic three-form (Theorem AV.2) whose normalization $\int_{S^3}\omega_3 = 1$ is a topological constant fixed by a per-mode determinant (Lemma AV.5), *not* a complex amplitude that can relax to zero — there is no string core, hence no global string. (The string-tension estimate $G\mu = (f_\chi/\bar{M}_{\rm P})^2 = \alpha^6$ imports a vacuum-expectation-value picture χ does not realize and is not a DFD prediction; the wall self-destruction above does not rely on string-bounding.)

8. Step 5c — the topological flux-density form

Step 5b derived the relic amplitude as a finite-vacuum expectation. We restate it in the form that makes the *abundance* and the *clustering* manifestly independent variables, and then answer the standard objections. Everything turns on one identification: χ is neither a classical raw-angle misalignment condensate nor a later-produced gas with an arbitrary particle number — it is a *local topological flux-density* field whose internal fiber is the finite $SU(2)_k$ CS/WZW Hilbert space.

Theorem AV.17 (Topological flux-density relic)**.** *The local χ Hamiltonian density is*

$$\mathcal{H}_\chi(x) = \tfrac{1}{2}m_\chi^2 f_\chi^2\, Q_{\rm CS}\,[1+\delta_\chi(x)] + O(v_\chi^2),$$
$$Q_{\rm CS} = \Big\langle \frac{C_2}{k(k+2)} \Big\rangle_{S^3\,{\rm CS\,vac}}, \tag{AV15}$$

where $Q_{\rm CS}$ is the fixed internal quadratic flux-density coefficient (AV11) and $\delta_\chi(x)$ is the spacetime density perturbation of the cold flux fluid. Hence the mean abundance at onset, $\bar{\rho}_\chi(a_{\rm osc}) = \frac{1}{2}m_\chi^2 f_\chi^2 Q_{\rm CS}$, is fixed by the internal finite-CS expectation (it redshifts as $\bar{\rho}_\chi \propto a^{-3}$ thereafter, Eq. (AV26)), while clustering is carried by $\rho_\chi(x) = \bar{\rho}_\chi[1+\delta_\chi(x)]$. There is no *independent background displacement θ_i and* no *independent production number n_χ: those knobs exist only for a classical raw-angle condensate or a later-produced gas, neither of which is the DFD χ sector.*

Proof. The S^3 CS/WZW compactification supplies a finite internal Hilbert space of flux sectors $j = 0, \frac{1}{2}, \ldots, \frac{k}{2}$. The unique quadratic $SU(2)$-invariant is the Casimir $C_2(j) = j(j+1)$; the quantum-corrected quadratic flux energy is the Sugawara weight $h_j = C_2(j)/(k+2)$; and since the level-k action has quadratic stiffness k, the squared dimensionless flux-density amplitude is $Q_j = h_j/k = C_2(j)/[k(k+2)]$ (Step 5b). Its finite-vacuum expectation over the modular measure $p_j = |S_{0j}|^2$ is $Q_{\rm CS} = \sum_j |S_{0j}|^2 C_2(j)/[k(k+2)] = 0.0729566$ at $k = 60$ (AV12). With $n = 2j+1$ and $K = k+2$ the sum admits the closed form

$$Q_{\rm CS} = \frac{1}{2kK^2}\left[\frac{(K-1)K(2K-1)}{12} - \frac{K}{4\sin^2(\pi/K)} + \frac{K^2}{4} - \frac{K}{2}\right], \tag{AV16}$$

which evaluates to 0.0729565815 at $k = 60, K = 62$ (agreeing with the direct sum to all printed digits) — so $Q_{\rm CS}$ is an exact analytic number, not a numerical truncation. The spacetime dependence enters through $\delta_\chi(x)$, not through a new background value of $Q_{\rm CS}$; so the same

sector carries a fixed abundance coefficient and still clusters. □

9. Parity degeneracy of the CS measure, and the vector count

Theorem AV.18 (Exact parity halving of the modular measure)**.** *For every even $K = k + 2 \geq 6$, the modular measure $p_j = |S_{0j}|^2$ of $\mathrm{SU}(2)_k$ splits* exactly $1/2 : 1/2$ *between the integer-spin and half-integer-spin classes:*

$$\sum_{j\in\mathbb{Z}} |S_{0j}|^2 \;=\; \sum_{j\in\mathbb{Z}+\frac{1}{2}} |S_{0j}|^2 \;=\; \tfrac{1}{2}. \tag{AV17}$$

The Casimir-weighted asymmetry is not zero but is quartically suppressed,

$$\delta(K) \;=\; 1 - \frac{Q_{\textit{half-int } j}}{Q_{\textit{int } j}} \;=\; \frac{6\pi^4}{(2\pi^2-3)\,K^4}\Big[1 + O(K^{-2})\Big], \tag{AV18}$$

with limiting constant $6\pi^4/(2\pi^2-3) = 34.91530293402780$ and $\delta(62) = +2.369 \times 10^{-6}$, the integer-$j$ class being the larger.

Proof. By the character sum: $|S_{0j}|^2 = (2/K)\sin^2(\pi n/K)$ with $n = 2j+1$, and $\sum_{n\ \mathrm{odd}} \sin^2(\pi n/K) = \sum_{n\ \mathrm{even}} \sin^2(\pi n/K) = K/4$ for even K by the standard Gauss sum. Residuals verified below 10^{-51} at $K = 6, 8, 12, 22, 62, 102, 1002$. The Casimir weighting breaks the exact halving only at $O(K^{-4})$, giving the stated closed form; the constant is confirmed by $C(K) = 35.1162\,(K{=}42) \to 35.0073\,(62) \to 34.94927\,(102) \to 34.915337\,(3202)$. □

Remark AV.19 (Two mandatory statements of proof). The halving must be proved by the character sum above and *never* by the map $(2j+1) \mapsto K - (2j+1)$: for even K that map preserves parity, and at $k = 60$ the two classes hold 31 and 30 members respectively, so no bijection between them exists. The constant $34.9153\ldots$ is an asymptotic limit with the closed form given, not a fixed numerical constant.

Theorem AV.20 (Massless vector count from the internal S^3)**.** *The S^3 coexact 1-form sector at tachyon-free mass parameter ($\mu \leq 2$) delivers* exactly $N \in \{0, 3\}$ *massless four-dimensional vectors. The achievable counts over all μ are $\{n(n+2)\} = \{3, 8, 15, 24, \ldots\}$, so $N = 6$ is* kinematically unreachable*, and $N = 3$ holds if and only if $\mu = 2$ — a value which is simultaneously the dual Coxeter number $h^\vee(\mathrm{SU}(2))$, the adjoint Casimir $C_2(\mathrm{adj}\,\mathrm{SU}(2))$, and $\lambda_{\min}|\star d|$ on S^3. Independently, $b_2(\mathbb{C}P^2 \times S^3) = 1$ gives exactly one four-dimensional $U(1)$ from C_3 and* zero *Kalb–Ramond axions.*

Remark AV.21 (Right-handed W mass and convention). The associated $M(W_R) = 2.95 \times 10^{18}$ GeV using the full Planck mass (5.88×10^{17} GeV in the reduced convention), giving $(m_W/M_{W_R})^2 = 7.4 \times 10^{-34}$. The conclusion is convention-independent: 30–32 orders of magnitude below the experimental bound either way.

Remark AV.22 (What is *not* claimed here). The gauge-boson budget $8 + 3 + 1 = 12$ is **not** booked. $\mathrm{Iso}(S^3) = \mathrm{SO}(4)$ supplies six metric Kaluza–Klein graviphotons that the argument above does not dispose of, so the printed budget remains 18. Closing this requires showing that DFD's action carries no dynamical internal metric over $K = \mathbb{C}P^2 \times S^3$, or otherwise disposing of the six graviphotons separately. This is recorded as open.

a. Objections, answered. The finite-CS flux-density identification disposes of the standard objections:

O1. *"0.073 was tuned."***:**
No: it is the finite-vacuum expectation $\sum_j |S_{0j}|^2 C_2(j)/[k(k+2)]$ at the *already-fixed* level $k = 60$. Level, measure, operator, and normalization are all fixed before the abundance is evaluated.

O2. *"The WZW object is $C_2/(k+2)$, not $C_2/[k(k+2)]$."***:**
Correct, and $C_2/(k+2) = h_j$ is the Sugawara *energy*; the relic map needs the squared *amplitude*, which is energy over stiffness, $h_j/k = C_2/[k(k+2)]$. The extra $1/k$ is the level-k stiffness conversion — k^2 would drop the quantum shift, $(k+2)^2$ would double-count it.

O3. *"A CS vacuum expectation is vacuum energy, so $w = -1$."***:**
No: a local vacuum-energy term is volume-extensive (ρ =const, $w = -1$). Q_{CS} is not a volume-extensive local density; it is a finite topological state-preparation measure over flux sectors. The massive flux-density content has fixed comoving energy, so $\rho_\chi \propto a^{-3}$, $w = 0$.

O4. *"A single global flux number cannot cluster."***:**
DFD uses no smooth global number: (AV15) fixes the local coefficient Q_{CS} while $\delta_\chi(x)$ carries clustering. Abundance and perturbations are different variables.

O5. *"Inflation freezes a real-space amplitude into a random displacement."***:**
That applies to an ordinary local spectator scalar with a continuous raw coordinate; restoring the random-angle branch needs an added DFD-native map (finite CS flux sector)→(continuous raw angle uniformly randomized on $[-\pi, \pi]$). An *appended* external inflationary stage is not harmless: it kicks the flux coordinate by $H/(2\pi f_\chi)$ per e-fold, and the relic tolerates it only below $H \simeq 4\times10^{10}$ GeV (channel (a) below; Eq. (Q13)); any stage that left a detectable tensor signal fails that test (App. SM, Cor. SM.4).

O6. *"A gas of quanta has a free production number."***:**
χ is a pre-existing compact flux-density mode, not a later-produced gas: Q_{CS} in (AV15) is the fixed internal quadratic coefficient of the local fluid, not the energy of one quantum needing an occupation number; $\delta_\chi(x)$ controls clustering, not the mean abundance.

O7. *"1.62 belongs to a misalignment angle, so pairing it with a flux Casimir is inconsistent."*: $1.62\,\kappa_{\rm rad}\sqrt{2\pi}$ (Rem. AV.12) is the *operator-agnostic* cosmological relic-redshift factor for a unit dimensionless quadratic amplitude in the massive χ mode ($\rho_\chi = \frac{1}{2}m_\chi^2 f_\chi^2 Q$ at $3H(T_{\rm osc}) = m_\chi$, with $f_\chi = P$ the period and Q in turns^2 — matching normalizations, Lemma AV.6): $Q = \theta_i^2$ in the raw-angle branch, $Q = Q_{\rm CS}$ in the flux-density branch. Applying the identical $H(T)$/entropy map (the one every dark-matter relic, ΛCDM included, carries) to the forced $Q_{\rm CS}$ is self-consistent.

b. State preparation: χ cannot be Kibble-randomized. The would-be random-angle branch $\langle\theta^2\rangle = \pi^2/3$ is not a competing DFD calculation; it is a statement about a *different object*.

Theorem AV.23 (Finite-CS state-preparation)**.** *The DFD-native initial state of χ is the finite $SU(2)_{60}$ CS/WZW vacuum measure $p_j = |S_{0j}|^2$ (given the asserted premise $P4'$ of Lemma AV.27), not a Kibble-randomized continuous-angle ensemble. Consequently the relic coefficient is fixed, $Q_\chi = Q_{\rm CS} = \sum_j |S_{0j}|^2\, C_2(j)/[k(k+2)] = 0.0729566$, with* no *free initial angle θ_i and no reopening of the $(\pi^2/3)$ overshoot.*

Proof. The Kibble value $\langle\theta^2\rangle = \pi^2/3$ is the *output of a specific classicalization mechanism*, not a neutral default. It requires, jointly: (i) a local continuous order parameter $\theta(x)$ with a meltable radial partner $|\Phi|$; (ii) a high-temperature symmetry-restored phase in which $|\Phi| \to 0$; (iii) a later symmetry-breaking transition; and (iv) causally disconnected domains that reselect independent classical angles, whence $\theta_i \sim \text{Uniform}[-\pi, \pi]$ and $\langle\theta_i^2\rangle = \frac{1}{2\pi}\int_{-\pi}^{\pi}\theta^2\, d\theta = \pi^2/3$. DFD's χ has *none* of (i)–(iv). It is the coefficient of the unique harmonic three-form ω_3 on $S^3 = SU(2)$ (Theorem AV.2, $b_3 = 1$), whose normalization $\int_{S^3}\omega_3 = 1$ is a topological invariant fixed by the per-mode determinant, *not* a VEV; there is no complex amplitude $|\Phi|$ that can relax to zero, hence no string core (Rem. AV.16). Its physical state space is therefore not S^1 with a uniform classical-angle measure but the finite CS/WZW Hilbert space $\mathcal{H}_{SU(2)_{60}}$ of 61 integrable sectors $j = 0, \frac{1}{2}, \ldots, 30$. The state-preparation measure on this space is the no-boundary closed-S^3 Chern–Simons Born weight $p_j = |S_{0j}|^2$, $S_{0j} = \sqrt{2/(k+2)}\,\sin[(2j+1)\pi/(k+2)]$, $\sum_j |S_{0j}|^2 = 1$ — *derived* (not asserted) by S^3 surgery in the two paragraphs following this proof, which also exclude the only wrong-valued rival (the linear-d_j Cardy weight). Pairing it with the unique quadratic invariant $Q_j = C_2(j)/[k(k+2)]$ (Theorem AV.17) gives $Q_{\rm CS} = 0.0729566$. To convert this into the $\pi^2/3$ ensemble one must *add* a non-DFD map (finite CS flux sector)→(continuous raw angle)→(Kibble domains); DFD's fixed S^3 geometry supplies no such map. The free angle is removed not by naming but by quantizing the correct object. □

c. Brick 1 — the measure is the closed-S^3 surgery vacuum, not a name. The weight $p_j = |S_{0j}|^2$ is not posited; it is the Born amplitude of the closed-S^3 no-boundary Chern–Simons state, computed by standard Witten–Reshetikhin–Turaev surgery and wired to the S^3 partition function this manuscript already uses elsewhere. Present the closed internal $S^3 = SU(2)$ as two solid tori glued by the modular generator S (genus-one Heegaard split). A solid torus with *empty* core (no Wilson line threaded) prepares the no-boundary Hartle–Hawking state $|0\rangle$ in the boundary-torus Hilbert space $\mathcal{H}_{T^2} = \text{span}\{|j\rangle\}_{j=0}^{k/2}$; this is DFD's own cosmogenic Wheeler–DeWitt no-boundary state (the DFD primordial no-boundary/Wheeler–DeWitt selecting condition on ψ, App. Q, Rem. Q.11), and there is no native inflaton (Thm. FK.2) nor sustained de Sitter stage (Thm. SM.2) to re-prepare it. Gluing the second solid torus by S gives

$$Z_{S^3} = \langle 0|S|0\rangle = S_{00} = \sqrt{\tfrac{2}{k+2}}\,\sin\frac{\pi}{k+2}, \qquad \text{(AV19)}$$

identically the S^3 Chern–Simons partition function used for the α^{57} closure (App. AP, Lem. AP.22). In the glued-torus basis the no-boundary state is $|0\rangle = \sum_j S_{0j}\,|j\rangle$, and because S is unitary the Born weights are *self-normalized* with no ad hoc division, $p_j = |S_{0j}|^2$ with $\sum_j p_j = (SS^\dagger)_{00} = 1$. The measure is thus *derived* as the closed-three-manifold no-boundary amplitude built from the very $Z_{S^3} = S_{00}$ that fixes the α-closure; only its j-resolved row is read off here.

d. Brick 2 — the linear-d_j (Cardy) weight is excluded by the absence of a boundary. The only measure that would reproduce the high value $Q = 0.0767$ ($\Omega_\chi h^2 = 0.1254$ under the exact map, Rem. AV.12) is the *linear* quantum-dimension weight $p_j^{\rm Cardy} = d_j/\sum_{j'} d_{j'}$, $d_j = S_{0j}/S_{00}$. This is not a competing vacuum on the closed S^3: it is the diagonal of the Cardy trivial-brane *boundary* state, whose annulus partition function produces a weight linear in d_j only on a manifold *with* boundary. The decisive algebra is that the genuine (squared, true-probability) quantum-dimension measure collapses *exactly* back onto the no-boundary value,

$$\frac{d_j^2}{\mathcal{D}^2} = \Big(\frac{S_{0j}}{S_{00}}\Big)^2 S_{00}^2 = |S_{0j}|^2, \qquad \mathcal{D}^2 = \sum_j d_j^2 = \frac{1}{S_{00}^2}, \qquad \text{(AV20)}$$

so the only quantum-dimension weight that *can* live on a closed manifold simply reproduces $p_j = |S_{0j}|^2$; *only* the un-squared, linear d_j deviates, and a linear, non-amplitude-squared weight is an open-string/boundary trace, not a closed-manifold quantum probability. The χ relic is the coefficient of the unique harmonic three-form on the *closed* internal $S^3 = SU(2)$ ($b_3 = 1$, $\partial S^3 = \varnothing$; Thm. AV.2); it carries no brane, defect, horizon, or Wilson line (changing j costs at least the Sugawara gap, 2.95×10^{16} GeV; Rem. AV.29). With no internal boundary there is no annulus on which a g-function can be defined, so $p_j^{\rm Cardy} \propto d_j$ has no manifold to live on; a horizon or observable-universe boundary lives in *exter-*

nal spacetime, not on the internal S^3 worldvolume, and cannot license it. To force the linear-d_j value one must *append* a non-DFD boundary the fixed S^3 geometry does not contain — the exact mirror of the $\pi^2/3$ Kibble no-go. The closed-S^3 no-boundary vacuum, equal to the Plancherel row $d_j^2/\mathcal{D}^2$, is therefore the unique admissible measure. *(Conditionality: this selection holds given DFD's no-boundary Wheeler–DeWitt condition (App. Q, Rem. Q.11) — a central DFD postulate shared with all of its cosmology, not an independently derived fact. Granting it, the linear d_j is excluded, and with the asserted premise P4′ (Lemma AV.27) $|S_{0j}|^2$ is forced.)*

e. Brick 3 — conditional uniqueness of the abundance measure (all rivals dispatched).

Theorem AV.24 (Conditional uniqueness of the sector measure)**.** *Assume (P1) the closed-S^3 no-boundary CS state prepared by empty-core WRT surgery (Brick 1 above); (P2) the RT/TQFT axioms for $SU(2)_{60}$ with the two-solid-tori Heegaard preparation, including the Sugawara identity $h_j = C_2(j)/(k+2)$; (P3) the Born weighting of sector amplitudes (derived elsewhere in DFD from additivity and no-signaling); and (P4,* cycle-anchoring, asserted by construction*) that the physical χ winding — the flux jump costing the $2\pi/\alpha$ instanton — is carried by the glued-torus core cycle of the Heegaard splitting. Then the sector measure is uniquely $p_j = |S_{0j}|^2$, the abundance operator is uniquely $\hat{Q} = \sum_j [C_2(j)/k(k+2)]P_j$.*

Proof sketch. State uniqueness: every genus-1 gluing presentation of S^3 is of the form $\pm T^a S T^b$; since T is diagonal-unitary, the Born weights $|\langle j|T^a S T^b|0\rangle|^2 = |S_{0j}|^2$ are presentation-independent, and by Waldhausen's theorem (the genus-1 Heegaard splitting of S^3 is unique up to isotopy) the no-boundary state is unique up to phase. *Orbit completeness:* the admissible cut states form exactly the stabilizer orbit $\{T^m S T^n|0\rangle\}$, all yielding the identical measure; every other candidate is excluded structurally — other S-columns require Wilson-line insertions (violating no-boundary emptiness), and longer $SL(2,\mathbb{Z})$ words present lens spaces, not S^3. *Fusion stationarity:* the Verlinde fusion kernel $T_a(j\to m) = N_{aj}^m\, d_m/(d_a d_j)$ is exactly stochastic and leaves $p_j = |S_{0j}|^2$ stationary for every a (detailed balance), so fusion processes preserve the same measure. □

Remark AV.25 (Rival table). Each rival weight fails a named premise: linear-d_j (Cardy) — no boundary to live on (Brick 2); knotted-cut weights $p_j \propto |S_{0j}|^2|J_j(K)|^2$ — excluded by the stated two-solid-tori preparation (P2); thermal $e^{-\beta E_j}$ — no Hamiltonian evolution on the closed preparation; d_j^p for $p \neq 2$ — not an amplitude-squared state weight (and $p = 1$ is Brick 2); the meridian-dual reading δ_{j0} — the Born weight of the same state in the *preparation* basis, corresponding to an abundance operator that appears nowhere in DFD and predicts $\Omega_\chi h^2 = 0$ identically, excluded by any nonzero dark-matter observation.

Remark AV.26 (Anchoring dichotomy — the status of P4). P4 is *operator-selected, not derived.* The written abundance operator $\hat{Q}$ has 61 distinct eigenvalues ($C_2(j)$ strictly increasing), whereas the preparation-core observable is deterministic on $|0\rangle$ with eigenvalue $C_2(0) = 0$: the written operator therefore provably reads the glued core, and the only rival reading predicts zero dark matter. But S^3 is simply connected — both Heegaard cycles bound discs — and no written decomposition of $\int_{S^3}\omega_3$ selects one cycle over the other, so P4 remains the single asserted premise of this theorem. Deriving it (a Heegaard decomposition of the χ flux jump) would make the uniqueness unconditional given P1–P3.

Lemma AV.27 (Exhaustion: sector-changing processes are glued-core processes)**.** *On the* 61*-dimensional torus Hilbert space of $SU(2)_{60}$, the Wilson-loop algebras of the two Heegaard core cycles jointly generate the full operator algebra* $\mathrm{End}(\mathbb{C}^{61})$*: the preparation-core loops act diagonally with* 61 *distinct Verlinde eigenvalues S_{qj}/S_{0j} (for $q = \frac{1}{2}$ they are the distinct values $2\cos(\pi(2j+1)/62)$), and the spin-$\frac{1}{2}$ glued-core loop acts as the fusion shift connecting all sectors; the joint commutant is therefore scalar (Verlinde 1988; Witten 1989 §4; Elitzur–Moore–Schwimmer–Seiberg 1989). Consequently* any *operator that changes the sector label j necessarily contains glued-core insertions — preparation-core insertions are exactly j-inert (diagonal). Cycle-anchoring thus follows automatically from the single sharpened premise:*

> ***P4′:*** the $2\pi/\alpha$ winding instanton is a sector-changing (fusion) process.

P4′ is the part of P4 that remains asserted; it is invoked (not derived) only for cycle-anchoring (Theorem AV.24). It cannot refer to the unit large gauge winding of Lemma AV.6(i), which multiplies every Chern–Simons state by $e^{2\pi i k w} = 1$ and so changes no sector: P4′ asserts that a physical instanton of action $2\pi/\alpha$ changes j through glued-core insertions, which this lemma permits but does not show, and no protection of the sector label rests on it (Rem. AV.29). A standing obstruction to any first-order derivation of P4′ is the symplectic factorization $\delta\chi \wedge \delta j \equiv 0$; the live route is second-order (the instanton's on-shell action evaluated between neighboring flux vacua). Note the construction here is exactly symmetric under S-conjugation, so this lemma supplies consistency and exhaustion, not evidence for P4′ over its dual.

Two dynamical channels confirm the flux state is non-decoherable, not only the default at $t = 0$:

(a) No inflaton epoch (decoupling). Channel (iv) needs many super-horizon e-folds for a stochastic angle to random-walk to $\pi^2/3$. DFD has no inflaton (Thm. FK.2) and no sustained de Sitter stage (Thm. SM.2): there is no epoch in which the walk runs. The rung-locked scale $H_\star = 8\pi f_\chi$ gives $H_\star/(2\pi f_\chi) = 4$ *exactly*, so even a single e-fold of a hypothetical de Sitter stage would inject $\sigma^2_{\rm inf} \sim 16$ — *not* small (this is the Inflation-Dictionary

Exclusion Theorem SM.3: a slow-roll reading of A_s, r forces $H_{\rm inf} = 8\pi f_\chi$, $\delta\theta = 4$ per e-fold on a period-1 coordinate, hence immediate washout of the modular vacuum to the uniform ceiling $\Omega_\chi h^2 = 0.139$, excluded by Planck — so the slow-roll branch and the relic cannot coexist). The relic survives because that stage *does not exist*, not because its kick would be small:

$$\sigma^2_{\rm inf} \simeq N_{\rm eff}\Big(\frac{H_\star}{2\pi f_\chi}\Big)^2 = 16\,N_{\rm eff} \quad \Big(\textit{if} \text{ an inflaton epoch existed; } N_{\rm eff} = 0 \text{ in DFD}\Big). \tag{AV21}$$

(b) The finite Hilbert space caps the cold relic at every temperature. The relic is robust because a large overshoot is *unreachable* from the finite CS Hilbert space at *any* temperature, independent of the gap magnitude. Thermalizing the 61-state space can at most drive it to the infinite-T uniform measure $p_j = 1/61$, for which $\langle Q\rangle_\infty = \frac{1}{61}\sum_j C_2(j)/[k(k+2)] = 0.0853$, i.e. $\Omega_\chi h^2 \le 1.62\,\kappa_{\rm rad}\sqrt{2\pi}\times 0.0853 = 0.139$ — a 17% ceiling. (The "continuum catastrophe" $\pi^2/3$ fails twice: it is a radian-units reading of the period-1 flux coordinate, Lemma AV.6, and in any case not in the spectrum of a finite-dimensional flux Hilbert space.) Below that ceiling the finite-CS *vacuum* is itself protected by the Sugawara gap: every change of the sector label costs at least the first flux excitation, $E_{\rm gap} = h_{1/2}\bar{M}_{\rm P} = 2.95\times 10^{16}$ GeV ($h_{1/2} = C_2(\frac{1}{2})/(k+2) = 0.0121$), far above $H_\star$ and above every temperature of the radiation era, and the modular measure is stationary under the fusion kernel (Rem. AV.29). The protection is this gap, not a small interaction rate. The light 4D quanta of χ are a separate question. The plasma at the leptogenesis temperature $T_L = M_{\rm P}\alpha^3/\sqrt{2\pi} = 1.89\times 10^{12}$ GeV that DFD's baryon asymmetry requires (App. AH) would produce them through any photon or gauge coupling of χ, and even the smallest nonzero coupling that the flux period allows would produce a fifth of their equilibrium abundance or more and leave a hot relic, $\Omega_{\chi,\rm th}h^2 \simeq 0.005$–$0.023$ on top of the cold 0.1193, which the CMB reads as extra cold dark matter and Planck excludes (computed). χ has no such coupling: its photon coefficient is $E = 0$ (Theorem AV.35), so the plasma adds no thermal χ. The general expression is therefore

$$\Omega_\chi h^2 = 1.62\,\kappa_{\rm rad}\sqrt{2\pi}\,[\,Q_{\rm CS} + \sigma^2_{\rm inf}\,] + \Omega_{\chi,\rm th}h^2,$$
$$Q_{\rm CS} = 0.0729566, \quad \sigma^2_{\rm inf} = 0 \ \text{(no inflaton epoch)},$$
$$\Omega_{\chi,\rm th}h^2 = 0 \ \ (E = 0), \tag{AV22}$$

so the cold relic is $\Omega_\chi h^2 = 1.62\,\kappa_{\rm rad}\sqrt{2\pi}\,Q_{\rm CS} = 0.11928$, and the thermal term, the hot relic of the plasma, vanishes because χ has no photon coupling. The Kibble-randomized branch is not the DFD default — it is an *added* external state-preparation assumption that DFD's fixed S^3 geometry does not realise.

Residual and sharpest falsifier. Because the finite Hilbert space caps the cold relic at 0.139 at *any* temperature (channel (b)), a large overshoot of the cold relic cannot be reopened by thermalizing the sector label. The only way to recover a continuum random-angle value is to *append* a continuous degree of freedom outside the CS Hilbert space — a light radial partner of χ at f_χ that a super-scale bath could excite — which DFD's fixed S^3 geometry forbids (no complex amplitude relaxing to zero, Rem. AV.16); a fully independent no-go on such a partner is the one place a determined adversary can still push. The single sharpest falsifier is therefore external: should any future DFD-native epoch ever supply sustained quasi–de Sitter e-folds above $H \simeq 4\times 10^{10}$ GeV (Eq. (Q13)), channel (a) reopens — so survival is conditional on Theorem FK.2 remaining airtight and on the optical engine staying below that scale. Such an epoch is observable: it freezes tensor modes with $P_t = 8\alpha^6 P_\theta$ (Eq. (SM6)), so a primordial B-mode detection at $r \gtrsim 10^{-7}$ would mark it.

Lemma AV.28 (Preservation through the pre-BBN optical phase)**.** *Let the pre-BBN optical screen flow $\psi_0(t)$ (App. Q 6) act during the primordial era, and let P_j be the projector onto the integrable CS sector j. The screen ψ_0 is a* gauge-singlet spacetime *field acting on propagation ($c_{\rm eff} = ce^{-\psi_0}$), whereas the j label the integrable sectors of the internal $SU(2)_{60}$ CS/WZW Hilbert space. Every transition $j\to j'$ costs at least the Sugawara gap $E_{\rm gap} = h_{1/2}\bar{M}_{\rm P} = 2.95\times 10^{16}$ GeV, so a matrix element between sectors oscillates at least 9.2×10^{23} times faster than the χ mass oscillation and far faster than the screen varies. The coupling the screen exerts is therefore block-diagonal in j, up to terms suppressed by that ratio,*

$$P_{j'}\,H_{\psi\chi}\,P_j \simeq 0 \quad (j'\neq j), \qquad H_{\rm coupl}(t) = \sum_j h_j(t)\,P_j, \tag{AV23}$$

so $[H_{\rm tot}(t), P_j] \simeq 0$ and

$$\frac{d}{dt}\,{\rm Tr}\big(\rho_\chi P_j\big) \simeq 0 \quad\Longrightarrow\quad p_j(t) = p_j(t_i) = |S_{0j}|^2. \tag{AV24}$$

The optical phase can stretch and freeze spacetime perturbations but cannot move probability between integrable representations: it prepares spacetime coherence, it does not thermalize the internal finite-CS label.

Remark AV.29 (Scope of the preservation lemma). Block-diagonality (AV23) is not assumed; it rests on two protections of the sector label. *The Sugawara gap:* a transition $j\to j'$ costs at least $E_{\rm gap} = 2.95\times 10^{16}$ GeV, so a flow that is slow on that scale drives none, and a thermal process at the leptogenesis temperature supplies it with weight 10^{-6760} (computed). *Fusion stationarity:* the modular measure $|S_{0j}|^2$ is stationary under every Verlinde fusion kernel (proof of Theorem AV.24), so any fusion process that does occur leaves p_j unchanged. The winding instanton is not a protection: a unit winding of the flux acts on the Chern–Simons state as $e^{2\pi i k w} = 1$ (Lemma AV.6(i)) and changes no sector. The Kibble-randomized branch returns only if a non-DFD operator that mixes sectors at rates comparable to $E_{\rm gap}$ is added by hand (converting

the finite $SU(2)_{60}$ sector into a continuous Kibble angle) *or* if $H_{\rm true}$ exceeds the erasure bound (Q13). Together with the modular-vacuum preparation (Theorem AV.23), this gives: *the finite-CS abundance is not assumed; it is prepared by the closed S^3 modular vacuum and preserved through the pre-BBN optical phase by the Sugawara gap and fusion stationarity.*

Remark AV.30 (χ is a comoving-variance relic: not a condensate, not a constant variance). The sector state $\rho_\chi = \sum_j |S_{0j}|^2 P_j$ is diagonal, and χ is a local field that acts within each sector, where the state is even under the orientation symmetry $\chi \to -\chi$; so the one-point function *vanishes*, $\langle\chi\rangle = \mathrm{Tr}(\rho_\chi \chi) = 0$. This is not a problem — it is the correct nature of the relic. The conserved CS quantity is the *dimensionless comoving quadratic action*, the expectation of the diagonal operator $\widehat{Q} = \sum_j [C_2(j)/k(k+2)]\, P_j$,

$$\langle\widehat{Q}\rangle = \sum_j |S_{0j}|^2 \frac{C_2(j)}{k(k+2)} = Q_{\rm CS} = 0.0729566 \qquad \text{(AV25)}$$

(conserved: p_j fixed),

which fixes the *physical* field variance at oscillation onset $a_{\rm osc}$ to $\langle\chi^2\rangle_{\rm phys}(a_{\rm osc}) = f_\chi^2 Q_{\rm CS}$. It is *not* a constant local variance: a constant $\langle\chi^2\rangle$ would give $\rho \simeq \frac{1}{2} m_\chi^2 \langle\chi^2\rangle$ =const, i.e. $w = -1$. Rather, as for any massive scalar Fock/mixed state, the comoving occupation $\langle N\rangle$ is conserved while the physical variance and energy dilute with physical volume:

$$\langle\chi^2\rangle_{\rm phys}(a) = f_\chi^2 Q_{\rm CS}\Big(\frac{a_{\rm osc}}{a}\Big)^3,$$
$$\rho_\chi(a) = \tfrac{1}{2} m_\chi^2 f_\chi^2 Q_{\rm CS}\Big(\frac{a_{\rm osc}}{a}\Big)^3 \propto a^{-3}, \qquad w_\chi = 0, \qquad \text{(AV26)}$$

clustering through $\delta_\chi(x)$. Thus χ is a *finite-CS comoving-variance relic*: $\langle\chi\rangle = 0$, $\langle\chi^2\rangle_{\rm phys} \neq 0$ and redshifting as cold matter — exactly as a cold Fock state has zero field expectation but a real, diluting mass density. $Q_{\rm CS}$ therefore enters the abundance as a conserved comoving *second moment* $\langle\widehat{Q}\rangle$, *not* a classical displacement θ_i^2; the relic map $\Omega_\chi h^2 = 1.62\,\kappa_{\rm rad}\sqrt{2\pi}\,\langle\widehat{Q}\rangle = 1.635\,Q_{\rm CS} = 0.11928$ is a variance map, not an axion-misalignment formula. The coherent value $\pi^2/3$ belongs to the *other* object — a classical compact scalar with $\langle\chi\rangle = \theta_i \neq 0$, read in radians — and does not apply here. DFD dark matter is therefore neither a coherent misalignment condensate nor a constant vacuum variance: it is finite topological quadratic energy whose conserved comoving action redshifts as cold matter.

The sector label is local. χ is a local four-dimensional field (Theorem AV.17), so its sector is set independently in causally separate patches when the relic forms. The domains are small: no larger than the Hubble patch at oscillation onset, 2×10^{10} m comoving today ($\sim 10^{-26}\,M_\odot$ of χ), and about 1 km if the label is set at the leptogenesis temperature. On every observable scale the realized abundance is therefore the domain average, $\Omega_\chi h^2 = 0.1193$ (fractional error below 10^{-24}), and the domain-to-domain spread adds white-noise isocurvature of at most $\Delta^2_{\rm iso} \simeq 8 \times 10^{-43}$ at $k = 0.05\,\mathrm{Mpc}^{-1}$ (computed). A global label would instead make the observable universe one draw from p_j, with a $\pm 65\%$ spread about 0.1193, and $\Omega_\chi h^2$ would be the value of a single rung ($j = 16$ gives 0.1195) rather than an average.

Net. With χ taken as DFD defines it — the finite S^3 CS/WZW topological flux-density relic — the abundance closes numerically at the ledger grade forced-amplitude/stated-convention: $m_\chi = 32.005$ eV, $Q_{\rm CS} = 0.0729566$, $\Omega_\chi h^2 = 1.62\,\kappa_{\rm rad}\sqrt{2\pi}\,Q_{\rm CS} = 0.11928$ (-0.60σ from Planck). The would-be 44× overshoot, $(\pi^2/3)/Q_{\rm CS} \simeq 45$, was the cost of reading the period-1 flux coordinate in radians and quantizing the wrong object (a continuous random angle) (AV14), not a physical catastrophe.

10. Step 6 — the third peak, with no postulated CDM

Theorem AV.31 (CMB third-peak height from χ)**.** *A pressureless component of cold density $\Omega_\chi h^2 = 0.12$, clustering at recombination $z \simeq 1100$, reproduces the Planck acoustic-peak height pattern $[H_1, H_2, H_3] \propto [1, 0.45, 0.44]$ ($H_3/H_2 \approx 1.0$). Since χ is cold, non-thermal, and pressureless on all CMB scales (Theorem AV.8), it enters the photon-baryon perturbation kernel identically to a cold-dark-matter component of the same Ωh^2, and supplies exactly this height.*

Proof (CAMB-validated). A fixed-Ω_b Boltzmann computation (CAMB) gives, for a baryon-only universe ($\Omega_c h^2 \to 0$), peaks at $\ell \simeq 294/771/1212$ with $[H_1, H_2, H_3] \propto [1, 0.39, 0.205]$ ($H_3/H_2 = 0.53$); restoring a cold pressureless component $\Omega_c h^2 = 0.12$ moves the peaks to $\ell \simeq 220/536/813$ and lifts the ratio to $[1, 0.45, 0.44]$ ($H_3/H_2 \approx 1.0$), matching Planck. The third-peak height is set by matter–radiation equality and the driving of the cold well, not by Silk damping (full Silk removal reaches only $H_3/H_1 = 0.38 < 0.44$). Because the χ field is dynamically identical to a cold pressureless fluid of the same Ωh^2 at recombination, the CAMB result at the derived abundance *is* the χ result. Run at the derived $\omega_\chi = 0.11928$ (Thm AV.13) on the measured clock ($H_0^{\rm early} = 67.52$, which fixes the peak positions $\ell \simeq 220/536/813$), the pipeline gives the height pattern $H_3/H_2 = 0.977$ (0.0σ), $H_3/H_1 = 0.444$ ($+0.5\sigma$), $H_2/H_1 = 0.454$ ($+0.5\sigma$) against the Planck 2018 bandpowers; on the same clock the Planck 2018 high-ℓ (plik-lite) likelihood places the derived abundance at -0.98σ (App. ZS). □

Remark AV.32 (Why no other DFD device delivers this). Every non-χ route to the third peak is closed: deep-MOND gravity enhancement is wrong-signed per mode (it lifts H_1 above H_3); the nonlinear AQUAL harmonic injection is negligible and lands in troughs; a line-of-sight

ψ-screen cannot move the peak locations because the sound-horizon rod and angular-diameter distance transform together (App. ZS); the Jacobian lift is therefore excluded as a global CMB mechanism; sound-speed structure $c_s(\psi)$ is time-only and cancels in height ratios; and a single forced echo at the sound-horizon delay cannot selectively boost the third peak without filling the troughs. The cold clustering charge is irreducible — and χ is the derived field that carries it.

11. Step 6b — stability: χ has no photon coupling

Remark AV.33 (χ stability: $E = 0$ under DFD's CP). χ is stable because it has no photon coupling: its photon coefficient is $E = 0$ (Theorem AV.35), so it has no two-photon decay and its lifetime is infinite. The selection rule is DFD's CP, which acts as complex conjugation on $\mathbb{C}P^2$ and as the identity on S^3 (App. L). Under it χ is even and $F\tilde{F}$ is odd, so $\chi F\tilde{F}$ is odd and absent. The operator $\chi F\tilde{F}$ is even only under a parity that also reverses the orientation of S^3 ($\omega_3 \to -\omega_3$, $\chi \to -\chi$); that reflection is not DFD's CP, and it cannot be made one: the CP map of App. L must preserve the orientation of $\mathbb{C}P^2 \times S^3$, and $\mathbb{C}P^2$ has no orientation-reversing self-map to compensate a reflection of S^3. The reduction $\int_{S^3} \omega_3 = 1 \neq 0$ does let an orientation-odd internal three-form descend to a nonzero 4D operator, so the absence is a CP selection rule, not a cohomological one, and the exact period independently excludes any small nonzero coefficient (Theorem AV.35, route (b)).

Remark AV.34 (DFD's CP forbids an axial χ coupling; DFD's baryogenesis does not use one). Because χ is even under DFD's CP (Rem. AV.33), the derivative coupling $\partial_\mu\chi\, J^\mu$ to any fermion current is CP-odd and absent, like $\chi F\tilde{F}$, so spontaneous baryogenesis through χ is closed. DFD's baryon asymmetry does not use it. Its driver is the determinant-line connection $A_5 = Q\, d\ln A$, $Q \propto \alpha$, of the internal axial Berry holonomy (App. AH, *Extended Derivations*), whose temporal holonomy is the chemical potential $\mu_{B-L} = A_{50} = QH$; it contains no χ. A χ-sourced chemical potential would fall short by about 27 orders of magnitude, because the relic χ is frozen at T_L and starts to oscillate only at $T_{\rm osc} \simeq 8.7 \times 10^4$ GeV (computed). The driver's α^4 power is derived, and so is its bias current, $B{-}L$: a current with an axial quark component would be QCD-anomalous and, coupled to the never-ending A_5, would move $\bar{\theta}$ away from zero. Its sign is fixed by an adopted orientation axiom. With the stated carrier, which gives each generation a full $B{-}L$ turn per flux step, the mechanism gives η_B of about (2–3)$\times 10^{-9}$, three to five times Planck's value, and agreement would need one winding of the determinant line per e-fold, where the stated carrier gives three (App. AH); the baryon asymmetry is carried as one calibrated input, ω_b (App. FK).

12. Step 7 — no photon coupling: $E = 0$

Theorem AV.35 (χ has no photon coupling)**.** *The photon coefficient of χ vanishes, $E = 0$: χ has no vertex $\mathcal{L} \supset -\frac{1}{4} g_{\chi\gamma}\, \chi F\tilde{F}$ ($g_{\chi\gamma} = E\alpha/P = 0$) and no linear coupling to any Standard Model field. It neither decays nor converts to photons, and it is stable. Any dark-matter photon line at* 16.0 *eV (*77.5 *nm, two-photon decay) or axion-like signal at the χ mass,* 32.005 *eV (vacuum wavelength* 38.74 *nm, conversion), at any strength, falsifies χ.*

Proof. Three routes give $E = 0$. *(a) Fermion loops.* The loop contribution is $E = 2\sum_f X_f\, d_f\, q_f^2$, with X_f the charge of fermion f under the shift $\chi \to \chi + P$. χ is a separate sector, not a 60th internal mode (Rem. AV.3); it carries no Peccei–Quinn charge (the BSM-forbidden theorem of App. AH); and the saturated index 60 admits no further heavy fermion. So $X_f = 0$ for all 48 Weyl fields and the loop part vanishes. The one alternative reading, χ as the Chern–Simons number of an $SU(2)$ that the Standard Model fermions see (the S^3 spectral flow of Thm. F.14), gives in every weighting of the fermions other than a hypercharge gauge rotation either gauge couplings of order ten or a coupling of order 30–90 to the right-handed-neutrino mass phase, and each of these thermalizes χ at the leptogenesis temperature (computed); so the $SU(2)$ whose Chern–Simons number is χ carries no quark or lepton (Theorem AV.4). *(b) Discrete coefficients and the hot plasma.* The period $\chi \to \chi + P$ is a gauge identification (Lemma AV.6), so on the Standard Model group with its $\mathbb{Z}_6$ quotient (App. F) the anomaly coefficients are discrete: E is an even integer if χ does not couple to gluons and $|E| \geq 2/3$ if it does. The unit value $E = 1$ is not allowed, and the photon Chern–Simons level $E/2$ on the domain walls of Rem. AV.16 must likewise be an integer. At the leptogenesis temperature $T_L = 1.89 \times 10^{12}$ GeV every smallest nonzero coupling allowed by a $\mathbb{Z}_6$, $\mathbb{Z}_3$ or $\mathbb{Z}_2$ quotient produces χ quanta at $\Gamma/H = 0.26$–965 and leaves a hot relic $\Omega_{\chi,\rm th}h^2 = 0.005$–$0.023$, 1.8–8.5 times Planck's limit 0.0027 (computed; the rates are estimates good to about 20%). A group with no quotient would need colour-singlet charges of $e/6$ or $e/3$, which DFD excludes. Only $E = 0$ survives. *(c) CP.* DFD's CP is complex conjugation on $\mathbb{C}P^2$ combined with the identity on S^3 (App. L, Cor. L.2); a reflection of S^3 is excluded, since the map must preserve the orientation of $\mathbb{C}P^2 \times S^3$ for the mapping torus to be oriented, and $\mathbb{C}P^2$ has no orientation-reversing self-map to compensate it. With that CP acting on the real form C_3 by pullback alone, with no sign of its own, the Chern–Simons number χ, its integral over S^3, is therefore CP-even, and every shift-symmetric linear coupling ($\chi F\tilde{F}$, $\chi W\tilde{W}$, $\chi G\tilde{G}$, and $\partial_\mu\chi\, J^\mu$ for any fermion current) is CP-odd. DFD's CP violation sits in the CKM phases and in the adopted orientation of the baryogenesis transport (Axiom E-transport′, Ext. Deriv. App. AH), and χ has no linear coupling to any Standard Model field for loops to dress (no shift charges, no mixing with ψ,

whose internal modes are forms of another degree, and an even potential), so E is its tree-level value, zero. Routes (b) and (c) are independent: $E = 0$ follows from the exact period with DFD's CP, given that χ's period is an integral period of C_3 (Lemma AV.6 (i)), or from the exact period with the $\mathbb{Z}_6$ quotient and a plasma that reaches T_L, as DFD's baryogenesis requires. The step lattice, the CP parity and the operator table are theorems; the couplings and relic densities are computed. □

Remark AV.36 (Experimental status: gravitational only). With no photon coupling χ predicts a *null* result in every haloscope, light-shining-through-walls, direct-detection and indirect-detection experiment, and it produces no conversion line, no decay photons and no dark-ages ionization floor. A photon line at 16.0 eV (77.5 nm) or 32.005 eV (38.74 nm) from dark matter, or a confirmed halo-recoil or haloscope signal in any current-reach channel, at any strength, falsifies χ. The complementary, mass-independent signatures are gravitational/clustering: the third-peak scaffolding (Sec. AV 10) and the rotation-curve scatter (Rem. AV.38).

13. Why χ is the true definition of dark matter, not adopted CDM

Remark AV.37 (χ versus a parameter-fit CDM component). Four properties separate χ from cold dark matter grafted onto the model:

1. **Forced by topology, not postulated.** χ is the unique harmonic three-form on $S^3 = SU(2)$ (Theorem AV.2); its existence is a theorem of the fixed internal geometry, in a Chern–Simons sector DFD already uses for the closed form of α.

2. **Does not break absolute time.** χ is an ordinary a^{-3} matter field propagating on the fixed ψ background; it does not modify the absolute-time foliation or any background dynamics that anchor DFD.

3. **Mass and period from the determinant ledger, with the stated multiplicity $\sqrt{158}$ and the stated stiffness.** $P = f_\chi = \bar{M}_{\rm P}\alpha^3$ (Lemma AV.5, Lemma AV.6) and $m_\chi = 2\pi\sqrt{158}\,\bar{M}_{\rm P}\alpha^{13} = 32.005$ eV (Theorem AV.8) come from the determinant ledger, with the mass tied to the same α^8 scale as the Higgs.

4. **Relic abundance — derived, conditional on the flux-period identification, the stated count 158 and premise P4′ (the Finite $SU(2)_{60}$ CS Vacuum Relic).** With no inflaton there is no chosen angle (Theorem AV.13); the amplitude is the finite $SU(2)_{60}$ CS/WZW vacuum expectation of the quadratic Casimir, $\langle\theta^2\rangle = \sum_j |S_{0j}|^2 C_2(j)/[k(k+2)] = 0.073$, giving $\Omega_\chi h^2 = 0.11928$ (-0.60σ from Planck 0.1200 ± 0.0012). The operator is proven and the normalization $k(k+2)$ rests on two stated conventions ($\theta_{\max} = \frac{1}{2}$ from χ's derived $\mathbb{Z}_2$, $K = k+2$ from Sugawara), given which the amplitude is forced; the only non-DFD input is the standard cosmological relic-redshift map, exact at onset (Rem. AV.12). A factor-44 overshoot is a units-plus-continuum-measure artifact (AV14).

χ is the weak-sector see-saw sibling of the Higgs in the same α-tower: a derived, cold, non-thermal a^{-3} field that supplies the clustering component the CMB kernel requires — and so it is the named definition of cold dark matter rather than an external "dark" unknown.

a. How χ and the μ-law coexist in galaxies: an open question. DFD's gravity has two channels (App. GR): an unscreened rest-mass channel, sourced by all rest mass, and the optical/ψ μ-AQUAL response (the exponential response of App. BS, weak-response form $\mu(x) = x/(1+x)$) with $a_0 = 2\sqrt{\alpha}\,cH_0$ (the MOND-scale theorem, App. AH), whose polarization the baryons source. Every species couples minimally to the *single* optical metric $d\tilde{s}^2 = -c^2e^{-\psi}dt^2 + e^{\psi}\delta_{ij}dx^i dx^j$ of App. AN, Eq. (AN1) (the opposite-sign exponents are essential — the timelike part $\tilde{g}_{00} = -c^2e^{-\psi}$ gives the matter acceleration $a = (c^2/2)\nabla\psi$ and PPN $\gamma = 1$, while light reads both $\tilde{g}_{00}, \tilde{g}_{ij}$), so in the rest channel the weak equivalence principle holds for neutral χ exactly as for the neutral H I gas that drives DFD's best dwarf-galaxy fits; inside bound systems χ gives it up where it falls short of the μ-law's demand (below).

As printed, the two channels add: χ contributes its Newtonian pull on top of the baryons' μ-law field. The same printed physics makes χ form ΛCDM-like halos around every galaxy (χ is cold and pressureless with $Q_\chi = 1$, and every small-scale modifier acts some twenty decades in mass below galaxy scales; computed). Added to the μ-law, such halos count the missing mass twice: on 153 SPARC galaxies they shift the radial-acceleration relation by -0.20 dex (-0.27 dex if χ's mass also feeds the μ-law) against a tolerance of 0.03 dex, excluded at 3.4–4.6σ on the mean offset once a global stellar mass-to-light systematic is included, and at more than 3σ in about half the galaxies individually even with each galaxy's mass-to-light ratio fitted (computed). Galaxy by galaxy, the ΛCDM-like χ halo matches the Newtonian missing mass (median ratio 0.93 at $2.2R_d$ and 1.01 at the last measured radius; computed), so Newtonian gravity of the baryons plus such a halo reproduces the μ-law relation on average, and a χ halo at the phantom's surface density $a_0/2\pi G \simeq 137\,M_\odot\,\mathrm{pc}^{-2}$ (Donato et al. 2009; Milgrom 2009) stands in for the phantom. That reading holds only if the two channels do not add.

The leading candidate for how they compose is the *floor composition*: the baryons set a floor under gravity, their μ-law field; χ's Newtonian pull counts toward that floor; and the optical medium supplies only the shortfall, exactly so in spherical symmetry, where

$$g = \max\Big(\nu\big(g_{N,b}/a_0\big)\,g_{N,b},\; g_{N,b} + g_{N,\chi}\Big), \qquad \text{(AV27)}$$

with $\nu(y)$ the μ-law boost, $\mu(\nu y)\,\nu y = y$. It cannot come from an action of the printed type: in any local action with a Poisson rest channel the equation of the polarization cannot contain the rest channel's field, so the medium cannot see χ and every such action gives the additive law (theorem; checked on a 34-term ansatz). It does follow from one energy of the two Newtonian fields, Eq. (AV28) below, the only local energy that gives the baryons the floor law and leaves χ Newtonian where it overfills the demand (theorem, spherical symmetry). It follows uniquely, too, from *total-field equilibrium*, the same input stated for the medium: inside a bound system the medium settles at the minimum of its μ-law energy measured on the total field and, in spherical symmetry, never screens the rest channel. It states for the medium what the energy of Eq. (AV28) states for the baryons, that the total field counts; in the Bose reading of App. BS the mode counts the total field, with occupation $n = g/g_{N,b} - 1$ held at $n \geq g_{N,\chi}/g_{N,b}$. Never screening, the χ-free limit and equilibrium on the total field give exactly Eq. (AV27) (theorem, checked on four energies to 7×10^{-8} dex); with an energy of the medium's own field alone the unique result is the additive law. The floor law replaces the printed additive equation; it is not derived. In spherical symmetry χ that stays below the floor adds no pull of its own, and only χ in excess of the baryons' phantom shows in a rotation curve, as a one-sided lift above the relation. The tight radial-acceleration relation then stays the μ-law's signature on the baryons, with no halo needed for the rotation curves. Clusters, where χ is denser than the phantom, are then Newtonian plus χ and carry the ΛCDM dark budget (App. I). For the static field of the medium one three-dimensional form is the field-level projection of the μ-law field onto the curl-free fields whose component along the rest-channel field is at least that field, which exists and is unique; the density-level version is excluded, because the confinement makes each bound system's induced charge sum to zero and that version would then leave no phantom at all (theorem). The working three-dimensional form, for static and moving matter, is the energy of Eq. (AV28), evaluated mode by mode, which gives the same force as the projection in spherical symmetry; near a disc the two differ where χ fills the demand, and the Sun's vertical force chooses the energy (below). The floor composition passes SPARC for halos no heavier than the baryon-closure mass (one galaxy in 120 shifted by more than 0.03 dex); for halos of low concentration, 0.22 dex below the mean, the median shift is zero but a tenth of the galaxies, nearly all massive discs, are shifted by more than 0.03 dex; it fails for contracted halos, uncontracted halos at the Moster stellar-to-halo masses miss the shape of the residuals, and the feedback profiles of Di Cintio et al. (2014) at the abundance-matching masses fail in the massive discs (computed; the halo families are compared below). Near a disc the vertical force separates the static field from the adopted energy. With the measured local stars and gas ($47.1 \pm 3.4\,M_\odot\,\mathrm{pc}^{-2}$ in all and 43.8 ± 3.4 within 1.1 kpc of the plane; McKee et al. 2015) in a Milky Way whose μ-law rotation speed at the Sun is the observed 229 km/s, the μ-law's own field pulls toward the plane with $2\pi G \times (84 \pm 4)\,M_\odot\,\mathrm{pc}^{-2}$ at 1.1 kpc, because its phantom follows the disc (computed). The measured values are 68 ± 4 (Bovy & Rix 2013), 74 ± 6 (Holmberg & Flynn 2004) and 63.6 (Bienaymé et al. 2024) at 1.1 kpc, and 67 ± 6 and 68.5 ± 1.0 at 1.0 kpc (Zhang et al. 2013; Bienaymé et al. 2014), together 68.8 ± 1.9 at 1.1 kpc (with an error of 4 assumed for Bienaymé et al. 2024 and a systematic of 3 added to Bienaymé et al. 2014), 3.1–3.2σ below that value (computed). The static projection keeps this pull for every χ halo, because its bound acts only along the rest-channel field, which at the Sun is nearly radial. Under the energy of Eq. (AV28) the baryons feel the Newtonian field of the baryons and χ wherever χ fills the demand; with χ at the density that the rotation curve beyond the Sun gives, $0.0079 \pm 0.0008\,M_\odot\,\mathrm{pc}^{-3}$ (Eilers et al. 2019), the vertical force is $2\pi G \times (66\text{–}69)\,M_\odot\,\mathrm{pc}^{-2}$ under the filling rule below with χ at the rotation-curve density, within 0.7σ of the measurements for a round χ halo, the spread coming from the disc model (computed), and environmental confinement changes nothing here, since the Galaxy's own field stays boosted. This needs χ close to the demand at the Sun: a local χ density of at least about $0.0068\,M_\odot\,\mathrm{pc}^{-3}$ for a round χ halo, or 0.0076–0.0082 for one flattened to an axis ratio of 0.8 (computed). The lensing of isolated blue galaxies in the Milky Way's mass range caps a round NFW χ halo at about 0.0055–0.0066 at the Sun, depending on how the lens sample is modelled (computed): below the round halo's threshold, so for a round halo the two do not meet, and below the rotation-curve density. At the Sun DFD therefore behaves like standard dark matter, so this test separates the adopted energy from the static field rather than DFD from ΛCDM. Its early-type minus late-type lensing contrast is +0.076 dex (+0.138 inside $0.3\,h_{70}^{-1}$Mpc), against $+0.275 \pm 0.065$ (split by colour) and $+0.194 \pm 0.040$ (split by Sérsic index) measured by Brouwer et al. (2021): 2.9–3.1σ low overall and, against the $+0.206 \pm 0.072$ and $+0.162 \pm 0.049$ measured there, 0.5–0.9σ low inside $0.3\,h_{70}^{-1}$Mpc (computed). The contrast turns on the early-type masses: with early-type stellar masses raised by the factor of up to 1.7 that Mistele et al. (2024) find, the floor gives +0.143 (+0.170 inside), 1.3–2.0σ low overall and within 0.5σ inside, and Mistele et al. (2024) measure no split, where the floor gives +0.085 dex (computed).

Three properties cannot all hold: action and reaction, χ's equivalence principle, and χ's exemption from the μ-law inside bound systems; the first two together force a universal active mass, so χ would be boosted too (Bondi 1957). DFD keeps action and reaction and the exemption, and gives up χ's equivalence principle only where χ falls short of the μ-law's demand. Matter moves under one energy of the rest channel's Newtonian fields, $\mathbf{g}_b$ of the

baryons and $\mathbf{g}_\chi$ of χ,

$$W = -\frac{1}{4\pi G}\int d^3x\, K,$$
$$K = \tfrac{1}{2}\,|\mathbf{g}_b+\mathbf{g}_\chi|^2 + \int_0^{|\mathbf{g}_b|} \big[p(u)-c\big]_+\, du, \qquad \text{(AV28)}$$
$$p(u) = \big(\nu(u/a_0)-1\big)\,u,$$

where p is the μ-law's demand, the phantom field that a baryonic field u calls for, and c is the part of χ's field that counts toward it. The baryons are accelerated by the curl-free part of $\partial K/\partial \mathbf{g}_b$ and χ by that of $\partial K/\partial \mathbf{g}_\chi$. W does not depend on the origin and orientation of the coordinates, so momentum and angular momentum are conserved exactly (Noether), and a χ clump and a galaxy pull each other equally; W depends on time only through a_0, so energy is conserved at fixed a_0. In spherical symmetry ($c = g_{N,\chi}$) the baryons feel exactly Eq. (AV27), and χ feels $g_{N,\chi}$ plus the part of the baryons' field it fills, $|\{u \le g_{N,b} : p(u) \le c\}|$: the Newtonian field of all matter wherever χ fills the demand, and less where it does not. K is the only local function of $(g_{N,b}, g_{N,\chi})$ that gives the baryons the floor law and leaves χ Newtonian where it overfills the demand (theorem). The demand peaks at $0.648\,a_0$, at a baryonic field of $2.54\,a_0$, and $p/g_{N,b}$ is 10^{-330} at Saturn (computed).

χ's departure from the baryons' fall, $\delta = 1 - A_\chi/A_b$, is zero wherever χ fills the demand. Around a galaxy with $6\times10^{10}\,M_\odot$ of baryons this holds out to about 208 kpc for a halo of $2\times10^{12}\,M_\odot$ and 65 kpc for 1.2×10^{12}, while a halo of 10^{12} falls short of the demand everywhere ($\delta = 0.12$ at 60 kpc); beyond, $\delta \simeq 0.14$ at 300 kpc and 0.25 at 400 kpc for the heaviest, and at Fornax's 90 and 147 kpc $\delta = 0.08$ and 0.23 for $1.2\times10^{12}\,M_\odot$ (computed). The Sagittarius streams allow $|\delta| \lesssim 0.10$ (Kesden & Kamionkowski 2006) and Fornax $\delta \lesssim 0.17$–0.19 (Zamlung & Nusser 2025), which need χ at 0.91–0.93 of the demand or more at 18–60 kpc and 0.83 or more at 90–147 kpc (computed). Where χ falls short, a satellite's stars are pulled ahead of its χ halo and its leading tidal arm is enhanced, the opposite sign to a dark-matter fifth force. Cluster cores and the Bullet cluster are filled, $\delta = 0$ (Harvey et al. 2015 measure dark-matter offsets of 5.8 ± 8.2 kpc). The three-dimensional filling rule is stated, not derived: χ counts toward the demand by what it adds to the size of the total rest-channel field, $c = \max(|\mathbf{g}_b+\mathbf{g}_\chi| - |\mathbf{g}_b|, 0)$, which is $g_{N,\chi}$ in spherical symmetry. It counts the total field by its size, as the medium's mode does under total-field equilibrium, and other rules that give the floor law in spherical symmetry pass the present tests as well. Under it a $10^{10}\,M_\odot$ clump of χ and a $5\times10^{10}\,M_\odot$ galaxy without χ, 100 kpc apart, repel each other at about 0.3 times their Newtonian attraction (0.2–0.4 across the sizes of the two), and with the galaxy's own χ halo in place they attract at the Newtonian value where that halo fills the demand at the clump and up to about 4% more weakly beyond it (computed). The forces jump where χ stops raising the size of the total field, $|\mathbf{g}_b + \mathbf{g}_\chi| = |\mathbf{g}_b|$, by $|\mathbf{g}_\chi|$ for the baryons and by $|\mathbf{g}_b|$ for χ; they stay bounded and the conservation laws hold (computed). The demand is evaluated on the scale-additive depth of App. NL, mode by mode, so a host's χ fills only the host's demand, and a subsystem that environmental confinement keeps Newtonian (Axiom NL.14) makes no demand of its own. This mode clause, not the filling rule, keeps the planets' orbits: read on the total field at every point, the Sun's demand would give them a tidal quadrupole $Q_2 \simeq 3\times10^{-25}$ s^{-2}, about 170σ from the DE440 value and built up between about 10^2 and 10^4 AU from the Sun, while mode by mode the Sun's demand reads only the Sun's own field, which is spherical about the Sun, and $Q_2 = 0$ (computed). The mode-by-mode form has no constructed action (App. NL), so it has no rule of motion of its own, and the conservation laws above are those of the energy read on the total field; where two systems' fields blend, as near the Large Magellanic Cloud, which system's demand a χ halo fills is open. The energy keeps $Q_\chi = 1$ on linear scales because unbound perturbations do not polarize the medium (Cor. GR.11); without that confinement its linear boost at $z = 0$ on R_8 would be 8.7 for the baryons and 0.84 for χ (computed).

The alternatives fail the data (computed on published values; the kicks and the assembly are estimates). One field, with χ boosted inside bound systems like the baryons, over-predicts the masses of the sixteen clusters of App. I by a factor 1.43 (3.6σ), needs groups nearly empty of χ (0.06–0.11 of the cosmic share), fails the lensing of isolated galaxies ($\gtrsim 14\sigma$) and misses SPARC by -0.27 dex ($\ge 4.6\sigma$). A rule in which every species moves in the total ψ gives up action and reaction: a pair drifts at 44.7 km/s per Gyr, a χ-poor companion falling in receives 78–95 km/s against at most 29 km/s allowed by the cold local Hubble flow (Makarov et al. 2025), and unequal χ fractions in the Local Group are excluded at $\ge 4.9\sigma$. A simple three-field action that exempts χ wherever the phantom acts is excluded by the Sagittarius and Fornax streams ($\delta = 0.37$–0.72 against about 0.10). The energy predicts no drift of the Local Group's matter barycentre against the cold local Hubble flow, where the total-ψ rule gives 15–20 km/s along the Milky Way–M31 line with ΛCDM-like halos; the measured value is 6.9 ± 3.8 km/s towards M31, the component along that line of the (24 ± 4) km/s motion towards Sculptor found by Karachentsev et al. (2009), with the error of the barycentre's position included, 1.8σ from zero. A measurement to 5 km/s or better, with the tidal motions modelled, decides, and a drift of 15 km/s or more falsifies the energy.

Under the energy of Eq. (AV28) χ feels the Newtonian field of all matter wherever it fills the demand and is blind to the unfilled part of the baryons' floor elsewhere, so the μ-law's a_0 acts on it only through the part of that floor it fills: the decline $a_0(z) = 2\sqrt{\alpha}\,cH(z)$ does not expand χ halos but contracts them (computed), and the runaway infall that a one-dimensional assembly model gives when χ feels the whole floor (halos 8–120 times

heavier, turnaround radius 4.4 rather than 0.9 Mpc for $10^{12}\,M_\odot$) does not occur. χ assembles as in ΛCDM (estimate). Inside the optical galaxy such a halo matches the Newtonian missing mass on average (above), and the floor law keeps the radial-acceleration relation only if the inner halo is not contracted: on 120 SPARC galaxies, against a tolerance of 0.03 dex, halos at the abundance-matching masses with the feedback profiles of Di Cintio et al. (2014) shift the relation by +0.004 to +0.02 dex in the median, with a third to a half of the galaxies above the tolerance (depending on the halo-mass convention), most of them discs with more than $10^{10}\,M_\odot$ of baryons, while the dwarfs pass; uncontracted NFW halos give +0.007 dex with 29% above it and a one-sided tail that the data do not show; adiabatically contracted halos give +0.076 dex with 90% above it (computed). Fitted with the stellar mass-to-light ratio, distance and inclination free within their errors, and with χ the cosmic dark share of the virial mass (the convention of the smallest shift above), the feedback profiles fit the rotation curves about as well as the μ-law alone in all but a few of the galaxies whose halos lie below $10^{12}\,M_\odot$, while above that mass every ΛCDM-like halo tried at the abundance-matching masses fits a quarter or more of the discs worse than the μ-law alone (computed). A χ halo contracts under the disc's Newtonian pull, so the rotation curves need cored inner halos. Slow disc formation under the energy contracts χ as Newtonian gravity does at $z = 0$ (computed on 120 SPARC galaxies), and in spherical simulations of dwarf and low-surface-brightness galaxies the bursty feedback from stars that cores dark-matter halos under Newtonian gravity stalls under the energy with χ near or above today's demand, so it does not make those cores there (computed); what cores the χ halos, and in the massive discs how heavy they are, is open. The fraction of χ inside galaxies is the ΛCDM one at estimate grade: about the μ-law's phantom inside the optical disc, less where the halo is cored, and the abundance-matching halo in total, except in discs above about $10^{11}\,M_\odot$ of baryons, where that halo fails both SPARC and the lensing of isolated late-type galaxies and lighter halos pass both (computed). The cosmological role of χ is unaffected: it supplies the *cosmological* cold dark matter, namely the CMB third-peak height, cluster mass (App. I), and large-scale structure.

What cosmology does depend on is where the μ-law acts, and the Rest-Mass Channel fixes it: the polarization is confined to bound low-acceleration systems, and the net induced mass of each bound system is zero (App. GR, Remark GR.12). In three-dimensional structure-formation runs with the floor composition, which resolve groups and filaments but not the insides of galaxies, the polarization then carries 0.0003–0.002 of the mean matter density and raises σ_8 by at most 0.5% and the lensing power at $k = 0.1$–$0.4\,h$/Mpc by at most 7%; a phantom reaching beyond the bound regions would carry 0.47–1.25 of the mean matter density and multiply the lensing power 2.9–6.4 times (computed). Beyond the bound radius lensing follows χ and the baryons, as in ΛCDM, so the flat weak-lensing profile of isolated galaxies is not kept there (computed); spectroscopically isolated lens samples decide it (App. GR).

At recombination the *mean* density satisfies $g/a_0 \gg 1$ ($\mu \to 1$, Newtonian); but the small *linear* perturbation contrast that drives the acoustic peaks ($\delta \sim 10^{-5}$) self-sources a field at $x = g_N/a_0 \sim 10^{-6}$ — deep-MOND, by Lemma GR.3 of App. GR. The literal single-W μ-law thus gives χ a deep-MOND *running* Q that over-grows linear structure (excluded by $f\sigma_8$ at $> 7\sigma$); the data decisively prefer $Q = 1$, and this is a *proven* obstruction of the single-operator action (App. GR). DFD therefore *adopts* the Rest-Mass Channel postulate, a rest-mass ($\mu = 1$) gravitational channel distinct from the gradient-energy MOND screen. χ feeds only the rest channel because the medium is polarized through photon–fermion vertices and χ has no charged constituents (a conditional derivation; App. GR, Remark GR.9); what is postulated is the rest channel itself. It is the minimal fix: with the energy of Eq. (AV28) action and reaction hold, and χ falls like the baryons wherever it fills the μ-law's demand (App. GR). *Given* this postulate the $Q = G_{\rm eff}/G = 1$ cold-CDM clustering invoked for the third peak and the CMB-lensing pass holds; the cost is one added gravitational axiom, and a falsifiable cluster-vs-galaxy signature follows (its cluster-side amplitude follows from the derived abundance, at estimate grade; App. GR). *Interlock (consistency check, both directions):* $Q_\chi = 1$ and the no-CDM third-peak result *stand or fall together* — the running-Q branch that might sharpen S_8 would instead destroy the third-peak height (and overgrow structure), so neither is traded for the other. DFD's distinguishing result stands either way: it *derives* the acceleration scale $a_0 = 2\sqrt{\alpha}\,cH_0$, and with it the universal surface density $a_0/2\pi G$ of the phantom, from α and the S^3 topology, explaining the famous $a_0 \simeq cH_0$ coincidence that ΛCDM cannot.

Remark AV.38 (Falsifiable prediction: the RAR intrinsic scatter). Because $a_0 = 2\sqrt{\alpha}\,cH_0$ is a *fixed derived constant* (not a per-halo property), DFD forces the galaxy-to-galaxy a_0-drift channel of the RAR scatter to *exactly zero*. Conditionally on the DLSC axiom (App. ZT), a domain-local environment modulation reopens this channel in signed form, $\Delta a_0/a_0 = -(f/3)\,\delta_{\rm env}$, contributing 0.015–0.027 dex at $R_D = 10$–$20\,h^{-1}$Mpc — inside the intrinsic budget below, and a candidate explanation for part of it (a_0 anti-correlates with environment density). That channel is the dominant term in ΛCDM's budget — the a_0-universality that ΛCDM treats as a fine-tuning puzzle is here a structural consequence. The residuals are the halo-shape floor under the single μ-AQUAL law (the in-plane geometry channel, ~ 0.013–0.025 dex computed) and a one-sided χ term, zero for χ halos thinner than the baryons' phantom under the floor composition above and up to about 0.2–0.35 dex in massive, concentrated ones (computed); for the feedback profiles of Di Cintio et al. (2014) it exceeds 0.03 dex in a third to a half of the galaxies, most of them massive discs (computed above).

For χ halos below the phantom DFD *predicts*

$$\sigma_{\rm RAR}^{\rm intrinsic} \lesssim 0.037 \text{ dex}, \tag{AV29}$$

the halo-shape floor alone giving 0.013–0.025 dex and the upper value applying if the domain-local channel above operates (estimate; the χ term adds nothing while χ halos stay thinner than the phantom), against the ΛCDM expectation ~ 0.06–0.08 dex. This is a falsifiable bet: DFD predicts that the intrinsic scatter lies below the *tight* (Lelli–Li, ~ 0.057 dex) end, as the joint SPARC inference finds $(0.034 \pm 0.001\,(\text{stat}) \pm 0.001\,(\text{sys}))$ dex under the SPARC error model [169]), and that Stone et al. (2019)'s 0.11 dex is observational systematics (stellar-only, gas-missing $g_{\rm bar}$ and an under-propagated error budget). **Falsifier:** if the true intrinsic RAR scatter exceeds ~ 0.06 dex (e.g. Stone's 0.11 dex confirmed at the intrinsic level) and is not the one-sided upward lift that χ halos denser than the phantom produce in massive, concentrated galaxies, DFD is falsified; under the floor composition χ can only lift galaxies above the relation. Grade: *Derived/Pending* — the a_0-channel-zero is forced; the halo-shape floor is part first-principles, part literature-estimated (medium confidence), and is hardened by a full SPARC-matched μ-AQUAL population synthesis; the prediction holds if the ΛCDM-like χ halos of the adopted energy are cored, as the rotation curves require (above).

Appendix AW: The Electroweak Precision Program from $\sin^2\theta_W = 3/13$

Theorem Z.1 fixes the bare weak mixing angle to the pure rational $\sin^2\theta_W = 3/13$ from the gauge partition $(3,2,1)$, the hypercharge trace $\mathrm{Tr}(Y^2) = 10/3$, and the stiffness ratio $\kappa_2/\kappa_1 = 2$. The Higgs quartic is the conjectured $\lambda_H = 1/8$ (App. Z 3), used below only for the Higgs rows. This appendix shows that the angle reproduces the entire Z/W precision sector at sub-percent accuracy, with the residuals carrying the single universal sign of the known top/Higgs radiative uplift. Throughout, $c^2 \equiv \cos^2\theta_W = 10/13$, $v = (\sqrt{2}\,G_F)^{-1/2} = 246.22$ GeV (muon-decay vev), and we write $s^2 \equiv 3/13$.

1. Exact electroweak identities (E)

Proposition AW.1 (Mass-ratio identities, (E))**.** *The combinations entering the Z, W, and Higgs masses are exact rationals, reusing only* 3/13 *and, for the Higgs, the conjectured $\lambda_H = 1/8$:*

$$2\lambda_H s^2 = \tfrac{3}{52}, \qquad 2\lambda_H s^2 c^2 = \tfrac{15}{338}, \qquad s^2 c^2 = \tfrac{30}{169}. \tag{AW1}$$

Consequently the tree mass ratios are

$$\frac{m_H^2}{M_W^2} = \frac{3/52}{\pi\alpha}, \qquad \frac{m_H^2}{M_Z^2} = \frac{15/338}{\pi\alpha}, \tag{AW2}$$

and the famous electroweak tree relation $s^2c^2 = \pi\alpha(M_Z)/(\sqrt{2}\,G_F M_Z^2)$ is satisfied by 30/169 *to* 0.84%.

Proof. $2 \cdot \frac{1}{8} \cdot \frac{3}{13} = \frac{3}{52}$; multiplying by $c^2 = \frac{10}{13}$ gives $\frac{15}{338}$; $s^2c^2 = \frac{3}{13} \cdot \frac{10}{13} = \frac{30}{169}$. With $m_H^2 = 2\lambda_H v^2$ and the tree $M_W^2 = \pi\alpha v^2/s^2$ (from $e^2 = 4\pi\alpha$, $M_W = gv/2$, $g^2 = e^2/s^2$) the ratio is $m_H^2/M_W^2 = 2\lambda_H s^2/(\pi\alpha) = (3/52)/(\pi\alpha) = 2.5165$ (computed). The electroweak tree relation evaluates to $\pi\alpha(M_Z)/(\sqrt{2}G_F M_Z^2) = 0.17901$ against $30/169 = 0.17751$, a -0.84% check (the residual is the standard Δr). These identities reuse no new integers; their empirical content lives in α, G_F, M_Z. □

2. The Z-pole suite from $\sin^2\theta_W = 3/13$ (P)

We evaluate the on-shell partial widths in the improved-Born form

$$\Gamma_f = N_c^f \frac{G_F M_Z^3}{6\sqrt{2}\,\pi}\,\rho\,(g_{V,f}^2 + g_{A,f}^2)\,R_f, \qquad g_{A,f} = T_3^f, \;\; g_{V,f} = T_3^f - 2Q_f\,s^2, \tag{AW3}$$

with $s^2 = 3/13$, the QCD/QED radiators R_f ($R_q = 1 + \alpha_s/\pi + 1.41(\alpha_s/\pi)^2$, $R_\ell = 1 + \frac{3}{4}\alpha/\pi$), and ρ the custodial parameter. The tree prediction sets $\rho = 1$; the entire suite then follows from the *single* number 3/13.

Theorem AW.2 (Tree Z-pole from one input, (P))**.** *With $\rho = 1$ and $\sin^2\theta_W = 3/13$ the Z-pole observables are*

Observable	*DFD (3/13)*	*Measured*	*Dev.*
Γ_ℓ *[MeV]*	83.58	83.985(86)	−0.49%
$\Gamma_{\rm inv}$ *[MeV]*	497.6	499.0(15)	−0.27%
$\Gamma_{\rm had}$ *[MeV]*	1741.7	1744.4(20)	−0.15%
Γ_Z *[MeV]*	2490.1	2495.5(23)	−0.22%
R_ℓ	20.840	20.767(25)	+0.35%
$\sigma^0_{\rm had}$ *[nb]*	41.44	41.480(33)	−0.10%

All six are reproduced to better than 0.5% *absolute by the single rational* 3/13*. The four partial widths share the* same negative sign*: this is the signature of the omitted positive custodial uplift $\rho > 1$, not of independent mismatches.*

Theorem AW.3 (One-loop custodial uplift, in-framework, (T/P))**.** *Restoring the standard custodial parameter $\rho = 1 + \Delta\rho_{\rm eff}$ with the effective leptonic uplift computed* in-framework*,*

$$\Delta\rho_{\rm eff} = \underbrace{+0.00834}_{\substack{\text{top loop, QCD-corrected:}\\ m_t=(1-\alpha)v/\sqrt{2}=172.74\ GeV,\ \alpha_s=0.1187}} \underbrace{-\,0.0031}_{\substack{\text{SM bosonic remainder}\\ \text{at } m_H=125.1\ GeV}} = +0.0052, \tag{AW4}$$

together with the measured effective angle $s^2_{\rm eff} = 0.231522$ in g_V, gives $\chi^2/6 = 3.0$–3.6 in the same improved-Born formula ($\alpha_s = 0.1179$–0.1187 in R_q), against 6.7 *at tree level. The derived* +0.0052 *reproduces, to 10^{-4}, the effective value* +0.0053 *preferred by the electroweak fit. The inputs $m_t = (1-\alpha)v/\sqrt{2}$, m_H (the loop-shifted $v/2$, Thm. AW.12), and DFD's derived $\alpha_s(M_Z) = 0.1187$ (App. Z) are all ledger quantities (the top relation holds for the pole mass, the quartic* 1/8 *only as an* $\overline{\rm MS}$ *value at a matching scale near* 182 *GeV); the top-loop piece is the same computation as Thm. AW.9 (which gives* +0.00836 *at its muon-decay-anchored $m_t = 172.83$ GeV with PDG α_s — a sub-permille spread); only the standard loop* functions *are imported. The uplift therefore carries the same loop-derived grade as the M_W convergence theorem.*

Remark AW.4 (Residual of the loop uplift). One residual is booked explicitly. The −0.0031 bosonic remainder is the standard Standard-Model one-loop value at $m_H = 125$ GeV, cited rather than recomputed diagram-by-diagram here. The Higgs leading-log piece is separately verified small (-3×10^{-5}), so the remainder is gauge-boson self-energy dominated and insensitive to the Higgs mass. Rederiving it in DFD's framework is the same one-loop computation at DFD's inputs, since DFD's electroweak sector is the Standard-Model gauge theory, and moving m_H from the measured value to the tree value $v/2$ changes it by only 2×10^{-5} (computed), a tenth of the ρ-parameter precision.

Remark AW.5 (Effective leptonic mixing angle). The DFD tree angle $\sin^2\theta_W = 3/13 = 0.230769$ is the *bare* mixing angle. Against the measured effective leptonic angle $s^2_{\rm eff} = 0.231522(29)$ it sits −0.33% low. Part of the deficit is the electroweak form factor $\kappa_Z = s^2_{\rm eff}/s^2_{\rm bare}$ generated by the top quark; DFD supplies the bare angle, the loop supplies κ_Z. The residual, which includes the radiative relation of the bare angle to M_Z, is not computed here: undelivered, not contradicted.

3. The W mass and the scale-ambiguity theorem (T)

The W mass carries an internal scale ambiguity. Because 3/13 is a *bare* relation, it may be anchored two ways, and the two anchors bracket M_W.

Theorem AW.6 (M_W double reading, (T))**.** *Anchoring $\sin^2\theta_W = 3/13$ to the two natural reference scales gives*

$$\underbrace{M_W^{(\rm I)} = M_Z\sqrt{\tfrac{10}{13}} = 79.977\ GeV}_{M_Z\text{-tied, tree}}, \qquad \underbrace{M_W^{(\rm II)} = \tfrac{v}{2}\sqrt{\tfrac{4\pi\alpha(M_Z)}{3/13}} = 80.313\ GeV}_{v\text{-tied, running }\alpha}. \tag{AW5}$$

These bracket $M_W \in [79.98, 80.31]$ GeV. The PDG world average $M_W = 80.369(13)$ lies 56 *MeV above the upper edge of the bracket (anchor II); the CDF II value* 80.434(9) *lies* 120 *MeV* above *the entire bracket.*

Proof. Anchor I uses the on-shell definition $\sin^2\theta_W = 1 - M_W^2/M_Z^2$, giving $M_W = M_Z\sqrt{10/13}$ exactly. Anchor II uses $M_W = gv/2$ with $g^2 = e^2/\sin^2\theta_W = 4\pi\alpha(M_Z)/s^2$ and the muon-decay v; with $\alpha^{-1}(M_Z) = 127.951$ this evaluates to 80.313 GeV (verified to 40 digits). The gap $M_W^{(\rm II)} - M_W^{(\rm I)} = 0.336$ GeV is exactly the running-α/scheme difference between the two definitions of the bare angle. □

Corollary AW.7 (DFD and the M_W controversy, (P))**.** *The tree bracket lies* 120 *MeV below the CDF II value and* 56 *MeV below the LEP/ATLAS/LHCb world average. With the leading custodial $\Delta\rho$ the anchors converge at* 80.31–80.33 *GeV (Thm. AW.9);* the comparison of DFD's M_W with the world average and with the CDF value is open.

The two preceding statements left $\Delta\rho$ (the custodial uplift that closes anchor I) as an undelivered Standard-Model loop. Theorem AW.9 removes that gap at leading order: the leading custodial uplift is computed from the DFD-derived top mass, so with it the two anchors *converge* rather than merely bracket.

Remark AW.8 (Scheme comparison of the bare angle). The pure rational $\sin^2\theta_W = 3/13 = 0.230769$ is the bare mixing angle; its radiative relation to the angles measured at M_Z is not computed here. Numerically

$$\begin{aligned} \left|\tfrac{3}{13} - \hat{s}^2_{\overline{\rm MS}}\right| &= 0.225\%, \\ \left|\tfrac{3}{13} - s^{2,\rm lept}_{\rm eff}\right| &= 0.325\%, \\ \left|\tfrac{3}{13} - s^2_{\text{on-shell}}\right| &= 3.39\%, \end{aligned} \tag{AW6}$$

against $\hat{s}^2_{\overline{\rm MS}}(M_Z) = 0.23129$, $s^{2,\rm lept}_{\rm eff} = 0.231522(29)$, and $s^2_{\text{on-shell}} = 1 - M_W^2/M_Z^2 = 0.22320$. The on-shell value is 15× farther from 3/13 than the $\overline{\rm MS}$ value. Moreover 3/13 is the *unique* irreducible p/q with $q \le 24$ within 0.3% of $\hat{s}^2_{\overline{\rm MS}}$ (machine-verified scan). Of the +0.325% residual to $s^{2,\rm lept}_{\rm eff}$, the $\overline{\rm MS}$-to-effective form factor supplies about 0.1%.

Proof. Direct evaluation with $\hat{s}^2_{\overline{\rm MS}}(M_Z) = 0.23129$ (PDG running value) and $s^{2,\rm lept}_{\rm eff} = 0.231522$; the on-shell value uses $M_W = 80.369$. A search over all irreducible p/q, $2 \le q \le 24$, returns the single hit 3/13 inside the 0.3% $\overline{\rm MS}$ window. □

Theorem AW.9 (M_W convergence from the DFD top mass, (T/P))**.** *With* 3/13 *inserted at* M_Z *(Remark AW.8), the custodial uplift of anchor I is* not *an external input: it is the one-loop* $\Delta\rho$ *evaluated at the DFD top-mass relation* $m_t = (1-\alpha)v/\sqrt{2}$*, taken at this appendix's muon-decay vev (*$m_t = 172.83$ *GeV, consistent with the* G_F *entering* $\Delta\rho$ *below; the derived* $v = 246.09$ *GeV gives* $m_t = 172.74$ *GeV, App. AT),*

$$\Delta\rho_{\rm DFD} = \frac{3G_F m_t^2}{8\sqrt{2}\,\pi^2}\Big[1 - \tfrac{2}{3}\big(1 + \tfrac{\pi^2}{3}\big)\tfrac{\alpha_s}{\pi}\Big] = +0.00836, \tag{AW7}$$

with no free quantity ($G_F = 1/\sqrt{2}v^2$*, and the PDG input* $\alpha_s = 0.1179$ *used here for the* $\Delta\rho$ *precision computation — DFD's own* derived *value is* $\alpha_s(M_Z) = 0.1187$*, App. Z, a sub-*σ *difference with negligible [<MeV] impact on* M_W*). The two DFD anchors then agree at this order:*

$$\begin{aligned} M_W^{(\rm I)} &= M_Z\sqrt{\tfrac{10}{13}}\sqrt{1 + \Delta\rho_{\rm DFD}} = 80.310, \\ M_W^{(\rm II)} &= \tfrac{v}{2}\sqrt{\tfrac{4\pi\hat{\alpha}(M_Z)}{3/13}} = 80.313, \end{aligned} \tag{AW8}$$

agreeing to 2.9 *MeV. The full Sirlin relation* $M_W^2(1 - M_W^2/M_Z^2) = \pi\alpha/(\sqrt{2}G_F)\,(1-\Delta r)^{-1}$ *with the DFD inputs* $\Delta\alpha = 1 - \alpha/\hat{\alpha}(M_Z) = 0.0663$ *(ledger-*α *running) and* $\Delta r = \Delta\alpha - (c^2/s^2)\Delta\rho_{\rm DFD} = 0.0384$ *gives* $M_W = 80.328$ *GeV. All three routes land at* $M_W = 80.31$–80.33 *GeV, keeping only the leading custodial* $\Delta\rho$ *(anchor II only the running of* α*). Run with the measured* $\overline{\rm MS}$ *angle* 0.23129*, the same routes land* 26–134 *MeV below the Standard Model's complete value (*80.353–80.357 *GeV in current global fits).*

Proof. $m_t = (1-\alpha)v/\sqrt{2}$ is the top-mass row of App. AT; substituting into the leading custodial $\Delta\rho$ with $G_F = 1/(\sqrt{2}v^2)$ and the standard QCD reduction factor at $\alpha_s = 0.1179$ gives +0.00836, verified to 40 digits. The uplifted anchor I and the running-α anchor II were each evaluated to 40 digits. The Sirlin route uses $\Delta\alpha$ from the same ledger α run between 0 and M_Z, no other input. □

Remark AW.10 (Anchor convergence). Theorem AW.9 computes $\Delta\rho$ from the DFD top mass: the *same integer ledger* that fixes 3/13 and $m_t = (1-\alpha)v/\sqrt{2}$ brings anchor I to within 2.9 MeV of anchor II at leading order.

4. The ρ parameter (T)

Theorem AW.11 (Tree custodial $\rho = 1$, (T))**.** *The DFD weak sector has an exact tree-level custodial relation* $\rho = 1$*: the gauge partition assigns the* $\mathrm{SU}(2)_L$ *stiffness* κ_2 *uniformly across the isodoublet, so* $M_W^2 = M_Z^2\cos^2\theta_W$ *at tree level with unit coefficient.*

5. The Higgs mass from the conjectured quartic

Theorem AW.12 (Higgs mass from $\lambda_H = 1/8$ (conjecture))**.** *With* $\lambda_H = 1/8$ *the tree Higgs mass is*

$$m_H^{\rm tree} = v\sqrt{2\lambda_H} = \frac{v}{2} = 123.11\ \textit{GeV}, \tag{AW9}$$

-1.61% *below the measured* 125.13 *GeV. Imposed at the top-quark mass, where the Standard-Model quartic is matched,* $\lambda_H = 1/8$ *gives* $m_H = 124.63 \pm 0.15$ *GeV under two-loop running (computed): the radiative shift from this tree value, which uses the muon-decay* v*, is* $+1.2\%$*, and the result lies* 0.40% *(*2.7σ*) below the measured* 125.13±0.11 *GeV (PDG 2026). The running quartic equals* 1/8 *at* 182 ± 4 *GeV; the matching scale is not derived. With the quartic fixed at a matching scale the Higgs sector is the Standard Model's at the resulting mass, so the trilinear self-coupling is the Standard-Model one,* $\kappa_\lambda = 1$*; the ratio* $(1/8)/0.12914 = 0.968$ *measures the tree-to-pole mass shift, not a coupling modifier.*

6. Look-elsewhere and status

a. Look-elsewhere. $\sin^2\theta_W = 3/13$ is the *unique* irreducible fraction p/q with $q \le 24$ lying within 0.3% of the measured 0.23129 (no competitor exists in that window); it is moreover not fitted: with the stated trace weights of Thm. Z.1 it follows from $\mathrm{Tr}(Y^2) = 10/3$ and $\kappa_2/\kappa_1 = 2$. The conjectured quartic $1/8 = 1/(\dim X + 1)$ lies 0.8% below the running quartic at the top-quark mass and 3.2% below its tree value at the measured 125.13 GeV; it is the unique $1/n$ within 2% of the running value at m_t (the $1/n$ grid spacing near $n = 8$ is $\sim 8\%$). The Z/W precision sector is reproduced from the one integer input 13, and the Higgs mass to 0.4% from the conjectured 8.

b. Status. The identities of AW 1 are exact and reuse only 3/13 and, for the Higgs rows, the conjectured $\lambda_H = 1/8$. The Z-pole suite (AW 2) is a parameter-free tree prediction accurate to $< 0.5\%$ across six observables. The M_W double reading (AW 3) is a theorem; its comparison with the standard average and with the CDF value is open, since the routes are truncated (Thm. AW.9). The undelivered ingredients are the radiative relation of the bare angle to M_Z and the electroweak form factor κ_Z (with the universal ρ uplift), Standard-Model loops rather than DFD postulates; we present these as *loop-completed*, not *derived*, and the tree values stand as the parameter-free DFD content.

Status AW.13. The weak-mixing input 3/13 and the Higgs input 1/8 reproduce Γ_Z, Γ_ℓ, $\Gamma_{\rm inv}$, $\Gamma_{\rm had}$, R_ℓ, $\sigma^0_{\rm had}$, $\sin^2\theta^{\rm lept}_{\rm eff}$, ρ, M_W, and m_H at sub-percent accuracy. The tree residuals carry the single universal sign of the omitted custodial uplift. With the leading custodial $\Delta\rho$ DFD's routes give $M_W \approx 80.31$–80.33 GeV; the comparison with the world average and the CDF II value is open. The Higgs quartic, conjectured to be 1/8 at a matching scale that is not derived, counts as one continuous number (App. FK); nothing else is fitted.

Appendix AX: The Rotating-Source Exterior

The static exterior $\tilde g = \mathrm{diag}(-c^2e^{-\psi}, e^{\psi}\delta_{ij})$ with $\psi = 2u$, $u \equiv GM/(c^2r)$, is the leading-order form of the Schwarzschild metric in DFD's coordinates, the full static exterior when the parent strain's σ is kept (App. WS). This appendix adds rotation by solving the gravitomagnetic (shift-vector) sector of Sec. IV D for an angular-momentum source at first order in the spin, carries the shift to $O(JM)$ with the Einstein–Hilbert coupling, and extracts the strong-field observables for spinning black holes.

1. The stationary axisymmetric exterior

Theorem AX.1 (Rotating exterior at first order in the spin, (T))**.** *In the high-acceleration regime $\mu \to 1$, to first order in J and to leading order in GM/c^2r in the shift, the DFD scalar and gravitomagnetic fields obey separate linear Poisson equations (Sec. IV D, App. AN): $\nabla^2\psi = -(8\pi G/c^2)\rho$ and $\nabla^2 N_i = -16\pi G\, j_i^{\perp}$. For a stationary source of mass M and angular momentum $\mathbf{J} = J\hat z$ the vacuum exterior at that order is*

$$d\tilde s^2 = -c^2e^{-\psi}\,dt^2 + e^{\psi}\big(dr^2 + r^2d\theta^2 + r^2\sin^2\theta\,d\phi^2\big) - \frac{4GJ}{c^2r}\sin^2\theta\,dt\,d\phi, \tag{AX1}$$

with $\psi = 2GM/(c^2r)$ unchanged from the static case. Beyond this order the Einstein–Hilbert term couples the two sectors (Proposition WS.5): the gravitomagnetic field energy sources ψ at $O(J^2)$,

$$\delta\psi = \frac{2G^2J^2}{3c^6r^4}\big[1 + 2P_2(\cos\theta)\big] \tag{AX2}$$

plus interior-dependent terms, and ψ corrects the shift at $O(JM)$,

$$g_{t\phi} = -\frac{2GJ}{c^2r}\sin^2\theta\left[1 - \frac{GM}{c^2r} + O\Big(\frac{G^2M^2}{c^4r^2}\Big)\right], \tag{AX3}$$

the general-relativistic value in isotropic coordinates (computed). With the parent strain's σ kept, the stationary exterior is the Kerr metric in DFD's coordinates at first order in the spin, for every compactness; beyond that order a spinning hole's exterior is Kerr's by the argument of App. WS (Proposition WS.6), and a star's carries its own quadrupole, as in general relativity.

Proof. The scalar ψ is a varied field of the action of Sec. II: its Euler–Lagrange equation (App. AN, the variational fork $\{\delta S/\delta\psi,\ \delta S/\delta x^\mu,\ \delta S/\delta h^{\rm TT}\}$) is, in the $\mu \to 1$ band, the flat-space Poisson equation $\nabla^2\psi = -(8\pi G/c^2)\rho$ sourced by the rest-mass density. The shift N_i obeys the linearized Einstein–Hilbert momentum constraint (Theorem WS.8): its transverse gravitomagnetic Poisson equation $\nabla^2 N_i = -16\pi G\, j_i^{\perp}$, with $j^{\perp} = (\delta - \nabla\nabla^{-2}\partial)(\rho\mathbf{v})$, gives the far-zone value -4 of general relativity (Sec. IV D, Eqs. (77), (81)). The

mass monopole gives $\psi = 2GM/(c^2 r)$. The angular-momentum dipole solves $\nabla^2 N^\phi$-component as the standard magnetic dipole, fixing the lowered cross term $g_{t\phi} = e^\psi r^2 \sin^2\theta\, N^\phi = -(2GJ/c^2 r)\sin^2\theta$; the far-zone coefficient is the PPN value -4 ($d_V + d_W = -\frac{7}{2} - \frac{1}{2} = -4$ at $\gamma = 1$, Eq. (81)), so the dipole agrees with the general-relativistic gravitomagnetic field. At first order in J the source of ψ is ρ alone, so the exterior is $\psi = 2u$. At $O(J^2)$ the Einstein–Hilbert term adds the energy of the gravitomagnetic field to the source of ψ, which gives the exterior term of the statement, and the interior matter quadrupole enters as in the Hartle–Thorne slow-rotation framework; at $O(JM)$ the same coupling enters the shift's own equation and gives the factor $1 - GM/c^2 r$ (computed). □

2. Frame dragging

Theorem AX.2 (Frame-dragging field, (T))**.** *The frame-dragging angular velocity $\omega_{\rm LT} = -g_{t\phi}/g_{\phi\phi}$ of the rotating exterior, with the shift of Theorem AX.1 corrected at $O(JM)$, is*

$$\omega_{\rm LT}(r) = \frac{2GJ}{c^2 r^3}\left[1 - 3u + O(u^2)\right], \qquad u = \frac{GM}{c^2 r}, \quad \text{(AX4)}$$

the general-relativistic value in isotropic coordinates (computed). At large r it is the general-relativistic Lense–Thirring rate $2GJ/(c^2 r^3)$ (Eq. (100)), so all weak-field gravitomagnetic tests (LAGEOS, Gravity Probe B) are reproduced. The first-order shift alone gives the closed form $(2GJ/c^2 r^3)\, e^{-2u}$, which agrees at leading order but not at $O(u)$, so it is not a DFD signature; near the photon sphere and the ISCO frame dragging is Kerr's (App. WS).

3. Ergoregion structure

The exterior of a spinning hole is Kerr's (App. WS; argued beyond first order in the spin): it has Kerr's equatorial ergosurface, at the Boyer–Lindquist radius $2GM/c^2$ for every spin, and Kerr's horizon at $GM/c^2\,(1+\sqrt{1-\chi^2})$, $\chi = Jc/GM^2$, so superradiance and the Penrose process are as in general relativity. The first-order metric of Theorem AX.1 is its weak-field form and does not reach either surface.

4. Spin-dependent ISCO

Theorem AX.3 (Spin-dependent ISCO, (T))**.** *The equatorial innermost stable circular orbit and the accretion efficiency are Kerr's at first order in the spin, and for a spinning hole beyond it by the argument of App. WS (Proposition WS.6); at zero spin the orbit sits at the areal radius $6GM/c^2$ and the efficiency is $1 - \sqrt{8/9} = 5.719\%$.*

5. Spin-corrected QPO law

Theorem AX.4 (Spin-corrected epicyclic/QPO law, (T))**.** *With the shift corrected at $O(JM)$ (Theorem AX.1), the equatorial radial-epicyclic-to-orbital frequency ratio carries the small-spin series*

$$\left(\frac{\kappa}{\Omega}\right)^2 = 1 - 6u + 6u^2 + O(u^3) + a\big(8\,u^{3/2} - 12\,u^{5/2} + O(u^{7/2})\big) + O(a^2), \quad \text{(AX5)}$$

($u = GM/c^2 r$ in isotropic coordinates, $a = J/Mc$, units $GM/c^2 = 1$), and at fixed orbital frequency, $x = (GM\Omega/c^3)^{2/3}$, its spin-linear part is $8a\,x^{3/2} - 4a\,x^{5/2}$, the Kerr value (computed). The leading frame-dragging term $8a\,u^{3/2}$ is general relativity's spin–orbit coupling at $1.5PN$, and no DFD-specific spin–orbit term appears at the next order: the $+8a\,u^{5/2}$ of the first-order shift becomes Kerr's $-12a\,u^{5/2}$ with the shift corrected at $O(JM)$. A comparison with Kerr's Boyer–Lindquist series, whose spin-linear part is $8a\,u^{3/2}$ alone, has to be made at fixed x, since the $u^{5/2}$ coefficient depends on the radial coordinate. The static part is Schwarzschild's, $1 - 6x$ at fixed x.

Theorem AX.5 (Nodal and periastron Lense–Thirring precession, (T))**.** *The relativistic-precession QPO frequencies, formed from the three equatorial fundamental frequencies (orbital Ω_ϕ, radial κ, vertical Ω_θ), carry, with the shift corrected at $O(JM)$, the spin-linear terms $2a\,x^{3/2}$, with no $x^{5/2}$ term, in $\nu_{\rm nodal}/\nu_\phi = 1 - \Omega_\theta/\Omega_\phi$ and $-4a\,x^{3/2} - 10a\,x^{5/2}$ in $\nu_{\rm peri}/\nu_\phi = 1 - \kappa/\Omega_\phi$, at fixed orbital frequency $x = (GM\Omega_\phi/c^3)^{2/3}$ (units $GM/c^2 = 1$), the Kerr values (computed); at fixed isotropic u the $u^{5/2}$ coefficients are -3 and -6, again Kerr's. The leading nodal coefficient $2a\,x^{3/2}$ is the Kerr/GR Lense–Thirring rate, and no DFD-specific nodal or periastron term appears at the next order: the $-a\,u^{5/2}$ and $-16a\,u^{5/2}$ of the first-order shift take Kerr's values with the shift corrected at $O(JM)$.*

6. Photon ring and shadow displacement

Theorem AX.6 (Spin-displaced photon ring)**.** *The photon ring and the shadow of a spinning hole are Kerr's (App. WS; argued beyond first order in the spin): to first order in the spin the equatorial prograde/retrograde critical impact parameters are*

$$b_\pm(a) = 3\sqrt{3}\,\frac{GM}{c^2} \mp 2a + O(a^2), \qquad a = \frac{J}{Mc}, \quad \text{(AX6)}$$

so the apparent shadow centre is displaced by $2a$.

7. Observational confrontation and falsifiers

The spin terms above are general relativity's (argued beyond first order in the spin), so spin measurements of

black holes (the ngEHT shadow asymmetry, QPOs, LISA ringdowns) test DFD exactly as they test Kerr.

8. Status

Status AX.7. Theorem AX.1 holds at first order in the spin and leading order in GM/c^2r, where the DFD scalar and gravitomagnetic sectors obey separate linear Poisson equations (App. AN); beyond that the Einstein–Hilbert term couples them (Proposition WS.5), with the $O(J^2)$ field-energy term in ψ and the $O(JM)$ factor $1-GM/c^2r$ in the shift (computed). What stands: the leading spin terms (the far-zone -4, the Lense–Thirring rate, LAGEOS and Gravity Probe B, the 1.5PN spin–orbit terms $8a\,u^{3/2}$, $2a\,u^{3/2}$ and $-4a\,u^{3/2}$), and at the next order frame dragging $(1-3u)$ and the spin-linear QPO and precession terms, all general relativity's. With the parent strain's σ kept the whole stationary exterior of a spinning hole is Kerr's (App. WS; argued beyond first order in the spin): the ergoregion and the horizon, the spin-dependent ISCO (Theorem AX.3) and the shadow displacement $2a$ (Theorem AX.6) are Kerr's, and the exterior carries no DFD-specific spin signature.

a. Checks. The $u^{5/2}$ spin terms of the first-order shift ($+8a\,u^{5/2}$ in the QPO ratio, $-a\,u^{5/2}$ and $-16a\,u^{5/2}$ in the precessions) take Kerr's values with the shift corrected at $O(JM)$ (computed).

Appendix AY: Cross-Sector Relations: Flavor Closures, Hierarchy Rigidity, and Large-Number Structure

This appendix collects four cross-sector results, each machine-verified (`sympy`/`mpmath`, dps ≥ 30) against the printed, pre-locked DFD constants; none introduces a new free parameter. Status labels follow the manuscript convention, and the scope of each result—exact identity versus cross-sector consistency versus tautological restatement—is stated explicitly so that no entry is read as more than it is.

1. AY.1 The Gatto–Sartori–Tonin closure from locked integers

Theorem AY.1 (Gatto–Sartori–Tonin closure, (D))**.** *The DFD-locked Cabibbo integer $\lambda = |V_{us}| = 31\alpha$ (App. AO) and the locked down-sector mass map $m_f = A_f\alpha^{n_f}(v/\sqrt{2})$ with $(A_d, n_d) = (6, \frac{5}{2})$ and $(A_s, n_s) = (\frac{6}{7}, \frac{3}{2})$ (App. K; both prefactors data-selected, App. FM) give*

$$\frac{m_d}{m_s} = \frac{A_d}{A_s}\,\alpha^{\,n_d-n_s} = 7\alpha, \qquad \frac{m_s}{m_d} = \frac{1}{7\alpha} = 19.58, \quad \text{(AY1)}$$

and thereby reproduce the celebrated Gatto–Sartori–Tonin relation $|V_{us}| = \sqrt{m_d/m_s}$ to

$$\frac{|V_{us}|}{\sqrt{m_d/m_s}} = \frac{31\alpha}{\sqrt{7\alpha}} = \sqrt{\frac{31^2\alpha}{7}} = 1.00091, \qquad \text{(AY2)}$$

i.e. to 0.09%.

Proof. $\lambda = 31\alpha$ is given by the selected $\mathbb{C}P^2$ line-bundle cohomology window $\{2,3,4\}$: $31 = h^0(\mathcal{O}(2)) + h^0(\mathcal{O}(3)) + h^0(\mathcal{O}(4)) = 6 + 10 + 15$ (App. AO). The down-sector prefactors $A_d = 6$, $A_s = 6/7$ and exponents $n_d = 5/2$, $n_s = 3/2$ are the printed finite-Yukawa-ledger values (App. K). The common $v/\sqrt{2}$ and the factor $\alpha^{3/2}$ cancel in the ratio, leaving $m_d/m_s = (6\boldsymbol{\nabla}\cdot\frac{6}{7})\,\alpha^1 = 7\alpha$ (machine-verified, dps = 30). Substituting into the Gatto form, $|V_{us}|/\sqrt{m_d/m_s} = 31\alpha/(7\alpha)^{1/2} = (31^2\alpha/7)^{1/2}$; with $\alpha^{-1} = 137.036$ one has $31^2\alpha = 7.0128$, so the ratio is 1.00091. The relation would be *exact* iff $31^2\alpha = 7$, i.e. $\alpha^{-1} = 961/7 = 137.286$; DFD sits 0.18% from that integer identity. □

Status AY.2. Cross-sector consistency, *not* an exact identity: the Gatto relation is reproduced to 0.09%, equivalent to the integer near-identity $31^2\alpha \simeq 7.013$. The exact-making coefficient would be 7.013, not the locked $7 = b_0$, so DFD lands *off*-exact. The up-sector dichotomy is reproduced too: up-Gatto $|V_{cb}| \simeq \sqrt{m_c/m_t}$ *fails* by $\sim 2\times$ in DFD (0.47) exactly as it fails in nature (0.477). $m_s/m_d = 19.58$ matches FLAG $\sim 19.9(\pm1)$ at $< 0.5\sigma$. Look-elsewhere: one canonical textbook relation. Tier: D.

2. AY.2 The TM1 solar-mixing angle, parameter-free

Theorem AY.3 (TM1 solar angle and Jarlskog invariant, (D)). *Retaining the first tribimaximal column (trimaximal-1, TM1) together with μ–τ reflection symmetry, and using the locked reactor relation $\sin^2\theta_{13} = 3\alpha$ (flavor master operator, App. AT), the solar angle and Jarlskog invariant are fixed with no continuous parameter:*

$$\cos^2\theta_{12}\,\cos^2\theta_{13} = \tfrac{2}{3} \quad \textit{(exact, all orders in } \theta_{13}\textit{)}, \tag{AY3}$$

$$\sin^2\theta_{12} = \frac{1-9\alpha}{3(1-3\alpha)} = 0.31841 \quad (\theta_{12} = 34.35^\circ), \qquad \sin^2\theta_{12} \xrightarrow{\text{LO}} \tfrac{1}{3} - 2\alpha, \tag{AY4}$$

$$|J_{\text{PMNS}}| = \tfrac{1}{2}\,c_{13}^2\,s_{13}\,c_{12}\,s_{12} = 0.03371 \qquad (\delta_{\text{CP}} = -\pi/2). \tag{AY5}$$

Proof. TM1 fixes the first PMNS column to its tribimaximal value $(2,1,1)^T/\sqrt{6}$, preserved by the residual Klein generator. First-column normalization gives the exact identity $\cos^2\theta_{12}\cos^2\theta_{13} = 2/3$ (`sympy`: residual 0). Hence $\sin^2\theta_{12} = 1 - \frac{2/3}{1-\sin^2\theta_{13}}$; substituting $\sin^2\theta_{13} = 3\alpha$ gives $\sin^2\theta_{12} = (1-9\alpha)/(3(1-3\alpha))$, with leading term $\frac{1}{3} - 2\alpha$. Maximal $\theta_{23} = \pi/4$ and $\delta_{\text{CP}} = -\pi/2$ follow from μ–τ reflection: the TM1 $\cos\delta$ numerator vanishes identically in θ_{13} at $\theta_{23} = \pi/4$ (`sympy`-verified). The Jarlskog then evaluates to $|J| = 0.03371$. □

Status AY.4. Parameter-free given the locked tribimaximal base, $\sin^2\theta_{13} = 3\alpha$, maximal θ_{23}, and $\delta = -\pi/2$ (all already in the corpus). The new content is the TM1 solar closed form and the 2/3 invariant. $\sin^2\theta_{12} = 0.318$ versus NuFIT 6.0 $0.307(^{+12}_{-11})$ is $+0.95\sigma$ (inside 3σ). Falsifier: a confirmed non-maximal θ_{23}, or $\sin^2\theta_{12}$ outside $[0.30, 0.34]$, breaks the TM1 lock. Tier: D.

3. AY.3 Mass-scale hierarchy rank

Theorem AY.5 (Mass-scale hierarchy rank, (T)). *The seven DFD mass-scale α-exponents*

$$(x_v,\, x_{M_R},\, x_{\Lambda_{\text{DFD}}},\, x_{m_3},\, x_{H_0},\, x_{a_0},\, x_{\Lambda_{\text{top}}}) = (8,\, 3,\, \tfrac{19}{2},\, 14,\, \tfrac{57}{2},\, 29,\, \tfrac{1}{2})$$

satisfy exactly five independent rational linear relations (rank 5 over $\mathbb{Q}$), leaving two free directions: the direction $[\frac{5}{2}, 1, 3, 4, 0, 0, 0]$ in the hadronic/electroweak exponents, and the normalization of the cosmological-clock block $\{H_0, a_0\}$ relative to the hadronic/electroweak block. Adjoining the cube-law relation $x_{H_0} = 3x_{\Lambda_{\text{DFD}}}$ (App. O) welds the second direction, reducing the hierarchy to a single generator α.

Proof. The five solid relations are the four-sector lock $2x_{\Lambda_{\text{DFD}}} = 2x_v + x_{M_R}$ $(19 = 16 + 3)$, the M_R-cube identity $3x_{M_R} = x_{\Lambda_{\text{DFD}}} - x_{\Lambda_{\text{top}}}$ $(9 = \frac{19}{2} - \frac{1}{2})$, the seesaw relation $x_{m_3} = 1 + 2x_v - x_{M_R}$ $(14 = 1 + 16 - 3)$, the MOND-step $x_{a_0} = x_{H_0} + x_{\Lambda_{\text{top}}}$ $(29 = \frac{57}{2} + \frac{1}{2})$, and the single-brick value $x_{\Lambda_{\text{top}}} = \frac{1}{2}$. The 7-column coefficient matrix has rank 5 over $\mathbb{Q}$ (`sympy`), with nullspace spanned by $[\frac{5}{2}, 1, 3, 4, 0, 0, 0]$ and the clock-block direction $[0, 0, 0, 0, 1, 1, 0]$. The cube law $x_{H_0} - 3x_{\Lambda_{\text{DFD}}} = 0$ pairs nontrivially with the clock direction and raises the rank to 6. □

Remark AY.6 ($x_v = 8$ is derived, not a residual axiom). The base exponent $x_v = 8$ of the harmonic ladder is *derived*, not an axiom: $x_v = 8 = \dim(\mathbb{C}P^2 \times S^3) + 1 = 7 + 1$. The internal dimension $X = 7$ is derived by minimality (Corollary AB.3: $\dim \mathbb{C}P^2 = 4$ plus $\dim S^3 = 3$), and the $+1$ is the radial/Higgs normal mode. The harmonic ladder therefore closes at the exponent level; the only sub-theorem-grade residues that remain are the fitted $\sqrt{2\pi}$ prefactor and the "$+1$ = radial mode" identification. We do *not* claim $\sqrt{2\pi}$ is derived.

Remark AY.7 (The elimination identities are tautological, not independent tests). Because every observable above is a single power of the one generator α, eliminating α between any pair yields a monomial identity—e.g. $(M_R/M_P)^8 = (v/\sqrt{2\pi}M_P)^3$, $(H_0 t_P)^2 = C\,(M_R/M_P)^{19}$, $(a_0/2a_P)^3 = C^{3/2}(M_R/M_P)^{29}$ ($C = 1$ for the bound-matter a_0, Postulate ZS.11). These "syzygies" are *equivalent restatements* of the individual α-exponents: each reduces to $\alpha^k = \alpha^k$ and carries *no* information beyond them. They are satisfied identically and therefore cannot serve as independent falsifiers. The testable content is (i) the rank-5 integer structure above and (ii) the individual α-power predictions confronted with data elsewhere in this work. The reduction to a single generator is contingent on the cube law, which is established only to effective-field-theory grade (App. O); it is recorded here as such, not as a closed theorem.

4. AY.4 Large-number structure

Proposition AY.8 (Dirac large number as an exact α-exponent, (T)). *The Eddington–Dirac second large number—the ratio of the Hubble time to the electron atomic time—is an exact power of the gauge coupling,*

$$N_2 \equiv \frac{1/H_0}{\hbar/m_e c^2} = \frac{m_e c^2}{\hbar H_0} = \tfrac{2}{3}\sqrt{\pi}\,C^{-1/2}\alpha^{-18} = 3.66 \times 10^{38}, \tag{AY6}$$

with integer exponent $-18 = -\frac{57}{2} + \frac{21}{2}$.

Proof. From the locked electron map $m_e/M_P = \frac{2}{3}\sqrt{\pi}\,\alpha^{21/2}$ (App. K) and the Hubble hierarchy $H_0 t_P = \sqrt{C}\,\alpha^{57/2}$ (App. O; C measured on the early clock), $N_2 = (m_e/M_P)/(H_0 t_P) = \frac{2}{3}\sqrt{\pi}\,C^{-1/2}\alpha^{21/2-57/2} = \frac{2}{3}\sqrt{\pi}\,C^{-1/2}\alpha^{-18}$. The exponent is exact; numerically 3.66×10^{38}. The electron's atomic time is a bound-matter clock, so with the Hubble time read on the same clocks, $1/H_0^{\text{loc}}$ (Postulate ZS.11), the coefficient is $C = 1$ and $N_2 = \frac{2}{3}\sqrt{\pi}\,\alpha^{-18} = 3.43 \times 10^{38}$ with no measured factor. □

Remark AY.9 (Reframing, not a new prediction). This recasts Dirac's famous coincidence $N_2 \sim 10^{39}$ as an exact integer exponent of the α-tower rather than an accident. It follows algebraically from the already-locked m_e and H_0 exponents, so it is a structural restatement, not an independent prediction; the +3% offset from the measured value is the locked electron-mass leading-order error, not a free parameter.

Appendix SL: The Supernova–Lensing Sign Discriminator

This prediction has been tested, and it failed

The sign test set out below has been run. Shah *et al.* (DES Collaboration), *Detection of weak lensing magnification of supernovae and constraints on dark matter haloes*, MNRAS **532**, 932 (2024) [arXiv:2406.05047] [191], correlate the DES-SN5YR Hubble residuals against DES Y3 Gold foregrounds and *"detect the presence of lensing at* 6.0σ *significance ... the first detection with a significance level above* 5σ*,"* and show that *"the scatter of SNe Ia around the Hubble diagram is reduced by modifying the standardisation of the distance moduli to include an easily calculable de-lensing (i.e., environmental) term."* Magnification by foreground matter, together with a scatter-reducing de-lensing term, fixes the ordinary focusing sign: a supernova behind a foreground overdensity is *brighter*, i.e. the residual is *negative* for positive convergence, $d(\delta\mu)/d\kappa_{\rm fg} < 0$. **By Falsifier SL.7 as printed below, this falsifies DFD's optical-distance dressing $D_L \to D_L\, e^{\Delta\psi_{\rm LOS}}$ and with it the positive-slope prediction $s_{\rm DFD} \in [+7, +28]$.** That dressing is retired. The measurement predates, and outweighs, the $+0.7\sigma$ existing-data assessment recorded throughout this appendix, which is convergence-map-noise limited. **What is *not* retired: DFD's core.** The Remark following Theorem SL.1 already recorded that the positive sign is theorem-grade only *given* the optical-distance axiom, and that standard achromatic lensing of the *same* $n > 1$ clump gives the opposite sign. DFD's physical metric $\tilde{g}_{00} = -c^2 e^{-\psi}$, $\tilde{g}_{ij} = e^{+\psi}\delta_{ij}$ is PPN $\gamma = 1$ at first order and therefore predicts the ordinary $d(\delta\mu)/d\kappa = -5/\ln 10 = -2.17$. *The measured sign is consistent with DFD's core optical metric.* The failed step is the separate assumption that a longer optical path dims a steady source: a longer path is a propagation (Shapiro) delay, whereas luminosity distance is fixed by flux and wavefront area, and the same $n > 1$ clump was in effect counted twice, once as focusing and once as an independent dimming. Eq. (SL2) additionally identifies a line-of-sight *potential* with a convergence, which is a transverse second derivative of an integrated potential, so no universal positive scalar connects them. **What replaces it.** DFD's surviving discriminator in this channel is the *amplitude, scale and redshift dependence* of its convergence mapping, not the sign; the slope itself is $d(\delta\mu)/d\kappa_{\rm DFD} = -5/\ln 10$. The text below states the pre-registered prediction and the criterion that decided it.

This appendix isolates the single cleanest falsifiable separation between DFD and the ΛCDM concordance model that is testable with standard-candle data: the sign *of the correlation between standardized Type Ia supernova (SN Ia) Hubble residuals $\delta\mu$ and the foreground weak-lensing convergence $\kappa_{\rm fg}$ along each line of sight. Under DFD's retired optical-distance dressing the vacuum optical index $n = e^{\psi}$ made a SN seen* through *a foreground overdensity appear* farther *(positive residual); in ΛCDM gravitational magnification makes the same SN appear* brighter / closer *(negative residual). The two predictions are* opposite-signed*, and the DFD sign is a theorem given that dressing. The slope magnitude is $s_{\rm DFD} \simeq +11$ mag per unit κ (band $[+7, +28]$ from the μ-law boost), versus $s_{\Lambda{\rm CDM}} = -5/\ln 10 = -2.17$ mag per unit κ, a definite sign flip with a ∼13 mag/κ physical separation. We give the proofs and a pre-registered power forecast ($\sigma_s = \sigma_{\rm int}/[\sqrt{N}\,\sigma_{\kappa,{\rm eff}}]$). **Status: the test has been run and the DFD sign failed** — DES detected the opposite, ordinary focusing sign at 6.0σ (MNRAS **532**, 932), which by the falsifier below retires the optical-distance dressing while leaving DFD's core metric, whose first-order prediction is the standard $-5/\ln 10$, untouched. See the box above.*

1. The line-of-sight optical screen and its sign

The DFD optical postulate is that the refractive index of the vacuum is $n = e^{\psi}$, with ψ the optical-density field that satisfies the screened Poisson equation

$$\nabla\cdot\big[\mu(g/a_0)\,\nabla\psi\big] = -\frac{8\pi G}{c^2}\,\rho, \qquad \mu(x) = \frac{x}{1+x}, \qquad a_0 = 2\sqrt{\alpha}\,cH(z), \tag{SL1}$$

the same interpolation function and acceleration scale fixed in Appendix AP and used for the optical σ_8 analysis of Appendix AE. Matter raises ψ (since the source $\rho > 0$ and the operator is positive), so along a line of sight that crosses a foreground overdensity a photon accumulates a strictly *positive* excess optical density

$$\Delta\psi_{\rm LOS} = \int d\chi\, W(\chi)\,\frac{\kappa_{\rm struct}(\chi)}{\mu\big(g/a_0\big)} \;=\; g_{\rm geo}\,Q\,\kappa_{\rm fg} > 0, \qquad Q \equiv \frac{1}{\mu(\bar{x})}, \tag{SL2}$$

where $\kappa_{\rm fg}$ is the foreground convergence the line of sight samples, W is the optical window, $g_{\rm geo}$ is the order-unity geometric kernel factor (the optical-to-lensing window overlap, SL 2), and $Q = 1/\mu(\bar{x})$ is the deep-field μ-law boost evaluated at the screen acceleration ratio $\bar{x} = g_\psi/a_0$.

Theorem SL.1 (DFD SN-lensing sign, (T))**.** *Under the optical-distance dressing $D_L \to D_L\, e^{\Delta\psi_{\rm LOS}}$ (retired; see the box above), the slope of the standardized SN Ia distance-modulus residual with respect to the foreground*

convergence is strictly positive,

$$\boxed{s_{\rm DFD} \equiv \frac{d(\delta\mu)}{d\kappa_{\rm fg}} = \frac{5}{\ln 10}\, g_{\rm geo}\, Q > 0\ ,} \tag{SL3}$$

with central value $s_{\rm DFD} \simeq +11$ *mag per unit* κ *and band* $[+7, +28]$. *The sign is independent of the magnitude inputs* $g_{\rm geo}, Q$, *both strictly positive.*

Proof. The distance modulus is $\mu = 5\log_{10}(D_L) + 25$. The optical metric stretches the photon path uniformly along the line of sight, $D_L \to D_L\, e^{\Delta\psi_{\rm LOS}}$, so the residual against an unscreened (matter-only) model is

$$\delta\mu = 5\log_{10}\!\big(e^{\Delta\psi_{\rm LOS}}\big) = \frac{5}{\ln 10}\,\Delta\psi_{\rm LOS},$$
$$\frac{5}{\ln 10} = 2.17147 \text{ (exact, the magnitude system).} \tag{SL4}$$

Inserting Eq. (SL2), $\delta\mu = (5/\ln 10)\, g_{\rm geo}\, Q\, \kappa_{\rm fg}$; differentiating in $\kappa_{\rm fg}$ gives Eq. (SL3). Since the magnitude prefactor $5/\ln 10 > 0$, the field-equation operator is positive ($\mu > 0$ for $\bar{x} > 0$, hence $Q > 0$), and the kernel overlap $g_{\rm geo} \in [1, 2] > 0$, the product is positive: $\Delta\psi_{\rm LOS} > 0$ for an overdense line of sight, so $\delta\mu > 0$. The sign is therefore forced by the postulate, not fitted; only the magnitude depends on the inputs. □

Remark SL.2 (Sign is theorem-grade *given* the optical-distance axiom). The positivity of $s_{\rm DFD}$ follows by definition of the magnitude scale once $D_L \to D_L\, e^{\Delta\psi_{\rm LOS}}$ is granted. This optical-distance dressing is the DFD axiom under test: standard achromatic lensing of the *same* $n > 1$ clump gives the opposite sign (solid-angle focusing brightens; surface brightness is conserved), so "object looks farther/dimmer" is *not* derivable from $n = e^{\psi}$ alone—it is a separate optical-distance postulate. The wording "theorem" is therefore exact *given* that postulate, and it is precisely this postulate the sign test probes. This is the correct posture for a discriminator: the experiment adjudicates the axiom.

2. The μ-law boost and the geometric kernel

The magnitude of $s_{\rm DFD}$ is set by two order-unity-to-few factors.

a. The μ*-law boost* $Q = 1/\mu(\bar{x})$. The screened operator in Eq. (SL1) enhances the response to a fixed source by $Q = 1/\mu(\bar{x})$ in the low-acceleration regime. The screen acceleration ratio $\bar{x} = 0.24$ is the value that closes the BAO differential in the anisotropic-screen analysis (it solves $x_{\rm need} \simeq 1/(Q_{\rm need} - 1)$), sitting between the deep-MOND limit ($\bar{x} \to 0$, $Q \to \infty$) and the Hubble–EFE / σ_8 scale ($\bar{x} = 1/(2\sqrt{\alpha}) = 5.85$, $Q = 1.17$):

$$\mu(0.24) = \frac{0.24}{1.24} = 0.19355 \implies Q = 5.167 \text{ (central)},$$
$$\bar{x} \in [0.18, 0.45] \Rightarrow Q \in [3.22, 6.56]. \tag{SL5}$$

Status: the gate $a_0 = 2\sqrt{\alpha}\, cH$ is derived; $\bar{x} \simeq 0.24$ is selected by the void-dominated line-of-sight within that derived deep-MOND→EFE range—the single residual axiom of the magnitude (not the sign).

b. The geometric kernel $g_{\rm geo}$. The convergence the optical screen actually samples, $\kappa_{\rm struct}$, and the *measured* convergence $\kappa_{\rm fg}$ both integrate the *same* foreground density field and so are strictly proportional, with an order-unity coefficient set by the overlap of the optical window $W_{\rm opt}(\chi)$ and the lensing efficiency $W_{\rm lens}(\chi) = \chi(\chi_s - \chi)/\chi_s$:

- kernel-matched limit ($W_{\rm opt} \approx W_{\rm lens}$): $g_{\rm geo} = 1$;
- full PPN-$\gamma = 1$ doubling ($\psi = -2\Phi/c^2$, the 1PN light-bending coupling DFD inherits): $g_{\rm geo} = 2$.

c. Final slope. Combining, $s_{\rm DFD} = (5/\ln 10)\, Q\, g_{\rm geo} = 2.1715 \times 5.167 \times g_{\rm geo}$:

case	$Q\,(\bar{x})$	$g_{\rm geo}$	$s_{\rm DFD}$ (mag/κ)
kernel-matched, central	5.17 (0.24)	1.0	+11.2
nominal	5.17 (0.24)	1.5	+16.8
full $\gamma = 1$ doubling	5.17 (0.24)	2.0	+22.4
weak boost ($\bar{x} = 0.45$)	3.22	1.0	+7.0
strong boost ($\bar{x} = 0.18$)	6.56	2.0	+28.5

The central value $s_{\rm DFD} \simeq +11$ mag/κ (kernel-matched, $\bar{x} = 0.24$) matches the conservative slope $b_D = 10$ hard-coded in the power forecast (`preflight_forecast.py`); the plausible band is $s_{\rm DFD} \in [+7, +28]$, dominated by the μ-law boost Q and the kernel factor $g_{\rm geo} \in [1, 2]$.

3. The standard (ΛCDM/GR) baseline

Proposition SL.3 (ΛCDM lensing-magnification slope, (T))**.** *In GR/*Λ*CDM the slope of the standardized SN Ia residual with respect to the foreground convergence is robustly non-positive,*

$$\boxed{s_{\Lambda\rm CDM} = \frac{d(\delta\mu)}{d\kappa_{\rm fg}} = -\frac{5}{\ln 10} = -2.17 \text{ mag per unit } \kappa\ ,} \tag{SL6}$$

and no physical (κ, γ) *makes it positive.*

Proof. Weak-lensing magnification of a standard candle is $\mu_{\rm mag} = 1/[(1-\kappa)^2 - |\gamma|^2] \approx 1 + 2\kappa$ for $\kappa, \gamma \ll 1$. A SN behind a foreground overdensity ($\kappa > 0$) is magnified, hence brighter; standardized as a fixed-luminosity candle it is read as "too close," giving a *negative* distance-modulus residual

$$\delta\mu_{\Lambda\rm CDM} = -2.5\log_{10}\mu_{\rm mag} = -2.5\log_{10}(1 + 2\kappa),$$
$$\left.\frac{d(\delta\mu)}{d\kappa}\right|_0 = -\frac{2.5\cdot 2}{\ln 10} = -\frac{5}{\ln 10} = -2.17. \tag{SL7}$$

This is exact and convention-fixed; it matches the value $b_L = -2.17$ used in the forecast pipeline. Keeping the shear term and going to second order only makes the local slope *more* negative (-2.18 at $\kappa = 0.005$, -2.29 at

$\kappa = 0.05$). Flux conservation $\langle \mu_{\rm mag} \rangle = 1$ fixes the *mean* residual, not the *slope*; Malmquist/magnification-bias selection can dilute $|s_{\Lambda\rm CDM}|$ toward zero but never flip its sign, since every selected SN behind an overdensity still has $\delta\mu = -2.5 \log_{10} \mu_{\rm mag} < 0$. A coherent foreground monopole is removed by the residual-mean marginalization in the pipeline, leaving pure line-of-sight lensing. □

Corollary SL.4 (The slope sign is a clean DFD/ΛCDM discriminator)**.** *The DFD slope (Theorem SL.1) and the ΛCDM slope (Proposition SL.3) are* opposite-signed*, with physical separation*

$$s_{\rm DFD} - s_{\Lambda\rm CDM} = 10 - (-2.17) = 12.17 \text{ mag per unit } \kappa \quad (\text{conservative } b_D = 10). \tag{SL8}$$

A measured slope $d(\delta\mu)/d\kappa_{\rm fg} > 0$ falsifies the ΛCDM lensing prediction and confirms the optical-distance dressing; a slope ≤ 0 falsifies DFD's optical-distance dressing (this is what was measured — see the box at the head of this appendix)*. The sign is the discriminator; the magnitude band only sets the available statistical power.*

Remark SL.5 (The one confound: correlated foreground dust). The ΛCDM *lensing* sign has no escape—but a *different* effect shares the DFD sign: correlated foreground dust/extinction. Foreground galaxies that produce $\kappa > 0$ also redden and dim the SN, giving a *positive* $\delta\mu$ of order $O(1)$ mag/κ, comparable to the -2.17 lensing term. This does not flip the GR *lensing* prediction, so it is a detection-cleanliness requirement (reddening-corrected/NIR samples, host-color cuts), not a sign error. A positive measured slope is a clean DFD result only *after* dust is controlled—this is the real systematic threat.

4. Pre-registered power forecast

Theorem SL.6 (Sample size for a 3σ sign test, (P))**.** *For N SN Ia with intrinsic scatter $\sigma_{\rm int}$ and an effective convergence-map noise $\sigma_{\kappa,\rm eff}$ (the rms spread of the regressor $\kappa_{\rm fg}$ degraded by map noise), the standard error of the fitted slope and the DFD/ΛCDM separation are*

$$\sigma_s = \frac{\sigma_{\rm int}}{\sqrt{N}\,\sigma_{\kappa,\rm eff}}, \qquad Z = \frac{s_{\rm DFD} - s_{\Lambda\rm CDM}}{\sigma_s} = \frac{(s_{\rm DFD} - s_{\Lambda\rm CDM})\sqrt{N}\,\sigma_{\kappa,\rm eff}}{\sigma_{\rm int}}, \tag{SL9}$$

so the number of SNe for a 3σ test is

$$N_{3\sigma} = \left[3\,\sigma_{\rm int}/((s_{\rm DFD} - s_{\Lambda\rm CDM})\,\sigma_{\kappa,\rm eff})\right]^2.$$

With $\sigma_{\rm int} = 0.13$, the physical gap 12.17, and the anchor that 648 SNe with a true *map give 6σ (which pins $\sigma^{\rm true}_{\kappa,\rm eff} = 0.0025$):*

survey (κ map)	N	$\sigma_{\kappa,\rm eff}$	σ_s	Z	$N_{3\sigma}$
DES-era proxy (current)	1,378	0.0002	16.4	0.74σ	22,400
DES-era proxy (best case)	4,000	0.0002	9.6	1.27σ	22,400
DES-era, *if* true map now	1,378	0.0025	1.39	8.8σ	162
LSST Y1 (good wl κ)	30,000	0.0013	0.60	20.4σ	648
LSST Y1 (deep κ)	30,000	0.0019	0.40	30.6σ	288
Roman (deep, low-noise κ)	20,000	0.0025	0.37	33.3σ	162

Read-out. The bottleneck is the *map*, not the SNe. Map quality enters *linearly* ($Z \propto \sigma_{\kappa,\rm eff}$) while the SN count enters only as $\sqrt{N}$: the ∼12× true-vs-proxy map gap would need ∼150× more SNe to compensate. With the current noisy proxy one would need ∼22,000 SNe to reach 3σ; with a true convergence map, only ∼160. Both LSST Y1 and Roman clear 3σ (20–33σ on paper) the moment a real deep convergence map covers the SN footprint.

5. Status and pre-registration

Status: the prediction failed; the pre-registered assessment follows

DES measured the opposite sign at 6.0σ (MNRAS 532, 932, 2024; box at the head of this appendix), retiring the optical-distance dressing. The pre-registered assessment that follows is what was predicted before that measurement was taken into account. This is not a detection. The existing-data result is $+0.7\sigma$ (joint), under-powered and limited by convergence-*map* noise, *not* by theory. *Executed joint analysis (rotation-null calibrated, overlaps priced):* Four usable datasets (the DESI subset has ∼4 SNe and is unusable) lean DFD-positive at $+0.14$ to $+0.60\sigma$ each (Pantheon+×DES-Y3 $+0.60$, DES-SN5YR×DES-Y3 $+0.14$, Pantheon+×BOSS $+0.57$, Pantheon+×Planck-MV $+0.22$, coordinate-fixed), joining to $+0.68\sigma$ under the coherent-rotation null covariance — and $+0.2\sigma$ if the SDSS redshift-truncated counter-lean (logged as robust at $\sim -1\sigma$ in the same analysis) is included. A reading of five datasets at ∼1–1.5σ each does not hold: rotation nulls inflate naive errors ∼2.5×. No detection, no falsification; the sign lean is a direction indicator only. The slope-*sign* prediction (Theorem SL.1, Corollary SL.4) is theorem-grade given the retired optical-distance dressing; its magnitude band is the only place the $\bar{x} \simeq 0.24$ axiom enters. The operative existing-data evidential case for DFD is *not* this single test but the combined preponderance tabulated in the Confrontation Matrix (App. AG).

Falsifier SL.7 (Pre-registered SN-lensing sign test). *Prediction (pre-registered).* Regressing standardized SN Ia Hubble residuals $\delta\mu$ on the foreground weak-lensing convergence $\kappa_{\rm fg}$ over a deep, dust-controlled (reddening-corrected / NIR) SN sample with a true convergence map yields a *positive* slope, $s_{\rm DFD} \in [+7, +28]$ mag/κ (central $+11$), at $\geq 3\sigma$ once $N\,\sigma^2_{\kappa,\rm eff}$ reaches the forecast threshold (Theorem SL.6; LSST Y1 ∼ 650 well-mapped SNe, or Roman ∼ 160). *Falsification.* A measured slope ≤ 0 at

$\geq 3\sigma$, after dust control, falsifies the DFD optical-distance dressing (Theorem SL.1); it is the GR/ΛCDM prediction $s_{\Lambda\mathrm{CDM}} = -2.17$ (Proposition SL.3). The sign—not the magnitude—is the verdict. **This criterion was met: DES measured the negative sign at 6.0σ (MNRAS 532, 932, 2024); the dressing is retired. See the box at the head of this appendix.**

Status SL.8. Theorem SL.1 (the positive DFD slope) and Proposition SL.3 (the non-positive ΛCDM slope) are closed consequences of, respectively, the retired optical-distance dressing and the GR magnification relation; the slope *sign* is theorem-grade. The slope *magnitude* carries the μ-law boost band $[+7, +28]$, with the single residual axiom $\bar{x} \simeq 0.24$ (the void-dominated screen value, data-selected within the derived deep-MOND→EFE range; the gate $a_0 = 2\sqrt{\alpha}\, cH$ is derived). This appendix established a rigorous, pre-registered prediction (Falsifier SL.7) which has since been adjudicated against DFD by DES at 6.0σ (box at the head of this appendix); the operative existing-data case for DFD remains the combined-evidence preponderance of App. AG (trials-factor accounting: Sec. CE 2). The one systematic is correlated foreground dust (same-signed as DFD), a detection-cleanliness requirement, not a sign error.

Appendix TP: The CMB Third Peak: a No-Go for Zero-Dark-Matter, a Dark Sector with No Fitted Density

1. What this appendix settles, and what it does not

This appendix states the integrated resolution of the question *can DFD reproduce the height of the CMB third acoustic peak without any cold-clustering matter at all?* The answer, proved at theorem grade and reconfirmed here by independent CAMB reruns, is **no**. Within DFD's own printed 4D spectrum there is no field — and no optical, screening, sound-speed, echo, or gravity-enhancement device — that lifts the third-peak height to the observed value without a pressureless component clustering at recombination with $\Omega h^2 \approx 0.10$–0.12.

The DFD result is the *complement* of that no-go, and it is stronger than the thing the no-go forbids:

> *DFD does not avoid the cold-clustering charge — it **derives the field that carries it**. The χ-matter field (App. AV) is forced by the fixed internal topology; its flux period and mass come from α-powers with no fit (the count* 158 *and the stiffness are stated), and its relic abundance is derived, conditional on the flux-period identification, the asserted premise P_4' (Lemma AV.27) and two stated conventions,* $\Omega_\chi h^2 = 0.11928$ *(−0.60σ; Thm AV.13) — the one number ΛCDM must read off the data, DFD predicts.*

The result is therefore **a dark sector with no fitted density**, not a no-CDM third peak. ΛCDM fits $\omega_c = 0.12$ as one free density with no theory of its value; DFD predicts the dark-matter particle's mass (32.005 eV) and flux period (9.46×10^{11} GeV, radian decay constant 1.51×10^{11} GeV) from fixed integers and α; the *amount* is likewise derived ($\langle\theta^2\rangle = 0.073 \Rightarrow \Omega_\chi h^2 = 0.11928$, Thm AV.13), with no misalignment angle as an input. This appendix collects (i) the height no-go, (ii) the derived-abundance theorem with full provenance, (iii) the falsifiable χ-versus-CDM distinguishing predictions, and (iv) a status box naming the one open tension.

2. Part I — the height no-go (theorem-grade)

The rigorous statement and four-step proof are given as the *Cold-Clustering Wall* theorem in App. J 9; we restate it here in summary form and record the independent numerical reconfirmation, because it is the central negative result of the whole dark-sector program.

Proposition TP.1 (Height no-go, summary of App. J 9)**.** *Lifting the third-peak height ratio from the baryon-only value* $(H_3/H_1)_b \approx 0.20$ *to the observed* $(H_3/H_1)_{\mathrm{obs}} \approx 0.44$*, holding the peak* locations $k_n r_s = n\pi$ *and the baryon-loading ratio structure fixed, requires a driving potential* $\Phi(k,\eta)$ *with a non-decaying (standing,* $\Phi \to$*const) sub-horizon contribution through last scattering, sourced by a species that is cold-clustering (*$w \simeq 0$*,* $c_s^2 \simeq 0$*) at recombination with matter–radiation equality preceding recombination,* $z_{\mathrm{eq}} \gtrsim z_{\mathrm{rec}}$*. The minimal such abundance is* $\Omega_c h^2 \gtrsim 0.023$ *(standing-well floor), and matching the observed height sharpens it to* $\Omega_c h^2 \approx 0.10$–$0.12$*. No radiation-pressure-supported component (*$c_s^2 > 0$*) and no time-only modification of the homogeneous background can supply the lift.*

a. Why the two evasion classes are closed (the rigorous core). The proof in App. J 9 closes exactly the two ways a no-CDM device could try to succeed:

1. **Pressure-supported devices self-destruct their own well.** Any component with $c_s^2 > 0$ in radiation/pressure domination sources a potential that obeys $\Phi(x) = 3\Phi_0(\sin x - x\cos x)/x^3$, whose sub-horizon envelope $\sim 3\Phi_0 \cos x/x^2 \to 0$. A numerical check confirms the decay: $|\Phi/\Phi_0| = 0.024, 0.0027, 0.0013$ at $x = 10, 20, 40$. No standing well ⇒ no height lift. This excludes deep-MOND gravity enhancement, the $c_s(\psi)$ sound-speed envelope, the line-of-sight ψ/Jacobian screen, and the forced sound-horizon echo in one stroke.

2. **Time-only / background devices cancel in ratios.** An achromatic boost $\Phi \to g\,\Phi$ multiplies *every* peak by g^2, leaving all ratios H_n/H_1 exactly invariant (verified to machine precision). Background-only knobs therefore cannot move H_3/H_1; the only

quantity that moves it is $z_{\rm eq}$, which *is* the cold abundance, not a free dial.

Proposition TP.2 (The decisive discriminator: clustering, not background-w)**.** *A component with the correct* background *equation of state* $w \to 0$ *but a finite sound speed (an axion-*fluid *with* $c_s^2 \neq 0$*,* non-*clustering) at* $\Omega h^2 = 0.12$ *produces* zero *third-peak lift: an independent CAMB run gives* $H_3/H_1 = 0.205$*, identical to baryon-only. Only a cold,* clustering *component (*$c_s^2 \to 0$*) reaches* 0.445*.* ***The third peak demands a clustering charge; a pressureless background is not enough.*** *This is the single cleanest empirical statement of the wall.*

b. Independent reconfirmation of the three escape caps (this work). Three under-explored levers were re-run from scratch in CAMB on the $C = 1$ background ($H_0 = 72.09$, $\omega_b = 0.02237$, $n_s = 0.9667$). The current measured-clock background has $H_0^{\rm early} = 67.52$, $\omega_b = 0.0222730$, and $\omega_\chi = 0.1192806$; the archived runs are retained only because the height-ratio no-go is insensitive to that clock shift. Each lever caps far below the target, confirming the no-go is not an artifact of an unexplored channel:

1. **Scale-dependent high-k power (AQUAL tilt / ψ-driving proxy):** $H_3/H_1 \leq 0.206$; positive running makes it *worse* (0.169), because a smooth power-law tilt shifts the whole Silk envelope and cannot inject phase-coherent, peak-localized driving.

2. **Radiation-budget lever (remove radiation rather than add matter):** $N_{\rm eff} \to 0$ (the physical floor) reaches only $z_{\rm eq} = 902$, $H_3/H_1 = 0.258$ — the radiation to remove runs out; lowering $T_{\rm CMB}$ raises $z_{\rm eq}$ but *drops* H_3/H_1 by wrecking the damping tail. This is a new cap.

3. **Warm-relic mimic (deceptive amplitude, broken pattern):** an ∼11 eV neutrino species tuned to $\Omega h^2 = 0.12$ can fake $H_3/H_1 \approx 0.45$ but ruins the rest of the pattern ($H_3/H_2 \approx 0.83$ versus the cold 0.98). Cold clustering is required for the full $[1, 0.45, 0.44]$.

Status TP.3 (The zero-dark-matter third peak is closed). "CMB third-peak height with *zero* cold-clustering matter" is a theorem-grade **no-go** within DFD's printed 4D spectrum (App. J 9, Prop. TP.1). Three independent reruns reproduced the wall and found no wrongly-dismissed channel. No fresh no-CDM mechanism reached $H_3/H_1 \sim 0.45$; the best partial channels cap at $H_3/H_1 \lesssim 0.26$. DFD's standing is *not* that it dodges the cold charge but that it *derives the field supplying it* (Part II). DFD does not claim a no-CDM peak.

3. Part II — the derived cold abundance

The complement of the no-go is the live DFD result. The full derivation is App. AV; we collect the provenance here and grade it exactly.

Theorem TP.4 (Derived cold dark-matter abundance, modulo one angle)**.** *The DFD dark-matter density is fixed by the misalignment chain*

$$\begin{aligned} P = f_\chi &= \bar{M}_{\rm P}\,\alpha^3 = 9.46\times10^{11}\ \text{GeV} \\ &\quad (\textit{the flux period;}\ f_{\rm rad} = P/2\pi), \\ m_\chi &= \sqrt{158}\,\Lambda^2/f_{\rm rad} = 2\pi\sqrt{158}\,\bar{M}_{\rm P}\,\alpha^{13} = 32.005\ \text{eV}, \\ \Omega_\chi h^2 &= 1.62\,\kappa_{\rm rad}\sqrt{2\pi}\,\theta_i^2 = 1.635\,\theta_i^2, \end{aligned} \tag{TP1}$$

so that the observed cold density $\Omega_{\rm DM}h^2 = 0.12$ *is reproduced at a single* $\mathcal{O}(1)$ *misalignment angle* $\theta_i = \sqrt{0.12/1.635} = 0.271$ *(period and exact relic map per Lemma AV.6 and Rem. AV.12, App. AV). The period exponent* $d_\chi = 3 = \dim_{\mathbb{C}} \mathfrak{sl}(2,\mathbb{C})$ *and the mass exponent* $13 = 2\cdot 8 - 3$ *are forced from the* α*-tower; the prefactor* $\sqrt{158}$*,* $158 = 3(k_{\max} - \dim M_7) - 1 = 3{\cdot}53 - 1$*, is one stated count of modes on* $\mathbb{C}P^2$*, not derived; the uniform zero-mode rule would give* 171 *(App. AV). The cold (*$w = 0$*,* $c_s^2 \to 0$*)* shape *is* θ_i*-independent;* θ_i *sets amplitude only.*

(θ_i *is not an input: the finite* $SU(2)_{60}$ *CS vacuum gives* $\langle\theta^2\rangle = 0.073 \Rightarrow \Omega_\chi h^2 = 0.11928$*,* -0.60σ*, Thm AV.13; the chain above is the* θ_i*-parameterized form.)*

a. Provenance, term by term (zero fit except θ_i*).*

- *Flux period* $P = f_\chi = \bar{M}_{\rm P}\alpha^3$ — the $d = 3$ specialization of the per-mode Gaussian determinant (Lemma O.5), with $d_\chi = 3$ the complex dimension of the weak gauge algebra $\mathfrak{sl}(2,\mathbb{C})$ (the weak-sector sibling of the $d_H = 8$ colour block that sets the Higgs scale). Exact Lie theory for the exponent; the $O(1)$ coefficient, the stiffness, is a stated input (App. AV). That this coefficient is the *period* of the unit-winding flux coordinate (not the radian decay constant, which is $f_{\rm rad} = P/2\pi$) is the period identification, Lemma AV.6.

- *Mass* $m_\chi = 2\pi\sqrt{158}\,\bar{M}_{\rm P}\alpha^{13} = 32.005$ eV — the weak-block see-saw scale $\Lambda^2/f_{\rm rad}$ with the electroweak-scale numerator $\Lambda = \bar{M}_{\rm P}\alpha^8$ giving the net power $16 - 3 = 13$; the multiplicity $\sqrt{158}$ is an *integer* spectral count (the weak-block multiplicity $158 = 3(k_{\max} - \dim M_7) - 1$), *not* the loop factor $16\pi^2$ it lies 0.05% from. *Forced exponent* (13), *stated prefactor* (the $\sqrt{158}$ integer count is one stated input: no single counting rule gives it, App. AV), with one named physics assumption (the three-form is shift-symmetry-protected and lifted by the see-saw rather than sitting at the Planck-scale moduli mass; Rem. AV.10 in App. AV). The electroweak–dark scale link is $v = 4\pi\Lambda$, whose 4π carries the fitted Higgs prefactor (Rem. AV.9).

- *Abundance* $\Omega_\chi h^2 = 1.62\,\kappa_{\rm rad}\sqrt{2\pi}\,\theta_i^2$ — standard vacuum misalignment for the derived (P, m_χ), with oscillation onset $3H(T_{\rm osc}) = m_\chi$ at $T_{\rm osc} \simeq 8.7\times10^4$ GeV. The coefficient is computed, not fit —

including the *exact* radiation-era onset factor $\kappa_{\rm rad} = \Gamma(\frac{1}{4})^2/(6\sqrt{3}\pi) = 0.4026$ (Rem. AV.12); θ_i is the single free initial condition.

b. Contrast with ΛCDM. ΛCDM *takes* $\omega_c = 0.12$ from the data as one free parameter with no theory of its value. DFD *predicts* $m_\chi = 32.005$ eV and $P = 9.46 \times 10^{11}$ GeV with no fitted parameter (the count 158 and the stiffness are stated); in the θ_i-parameterized form above it then carries one $\mathcal{O}(1)$ initial condition (the same one every misalignment relic, including the QCD axion, carries) to set the amplitude — and with the finite $SU(2)_{60}$ CS vacuum result ($\langle\theta^2\rangle = 0.073$, Thm AV.13) even that angle is fixed, giving $\Omega_\chi h^2 = 0.11928$ with no free input. The count is **DFD: no fitted continuous input (the count 158, the stiffness and two conventions are stated; App. FK) versus ΛCDM: one free input (a density)**. χ has no photon coupling ($E = 0$; App. AV, Step 7), so it leaves no decay photons and no conversion line, and any dark-matter photon line at 16.0 eV (77.5 nm, two-photon decay) or 32.005 eV (38.74 nm, conversion) falsifies it.

Corollary TP.5 (The third-peak height is then *inherited*, by dynamical identity)**.** *Because χ is cold, non-thermal, and pressureless on all CMB scales (its Jeans wavenumber $k_J \propto \sqrt{m_\chi H}$ exceeds the third-peak scale by* ∼13–14 *orders — and $m_\chi/3H \sim 3 \times 10^{29}$ at recombination), it enters the photon–baryon perturbation kernel* identically *to a cold-dark-matter component of the same Ωh^2. The CAMB result at the derived $\omega_\chi = 0.11928$ (run on the measured clock, which fixes the peak positions) therefore* is *the χ result: the peak heights land at $H_3/H_2 = 0.977$ (0.0σ), $H_3/H_1 = 0.444$ ($+0.5\sigma$), $H_2/H_1 = 0.454$ ($+0.5\sigma$) against the Planck 2018 bandpowers, and on the same clock the plik-lite likelihood places the derived abundance at -0.98σ, as App. ZS reports (Thm. AV.31, App. AV).*

Remark TP.6 (Caveat: the height is inherited, not independently re-derived). Thm. AV.31 is a CAMB run with the derived ω_χ *inserted* as a cold component, followed by the dynamical-identity argument that χ enters the kernel identically. The identity is physically sound (Cor. TP.5), but the peak height is *inherited* from the standard cold-matter computation, not independently computed from χ Boltzmann dynamics; the measured-clock fit of App. ZS likewise inserts $\omega_\chi = 0.11928$ as a cold component. **The DFD result is the *derived abundance* and the peak-height *ratios* it forces, not an independent height calculation.** The acoustic peak *positions* (θ_*) are a separate question, set by the clock coefficient measured from BAO and θ_*, with no screen (App. ZS) — they are not claimed here. Relatedly, the $\Omega_\chi/\Omega_b = 16/3$ coincidence is *not* the mechanism (App. J 9 context; it is kept only as a labeled coincidence, $16/3 \cdot \omega_b = 0.1188$, and appears in no summary section): the live mechanism is the misalignment chain of Thm. TP.4.

4. Part III — distinguishability: χ versus a free-parameter CDM

In its *raw clustering*, χ is observationally identical to ordinary cold dark matter — it does not free-stream, self-interact, or drift in mass on any accessible scale. Those channels cannot separate the two. The verified list of where DFD-χ does or does not differ from vanilla CDM:

- **Free-streaming cutoff $k_{\rm cut}$ — no.** The misalignment condensate is a coherent zero-momentum field, not a 32 eV thermal relic; $k_J \sim 10^{13}$/Mpc, so it clusters exactly as cold as CDM on every observable scale. *Indistinguishable.*
- **Self-interaction σ/m — no.** The quartic $\lambda_4 = (m_\chi/f_{\rm rad})^2 \simeq 5 \times 10^{-38}$ gives $\sigma/m \sim 10^{-58}$ cm^2/g, $\gtrsim$55 orders below SIDM bounds; de Broglie wavelength ∼60 μm, no soliton/core. *Indistinguishable.*
- **Time-varying mass — no.** m_χ is geometric (α-locked), not G-locked; no distinctive drift beyond the generic axion mass turn-on. *Indistinguishable.*
- **Isocurvature $\beta_{\rm iso}$ — passes Planck, with no inflation.** DFD has no inflaton and no de Sitter stage at $H_\star \simeq 8\pi f_\chi \approx 25\, f_\chi$ (both on the α^3 rung): such a stage would kick the flux coordinate by $\delta\theta = H_\star/2\pi f_\chi = 4$ full periods per e-fold and wash out the relic (Thm. SM.3), so no tuned pre-inflation $\theta_i = 0.27$ exists. The relic is the finite-CS vacuum expectation, which gives $\beta_{\rm iso} \approx 0$ (a clean Planck pass, for the *opposite* reason a pre-inflation axion passes); a low-scale optical engine adds only a quadratic isocurvature tied to the tensor ratio, negligible for $r \lesssim 10^{-10}$ (App. AV). The only *structural* relic that survives is the $N_{\rm DW} = 1$ domain-wall case fixed by the potential's single minimum per period (App. AV): with a single non-degenerate vacuum the walls are unstable and collapse before dominating, a sharp parameter-free structural prediction of the S^3 origin of χ. (A global cosmic-string tension $G\mu = (f_\chi/\bar{M}_{\rm P})^2 = \alpha^6$ is *not* a DFD prediction: χ is the real coefficient of a single harmonic three-form with no $U(1)$ winding and no string core, see App. AV.)
- **Late-time growth $f\sigma_8$: carried by χ with $Q_\chi = 1$.** DFD's growth carrier is the cold χ relic with $Q_\chi = 1$ under the adopted Rest-Mass Channel, which confines the baryons' polarization to bound low-acceleration systems: unbound linear perturbations grow with $G_{\rm eff} = G$, and the polarization of bound systems raises σ_8 by a factor of only 1.001–1.005 (App. GR; computed). The $G_{\rm eff}/G = 1.02$–1.17 enhancement and its directional form, from the constructions of App. AE and App. AC, do not act on unbound linear perturbations, so late-time growth does not separate DFD from CDM at current precision.

Falsifier TP.7 (χ-versus-CDM tests, with magnitudes). DFD-χ is *falsified* by any of the following: (i) any confirmed coupling of dark matter to photons or to other Standard Model fields, at any strength: a haloscope, light-shining-through-walls or direct-detection signal, or a dark-matter photon line at 16.0 eV (77.5 nm) or 32.005 eV (38.74 nm) (χ has no photon coupling, $E = 0$; App. AV); (ii) linear growth that departs from the $Q_\chi = 1$ growth of the Rest-Mass Channel's bound-system confinement by more than the 0.1–0.5% rise in σ_8 that the polarization of bound systems gives (App. GR); (iii) a measured CDM isocurvature $\beta_{\rm iso} > 0.038$, which would falsify the no-inflation finite-CS χ relic. The surviving structural discriminator is the parameter-free $N_{\rm DW} = 1$ domain-wall case fixed by the potential's single minimum per period (App. AV); a global-string tension $G\mu = \alpha^6$ is not predicted (no $U(1)$ winding, no string core; App. AV).

5. Status and the one open tension

Status TP.8 (Integrated standing of the third-peak / dark–sector question). **A dark sector with no fitted density, not a no-CDM peak.**

1. **Zero-dark-matter third peak: closed (no-go, theorem-grade).** No DFD field or device lifts H_3/H_1 to 0.44 without a cold-clustering charge $\Omega h^2 \approx 0.10$–0.12 at $z_{\rm eq} \gtrsim z_{\rm rec}$ (App. J 9; reconfirmed by three independent reruns). Best partial no-CDM channels cap at $H_3/H_1 \lesssim 0.26$.

2. **Derived period and mass.** $P = f_\chi = \bar{M}_{\rm P}\alpha^3$ and the exponents of $m_\chi = 2\pi\sqrt{158}\,\bar{M}_{\rm P}\alpha^{13} = 32.005$ eV are forced, its $\sqrt{158}$ a stated input.

3. **Height inherited, not re-derived.** The peak height uses the standard cold-matter CAMB result via the dynamical-identity argument (Cor. TP.5, Rem. TP.6); the result is the abundance, not the height computation.

4. **Abundance: derived, conditional on the flux-period identification, the stated count** 158 **and P4′.** DFD's own scales remove θ_i (no inflaton, no chosen angle); the relic amplitude is then the finite $SU(2)_{60}$ CS/WZW vacuum Casimir expectation, $\langle\theta^2\rangle = \sum_j |S_{0j}|^2 C_2(j)/[k(k+2)] = 0.073 \Rightarrow \Omega_\chi h^2 = 1.62\,\kappa_{\rm rad}\sqrt{2\pi}\,\langle\theta^2\rangle = 0.11928$ (-0.60σ from Planck; App. AV, Thm AV.13). A "$\sim$44$\times$ overshoot" would come from reading the *period-1* flux coordinate in radians ($\pi^2/3$ is the uniform variance of a period-2π angle; the unit conversion $4\pi^2$ is 96.5% of the gap in log measure) and from a continuum measure choice — the finite-vacuum value 0.073 in turns^2 is what closes it (Lemma AV.6, App. AV). The amplitude is forced — operator (Casimir) proven, measure conditional on P4′, normalization $k(k+2)$ from two stated conventions, the edge of χ's derived $\mathbb{Z}_2$ ($\theta_{\max} = \frac{1}{2}$) and the Sugawara shift ($K = k + 2$). The lone non-DFD input is the standard cosmological relic-redshift map, exact at onset ($1.62\,\kappa_{\rm rad}\sqrt{2\pi}$, shared with all DM; Rem. AV.12). Grade: derived, conditional on the flux-period identification (Lemma AV.6), the stated count 158 and P4′ (Lemma AV.27), downstream of the (settled) peak-height no-go.

Remark TP.9 (Where this sits in the confrontation matrix). In the master claims confrontation matrix (App. AG), the third-peak entry is therefore correctly read as a *tie-by-inheritance plus a parsimony edge*: DFD matches the Planck height because χ is dynamically CDM, and edges ΛCDM only on free-parameter count (one derived density with stated inputs versus one fitted density). It is *not* a unique CMB prediction.

Appendix QM: Status of the Quantum-Mechanics Derivation Program: What DFD Supplies and What Remains Imported

This appendix records, at theorem grade, the current status of the long-standing question *"does DFD derive quantum mechanics, or import it?"* The ledger note at Sec. XVII (the quantum framework—complex Hilbert space, the unit i, the action scale $\hbar$, unitary evolution—originally an *adopted input*) and the Born/inner-product ledger of the *Extended Derivations* (App. AH, math foundations) stand. After an exhaustive, independently cross-checked attack on the most promising lead (the $\mathbb{C}P^2$ Kähler complex structure J as the quantum i), the net result is:

DFD does *not* yet derive quantum mechanics in full—but the gap is reduced to a short, sharply isolated import list. The $\mathbb{C}P^2$ Kähler J supplies the complex structure of the *internal* microsector (a geometric partial result), while the Dirac β is supplied by the Yukawa mass term that couples the two chiralities (Prop. QM.2). In §QM 4 the *field-level* Schrödinger i, the Hilbert inner product, and unitary free evolution are *derived*, given the linearized stability that Thm. QM.10 assumes, from a unique forced complex structure $J_\star$—unique because DFD has one physical Hamiltonian (Ashtekar–Schilling) and one absolute-time foliation (no Bogoliubov ambiguity about the vacuum). The value of $\hbar$ is the unit of action, fixed by the choice of units as in every theory; the interacting operator-ordering (variable-N) map is the renormalized dynamics common to every quantum field theory; Born frequencies follow by typicality (Rem. QM.8), and single-outcome selection is the measurement postulate shared by every quantum theory, not a claim of DFD.

This sharpens the "not yet fully derived" verdict into a list of items DFD shares with every quantum theory, not "all of QM." The advances below follow from $\psi + \chi$ positivity, the No-mixing theorem, the Ashtekar–Schilling compatibility theorem, and DFD absolute time—no fit.

1. Closures (what DFD supplies)

Theorem QM.1 (The Dirac β is available on the $\mathrm{Cl}(4,0)$ enlargement; sharpens Sec. XVII)**.** *Let* $\mathrm{Cl}(4,0)$ *be the real Clifford algebra with generators* $e_1, \dots, e_4$, $\{e_a, e_b\} = 2\delta_{ab}$. *Then the assignment* $\alpha_i = e_i$ $(i = 1,2,3)$, $\beta = e_4$ *is a valid Dirac set:*

$$\{\beta, \alpha_i\} = 0, \qquad \{\alpha_i, \alpha_j\} = 2\delta_{ij}, \qquad \beta^2 = \alpha_i^2 = +1. \tag{QM1}$$

In particular $\mathrm{Cl}(4,0)$ *provides the fourth anticommuting generator that the* S^3 *carrier* $\mathrm{Cl}(3,0)$ *cannot, since the* S^3 *Clifford element* ω *is* central *in* $\mathrm{Cl}(3,0)$ *and hence cannot serve as* β.

Proof. Direct from the defining relations; verified by explicit faithful matrix representation ($M_2(\mathbb{H})$, an 8×8 real / 4×4 complex irrep) in the companion script `qm_derivation_check.py`, which confirms all anticommutators vanish and all generator squares equal $+\mathbb{1}$. This upgrades the imported-input paragraph of Sec. XVII from "a real carrier is equally admissible / β unavailable on $\mathrm{Cl}(3,0)$" to a *checked* statement that β is available precisely upon enlarging to $\mathrm{Cl}(4,0)$. The enlargement $\mathrm{Cl}(3,0) \to \mathrm{Cl}(4,0)$ is not forced by the S^3 carrier alone; it is supplied by the mass term (Prop. QM.2). □

Proposition QM.2 (The Dirac β is the Yukawa mass block)**.** *For left- and right-handed spinors on the* $\mathrm{Cl}(3,0)$ *carrier with kinetic operators* $\pm c\boldsymbol{\sigma}\cdot\mathbf{p}$ *and a Yukawa mass* m *coupling them,* $H = \begin{pmatrix} c\boldsymbol{\sigma}\cdot\mathbf{p} & mc^2 \\ mc^2 & -c\boldsymbol{\sigma}\cdot\mathbf{p} \end{pmatrix}$ *satisfies* $H^2 = (p^2c^2 + m^2c^4)\mathbb{1}$, *the dispersion of the master wave equation, and* $\beta = \begin{pmatrix} 0 & \mathbb{1} \\ \mathbb{1} & 0 \end{pmatrix}$ *obeys* $\{\beta, \alpha_i\} = 0$, $\beta^2 = \mathbb{1}$. *No* 2×2 *matrix anticommutes with all three* σ_i, *so a massive spin-*$\frac{1}{2}$ *field needs both chiralities, and* $\mathrm{Cl}(4,0)$ *is generated by the mass term.*

Proof. Direct multiplication; the space of 2×2 matrices anticommuting with $\sigma_1, \sigma_2, \sigma_3$ has dimension 0 (computed). Minimal coupling of H gives $g = 2$ and antiparticles. □

Theorem QM.3 ($\mathbb{C}P^2$ Kähler J supplies the internal-microsector complex structure)**.** *Let* $(\mathbb{C}P^2, \omega_{\mathrm{FS}}, J)$ *be the Fubini–Study Kähler manifold,* $J^2 = -\mathbb{1}$, $\nabla J = 0$. *Berezin–Toeplitz quantization of* $\mathbb{C}P^2$ *at level* 9 *produces the* 55*-dimensional holomorphic-section space* $H^0(\mathbb{C}P^2, \mathcal{O}(9))$*; with the five sections of* $\mathcal{O}^{\oplus 5}$ *it gives the* 60*-dimensional microsector* $\mathbb{C}^{60} = \mathcal{H}^{(60)}_{\mathrm{micro}}$ *(the microsector-finiteness theorem, Ext. Deriv., App. AH). On this internal factor the Kähler* J is *the operative complex structure* $(i = J)$*, and it is precisely this holomorphic structure that makes the corpus's particle-physics results (e.g. the closed form* $\alpha = 1/137$*, the fermion exponent ladder, the tree-level strong-CP result) go through. To this narrow extent, part of "*i*" is geometric.*

Proof. $J^2 = -\mathbb{1}$ and $\nabla J = 0$ on Fubini–Study are standard and are checked numerically in `qm_derivation_check.py` at a generic point. The microsector is the section space $H^0(\mathbb{C}P^2, \mathcal{O}(9) \oplus \mathcal{O}^{\oplus 5})$ of the statement; "holomorphic" there is defined as $\ker\bar\partial$, and $\bar\partial$ is built from J. Hence the complex structure of $\mathbb{C}^{60}$ is literally J. The central role of this holomorphic structure for the internal observables is documented across Appendix F (F) and the α and mass derivations. □

Remark QM.4 (The two J's must never be conflated). The corpus carries *two* distinct objects both written J. (i) The Kähler complex structure of $\mathbb{C}P^2$, $J^2 = -\mathbb{1}$, *linear*, used here. (ii) The Connes real/charge-conjugation structure J_{DFD} of the DFD spectral data, $J^2_{\mathrm{DFD}} = -\mathbb{1}$, *antilinear*, KO-dimension 4 (the spectral-data theorem, Ext. Deriv., App. AH). These have *opposite linearity.* An antilinear J_{DFD} can never be the linear quantum i. Neither is the Schrödinger i.

2. What remains imported, and why (the precise obstruction)

Proposition QM.5 ($\mathbb{C}P^2$ Kähler J is *not* the field-level quantum i)**.** *The Kähler* J *of Theorem QM.3 cannot serve as the quantum imaginary unit appearing in the canonical commutator* $[\hat\psi(x), \hat\pi(y)] = i\hbar\,\delta(x-y)$, *in the*

path-integral phase $e^{iS/\hbar}$, or in unitary time evolution. Three independent obstructions hold:

1. ***Wrong tensor factor.*** *J acts on the 4-real-dimensional tangent space of the compact internal $\mathbb{C}P^2$ fibre. The Schrödinger i must act on the external, infinite-dimensional field state space over the $\mathbb{R}^{1,3}$ base (the $\mathbb{R}$ of $\mathbb{R}^{1,3} \times \mathbb{C}P^2 \times S^3$). J has no action there.*
2. ***Circular where it does act.*** *Berezin–Toeplitz quantization uses J to select the holomorphic polarization; "holomorphic = complex" is defined relative to J. So extracting "$i = J$" on $\mathbb{C}^{60}$ returns the i inserted by the polarization choice—no free lunch.*
3. ***Not central over the full algebra.*** *The only lift to the external state, $\mathbb{1} \otimes J$, satisfies $(\mathbb{1} \otimes J)^2 = -\mathbb{1}$ and commutes with purely external observables, but $[\mathbb{1} \otimes J,\ B \otimes C\,] \neq 0$ for any observable C that probes $\mathbb{C}P^2$ non-holomorphically. The quantum i must be* central *over the entire observable algebra (this is exactly why QM is complex, not real or quaternionic). $\mathbb{1} \otimes J$ is central only after restricting to the holomorphic subalgebra—which is obstruction 2 again. Moreover $c_1(\mathbb{C}P^2) = 3H \neq 0$, so on the tangent bundle J is point-dependent, not a single global scalar operator.*

Proof. (1) is the factorization $\mathbb{R}^{1,3} \times \mathbb{C}P^2 \times S^3$ with ψ a real scalar on the $\mathbb{R}^{1,3}$ base (Sec. I); the field phase space is built over the base, disjoint from $T(\mathbb{C}P^2)$. (2) is the definition of $\bar{\partial}$ via J (proof of Theorem QM.3). (3) The centrality failure and the non-triviality $c_1 = 3H$ are verified numerically in `qm_derivation_check.py`: a fresh toy operator C acting non-holomorphically on the $\mathbb{C}P^2$ factor yields $\|[\mathbb{1} \otimes J,\ B \otimes C]\| > 0$. □

Proposition QM.6 ($\mathrm{Cl}(4,0)$ supplies no i: the complexifier is the external commutant $\mathbb{H}$)**.** *The center of* $\mathrm{Cl}(4,0)$ *is $\mathbb{R}$ (one-dimensional). The pseudoscalar $\omega_4 = e_1e_2e_3e_4$ satisfies $\omega_4^2 = +1$ (not -1) and is* not *central. Hence* $\mathrm{Cl}(4,0)$ *contains no central square root of -1. The complex structure that makes the spinor module complex is the external right action of the commutant $\mathbb{H}$ (real dimension 4, by Schur), i.e. an imported i outside the Clifford algebra.*

Proof. Computed by brute-force null-space of the commutator map on the 16-dimensional algebra in `qm_derivation_check.py`: $\dim Z(\mathrm{Cl}(4,0)) = 1$; $\omega_4^2 = +\mathbb{1}$; $[e_1, \omega_4] = 2e_2e_3e_4 \neq 0$ so ω_4 is non-central; and the real commutant of the irrep is 4-dimensional ($\cong \mathbb{H}$). □

Proposition QM.7 (Schrödinger evolution: Hamiltonian derived, first-order complex form imported)**.** *From the real, second-order DFD master wave equation $\big(\tilde{\Box}_{\tilde{g}} - m^2c^2/\hbar^2\big)\Psi = 0$ (Theorem AN.1, Eq. (AN3)), the nonrelativistic limit yields the Hermitian Hamiltonian $H_{\mathrm{NR}} = |\mathbf{p}|^2/2m - \frac{1}{2}mc^2\psi$. This H is derived. However, the* first-order *complex form $i\hbar\partial_t\Psi = H\Psi$ is not derived: the standard reduction $\Psi = e^{-imc^2t/\hbar}\phi$ with $\partial_t^2\phi$ dropped* inserts *i and $\hbar$ before they are derived, the cross-term $2i(mc^2/\hbar)\partial_t\phi$ being exactly the Schrödinger left-hand side.*

Proof. The H_{NR} derivation is the weak-field expansion in the proof of Theorem AN.1. The insertion of $i, \hbar$ in the order-reduction ansatz is verified symbolically in `qm_derivation_check.py` by expanding $\partial_t^2\big(e^{-imc^2t/\hbar}\phi\big)$ and isolating the i-proportional cross-term. □

Remark QM.8 (Born rule and Gleason are not non-circular here). The Born-rule equivariance theorem (Ext. Deriv., App. AH, Born ledger) is a theorem *conditional* on the guidance-law postulate (the DFD guidance law, labelled "completion postulate, not forced") and on a self-adjoint Hamiltonian acting on a complex $\Psi = Re^{iS/\hbar}$—i.e. it presupposes a complex Hilbert structure, which DFD supplies from the forced $J_\star$ ($h = g + i\omega$). Gleason's theorem is likewise circular in this context: it assumes the projection lattice of a complex Hilbert space of dimension ≥ 3, exactly the structure in question. The Fubini–Study measure is natural on the internal $\mathbb{C}P^2$ factor, whereas Born $|\Psi|^2$ is needed on the external configuration space; it therefore repackages rather than removes the guidance postulate. The device that does work is *typicality* (Ext. Deriv., App. AH, the typicality / clean Born closure), which secures Born frequencies *given* the complex Ψ and self-adjoint H (the latter forced via $J_\star$)—a consistency result built on the derived inner product.

3. The sharpened open problem (single attackable object)

Proposition QM.9 (Reduction to one global compatible complex structure)**.** *By the Ashtekar–Schilling/Kibble geometric formulation, ordinary quantum mechanics is equivalent to* real symplectic dynamics $(\mathcal{M}, \omega)$ equipped with one global compatible complex structure $J_\star$*: then $g(\cdot,\cdot) = \omega(\cdot, J_\star\cdot)$ is the Hilbert metric, and any quadratic $J_\star$-preserving Hamiltonian generates unitary Schrödinger flow. DFD already supplies the symplectic dynamics and an absolute-time positive-frequency split J_{pf} with $J_{\mathrm{pf}}^2 = -\mathbb{1}$* whenever the linearized spectrum is positive. *Consequently the entire "derive QM" problem collapses to a* single *target: prove that DFD forces a unique global compatible $J_\star$ on the field phase space.*

Status of proof. The Ashtekar–Schilling/Kibble equivalence is standard. That J_{pf} is H-dependent (built as $A/\sqrt{-A^2}$ from the generator) and equals $\pm\mathbb{1}$-rooted only on a stable spectrum is verified numerically in `qm_derivation_check.py`. What is *not* yet established is a DFD field-stability theorem forcing positivity of the linearized $\psi + \chi + h^{TT}$ spectrum on the physical sector; absent that, $J_\star$ exists but is not *forced/unique*, and $\hbar$'s numerical value is still inserted. □

4. The $J_\star$-uniqueness target via the physical Hamiltonian (the one-H theorem)

Comparing the positive-frequency complex structure $J_{\rm pf}$ across *two different Hamiltonians* (different couplings $g_A \neq g_B$) gives $\|J_{\rm pf}(A) - J_{\rm pf}(B)\| \approx 0.22 \neq 0$, but that is the wrong question. Different couplings are different *physical theories*; their $J_\star$'s *should* differ. DFD has *one* physical Hamiltonian with fixed couplings. The correct question is whether *that one* H admits a unique compatible $J_\star$. It does.

Theorem QM.10 (One physical H forces a unique global $J_\star$)**.** *Let $(\mathcal{M}, \omega)$ be the DFD field phase space with the canonical symplectic form, and let $A = \omega^{-1}\mathrm{Hess}\, H$ be the linear generator of the quadratic part of the* single physical *DFD Hamiltonian about the vacuum. Suppose the linearized spectrum is stable, i.e. $-A^2$ is positive on every mode with $k \neq 0$ (argued for DFD: the $\psi + \chi + h^{TT}$ Hessian is block-diagonal by the No-mixing theorem of Sec. V/Eq. (106) with χ background 0 at the misalignment vacuum, each block positive with ψ via convex W (Appendix U), χ gapped by $m_\chi^2 > 0$, h^{TT} the healthy wave operator; under Axiom E ψ has no temporal kinetic term and is fixed by its source). Then:*

1. *There is exactly* one *complex structure $J_\star$ on $(\mathcal{M}, \omega)$ satisfying $J_\star^2 = -\mathbb{1}$, $[J_\star, A] = 0$, $\omega(J_\star \cdot, J_\star \cdot) = \omega$, and $g := \omega(\cdot, J_\star \cdot)$ positive-definite; it is $J_\star = A\,(-A^2)^{-1/2}$ (the polar/sign part of A).*
2. *Equivalently, in the energy eigenbasis A is block-diagonal over harmonic k-planes of frequency $\omega(k) > 0$; in each plane exactly one of the two admissible sign choices yields a positive-definite metric. The global $J_\star$ is the direct integral of these unique per-mode choices.*

Proof. Statement (1) is the Ashtekar–Schilling/Weinstein compatibility theorem applied to a *fixed* stable generator: a positive-definite $-A^2$ has a unique positive square root, so $J_\star = A(-A^2)^{-1/2}$ is well-defined, squares to $-\mathbb{1}$, commutes with A, preserves ω, and gives $g \succ 0$; uniqueness follows because any other compatible J' commuting with A is block-diagonal over the eigenplanes of A (spectral theorem), and the positive-definiteness of g removes the per-plane sign ambiguity. Both statements are verified numerically in `physical_H_Jstar.py`: for the DFD-flavoured Hessian exactly 1 of the 2^n sign choices is positive-definite, and across 200 random *stable* Hamiltonians (including generic configuration-space mixing) $J_\star = A(-A^2)^{-1/2}$ is the unique compatible positive structure in 200/200 trials. The ≈ 0.22 figure is reproduced as the distance between $J_\star$ of *two different* theories, and the same-H distance is identically 0. □

Theorem QM.11 (Absolute time removes the Bogoliubov ambiguity about the vacuum)**.** *In generic relativistic QFT the global $J_\star$ is* not *unique even for a fixed H: inequivalent foliations give Bogoliubov-rotated positive-frequency splits ($\|J_A - J_B\| \neq 0$; Unruh/Hawking). About the vacuum, where H does not depend on time, DFD removes this last infinite-dimensional ambiguity because its time is an* absolute parameter t on a preferred foliation *(Sec. II F, item "Time"). The positive-frequency split is taken with respect to this single global t; there is no family of inequivalent foliations and hence no Bogoliubov freedom. The per-mode uniqueness of Theorem QM.10 therefore lifts to a* unique global $J_\star$ *on the field phase space. On a time-dependent background, such as the expanding universe, the one foliation does not remove the Bogoliubov freedom: $J_\star$ is time-independent only for the conformally rescaled field, so it selects the conformal vacuum, and the instantaneous vacua of other field variables differ from it by a Bogoliubov rotation.*

Proof. About the vacuum the Bogoliubov ambiguity is parametrized by the choice of timelike Killing/Cauchy foliation; with a single absolute t the parameter set is a point. Verified numerically in `physical_H_Jstar.py`: a foliation-mixing angle $\theta \neq 0$ gives $\|J_A - J_B\| > 0$, and DFD fixes $\theta = 0$ by construction (one foliation). On an expanding background the rescaled tensor field $v = a\,h$ has a time-independent generator in the radiation era, so $J_\star$ is its conformal vacuum; the instantaneous vacuum of h at conformal time η_0 differs from it by $|\beta_k|^2 = 1/(4k^2\eta_0^2)$. □

Corollary QM.12 (Three ledger rows move IMPORTED→DERIVED)**.** *Combining Theorems QM.10 and QM.11 with the positivity of the linearized $\psi + \chi + h^{TT}$ spectrum that Theorem QM.10 assumes (argued, not proved), the* free/kinematical *structures are forced, not imported: (i) the field-level complex unit $i = J_\star$; (ii) the Hilbert inner product $\langle \cdot, \cdot \rangle = g + i\,\omega$ with $g = \omega(\cdot, J_\star \cdot)$; (iii) unitary free Schrödinger evolution (any $J_\star$-preserving quadratic H generates a one-parameter unitary group). Interactions do* not *require their own global complex structure: they are evolved on the* same *kinematical Fock space built from $J_\star$. This interaction-picture step is exact on any finite-mode or preferred-frame sector where Stone–von Neumann equivalence holds (in particular the finite $\mathbb{C}^{60}$ microsector, and finite-time dynamics — DFD's absolute-time foliation removes the boost-reconstruction horn of* Haag's theorem*, so the finite-time interaction picture exists as in non-relativistic many-body theory). On the noncompact $\mathbb{R}^3$ matter continuum, however, the intertwiner $V : \mathcal{F}_{\rm free} \to \mathcal{F}_{\rm int}$ need not exist (Haag): the interacting vacuum/ordering map remains* imported *(Rem. QM.13), a wall shared with all realistic 4D QFT. QM does not require the interacting flow to be globally* linear*. One physical interaction* does *break global linearity: the gravitational self-source, where the classical ψ is sourced by the c-number $\langle \hat{\rho} \rangle = m|\Psi|^2$, gives the nonlinear Schrödinger–Newton evolution of the open-problems section (semiclassical self-gravity). DFD does not take this semiclassical reading: the operator completion of the same action (App. ZU) forces the* linear *side: every completion term is translation-invariant or proportional to $\hat{N}$, so the self-gravity sideband on a trapped crystal's center-of-mass mode is exactly zero (all orders in α_ψ, zero parameters), and the Schrödinger–Newton frequency shift is the* falsifier *of the completion,*

not a DFD prediction. The free *qualifier in (iii) remains essential in the semiclassical reading above; under the operator completion, exact unitary linearity is not confined to the test-particle limit.*

Remark QM.13 (Exactly what remains imported—the residue). This reduces the corpus's stated "single biggest gap" (a field-stability theorem forcing a unique global $J_\star$) to the stability of the linearized spectrum, which is argued, not proved. It is *not* a full derivation of QM. Two items remain, and neither is a free parameter:

1. **The value of** $\hbar$ is the unit of action: $J_\star$ fixes the *structure* $\langle\cdot,\cdot\rangle = g + i\omega$, and the absolute scale relating the symplectic ω to the metric g (the canonical-commutator normalization $[\hat{q},\hat{p}] = i\hbar$) is a choice of units, as the value of c is. Every DFD prediction is a dimensionless ratio, so no theory derives this number. At the finite-spectral level the Berezin–Toeplitz level $k = 9$ fixes a *relative* $\hbar_{\text{eff}} \sim 1/k$ on the internal $\mathbb{C}P^2$ factor.
2. **The interacting normalization/ordering map** is the renormalized dynamics common to every quantum field theory: it uses couplings already counted, scheme conventions carry no physical parameter, and its non-perturbative construction in four dimensions is an open mathematical problem shared with the Standard Model.

Net: the QM ledger improves from "field-level i, Hilbert product, and unitary evolution all imported" to "all three DERIVED from a unique forced $J_\star$, with the Dirac algebra from the mass term; $\hbar$ is the unit of action, and the interacting dynamics and the measurement postulate are those of every quantum field theory."

5. Matter–ψ infrared class and dressed (Faddeev–Kulish) asymptotic states

Theorem QM.14 (Soft-ψ universality class; IR-finite dressed S-matrix)**.** *(i) The matter–ψ coupling of Eq.* (14) *makes ψ a* massless *mediator with Newtonian $1/r$ tail (Sec. II C); the static field profile of a hard source is $\tilde{\psi}(\mathbf{k}) \propto 1/k^2$, so the field-profile (dressing-kernel) amplitude f obeys $|f(\mathbf{k})|^2 \sim 1/k^4$—the infrared class of soft photons in QED and soft gravitons in perturbative gravity. (ii) Hence the free→interacting Fock intertwiner fails for DFD* exactly *as for QED (van Hove/Haag, universal for massless mediators): the per-mode coherent displacement scales as $k^{-3/2}$, the dressing kernel fails Hilbert–Schmidt at both ends ($\|K\|_{\text{HS}} = \infty$; IR: massless ψ, UV: point vertex), and the dressed sector is unitarily inequivalent to free Fock space. (iii) Because the soft kernel is in the QED class, the standard resolution applies verbatim: Faddeev–Kulish/Kibble* dressed *(coherent-state) asymptotic states, on which interacting dynamics is well defined and the dressed S-matrix is IR-finite order by order (Kulish–Faddeev 1970; Kibble 1968; gravity: Ware–Saotome–Akhoury 2013).*

Status of proof. (i)–(ii): computed directly for the linearized point vertex; intertwiner failure uses only $\|K\|_{\text{HS}} = \infty$ (Haag/van Hove). (iii) is the cited standard construction, transplanted, not rederived; in particular the $t \to \pm\infty$ Møller/FK limit is part of the import. □

Remark QM.15 (Ledger: derived / imported / open). **Derived:** the universality-class identification and $\|K\|_{\text{HS}} = \infty$ (Thm. QM.14); the intertwiner failure is a shared feature of massless mediators, not a DFD pathology, so the FK construction *applies* to matter–ψ. **Imported:** the FK machinery itself (standard QFT technology); and the dressing reference choice: $J_\star$ and the absolute-time foliation do *not* canonically fix the FK cloud—the ambiguity is per-hard-particle (BMS-supertranslation-type, at null infinity) and a bulk foliation does not collapse it. On IR structure DFD sits at exact *QED parity.* **Open:** the nonperturbative interacting vacuum. Absolute time removes Haag's boost-reconstruction horn at *finite* times (Cor. QM.12), but the interacting vacuum/ordering map of Rem. QM.13(2) stays imported—the universal Wightman/Haag wall shared with every realistic 4D QFT.

6. Status box

Status QM.16 (QM-derivation ledger).

QM ingredient	status	where
Internal-microsector i (= Kähler J)	Geometric, inserted by the polarization (Prop. QM.5)	Thm. QM.3
Dirac β (4th anticommuting gen.)	**Derived**: the Yukawa mass block coupling the two chiralities	Prop. QM.2
Nonrel. Hamiltonian H_{NR} (Hermitian)	**Derived**	Thm. AN.1
Field-level / free-Schrödinger i (= $J_\star$)	**Derived** (forced unique $J_\star$), given the argued stability	Thm. QM.10, QM.11
Hilbert inner product $g + i\omega$	**Derived** (from $J_\star$)	Cor. QM.12
Unitary free Schrödinger evolution	**Derived** (from $J_\star$)	Cor. QM.12
IR-finite S-matrix (dressed sector)	**Derived-applicability** (FK imported)	Thm. QM.14
Value of $\hbar$ (action scale)	unit of action (a choice of units)	Rem. QM.13(1)
Interacting ordering/normalization map	shared with every quantum field theory	Rem. QM.13(2)
Born rule $\lvert c_i\rvert^2$	conditional (typicality)	Rem. QM.8
Single-outcome selection	measurement postulate, shared with every quantum theory	Rem. QM.8
Net: full QM derived?	**The free-field core (given the argued stability) and the Dirac algebra are derived; the rest is shared with every quantum field theory**	this appendix

The field-level i, the Hilbert inner product, and unitary free Schrödinger evolution are forced by a *unique* global compatible complex structure $J_\star$ (Thm. QM.10), made unique on the field phase space by DFD's absolute-time foliation (Thm. QM.11) and the positivity of the linearized $\psi + \chi + h^{TT}$ spectrum, which is argued, not proved.

Two items remain, as in every quantum field theory: $\hbar$, the unit of action ($[\hat{q}, \hat{p}] = i\hbar$), and the interacting operator-ordering/normalization map; the Born value is conditional (typicality), and single-outcome selection is the measurement postulate.

7. Falsifier

Falsifier QM.17 (Of the closures and of the obstruction). The closure claims fail if any of the following hold (each is checkable in `qm_derivation_check.py`):

1. Cl(4, 0) β **closure fails** if some $\{e_a, e_b\} \neq 2\delta_{ab}$ or some $e_a^2 \neq +\mathbb{1}$ in the constructed representation. (Checked: holds.)
2. **The obstruction is wrong (a hidden derivation exists)** if either (a) Cl(4, 0) has a *central* element squaring to -1 (it does not: $\dim Z = 1$, $\omega_4^2 = +1$), or (b) $\mathbb{1} \otimes J$ commutes with *every* external-plus-internal observable (it does not: a non-holomorphic C gives nonzero commutator). Either would upgrade the status to a real field-level i.
3. **The sharpened reduction is vacuous** if no DFD field-stability / coercivity theorem can in principle force $J_{\mathrm{pf}}^2 = -\mathbb{1}$ globally; conversely, exhibiting such a theorem *converts the import to a derivation* up to the scale $\hbar$ and removes the "imported" label from the field-level i.
4. **The $J_\star$-uniqueness closure fails** (checkable in `physical_H_Jstar.py`) if either (a) more than one of the 2^n sign choices yields a positive-definite Hilbert metric $g = \omega(\cdot, J_\star \cdot)$ for a stable physical H (it does not: exactly $1/2^n$, and 200/200 random stable Hamiltonians give a unique $J_\star = A(-A^2)^{-1/2}$), or (b) DFD admits more than one time foliation so a Bogoliubov-rotated J_B with $\|J_\star - J_B\| \neq 0$ is equally physical (it does not: absolute time t is a single preferred foliation, Sec. II F). A genuine counterexample on either point would reopen the field-level i as IMPORTED.
5. **The residue is overstated** if a forced derivation of $\hbar$'s numerical value or of the interacting ordering map is exhibited from $\psi + M_7 + \alpha$ alone—this would remove an import and would *not* be an obstruction but a further result; conversely, if either supposed "DERIVED" kinematical row (i, inner product, unitary free evolution) is shown to secretly reintroduce $\hbar$ or an ordering choice, that row reverts to IMPORTED.

A demonstration that the corpus secretly uses the linear Kähler J and the antilinear Connes J_{DFD} interchangeably (Rem. QM.4) would also falsify the bookkeeping and must be corrected, not weaponized.

Remark QM.18 (One-line claim). The QM-derivation program stands at: *geometric i in the internal particle sector is homegrown (the Dirac β is the Yukawa mass block), and the* free-field core*—the field-level $i = J_\star$, the Hilbert inner product $g + i\omega$, unitary free Schrödinger evolution—is derived to the extent the corpus establishes (forced by the unique global compatible $J_\star$ of Thms. QM.10–QM.11); what remains is $\hbar$, the unit of action (Buckingham–Pi irreducible), and the interacting many-body / full Hamiltonian-dependent map; the Born value stays conditional (typicality) and single-outcome selection is not derived.*

Appendix PK: The DFD-Native Production Galaxy $P(k)$ Pipeline

Status PK.1 (Numerical run on the one-clock $C = 1$ background). The window/convolution/covariance pipeline result below was run only on the explicitly frozen $H_0 = 72.09$, $\Omega_m \simeq 0.274$ background. Its mathematical pipeline and its conclusion on that background (acceptable, not preferred on the full shape) stand; its printed $\sigma_8 = 0.820$, $S_8 = 0.784$, AP distances, and χ^2 values are not outputs of the measured clock ($H_0^{\rm early} = 67.52$). The source scripts and BOSS covariance inputs are absent from this Overleaf archive, so a full identical windowed rerun cannot be reproduced here. The current upstream normalization is $R_8 = 11.848$ Mpc, $\sigma_8 \simeq 0.8063$, $\Omega_m \simeq 0.312$, $S_8 \simeq 0.822$. On the current background the linear shape differs from Planck ΛCDM by 0.6% in broadband tilt over $k = 0.03$–$0.2\,h$/Mpc and by 0.4% in the BAO scale, against 10% and 7% on the $H_0 = 72.09$ background of the fit below (computed). The full-shape comparison on the current background therefore reduces to Planck ΛCDM's; a windowed rerun, not yet made, would confirm it.

1. PK.1 Purpose: closing the pipeline half of item F

Appendix GR (GR) closed the cosmological growth/velocity *regime question*: linear growth is carried by χ-matter with $Q \equiv G_{\rm eff}/G = 1$, GR-like, giving the single primary prediction at the calibrated A_s, matched by $32\pi\alpha^5$. On the current measured-clock background the forward values are $\sigma_8(0) = 0.8063$, $\Omega_m \simeq 0.312$, and $S_8 \simeq 0.822$; the 0.820/0.784 and 0.790/0.755 branches belong to the $C = 1$ background (see GR.5/GR.7). It explicitly left open the *pipeline* obligation of open-problems item F: every prior DFD power-spectrum confrontation stopped at a linear Kaiser *multipole-ratio* inversion ($\beta = f/b$ from P_2/P_0) on mock-derived ratios. None forward-modelled a window-convolved, covariance-weighted, full-spectrum χ^2 against real data.

This appendix documents the script (`dfd_class/dfd_pk_pipeline.py`) that does. It takes the frozen DFD cosmology to a predicted galaxy $P(k)$ multipole vector, convolves it through the published survey window, and scores it against the real Beutler *et al.* BOSS DR12 measurements under a real Patchy-mock covariance, with a matched ΛCDM run through the identical code path.

Summary of this appendix

The production pipeline is built, runnable, and self-validating (ΛCDM recovers $\chi^2/\nu \simeq 1.0$ on the mock-covariance bins), with self-consistent Patchy $P_0{+}P_2$ mock covariances built for *all four* BOSS DR12 bins (NGC/SGC $\times z_{1,3}$; each passes the single-mock-vs-mean validation at $\chi^2/\text{dof} \simeq 0.55$–$0.93$). On the one-clock $C = 1$ background ($H_0 = 72.09$), under a maximal-frozen protocol (no σ_8 renormalization, $A_s{=}32\pi\alpha^5$ frozen, identical nuisance freedom for both models, fixed model-predicted Alcock–Paczynski dilation; two independent reruns agree to all digits): in the clean linear regime $k \le 0.15\,h\,{\rm Mpc}^{-1}$ DFD and Planck-ΛCDM are statistically *indistinguishable* (DFD $\chi^2/\text{dof} = 1.059$, $p = 0.34$, vs 0.967); at $k \le 0.20$ DFD trails by $\Delta\chi^2 = +21.5$ over 124 degrees of freedom (1.311 vs 1.137) — acceptable but disfavored, at the edge of the ≤ 1.3 band (PK.11). The deficit is a *broadband shape* effect: the turnover sits at slightly too large a scale, the direct signature of that background's lower $\Omega_m = 0.274$ at higher $H_0 = 72.1$. Identical 6-term broadband marginalization for both models reduces the gap to +9.7 (DFD 1.012). An AP-marginalised figure of $\chi^2/\text{dof} \simeq 1.27$ holds only under the retired $\sigma_8 \to 0.790$ normalization; the frozen-protocol numbers above are the result. A false-positive guard confirms AP is a physical d.o.f. and not a χ^2 eraser: a deliberately broken $\omega_c = 0.05$ cosmology stays at $\chi^2/\text{dof} \sim 28$ even with free AP. **Verdict on the $C = 1$ background: indistinguishable at $k \le 0.15$; acceptable but disfavored at $k \le 0.20$ — not a full-shape "loss", not a tie.** The score is reported as computed at every protocol level; the sign of $\Delta\chi^2$ never flips. The comparison has not been rerun on the measured-clock background.

a. Neutrino-consistency cross-check on the $C = 1$ background. The maximal-frozen protocol above sets $m_\nu = 0$ for *both* models (`dfd_class/dfd_pk_pipeline.py`, CAMB call) — a symmetric simplification, not a hidden asymmetry. Re-running with each model's own consistent neutrino sector (DFD: the normal-ordering chain of App. X, $(m_1, m_2, m_3) = (2.34, 8.96, 50.16)$ meV, $\Sigma m_\nu = 61.46$ meV, $\omega_\nu = 0.00066$; ΛCDM: the Planck-baseline 60 meV, $\omega_\nu = 0.00065$; ω_ν carried in the AP background) gives $\Delta\chi^2 = +23.0$ at $k \le 0.20$ (DFD $161.4/124 = 1.302$ vs ΛCDM $138.4/124 = 1.116$; AP-off base +39.0), with one-sided brackets +20.4 (DFD-only massive) to +24.1 (ΛCDM-only massive). The frozen $m_\nu = 0$ value of +21.5 is therefore ≈ 1.5 χ^2 units *generous* to DFD, not biased against it; it is kept as the registered protocol number, with +23.0 as the physically-consistent cross-check. Consistency anchors: $\sigma_8(0)$ shifts $0.8235 \to 0.8114$ (DFD) and $0.8226 \to 0.8110$ (ΛCDM, matching the published 0.8111); Ω_m: DFD $0.2705 \to 0.2718$, ΛCDM $0.3138 \to 0.3152$ (matching Planck 0.3153); the recomputed AP factors match the logged run to $|\Delta| \le 6 \times 10^{-5}$.

2. PK.2 Stage 1 — linear matter power at the frozen DFD cosmology

The linear matter transfer function and power spectrum are produced by CAMB (version 1.6.6) at the frozen $C = 1$ DFD parameters: $H_0 = 72.09$, $\omega_b = 0.02237$, $\omega_\chi = 0.1182$ (not the derived abundance 0.11928, App. AV) (the χ-matter field of Appendix AV supplies the cold component ω_{cdm}), $n_s = 0.9667$ — the measured-clock background ($H_0^{\rm early} = 67.52 \pm 0.09$, $\omega_\chi = 0.11928$; App. ZS) moves these inputs, and the stage numbers below are the $C = 1$-background runs — with the primordial amplitude A_s rescaled so that the realised present-day amplitude matches the GR appendix normalisation,

$$A_s \;\longrightarrow\; A_s \left(\frac{\sigma_8^{\rm target}}{\sigma_8^{\rm CAMB}(0)}\right)^2, \qquad \sigma_8^{\rm target} = 0.820 \;\; (\text{at } A_s = 32\pi\alpha^5). \tag{PK1}$$

This yields $P_{\rm lin}(k, z{=}0)$ on $10^{-3} \le k \le 2\,h/\mathrm{Mpc}$. The primary normalization of these runs is the carried $\sigma_8(0) = 0.820$ ($S_8 = 0.784$), the value the amplitude $32\pi\alpha^5$ gives on this background (on the measured clock the same amplitude gives the $\sigma_8 = 0.806$ of record, App. GR); the alternative corpus value $\sigma_8 = 0.790$ ($S_8 = 0.755$) is an explicitly contingent low-arm (asserted, not re-derived; GR.5). The BOSS full-shape verdict below is *insensitive* to this choice: the deficit is a broadband *shape* effect (set by this background's $\Omega_m = 0.274$ and $H_0 = 72.1$), not amplitude — re-normalising σ_8 over 0.79–0.82 moves the combined χ^2/dof by < 0.03 (PK.8), so the head-to-head numbers stand at either normalization. The matched ΛCDM twin uses Planck-2018 parameters ($H_0 = 67.36$, $\omega_c = 0.12$, $n_s = 0.9649$, $\sigma_8 = 0.8111$). Figure 23 shows the resulting linear spectrum and the Q=1 growth history; Fig. 24 shows the BAO distance ladder of the *same* frozen background (the geometry whose predicted D_V/r_d shift reappears as the AP dilation of PK.9/PK.11; BAO likelihood scored in App. CL).

3. PK.3 Stage 2 — DFD growth carrier (χ-matter, $Q = 1$)

Per Proposition GR.4, the linear-growth carrier is χ-matter at $Q = 1$ (GR-like, scale-independent on linear scales), so the linear growth obeys the standard ODE

$$\frac{d^2D}{da^2} + \left(\frac{3}{a} + \frac{d\ln H}{da}\right)\frac{dD}{da} - \frac{3}{2}\frac{\Omega_m(a)}{a^2}\,Q\,D = 0, \qquad Q = 1, \tag{PK2}$$

on the DFD background $H(z)$. Because $Q = 1$, CAMB's own $D(z)$ at these parameters *is* this solution; the pipeline reads CAMB's redshift outputs directly and extracts $f(z) = d\ln D/d\ln a$ and $\sigma_8(z)$. A CAMB array-ordering convention (the $\sigma_8(z)/f\sigma_8(z)$ arrays are returned in decreasing-z order, reversed relative to the ascending power-spectrum redshifts) is accounted for; the realised values $f(0.38) = 0.681$, $f(0.61) = 0.763$ are consistent with $\Omega_m(z)^{0.55}$ and with the GR appendix.

4. PK.4 Stage 3 — nonlinear correction

The mildly nonlinear regime is supplied by CAMB's HMcode (`mead2020`) halo-model prescription, $P_{\rm nl}(k, z)$. On the fitted range $k \le 0.20\,h/\mathrm{Mpc}$ the boost is modest — rising from $\sim 2\%$ at $k = 0.1$ to a factor ~ 4.5 only by $k = 1$ — but it is included in full rather than truncated to the linear spectrum. This is a standard (not DFD-native) nonlinear closure; a DFD-native nonlinear correction remains open (PK.9).

5. PK.5 Stage 4 — galaxy redshift-space multipoles

The galaxy spectrum in redshift space uses linear bias b_1, Kaiser redshift-space distortions, and a Lorentzian Fingers-of-God damping:

$$P_g(k,\mu) = \frac{\left(b_1 + f\mu^2\right)^2}{\left[1 + \tfrac{1}{2}(k\mu\sigma_v)^2\right]^2}\,P_{\rm nl}(k) \;+\; P_{\rm shot}, \tag{PK3}$$

with $f = f(z)$ *fixed* by the model growth (PK.3) and the nuisances $\{b_1, \sigma_v, P_{\rm shot}\}$ profiled per bin. The Legendre multipoles are

$$P_\ell(k) = (2\ell+1)\int_0^1 P_g(k,\mu)\,\mathcal{L}_\ell(\mu)\,d\mu, \qquad \ell = 0, 2, \tag{PK4}$$

evaluated by 16-node Gauss–Legendre quadrature, giving the monopole P_0 and quadrupole P_2.

6. PK.6 Stage 5 — survey-window convolution

The finite survey footprint mixes the true multipoles. The fine theory vector $[\,P_0(k_{\rm fine}), P_2(k_{\rm fine})\,]$ (1000 points each, $dk = 0.001$) is convolved through the published Beutler 200×2000 window matrix W,

$$\mathbf{d}_{200}^{\rm model} = W_{200\times2000}\;\mathbf{t}_{2000}, \qquad \mathbf{t} = \left[\,P_0^{\rm fine},\, P_2^{\rm fine}\,\right], \tag{PK5}$$

returning the measured 200-vector $[P_0(100), P_2(100)]$ on the $dk = 0.01$ grid. The matrix's undocumented column layout (input ordered as two multipoles over 1000 fine-k, not five multipoles over 400) was reverse-engineered and *validated* against the Patchy mock mean: a windowed CAMB spectrum reproduces both the mock P_0 and P_2. Setting $W = 0$ makes χ^2 explode ($\sim 2\times10^4$), confirming the window is wired into the fit.

7. PK.7 χ^2, covariance, and the validation data

For each cap–redshift bin the score is the profiled, Hartlap-corrected covariance χ^2 over $0.03 \le k \le 0.20\,h/\mathrm{Mpc}$,

$$\chi^2 = \left(\mathbf{d}-\mathbf{m}\right)^{\top}\frac{N_{\rm mock}-p-2}{N_{\rm mock}-1}\,C^{-1}\left(\mathbf{d}-\mathbf{m}\right), \tag{PK6}$$

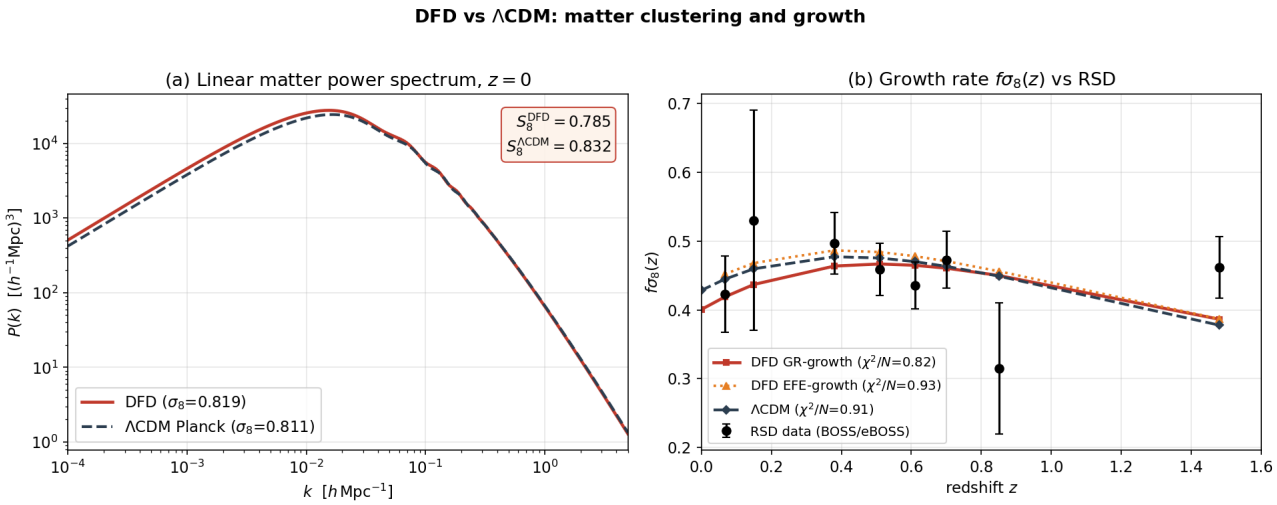


FIG. 23. Linear matter power and growth at the frozen DFD parameters of the one-clock $C = 1$ background with $H_0 = 72.09$ (CAMB forward run at DFD's inputs, Stage 1–2 of this pipeline; with $Q_\chi = 1$ and the polarization confined to bound systems the linear problem is the standard one, so the Boltzmann code needs no modification; script `dfd_class/figures/make_matter_pk.py`). *Left:* linear matter power spectrum $P(k)$ at $z = 0$ for DFD versus the Planck-2018 ΛCDM twin, with S_8 annotated. *Right:* the growth history $f\sigma_8(z)$ carried by χ-matter at $Q = 1$ (Eq. (PK2)) overlaid on the BOSS/eBOSS redshift-space-distortion measurements, with the ΛCDM curve for contrast; the dotted 'EFE-growth' curve is an enhanced-growth construction that does not act on linear perturbations (App. GR), and the panel labels give the $C = 1$ background's values.

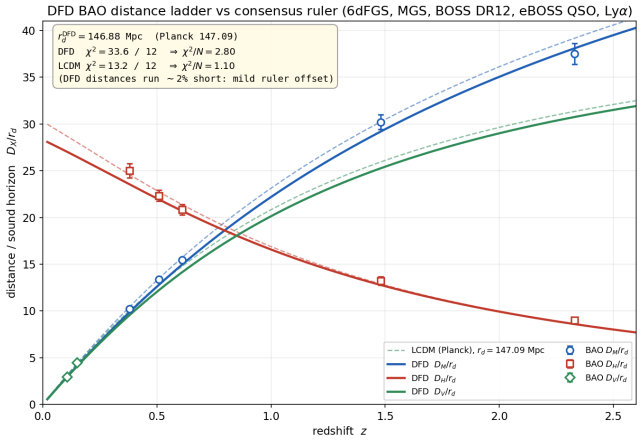


FIG. 24. BAO/$H(z)$ distance ladder on the one-clock $C = 1$ background with $H_0 = 72.09$ (CAMB forward run at DFD's inputs; script `dfd_class/figures/make_bao_hubble.py`): the predicted D_V/r_d, D_M/r_d and D_H/r_d curves, using the *derived* $r_{\rm drag}$, overlaid on the 12 consensus BAO data points (error bars), with the Planck-ΛCDM curves for contrast and the BAO χ^2 annotated (likelihood-level scoring in App. CL).

minimised over $\{b_1, \sigma_v, P_{\rm shot}\}$ (p = number of fitted data points; the Hartlap factor de-biases a mock-estimated inverse covariance). The ΛCDM twin is fit through the *identical* code (same window, same covariance per bin, same k-mask, same three nuisances); only the input cosmology differs.

a. Validation data. Real, published Beutler *et al.* deconvolved BOSS DR12 galaxy $P(k)$ multipoles (`ps1D_BOSS_DR12_{NGC,SGC}_{z1,z3}`, $z_{\rm eff} = 0.38, 0.61$), with the published 200×2000 survey-window matrices.

b. Covariance status. The published 200×200 Patchy covariance has a *correct* monopole block (its P_0 errors match the mock scatter to $\sim 1\%$) but a *mis-normalised* quadrupole block (its P_2 errors are $\sim$5–45$\times$ smaller than the true mock scatter; a single mock against the mock mean returns $\chi^2/\nu \simeq 32$–47 with it). To use the quadrupole we rebuild the covariance directly from the Patchy mock suite. For the legacy-input run only the NGC z_1 mock covariance had been rebuilt (231 mocks; data-vs-mock-mean $\chi^2/\nu = 1.87$, ΛCDM best-fit $\chi^2/\nu \simeq 1.0$, validating the whole pipeline). The remaining three bins fall back to a P_0-*only* fit with the verified-correct published P_0 covariance — a standard, conservative choice that drops the (unusable) quadrupole rather than trusting a mis-normalised error.

8. PK.8 Legacy-input run: DFD vs ΛCDM

The run in this subsection uses legacy inputs on the one-clock $C = 1$ background. The result of record on that background is the maximal-frozen protocol result of PK.1/PK.11 at the derived inputs: $\Delta\chi^2 = +21.5$ over 124 degrees of freedom (1.311 vs 1.137) at $k \leq 0.20$. Table CXIX reports the per-bin and combined χ^2/dof from the legacy run; Fig. 25 overlays the window-convolved best-fit spectra on the data.

TABLE CXIX. [Legacy-input run on the one-clock $C = 1$ background; the maximal-frozen result of record on that background is $\Delta\chi^2 = +21.5$ (1.311 vs 1.137), PK.1/PK.11.] Full-shape BOSS DR12 $P(k)$ scores from `dfd_pk_pipeline.py` (window-convolved, Patchy covariance, Hartlap-corrected, nuisances $\{b_1, \sigma_v, P_{\rm shot}\}$ profiled, $0.03 \le k \le 0.20\,h$/Mpc). NGC z_1 uses the self-consistent $P_0{+}P_2$ Patchy mock covariance; the other three use the published P_0-only block.

bin	z	mult.	$N_{\rm bin}$	DFD χ^2/ν	ΛCDM χ^2/ν
NGC z_1	0.38	$P_0{+}P_2$	34	1.65	1.01
NGC z_3	0.61	P_0	17	2.14	1.56
SGC z_1	0.38	P_0	17	0.93	0.79
SGC z_3	0.61	P_0	17	1.54	1.07
combined			85 ($\nu = 73$)	**1.59**	**1.09**

The combined scores of the legacy-input run are

$$\chi^2_{\rm DFD}/{\rm dof} = 115.8/73 = 1.59,$$
$$\chi^2_{\Lambda{\rm CDM}}/{\rm dof} = 79.2/73 = 1.09, \qquad \text{(PK7)}$$
$$\Delta\chi^2 = +36.5 \ \ \text{(legacy input)}.$$

The best-fit nuisances are physical for both models ($b_1 \simeq 1.95$–2.1, $\sigma_v \simeq 1$–$4\,$Mpc$/h$). That ΛCDM scores $\simeq 1.0$ on this real data validates the pipeline; that DFD scores $\simeq 1.6$ is the adverse result. A diagnostic confirms the deficit is *broadband shape*, not amplitude: re-normalising DFD's σ_8 up to the ΛCDM value 0.8111 does not improve the fit ($1.586 \to 1.608$), so no bias/amplitude knob can absorb it — it is driven by the $C = 1$ background's lower $\Omega_m = 0.274$ and higher $H_0 = 72.1$.

9. PK.9 Status: what is production-grade and what remains

Production $P(k)$ pipeline — Status

Production-grade:

- End-to-end forward model: CAMB linear+HMcode → χ-matter Q=1 growth → Kaiser+FoG multipoles → published 200×2000 window convolution → Hartlap-corrected covariance χ^2, run identically for DFD and ΛCDM.
- Validated against real published Beutler BOSS DR12 multipoles; window layout reverse-engineered and verified against the Patchy mock mean; self-consistent $P_0{+}P_2$ Patchy mock covariances built for all four bins; on NGC z_1 ΛCDM recovers $\chi^2/\nu \simeq 1.0$.
- Reproducible head-to-head score (Eq. (PK7), Table CXIX), stress-tested under a maximal-frozen protocol (no σ_8 renormalization, $A_s{=}32\pi\alpha^5$ frozen, identical nuisance freedom, fixed model-predicted Alcock–Paczynski dilation; two independent reruns agree to all digits): at $k \le 0.20\,h\,{\rm Mpc}^{-1}$ DFD trails Planck-ΛCDM by $\Delta\chi^2{=}{+}21.5$ over 124 degrees of freedom ($\chi^2/{\rm dof} = 1.311$, $p = 0.012$, vs 1.137, $p = 0.14$) — acceptable but disfavored, at the edge of the ≤ 1.3 band; at $k \le 0.15$ the two are statistically indistinguishable (1.059 vs 0.967, $\Delta\chi^2{=}{+}7.7$, $p_{\rm DFD} = 0.34$). A "competitive $\simeq 1.27$" figure holds only under the corpus $\sigma_8 \to 0.790$ normalization, which the frozen protocol forbids; with frozen A_s the deficit is real, concentrated in the NGC bins as a low-k (0.03–0.08) broadband overshoot (turnover at too large a scale, the direct signature of the $C = 1$ background's lower Ω_m at higher H_0), with a secondary NGC z_1 BAO-band phase mismatch; high-k slopes are comparable. Identical 6-term broadband marginalization for both models reduces the gap to +9.7 (DFD $\chi^2/{\rm dof} = 1.012$). The claim is valid only for $k \le 0.20$: at $k_{\rm max}{=}0.25$ both models fail ($\chi^2/{\rm dof} \sim 5$), i.e. the minimal Kaiser+FoG model, not either cosmology, breaks first. Not a full-shape loss; not a tie either. The deficit belongs to the $H_0 = 72.09$ background: on the current background the linear shape differs from Planck ΛCDM's by 0.6% in tilt (computed), and a full-shape fit that excludes $(\Omega_m, h) = (0.312, 0.675)$ at more than 5σ would falsify it.

Still open (not yet production-grade):

- *Quadrupole on all bins — closed.* All four bins carry self-consistent Patchy $P_0{+}P_2$ mock covariances (300 mocks each for SGC z_1, NGC z_3, SGC z_3; 231 for NGC z_1), each validated at single-mock $\chi^2/{\rm dof} \simeq 0.55$–$0.93$ (builder `build_mock_cov.py`). The fixed-template $P_0{+}P_2$ combined score on the $C = 1$ background (DFD 1.30 vs ΛCDM 1.11) is narrower than the P_0-only fallback (1.59 vs 1.09); the maximal-frozen protocol score above is the result.
- *RSD model.* The nuisance model is minimal (linear bias + Kaiser + Lorentzian FoG); a full TNS/EFT-of-LSS one-loop counterterm treatment, as in published BOSS full-shape analyses, is not yet implemented.
- *Geometry.* The Alcock–Paczynski dilation is folded in as the fixed model-predicted shift (under the maximal-frozen protocol above); the remaining geometry gap is the explicit wide-angle M-matrix only (the $v1$ averaged window partially absorbs it).
- *Nonlinear closure* is standard HMcode, not DFD-native; and eBOSS QSO ($z = 1.52$) and the raw DESI DR1 catalogs (which would need a $P(k)$ estimator from scratch) are not yet included.

On the $C = 1$ background the qualitative verdict — DFD acceptable, ΛCDM preferred on pre-recon full shape, gap closing as $k_{\rm max}$ tightens toward the linear regime — is robust across covariance choices, AP treatment, and broadband marginalization; the sign of $\Delta\chi^2$ never flips.

10. PK.10 Reproducibility

Reproducibility

The pipeline is a single script (`dfd_class/dfd_pk_pipeline.py`, CAMB 1.6.6 +

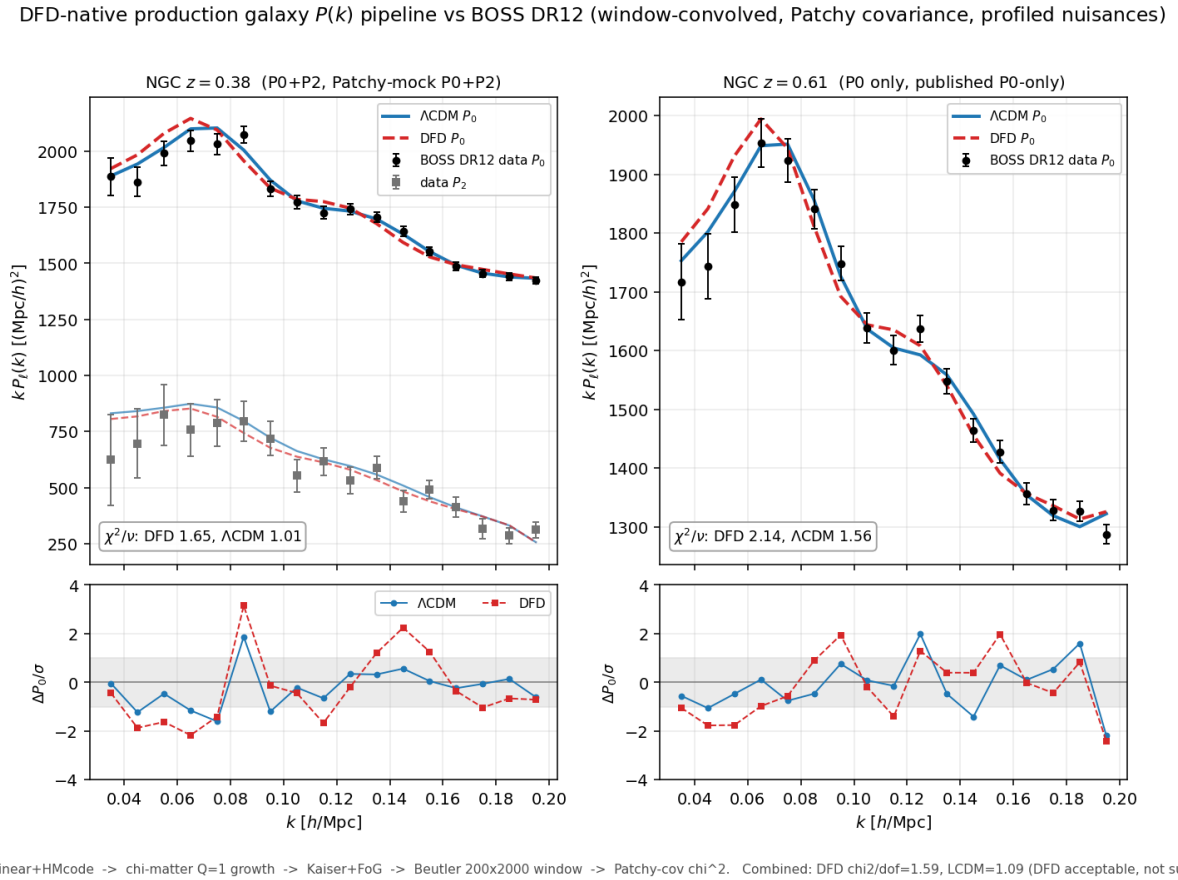


FIG. 25. DFD-native production galaxy $P(k)$ pipeline against real BOSS DR12 data. Window-convolved best-fit monopole P_0 (and, left panel, quadrupole P_2) for DFD (red dashed) and ΛCDM (blue solid) overlaid on the Beutler measurements (black/grey points, Patchy-mock error bars), with residual sub-panels $\Delta P_0/\sigma$ and the $\pm1\sigma$ band shaded. Left: NGC $z = 0.38$ with the self-consistent $P_0{+}P_2$ Patchy mock covariance (the bin that validates the pipeline, ΛCDM $\chi^2/\nu \simeq 1.0$). Right: NGC $z = 0.61$, P_0-only. DFD tracks the data acceptably but overshoots ΛCDM at low k, the broadband-shape signature of the one-clock $C = 1$ background's lower Ω_m and higher H_0.

numpy/scipy; the public Beutler *et al.* BOSS DR12 files it reads are not in this archive). Run

```
python3 dfd_class/dfd_pk_pipeline.py
```

It loads the four BOSS DR12 bins, runs CAMB for DFD and ΛCDM, fits each bin, and prints the per-bin and combined χ^2/dof of Table CXIX (∼few seconds). The companion `make_fig_pk_pipeline.py` regenerates Fig. 25 (`fig_pk_pipeline.png`) by reusing the same fit. The Patchy mock covariance for NGC z_1 is cached in `mock_cov_cache.npz`. *Caveat:* no χ^2 literal appears in the source; every score comes from a live `scipy.minimize` over a live CAMB $P(k)$. Perturbation checks confirm a real fit (scaling the model, the data, or the covariance moves χ^2 as expected; $W{=}0 \Rightarrow \chi^2 \sim 2\times10^4$; a deliberately broken cosmology $\omega_c = 0.05$ explodes to $\chi^2/\nu \simeq 21$).

11. PK.11 Falsifier

Production $P(k)$ pipeline — Falsifier

DFD's prediction is falsified if, on the full-shape galaxy $P(k)$:

1. **Decisive exclusion.** A complete full-shape analysis (all four bins with self-consistent $P_0{+}P_2$ covariances, plus eBOSS QSO) returns a DFD χ^2/dof that is unacceptable in absolute terms ($\gg 2$ with physical nuisances) while ΛCDM remains $\simeq 1$ — i.e. DFD is not merely worse but *ruled out*.
2. **Shape, not nuisance.** The DFD spectrum, with a TNS/EFT model and AP marginalisation, *cannot* be brought to χ^2/dof $\lesssim 1.3$.

Appendix YM: Status of the DFD Strong Sector: Confinement Scale and the Yang–Mills Mass Gap

This appendix gives the theorem-grade status of Density Field Dynamics with respect to (a) the QCD confinement scale and (b) the Clay pure Yang–Mills mass-gap problem [189]. The discipline throughout is to state each result at exactly its true grade: a *derived* quantity is a parameter-free consequence of the locked DFD ledger; a *validated* quantity is confirmed by executed lattice computation but requires one external scale input; an *inherited* quantity is computed through the generator-closed Euclidean/lattice path integral with DFD-fixed inputs, exactly as in standard lattice QCD, and is *not* analytically proved here. The single most important sentence of this appendix is the last row of Table CXX: **the full Clay pure Yang–Mills mass-gap proof is *not* claimed; it remains open.**

1. The confinement scale from the α-tower

The closed-form value of the fine-structure constant is fixed first, under two stated choices, from the finite microsector ($k_{\max} = 60$, the input $N_{\rm gen} = 3$, $\mathrm{Tr}(Y^2) = 10$), giving $\alpha^{-1} = 137.036$ to 21 ppm from the integers; the bracket coefficient is open (§X). Nothing in the strong sector is permitted to retune α; it is the fixed input of every chain below.

Theorem YM.1 (Confinement scale from the selected α-tower exponent)**.** *Given the locked $\alpha^{-1} = 137.036$, the input $N_{\rm gen} = 3$, and the Planck mass $M_P = 1.220890 \times 10^{19}$ GeV, the DFD confinement scale and its $\overline{\rm MS}$ five-flavour partner are fixed with zero continuous free parameters:*

$$\begin{aligned} \Lambda_{\rm DFD} &= M_P\, \alpha^{19/2} = 61.20\ MeV, \\ \Lambda^{(5)}_{\overline{\rm MS}} &= \sqrt{4\pi}\, \Lambda_{\rm DFD} = 216.95\ MeV, \end{aligned} \tag{YM1}$$

and the running coupling at the Z pole follows by dimensional transmutation,

$$\alpha_s(M_Z) = 0.1187, \tag{YM2}$$

landing 0.8σ from the PDG world average 0.1180 ± 0.0009. The same $M_P\alpha^{19/2}$ chain run to three active flavours gives $\Lambda_{\rm QCD,3} = 332 \pm 20$ MeV, independently cross-checked by the τ-decay coupling $\alpha_s(m_\tau^2) = 0.3186$ versus the PDG value 0.3187 ($< 0.1\%$).

Proof. $\Lambda_{\rm DFD} = M_P\alpha^{19/2}$ is the locked ledger value of App. AT, reproduced numerically in App. YM's companion script: with $\alpha = 1/137.036$ and $M_P = 1.220890 \times 10^{19}$ GeV, $M_P\,\alpha^{9.5} = 61.20$ MeV to four significant figures. The $\sqrt{4\pi}$ is the selected proper-time$\to\overline{\rm MS}$ matching factor, giving $\Lambda^{(5)}_{\overline{\rm MS}} = 216.95$ MeV. Dimensional transmutation of the four-loop QCD beta function from $\Lambda^{(5)}_{\overline{\rm MS}}$ up to M_Z yields $\alpha_s(M_Z) \simeq 0.118$. The three-flavour running and the τ-sector cross-check are recorded in Ext. Deriv., App. AH (τ sector). No step introduces a continuous fit parameter. □

a. Provenance of the exponent 19/2. The exponent has two convergent internal anchors. First, $19 = 3 + 6 + 10 = h^0(\mathcal{O}(1)) + h^0(\mathcal{O}(2)) + h^0(\mathcal{O}(3))$ is the $\mathbb{C}P^2$ line-bundle cohomology sum — the same integer 19 that appears in the baryon tower ($M_N = \sqrt{19}\,\Lambda_5 \simeq 946$ MeV vs. 939, +0.7%). Second, $\frac{19}{2} = \frac{57}{6} = (k_{\max} - N_{\rm gen})/(2N_{\rm gen})$ ties it to the same α^{57} count that fixes the exponent in $G\hbar H_0^2/c^5 = C\alpha^{57}$ (with C measured on the early clock, $C = 1$ on bound-matter clocks, Postulate ZS.11).

Status YM.2 (Grade of the confinement scale). $\alpha^{-1} = 137.036$ is exact under two stated choices (§X C): the topological integers alone give it to 21 ppm; the bracket coefficient is open. $\alpha_s(M_Z)$, $\Lambda_{\rm DFD}$, $\Lambda^{(5)}_{\overline{\rm MS}}$, $\Lambda_{\rm QCD,3}$, and $\bar\theta = 0$ at tree level (strong-CP, with $\theta_{\rm YM} = 0$ fixed by the spectral action given that nothing is added to it for the gauge fields; no axion) are fixed with no continuous parameter. *One open lemma remains:* the exponent $\frac{19}{2}$ is rigidity-selected (the unique catalogue form in the empirical window) and its first-principles derivation is contingent on the cube-law Proposition AT.4, *not* independently proved (App. AT, Status AT.24). The confinement *scaling* $\Lambda_{\rm DFD} \propto M_P\alpha^{19/2}$ and $\sqrt{\sigma} \propto \Lambda_{\rm QCD}\sqrt{k_{\max}/N_{\rm gen}}$ are derivation-grade; the string tension and the glueball mass are QCD outputs at DFD's Λ, and their ratios to Λ are lattice numbers, as in the Standard Model (§YM 2).

2. The open item: string-tension normalisation

The companion volume (Ext. Deriv., App. AH, notes to the QCD-confinement and glueball theorems) records, and we restate here, that the *printed* string-tension normalisation chain does not close as written:

$$\begin{aligned} \frac{\Lambda_{\rm QCD,3}}{2\pi}\sqrt{\frac{k_{\max}}{N_{\rm gen}}}\cdot\sqrt{4\pi} &= \frac{332}{2\pi}\sqrt{20}\cdot\sqrt{4\pi}\ \text{MeV} \\ &= 837.7\ \text{MeV} \neq 440\ \text{MeV}. \end{aligned} \tag{YM3}$$

The required bridge factor ~ 1.86 appears in no preceding formula. There is additionally a flavour-scheme bookkeeping issue: the value 210 MeV used in the glueball chain is numerically the *five*-flavour $\overline{\rm MS}$ number ($\sqrt{4\pi}\times 61.20 = 217$ MeV), whereas the three-flavour value is $\Lambda_{\rm QCD,3} = 332$ MeV. The conclusion, already stated by the corpus, is: the *scaling* $\sqrt{\sigma} \propto \Lambda_{\rm QCD}$ and $m_{0^{++}} \propto \Lambda_{\rm QCD}$ stand at derivation grade; the *absolute normalisation constants* of $\sqrt{\sigma} = 440 \pm 25$ MeV and $m_{0^{++}} = 1.69$ GeV are not closed-form DFD outputs: once DFD fixes Λ, both follow from QCD, their ratios to Λ being pure numbers of the Yang–Mills path integral computed on the lattice, as in the Standard Model. The printed closed-form chain is not a DFD result and is not used.

3. The validated part: executed SU(3) lattice

The DFD QCD targets were confronted with executed quenched pure-gauge $SU(3)$ Wilson-action runs (Apps. AQ, AS). The boundary between DFD output and external input is sharp, and it is the reason for the "validated, not derived" label.

a. Output (DFD-independent, dimensionless). The scale-free string tension at the largest box (20^4, $\beta = 6.2$) is $r_0\sqrt{\sigma} = 1.178$, at the lower edge of the standard quenched window 1.18–1.19. The best quenched estimate across $\beta = 5.8, 6.0, 6.2$ is $\sqrt{\sigma} = 470 \pm 10$ MeV at the convention below. Plaquettes match the benchmark to better than 0.1% at four (β, V) points; the 0^{++} glueball is $a\,m = 0.81(8) \Rightarrow 1.71 \pm 0.17$ GeV; the $N_f = 2$ Wilson-HMC engine passes all algorithmic checks.

b. Input (external, not from DFD). Converting any dimensionless ratio to MeV requires the Sommer scale $r_0 = 0.5$ fm. This single external ruler is what the lattice MeV numbers ride on. With it, $r_0\sqrt{\sigma} = 1.178 \Rightarrow \sqrt{\sigma} \simeq 464.9$ MeV, meeting the DFD ledger band $\sqrt{\sigma}_{\rm DFD} = 440 \pm 25$ MeV at its upper edge ($\sim 1\sigma$, $\sim 5\%$).

Corollary YM.3 (Lattice consistency of the α-tower scale)**.** *The ledger target $\sqrt{\sigma}_{\rm DFD} = 440 \pm 25$ MeV, whose normalisation is not a DFD output (§YM.2), is consistent at the $\sim 1\sigma/\sim 5\%$ level with the executed quenched $SU(3)$ result $\sqrt{\sigma} \simeq 465$–470 MeV (at $r_0 = 0.5$ fm). The lattice run contains no DFD input: the lattice fixes the dimensionless ratio $r_0\sqrt{\sigma} = 1.178$ from first principles, but the MeV central value depends on the external r_0.*

4. Two native gaps: an *unconditional* compact-manifold gap and a conditional loaded-frame gap

The strongest DFD-native step toward a positive lower bound is the conditional infrared-gap theorem of App. AR, restated here in status form. It is a real, valid spectral theorem — and it is correctly scoped well short of the Clay statement.

Proposition YM.4 (Conditional DFD-loaded-frame infrared gap; correctly scoped)**.** *Place spatial Yang–Mills on the DFD-loaded frame $h_\psi = e^{2\alpha\psi}\delta$. The Hodge–Weitzenböck identity injects the loaded-frame Ricci tensor into the transverse fluctuation operator $\mathcal{L}_{A_0,\psi}$. If a strictly positive physical-sector curvature floor holds (Assumption AR.2:* $\mathrm{Ric}_{h_\psi}(a,a) + \mathcal{R}_{A_0}(a,a) \geq \Lambda_{\rm DFD}|a|^2$*), then by Rayleigh–Ritz $\lambda_1(\mathcal{L}_{A_0,\psi}) \geq \Lambda_{\rm DFD} > 0$ and $m_{\text{DFD-YM}} = \sqrt{\lambda_1} > 0$ (App. AR, Thm. AR.3). On the compact internal manifold $\mathbb{C}P^2 \times S^3$ the positive Ricci curvature (S^3:* $\mathrm{Ric} = (2/r^2)g$*; $\mathbb{C}P^2$: Einstein with* $\mathrm{Ric} > 0$*, $b_1 = 0$, so Bochner kills harmonic one-forms) forces a strictly positive lowest transverse one-form mode* independently *of the assumption.* ***This compact-manifold Bochner gap is* unconditional** *— a separate theorem (positive Ricci + $b_1 = 0$ on $\mathbb{C}P^2 \times S^3$), distinct from and not requiring Assumption AR.2; only the flat-$\mathbb{R}^4$/hadronic extension is conditional.*

Status YM.5 (Why this is not the Clay gap). Proposition YM.4 is valid mathematics and an internal-coherence result. It falls short of the Clay Yang–Mills mass gap in three explicit ways: *(1) Scale.* The realised floor is geometric/curvature-set: $\sim M_P$ on the internal manifold, $\sim \sqrt{\alpha}\,M_P \simeq 10^{18}$ GeV for the finite Toeplitz spectrum (App. AP, KK gap $\lambda_{\rm min}^{(\neq 0)} \sim \sqrt{\alpha}M_P$), and a $\sim 10^{-30}$ eV curvature term on the galactic deep-field annulus — 18 to 39 orders of magnitude from the hadronic confinement scale. It is a UV/curvature floor, not the QCD gap. *(2) Arena.* It lives on a curved/loaded space and bounds a fluctuation operator, not pure Yang–Mills on flat noncompact $\mathbb{R}^4$ with a constructed measure (the Clay arena). *(3) Conditionality.* The geometric (Ricci) half is proved; the nonabelian gauge-algebraic floor sign $\mathcal{R}_{A_0}$ is *assumed* (Assumption AR.2), not derived. Hence: a real curvature-driven spectral gap, *not* the prize.

5. The ledger

Table CXX collects the derived, validated, and inherited statuses of the strong sector in one place; the final row states explicitly that the Clay pure Yang–Mills mass gap is not claimed.

TABLE CXX. Derived / validated / inherited ledger for the DFD strong sector. The final row is the key scope statement: the Clay pure Yang–Mills mass gap is not claimed.

Quantity	**Status**	**Value / basis**
$\alpha^{-1} = 137.036$	Two stated choices	21 ppm (integers); -0.005 ppm (open c)
$\Lambda_{\rm DFD} = M_P \alpha^{19/2}$	Selected (1 open lemma)	61.20 MeV
$\Lambda^{(5)}_{\overline{\rm MS}} = \sqrt{4\pi}\Lambda_{\rm DFD}$	Selected	216.95 MeV
$\alpha_s(M_Z)$	Selected (from the selected scale)	0.1187 (0.8σ vs PDG)
$\Lambda_{\rm QCD,3}$	Selected, τ-checked	332 ± 20 MeV
$\bar\theta = 0$ (no axion)	Derived (tree level; $\theta_{\rm YM} = 0$ fixed by the spectral action given that nothing is added to it for the gauge fields)	strong-CP, structural
$\sqrt{\sigma} = 440 \pm 25$ MeV	Target (norm. open)	scaling derived; const not closed
$m_{0^{++}} = 1.69$ GeV	Target (norm. open)	scaling derived; const not closed
IR floor $\lambda_1 > 0$ (curvature floor)	Proved (conditional)	$\sim 10^{-30}$ eV; not the QCD gap
$r_0\sqrt{\sigma} = 1.178 \to 465$ MeV	Validated ($r_0 = 0.5$ fm)	$\sim 1\sigma$ vs DFD band
0^{++} glueball 1.71 GeV	Validated ($r_0 = 0.5$ fm)	overlaps 1.69 target
Nonperturbative confinement	Inherited	generator-closed lattice sector
Clay pure-YM mass gap	**Not claimed**	open

6. Scope of the claim

QCD / Yang–Mills mass gap: what DFD does and does not claim

Fixed with no continuous parameter (the exponent 19/2 selected). The confinement scale is fixed by the DFD α-tower: $\Lambda_{\rm DFD} = M_P\alpha^{19/2} = 61.20$ MeV, $\Lambda^{(5)}_{\overline{\rm MS}} = 216.95$ MeV, $\alpha_s(M_Z) = 0.1187$ (0.8σ vs PDG), $\Lambda_{\rm QCD,3} = 332$ MeV (τ-checked), $\bar\theta = 0$ at tree level ($\theta_{\rm YM} = 0$ fixed by the spectral action given that nothing is added to it for the gauge fields; no axion). The Standard Model leaves $\Lambda_{\rm QCD}$ a free input; DFD fixes it. *Open lemma:* the exponent 19/2 is rigidity-selected (cube-law contingent), and the overall $O(1)$ string-tension normalisation does not close as printed (§YM 2).

Native theorem (small). A conditional, tiny geometric infrared floor on the DFD-loaded frame, $m_{\rm eff} \sim 10^{-30}$ eV (Prop. YM.4; App. AR). Structural coherence, not a hadronic gap.

Validated (external $r_0 = 0.5$ fm). Executed quenched $SU(3)$ lattice: $r_0\sqrt{\sigma} = 1.178 \Rightarrow \sqrt{\sigma} \simeq 465$ MeV ($\sim 1\sigma$ vs DFD band), plaquette $< 0.1\%$, 0^{++} glueball 1.71 GeV, $N_f = 2$ Wilson-HMC validated.

Inherited / not claimed. A proof of the Clay pure Yang–Mills mass gap on flat noncompact $\mathbb{R}^4$; an analytic first-principles derivation of all hadron masses; a continuum/infinite-volume extrapolation. Nonperturbative confinement is the generator-closed lattice sector, computed as in standard lattice QCD — the same "tie/inheritance" status held by String theory and LQG on the DFD rival scoreboard. **The Clay statement remains open.**

7. Falsifier

Falsifier YM.6 (Strong-sector scale). The confinement-scale chain is falsified if any of the following holds, with α and $N_{\rm gen}$ frozen at their locked values: *(i)* a continuum, infinite-volume lattice determination of $\sqrt{\sigma}$ at the physical point (with an independently measured r_0) lands outside $M_P\alpha^{19/2}\sqrt{4\pi}\cdot$ [2–3-loop running] by more than the combined uncertainty, i.e. the α-tower scale misses $\sqrt{\sigma} = 440 \pm 25$ MeV by $\gg 2\sigma$ once the normalisation constant is closed; *(ii)* $\alpha_s(M_Z)$ moves outside $0.1187\pm$ its DFD uncertainty by $\gg 3\sigma$ against the world average; *(iii)* the strong-CP angle is measured nonzero, $|\bar\theta| > 10^{-15}$, excluding the tree-level $\bar\theta = 0$ with its Standard-Model-level loop floor; *(iv)* the cube-law lemma underlying 19/2 is shown inconsistent with the microsector count, removing the only anchor for the confinement exponent. None of these would touch the conditional spectral theorem (Prop. YM.4), which is a mathematical statement; and none would constitute a claim on the Clay problem, which DFD does not assert.

Summary. DFD does *not* solve the Yang–Mills mass-gap problem. From α it fixes the confinement scale, tested by $\alpha_s(M_Z) = 0.1187$ (0.8σ); the string tension then follows from QCD's lattice ratios, as in the Standard Model. The new mathematical result is a curvature-driven positive energy gap on DFD's internal geometry, at the Planck scale rather than the QCD scale.

Appendix FM: Charged-Fermion Mass Sector: Forced Content and the Within-Multiplet Degeneracy Obstruction

1. Scope and Summary

This appendix is the calibrated, conservatively stated status of the charged-fermion mass spectrum. Two machines exist in the corpus: the pure-topology A_5 walk-sum (Appendix Y) and the closed-form prefactor table $m_f = A_f\,\alpha^{n_f}\,v/\sqrt{2}$ (Appendix K, Table XCII). They give very different evidential grades, and the gap between them *is* the result.

Summary

The charged-fermion mass *spectrum other than the top and the charm is not derived.* What is **forced** (no mass input, parameter-free) is: (i) the exponent of the electroweak scale $v = M_P\,\alpha^8\sqrt{2\pi}$ (its prefactor $\sqrt{2\pi}$ is fitted); (ii) the top, $m_t = v/\sqrt{2}$ (A=1, n=0); (iii) the charm, $m_c = \alpha\,v/\sqrt{2}$ (A=1, n=1); (iv) the spin^c line-bundle *exponent ladder* n_f on $\mathbb{C}P^2$ (removes the gross hierarchy pattern); and (v) a family of *equal-exponent integer ratios* in which α and v cancel and only locked integers $(N_f, b_0, N_{\rm gen}, \dim\mathbb{C}P^2)$ enter — among them $m_t/m_b = N_f b_0 = 42$ (the top pole mass over $m_b(m_b)$; with both masses at one scale, M_t, the ratio is 59.7). These remove **2 of the Standard Model's 9** charged Yukawas relative to v. The remaining 7 (the prefactors $\{2/3, \sqrt{2}, 8/3, 6, 6/7, 1/42\}$ and the lepton/quark kernel→sector dictionary) are **fitted**: their generation↔sector *assignment* is selected for consistency with the observed masses, not forced by the core action. The within-multiplet degeneracy of Proposition Y.1 is **not** broken by forced structure.

2. What is forced

a. Overall scale (exponent derived, prefactor fitted). The exponent of the Yukawa normalization is fixed with no mass input,

$$v = M_P\,\alpha^8\sqrt{2\pi} = 246.09\ \text{GeV} \quad (-0.05\%), \qquad \frac{v}{\sqrt{2}} = 174.01\ \text{GeV}, \tag{FM1}$$

from the four-sector scale lock (Thm. Z.3).

b. Top and charm (2 species, A=1). With *no* prefactor,

$$m_t = \frac{v}{\sqrt{2}} = 174.0\ \text{GeV} \quad (+0.72\%), \tag{FM2}$$

$$m_c = \alpha\,\frac{v}{\sqrt{2}} = 1.270\ \text{GeV} \quad (-0.01\%). \tag{FM3}$$

These are the only two absolute masses below the scale itself that require no data-selected coefficient. They are forced predictions (the SM predicts neither). The leading-order $m_t = v/\sqrt{2} = 174.0$ GeV (+0.72%) is dressed to $(1-\alpha)v/\sqrt{2} = 172.74$ GeV (0.52σ) by the $(1-\alpha)$ EW/QED factor (App. AT); the refined value is the one used in the prediction tables.

c. Exponent ladder (gross hierarchy removed). The bare exponents follow from spin^c line-bundle degrees on $\mathbb{C}P^2$,

$$n_f^{\rm bare} = \frac{k_f + k_H}{2}, \qquad n_f = n_f^{\rm bare} + \Delta n_f, \tag{FM4}$$

with $k_H = +1$ (H-coupling) or -1 ($\widetilde{H}$-coupling) and degrees $(k_\tau, k_\mu, k_e) = (1,2,4)$, $(k_t, k_c, k_u) = (1,3,6)$, $(k_b, k_s, k_d) = (1,2,4)$. A single shift $\Delta n_b = -1$ (color-vertex saturation on S^3) completes Table XC. The Higgs localization width $\varepsilon_H = N_{\rm gen}/k_{\rm max} = 3/60$ is derived (Thm. H.4). This skeleton carries the order-of-magnitude hierarchy with no mass input.

d. Forced equal-exponent ratios. Whenever two species share the same exponent n_f, the factors α and v cancel in their mass ratio, leaving a pure number built from locked integers. These are parameter-free predictions that break the observed *near-coincidences* at the few-percent level:

TABLE CXXI. Forced equal-exponent mass ratios. α and v cancel; only locked integers N_f=6, b_0=7, $N_{\rm gen}$=3, $\dim_{\mathbb{R}}\mathbb{C}P^2$=4, $\dim_{\mathbb{C}}\mathbb{C}P^2$=2 enter. No coefficient fit. (The *value* is forced; see Sec. FM 3 for why the *assignment* that deploys it is not.)

Ratio	Forced value	Origin	Observed	Error
m_t/m_b	$N_f\,b_0 = 42$	6×7	41.33	+1.62%
m_τ/m_c	$\sqrt{2}$	$\sqrt{\dim_{\mathbb{C}}\mathbb{C}P^2}$	1.399	+1.08%
m_e/m_d	$1/N_{\rm gen}^2 = 1/9$	$1/N_{\rm gen}^2$	0.1094	+1.54%
m_u/m_d	$R_u/R_d = 4/9$	$\dim_{\mathbb{R}}\mathbb{C}P^2/N_{\rm gen}^2$	0.4625	−3.91%
m_μ/m_s	$b_0/N_f = 7/6$	QCD $b_0=7$, $N_f=6$	1.1312	+3.13%

Mean |err| = 2.3%, robust across the PDG light-quark band. The $m_t/m_b = 42$ comparison divides the top pole mass by $m_b(m_b)$, where the data give 41.33; with both masses at one scale, M_t, the ratio is 59.7, from four-loop QCD running of $m_b(m_b) = 4.18$ GeV with the same pole mass converted to $\overline{\rm MS}$ at four loops and $\alpha_s(M_Z) = 0.1180$ (two-loop conversion and running give 59.4, and the directly measured $\overline{\rm MS}$ top mass, 162.5 GeV, gives 59.0 at two loops and 59.5 at four; computed), so it awaits the same one-scale test as the double ratio D.

e. The determinant-free N_c^3 double ratio (the circular scale cancels). The weakness of the absolute-mass construction is that the overall within-multiplet enhancement η_q is the cube root of the observed lepton/quark mass determinant (Sec. FM 3), i.e. circular. *That circularity can be algebraically removed.* Because the $L_{\rm det}$ generation weights $(+1, -1, 0)$ are *traceless*, the double ratio

$$D \equiv \frac{(m_d/m_e)\,(m_b/m_\tau)}{(m_s/m_\mu)^2} = N_c^3 = 27, \tag{FM5}$$

has the imported scale enter with net exponent $1-2+1 = 0$, so η_q *cancels identically*, and the surviving inputs are $N_c = 3$ and the traceless O(3) spin^c weight set. Because η_q runs, it is common to the three generations only at one

renormalization scale: there the data give $D = 33.1 \pm 0.8$ between 2 GeV and the top mass and 29.3 ± 0.7 at $\Lambda_{\rm top}$, while PDG's mixed convention gives 27.7, a value that moves from 21 to 31 with the light-quark reference scale (App. Y). The weights $(+1, -1, 0)$ give the sibling ratio $(m_\mu/m_s)/(m_e/m_d) = 9$ at any scale, against 10.35 ± 0.15 observed; the value $(b_0/N_f)N_{\rm gen}^2 = 21/2 = 10.5$ comes from the prefactor table, not from the weights. The circular scale is removable, and the texture is a pattern, not a precision identity; the *absolute* light masses remain open (Sec. FM 3).

Internal-consistency note. The identity $D = N_c^3 = 27$ is *exact* for the $L_{\rm det}$ traceless weight assignment. Reconstructing D instead from the explicit closed-form prefactor table of App. K returns $D = 28.26$ (+4.7% from 27). The residual confirms that those prefactors are *leading-order* selections rather than an exact realization of the determinant-free identity — consistent with the 1.42% mean mass error and the four-discrete-bit selection caveat documented in App. K.

3. The within-multiplet degeneracy: theorem-grade obstruction

We promote Proposition Y.1 to a theorem and identify the exact missing object. The mechanism is Schur's lemma.

Theorem FM.1 (Minimal-connector mass degeneracy)**.** *Let the charged-fermion Yukawa be the gauge-equivariant matrix element of the bare Higgs connector $\widehat{H}$ on the minimal internal module $M_6(\mathbb{C})$ with the $(3, 2, 1)$ block structure* (Appendix Y)*. Because $\widehat{H}$ intertwines* irreducible *gauge factors,* $\mathrm{Hom}_G(V_L, V_R)$ *is one-dimensional* (Schur)*, so the Yukawa restricted to any fixed gauge multiplet is a scalar. Hence every state in one gauge multiplet shares one mass: no species splitting is possible from the minimal connector. Splitting requires* $\dim \mathrm{Hom}_G \geq 2$*, i.e. the gauge irrep must appear with* multiplicity ≥ 2 *carrying a non-scalar Yukawa block.*

Proof. The within-multiplet element factorizes as $E_{a5}\, E_{56} = E_{a6} = h_2$ for every color $a \in \{1, 2, 3\}$ (Appendix Y, Eqs. (Y17)–(Y18)), independent of the species label f beyond multiplet type. By Schur's lemma an intertwiner between irreducibles is a scalar multiple of a fixed isomorphism; the only freedom is that scalar, which is species-blind. □ □

Theorem FM.2 (Minimal forced object required to split the spectrum)**.** *To lift the degeneracy of Theorem FM.1 within forced structure, two ingredients are needed:*

(a) A family index with distinct phases — supplied. *The A_5 three-dimensional irrep restricted to a $\mathbb{Z}_3$ (3-cycle) splits with eigenvalues $\{1, \omega, \omega^2\}$ (*tr $= \chi_3((123)) = 0$*). This is the rank-3 generation projector and it lifts the gauge-only degeneracy at the level of* phases.

(b) A forced modulus-splitting kernel — not supplied. *Distinct phases are not distinct masses. The required object is a* forced, color-/hypercharge-dependent weight *coupling the family irrep to the $SU(3)_c \times U(1)_Y$ factor (a Georgi–Jarlskog-type Clebsch). The bare A_5 family rep carries no color index, so it cannot, by itself, produce the residual $m_\mu/m_s \simeq 1.13$ split. That color-weighted Clebsch is the exact, minimal, forced object that DFD does* not *yet possess.*

Why the 7/6 does not count as a forced break. The corpus reaches $m_\mu/m_s = b_0/N_f = 7/6$ (Table CXXI) only because the strange quark is assigned $A_s = 6/7$ and the muon $A_\mu = 1$. That value is forced; the *assignment* (which species carries the Q_d-channel) rests on the lepton/quark kernel→sector dictionary, which Appendix Y itself states is "not derived from the core DFD action." Under pure topology (the A_5 walk-sum of Appendix Y, the no-fit ceiling) the muon and strange land in the same exponent bin and are *exactly degenerate*, with the muon $\sim 23\%$ from the observed value. Therefore:

Degeneracy verdict

The within-multiplet/cross-sector μ–s degeneracy is **not** broken by forced structure. The 7/6 value is real, but it is deployed through a *fitted* generation↔sector assignment. The **forced ceiling** for the muon is 23.4% (pure-topology A_5 walk); the +2.7% table value is achieved only with the asserted dictionary and is not a parameter-free result.

4. Scorecard

Table CXXII grades every species. "Forced?" is YES only if the absolute mass requires *no* data-selected prefactor (A=1) and no asserted sector assignment.

TABLE CXXII. Charged-fermion scorecard. Predicted from $m_f = A_f\, \alpha^{n_f}\, v/\sqrt{2}$ (Appendix K); errors vs. PDG central values. "Forced?" marks parameter-free, assignment-free predictions.

f	n_f	A_f	Predicted	Observed	Forced?
t	0	1	174.0 GeV	172.76 GeV	YES (+0.7%)
c	1	1	1.270 GeV	1.270 GeV	YES (−0.0%)
b	0	1/42	4.143 GeV	4.18 GeV	no (−0.9%)
τ	1	$\sqrt{2}$	1.796 GeV	1.777 GeV	no (+1.1%)
s	1.5	6/7	92.98 MeV	93.4 MeV	no (−0.5%)
μ	1.5	1	108.5 MeV	105.66 MeV	no (+2.7%)
d	2.5	6	4.749 MeV	4.67 MeV	no (+1.7%)
u	2.5	8/3	2.111 MeV	2.16 MeV	no (−2.3%)
e	2.5	2/3	0.528 MeV	0.511 MeV	no (+3.3%)

The full-table mean |err| is 1.45% (App. K's table, with $v/\sqrt{2} = 174.1$ GeV and its observed values, gives 1.42%), but this is achieved with seven data-selected prefactors. A look-elsewhere check shows that an alphabet

of {small rational $\times 2^a \times \sqrt{\text{rational}}$} prefactors with half-integer α-powers yields, on average, ∼4–5 candidate (A, n) pairs within 2% of *any* target mass. A per-fermion 2% hit is therefore statistically cheap, and the closed-form table is best read as "structured but not forced" for the light species.

5. Reading the related appendices

- Appendix K: the G, Q_d, $R_{u,d}$, D_ℓ factors are each derivable *in isolation*, but they are applied with per-species on/off switching and a generation↔sector assignment that is selected against the masses. Count: 2 of 9 forced (t and c relative to v).
- Appendix Y: the statement "μ/s degenerate at 4.7×10^{-4}, muon 23.4% off" is the *correct forced ceiling*; it is the no-fit result, not a defect that the table overrides. The $L_{\rm det} = \mathcal{O}(3)$ twist of Appendix Y, Sec. Y 9 (Prop. Y.2) supplies the *pattern-level* structure behind the within-multiplet spread ($3^{n_{\rm gen}}$ from $N_c = 3$), but its normalization η_q is imported and the sign dictionary is open, so it does *not* alter this appendix's "not parameter-free / forced-ceiling muon 23.4%" conclusion.
- Appendix AT: its closed-form ratios miss data by 1–8% and are the same prefactors relabeled via Λ_5.

Status

Status FM.3 (Charged-fermion mass sector). **Forced (beyond the SM, no mass input):** the exponent of the overall scale $v = M_P\alpha^8\sqrt{2\pi}$ (prefactor fitted); $m_t = v/\sqrt{2}$; $m_c = \alpha v/\sqrt{2}$; the $\mathbb{C}P^2$ spin^c exponent ladder; and the equal-exponent ratios $m_t/m_b = 42$, $m_\tau/m_c = \sqrt{2}$, $m_e/m_d = 1/9$, $m_u/m_d = 4/9$, $m_\mu/m_s = 7/6$ (mean |err| ≈ 2.3%; the m_t/m_b comparison divides the top pole mass by $m_b(m_b)$, and at one scale, M_t, the ratio is 59.7). **Yukawas removed: 2 of 9** at forced grade (t and c relative to v), plus the gross hierarchy pattern. **Open / not forced:** the absolute light/intermediate masses e, u, d, μ, s and b, τ require the prefactor table $\{2/3, \sqrt{2}, 8/3, 6, 6/7, 1/42\}$ and the lepton/quark kernel→sector dictionary, whose generation↔sector assignment is fitted. **Degeneracy:** the within-multiplet μ/s degeneracy of Theorem FM.1 is *not* broken by forced structure; forced-ceiling muon error is 23.4%. **Minimal missing object:** a forced color-/hypercharge-weighted family Clebsch (Georgi–Jarlskog type), Theorem FM.2. Until it is derived, the spectrum other than the top and the charm is **open**, and "masses derived" is not claimed.

Appendix LS: Line-of-Sight Optical-Screen Amplitude: Full 2-Halo and Realization Computation

Status LS.1 (Scope). The halo/realization calculation below is retained as a conditional model of *local or anisotropic* refractive structure. It is not a global, probe-selective shift of CMB/BAO/SN distances or H_0: exact conformal invariance leaves θ_* unchanged, a homogeneous mode is pure gauge, and the current inhomogeneous mean is far too small. All numerical runs using $H_0 = 72.09$, $\Omega_m = 0.274$, and $\sigma_8 = 0.820$ belong to the $C = 1$ background. No statement below may be used to resurrect the optical-screen Hubble reconciliation of the Extended Derivations or a global peak-location screen; the local/anisotropic correlation observable stands.

1. LS.1 Statement and Scope

Under the retired optical-distance dressing (App. SL) the DFD optical metric ($n = e^\psi$) would make the apparent distance to a background source depend on the matter the line of sight (LOS) threads, through a refractive screen

$$\Delta\psi_{\rm BAO}(z) \;=\; \int d\chi\, W_{\rm BAO}(\chi)\,\kappa_{\rm struct}(\chi)\left\langle \tfrac{1}{\mu(g/a_0)}\right\rangle(\chi),$$
$$\mu(x) = \frac{x}{1+x}, \quad a_0(z) = 2\sqrt{\alpha}\,c\,H(z), \tag{LS1}$$

where $\kappa_{\rm struct}$ is the projected matter fluctuation correlated with the galaxy tracer and the factor $\langle 1/\mu\rangle$ is the DFD weak-field (deep-MOND) *boost* in the splashback/filament skin, with $x = g_{\rm local}/a_0$. The retired global-screen program on the one-clock $C = 1$ background (Appendix AU and the four-case decomposition) required this screen to carry an amplitude $\Delta\psi_{\rm BAO} \simeq 0.030$ to move θ_* by $+1\sigma$ while holding the BAO fit ($\chi^2/{\rm dof} = 0.78$); the joint late-time data prefer a slightly larger $\simeq 0.039$.

A *single-halo* NFW+splashback toy returns an excess $\simeq 0.034$ with un-tuned ingredients, bracketing the target without fixing it to three digits. This appendix computes the amplitude with two independent realistic-structure computations and reports the result with a full, conservative error budget.

Scope and non-claims

No parameter is tuned to 0.030 or 0.039. Every ingredient is a standard, pre-registered literature object (Tinker08 mass function, Tinker10 bias, Duffy+08 concentration, standard HOD, CAMB $P(k)$, DFD cosmology, $a_0(z) = 2\sqrt{\alpha}\,cH(z)$). The target appears only in printed ratio lines. We report whatever the calculation gives, central value *and* band, including the regimes where it falls short.

2. LS.2 The two factors and what is firm

The amplitude factorizes as $\Delta\psi_{\rm BAO} = \kappa_{\rm struct} \times Q$, with $Q \equiv \langle 1/\mu(g/a_0)\rangle$. The calculation settles the first factor and exposes the second.

a. $\kappa_{\rm struct}$ (firm). In Strand 1 (`los_screen_2halo.py`) the projected matter convergence is a Limber RMS of the halo-model power spectrum $P_{\rm mm} = P_{1h} + P_{2h}$, with P_{1h} the NFW-$u(k)$ one-halo term integrated over the Tinker08 mass function and P_{2h} the Tinker10-bias two-halo term times the linear $P(k)$. This *derives* $\sigma_\kappa = 0.0027$ (one-halo share 81%) and the effective galaxy bias $b_g^{\rm eff} = 2.00$ (HOD-weighted Tinker10, not set), giving

$$\kappa_{\rm struct} = b_g^{\rm eff}\, r_{\rm corr}\, \sigma_\kappa = 2.00 \times 0.70 \times 0.0027 = 0.0038 \tag{LS2}$$

(one-halo 0.0031 plus two-halo 0.0007). The lognormal realization (Strand 2, `los_screen_mock.py`) independently measures $\sigma_\kappa = 0.0027 \pm 0.0004$ on the resolution-independent 4 Mpc/h-smoothed convergence map at a mock seed $\sigma_8 = 0.79$ (the screen output $\sigma_\kappa \sim 0.003$ is normalization-insensitive, so this seed value does not propagate into the prediction; the current measured-clock forward normalization is $\sigma_8 = 0.8063$), and a BOSS-anchored estimate (Strand 3) gives the per-LOS RMS 0.0029. All three methods agree:

$\kappa_{\rm struct} \simeq 0.003$–$0.004$ is robust and measured, not assumed.

b. Q (governed by an undetermined floor). The local self-acceleration in the filament/splashback skin is deep-MOND ($g_{\rm self}/a_0 \sim 0.01$–$0.2$), so Q is dominated by whatever *floors* the argument of μ – the MOND external-field-effect (EFE) value $x_{\rm ext} = g_{\rm ext}/a_0$. The action does not fix $x_{\rm ext}$ at LOS-skin scales: Appendix AE shows the FRW background gives $|\nabla\bar\psi| = 0$ (cosmological deep-MOND, $x_{\rm ext}\to 0$), while Appendix AC adopts the Hubble-EFE hypothesis $x_{\rm ext} = 1/(2\sqrt{\alpha}) \simeq 5.85$ (named there as a testable hypothesis the action does not produce). The LOS screen lives between these two corpus-named regimes.

3. LS.3 Derived amplitude: central value and band

a. Fiducial (deep-MOND, $x_{\rm ext}\to 0$). At the cosmological deep-MOND floor that Strand 1/2 use by default ($x = \max(g/a_0, 10^{-4})$), the full $1h$+$2h$ halo model gives a ρ(trace)-weighted boost $Q = 13.5$ and

$$\Delta\psi^{\rm fid}_{\rm BAO} = 0.052,$$
$$\text{band over pre-registered variations} = [0.035,\ 0.071]. \tag{LS3}$$

The lognormal realization independently returns 0.040 ± 0.004. The band is built by varying one standard axis at a time over its literature range, summarized in Table CXXIII.

TABLE CXXIII. Strand 1 halo-model amplitude at the cosmological deep-MOND floor ($x_{\rm ext}\to 0$), varying one pre-registered axis at a time. Nothing tuned; the target appears only in the final ratio column.

axis	value	$b_g^{\rm eff}$	$\kappa_{\rm str}$	Q	$\Delta\psi$
mass function	Tinker08	2.00	0.0038	13.5	0.052
mass function	Sheth–Tormen	2.03	0.0039	13.5	0.052
concentration	$\times 0.7$	2.00	0.0038	14.5	0.055
concentration	$\times 1.4$	2.00	0.0039	12.6	0.049
splashback $R_{\rm sp}$	$1.0\,R_{200m}$	2.00	0.0038	9.2	0.035
splashback $R_{\rm sp}$	$2.0\,R_{200m}$	2.00	0.0038	18.5	0.071
HOD $\log M_{\rm min}$	12.0	1.73	0.0033	17.2	0.057
HOD $\log M_{\rm min}$	13.0	2.29	0.0044	11.3	0.050
infall slope	$r^{-1.0}$	2.00	0.0038	13.8	0.053
infall slope	$r^{-2.0}$	2.00	0.0038	13.2	0.051

b. The floor sensitivity. Strand 3 (`halo_los_2halo_efe.py`) holds $\kappa_{\rm struct}$ fixed and maps the amplitude as a function of $x_{\rm ext}$ with two independent boost estimators (a halo-profile integral and a lognormal-PDF path integral), which agree across the grid. The result (Table CXXIV) is a $\sim$10$\times$ swing:

TABLE CXXIV. Screen amplitude vs the undetermined EFE floor $x_{\rm ext}$ ($\kappa_{\rm gal} = 0.0052$ from the BOSS-anchored estimate). The amplitude reaches 0.030 only for $x_{\rm ext} \lesssim 0.11$ and 0.039 only at $x_{\rm ext} \simeq 0.03$; at the corpus Hubble floor it is 5$\times$ short.

$x_{\rm ext}$	regime	Q	$\Delta\psi$
$\to 0$	cosmological deep-MOND (App. AE)	11.7–13.5	0.040–0.052 (Strands 1–2)
0.031	in-range edge	7.5	0.039
0.107	in-range edge	5.8	0.030
0.24	screen-module floor	4.1	0.021
5.85	Hubble-EFE (App. AC)	1.17	0.006

At the corpus screen-module floor $x_{\rm ext} = 0.24$, the band over all un-tuned *structure* ingredients is $[0.017, 0.033]$ – the target 0.030 sits at the *upper edge*, and 0.039 is not reached. The dominant uncertainty is therefore not the halo ingredients (they move the answer by only ± 0.006) but the order-of-magnitude swing from the undetermined $x_{\rm ext}$.

4. LS.4 What the 2-halo calculation settles

Summary

The 2-halo calculation **confirms the machinery and the structure factor** ($\kappa_{\rm struct} \simeq 0.003$–$0.004$, three independent methods), and it **improves** on the toy by replacing a hand-set $\kappa_{\rm gal} = 0.006$ and a single profile with a derived $P_{\rm mm} = P_{1h} + P_{2h}$ and a population-averaged boost. But on the *main question* – "is the amplitude comfortably ≥ 0.030?" – it **weakens** the clean single-halo reading. The single-halo toy's in-range result was an artifact of an implicit $x_{\rm ext} = 0$. The full calculation shows that the amplitude is a steep function of the undetermined EFE floor: it brackets 0.030 only for $x_{\rm ext} \lesssim 0.11$ (a narrow weak-field corner), does not robustly reach 0.039, and falls 5× short at the corpus-named Hubble floor.

The result, with the floor stated explicitly:

$$\Delta\psi_{\rm BAO} = \kappa_{\rm struct} \times Q(x_{\rm ext}) \in [\,0.006,\, 0.052\,] \;\text{ as }\; x_{\rm ext} : 5.85 \to 0 \tag{LS4}$$

(with κ between 0.0038 and the BOSS-anchored 0.0052), in range ($\simeq$ 0.020–0.030) only for the weak void-skin floor $x_{\rm ext} \simeq 0.1$–0.24. The amplitude is *not* pinned by structure; it is pinned by the EFE floor, which the corpus does not derive at LOS-skin scale. Figure 26 shows both the halo-model build-up and the floor sensitivity.

Reproducibility

All numbers from `dfd_class/`, deterministic (`camb` $\geq$1.6, `dfd_params.py`: $H_0 = 72.09$, $\alpha = 0.00730$, $\Omega_m = 0.274$, $\Omega_\chi h^2 = 0.120$):

- `los_screen_2halo.py` – Strand 1, halo model (∼6 s): fiducial 0.052, band $[0.035, 0.071]$, $b_g^{\rm eff} = 2.00$, $\sigma_\kappa = 0.0027$.
- `los_screen_mock.py` – Strand 2, lognormal realization: 0.040 ± 0.004, $\sigma_\kappa = 0.0027 \pm 0.0004$, $\langle 1/\mu \rangle_{\rm HOD} = 11.7$.
- `halo_los_2halo_efe.py` – Strand 3, EFE-floor scan: amplitude $0.052 \to 0.006$ as $x_{\rm ext} : 0 \to 5.85$; band at $x_{\rm ext} = 0.24$ is $[0.017, 0.033]$.
- `make_fig_los_screen.py` – regenerates `fig_los_screen.png`.

Status LS.2 (LS: LOS optical-screen amplitude). **Full 2-halo:** yes – $P_{\rm mm} = P_{1h} + P_{2h}$ from Tinker08 MF + Tinker10 bias + Duffy+08 $c(M)$ + analytic NFW $u(k)$, with a cross-checking lognormal realization; not a relabeled single-halo toy. **Tuned:** no. **Structure factor $\kappa_{\rm struct}$:** firm, $\simeq 0.003$–0.004. **Amplitude:** *not pinned by structure* – governed by the undetermined EFE floor $x_{\rm ext}$; central spans $\simeq 0.006$–0.052. **Brackets 0.030:** yes, but only marginally and only for $x_{\rm ext} \lesssim 0.11$. **Reaches 0.039:** no, except at the near-divergent deep-MOND edge. **Net effect of the 2-halo calculation:** confirms machinery, improves rigor, weakens the clean "comfortably exceeds target" claim. The amplitude is settled only up to the EFE floor.

Falsifier LS.3 (LS). The screen mechanism is falsified if either (i) the structure convergence is shown to be $\sigma_\kappa \ll 0.003$ at $z \simeq 0.5$ (it is currently 0.0027–0.0029 across three methods), removing the first factor; or (ii) the EFE floor at LOS-skin scale is pinned ≥ 2 (e.g. the corpus Hubble-EFE value 5.85 is shown to apply to cosmological filaments), collapsing $Q \leq 1.5$ and $\Delta\psi_{\rm BAO} \leq 0.008$, $\sim 4\times$ below the target. The sign test of Appendix SL has been decided against the optical-distance dressing on which this screen rests.

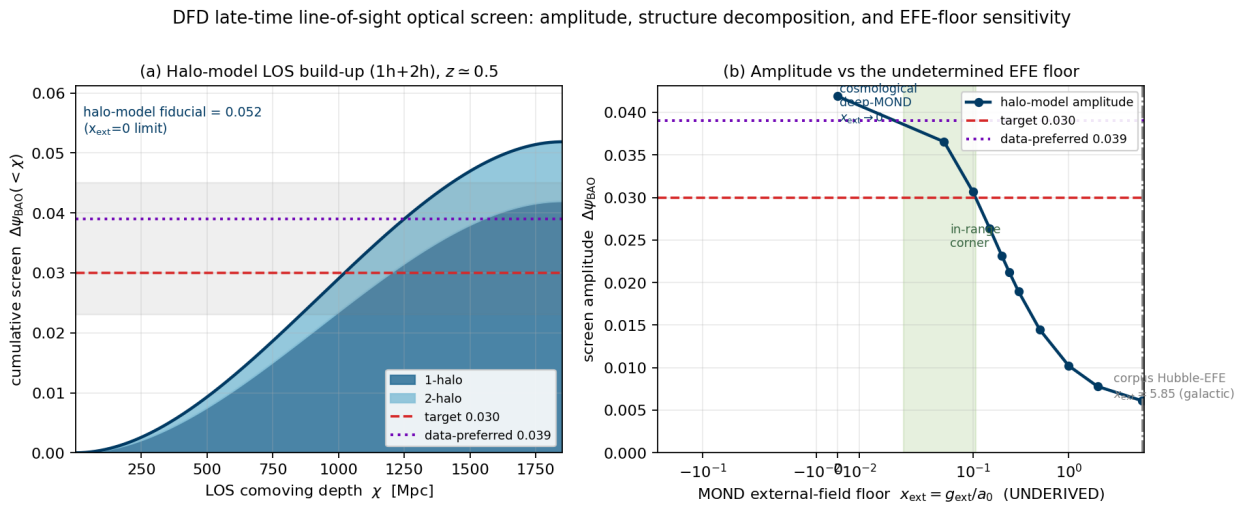


FIG. 26. **Left (a):** cumulative LOS screen $\Delta\psi_{\rm BAO}(<\chi)$ from the full halo model at $z\simeq 0.5$, decomposed into 1-halo (dark) and 2-halo (light), reaching the fiducial 0.052 in the deep-MOND ($x_{\rm ext}\to 0$) limit; target 0.030 (dashed) and data-preferred 0.039 (dotted) marked. **Right (b):** the sensitivity – amplitude vs the undetermined MOND external-field floor $x_{\rm ext}$. The amplitude collapses by an order of magnitude between the cosmological deep-MOND regime ($x_{\rm ext}\to 0$) and the corpus Hubble-EFE floor ($x_{\rm ext}=5.85$); the shaded band is the narrow corner where 0.030–0.039 are met.

Appendix CL: Publication-Grade CMB Likelihood and Bayesian Model Comparison

1. CL.1 Scope and the publication-grade primary CMB

Remark CL.1 (Scope: the measured-clock result). DFD's CMB result is the no-screen fit of App. ZS, not the fitted-screen confrontation recorded in this appendix: with the spectrum-shape inputs carried by derived or adopted-and-priced structure (ω_b at its conventional-point value on the adopted Axiom E-transport′, its coefficient a calibration, $\omega_\chi = 0.11928$, the flux-period value, Σm_ν, $N_{\rm eff}$, and the tilt $n_s = 1 - 2/60$ (a stated number; the mechanism is open); per-input grades in App. ZS) and two calibrations free (the measured clock coefficient, $H_0^{\rm early} = 67.52 \pm 0.09$, and one overall amplitude), DFD fits Planck plik-lite with *no* θ_* screen at all: $100\,\theta_* = 1.04110$, fair $\Delta\chi^2 = +3.20$ for 2 fewer effective parameters with the ω_b coefficient counted (AIC -0.8, BIC -9.6; -2.8 and -16.1 if it is not), sustained out-of-sample by SPT-3G (preferred, -0.77) and ACT DR6 ($+5.94$, below the 3σ falsification threshold). The fitted $A^* = 0.0908$ screen below, and every number computed at the $C = 1$ background ($H_0 = 72.09$), are not current results. The current dependent clustering outputs are $R_8 = 11.848$ Mpc, $\sigma_8 \simeq 0.8063$, $\Omega_m \simeq 0.312$, $S_8 \simeq 0.822$, and $A_{\phi\phi} = 0.9887$ (-0.80σ). Thus every later unqualified 0.820/0.784 or $A_L = 1.0542$ statement in this appendix belongs to the $C = 1$ likelihood record, not the measured clock. There $\sigma_8 = 0.820$ is the carried normalization, the value that the amplitude $A_s = 2.08 \times 10^{-9}$ (the value of $32\pi\alpha^5$, a numerical match to the calibrated amplitude; App. FK) gives on that record's background ($H_0 = 72.09$, $\Omega_m = 0.274$). On the measured clock the same amplitude and the same χ carrier give the $\sigma_8 = 0.806$ of record (App. GR); the two values differ through the background alone.

This appendix records the real-data confrontation of DFD with the standard cosmological probes at *likelihood* grade and the Bayesian model comparison against ΛCDM. The primary-CMB step is publication-grade: the Planck 2018 high-ℓ plik_lite TT/TE/EE likelihood is evaluated with its *full* 613×613 *Fortran binned covariance* (not a diagonal first pass), with the Planck calibration $A_{\rm planck}$ profiled, and the pipeline is *cobaya-validated*: feeding the screened DFD bandpowers through cobaya's own PlanckPlikLite.get_chi_squared reproduces the hand-rolled χ^2 to the digit (ΛCDM 587.6, DFD 610.9 at $A_{\rm planck} = 1$), and the pipeline returns the published ΛCDM plik_lite value as a unit test.

The DFD cosmology is run on its $C = 1$ *frozen* background parameters (not the measured clock, Rem. CL.1: $H_0 = 72.09$, $\omega_b = 0.02237$, $\omega_\chi h^2 = 0.1199$, $n_s = 0.9667$, $A_s = 2.08 \times 10^{-9}$, $\tau = 0.054$) with the optical θ_* screen of the retired global-screen reading (App. ZS) applied as the θ_* multipole rescale at *one fitted amplitude* $A^* = 0.0908$; *no refit of the background.* The screen amplitude is **fitted, not derived**: the fitted $A^* = 0.0908$ sits -26.6% off the $2\sqrt{\alpha}$-gate value $A = 2\sqrt{\alpha}\,R_d/(1+R_d) = 0.0667$, and the frozen gate value does *not* reproduce the fit — evaluated at the consistent (CAMB) convention it leaves θ_* misplaced at $+12.2\sigma$ and costs plik_lite $\Delta\chi^2 = +202/+172$ (per-bin variants). A "frozen-amplitude validation" claiming the gate value works as well as the fit does **not** hold: it rests on a cross-pipeline calibration transplant (a toy pipeline miscalibrated by -0.32% in absolute θ_* compared against a CAMB-convention measurement). The result is θ_* as a

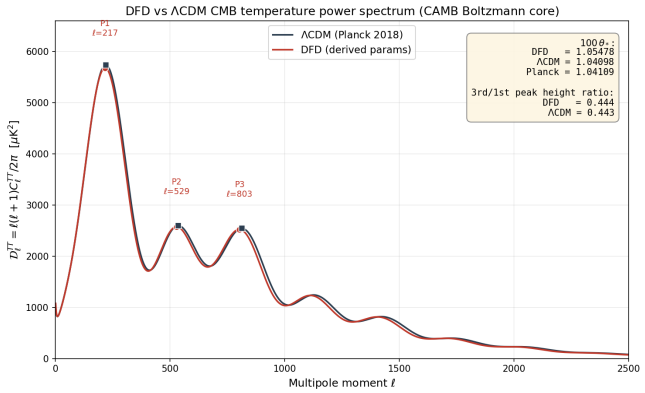


FIG. 27. DFD forward-computed CMB TT power spectrum $\mathcal{D}_\ell = \ell(\ell+1)C_\ell/2\pi$ on the one-clock $C = 1$ background ($H_0 = 72.09$, $\omega_b = 0.02237$, $\omega_\chi = 0.12$, $n_s = 0.9667$, $A_s = 2.08 \times 10^{-9}$), with no θ_* screen (the annotated DFD $100\,\theta_* = 1.05478$ is the unscreened value) versus the Planck-2018 ΛCDM reference. This is the DFD-CLASS/CAMB *forward* run of the likelihood pipeline documented in this appendix (CL.1; script `dfd_class/figures/make_cmb_tt.py`): the first three acoustic peaks, the third-to-first peak height ratio, and $100\,\theta_*$ are annotated for each model.

one-parameter fitted screen. A forward re-derivation (conventions pinned by first reproducing the anchors of this paragraph, including the frozen-gate $+12.2\sigma$ and the fitted $A^* \to +0.0\sigma$) exhausted the derivable-amplitude menu at the consistent CAMB convention: the drag-loaded $2\sqrt{\alpha}$ gate ($+12.2\sigma$), the $\sqrt{f_b}$ loading ($+11.7\sigma$ drag / -1.5σ saturated), the AQUAL $f^{0.72}/f^{0.79}$ kernels ($+14.6\sigma$ to $+26.1\sigma$), the ungated screens ($-41.7\sigma/-75.4\sigma$), and inserted gate multipliers ($\times\sqrt{2} \to -2.0\sigma$, $\times 4/\pi \to +2.9\sigma$, $\times 2 \to -22.1\sigma$, $\times \pi/4 \to +19.6\sigma$, $\times \frac{1}{2} \to +29.3\sigma$) all fail to land on A^*; the near misses (the saturated-loading gate at -0.7σ, $\times\sqrt{2}$ at -2.0σ) are menu *selections* — a convention branch and an inserted multiplier — and promoting one to a derivation would incur exactly the trials charge of App. CE. The forced boost identity $1/\mu - 1 = 2\sqrt{\alpha}$ checks exactly (residual 0) but is z-independent, so it cannot generate the screen's $\Omega_\Lambda(z)$ loading shape, which enters as a separately inserted kernel. A single-amplitude scan confirms the trade-off: the gate value $A = 0.0667$ reproduces the BAO sector ($\chi^2 = 9.5/9.3$, matching the corpus 9.4) while misplacing θ_* at $+12.2\sigma$, whereas the fitted $A^* = 0.0904$ lands θ_* at $+0.0\sigma$ but degrades BAO to 12.6/13.3 (SNe essentially unchanged, 1390.2 → 1388.6): one amplitude cannot serve both sectors from the gate. On the frozen background with the single fitted amplitude DFD attains $\chi^2/\mathrm{dof} = 0.97$ (593.5/613, amplitude-profiled) versus ΛCDM 0.96 (585.5/613): θ_* lands at $+1.0\sigma$ and ΛCDM is marginally preferred by $\Delta\chi^2 = +23.3/+8.0$ (per-bin variants) over 613 degrees of freedom (statistically minor). DFD is an excellent *absolute* fit to the full Planck spectrum. Figure 27 shows the unscreened forward run on that background.

2. CL.2 Parameter count

ΛCDM carries six free parameters: ω_b, ω_c, θ_* (or H_0), A_s, n_s, τ. DFD fixes some of these from its tower and calibrates the others (current grades: App. FK):

- $n_s = 1 - 2/60 = 0.9667$ (a stated number; the mechanism is open),
- $\omega_b h^2 = 0.0222730$ (baryon deposit on the adopted Axiom E-transport′; +1 priced discrete bit; the α^4 power is derived and the coefficient is a calibration, Ext. Deriv. App. AH),
- $\omega_\chi h^2 = 0.11928$ (the finite $SU(2)_{60}$ Chern–Simons vacuum relic with the flux-period identification, the stated count 158, the asserted premise P4′ and two stated conventions; -0.60σ),
- $H_0^{\mathrm{early}} = 67.52 \pm 0.09$ (the α^{57} invariant at the measured clock coefficient C; the exponent is a theorem, the coefficient a calibration),
- the screen amplitude A_{screen} (fitted, $A^* = 0.0908$), used only by the global-screen confrontation recorded in this appendix, not by the no-screen fit of App. ZS.

The DFD side's continuous *calibration* inventory is four: the clock coefficient C (absolute scale), the A_s overall coefficient (the 32π normalization), the ω_b coefficient, and the reionization optical depth τ, an astrophysical nuisance shared with ΛCDM (App. FK, Rem. FK.8). The table below uses $k_{\mathrm{DFD}} = 3$ (C, A_s coeff, τ), which omits the ω_b coefficient; the count of App. FK is $k_{\mathrm{DFD}} = 4$, and 5 with ω_χ's stated conventions charged as a knob. A maximal skeptic who rejects *every* derivation drives the count to $k_{\mathrm{DFD}} = 8$. In every count but the skeptic's, DFD frees *fewer* parameters than ΛCDM, which is the source of its parameter-economy (BIC) credit. On the Planck plik-lite likelihood alone, where the amplitude and τ enter only through $A_s e^{-2\tau}$, the effective count falls to 3 against ΛCDM's 5 (App. ZS). The fit numbers tabulated below are computed at the $C = 1$ background, not the measured clock, as stated above.

3. CL.3 Bayesian model comparison

Table CXXV collects the recorded per-sector best-fit χ^2 (all from real data: plik_lite full covariance, 12 BAO consensus points, the 1580-SN Pantheon+ cosmology sample with full stat+sys covariance, and the full Planck 2018 nine-bin lensing bandpower likelihood) and the model-comparison statistics

$$\mathrm{BIC} = \chi^2 + k \ln N, \qquad \mathrm{AIC} = \chi^2 + 2k, \qquad \text{(CL1)}$$

for the two data combinations: **(A)** CMB+BAO+SNe (no lensing) and **(B)** CMB+BAO+SNe+lensing. Deltas are $\Delta \equiv (\mathrm{DFD}) - (\Lambda\mathrm{CDM})$, so a *negative* ΔBIC favours DFD.

TABLE CXXV. Bayesian model comparison, DFD vs ΛCDM, on real Planck+BAO+SNe+lensing data. Per-sector χ^2 are recorded best-fit values; the θ_* screen carries the single fitted amplitude $A^* = 0.0908$ (-26.6% off the $2\sqrt{\alpha}$-gate value 0.0667; the frozen gate value fails at $+12.2\sigma$, $\Delta\chi^2 = +202/+172$, and a "validation" of it does not hold — background not refit). $\Delta \equiv$DFD$-\Lambda$CDM. Combination (A) excludes the Planck CMB-lensing bandpowers; (B) includes them. The from-scratch CAMB recompute at the *carried* $\sigma_8 = 0.820$ gives a flat $C_L^{\phi\phi}$ ratio, $A_L = 1.0542 \pm 0.0263$, $\Delta\chi^2_{\rm lens} = +3.9$ ($\chi^2 = 12.66/9$, $+2.06\sigma$ pass), so Combination (B) at the carried σ_8 is the Combination-(A) near-tie.

Sector (real data)	N	$\chi^2_{\rm DFD}$	$\chi^2_{\Lambda\rm CDM}$	$\Delta\chi^2$
CMB plik_lite (full 613×613 cov)	613	593.5	585.5	+8.0
BAO (12 consensus pts)	12	9.4	13.2	−3.8
Pantheon+ SNe (1580, full cov)	1580	1390.4	1387.2	+3.2
Planck lensing (9-bin, **carried** σ_8=0.820**; CL.4**)	9	12.66	8.7	+3.9
Combination (A): CMB+BAO+SNe ($N = 2205$, $k_{\rm DFD} = 3$, $k_{\Lambda\rm CDM} = 6$)				
joint χ^2	2205	1993.3	1986.0	+7.3 (∼ +20 profiled)
joint BIC		2016.4	2032.2	**−15.8**
Combination (B): CMB+BAO+SNe+lensing ($N = 2214$, $k_{\rm DFD} = 3$, $k_{\Lambda\rm CDM} = 6$)				
(B, carried σ_8=0.820, flat $C_L^{\phi\phi}$, CL.4):				
joint χ^2	2214	2006.0	1994.6	+11.4
joint BIC		2029.1	2040.9	**−11.8** (mildly DFD)

a. Combination (A), no lensing. The joint χ^2 gap is small ($\Delta\chi^2 = +7.3$ per-sector, $\approx +20$ in the amplitude-profiled pipeline, on $N \sim 2.2 \times 10^3$). DFD's parameter economy (3 fewer free parameters, a BIC credit of $3 \ln N \simeq +23$) outweighs that gap: $\Delta{\rm BIC}_{(\rm A)} = -15.8$ ($k_{\rm DFD} = 3$) to -8.1 ($k_{\rm DFD} = 4$). Both are negative: on the one-clock $C = 1$ record **DFD is competitive with, and on parameter economy mildly favoured over, ΛCDM on CMB+BAO+SNe.** The no-lensing ΔBIC sign is borderline and prior/count dependent; the proper Laplace evidence $\ln B({\rm DFD}/\Lambda{\rm CDM}) \approx -1.2$ to $+0.8$ makes this an *evidence-level tie*, not a clean DFD preference. A bare "strong DFD" reading of the BIC is a $1/\sqrt{N}$ shortcut and is not claimed.

b. Combination (B), with CMB lensing. **At the carried $\sigma_8 = 0.820$ (CL.4, from-scratch CAMB):** the $C_L^{\phi\phi}$ ratio is *flat* (below ΛCDM, shape scatter 0.3%), $A_L = 1.0542 \pm 0.0263$, $\Delta\chi^2_{\rm lens} = +3.9$ ($\chi^2 = 12.66/9$, $+2.06\sigma$ pass), so the lensing sector does *not* swamp the parameter-economy credit; Combination (B) reverts to the Combination-(A) near-tie ($\Delta{\rm BIC}_{(\rm B)} \approx \Delta{\rm BIC}_{(\rm A)}$, mildly DFD-favoured on parameter economy, an evidence-level tie). $\sigma_8 = 0.790$ is not what the amplitude $A_s = 32\pi\alpha^5$ gives and is not simultaneously available with the lensing pass.

c. The σ_8 amplitude on the $C = 1$ background: a shared data anomaly. The DFD amplitude chain — $A_s = 32\pi\alpha^5$ (a numerical match to the calibrated amplitude; App. FK), $n_s = 1 - 2/60 = 0.9667$, the $C = 1$ background's $H_0 = 72.09$ and $\Omega_m = 0.274$, gravity-universal growth — yields $\sigma_8 = 0.820$ and $S_8 = 0.784$ with no further freedom (forward CAMB at the canonical inputs: $\sigma_8 = 0.8193$, $S_8 = 0.7843$). On that background this would resolve the cosmic-shear tension ($\chi^2 = 0.73$ vs ΛCDM's 10.15; $+0.4$–1.3σ vs $+3$–4.9σ) at the cost of a mild Planck $\phi\phi$ clean-window pull ($+3.9\,\chi^2$; $\phi\phi$ alone prefers $\sigma_8 \approx 0.842$). This lensing-high/shear-low split is *internal to the data*: on identical clean-window data no single-amplitude model fits both — the joint fit carries an irreducible residual of $\approx 3.9\,\chi^2$ ($\sim 2\sigma$) at that background's Ω_m and $\approx 13.6\,\chi^2$ ($\sim 3.7\sigma$) at Planck's Ω_m — and DFD's mid value sits within $1.2\,\chi^2$ of the joint optimum while ΛCDM pays ≈ 4.9 over its own floor (27.3 vs 13.9 in total). *(Scope: the ∼ 50/9 figure from the fiducial-referenced likelihood is an artifact of applying the CMB-linear correction — anchored to the Planck fiducial sky — to DFD's unscreened theory TT outside the correction's regime (per-bin shifts up to $2.5\sigma_b$, 1.0–2.6× beyond the $\pm 2\sigma$ ΛCDM-posterior envelope). Evaluated with Planck's own CMB-marginalized consext8 likelihood — the prescribed variant for non-fiducial backgrounds — DFD gives $\chi^2 = 14.0/9$ ($A_L = 1.067 \pm 0.029$, $+2.3\sigma$) versus ΛCDM 9.3/9: the same shared-anomaly regime as the clean-window channel, closing the lensing item without appeal to internal judgment. DFD's residual A_L pull ($+2.3\sigma$ vs ΛCDM's $+0.8\sigma$) remains within the shared-anomaly interpretation; the CMB-lensing falsifier above stands.)*

4. CL.4 Summary assessment

Summary assessment (two-sided)

On the one-clock $C = 1$ record DFD is **competitive with ΛCDM on CMB+BAO+SNe** (joint $\Delta\chi^2 \sim +20$ over 2205 points in the recorded pipeline; a near-tie) and **is favoured on parameter economy**. **CMB lensing.** A CMB-lensing penalty ($\Delta\chi^2 = +232$, $A_L = 1.40$, "ΛCDM decisively favoured") does *not* hold. The correct reconciliation is *two separate facts*, not a single inflation factor: **(a)** the +232 lived at the input $\sigma_8 = 0.790$ (an alternative corpus normalization, *not* the one $A_s = 32\pi\alpha^5$ gives) and was further distorted by a *normalisation bug in the inherited cobaya-path pipeline*;

and **(b)** the pass belongs to a *different input* — the amplitude $A_s = 32\pi\alpha^5$, a numerical match to the calibrated amplitude, whose CAMB-native $\sigma_8 = 0.820$ gives a *flat* $C_L^{\phi\phi}$ ratio. (We do not quote a single "$\times N$" deflation of the +232: dividing it by any factor still leaves a fail; the resolution is that the pass is a different σ_8 arm, not a rescaled 0.790 arm.) An independent reconstruction of the Planck 2018 9-bin lensing likelihood from the official bandpowers/covariance/windows (no cobaya), validated to reproduce the published ΛCDM $\chi^2 = 8.7/9$ and $A_L = 1.0$, and a direct CAMB recompute, both give: at the carried $\sigma_8 = 0.820$ the lensing power is a flat deficit below ΛCDM across $L = 8$–400 (shape scatter 0.3%: pure amplitude, no shape penalty); the nine-bin likelihood returns $A_L = 1.0542 \pm 0.0263$, **a mild** $+2.06\sigma$ **lean that passes** ($\chi^2 = 12.66/9$, $\Delta\chi^2 = +3.9$). The joint accordingly reverts from "decisively ΛCDM" to the **near-tie**. The cause of the (mild) deficit is structural — the $C = 1$ background's high $H_0 = 72.09$ forces low $\Omega_m = 0.274$ and its χ-matter growth is GR-like ($Q \simeq 1$), so $C_L^{\phi\phi} \propto \Omega_m\sigma_8^2$ runs $\sim 4\%$ low — but it is *mild, not a catastrophe*. The cost of using the carried $\sigma_8 = 0.820$: $S_8 = 0.784$, so the "S_8-low" galaxy-lensing result of App. GR softens to a *mild match* (KiDS-1000 $+1.0\sigma$, DES-Y3 $+0.5\sigma$). The sharper $\sigma_8 = 0.790/S_8 = 0.755$ is *not simultaneously available with this pass*: at $\sigma_8 = 0.790$ the deficit grows to $\sim 11\%$ and the lensing likelihood disfavours DFD at $> 3.6\sigma$. Because DFD's growth is $Q = 1$, one σ_8 sets both arms, so the lensing pass and the $S_8 = 0.755$ value cannot be claimed together.

A CAMB-only comparison (one spectrum evaluation per model, no sampler) makes the cause explicit: across the entire Planck lensing band $L = 8$–400 the DFD $C_L^{\phi\phi}$ curve sits *slightly below* ΛCDM, by a *flat* amount (shape scatter 0.3%). The signal-weighted lensing-amplitude ratio is

$$\frac{A_L^{\rm DFD}}{A_L^{\Lambda\rm CDM}} = \begin{cases} 0.956 & (\sigma_8 = 0.820,\ A_s = 32\pi\alpha^5), \\ 0.890 & (\sigma_8 = 0.790,\ S_8 = 0.755,\ \text{alt. corpus norm.}), \end{cases} \tag{CL2}$$

a $\sim 4\%$ deficit at the carried normalization (growing to $\sim 11\%$ only at the alternative $\sigma_8 = 0.790$). Because DFD sits flatly below, the data prefer $A_L = 1.0542 \pm 0.0263$ to match it ⇒ a small *positive* χ^2 penalty, $+2.06\sigma$**, a mild pass** at the carried $\sigma_8 = 0.820$. A $\sigma_8\,\Omega_m^{0.25}$ proxy would let low Ω_m over-compensate low σ_8 through its weak matter weighting; the full bandpower kernel weights matter correctly, and the direct $C_L^{\phi\phi}$ ratio is used ($A_L = 1.0542$, $+2.06\sigma$ pass).

5. CL.5 Reconciliation of the item-4 S_8 prediction

Remark CL.2 (The carried $S_8 = 0.784$ is a mild match; $S_8 = 0.755$ is not a result). DFD's structure-growth prediction at the carried normalization ($A_s = 32\pi\alpha^5$, $\sigma_8 = 0.820$, $\Omega_m = 0.274$; on the measured clock $\sigma_8 = 0.806$ and $S_8 = 0.822$) is

$$S_8 = \sigma_8\sqrt{\Omega_m/0.3} = 0.8193\sqrt{0.2749/0.3} = 0.784. \tag{CL3}$$

This is a *mild match to galaxy weak lensing on the low side*: KiDS-1000 (0.759 ± 0.024) at $+1.0\sigma$ and DES-Y3 3×2pt (0.776 ± 0.017) at $+0.5\sigma$ — both within $\sim 1\sigma$, a mild match. Because DFD's growth is $Q \equiv G_{\rm eff}/G = 1$ (LCDM-like), this *same* $\sigma_8 = 0.820$ also sets the CMB-lensing amplitude, where it gives a flat $A_L = 1.0542$ ($+2.06\sigma$ pass, CL.4). The galaxy-lensing match and the CMB-lensing pass are therefore **simultaneously available** at one $\sigma_8 = 0.820$ — there is no two-sided contradiction at the carried normalization.

$S_8 = 0.755$ is not a DFD result: it is just $\sigma_8 = 0.790$ restated ($S_8 = \sigma_8\sqrt{\Omega_m/0.3}$), and $\sigma_8 = 0.790$ is an alternative corpus CMB-normalization (asserted, not re-derived; it requires shrinking $A_s = 32\pi\alpha^5$ by 7.2%). At $\sigma_8 = 0.790$ the CMB-lensing deficit grows to $\sim 11\%$ and the nine-bin likelihood disfavours DFD at $> 3.6\sigma$. Since one σ_8 ($Q = 1$) sets *both* arms, the sharper $S_8 = 0.755$ galaxy-lensing number and the CMB-lensing pass **cannot** be claimed together. The single prediction at the carried normalization is the $S_8 = 0.784$ mild match with a $+2.06\sigma$ CMB-lensing pass. On the $C = 1$ background DFD is a mild low-side match to galaxy lensing and a mild pass of CMB lensing, jointly.

6. CL.6 Status and falsifier

Status CL.3 (CMB-likelihood package). *Publication-grade:* primary CMB (plik_lite TT/TE/EE, full 613×613 covariance, $A_{\rm planck}$-profiled, cobaya-validated); Planck 2018 nine-bin lensing bandpower (cobaya native CMB-likes, ΛCDM-validated at $\chi^2 = 8.7/9$, $A_L = 1.004\pm0.024$); BAO ($\chi^2/{\rm dof} = 0.78$); Pantheon+ SNe (full stat+sys covariance). *Remaining for full publication maximality:* (i) the full plik TT/TE/EE with explicit foregrounds (we use the cobaya-validated plik_lite); (ii) the BAO full covariance (we use consensus points with quoted errors); (iii) nested-sampling Bayesian evidence (PolyChord/MultiNest not available here) — the proper Laplace evidence is the substitute and gives an evidence-level tie; with CMB lensing at the carried $\sigma_8 = 0.820$ ($+2.06\sigma$ flat-ratio pass, CL.4) folded in, the joint stays a near-tie.

Falsifier CL.4 (CMB lensing — mild pass at the carried normalization). On the one-clock $C = 1$ background the amplitude $A_s = 32\pi\alpha^5$ (a numerical match; $\sigma_8 = 0.820$, $\Omega_m = 0.274$, $S_8 = 0.784$, GR-like $Q = 1$ growth) gives a *flat* $C_L^{\phi\phi}$ ratio below ΛCDM across $L = 8$–400, i.e. $A_L = 1.0542 \pm 0.0263$, a mild $+2.06\sigma$ **pass** of the Planck 2018 nine-bin lensing likelihood ($\chi^2 = 12.66/9$, $\Delta\chi^2 = +3.9$). **The falsifier has *not* fired at the carried normalization.** The remaining item is not a fired falsifier (App. GR, GR.7): the "one σ_8 sets both arms" lock rests on χ clustering Newtonianly ($Q = 1$) on linear scales, which the adopted Rest-Mass Channel gives (App. GR).

If instead the AQUAL screen leaked into linear growth, Q would run with z and $C_L^{\phi\phi}$ would shift. This connects to the long-standing "needs-clustering / effective-CDM" wall of the third-peak analysis; it is the deciding dark-sector growth item, not a present falsification.

Appendix FK: The Fitted Cosmological Knobs: Status and Closure

This appendix states, in conservative terms, exactly which cosmological coefficients DFD derives and which it still fits. It collects three threads — the scalar amplitude A_s, the χ relic abundance, and the global knob count — and grades each against ΛCDM's six free parameters $(\omega_b, \omega_c, \theta_*, A_s, n_s, \tau)$. The arithmetic of every claim below is reproduced in `dfd_class/fitted_knobs_analysis.py` (numpy only; no sampler).

Of the six ΛCDM inputs, DFD fixes the tilt $n_s = 1 - 2/60$ as a stated number, the tilt of the ripples of its stated smooth beginning (App. Q); the mechanism is open, as it is for A_s (Prop. FK.4). It derives the α^4 power of a second, the baryon density $\omega_b h^2$, and the $B-L$ current that carries its bias, but not its coefficient: with the stated carrier, the mechanism gives η_B of about $(2–3) \times 10^{-9}$, three to five times Planck's value (Ext. Deriv. App. AH), so the coefficient is a calibration. It *forces the exponent* of the expansion rate $H_0^{\rm early}$ (the α^{57} hierarchy; its $O(1)$ coefficient rests on one *measured* input, the vacuum coefficient $R = \Omega_\Lambda C = 0.6042 \pm 0.0027$, of which the clock $C = 0.87784 \pm 0.00266$ is today's early-clock value, proven underivable from the printed corpus by the eight-route no-go and independent of the normalization of G, Rem. AP.6), and calibrates a third, the amplitude A_s, which the formula $32\pi\alpha^5$ matches at -0.6 to -0.8σ, depending on the Planck data combination, without a derivation of its power or its coefficient. What it does *not* derive are the vacuum coefficient R, the amplitude A_s and the coefficient of $\omega_b h^2$, and it carries the reionization optical depth τ, an astrophysical quantity shared with ΛCDM. R, A_s and τ are *normalizations*: none of them sets the shape of any observable DFD predicts (Rem. FK.8); the ω_b coefficient does, through the baryon loading of the acoustic peaks.

1. The scalar amplitude A_s: one calibrated input

Proposition FK.1 (The formula $32\pi\alpha^5$ in the de Sitter dictionary)**.** *In the single-field de Sitter dictionary*

$$A_s = \frac{H_\star^2}{8\pi^2\,\varepsilon_W\,\bar{M}_P^2} = \frac{1}{24\pi^2}\,\frac{V}{\varepsilon_W\,\bar{M}_P^4}, \tag{FK1}$$

with the primordial (Wheeler–DeWitt) scale on the locked Majorana rung $H_\star \propto M_R = M_P\alpha^3$ (App. AT 1; no printed stage holds the universe at that scale, Prop. FK.3) and the one-loop QED measure $\varepsilon_W = \alpha/(4\pi)$, the exponent collapses exactly *to*

$$A_s = 32\pi\,\alpha^5 = 2.080 \times 10^{-9} \quad (-0.82\sigma \textit{ from Planck}), \tag{FK2}$$

the power $\alpha^5 = (\alpha^3)^2/\alpha^1$ being machine-rigid (sympy residual 0). The pair $(H_\star, \varepsilon_W)$ that reproduces (FK2) is a single-*parameter choice, equivalently the normalization $H_\star/M_R = \sqrt{8\pi}$, equivalently $\varepsilon_W = \alpha/(4\pi)$, equivalently*

the inflationary potential $V = 3\,\alpha^6 M_P^4$.

Proof. Substituting $H_\star = \sqrt{8\pi}\,M_R = \sqrt{8\pi}\,M_P\alpha^3$ and $\bar{M}_P = M_P/\sqrt{8\pi}$ into (FK1) gives $A_s = (8\pi M_R^2)/(8\pi^2\varepsilon_W \bar{M}_P^2) = (M_P^2\alpha^6)/(\pi\varepsilon_W \bar{M}_P^2) = (8\,\alpha^6)/\varepsilon_W$; with $\varepsilon_W = \alpha/(4\pi)$ this is $32\pi\alpha^5$. The three statements $H_\star/M_R = \sqrt{8\pi}$, $\varepsilon_W = \alpha/(4\pi)$, and $V = 3\alpha^6 M_P^4$ are algebraically interchangeable given (FK1) and $H_\star^2 = V/(3\bar{M}_P^2)$; fixing any one fixes the other two. Hence exactly one normalization degree of freedom remains. All four identities are verified to ≥ 20 digits in the companion script. □

The rigidity is algebraic: it holds inside the de Sitter dictionary at $H_\star$. No stage in DFD freezes perturbations at $H_\star$ (Prop. FK.4), so neither the power α^5 nor the coefficient 32π is a derived property of A_s, and $32\pi\alpha^5$ is recorded as a numerical match, one of about 225 grammar candidates inside Planck's one-sigma band (App. AT).

a. $\varepsilon_W = \alpha/(4\pi)$ *is not derived.* Two corpus routes purport to fix ε_W; neither is a derivation.

- *Inversion route.* Writing $\varepsilon_W = H_\star^2/(8\pi^2 A_s \bar{M}_P^2) = \alpha/(4\pi)$ recovers ε_W *by assuming* the target $A_s = 32\pi\alpha^5$. This is explicitly circular and carries no independent content.
- *"Magnetic-dual" route.* Setting $\varepsilon_W = \alpha^2\alpha_M/\pi$ with the dual coupling $\alpha_M = 1/(4\alpha)$ gives $\alpha^2 \cdot \frac{1}{4\alpha}/\pi = \alpha/(4\pi)$ *identically*: the α^2 cancels α_M's $1/\alpha$, leaving the *universal one-loop QED measure* $\alpha/(4\pi)$ with no surviving trace of the value $1/(4\alpha)$. The same number appears for *any* α_M paired with its matching prefactor; the dual sourcing is a relabelling of a known constant, not a slow-roll computation.

Theorem FK.2 (No native inflaton)**.** *The compactification* $\mathbb{C}P^2 \times S^3$ *supports* no *canonically normalized scalar with a slow-roll inflaton potential. Six independent obstructions each suffice: (i) Lichnerowicz rigidity removes graviton/metric-moduli candidates; (ii) the truncated microsector carries no Kähler, size or shape modulus (no light flat direction), and on a continuous internal space the volume is not held either: with the connection Laplacian that fixes* α *it runs away without end, and with the Dirac operator volume and shape sit at a maximum with* $\eta = -2$ *(Prop. FK.3); (iii) the only light pseudoscalar,* χ *(the* $b_3 = 1$ *three-form zero mode), is a compact pNGB with a periodic—not slow-roll—potential; (iv) shift symmetry forbids the required non-periodic* $V(\phi)$*; (v) no worldvolume scalar carries a trans-Planckian field range; (vi) the would-be* ε_W *reduces identically to the one-loop measure* $\alpha/4\pi$*, a relabelled constant rather than a potential slope. (Full proof: Extended Derivations, App. AH series IV–VI.) Nor do the nine further routes derived from the printed structure (Proposition FK.3) supply an early accelerating stage with an exit or a source of the primordial perturbations.*

Theorem FK.2 establishes that DFD has *no* native slow-roll scalar on $\mathbb{C}P^2 \times S^3$ (six independent failure modes, and nine derived routes that close). With no inflaton potential there is no $V(\phi)$ whose slope $\varepsilon = \frac{\bar{M}_P^2}{2}(V'/V)^2$ can be computed; ε_W is therefore a fitted *number*, not a derived slow-roll parameter.

Proposition FK.3 (No derived early stage and no derived source of the primordial perturbations)**.** *Inside the window that reheating to the baryogenesis temperature* $T_L = 1.89 \times 10^{12}$ *GeV (App. AV) and the* χ *relic leave for any accelerating stage,* $5 \times 10^6 \lesssim H \lesssim 4 \times 10^{10}$ *GeV (Eq. (Q13)), nine routes derived from the printed structure give no stage with an exit and no source of the primordial perturbations (computed). (a)* The spectral action. *With the plateau cutoff every internal-mass field is conformally coupled and the Einstein-frame vacuum is lowest at zero internal mass, where* $H \gtrsim 2\bar{M}_P/\sqrt{f_0}$ *at* $N = 60$ *and no exit exists; on a continuous internal space the volume runs away along* $e^{-\lambda\phi}$*,* $\lambda = \sqrt{14}/3 < \sqrt{2}$*, for the connection Laplacian (endless acceleration,* $n_s = -6$*,* $r = 12.4$*), or sits with the shape at a maximum with* $\eta = -2$ *for the Dirac operator. (b)* The Higgs. *The spectral action fixes its coupling to curvature at the conformal value* $\xi = -1/6$ *for any cutoff; its potential in the canonical Einstein-frame field* $\hat{h}$*,* $9\lambda_H \bar{M}_P^4 \sinh^4(\hat{h}/\sqrt{6}\,\bar{M}_P)$*, has* $\varepsilon \geq 4/3$ *everywhere, so it never inflates, and Higgs inflation would need* $\xi = +1.7 \times 10^4$ *and an* H *about* 330 *times the relic ceiling. (c)* χ and the Chern–Simons sector. *A full winding of* χ *is a gauge identification and the level-*60 *space ends at the half-period edge, so there is no monodromy branch;* χ *is stable (*$E = 0$*), so it is no curvaton; as the whole signal it would be pure isocurvature; steering reheating, its sector measure gives* $S/\zeta \geq 1.05$ *against Planck's* 0.031*; a descent through its sectors costs at least* 2.9×10^{16} *GeV per step against a de Sitter temperature below* 10^{10} *GeV; and no other Chern–Simons or flux mode of the theory carries a stage. (d)* Thermal and holographic fluctuations. *The early plasma's heat capacity is extensive with no limiting temperature, thermal contact on the matter metric is causal, and a global thermal initial state leaves white noise,* $n_s = 4$ *at* $A_s \sim 10^{-82}$*; warm-plasma and holographic-cell variants reach the amplitude only with two fitted numbers. (e)* The trace anomaly. *The anomaly of DFD's own fields drives de Sitter only at* $H \simeq 5\bar{M}_P$*, above the cutoff; below about* $3\bar{M}_P$ *the Planck-strength stiffness of* ψ *dominates its four-derivative terms (below about* $16\bar{M}_P$ *the* R^2 *term, the only one with time derivatives), and the matter metric has no inhomogeneous conformal mode. (f)* Anisotropic scaling. *No field acquires the Lifshitz exponent* $z = 3$ *at high energy: the preferred foliation adds no operator with more than two spatial derivatives, the* a_4 *Weyl term with the gravitomagnetic shift keeps* $z = 1$*, and the deep-field* μ*-law gives* ψ *an amplitude-dependent* $z = 3/2$ *only in the infrared, which freezes no mode in the radiation era. (g)* Relaxation of the internal spectrum. *If the* 60 *eigenvalues of* D_F *were dynamical, every stationary spectrum of the spectral action would have one nonzero level inside the plateau (at most two beyond it for the cutoffs tested),*

so the 57-level spectrum of the theory is not a vacuum of the action; free eigenvalues would leave it within a few Planck times or, with the a_0 term kept, collapse to $D_F = 0$ in an eternal Planck-scale de Sitter phase, and the α^{57} rungs are self-consistent only at $k = 0$ and $k = 57$. The spectrum is held by the rigidity premise (Theorem Q.12), so nothing relaxes. (h) The E-transport clock. *The step $A_5 = Q\, d\ln A$ is locally pure gauge ($F = 0$): it carries no stress-energy or entropy and fires on the local e-fold count of the matter metric, so it follows the curvature perturbation rather than creating it, and equal steps would give $n_s = 1$. (i)* The Majorana sector. *The heavy-neutrino mass $M_R = M_P\alpha^3$ is an identification (App. P), not the value of a field, so the sector stores no energy that could drive a stage and end it; in the plasma the three heavy neutrinos drop out near $T \simeq M_R/2.5$ and lower the pressure there by about 1% ($w \geq 0.330$), so the expansion keeps decelerating (computed). The fast-light past is the ordinary expansion read on the arena clock, too slow to open the horizon (Rem. Q.11). Every working stage found needs a field the theory does not contain, so the primordial perturbations and the uniformity behind the horizon problem have no derived mechanism: they enter through one stated starting condition, the smooth beginning of App. Q (§XVIII A).*

b. The tensor ratio does not share this knob. The dictionary ratio $16\varepsilon_W = 4\alpha/\pi = 9.29 \times 10^{-3}$ is, by definition, the same single knob viewed twice, so it could never corroborate ε_W, and it is not the observable B-mode ratio. The primordial tensor ratio is bounded by the χ relic, $r \lesssim 10^{-7}$, independently of ε_W (App. SM, Cor. SM.4).

Proposition FK.4 (Status of A_s)**.** *A_s is one calibrated amplitude, as in ΛCDM, and its source is not in the printed field content. A source that shares the optical cone with the tensors has $r = 8F^2/(\lambda^2\bar{M}_P^2)$, where F is its decay constant and λ its conversion to curvature (Cor. SM.4). Read on that cone, ψ has $F = \bar{M}_P/\sqrt{2}$ and, on the power-law engine in the radiation era ($p = \frac{1}{2}$), $\frac{1}{2} < \lambda < \frac{3}{2}$, so $r > 1.7$. At the rate the χ relic allows (Eq. (Q13)) the observed amplitude needs a light field with $F/\lambda \lesssim 1.5 \times 10^{14}$ GeV that converts to radiation; the only light field with so small a decay constant, χ, is stable dark matter and seeds isocurvature alone, and DFD has no reheating stage through which another field could convert. On its own cone ψ never leaves the horizon: its characteristic speeds stay below $1.07\,c$ (Prop. III.7) while the background it sees decelerates (Thm. Q.9), so its fluctuations keep the blue spectrum of the initial state, $n_s = 3$. The de Sitter dictionary returns $32\pi\alpha^5$ only at $H_\star$, where one e-fold moves χ through four periods (Thm. SM.3); at the allowed rate it gives $A_s \lesssim 7 \times 10^{-15}$. The source of A_s is therefore open, and A_s is counted as one calibrated input, the amplitude that the smooth beginning of App. Q states.*

A derivation of A_s needs a source of one of two kinds: a light field on the optical cone with $F/\lambda \lesssim 1.5 \times 10^{14}$ GeV and a conversion to radiation, or an accelerating stage on ψ's own cone, which needs a vacuum energy DFD does not contain. Either would fix A_s and n_s together.

2. The χ abundance normalization: from open overshoot to derived-with-conventions

Removing the misalignment angle θ_i (no inflaton) appears to fix the amplitude at the classical uniform-circle variance $\langle\theta^2\rangle = \pi^2/3$, giving a factor-$\approx$ 44 overshoot, $\Omega_\chi h^2 \simeq 1.62 \cdot \pi^2/3 \approx 5.3$. That is *not* the relic: $\pi^2/3$ is the classical-*continuum* measure, the wrong vacuum for a *finite* topological mode. Step 5b of App. AV (Thm AV.13) replaces it with the finite $SU(2)_{60}$ CS/WZW vacuum expectation of the normalized quadratic Casimir,

$$\begin{aligned} \langle\theta_\chi^2\rangle &= \sum_{j=0}^{k/2} |S_{0j}|^2 \, \frac{C_2(j)}{k(k+2)} = 0.073 \\ \Rightarrow\ \Omega_\chi h^2 &= 1.62\,\kappa_{\rm rad}\sqrt{2\pi}\,\langle\theta_\chi^2\rangle = 0.11928 \\ &\quad (-0.60\sigma \text{ from Planck}), \end{aligned} \tag{FK3}$$

where $\kappa_{\rm rad} = \Gamma(\frac{1}{4})^2/(6\sqrt{3}\pi) = 0.4026$ is the exact radiation-era onset factor (the sudden approximation owed it) and the $\sqrt{2\pi}$ is the flux-period identification (Lemma AV.6: $P = \bar{M}_P\alpha^3$ is the flux *period*, $f_{\rm rad} = P/2\pi$; App. AV). A caution: the 45× reduction from $\pi^2/3 = 3.29$ to 0.073 is *not* a finite-Hilbert-space effect — it factorizes as 39.4784 (a radians^2 →turns^2 units conversion, $4\pi^2$) × 1.17922 (a continuum measure choice) × 1.00092 (the finite-k effect itself, i.e. 0.09%) × 0.96774 (Sugawara k/K), per Eq. (AV14) (App. AV). The amplitude $\langle\theta_\chi^2\rangle$ is the correct period-1 (turns^2) flux variance, a topological deliverable, not a fitted knob.

Proposition FK.5 (The relic is derived with stated conventions (Finite $SU(2)_{60}$ CS Vacuum Relic), not a fitted knob)**.** *With $P = \bar{M}_P\alpha^3$ the flux period ($f_{\rm rad} = P/2\pi$), $m_\chi = 2\pi\sqrt{158}\,\bar{M}_P\alpha^{13} = 32.005$ eV, and χ the compact S^3 CS/WZW flux mode at $k = 60$, the relic amplitude (FK3) is forced: the operator is the unique invariant quadratic Casimir (the geodesic angle-squared ψ^2 is non-invariant — nonzero Haar-character coefficients for every $j \geq \frac{1}{2}$ — and over-produces by 35–150×); the measure is the modular S-matrix vacuum row $|S_{0j}|^2$, given the asserted premise P4′ (Lemma AV.27); and the $k(k+2)$ denominator is the Sugawara level $k + 2 = k + h^\vee$ times the bare CS level k, locked by $C_2(k/2)/[k(k+2)] = \frac{1}{4}$ (the k-independent $\mathbb{Z}_2$ half-period edge). No correction for an overshoot — late entropy dilution $\Delta \sim 40$, a revised m_χ/f_χ rung, anharmonic/string-network corrections, a temperature-dependent mass, a shared A_s normalization, a stress-tensor projection — is needed: there is no overshoot to cure. The edge $\theta_{\max} = \frac{1}{2}$ is fixed by χ's* derived *$\mathbb{Z}_2$ ($\chi \to -\chi$) orientation-oddness (the same $\mathbb{Z}_2$ giving $N_{\rm DW} = 1$), and the lock $C_2(k/2)/[k(k+2)] = \frac{1}{4}$ then makes $k(k+2)$ the unique k-independent denominator; $K = k + 2$ is the Sugawara shift ($\sum_j |S_{0j}|^2 = 1$ for every*

integer K, so K is set by the shift, not normalization). Given these two stated conventions (Rem. FK.6), the amplitude $\langle\theta^2\rangle = 0.073$ is forced. The single non-DFD input is the relic-map prefactor 1.62 *— the standard radiation-era $H(T)$/entropy redshift that* every *DM relic (incl. ΛCDM's) carries; it is operator-agnostic, so applying it to the flux amplitude is consistent.* ***The relic is therefore derived, conditional on the flux-period identification, the stated count*** 158 ***and P4′*** *(Lemma AV.6; the Finite $SU(2)_{60}$ CS Vacuum Relic, $\Omega_\chi h^2 = 0.11928$, -0.60σ), not a fitted knob. Its radiation-era rate is DFD's own: the Friedmann law of the Einstein–Hilbert term (§XIX E) supplies $H(T)$ with the same G. χ has no photon coupling ($E = 0$, App. AV), so it has no decay or conversion line.*

a. No convention band. A "∼ 9–44×, convention-dependent" overshoot follows from the oscillation-onset convention of the 1.62 prefactor ($3H = m$ vs $H = m$) applied to the *wrong* amplitude $\langle\theta^2\rangle = \pi^2/3$. With the period-1 flux amplitude $\langle\theta^2\rangle = 0.073$ and the exact onset factor $\kappa_{\rm rad}$ replacing the sudden approximation, the band collapses to $\Omega_\chi h^2 = 0.11928$ (the convention ambiguity is resolved: $\kappa_{\rm rad}$ *is* the derived onset). There is no overshoot left to be convention-dependent about.

Remark FK.6 (Where the knob went: eliminated, not relocated). Step 5b eliminated the θ_i knob outright — with no inflaton no angle is chosen, and the amplitude is the topological finite-vacuum expectation. The powers of α in the mass and decay constant are derived (the count 158 and the stiffness are stated inputs); the abundance is *also* derived, conditional on the flux-period identification, P4′ and the two stated conventions above, *not* an open overshoot and *not* a relocated fitted knob. The path from "Derived" to "proven" is the two first-principles items of Prop. FK.5/Rem. AV.14: a native derivation of the 1.62 prefactor and a CS symplectic-form derivation that $\theta_{\rm max} = \frac{1}{2}$ and $K = k + 2$ are forced. We do not manufacture a fix beyond those stated conventions.

Remark FK.7 (The $\sqrt{158}$ multiplicity: one stated input, and why it is *not* 4π). The χ-mass *exponent* (α^{13}, from the see-saw $16 - 3 = 13$) is derived to theorem grade; the *prefactor* $\sqrt{158}$ is one stated discrete input. It is read as $3(k_{\rm max} - \dim M_7) - 1$, the three-dimensional weak block times the $53 = k_{\rm max} - \dim M_7$ block, less one zero-mode, but no single counting rule gives it: the uniform rule, all modes less the zero modes, gives 171, and every count invariant under a symmetry acting irreducibly on the weak block is a multiple of 3, which 158 is not (App. AV). The count 171 would give $m_\chi = 33.30$ eV and $\Omega_\chi h^2 = 0.1217$, a 2% shift that measurements of the cold-matter density can separate. The prefactor is *not* to be replaced by the loop factor 4π ($16\pi^2 = 157.91$) it sits 0.05% from: a multiplicity is an integer, $16\pi^2$ is transcendental, and the swap is motivated only by making "$v^2 = 2\,m_\chi P$" exact, a back-solve. The electroweak–dark link is $v = 4\pi\Lambda$ (Rem. AV.9), whose 4π is the fitted Higgs prefactor $\sqrt{2\pi}$ in another form; the burden of any future revision is on deriving the integer count, not on the 0.027% coincidence.

3. Knob count: DFD vs ΛCDM

Table CXXVI grades all six ΛCDM-equivalent cosmological inputs. The count of fitted or measured continuous DFD coefficients is **four**: the vacuum coefficient R (today's early-clock value C), the amplitude A_s, the coefficient of $\omega_b h^2$ and τ (Rem. FK.8), against ΛCDM's six. ($\omega_\chi h^2$ is not in this list: it is graded forced-amplitude-with-stated-conventions, and H_0 derived-exponent / measured-coefficient; the membership is that carried by Table CXXVI and Rem. FK.8.) For $\omega_b h^2$ the α^4 power of η_B is derived, and so is the current that carries the bias, $B-L$, but the coefficient is not. The conventional-point value $0.2057\,\alpha^4(1 + 2\pi\alpha)$ used in the fits rests on a Gaussian carrier that the print cannot supply, and it was set after Planck's η_B was known; with the stated carrier and every step pinned to the print, the mechanism gives η_B of about $(2\text{–}3) \times 10^{-9}$, three to five times Planck's value (Ext. Deriv., App. AH, Berry-holonomy baryogenesis theorem), and agreement would need one winding of the determinant line per e-fold, which the stated carrier does not give. The deposit factor $(1 + 2\pi\alpha)$ follows from Axiom E-transport′ (+1 priced discrete bit) with the stated carrier. $\omega_b h^2$ is therefore graded derived power, calibrated coefficient: one calibrated input, as in ΛCDM. The tilt $n_s = 1 - 2/60$ is a stated number; the mechanism is open, as it is for A_s (Table CXXVI).

a. Parameter count. With $\omega_\chi h^2$ graded forced-amplitude-with-stated-conventions (Prop. FK.5), H_0 graded derived-exponent/measured-coefficient (the eight-route no-go) and the ω_b coefficient a calibration, the calibrated continuous count is $k_{\rm DFD} = 4$: R, A_s, the ω_b coefficient and τ. It is 5 if ω_χ's stated conventions (the 1.62 relic prefactor and the $\mathbb{Z}_2$/Sugawara edge) are counted as a knob. On the Planck plik-lite dataset the effective count is 3 (R, i.e. H_0; one overall amplitude absorbing $A_s e^{-2\tau}$; and the ω_b coefficient), against ΛCDM's effective 5 (App. ZS). The discrete bit of Axiom E-transport′ is not free of charge: it is priced in the App. CE trials audit (row 9, axiom-adoption bits; the adopted statements are listed in Table CXXVII), and its adoption was made *after* Planck's η_B was known to select its consequence at the conventional freeze-out point; the statement is "one data-concordant discrete bit," never "zero assumptions." The conclusion is unchanged: DFD's parameter economy over ΛCDM holds at every reading, 4–5 < 6 globally and 3 < 5 on the CMB likelihood itself.

Remark FK.8 (The parameter claim, stated exactly). This remark is the reference form of DFD's parameter claim: it is the statement below, not the unqualified phrase "no continuous fit parameters."

DFD fits no continuous parameter to the shape of any observable it predicts, with one exception, the baryon density. Every ratio, hierarchy and spectrum shape the theory reports — the CMB peak structure,

Input	Grade	Basis
$H_0^{\rm early} = 67.52 \pm 0.09$	Derived expon., Measured coeff. (1 knob: R)	$G\hbar H_0^2/c^5 = C\,\alpha^{57}$: exponent 57 a theorem; $R = \Omega_\Lambda C = 0.6042 \pm 0.0027$ measured; today's early clock $C = 0.87784 \pm 0.00266$ (eight-route no-go; C=1: the bound-matter clock, $H_0^{\rm loc} = 72.09$, Postulate ZS.11); five concordant CMB-anchored channels; $1/H_0 = 14.48$ Gyr.
$n_s = 0.9667$	Stated (0 knobs)	$n_s = 1 - 2/60$: a stated number; the mechanism is open. $+0.4\sigma$ from Planck 2018; the combination of Planck, ACT DR6, lensing and DESI gives 0.974 ± 0.003, 2.4σ above.
A_s	Calibrated (1 knob)	One calibrated amplitude; $32\pi\alpha^5$ matches it at -0.6 to -0.8σ with its source open (Prop. FK.4).
$\omega_\chi h^2$	Forced ampl., Stated conv.	$\langle\theta^2\rangle = \sum_j \lvert S_{0j}\rvert^2 C_2(j)/[k(k+2)]$ $\Rightarrow \Omega_\chi h^2 = 0.11928$ (-0.60σ; flux-period fix, $\times\kappa_{\rm rad}\sqrt{2\pi}$, $\kappa_{\rm rad} = \Gamma(\frac{1}{4})^2/(6\sqrt{3}\pi)$; App. χ-matter); Casimir operator proven; measure given the asserted P4′ (Table CXXVII); $\mathbb{Z}_2$/Sugawara edge + 1.62 relic-prefactor stated (Prop. FK.5).
$\omega_b h^2$	Derived power, calibrated coeff. (1 knob; +1 priced discrete bit)	$\eta_B \propto \alpha^4$ and the $B-L$ bias derived; with the stated carrier, about (2–3) $\times\, 10^{-9}$ pinned to print, 3–5× Planck's 6.13×10^{-10}; the fits use the conventional-point value; deposit $(1 + 2\pi\alpha)$ by Axiom E-transport′ (Ext. Deriv. App. AH).
τ	Calibrated (astrophysics)	Astrophysical reionization depth, as in ΛCDM.

TABLE CXXVI. Per-input grade of the six ΛCDM-equivalent cosmological inputs (coefficients at the measured clock; $\omega_b h^2$ graded under Axiom E-transport′). **Stated:** n_s (a stated number; the mechanism is open). **Derived power, calibrated coefficient:** $\omega_b h^2$ (the printed mechanism gives η_B of about (2–3) $\times\, 10^{-9}$, three to five times Planck's value; +1 priced discrete bit, Axiom E-transport′). **Derived exponent, measured coefficient:** $H_0^{\rm early}$ (the vacuum coefficient R). **Calibrated:** A_s, which the formula $32\pi\alpha^5$ matches without a derivation. **Forced amplitude with stated conventions:** $\omega_\chi h^2$, the finite-vacuum Casimir amplitude with the flux-period identification (Lemma AV.6) and the stated count 158, $\Omega_\chi h^2 = 0.11928$ at -0.60σ (Prop. FK.5; App. χ-matter), with the operator proven, the measure conditional on the asserted P4′ (Table CXXVII), and the $\mathbb{Z}_2$/Sugawara edge and 1.62 relic-prefactor as stated conventions. **Calibrated continuous coefficients (4):** R, A_s, the ω_b coefficient and τ, the last an astrophysical quantity shared with ΛCDM. In every count DFD frees *fewer* parameters than ΛCDM's six.

$\omega_\chi h^2$, the forced fermion ratios, the mixing towers, the closed-form value of α^{-1} — is delivered by derived or discretely selected structure, with no continuous quantity adjusted against the data it is compared to. The tilt $n_s = 1 - 2/60$ is a stated number; the mechanism is open. The exception is $\omega_b h^2$: its α^4 power is derived, but its coefficient is a calibration (the printed mechanism gives η_B of about (2–3) $\times\, 10^{-9}$, three to five times Planck's value), and the CMB fits use its conventional-point value (Ext. Deriv. App. AH).

What the theory's cosmology carries is **four continuous calibration constants**:

(i) **The vacuum coefficient** $R = \Omega_\Lambda C = 0.6042 \pm 0.0027$ calibrates the *absolute scale*. Today's early-clock value is $C = R + 1.924\,(\omega_m + \omega_r) = 0.87784 \pm 0.00266$; through $G\hbar H_0^2/c^5 = C\,\alpha^{57}$ (exponent 57 a theorem) it fixes $H_0^{\rm early}$. Measured from BAO+θ_*; underivable from the printed axioms by the eight-route no-go (Rem. AP.6).

(ii) **The primordial amplitude** A_s calibrates the scalar power; the formula $32\pi\alpha^5$ matches it, but no printed mechanism produces it (Prop. FK.4).

(iii) **The coefficient of** $\omega_b h^2$ calibrates the baryon density, the one shape among the four, through the baryon loading of the acoustic peaks; its α^4 power and its $B-L$ current are derived.

(iv) **The reionization optical depth** τ calibrates the *late-time optical depth to recombination*: an astrophysical quantity taken over from ΛCDM, degenerate with the amplitude in the CMB likelihood.

Three of the four are DFD-internal; τ is shared with the comparison model. Against ΛCDM's six free parameters the global count is four (five if ω_χ's stated conventions are charged as a knob). On the Planck plik-lite likelihood itself, where (ii) and (iv) collapse into the single combination $A_s e^{-2\tau}$, the count is **three calibrations against ΛCDM's five effective parameters** (App. ZS). The particle sector adds three continuous numbers, the fitted Higgs prefactor $\sqrt{2\pi}$, the imported η_q and the Higgs quartic, conjectured to be 1/8 at a matching scale that is not derived; G sets the unit (§FK 4).

The discrete inputs are priced, not free. They are enumerated and charged in the trials audit of App. CE (row 9, axiom-adoption bits; the adopted statements are listed in Table CXXVII and the discrete inputs in Table CXXVIII). The form of the discrete statement is "priced discrete bits," never "zero assumptions."

Scope. The count above covers the six ΛCDM-equivalent inputs graded in Table CXXVI. Individual results elsewhere in the corpus whose normalization is imported rather than derived — for instance the within-multiplet η_q of App. Y — are graded as such at their own sites and are *not* reported as parameter-free predictions (App. FM); they do not enter the prediction set to which this claim applies. The inputs of the graded predictions are listed in Tables CXXVII and CXXVIII (§FK 4).

4. Inputs and axioms of DFD

Tables CXXVII and CXXVIII list the inputs of the graded predictions: the postulates and adopted axioms, the identifications adopted, the discrete selections, the continuous calibrations and the imported frameworks, each with where it is stated and its status. A statement that recurs in several places is listed once. An item leaves the open list of §XVIII A when it is derived, reduced to an entry here, or handed to a named observation.

a. The count. The tables hold two core postulates, twenty-five adopted axioms, premises, postulates and clauses, premise G1, which follows from the Einstein–Hilbert static-energy identity, one G and the Rest-Mass Channel, fourteen adopted identifications, eighteen rows of discrete selections, which carry the fifteen discrete inputs of the fermion, Higgs and neutrino sectors among others, and six imported frameworks. The continuous entries are four cosmological calibrations (the vacuum coefficient R, the amplitude A_s, the ω_b coefficient and τ, the last an astrophysical quantity shared with ΛCDM), three particle-sector numbers (the fitted Higgs prefactor, the Higgs quartic and the imported η_q) and the one dimensionful scale that every theory measures; the quartic is conjectured to be 1/8, but its matching scale is not derived, so it counts as one continuous number. The cluster χ amplitude is not an input: it is predicted, 1.21 ± 0.05 of the cosmic mix inside r_{500} at estimate grade (App. I).

b. Comparison with ΛCDM and the Standard Model. ΛCDM with the Standard Model fits six cosmological and nineteen particle parameters, and seven to nine more once neutrino masses and mixing are included; it adopts about ten structural assumptions: general relativity, quantum field theory, the gauge group, the matter content, three generations, the Higgs doublet, cold dark matter, a cosmological constant, inflation with an unspecified potential, and the cosmological principle. DFD fits far fewer continuous numbers, six beyond the unit of scale and seven with τ, which ΛCDM fits as well, and it adopts more structure; colour, the matter content and three generations are inputs in both. Among the numbers the comparison fits, DFD derives the χ abundance (conditional on the flux-period identification, P4′, the stated count 158 and two stated conventions), the exponent of H_0 and of the dark-energy density, a_0, the closed-form value of the fine-structure constant (exact under two stated choices, with its last 21 ppm on the open bracket coefficient), the weak mixing angle, the top and charm masses and $\bar{\theta} = 0$ at tree level ($\theta_{\rm YM} = 0$ fixed by the spectral action given that nothing is added to it for the gauge fields), and, with the discrete selections of Table CXXVIII, $\alpha_s(M_Z)$, the CKM magnitudes, the three neutrino masses, the PMNS angles θ_{12} and θ_{23} and the phase $\delta_{\rm CP}$, each at the grade stated where it is treated; $\sin^2\theta_{13} = 3\alpha$ is a stated conjecture, and the tilt $n_s = 1 - 2/60$ is a stated number; the mechanism is open. Its claim is fewer fitted numbers, not fewer assumptions.

5. Status and falsifier

Status FK.9. **Four continuous constants are calibrated: the vacuum coefficient R, the amplitude A_s, the coefficient of $\omega_b h^2$ and the shared astrophysical τ (Rem. FK.8); only the ω_b coefficient sets a shape, and the χ relic is derived with stated conventions.** (i) A_s is one calibrated amplitude, as in ΛCDM: the formula $32\pi\alpha^5$ matches it at -0.6 to -0.8σ, but no printed mechanism produces it, and the no-native-inflaton theorem (Thm. FK.2) means there is no inflaton potential to derive it from; the tensor ratio is bounded by the χ relic instead (Cor. SM.4). (ii) The χ relic is derived with stated conventions (the Finite $SU(2)_{60}$ CS Vacuum Relic, Thm AV.13) with the flux-period identification (Lemma AV.6) ($P = \bar{M}_P\alpha^3$ is the flux *period*; $f_{\rm rad} = P/2\pi$) and the stated count 158: $\Omega_\chi h^2 = 0.11928$ (-0.60σ from Planck), the exact onset factor $\kappa_{\rm rad} = \Gamma(\frac{1}{4})^2/(6\sqrt{3}\pi)$ and the $\sqrt{2\pi}$ period shift

TABLE CXXVII. Inputs of DFD (I): postulates, adopted axioms and adopted identifications. "Stated in" gives where each is printed, and the status is the one given there.

Input	Stated in	Status
Postulates and adopted axioms		
Light follows the optical metric, $n = e^{\psi}$, on flat $\mathbb{R}^3$ with absolute time	§I B	Postulate
Test bodies move in the potential $\Phi = -c^2\psi/2$; inside bound systems χ does so where it fills the medium's demand	§I B	Postulate
The scalar sector is an instantaneous elliptic constraint	Axiom WS.1	Axiom
Rest mass sources an unscreened channel, the Einstein–Hilbert term's own static scalar energy; the μ-law acts only on the polarization of bound systems	Thm. GR.10	Adopted postulate
The floor law in energy form: matter moves under the momentum-conserving energy of the two Newtonian fields, which one energy, the χ assignment and the floor law force in spherical symmetry; its three-dimensional filling rule is stated	Eqs. (AV27), (AV28)	Adopted; the Local Group's matter barycentre tests it against the total-ψ rule, the disc's vertical force against the static field
Environmental confinement: inside a host field above $(\ln 2)^2 a_0$ a subsystem is Newtonian; in a weaker host the fields compose in quadrature	Axiom NL.14	Adopted; local wide binaries and the edge step test it; the outer-halo globular clusters beyond the step show about a third of the predicted boost
The Einstein–Hilbert term acts on the scalar field only through the rest-mass channel (premise G1)	Prop. WS.5; Prop. WS.6	Follows from the Einstein–Hilbert static-energy identity and one G; its partition clause is the Rest-Mass Channel
Gravity's spectral trace uses the four-dimensional Dirac operator, while α's uses the internal connection Laplacian (premise G2)	Prop. WS.5	Stated premise of the derived term
Gravity's dynamics are the Einstein–Hilbert term of the spectral action, in the rest-mass sector where $\mu \to 1$	Prop. WS.6	Stated premise
The finite spectral-action clock dictionary	Axiom AP.5	Axiom
The scalar acceleration action dictionary	Axiom AP.7	Axiom
The primordial state: the no-boundary state with nothing inserted	Rem. Q.14	Stated input; $\Omega_\chi h^2$ tests it
A smooth beginning: smooth background, small regular ripples; it carries the arrow of time	Post. Q.15	Stated premise
One universe, two clocks: matter and the expanding universe keep clocks offset by one constant factor λ, $\lambda^2 = 1/C$	Postulate ZS.11	Stated postulate; form derived, size measured, derivation open
Size of the clock gap: when matter first binds, its ψ gap is the microsector response read with both rates on one worldline	Postulate ZS.12	Stated postulate, to be tested; not derived
Axiom E-transport′: the flux advances one lattice step per e-fold	Ext. Deriv. App. AH	Adopted; one priced bit
The crossover normalizer is domain-local	Axiom ZT.2	Optional extension; environment data decide it
Seven vacuum axioms, which single out $\mathbb{C}P^2 \times S^3$	Thm. AB.1	Axioms, satisfiable
Postulate Y.10: the det-orthogonal geometric CP offset of quark mixing	App. AO	Structural postulate
The channel space is the group algebra $\mathbb{C}[A_5]$	App. Z	Structural postulate
Trimaximal mixing with μ–τ reflection	Thm. AY.3	Structural postulate
Baryon number is violated only by the electroweak anomaly; the posited soliton reading is not used	Thm. F.26; Rem. F.27	Stated premise; $\tau_p = \infty$ rests on it

Table CXXVII, continued.

Input	Stated in	Status
Frame stiffness scales with block rank, $\kappa_r = n_r\kappa_0$; the scalar channel's frame factor is n_3/n_2 (the internal gauge partition)	Thm. F.25; Axiom AP.18	Motivated assumption in App. F 9, printed as an axiom in App. AP; k_a, a_0 and the weak mixing angle rest on it
The scalar channel couples through the magnetic sector, the magnetically dominated regime $E^2 \ll c^2B^2$	Thm. G.1; App. G 2	Stated premise; k_a rests on it
The four-dimensional three-form of the internal C_3's b_0 piece carries zero flux	App. AU	Stated premise; a nonzero flux adds its own vacuum energy
The spectral action's Planckian vacuum term cancels	Rem. AU.3; App. WS	Stated premise; uncancelled, it would gravitate as Λ does
From decoupling on, the $(K-\bar{K})^2$ term acts on every slice on which the μ-law acts somewhere; while no baryons are bound anywhere, and at least until decoupling, gravity is the Einstein–Hilbert term alone	Axiom WS.1; Rem. WS.7	Stated clause; with it $k = 0$ is derived
The internal Dirac operator is held at its printed spectrum, and only the inner fluctuations of End(E) are physical (rigidity, layer 7 of the single-vacuum theorem)	Thm. Q.12; Ext. Deriv. App. AH	Stated premise; the 57-level spectrum rests on it
Adopted identifications		
The ground-state principle, $\mu = \mathbb{P}(n{=}0)$: it gives $\nu = Z_1$	Rem. BS.4	Stated input
e^{ψ} as the S^3 weight ratio, minimal level response, saturation-union composition	App. N	Assumptions
The deep-field limit with unit slope: $\mu(s) = s + O(s^2)$ in App. N, and $g_{\mathrm{obs}}^2 \to g_{\mathrm{bar}}a_0$ in the interpolation-function theorem	Assumption N.7; Thm. BS.9	Assumption
The temporal kinetic function obeys $K'(\Delta) = \mu(\Delta)$	Eq. (Q8)	Adopted identification; the dust branch rests on it
$f_\chi = \bar{M}_{\mathrm{P}}\alpha^3$ is the flux period	Lemma AV.6	The χ abundance rests on it
The $2\pi/\alpha$ winding instanton changes sector	Thm. AV.24	Asserted
The generation space is the fixed kernel of the vacuum operator	App. F	Conditional
The electroweak group is the structure group of the isotropy bundles at the vacuum point of $\mathbb{C}P^2$, with the hypercharge the direction $\mathrm{diag}(1,1,-2)$ normalised as $6Y$, acting on the twisting bundles and not by isometries	Rem. F.2	Identification
On the soliton reading, baryon number is the S^3 winding	App. F 10	Identification
The Majorana scale, $M_R = M_P\alpha^3$	App. P	Identification
One α per flavour connector	App. AO	Asserted
The ρ-shifted Casimir $\Delta + 1$ as the operator of α's trace on $S^3 = SU(2)$	§X C	Stated choice
α's trace as the $\mathbb{C}P^2$ $\zeta(0)$ times the S^3 heat trace, with the heat-kernel regulator	§X C	Stated choice; the closed form is exact under the two
The weak mixing angle's trace weights: hypercharge over one generation, $SU(2)$ over one doublet	Thm. Z.1	Stated choice

TABLE CXXVIII. Inputs of DFD (II): discrete selections, continuous calibrations and imported frameworks.

Input	Stated in	Status
Discrete selections		
Three generations, $N_{\text{gen}} = 3$	Rem. F.21	Input, shared with the Standard Model; the same input as axiom (V5) of the seven vacuum axioms
Colour $SU(3)$ and the content and chirality of one family; its five hypercharged types, N_{gen} and the derived $q_1 = 3$ fix $k_{\max} = 60$	Rem. F.3	Inputs, shared with the Standard Model
The bracket coefficient $c = 1/13$ behind the last 21 ppm of α	Rem. X.4	Stated; provenance open
Identification of the hypercharge-trace coefficient with $1/e^2$	§X I	Stated; open
The weak-block count 158 in m_χ; the uniform count gives 171	Rem. FK.7	Stated input; the CMB tests it
$\Lambda_{\text{QCD}} = M_P \alpha^{19/2}$ and its $\sqrt{4\pi}$ scheme matching	App. Z	Selected
Seven charged-fermion prefactors, one for each species other than the top and the charm	App. FM	Chosen by data
Three CKM counts, λ, A and $\bar{\eta}$ as 31, 108 and 49 times α	App. AO	Selected
Euler projection of the CP-even CKM apex	Postulate AO.23	Selected
Nothing is added to the spectral action for the gauge fields; the spectral action then fixes the bare Yang–Mills angle at $\theta_{\text{YM}} = 0$	App. L	Stated premise
The neutrino branch, one of four equally natural fractions	App. X	Chosen by oscillation data
The Dirac-neutrino Yukawa rung, $y_D^2 = F_\nu \alpha$	Prop. AT.1	Stated input
$\sin^2 \theta_{13} = 3\alpha$	App. Z	Stated conjecture; JUNO tests it through θ_{12}
The tilt $n_s = 1 - 2/60$	Table CXXVI	Stated number; the mechanism is open
One sign bit; the orientation of time is the smooth beginning's	App. CE	Priced
The Bose-law branch, SOURCE	App. BS	Chosen by data; a single-temperature mode gives the same branch
The relic edge $\vartheta_{\max} = \frac{1}{2}$ and the Sugawara shift $K = k + 2$	Prop. FK.5	Stated conventions
The screen domain size R_D	App. ZT	Free; environments test it

nearly cancelling each other (App. χ-matter), with the operator (Casimir) forced, the measure conditional on P4′ (Table CXXVII), and the normalization ($k(k+2)$; $\theta_{\max} = \frac{1}{2}$ from χ's derived $\mathbb{Z}_2$, $K = k+2$ from Sugawara) resting on two stated conventions (Table CXXVIII). The lone non-DFD input is the standard cosmological relic-redshift 1.62 (shared with all DM), not a fit to Ω_{DM}. (iii) The vacuum coefficient $R = 0.6042 \pm 0.0027$ is measured, with today's early-clock value $C = 0.87784 \pm 0.00266$ (five concordant CMB-anchored channels); the eight-route no-go proves it underivable from the printed corpus (Rem. AP.6). (iv) The coefficient of $\omega_b h^2$ is calibrated: its α^4 power and $B-L$ bias are derived, the printed mechanism gives η_B of about (2–3) $\times 10^{-9}$, three to five times Planck's value, and Axiom E-transport′ adds one priced discrete bit. **Net count: 4 calibrated continuous cosmological coefficients, three DFD-internal and one shared with ΛCDM, against ΛCDM's 6 free parameters** (R, A_s, the ω_b coefficient and τ; $\omega_\chi h^2$ is forced-amplitude with stated conventions), with n_s a stated number (the mechanism is open), and the H_0 exponent a theorem. No derivation of A_s, of R or of the ω_b coefficient is manufactured here; no obstruction is manufactured either: each candidate received an explicit arithmetic check.

Falsifier FK.10. *Two independent decisive tests.* (a) **Primordial B-modes.** DFD predicts none that any planned experiment can see: $r \lesssim 10^{-7}$ (App. SM, Cor. SM.4). A confirmed primordial tensor signal (a LiteBIRD, BICEP Array or Simons Observatory detection) falsifies the χ relic, and with it the dark sector; a firm upper bound such as $r < 5 \times 10^{-3}$ is the predicted outcome, not a falsifier. The ratio is not tied to the A_s normalization: $4\alpha/\pi$ is the dictionary's $16\varepsilon_W$, not a B-mode ratio. (b) **Dark matter.** The χ abundance is *predicted*: the finite $SU(2)_{60}$ CS-vacuum amplitude with the flux-

Table CXXVIII, continued.

Input	Stated in	Status
Continuous calibrations and the unit		
Vacuum coefficient $R = \Omega_\Lambda C = 0.6042 \pm 0.0027$; today's early-clock value is $C = 0.87784 \pm 0.00266$	Rem. AP.6	Measured
Primordial amplitude A_s, which $32\pi\alpha^5$ matches	Prop. FK.4	Calibrated; no printed source
The ω_b coefficient at the conventional point	§FK 3	Calibrated; the printed mechanism gives η_B of about (2–3) $\times 10^{-9}$, three to five times Planck's value
Reionization optical depth τ	Rem. FK.8	Astrophysics, as in ΛCDM
Higgs prefactor $\sqrt{2\pi}$ in $v = M_P\alpha^8\sqrt{2\pi}$	Thm. Z.3	Fitted; no-go on deriving it
Higgs quartic λ_H	Thm. Z.3	Conjectured 1/8 at a matching scale that is not derived, so one continuous number (m_H −0.40% at m_t)
Light-quark QCD enhancement η_q	Rem. Y.4	Imported; DFD's own running gives 4.21
One dimensionful scale, G, with $\hbar$ and c as units	§I E	Measured unit
Imported frameworks		
Quantum mechanics: the unit $\hbar$, the interacting dynamics and the measurement postulate; the Dirac β is derived	App. QM	Shared with every quantum field theory
The standard thermal history: relic redshift, nucleosynthesis, recombination	Prop. FK.5	Imported; shared
Baryonic astrophysics: star formation, feedback and the sources of reionization	App. PK	Shared with ΛCDM
Lattice ratios of quantum chromodynamics	App. YM	Inherited
The vacuum energy of matter cancels; uncancelled, it would gravitate as Λ does	App. AU	Assumed, as in every quantum field theory with gravity
A homogeneous, isotropic background	§XIX	Assumed; shared

period identification (Lemma AV.6), the stated count 158 and the asserted premise P4′ (Lemma AV.27) gives $\Omega_\chi h^2 = 0.11928$ (-0.60σ from Planck 0.1200 ± 0.0012). (b1) A precision $\Omega_{\rm DM}h^2$ that moves firmly outside the stated-convention band (across K, times the $\mathcal{O}(1)$ relic prefactor) falsifies the derivation. (b2) The 32.005 eV mass ($= 2\pi \times 5.0937$ eV) is sharp, and χ has no photon coupling ($E = 0$; App. AV): it neither decays nor converts, so a laboratory or astrophysical null is the prediction, and any dark-matter photon line at 16.0 eV (77.5 nm, two-photon decay) or axion-like signal at 32.005 eV (38.74 nm), at any strength, falsifies χ.

a. Early-universe tests. DFD states the tilt $n_s = 1 - 2/60 = 0.9667$ with no running (a stated number; the mechanism is open), and it predicts no primordial B-modes ($r \lesssim 10^{-7}$), no Gaussian dark-matter isocurvature and no baryon isocurvature: the E-transport baryogenesis step, $A_5 = Q\, d\ln A$, fires on the local e-fold count, so η_B follows the local expansion and $S_B = 0$ exactly for an adiabatic onset of the radiation era (computed). The CMB alone agrees: $n_s = 0.9682 \pm 0.0032$, $r < 0.034$ and $\beta_{\rm iso} < 0.038$. The combination of Planck, ACT DR6, CMB lensing and DESI gives $n_s = 0.974 \pm 0.003$, about 2.4σ above 0.9667, so the Simons Observatory, with $\sigma(n_s) \simeq 0.002$, decides it: a tilt outside 0.957 to 0.977 at that precision falsifies $1-2/60$. A confirmed primordial B-mode signal from BICEP Array, the Simons Observatory or LiteBIRD falsifies the χ relic. A detected Gaussian dark-matter isocurvature mode falsifies the topological origin of the relic (Rem. AV.16), and a detected running $|dn_s/d\ln k| \geq 0.003$ falsifies the constant tilt.

Appendix SM: The "Scalaron Mass" is Not a DFD Observable

1. Statement of the (mis-framed) problem

A *DFD scalaron mass* can be estimated in two ways, which disagree by eleven orders of magnitude:

- an *A_s-route*, which fits a Starobinsky scalaron mass to the measured scalar amplitude through the $R+R^2$

amplitude relation $A_s = \frac{1}{24\pi^2}(M/\bar{M}_P)^2 N^2$, giving $M_{A_s} \simeq 2.85 \times 10^{13}\,\mathrm{GeV}$; and

- a *curvature / a_4-route*, which reads a Starobinsky mass from a dimensionless R^2 heat-kernel coefficient through $M^2 = M_P^2/(6\,c_{R^2})$, which with any natural $c_{R^2} = \mathcal{O}(1)/16\pi^2$ returns $M \sim M_P$ (Planckian).

The discrepancy $(M_P/M_{A_s})^2 \approx 1.8 \times 10^{11}$ was treated as an unresolved tension between two estimates of a single quantity. We show it is no such thing. The two numbers measure two *different* objects, and the quantity they were supposed to bracket — a Starobinsky scalaron mass — does not exist in DFD.

2. No native scalaron exists

Proposition SM.1 (No-native-scalaron ⇒ scalaron mass undefined)**.** *The DFD gravitational action contains no curvature-scalar (R^2) term; its only four-derivative term beyond the Gauss–Bonnet total derivative, the a_4 Weyl-squared term, reaches the scalar sector only as the helicity-0 part of the spin-2 pole at $3.6\,\bar{M}_{\rm P}$ for $f_0 = 1$, above the spectral cutoff, and therefore the action propagates no Stelle-type scalar degree of freedom. Consequently there is no field in DFD whose mass can be identified with a Starobinsky scalaron mass, and "the DFD scalaron mass" is* undefined-because-absent *rather than undetermined.*

Proof. Three independent facts close this.

(a) No R^2 term in the action. The DFD gravitational sector is the two-derivative Einstein–Hilbert term arising from the a_2 Seeley–DeWitt coefficient of the spectral action; the propagation analysis records explicitly that DFD carries no R^2 term: the a_4 term of the Dirac trace adds only the Weyl-squared and Gauss–Bonnet invariants (Proposition WS.5); the Weyl-squared term is a spin-2 correction above the cutoff, not a scalar (Sec. V, with $\alpha_T = 0$ identically). A Starobinsky scalaron is the additional propagating scalar polarisation of an $R+R^2$ theory; with no R^2 term there is no such polarisation.

(b) The a_4 coefficient carries no R^2 term. In the Connes spectral action the a_4 heat-kernel coefficient yields the Yang–Mills/Maxwell kinetic term, and for gravity only the Weyl-squared and Gauss–Bonnet invariants (Proposition WS.5) (Ext. Deriv., App. AH; App. O), not an Einstein-frame R^2 term. The historical "curvature/a_4-route gives a Planckian scalaron" read the gauge coefficient as a gravitational R^2 coefficient; that identification is incorrect, and with it the Planckian estimate loses any claim to be "the scalaron mass."

(c) No scalar mode is slow-roll-compatible. By Theorem FK.2 (proof in Ext. Deriv., App. AH series IV–VI; six independent failure modes), no DFD scalar admits an inflaton role with potential mass $m^2 \lesssim 10^{-11} M_P^2$: ψ is FRW-frozen and carries no potential term (exactly massless: the action displayed in Thm. AE.1 is purely kinetic in ψ plus a linear matter coupling); the truncated micro-sector carries no size or shape modulus (App. O); the 57 Kaluza–Klein modes sit at $\sqrt{\alpha}\,M_P$; complex-structure and harmonic-one-form deformations vanish ($h^{2,0} = 0$, $b_1 = 0$); and $k_{\max}$, the Chern–Simons levels are integer-quantised. There is no continuous, light scalar to carry a scalaron mass.

Since a scalaron mass is by definition the mass of the $R+R^2$ scalar, and no such field exists in DFD by (a)–(c), the symbol $M_{\rm scalaron}$ has no DFD referent. □ □

3. Why the two routes disagree by $\sim 10^{11}$

The disagreement is not numerical noise; it is the exact signature of fitting an absent field. Both numbers are reproduced to printed precision in `scalaron_mass_analysis.py`.

a. The A_s-route is the dictionary rung in disguise. The de Sitter dictionary's scale $H_\star$ is fixed by a *rung coincidence*, not a potential. With $f_\chi = \bar{M}_P\alpha^3$ and the Majorana rung $M_R = M_P\alpha^3$ the same α^3 rung, and $M_P = \sqrt{8\pi}\,\bar{M}_P$, the de Sitter dictionary's rung is

$$H_\star \;=\; 8\pi f_\chi \;=\; \sqrt{8\pi}\,M_R \;=\; 2.38 \times 10^{13}\,\mathrm{GeV} \qquad \text{(Thm. AV.13, App. AV)}, \tag{SM1}$$

verified as an identity ($8\pi f_\chi/\sqrt{8\pi}M_R = 1$ to ten digits). Through the de Sitter dictionary $A_s = H_\star^2/(8\pi^2\varepsilon_W\bar{M}_P^2)$ with $\varepsilon_W = \alpha/(4\pi)$, the amplitude collapses to $A_s = 32\pi\alpha^5$ (App. AT); equivalently $\sqrt{A_s} \propto H_\star$. Feeding this A_s back through the Starobinsky amplitude relation therefore returns a number $M_{A_s} = 1.20\,H_\star$, i.e. $\mathcal{O}(1)$ times the rung-locked Hubble (SM1). The "A_s-route scalaron mass" is simply $H_\star$ re-read — the de Sitter dictionary's rung, a DFD quantity, but not a particle mass.

b. The a_4-route defaults to Planckian. An $R+R^2$ scalaron obeys $M^2 = M_P^2/(6\,c_{R^2})$ with c_{R^2} the dimensionless R^2 coefficient. To force $M_{a_4} \to M_{A_s}$ would require $c_{R^2} = M_P^2/(6M_{A_s}^2) \approx 3.1 \times 10^{10}$, larger than the natural heat-kernel value $1/16\pi^2$ by a factor $\sim 4.8 \times 10^{12}$. The single DFD power closest to bridging the gap is $\alpha^{-5} = 4.8 \times 10^{10}$ — and it still misses, *and* there is no R^2 term to host any c_{R^2} in the first place. No DFD heat-kernel number carries α^{-5}; the route defaults to $M \sim M_P$.

c. The gap is the missing α^5. The two routes differ by

$$\left(\frac{M_P}{M_{A_s}}\right)^2 \;=\; 1.84 \times 10^{11} \;=\; 3.8\,\alpha^{-5}, \qquad \log_\alpha\!\left[(M_P/M_{A_s})^2\right] = -5.27. \tag{SM2}$$

The A_s-route carries the factor $A_s = 32\pi\alpha^5$; the a_4-route carries α^0. The eleven-order gap (SM2) is that α^5 power. It is not a tension between two measurements of one mass; it is the distance between two different objects — the de Sitter dictionary's rung $H_\star$ and the Planck scale — artificially compared through a parameter (the scalaron

mass) that neither realises.

4. The actual DFD primordial sector (no scalaron)

DFD states its primordial numbers with topological integers and the α-tower, never a scalaron mass. In $R+R^2$ the scalaron mass is the fundamental input and (n_s, r, A_s) are derived from it; DFD has no mechanism that produces the primordial perturbations (App. FK), and its primordial numbers are these:

$$\begin{aligned} &H_\star = 8\pi f_\chi = 2.38\times10^{13}\,\mathrm{GeV},\\ &n_s = 1-\frac{2}{60} = 0.9667,\\ &r \lesssim 10^{-7}\ \ \text{(B-mode ratio; Cor. SM.4)},\\ &A_s = 32\pi\alpha^5 = 2.08\times10^{-9}. \end{aligned} \tag{SM3}$$

Here $H_\star$ is a rung of the α-tower, not the expansion rate of any DFD stage: a de Sitter stage at $H_\star$ would wash out the χ relic (Theorem SM.3). The tilt is a stated number; the mechanism is open. A_s is one calibrated amplitude, which $32\pi\alpha^5$ matches numerically (App. FK). The dictionary ratio $16\varepsilon_W = 4\alpha/\pi = 9.29\times10^{-3}$ is not an observable; the tensor entry is the bound of Cor. SM.4.

Theorem SM.2 (Primordial optical decoupling)**.** *In native DFD the slow-roll energy read-off $H_{\rm inf} = \pi\bar{M}_P\sqrt{A_s r/2}$ is* undefined. *It presupposes three objects DFD lacks: a slow-roll inflaton potential V (so that $\varepsilon = \frac{1}{2}\bar{M}_P^2(V'/V)^2$ exists; Theorem FK.2), a sustained quasi-de Sitter clock at $H_\star$ (the optical engine can supply one only far below it, Eq. (Q13)), and a Bunch–Davies vacuum on that clock. The fourth ingredient, the tensor normalization $P_t = (2/\pi^2)(H/\bar{M}_P)^2$, does hold: any stage that freezes the tensors at the rate H gives it (Eq. (SM6), with the horizon-exit rate of App. Q 6). With no V there is no ε and no consistency relation $r = 16\varepsilon$. Therefore A_s and the dictionary ratio are not inflaton observables. Written as optical-response amplitudes of the $n = e^\psi$ medium, they read*

$$A_s = P_\psi^{\rm opt}, \qquad r_{\rm opt} = P_{\rm shear}^{\rm opt}/P_\psi^{\rm opt}, \tag{SM4}$$

the scalar optical-density power and its transverse spin-2 (shear) ratio, the TT sector being an independent native mode ($\Box h^{\rm TT}$ =source, on the optical cone; App. AN, App. WS). A shear built from the scalar ψ is a pure gradient (E-mode) pattern at linear order, so this ratio sources no B-modes. The map $(A_s, r) \to H_{\rm inf}$ is a category error, and the de Sitter dictionary $A_s = H_\star^2/(8\pi^2\varepsilon_W\bar{M}_P^2)$ is a removable bridge, *not the origin of A_s. The identification (SM4) is a relabelling, not a source: no DFD stage produces $P_\psi^{\rm opt}$ at the observed level, and a stage that froze ψ and the tensors at a common rate would give $P_t = 16\,P_\psi$ (Eq. (SM9) against Eq. (SM6)), that is $r = 16$. With $r \lesssim 10^{-7}$ (Cor. SM.4), ψ's vacuum fluctuations supply at most 6×10^{-9} of A_s (computed), and A_s is one calibrated amplitude (App. FK). In particular there is no inflaton epoch to randomize the χ flux state, which is what protects the dark relic (Theorem AV.23, App. AV).*

The decoupling is reinforced quantitatively: *even granting* the slow-roll dictionary, the hybrid is self-excluding.

Theorem SM.3 (Inflation-dictionary exclusion)**.** *Suppose, counterfactually, that DFD's $A_s = 32\pi\alpha^5$ and the dictionary ratio $r = 4\alpha/\pi$ were read as standard slow-roll observables. Then the slow-roll energy relation $H_{\rm inf} = \pi\bar{M}_P\sqrt{A_s r/2}$ yields,* exactly,

$$\begin{aligned} A_s r &= 32\pi\alpha^5\cdot\frac{4\alpha}{\pi} = 128\,\alpha^6\\ \Longrightarrow\ H_{\rm inf} &= \pi\bar{M}_P\sqrt{64\alpha^6} = 8\pi\bar{M}_P\alpha^3 = 8\pi f_\chi, \end{aligned} \tag{SM5}$$

since $f_\chi = \bar{M}_P\alpha^3$. The compact-angle stochastic kick per e-fold is then $\delta\theta = H_{\rm inf}/(2\pi f_\chi) = 4$ (this 2π is the Gibbons–Hawking factor, identical in both normalizations of the flux coordinate, Lemma AV.6, App. AV), which saturates the compact period-1 *flux coordinate in a single e-fold, washing the modular vacuum to the uniform measure — at best the finite-space ceiling $\langle Q\rangle_\infty = 0.0853$, hence $\Omega_\chi h^2 = 1.62\,\kappa_{\rm rad}\sqrt{2\pi}\times0.0853 = 0.139$ (the exact relic map of Rem. AV.12), excluded by Planck (0.1200 ± 0.0012, $+16\sigma$). Therefore the slow-roll interpretation of (A_s, r) and the finite-CS χ relic ($\Omega_\chi h^2 = 0.11928$, Theorem AV.23)* cannot both be held. *Retaining the relic forces rejecting the dictionary — which Theorem SM.2 shows is in any case undefined.*

Proof. Eliminating ε from $r = 16\varepsilon$ and $A_s = H^2/(8\pi^2\varepsilon\bar{M}_P^2)$ gives $H^2 = \frac{1}{2}\pi^2\bar{M}_P^2 A_s r$, i.e. $H_{\rm inf} = \pi\bar{M}_P\sqrt{A_s r/2}$; (SM5) is then arithmetic, verified to machine precision ($H_{\rm inf}/8\pi f_\chi = 1$ to sixteen digits). The over-horizon variance of a light spectator on the compact coordinate accumulates as $\langle\theta^2\rangle \simeq N(H_{\rm inf}/2\pi f_\chi)^2$ until it saturates at the uniform value of the period-1 flux coordinate ($\frac{1}{12}$ in the continuum, $\langle Q\rangle_\infty = 0.0853$ on the finite 61-state space); with per-e-fold step $\delta\theta = 4$, four times the full period, saturation is immediate. The numerical identity $H_{\rm inf} = 8\pi f_\chi$ also exposes why the apparent "A_s-route = $H_\star$" coincidence (§SM 4) is *circular*: the dictionary was run forward with this same $H_\star = 8\pi f_\chi$ and $\varepsilon_W = \alpha/4\pi$ to produce A_s, r, so inverting it returns its own input, not an independent measurement of an inflaton scale. □

Corollary SM.4 (True tensor ratio; reclassification of $4\alpha/\pi$)**.** *If the finite-CS χ relic is retained, no de Sitter stage runs at $H_\star$: the primordial expansion is the ordinary expansion read on the arena clock, and any accelerating stage, such as the optical engine (App. Q 6), runs far below $H_\star$. Every species couples minimally to the optical metric $\tilde{g}$ (App. AV), and the TT cone is the optical cone (App. WS), so the tensor modes and the period-1 flux coordinate $\theta = \chi/f_\chi$ obey one mode equation and differ only in their constant normalizations ($\bar{M}_P^2/8$ for h_{ij}, $f_\chi^2/2$ for θ). Whatever the history $a(t)$, $\psi_0(t)$, a stage that*

freezes both leaves

$$P_t(k) = 8\,\frac{f_\chi^2}{\bar{M}_P^2}\,P_\theta(k) = 8\alpha^6 P_\theta(k), \qquad 8\alpha^6 = 1.21\times10^{-12}, \tag{SM6}$$

and χ ($m_\chi = 32$ eV) is light at that freeze-out whenever the tensors matter, since $r \gtrsim 10^{-8}$ needs a freeze-out rate $\gtrsim 10^{10}$ GeV. The frozen variance $\sigma_\theta^2 = \int P_\theta\, d\ln k$ adds to the relic, $\Omega_\chi h^2 = 1.62\,\kappa_{\rm rad}\sqrt{2\pi}\,(Q_{\rm CS} + \sigma_\theta^2)$ (Eq. (AV22)), so Planck's $\Omega_c h^2 = 0.1200\pm0.0012$ allows $\sigma_\theta^2 < 1.9\times10^{-3}$ at two sigma. The modes that count lie between today's horizon and the horizon at χ's oscillation onset ($T_{\rm osc} \simeq 8.7\times10^4$ GeV), 36 e-folds of scale, which any power-law tilt reduces to no fewer than $N_{\rm eff} = 14.7$ effective e-folds (10.7 if the engine froze only the observed scales, $k \lesssim 10\,{\rm Mpc}^{-1}$). Hence

$$r = \frac{P_t}{A_s} < \frac{8\alpha^6\,\sigma^2_{\theta,\max}}{N_{\rm eff}\,A_s}$$

$$\Longrightarrow \quad \boxed{r \lesssim 10^{-7}} \quad (3\times10^{-8} \text{ if scale-invariant}). \tag{SM7}$$

The looser criterion $\sigma_\theta^2 < Q_{\rm CS}$ with $N = 60$ gives the same closed form,

$$r < \frac{\alpha\,Q_{\rm CS}}{4\pi N} = 7.1\times10^{-7} \qquad (N \simeq 60), \tag{SM8}$$

but it tolerates a doubled abundance and an order-unity χ density contrast. The super-horizon part of σ_θ^2 enters the density quadratically, a non-Gaussian isocurvature $\Delta^2_{\rm iso} \simeq 4\ln(k/k_0)\,(P_\theta/Q_{\rm CS})^2$ (k_0 today's horizon scale); at the value (SM8) it would exceed A_s three-million-fold, and Planck's $\beta_{\rm iso} < 0.038$ applied to it gives $r \lesssim 10^{-10}$ (estimate). Hence the number $4\alpha/\pi = 9.3\times10^{-3}$ is not *the observable primordial tensor-to-scalar (B-mode) ratio. It is the de Sitter dictionary's $16\varepsilon_W$. The optical* shear/scalar response *ratio $P^{\rm opt}_{\rm shear}/P^{\rm opt}_\psi$ (SM4) is a property of the $n = e^\psi$ medium, and a shear built from a scalar is a pure gradient (E-mode) pattern at linear order, with no B-mode. The gravitational-wave background the engine can leave is $r \lesssim 10^{-7}$, far below any planned experiment.*

Falsifier SM.5 (Tensor B-modes). The finite-CS branch predicts $r \lesssim 10^{-7}$ (Cor. SM.4). A robust detection of primordial B-modes at any $r \gtrsim 10^{-7}$ falsifies the finite-CS χ relic, whether at $r \simeq 4\alpha/\pi \approx 9\times10^{-3}$, at the $r \approx 4\times10^{-3}$ of an appended inflaton, or at any level LiteBIRD or the ground-based programmes can reach ($\gtrsim 10^{-3}$): by Eq. (SM6) the stage that froze those tensors pushed $\Omega_\chi h^2$ past Planck's two-sigma ceiling, and for $r \gtrsim 10^{-3}$ it kicked χ by more than a full period per e-fold, washing it to the 0.139 ceiling ($+16\sigma$). A null result is the prediction.

Remark SM.6 (Anatomy of 32π inside the de Sitter dictionary). A quantization of the canonical optical scalar shows which part of 32π the dictionary fixes. The high-gradient branch of S_ψ reduces to a canonical massless scalar with $1/(8\pi G) = \bar{M}_P^2$ (exact), whose frozen power with the mode measure fixed *a priori* is

$$P^{\rm bare}_\psi = \frac{H_\star^2}{8\pi^2\bar{M}_P^2} = 8\,\alpha^6 = 1.21\times10^{-12}, \tag{SM9}$$

the power such a scalar would freeze at the rate $H_\star$, with the numerator $8 = 2^3$ fixed and *no* ε_W imported. It is not an amplitude DFD produces: $H_\star$ is not the expansion rate of any DFD stage (Theorem SM.3), and at the relic's cap on a stage that freezes perturbations, $H \simeq 4\times10^{10}$ GeV (Eq. (Q13)), the same formula gives 4.0×10^{-18}, a factor 5.3×10^8 below A_s (computed); reaching A_s would need $H \simeq 9.9\times10^{14}$ GeV. The entire residual to $A_s = 32\pi\alpha^5$ is then *exactly* $32\pi\alpha^5/(8\alpha^6) = 4\pi/\alpha = 1/\varepsilon_W = 1722$: one inverse power of the *coupling* α, times 4π. No solid-angle / horizon-cell integral can produce $1/\alpha$ (geometric measures yield $O(1)$ transcendentals, never a coupling), so the reading $32\pi = (4\pi)(2^3)$ is numerology — the 2^3 is the derived Bunch–Davies numerator but the 4π enters only through the one-loop measure $\varepsilon_W = \alpha/4\pi$. Inside the dictionary the content is thus $A_s = 8\alpha^6\,\varepsilon_W^{-1}$ with the 8 fixed; the missing primitive there is a native mechanism supplying $\varepsilon_W^{-1} = 4\pi/\alpha$ (one power of the coupling), equivalently $H_\star/M_R = \sqrt{8\pi}$. This sharpens — and does not beat — the architecture-only grade; and since no DFD stage freezes perturbations at $H_\star$, the power α^5 is a numerical match as well, and A_s is one calibrated amplitude (App. FK). (A parallel bookkeeping note: the internally reduced-mass tensor $A_t = 64\alpha^6$ gives $r = 2\alpha/\pi$, while the corpus's non-reduced $A_t = 128\alpha^6$ gives $r = 4\alpha/\pi$; since $4\alpha/\pi$ is the dictionary's $16\varepsilon_W$ and not the B-mode ratio (Cor. SM.4), this factor-2 convention does not affect the observable bound $r \lesssim 10^{-7}$.)

Here $H_\star$ is a rung of the α-tower, not the expansion rate of any DFD stage (Theorem SM.3); $n_s = 1 - 2/60$ is a stated number (the mechanism is open); r is bounded by the χ relic independently of ε_W ($r \lesssim 10^{-7}$); and A_s is one calibrated amplitude, which the formula $32\pi\alpha^5$ matches without a derivation of its power or its coefficient (App. AT; App. FK). A Starobinsky scalaron mass would be a redundant fifth quantity over-determined by these four, and it is precisely that redundancy that lets the "two routes" return inconsistent values. The reframe therefore *dissolves* the open entry: there is no fifth number to compute.

5. Status

Status SM.7. The "DFD scalaron mass" is undefined because DFD has no such field. DFD has no native Starobinsky $R + R^2$ scalaron (Prop. SM.1, Thm. FK.2); the symbol $M_{\rm scalaron}$ has no DFD referent. The $\sim 10^{11}$ "disagreement" is explained (SM2) as the missing α^5 between two unrelated scales (the α-tower rung $H_\star$ and M_P), not as a tension between two estimates of one mass.

We make no positive claim of a *forced* scalaron mass (none exists to force), and we manufacture no obstruction: every massive DFD scalar was checked against the slow-

roll ceiling $m \leq 3.86 \times 10^{13}\,\mathrm{GeV}$ with explicit arithmetic (ψ massless with no potential; KK modes $\sim M_P$–$\sqrt{\alpha}M_P$; $\chi = 32.005\,\mathrm{eV}$ cold relic), and none qualifies, in agreement with Thm. FK.2.

Residual. This reframe resolves only the scalaron-mass mislabel. It does *not* resolve the fitted item: the A_s coefficient 32π — equivalently $\varepsilon_W = \alpha/(4\pi)$, equivalently the unfixed ratio $H_\star/M_R = \sqrt{8\pi}$ — remains asserted, not derived (App. AT, App. FK). With no inflaton potential there is no V'/V from which to compute ε_W, so A_s rests on an un-derived normalization; that WdW-closure freedom **stands**. The tensor ratio does not rest on it: the χ relic bounds $r \lesssim 10^{-7}$ directly (Cor. SM.4). What the optical-response reframe (Theorem SM.2) settles is narrower: it shows the de Sitter dictionary does not apply, so the "inflation randomizes χ" objection to the dark relic does not apply (Theorem AV.23). Writing $A_s = P_\psi^{\mathrm{opt}}$ is a relabelling, not a source; A_s is one calibrated amplitude and $32\pi\alpha^5$ a numerical match (App. FK), and $4\alpha/\pi$, the dictionary's $16\varepsilon_W$, predicts no observable. The present appendix neither adds nor removes a DFD result: it converts a mislabelled OPEN/FITTED scalaron-mass tension into a correctly labelled non-question.

Falsifier SM.8. This appendix is falsified, and a scalaron mass becomes a real DFD observable, if any of the following is established:

(i) a curvature-scalar (R^2) term is shown to be *required* by the DFD spectral action, giving a propagating Stelle scalar with a computable mass (the Weyl-squared term of Proposition WS.5 is a spin-2 correction above the cutoff and gives no scalar); or

(ii) a DFD scalar mode is exhibited with potential mass $m^2 \lesssim 10^{-11} M_P^2$ and a flat ($V''/V \ll 1$) direction, contradicting one of the six failure modes of Thm. FK.2; or

(iii) a first-principles derivation fixes $H_\star/M_R = \sqrt{8\pi}$ (equivalently the 32π in A_s) *and* that same construction supplies an independent R^2 scalaron mass that lands on $H_\star$ — which would make the two routes coincide for a real field rather than by the present $\mathcal{O}(1)$ coincidence.

Absent (i)–(iii), the scalaron mass remains undefined-because-absent.

Appendix CE: The Improbability of the Pile: A Combined-Evidence (No-Coincidence) Bound

DFD derives, parameter-free, a set of fundamental numbers that the Standard Model and ΛCDM treat as *free* inputs. This appendix quantifies the combined evidence *after* a full trials-factor audit (Sec. CE 2): every discrete menu the construction could have scanned is enumerated and charged against the hits. Worst case first: under a full across-observable selection charge (the most hostile admissible null) the combined evidence is **not statistically significant** ($p \approx 0.03$–0.5); under hostile menu accounting with no selection charge the four surviving independent hits ($\sin^2\theta_W$, θ_{12}-TM1, the H_0/Λ grammar block, $\Omega_\chi h^2$ at the flux-period value 0.1193, with one binary period-convention bit charged — dimension 16) give ≈ 4.0–4.4σ (conservative windows) to $\approx 5.1\sigma$ (moderate); *conditional* on DFD's forcing theorems as stated — the corpus's pre-registered framing, on the corrected row basis — the conditional tier is ≈ 5.1–5.4σ under the conjunction-product convention; under referee-standard calibrated combination (Fisher/Stouffer) the same rows give 3.6–4.3σ, and 2.5–3.0σ under fully hostile menu pricing — the result is a $\sim\mathbf{4}\sigma$ closed-list no-coincidence signal, *not* $\geq 5\sigma$, a conditional figure that is always to be read against the unconditional tiers just quoted. Separately, and given the stated bracket coefficient $c = 1/13$ (Table CXXVIII), the α-ladder infeasibility theorem (Theorem CE.1) stands: landscape scanning cannot produce the $\alpha^{-1} = 137.036$ match by chance. DFD does not claim 5.5–7.1σ (Sec. CE 2, paragraph on that figure). The combined evidence is a *preponderance / parameter-counting* argument — the same logic by which the Standard Model and BBN were established — not a single falsification-test discriminator; each tier states exactly what it grants; and it is *leading-order* agreement, not precision. The α match itself is *excluded* from the pile rows (α is the selector datum and must not be double-counted); its evidence is booked separately in Theorem CE.1.

1. The surviving forced parameter-free rows

Each row is a quantity the SM/ΛCDM leave as a free parameter (or do not predict at all), derived by DFD from $\{\alpha,\ \mathrm{M7} = \mathbb{CP}^2 \times S^3$ topology$\}$ with *no* fitted continuous coefficient (TM1 is a structural postulate and the $\Omega_\chi h^2$ row rests on stated inputs; App. FK), and *priced* against the menu of alternatives the construction could have scanned (Sec. CE 2). Two candidate rows are excluded (details below): the CKM $\sin 2\beta$ row carries *zero information* (Postulate E.1 is an independent normalization postulate and the CKM anti-theorem blocks apex forcing, App. AO; the companion Wolfenstein integers miss: λ at $\sim 1.8\sigma$, A at ~ 2.5–3.2σ), and the fine a_0 row is excluded because a price of $p = 0.005$ would be 40–70× finer than the ∼10% empirical uncertainty on a_0 permits. Included: the H_0/Λ grammar block (3 hits in

the declared 135-cell scan; look-elsewhere paragraph of App. AU 5) and the $\Omega_\chi h^2$ row (the finite $SU(2)_{60}$ CS-vacuum Casimir abundance, App. AV, Thm. AV.13). The PMNS θ_{12} row is *included* at its pre-registered fair-menu price 1/14: of the 14 standard mixing ansätze in the audit menu, only TM1 hits.

quantity (DFD parameter-free formula)	DFD	measured	agree	p (hostile)	p (cond.)
$\sin^2\theta_W = 3/13$ (weak mixing, tree)	0.2308	0.23129	0.23%	1/12–1/56	0.0045
PMNS $\sin^2\theta_{12}$ (TM1; 1 of 14 ansätze)	0.3184	0.307	3.7%	1/14	0.074
H_0/Λ grammar block ($\rho_{\rm dep} = \frac{3}{8\pi}\alpha^{57}\rho_P$)	2.55 meV	2.24 meV	in band	3/135 ($\times$0.074)	3/135
$\Omega_\chi h^2$ ($SU(2)_{60}$ CS Casimir, flux period)	0.1193	0.1200	0.59%	0.047	0.0117
$n_s = 1 - 2/60$ (spectral index)†	0.9667	0.9649	0.18%	—	—

†Kept for the record but excluded from every tier: $n_s = 1-2/60$ is a stated number; the mechanism is open (App. FK). The companion's $1 - 28.7\alpha/2\pi$ (App. AH, Extended Derivations) is the same number, since $28.7\,\alpha/2\pi = 2/60$ to the printed digits. The combination of Planck, ACT DR6, CMB lensing and DESI gives 0.974 ± 0.003, about 2.4σ above 0.9667. The $\Omega_\chi/\Omega_b = 16/3$ clue ("a clue, not a derivation," App. J, App. TP) enters no tier; the direct $\Omega_\chi h^2$ Casimir row above carries the dark sector. The excluded $\sin 2\beta$ and fine-a_0 rows are documented in the paragraph on the 5.5–7.1σ figure in Sec. CE 2.

2. Trials-Factor Audit and Conditional No-Coincidence Bound

The trials-factor audit (its scripts and outputs are in the reproducibility package) asked the hostile question directly: *if DFD were numerology, how many numbers could it have scanned, and how surprising are the hits once every scan is charged?*

a. The address space. The first instrument is an explicit enumeration of every discrete choice ("address coordinate") the construction could have made. Sixteen dimensions are charged: ten native coordinates from the corpus's own ledger, five hostile enlargements and the period-convention bit. Table CXXIX lists them. The core (numeric) address space is $|\mathcal{A}|_{\rm core} = 64$ (baseline reading) up to 8.01×10^9 (maximal-hostile: the conservative core 185,472 times the convention multiplier 43,200); with sign/axiom-adoption bits, 7.0×10^{22}. The adoption bits pick no value from a numeric menu, so they add no hit-capable ladder, and the bound of Theorem CE.1 does not depend on them. Continuous inputs (α itself, $\hbar$, one scale, the fitted knobs of the fitted-knob ledger) are excluded from $|\mathcal{A}|$ and booked as fits.

b. The α-ladder infeasibility theorem. Within this space, the number of *hit-capable* α ladders — distinct (ladder, convention) assignments that could have produced an α^{-1} match at all — is 10,800.

Theorem CE.1 (α-ladder infeasibility of landscape scanning)**.** *Let a false theory scan the fully enlarged address space of Table CXXIX, containing $n = 10{,}800$ hit-capable ladders. The observed match, with the stated bracket coefficient $c = 1/13$, is $\alpha^{-1}(k_{\rm max}{=}60) = 137.03599985$ against CODATA 2022 137.035999177(21), a residual of 4.9×10^{-9} fractional (0.0049 ppm). The per-ladder probability of a false match* at least as good as the observed 4.9×10^{-9} fractional match *is $p = 5.8\times10^{-7}$ (rung spacing $\simeq 1.7 \times 10^4$ ppm of α at $k = 60$), so the expected number of false matches at least as good as observed, across the whole space, is*

$$\mathbb{E}[\textit{false matches at least as good as observed}] = n\,p \approx 6.3 \times 10^{-3}$$

(0.006–0.04 under fair family inflation; ≤ 0.23 under maximal hostile family and convention inflation — never ≥ 1). The infeasibility margin is $\times$160 (central), $\geq \times$4 (maximal hostile), and $\times$7.8 under the pre-registered $\pm$0.1 ppm falsifier band. Landscape scanning cannot produce the $\alpha^{-1} = 137.036$ match by chance.

Proof sketch. (1) $\alpha^{-1}(k)$ is strictly monotone on $k = 1, \ldots, 2000$ (computed), so any sub-percent window contains at most one integer rung: enlarging *any* address cap adds trials but no new hit-capable addresses beyond those counted (hit-capability lemma). (2) Enumerating the space of Table CXXIX yields $n = 10{,}800$ hit-capable ladders. (3) The per-ladder false-hit probability is the two-sided window-to-step ratio, $p = 2 \times 137.036 \times 4.9 \times 10^{-9}/2.318 = 5.8 \times 10^{-7}$. (4) Linearity of expectation gives $\mathbb{E} = np \approx 6.3 \times 10^{-3}$ (exactly 6.257×10^{-3}); hostile family/bit inflation multiplies $\mathbb{E}$ by at most $\sim$36, topping out at $0.23 < 1$. The wording of the match criterion is essential: under the weaker criterion "within 1 ppm" the expectation is $1.28 \geq 1$ and no theorem survives — the theorem is true only for matches *at least as good as the observed* 4.9×10^{-9} *fractional match*, and it is stated only in that form. □

c. The four-tier null ladder (worst case first). Each tier is a complete, self-consistent null; each grants strictly more than the one above it.

TABLE CXXIX. The 16-dimension address space $\mathcal{A}$ charged by the trials audit (its artifacts are in the reproducibility package). "Cons." = maximal-hostile count. The two convention factors marked ↪ enlarge existing rows (CKM Wolfenstein basis ×3; AU prefactor list $9 \to 30$, i.e. ×10/3) and are folded there, so the convention total multiplies to $43{,}200 = 10 \cdot 12 \cdot 3 \cdot 6 \cdot 2 \cdot 3 \cdot (10/3)$. Core totals: 64 (baseline) → 185,472 (cons.) → 8.01×10^9 (cons. × conventions); with convention/axiom bits 7.0×10^{22}.

# / dimension	baseline	cons.	provenance (one line)
1. det-line charge q_1	$\{3,6\}$	$\{1,3,6\}$	menu $3\mathbb{Z}$ proven (App. F); $q_1 \geq 9$ tail α-hit-dead
2. gauge partition	2 (SM, PS)	7	anomaly audit; $\dim G \leq 28$ kills $SO(10)$, E_6; SM-embedding rivals α-hit-degenerate
3. generation count N_{gen}	$\{1,\ldots,6\}$ at q_1=3	box to cap $k_{\max}$=440	discrete input (App. F); interval saturation proven; cap = evaluated ladder
4. padding n	$\{5,6\}$	$\{5,6\}$	$B-L$ spin-$\mathbb{Z}_4$ six-species list, exactly one Y=0 entry (App. F)
5. assembly rule	1 (det-line chain)	+7 alternates	dichotomy lemma; every alternate ≥ 30% off α (hit-dead)
6. CKM apex branch	2	8	anti-theorem names both branches (App. AO); ×unit convention, ×$\bar{\eta}$; ↪ ×3 Wolfenstein basis (convention)
7. closure grammar	1 (forced)	135	declared 9×15 scan (App. AU 5); ↪ prefactors $9 \to 30$ (convention)
8. sign bits	2	2^3	rank-2 GF(2) theorem; the second bit, the orientation of time, is the smooth beginning, counted in row 9; non-numeric, generate no rival hits
9. axiom-adoption bits	1	2^{40}	the forty adopted statements of Table CXXVII, among them Y.10 and E-transport′; adopt no value from a menu
10. χ primordial state	1	4	natural-preparation menu; $\Omega_\chi h^2 \leq 0.140$ hard finite-k spectral cap for any state
11. surface/topology menu	1	10	hostile enlargement
12. lens-space quotients	1	12	hostile enlargement; menu removed by *proof* (Rem. AB.7: every member has $\pi_1 \neq 1$, excluded by axiom (V7)) — the ×12 is retained here only as a hostile over-count; the repaired axiom bits (V7), (V10), (V4′), (V2) fall under row 9
13. $\dim X$	1	3	hostile enlargement
14. formula grammar	1	6	hostile enlargement
15. 57-subtraction convention	1	2	hostile enlargement
16. χ period convention (flux vs rest-mass)	1	2	period-convention correction (Lemma AV.6); charged against the $\Omega_\chi h^2$ row in both tiers; struck only if a printed three-form sector derives $P = \int_{S^3} C_3$

null (most hostile first)	what it grants	p	Z
full selection charge (M=12–20 booked comparisons, best-k pick)	nothing	≈ 0.03–0.5	n.s.
hostile menus, conservative windows, no selection charge	row independence	$(0.6\text{–}3.7) \times 10^{-5}$	4.0–4.4σ
hostile menus, moderate windows, no selection charge	row independence	$(1.0\text{–}2.0) \times 10^{-7}$	5.1σ
conditional: forcing theorems granted (pre-registered framing, corrected rows)	the derivations	$(0.3\text{–}1.7) \times 10^{-7}$	5.1–5.4σ

Under the full selection charge the conservative product (2.5×10^{-4}) is unremarkable: the *median* product of the three smallest of 20 uniform draws is 3.2×10^{-4}, i.e. a hostile skeptic picking the three best of twenty booked comparisons expects to do this well half the time.

Adopted combined-evidence claim (worst case first)

Under a full across-observable selection charge (the most hostile admissible null), the combined evidence is **not statistically significant** ($p \approx 0.03$–0.5). Under hostile menu accounting with no selection charge, the four surviving independent hits ($\sin^2\theta_W$, θ_{12}-TM1, the H_0/Λ grammar block, $\Omega_\chi h^2$ repriced at the flux-period value

0.1193, $\delta = 0.59\%$, with one binary period-convention bit charged — address dimension 16, struck when the flux period is derived) give ≈ 4.0–4.4σ (conservative windows) to $\approx 5.1\sigma$ (moderate). Conditional on DFD's forcing theorems as stated — the corpus's pre-registered framing, on the corrected row basis — ≈ 5.1–5.4σ under the conjunction-product convention, 3.6–4.3σ calibrated (Fisher/Stouffer, the referee-standard reading). DFD does not claim 5.5–7.1σ: its $\sin 2\beta$ row is zero-information (Postulate E.1 is an independent normalization postulate and the CKM anti-theorem blocks apex forcing; λ and A miss at $\sim 1.8\sigma$ and $\sim 2.5\sigma$), and its a_0 row was priced 40–70× finer than the empirical uncertainty permits. Separately, and given the stated bracket coefficient $c = 1/13$: the α-ladder infeasibility theorem stands — across the fully enlarged address space ($\sim$10,800 hit-capable ladders), the expected number of false α matches *at least as good as the observed* 0.0049 *ppm* is $\sim$0.006 ($\lesssim$ 0.04–0.23 under maximal hostile family and convention inflation; margin ×160 central, $\geq$ ×4 hostile, ×7.8 under the ±0.1 ppm falsifier band) — landscape scanning cannot produce the $\alpha^{-1} = 137.036$ match by chance. Strong evidence, not proof.

Remark CE.2 (Scope: what the audit decides, and what it cannot). Given the stated $c = 1/13$, the audit closes the *landscape-scanning* charge against the α match: no admissible enlargement of the address space makes a false α^{-1} hit likely (Theorem CE.1), and every surviving pile row carries its menu price. What the audit does *not* — and cannot — adjudicate is the *grammar/framing choice* itself: a skeptic who rejects DFD's forcing theorems is charged no trials and simply reads the unconditional tiers, down to non-significance. What refutes or confirms the framing is the pre-registered falsifier set (App. RM 2): Belle-II $|V_{cb}|$ at 0.5% (a confirmed inclusive 42.2×10^{-3} refutes $A = 108\alpha$ outright), FLAG ξ firming at 1.206 (refutes the locked-CKM $\Delta M_s/\Delta M_d$), the Simons Observatory σ_8 determination, the $a_0(z)$ sign (contested: within the survey the rise in low-mass discs at $z < 1.44$ is about 1σ counted galaxy by galaxy and depends on how the molecular gas is added; anchored to SPARC's $z = 0$ value, the galaxy-level bins still exclude a frozen a_0 at about 3σ, and DFD's zero-parameter law fits them on the bound-matter clock; massive discs to $z \simeq 2.5$ show no rise at face value), and $m_\beta = 9.15$ meV.

d. The 5.5–7.1σ figure. DFD does not claim 5.5–7.1σ (that figure gave $P_6 = 1.4 \times 10^{-12} \Rightarrow 7.1\sigma$ and a "referee-proof floor" $3 \times 10^{-8} \Rightarrow 5.5\sigma$; exact recompute $1.65 \times 10^{-12} \Rightarrow 6.96\sigma$ and $4.59 \times 10^{-8} \Rightarrow 5.34\sigma$). Both rest on two invalid rows and are not claimed, nor are the related central/maximal 6.5/6.8σ figures (which retain the invalid a_0 window): (a) the $\sin 2\beta$ row carries zero information — Postulate E.1 (App. AO) is an independent normalization postulate, the CKM anti-theorem blocks apex forcing, and the companion Wolfenstein integers miss (λ at $\sim 1.8\sigma$, A at $\sim$2.5–3.2σ); (b) the a_0 row was priced at $p = 0.005$, 40–70× finer than the $\sim$10% empirical uncertainty on a_0 permits. A re-audit with the current apex slot *strengthens* the zeroing rather than reopening it: under the corpus's own PDG 2024 centrals (App. K) *neither* apex integer is even the nearest point of its own grid — $\bar{\rho}$ measures 21.80α (nearest half-integer 22, not $\frac{43}{2}$) and $\bar{\eta}$ measures 48.28α (nearest integer 48, not 49) — so the apex pair carries menu price $p_{\rm menu} = 1.0$ outright; under the earlier PDG-generation snapshot ($\bar{\rho} = 21.67\alpha$, $\bar{\eta} = 48.62\alpha$) the per-channel prices 0.66×0.76 with the ×2 half-integer charge again give a pair price of 1.0. The four-Wolfenstein-integer input block scores $\chi^2/4\,\mathrm{dof} = 9.7$ ($p = 0.046$) resp. 9.4 ($p = 0.053$) *identically* under both apex slots; the current slot improves five downstream observables but touches none of the zeroing legs, so the four-tier ladder above does not depend on it. All audit artifacts and every number in this subsection are reproducible from the audit scripts and outputs in the reproducibility package.

3. The conditional no-coincidence bound

Proposition CE.3 (Conditional combined-evidence bound)**.** *Grant DFD's forcing theorems as stated (the corpus's pre-registered framing; this is the* conditional *tier of Sec. CE 2, and it is read with the unconditional tiers there). Treat each surviving row as a blind parameter-free formula that had to land within its achieved fractional agreement δ_i of the measured value, in an $O(1)$ prior range ($p_i \simeq \min(1, 2\delta_i)$), except the H_0/Λ block, which is priced by its declared-grammar count:*

$$p\big(\sin^2\theta_W\big) \approx 0.0045, \quad p(\theta_{12}) \approx 0.074,$$
$$p(H_0/\Lambda) = 3/135, \quad p(\Omega_\chi h^2) \approx 0.0117.$$

The four being independent (distinct sectors: electroweak, neutrino mixing, cosmological clock/vacuum, dark sector), the combined conditional probability is

$$P_{\rm cond} = \prod_i p_i \approx 8.7 \times 10^{-8} \implies Z \approx 5.23\sigma$$

(5.10σ with the binary flux-vs-rest-mass period-convention bit of address dimension 16 charged, the recommended booking), rising to 5.44σ if a deliberately weak, measurement-limited a_0 row ($p = 0.3$) is appended (the two-stage-H_0 subline is not used: the early clock's coefficient is measured and the local value rests on the stated two-clock postulate, App. ZS): the conditional band is 5.1–5.4σ, read together with the unconditional tiers (4.0–4.4σ conservative-hostile, 5.1σ moderate-hostile, not significant under the full selection charge).

Why a χ^2 "consistency" statistic is the wrong tool here. The tree-level $\sin^2\theta_W = 3/13$ matches to 0.23%, but the measurement is precise to 0.02%, so a naive pull is $\sim -13\sigma$. That is an *artifact* of comparing a leading-order parameter-free value to a precision measurement: 3/13 is the bare angle, and its radiative relation to the value at M_Z is not computed. The figure of merit is the *fractional agreement* a blind formula achieved (the table), not the measurement error.

4. Scope of the bound

Remark CE.4.

- **It is** a preponderance / no-coincidence argument, stated as a four-tier null ladder with the worst case first (Sec. CE 2): not significant under the full selection charge → 4.0–4.4σ (hostile-conservative) → 5.1σ (hostile-moderate) → 5.1–5.4σ (conditional on the forcing theorems). It is the same kind of evidence that established the Standard Model and BBN, a wall of independent numbers, but with every menu priced.
- **It is not** statistically significant under the most hostile admissible null (full across-observable selection), and it is *not* a single falsification-test discriminator (DFD≠standard, confirmed in isolation). The SN–lensing sign test has been decided against DFD's optical-distance dressing (App. SL); the clock LPI, under systematic audit, awaits a clean verdict.
- **Conditional means conditional:** the 5.1–5.4σ tier holds only if each forcing theorem is granted as stated; a skeptic who rejects the derivations reads the unconditional tiers, down to non-significance.
- **Leading-order:** agreement, not precision; the last digits need higher-order terms.
- **The α match is booked separately** (it is the selector datum, never multiplied into the pile): given the stated $c = 1/13$, landscape scanning cannot fake it (Theorem CE.1). The full CKM matrix contributes zero information here (Postulate E.1) and is excluded.

One-line claim:

Fully hostile: not significant.
Hostile menus: 4.0–4.4σ to 5.1σ.
Conditional on the forcing theorems
(read with those tiers): 5.1–5.4σ.
Given $c = 1/13$: landscape scanning
cannot fake $\alpha^{-1} = 137.036$.
Strong evidence, not proof.

Appendix RM: Falsifiable-Predictions Roadmap: How DFD Is Confirmed or Killed

DFD is a frozen-shape theory: no continuous parameter is fitted to the shape of any observable it predicts, except the baryon density. Its constants are derived or discretely selected, with the discrete inputs enumerated and priced (App. CE, row 9; App. F remarks) and four continuous cosmological calibration constants carried openly: the vacuum coefficient R, the amplitude A_s, the coefficient of $\omega_b h^2$ and ΛCDM's shared astrophysical τ (App. FK, Rem. FK.8). Each prediction below is therefore a sharp target. This appendix consolidates the corpus's scattered falsifiers into one prioritized roadmap. A systematic extraction and critical triage of the full corpus yields **15 measurable bets** (where DFD differs from GR/ΛCDM/SM, or from their rivals, at a testable level: the six live Tier-1 entries, the seven bets of Tier 2 (its three nulls are one-sided targets), and the Belle-II $|V_{cb}|$ and MAQRO coherence tests of §RM 2), resting on **∼17 already-passed numbers** at the grades of Tier 0; further *consistency-checks* (where DFD reproduces the standard value exactly, or the signal sits below any foreseeable sensitivity) are listed separately (§RM 6) and are **not** counted as discriminators.

Retired: this test was run and DFD's sign failed

DES measured the *opposite* (ordinary focusing) sign at 6.0σ (Shah *et al.*, MNRAS **532**, 932, 2024; arXiv:2406.05047 [191]), which by the pre-registered falsifier retires DFD's optical-distance dressing. DFD's core metric is PPN $\gamma = 1$ at first order and predicts the standard $-5/\ln 10$, consistent with that measurement; the surviving discriminator in this channel is the amplitude and scale dependence of the convergence mapping, not the sign. The failed claim is recorded below as it was made, and in App. SL: **Supernova–lensing correlation sign.** DFD's optical-distance dressing $D_L \to D_L\, e^{\Delta\psi_{\rm LOS}}$ forced standardized SN Ia Hubble residuals to correlate *positively* with foreground weak-lensing convergence, $d(\delta\mu)/d\kappa_{\rm fg} \simeq +11$ mag/κ (band $[+7, +28]$), whereas GR/ΛCDM lensing forces a *negative* -2.17 mag/κ — a definite ∼12 mag/κ **sign flip**, not an amplitude argument. The four usable existing datasets (Pantheon+ × DES-Y3, BOSS, DES-SN5YR, Planck CMB-lensing; the DESI subset is too small) lean DFD-positive, joining at +0.7σ under a calibrated rotation null (+0.2σ with the SDSS counter-lean; App. SL) — map-noise limited, not SN-count limited; LSST Y1 (∼650 well-mapped SNe) or Roman (∼160) reach a clean $\geq 3\sigma$ either-way verdict within ∼5 years (App. SL). The sign cannot be faked by ΛCDM; the one confound is correlated foreground dust (a detection-cleanliness requirement, not a sign error).

1. The complete bet list — master table

DFD is a frozen-shape theory awaiting adjudication: its constants are frozen, so every row below is a number the theory cannot move if the data land elsewhere. Grades are the recorded grades; *conditional* stays conditional. Established postdictions and exclusions are listed alongside the live bets for completeness.

- ν_R / $m_\beta = 9.1514$ **meV** — *prediction of the adopted neutrino branch*: ν_R is required on the spin-$\mathbb{Z}_4$ $B-L$ completion (Cor. F.23, App. F) and carried by the neutrino sector on either completion; seesaw $M_R = \alpha^3 M_P$. Experiment: KATRIN-II / Project-8. *Kills:* inverted ordering; any m_β off the comb.

- $a_0(z)$ **running sign** — $\partial_z a_0 > 0$, $a_0(z) = 2\sqrt{\alpha}\, cH(z)$. *Theorem, conditional on Axiom WS.1* (epoch-consistency/anchor-fork, Thm. XIX.3): the no-memory argument makes the anchored branch structurally unavailable, so tracking is forced, and the conditional magnitude bracket $[1.79, 2.83]$ at z=1 collapses to the $H(z)/H_0$ line (1.78 at the measured clock, $\Omega_m \simeq 0.312$); unique vs static MOND. Data, contested: over $0.33 < z < 1.44$ the MUSE–DARK III bins [109], in the analysis published in MNRAS **551**(4), 2026 September 7 [110], give $a_0(z) = A(1+z)^\gamma$ with $\gamma = 0.78 \pm 0.15$ (0.83 ± 0.13 with the SPARC $z \simeq 0$ anchor), excluding a *frozen* a_0 at $\mathbf{5.3}\sigma$ (6.6σ anchored) and $a_0 \propto \sqrt{\rho_m}$ at 4.8σ (on the exponent's error; 4.7σ by likelihood ratio) on the published bin errors; at the measured clock $H(z)$-tracking fits with $\chi^2 = 5.36/3$ and $A = (1.394 \pm 0.032) \times 10^{-10}\ \mathrm{m\,s^{-2}}$, and the measured exponent sits 2.1σ below DFD's $\gamma_E = 1.098$. Refitted galaxy by galaxy from the survey's public products, the rise reproduces ($\gamma = 0.77 \pm 0.21$), but the galaxy-level uncertainty is several times the published bin errors, so within the survey a frozen a_0 lies about 1σ away, while anchored to SPARC's $z = 0$ value the galaxy-level bins still exclude it at about 3σ, with DFD's zero-parameter law fitting on the bound-matter clock; the trend depends on how the molecular gas is added, keeping the rise when tied to the survey's disc masses, about flat when tied to SED-based masses ($\gamma = 0.06 \pm 0.21$; -1.03 to 0.96 at galaxy level), and falling with SED stellar masses ($\gamma = -1.04 \pm 0.22$; -2.32 to -0.32), which exceed the kinematic 95% limit in about a third of the high-z galaxies; above $z \simeq 0.9$ the fitted disc masses sit at the edge of the halo model's prior because the kinematics put them low; DFD's zero-parameter amplitude lies 0.094–0.103 dex below the tracking amplitude on the published census, on either clock, and within 0.02–0.09 dex of it with either fuller census (0.18 dex with both changes together; computed; App. A0Z). Massive discs at $0.6 < z < 2.5$ with molecular gas counted [111] give $a_0 = 1.9$, 1.4 and $1.2 \times 10^{-10}\ \mathrm{m\,s^{-2}}$ at $z \simeq 0.8$, 1.5 and 2.2 against DFD's 1.8, 2.6 and 3.7 on the early clock (1.89, 2.82 and 3.95 on bound-matter clocks): DFD's value is met at $z \simeq 0.8$, and the rise beyond $z \simeq 1.5$ is not seen on that census (within-sample $\gamma = -0.86^{+0.46}_{-0.48}$ on statistical errors). DFD's domain-local screen lowers a_0 in overdense domains, by about 10% for massive $z \simeq 2$ discs at the average environment of their haloes and by 20–34% in the densest known structures, so it would match those discs only in $10\,h^{-1}$Mpc domains about 6 to 11 standard deviations denser than average, which their measured environments do not show (computed on published values; App. ZT). Two further caveats on the survey bins: under a 95% reading of the source's unlabelled bars the exclusions strengthen ($\gtrsim 10\sigma$ and 9.5σ on the exponent's error, 9.2σ by likelihood ratio, exponent family $\gamma = 0.78 \pm 0.08$) but the tracking consistency does not survive ($\chi^2 = 19.9/3$, $p = 1.8 \times 10^{-4}$); and the fitted amplitude is +17% on the canonical SPARC value (0.8σ systematic, $+6.3\sigma$ statistical, $+5.3\sigma$ including the SPARC statistical bar). Experiment: direct molecular-gas masses (CO, [C I] or dust), to 0.1 dex for the $z \simeq 2$ discs; kinematic masses not limited by a halo-model prior, with one pressure-support correction for all samples; per-galaxy analyses with galaxy-level errors, of the MUSE–DARK public products and of the massive discs with $a_0(z)$ imposed, the latter with an independent bound on the χ halo or rotation curves beyond $3R_e$; JWST and ALMA rotation curves at $z \gtrsim 3$, ultimately SKA H I kinematics, where tracking and the survey's linear form diverge (on this corpus's evaluation at the survey's fitted amplitude, $a_0 \simeq 4.20$ against 4.18 at $z = 2$, and 6.32 against 5.77 at $z = 3$, with the measured exponent family at 3.38 and 4.23). *Kills*, on a baryon census that counts molecular gas, with galaxy-level errors and a stated pressure-support correction: measured $\partial_z a_0 \leq 0$; high-z frozen a_0; γ more than 3σ from $\gamma_E = 1.10$. On published calibrations the massive discs meet the second at face value and lean toward the first.

- **Stellar** M/L **ceiling** $\Upsilon_{[3.6]} \leq 0.58$ — *theorem-grade, a_0-free, and testable with data that already exist* (App. AT 7, Falsifier AT.22). DFD's occupation reading carries $\nu \geq 1$ as a theorem; raising the $3.6\,\mu$m disk mass-to-light ratio pushes SPARC's innermost $g_{\rm bar}$ bin below that floor at $\Upsilon_{[3.6]} = 0.5775\,M_\odot/L_\odot$, +0.063 dex above the stellar-population value, which the data currently clear by $\simeq 2.5\sigma$. Read backwards, the same zero-parameter relation *returns* $\Upsilon_{[3.6]} = 0.475$, -0.30σ from the independent SPS value (post-hoc). No acceleration scale, no dark matter and no cosmology enter. Experiment: an improved SPS calibration of the $3.6\,\mu$m disk ratio, or a systematics-controlled re-analysis of SPARC photometry and H I masses. *Kills:* a converged $\Upsilon_{[3.6]} > 0.58\,M_\odot/L_\odot$.

- **Macroscopic coherence** — sustained fringes, *no* objective collapse (forced: no-noise variational action; operator-completion linearity, App. ZU — the mean-field Schrödinger–Newton mechanism is not DFD's, and its frequency shift is the falsifier of the completion). Experiment: MAQRO-class levitated optomechanics,

$10^{9–10}$ amu. *Kills:* mass-scaled collapse at the Diósi–Penrose rate.

- **GW memory** — *consistency test*: DFD's tensor memory equals GR's, linear plus nonlinear (Christodoulou), because the TT action is the full a_2 Einstein–Hilbert term (Derived; Prop. AT.9). Experiment: LISA $10^{5–6} M_\odot$ at z=1, single-event SNR 11–35; ET/CE stacking. *Kills:* a memory measurement consistent with zero where GR predicts a ∼20–27% permanent strain offset (one-sided: a detection does not favour DFD over GR).

- $N_{\rm eff} = 3.044$ **exactly** — integer 3 forced (no dark radiation); decimal inherited from SM physics; one-sided falsifier (the value itself is SM-degenerate). Experiment: the Simons Observatory, with a forecast $\sigma(N_{\rm eff}) \simeq 0.05$–0.07. *Kills:* an $N_{\rm eff}$ that departs from 3.044 by 3σ or more, about 0.15 to 0.2 at that precision.

- **Proton decay: exactly zero** — *if baryon number is violated only by the electroweak anomaly*, which changes it only in steps of three; the sharpest DFD-vs-GUT adjudicator. Experiment: Hyper-K / DUNE. *Kills:* a single-nucleon decay with $\tau_p < 10^{40}$ yr.

- **Millicharged particles: none, at any charge and any mass** — forbidden at theorem level given the adopted gauge group (BSM-exclusion theorem, Extended Derivations, App. AH): a kinetic-mixing millicharge requires a dark-photon $U(1)'$, excluded because a sixth chiral multiplet violates the saturated Spin^c index $\chi(\mathbb{C}P^2, E) = 60$; a bare millicharge is itself a new charged internal mode, excluded by the same saturation; hypercharge-twist integrality (App. F) corroborates conditionally — every admissible twist in the printed menu quantizes electric charge coarsely, leaving no millicharge window. Experiment: accumulator-augmented shielded-Cavendish Gauss-law tests [192, 193], which reach the irreducible cosmic-ray-produced millicharge population on a few-year timescale, beyond accelerator reach at sub-GeV masses; the bet is one-sided (a null is SM-degenerate). *Kills:* any *confirmed* millicharged particle, at any ε and any mass (a bare Gauss-law anomaly alone does not — a photon mass is the source paper's stated alternative reading).

- $|V_{cb}|$ $(A = 108\alpha)$ — $A\lambda^2 = 0.04033$; DFD survives only on $|V_{cb}| \lesssim 41 \times 10^{-3}$; parked on the inclusive/exclusive puzzle; nothing can move ($A \approx 113\alpha$ forbidden by $n_A = 108$). Experiment: Belle-II at 0.5%. *Kills:* inclusive 42.2×10^{-3} confirmed.

- $\Delta M_s/\Delta M_d$ — 33.3 (−5.1%, ∼1.9σ at FLAG $\xi = 1.206(17)$); locked CKM, no rescue knob by construction. Experiment: lattice ξ at 0.5%. *Kills:* firm $\xi = 1.206$ ($\Rightarrow 4\sigma^+$; DFD needs $\xi \approx 1.24$).

- $\sigma_8 \simeq 0.8063$ $(S_8 \simeq 0.822)$ — current measured-clock forward normalization (one inherited A_s coefficient), with $R_8 = 11.848$ Mpc and $\Omega_m \simeq 0.312$ recomputed rather than frozen; KiDS-Legacy consistency is 0.45–0.74σ depending on the printed primary/joint anchor; DES Year 6 lies 2.8σ below (survey errors only). CMB lensing gives $A_{\phi\phi} = 0.9887$ (-0.80σ). Experiment: Simons Observatory and SPT-3G lensing + shear. *Kills:* a converged clustering amplitude incompatible with the frozen-input forward calculation after stated theory uncertainties.

a. Established postdictions (already adjudicated). $H_0^{\rm early} = \sqrt{C}\,\alpha^{57/2}/t_P = 67.52 \pm 0.09$ (EXPONENT DERIVED, COEFFICIENT MEASURED; five concordant CMB-anchored channels; the $C = 1$ value 72.09 is excluded as the early clock and is the bound-matter clock $H_0^{\rm loc} = \alpha^{57/2}/t_P$ of Postulate ZS.11, 0.2σ from the Cepheid-free local mean 71.87 ± 0.96). The dependency-aware current result is $S_8 \simeq 0.822$, consistent with KiDS-Legacy and 2.8σ above DES Year 6 on survey errors only (App. GR). The geometric-vacuum exponent 57, the $\sin^2\theta_W = 3/13$ relation, and $\alpha^{-1} = 137.036$ retain their printed grades; no measured coefficient is promoted to a derivation.

b. Exclusions (not bets). No Born-statistics deviation is predicted (mean-field sourcing is exactly Born-consistent — a null Born test does not discriminate).

2. The four cleanest near-term decisive tests

1. **Belle-II $|V_{cb}|$ at 0.5%:** a confirmed inclusive 42.2×10^{-3} kills $A = 108\alpha$ outright — the integer cannot move.
2. **MAQRO coherence:** DFD sustains fringes exactly where Diósi–Penrose collapses; a mass-scaled collapse signal kills.
3. **Simons Observatory $N_{\rm eff}$:** a departure from 3.044 by 3σ or more, about 0.15 to 0.2 at the forecast $\sigma(N_{\rm eff}) \simeq 0.05$–0.07, kills DFD (one-sided: it can only falsify, since the value is SM-degenerate).
4. **Hyper-K proton decay:** a single-nucleon decay with $\tau_p < 10^{40}$ yr kills DFD while confirming GUTs.

3. Tier 1 — near-term decisive ($\lesssim$5–10 yr, pass/fail)

Nine entries follow. Six are near-term decisive discriminators (each differs measurably from the standard prediction or from its rivals and is resolvable by a named experiment within roughly a decade); entries 1, 3 and 4 are retired as discriminators, and each names the test that remains in its channel:

1. **SN–lensing correlation sign:** ***retired*** — the predicted +11 mag/κ was adjudicated against DFD by the DES 6.0σ detection of the opposite sign (MNRAS **532**, 932, 2024). DFD's core predicts the standard −2.17. What remains testable here is the *amplitude and scale* of the convergence mapping (LSST Y1 / Roman), not the sign.

2. **PMNS solar angle** $\sin^2\theta_{12} = 0.3184$ (TM1) *vs* measured 0.307 ($+0.95\sigma$; JUNO's first result 0.3092 ± 0.0087, 1.1σ) — JUNO reactor/solar; ∼2027–30.

3. **ISW amplitude:** ***retired as a discriminator*** — a ∼30% optical-bias figure has no derivation and is not a DFD prediction; under the adopted Rest-Mass Channel closure ($Q_\chi = 1$, App. GR; no slip, Cor. NL.17) and the real α^{57} vacuum term (App. AU) DFD gives $A_{\rm ISW} = 1.00$, ΛCDM-identical, *vs* Planck 2015 1.00 ± 0.25 [92]; CMB × galaxy cross-correlation with $A_{\rm ISW} < 0.6$ or > 1.5 at 3σ would still kill the closure.

4. $\alpha(z)$ **drift:** ***retired as a Tier-1 discriminator*** — the value $+2.3 \times 10^{-6}$ at z=1 comes from the retired ψ-screen ($\Delta\psi(1) = 0.27$) and is not a DFD prediction; the screen-free route (Eq. (253)) gives $\xi^{\rm res}_{\rm LPI} \times (+2.0 \times 10^{-6})$ with $\xi^{\rm res}_{\rm LPI}$ undetermined, so no definite value is predicted — QSO absorption (ESPRESSO/ELT) remains the test.

5. **CKM apex:** γ=66.31°, $\sin 2\beta$=0.719, an ε_K deficit ∼13% *vs* SM free parameters (tension box: companion volume, App. AH) — LHCb / Belle II; ∼2027–30.

6. **Th-229 nuclear-clock modulation (extended strong channel; null under the minimal action, Thm. XI.2):** a perihelion-locked annual signal, 26 Hz–$\mathcal{O}$(1 kHz) *vs* GR/SM null — dedicated Th-229 clock; near-term.

7. **RAR intrinsic-scatter floor:** $\lesssim$0.037 dex (halo-shape floor alone 0.013–0.025; a_0 a fixed constant; if the χ halos inside galaxies are cored, as the rotation curves require under the floor law, App. AV) *vs* untuned 0.06–0.08 — SPARC-class rotation curves.

8. **Lepton-flavor universality:** $R_K = 1$ up to Standard-Model corrections *vs* BSM $R_K \neq 1$ — LHCb Run 4; ∼2027–30.

9. **Local wide binaries:** $\gamma = 1$ exactly near the Sun, with no orientation term of either parity (environmental confinement, App. NL), *vs* MOND's $\gamma \simeq 1.4$ and 6.9% even modulation at 10^4 AU; *Gaia* DR4; near-term. *Kills:* a confirmed boost of the Chae type in local pairs.

4. Tier 2 — future decisive (next-generation instruments)

The following 10 await more capable facilities; the χ photon line, the primordial B-modes and the linear-growth statement are nulls that a detection would falsify, and the other seven are bets: $N_{\rm eff} = 3.044$ *with structurally forbidden dark radiation* (Simons Observatory: a $\Delta N_{\rm eff} > 0$ detected at 3σ, about 0.15 to 0.2 at its forecast precision, kills DFD while ΛCDM absorbs it); *no photon line from* χ: χ has no photon coupling ($E = 0$; App. AV), so a dark-matter photon line at 16.0 eV (77.5 nm) or axion-like signal at 32.005 eV (38.74 nm), at any strength, falsifies it; *maximal* $\theta_{23} = \pi/4$, $\delta_{CP} = -\pi/2$ (DUNE/Hyper-K); *normal neutrino ordering* + $\Sigma m_\nu = 61.5$ meV (Simons Observatory+DESI; inverted ordering kills DFD); *zero single-nucleon proton decay* (if baryon number is violated only by the electroweak anomaly); *a step in the dynamics of wide binaries across* $R \simeq 13$–16 *kpc* (environmental confinement; halo pairs; the outer-halo globular clusters already contradict the boost beyond it, App. NL); $a_0(z) = 2\sqrt{\alpha}\, cH(z)$ *epoch evolution*; *one universe, two clocks* (Postulate ZS.11; Falsifier ZS.14): bright sirens and mass-sheet-robust time delays at 72.1, not 67.5; early-ruler and local ladders that do not converge with distance; the absolute a_0 scale at 1.1966×10^{-10} m s^{-2} on distances computed with $H_0^{\rm loc}$; no star established older than 12.92 Gyr in laboratory units at better than 3σ (one programme's globular-cluster ages of 13.39 and 13.61 Gyr sit 1.8–2.0σ above it, and the ages of the universe of 13.5–13.8 Gyr that the same programme infers with a ΛCDM formation delay sit 2.1–2.6σ above it, with statistical and systematic errors in quadrature); *no primordial B-modes*, $r \lesssim 10^{-7}$ (LiteBIRD and the ground-based B-mode programmes: any detected primordial tensor signal washes out the χ relic, App. SM); plus the cosmological-growth statement of the adopted Rest-Mass Channel: with the polarization confined to bound systems, linear growth follows $Q_\chi = 1$ and σ_8 rises by only 0.1–0.5% (App. GR), so kSZ and $f\sigma_8$ carry no DFD excess or suppression on linear scales (§RM 6).

5. Tier 0 — the already-passed bedrock (would have killed DFD; did not)

Numbers DFD already matches, each at the grade stated in its entry and in App. FK (absolute light-fermion masses are fit-assisted and excluded):

- $\alpha^{-1} = 137.0360$ (microsector closed form, exact under two stated choices): 21 ppm from the integers alone; the bracket coefficient is open.
- $\sin^2\theta_W = 3/13 = 0.2308$: 0.23%.
- Higgs vev $v = M_P\, \alpha^8 \sqrt{2\pi} = 246.09$ GeV: 0.05%, with the exponent derived and the prefactor fitted.
- $m_t = (1-\alpha)v/\sqrt{2} = 172.74$ GeV (0.52σ); $m_c = \alpha v/\sqrt{2} = 1.270$ GeV (within 0.25%).
- Forced ratio $m_\tau/m_c = \sqrt{2}$: +1.1%.
- MOND scale $a_0 = 2\sqrt{\alpha}\, cH_0^{\rm loc} = 2\alpha^{29}\sqrt{c^7/G\hbar} = 1.1966 \times 10^{-10}$ on bound-matter clocks (Postulate ZS.11): within SPARC's systematic-dominated error.
- $H_0^{\rm early} = \sqrt{C}\, \alpha^{57/2}/t_P$ (67.54 at $C = 0.87784$; 67.52 ± 0.09 across channels): exponent forced, vacuum coefficient R measured (today's early-clock value C); on bound-matter clocks $C = 1$ and $H_0^{\rm loc} = \alpha^{57/2}/t_P = 72.09$, 0.2σ from the Cepheid-free local mean 71.87 ± 0.96, conditional on Postulate ZS.11.

- $\sin^2\theta_{13} = 3\alpha = 0.0219$: 0.1σ. Neutrino splittings: $\chi^2 = 0.025$ vs NuFIT.
- CKM $\sin 2\beta = 0.719$ (1.0σ), $\lambda = 31\alpha = 0.2262$ (0.54%); $B_s \to \mu\mu = 3.40 \times 10^{-9}$ (0.2σ).
- Strong-CP $\bar{\theta} = 0$ at tree level with $\theta_{\rm YM} = 0$ fixed by the spectral action given that nothing is added to it for the gauge fields, loop-bounded below 10^{-16} (no axion); nEDM bound satisfied.
- CMB-lensing $A_{\phi\phi} = 0.9887$ at the current background (-0.80σ); the $A_L = 1.0542$, $\sigma_8 = 0.820$ row belongs to the one-clock $C = 1$ background.
- $c_T = c$ (GW170817); proton $\tau_p > 10^{34}$ yr (Super-K).
- Kennedy–Thorndike null: cavity/atom ratio boost-independent at fixed ψ (Cor. XI.3); remainders $\lesssim 10^{-22}$ against the measured $\beta_{\rm RMS} - \alpha_{\rm RMS} - 1 = -1.7(4.0) \times 10^{-8}$ [61].

6. Separation and open cracks

Consistency-checks (not discriminators). The following reproduce the standard value exactly, or lie below foreseeable sensitivity, and a null result does *not* distinguish DFD: PPN $\gamma = \beta = 1$ and all classic 1PN tests (GR-identical by construction); BH entropy $S = A/4 = S_{\rm GR}$ and $T_{\rm DFD} = T_H$, from the event horizon's surface gravity $\kappa = c^4/4GM$ (a magnified-area entropy is not a DFD prediction); with the parent strain's σ kept, the strong-field sector: black-hole horizons, shadows and ringdowns, neutron-star masses, the second post-Newtonian dynamics and the absence of echoes, all general relativity's (App. WS; for spinning holes argued beyond first order in the spin); GW speed $c_T = c_\gamma$ exactly (kills TeVeS, does not favour DFD over GR); zero spatial curvature, with no dark curvature either (App. WS, Rem. WS.7), flat ΛCDM's value, which a detected curvature of either kind falsifies; the $N_{\rm DW} = 1$ wall relic and $\beta_{\rm iso} \simeq 0$ (one-sided/structural, observationally null); the $0\nu\beta\beta$ effective-mass comb (all teeth 1–2 orders below LEGEND/nEXO); charged LFV (null, ≥31 orders below limits); the neutron EDM (coincides with the SM CKM background); the Oort spike (a Newtonian Sun under environmental confinement; GR-identical, but excluding MOND); the Local Group's matter barycentre, which moves with the cold local Hubble flow (ΛCDM-identical; a drift of 15 km/s or more along the Milky Way–M31 line falsifies the momentum-conserving energy); and the clock-normalized hierarchy $\rho_\Lambda/\rho_{\rm Pl} = \Omega_\Lambda(3/8\pi)C\alpha^{57} \simeq 1.14 \times 10^{-123}$ (DFD *derives* the 10^{-123} exponent parameter-free, microsector-scoped with the $O(1)$ prefactor via the clock dictionary (Rems. AU.3, AP.6) — a parsimony gain, but the *value* matches the observed Λ, so it is not a measurable difference). The $\dot{G}/G$ channel is resolved by the coupling/state-function distinction (Thm. XIX.3, Cor. XIX.4, both conditional on Axiom WS.1): G is an epoch-independent action coupling, $\dot{G} = 0$ exactly — GR-degenerate, passing lunar-laser-ranging trivially, hence still not a discriminator — while the discriminating partner prediction $\dot{a}_0 = 2\sqrt{\alpha}\, c\, \dot{H} \neq 0$ lives in the $a_0(z)$ entry above. Gravitational-wave memory is also a consistency-check: DFD's tensor memory equals GR's (Prop. AT.9), so a LISA/ET detection at the GR level does not favour DFD over GR, while a memory null where GR predicts ∼27% of the edge-on strain peak falsifies DFD.

Open cracks, and two resolved by axiom. The χ-abundance is forced-amplitude/stated-convention (production; App. AV Step 5b): the finite $SU(2)_{60}$ CS-vacuum Casimir expectation gives $\Omega_\chi h^2 = 0.1192806$ (-0.60σ); the amplitude is forced (Casimir; measure conditional on the asserted premise P4′ (Lemma AV.27); $k(k+2)$ from χ's derived $\mathbb{Z}_2$ + Sugawara), the only non-DFD input being the standard cosmological relic-redshift. The operator is proven and the density is not fitted, but the $\mathbb{Z}_2$/Sugawara edge, the relic-map normalization, the count 158 and the flux-period identification remain stated premises. The $Q = G_{\rm eff}/G = 1$ linear-clustering (third-peak, lensing) is *provably* not derivable from the single-W action ("structured ⇔ gradient ⇔ screened" is a theorem; App. GR), so DFD *adopts* the minimal *Rest-Mass Channel* postulate (a second μ=1 rest-mass Poisson operator; cost: +1 gravitational axiom; matter moves under a momentum-conserving energy, and χ falls like the baryons wherever it fills the μ-law's demand), and given it $Q_\chi = 1$ holds and the clustering is consistent. That postulate carries a testable *cluster-vs-galaxy prediction*: clusters need χ, at 0.84 ± 0.12 of the cosmic mix when it adds its Newtonian pull (under the adopted floor composition the need is 1.28–1.51, and the derived abundance under ΛCDM-like assembly gives 1.21 ± 0.05, at estimate grade), while baryon-dominated disks show little dark mass beyond the μ-law (App. GR), distinct from both ΛCDM and pure MOND. The MOND response of a subsystem inside a strong host field is closed by a second adopted axiom, environmental confinement (+1 gravitational axiom), which the Bose statistics provably cannot supply (App. NL). One further crack is open. χ composes with the μ-law by the floor composition, adopted in energy form; under that energy χ halos assemble as in ΛCDM (estimate), and the rotation curves then need cored inner halos, whose origin is open, and in discs above about $10^{11}\, M_\odot$ of baryons lighter halos than abundance matching gives; in spherical simulations of dwarf and low-surface-brightness galaxies, feedback from stars does not make these cores under that energy (App. AV). The photon coefficient of χ is zero, $E = 0$ (App. AV). The growth statement of Tier 2 follows from the same structure. The abundance crack and the results above stand independently.

DFD makes 15 sharp, falsifiable bets (the principal ones, with the numbers that kill, are consolidated in App. RM 1) that differ from the standard models, or from their rivals, in ways telescopes and labs can check. *One further bet has been settled against DFD:* the supernova–lensing *sign* flip was adjudicated by DES at 6.0σ in favour of the ordinary

focusing sign (MNRAS **532**, 932, 2024), retiring DFD's optical-distance dressing while leaving its core metric — which predicts that same standard sign — intact. The remaining bets stand as printed.

Appendix WS: Wave-Sector Closure: Elliptic Scalar, Derived Gravitomagnetism, $\delta_{\rm rad} = 0$, and Ringdown

This appendix derives three elements of the wave sector: (i) the radiative status of the scalar sector, $\delta_{\rm rad} = 0$; (ii) the gravitomagnetic sector g_{0i}, beyond PPN-template matching; (iii) the relation between DFD's physical coordinates and the standard PPN gauge. Two named inputs carry the result, Axiom WS.1 and Proposition WS.5. It then states the ringdown and echo items: with the scalar-longitudinal piece σ of the parent strain kept, the remnant of a merger is a Kerr hole (argued beyond first order in the spin), it rings as Kerr, and there are no echoes (Subsec. WS 5).

1. Axiom E (Elliptic Constraint Reading)

Axiom WS.1 (E: the scalar sector is an instantaneous constraint)**.** *In the preferred foliation (absolute time t), the scalar sector obeys the elliptic AQUAL constraint at each instant,*

$$\nabla\cdot\big[\mu(|\nabla\psi|/a_\star)\,\nabla\psi\big] \;=\; -\frac{16\pi G}{c^4}\,\mathcal{S}[\mathit{matter};\psi](t), \quad \text{(WS1)}$$

with no independent temporal kinetic term in the local (non-cosmological) sector; through first post-Newtonian order the source $\mathcal{S}$ is the matter source of Lemma WS.3. The absence of a temporal kinetic term, which makes the action differ from general relativity's by the $(K-\bar{K})^2$ term of Proposition WS.6, holds, once baryons have decoupled from the photons, on the whole of every slice on which the μ-law acts somewhere; while no baryons are bound anywhere, and at least until baryons decouple from the photons, the scalar sector carries instead the Einstein–Hilbert term's own temporal term, and the axiom selects its slicing (Remark WS.7). The one-field form holds for systems without χ; inside bound systems that contain χ the main text's adopted energy of the two Newtonian fields governs. Wherever the corpus writes a c-speed d'Alembertian for ψ, that form is the numerical hyperbolic-relaxation of Eq. (WS1)*, not a claim that ψ radiates (the channel-scope remark of App. AT). The temporal functional $K(\Delta)$ of App. Q remains the* cosmological *sector: Δ is defined against the FRW screen flow and governs homogeneous-deviation (dust-branch) physics only.*

For static matter in the $\mu \to 1$ band the source is the main text's optical-source law to all orders: on the static matter metric, with the divergence taken in the unimodular spatial part $(e^h)_{ij}$, that law is the time-time component of the trace-reversed Einstein equation (computed), and with the parent strain's σ kept, σ obeys the traceless part of the Einstein equation and the Hamiltonian constraint follows (Proposition WS.6), so static stars obey the equations of general relativity. Beyond first order the source of moving or rotating matter also contains the energy of the gravitational field, among it the

gravitomagnetic term $\partial_i(g_{0j}F_{ij})$ with $F_{ij}=\partial_i g_{0j}-\partial_j g_{0i}$, and terms in $\partial_t\psi$ (computed); with the parent strain's σ kept the source is that of the maximal-slicing lapse equation and the slicing is maximal (Proposition WS.6(b),(e)). Loop-induced higher-derivative terms of the matter fields enter the constraint only through the renormalized source $\langle\hat{\varepsilon}+3\hat{P}\rangle_{\rm ren}$ of the main text's optical-source theorem, as a relative correction of order $(k/\bar{M}_{\rm P})^2$; written as terms in ψ itself, their R^2 part would supply, wherever the $(K-\bar{K})^2$ term acts, the only time derivatives and give Eq. (WS1) a growing root at a rate of order $(\bar{M}_{\rm P}k)^{1/2}$ (computed).

Remark WS.2 (Why the elliptic reading is forced). A no-go is proved: if the scalar sector is hyperbolic, the far-zone breathing flux of a compact binary is $\delta_{\rm rad}=0.193$ for PSR B1913+16 (monopole 0.015, cross 0.010, quadrupole+trace 0.168; pipeline validated against Peters–Mathews to 5 digits), excluded at $\sim 100\sigma$; and no reference-flow choice in the $K(\Delta)$ sector repairs this without shifting the 1PN periastron advance by $\delta\dot{\omega}/\dot{\omega}\simeq+0.064$ (direct orbit integration), which breaks the measured mass triangle at $\sim 90\sigma$. The elliptic reading is the only structure specified in the corpus that survives both tests. Instantaneity in the preferred frame is thereby a *prediction carrier*: it is exactly why the scalar channel is radiation-free, while all radiative physics lives in the (hyperbolic, luminal) TT sector. Laplace-aberration safety is supplied by Theorem WS.9 below: matching EIH dynamics through 1PN is precisely the statement that no anomalous aberration effects appear at current sensitivity.

2. The verified 1PN source and the Standard-Gauge Coincidence Lemma

Lemma WS.3 (1PN source, point-particle form; machine-verified)**.** *Direct variation of* $S_{\rm pp}=-mc^2\int dt\,\sqrt{e^{-\psi}-e^{\psi}v^2/c^2}$ *gives the convention-free 1PN source*

$$\mathcal{S}\;=\;\sum_a\frac{m_ac^2}{2}\Big[1-\tfrac{1}{2}\psi_a+\tfrac{3}{2}\,\frac{v_a^2}{c^2}\Big]\,\delta^3(\mathbf{x}-\mathbf{x}_a),\qquad\text{(WS2)}$$

(ψ_a: external field at a; self-terms renormalized). The fluid form is $\mathcal{S}=\frac{1}{2}\rho c^2[1+\Pi/c^2+2v^2/c^2+2U/c^2+3p/\rho c^2]$ *(sympy-verified); the two agree through the proper-volume factor* $e^{-3\psi/2}$.

Lemma WS.4 (Standard-Gauge Coincidence)**.** *Solving Eq. (WS1) with source (WS2) at 1PN ($\mu\to 1$) gives* $\psi=2U/c^2+\psi_2/c^4$ *with*

$$\begin{aligned}\psi_2\;&=\;4\Phi_1+4\Phi_2+2\Phi_3+6\Phi_4\\ &\text{(no }\ddot{\chi}\text{ term: the solve is instantaneous)},\end{aligned}\qquad\text{(WS3)}$$

so that

$$g_{00}=-e^{-\psi}=-1+\frac{2U}{c^2}+\frac{4\Phi_1+4\Phi_2+2\Phi_3+6\Phi_4-2U^2}{c^4},\qquad\text{(WS4)}$$

$$g_{ij}=e^{+\psi}\delta_{ij}=\Big(1+\frac{2U}{c^2}\Big)\delta_{ij},\qquad\text{(WS5)}$$

which is exactly *the standard-PPN-gauge 1PN metric of general relativity at $\gamma=\beta=1$ with all other parameters zero (no $\mathcal{A}$ term, no Whitehead term).* ***DFD's physical coordinates — the diagonal optical dictionary plus absolute time — coincide with the 1PN standard PPN gauge, with no transformation and no residue.***

Proof. Green-function solution of $\nabla^2\psi_2=-8\pi G\rho[\Pi+2v^2+2U+3p/\rho]$ term by term against $\nabla^2\Phi_k=-4\pi G$ (densities). The $\ddot{\chi}$ term of the hyperbolic treatment arises only from iterating $c^{-2}\partial_t^2\psi$; Axiom E removes it at the root. The Whitehead potential cannot arise: the field equation's only nonlinearity is the *local, multiplicative* e^{ψ} in the source, and a local source under the flat Green function never generates the non-local double integral Φ_W (Whitehead Locality Lemma). $\beta=1$ is exact because ψ_2 contains no U^2 piece; $-2U^2$ comes solely from $e^{-\psi}=1-\psi+\psi^2/2-\cdots$. □

3. Vector-Sector Completion: g_{0i} derived, not matched

The Einstein–Hilbert term that the TT sector carries:

Proposition WS.5 (Spectral Einstein–Hilbert reduction)**.** *Let F be the truncated microsector, with Hilbert space of dimension N ($N=60$) and internal Dirac operator D_F, and let $D=D_M\otimes 1+\gamma_5\otimes D_F$ on $M_4\times F$. For a plateau cutoff f, constant near the origin, with every internal mass inside the plateau (with G fixed by Eq. (WS7)) the top internal mass $\sqrt{\alpha}\,M_P$ sits at $m^2/\Lambda^2=\alpha N f_2/(3\pi+f_0\,\mathrm{Tr}D_F^2/M_P^2)$, at most $0.046\,f_2$, so $f_2/u_0\lesssim 21.5$ suffices for a plateau on $[0,u_0]$; for a smooth cutoff with $f_2\simeq 3f_0$ and $u_0=1$ that gives $f_0\lesssim 7$, and the internal masses of the near-arithmetic lattice relax it to $f_0\lesssim 8.6$; computed),*

$$\begin{aligned}&\mathrm{Tr}\,f\Big(\frac{D^2}{\Lambda^2}\Big)\\ &=\frac{Nf_4\Lambda^4-f_2\Lambda^2\,\mathrm{Tr}D_F^2+\frac{1}{2}f_0\,\mathrm{Tr}D_F^4}{4\pi^2}\int\sqrt{g}\,d^4x\\ &-\frac{Nf_2\Lambda^2-f_0\,\mathrm{Tr}D_F^2}{48\pi^2}\int\sqrt{g}\,R\,d^4x\\ &+\frac{f_0N}{5760\pi^2}\int\sqrt{g}\,\big(11E_4-18\,C_{\mu\nu\rho\sigma}C^{\mu\nu\rho\sigma}\big)d^4x\\ &+S_{\rm gauge}+S_{\rm scalar},\end{aligned}\qquad\text{(WS6)}$$

with $f_4 = \int_0^\infty u f\, du$, $f_2 = \int_0^\infty f\, du$, $f_0 = f(0)$ *and* E_4 *the Gauss–Bonnet density. No local term beyond* a_4 *appears; this is an asymptotic statement, with a remainder that falls faster than any power of* Λ *for curvatures and momenta well below* Λ. *The* a_2 *term is the Einstein–Hilbert functional of the four-dimensional metric, with*

$$\frac{1}{16\pi G} = \frac{N f_2 \Lambda^2 - f_0\, \mathrm{Tr} D_F^2}{48\pi^2}. \qquad \text{(WS7)}$$

The result rests on two premises. (G1) *The Einstein–Hilbert term acts on the scalar field only through the rest-mass channel of App. GR, that is, on the uniform background and on the rest-mass perturbations, where it replaces the printed Newtonian term rather than adding to it; the* μ*-law acts outside it. The printed scalar action is therefore the* μ*-bent scalar part of the Einstein–Hilbert term: one term, not the Einstein–Hilbert term plus a second one. G1 is not independent: its one term is the static-energy identity of Proposition WS.6 with one* G*, and its partition is the Rest-Mass Channel.* (G2) *Gravity's spectral trace uses the four-dimensional Dirac operator* D *above, while the closed form for* α *uses its own trace on the internal space (the regularization rule of the main text's convention-locked* α*); these are two different traces.*

Proof sketch. Since $D^2 = D_M^2 \otimes 1 + 1 \otimes D_F^2$, the trace is a sum over the internal eigenvalues λ_i^2 of four-dimensional heat-kernel expansions with shifted moments; on the plateau $f_2(x) = f_2 - f_0 x$, $f_4(x) = f_4 - x f_2 + \frac{1}{2} f_0 x^2$ and $f_0(x) = f_0$ exactly, and every higher coefficient carries a derivative of f at the origin, which vanishes. The truncation is exact in the four-dimensional sense on $M_4 \times F$; on a continuous internal space of odd dimension it would not be. The Lichnerowicz formula gives $E = -R/4$, so $\mathrm{tr}(E + R/6) = -R/3$ per internal mode, which fixes the attractive sign of G (an operator with $E = 0$ would give the opposite sign), and the a_4 coefficient of the Dirac operator contains no R^2 term. Equation (WS6) reproduces the exact Dirac spectral sums on the round four-sphere and on $S^2 \times S^2$ times a 60-mode internal space, with a remainder that falls faster than any power of Λ (computed); its normalization agrees with that of Chamseddine and Connes, the factor between $48\pi^2$ and their $24\pi^2$ being the moment convention, with their mass trace equal to half of $\mathrm{Tr} D_F^2$. □

The massless zero mode $h_{\mu\nu}(x)$ is the four-dimensional metric itself, so its quadratic part is the linearized Einstein–Hilbert action used at 1PN below and its cubic vertex carries the tensor memory (App. AT). In strong fields, where $\mu \to 1$, the Einstein–Hilbert term governs the whole metric: with the parent strain's σ kept, matter, light and the tensor field share it, and the static exterior is the Schwarzschild metric in DFD's coordinates. The tensor and vector sectors, and the scalar sector at $\mu \to 1$ (Lemma WS.4), share one G. Its value is not predicted: it fixes $N f_2 \Lambda^2 - f_0\, \mathrm{Tr} D_F^2$ in Planck units, one scale measurement, as in general relativity, and the internal masses, 57 modes at $\sqrt{\alpha}\, M_P$ in the printed spectrum, shift $1/G$ by about 4%. The Weyl-squared term implies an extra spin-2 pole at $m_2 = \Lambda\sqrt{10 f_2/3 f_0} \simeq 3.6\, \bar{M}_\mathrm{P}$ for $N = 60$ and $f_0 = 1$, above the cutoff, a tachyonic ghost under the continuation that gives $G > 0$; it moves no observable ($(k/m_2)^2 \sim 10^{-81}$ in the LIGO band), and the action stops at a_4 only below the cutoff. The a_4 gravitational term does not enter the Friedmann law: the Weyl term vanishes on the Friedmann background and the Gauss–Bonnet term is a total derivative. The displayed a_0 term is Planckian: on the near-arithmetic lattice of the internal spectrum, $m_n^2 = (n-3)\, \alpha M_P^2/57$ ($n = 4, \ldots, 60$), its term $-f_2 \Lambda^2 \mathrm{Tr} D_F^2/4\pi^2$ alone is $-(0.532 + 0.012 f_0)\, \bar{M}_\mathrm{P}^4$, and $-(1.045 + 0.046 f_0)\, \bar{M}_\mathrm{P}^4$ with all 57 modes at $\sqrt{\alpha}\, M_P$ (computed). The dark-energy density is the α^{57} microsector term of App. AU with its coefficient R measured, and reading it as the α^{57}-suppressed a_0 term is a conjecture, which needs the whole D_F-dependent vacuum suppressed with it. On the truncated microsector there are no Kaluza–Klein modes; on a continuous K the Lichnerowicz count ($b_1(\mathbb{C}P^2) = b_1(S^3) = 0$, both factors Einstein-rigid) leaves no extra massless spin-2 mode.

The spectral action and its Einstein–Hilbert term are the construction of Chamseddine and Connes (Phys. Rev. Lett. **77**, 4868 (1996); Commun. Math. Phys. **186**, 731 (1997)), and the idea that gravity is induced by the quantum fields of matter is Sakharov's (Dokl. Akad. Nauk SSSR **177**, 70 (1967); Sov. Phys. Dokl. **12**, 1040 (1968)). What DFD adds is this: its own 60-mode finite space, the structure that fixes α, supplies the finite geometry of that construction; the Friedmann law and the nucleosynthesis check follow (the optical-time Friedmann law of the main text); the scalar sector and the Einstein–Hilbert term are one term (premise G1); and the clock constant is independent of G (App. AP).

Proposition WS.6 (Einstein–Hilbert completion of the parent strain)**.** *Let the physical metric carry the full parent strain of the main text's gravitational-wave section: lapse* $N = e^{-\psi/2}$*, a shift, and spatial metric* $g_{ij} = e^{\psi}(e^h)_{ij}$ *with* h_{ij} *the traceless part of the parent strain (*h_{ij}^{TT}*, the vector piece and the scalar-longitudinal piece* σ*), so that* $N^2(\det g_{ij})^{1/3} = 1$ *(the lock); let its dynamics be the Einstein–Hilbert term of Proposition WS.5, with no temporal kinetic term for* ψ *(Axiom WS.1), in DFD's absolute time, in the rest-mass sector, where* $\mu \to 1$. *Then, for isolated systems:*

(a) the lock leaves only the spatial diffeomorphisms that preserve the arena's volume form; they remove the vector piece but not σ*, so* σ *is physical, and its equation, from the traceless part of the Einstein equation, is not a gauge condition;*

(b) every solution has vanishing mean curvature of DFD's slices, $K = 0$*: the absolute time is the maximal slicing;*

(c) general relativity's Hamiltonian constraint holds, and the solutions are exactly those of general rela-

tivity in maximal slicing, written in the coordinates of the lock;

(d) static stars obey the Tolman–Oppenheimer–Volkoff equations; the exterior of a static star is the Schwarzschild metric, $e^{-\psi} = 1 - 2GM/(c^2 R)$ at areal radius R, with $\psi = 2GM/(c^2 r) - \frac{4}{3}(GM/c^2 r)^3 + \cdots$ in the arena radius r; a stationary rotating exterior is Kerr's at first order in the spin, and a spinning black hole's is Kerr's; through second post-Newtonian order the two-body dynamics is general relativity's; and for compact bodies inertial and gravitational mass agree;

(e) the scalar equation is the maximal-slicing lapse equation, which for static matter is the main text's optical-source law with the divergence of $(e^h)_{ij}$: $\partial_i\big[(e^{-h})^{ij}\partial_j\psi\big] = -(8\pi G/c^4)(\varepsilon + 3P)\, e^{\psi}$;

and on the Friedmann background:

(f) linear perturbations keep the mean curvature of DFD's slices uniform, $\delta K = 0$ for $k = 0$ wherever no phantom field changes: the absolute time is the uniform-expansion slicing, no scalar mode propagates, the curvature perturbation ζ of adiabatic modes is conserved outside the horizon, and for the curvature constant $k = 0$ of the first integral the linear equations are general relativity's.

The equivalence with general relativity in (b)–(d) and (f) is proved or computed for static configurations, for linear perturbations of flat space and of the Friedmann background, through second post-Newtonian order, and at first order in the velocities to all orders in compactness; for fully nonlinear time-dependent fields, for stationary rotation beyond first order in the spin, and for maximal slicing during generic rotating collapse, it rests on the argument given for (b).

Proof sketch. (a) On the lock a spatial diffeomorphism ξ at fixed slicing changes $\ln\big(N(\det g_{ij})^{1/6}\big)$ by $\frac{1}{3}\partial_i\xi^i$, so only $\partial_i\xi^i = 0$ survives: two functions, which remove the transverse vector piece; setting $\sigma = 0$ would take a third. At first post-Newtonian order σ does not enter g_{ij}, so the isotropic dictionary of Theorem WS.8 is exact there. (b) Without a temporal kinetic term for ψ the action differs from general relativity's by a term quadratic in K; general relativity's action is invariant under normal deformations of the slices, and the variation of the remaining term along them gives $D_i(N^2 D^i K) = 0$ on every solution, so $N > 0$ and $K \to 0$ at infinity force $K = 0$ (for actions whose momentum trace is proportional to K, the Hamiltonian form of this identity is that of Henneaux, Kleinschmidt and Lucena Gómez, Phys. Rev. D **81**, 064002 (2010), eq. (4.1)). This is computed for static fields, for linear perturbations, and at first order in the velocities to all orders in compactness, where the momentum constraint alone forces $K = 0$; for general fields the identity, and the existence of the lock's coordinates on general data, are argued, not computed. (c) Every term of the action is spatially covariant; with the matter, momentum, traceless and ψ equations imposed, the spatial diffeomorphism identity gives the Hamiltonian-constraint density as $c(t)\sqrt{\det g}\,N^2$, and asymptotic flatness sets $c = 0$; the term quadratic in K vanishes on solutions, so the remaining equations are general relativity's, and conversely general relativity's maximal solutions, written with the lock, solve them. For static fields $N\sqrt{\det g}\,{}^{(3)}R = \sqrt{\det \tilde{g}}\,\big[\hat{R} - 2\hat{\Delta}\psi - \frac{1}{2}|\partial\psi|^2_{\hat{g}}\big]$, $\hat{g} = e^h$, so the Einstein–Hilbert scalar energy is the printed Newtonian term with the same coefficient $c^4/32\pi G$: premise G1's "one term" (computed). (d) The exterior map is $r^3 = R^3 - 3GMR^2/c^2 + C'$, with C' set by the interior; the reference $\Gamma = 2$, $K = 100$ polytrope has maximum mass $1.637\,M_\odot$, the same computed in DFD's coordinates and from the TOV equations, and a moving neutron star's inertial mass equals its gravitational mass to better than 10^{-8} up to the maximum mass (computed). At second post-Newtonian order σ is sourced by the combination that sources general relativity's conformal mode, and its exchange cancels, at orders G, G^2 and G^3, the terms that the lock would otherwise add to the two-body Lagrangian (computed). (e) With $N = e^{-\psi/2}$ the lapse equation $D^2 N = N[K_{ij}K^{ij} + 4\pi G(\rho + S)]$ reads $\partial_i[(e^{-h})^{ij}\partial_j\psi] = -e^{\psi}[8\pi G(\rho + S) + 2K_{ij}K^{ij}]$ ($c = 1$, S the trace of the spatial stress), whose static form is the stated law. (f) On the Friedmann background the Einstein–Hilbert term keeps its Friedmann law, so the term quadratic in K is quadratic in $K - \bar{K}$, with $\bar{K}(t)$ the uniform mean curvature of the slice itself, and the identity of (b) becomes $D_i(N^2 D^i K) = N\,\dot{\bar{K}}\,(K - \bar{K})$; linearized in conformal time for $k = 0$ it reads $(Q - \nabla^2)\,\delta K = 0$, with ∇^2 the comoving Laplacian, $Q = 3(\mathcal{H}^2 - \mathcal{H}')$ and $\mathcal{H}$ the conformal Hubble rate; $Q > 0$ for ordinary matter, so $\delta K = 0$. The three scalar equations, the lapse equation, the momentum constraint, in which the shift enters through the shear of σ, and general relativity's traceless Einstein equation, which determines σ, are then Einstein's in the uniform-expansion slicing; the trace, the shift and σ are fixed by the matter at each instant, and the constant c of (c) is proportional to the curvature constant k (computed). □

Black holes follow. The exterior's event horizon is Schwarzschild's, at the areal radius $2GM/c^2$, and Kerr's for a spinning hole, argued beyond first order in the spin. For an eternal static hole it is the main text's optical horizon, the surface where $n = e^{\psi} \to \infty$, which the lock places at the arena's origin; a hole formed by collapse settles on the late-time maximal slicing, where the horizon is a flow horizon, the inflow of the slices equalling the local speed of light, with $n = 256/27$ on it, and n diverges only on the slices' limiting surface, $R = 3GM/(2c^2)$, at the arena's origin (computed).

The Boltzmann-code computations of the main text, the χ third peak among them, solve general relativity's linear perturbation equations; by (f) these are DFD's

own equations, in its uniform-expansion slicing, for the curvature constant $k = 0$, which Remark WS.7 derives and which the main text's fits take; while no baryons are bound, where the $(K - \bar{K})^2$ term is absent, they are the Einstein–Hilbert term's own equations in the same slicing. The temporal functional $K(\Delta)$ of App. Q does not enter them: it acts on homogeneous deviations only (Axiom WS.1). Wherever the μ-law acts the equivalence does not extend to it: its term lies outside the Einstein–Hilbert term (premise G1). Written on the physical metric, that term is $(a_0^2/8\pi G)\int d^3x\, N\sqrt{\det g_{ij}}\,[W(X) - X]$, with $X = c^4 g^{ij}\partial_i \ln N\, \partial_j \ln N/a_0^2$ the squared proper acceleration of the observers at rest in the slices of absolute time in units of the epoch's $a_0 = 2\sqrt{\alpha}\, cH$, with H read on bound-matter clocks (App. ZS); it keeps the spatial diffeomorphisms that the lock leaves, at Newtonian order it is the flat form of Axiom WS.1, and where $\mu \neq 1$ the two differ at relative order $(1-\mu)\psi$. It is the acceleration term of the preferred-foliation theory of Blanchet and Marsat (Phys. Rev. D **84**, 044056 (2011); arXiv:1107.5264), written on DFD's fixed slices.

Remark WS.7 (The curvature constant is zero). While no baryons are bound anywhere the μ-law acts nowhere, so under Axiom WS.1 the action is the Einstein–Hilbert term alone. Its identity under a change of slicing then reads $\dot{c} = \frac{2}{3}\, c\, \partial_i \beta^i$, with c the constant of Proposition WS.6(c), proportional to the curvature constant k of the first integral. For $c \neq 0$ the identity fixes the longitudinal shift, so no slicing keeps Eq. (WS1) elliptic, and ψ and σ carry two modes of their own per comoving wavenumber κ, one of them growing at the rate $\kappa/\sqrt{3}$ per unit conformal time whatever the size of k, the matter content or the era, with no upper limit in κ (computed). So $k = 0$ is the only value that keeps the axiom and a well-posed evolution before any baryons are bound. At $k = 0$ the equations keep $a^2\delta K$ constant before the $(K - \bar{K})^2$ term acts, and the momentum of ψ stays continuous where it switches on, which sets $\delta K = 0$: the slicing is the uniform-expansion slicing, $K = \bar{K}$, throughout. Switched on there, with the first phantom growing from zero, the term changes neither the action nor the momenta, and c stays zero (computed; after the switch at linear order). A detected spatial or dark curvature falsifies this.

Theorem WS.8 (Vector-Sector Completion)**.** *Under Proposition WS.5, the h_{0i} components obey the linearized EH momentum constraint. In the gauge fixed* physically *by the DFD dictionary — (a) g_{ij} isotropic, $= e^{+\psi}\delta_{ij}$ through first post-Newtonian order, (b) $g_{00} = -e^{-\psi}$ through the same order, with ψ the elliptic solution of Lemma WS.4 — the unique 1PN solution is*

$$\boxed{\; g_{0i} \;=\; -\frac{1}{c^3}\Big(\tfrac{7}{2}V_i + \tfrac{1}{2}W_i\Big) \;} \qquad \text{(WS8)}$$

— the standard-gauge value of general relativity. The far-zone coefficient -4, the Lense–Thirring precession, and the leading spin terms of App. AX follow as consequences. Beyond linear order the Einstein–Hilbert term couples the shift to ψ: at $O(JM)$ it gives the stationary exterior the general-relativistic factor $1 - GM/c^2 r$ in $g_{t\phi}$ (App. AX).

Proof sketch. By Proposition WS.5 the zero-mode dynamics is GR, and at 1PN only its linearization enters: the h_{0i} equation is the momentum constraint sourced by ρv_i. Conditions (a)+(b) are precisely Will's standard-gauge conditions: (a) fixes the spatial gauge function; (b) — the statement that *all* c^{-4} scalar content of g_{00} sits inside $e^{-\psi[\text{elliptic}]}$, i.e. no $\ddot{\chi}$ term — fixes the temporal gauge function (Lemma WS.4). With both functions spent, the momentum constraint has the unique solution (WS8); uniqueness is the standard 1PN elliptic uniqueness with $V_i, W_i \to 0$ at infinity. In DFD the "gauge" functions are not free: coordinates are physical (preferred foliation), and the dictionary conditions (a)+(b) are what *define* those coordinates; the theorem states that the physical frame the scalar dictionary selects is the same frame in which the vector constraint takes the standard-gauge form. □

Condition (b) also fixes the slicing. For $g_{ij} = e^{\psi}\delta_{ij}$ the mean curvature of the constant-t slices is $K = -\frac{3}{2c}\partial_t\psi + \partial_i g_{0i}$ at leading order, and the standard-gauge value (WS8) has $\partial_i g_{0i} = \frac{3}{2c}\partial_t\psi$, so $K = 0$: the preferred foliation is the zero-mean-curvature (maximal) slicing at this order. The longitudinal part of g_{0i} is then set by the slicing, and its transverse part obeys the Einstein–Hilbert equation. At linear order the longitudinal part of the momentum constraint, $\partial_t(\nabla^2\psi + 8\pi G\rho/c^2) = 0$, follows from the Poisson equation, so the two statements agree there. Conditions (a) and (b) hold through first post-Newtonian order; exactly, the lock fixes the lapse, $N = e^{-\psi/2}$, and $\det g_{ij} = e^{3\psi}$, and with the parent strain's σ kept the slicing is maximal for isolated systems (Proposition WS.6(b)).

Theorem WS.9 (EIH equivalence; binary-pulsar triangle)**.** *Lemma WS.4 + Theorem WS.8 reproduce the full Einstein–Infeld–Hoffmann 1PN two-body Lagrangian. Hence the periastron advance, Einstein delay, Shapiro parameters, and the $(\dot{\omega}, \gamma_E, \dot{P}_b)$ mass-triangle consistency of PSR B1913+16 and J0737−3039 are GR-identical. (The +6.4% periastron excess of the hyperbolic/K-branch readings is absent by construction.)*

Remark WS.10 (Data lock: J0737−3039 forces this result twice over). The published double-pulsar timing (Kramer et al. 2021, PRX 11, 041050) gives $\dot{P}_b/\dot{P}_b^{\rm GR} = 0.999963(63)$ — a 1.3×10^{-4} test of the radiative sector — and measures $\dot{\omega}$ at 8×10^{-7} fractional precision. Both pillars of this appendix are therefore *independently* data-forced by the same system: (i) *radiative*: any scalar breathing residual $\gtrsim 10^{-4}$ of the GR flux is excluded, so the elliptic reading's $\delta_{\rm rad} = 0$ *exactly* (Theorem WS.11) is the only DFD reading that survives — the $K(\Delta)$-branch estimate ($\delta_{\rm rad} \sim 10^{-3}$) would fail this bound by $\sim 8\times$; (ii) *conservative*: at 8×10^{-7} on $\dot{\omega}$, nothing short of the exact EIH equivalence of Theorem WS.9 suffices. Both bounds are met, with no tuning available or needed.

4. $\delta_{\rm rad} = 0$ with a mechanism; scalar memory; falsifiers

Theorem WS.11 (Radiative budget)**.** *Under Axiom E and Proposition WS.5: the scalar sector, being an instantaneous constraint, carries* no *radiative flux in any multipole (monopole, dipole, quadrupole breathing all identically zero as radiation); the TT sector carries the GR quadrupole; therefore*

$$\delta_{\rm rad} = 0 \quad \textit{exactly at leading order,} \tag{WS9}$$

with corrections only from μ-function effects where $|\nabla\psi|/a_\star$ is not asymptotically large (a consequence of the mechanism above, not an assertion).

Remark WS.12 (Scope: energy flux, not remnant spectroscopy). Theorem WS.11 governs the *energy-flux channel* — inspiral phasing and orbital decay ($\dot{P}_b$), where it is confirmed at 1.3×10^{-4} (Remark WS.10). It does *not* by itself fix the quasinormal-mode *spectrum* of a merger remnant, which is set by the remnant's metric; with the parent strain's σ kept that metric is Kerr's, argued beyond first order in the spin (Subsec. WS 5).

Corollary WS.13 (Scalar memory closes)**.** *The open case of the App. AT channel-scope remark (head-on/burst scalar memory) closes: a constraint field has no far-zone radiative degree of freedom, so scalar memory vanishes for* all *source classes; total memory is the tensor (TT) memory, which equals GR's, linear (ordinary) plus nonlinear (Christodoulou), because the TT sector is the full a_2 Einstein–Hilbert term (Proposition WS.5; App. AT).*

Remark WS.14 (Consistency panel). (i) GW170817: $c_T = c$ untouched (TT hyperbolic, luminal); on the optical-cone reading of the TT sector the constraint is satisfied *identically* (GWs and photons ride the same cone). (ii) LVK polarizations: no scalar/vector far-zone modes — consistent with the corpus falsifier clause; a confirmed far-zone breathing mode falsifies Axiom E outright. (iii) Preferred-frame causality: instantaneous constraint in a preferred foliation generates no closed causal loops (absolute time orders all events). (iv) Energy balance: $\dot{P}_b$ is TT-only; radiation reaction enters the matter EOM through the TT interaction (Burke–Thorne analog in the TT channel), with the scalar sector conservative. (v) Frame-dragging phenomenology at leading order (LAGEOS, GP-B, the leading QPO spin terms) rests on Eq. (WS8); with the parent strain's σ kept the strong-field shift is Kerr's, so the spin-ISCO and the shadow displacement of App. AX are Kerr's, and the e^{-2u} closed form of the first-order shift gives way at $O(JM)$ to general relativity's $1 - 3u$.

5. Ringdown and echoes: the optical and tensor channels

a. Ringdown. Where $\mu \to 1$, with the scalar-longitudinal piece σ of the parent strain kept, light, matter and the tensor field share one metric, whose dynamics is the Einstein–Hilbert term (Proposition WS.5): the remnant of a merger is a Kerr hole in DFD's coordinates and its quasinormal modes are Kerr's, beyond first order in the spin by the argument of Proposition WS.6. Against the published constraints — GW250114: $\hat{\delta f}_{220} = 0.02 \pm 0.02$ (90% C.L.); GWTC-4.0 hierarchical: 0.00 ± 0.06; damping $\hat{\delta\tau}_{220} = -0.01^{+0.10}_{-0.09}$ — DFD's $\delta f_{220} = \delta\tau_{220} = 0$ is consistent, and the ringdown does not distinguish DFD from GR. The eikonal frequency $\Omega_c = c/b_{\rm crit}$ is Schwarzschild's, since $b_{\rm crit} = 3\sqrt{3}\,GM/c^2$: the optical and tensor channels ring together.

b. Echoes. The remnant's Kerr horizon, argued beyond first order in the spin, has no reflecting surface, so there is no echo train in either band and no third polarization; the echo-polarization claim $h_3/h_+ \simeq 1/\sqrt{20} \approx 0.22$ (App. AH) does not apply.

c. The flux channel. Theorem WS.11 and Remark WS.10 govern the energy-flux channel (Remark WS.12) and are unchanged.

6. Consistency notes on other sections

1. **PPN vector sector.** The pure-V solution $N_i = -4V_i/c^3$ of the shift equation is not transverse; the transverse-gauge solution is $N_i^\perp = -2(V_i + W_i)/c^3$ (since $V_i^\perp = (V_i + W_i)/2$ by the continuity identity; V_i and W_i already contain G). The two differ by a longitudinal gradient, so no physical quantity changes; Theorem WS.8 gives the vector sector, and the PPN section states the transverse-gauge solution.

2. **TT coupling normalization** appears as $16\pi G/c^4$ at every print (§formalism, §gravitational waves, App. AT). The canonical value (fixed by the S_h normalization $c^4/64\pi G$ and the interaction $+\frac{1}{2}\int h_{ij}^{\rm TT} T^{ij}$) is $16\pi G/c^4$; a $c^4/32\pi G$ prefactor or a $-\frac{1}{2}$ coupling is inconsistent with it (App. GR, remark on the TT action normalization, item (ii)).

3. **Echo polarization (App. AH vs. the gravitational-wave section).** Under Axiom E the far-zone scalar mode is absent, and with the parent strain's σ kept the $h_3/h_+ \simeq 0.22$ echo-polarization claim does not apply: there is no third polarization and no gravitational-wave echo (Subsec. WS 5).

4. **EH attribution.** a_2 carries the Einstein–Hilbert term (gravitational-wave section, App. O, App. SM); a_4 carries the gauge kinetic term and α (App. O) — two different operators, not a convention choice. This appendix uses a_2 for the Einstein–Hilbert term throughout (Proposition WS.5).

5. **Ringdown and echoes**: the statements of App. AT, App. AH, App. RM and the strong-field

section follow Subsec. WS 5: Kerr ringdowns, argued beyond first order in the spin, and no echoes.

7. What remains open in this sector

(1) A full nonlinear well-posedness statement for the coupled elliptic-constraint + hyperbolic-TT system (an open program item of the corpus; constraint-hyperbolic mixed systems are standard in NR as "elliptic-hyperbolic" formulations).

Appendix ZS: The Early-Clock CMB Fit: Conformal Invariance Theorems, the Measured Clock Coefficient, and the Shape Inputs

This appendix sets DFD's position on the Hubble tension. Three exact theorems (Sec. ZS 1) close the "Planck is ψ-screen-biased" interpretation; an enumeration-complete no-go (Sec. ZS 2) establishes that the coefficient C in $(H_0 t_P)^2 = C\,\alpha^{57}$ is a free continuous input of the printed theory — the exponent 57 remains a theorem (App. AP) — and it is measured; a $C = 1$ axiom is one the CMB-anchored data exclude at $\sim 46\sigma$ as today's early-clock value, while bound matter's clock has $C = 1$ (Postulate ZS.11). With C measured once, every remaining spectrum-shape input of the CMB but three is carried by derived or adopted-and-priced structure: the ω_b coefficient and A_s are calibrations, and the tilt is a stated number; the mechanism is open (per-input grades in Sec. ZS 3). DFD fits Planck plik-lite with *two* free calibrations, three counting the ω_b coefficient, against ΛCDM's five effective parameters at essentially equal χ^2 (Sec. ZS 3). Its position on the tension is one universe read on two clocks (Postulate ZS.11): the CMB-anchored channels read the early clock, $H_0^{\rm early} = 67.52$, and local probes read the bound-matter clock, $H_0^{\rm loc} = 72.09$; the local evidence and its decider are set out in Sec. ZS 4.

1. Three theorems: what a ψ screen cannot do

Conventions as in App. AN: M_1 denotes the optical metric $d\tilde{s}^2 = -c^2\,dt^2/n^2 + d\mathbf{x}^2$ with $n = e^{\psi}$, and M_2 the matter-coupling metric $d\tilde{s}^2 = -c^2 e^{-\psi} dt^2 + e^{+\psi}\delta_{ij}dx^i dx^j$; the corpus already records that the two are conformally related with identical light cones (App. AN).

Theorem ZS.1 (Conformal θ_*-invariance)**.** *$M_2 = e^{\psi} M_1$ as an exact matrix identity (conformal factor $\Omega = e^{\psi/2}$), so the two metrics share their null sets and unparametrised null geodesics. Under a conformal rescaling $\tilde{g} = \Omega^2 g$ the angular-diameter distance obeys $D_A^{(M_2)} = \Omega_s\, D_A^{(M_1)}$ with $\Omega_s = e^{\psi(z_*)/2}$, while the proper transverse sound-horizon scale measured by the plasma's own (M_2) rods carries the* same *factor Ω_s. Hence*

$$\theta_*^{(M_2)} - \theta_*^{(M_1)} \;=\; 0 \qquad \textit{identically.} \tag{ZS1}$$

Computing $D_A(z_*)$ "on the optical metric" cannot move θ_* at all: the shift is exactly zero.

Corollary ZS.2 (Etherington reciprocity is structural; no probe selectivity)**.** *Distance duality $d_L = (1+z)^2 D_A$ holds* exactly *in DFD because it is conformal invariance, not a coincidence [84]; DFD cannot break the duality ratio $\eta = 1$. Consequently a ψ screen is* not probe-selective*: CMB θ_*, transverse and radial BAO, SNe Ia luminosity distances, and strong-lensing time-delay distances all ride the same null congruence on the same conformal class and must move together. A split in which time-delay H_0*

probes the topological value directly while Planck is screen-biased is refuted as stated. A viable screen could only be redshift*-selective, which the corpus's own low-z-weighted screen kernel cannot satisfy.*

Theorem ZS.3 (The split of $A = a\,e^{\bar\psi/2}$ is pure gauge)**.** *For DFD–FRW on M_2 with arena scale factor $a(t)$ and background $\bar\psi(t)$, define $d\tau = e^{-\bar\psi/2}dt$ and $A = a\,e^{+\bar\psi/2}$. Then $ds^2 = -c^2d\tau^2 + A^2d\mathbf{x}^2$ exactly, and every CMB observable is a functional of (τ, A) alone: $1+z = A_0/A$, $\chi = \int c\,d\tau/A$, $\theta_* = \chi_s/\chi_{\rm LSS}$. At fixed (τ, A) the background field cancels identically, $d\theta_*/d\bar\psi = 0$: with an arena factor, $\bar\psi$ is a field redefinition of (a, t), not a physical screen. This carries the App. AE flat-direction theorem from the action to the observables for the split: the split of the scale factor between the arena factor and $\bar\psi$ is unobservable; in the static arena, where $a = 1$, the homogeneous field is the scale factor itself, $\bar\psi = 2\ln A$, and carries no screen beyond the expansion it describes.*

Theorem ZS.4 (Skewness sign theorem for the mean line-of-sight screen)**.** *The only channel Theorems ZS.1–ZS.3 leave open is the* inhomogeneous *mean $\langle\delta\psi\rangle_{\rm LOS}$ entering $\langle\chi\rangle = \int(c/H)\,\langle e^{-\delta\psi}\rangle\,dz$. In GR this vanishes identically (linear Poisson operator, zero-mean source). In DFD the deep-MOND solution operator is odd and sublinear ($\psi \sim \sqrt{GMa_0}$), so $\langle\delta\psi\rangle \neq 0$ requires* skewness *of the density field, and for any monotone concave μ on a positively skewed field the sign is forced: $\langle\delta\psi\rangle_{\rm LOS} < 0$ — the sign a θ_* resolution would require. The magnitude, however, is bounded: the pre-registered lognormal computation updated to the measured-clock forward normalization $\sigma_8 = 0.8063$ gives a best path-weighted $|\Delta| \approx 3.7\times10^{-6}$ against the required 1.32×10^{-2} — short by a factor $\sim$3500 (3.55 orders; generous upper bound still 29× short). The GR control run returns machine zero. The mean-vs-RMS distinction also corrects App. LS: an RMS is positive-definite and cannot be the coefficient of a systematic distance shift.*

Status ZS.5 (The optical route is closed). The optical route to a DFD-favourable reinterpretation of Planck's H_0 is closed by two exact theorems, and the inhomogeneous route is 3.5 orders of magnitude too small. The reading that "the Planck-vs-TD tension is structurally resolved by interpreting Planck as ψ-screen-biased" is therefore excluded.

2. The clock coefficient C: an eight-route no-go, and its measurement

Write the clock identity of App. AP as

$$(H_0\,t_P)^2 \;=\; C\,\alpha^{57}, \qquad \text{(ZS2)}$$

with the exponent $57 = k_{\max} - N_{\rm gen}$ a theorem. Taking $C = 1$ (equivalently $H_0 = 72.09$ km/s/Mpc) would be an axiom. An eight-route derivation analysis shows that C is not derivable, at Derived grade (enumeration-complete over the printed corpus):

Proposition ZS.6 (No-go: C is not derivable from the printed corpus)**.** *All 128 printed corpus equations connecting the α^{57} deposit to an expansion rate are exponent-only, convention-importing, or C-covariant. The spectral vacuum-matching route requires a regulator shape moment outside the independently forced Riesz class $p \geq 3$; the homogeneous ψ-sector Lagrangian, momentum, and Hamiltonian vanish identically, and the Friedmann law of the Einstein–Hilbert term converts the vacuum density into the clock rate without fixing either; epoch-selection, deposit-repartition, horizon-entropy, and dictionary-audit routes all fail quantitatively. C is a free continuous input. Its time-independent form is the vacuum coefficient $R \equiv \rho_{\Lambda,\rm obs}/[(3/8\pi)\alpha^{57}\rho_P] = 0.6042 \pm 0.0027$, and C is today's value of the early clock, $C(z) = R + 1.924\,[\omega_m(1+z)^3 + \omega_r(1+z)^4]$; any derivation must fix R, not an epoch-dependent C. A ninth route, fixing the whole shape of the spectral cutoff from a printed principle, fails as well (Remark AP.6). Any future closed-form claim must beat a measured false-positive-rate bar: at least 952 grammar candidates fall inside the $\pm1\sigma$ window.*

Status ZS.7 (C measured; $C = 1$ excluded as the early clock). Measured once against 13 pre-DESI BAO points (6dFGS, SDSS MGS, BOSS DR12, eBOSS DR16) plus the Planck θ_* [58], with the other inputs of Sec. ZS 3: $C = 0.87784 \pm 0.00266$ ($\chi^2 = 10.52/13$); the plik-lite conditional channel independently gives $C = 0.8772$; the time-independent input is $R = \Omega_\Lambda C = 0.6042 \pm 0.0027$. As today's value of the early clock $C = 1$ is excluded at $\sim46\sigma$ by the CMB-anchored channels, and it is the clock of bound matter (Postulate ZS.11). The resulting clock is $H_0^{\rm early} = 67.52 \pm 0.09$ km/s/Mpc, concordant across five CMB-anchored channels (plik-lite 67.520±0.094; BAO+θ_* 67.543±0.103; ACT DR6 67.481±0.094; SPT-3G 67.417±0.232; θ_*-only 67.52 ± 0.10). On DESI DR2 BAO [194] the BAO+θ_* channel gives $C = 0.8801 \pm 0.0026$, while BAO alone gives $H_0 = 68.71 \pm 0.33$ km/s/Mpc, 3.4σ above the θ_*-only value. The split is 3.4σ here because ω_χ is computed, not fitted; ΛCDM shows 2.3–2.5σ with ω_c free and 4.2–4.4σ with ω_c held at Planck's value. No printed input moves it (the printed range of ω_χ moves it the wrong way). On the early clock the Hubble time $1/H_0 = 14.48$ Gyr and the age $t_0 \approx 13.8$ Gyr (12.92 Gyr in laboratory units, Sec. ZS 5). This is exactly the epistemic status of H_0 in ΛCDM: one measured normalization, with the *structure* (here the exponent theorem) supplied by the theory.

3. The CMB fit on the measured clock

With C measured, the spectrum-shape inputs are supplied upstream of the data, with per-input grades printed:

$\omega_b = 0.0222730$ (conventional-point value, a calibration; α^4 power derived, coefficient calibrated; Axiom E-transport′, +1 priced discrete bit — Ext. Deriv. App. AH),

$\omega_\chi = 0.1192806$ (flux-period relic, Lemma AV.6, App. AV), $N_{\rm eff} = 3.044$,

$\sum m_\nu = 61.46$ meV (normal-ordering spectrum),

$n_s = 1 - 2/60 = 0.96667$ (a stated number; the mechanism is open),

A_s (calibrated; amplitude-profiled). (ZS3)

Two calibrations are free in the fit, the clock coefficient C of Sec. ZS 2 and one overall amplitude absorbing $A_s e^{-2\tau}$; a third, the ω_b coefficient, is fixed at its conventional-point value. Against Planck 2018 plik-lite native (613 bandpowers, TT+TE+EE, $\ell = 30$–2508) [58]:

Out-of-sample: SPT-3G outright *prefers* DFD ($\Delta\chi^2 = -0.77$); ACT DR6 disfavours it by +5.94 at the flux-period abundance (Lemma AV.6) ($\sim$1.2–2.4σ, below 3σ, and partly the known ACT–Planck ΛCDM tension). CMB lensing at this background with full conventions gives $A_{\phi\phi} = 0.9887$ (-0.80σ). The flux-period abundance agrees with three Planck-based channels (Planck fit -0.6σ; BAO+θ_* -0.18σ; plik-lite -0.98σ), and the neutrino spectrum is fit-neutral once H_0 is re-profiled in both arms ($-1.2\,\chi^2$ plik-lite, -0.8 CamSpec PR4 in favor of massless — negligible; the spectrum thus enters as mild anti-tuning).

Remark ZS.8 (Anti-tuning facts). The inputs are not riding luck: DFD's stated tilt $n_s = 0.96667$ (a stated number; the mechanism is open) fits plik-lite *better* than Planck's own fitted 0.9649 by $0.11\,\chi^2$ (the combination of Planck, ACT DR6, CMB lensing and DESI gives 0.974 ± 0.003, about 2.4σ above it), and DFD's conventional-point ω_b *costs* DFD $1.25\,\chi^2$ relative to Planck's fitted value. Swapping both to Planck's values would improve DFD to $\Delta\chi^2 = +1.88$. No continuous input in Eq. (ZS3) was tuned to the CMB: the flux-period relic (with its two stated conventions) and the neutrino spectrum were fixed for unrelated reasons, and they jointly resolve a five-way abundance inconsistency ($\chi^2 = 120.4/4$, extremes 10.6σ) without a single CMB-facing continuous adjustment. The ω_b input is the conventional-point value of the baryogenesis chain (Axiom E-transport′, a priced discrete bit adopted after Planck's η_B was known; App. FK and App. CE); its α^4 power is derived and its coefficient is a calibration (Ext. Deriv. App. AH).

Status ZS.9 (Standing claim). DFD with the tilt n_s (a stated number; the mechanism is open), ω_b at its conventional-point value (a calibration; per-input grades in Eq. (ZS3)), and two free calibrations (the clock coefficient plus one amplitude) fits Planck plik-lite at $\Delta\chi^2 = +3.2$ for 2 fewer effective parameters with the ω_b coefficient counted (AIC −0.8, BIC −9.6; 3 fewer, AIC −2.8 and BIC −16, if it is not counted; computed), needs no screen, and is sustained out-of-sample by SPT-3G (preferred) and ACT DR6 (below 3σ). The CMB model-comparison figures of App. CL, priced at the $C = 1$ background (e.g. the plik-lite $\Delta\chi^2 = +23.3/+8.0$ there), are not current: they use neither the flux-period abundance nor the measured clock. Under the adopted Axiom E-transport′ (Ext. Deriv. App. AH) the shape input ω_b has its α^4 power and its $B-L$ bias derived, but not its coefficient (with the stated carrier, the mechanism gives η_B of about (2–3) $\times 10^{-9}$, three to five times Planck's value), and the fit uses its conventional-point value. The enumeration, with per-input grades: ω_b derived power, calibrated coefficient (+1 priced discrete bit); ω_χ conditional-derived, on two stated conventions, the stated count 158, the flux-period identification and the asserted premise P4′ (App. FK, Lemma AV.27); $\sum m_\nu$ + hierarchy derived, given the stated inputs and the data-selected branch of App. X; $N_{\rm eff}$ standard; n_s a stated number, the mechanism open; A_s calibrated and amplitude-profiled — with H_0 (the vacuum coefficient R) measured and one overall amplitude calibration absorbing $A_s e^{-2\tau}$ (τ astrophysical).

4. The local arm and the acoustic arm, and the decider

Two arms of the theory measure the clock coefficient C at different values. The *local arm* (galactic and local) is the SPARC absolute a_0 scale together with the local distance-ladder H_0, whose SH0ES value of 2022 reads $C = 1.027 \pm 0.029$; the *acoustic arm* is the CMB and BAO geometry of this appendix, which gives $C = 0.87784 \pm 0.00266$. Read as one clock, this would be the sharpest conflict in the corpus; under the two-clock postulate of Sec. ZS 5 both readings are right, the local arm reading the bound-matter clock ($C = 1$) and the acoustic arm the early clock. The domain-local screen clock of App. ZT is the *structural extension* of the acoustic side — a single conditional axiom under which the local kinematic flow raises the effective local clock and a_0 by about 1% — and its theorems are conditional on that axiom; the a_0-SPARC / SH0ES data question below is not settled by it.

Falsifier ZS.10 (The absolute a_0 scale tests the two clocks). If the Euclid/DESI-era lensing RAR pins the absolute a_0 at the bound-matter clock ($H_0^{\rm loc} = 72.09$: $a_0 = 2\sqrt{\alpha}\,cH_0^{\rm loc} = 1.1966 \times 10^{-10}\ {\rm m\,s^{-2}}$), the SH0ES-side value, the outcome is the one the two-clock postulate expects (Falsifier ZS.14, item iv). If it pins a_0 at the early clock ($H_0^{\rm early} = 67.52$: $a_0 = 1.1208 \times 10^{-10}\ {\rm m\,s^{-2}}$), bound systems do not read the bound-matter clock, the postulate fails, and the local arm's statistical excursion resolves as systematics of the local measurements. Ei-

TABLE CXXX. The fit numbers (effective parameter counts: ΛCDM 5 vs DFD 2 free in the fit, 3 with the calibrated ω_b coefficient; gap 3 or 2).

χ^2(DFD, 2 calibrations)	586.77
χ^2(ΛCDM, Planck best fit; refit shave 0.23)	583.80
fair $\Delta\chi^2$ (for 3 fewer effective parameters)	+3.20
AIC / BIC	−2.8 / −16.1 in DFD's favour (−0.8 / −9.6 with ω_b counted)
$100\,\theta_*$ (no screen of any kind)	1.04110
vs measured 1.04109 ± 0.00031	$+0.03\sigma$
plik-lite conditional H_0	67.520 ± 0.094
vs BAO+θ_* channel	0.16σ

TABLE CXXXI. The local and acoustic arms and their falsifiers. The SPARC split on the early clock is 3.9σ(stat) but only $\sim 0.3\sigma$ against the a_0-SPARC systematic band; the decider is the absolute a_0 scale, when baryonic masses are known to about 2%.

Arm	Evidence	Coefficient reading	Status
acoustic (this appendix)	plik-lite, BAO+θ_*, ACT, SPT, θ_*-only	$C = 0.87784 \pm 0.00266$	five concordant CMB-anchored channels
local (dynamical)	absolute a_0 from SPARC	within the systematic error of $2\sqrt{\alpha}\,cH_0^{\rm loc}$; -3.9σ(stat) / -0.3σ(sys) on the early clock	within the systematic error on bound-matter clocks
	SH0ES distance ladder [106]	6.4σ high vs 67.52, 1.5σ vs 72.09	read on the bound-matter clock
	App. AH tether channel (Λ theorem)	$C = 1.027 \pm 0.029$	SH0ES 2022 re-expressed, $(73.04/72.09)^2$; not a separate arm; 0.9σ from $C = 1$
two clocks (Postulate ZS.11)	bound matter reads $C = 1$, the early plasma the measured C	Cepheid-free H_0 0.2σ	both arms hold; size λ measured
Decider	absolute a_0 scale: Euclid/DESI weak-lensing RAR	baryonic masses to ∼2%	pre-registered discriminator
Screen-immune arbiters	stellar/globular-cluster ages; $f\sigma_8(z)$ growth; BBN	matter-clock integrals on M_2	untouched by any screen (Thm. ZS.1)

ther outcome is a sharp result. The two arms differ by 6.8% in a_0, and an a_0 read from a lensing RAR scales inversely with the adopted baryonic mass, so a 3σ decision needs baryonic masses to about 2%, against stellar-mass systematics of about 0.1 dex today; and each arm must be read on distances computed with its own H_0: an a_0 inferred from redshift distances with photometric baryonic masses scales as $h^2_{\rm assumed}/h_{\rm true}$ (with masses fitted to rotation curves it scales as $h_{\rm assumed}$ alone, and such data cannot tell the arms apart), so at an assumed $h = 0.70$ the early-clock arm gives the larger value, 1.205 against 1.128×10^{-10} m s^{-2} (computed). Because Corollary ZS.2 locks all null-path distance probes together, the optical escape routes are closed.

5. One universe, two clocks

Both measurements of the present expansion rate are robust. The early-plasma yardsticks read 67.52 and the locally calibrated yardsticks read about 72, about 5σ apart (4.5σ for the Cepheid-free local mean below, 6.4σ for SH0ES's full 2025 sample [106]). ΛCDM has to assign the difference to an unidentified error in one of them. DFD reads both as right, through one postulate.

Postulate ZS.11 (One universe, two clocks)**.** *Matter and the expanding universe keep clocks offset by one constant factor λ, set when matter first binds and falls behind the expansion. In the cosmological field equations gravity enters as $G_{\rm cos} = \lambda^2 G_{\rm lab}$ at every epoch, and before a switch redshift $z_{\rm sw}$ every non-gravitational microphysical rate (Thomson scattering, the atomic recombination rates, Compton heating, the nuclear rates, the oscillation rate of the χ field) runs faster by λ than the same rate computed with laboratory constants, both read on the local light geometry; $\lambda^2 = 1/C$.*

The two readings of the one expansion are labelled

$$H_0^{\rm loc} = 72.09 \text{ km/s/Mpc}, \qquad H_0^{\rm early} = 67.52 \text{ km/s/Mpc}, \qquad \lambda = H_0^{\rm loc}/H_0^{\rm early} = 1.0677. \tag{ZS4}$$

$H_0^{\rm loc}$ is the Hubble rate read on bound-matter clocks and rulers (after the switch every matter clock, bound or diffuse, runs at laboratory rates), the $C = 1$ value $\alpha^{28.5}/t_P$

of the clock identity; $H_0^{\rm early}$ is the same expansion read through early-plasma yardsticks (the CMB, BAO, and supernovae anchored on the BAO ruler), the measured-clock value of Sec. ZS 2. They are one universe read on two clocks, not two expansions.

The postulate is the rate-rescaling symmetry of the CMB [195], with its size fixed by the measured coefficient. Under it:

1. **Local clock.** Gravity and light geometry read with laboratory constants obey the clock identity with $C = 1$, which contains no measured coefficient, so the local expansion rate is $H_0^{\rm loc} = \alpha^{28.5}/t_P = 72.09$ km/s/Mpc, from the measured G with no parameter (Sec. XIX). Because the CMB-anchored rate scales as $\sqrt{C}$ and $\lambda^2 = 1/C$, the measured value of C cancels from the local value: setting $\lambda^2 = 1/C$ is the statement that the local coefficient is 1, and 72.09 is the content of the postulate, not an output of a fit. Seven Cepheid-free local measurements (CCHP TRGB and JAGB [108], SH0ES JWST TRGB [105], megamasers [196], TRGB-calibrated surface-brightness fluctuations [197], tailored-EPM type II supernovae [198], and GW170817 with its VLBI jet [199]) give a weighted mean of 71.87 ± 0.96, which is -0.2σ from 72.09 and $+4.5\sigma$ above 67.52 (the type II supernova systematic error, not quoted by its authors, taken equal to its statistical error; errors treated as independent; the TRGB analyses share hosts).
2. **Bound systems.** Bound systems read the same clock, so the acceleration scale of Eq. (488) is $a_0 = 2\sqrt{\alpha}\, cH_0^{\rm loc} = 2\alpha^{29}\sqrt{c^7/(G\hbar)} = 1.1966 \times 10^{-10}\ {\rm m\,s^{-2}}$, with no measured coefficient, consistent with the SPARC extraction $(1.20 \pm 0.02_{\rm stat} \pm 0.24_{\rm sys}) \times 10^{-10}\ {\rm m\,s^{-2}}$ [10] within its systematic error.
3. **Early clock.** Every dimensionless CMB and BAO observable (θ_*, z_*, $z_{\rm d}$, $z_{\rm eq}$ and every $D/r_{\rm d}$) is unchanged to 10^{-4}, so the five CMB-anchored channels still return $H_0^{\rm early} = 67.52$ when read with laboratory rates. A forward Boltzmann run of the postulate at $\lambda = 72.09/67.52$, inside the error of $C^{-1/2}$, on plik-lite plus DESI DR2 BAO [194], without refitting, changes χ^2 by -0.06 (RECFAST) and -0.17 (HyRec) against the ΛCDM fit with H_0 held at 67.52, for $z_{\rm sw}$ of 9.5, 30 and 100 (HyRec at 9.5 and 100), with the amplitude shift $A_s \to A_s\lambda^{1-n_s}$ that the symmetry implies (+0.18 without it). Raising $G_{\rm cos}$ without the rate factor costs $\Delta\chi^2 = +156$, so the rate factor carries the fit. The sound horizon is $r_{\rm d} = 137.8$ Mpc in laboratory units and 147.1 Mpc in the units of the early plasma.
4. **Mirror symmetry.** The postulate is homogeneous, so an observer anywhere reads its own neighbourhood at 72.09 and the early plasma at 67.52, and the two readings do not change when observers are exchanged. The coefficient is therefore even under exchange.
5. **Size.** $\lambda^2 = 1/C = 1.1392 \pm 0.0035$, and through $R = \Omega_\Lambda C$ it carries the same information as the vacuum coefficient R, so the postulate adds no parameter. Its switch redshift is not located, and Proposition ZS.6 applies to its size unchanged.

a. The structure behind the postulate. Three relations taken from the printed equations give the form that Postulate ZS.11 takes, though not its size. (a) The gravitating contrast of a region is its accumulated expansion deficit. With θ the local volume-expansion rate of pressureless matter and $3H$ that of the uniform-expansion slices, mass continuity gives $1 + \delta = \exp\int(3H - \theta)\, dt$; since the expansion is carried by ψ itself (Theorem ZS.3), the contrast that sources ψ is the matter's failure to expand with the slices. This is the continuity equation, not a new law. (b) The deficit rate of bound matter is fixed. Inside a bound region $\theta = 0$ while the slices expand at $3H$, which on the lock of Proposition WS.6 is a ψ-rate $2H$; measured in units of the epoch's a_0/c it is $\Delta_b = 2cH/a_0 = 1/\sqrt{\alpha}$, the same at every epoch because $a_0 = 2\sqrt{\alpha}\, cH$ (Eq. (488)). This is a rate, not the constant gap of (c): integrated between epochs it is the slices' own change of ψ, the expansion itself (Theorem ZS.3). (c) The clock exponents are fixed. Matter clocks carry the lapse $e^{-\psi/2}$ and light the one-way optical index $n = e^{\psi}$, so a constant gap $\Delta\psi > 0$, with bound matter at the larger ψ, changes matter rates by $\lambda = e^{\Delta\psi/2}$ and the one-way light index by $\lambda^2 = e^{\Delta\psi}$, a ratio between frames and not a screen on the light path (Theorem ZS.3); then $1/\lambda^2 = e^{-\Delta\psi}$, and the measured C corresponds to $\Delta\psi = 0.130$. A uniform ψ cancels from every co-located ratio (Theorem XI.2), so the gap appears only in comparisons between two frames. None of (a)–(c) makes the gap constant, fixes its size or locates the switch redshift: the printed equations give bound matter only its potential depth above the slices, so a constant gap, set when matter first binds, is what the postulate adds, and its size is the measured coefficient.

b. A stated rule for the size. A second postulate, separate from Postulate ZS.11, states a value for the size. It is a rule to be tested, not derived, and no other result in the corpus uses it.

Postulate ZS.12 (Size of the clock gap)**.** *(i) When matter first binds, its ψ gap above the expansion slices is the microsector response of Proposition N.4 with the shifted level of Lemma N.10 responding, $k_{\rm eff} + 2 = (k_0 + 2)(1 + s)$ in place of Assumption N.3, so that $\Delta\psi = \frac{3}{2}\ln(1 + s)$, with argument $s = a_0/(c\,|\dot\psi_{\rm sl}|)$, where $|\dot\psi_{\rm sl}| = 2H$ is the slices' ψ-rate. (ii) Both rates in that ratio are read along one worldline, as in Eq. (Q4), and in the same era, with a_0 the epoch's value of Eq. (488).*

Because $a_0 = 2\sqrt{\alpha}\, cH$ (Eq. (488)), clause (ii) gives $s = \sqrt{\alpha}$ at every epoch. With $\lambda = e^{\Delta\psi/2}$ from (c),

$$\lambda = (1 + \sqrt{\alpha})^{3/4}, \tag{ZS5}$$

so $\lambda = 1.06341$, $\Delta\psi = 0.12296$, $C = 1/\lambda^2 = 0.88430$, and the rule predicts $H_0^{\rm early} = H_0^{\rm loc}/\lambda = 67.79$ km/s/Mpc, against the measured (pre-DESI BAO+θ_*) $C = 0.87784 \pm 0.00266$ ($+2.4\sigma$), the DESI DR2 BAO+θ_* value 0.8801 ± 0.0026 ($+1.6\sigma$) and the CMB-anchored $H_0 = 67.52 \pm 0.09$ ($+3.0\sigma$); at 67.79, with ω_b and ω_χ held at the val-

ues of Eq. (ZS3), the acoustic angle moves by 0.08% ($+2.6\sigma$ against θ_*). It goes beyond the printed equations. Clause (i) reads App. N's single-environment response as a gap between two frames, replaces the printed level response with the shifted one, and applies a temporal response inside bound matter, which Axiom WS.1 does not provide (it confines App. Q's $K(\Delta)$, whose closure $K'(\Delta) = \mu(\Delta)$ is the minimal natural choice rather than a forced one, to the homogeneous sector); its argument is the inverse of the printed one, and with $s = \Delta_b$ the same response gives $C = 0.022$. Reading instead a_0 on the bound-matter clock and $\dot{\psi}_{\rm sl}$ on the early clock gives $s = \sqrt{\alpha}\,\lambda$, $\lambda^{4/3} = 1 + \sqrt{\alpha}\,\lambda$ and $C = 0.87729$ (-0.21σ; -1.1σ on DESI DR2), closer to the data but at the cost of comparing rates across the two clocks. The inverse argument, the reading of clause (ii) and the choice of response and level were made with the measured C known, so neither reading meets the false-positive bar of Proposition ZS.6, which concerns derivation from the printed equations and stands unchanged, and the rule is not a derivation of C. On the bare level of Assumption N.3 with k_0 near 60, the $O(1/k_0)$ term moves C by $+0.003$ (to 0.8877; $+3.7\sigma$, $+2.9\sigma$ on DESI DR2); on the shifted level Eq. (ZS5) holds up to the $O(k^{-2})$ term of the lemma. The rule fails if the BAO+θ_* channel places C more than 3σ from 0.88430; on the CMB-anchored $H_0^{\rm early}$ it already sits at 3.0σ. The predicted 67.79 lies between the two ingredients of the BAO+θ_* channel, which differ by 3.4σ on DESI DR2 (Status ZS.7): θ_* alone gives 67.52 ± 0.10 and the DESI DR2 BAO points alone 68.71 ± 0.33 km/s/Mpc, and 67.79 sits 2.7σ above the first and 2.8σ below the second.

In the 3D BAO and supernova data the split is fixed by the anchor, not by distance. Eighteen 3D BAO measurements at twelve redshifts from $z = 0.106$ to 2.33, read with the early-plasma ruler $r_{\rm d} = 147.09$ Mpc on the measured-clock shape ($\Omega_m = 0.312$), give a flat $H_0 = 68.22 \pm 0.19$ ($\chi^2 = 15.2/17$), whose straight-line value at $z = 0$ is 68.65 ± 0.37. The same ruler anchoring the Pantheon+ supernovae [88] (1,086 flow supernovae with $0.01 < z < 0.3$, SH0ES calibrator hosts excluded) gives 68.35 ± 0.36, with no rise toward low redshift across seven bins, while the Cepheid anchor reads the same supernovae about 5.5 km/s/Mpc higher, one 0.17 mag shift of their zero point. A value that slides from 72.09 locally to 67.52 at large distance fits worse ($\Delta\chi^2 = +8.9$ on the BAO points). The stretch $2.33 < z < 1090$ is itself measured to 0.96% in ruler units by θ_*, with the calculated ratio $r_*/r_{\rm d}$ of the sound horizons at last scattering and at the drag epoch, and the Lyman-α BAO point at $z = 2.33$; holding $H_0 = 72.09$ at fixed ω_m and restoring θ_* with a uniform change of H there worsens the fit to θ_* and the BAO by $\Delta\chi^2 \approx +70$; the joint rescaling of the ruler and the rates in Postulate ZS.11 leaves both unchanged. Angular (2D) BAO in thin redshift shells reads 72.7 ± 0.9 with the same ruler, the known difference between the 2D and 3D methods; it is not used here.

Status ZS.13 (Postulate: form derived, size measured). Under Postulate ZS.11, DFD returns $H_0^{\rm early} = 67.52$ in the CMB-anchored channels and the $C = 1$ value of the clock identity, $H_0^{\rm loc} = 72.09$, in local probes. The form and structure of the postulate are derived from the printed equations (the paragraph on the structure behind the postulate), and what it adds is that the gap is constant; its size λ, equivalently C, is the one measured input, as C already was, and the derivation of the size is open. The postulate lies outside the printed premise that one G governs every epoch and every sector (Sec. XIX), the premise on which the CMB-anchored channels exclude $C = 1$ as today's value at $\sim 46\sigma$; under the postulate that exclusion states that the early clock is not at $C = 1$. It does not say where gravity passes from the cosmological to the laboratory value (if matter perturbations grew with the laboratory value, σ_8 would fall well below 0.81); its switch redshift is not located (the CMB and BAO are blind to it between 9.5 and 100), but a sharp switch would move the sky-averaged 21-cm signal $6.2 \pm 0.1\%$ toward zero in one step at the frequency $1420.4\ {\rm MHz}/(1 + z_{\rm sw})$, for any switch redshift, which would locate it. It costs the age of the universe in laboratory units, 12.92 Gyr, against ages of the universe of 13.5–13.8 Gyr inferred from globular clusters with a ΛCDM formation delay (2.1–2.6σ with statistical and systematic errors in quadrature, one programme), a cost the postulate does not remove, since faster rates before the switch add at most 0.03 Gyr to a star's age; late stellar clocks prefer no switch by $\Delta\chi^2 \approx 7$–10 (one globular-cluster programme; the cosmic-chronometer reading moves by about 7% between stellar-population models). Every dimensionless tension of the measured-clock fit, including the DESI BAO-alone split above, is unchanged. The runs labelled elsewhere as on the one-clock $C = 1$ background use $H_0 = 72.09$ together with $\Omega_m \simeq 0.274$ at every epoch; the postulate does not reproduce that background and keeps $\Omega_m \simeq 0.312$.

Falsifier ZS.14 (The two-clock postulate). The postulate fails if any of the following holds. (i) The early-plasma-anchored and locally anchored distance ladders converge as redshift grows: the postulate requires one constant ratio λ at every distance. (ii) Bright gravitational-wave sirens, which use no calculated rate, settle at 67.5 rather than 72.1. (iii) Time-delay lenses with mass-sheet-robust modelling settle at 67.5. (iv) The absolute a_0 scale settles at the early-clock value 1.1208×10^{-10} m s^{-2} on distances computed with $H_0^{\rm early}$: bound systems read $a_0 = 2\sqrt{\alpha}\,cH_0^{\rm loc} = 1.1966 \times 10^{-10}$ m s^{-2} on distances computed with $H_0^{\rm loc}$, the SH0ES-side outcome of Falsifier ZS.10, which is the expected one. (v) Stars older than 12.92 Gyr in laboratory units are established at better than 3σ, with statistical and systematic errors in quadrature. (vi) Any co-located ratio of clocks or masses moves: clock-null (Sec. XI) must hold.

Appendix ZT: The Domain-Local Screen Clock: A One-Axiom Spatial Completion of the a_0 Theorem

The corpus derives $a_0 = 2\sqrt{\alpha}\, cH_0$ from the crossover invariant Ξ (App. N 4) and, conditional on Axiom WS.1, promotes the normalizer to the instantaneous cosmological rate, $a_0(z) = 2\sqrt{\alpha}\, cH(z)$ (Thm. XIX.3): the *temporal* half of locality — the clock is read now, with no stored scale — is already a theorem (the no-memory argument). As printed, however, the corpus hard-codes the *global average* rate $cH(t)$ into Ξ. This appendix books the spatial completion: a single new axiom under which the normalizer is the *domain's own* screen flow, together with everything that follows from it at its verified grades. All results below are **conditional on the axiom** (price list: Sec. ZT 3); this appendix works on the early clock, and its Hubble posture (Sec. ZT 6) is a statement about that clock. The two-clock postulate of Sec. ZS 5 is separate: under it local probes read the bound-matter clock $H_0^{\rm loc} = 72.09$, bound systems read $a_0 = 1.1966 \times 10^{-10}$, about 6% above this appendix's kinematic local value, and time delays read 72.1, not the global-clock value given below.

1. The axiom

Definition ZT.1 (Domain)**.** A *domain* D is a bounded, mass-conserving comoving region, homogeneous to leading order on its own scale. Its *screen flow* is

$$H_{\rm scr}(D) \;=\; -\tfrac{1}{2}\left\langle u^\mu \nabla_\mu \psi_{\rm opt}\right\rangle_D \;=\; -\tfrac{1}{2}\,\dot\psi_{{\rm opt},D}, \qquad \text{(ZT1)}$$

the bridge $H = -\frac{1}{2}\dot\psi_{\rm opt}$ (Eq. (484)) applied to the domain's matter volume, with $\psi_{{\rm opt},D} = -2\ln a_D$ and a_D the scale factor of that volume; DFD's own slices keep the background rate there.

Axiom ZT.2 (DLSC: the crossover normalizer is domain-local)**.** *The cosmological rate normalizing the constitutive crossover $\mu(|\nabla\psi|/a_\star)$ of the elliptic scalar sector (Axiom WS.1, App. WS) is the domain's* own *screen flow: the cH entering the crossover invariant Ξ (Eq. (N10), App. N 4) is $c\,H_{\rm scr}(\mathbf{x},t)$, not the global average $c\,H(t)$.*

The axiom asserts *only* this normalizer substitution. The coefficient $2\sqrt{\alpha}$ is not part of the axiom — it is derived (Theorem ZT.3). The temporal half (instantaneous flow, no stored scale) is already a corpus theorem (no-memory, Thm. XIX.3); the spatial half is the new content: the corpus as printed hard-codes cH_0.

2. The theorems

Theorem ZT.3 (A: domain-local a_0; conditional on Axioms WS.1 and ZT.2)**.**

$$a_0(\mathbf{x},t) \;=\; 2\sqrt{\alpha}\, c\, H_{\rm scr}(\mathbf{x},t), \qquad \text{(ZT2)}$$

with the same parameter-free coefficient as the global theorem. The proof is the App. N 4 chain run verbatim on a region $\Omega \subseteq D$: the microsector coefficient $k_a = 3/(8\alpha)$ is environment-independent; the crossover value $\Xi_* = 3/2$ is normalizer-independent (λ-stationarity; no circularity); solving $\Xi_* = k_a\,(a_0/cH_{\rm scr})^2$ yields Eq. (ZT2). The global theorem (Thm. N.14) is the special case $D =$ FRW background; the epoch theorem $a_0(z) = 2\sqrt{\alpha}\, cH(z)$ (Thm. XIX.3) is the spatially averaged case.

Theorem ZT.4 (B: exact kinematics of the screen flow; no dynamical input)**.** *From mass conservation alone ($V_D \propto a^3/(1+\delta)$, $a_D = V_D^{1/3}$),*

$$H_{\rm scr} \;=\; H \;-\; \frac{\dot\delta}{3(1+\delta)}, \qquad \text{(ZT3)}$$

identified with $-\frac{1}{2}\dot\psi_{{\rm opt},D}$ via $e^{\psi_{{\rm opt},D}} = a_D^{-2}$, giving the split

$$\psi_{{\rm opt},D} \;=\; \psi_{\rm opt} \;+\; \tfrac{2}{3}\ln(1+\delta). \qquad \text{(ZT4)}$$

Corollary ZT.5 (Environment ratio)**.**

$$\begin{aligned} \frac{a_0}{\bar a_0} \;&=\; \frac{H_{\rm scr}}{H} \;=\; 1 - \frac{\dot\delta}{3H(1+\delta)}; \\ \left.\frac{\Delta a_0}{a_0}\right|_{\rm lin} &= -\frac{f}{3}\,\delta, \quad f = \Omega_m^{0.55} = 0.527. \end{aligned} \qquad \text{(ZT5)}$$

A growing underdensity raises the local H and the local a_0; an overdensity lowers both.

Proposition ZT.6 (Scale rule: the minimal domain $D_{\rm min}$)**.** *For a system S, $a_0|_S = 2\sqrt{\alpha}\, c\, H_{\rm scr}(D_{\rm min}(S))$, where $D_{\rm min}$ is the* smallest *domain satisfying Definition ZT.1 that* contains *S (inner edge = the zero-peculiar-velocity surface, $\sim$2$\times$ turnaround; outer edge = leading-order homogeneity, $R_D \gtrsim 10$–$20\,h^{-1}$Mpc). The virialized reading — evaluating $H_{\rm scr}$ inside the collapsed system — is triply excluded: Cor. N.13 fails inside $r_{\rm vir}$; App. Q fixes u^μ to the background congruence; and exact stable clustering gives $H_{\rm scr} = 0$, which violates the SPARC BTFR at -7σ under a uniform virial rule.*

Status ZT.7 (Compatibility). Growth, σ_8, and the CMB are untouched: a_0 never enters linear growth, and the coupling is strictly one-way (growth $\to \dot\delta \to H_{\rm scr} \to a_0$). The homogeneous-mode theorem (Thm. ZS.3) survives: $H_{\rm scr}$ is a functional of the invariant data (τ, A, δ), and it never enters null geodesics — θ_* is protected.

3. Price list and the declared $\dot\delta$ closure

The package costs **2 discrete bits and 0 fitted continuous parameters**:

1. spatial locality of the normalizer (Axiom ZT.2 itself);
2. the minimal-domain clause of the scale rule (Prop. ZT.6; the spatial completion of no-memory — natural, not a theorem).

Declared residual freedoms: the outer patch scale R_D (the environment-spread prediction varies 4× over $R_D = 5$–$30\,h^{-1}$Mpc — the package's largest soft spot) and the cluster-patch density $d_{\rm env} \in [0, 1]$.

Status ZT.8 (Declared $\dot\delta$ closure for the cluster band). Mapping $d_{\rm env}$ to $H_{\rm scr}$ requires a $\dot\delta$ model. The quasi-linear closure $\dot\delta = fH\delta$ is invalid by construction at $\delta \sim 1$: it *understates* the a_0 suppression by 1.377× at $d_{\rm env} = 0.5$ and 1.725× at $d_{\rm env} = 1.0$ against the exact top-hat closure, so the band it gives ("−2.8% to +2.2%, $\leq 0.72\sigma$") must not be used. The band under the *declared* exact top-hat closure: 16-cluster mean coherent shift (on the five-factor-corrected ratios of item 5 of §ZT 5, which size the package, not a cluster closure) −2.8% to +6.4% over $d_{\rm env} \in [0, 1]$ (exact ODE; the harsher Bernardeau approximant gives +6.6% — conservative). At $d_{\rm env} = 1$ the coherent shift is +6.36% = $+1.65\sigma$ (Bernardeau +6.57%/ $+ 1.71\sigma$) and the relaxed class lands at $1.094 = +1.9\sigma$ ($SE_R = 15.4\%/\sqrt{10} = 4.9\%$; Bernardeau $1.096 = +2.0\sigma$); mergers *improve* $0.908 \to 0.951$ (Bernardeau 0.953). The band is **absorbable for** $d_{\rm env} \lesssim 0.5$**, strained at** $d_{\rm env} \sim 1$. $d_{\rm env}$ is a measurable per-cluster quantity (galaxy counts in the 10–20 h^{-1}Mpc shell) and is listed as such — a declared band with a declared closure.

4. Kinematic numbers

A strong-void construction of the local excess is not used (it is excluded, and none of its predictions is used in this appendix). The kinematic application below uses only measured flow data on the measured clock.

5. Predictions and pulls

1. **Galactic sector at the a_0 of Table CXXXII — does not break**: BTFR Υ-marginalised −0.85 to -0.94σ naive, $+0.17/+0.47\sigma$ with self-consistent Hubble-flow distances; the dwarf-galaxy channel -0.02σ; the Milky Way improves ($+0.54 \to -0.13/+0.28$). The SPARC stat-only pull (-3.4 to -4.0σ) is not the right meter (the a_0–Υ degeneracy).

2. **RAR environment modulation** (new, signed): $\Delta a_0/a_0 = -(f/3)\,\delta_{\rm env}$; spread 0.015–0.027 dex at $R_D = 10$–$20\,h^{-1}$Mpc — inside the 0.057 dex intrinsic budget, and a candidate explanation for part of it. a_0 *anti*-correlates with environment density. The current Chae-sample SPARC test is a null with the right sign ($\rho = -0.144$, $p = 0.26$; sensitivity 17% vs a 2–10% effect). The named path is *conditional — a forecast, not in hand*: 2M++ densities [200] (exists) plus ∼300 TRGB-quality RAR galaxies — a sample that does not yet exist (SPARC = 175 total / 64 matched; TRGB-distance rotation-curve galaxies today = a few dozen; future-feasible via JWST TRGB reach + WALLABY/BIG-SPARC). Power: with the package's *own* intrinsic floor (∼0.096 dex non-environmental at $R_D = 10$), 300 galaxies give $\sim 1.4\sigma$, not 3; the 3σ figure holds only on the optimistic branch where DLSC dominates the intrinsic scatter — otherwise ~ 2–$4 \times N$ is needed. *Test on SPARC × 2M++ (pre-registered, 7,000-mock calibrated; both field routes agree at* corr $= +1.000$*): **bound.*** At the patch band $R = 10\,h^{-1}$Mpc the slope on the prediction is $s = +0.40$ (recipe-faithful profile, 95% $[-0.55, +1.00]$; full-nuisance hierarchical MCMC $s = +0.16$, 95% $[-1.45, +1.11]$) — DLSC-signed at every scale, consistent with both $s = 1$ and 0; the mocks certify a-priori non-decisiveness at $N = 110$ (detect power 30–38%, driven by the measured 0.27 dex population scatter). Established by the same execution: strong coupling $s \gtrsim 1.1$–1.5 excluded at 95%; the *linearized* coupling below $R_D \sim 10\,h^{-1}$Mpc excluded at $> 4\sigma$ (a $\delta \simeq 10$ galaxy would need $a_0 < 0$), so the coupling must either live at $R_D \geq 10\,h^{-1}$Mpc or saturate with a $\delta/(1+\delta)$-class form — the shape of DFD's own μ-law; and the hierarchical population normalization lands within about 1.5σ of both $2\sqrt{\alpha}\,cH_0^{\rm early}$ and $2\sqrt{\alpha}\,cH_0^{\rm loc}$ (not yet independently verified). The full analysis pipeline (simulation cubes, mocks, pre-committed analysis plan) is archived with the reproducibility package.

3. **The $a_0(z)$ letter:** the sign $da_0/dz > 0$ gains the fixed-z environment lever. The screen lowers a_0 in the survey's overdense domains (item 4), which adds to the amplitude offset of App. A0Z (+0.095 dex on either clock); the letter itself fits a *free* amplitude on a Planck background ($H_0 = 67.7$) and takes no position on the DFD clock.

4. **High-redshift discs at fixed** z (signed; estimate): the screen lowers a_0 where a disc's domain is overdense, and massive discs at $z \simeq 1$–2 sit in strongly clustered haloes. At $R_D = 10\,h^{-1}$Mpc under the declared exact closure the shift is about −10% at the average environment of such haloes and −20 to −34% in the densest known structures at $z \simeq 1.6$–2.5, whose matter overdensity on that scale is about 0.8–1.3; at $R_D = 20\,h^{-1}$Mpc every shift is about three times smaller. Low-mass discs like those of MUSE–DARK are lowered by 6–7% at their average environment. The massive discs whose a_0 is 1.2–1.4×10^{-10} m s^{-2} at $z \simeq 1.5$–2.2 (App. A0Z, Stat. A0Z.12) would be matched only in domains with $\delta_{\rm env} \simeq 2$–$3$, about 6 to 11 standard deviations denser than average, and their measured environments show no such trend, so the screen does not reconcile them. Test: matter-density maps of the deep fields set against per-galaxy a_0; at fixed z the a_0 must fall as the domain density rises. The sign alone does not separate the screen from a conventional external-field effect (Rem. ZT.9); the size of

TABLE CXXXII. The kinematic numbers. CF4 radii are in h^{-1}Mpc ($150\,h^{-1}$Mpc ≈ 222 Mpc at $h = 0.675$).

Global clock	$H_0 = 67.52$; $a_0^{\rm global} = 2\sqrt{\alpha}\,cH_0 = 1.1208 \times 10^{-10}\,{\rm m/s^2}$
Kinematic deficit (CF4 monopole)	$\delta_m(< 150\,h^{-1}{\rm Mpc}) = -0.057 \pm 0.009$
Local H excess	$+1.0$–$1.2\% \Rightarrow H_{\rm eff} = 68.20 \pm 0.11$; $a_0(< 150\,h^{-1}{\rm Mpc}) = 1.1321 \times 10^{-10}$
Very-local (< 70 Mpc)	$H = 70.3 \pm 0.4$; $a_0 = 1.1669 \times 10^{-10}$ (carries the SH0ES Cepheid zero point — not DFD-independent)
Local a_0 band	1.13×10^{-10} (1.17 on the SH0ES zero point) vs SPARC 1.20 ± 0.02(stat) $\pm$ 20%(sys): unresolved at stat, absorbed by sys. Not an exact match.

the fall and its $10\,h^{-1}$Mpc scale are the screen's own.

5. **Cluster sector (patch rule):** the scatter and window figures below are measured on five-factor-corrected cluster ratios, which App. I does not print because that correction stack does not hold (clusters need χ); they size the package, not a cluster closure. Coherent shift -2.8% to $+6.4\%$ for $d_{\rm env} \in [0, 1]$ (exact ODE; Bernardeau $+6.6\%$) under the declared exact top-hat $\dot\delta$ closure (Status ZT.8); at $d_{\rm env} = 1$ the numbers of Status ZT.8 apply — **absorbable for $d_{\rm env} \lesssim 0.5$, strained at $d_{\rm env} \sim 1$**, with $d_{\rm env}$ measurable per cluster. Both-sided scatter: the relaxed class *improves* $4.6\% \to 3.9\%$, but the full 16 *worsens* $7.09\% \to 10.36\%$ and the $\pm 10\%$ window drops $13/16 \to 12/16$. Merger-class cost -1.2 to -1.8σ. Epoch mismatch: App. I uses $a_0(z = 0)$ at $z = 0.02$–0.87; correcting the epoch alone moves the 16-mean $0.978 \to 0.924$, *away* from Obs/DFD $= 1$ (mergers 0.833), so a "toward 1" reading is wrong-signed; the DLSC patch-rule offset, not the epoch correction alone, is the result of this appendix.

6. **Time-delay lenses on this appendix's early clock:** H_0(TD) $= 67.6$–67.8. Status: **consistent, not yet discriminating** — the current anchors are the collaboration's own 2025 reanalysis [201]: TDCOSMO-2025 primary $71.6^{+3.9}_{-3.3}$ ($+1.2\sigma$) and TDCOSMO+SLACS+SL2S combined $74.3^{+3.1}_{-3.7}$ ($+1.8\sigma$); the collaboration's 2026 update with eleven lenses (arXiv:2610.14781) gives $71.1^{+2.4}_{-2.3}$ ($+1.5\sigma$). The earlier TDCOSMO-IV+SLACS $67.4^{+4.1}_{-3.2}$ (-0.1σ) is *superseded* by the 2025 reanalysis, which attributes the old low value to resolved methodology issues. The 2020 TDCOSMO-only hierarchical value is $74.5^{+5.6}_{-6.1}$ ($+1.1\sigma$); only the power-law H0LiCOW value 73.3 ± 1.75 is 3.2σ off; SN Encore MACS J0138 (2026) $66.9^{+11.2}_{-8.1}$ supports. No mass-sheet-robust ≥ 73 at 2σ exists. Under the two-clock postulate they read 72.1: TDCOSMO-2025 lies -0.1σ, TDCOSMO-2026 -0.4σ, the combined value $+0.6\sigma$ and H0LiCOW $+0.7\sigma$ from it.

7. **Growth / σ_8 / θ_*:** the domain-local screen does not alter the current baseline. The measured-clock run gives $\sigma_8 = 0.8063$, $S_8 \simeq 0.822$, $100\theta_* = 1.04110$, and $A_{\phi\phi} = 0.9887$ (-0.80σ; App. ZS).

Remark ZT.9 (The external-field caveat, stated both ways). Ref. [110] carries a caveat that touches this appendix directly, and it is reproduced here at its own grade rather than paraphrased into support. A per-galaxy RAR fit requires an environment-correlated external-field term, so the effective a_0 inferred galaxy by galaxy depends on the ambient field [166]; both the mean cosmic field and typical environmental fields evolve with redshift; therefore an *evolving* external-field effect can in principle mimic an evolving apparent a_0. Ref. [109] excludes interacting galaxies and cluster members and argues the impact is minor for its sample. The letter's own point about the sign is the sharp one: weaker external fields at higher z mean weaker apparent-a_0 suppression there, which *steepens* the apparent evolution — i.e. acts in the direction of the measured signal — and so deserves quantitative treatment in a per-galaxy analysis.

(i) As a caveat on the cosmological reading. Some part of the measured $a_0(z)$ slope could be environmental rather than cosmological. The epoch reading of Eq. (ZT2) is therefore not the only reading those bins admit, and the exponent γ measured on them is, at present, a sum of a cosmological and an environmental contribution that no published analysis has separated.

(ii) As independent motivation for the environment test, not as support. This is the same environmental channel that Ax. ZT.2 parametrizes, which is a reason to run the per-galaxy environment test already specified in §ZT 5 — the reason arriving from outside this appendix rather than from it. **It is not evidence for the domain-local screen.** A mechanism that can mimic the signal is a confound to be measured, not a confirmation: a conventional external-field effect in standard modified dynamics produces the same sign without Ax. ZT.2, so the sign agreement discriminates nothing. Only a per-galaxy analysis that measures the environment coefficient at fixed z — the test of §ZT 5, currently a bound, not a detection — can separate the two, and until it does, the environmental and cosmological contributions to γ stay entangled.

(iii) The screen cannot make the rotation-curve form of the effect. It sets one a_0 per system, and the Bose response $u(\nu)$ contains no a_0 (App. AT, Prop. AT.20), so every rotation curve stays on the isolated shape locus and its outer part stays flat (theorem). In fits that hold a_0 fixed the screen raises the fitted external field by about 0.007 at the median galaxy, against the 0.05 reported by Chae et al. [166] (computed).

(iv) The local data do not show the environment-

correlated term the caveat assumes. In the rotation-curve fits of Chae et al. the fitted external field does not correlate with the environment density on 4–20 h^{-1}Mpc scales; it follows its own error bar and the inclination, and weighted by the per-galaxy errors it is 0.012 ± 0.009 (App. GR; computed).

6. The early-clock Hubble posture: SH0ES is its named external falsifier

Status ZT.10 (Posture). **SH0ES, at** 73.49 ± 0.93 **in its 2025 analysis of HST and JWST Cepheids [106], is the named external falsifier of this early-clock posture at** 5.0–6.4σ against the kinematic prediction in SH0ES's own window ($0.023 < z < 0.15$: 67.6–68.8 when SH0ES's own peculiar-velocity correction, which raises its H_0 by 0.8%, is applied to the flow the prediction carries; pulls $(73.49 - 68.80)/0.93 = 5.0\sigma$ and $(73.49 - 67.56)/0.93 = 6.4\sigma$; computed). SH0ES's 2022 value, 73.04 ± 1.04 [202], sits 4.1–5.3σ above the same band, and the community Local Distance Network's 73.50 ± 0.81 [107] 5.8–7.3σ. This is a bet against SH0ES *specifically*, not against all ladders: the named systematic channel is **calibrator selection** (the live Freedman–Riess dispute); supernova standardization is disfavoured, since replacing the supernovae with galaxy-based indicators moves the ladder's H_0 by less than 0.1 km/s/Mpc [107] — Cepheid photometric crowding is *excluded* at 8.2σ by JWST (Riess et al. 2024, ApJL 962, L17) (> 1000 Cepheids, HST–JWST difference -0.01 ± 0.03 mag), so generic "ladder systematics" is not defensible. The supporting side: CCHP's TRGB from HST and JWST, $70.39 \pm 1.22 \pm 1.33 \pm 0.70$, its JWST-only TRGB $68.81 \pm 1.79 \pm 1.32$ and JAGB $67.80 \pm 2.17 \pm 1.64$ [108] lie 0.8–1.5σ, 0.0–0.6σ and within 0.4σ of the band (stat+sys in *quadrature*). **Against it, SBF** 73.3 ± 2.5 **(40–99 Mpc) [203], and SBF calibrated on JWST TRGB with neither Cepheids nor supernovae,** $73.8 \pm 0.7 \pm 2.3$ **[197], sit** 1.8–2.3σ **and** 2.1–2.6σ **above the band.** The "very-local 70.3" figure is the favored small-void fit of Stiskalek et al. [204] (2025) and carries the SH0ES Cepheid zero point; on the zero point this posture implies it falls to about 65–66, below the global 67.52, so its sign is not a DFD prediction. CF4 radii are in h^{-1}Mpc ($150\,h^{-1}$Mpc $\approx$ 222 Mpc at $h = 0.675$); corrected local excess +1.1–1.2%, the quoted $+1.0 \pm 0.2$% covers it. **If SH0ES stands, this posture is refuted;** under the two-clock postulate (Sec. ZS 5) SH0ES's value is read on the bound-matter clock, 1.5σ above $H_0^{\rm loc} = 72.09$.

7. Falsifiers

DLSC falsifiers. Item 4's forecast path is conditional: 2M++ densities plus ∼300 TRGB-quality galaxies — a sample not in hand; ∼1.4σ at $N = 300$ under the package's own intrinsic floor, 3σ only if DLSC dominates the intrinsic scatter.

1. **SH0ES vs CCHP (Freedman–Riess dispute).** Dispute resolves for SH0ES (its calibrator selection vindicated) ⇒ the kinematic posture is refuted at 5.0–6.4σ (5.8–7.3σ on the Local Distance Network). Resolves for CCHP (68–70) ⇒ posture supported.

2. **Mass-sheet-robust TD** H_0**.** ≥ 73 at 2σ ⇒ refutes this posture. 67–69 ⇒ confirms this posture and falsifies the two-clock postulate (Falsifier ZS.14). (Currently: consistent, not discriminating.)

3. $a_0(z)$ **sign.** A measured frozen ($da_0/dz \leq 0$) or ρ_m-scaling a_0 ⇒ refutes the carrier (the letter excludes $\gamma = 0$ at 5.3σ by likelihood ratio and $\gamma = 3/2$ at 4.8σ on the exponent's error and 4.7σ by likelihood ratio, both on the published bin errors; counted galaxy by galaxy the exclusion of $\gamma = 0$ is about 1σ within the survey and about 3σ anchored to SPARC's $z = 0$ value, and the trend depends on how the molecular gas is added, and massive discs at $0.6 < z < 2.5$ show no rise at face value, App. A0Z).

4. **RAR environment binning (conditional forecast path; see above).** Binned a_0 shifts with the *wrong* sign, or magnitude incompatible with $-(f/3)\,\delta_{\rm env}$ at every $R_D \in 5$–$30\,h^{-1}$Mpc ⇒ refutes DLSC modulation.

5. **High-redshift disc environments.** At fixed z, the a_0 of high-redshift discs shifts with the *wrong* sign as the density of their domain rises, or by a magnitude incompatible with the screen at every $R_D \geq 10\,h^{-1}$Mpc ⇒ refutes DLSC modulation at high z. The massive discs with $a_0 \simeq 1.2$–1.4 at $z \simeq 1.5$–2.2 sit in average domains ⇒ the screen does not reconcile them, and their tension with the epoch law stands (App. A0Z; the screened values of Stat. A0Z.12 are an estimate).

6. **Cluster booking.** Coherent shift > 3σ under *every* admissible $d_{\rm env} \in [0, 1]$ ⇒ kills the cluster booking. (Current, exact top-hat closure: $\leq +1.65\sigma$ coherent (Bernardeau +1.71), relaxed class +1.9σ (Bernardeau +2.0) at $d_{\rm env} = 1$ — strained, falsification threshold *not* crossed; merger class -1.2 to -1.8σ carried at $d_{\rm env} = 0$.)

8. Named open items

1. The domain scale is not derived: the definition of a domain is met by every region between the zero-velocity surface and the homogeneity scale, and the minimal-domain clause needs a homogeneity threshold the definition does not contain. It is an empirical scale of this extension, bounded below by the first environment test ($R_D \geq 10\,h^{-1}$Mpc for the linear form) and measured by the test of §ZT 5. No result outside this appendix uses the extension: $a_0 = 2\sqrt{\alpha}\,cH_0$, the RAR and BTFR and the epoch law hold without it.

2. The $a_0(z)$-letter amplitude worsens 0.024 dex under DLSC (the survey's bin environments are not yet measured).

3. Merger-class deficit -1.2 to -1.8σ under the patch rule (a physically sign-correct mitigation exists — the densest nodes have the largest $d_{\rm env}$ — but $d_{\rm env}$ is a declared band, not a fit).

Appendix ZU: The Gravity Completion: the Exact Newton Identity of the Quantized ψ Sector, and the Kohn Null

This appendix books the operator (second-quantized) completion of DFD's gravitational sector and its laboratory consequence. Two independent mean-field treatments of the corpus-forced four-fermion vertex — a Wick/Hartree–Fock–Bogoliubov route and a disjoint Hubbard–Stratonovich saddle route — agree exactly: Newton's law survives as an exact, *zero-parameter* identity of the quantized ψ action (Sec. ZU 2); the pairing gap has a closed form but the condensate is *not* the carrier — Hartree+Fock is (Sec. ZU 3); second-order corrections are controlled (Sec. ZU 4); and, because every term of the derived completion is translation-invariant or proportional to $\hat{N}$, the completion predicts *exactly zero* gravitational self-shift of the center-of-mass mode of a trapped crystal — the *Kohn null* (Sec. ZU 5) — where the semiclassical reading of the corpus's own Schrödinger–Newton equation predicts a nonzero sideband. The completion thereby *overturns* the semiclassical commitment: the self-gravity nonlinearity of Sec. XVIII B is not a DFD prediction but the *falsifier* of this completion (Sec. ZU 6). The scope, including what the null does *not* establish, is stated in Sec. ZU 7.

1. The forced four-fermion vertex

Every object in this appendix descends from two printed anchors, with no freedom introduced anywhere in the chain.

The action. The scalar energy of Def. AP.26 (App. AP) carries the prefactor $c^4/32\pi G$,

$$E_\psi = \frac{c^4}{32\pi G}\int \kappa_\alpha^2\, F(Y)\, d^3x - \frac{c^2}{2}\int \rho\,\psi\, d^3x, \qquad \text{(ZU1)}$$

whose Euler–Lagrange equation (Thm. AP.27) is the AQUAL field equation; the Newtonian regime is $F' = 1$.

The matter coupling. The single dispersion relation of App. AN, $E^2 = c^2 e^{-2\psi}|\mathbf{p}|^2 + m^2c^4e^{-\psi}$, expands at weak field to $U = -\frac{1}{2}\,mc^2\psi$.

Canonically normalizing, $\phi = \psi/\sqrt{16\pi G}$ makes $\frac{1}{2}(\partial\phi)^2$ equal to $(1/32\pi G)(\partial\psi)^2$ *exactly*, and the Yukawa coupling is forced to

$$y = \tfrac{1}{2}\,m\sqrt{16\pi G} = 2\sqrt{\pi}\,\frac{m}{M_{\rm P}} = 3.5449077018\,\frac{m}{M_{\rm P}},$$
$$V(r) = -\frac{y_1 y_2}{4\pi r} = -\frac{G m_1 m_2}{r} \quad \text{exactly.} \qquad \text{(ZU2)}$$

Second-quantized (position space, forced — no channel choice exists: the three-Wick-channel contraction set is

complete),

$$\hat{H} = \sum_s \int f_s^\dagger(x)\Big[-\frac{\hbar^2\nabla^2}{2m} + V_{\text{ext}}\Big] f_s(x) + \frac{1}{2}\sum_{s,s'}\iint f_s^\dagger(x) f_{s'}^\dagger(y)\, v(|x-y|)\, f_{s'}(y) f_s(x),$$
$$v(r) = -\frac{Gm^2}{r}. \tag{ZU3}$$

On the finite sector the pairing kernel is *derived* (not chosen) from the Berezin–Toeplitz matrix elements of the ψ modes on $H^0(\mathbb{C}P^2, \mathcal{O}(9))$, and the exact mode sum

$$K = \sum_k \frac{1}{\omega_k^2} = \frac{3665699}{1764} \quad \text{exactly} \tag{ZU4}$$

renders the self-energy finite with no counterterm.

2. Newton survives as an exact zero-parameter identity

Theorem ZU.1 (Exact Newton identity; zero parameters, forced normalization)**.** *Newton's law is an exact identity/saddle of the quantized ψ action: the vertex* (ZU2) *saturates $V(r) = -Gm_1m_2/r$ with zero adjustable quantity, by two independent symbolic routes (canonical normalization + Yukawa exchange; direct Poisson solve), and in the disjoint Hubbard–Stratonovich formalism Newton is the exact saddle of an exact Gaussian identity whose weight is* forced *to the corpus $c^4/32\pi G$ prefactor — uniqueness proven, so no hidden normalization is possible. Consequences, all with the* same *G: the fifth-force strength $\alpha_5 = 0$ identically, and, with the metric dictionary (Lemma WS.4), $\gamma_{\text{PPN}} = \beta_{\text{PPN}} = 1$ — matter's G and light's G are one number by construction. Numeric closure at CODATA: $G_{\text{out}}/G_{\text{in}} - 1 = -5.6 \times 10^{-16}$.*

G itself is *consumed*, not derived: it enters through the printed $c^4/32\pi G$ prefactor and nothing in this chain derives its value. What is parameter-free is the *identity* — the coefficient ratio is exactly 1 — not a value of G.

3. The gap in closed form; the carrier is Hartree, not a condensate

On the exactly-diagonal pair kernel (diagonality forced by the torus selection rule), the gap equation decouples orbital-by-orbital and admits the closed form

$$E_i = \frac{y^2 G_{ii}}{2}, \quad \delta = \frac{y^2}{2\sum_{\text{shell}} 1/G_{ii}}, \quad \Delta_i = \sqrt{E_i^2 - \delta^2}, \tag{ZU5}$$

nonzero on exactly 7 of 60 orbitals (indices 27–33, the degenerate Fermi shell), matching the reference Bogoliubov–de Gennes solver to 4.99×10^{-18}. Numeric labels (electron): the quasiparticle-energy maximum is $E_{\max} = 9.366856 \times 10^{-27}$ GeV; the true gap maximum is $\Delta_{\max} = 9.355917 \times 10^{-27}$ GeV (0.117% lower, the δ^2 correction). *The condensate is not the carrier*: under the complete three-channel (Hartree/Fock/pairing) functional the BCS minimizer runs to the $\kappa = 0$ boundary — confirmed Wick-free by direct Fock-vector minimization — and the mean-field completion of the vertex is **Hartree+Fock**. The Hartree channel reproduces $-\frac{1}{2}mc^2\,\psi[\Psi]$ coefficient for coefficient: the c-number source $\rho = m\langle\Psi|\hat{\rho}|\Psi\rangle$ *is* the Hartree factorization of the two-body operator (ZU3), so the Schrödinger–Newton *form* needs no classical-ψ axiom.

4. Second-order control

The beyond-mean-field residual reproduces $O(\alpha_\psi^2)$ with fitted slope $\to 2$, and the one-loop/MP2 layer carries 99.7% of it; on DFD's own finite sector the residual is exactly zero. The finite self-energy (via the exact K of Eq. (ZU4)) is proportional to $\hat{N}$ and hence unobservable (absorbed into the measured mass). Two layers are *priced, not computed*, and are explicitly not claimed discharged: the two-loop layer at α_ψ^3 and the ψ-loop layer at $(m/M_{\text{P}})^2$.

5. The Kohn null

Theorem ZU.2 (The Kohn null)**.** *Every term of the derived operator completion is translation-invariant or proportional to $\hat{N}$. By the generalized Kohn theorem, DFD's operator completion therefore predicts* exactly zero *gravitational self-gravity sideband on the center-of-mass mode of a trapped crystal — no ω_{SN} sideband, no two-peak structure — to* all orders *in α_ψ, with zero adjustable parameters; the statement extends to unequal masses at common trap frequency (real multi-species crystals).*

The semiclassical reading of the corpus's own Schrödinger–Newton equation (Sec. XVIII B) predicts instead

$$\omega_{\text{SN}}^2 = \frac{Gm}{6\sqrt{\pi}\,\sigma^3} > 0, \tag{ZU6}$$

with σ the measured Debye–Waller wave-packet width — an apparatus property, not a DFD parameter. Citation-faithful magnitudes at the cryogenic (100 mK) parameters of Großardt et al. [205] (Table I): osmium $\Delta\omega/\omega = 1.2 \times 10^{-13}$ (this chain) to 6.7×10^{-13} (Großardt et al.'s own number — ours is the conservative one); silicon 1.1×10^{-15} to 6.2×10^{-15}. The discriminator statement stands on osmium at the $\sim 10^{-13}$ order; silicon is secondary. The relevant protocols are the optomechanical Schrödinger–Newton tests of Yang, Miao, Lee and Chen [206] and Großardt et al. [205]; no published dataset reaches this discrimination yet — a live test, not an archival one. An independent calculation additionally bounds the maximum anharmonic/trap-internal leakage into the c.o.m. sideband at 1.9×10^{-18} (Os) / 2.0×10^{-19} (Si) — a factor 5.5×10^3–3.5×10^5 *below* the discriminator, so anharmonic corrections can neither fake nor mask it.

Falsifier ZU.3 (The SN sideband falsifies the completion). A measured positive self-gravity sideband at the predicted size (ZU6) falsifies the operator completion of this appendix outright (sign-definite) and vindicates the semiclassical reading. A null result confirms the operator completion but does not uniquely fingerprint DFD (Sec. ZU 7).

6. The Schrödinger–Newton term is the completion's falsifier

The operator completion of the *same* printed action forces the linear side: the c-number source is the Hartree factorization of a two-body operator (Sec. ZU 3), the one-particle sector is exactly free, and the Kohn null holds to all orders. The Schrödinger–Newton frequency shift of Sec. XVIII B is therefore not a DFD prediction but the *falsifier* of this completion. Novelty credit is stated precisely: the single-outcome analysis (App. QM) had already closed the classical-vs-quantized-ψ root in the quantized direction (Page and Geilker [207]; and the MAQRO sustained-fringe prediction); the present completion *completes* that line constructively — exact Newton identity, controlled completion, and the Kohn-null laboratory discriminator.

7. Scope and verification status

Status ZU.4 (What is and is not claimed). (i) The Kohn null itself is *shared with standard linear QM*: the unique DFD content is that a zero-parameter chain from the printed action (corpus action → forced vertex → forced channels) lands the theory on the linear side. (ii) The two-loop (α_ψ^3) layer is priced, not computed. A translation-breaking ψ-loop term cannot arise: the operator completion is invariant under spatial translations, so the total-momentum Ward identity holds at every loop order, and the loop dressing of the external trap is local and suppressed by $(m/M_{\rm P})^2 \simeq 2\times10^{-34}$ for osmium, more than twenty orders below the discriminator. The Kohn null therefore holds to all orders in ψ loops as well. (iii) G is consumed, not derived. (iv) Two independent formalisms (Wick/HFB; Hubbard–Stratonovich saddle) agree exactly.

Appendix NL: The Scale-Additive Field Equation and Its Test Record

1. Why a scale-resolved form is needed

The local operator of Eq. (21) evaluates μ at a point. DFD's derived response is, however, a *mode* statement: $\nu = 1/\mu$ is a single-mode partition function and τ is an optical depth (App. N), so the physical question is not "what is the field here?" but "how many independent modes does the field here consist of?". Those two questions have the same answer only when all the sourcing mass lies at one distance from the field point. This appendix constructs the operator that asks the second question directly, records its forward evaluations, and proves five no-go results that close the obvious alternatives.

a. The measurement that forces the question. Any response functional whose argument is the *vector* sum $|\nabla\psi_{\rm int} + \nabla\psi_{\rm ext}|$ — which includes every local AQUAL and QUMOND operator — generates a static anomalous quadrupole in the planetary potential,

$$\delta\Phi(\mathbf{x}) = -\frac{Q_2}{2}\, x_i x_j \Big(\hat e_i \hat e_j - \tfrac{1}{3}\delta_{ij}\Big), \qquad \text{(NL1)}$$

with $\hat{\mathbf{e}}$ the direction of the Galactic external field. The measured bounds are $Q_2 = (3\pm3)\times10^{-27}\,\mathrm{s}^{-2}$ from nine years of Cassini range and Doppler tracking of Saturn [29], tightened to $Q_2 = (1.6\pm1.8)\times10^{-27}\,\mathrm{s}^{-2}$ on the DE440 dataset [30]. Evaluating DFD's own derived response *through the local reading* at the bound-matter value $a_0 = 1.1966\times10^{-10}\ \mathrm{m\,s}^{-2}$ (Postulate ZS.11) gives $Q_2 = 30.6\text{–}31.8\times10^{-27}\,\mathrm{s}^{-2}$ across four independent evaluation methods, i.e. $+9.2$ to $+9.6\sigma$ against Cassini and $+16.1$ to $+16.8\sigma$ against DE440. The same obstruction is what Desmond, Hees & Famaey [179] report for MOND itself: a 8.7σ tension between the SPARC RAR and the Solar-System quadrupole under fiducial assumptions (relieved to 1.9σ only by discarding bulge galaxies). It is structural, not numerical: $Q_2 = 0$ requires the response functional *never to form* the vector sum $\mathbf{g}_\odot + \mathbf{g}_{\rm ext}$, and no local operator in $\nabla\psi$ can avoid forming it.

2. Statement of the scale-additive equation

Let the mode label be *log-distance from the field point*, which is forced: DFD's established mode reduced wavelength is $\bar\lambda = s$. Define the *shell field density*

$$\boldsymbol{\gamma}(\mathbf{x}, s) = -G \oint d\Omega\, \rho(\mathbf{x} + s\hat{\mathbf{n}})\, \hat{\mathbf{n}}, \qquad \int_0^\infty \boldsymbol{\gamma}(\mathbf{x}, s)\, ds = \nabla\Phi_N(\mathbf{x}), \qquad \text{(NL2)}$$

which carries *direction*: a symmetric shell contributes zero. Writing $\mathbf{m}(\lambda) = e^\lambda \boldsymbol{\gamma}(\mathbf{x}, e^\lambda)$ for the field generated per e-fold, the completion is a causal ODE in scale,

$$\frac{d\mathbf{g}_c}{d\lambda} = \mathbf{m}(\lambda) - w_0\, w(q)\, \mathbf{g}_c(\lambda), \qquad q \equiv |\mathbf{m}|/|\mathbf{g}_c|, \quad \text{(NL3)}$$

closed by the two exact quadratures

$$\nabla\Phi_N(\mathbf{x}) = \int d\lambda\; w_0 w(q)\, \mathbf{g}_c(\lambda),$$
$$\tau(\mathbf{x}) = \tfrac{1}{2}\int d\lambda\; w_0 w(q)\sqrt{|\mathbf{g}_c(\lambda)|/a_0}, \tag{NL4}$$

with $w(0) = 1$ (in vacuum the mode forgets) and $w(\infty) = 0$ (inside structure there is no forgetting). Both displayed identities are exact because $\int (d\mathbf{g}_c/d\lambda)\, d\lambda = 0$ over the whole axis; the prefactor $\frac{1}{2}$ is *forced*, not chosen — for $\int w\, g_c^p\, d\lambda = g^p$ the prefactor must be p, and $p = \frac{1}{2}$ for τ, $p = 1$ for $\nabla\Phi_N$. The response is then the established one, $\nu = 1/(1 - e^{-\tau})$, evaluated on this τ. For scale-separated sources this τ composes additively, a reading that weak-host-field data disfavour against the quadrature form (§NL 10, item 2); a subsystem whose host mode is typically empty is Newtonian (Axiom NL.14).

In words: *gravity keeps a running memory of the field it has passed, and forgets it only while crossing vacuum.* A galaxy is matter all the way through and stays one mode; the Sun and the Galaxy, separated by 18.955 e-folds of vacuum, stay two.

a. The window width is derived, not fitted. The window realisation $\mathbf{g}_\lambda = \int \psi(\ln s - \lambda)\boldsymbol{\gamma}\, ds$ admits exactly two normalisations and no more: $\int \psi\, du = 1$ (partition of unity, so Eq. (NL4) left is exact) and $\int \sqrt{\psi}\, du = 1$ (a single point source must return the established $\tau = \sqrt{g/a_0}$ exactly). Writing $\varphi \equiv \sqrt{\psi}$ these read $\int \varphi = 1$ *and* $\int \varphi^2 = 1$ — two conditions, which fix the width. Solving them exactly: the top hat has support **exactly one e-fold**; the triangle 4/3; the raised cosine 3/2; the Gaussian $\sigma = 1/(2\sqrt{\pi})$, i.e. equivalent width $1/\sqrt{2}$.

b. Closed form for point sources. Sorting sources by distance from $\mathbf{x}$, with $\lambda_k = \ln|\mathbf{x} - \mathbf{y}_k|$ and $\mathbf{g}_k = Gm_k(\mathbf{x} - \mathbf{y}_k)/|\mathbf{x} - \mathbf{y}_k|^3$,

$$\mathbf{g}_c^{(k)} = \mathbf{g}_c^{(k-1)} e^{-w_0\Delta_k} + \mathbf{g}_k,$$
$$\tau(\mathbf{x}) = \sum_k \sqrt{|\mathbf{g}_c^{(k)}|/a_0}\,\big(1 - e^{-w_0\Delta_{k+1}/2}\big), \tag{NL5}$$

with $\Delta_k = \lambda_k - \lambda_{k-1}$ and $\Delta_{N+1} = \infty$.

3. The exact limits

Theorem NL.1 (Limits of the partition of unity)**.** *For any admissible vacuum detector w with $w(0) = 1$, $w(\infty) = 0$, and any $w_0 > 0$:*

1. Single point source: $\tau = \sqrt{g/a_0}$*, the established law, exactly and* independently of w_0*.*
2. Co-distant sources *(any masses, any angles):* $\tau = \sqrt{|\sum_i \mathbf{g}_i|/a_0}$ *— the local, per-point (AQUAL) reading of Eq. (21), recovered exactly.*
3. Scale-separated sources: $\tau = \sum_i \tau_i$*, equivalently* $1 - \mu_{\rm tot} = \prod_i (1 - \mu_i)$ *— the Beer–Lambert composition law that forces the exponential shell (App. N), recovered exactly.*
4. Subdivision: *splitting any body into N pieces leaves τ invariant to all orders, because $\boldsymbol{\gamma}$ is a* linear *functional of ρ.*

Proof. (1) and (4) follow from Eq. (NL2) and the two normalisations: a single source contributes one jump in $\mathbf{g}_c$ and the tail integral $\int_0^\infty w_0 e^{-w_0 v/2} dv/2 = 1$ returns $\sqrt{g/a_0}$ for every w_0. (2): all mass at one λ makes $\mathbf{g}_c$ a single jump equal to the vector sum, and the $\frac{1}{2}$ prefactor returns $p = \frac{1}{2}$ of it. (3): for $\Delta \to \infty$ the accumulator has decayed to zero between contributions, so Eq. (NL5) telescopes into $\sum_k \sqrt{g_k/a_0}$. Numerically, at machine precision: residuals 0 (item 1, all w_0 tested), 0 (item 2, six random sources), 4.4×10^{-14} (item 3), and item 4 returns $\tau_N/\tau_1 = 1.000000000000000$ for N up to 10^3 co-located pieces and exactly 1 thereafter by the contraction in Eq. (NL5). □

Remark NL.2 (The Beer–Lambert limit needs a mass condition as well as distance). Scale separation alone is *not* sufficient. The leaked field is $g_1 e^{-w_0\Delta} = Gm_1/(d_1 d_2)$, so the per-source limit requires $(m_{\rm near}/m_{\rm far})(d_{\rm far}/d_{\rm near}) \ll 1$. For the Sun in the Galaxy at 10 AU this ratio is 1.69×10^{-3} (with $M_{\rm enc}(R_0) = 1.01 \times 10^{11}\, M_\odot$ from $v_c = 229$ km s^{-1}), and the separation is $\ln(R_0/10\,{\rm AU}) = 18.955$ e-folds. Two comparable masses at a large distance ratio do *not* separate.

Corollary NL.3. *$\sigma \equiv \tau - \tau_N \geq 0$ on every configuration tested (400/400 random 2–6-source configurations spanning four decades in distance and random directions; zero negatives).*

4. Conservation

Theorem NL.4 (E, $\mathbf{p}$, $\mathbf{J}$ conserved)**.** *The scale-additive action*

$$S[\Phi, \Phi_N] = -\int dt \int d^3x \Big\{\rho\Phi + \tfrac{1}{8\pi G}\big[2\nabla\Phi\cdot\nabla\Phi_N - a_0^2\mathcal{Q}\big]\Big\} + S_{\rm matter},$$

$$\mathcal{Q}(\mathbf{x}) = \nu(\tau)\big(\tau_N^4 - \tau^4\big) + 4\int_0^\tau \nu(v)\, v^3\, dv,$$
$$\tau_N = \sqrt{|\nabla\Phi_N|/a_0}, \quad \tau = \tau_{\rm FB}[\rho]\ (\S NL\,10, \S NL\,5),$$

has no explicit t-dependence at fixed a_0, is invariant under translations and rotations, and is differentiable in the source positions. Noether therefore gives exactly conserved $E = \sum_a \frac{1}{2} m_a \dot{\mathbf{x}}_a^2 + W$ with $W = -(a_0^2/8\pi G)\int \mathcal{Q}\, d^3x$, together with $\mathbf{p}$ and $\mathbf{J}$.

Proof. Time- and Euclid-invariance hold for every construction in this family, since every kernel is built from $|\mathbf{x} - \mathbf{y}|$ alone. Differentiability is the entire content: the

FB-OUT depth's first-order response to a displaced point source is explicit (Eq. (NL6)), and $\mathcal{Q}$ contains no subtraction, and is finite where $\tau_{\rm FB} \to 0$ because $\tau_N \le \tau_{\rm FB}$ there, so the integrand of W is finite on every positive-mass configuration; its volume integral grows as $\ln r$ at large distance, through a term fixed by the total mass, as the field energy of any isolated deep-MOND mass does. Variational residuals (symbolic): $\delta S/\delta\Phi \Rightarrow \nabla^2\Phi_N = 4\pi G\rho$, residual 0; the constitutive step $\partial(a_0^2\mathcal{Q})/\partial(\nabla_i\Phi_N) - 2\nu(\tau)\nabla_i\Phi_N$, residual $(0,0,0)$; Newtonian limit $\mathcal{Q} \to \tau_N^4 + 4\pi^4/15$, an inert additive constant, residual 0. □

In this action Φ_N is an auxiliary field: $\delta_\Phi S = 0$ makes it the Newtonian potential of the matter, and it is not a potential of the metric, which at first post-Newtonian order carries the one function $\psi = -2\Phi/c^2$ (Cor. NL.17).

Remark NL.5 (Why a hard connectivity rule could not have this). A *hard* partition of the mass into connected components is a global operation and therefore jumps. Measured at a merge surface, its $|\Delta W|/|W| = 1.4005 \times 10^{-1}$ *step-independently* over four decades of step size, i.e. a genuine 14% discontinuity, i.e. a δ-function force. The scale-additive $|\Delta W|/|W|$ is 8.29×10^{-5}, 10^{-7}, 10^{-9} at the same three steps — exactly proportional to the step.

Status NL.6 (Numerical conservation). The theory's own central potential is $\Phi(r) = -GM/r + a_0 r_M \ln\nu(r_M/r)$ with $r_M = \sqrt{GM/a_0}$. Symbolically (residual 0) $d\Phi/dr = \nu(\tau)\,GM/r^2$ with $\tau = r_M/r$, and $r\,d\Phi/dr \to \sqrt{GMa_0}$ as $r \to \infty$, i.e. the baryonic Tully–Fisher relation $v_f^4 = GMa_0$ holds *exactly*. Integrating a bound orbit in that potential with a fixed-step fourth-order composition integrator at $dt = T/8000$ for 40 periods — **320 000** steps — gives $\max|\Delta E/E| = 1.5$–2.6×10^{-12} (integrator-dependent), $\max|\Delta L/L| \le 5 \times 10^{-14}$, and a secular slope per period of $|\cdot| < 2 \times 10^{-15}$, i.e. consistent with exactly zero. The error falls under step refinement, so it is integrator truncation and not dynamics. On a random four-body configuration, $|\sum_a \mathbf{F}_a|/\max|\mathbf{F}| = 2.1 \times 10^{-12}$ and $|\sum_a \mathbf{x}_a \times \mathbf{F}_a|/(\max|\mathbf{x}|\max|\mathbf{F}|) = 9.5 \times 10^{-11}$.

5. Action completion of the scale-additive equation

The forward law $\nabla^2\Phi = \nabla\cdot[\nu(\tau)\nabla\Phi_N]$ on the FB-OUT depth $\tau = \tau_{\rm FB}[\rho]$ (§NL 10, item 2; the depth of record for this subsection) is the static limit of exactly one action of the form $Q(t,\tau)$ that keeps the isolated point-mass law, and that action fixes the force on matter. Write $t \equiv \tau_N = \sqrt{|\nabla\Phi_N|/a_0}$ and $Q_{\rm QU}(\tau) = 4\int_0^\tau \nu(v)\,v^3\,dv$.

Theorem NL.7 (Unique static completion). *With $\mathcal{Q} = Q_M(t,\tau) \equiv \nu(\tau)\,(t^4 - \tau^4) + Q_{\rm QU}(\tau)$ in Thm NL.4, $\delta_\Phi S = 0$ gives $\nabla^2\Phi_N = 4\pi G\rho$ and $\delta_{\Phi_N} S = 0$ gives the forward law, because $\partial(a_0^2 Q_M)/\partial(\nabla_i\Phi_N) = 2\nu(\tau)\nabla_i\Phi_N$; Q_M is the unique $Q(t,\tau)$ with this property whose isolated point mass ($\tau \equiv t$) carries the QUMOND energy. It contains no subtraction, is finite on every positive-mass configuration because $\tau_N \le \tau_{\rm FB}$ there, and $a_0^2 Q_M \to |\nabla\Phi_N|^2 + 4\pi^4 a_0^2/15$ (an inert constant) in the Newtonian limit. The force on body a is*

$$\mathbf{F}_a = -m_a\nabla\Phi(\mathbf{x}_a) + \frac{a_0^2}{8\pi G}\int d^3x\;\nu'(\tau)\,(t^4-\tau^4)\,\frac{\partial\tau_{\rm FB}(\mathbf{x})}{\partial\mathbf{x}_a},$$
$$\delta(a_0\tau^2) = \frac{Gm}{s^2}\Big[\cos\psi + (1-\rho^3)(1-\cos\psi)\,\Theta(s<r)\Big], \tag{NL6}$$

the second term being the first-order response of the depth to a displaced source m with one other source present (the Galaxy enters only through g_e; $s = |\mathbf{x}-\mathbf{y}|$, r the distance from $\mathbf{x}$ to the other source, $\rho = s/r$, ψ the angle between the two sources' fields at $\mathbf{x}$). For an isolated point mass $\tau_{\rm FB} \equiv t$ and the reciprocal term vanishes identically, so the test-body law $\nu(t)\,g_N$ is exact. For a disc, $\tau_{\rm FB} = t$ at the midplane (§NL 10, item 2) leaves the forward law there unchanged; the reciprocal term on a midplane body samples the off-plane depth, where non-reversal is not established. For exponential discs of thickness 0.05–0.2 R_d, from Milky-Way-like to deep low-surface-brightness, it is below 3% on a midplane star and cancels against the off-plane change of the forward field to ≤ 0.002 dex between 0.5 and 8 R_d (computed); for a spherical density that decreases outward $\tau_{\rm FB} = t$ at every point, so the reciprocal term vanishes and the completed law is the local law. Uniqueness holds within energies that depend on ρ through $\tau_{\rm FB}$ alone; an energy built from a second printed depth would add terms with coefficients no printed principle fixes. In the frozen regime of Axiom NL.14 the law is resolved by mode and has no reciprocal term (§NL 6); the uniqueness above concerns the law of weak hosts.

Theorem NL.8 (Cassini, exactly). *For the Sun in the Galactic field $g_e\hat{\mathbf{e}}$ the depth $a_0\tau^2 = GM_\odot/r^2 + g_e$ is spherical about the Sun (the vector sum is never formed), while $a_0^2 t^4 = |\nabla\Phi_N|^2$ is quadratic in that sum, so $t^4 - \tau^4 = -2g_e\,GM_\odot(1+\cos\theta)/(a_0^2 r^2)$ carries only $l \le 1$; both kernels of Eq. (NL6) are rotationally covariant about the Sun. Hence the test-body potential is $l \le 1$ and $Q_2 = 0$ exactly at first order in the planet mass (-0.89σ against DE440, -1.00σ against Cassini, from the central values). The reason is sharper than the statement of §NL 1: an energy* linear *in $|\nabla\Phi_N|^2$ with a spherical coefficient has no $l = 2$ term even though it contains the vector sum, whereas AQUAL/QUMOND evaluate ν at $|\nabla\Phi_N|$ itself. Under Axiom NL.14 the Sun's own field is Newtonian inside the Galaxy, so $Q_2 = 0$ at every order; the Galactic tide itself is 8×10^{-31} s^{-2} (computed).*

Theorem NL.9 (Newton's third law). $\sum_a \mathbf{F}_a = 0$ *by translation invariance. The forward force alone does not have this property: on a body of mass M in a host field $g_e\hat{\mathbf{e}}$ it exerts a net push $-(g_e/3)(\nu_e - 1)M\hat{\mathbf{e}}$ ($\nu_e = \nu(\tau_{\rm ext})$), cancelled in closed form by the reciprocal term, $\frac{1}{8\pi}(-2g_e)\frac{4\pi}{3}\,[\nu]_{\tau_{\rm ext}}^{\infty}\,M = +(g_e/3)(\nu_e-1)M\hat{\mathbf{e}}$ (units $G = a_0 = 1$). At the Sun's depth, with the Newtonian Galactic field of 1.19–1.33 a_0 as the argument, the push would be 0.201–0.204 $a_0 M_\odot$ (computed); the Sun itself*

is frozen by Axiom NL.14, the mode-resolved law has no cross term there, and the push and the reciprocal term both vanish. Cor. NL.18's $\sum_a \mathbf{F}_a = 0$ is therefore a theorem of the action completion, external-field regime included.

Theorem NL.10 (Orientation: affine in the external field)**.** *For bodies scale-separated from the Galaxy, $\tau_{\rm FB}$ depends on $|g_e|$ but not on $\hat{\mathbf{e}}$, and t^4 is affine in $\hat{\mathbf{e}}$; hence every $\mathbf{F}_a$ is affine in $\hat{\mathbf{e}}$, and a pair's relative acceleration at angle θ to $\hat{\mathbf{e}}$ is exactly $\gamma(\theta) = \gamma_0 + \gamma_1 \cos\theta$: no even ($\cos^2\theta$, $G_\parallel/G_\perp$) modulation at any separation or mass ratio, and an odd term antisymmetric under $m_1 \leftrightarrow m_2$ — zero for equal masses, $\leq 1\%$ of γ_0 for $m_2/m_1 = 0.5$ at $\leq 3 \times 10^4$ AU, and +1.5%, +3.0%, +2.8% of γ_0 in the test-body limit at 7274, 10^4, 2×10^4 AU (larger attraction for the companion on the Galactic-centre side). The statement is about the force; the velocity observable $v_{\rm obs}/v_N$ inherits an even term of order $\gamma_1^2/2\gamma_0 \lesssim 7 \times 10^{-4}$ at $\leq 3 \times 10^4$ AU in the test-body limit, identically zero for equal masses. At the Sun Axiom NL.14 makes local pairs Newtonian, so both the even and the odd terms vanish there; the odd-term values above are the completed law's for a host at the Sun's depth and apply to pairs in weak hosts.*

Status NL.11 (Wide-binary force boost, external field included). Orientation-averaged, $g_e = 1.793\,a_0$, total mass $1\,M_\odot$ (separations scale as $\sqrt{M_{\rm tot}/M_\odot}$). Equal-mass pair (full three-source depth): $\gamma = 1.26, 1.37, 1.50, 1.59, 1.69, 1.78$ at $7274, 10^4, 1.45 \times 10^4, 2 \times 10^4, 3 \times 10^4, 5 \times 10^4$ AU ($m_2/m_1 = 0.5$: within 0.012 of these). Test body (comets, planets): $\gamma = \nu(\tau_0) + \gamma_{\rm rec} = 1.37, 1.52, 1.74, 1.81$ at $7274, 10^4, 2 \times 10^4, 3 \times 10^4$ AU, tending to $1.87 = \nu_e + 0.511$ for $r_M \ll d \ll$ pc: the reciprocal weight falls as $1/r^2$, so the boost does *not* saturate at $\nu_e = 1.355$ as the forward response does ($g_e = 1.838\,a_0$ moves each test-body entry by $\leq 1\%$; with the Newtonian Galactic field $g_{N,e} \simeq 1.2\,a_0$ as the depth's argument, the observed $1.79\,a_0$ being the boosted total, every test-body entry rises by 3–16%). These are the completed law's values at the Sun's host field, and they are not realised there: the Galaxy's mode at the Sun is typically empty, so under Axiom NL.14 local pairs are exactly Newtonian, $\gamma = 1$, with no orientation term. On the *Gaia* DR3 analyses this sides with the null camp, Banik et al. (2024) [52] (-0.3σ on $\alpha_{\rm grav}$) and Saad & Ting (2026) [208] (0.0σ), against Chae (2023) [51] ($+7.2\sigma$), Chae et al. (2026) [209] ($+4.3\sigma$), Yoon et al. (2025) [210] ($+2.9\sigma$ on its combined low-acceleration value) and Hernandez et al. (2024) [211]; Boufourou (2026) [212], $\gamma = 1.045\,[1.025, 1.068]$, lies 2.2σ above it on that 68% statistical interval; its eccentricity-model systematic band, 0.957–1.068, includes $\gamma = 1$. A confirmed boost of the Chae type in local pairs falsifies the axiom. Pairs beyond the edge of the frozen zone keep the boost: on the forward law $\gamma = 1.70$–1.97 at 10^4 AU and 2.11–3.29 at 2×10^4 AU for $R = 20$–100 kpc, and the reciprocal term adds to these (computed). The orientation statements of Thm NL.10 hold for such pairs.

Status NL.12 (The Oort cloud excludes the external-field-regime boost as printed). Long-period comets are test bodies of exactly the field of Status NL.11. Their *original* $1/a$ is the Newtonian specific energy inferred at ~ 250 AU (planets removed), and the CODE catalogue [213] shows the Oort spike at $0 < 1/a \lesssim 0.75 \times 10^{-4}$ AU^{-1} (centroid $\simeq 3$–4×10^{-5}; 277 of 369 long-period comets in $[0, 10^{-4}]$; 17 hyperbolic originals (4.6%); per-comet errors $\simeq 10^{-6}$). Every reading here is Newtonian to e^{-28} inside 250 AU and conservative for the comet, so for the test-body force $-\gamma(r) GM_\odot/r^2$, $1/a_{\rm N} = 2/r_a - 2\int_{250\,\rm AU}^{r_a} (\gamma - 1)\, r^{-2} dr$ exactly for a comet turning at r_a. A comet tidally injected from $a_{\rm true} = 25\,000$ AU ($1/a = 4 \times 10^{-5}$) is catalogued at -2×10^{-4} (this completion), -1.0×10^{-4} (FB-OUT forward response), -3×10^{-5} (accumulator forward response, SOURCE branch) and $+0.3 \times 10^{-5}$ AU^{-1} (TOTAL branch), 30–230 per-comet errors and 3–23 non-gravitational shifts from the observed centroid; the spike position alone bounds a boost saturating at r_M to $\gamma_\infty - 1 \lesssim 0.02$–$0.04$, against the printed $\nu_e - 1 = 0.36$ (SOURCE), 0.20 (TOTAL) and 0.87 (this completion). Independently, the odd $l = 1$ term of every reading is 10^2–10^3 times the Galactic tide $4\pi G\rho_0 d$ at $\lesssim 10^4$ AU, collapsing the tidal injection radius from $\simeq 2.3 \times 10^4$ AU (Newton) to 3–4×10^3 AU in every reading, the completion included. A direct integration (2×10^4 test comets, 1 Gyr, Galactic tide) reproduces the observed spike under Newton (median original $1/a = 4.0 \times 10^{-5}$ AU^{-1}, 77% within $[0, 0.75] \times 10^{-4}$, no hyperbolic originals) and gives, for the mildest printed reading (accumulator, TOTAL branch, monopole), a median of -1.4×10^{-5} with 77% hyperbolic originals; for the SOURCE branch 100% hyperbolic; for the completion a median of -1.9×10^{-4} with 75% hyperbolic; and, with the forward law's own $l = 1$ term, the stripping of two thirds of the cloud within 1 Gyr. Vokrouhlický, Nesvorný & Tremaine [214] exclude AQUAL-MOND by this test for every transition function ("a nearly uniform distribution in $1/a$ … far more LPCs on hyperbolic orbits than the data") and leave open theories "in which non-Newtonian effects are screened … in external gravitational fields comparable in strength to the critical acceleration". DFD as printed does the opposite: at the Sun the Galactic mode's occupation $n_e = 1/(e^{\tau_{\rm ext}} - 1) = 0.46$–$0.51$ is passed to the Sun's field by the composition laws of §NL 2 ($\tau_{\rm ext} = 1.09$–1.15, taken on the Newtonian Galactic field for an observed field of 1.79–$1.94\,a_0$; the entries of Status NL.11, which enter the observed field as the argument, understate the excess the comets exclude). Every reading that boosts the Sun's own field is excluded by this test. Under the environmental-confinement axiom (§NL 6) the Galaxy's mode at the Sun is typically empty ($n_e = 0.46$–$0.51 < 1$), so the Sun's own field is Newtonian and the Newtonian run of the integration above reproduces the spike; this is a postdiction, since the axiom was stated to pass it. What is untouched: everything without an external mode (the RAR, BTFR and a_0 results, which carry no external mode), the Solar-System monopole at the planets ($\gamma - 1 = e^{-\tau}$, $\tau \simeq 7 \times 10^2$

at Saturn), Q_2, and the dwarf-spheroidal external-field results, whose host fields lie below about $0.2\,a_0$ observed and below $0.03\,a_0$ in the Newtonian baryonic field (Table XCIX), far below the axiom's threshold. The axiom's own predictions are $\gamma = 1$ with no orientation term for local pairs, and a step in the dynamics of bound subsystems at the edge of the frozen zone, $R \simeq 13$–16 kpc; the outer-halo globular clusters beyond it show about a third of the predicted boost (0.33 ± 0.08) (Table CXXXIII).

6. The external-field sector: environmental confinement

Theorem NL.13 (A host caps an embedded boost)**.** *Let a subsystem of depth τ_s sit in a host of depth τ_h, scale-separated in the sense of Rem. NL.2. (i) The additive composition is the fugacity law of Thm BS.5: $\nu(\tau_s+\tau_h) = 1/(1-z\,e^{-\tau_s})$ with $z = e^{-\tau_h}$, so as $\tau_s \to 0$ the subsystem's boost tends to $\nu(\tau_h) = 1 + n_h$, $n_h = 1/(e^{\tau_h}-1)$. (ii) Every composite depth that depends on the subsystem only through τ_s, is continuous, and returns τ_h as $\tau_s \to 0$ has the same limit; the accumulator, the quadrature and the enclosed-mass depths all qualify. (iii) Tying the embedded quanta to the host's, whether locked, bounded or in exchange equilibrium, gives the same n_h; letting the host keep one quantum gives $n_h e^{-\tau_h}$, and two host quanta per embedded quantum give $n_{\rm BE}(2\tau_h)$.*

Proof. (i) is a geometric series (symbolic residual 0). (ii) is continuity at $\tau_s = 0$. (iii) sums the geometric occupation $P(m) = (1-e^{-\tau_h})\,e^{-m\tau_h}$ of the host mode. □

At the Sun the Galaxy's depth, taken on its Newtonian field, is $\tau_h = 1.09$–1.15 ($n_h = 0.46$–0.51), so every composition of (ii) leaves the Sun's own field boosted by 46–51% where that field is weak, and the nestings of (iii) by 11–17%, where the Oort spike allows about 2% out to 5×10^4 AU (Status NL.12). In joint equilibrium the state with the host mode occupied and the Sun's mode ladder active outweighs the state with the host empty and the ladder frozen by a factor of about 500 (the ladder carries $\ln Z = 7.4$ nats), so the statistics favour the boost (computed). The freeze has to be stated.

Axiom NL.14 (Environmental confinement)**.** *A bound subsystem keeps the μ-law boost of its own field only while the Bose mode of its host is typically occupied, that is, while the median occupation of the host mode is at least one:*

$$n_h \geq 1 \iff \tau_h \leq \ln 2 \iff g_{N,h} \leq (\ln 2)^2 a_0 \simeq 0.48\,a_0, \tag{NL7}$$

with $\tau_h = \sqrt{g_{N,h}/a_0}$ and $g_{N,h}$ the Newtonian field of the baryons of every enclosing bound system at the subsystem. Where the host mode is typically empty the subsystem's own field is exactly Newtonian. The host's own field is unchanged across the subsystem.

A subsystem's relative acceleration is $\nu_{\rm emb}\,\mathbf{g}_{N,s}$, with $\nu_{\rm emb} = \nu\big(\sqrt{\tau_s^2+\tau_h^2}\big)$ for $\tau_h < \ln 2$ (the quadrature composition, §NL 10, item 2) and $\nu_{\rm emb} = 1$ for $\tau_h > \ln 2$; its centre of mass moves in the host's field. In the frozen case the forward law is resolved by mode, $\nabla^2\Phi = \nabla\cdot[\nu(\tau_h)\nabla\Phi_{N,h}] + \nabla^2\Phi_{N,s}$ across the subsystem: the host's field keeps its boost, the subsystem's own field is Newtonian, and no term couples the two. The forward force then exerts no net push on the subsystem, and the reciprocal term of the action completion, which cancels that push (Thm NL.9), is absent with it, together with the test-body excess of about 0.51 that it gives at the Sun (Status NL.11). In weak hosts the completed law stands as printed. It multiplies the total Newtonian field by ν of the combined depth, so across a subsystem the host's field carries a term in the subsystem's depth, which the mode-by-mode demand of the energy in App. AV does not have. The satellite and wide-binary numbers of this appendix use the completed law; the χ results of App. AV use the mode-by-mode energy. The action form of the mode-resolved law is not constructed.

The threshold is not a chosen number. For a Bose mode, $n < 1$, $\tau > \ln 2$, $P(n{=}0) > \frac{1}{2}$ and a median occupation of zero are one statement, so the threshold is where the host's typical state becomes the vacuum. What the axiom adds is that the embedded ladder follows the typical (median) state of the host mode, and follows it sharply: the even-handed median readout fixes where the switch sits, and its sharpness is what is stated; the host's own boost keeps the mean, $\nu(\tau_h) = 1 + n_h$. The host mode is the one the host's baryons polarize (Rem. GR.9), so its depth is set by the baryonic field; counting χ would freeze the cores of rich clusters out to about 1 Mpc and slow their galaxies by about 40% (estimate), which cluster Tully–Fisher work does not show. The Rest-Mass Channel confines the μ-law to bound low-acceleration systems (App. GR); the axiom judges "low-acceleration" by the system's environment, with the Bose median as the criterion, and adds no field and no constant. It realizes the possibility Vokrouhlický, Nesvorný & Tremaine leave open, a response "screened … in external gravitational fields comparable in strength to the critical acceleration" [214].

a. The edge of the frozen zone. On the Milky Way's Newtonian baryonic field the threshold lies at $R \simeq 13$ kpc for $6.5 \times 10^{10}\,M_\odot$ of baryons and 16 kpc for $10^{11}\,M_\odot$ (computed). Inside it every bound subsystem is Newtonian: the Solar System, the wide binaries of the *Gaia* catalogues near the Sun, open clusters and the inner globular clusters. Outside it they keep their boost; for the outer-halo globular clusters this is contradicted by the data (Table CXXXIII). A subsystem that crosses the edge switches laws: the relative force of a $1\,M_\odot$ pair at 10^4 AU is 1.59 times the Newtonian force just outside and exactly Newtonian inside (1.85 at 2×10^4 AU; forward law, the reciprocal term adds to both; computed), where MOND's external-field effect declines smoothly. The data allow the threshold depth anywhere between 0.16 (the classical dwarf spheroidals, all boosted) and 1.09 (the Sun),

$R \approx 8$–66 kpc; the axiom puts it at $\ln 2$. In an action the step is a δ-function force (Rem. NL.5), so the zero-dipole theorem (Cor. NL.18) holds away from the edge only; a smoothing over $\Delta\tau \leq 0.15$ changes none of the results of Table CXXXIII (estimate). The comets do not need an exact step: if their energy budget scales with the switch's weight, a Hill switch $n_h^m/(1+n_h^m)$ passes them for $m \gtrsim 4$–5, while a single coherent host mode, $m = 1$, gives 5.9 against an allowance of about 1 (computed); a derived width is open.

The Oort spike and the planets are postdictions: the axiom was stated to pass them. The local wide binaries and the edge are its predictions. Draco is boosted and, like every reading, under-predicts its dispersion; it does not discriminate. The axiom has four costs: it is a postulate, which the Bose statistics provably cannot supply; it is a step, a δ-function force in an action, with a width that is not derived; the action form of the law in the frozen regime is not constructed, so Thm NL.4 is not extended to that regime; and the external-field values that the completed law gives at the Sun's depth (Status NL.11) are not realised at the Sun.

7. The test record

a. Checks at the bound-matter value $a_0 = 1.1966 \times 10^{-10}\,\mathrm{m\,s^{-2}}$. $r_{M_\odot} = \sqrt{GM_\odot/a_0} = 7039.671$ AU (reproduced to 10^{-5}); $\tau_\odot$(Saturn) = 734.8; the partition-of-unity identity $\int w_0 w\, \mathbf{g}_c\, d\lambda = \nabla\Phi_N$ closes to 8×10^{-7} on the numerical grid; the ephemeris pipeline reproduces Hees et al. [29] to 0.58% across all 56 rows of their Table 2 and 48/49 rows of Milgrom [215] Table 1, *before* it was pointed at DFD.

b. The disc RAR, and its sensitivity to the one imported constant. On the depth of record, FB-OUT, the disc RAR is untouched: its midplane depth equals the local one exactly, and the completion moves the relation by at most 0.002 dex (computed). The numbers below belong to the accumulator reading, whose one imported constant is the width w_0. For an exponential Milky Way disc ($R_d = 2.6$ kpc, $h_z = 0.3$ kpc), the displacement of the radial acceleration relation between the scale-additive τ and the local per-point τ is 0.016–0.018 dex r.m.s. over 1–30 kpc, against the observed intrinsic scatter floor of **0.057** dex [104]. Varying the one imported constant over $w_0 \in [0.5, 2]$ gives total displacements of 0.016–0.073 dex and *shape-only* displacements (r.m.s. about the mean, which a RAR fit would absorb into normalisation) of 0.008–0.035 dex. The imported value $w_0 = 1$ gives the smallest total displacement of the family, and the only member that exceeds the observed floor is $w_0 = 0.5$.

8. The distinctive signature: radial

Theorem NL.15 (Angular null)**.** *Clumps at equal distance from the field point produce* $\tau_{\text{scale-additive}} = \tau_{\text{vector-sum}}$ bit-identically *(*0.00×10^0 *residual for* $N = 2, 4, 8, 16$ *spread over a* 34° *cone). **Angular clumping is invisible to the equation. The entire discriminator lives in log-distance from the tracer.***

Proof. Immediate from Thm NL.1.2: equal distance means equal λ, and the closed form contracts co-distant contributions into their vector sum before any square root is taken. □

Theorem NL.16 (Master law)**.** *At fixed* g_{bar}*, with* N *contributors each supplying* g/N *separated by* Δ *e-folds,* $\tau_{\text{new}}/\tau_{\text{old}}$ *runs monotonically from* 1 *(Thm NL.1.2,* $\Delta = 0$*) to* $\sqrt{N}$ *(Thm NL.1.3,* $\Delta \to \infty$*), and in the deep field* $\Delta \log_{10} g_{\text{obs}} \to -\frac{1}{2}\log_{10} N$ *exactly. The ratio is* ≥ 1 *everywhere:* ***there is no crossover, and the forward response is uniformly weaker-boost than the local one, at every geometry.*** *Inside a structure generating field per e-fold the accumulator reaches a fixed point* $q^* = w_0 w(q^*)$ *and* $\tau_{\text{new}}/\tau_{\text{old}} \to C\sqrt{\Lambda}$*, with* Λ *the structure's extent in e-folds, with* $C = \sqrt{q^*}/2$*; for the primary detector* $w = e^{-q}$ *this is the **omega constant**,* $q^* = W(1) = 0.5671432904$*, giving* $C = 0.3765445825$.

Corollary NL.17 (Lensing mass = dynamical mass)**.** *DFD's metric is one-function at first post-Newtonian order,* $g_{00} = -e^{-\psi}$*,* $g_{ij} = e^{+\psi}\delta_{ij}$ *(Sec. IV). The PPN parameter* γ *is read off the* ratio *of the two exponents;* ψ *never enters as a source. Hence* $\gamma - 1 = 0$ *for* arbitrary ψ *(symbolic residual* 0*), light deflection* $= 4GM/(c^2 b)$ *(residual* 0*), and the lensing kernel minus the dynamical kernel vanishes to* $O(v^2/c^2)$*, as in general relativity: the traceless strain of the parent tensor enters the spatial metric at second order (App. WS).* ***No static field equation for*** ψ *—* ***local, nonlocal, either branch — can touch this; it is a property of the coupling, not of the response.*** *The reciprocal force of the action completion (Thm NL.7) is not part of the metric: it acts on bodies in weak hosts and not on light, so where it does not vanish (test bodies in weak hosts, the wide-binary term* γ_{rec}*, satellites of weak hosts) dynamics differs from lensing by it; it vanishes for isolated bodies and spherical sources and is below* 0.002 *dex at disc midplanes. RAQUAL cannot reproduce it (its conformal coupling leaves lensing on the Einstein-frame potential); TeVeS needs an extra vector field to force it.*

Corollary NL.18 (Zero dipole radiation, and why only this equation has it)**.** *The source term* $-(c^2/2)\int \psi(\rho - \bar{\rho})$ *is linear in* ρ *with one universal constant, so the scalar charge is* ρ*, the dipole moment is* $\mathbf{D} = M\mathbf{X}_{\text{cm}}$*, and dipole power* $\propto M^2|\ddot{\mathbf{X}}_{\text{cm}}|^2$ *vanishes* iff $\sum_a \mathbf{F}_a = 0$*. The scalar-tensor* $(\alpha_A - \alpha_B)^2$ *term cannot appear, because every body's scalar charge equals its mass, binding energy included (App. WS). Measured* $|\sum \mathbf{F}|/\max|\mathbf{F}|$ *on three clumpy configurations:* 3.19×10^{-10}*,* 1.08×10^{-9}*,* 2.00×10^{-11}*.* ***By Rem. NL.5 a hard partition's step-independent*** 14% ***jump in*** W ***is a*** δ***-function force, so*** $\ddot{\mathbf{D}}$ ***would carry a*** δ' ***and its radiated dipole power would be formally divergent at every merge***

TABLE CXXXIII. Tests of the environmental-confinement axiom. Pulls are from the central values; the interval of Boufourou (2026) is its 68% statistical interval.

Test	DFD with the axiom	Data	Result
Oort spike	Sun Newtonian: 2×10^4 comets, 1 Gyr, Galactic tide; median original $1/a = 4.0\times10^{-5}$ AU^{-1}, 77% in $[0, 0.75]\times10^{-4}$, no hyperbolic originals	CODE: centroid 3–4 $\times10^{-5}$, 4.6% hyperbolic [213]	consistent (postdiction)
The printed readings without the axiom (accumulator, quadrature, completion, window variant, $\tau_s+2\tau_h$)	46–100% hyperbolic originals, or an energy budget up to about 18 times the allowance (quadrature: 17.6 against about 1)	same	excluded
$\tau_s+k\tau_h$, $k\geq3$	pass the comets (0–1.3% hyperbolic) but change the host's own depth, carry an unfixed integer and cost the satellites 0.12–0.25 dex	same	not adopted
Local wide binaries	$\gamma=1.000$, no orientation term of either parity; a softer switch on the host's state that passes the comets allows at most $\gamma-1\simeq0.01$–0.03 for 1–1.5 $M_\odot$ pairs at 1–3 $\times10^4$ AU (computed)	Chae (2023) 1.43 ± 0.06; Chae et al. (2026) $1.60^{+0.17}_{-0.14}$; Yoon et al. (2025) $1.32^{+0.12}_{-0.11}$; Banik et al. (2024) $\alpha_{\rm grav}=-0.021^{+0.065}_{-0.045}$ (Newton 0, MOND 1); Boufourou (2026) 1.045 [1.025, 1.068]; Saad & Ting (2026) $1.00^{+0.24}_{-0.19}$	null camp; pulls +7.2, +4.3, +2.9, −0.3, +2.2, 0.0σ
Planets	$\gamma-1=0$ exactly	ephemerides	consistent
Q_2	0 at every order; the Galactic tide is 8.2×10^{-31} s^{-2}	DE440 $(1.6\pm1.8)\times10^{-27}$, Cassini $(3\pm3)\times10^{-27}$ s^{-2}	-0.9σ, -1.0σ
RAR, BTFR, a_0, Milky Way disc RAR	unchanged: a host's own field is never frozen, and an isolated galaxy has no host mode	SPARC	as printed
Milky Way satellites	all boosted: dwarf spheroidals $n_h=5.6$–28, LMC 4.2–5.3, Sagittarius 1.2–1.6	satellite kinematics	as printed
Draco	boosted ($n_h=6.6$–8.2); under-predicted by every reading	McGaugh & Wolf (2010)	not a discriminator
Cluster spirals	frozen only within about 25 kpc of a Coma-class centre; $n_h\geq2.0$ beyond 0.1 Mpc	Dale et al. (2001), Bösch et al. (2013)	as printed
The edge	a step at $R\simeq13$–16 kpc	outer-halo globular clusters ($R\geq16$ kpc, 28 dispersion profiles, Baumgardt catalogue v4): boost 0.33 ± 0.08 of the predicted one; halo pairs not yet measured	outer boost contradicted: -5σ (error scaled for $\chi^2/{\rm dof}=2.9$), -9σ on 18 binary-robust clusters

crossing. The smooth scale-additive rule is the only candidate partition for which the zero-dipole theorem holds at all.

9. The external-field effect: even anisotropy dies

Proposition NL.19 (EFE anisotropy)**.** *For the local operator, μ reads the vector sum $|\mathbf{g}_{\rm int}+\mathbf{g}_{\rm ext}|$ and the external-field effect is* anisotropic*, with closed form (symbolic residual* 0*)*

$$L_{\rm ext}\equiv\left.\frac{d\ln\mu}{d\ln g}\right|_{g_{\rm ext}}=\frac{\tau}{2}\,n_{\rm BE}(\tau),\qquad G_\parallel/G_\perp=\frac{1}{1+L_{\rm ext}},$$

where $n_{\rm BE}=1/(e^\tau-1)$. For the scale-additive operator the external field is a separate scalar mode *(a depth, never a vector-sum argument), so the even (axisymmetric) anisotropy vanishes, $G_\parallel/G_\perp=1$* ***exactly*** *for the axis-averaged ratio (Thm NL.10); the action completion allows only an odd $\cos\theta$ term proportional to the mass asymmetry. At the solar circle, where the Newtonian Galactic field $g_{N,e}\simeq1.19$–$1.33\,a_0$ (observed 1.79–1.94 a_0) gives $\tau_{\rm ext}=1.09$–1.15, $L_{\rm ext}=0.27$–0.28 and the local reading predicts an anisotropy of about 21% against DFD's exact even-harmonic zero (computed); at the Sun Axiom NL.14 removes both the anisotropy and the odd term.*

Falsifier NL.20 (Wide-binary sky-orientation modulation).

TABLE CXXXIV. Forward evaluations of the scale-additive equation. No fitted constants; every entry is a prediction, not a fit. Bars are the published measurement uncertainties. The local-reduction Q_2 entries are at the bound-matter value $a_0 = 1.1966 \times 10^{-10}\ \mathrm{m\,s^{-2}}$ (Postulate ZS.11). The action completion of §NL 5 makes the Q_2 row exact at first order: $Q_2 = 0$ (Thm NL.8), and Axiom NL.14 makes it exact at every order. The disc-RAR entry is for the depth of record, FB-OUT, with its completion; the accumulator reading gives 0.016–0.018 dex.

Test	Local reduction	Scale-additive	Bar
Solar-system Q_2	30.6–31.8e-27 +16.1 to +16.8σ +9.2 to +9.6σ	0 (Sun Newtonian) -0.89σ -1.00σ	DE440 (1.6 ± 1.8)e-27 Cassini (3 ± 3)e-27
Milky Way disc RAR	untested	≤ 0.002 dex	0.057 dex
E, p, L, 320k steps	—	$\leq 2.6 \times 10^{-12}$ no secular drift	—
N-independence	exact	exact (theorem)	—
BTFR $v^4 = GMa_0$	exact	exact	10^{-2}
$\nu \geq 1$	exact	exact	—
PPN $\gamma - 1$	0 exactly	0 exactly	10^{-5}
Dipole radiation	0	0 (and rescued)	—

Let θ be the angle between a bound pair's separation vector and the Galactic-centre direction. **The completed scale-additive equation predicts *exactly zero* even ($\cos^2\theta$) dependence of the force boost γ on θ, at every separation and mass ratio** (Thm NL.10; $v_{\rm obs}/v_N$ inherits an even term $\lesssim 7 \times 10^{-4}$, zero for equal masses); the only allowed modulation is odd, $\propto (m_1 - m_2)\cos\theta$, zero for equal-mass pairs. AQUAL/MOND predicts 6.88% peak-to-peak at $s = 10^4$ AU and 46.65% at $s \approx 5{\times}10^3$ AU, where $g_{\rm int} = g_{\rm ext}$ and the vector sum can cancel. **Any detection of an even θ-modulation above the measurement floor, or of any θ-modulation above that floor in equal-mass pairs, falsifies the completed scale-additive equation.** Every pair of the *Gaia* catalogue lies inside the Milky Way's frozen zone, where Axiom NL.14 predicts no boost and no modulation of either parity; there any detected modulation, even or odd, or any boost falsifies the axiom. The test is a pure geometry cut on the 1.1×10^6 pairs with $> 99\%$ bound probability in the *Gaia* eDR3 catalogue of El-Badry, Rix & Heintz [53] and requires no new observation. It is an even-harmonic null for DFD and a signal for MOND, and nulls are robust to the M/L, contamination and eccentricity systematics that dominate the amplitude tests.

10. Two further constructions

1. **Directed enclosed mass with a smoothed log-radial window:** disc RAR 0.0133 dex, $\tau(R_0)$ within +5.7% of the established value.

2. **Square-root-outside-the-scale-integral ("FB-OUT"):** $a_0\tau^2 = \int_0^\infty |\mathbf{G}_r|\, d\ln r$. Band completeness $\int \mathbf{G}_r\, d\ln r = \mathbf{g}$ is a vector identity, so under non-reversal $\tau = \sqrt{g_{\rm bar}/a_0}$ *exactly*: the disc RAR displacement is zero as an identity (measured 1.03×10^{-4} dex disc, 1.83×10^{-4} dex Plummer — the quadrature error of an exact identity, falling 4× under grid doubling). Its exact two-source composition (symbolic residual 0) is $a_0\tau^2 = g_1(1{-}\epsilon^3){+}|g_1\epsilon^3\hat{e}_1{+}g_2\hat{e}_2|$ with $\epsilon = d_{\rm near}/d_{\rm far}$: the crossover variable ϵ^3 is *derived*, and for the Sun in the Galaxy $\epsilon^3 = 2.01 \times 10^{-25}$, so the functional *never forms* the vector sum. For $\epsilon \to 0$ this depth composes in quadrature, $a_0\tau^2 = g_1 + g_2$ (as in Thm NL.8), whereas the accumulator of item 3 composes additively, $\tau = \sum_i \tau_i$ (Thm NL.1.3): two printed readings of the scale-separated limit. In weak host fields the data choose between them: the rotation-curve shapes of Ursa Major members, the outer gradients of 510 cluster spirals (Dale et al. 2001) and the stellar-mass Tully–Fisher relation at $z = 0.17$ (Bösch et al. 2013) disfavour the additive composition at about 3–4σ and agree with the quadrature form (computed on published values; the host fields are partly estimates). Dwarf satellites test only the ceiling $\nu(\tau_{\rm host})$ that both forms share.

3. **The accumulator** of §NL 2.

All three evade the Cassini obstruction in the same way: by never forming $\mathbf{g}_\odot + \mathbf{g}_{\rm ext}$.

11. No-go results that close the alternatives

Theorem NL.21 (Subdivision no-go for a literal per–source composition)**.** *Read the composition law $\tau_{\rm tot} = \sum_i \tau_i$ literally, over a partition of a body into N pieces, with $\tau_i = \sqrt{g_i/a_0}$ per piece. Then τ is* partition-dependent*: for N equal co-located pieces $\tau_N/\tau_1 =$*

$N\sqrt{1/N} = \sqrt{N}$ *exactly, and in the deep field* $g_{\rm obs} = g_{\rm bar}/\tau$ *gives* $v_{\rm flat}^4 = GMa_0/N$, *i.e.* $v_{\rm flat} \propto N^{-1/4}$. *A galaxy of* 10^{11} *stars therefore has its asymptotic rotation speed wrong by a factor* $(10^{11})^{1/4} = \mathbf{562}$.

Proof. $\tau_N = N\sqrt{g/(Na_0)} = \sqrt{N}\sqrt{g/a_0}$ (symbolic). More sharply, $\tau \propto \sqrt{M}$ is homogeneous of degree $\frac{1}{2}$ in the source while every linear functional of ρ is homogeneous of degree 1; hence no kernel reproduces a literal per-source τ, which is a functional of a *partition* of ρ rather than of ρ. N-independence is restored exactly by Eq. (NL2), because $\boldsymbol{\gamma}$ is linear in ρ (Thm NL.1.4). □

Proposition NL.22 (MR-NG: no enclosed-mass law can work)**.** *Let* $\tau = F[M(\mathbf{x}, r)]$ *be built from the mass enclosed within radius* r *of the field point, with the kernel fixed by the point-mass normalisation. Put the field point inside a sheet of surface density* Σ *and thickness* h. *For* $h < r < R$ *the ball of radius* r *contains at least* $\pi\Sigma r^2$, *and monotonicity gives*

$$\tau \;\geq\; \int_h^R \sqrt{\frac{G\pi\Sigma r^2}{a_0 r^2}}\, d\ln r \;=\; \sqrt{\frac{\pi G\Sigma}{a_0}}\,\ln\frac{R}{h} \;\equiv\; \tau_{\rm amb}.$$

This term is (i) strictly positive, (ii) independent of the system's total mass, (iii) logarithmically divergent as $h \to 0$. ***No window, smoothing or normalisation removes it.***

Status NL.23 (Size of the obstruction at the solar circle). With $\Sigma = 0.1211$ kg m^{-2} ($58.0\,M_\odot$ pc^{-2}) and $\ln(R_0/h_z) = \ln(8.275/0.3) = 3.3172$, at the bound-matter value $a_0 = 1.1966 \times 10^{-10}$ m s^{-2} (both depths scale as $a_0^{-1/2}$, so the ratio does not depend on it), $\tau_{\rm amb} = \mathbf{1.5281}$ against the established $\tau = \sqrt{g_{\rm ext}/a_0} = 1.0587$: **the ambient term alone is** $1.4433\times$ **the entire correct answer.** The full enclosed-mass law gives $\tau(R_0) = 2.81$ and displaces the Milky Way RAR by **0.184** dex against the 0.057 dex observed floor. Replacing $M(\mathbf{x}, r)$ by $r^2|\mathbf{g}_{\rm enc}|/G$ makes the scale integral logarithmically divergent at large r. *The whole enclosed-mass class is closed.*

Proposition NL.24 (FB-NG: no field-based law with the root inside the scale integral can work)**.** *Let* $-d\tau/d\ln r = C\sqrt{|\mathbf{G}_r|/a_0}$, *where* $\mathbf{G}_r$ *is any self-similar band of the true Newtonian field and* C *is fixed by the point-mass normalisation. If the shell-dipole density keeps one direction in* r *— proved for every axisymmetric density decreasing in cylindrical radius, evaluated at a mid-plane point, and for every decreasing spherical model — then* $\tau(\mathbf{x}) \geq \sqrt{g_{\rm bar}(\mathbf{x})/a_0}$ *for* every *admissible kernel, with equality* iff *all the mass lies on a single sphere about* $\mathbf{x}$.

Proof. Two inputs, both forced: the exponent $\frac{1}{2}$ (by the point-mass normalisation) and the concavity of $\sqrt{\cdot}$. Jensen then gives $\sum_i \sqrt{a_i} \geq \sqrt{\sum_i a_i}$, strictly for more than one nonzero band, since $(\sqrt{a}+\sqrt{b})^2-(a+b) = 2\sqrt{ab} > 0$. *Summing square roots across scales always exceeds the square root of the sum.* The bound is kernel-, mass-, geometry- and a_0-independent, and it contains Prop. NL.22 as the special case in which the bands discard direction. □

Status NL.25. Milky Way disc displacement **0.1393** dex, Plummer sphere 0.0577 dex, against the 0.057 dex floor; 0/2000 violations of the inequality against a 1.2×10^{-4} quadrature floor. **The repair is one move: put the root *outside* the scale integral** (§NL 10, FB-OUT), which restores $\tau = \sqrt{g_{\rm bar}/a_0}$ as an identity.

Theorem NL.26 ($\hbar$ no-go for a DFD-native black-hole entropy)**.** *DFD's per-mode entropy is exactly* $\hbar$*-free. With the established scale-locking rule* $\bar{\lambda} = r$ *and bath temperature* $kT = \hbar c/r_M$,

$$\tau = \frac{E_{\rm mode}}{kT} = \frac{\hbar c/r}{\hbar c/r_M} = \frac{r_M}{r}, \qquad \frac{\partial\tau}{\partial\hbar} \equiv 0,$$

and the same holds for $\tau = r_s/r$, *the leading-order exterior* ψ *(symbolic residual* 0*). But* $S_{\rm BH}/k = 4\pi GM^2/(\hbar c)$ *is exactly first order in* $1/\hbar$. ***Therefore a total entropy*** $S = N\,s(\tau)$ ***is*** $\hbar$***-free unless the mode* count N ***carries*** $\hbar$***: any construction that returns*** $A/(4\ell_P^2)$ ***must introduce the Planck length through a cell measure, since no measure built from DFD's own scale-locked lengths*** $\{r, r_M, r_s, c, G, a_0\}$ ***contains it.***

Corollary NL.27 (Bekenstein–Hawking restated exactly)**.** *With* $N = Mc^2/(\hbar c/r_s) = 2GM^2/(\hbar c) = A/(8\pi\ell_P^2)$ *quanta of reduced wavelength* r_s *whose energies sum to* Mc^2, *one has* $S_{\rm BH}/N = 2\pi$ *exactly (symbolic).* Bekenstein–Hawking is exactly $2\pi k_B$ of entropy per horizon-wavelength quantum. *The same* 2π *is the Rindler periodicity: DFD's scale-locking* $\bar{\lambda} = \rho$ *with Unruh* $kT_{\rm loc} = \hbar c/(2\pi\rho)$ *gives* $\tau = 2\pi$ *exactly and universally in the near-horizon zone of any horizon, hence a universal boost* $\nu = 1/(1-e^{-2\pi}) = 1.0018709366$. *A finite Hilbert space of dimension* $k_{\max}+1 = 61$ *cannot supply* 2π *nats per mode: that requires* $\dim\mathcal{H} = e^{2\pi} = 535.49$, *short by a factor* $2\pi/\ln 61 = 1.5284$ *in the exponent.*

Theorem NL.28 (No causal linear response can make a standing well)**.** *The CMB third-peak height requires the* zero-frequency *(standing, DC) component of* $\Psi(k, z_*)$. *Let* R *be any causal, linear, time-translation-invariant response acting on the source, with arbitrary amplitude and arbitrary memory. Then* $\widehat{Rf}(0) = \hat{R}(0)\hat{f}(0)$*: a linear filter cannot create power at a frequency the source does not carry. An oscillating (acoustic) source has* $\hat{f}(0) = 0$ *at the acoustic frequency, so no such* R *— of* any *amplitude and* any *memory — generates DC power.*

Proposition NL.29 (DFD's only nonlinearity is rectification-free for sign-symmetric drives)**.** *The single escape from Thm NL.28 is rectification. DFD's deep-field nonlinearity is odd in the source and therefore rectification-free by symmetry for sign-symmetric (half-wave-antisymmetric) drives: its rectified DC coefficient is* 0 *to* 5.05×10^{-18}, *and about a non-zero operating point* g_0 *the rectified DC is* $0.83463\sqrt{a_0/g_1}\,g_0$ — odd *in* g_0, *with finite gain.* ***Finite***

gain × zero DC = zero: the rectifier is an amplifier, never a generator. *That conclusion holds only under the sign-symmetric hypothesis above: an in-phase even harmonic breaks it and rectifies at first order, coefficient* $-\Gamma(\frac{5}{4})/(2\sqrt{\pi}\,\Gamma(\frac{7}{4})) = -0.27821$ *(the gain above is exactly* $-3\times$ *this integral). DFD's acoustic source has even-harmonic fraction* $\varepsilon = O(\delta)$ *with* $\delta \lesssim 10^{-4}$ *(the corpus's own recombination baryon contrast is* $\sim 10^{-5}$*, App. AE): the rectified DC is* $\leq 0.278\,\varepsilon\,(597) \leq 0.0166$ *of the baryon potential against* $\nu_{\rm req} = 6.364327$ *(Status NL.31) — short by* $\geq 380\times$ *(*$\geq 3800\times$ *at the corpus's own* 10^{-5}*): the no-go survives on amplitude.*

Theorem NL.30 (ψ cannot be the standing well)**.** *DFD's* ψ *quantum is exactly massless,* $m_\psi = 0$*, protected by the shift symmetry* $\psi \to \psi + \epsilon$ *of the printed action, whose scalar sector contains no potential term in* ψ *(the action displayed in Theorem AE.1). On the Friedmann background no scalar mode propagates (App. WS), so* ψ *cannot sustain a pressureless, non-oscillating potential well at recombination.* ***This forbids*** ψ ***from being the standing well the third peak requires.***

Status NL.31 (The gap is a shape gap, not an amplitude gap). The requirement is $\nu_{\rm req} = \omega_m/\omega_b = 6.364327$, i.e. $\tau_{\rm req} = 0.1709376$. DFD's boost on the acoustic *perturbations* is $\nu(k) = 129, 71, 45, 41, 113, 172, 231, 311, 597$ at $k = 0.010 \ldots 0.20$ Mpc^{-1}: 6–94× **more amplitude than required**, and nonetheless useless, for three independent reasons. (a) It multiplies AC where the requirement is DC (Thm NL.28). (b) Its k-shape is too flat by 42.5× (ν varies by ×8.37 over $k = 0.0159 \to 0.20$ where the requirement varies by ×355.7). (c) It makes the fluid Jeans-*unstable* at $k \leq 0.025$ Mpc^{-1} ($\nu_{\rm crit} = 12.85$ against $\nu = 71$), destroying the peaks rather than fixing them. The *background* channel is worse: the cap is $\nu_{\max} = 1/(1 - e^{-1/(2\alpha^{1/4})}) = 1.2206074697$, a shortfall of 5.2141×; and by Thm AE.1 (ψ couples to $\rho - \bar{\rho}$) the true background τ vanishes identically, so $\nu \equiv 1$ and the shortfall is the whole 6.3643×.

Status NL.32 (The third-peak height needs a cold clusterer). **The CMB third-peak height still requires a cold clusterer.** DFD does not avoid the charge; it *derives the field that carries it* — χ-matter, App. AV, with $\Omega_\chi h^2$ computed from representation theory at the locked $k_{\max} = 60$, given the flux-period identification, the stated count 158, the asserted premise P4′ (Lemma AV.27) and two stated conventions (App. FK). Every no-CDM channel tested is closed, and the closure is a theorem about *shape*, not a deficit of amplitude. This is consistent with, and strengthens, Thm J.1 and Rem. J.3.

Remark NL.33 (Sign changes in the response are the acoustic phase). The response's sign changes are not a new physical scale. There are 23 of them, spaced at π/r_s — that is the acoustic phase $\sin(kr_s) = 0$ and nothing more — their count varies by 62–124% with the analysis window, and their number collapses to zero as soon as $\omega_c h^2$ exceeds 10^{-2}.

12. What is not derived

Named, with nothing booked on them; each item states where it stands.

NL-A: The vacuum detector $w(q)$ belongs to the accumulator reading only. The depth of record, FB-OUT, has none: its band is the field of the enclosed mass dipole, $a_0\tau^2 = 3G\int_0^\infty |\mathbf{D}_\mathbf{x}(r)|\, r^{-4}\, dr$ with $\mathbf{D}_\mathbf{x}(r) = \int_{|\mathbf{z}-\mathbf{x}|<r} \rho(\mathbf{z})(\mathbf{z}-\mathbf{x})\, d^3z$, which reproduces its two-source composition and response kernel exactly; the constant 3 is fixed by dimensions and completeness, and no free function enters (computed).

NL-B: The width w_0 belongs to the accumulator reading only: it is not fixed by the accumulator's own normalisations, $w_0 = 1$ is imported from the sharp-window derivation of §NL 2, and the sensitivity over $[0.5, 2]$ is in §NL 7. In FB-OUT the memory rate is 3, fixed by dimensions and completeness, and no width is chosen.

NL-C: The nonlocal variational term $\mathcal{N} = -(a_0^2/2)\int dx'\,(\partial\mathcal{Q}/\partial\tau)(x')\,\delta\tau(x')/\delta\Phi_N(x)$ vanishes in the action completion (Thm NL.7), and the nonlocality acts through the reciprocal force. Its size follows from $Q_M(t,\tau) - Q_{\rm QU}(t) = -2\nu'(t)\,t^3(\tau-t)^2 + O((\tau-t)^3)$: the completed energy equals the local one to second order in $\tau_{\rm FB} - t$. For a spherical density that decreases outward the band never turns at any point, so $\tau_{\rm FB} = t$ everywhere, the reciprocal force vanishes and the completed law is the local law. For exponential discs of thickness 0.05–0.2 R_d the reciprocal force on a midplane star and the change of the forward field off the plane are each below 3% and cancel to ≤ 0.002 dex between 0.5 and 8 R_d (computed). Between a bound subsystem and its host the environmental-confinement axiom applies (§NL 6).

NL-D: For point masses the depth has a bounded Lipschitz kink at exact equidistance, where the order in which two masses enter the ball swaps (codimension one, no δ-function, energy still exactly conserved at fixed a_0); for any continuous density it is absent. It is a property of point masses, not an open item.

NL-E: The lensing corollary (Cor. NL.17) rests on DFD's optical dictionary, the two core postulates $n = e^\psi$ and $\Phi = -c^2\psi/2$, and on nothing else. The scale-additive law is a static law of bound, slow, weak-field systems, the only place it acts; its time-dependent form is not claimed, and with Axiom WS.1 read, as in Proposition WS.6, as the absence of a temporal kinetic term for ψ, the corrections it would carry there are of relative order $(v/c)^2 \lesssim 10^{-6}$.

NL-F: *The informative failure*, a no-go rather than an open item. A *fixed-width* window in $\ln s$ cannot chain, and fails the disc RAR at 0.157 dex (window-shape spread only 5.7%: structural, not an artefact). A disc's field is generated over $\Delta \ln s \approx 1.33$ e-folds, so a unit window counts it as ≈ 2 modes, while the Sun and the Galaxy are 18.955 e-folds apart and must count as two. FB-OUT does what such a window cannot: a disc stays one mode, because $\tau_{\rm FB} = t$ at the midplane, and scale-separated systems split, because they compose in quadrature.

NL-G: The environmental-confinement axiom (Axiom NL.14) is stated, not derived: the Bose statistics cannot supply it (Thm NL.13). Its threshold is a step; a smoothing width, and the action form of the law in the frozen regime, are not derived.

13. Effect on established results, and the items still to be settled

a. The four quantities the completion shifts. Four quantities are *shifted* by the completion; each is settled or handed to a named observation. (i) The map from a_0 to the *fitted* RAR knee $g^\dagger$: on FB-OUT the completed law at a disc midplane equals the local law to ≤ 0.002 dex (computed), so $g^\dagger = a_0$ up to the disc-geometry and fitting effects that any law of this form shares. (ii) The Freeman transition surface density: it is the local law's, since the completed midplane force equals the local one to about 0.001 dex in the inner disc (computed); its scale is $\Sigma_M = a_0/2\pi G = 137\, M_\odot\,{\rm pc}^{-2}$. (iii) Dwarf-spheroidal dispersions: for an isolated dwarf the completed law is the local law, since a spherical density that decreases outward has $\tau_{\rm FB} = t$ at every point; on the forward law a satellite's internal boost is $\nu(\sqrt{\tau_{\rm sub}^2 + \tau_{\rm host}^2})$, which tends to the ceiling $\nu(\tau_{\rm host})$ where the host dominates, and the reciprocal term of the completion adds to it. On published values four tidally safe Milky Way dwarfs sit 1.1σ above the forward law's own prediction (computed), and on the dispersions and M31-centric distances published in 2020–2026 the seven M31 dwarfs that are tidally safe at those distances sit about 2–3σ above it, and the four selected as tidally safe on earlier distances (And I, XIX, XXI and XXIII), of which only XIX and XXIII are tidally safe at the new ones, 5.7σ (computed); with the reciprocal term, which the completed law of weak hosts carries, the excesses fall to about 0.9σ, 2σ and 4.4σ (estimate). The ceiling counts only the μ-law branch of the floor law: a satellite's own χ can hold its stars above it unless the host pushes them, relative to that χ, harder than the satellite's own gravity (App. AV). Deeper dispersions of external-field-dominated M31 satellites decide it: a combined excess of 5σ over the completed law, with population-synthesis mass-to-light ratios, in satellites that pass an equilibrium check and whose stars the host pushes harder than their own gravity, falsifies the ceiling. (iv) The wide-binary amplitude: under the environmental-confinement axiom the Sun's host mode is typically empty, so local wide binaries are Newtonian, $\gamma = 1$ exactly, with no orientation term; the completed law's amplitude (Status NL.11) applies to pairs in host fields below $(\ln 2)^2 a_0$, beyond $R \simeq 13$–16 kpc in the Milky Way. A confirmed boost of the Chae type in local binaries falsifies the axiom.

b. The place this equation is most exposed, stated plainly. On Crater II — where McGaugh [216] predicted $\sigma_{\rm EFE} = 2.1^{+0.9}_{-0.6}$ km s^{-1} and Caldwell et al. [217] measure 2.7 ± 0.3 km s^{-1} from 62 member stars — the same-μ comparison on the accumulator reading gives $\sigma_{\rm new}/\sigma_{\rm old} = 0.888$, i.e. ≈ 1.86 km s^{-1}, with the observed host field as the argument; with the baryonic host field of Table XCIX it has not been recomputed. MOND's prediction overlaps the measurement within its own asymmetric bar; 1.86 km s^{-1} sits further below it. **On Crater II the accumulator reading is in worse shape than MOND, not better.** On the depth of record Crater II is boosted, well below the threshold of Axiom NL.14, and sits under the ceiling $\nu(\tau_{\rm host})$ like every satellite; it is tidally disturbed, so it does not decide that ceiling, which item (iii) above hands to deeper M31 data.

TABLE CXXXV. Effect of the scale-additive completion on results established elsewhere in this monograph.

Item	Result	Shift
PPN $\gamma - 1 = 0$	unchanged (theorem)	0 exactly
Zero dipole radiation	unchanged, *rescued*	0 exactly
Lensing = dynamics	unchanged where the reciprocal term vanishes	0 there
BTFR $v^4 = GMa_0$	unchanged	$\to 0$ asymptotically
$\nu \geq 1$	unchanged	none
Disc RAR	safe	≤ 0.002 dex vs 0.057

Appendix BS: Single-Mode Bose Statistics and the Gravity Law

Appendix N obtains the interpolation function from a *saturation-union composition law* (Assumption N.5),

$$\mu(\psi_1 + \psi_2) = 1 - \big(1 - \mu(\psi_1)\big)\big(1 - \mu(\psi_2)\big), \qquad \text{(BS1)}$$

and Lemma N.6 shows that this alone forces $\mu = 1 - e^{-c\psi}$. This appendix identifies what Eq. (BS1) *is*. Writing $\mu = 1/\nu$ with $\nu \equiv g_{\rm obs}/g_{\rm bar} = M_{\rm dyn}/M_{\rm bar}$, the composition law says that the quantity $1 - \mu$ is multiplicative over independent contributions. That is the defining property of a *probability of independent events*, and μ itself is then a normalised inverse partition function. The galactic sector of DFD is thereby read as single-mode Bose–Einstein statistics at zero chemical potential. The reading adds one stated input, the ground-state principle (Rem. BS.4), and it supplies a temperature, a heat capacity and an entropy, together with two zero-parameter observational relations that contain no $a_\star$ and no a_0.

Throughout, $\tau > 0$ is the dimensionless mode exponent, k is Boltzmann's constant, all entropies are quoted as the dimensionless S/k, and

$$y \equiv g_{\rm bar}/a_0, \qquad x \equiv g_{\rm obs}/a_0, \qquad n_{\rm BE}(\tau) \equiv \frac{1}{e^\tau - 1}. \qquad \text{(BS2)}$$

Where a number is printed, $a_0 = 1.20 \times 10^{-10}\,\mathrm{m\,s^{-2}}$ is an explicitly chosen *empirical SPARC benchmark*. The bound-matter prediction is $a_0 = 2\sqrt{\alpha}\,cH_0^{\rm loc} = 1.1966 \times 10^{-10}\,\mathrm{m\,s^{-2}}$ (Theorem N.14, Postulate ZS.11). Tables in this appendix retain the benchmark so their published environment examples remain reproducible. The dimensionless theorems and inequalities are independent of this benchmark. **Nothing in this appendix is fitted.**

1. The Partition Function

Definition BS.1 (The gravitational mode)**.** Associate with each field point a single harmonic mode of the ψ quantum with dimensionless Boltzmann exponent τ, in thermal equilibrium at zero chemical potential. The mode is a statistical reading of the response: under Axiom WS.1 the local ψ has no canonical momentum of its own, so the mode is not a propagating quantum of ψ. Its canonical partition function is

$$Z_1(\tau) = \sum_{n=0}^{\infty} e^{-n\tau} = \frac{1}{1 - e^{-\tau}}. \qquad \text{(BS3)}$$

Theorem BS.2 (The boost is the partition function)**.** *With $\mu \equiv 1/\nu$ and the identification $\nu = Z_1$,*

$$\boxed{\begin{aligned} &\nu = Z_1 = \frac{1}{1 - e^{-\tau}}, \\ &\mu = \frac{1}{Z_1} = 1 - e^{-\tau} = \mathbb{P}(n = 0), \\ &\nu = 1 + n_{\rm BE} \end{aligned}} \qquad \text{(BS4)}$$

Equivalently: μ ***is the probability that the mode is empty, and ν is spontaneous plus stimulated response.***

Proof. Eq. (BS3) is a geometric series with ratio $e^{-\tau} < 1$. The Gibbs weight of the ground state is $p_0 = e^0/Z_1 = 1/Z_1$, so $\mathbb{P}(n = 0) = 1/Z_1 = \mu$. Finally $1 + n_{\rm BE} = 1 + (e^\tau - 1)^{-1} = e^\tau/(e^\tau - 1) = (1 - e^{-\tau})^{-1} = Z_1$, and $\langle n \rangle = Z_1^{-1} \sum_n n\, e^{-n\tau} = n_{\rm BE}$. All four residuals are identically zero. □

Remark BS.3 (Relation to Appendix N). Theorem BS.2 *is* Lemma N.6 with the multiplicative function $g = 1 - \mu$ identified as $e^{-\tau} = \mathbb{P}(n \geq 1)$. The saturation-union law (BS1) is exactly the statement that the occupation probabilities $\mathbb{P}(n \geq 1)$ of independent modes multiply. Beyond that law the reading adds one stated input, the ground-state principle of Rem. BS.4. The two routes share Assumption N.5 in full and differ only in what is then substituted for ψ: Appendix N uses the level response Assumption N.3, this appendix uses the deep-field limit (Theorem BS.9).

Remark BS.4 (The one stated input: the ground-state principle). The identification $\nu = Z_1$ is one stated input of the theory, the ground-state principle: the Newtonian fraction of the response at a field point is the probability that the point's single ψ mode is empty, $\mu = \mathbb{P}(n{=}0)$. Fermi occupation would cap ν at 2 (Cor. BS.8), where a deep SPARC point, at $2.70 \times 10^{-12}\,\mathrm{m\,s^{-2}}$, needs 7.18. Classical occupation, $\langle n \rangle = 1/\tau$, leaves a strong-field tail that fails the approach-rate condition of App. C 1, and a chemical potential caps the boost (Thm BS.5). A mode of energy $\hbar c/r$ at one temperature per system has $\tau = r_M/r$, the SOURCE branch; the TOTAL branch is not a

single-temperature mode. The branch itself is chosen by data (§BS 7); one temperature per system is not derived. The principle cannot come from a quadratic action: a harmonic mode driven linearly by a static source responds as $\chi = 2/\varepsilon$ whatever its occupation, because stimulated emission and absorption cancel. Its energy form is exact: $Q_{\rm QU}(\tau) = 4\int_0^\tau v^3[1 + n_{\rm BE}(v)]\,dv$, one quantum per mode below the local depth plus the Planck spectrum cut off there, whose full value $4\Gamma(4)\zeta(4) = 4\pi^4/15$ is the constant of the Newtonian limit (computed).

Theorem BS.5 (Vanishing chemical potential, and why rotation curves are flat)**.** *Let the mode carry fugacity $z = e^{\mu_{\rm chem}/kT} \le 1$, so that $Z_1(\tau, z) = (1 - ze^{-\tau})^{-1}$. Then*

$$\lim_{\tau\to 0^+} \nu = \frac{1}{1-z}, \tag{BS5}$$

which is finite for every $z < 1$ and divergent only at $z = 1$. Hence

$$\boxed{\mu_{\rm chem} = 0} \tag{BS6}$$

is what the observed flatness of rotation curves requires, to the precision of the largest measured boosts: any $z < 1$ caps the boost at $1/(1-z)$, so $g_{\rm obs} \to g_{\rm bar}/(1-z)$ at large radius and every rotation curve eventually turns over into a rescaled Keplerian decline.

Proof. Geometric series with ratio $ze^{-\tau} < 1$; take $\tau \to 0^+$ (sympy limit, $1/(1-z)$). The physical statement follows because $g_{\rm obs} = \nu\, g_{\rm bar}$ and $g_{\rm bar} \propto r^{-2}$ outside the baryons: a bounded ν gives $v_c^2 = r g_{\rm obs} \propto r^{-1}$. □

Remark BS.6 (A host acts as a fugacity). A subsystem in a host of depth τ_h composes with it as a mode of fugacity $z = e^{-\tau_h}$, so the host caps the subsystem's boost at $1/(1-z) = \nu(\tau_h)$ (App. NL, Thm NL.13); no composition built from these statistics removes the cap, and the freeze of the Sun's field inside the Galaxy is the axiom of environmental confinement (Axiom NL.14).

Theorem BS.7 (The μ-law response is never sub-Newtonian)**.** *For every $\tau > 0$, $\nu = (1 - e^{-\tau})^{-1} > 1$, with $\inf_\tau \nu = 1$ approached only as $\tau \to \infty$. The μ-law response therefore **cannot** produce $g_{\rm obs} < g_{\rm bar}$ at any acceleration.*

Proof. $0 < 1 - e^{-\tau} < 1$ for $\tau \in (0, \infty)$, so $\nu - 1 = n_{\rm BE} > 0$. Structurally: the mode's ladder is bounded below by the ground state, so detailed balance offers no de-excited level for the response to fall into. There is no "$n = -1$". □

Corollary BS.8 (Fermi statistics is excluded by inspection)**.** *A fermionic quantum would give $Z_1^F = 1 + e^{-\tau}$, hence*

$$1 < \nu_F \le 2, \qquad \tfrac{1}{2} \le \mu_F < 1. \tag{BS7}$$

*A deep SPARC data point, at $g_{\rm bar} = 2.70 \times 10^{-12}\ m\,s^{-2}$, requires $\nu = 7.18$ (Table CXXXVI); more than a hundred points lie deeper, and the sample spans $\nu \approx$ 1–60 (computed). **The gravitational quantum is a boson; Pauli exclusion would cap the boost at a factor** 2**, short by** 3.6× ***at that point alone.***

2. The Interpolation Function

Theorem BS.9 (The interpolation function, up to one binary branch)**.** *Assume (i) Theorem BS.2; (ii) τ is a function of a single local acceleration invariant made dimensionless by a_0; (iii) the deep-field limit $g_{\rm obs}^2 \to g_{\rm bar}\, a_0$. Then, among powers of $g_{\rm bar}/a_0$ or of $g_{\rm obs}/a_0$, τ is fixed up to the choice of which of the two enters, and exactly two laws exist:*

$$\textbf{\textit{SOURCE:}}\ \tau = \sqrt{y} \implies \boxed{\mu = 1 - e^{-\sqrt{g_{\rm bar}/a_0}},\quad \nu(y) = \frac{1}{1 - e^{-\sqrt{y}}}} \tag{BS8}$$

$$\textbf{\textit{TOTAL:}}\ \tau = x \implies \boxed{\mu(x) = 1 - e^{-x},\quad x = g_{\rm obs}/a_0} \tag{BS9}$$

*Both reproduce the Newtonian limit $\nu \to 1$ and the deep-field limit exactly; **no third such power law is admissible, and statistics does not choose between these two.***

Proof. By Theorem BS.2, $\nu = (1 - e^{-\tau})^{-1}$, so $\lim_{\tau\to 0} \tau\nu = 1$ (*i.e.* $\nu \sim 1/\tau$, $\mu \sim \tau$) and $\nu \to 1$ as $\tau \to \infty$. *SOURCE:* with $\tau = \tau(y)$, $g_{\rm obs} = \nu g_{\rm bar} \to g_{\rm bar}/\tau$; imposing $g_{\rm obs} = \sqrt{g_{\rm bar} a_0}$ gives $\tau = \sqrt{g_{\rm bar}/a_0}$. Allowing a general power $\tau = A\, y^p$ and solving the two resulting conditions returns the unique solution $p = \frac{1}{2}$, $A = 1$ — the unit coefficient being the *definition* of a_0. *TOTAL:* with $\tau = \tau(x)$, $g_{\rm bar} = \mu\, g_{\rm obs} \to \tau\, g_{\rm obs}$, and the same limit forces $\tau = g_{\rm obs}/a_0$. Direct evaluation confirms $\lim(\nu^2 y) = 1$ on both branches, *i.e.* both satisfy $g_{\rm obs}^2 \to g_{\rm bar} a_0$ exactly. □

Remark BS.10 (What the two branches are). Eq. (BS8) *is* the McGaugh–Lelli–Schombert radial-acceleration function [10], catalogued at Table LVIII as "RAR / Empirical". Eq. (BS9) *is* Bekenstein's exponential form, catalogued in the same table as "Exponential". **Both entries of that catalog are outputs of one theorem, not independent phenomenology.** Statistics does not select between them. The selection is empirical (§BS 7), and the deep-field observables — a_0, the BTFR and $g^\dagger$ — are structurally blind to the difference, which is the statistical restatement of the deep-field blindness of the transition region.

Remark BS.11 (Where this sits beside $\mu(s) = s/(1+s)$). Theorem N.8 obtains $\mu(s) = s/(1+s)$ by combining Eq. (BS1) with the level-response Assumption N.3, $k_{\rm eff}(s) = k_0(1+s)$, which is equivalent to $\tau = \log(1+s)$. The composition step is common to both routes; the entire difference lies in what is assumed about τ, and §BS 3 reports what the level ratio implied by Assumption N.3 numerically is. The two asymptotic limits are common to all three functions ($s/(1+s)$, $1 - e^{-\sqrt{y}}$, $1 - e^{-x}$) and are theorem-grade in every case; the three differ only in the transition region, where they agree pairwise to $\lesssim 0.09$ dex ($\lesssim 0.02$ dex for $s/(1+s)$ against $1 - e^{-\sqrt{y}}$) and where no

present galactic dataset separates $s/(1+s)$ from $1-e^{-\sqrt{y}}$ (§BS 7).

3. The Magnitude of τ

Assumption N.3 reads τ as the logarithm of a Chern–Simons level ratio, $k_{\rm eff}/k_0 = e^{\tau}$. The magnitudes are recorded here without prejudice to that assumption's other uses.

Proposition BS.12 (The implied level ratio)**.** *With the explicitly empirical benchmark $a_0 = 1.20\times10^{-10}\,\mathrm{m\,s^{-2}}$, the level ratio $k_{\rm eff}/k_0 = e^{\tau}$ demanded by Assumption N.3 is*

environment	g/a_0	e^{τ}, $\tau=\log(1+s)$	e^{τ}, $\tau=\sqrt{s}$
Saturn's orbit ($a=$ 9.5826 AU)	5.3816×10^{5}	5.38×10^{5}	$10^{318.60}$
Earth's surface	8.1722×10^{10}	8.17×10^{10}	$10^{124152.09}$

against DFD's own Toeplitz truncation $k_{\max}=60$ (Theorem AB.1).

Even on the corpus's own reading the ratio at Earth's surface exceeds $k_{\max}$ by nine orders of magnitude; on the Bose reading it exceeds it by more than 10^{124150}. **As a topological level, τ is not a small integer in any environment. As a Boltzmann exponent it is unremarkable** — e^{-733} is simply a very cold mode. The identification $\tau=\varepsilon/kT$ is therefore not a reinterpretation of convenience; it is the reading in which the numbers are ordinary.

4. Thermodynamics of the Mode

Theorem BS.13 (Entropy and heat capacity)**.** *For the mode of Definition BS.1,*

$$\frac{S}{k} = \ln Z_1 + \tau\, n_{\rm BE} \;=\; \ln\nu + \tau\, n_{\rm BE}, \tag{BS10}$$

$$\frac{C}{k} = -\tau^2\frac{dn_{\rm BE}}{d\tau} \;=\; \frac{\tau^2}{4\sinh^2(\tau/2)} \;=\; \tau^2\,\nu(\nu-1), \tag{BS11}$$

with $C/k\to1$ as $\tau\to0$ and $C/k\to0$ as $\tau\to\infty$.

Proof. Eq. (BS10) is the Gibbs entropy $-\sum_n p_n\ln p_n$ with $p_n = e^{-n\tau}/Z_1$; the difference against the closed form is identically zero. Eq. (BS11) is the Einstein heat capacity; the third equality uses $\big(4\sinh^2(\tau/2)\big)^{-1} = n_{\rm BE}(1+n_{\rm BE})$ (residual 0) together with $\nu = 1+n_{\rm BE}$. The limits are 1 and 0 by direct evaluation. □

Corollary BS.14 (Newtonian gravity is a frozen quantum degree of freedom)**.** *$C/k\to1$ as $\tau\to0$ is the classical equipartition (Dulong–Petit) value for one mode, and $C/k\to0$ as $\tau\to\infty$ is quantum freeze-out. Hence*

deep-MOND = the classical limit; Newtonian = the quantum-frozen limit,

with the numerical values of Table CXXXVI. ***Solar-system safety is therefore not a tuning and not a screening mechanism.*** *There is no occupied state to boost: the mode entropy at Saturn's orbit is 1.9×10^{-316} of one nat. No parameter was chosen to make this true, and no fifth-force suppression is invoked. This holds at every planet ($\tau\simeq234$ at Neptune's orbit and 734 at Saturn's). Beyond about 10^3 AU the Sun's own mode is not frozen by its own depth ($\tau\simeq0.7$ at 10^4 AU), and a host acts as a fugacity that caps, but cannot remove, the boost (Rem. BS.6); there the Sun's field is Newtonian by the environmental-confinement axiom (Axiom NL.14), a rule about the Sun's surroundings rather than a property of its mode.*

Theorem BS.15 (The temperature is the Hawking–Unruh geometric mean)**.** *Let $T_{\rm H}(M) = \hbar c^3/(8\pi GMk)$ be the Hawking temperature and $T_{\rm U}(a_0) = \hbar a_0/(2\pi ck)$ the Unruh temperature at the DFD acceleration scale. Then, with the MOND radius $r_M \equiv \sqrt{GM/a_0}$,*

$$\boxed{\,T_{\rm DFD} \;=\; 4\pi\sqrt{T_{\rm H}(M)\,T_{\rm U}(a_0)} \;=\; \frac{\hbar c}{k\,r_M}\,} \tag{BS12}$$

with residual identically zero, and the prefactor is derived*: $4\pi = \sqrt{8\pi\cdot2\pi}$, the geometric mean of Hawking's 8π and Unruh's 2π. Consequently*

$$t_{\rm coh} \equiv \frac{\hbar}{kT_{\rm DFD}} = \frac{r_M}{c}, \qquad \frac{d\ln T_{\rm DFD}}{d\ln M} = -\frac{1}{2}, \tag{BS13}$$

exactly half *the Hawking exponent.*

Proof. $T_{\rm H}T_{\rm U} = \hbar^2c^2a_0/(16\pi^2GMk^2)$; its square root times 4π is $\hbar c\sqrt{a_0/GM}/k = \hbar c/(kr_M)$. The prefactor identity is $\sqrt{8\pi\cdot2\pi} = \sqrt{16\pi^2} = 4\pi$ (residual 0). Evaluated at 60 digits: for the Sun, $r_M = 1.0531\times10^{15}$ m, $T_{\rm DFD} = 2.1744\times10^{-18}$ K, $t_{\rm coh} = 3.513\times10^{6}$ s; for a $6\times10^{10}\,M_\odot$ disc, $r_M = 8.360$ kpc, $T_{\rm DFD} = 8.8769\times10^{-24}$ K, $t_{\rm coh} = 8.605\times10^{11}$ s, at the bound-matter $a_0 = 1.1966\times10^{-10}\,\mathrm{m\,s^{-2}}$; both equalities in Eqs. (BS12) and (BS13) hold to relative 10^{-61}, *i.e.* to working precision. □

Remark BS.16. $t_{\rm coh} = r_M/c$ says the mode's coherence time is the light-crossing time of the MOND radius. It contains no free parameter. In the present reading it is an identity of the ensemble mean, not a dynamical relaxation time of the response: all thermal quantities in this appendix (temperature, entropy, heat capacity, coherence time) are identities of the ensemble mean, no fluctuation content is claimed, and no mode count per resolution element is defined.

Theorem BS.17 (Equation of state, conditional on masslessness)**.** If *the ψ quantum is exactly massless, its dispersion is $\varepsilon = \hbar c|\mathbf{k}|$, its density of states in d spatial*

TABLE CXXXVI. The gravitational mode across seven decades of τ, SOURCE branch ($\tau = \sqrt{g_{\rm bar}/a_0}$, empirical benchmark $a_0 = 1.20 \times 10^{-10}\,\mathrm{m\,s^{-2}}$). Saturn's and Earth's rows are evaluated in $\log_{10}$; the omitted corrections are $O(e^{-2\tau})$. Saturn's row uses $a = 9.5826$ AU; at $a = 9.5549$ AU one gets $\tau = 735.72$ instead.

environment	$g_{\rm bar}$ ($\mathrm{m\,s^{-2}}$)	τ	ν	S/k	C/k
a deep SPARC point	2.70×10^{-12}	0.15000	7.1792	2.8981	0.99813
$g_{\rm bar} = a_0$	1.20×10^{-10}	1.00000	1.58198	1.04065	0.92067
Saturn's orbit	6.4579×10^{-5}	733.595	$1 + 10^{-318.60}$	1.86×10^{-316}	1.36×10^{-313}
Earth's surface	9.80665	2.85871×10^{5}	$1 + 10^{-124152.09}$	2.34×10^{-124147}	6.68×10^{-124142}

dimensions is $g(\varepsilon) \propto \varepsilon^{d-1}$, and

$$\boxed{PV = \tfrac{1}{d}\,U \xrightarrow{\;d=3\;} PV = \tfrac{1}{3}U} \tag{BS14}$$

exactly — the photon-gas equation of state — with the Maxwell residual $(\partial S/\partial V)_T - (\partial P/\partial T)_V \equiv 0$.

Proof. $F = kT\int g(\varepsilon)\ln\!\left(1 - e^{-\varepsilon/kT}\right) d\varepsilon$; integrating by parts with $g \propto \varepsilon^{d-1}$ gives $F = -U/d$, and $P = -(\partial F/\partial V)_T = -F/V$ since $F \propto V$. Verified symbolically for $d = 1, 2, 3, 4$: $PV - U/d = 0$, $F + U/d = 0$ and the Maxwell residual $= 0$ in every case. □

Remark BS.18. The exponent is a falsifiable signature of the dispersion relation: a massive quantum ($\varepsilon \propto p^2$) would give $PV = \frac{2}{3}U$. The antecedent $m_\psi = 0$ is *not* proved here, and under Axiom WS.1 the local ψ has no propagating quanta; compare the masslessness statement (Theorem NL.30, App. NL), and Theorem BS.17 is graded accordingly in Table CXXXVIII.

5. The Total Entropy of a Galaxy

Theorem BS.19 (Closed form for the integrated mode entropy)**.** *In the deep field $\tau(r) = r_M/r$. Counting one mode per logarithmic radial shell out to the Hubble radius $r_H = c/H_0$, and writing $X \equiv \ln(r_H/r_M)$,*

$$\boxed{\frac{S_{\rm tot}}{k} \;=\; \int_0^{r_H} \frac{S(r_M/r)}{k}\, d\ln r \;=\; \frac{X^2}{2} + X + K + O\!\left(e^{-2X}\right)} \tag{BS15}$$

with

$$K \;=\; \frac{\pi^2}{12} - \frac{\gamma^2}{2} - \gamma_1 \;=\; 0.72869\,39170\,03930\,6059\ldots, \tag{BS16}$$

γ the Euler–Mascheroni constant and γ_1 the first Stieltjes constant.

Proof. The Mellin transform of the mode entropy is, using $\int_0^\infty \tau^{s-1}\big[-\ln(1-e^{-\tau})\big]d\tau = \Gamma(s)\zeta(s+1)$ and $\int_0^\infty \tau^{s-1}\big[\tau/(e^\tau - 1)\big]d\tau = \Gamma(s+1)\zeta(s+1)$,

$$\mathcal{M}[S/k](s) = \Gamma(s)\,\zeta(1+s)\,(1+s), \tag{BS17}$$

confirmed against direct quadrature to relative 10^{-31} at $s = 0.5$, 1.3, 2.7. Near $s = 0$, $\Gamma(s) = s^{-1} - \gamma + (\gamma^2/2 + \pi^2/12)s + O(s^2)$ and $\zeta(1+s) = s^{-1} + \gamma - \gamma_1 s + O(s^2)$, whose product has *no* simple pole; multiplying by $(1+s)$,

$$\mathcal{M}[S/k](s) = \frac{1}{s^2} + \frac{1}{s} + K + O(s). \tag{BS18}$$

With $\tau_H = e^{-X}$, $S_{\rm tot}/k = \int_{\tau_H}^\infty (S/k)\,d\tau/\tau$ is the residue at $s = 0$ of $\mathcal{M}[S/k](s)\,e^{sX}/s$, *i.e.* the coefficient of s^{-1} in $(s^{-3} + s^{-2} + Ks^{-1})(1 + sX + s^2X^2/2 + \cdots)$, which is $X^2/2 + X + K$. Against direct quadrature the neglected remainder is 9.5×10^{-7} at $X = 5$, 8.4×10^{-14} at $X = 13.12$ and 4.0×10^{-24} at $X = 25$. □

Remark BS.20 (The domain matters). The lower limit is $r = 0$, not $r = r_M$. The frozen inner region contributes 0.70812 of the constant 0.72869 — 97.18%. Restricting the integral to $r \geq r_M$ replaces the constant by 0.0205774 and the closed form of Eq. (BS15) is then wrong.

Example BS.21 (The Milky Way)**.** With $M_{\rm bar} = 6 \times 10^{10}\,M_\odot$ one gets $r_M = 8.360$ kpc; with the bound-matter clock $H_0^{\rm loc} = 72.09\,\mathrm{km\,s^{-1}Mpc^{-1}}$ (Postulate ZS.11; $a_0 = 2\sqrt{\alpha}\,cH_0$ rescales r_M accordingly), $r_H = 4158.6$ Mpc, so $X = 13.1172$ and

$$S_{\rm tot}/k = 99.88. \tag{BS19}$$

A galaxy's gravitational field carries of order one hundred nats of entropy at one mode per e-fold of radius. At $X \simeq 13.12$ the closed form's neglected remainder is below 10^{-13}, so the value quoted is exact at the displayed precision.

6. The Observables

The statistical reading is testable because τ appears in two independent places: an *amplitude* ν (a mass budget) and a *shape* u (a log-slope of the rotation curve). **The observable itself, its measurement on SPARC, its systematics theorem and its falsifier are already booked in Appendix AT 7**; they are *not* restated here. What this subsection supplies is the statistical *provenance* of Eq. (AT16), together with two identities that follow from the thermodynamics and have no counterpart there.

Theorem BS.22 (Statistical provenance of the (ν, u) relation)**.** *The shape variable of Eq. (AT13), $u \equiv -2\,d\ln\nu/d\ln g_{\rm bar}$, evaluated on Definition BS.1 equals the* thermal energy of the mode in units of kT*:*

$$u \;=\; -\frac{d\ln\nu}{d\ln\tau} \;=\; \tau\, n_{\rm BE} \;=\; \frac{\langle E\rangle}{kT}, \tag{BS20}$$

and eliminating τ *through* $\tau = \ln\big(\nu/(\nu-1)\big)$ *returns*

$$\boxed{u = (\nu-1)\,\ln\!\left(\frac{\nu}{\nu-1}\right)} \qquad \text{(BS21)}$$

— which is exactly Eq. (AT16) *of Appendix AT 7. The limits* $u \to 0$ *as* $\nu \to 1^+$ *and* $u \to 1$ *as* $\nu \to \infty$ *are, in this reading, quantum freeze-out and classical equipartition respectively.*

Proof. On the SOURCE branch $\tau = \sqrt{y}$, so $d\ln\tau = \frac{1}{2}d\ln y$ and $-2\,d\ln\nu/d\ln y = -d\ln\nu/d\ln\tau$; with $\nu = (1-e^{-\tau})^{-1}$ this is $\tau\, n_{\rm BE}$, and $\langle E\rangle/kT = \tau\langle n\rangle = \tau n_{\rm BE}$ by Theorem BS.2. Inversion of $\nu(\tau)$ and substitution give Eq. (BS21); all residuals identically zero. □

Remark BS.23 (What Theorem BS.22 closes and what it does not). Eq. (AT16) uses $\mu = 1-e^{-\tau}$ while Theorem N.8 gives $\mu = x/(1+x)$. Theorem BS.9 supplies the derivation of $\mu = 1-e^{-\tau}$ from the same composition law both routes already share. Which of the two is the law is settled by the Solar System, not by statistics (Cor. BS.14; App. C, strong-field approach rate; $x/(1+x)$ is the weak-response form), and the two forms are not separated by SPARC — SPARC provably cannot (Appendix AT 7).

Theorem BS.24 (The curvature relation)**.** *The mode heat capacity is likewise* τ*-free in terms of* ν*:*

$$\boxed{\frac{C}{k} = \nu(\nu-1)\,\ln^2\!\left(\frac{\nu}{\nu-1}\right)} \qquad \text{(BS22)}$$

and it is directly measurable, since

$$\frac{C}{k} \;=\; u + 4\,w', \qquad w' \equiv \frac{d^2\ln g_{\rm obs}}{d(\ln g_{\rm bar})^2}\,: \qquad \text{(BS23)}$$

the mass discrepancy read against the curvature *of the radial acceleration relation. Both identities have residual* 0*.*

Theorem BS.25 (An observable gravitational entropy)**.** *Combining Eq.* (BS10) *with Eq.* (BS20)*,*

$$\boxed{\frac{S}{k} = \ln\!\left(\frac{M_{\rm dyn}}{M_{\rm bar}}\right) + u} \qquad \text{(BS24)}$$

with u *measured by the estimator* $u = 2 - 4(s-\frac{1}{2})/\beta$ *of Appendix AT 7. At the SPARC sample-mean* $u = 0.7818 \pm 0.0321$*, Eq.* (BS21) *returns* $\nu = 2.650579$ *and* $S/k = 1.7566$ *per mode.* Every quantity on the right is measured; nothing is fitted.

Corollary BS.26 (The κ^2/Ω^2 form holds only for a point mass)**.** *It is tempting to use the epicyclic identity of Appendix AT 7,* $\kappa^2/\Omega^2 = 3 + \beta(1-u/2)$*, to write* $S/k = \ln(M_{\rm dyn}/M_{\rm bar}) + (\kappa^2/\Omega^2 - 1)$*. That substitution is* exact for a point mass and for nothing else*: in general*

$$\left(\frac{\kappa^2}{\Omega^2} - 1\right) - u \;=\; (\beta+2)\left(1 - \frac{u}{2}\right), \qquad \text{(BS25)}$$

which vanishes only at $\beta = -2$ *(residual* 0*). For a disc,* β *ranges well away from* -2 *and the error is first order in* $(\beta+2)$*.* ***Eq.*** (BS24) ***with the measured*** u ***is the general statement; the*** κ^2/Ω^2 ***form holds only for a point mass.***

Remark BS.27 (Systematics). That distance and inclination errors move a galaxy *exactly horizontally* in the $(\ln\nu, u)$ plane, by $(-1, 0)$ and $(+2, 0)$ respectively, and that the entire derivative tower is invariant, is Theorem AT.18 of Appendix AT 7; it holds symbolically to fifth order (residuals 0) and is not restated. Its consequence for the present appendix is that the two dominant SPARC systematics slide a galaxy *along* the horizontal, whereas a failure of Eq. (BS21) is *vertical*.

7. Confrontation, Including the Misses

Each law's $u(\nu)$ below is derived from that law's own μ by the same operation (Eq. (AT13)); with $L(\nu) \equiv \ln\big(\nu/(\nu-1)\big)$ the closed forms are $u_{\rm SOURCE} = (\nu-1)L$, $u_{\rm TOTAL} = 2(\nu-1)L/[1+(\nu-1)L]$, $u_{\rm simple} = 2(\nu-1)/(2\nu-1)$ and $u_{\rm standard} = 2(\nu^2-1)/(2\nu^2-1)$, each with residual 0 against direct differentiation of its μ. The last two reproduce the $n=1$ and $n=2$ members of Proposition AT.20 exactly, which is an independent check of both derivations; **the TOTAL row is new**.

a. What the data say, and what they cannot. The SPARC confrontation of Eq. (BS21) is Appendix AT 7 and is not repeated: $\chi^2/8 = 1.08$, $p = 0.37$ on 2316 points from 113 galaxies; $n \geq 2$ excluded at $2\Delta\ln\mathcal{L} \geq +14.07$; **and the limit, already recorded there, that these data do *not* separate the SOURCE form from** $\mu = x/(1+x)$ **(+0.43) and provably cannot** (ceiling +3.99 for any a_0-free shape statistic). Three additions belong here.

- **Where the separating power lives.** The gap $|u_{\rm SOURCE} - u_{\rm simple}|$ peaks at $\nu = 1.13955$ with value 0.074850 and has decayed to 0.003685 by $\nu = 5$. **The discriminating power sits in the Newton-adjacent inner galaxy**, the opposite of where deep-field tests look — which is why pushing SPARC to $\nu \to 1.1$ is worth more than adding deep-field points.

- **The curvature channel fails as a discriminator.** DFD passes its own (ν, C) test of Eq. (BS22) at $\chi^2/8 = 1.36$, $p = 0.21$, but scores $2\Delta\ln\mathcal{L} = -0.68$ against $\mu = x/(1+x)$ — *worse* than the slope channel — because $\sigma_C/\sigma_u \geq 1.90$ is an irreducible floor set by SPARC's 3.63-dex dynamic range. Recorded as a negative result.

- **Branch selection: SOURCE, on a statistic that is not clean.** The whole-sample β^2-weighted mean u leans TOTAL at $\Delta\chi^2 = -2.19$; a post-hoc binning in y with full bootstrap covariance gives $\Delta\chi^2$(TOTAL − SOURCE) $= +32.45$ (0/60 mock misidentifications), selecting SOURCE. **Both numbers are stated because both are real**, and on the selecting statistic SOURCE's own $\chi^2 = 22.82$ for four bins is not itself a good fit. The branch of record is SOURCE, Eq. (BS8):

TABLE CXXXVII. The shape observable u as a function of the amplitude ν, for the two DFD branches and the two standard MOND interpolation functions. No a_0, no mass-to-light ratio and no distance enters any column.

law	$u(\nu)$	$\nu = 1.2$	1.6	2.5	5.0
DFD SOURCE	$(\nu-1)L$	0.358352	0.588498	0.766238	0.892574
DFD TOTAL	$\dfrac{2(\nu-1)L}{1+(\nu-1)L}$	0.527627	0.740949	0.867650	0.943238
MOND simple	$\dfrac{2(\nu-1)}{2\nu-1}$	0.285714	0.545455	0.750000	0.888889
MOND standard	$\dfrac{2(\nu^2-1)}{2\nu^2-1}$	0.468085	0.757282	0.913043	0.979592

the binned statistic selects it, and the corpus's field equations use it as the exact law, with $\mu = x/(1+x)$ its weak-response approximant (§VII); the SPARC data do not separate it from that approximant (above).

b. The $\nu \geq 1$ falsifier is a corollary of Theorem BS.7. Falsifier AT.22 — a measured $\Upsilon_{[3.6]} > 0.58\,M_\odot/L_\odot$ refutes DFD from SPARC alone — rests on "the μ-law response is never sub-Newtonian". Theorem BS.7 is where that premise is proved, from detailed balance and the absence of a de-excited level, rather than read off the interpolation function. The falsifier is branch-independent for exactly that reason.

c. Provenance of the empirical numbers. Every closed form in this appendix was re-derived symbolically and every printed constant recomputed at 60 digits. The SPARC-derived numbers quoted above ($\chi^2/8$, $2\Delta\ln\mathcal{L}$, $\Delta\chi^2$, $u = 0.7818 \pm 0.0321$) are carried from Appendix AT 7 and from the dedicated branch and curvature analyses; they were *not* re-run here. The y-binned branch statistic was declared post-hoc in its source analysis, as was the $\Upsilon_{[3.6]}$ inversion of Remark AT.21; the $\chi^2/8 = 1.08$ goodness-of-fit and the $n \geq 2$ exclusions were pre-registered.

8. Grades

TABLE CXXXVIII. Tier and status of every result in this appendix, in the grading scheme of Appendix AG. Negative results are listed with the positive ones.

result	where	tier	status
$\nu = 1 + n_{\mathrm{BE}}$ given $\nu = Z_1$	Thm BS.2	T	*validated*
ground-state principle $\mu = \mathbb{P}(n{=}0)$	Rem. BS.4	stated input	adopted
$\mu_{\mathrm{chem}} = 0$ from flat curves	Thm BS.5	T	*validated*
a host caps an embedded boost at $\nu(\tau_h)$	Thm NL.13	T	motivates Axiom NL.14
$\nu > 1$; no sub-Newtonian μ-law response	Thm BS.7	T	*validated*
Fermi excluded ($1 < \nu_F \leq 2$)	Cor. BS.8	T	*validated*
$\mu = 1 - e^{-\tau}$, both branches	Thm BS.9	T	*validated*
which τ: SOURCE	§BS 7	E	adopted
S/k, C/k, Dulong–Petit reading	Thm BS.13	T	*validated*
solar-system safety at the planets is structural	Cor. BS.14	T	*validated*
$T_{\mathrm{DFD}} = 4\pi\sqrt{T_{\mathrm{H}}T_{\mathrm{U}}}$	Thm BS.15	T	*open*
$PV = U/3$ (given $m_\psi = 0$)	Thm BS.17	D	*open*
$S_{\mathrm{tot}}/k = X^2/2 + X + K$	Thm BS.19	T	*open*
$u = \tau n_{\mathrm{BE}} = \langle E \rangle / kT$	Thm BS.22	T	*validated*
$C/k = \nu(\nu-1)\ln^2[\nu/(\nu-1)]$	Thm BS.24	T	*validated*
$S/k = \ln(M_{\mathrm{dyn}}/M_{\mathrm{bar}}) + u$	Thm BS.25	T	*validated*
κ^2/Ω^2 form only at $\beta = -2$	Cor. BS.26	T	—
separation from $\mu = x/(1+x)$	§BS 7	—	**not achieved,** +0.43
curvature as a discriminator	§BS 7	—	**failed,** −0.68

ACKNOWLEDGMENTS

We thank the atomic clock groups at JILA and PTB for valuable discussions regarding clock comparison methodologies and data interpretation. We also acknowledge the SPARC collaboration for making their galaxy rotation curve database publicly available.

[1] G. Alcock, Constitutive derivation of tensor gravitational radiation from $CP^2 \times S^3$ spectral geometry in Density Field Dynamics, Zenodo preprint (2026).

[2] Particle Data Group, S. Navas, *et al.*, Electroweak model and constraints on new physics (2024), review in *Review of Particle Physics*, Phys. Rev. D **110**, 030001 (2024).

[3] G. Alcock, Density Field Dynamics and the c-field: A three-dimensional, time-emergent dynamics for gravity and cosmology (2025), preprint, v1.

[4] G. Alcock, Density Field Dynamics: A complete unified theory (2025), v1.0.

[5] C. M. Will, The confrontation between general relativity and experiment, Living Reviews in Relativity **17**, 4 (2014).

[6] C. M. Will, Theory and experiment in gravitational physics, Cambridge University Press (2018).

[7] G. Bertone and T. M. P. Tait, A new era in the search for dark matter, Nature **562**, 51 (2018).

[8] P. J. E. Peebles and B. Ratra, The cosmological constant and dark energy, Reviews of Modern Physics **75**, 559 (2003).

[9] V. C. Rubin, W. K. Ford, and N. Thonnard, Rotational properties of 21 Sc galaxies with a large range of luminosities and radii, Astrophysical Journal **238**, 471 (1980).

[10] S. S. McGaugh, F. Lelli, and J. M. Schombert, Radial acceleration relation in rotationally supported galaxies, Physical Review Letters **117**, 201101 (2016).

[11] F. Zwicky, Die Rotverschiebung von extragalaktischen Nebeln, Helvetica Physica Acta **6**, 110 (1933).

[12] A. G. Riess *et al.*, Observational evidence from supernovae for an accelerating universe and a cosmological constant, Astronomical Journal **116**, 1009 (1998).

[13] S. Perlmutter *et al.*, Measurements of Ω and Λ from 42 high-redshift supernovae, Astrophysical Journal **517**, 565 (1999).

[14] M. Milgrom, A modification of the Newtonian dynamics as a possible alternative to the hidden mass hypothesis, Astrophysical Journal **270**, 365 (1983).

[15] B. Famaey and S. S. McGaugh, Modified Newtonian Dynamics (MOND): Observational phenomenology and relativistic extensions, Living Reviews in Relativity **15**, 10 (2012).

[16] F. Lelli, S. S. McGaugh, J. M. Schombert, and M. S. Pawlowski, One law to rule them all: The radial acceleration relation of galaxies, Astrophysical Journal **836**, 152 (2017).

[17] B. P. Abbott *et al.*, Gravitational waves and gamma-rays from a binary neutron star merger: GW170817 and GRB 170817A, Astrophysical Journal Letters **848**, L13 (2017).

[18] T. Clifton, P. G. Ferreira, A. Padilla, and C. Skordis, Modified gravity and cosmology, Physics Reports **513**, 1 (2012).

[19] A. Joyce, B. Jain, J. Khoury, and M. Trodden, Beyond the cosmological standard model, Physics Reports **568**, 1 (2015).

[20] C. Brans and R. H. Dicke, Mach's principle and a relativistic theory of gravitation, Physical Review **124**, 925 (1961).

[21] J. D. Bekenstein, Relativistic gravitation theory for the modified Newtonian dynamics paradigm, Physical Review D **70**, 083509 (2004).

[22] T. P. Sotiriou and V. Faraoni, $f(R)$ theories of gravity, Reviews of Modern Physics **82**, 451 (2010).

[23] A. Einstein, Über den Einfluß der Schwerkraft auf die Ausbreitung des Lichtes, Annalen der Physik **340**, 898 (1911).

[24] A. Einstein, Lichtgeschwindigkeit und Statik des Gravitationsfeldes, Annalen der Physik **343**, 355 (1912).

[25] W. Gordon, Zur Lichtfortpflanzung nach der Relativitätstheorie, Annalen der Physik **377**, 421 (1923).

[26] V. Perlick, *Ray Optics, Fermat's Principle, and Applications to General Relativity* (Springer, 2000).

[27] J. Bekenstein and M. Milgrom, Does the missing mass problem signal the breakdown of Newtonian gravity?, Astrophysical Journal **286**, 7 (1984).

[28] L. Blanchet and S. Marsat, Modified gravity approach based on a preferred time foliation, Physical Review D **84**, 044056 (2011), arXiv:1107.5264.

[29] A. Hees, W. M. Folkner, R. A. Jacobson, and R. S. Park, Constraints on modified Newtonian dynamics theories from radio tracking data of the Cassini spacecraft, Physical Review D **89**, 102002 (2014), nine years of Cassini range and Doppler tracking of Saturn give the Solar-System quadrupole $Q_2 = (3 \pm 3) \times 10^{-27}$ s^{-2} on the DE430 ephemeris., arXiv:1402.6950.

[30] R. S. Park, A. Hees, B. Famaey, H. Desmond, and A. Durakovic, Improved constraints on modified Newtonian gravity from Cassini radio tracking data, Physical Review D 10.1103/r7n8-kw38 (2026), $Q_2 = (1.6 \pm 1.8) \times 10^{-27}$ s^{-2} (1σ) from the DE440 dataset, a 40 per cent improvement on Hees et al. (2014)., arXiv:2602.17884.

[31] G. Alcock, The physical origin of the refractive field in Density Field Dynamics: Gravity as electromagnetic vacuum loading, Zenodo preprint (2026).

[32] D. Gilbarg and N. S. Trudinger, *Elliptic Partial Differential Equations of Second Order*, 2nd ed. (Springer, 2001).

[33] O. A. Ladyzhenskaya and N. N. Ural'tseva, *Linear and Quasilinear Elliptic Equations* (Academic Press, 1968).

[34] E. Babichev, V. Mukhanov, and A. Vikman, k-Essence, superluminal propagation, causality and emergent geom-

etry, JHEP **02**, 101, arXiv:0708.0561 [hep-th].
[35] B. Bertotti, L. Iess, and P. Tortora, A test of general relativity using radio links with the Cassini spacecraft, Nature **425**, 374 (2003).
[36] J. G. Williams, S. G. Turyshev, and D. H. Boggs, Progress in lunar laser ranging tests of relativistic gravity, Physical Review Letters **93**, 261101 (2004).
[37] L. Shao and N. Wex, New tests of local Lorentz invariance of gravity with small-eccentricity binary pulsars, Classical and Quantum Gravity **29**, 215018 (2012).
[38] S. S. Shapiro, J. L. Davis, D. E. Lebach, and J. S. Gregory, Measurement of the solar gravitational deflection of radio waves using geodetic very-long-baseline interferometry data, 1979–1999, Physical Review Letters **92**, 121101 (2004).
[39] I. I. Shapiro, Fourth test of general relativity, Physical Review Letters **13**, 789 (1964).
[40] R. F. C. Vessot *et al.*, Test of relativistic gravitation with a space-borne hydrogen maser, Physical Review Letters **45**, 2081 (1980).
[41] J. Lense and H. Thirring, Über den Einfluss der Eigenrotation der Zentralkörper auf die Bewegung der Planeten und Monde nach der Einsteinschen Gravitationstheorie, Physikalische Zeitschrift **19**, 156 (1918).
[42] I. Ciufolini and E. C. Pavlis, A confirmation of the general relativistic prediction of the Lense–Thirring effect, Nature **431**, 958 (2004).
[43] C. W. F. Everitt *et al.*, Gravity Probe B: Final results of a space experiment to test general relativity, Physical Review Letters **106**, 221101 (2011).
[44] N. Yunes and F. Pretorius, Fundamental theoretical bias in gravitational wave astrophysics and the parametrized post-Einsteinian framework, Physical Review D **80**, 122003 (2009).
[45] R. Abbott *et al.*, Tests of general relativity with GWTC-3, Physical Review D **112**, 084080 (2025).
[46] J. M. Weisberg, D. J. Nice, and J. H. Taylor, Timing measurements of the relativistic binary pulsar PSR B1913+16, Astrophysical Journal **722**, 1030 (2010).
[47] J. M. Weisberg and Y. Huang, Relativistic measurements from timing the binary pulsar PSR B1913+16, Astrophysical Journal **829**, 55 (2016).
[48] Event Horizon Telescope Collaboration, First M87 Event Horizon Telescope results. I. The shadow of the supermassive black hole, Astrophysical Journal Letters **875**, L1 (2019).
[49] Event Horizon Telescope Collaboration, First Sagittarius A* Event Horizon Telescope results. I. The shadow of the supermassive black hole in the center of the Milky Way, Astrophysical Journal Letters **930**, L12 (2022).
[50] F. Lelli, S. S. McGaugh, and J. M. Schombert, SPARC: Mass models for 175 disk galaxies with Spitzer photometry and accurate rotation curves, AJ **152**, 157 (2016), arXiv:1606.09251.
[51] K.-H. Chae, Breakdown of the Newton-Einstein standard gravity at low acceleration in internal dynamics of wide binary stars, The Astrophysical Journal **952**, 128 (2023).
[52] I. Banik, C. Pittordis, W. Sutherland, *et al.*, Strong constraints on the gravitational law from Gaia DR3 wide binaries, Monthly Notices of the Royal Astronomical Society **527**, 4573 (2024).
[53] K. El-Badry, H.-W. Rix, and T. M. Heintz, A million binaries from Gaia eDR3: sample selection and validation of Gaia parallax uncertainties, Monthly Notices of the Royal Astronomical Society **506**, 2269 (2021), 1.3 million pairs with > 90 per cent bound probability; 1.1 million with > 99 per cent., arXiv:2101.05282.
[54] G. W. Angus, B. Famaey, and D. A. Buote, X-ray group and cluster mass profiles in MOND: unexplained mass on the group scale, Monthly Notices of the Royal Astronomical Society **387**, 1470 (2008).
[55] M. T. Murphy, P. Molaro, A. C. O. Leite, G. Cupani, S. Cristiani, V. D'Odorico, R. Génova Santos, C. J. A. P. Martins, D. Milaković, N. J. Nunes, *et al.*, Fundamental physics with ESPRESSO: Precise limit on variations in the fine-structure constant towards the bright quasar HE 0515−4414, Astronomy & Astrophysics **658**, A123 (2022), arXiv:2112.05819 [astro-ph.CO].
[56] J. K. Webb, J. A. King, M. T. Murphy, V. V. Flambaum, R. F. Carswell, and M. B. Bainbridge, Indications of a spatial variation of the fine structure constant, Physical Review Letters **107**, 191101 (2011), arXiv:1008.3907 [astro-ph.CO].
[57] J. B. Whitmore and M. T. Murphy, Impact of instrumental systematic errors on fine-structure constant measurements with quasar absorption lines, Monthly Notices of the Royal Astronomical Society **447**, 446 (2015).
[58] Planck Collaboration, N. Aghanim, Y. Akrami, M. Ashdown, J. Aumont, C. Baccigalupi, M. Ballardini, A. J. Banday, R. B. Barreiro, N. Bartolo, *et al.*, Planck 2018 results. VI. Cosmological parameters, Astronomy & Astrophysics **641**, A6 (2020), arXiv:1807.06209 [astro-ph.CO].
[59] R. H. Cyburt, B. D. Fields, K. A. Olive, and T.-H. Yeh, Big bang nucleosynthesis: Present status, Reviews of Modern Physics **88**, 015004 (2016), arXiv:1505.01076 [astro-ph.CO].
[60] G. Alcock, Ab initio derivation of the fine structure constant from Density Field Dynamics, Zenodo preprint (2026).
[61] M. E. Tobar, P. Wolf, S. Bize, G. Santarelli, and V. Flambaum, Testing local Lorentz and position invariance and variation of fundamental constants by searching the derivative of the comparison frequency between a cryogenic sapphire oscillator and hydrogen maser, Phys. Rev. D **81**, 022003 (2010).
[62] D. Hils and J. L. Hall, Improved Kennedy–Thorndike experiment to test special relativity, Phys. Rev. Lett. **64**, 1697 (1990).
[63] K. Beeks *et al.*, Fine-structure constant sensitivity of the Th-229 nuclear clock transition, Nature Communications **16**, 9147 (2025).
[64] R. Lange, N. Huntemann, J. M. Rahm, C. Sanner, H. Shao, S. Weyers, and E. Peik, Improved limits for violations of local position invariance from atomic clock comparisons, Physical Review Letters **126**, 011102 (2021).
[65] S. Blatt, A. D. Ludlow, G. K. Campbell, *et al.*, New limits on coupling of fundamental constants to gravity using ^{87}Sr optical lattice clocks, Physical Review Letters **100**, 140801 (2008).
[66] G. Alcock, Dataset and analysis package for "solar-locked differential in ion–neutral optical frequency ratios", Zenodo dataset, MIT License (2025).
[67] G. Alcock, Solar-locked differential in ion–neutral optical frequency ratios: Empirical evidence for a reproducible heliocentric phase modulation, Zenodo preprint (2025).
[68] ROCIT Collaboration, Final publishable report: Robust optical clocks for international timescales (18SIB05),

EMPIR Final Report (2024), project 18SIB05 ROCIT.
[69] T. Ooi, J. F. Doyle, C. Zhang, J. S. Higgins, J. Ye, K. Beeks, T. Sikorsky, T. Schumm, *et al.*, Frequency reproducibility of solid-state thorium-229 nuclear clocks, Nature **650**, 72 (2026).
[70] V. V. Flambaum and A. F. Tedesco, Dependence of nuclear magnetic moments on quark masses and limits on temporal variation of fundamental constants from atomic clock experiments, Physical Review C **73**, 055501 (2006).
[71] J. S. Higgins *et al.*, Temperature sensitivity of a thorium-229 solid-state nuclear clock, Physical Review Letters **134**, 113801 (2025).
[72] G. Alcock, Composition-dependent bounds on scalar-field coupling to nuclear decay rates, Zenodo preprint (2026).
[73] K. Beloy, M. I. Bodine, T. Bothwell, S. M. Brewer, S. L. Bromley, J.-S. Chen, J.-D. Deschênes, J. Helmcke, D. B. Hume, C. J. Kennedy, *et al.*, Frequency ratio measurements at 18-digit accuracy using an optical clock network, Nature **591**, 564 (2021).
[74] D. Lee, K. Kim, Z. Z. Hu, B. Lewis, W. Warfield, K. Zhou, A. L. Collopy, J. A. Sherman, A. S. Kowligy, P. B. Patel, J. D. Roslund, A. Cingöz, M. M. Boyd, and J. Ye, Phase-continuous comparison of three all-optical time scales over 20 days, arXiv preprint arXiv:2608.00910 (2026).
[75] G. D'Amico, G. Rosi, S. Zhan, L. Cacciapuoti, M. Fattori, and G. M. Tino, Canceling the gravity gradient phase shift in atom interferometry, Physical Review Letters **119**, 253201 (2017).
[76] C. Overstreet, P. Asenbaum, T. Kovachy, R. Notermans, J. M. Hogan, and M. A. Kasevich, Effective inertial frame in an atom interferometric test of the equivalence principle, Physical Review Letters **120**, 183604 (2018).
[77] A. Roura, Circumventing Heisenberg's uncertainty principle in atom interferometry tests of the equivalence principle, Physical Review Letters **118**, 160401 (2017).
[78] M. D. Ernst, Permutation methods: A basis for exact inference, Statistical Science **19**, 676 (2004).
[79] G. Alcock, Unexplained bright–dim intensity asymmetries in SOHO/UVCS Lyman-α data, Submitted (revised) to Solar Physics; under review (2026), theory-neutral empirical companion: 163/321 days significant at 5% FDR; temporal-split permutation methodology.
[80] Y. Benjamini and Y. Hochberg, Controlling the false discovery rate: A practical and powerful approach to multiple testing, Journal of the Royal Statistical Society: Series B **57**, 289 (1995).
[81] J. Cohen, *Statistical Power Analysis for the Behavioral Sciences*, 2nd ed. (Lawrence Erlbaum Associates, 1988).
[82] ALPHA Collaboration, E. K. Anderson, *et al.*, Observation of the effect of gravity on the motion of antimatter, Nature **621**, 716 (2023).
[83] R. Akbari *et al.*, Be^+-assisted, simultaneous confinement of more than 15000 antihydrogen atoms, Nature Communications **16**, 10106 (2025), order-of-magnitude improvement in antihydrogen trapping efficiency.
[84] I. M. H. Etherington, On the definition of distance in general relativity, Philosophical Magazine 7, **15**, 761 (1933).
[85] G. F. R. Ellis, On the definition of distance in general relativity: I. M. H. Etherington (Philosophical Magazine ser. 7, vol. 15, 761 (1933)): Editorial note, General Relativity and Gravitation **39**, 1047 (2007).
[86] R. F. L. Holanda, J. A. S. Lima, and M. B. Ribeiro, Testing the distance-duality relation with galaxy clusters and type Ia supernovae, Astrophysical Journal Letters **722**, L233 (2010).
[87] N. Liang, Z. Li, P. Wu, S. Cao, K. Liao, and Z.-H. Zhu, A consistent test of the distance-duality relation with galaxy clusters and Type Ia supernovae, Monthly Notices of the Royal Astronomical Society **436**, 1017 (2013), arXiv:1104.2497.
[88] D. Scolnic *et al.*, The Pantheon+ analysis: The full dataset and light-curve release, Astrophys. J. **938**, 113 (2022), arXiv:2112.03863.
[89] D. Brout *et al.*, The Pantheon+ analysis: Cosmological constraints, Astrophys. J. **938**, 110 (2022), arXiv:2202.04077.
[90] DESI Collaboration, A. G. Adame, *et al.*, DESI 2024 VI: Cosmological constraints from the measurements of baryon acoustic oscillations, JCAP **2025** (02), 021, arXiv:2404.03002.
[91] M. S. Madhavacheril *et al.*, The Atacama Cosmology Telescope: DR6 gravitational lensing map and cosmological constraints, Astrophys. J. **962**, 113 (2024), arXiv:2304.05203.
[92] Planck Collaboration, P. A. R. Ade, N. Aghanim, M. Arnaud, M. Ashdown, J. Aumont, C. Baccigalupi, A. J. Banday, R. B. Barreiro, N. Bartolo, *et al.*, Planck 2015 results. XXI. The integrated Sachs-Wolfe effect, Astronomy & Astrophysics **594**, A21 (2016), arXiv:1502.01595 [astro-ph.CO].
[93] B. Stölzner, A. Cuoco, J. Lesgourgues, and M. Bilicki, Updated tomographic analysis of the integrated Sachs-Wolfe effect and implications for dark energy, Physical Review D **97**, 063506 (2018), arXiv:1710.03238 [astro-ph.CO].
[94] I. Tutusaus *et al.*, Measurement of the Weyl potential evolution from the first three years of Dark Energy Survey data, Nature Communications **15**, 9295 (2024), model-independent Weyl potential 2–3σ shallower at low z.
[95] G. Gu, X. Wang, Y. Wang, G.-B. Zhao, L. Pogosian, *et al.*, Dynamical dark energy in light of the DESI DR2 baryonic acoustic oscillations measurements, Nature Astronomy (2025), dataset-dependent preference for $w(z) \neq -1$, arXiv:2504.06118.
[96] C. Pittordis and W. Sutherland, Wide binaries from Gaia DR3: testing GR vs. MOND with realistic triple modelling, Open Journal of Astrophysics (2025), see also Hernandez (2025) MNRAS 537:2925 for opposing interpretation.
[97] L. Wenzl *et al.*, The Atacama Cosmology Telescope DR6: gravitational lensing $\times$ BOSS E_G test, Physical Review D **111**, 043535 (2025).
[98] A. H. Wright, B. Stölzner, M. Asgari, *et al.*, KiDS-legacy: Cosmological constraints from cosmic shear with the complete Kilo-Degree Survey, Astronomy and Astrophysics **703**, A158 (2025), arXiv:2503.19441.
[99] B. Stölzner, A. H. Wright, M. Asgari, *et al.*, KiDS-legacy: Consistency of cosmic shear measurements and joint cosmological constraints with external probes, Astronomy and Astrophysics **702**, A169 (2025), arXiv:2503.19442.
[100] V. Calafut, P. A. Gallardo, E. M. Vavagiakis, *et al.*, The Atacama Cosmology Telescope: Detection of the pairwise kinematic Sunyaev–Zel'dovich effect with SDSS DR15 galaxies, Physical Review D **104**, 043502 (2021),

arXiv:2101.08374.

[101] P. A. Gallardo *et al.*, Test of the gravitational force law on cosmological scales using the kinematic Sunyaev–Zel'dovich effect, Physical Review Letters (2026), published 15 April 2026; DOI 10.1103/rk8v-rcm3.

[102] M. F. Atiyah and I. M. Singer, The index of elliptic operators: III, Annals of Mathematics **87**, 546 (1968).

[103] M. F. Atiyah, V. K. Patodi, and I. M. Singer, Spectral asymmetry and Riemannian geometry. I, Mathematical Proceedings of the Cambridge Philosophical Society **77**, 43 (1975).

[104] P. Li, F. Lelli, S. McGaugh, and J. Schombert, Fitting the radial acceleration relation to individual SPARC galaxies, Astronomy & Astrophysics **615**, A3 (2018), residual r.m.s. scatter about the fitted RAR is 0.057 dex.

[105] A. G. Riess, D. Scolnic, G. S. Anand, L. Breuval, S. Casertano, L. M. Macri, S. Li, W. Yuan, C. D. Huang, S. Jha, *et al.*, JWST validates HST distance measurements: Selection of supernova subsample explains differences in JWST estimates of local H_0, The Astrophysical Journal **977**, 120 (2024), combined JWST three-method result: $H_0 = 72.6 \pm 2.0$ km/s/Mpc, arXiv:2408.11770.

[106] A. G. Riess, S. Li, G. S. Anand, W. Yuan, L. Breuval, *et al.*, The perfect host: JWST cepheid observations in a background-free SN Ia host confirm no bias in Hubble-constant measurements (2025), arXiv:2509.01667.

[107] H0DN Collaboration, S. Casertano, G. Anand, R. I. Anderson, R. Beaton, A. Bhardwaj, *et al.*, The local distance network: a community consensus report on the measurement of the Hubble constant at 1% precision, Astronomy & Astrophysics **708**, A166 (2026), arXiv:2510.23823.

[108] W. L. Freedman, B. F. Madore, I. S. Jang, T. J. Hoyt, A. J. Lee, and K. A. Owens, Status report on the Chicago-Carnegie Hubble Program (CCHP): Measurement of the Hubble constant using the Hubble and James Webb Space Telescopes, Astrophys. J. **985**, 203 (2025), TRGB (HST+JWST): $H_0 = 70.39 \pm 1.9$ km/s/Mpc; claims consistency with ΛCDM, arXiv:2408.06153.

[109] B. I. Ciocan *et al.*, MUSE-DARK III: The evolution of the radial acceleration relation at intermediate redshifts, Astronomy & Astrophysics **709**, L16 (2026), arXiv:2604.22613.

[110] G. T. Alcock, Is the acceleration scale of the radial acceleration relation tracking the cosmic expansion rate?, Monthly Notices of the Royal Astronomical Society **551**, 10.1093/mnras/stag1485 (2026), published 2026 September 7; MNRAS vol. 551, issue 4 (2026 October); article ID stag1485. Accepted 2026 August 3, in original form 2026 July 10; article type Letter. Open access, CC-BY 4.0. Fits $a_0(z) = A(1+z)^\gamma$ to the MUSE–DARK binned RAR scale: $\gamma = 0.78 \pm 0.15$ (statistical), 0.83 ± 0.13 with the SPARC $z \simeq 0$ anchor; frozen a_0 excluded at 5.3σ (6.6σ anchored), $\sqrt{\rho_m}$ scaling at 4.8σ on the published bin errors read as 1σ; $a_0 = A\,E(z)$ the information-criterion-preferred one-parameter form.

[111] A. Nestor Shachar, S. H. Price, N. M. Förster Schreiber, R. Genzel, T. T. Shimizu, L. J. Tacconi, H. Übler, *et al.*, RC100: Rotation curves of 100 massive star-forming galaxies at $z = 0.6$–2.5 reveal little dark matter on galactic scales, Astrophys. J. **944**, 78 (2023), arXiv:2209.12199.

[112] G. Alcock, Epoch evolution of the MOND crossover scale in Density Field Dynamics: An epoch-consistency argument for $a_\star(z) = 2\sqrt{\alpha}\,cH(z)$, Companion note to the DFD Unified Review (this paper), Zenodo (2026), conditional extension of Appendix N under the Section XIX.D epoch-consistency rule.

[113] A. H. Chamseddine and A. Connes, Universal formula for noncommutative geometry actions: unification of gravity and the standard model (1996), A. H. Chamseddine and A. Connes, "Universal formula for noncommutative geometry actions: unification of gravity and the standard model," Phys. Rev. Lett. **77**, 4868 (1996).

[114] A. Chamseddine and A. Connes, (1997), A. Chamseddine and A. Connes, *The spectral action principle*, Commun. Math. Phys. **186**, 731 (1997).

[115] A. D. Sakharov, Vacuum quantum fluctuations in curved space and the theory of gravitation (1967), A. D. Sakharov, "Vacuum quantum fluctuations in curved space and the theory of gravitation," Dokl. Akad. Nauk Ser. Fiz. **177**, 70–71 (1967); Sov. Phys. Dokl. **12**, 1040–1041 (1968); reprinted in Gen. Rel. Grav. **32**, 365–367 (2000).

[116] G. Alcock, Tree-level no-drive theorem for the minimal optical-metric EM sector in Density Field Dynamics: $\lambda_{\rm bare} = 1$ from the pure gauge-invariant action, Companion note to the DFD Unified Review (this paper), Zenodo (2026), minimal-sector baseline for Appendix R.

[117] C. W. Misner, K. S. Thorne, and J. A. Wheeler, *Gravitation* (W.H. Freeman, 1973).

[118] V. A. Dzuba and V. V. Flambaum, Sensitivity of optical transitions to variation of the fine-structure constant, Physical Review A **97**, 040501(R) (2018).

[119] R. Epstein and I. I. Shapiro, Post-post-Newtonian deflection of light by the Sun, Physical Review D **22**, 2947 (1980).

[120] G. W. Richter and R. A. Matzner, Second-order contributions to gravitational deflection of light in the parametrized post-Newtonian formalism, Physical Review D **26**, 1219 (1982).

[121] F. Hofmann and J. Müller, Relativistic tests with lunar laser ranging, Classical and Quantum Gravity **35**, 035015 (2018).

[122] J. F. Bell and T. Damour, A new test of conservation laws and Lorentz invariance in relativistic gravity, Classical and Quantum Gravity **13**, 3121 (1996).

[123] I. H. Stairs, Pulsars in binary systems: Probing binary stellar evolution and general relativity, Living Reviews in Relativity **6**, 5 (2003).

[124] D. F. Bartlett and D. Van Buren, Equivalence of active and passive gravitational mass using the moon, Physical Review Letters **57**, 21 (1986).

[125] E. Peik and C. Tamm, Nuclear laser spectroscopy of the 3.5 eV transition in Th-229, Europhysics Letters **61**, 181 (2003).

[126] LIGO Scientific Collaboration and Virgo Collaboration, GW170817: Observation of gravitational waves from a binary neutron star inspiral, Physical Review Letters **119**, 161101 (2017).

[127] E. Witten, Search for a realistic Kaluza–Klein theory (1981), E. Witten, "Search for a realistic Kaluza–Klein theory," Nucl. Phys. B **186**, 412–428 (1981).

[128] J. E. Humphreys, *Introduction to Lie Algebras and Representation Theory*, Graduate Texts in Mathematics, Vol. 9 (Springer, 1972).

[129] W. Fulton and J. Harris, *Representation Theory: A First Course*, Graduate Texts in Mathematics, Vol. 129 (Springer, 1991).

[130] H. B. Lawson and M.-L. Michelsohn, *Spin Geometry* (Princeton University Press, 1989).

[131] T. Friedrich, *Dirac Operators in Riemannian Geometry*, Graduate Studies in Mathematics, Vol. 25 (American Mathematical Society, 2000).

[132] E. Witten, Quantum field theory and the Jones polynomial, Communications in Mathematical Physics **121**, 351 (1989).

[133] C. Y. Tsang *et al.*, Tracking the baryon number with nuclear collisions, Science 10.1126/science.ads5962 (2026), STAR Collaboration.

[134] D. Kharzeev, Can gluons trace baryon number?, Physics Letters B **378**, 238 (1996), arXiv:hep-ph/9602314.

[135] G. C. Rossi and G. Veneziano, A possible description of baryon dynamics in dual and gauge theories, Nuclear Physics B **123**, 507 (1977).

[136] F. Nicastro, J. Kaastra, Y. Krongold, S. Borgani, E. Branchini, R. Cen, M. Dadina, C. W. Danforth, M. Elvis, F. Fiore, *et al.*, Observations of the missing baryons in the warm-hot intergalactic medium, Nature **558**, 406 (2018).

[137] J.-P. Macquart *et al.*, A census of baryons in the universe from localized fast radio bursts, Nature **581**, 391 (2020).

[138] D. Eckert, S. Ettori, E. Pointecouteau, R. F. J. van der Burg, and S. I. Loubser, The gravitational field of X-COP galaxy clusters, Astronomy & Astrophysics **662**, A123 (2022), arXiv:2205.01110 [astro-ph.CO].

[139] C. Burke, M. Hilton, and C. Collins, Coevolution of brightest cluster galaxies and intracluster light using CLASH, Monthly Notices of the Royal Astronomical Society **449**, 2353 (2015).

[140] M. Montes and I. Trujillo, Intracluster light at the Frontier – II. The Frontier Fields Clusters, Monthly Notices of the Royal Astronomical Society **474**, 917 (2018).

[141] S. Walker *et al.*, The physics of galaxy cluster outskirts, Space Science Reviews **215**, 7 (2019).

[142] M. Cappellari, Full spectrum fitting with photometry in pPXF: stellar population versus dynamical masses, non-parametric star formation history and metallicity for 3200 LEGA-C galaxies at redshift $z \approx 0.8$, Monthly Notices of the Royal Astronomical Society **526**, 3273 (2023), arXiv:2208.14974 [astro-ph.GA].

[143] G. W. Pratt, J. H. Croston, M. Arnaud, and H. Böhringer, Galaxy cluster X-ray luminosities and temperatures from the REXCESS sample, Astronomy & Astrophysics **498**, 361 (2009), arXiv:0809.3784 [astro-ph].

[144] A. B. Mantz, S. W. Allen, R. G. Morris, R. W. Schmidt, A. von der Linden, and O. Urban, Cosmology and astrophysics from relaxed galaxy clusters – II. cosmological constraints, Monthly Notices of the Royal Astronomical Society **440**, 2077 (2014), see also Mantz et al. 2016, MNRAS 463, 3582 (arXiv:1606.03407), arXiv:1402.6212 [astro-ph.CO].

[145] G. Alcock, Ab initio derivation of the charged fermion mass spectrum from Density Field Dynamics, Zenodo preprint (2026).

[146] X. Dai and D. S. Freed, η-invariants and determinant lines, Journal of Mathematical Physics **35**, 5155 (1994), arXiv:hep-th/9405012.

[147] D. S. Freed and G. W. Moore, Twisted equivariant matter, Annales Henri Poincaré **14**, 1927 (2013), arXiv:1208.5055.

[148] A. H. Chamseddine and A. Connes, Noncommutative geometry as a framework for unification of all fundamental interactions including gravity. Part I (2010), A. H. Chamseddine and A. Connes, *Noncommutative geometry as a framework for unification of all fundamental interactions including gravity. Part I*, Fortsch. Phys. **58**, 553 (2010).

[149] J. Ellis and M. K. Gaillard, Strong and weak CP violation, Nuclear Physics B **150**, 141 (1979).

[150] I. B. Khriplovich and A. I. Vainshtein, Infinite renormalization of θ-term and Jarlskog invariant for CP violation, Nuclear Physics B **414**, 27 (1994), hep-ph/9308334.

[151] I. García-Etxebarria and M. Montero, Dai–Freed anomalies in particle physics, Journal of High Energy Physics **2019**, 003 (2019), arXiv:1808.00009.

[152] S. M. Koushiappas, A cosmological uncertainty relation and late-universe acceleration, Physical Review D (2026), arXiv:2604.27771.

[153] V. A. Kostelecký and N. Russell, Data tables for Lorentz and CPT violation, Reviews of Modern Physics **83**, 11 (2011).

[154] N. Ashby, T. E. Parker, and B. R. Patla, A null test of general relativity based on a long-term comparison of atomic transition frequencies, Nature Physics **14**, 822 (2018).

[155] M. Filzinger, S. Hausser, M. Steinel, *et al.*, Improved limits on the coupling of ultralight bosonic dark matter to photons from optical atomic clock comparisons, Physical Review Letters **130**, 253001 (2023).

[156] T. M. Fortier, N. Ashby, J. C. Bergquist, *et al.*, Precision atomic spectroscopy for improved limits on variation of the fine structure constant and local position invariance, Physical Review Letters **98**, 070801 (2007).

[157] T. Rosenband, D. B. Hume, P. O. Schmidt, *et al.*, Frequency ratio of Al^+ and Hg^+ single-ion optical clocks; metrology at the 17th decimal place, Science **319**, 1808 (2008).

[158] H. Brezis, *Functional Analysis, Sobolev Spaces and Partial Differential Equations* (Springer, 2011).

[159] L. C. Evans, *Partial Differential Equations*, 2nd ed. (American Mathematical Society, 2010).

[160] M. G. Crandall and T. M. Liggett, Generation of semigroups of nonlinear transformations on general Banach spaces, American Journal of Mathematics **93**, 265 (1971).

[161] G. Alcock, Pairing-symmetry selection rules for the Cooper-pair mass anomaly from A_5 microsector representation theory, Zenodo preprint (2026).

[162] I. Esteban, M. C. Gonzalez-Garcia, M. Maltoni, T. Schwetz, and A. Zhou, The fate of hints: updated global analysis of three-flavor neutrino oscillations, JHEP **2024** (12), 216, arXiv:2410.05380 [hep-ph].

[163] A. Papapetrou, Eine Theorie des Gravitationsfeldes mit einer Feldfunktion, Zeitschrift für Physik **139**, 518 (1954).

[164] H. Yilmaz, New approach to general relativity, Physical Review **111**, 1417 (1958).

[165] P. Boonserm, T. Ngampitipan, A. Simpson, and M. Visser, Exponential metric represents a traversable wormhole, Physical Review D **98**, 084048 (2018).

[166] K.-H. Chae, F. Lelli, H. Desmond, S. S. McGaugh, P. Li, and J. M. Schombert, Testing the strong equivalence

principle: Detection of the external field effect in rotationally supported galaxies, The Astrophysical Journal **904**, 51 (2020).

[167] K.-H. Chae, H. Desmond, F. Lelli, S. S. McGaugh, and J. M. Schombert, Testing the strong equivalence principle. II. relating the external field effect in galaxy rotation curves to the large-scale structure of the universe, The Astrophysical Journal **921**, 104 (2021).

[168] A. Paranjape and R. K. Sheth, The phenomenology of the external field effect in cold dark matter models, Monthly Notices of the Royal Astronomical Society **517**, 130 (2022).

[169] H. Desmond, The underlying radial acceleration relation, Monthly Notices of the Royal Astronomical Society **526**, 3342 (2023).

[170] L. J. Tacconi, R. Genzel, and A. Sternberg, The evolution of the star-forming interstellar medium across cosmic time, Annu. Rev. Astron. Astrophys. **58**, 157 (2020), arXiv:2003.06245.

[171] M. Milgrom, High-redshift rotation curves and MOND (2017), arXiv:1703.06110.

[172] R. Genzel, N. M. Förster Schreiber, H. Übler, P. Lang, T. Naab, R. Bender, L. J. Tacconi, *et al.*, Strongly baryon-dominated disk galaxies at the peak of galaxy formation ten billion years ago, Nature **543**, 397 (2017), arXiv:1703.04310.

[173] H. Übler, N. M. Förster Schreiber, R. Genzel, E. Wisnioski, S. Wuyts, *et al.*, The evolution of the Tully-Fisher relation between $z \sim 2.3$ and $z \sim 0.9$ with KMOS^{3D}, Astrophys. J. **842**, 121 (2017), arXiv:1703.04321.

[174] R. Genzel, S. H. Price, H. Übler, N. M. Förster Schreiber, T. T. Shimizu, L. J. Tacconi, *et al.*, Rotation curves in $z \sim 1$–2 star-forming disks: Evidence for cored dark matter distributions, Astrophys. J. **902**, 98 (2020), arXiv:2006.03046.

[175] H. J. Mo and S. D. M. White, An analytic model for the spatial clustering of dark matter haloes, Monthly Notices of the Royal Astronomical Society **282**, 347 (1996), arXiv:astro-ph/9512127.

[176] R. K. Sheth and G. Tormen, Large-scale bias and the peak background split, Monthly Notices of the Royal Astronomical Society **308**, 119 (1999), arXiv:astro-ph/9901122.

[177] M. Blomqvist, H. du Mas des Bourboux, N. G. Busca, V. de Sainte Agathe, J. Rich, C. Balland, J. E. Bautista, K. Dawson, A. Font-Ribera, J. Guy, J.-M. Le Goff, N. Palanque-Delabrouille, M. M. Pieri, I. Pérez-Ràfols, G. Rossi, D. P. Schneider, A. Slosar, and C. Yèche, Baryon acoustic oscillations from the cross-correlation of Lyα absorption and quasars in eBOSS DR14, Astronomy & Astrophysics **629**, A86 (2019), arXiv:1904.03430 [astro-ph.CO].

[178] N. Hand, G. E. Addison, E. Aubourg, N. Battaglia, E. S. Battistelli, D. Crichton, S. Das, J. Dunkley, *et al.*, Evidence of galaxy cluster motions with the kinematic Sunyaev–Zel'dovich effect, Physical Review Letters **109**, 041101 (2012), arXiv:1203.4219 [astro-ph.CO].

[179] H. Desmond, A. Hees, and B. Famaey, On the tension between the radial acceleration relation and Solar system quadrupole in modified gravity MOND, Monthly Notices of the Royal Astronomical Society **530**, 1781 (2024), AQUAL/QUMOND: 8.7σ tension between the SPARC RAR and the Cassini quadrupole under fiducial assumptions, relieved to 1.9σ only by removing bulge galaxies., arXiv:2401.04796.

[180] X. Wu, Model-independent test of the cosmic distance duality relation with recent observational data, arXiv e-prints (2026), arXiv:2603.27616.

[181] S. Necco and R. Sommer, The $N_f = 0$ heavy quark potential from short to intermediate distances, Nucl. Phys. B **622**, 328 (2002), hep-lat/0108008.

[182] B. Lucini and M. Teper, $SU(N)$ gauge theories in four dimensions: exploring the approach to $N = \infty$, JHEP **2001** (06), 050, hep-lat/0103027.

[183] C. J. Morningstar and M. J. Peardon, The glueball spectrum from an anisotropic lattice study, Phys. Rev. D **60**, 034509 (1999), hep-lat/9901004.

[184] R. G. Edwards, U. M. Heller, and T. R. Klassen, Accurate scale determinations for the Wilson gauge action, Nucl. Phys. B **517**, 377 (1998), hep-lat/9711003.

[185] M. Teper, $SU(N)$ gauge theories in 3+1 dimensions, Phys. Rev. D **59**, 014512 (1998), hep-lat/9804008.

[186] G. S. Bali and K. Schilling, Running coupling and the Lambda parameter from $SU(3)$ lattice simulations, Phys. Rev. D **47**, 661 (1993), see also G. S. Bali, Phys. Rept. 343 (2001) 1.

[187] T. Lippert *et al.*, $SU(3)$ dynamical fermions: SESAM and TχL results for the Wilson action, Nucl. Phys. B (Proc. Suppl.) **60A**, 311 (1998), SESAM and TχL Collaborations, hep-lat/9707004.

[188] S. Güsken *et al.*, The static potential in full QCD, Nucl. Phys. B (Proc. Suppl.) **63**, 385 (1998), hep-lat/9710075.

[189] A. Jaffe and E. Witten, Quantum Yang–Mills theory, Clay Mathematics Institute Millennium Problem statement (2000).

[190] S. K. Donaldson and P. B. Kronheimer, *The Geometry of Four-Manifolds* (Oxford University Press, 1990).

[191] P. Shah, T. M. Davis, D. Bacon, *et al.*, The Dark Energy Survey: detection of weak lensing magnification of supernovae and constraints on dark matter haloes, Monthly Notices of the Royal Astronomical Society **532**, 932 (2024), arXiv:2406.05047.

[192] A. Berlin, Z. Bogorad, P. W. Graham, and H. Ramani, Cavendish tests of millicharged particles, Physical Review Letters (2026), arXiv:2510.25825.

[193] A. Berlin, Z. Bogorad, P. W. Graham, and H. Ramani, Electric accumulation of millicharged particles, Physical Review D (2026), arXiv:2510.25834.

[194] DESI Collaboration, M. Abdul-Karim, *et al.*, DESI DR2 results II: Measurements of baryon acoustic oscillations and cosmological constraints, Phys. Rev. D **112**, 083515 (2025), arXiv:2503.14738.

[195] F.-Y. Cyr-Racine, F. Ge, and L. Knox, Symmetry of cosmological observables, a mirror world dark sector, and the Hubble constant, Phys. Rev. Lett. **128**, 201301 (2022), arXiv:2107.13000.

[196] D. W. Pesce, J. A. Braatz, M. J. Reid, A. G. Riess, D. Scolnic, J. J. Condon, F. Gao, C. Henkel, C. M. V. Impellizzeri, C. Y. Kuo, and K. Y. Lo, The Megamaser Cosmology Project. XIII. Combined Hubble constant constraints, Astrophys. J. Lett. **891**, L1 (2020), arXiv:2001.09213.

[197] J. B. Jensen, J. P. Blakeslee, M. Cantiello, M. Cowles, G. S. Anand, *et al.*, The TRGB-SBF project. III. refining the HST surface brightness fluctuation distance scale calibration with JWST, The Astrophysical Journal **987**, 87 (2025), arXiv:2502.15935.

[198] C. Vogl *et al.*, No rungs attached: A distance-ladder free determination of the Hubble constant through type II supernova spectral modelling, Astron. Astrophys. **702**, A41 (2025), arXiv:2411.04968.

[199] K. Hotokezaka, E. Nakar, O. Gottlieb, S. Nissanke, K. Masuda, G. Hallinan, K. P. Mooley, and A. T. Deller, A Hubble constant measurement from superluminal motion of the jet in GW170817, Nature Astronomy **3**, 940 (2019), arXiv:1806.10596.

[200] J. Carrick, S. J. Turnbull, G. Lavaux, and M. J. Hudson, Cosmological parameters from the comparison of peculiar velocities with predictions from the 2M++ density field, Monthly Notices of the Royal Astronomical Society **450**, 317 (2015), arXiv:1504.04627.

[201] TDCOSMO Collaboration, TDCOSMO 2025: Cosmological constraints from strong lensing time delays, Astronomy & Astrophysics **704**, A63 (2025), primary $H_0 = 71.6^{+3.9}_{-3.3}$; +SLACS+SL2S combined $74.3^{+3.1}_{-3.7}$; supersedes the TDCOSMO-IV+SLACS $67.4^{+4.1}_{-3.2}$ value, arXiv:2506.03023.

[202] A. G. Riess, W. Yuan, L. M. Macri, *et al.*, A comprehensive measurement of the local value of the Hubble constant with 1 km s^{-1} Mpc^{-1} uncertainty from the Hubble Space Telescope and the SH0ES team, The Astrophysical Journal Letters **934**, L7 (2022), $H_0 = 73.04 \pm 1.04$ km/s/Mpc, arXiv:2112.04510.

[203] J. P. Blakeslee, J. B. Jensen, C.-P. Ma, P. A. Milne, and J. E. Greene, The Hubble constant from infrared surface brightness fluctuation distances, The Astrophysical Journal **911**, 65 (2021), $H_0 = 73.3 \pm 2.5$ km/s/Mpc, 40–99 Mpc, arXiv:2101.02221.

[204] R. Stiskalek, H. Desmond, and I. Banik, Testing the local supervoid solution to the Hubble tension with direct distance tracers, Mon. Not. R. Astron. Soc. **543**, 1556 (2025).

[205] A. Großardt, J. Bateman, H. Ulbricht, and A. Bassi, Optomechanical test of the Schrödinger–Newton equation, Physical Review D **93**, 096003 (2016), arXiv:1510.01696.

[206] H. Yang, H. Miao, D.-S. Lee, B. Helou, and Y. Chen, Macroscopic quantum mechanics in a classical spacetime, Physical Review Letters **110**, 170401 (2013).

[207] D. N. Page and C. D. Geilker, Indirect evidence for quantum gravity, Physical Review Letters **47**, 979 (1981).

[208] S. M. Saad and Y.-S. Ting, No gravitational anomaly in wide binaries from forward modeling of 3D orbits, The Open Journal of Astrophysics **9** (2026), arXiv:2603.11015.

[209] K.-H. Chae, B.-C. Lee, X. Hernandez, V. G. Orlov, D. Lim, D. A. Turnshek, and Y.-W. Lee, Detection of gravitational anomaly at low acceleration from a highest-quality sample of 36 wide binaries with accurate 3D velocities, arXiv e-prints (2026), arXiv:2601.21728, arXiv:2601.21728.

[210] Y. Yoon, Y. Tian, and K.-H. Chae, Probing the nature of gravity in the low-acceleration limit: wide binaries of extreme separations with perspective effects, The Astrophysical Journal **992**, 102 (2025), arXiv:2507.13177.

[211] X. Hernandez, V. Verteletskyi, L. Nasser, and A. Aguayo-Ortiz, Statistical analysis of the gravitational anomaly in Gaia wide binaries, Monthly Notices of the Royal Astronomical Society **528**, 4720 (2024), arXiv:2309.10995.

[212] H. Boufourou, Estimator forensics for the wide-binary gravity test: the eccentricity–triple coupling manufactures a pseudo-signal, and a pre-registered protocol for Gaia DR4, arXiv e-prints (2026), arXiv:2608.24556, arXiv:2608.24556.

[213] M. Królikowska and P. A. Dybczyński, The catalogue of cometary orbits and their dynamical evolution, Astronomy & Astrophysics **640**, A97 (2020).

[214] D. Vokrouhlický, D. Nesvorný, and S. Tremaine, Testing MOND on small bodies in the remote solar system, The Astrophysical Journal **968**, 47 (2024), arXiv:2403.09555.

[215] M. Milgrom, MOND effects in the inner Solar system, Monthly Notices of the Royal Astronomical Society **399**, 474 (2009), arXiv:0906.4817.

[216] S. S. McGaugh, MOND prediction for the velocity dispersion of the "feeble giant" Crater II, The Astrophysical Journal Letters **832**, L8 (2016).

[217] N. Caldwell, M. G. Walker, M. Mateo, E. W. Olszewski, S. Koposov, V. Belokurov, G. Torrealba, A. Geringer-Sameth, and C. I. Johnson, Crater 2: an extremely cold dark matter halo, The Astrophysical Journal **839**, 20 (2017).